The VELA Program

A Twenty-Five Year Review of Basic Research

The VELA Program

A Twenty-Five Year Review of Basic Research

Printed in the United States of America.
First Printing: 1985

Library of Congress Catalog Card Number: 85-080931

Dianne L. Carlson, Publisher
Executive Graphic Services

The views and opinions of authors expressed herein do not necessarily state or reflect those of the United States Government.

The VELA Program

A Twenty-Five Year Review of Basic Research

Ann U. Kerr
Editor

DEFENSE ADVANCED RESEARCH PROJECTS AGENCY

Editors Note

The Defense Advanced Research Projects Agency (DARPA) initiated the VELA Research Program in 1959 in response to a national need for development of a scientific basis for monitoring nuclear testing in all environments. From program inception, DARPA has developed the technical basis for all U.S. test ban treaty negotiations. The current focus of the program is aimed at improving capability to monitor underground nuclear explosions.

On the occasion of the twenty-fifth year of the VELA Program, a special review meeting was held to assess progress in the program throughout its history, to review the state-of-the-art in key areas, and to identify potential new improvements. This special volume commemorates the twenty-five years of the VELA Program. It includes talks and papers presented at the DARPA Review meeting and additional contributions of significance.

I would like to express appreciation to the authors for their cooperation and time taken for careful reading of the draft articles. Special thanks are due to several individuals for their efforts. George Duffin and his staff at Teledyne Geotech prepared two volumes of abstracts and materials for the special review meeting. Nancy Davis and her staff at Science Applications International Corporation typed all the manuscripts for this book.

Special acknowledgement is due to Dianne Carlson and her staff at Executive Graphic Services who redrew all the artwork and typeset the entire book. Without Dianne's tireless efforts and dedication, this volume would not be possible.

Ann U. Kerr
Editor

Special Recognition

Throughout the history of the VELA Nuclear Monitoring Research Program, many individuals from numerous academic institutions, industrial research groups, and government agencies have made major contributions to its success. There are two who have been instrumental, each in his own way, helping establish and shape the program through its various phases.

Carl F. Romney

Carl Romney has been uniquely involved in every facet of the VELA and DARPA programs since their beginning and continues his close involvement as Technical Director of the Center for Seismic Studies. He was a member of the United States Delegation to the 'Conference of Experts to study the " Possibility of Detecting Violations of Possible Agreement on Suspension of Nuclear Tests' in 1958. He was also a member of the Berkner Panel. These were two landmark efforts to consider international monitoring of nuclear testing and the scientific and technical issues related to monitoring. In both these roles he was instrumental in formulating the concepts, goals and requirements for a national program in nuclear monitoring, the catalyst for the VELA program. During a period of rapid and frequent changes in global nuclear testing he served as an Assistant Technical Director of AFTAC and provided the essential scientific leadership instrumental in shaping its organizational character emphasizing technical and analytical expertise. At the urging of ARPA, he served as the First Director of the VELA Seismological Center, establishing it as a strong technical force during its more than twenty years in the VELA program. Throughout his career he has served as a member of or Senior Technical Leader of every major United States test ban treaty negotiating delegation.

As Deputy and then Director of the Nuclear Monitoring Research Office at DARPA, his leadership in the field continued to set high standards of scientific excellence and champion the research program, especially in periods of budget uncertainties. In his role as Deputy Director for Research at DARPA he continued his interest in and support of basic research, highlighting the need for and strengthening the place of basic sciences within the Department of Defense.

During his federal career he received numerous awards and commendations. He is specially distinguished having been one of the first to receive the award of Presidential Executive.

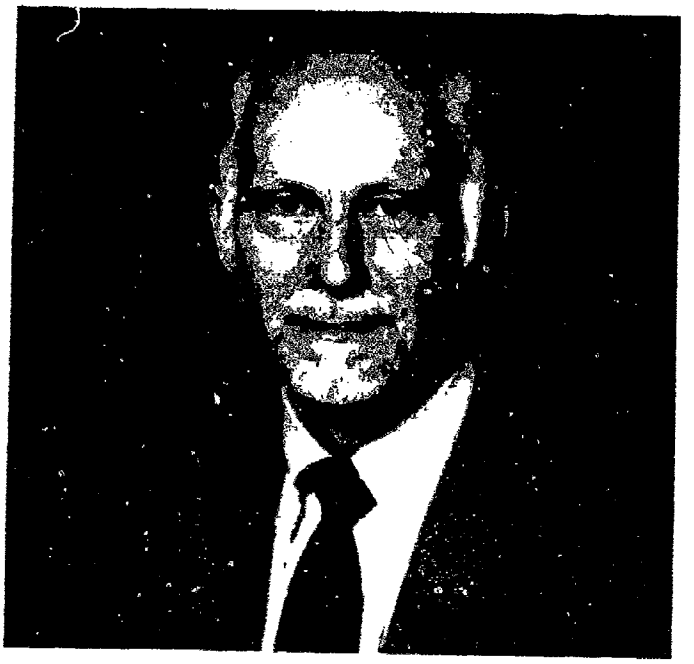

Carl F. Romney

William J. Best

Bill Best's contributions are many and unique and impossible to catalog here. His first career spanned twenty years as an Air Force Officer from which he retired as a Colonel in 1964. His second career as a Program Manager in the Air Force Office of Scientific Research also spanned twenty years. In both these careers he has received numerous citations and awards recognizing his contributions. He is one of the very few persons in the country who have been associated with the DARPA Research Program since its inception. In his various roles he has helped the science of seismology with his sponsorship of university research and the many scientists he funded and guided through the years.

The strong academic component of the VELA program and its emphasis on fundamental research is a hallmark of the program and of Bill's involvement and personal philosophy. Bill's management and foresight provided university scientists with facilities to advance seismology from a 'sleepy little science' in the 1950's to the dynamic field it is today; in its evolution influencing a broad spectrum of solid earth geophysics. Throughout the years, he provided key support at the university level to encourage and maintain a critical mass of fundamental research in solid earth geophysics. Two generations of seismologists were guided and supported through his efforts. Beyond the contributions of the university research program to nuclear test ban monitoring are the many careers in seismology fostered by Bill. Two generations of seismologists were guided and supported through his efforts. Many of today's key researchers in the field began and continued their individual careers as a result of Bill's stewardship.

It is not only what Bill has accomplished but how. His many accomplishments are well known but what is most cherished about Bill is his personal and unique style. Even in retirement from his second career he maintains strong ties with the program and his former "kids", a privileged title, indeed.

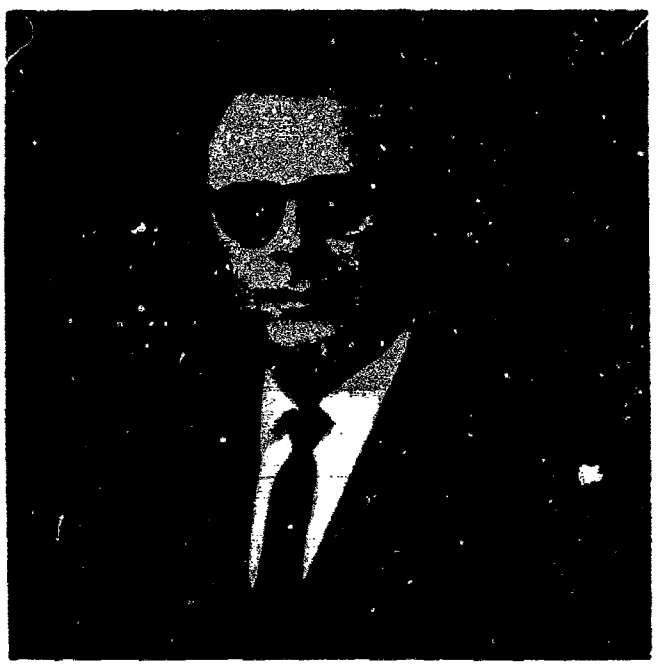

William J. Best

Foreward

The International Conference of Experts meeting in Geneva in 1958 explored a number of methods for monitoring a proposed suspension of nuclear testing and recommended a global control system for this purpose. Following this conference, and in the ensuing negotiations, it became quickly apparent how little was understood about the problems such a verification system would present. To remedy this situation, President Eisenhower formed a special Science Advisory Committee to review these proposals and to give recommendations on a broad range of issues concerning the capability to detect and identify nuclear explosions. One recommendation adopted by President Eisenhower, and given the highest priority, was the establishment of a comprehensive research effort to 'provide a full understanding of both the capabilities of presently proposed nuclear detection systems and the potential for improvements in such systems.' The newly formed Advanced Research Projects Agency within the Department of Defense was given the responsibility for developing this program. On 18 September 1959, ARPA Order Number 102 was signed providing funding to the U.S. Air Force for research in nuclear test monitoring technologies. Thus began project VELA. Other Orders followed quickly to the Atomic Energy Commission, the U.S. Coast and Geodetic Survey and the National Aeronautics and Space Administration. The incipiant VELA Program turned early to the National Academy of Sciences for assistance in mobilizing the U.S. academic geophysical community behind this effort. The continued funding by DARPA to this project over the twenty-five years that we now celebrate has profoundly changed the course of seismology and geophysics in both this country and around the world. Indeed, numerous present-day concepts about the constitution and dynamic processes of the earth owe their origins to this program.

Many of the papers in this review plot the course of steady improvements in the nuclear test detection field. Initial hopes for quick technological solutions to the overall verification problem for use in the Comprehensive Test Ban negotiations in the early 1960's proved unreachable. However, the program has served the country extremely well by providing the fundamental technical basis of the current U.S. nuclear monitoring system as well as supplying the sound technical advice necessary in the ensuing nuclear test ban negotiations. The idealism

and dedication to this project by the current generation of researchers is no less than those at the founding.

Much thanks goes to the participants in this review for their efforts in summarizing the state of the VELA research. Ms Ann Kerr must be particularly singled out for her organization and planning of the twenty-five year review and her commitment to produce a first class document.

Dr. Ralph W. Alewine, III
Defense Advanced Research
Projects Agency

Table of Contents

Introductory Talks Presented at the VELA 25th Anniversary Conference

Explosion/Earthquake Source Theory

Seismic Wave Propagation Effects
Development of Theory and Numerical Modeling

Appendices

A Review of Test Ban Research

Dr. Ralph W. Alewine, III

Within the DOD, the responsibility for these research and development activities to improve national capabilities to detect, identify, and determine characteristics of foreign nuclear explosions has been assigned to the Defense Research Projects Agency (DARPA). DARPA's charter includes responsibility for basic research and development to solve fundamental problems of nuclear test monitoring, as well as providing scientific support to U.S. arms control activities.

In recent years, the emphasis of verification research has been on improving the capability to detect and identify underground nuclear tests and on determining their yields. Currently, seismological methods are the primary means for the detection of such tests and the determination of yield. Other remote sensing means are likely to play a critical role by providing corroborating evidence of a treaty violation. Therefore, surveillance by, for example, satellite photography certainly would make clandestine testing more difficult. Under a comprehensive test ban treaty, it will be necessary to verify compliance in all environments: that is, in the atmosphere, in space, and in the oceans. Unlike underground nuclear tests, there is the additional problem of unambiguously attributing a detected nuclear explosion to the responsible nation.

A key point is that the verification of any nuclear test limitation agreement must be based on solid technical grounds. From a monitoring perspective, it is especially important that this technical foundation be established either before or concurrent with consideration of such agreements. Developing the foundations for verification technology *ex post facto* can lead to serious difficulties.

As a case in point, the Threshold Test Ban Treaty was negotiated with the Soviet Union in 1974 and set a 150-kiloton limit on the maximum size of underground nuclear explosions. Some provisions were made in the protocols of the treaty for the exchange of geophysical data and yields of two calibration explosions to aid in the monitoring of this treaty. Since the only practical way to estimate the yield of Soviet

underground nuclear tests at that time were seismological techniques, it fell to this method to serve as the primary monitoring tool. Prior to this time, U.S. policy was specifically aimed at seeking a Comprehensive Test Ban Treaty and, therefore, research on developing the methodology to achieve the level of yield accuracy required was a relatively neglected research area. As a result, the research base was insufficient to anticipate the yield estimation problems which subsequently have arisen with monitoring this treaty.

As a result of an intensive research effort, the technology and scientific basis for monitoring the Threshold Test Ban Treaty has advanced considerably since the time the treaty was negotiated. Our understanding about the processes which affect yield estimation has increased and additional measuremen chniques have been developed which can be used for on-site verification of the yields. Improvements to our monitoring techniques have been made and are continuing. However, these unilateral improvements to the current methods are inherently limited by the lack of sufficiently complete and reliable geophysical and other information concerning the Soviet nuclear test sites. If the uncertainties in our yield estimates are to be significantly reduced, more direct information is needed than is currently available, or is specified for exchange in the current treaty protocols.

The Soviets and others in this country have suggested that adequate verification of the TTBT will result from the exchange of the data called for when the treaty is ratified. Unfortunately, these data will be of limited use unless they can be independently verified. Even if these data were verified, they would not provide the required information to achieve the yield accuracies for other large tests.

In the Comprehensive Test Ban Treaty (CTBT) talks of 1977 through 1980, the discussions focused on three verification measures which would be placed into operation to supplement the national technical means of each country. These were:

- a network of seismic stations and arrays in the U.S., the U.K., and in the Soviet Union, specifically designed for treaty monitoring purposes;
- a system of International Seismic Data Exchange which would draw upon the work of the Conference on Disarmament; and,
- a provision for limited on-site inspections.

Since the CTBT talks were suspended, research has continued to develop the technology base in each of these three general areas. Most

of the recent efforts in on-site inspection technology have been undertaken by the Department of Energy national laboratories.

In a comprehensive or very low yield test ban situation, as we shall see, there would be inherent risks in relying on seismological techniques to provide definitive evidence of a concealed underground nuclear explosion. It must be emphasized that seismological methods, by themselves, may not be able to provide sufficiently conclusive evidence of a carefully concealed nuclear test. However, the seismological data can be used very effectively to quickly detect and locate suspicious events so that other verification methods can be focused on them.

The fundamental technical basis for monitoring underground nuclear explosions has not changed dramatically over the past decade. The concepts underlying the detection and identification of explosions and the techniques which can be used to attempt to evade detection and identification remain generally as they were described in some detail in the mid-1970's. However, there have been some important changes in capability resulting from steady progress in our research program in geophysics and explosion seismology. We now have a more complete understanding of the nature of explosions and earthquakes as sources of seismic signals, as well as the effect of the earth's structure on the propagation of these signals.

Most of the research emphasis before 1980 was on methods for detecting, identifying, and characterizing explosions from seismic signals collected at long ranges. These are primarily the signals which we can record with existing national technical means (NTM) based on seismic stations outside the USSR. With agreement in principle during the CTBT talks to establish seismic stations on Soviet territory, research has been redirected toward methods based on the use of data collected at regional distances (that is less than 2,000 km) from events of interest. Signals from these shorter distances turn out to be much more complicated than those from the longer ranges, but they can be exploited for the detection of much smaller events. It is these complicated signals that we must use from stations inside the Soviet Union under a nuclear test ban treaty. One of the key topics for research is development of robust techniques to identify explosion-like events using these regional signals. Since the character of these signals depends on each specific region, this research is handicapped by the lack of adequate data from the Soviet Union.

The most dramatic improvements in seismic monitoring capability have been in two major areas: (1) data collection capabilities, that is, improved seismic instrumentation, electronics, and high dynamic range digital data recording; and (2) development and implementation of automated

and more powerful data processing techniques. In reviewing this progress, a highlight is the development of ultra-sensitive seismometers with extremely great resolution and low noise electronics.

The shift to high quality digital data collection has made it possible to automate much of the data processing, and therefore to handle the large volumes of data that will be required with consistent procedures. The capability for automated processing and data analysis is still at a relatively early stage of development, but is being improved and demonstrated at the DARPA Center for Seismic Studies in Arlington, Virginia.

This promising new technology is being exploited as quickly as possible. Improved sensors developed in this program have been incorporated by the Department of Energy into engineering prototypes of seismic stations which could be used inside the Soviet Union or elsewhere. A network of these stations has been deployed in the U.S. and Canada for test and evaluation purposes. The digital data from these stations are broadcast directly by satellite to the DARPA Center, where they are used to test the automated data handling methods under development. The ability to handle the large volumes of data from a network of stations inside the Soviet Union is reasonably advanced. In addition, this development is providing a thorough evaluation of the prototype seismic sensor systems.

Under the auspices of the Conference on Disarmament (CD) work has continued on the development of methods for "International Seismic Data Exchange." The concept is to collect, organize, and make available seismic data voluntarily submitted by existing seismic stations at many locations around the world. These data could be used by countries that do not possess sophisticated National Technical Means to monitor for major treaty infractions, and they could supplement U.S. monitoring systems in certain remote areas. With the support of the DOD research program, the U.S. has been very active in the development, specification, and testing of procedures that could be used for these purposes. We have undertaken a number of technical initiatives within the CD to improve the overall global monitoring capabilities and to introduce advanced technical methods into the proposed international system.

With the firm backing of the U.S., the CD undertook last fall a two-month test of elements of the proposed system. Altogether, more than 37 countries took part, contributing data from almost 80 globally distributed seismic stations. Prototype International Data Centers were established in Washington, Stockholm, and Moscow to receive and analyze data from the network and to distribute the results to all participants. The Washington International Data Center used the facilities of the DARPA

research center and made extensive use of the automated data acquisition and processing methods developed for monitoring purposes. An evaluation of this test is now underway by the CD, but it is clear that a number of deficiencies must be corrected and the overall technology upgraded before such a system can play any meaningful role in a nuclear test ban situation.

During this international data exchange experiment, a number of nuclear explosions in the Soviet Union, French Polynesia, and the U.S. were detected and reported by participating stations, and locations and magnitudes were determined by the Washington and Stockholm data centers. However, the Soviet Union limited its participation to a single seismic station and, contrary to the agreed procedures, withheld data from all Soviet nuclear tests. Such actions reinforce the long-held U.S. position that any verification arrangement for seismic installations inside the Soviet Union must have the provision for direct access to the data produced by those stations.

It has been known for some time that special measures might have to be employed to achieve effective monitoring in the Kurile-Kamchatka area of the Soviet Union. This is an area of concentrated military activities, as well high seismic activity, and thus an area where evasion must be considered a possibility. One promising approach for improving the monitoring capabilities in this area was to implant seismic sensors deep beneath the sea bed in international waters in the northwest Pacific. The technology in instrumentation, marine engineering, and deep sea drilling has only recently been developed to a point where such a challenging project could be undertaken. An experiment was successfully conducted, using the drill ship *Glomar Challenger* to implant the sensors and recording systems, to demonstrate that effective monitoring data could be obtained from carefully chosen sites in the deep ocean. The results of this experiment open large new areas of the world, previously considered inaccessible, to installation of high quality monitoring stations.

A highly promising development in the research program has been the design and testing of a prototype advanced seismic array. This new array, called NORESS, offers the potential of providing much greater sensitivity for signal detection than any existing station. It also provides valuable information to help locate events. The superiority of such installations for the detection and identification of low-magnitude events in a test ban context is evident. After several years of design and experimentation in cooperation with scientists in Norway, the prototype NORESS array began operation in a research mode earlier this year in southern Norway, an area which is thought to be geologically similar to the western part of the USSR. This seismic research station, which is

the most advanced in the world, has been specially designed to detect and locate signals of higher frequency which propagate in the regional distance range. Initial indications are that NORESS can achieve about an order of magnitude improvement in signal detection capabilities in the regional range of interest. A very preliminary analysis indicates that the regional array has a detection threshold in the 2.5 to 3.0 magnitude range for certain regional paths extending into the Soviet Union. A full evaluation and exploitation of these results is underway.

Within the past decade, the research program has included a major effort to maintain and improve the global seismic monitoring capabilities and to provide a high quality data base for research and technique development. Eighteen advanced seismic observatories have been installed around the globe and other existing stations equipped with improved digital equipment. In addition, we have supported several international cooperative efforts to improve the available global data base for research purposes, including efforts with Australia and the Peoples Republic of China.

One major objective of the research efforts discussed thus far has been to reduce the threshold for signal detection to as low a level as possible. This is the area in which the research program has been most successful. For example, if the monitoring objective is to detect all nuclear tests as small as one kiloton or more, it now appears that a detection threshold of about magnitude 2.5 is required. At the present time, we have insufficient information about the geophysical characteristics of the Soviet Union to determine with any certainty the exact number and placement of seismic monitoring installations which would be necessary to achieve such a monitoring goal. Only rough estimates, based on imprecise assumptions, can be made.

In any case, a requirement for monitoring large portions of the entire Soviet Union at this level would be a formidable task in data processing and analysis because of the very large number of natural events of this size which occur. At the present time in our research program, the capability developed to detect small events has far exceeded our capability to differentiate small, or muffled, nuclear explosions from natural seismic events. This is especially true when only the complex data from regional distances are available. It has been estimated that, based on the technology available today, at least 1,000 natural seismic events per year at the one kiloton monitoring level would require special attention and analysis. With the current capability to discriminate between nuclear explosions and earthquakes, a significant fraction could not be confidently identified as non-nuclear. Some of these would actually be earthquakes that have seismic characteristics that do not easily distinguish themselves from explosions, and some would be chemical explosions.

Chemical explosions pose an especially difficult problem for a low yield nuclear test ban treaty. A large number of them are routinely conducted for civil and engineering purposes. In fact, there are occasional chemical explosions with yields of several kilotons or more. Current seismic verification capabilities are not adequate to distinguish between chemical and low yield nuclear explosions, or to provide the assurance that a *bona fide* chemical explosion is not disguising a nuclear test. Barring some unforeseen technical breakthrough, some alternative provisions will be required to deal with this problem.

A signatory to a nuclear test ban who is determined to conduct clandestine nuclear tests could attempt to do so in any environment — in space, in the atmosphere, in the ocean, or underground. The safest way to attempt clandestine underground testing is to design the test to produce seismic signals which are below the detection capability of the monitoring network. The most effective way to reduce seismic signals is to conduct the nuclear explosion in a large underground cavity (cavity decoupling). Large cavities, which can be used to reduce the signals of militarily significant yields, are not uncommon and can be constructed most easily in areas of underground salt deposits. Such areas are quite extensive in the Soviet Union. Cavities of the volume required for such tests exist, although all may not have the optimum shape for decoupling. In the United States they are used for storing petroleum reserves. Foiling such an evasion attempt requires a very sensitive monitoring network which is reliably deployed. This threat is the primary reason for the need for high quality stations and arrays inside the Soviet Union.

The U.S. has long recognized the threat imposed by the cavity decoupling method and has fully taken this into account in our monitoring capability estimates. However, it must be said that the current understanding of the seismic effects of cavity decoupling is incomplete and is based on a relatively sparse set of experiments. Inconsistencies remain between actual experience and theoretical possibilities. A full-scale feasibility test of this concept was conducted a number of years ago using a small nuclear explosion, and data from this experiment have been supplemented with laboratory and numerical models and other theoretical work.

There are indications from this experience and from theory that the cavity decoupling evasion method loses its effectiveness at frequencies higher than those now normally used for signal detection. Thus, if these high frequencies can propagate efficiently over certain paths, it may be possible to reduce the effectiveness of this evasion scheme in some circumstances. Several years ago, we discovered through our research program that seismic energy does propagate very efficiently across the

western portion of the Soviet Union, at least when the signals do not cross major geological boundaries. Stations deployed inside the Soviet Union could presumably take advantage of this. We are now collecting and evaluating such high frequency data from events originating in the Soviet Union to determine the propagation characteristics of very high frequency signals such as might leak out of a cavity-decoupled explosion. Much is left to be learned about this.

It is known that the Soviets have conducted a number of nuclear tests in areas where cavity decoupling is possible. They certainly have information on the propagation of high frequency energy in these regions. Such information, if available to the U.S. research program, would greatly reduce our uncertainties about the effectiveness of this evasion possibility and contribute to a better understanding of our verification capabilities.

A substantial number of high quality stations and arrays within the Soviet Union is necessary for effective counter evasion. Without these stations, evasion of the nuclear test ban would be relatively easy and with decoupling could involve explosions with fairly large yields, *i.e.*, more than ten kilotons. If there were a sufficient number of properly sited stations and arrays, evasion would not be impossible, but it would be much more difficult, complex, and expensive, especially for yields greater than a few kilotons.

One should bear in mind that no realistic seismic verification system will be able to monitor a zero yield test ban with 100% certainty. We also must realize that seismic evidence by itself cannot provide all of the stringent data that will be required to ensure compliance. Other methods must supplement this system. A realistic goal for our research program has been to provide the technology to deter cheating by maintaining a high probability of detecting and identifying nuclear tests of militarily significant yields. It is important that any verification measure be viable and contribute to confidence building by minimizing the number of natural earthquakes and man-made non-nuclear events (for example, chemical explosions) that could be mistaken for nuclear explosions.

A comprehensive test ban would be, from a monitoring point of view, a low-yield threshold treaty with a vague and undefined threshold. Consideration of an explicitly defined low-yield threshold test ban, rather than a comprehensive test ban, presents a different set of verification problems. As we have found out, monitoring the current 150-kiloton limitation on testing, which demands the precise determination of yield, is a very complex undertaking and requires considerable information about the geophysical conditions near the explosion site. As the yield limit becomes smaller, the range of possible variation in emitted seismic signals grows larger. Direct determination of yield by measuring the

hydrodynamic shock front can provide a relatively precise yield estimate for underground tests. This method could also provide a seismic calibration for small geophysically homogeneous sites and thus reduce the uncertainties of the seismically determined yield estimates of other tests. Such measures were discussed in the PNET negotiations and more recently by President Reagan as a means for improving the verification of the current 150-kiloton limit on testing.

In summary, DARPA has been conducting a vigorous research and development program to improve nuclear test ban verification capabilities. Significant improvements to our monitoring capabilities have been made through the research and development effort and they are continuing. Technology is being developed and improved, both for existing monitoring resources and for potential systems whose installation in the Soviet Union which would have to be negotiated. If successfully negotiated, the installation of a number of high quality tamper-resistant seismic stations and arrays in the Soviet Union would significantly lower the verification threshold of a nuclear test ban treaty. The amount of improvement that such facilities in the Soviet Union would provide depends on the number and siting of the installations, on the actual geophysical conditions within the USSR, and other factors. At the present time, the research efforts are handicapped by the lack of adequate geophysical and seismological data from key regions in Eurasia. Any action to make such data available would provide a major contribution to the effort to improve our seismic monitoring capabilities.

As technical experts, it is our role to realistically portray the capability and limitations to monitor compliance with proposed nuclear test limitation agreements. This is crucial for assessing the risks. There remain problems in detecting and, especially, identifying underground nuclear tests, particularly if they are carefully designed for evasion. Until these problems are solved, they will present a degree of risk. The potential for deliberate evasion must be balanced with stringent verification measures to reduce these risks, which should not be understated. These are the key problems to which our research efforts are directed.

10

Underground Nuclear Weapons Testing and Seismology — a Cooperative Effort

Gerald W. Johnson

As you know, I didn't come here to make a speech. I came here to listen. But I am pleased to have the opportunity to make a few comments. It has been my pleasant fate to have become associated with the seismic community almost 30 years ago. With respect to the seismic community, I would class myself as having been primarily a user of your product. I have learned to appreciate the fact that seismology is not an accurate science in the sense that safety requirements need to be implemented and treaties need to be verified. There is always a demand for less uncertainty. Rather than to go through a mass of detail, I would like to pick out a few points here and there and pick up on Hal Thirlaway's talk with respect to the history of the interaction between your seismologists and the nuclear weapon test program. My contact with you began in 1956—while I was in charge of the nuclear weapons test program in Nevada for Lawrence Livermore Laboratory.

The development of the technique of underground testing was stimulated in the latter 1950's because of the rising concerns about radioactive fallout both locally and worldwide from atmospheric testing. These concerns were brought forcibly to my attention in 1956 during our test operations in Nevada when we experienced delays of up to three weeks awaiting favorable wind patterns which would result in acceptable local fallout. Steps were taken to reduce the local fallout by firing the test devices on top of steel towers up to 500 feet high or alternatively suspended from tethered balloons at altitudes up to 1500 feet. While these approaches were successful in alleviating the problem, as time went on and political sensitivity increased our operational constraints actually increased.

To assure that operations were carried out in accord with guidelines established by the Atomic Energy Commission for maximum allowed exposure of test personnel as well as offsite individuals and communities to radioactivity and other offsite potential hazards arising from flash,

airblast, and—to some degree—ground shock, it was necessary to establish a large task force. As a consequence, when the operations were carried out there were thousands of people on the site. Because so many individuals were involved costs were very high and as a consequence the operations were carried out as expeditiously as possible. Such crash efforts carried out at intervals of about eighteen months were a complication to those of us who were responsible for the development of nuclear weapons. We concluded that development could advance more expeditiously if it were possible to establish a "laboratory" in which tests or experiments could be conducted at times dictated only by the test program.

Because of all of these concerns and based on a suggestion by Edward Teller and David Griggs, the test division at the Lawrence Livermore National Laboratory designed an underground nuclear test to evaluate the practicability of such testing for nuclear weapons. If the required technical data could be successfully recovered at acceptable cost we would have available the laboratory we desired and we would be able to fire without serious concern for the winds or for off-site hazards to people or property, with the possible exception of the effects of ground shock on structures off-site for sufficiently large explosions.

Since this event, code-named RAINIER, was to be an experiment, the explosive selected was a production unit which would give a known yield of 1.7 kilotons. For convenience and, we thought, simplification of instrumentation, it was decided to place the explosive at the end of a long tunnel driven into the side of a mountain on the Nevada Test Site, now known as Rainier Mesa. The tunnel was terminated in a spiral designed to be self-sealing with respect to radioactivity and the explosive was placed in a small cubical room at the end of the spiral. The tunnel immediately outside the room was sealed with several feet of sandbags. The physical, chemical, and mineralogical properties of the medium surrounding the emplacement chamber were characterized in detail as well as the geological structure out to the mouth of the tunnel. With all of this detail in hand it was hoped that the post-shot results could ultimately be amenable to theoretical analysis and interpretation.

It was early recognized that the explosion would be measurable over large distances with seismographs and could be useful to the seismological community. In addition, the closer-in strong motion measurements could be applied to assessment of damage to local structures as well as characterization of the near field. In response to their suggestions, to be most helpful to the scientific community we arranged to announce, prior to detonation, what the total expected energy release would be and to provide the geographical coordinates of the center of detonation.

It was also agreed that the detonation time would be announced ahead of time and that the event would take place within one-tenth second of the announced time. In the event that the firing was delayed for any reason, the delay would be twenty-four hours at a time.

As operators we were interested in encouraging the seismic measurements which would form the basis for establishment of allowable yields to be tested at the Nevada Test Site. The cooperative arrangements worked out at that time formed a precedent for subsequent activities of a similar nature.

However, our good intentions almost got us into trouble. The publicity attendant to the announcements to be made to the scientific world almost cost us the test. In early September of 1957 when we were making final preparations, in the course of an international meeting on geophysics in Toronto this experiment was described to the assembled scientists as all of us desired. However, when the press picked it up the subject hit the headlines with the announcement that the Atomic Energy Commission was planning to fire a small "Earthquake Maker" in Nevada.

This unfortunate description of the event led to a number of difficulties for us. First ' all Louis Strauss, the Chairman of the Atomic Energy Commission wno had the final approval authority for us to proceed, called me to state that the Commission would only approve the event if we could assure them with respect to the following three questions:

1. The detonation would not directly cause seismic damage.
2. It would not trigger an earthquake.
3. If a natural earthquake occurred at the same time with an epicenter in the vicinity of the test, we had to be able to prove it had not been caused by the detonation.

Since none of us were qualified to answer these questions and also since we were advocates for the tests our objecti-ity might be subject to question, we asked the seismologists for help. A small advisory group was established under the chairmanship of Professor Perry Byerly of the University of California at Berkeley. This group was able to successfully reassure the Commission on all questions raised for an energy release of 1.7 kilotons. In fact, in response to a question from Chairman Strauss, the spokesman for the committee stated that up to one megaton could probably be fired underground at the Nevada Test Site without undue risk to property off-site in Nevada.

The test shot was successfully fired on September 19, 1957 without measurable release of radioactivity and subsequent analysis of the

measurements indicated that nuclear weapons development could be successfully carried out underground at yields of interest and under conditions which would protect public safety—the basis for the underground "laboratory" had been established. The seismic measurements were accomplished by the community out to a few thousand kilometers and the cooperative precedent was established between the underground nuclear program and the earth scientists.

Now that underground testing was initiated we felt we were in the clear to continue with weapons development and as the understanding of the phenomenology of RAINIER unfolded a new program to explore the possible constructive uses of nuclear explosions was initiated—The Plowshare Program. An important component of the program was the hoped use of explosions in various parts of the world as seismic sources for purely scientific purposes.

However, our joy was short-lived because a little more than a year later on November 1, 1958, President Eisenhower directed that the U.S. would abstain all nuclear weapons testing unilaterally provided the Soviet Union would do likewise. A few days later the Soviets completed their test series and Brezhnev made a parallel statement for the Soviet Union. The test moratorium had begun. While testing was being held in abeyance by both sides, they agreed to discuss the negotiation of a comprehensive nuclear test ban—the CTB.

The initiation of the talks with the Soviets began in Geneva in early 1958 and continued in various forms until 1961 when atmospheric testing was resumed. The test ban discussions focused early on the verification issues in the atmosphere, in outer space, underwater, and underground. Since underground testing was new and offered promise as a test procedure eliminating the politically sensitive issue of radioactive fallout it received special attention. Questions raised were the now-familiar ones of the limit of capabilities of seismic systems to detect and identify underground nuclear explosions which meant most importantly to distinguish between such events and earthquakes taking into account a number of possible evasion scenarios. One of the questions raised was the need for calibration explosions of known yields at the test sites of both sides.

To explore the technical aspects of the proposed arrangements a small group of us met with the Soviet scientific team several times in Geneva to discuss the capabilities and limitations of verification by seismic means. A seismic improvement program was discussed involving improved instrumentation, use of arrays, and a substantial list of calibration tests world-wide with explosions up to the megaton energy range. While none of this effort resulted in a cooperative program with the Soviets or in

a test ban, it did provide the basis for a substantial boost in the U.S. seismological program and for cooperative work with other nations.

The resumption of atmospheric testing in 1961 implied that the Plowshare program could proceed, which it did with primary emphasis on cratering since the Panama Canal Company and the Corps of Engineers were interested in the possible use of nuclear explosives for canal construction. At the same time a number of events were carried out in various geological structures for a number of different justifications and in different parts of the United States. All of the events were coordinated with the seismic community for scientific purposes and to generate data for possible future test ban considerations.

As an aside, all during this period and beginning with an exchange I had with the head of the Soviet atomic energy program, Emelyanov, at the Atoms for Peace Meeting in Geneva in 1958, the Soviet attitude toward Plowshare—now referred to as peaceful nuclear explosives applications—was militantly negative. The Soviet position was that this talk of constructive uses of nuclear explosives was a subterfuge by the United States to continue nuclear weapons testing under the guise of peaceful uses. It was not until 1964 that the Soviets first hinted that they were developing an interest in Peaceful Nuclear Explosives (PNEs), which I believe was the original designation of the program by the Soviets and was the name later adopted by the U.S.

With the completion of the test series in 1963 by the Soviet Union and the United States, the sides agreed that it was time again to consider limiting nuclear weapons testing especially in the atmosphere. As a consequence, recognizing that a comprehensive treaty was difficult to negotiate but still the ultimate goal, the Limited Test Ban Treaty (LTBT) was signed and ratified. The treaty limited all nuclear weapons testing to the underground environment.

The entry into force of the LTBT forced both the U.S. and the USSR to conduct all of their testing underground subject only to the condition that the tests would be conducted in such a manner that radioactivity would not be deposited (USSR position) or present (U.S. position) outside the territorial limits of the state in which the test had taken place. Under these guidelines over the ensuing years hundreds of explosions have taken place at the test sites of the two powers with energy releases up to the megaton range. Although the U.S. continued its program for only a few more years the Soviet Union embarked on an ambitious PNE program involving several events per year and with tests taking place over widely separated parts of the Soviet Union. The experiments covered a wide range of interests including excavation, gas and oil stimulation, mining, production of underground cavities, and a major continental deep

seismic sounding program. While some of the nominal yields of Soviet PNE events have been announced most have not. They did not at any time pick up on the Rainier cooperative precedent with the seismic community. As a consequence, today we still do not have a confirmed yield on any Soviet event, so calibrations for scientific and verification purposes still are needed.

The next challenge to the seismic community came with the negotiation and signing of the Threshold Test Ban Treaty between the U.S. and the USSR in 1974, which among other things limited underground tests to yields of 150 kilotons. Monitoring this limitation required that, in addition to detecting and locating nuclear tests by teleseismic means, it was also necessary to measure their yields. An additional related treaty, the Peaceful Nuclear Explosion Treaty (PNET), signed in 1976, included the 150 kiloton limitation for single explosions but permitted group explosions up to 1500 kilotons provided the yields of the individual explosions comprising the group could each be measured. To be able to verify the yields of individual explosions in a group would require intrusive on-site measurements to satisfy compliance conditions. Neither treaty has been ratified but both sides have behaved as if the 150 kiloton limit provision were in-force and both sides have on occasion challenged the other when their teleseismic measurements suggested there might have been a violation. The diplomatic problem has been complicated by the fact that it has not been possible to develop a technique for the accurate enough measurement of yield teleseismically.

With the inauguration of the Carter administration in 1977 a new thrust was initiated to negotiate a Comprehensive Test Ban Treaty banning all nuclear weapons testing. In principle this would have implied that the National Technical Means would need to have the capability of measurements of yield approaching zero—which of course would be quite a technical challenge. In practical terms this requirement was interpreted operationally to mean that best efforts would be made using seismic methods and to negotiate cooperative procedures to improve the monitoring capability.

One approach explored to improve detection and identification and, perhaps to improve modestly the yield measurement, was the concept of unmanned seismic stations in the testing countries. The stations would be in operation continuously and all data would be transmitted in near-real time to the signatories of the treaty. The design provided that all data would be automatically authenticated and the seismometers were to be installed in tamper-proof configurations at the bottom of sealed drill holes. While the negotiations were not successfully completed, the delegations had agreed to 10 stations each in the U.S. and the USSR and the

general locations were selected. The United Kingdom agreed to have one station on their territory.

Toward the end of the CTB negotiation in early 1979 in the course of a reception at the British Mission, Petrosyants, the head of the Soviet CTB delegation, and his deputy, Timerbaev, pulled me aside for a conversation. They inquired whether it would be possible to arrange for the USSR to buy two of the American national seismic stations, one of which they would install at the site of one of their seismic installations and would be jointly manned by a USSR, UK, and U.S. team as a research endeavor to assess the performance of the system in the Soviet Union. It later developed that the proposed installation would be located in Obninsk, some 80 miles southwest of Moscow. The other NSS would be examined in detail by the Soviet Union. What was of interest to me at that point was that they did not link the deal to completion of the negotiation—it was to be a separate activity.

The Soviet proposal was consistent with our concept of the application of the NSS and the experience gained by the joint experiment was deemed desirable. It required several months of discussion to work out details of technology transfer as well as visits of a Soviet technical team to the U.S. to see the equipment and a visit of U.S. personnel to Moscow and Obninsk. Toward the end of 1979 it appeared that it might be possible to proceed but then concern over the presence of the Soviet Brigade in Cuba was revived and the invasion of Afghanistan began. These events stopped all further activity on the possible cooperative effort which had appeared so promising. In the meantime, the development and testing of the NSS approach continues in the United States which could permit implementation of the idea if another opportunity were to appear.

These recollections serve to illustrate the intimate association between all of the varied aspects of underground testing and seismology that has developed and continued for a quarter of a century to the benefit of both endeavors. That such mutually profitable cooperative activities will continue with increasing challenges there can be no doubt and they should continue to be encouraged in every way.

Forensic Seismology

H.I.S. Thirlaway

Forensic, (from forensis) formally means a forum or market place, and I shall give some personal impressions of the way in which seismologists have been drawn into the political market place, and how they and their science have performed and continue to fare in the complex negotiations which precede the adoption and control of international treaties.

Efforts to ban the testing of nuclear weapons was thought to be a logical step to inhibit the development of nuclear armaments. In these endeavours, geophysicists have been required to act as expert witnesses in a variety of unfamiliar forums—conferences of experts, congressional hearings, technical working groups attached to policy-making delegations — to name a few. Seismologists have been concerned with the problem of proof, beyond all *reasonable* doubt, of the nature of seismic events in the context of a total ban on nuclear weapon testing—that is to say, with differences between earthquakes and explosions as observed on seismograms.

Nuclear tests in other media—water, the atmosphere and outer space—are prohibited by the provisions of a treaty which was signed in Moscow by the UK, USA, and USSR on August 5, 1963, and subsequently ratified by over 100 countries. Indeed, there are several other treaties in which the capacity of the geophysical and other sciences to detect possible violations have played, and continue to play, some part. These are the Antarctic Treaty (1959), the Treaty on Principles Governing the Activities of States in the Exploration and Use of Outer Space (1967), the Treaty for the Prohibition of Nuclear Weapons in Latin America (Treaty of the Tlatelolco 1967), the Treaty of the Non-Proliferation of Nuclear Weapons (1968), the Treaty on the Prohibition of Emplacement of Nuclear Weapons and other Weapons of Mass Destruction on the Sea-Bed, and the Treaty on the Limitation of Anti-Ballistic Missile Systems (1972). That there may be important omissions among the countries adhering to any of these treaties is irrelevant to the fact that the treaties are in force, and open to any state to join, so that, on the face of it, scientists have convinced each other, and their governments have accepted, that violations of these treaties could be verified. Consequently, it is not too unlikely to suppose that one day geophysicists may be required to give evidence before juries of some kind as to whether or not violations have occurred. The history of technical negotiations associated with the test-ban treaty, as well as

of forensic medicine, warns us that it is not a task to be undertaken lightly, and without training and experience beyond the normal professional experience of the witness.

The Antarctic, Non-Proliferation, and Sea-Bed Treaties provide for on-site inspections of one kind or another to verify suspected violations. Others either make no specific mention of procedures for verification, or, as in the case of the limitation of anti-ballistic missiles, for example, the USA and the USSR will rely on their "national technical means" of verification. This is the formula required for converting the provisions of the Test Ban Treaty of 1963 to a comprehensive ban by including underground explosions, but seismologists have so far been unsuccessful in convincing themselves and their governments that national means of verification by "remote seismographs" is an adequate safeguard against undetected but important nuclear weapon tests, as well as tests, which by natural causes or by intention, appear to be earthquakes. Even more embarrassing for a seismologist would be the earthquake, which appearing to be an explosion, would thereby lead a state to be falsely accused of violating a treaty.

From time to time, and especially in the early 1960's when enthusiastic attempts were made to reach agreement, politicians voiced their impatience with this apparent lack of professional expertise. The blame was put on the science. Seismology, they said, had been so neglected as to be still in the Stone Age compared with nuclear and space research. Some of the blame might more properly have been ascribed to the inexperience of seismologists in applying their knowledge to the special case of the manifold procedures necessary for the control of treaties of this category. Forensic seismology, in other words, was an unknown art, and no one thought to learn from medical colleagues who were in a similar fix 200 years ago.

It was in 1791 that a leading physician, John Hunter, made apparent that special experience was required before a medical man was fit to act as a witness in a court of law. The case was Rex *vs*. Dunellan at the Warwick Lent Assizes. The prisoner was accused of poisoning by use of laurel water and the evidence was overwhelmingly in favour of the prosecution. John Hunter, acting as expert witness for the prosecution, and in answer to the following question by the Court, "Give your opinion in the best manner you can, one way or the other; whether upon the whole of the symptoms described, death proceeded from the medicine or any other cause?" replied, "I do not mean to equivocate; but when I tell the sentiments of my own mind, what I feel at the time, I can give nothing decisive". Seismologists were in much the same dilemma 25 years ago when governments first availed themselves of their knowledge and experience for the purpose of formulating a nuclear test-ban treaty. Like

our medical colleagues, before they created a formal branch of their science dedicated to aid law in fixing the perpetration of a crime, or to rescue an innocent person from a falsely imputed crime (in test-ban terms, to detect a violation and avoid a false alarm), we approached our new duties with some apprehension. Conscious of the importance which might be attached to the evidence, we were only too aware of the narrow basis on which the science rested. We did not enjoy the public gaze in which often we had to work; we had little or no experience in handling journalists and, in our innocence, resented what we thought was the unreasonable license allowed them, and the occasional disparaging comments they made. We were not careful enough to separate fact from opinion and comment for the benefit or our officials; we did not give sufficiently direct answers to simple questions; we filled our answers with technical terms and jargon as though addressing professional societies rather than civil servants and politicians and to cover our deficiencies we tended to exaggerate.

If you think I exaggerate, listen to one Soviet seismologist commenting, in 1960, on the apparently straightforward relationship between seismic magnitudes and yields of explosions in the form

$$m = C + n \log Y$$

"It is possible that in the American treatment of 'New Seismic Data', some role was played by the circumstance that an increase of n to 1.0 leads to a considerable increase in the computed annual number of earthquakes, exceeding in magnitude nuclear explosions with yields approximately up to 20 kilotons, as compared with the previous Geneva evaluations, and leads to the development of the view that there is much greater difficulty in recognizing such nuclear explosions among the 'tremendous' number of earthquakes." Again: "The failure of the American experts in analysing and discovering the causes of the 'unexpected' (to them) agreement between local and teleseismic magnitudes in the indicated experiment, can only be explained, in this case, by the hypnotic effect of the very fact that numerical values, obtained by different means, were the same". The author ends in "friendly" terms when he "expresses his heartfelt thanks to his fellow workers...and also to his American colleagues...for their ardent discussions, which aided considerably in allowing us...to distinguish what was essential from what was secondary". If these polemics were possible between professional colleagues, what could the political delegations make of the witnesses? It is instructive to look in retrospect at the basis of these comments on the seismic magnitude problem; they illustrate how a variety of contentious issues concerned with detection and discrimination thresholds stemmed from the inadequate scientific base.

The technical working group of the Geneva Conference on the Discontinuance of Nuclear Weapon Tests was composed of the Soviet Union, the United Kingdom , and the United States, and was attended by the Personal Representative of the Secretary General of the United Nations. It opened on 31 October, 1958, and ceased in January, 1962. The discussions were published verbatim by the United Nations; they are essential reading for all forensic seismologists. The delegates enjoyed the benefit of a moratorium on testing until September, 1961, when the Soviet Union effectively destroyed confidence in further negotiations by unilaterally resuming testing over Novaya Zemlya.

The magnitude problem arose from specially recorded seismograms of a number of nuclear explosions conducted in Nevada in the autumn of 1958, almost a year after the first underground nuclear explosion, named Rainier, and having a yield of 1700 tons. The Atomic Energy Commission of the United States had given pre-shot details of RAINIER immediately after Professor Bullen's address at the IUGG in Toronto on the value of atomic explosions for seismology. (The Soviet delegation, led by Professor Beloussov, walked out of the meeting called by Keith Bullen to agree a telegram of thanks to the AEC). The experts at the initial conference on the test ban in August, 1958, relied heavily on the RAINIER data when assessing the relationship between seismic magnitude, yield and the number of earthquakes occurring annually at a given magnitude threshold. The magnitude adopted by the Geneva conference was 4¼. The number of earthquakes of this magnitude had to be estimated because the RAINIER seismograms showed no characteristics unique to explosions, so the experts were forced to accept a rarefaction, or downward first motion of the ground, and depth of focus as positive evidence for earthquakes. Earthquakes were thereby eliminated one by one and the remaining unidentified events were to be verified by inspection of the epicentral areas. The number of unidentified events depended on the total number of events recorded at given magnitude thresholds. Accord on these matters was reached in the summer of 1958, and the design of a network or seismographs to control the treaty was specified.

Meanwhile, the United States government had decided to supplement existing stations in the USA by deploying a special network of Benioff seismographs to observe the series of underground nuclear tests which were already planned for the autumn; the yields in terms of TNT equivalents ranged from a few hundred to 20,000 tons. The observations did not confirm the interpretations and extrapolations made from the RAINIER data and, after some reluctance on the part of the Soviets, the seismograms were tabled for discussion in the technical working group at Geneva.

The contentious issue central to the problem was the magnitude-yield

relation to which I have referred. Three Soviet seismographs had detected the explosion of nearly 20,000 tons at distances in excess of 6000 km. They gave a magnitude of about 5.2, roughly in agreement with three American observations from stations between 2500 and 4000 km from the explosion. This value did not agree with the local magnitudes estimated from the nearer stations of the newly established network of the western United States. A value for M_L of just over 4¾ was derived from recordings at stations between 180 and 600 km distance to compare with the M_L value for RAINIER (yield 1700 tons) of 4¼ accepted by the first experts' conference. Attempts to relate the magnitude scales for local and distant events had already been made by Gutenberg, who warned us not to place too much reliance on the result, but because seismographs had been specially deployed in the United States up to distances of 4000 km, a comparison of the two scales was possible by direct observation. Eight of these, including the three most distant American stations referred to earlier, recorded the explosion, and, a mean of just over 4.8 was estimated as a teleseismic magnitude. Accordingly, the American local and teleseismic values were accepted as a homogeneous set and an "official" magnitude of about 4¾ was assigned to the 20,000 ton explosion in conflict with the Soviet value (from their three stations) of just under 5.2. Views hardened round this difference of nearly ½ magnitude. It followed that the Soviets could not accept the American view that explosions (earthquakes) of given yield (magnitude) were more difficult to detect than had been thought from the RAINIER data; nor could they accept the larger number of earthquakes (and therefore greater number of unidentified events for a given yield equivalence) which the lower magnitude estimate implied. They argued that five of the stations from which the teleseismic magnitude had been estimated were located in an anomalous distance range—the so-called shadow or second zone between 10° and 20°, and that the low magnitudes derived from them were due to a systematic error in the amplitude-distance normalizing function.

Why had the RAINIER data misled seismologists just a few months earlier? Simply because of the scatter of data. Three well-regarded stations in the California (local) network turned out to be singularly poor receptors for *P*-waves originating from explosions in Nevada. For the explosion in question, the mean local magnitude of two of these stations was as much as one unit less than the mean of the eight near stations first used to estimate RAINIER's magnitude. When considering RAINIER in the summer of 1958, the Conference of Experts did not have data from the three stations; by including them, the average magnitude was made just over 4. In retrospect, it does seem extraordinary that we fell into the trap, especially when you remember that seismic magnitude—an empirical number without theoretical basis—in some quarters is not regarded as a respectable research activity

for seismologists. We did what every medical student is taught to avoid—we were persuaded to appear as witnesses to testify about what we did not know.

Sadly, there are several other instances of our inexperience in these early days. One eminent physicist seriously argued the feasibility of muffling seismic signals from a megaton of nuclear explosives. The same man claimed it would need the most powerful computers of the day (the IBM "Stretch") to process the UK delay-and-sum arrays. A well-known (though less eminent) seismologist advocated using complexity differences to discriminate between earthquake and explosion seismograms.

In retrospect again, the latter is another example of a witness testifying about what he does not know. The criterion was founded on data recorded by the first large array of seismometers between Laramie and Cheyenne on the Pole Mountain granite of Wyoming. The *P*-wave trains of some 90 percent of earthquakes recorded there spread over a significantly greater time than those of explosions. Earthquakes were said to be more "complex" than explosions and the "complexity criterion" was invented. From the accepted notions of the two source mechanisms, there were plausible reasons why earthquakes should generate more complex wave trains than explosions. At first, these were not matched quantitatively when modeled and when the first large underground explosion in the Lower Palaeozic structure of Novaya Zemlya generated relatively complex *P*-wave trains at North American stations, the criterion was destroyed.

Subsequent explosions at many places have thrown some light on what it was we did not know at the time: it is not the source mechanisms but the structures underlying seismographs and/or distant sources that are the principal reasons for complex short-period explosion seismograms.

The questions raised by this conclusion have been studied in detail. It turns out that abnormally long *P*-wave trains from distant events are structured by differences in phase velocity and frequency as well as amplitude; discrete signals were identified, and phase velocities and travel times assigned to them. The simplest explanation of the data is that the *P*-wave scattered below the source and/or seismograph; *P*-waves following a *single* path of low absorption throughout their travel arrive as simple high frequency, large amplitude pulses. Kazakh to Pole Mountain is such a path, Novaya Zemlya to North America is not. In general, maximum absorption, low m_b and complexity is observed on paths between recent fold structures.

Paths between Shields or sometimes between ancient fold mountain structures, for example that of Kazakh to Uppsala, are paths of minimum absorption and complexity. This is the reason for the exaggerated yields Uppsala Observatory published of explosions in Kazakh. When these ideas are incorporated in computer codes the model predicts basic features of

a seismogram given the Q structures of source and receptor areas. A useful contribution to the world wide values of local Q is the correlation with P_n velocities predicted by Marshall and Springer.

It is worth noting that studies of explosions in "normal" areas of the earth were responsible for these advances in the understanding of forensic seismology. Earthquakes make poor sources not only because of the uncertainties about their source mechanism, to which we formerly ascribed magnitude and complexity anomalies, but also for the reason they occur in anomalous and restricted areas of the earth. Many ideas about the Upper Mantle have their basis in seismograms of events occurring in seismic zones and, what is more, are recorded by stations which by and large are sited in or near such zones: the relatively old and stable interiors of continents are thinly populated by seismographs. In contrast, the greater proportion of the data of forensic seismology are from sources in many different aseismic areas recorded by seismographs on shields on which the UK arrays are sited.

Meanwhile rapid advances were made in the development of long-period seismometers. The use of spring materials with nearly zero temperature and creep coefficients, which were developed for the oil industry's gravity meters, and the appreciation that much of the ambient long-period noise was due to small fluctuations of the ambient pressure, was largely responsible for the order-of-magnitude increase in the gain at which long-period seismometers can now be operated. This means that surface waves, in particular Rayleigh waves, of small seismic events can now be recorded at great distances. This has advantages for estimating yields and the recordings have also provided data which seem to confirm early intuitive ideas, and later theoretical studies, that there is a fundamental difference between the two sources in the ratio of the P-wave/Rayleigh wave spectrum. The literature of this period is sprinkled with the scatter diagrams of P-wave *vs.* Rayleigh magnitudes, and they generally demonstrate two well-defined populations—one of explosions, the other of earthquakes.

For the first time, these observations provided the basis of a criterion which allowed explosions to be identified and to dispense with the primitive procedures leading to a residue of unidentified earthquakes or explosions, and perhaps even with on-site inspections. Sir Solly (now Lord) Zuckermann, then Chief Scientific Adviser to the Prime Minister, decided that the results sufficiently advanced the powers of forensic seismology to justify re-opening negotiations to agree a treaty to ban testing of nuclear warheads. To this end he persuaded Professors Millionchekov, Emalyanov and Artsimovich, supported by Dr. Keilis-Borok, to meet him, Dr. Bob Press and myself in the Soviet Academy of Science, Moscow, during a week in September, 1966. He succeeded in his purpose of convincing his Soviet

colleagues that the results deserved an initiative. Sadly, when the UK Foreign Secretary of the time met Mr. Gromyko shortly afterwards, the latter did not agree to approach the USA with a joint proposal to re-open formal negotiations.

The criterion remains one of the most powerful of forensic tools given that the technical difficulty of detecting Rayleigh waves is solved by siting stations within 1000 km of sources. Together with many other data, which have been presented as working papers to the political forum of the Conference of the Committee on Disarmament, it has been informally discussed and explained by seismologists to the delegates. The Committee has met in Geneva each year since March, 1962, when an initiative by the Soviet Union and United States to resume general disarmament talks (which had ceased with the technical working groups in January, 1962) was endorsed by the General Assembly of the United Nations. In those days, it was the Eighteen Nation Committee on Disarmament. It was enlarged in 1969 and changed its name. It reports progress each year to the United Nations and several of the disarmament measures now in force are due, in some degree, to its labours.

In recent years, an "Ad hoc working group of scientific experts" has been recognised by the committee and has succeeded in designing experiments having the object of testing the general validity of forensic methods developed nationally. At the same time, confidence in these advances led to serious negotiations between UK, USA and USSR which attempted to translate them into treaty language. Agreements on international exchange of data, siting of national stations in the Soviet Union and USA (but not unfortunately so far, in UK territories) and on-site inspection of otherwise unverified seismic sources were agreed at least in principle. There remains the ways and means of transmitting and processing the enormous quantity of data (for which recent developments are demonstrating the solutions) and of establishing the format of the jury to which seismologists would "give their opinion in the best manner they can...upon the whole of the symptoms described."

Alas, progress was too fast and these negotiations are adjourned to allow some participants to catch their breath. Perhaps forensic seismologists have come of age. Certainly we have learned from the bruising I described when I gave the 10th Anniversary Lecture in honour of Sir Harold Jeffreys on 8 December, 1972, in London. I feel equally privileged to be invited to give it, slightly modified, for the second (and certainly the last) time at the 25th Anniversary of the VELA Uniform program in Santa Fe, a program with which my own group has the honour to cooperate and which has blessed me with life-long friends and many after dinner tales.

References

1. "World Armaments and Disarmaments", *SIPRI Yearbook 1972*. Paul Elek, London.
2. *The United Nations and Disarmament 1945 - 1970*, United Nations, New York 1970.
3. *Strategic Arms Limitations. Pt. I*, SIPRI Research Report 1972. Paul Elek, London.
4. Sir Michael Wright, *Disarm and Verify*, Chatto and Windus, London 1964.
5. *Taylor's Principles and Practice of Medical Jurisprudence*, ed. Fred J. Smith: J. and A. Churchill, 1905.
6. Riznichenko, Yu V., 1960. "Seismic Magnitudes of Underground Explosions", *Transactions of the O Yu Shmidt Institute of Geophysics* No. **15** (182) Acad of Sci. Press, Moscow.
7. *The Detection and Recognition of Underground Explosions*, UKAEA (HMSO) December, 1965.
8. *Report of the Conference of Experts to Study the Methods of Detecting Violations of a Possible Agreement on the Suspension of Nuclear Tests*, HMSO, Cmnd **551**, 1958.
9. Davies, D. and Julian, B.R., 1972. "A Study of Short-Period *P*-Wave Signals from Longshot", *Geophys. J R Astr. Soc.* **29**, 185-202.
10. Romney, C., 1959. "Amplitudes of Seismic Body Waves from Underground Nuclear Explosions", *J Geophys. Res.* **64**, 1489-1498.
11. Gutenberg, B., and G. F. Richter, 1956. "Magnitude and Energy of Earthquakes." *Ann. Geofis.* **9**, 1-15.
12. Marshall, P. D., A. Douglas, and J. A. Hudson, 1971. "Surface Waves from Underground Explosions", *Nature* **234**, 8-9.
13. Marshall, P. D., and P. W. Basham, 1972. "Discrimination between Earthquakes and Underground Explosions Employing an Improved M_s Scale", *Geophys. J R Astr. Soc.*, **28**, 431-458.
14. Thirlaway, H. I. S., 1965. "Interpreting Array Records: Explosion and Earthquake *P*-Wave Trains which have Traversed the Deep Mantle", *Proc. Roy. Soc. A.* **290**, 385-395.
15. Douglas, A., P. D. Marshall, and D. J. Corbishley, 1971. "Absorption and the Complexity of *P* Signals", *Nature Phys. Sci.* **233**, 50-51.
16. Woodhouse, J. H., 1972. "Diffraction by Anomalous Regions in the Earth's Mantle", *Geophys. J R Astr. Soc.*, **32**, 295.
17. Douglas A., P. D. Marshall, P. G. Gibbs, J. B. Young, and C. Blamey, 1973. *P*-Wave Complexity Re-examined", *Geophys. J R Astr. Soc.* **33**, 195.
18. Marshall, P. D., and D. L. Springer, 1976. "Is the Velocity of P_n an Indicator of Q?", *Nature*, **264**, 531-533.
19. Pearce, R. G., 1977. "Fault Plane Solutions Using Relative Amplitude of *P* and *pP*", *Geophys. J R Astr. Soc.* **50**, 381-394.
20. Douglas, A., J. A. Hudson, and C. Blamey, 1972. "A Quantitative Evaluation of Seismic Signals at Teleseismic Distances - III. Computed *P* and Rayleigh Wave Seismograms." *Geophys. J R Astr. Soc.* **28**, 385-410.

26

Technical Issues Related to Test Ban Treaties

Edward Giller

There are certainly a lot of old friends in the audience today and I hope they will bear with me as I am going to talk about CTB—or nuclear testing in general. CTB is a classic example, I think, of a concept that, on the surface, sounded beneficial or useful and simple to implement. However, after some 30 years now we have been trying to do this and it has involved several serious attempts. I was involved in the recent one. We now understand, really for the first time, the scientific and political complexity inherent in this idea. With the advantage of hindsight we can see more clearly those technical areas that we should have examined before we entered into these negotiations, but we all know that it is impossible to foresee all the technical issues. Therefore, continuous technical support, which Hal spoke a lot about earlier, is necessary for any negotiation and has the attendant possibility of dramatically changing the outcome. I am going to ask the experts in the audience—there are at least ten or twelve here who have had years of experience in this general subject—to bear with me on some of my details because I am trying to draw a broader picture. I am going to try to do it by drawing on a chronology of nuclear testing to bring in the political, military, and the scientific or engineering aspects of how they relate to policy formulation. Because of all these experts in the room, I feel a little like the fellow in the story of the Jamestown flood.

Now for our visitors, Jamestown, Pennsylvania, at the turn of the century, had a dam break above the town and wipe out a very large percentage of the people. There were some survivors of course. However, one gentleman who survived it had a very dramatic experience as you might expect. He was always telling the story of the flood and how bad things were and how dramatic his survival. He told it to all the natives that were left until they got tired of hearing it. Also every time some tourist came through town and stopped to read the sign, he would be there to tell them about the flood and he became the town bore. Eventually, he passed on and came to the pearly gates whereupon St. Peter said, "We have a rule

up here—a practice—you get fifteen minutes on the stage to explain one item in your life that is most interesting". His eyes lit up and he said, "Great! I'll tell them about all the details of this great Jamestown flood that I was in." St. Peter said, "Just remember, Noah's in the audience." So, I have fifteen or twenty Noahs out there at least. If they complain I'm going to bring them up here on stage afterwards and you can question them directly.

The concept of outlawing nuclear weapons goes way back to right after World War II with the Barauch plan in 1946, which was a broad approach to the problem—very broad. The U.S. proposed to outlaw weapons, put them under international control—the U.N. Even then intrusive verification was realized as a major problem, which was to be viewed mainly in a world political context. Between 1946 and 1954, there was a lot of emphasis on general sweeping disarmament proposals. They came from every corner of the globe—mostly into the U.N. but also in a bilateral, trilateral forum. These proposals didn't fit with each other and they didn't go anywhere as history tells us. But in 1954 the U.S. exploded its biggest-ever nuclear test in the Pacific called BRAVO, about 15 megatons. It was from that that the famous fallout sequence took place on a Japanese ship and on the islands which completely surprised the test managers. It created a major uproar— nationally and internationally. Radioactive fallout, concern for which up to this time had not really been seriously voiced publicly, raised the whole question of radiobiology, and exposure of man to radiation began to take on a more political drive. Between 1954 and 1957 there was a lot of discussion about the hazards of testing but it wasn't until 1957 that various ideas for a true comprehensive test ban—CTB I'll call it—emerged. During this period the USSR proposed a two- to three-year moratorium on testing, including an international commission. This included a number of in-country stations for atmospheric sampling. Many were worried about the atmospheric testing and its fallout; therefore, sampling was to be the main verification activity. The engineer now enters the picture in the form of Gerry Johnson, who is in the audience, among others. It was decided to test underground due to the political pressure against atmospheric bursts. We fired the first underground shot, RAINIER, in Nevada. The AEC dug back into the cavity and there is a famous picture of Gerry standing and staring at the walls of this radioactive cavity. I don't know how long he stayed, maybe he left in a hurry. You can see where this type of testing changed the verification problem rather dramatically, *i.e.*, going from atmospheric sampling to the underground problem of seismic measurements. Currently in the U.S., seen on television programs on Monday and Tuesday nights in the Washington area, is a subject called T.V. Bloopers. These are T.V. takes never seen on the regular screen, either commercials or

programs, during which they make terrible, but funny, mistakes which require retakes. If you have ever seen any movies of the early days of flying where the wings fell off of the plane or an airplane ran in circles (some had really weird designs) you would appreciate a short T.V. Blooper, well movie actually, of some of Gerry's earliest experiences.

I should not put all the blame on him, however. In one instance in the early days of trying to figure out how to contain a nuclear test, they drilled a tunnel horizontally into a mountain, and then at the end of the tunnel made a little loop. They put the bomb in the loop, sealed it off, and two miles away put their cameras, with a place for people to stand and observe from three or four miles away. The world's biggest blunderbuss followed. Everything came shooting out of this mountain—it shows a 3-foot-diameter boulder coming right for the camera—but it didn't show what happened to the sightseers. They may have run for cover. There are a series of such movies which are really interesting to see and I hope some day we can put them together in the proper context and show them. Anyway, underground testing radically changed the course of CTB verification. In 1958, the first conference of experts, which was convened for which Hal gave you a short title. I am always intrigued by its full formal title, 'The Conference of Experts to Study the Possibility of Detecting Violations of a Possible Agreement on Suspension of Nuclear Tests'. It surely was written by the Russians as it's the classical way Russians describe things. This was the first meeting of experts to try and see if there was some way to detect violations. In other words, everything centered on verification. They proposed 180 stations that Hal mentioned with about forty people each. Gosh, what a career could have come out of this organization; ships worldwide and aircraft, as well as in-country activities. This is the first time we thought about verification supported by a worldwide network of detectors. They thought they could detect one kt atmospheric—this would be from fallout—and detect and identify 5 kt underground. But this would leave 20 to 100 uncertain events per year in the Soviet Union. Maybe you would need an OSI (on-site inspection). Certain experiments in the HARDTACK Series, which Hal explained, raised the detection level to 20 kt, not 5.

During this period, the so-called black box concept was born. This is the use of unmanned, unattended remote measuring and data recording equipment, perhaps including some form of transmission of the data, for the purpose of verification. It was during this period that the concept of 'Decoupling' entered the picture. I think it was Al Latter who first conceived the idea. Decoupling, as you may know, involves firing a weapon or device in a large cavity which can be made in salt. This will muffle the seismic signal by a factor of 20, 50, or 100. Thus was born the first so-called "evasion concept". This is one way to evade detection by reducing

the signal level. Several others were invented later, including the simulation of an earthquake or by firing during a large natural earthquake. It would be necessary to wait for a big, *i.e.* Richter 7, 7.2 earthquake to come along and then fire so that the signal looks like an aftershock. As a practical matter, I would hate to be in charge of the operation, sitting there year after year waiting for the right earthquake in the right place to come along and hoping it didn't explode before it was time, and that it would go off at the intended time. However, the evasion scenarios do interact with the political aspects of any treaty. It was during this period that the U.S. and USSR agreed to a moratorium with the UK. During this period of time there was a strong national will in favor of a treaty. If you read Seaborg's book, *Kennedy, Krushchev, and the Test Ban*, you will see that Seaborg, who was head of the AEC, does a very careful job describing the intentions of the various political figures in the U.S., UK and Russia. There were severe verification problems then. Also, there had been little thought given to the national security implication of the CTB. I think, in spite of what Hal says, there was more national will during that period than you are going to see again for a long time. National will? I don't know what it means in the context of treaty writing. It seems to be a phrase people use to say "let's get on with finishing our negotiation even if it means setting aside important concerns". It's an emotional political statement which I think has little meaning. If there ever was a time for national will for a CTB, it existed during that period. I think Hal will agree with me on that. I wasn't involved then but I get this impression from reading Seaborg's book.

In 1961 the moratorium was broken by the Soviets. However, it is true that the U.S. had previously announced that we would no longer be bound by it. The Soviets fired after a very short notice, perhaps 24 or 48 hours. I don't remember if the first one was the biggest but in that series they fired a 50 Mt dropped from an airplane—I'm glad I wasn't the pilot. And it seems clear that for a year or more they had been buying and building hardware because you cannot put together a test series in less than a year; there is a lead time for everything, such as, the measuring equipment, the bomb itself and the necessary practice. To show you how the U.S. reacted, and we still do under similar circumstances, we forbid Los Alamos to buy coax cable during this period because it might signal an intent to test. That is the difference between the two countries' approach to that situation. During all that time, Seaborg writes, there were at least 200 meetings of the Geneva delegates that kept going on, but slowly ran down because it was clear that it wasn't going to accomplish much. They were still meeting while these tests were being conducted. The political side had run down, it was unproductive then and again in 1979-1980. Out of this grew the Limited Test Ban Treaty. This is the treaty which restricts explosions in all

environments except underground, *i.e.*, underwater, in the atmosphere, and in space.

Underground testing would be permitted, however no debris shall be permitted to escape the boundaries of the state conducting the event. The meterologists and the people who build geiger counters now enter the picture. Every time a geiger counter improves by another factor of 10 in sensitivity, the debris can be measured at greater distances. The U.S. fired a peaceful nuclear explosion from which all the American debris went up to the Canadian border and stopped—it didn't go across the border. The Soviets didn't quite accept that but they weren't doing any better then and they certainly aren't today. Buried in that treaty language is a lesson involving a technical point, *i.e.*, the treaty uses the word "debris" and leaves it at that. The Soviets interpret this to mean particulate, not gaseous, matter which must not escape the boundary. The Americans insist that their interpretation means both particulate and gaseous debris. As a result, we have written each other letters over the last twenty years, claiming that the other has violated this part of the treaty. It was an ambiguous point which was left for later interpretation. I have been told that it was known at the time and it was decided to leave it that way. Not much happened on CTB or nuclear testing until 1970 when the non-proliferation treaty came into force with a CTB included in its preamble. Preambles of treaties often contain broad promises of things to come—usually in the indefinite future. The operational sections of treaties contain the activities to which you are legally bound. This has created a rather interesting debate over the NPT preamble which promises to make the attempt to find a complete ban on all nuclear tests. The Soviets, to a certain extent, numerous delegations in Geneva, and some people associated with the various "Ban the Bomb" organizations in the United States, insist that the preamble is legally binding on the United States and therefore we are in violation of the nonproliferation treaty. Every five years there is a review conference of the nonproliferation treaty by all the signatories. There are about 135 or 140 members which makes it one of the largest treaties. It will have its third review next year. Already there is a lot of concern that since the CTB negotiations are dormant, this lack of progress will impact very negatively on the nonproliferation treaty review. However, they said that five years ago and nobody withdrew from the treaty. I don't know what will happen this time. The NPT Treaty also contains an Article 6 which is an operative paragraph which has to do with disarmament. It says that the super powers shall find ways to reduce their nuclear armaments. This is a second item which will be used to critique the nonperformance of the super powers at the NPT review.

The U.S. is predicting a major international discussion of these two sections when the NPT comes up for review next summer. I'm going to

digress for a moment on this point. It is said that one reason for a CTB is that it will assist the NPT in controlling proliferation. Most of the countries which cause us concern over proliferation and have not signed the NPT have a major national security problem in their region. This administration has said that it is more important to support the national security of these countries than it is to try to prevent them from getting their hands on some technology which might lead to building a bomb. There is a general agreement that a simple, reliable and certainly large enough for its purpose weapon can be built without testing providing you have the materials. There is a debate about whether CTB really contributes to non-proliferation. It has been said in the 40 nations CD (Conference on Disarmament) that meets every year in Geneva that those who think the NPT is discriminatory can sign the CTB and thereby meet their commitment to nonproliferation. That's the worst logic I've heard. The NPT requires full-scope safeguards, which means nuclear facilities shall be opened to international safeguards inspections by the IAEA (the International Atomic Energy Agency in Vienna). The CTB treaty does not require such inspections and therefore you could sign up for CTB, build your bomb, and still get your international seal of approval. That isn't what you want; you want them to sign the NPT which requires an inspection, which will be as much of a deterrent as possible.

The threshold test ban treaty was signed after a very short negotiation period in 1974. It has a technical annex that requires the exchange of considerable geophysical data, which brings your profession to the front to tell us what it is we should ask for. The TTBT contains a problem, not in the preamble, but in Article 1 which states that the parties to the treaties shall continue their negotiations toward the end of a CTB. This would be legally binding, however, our lawyers indicate that it doesn't tell you when to move forward. There is another problem in that the treaty calls for each side to furnish the other with calibration data of the yield of a pair of explosive devices, which is spelled out in some detail, to be conducted in designated high-yield weapons testing areas. It doesn't provide any way to verify that they gave you the right yield.

The TTBT is on the middle burner right now. This administration has decided that the accuracy which we accepted in 1974 is insufficient, *i.e.*, plus or minus a factor of 2 in yield. Which means that if the central value from our national seismic net is 200 kt, the true yield is between 100 and 400. A simple multiply by or divide by 2 is the kind of layman's language we need in Washington. What the Soviets have done is consistent with their exceeding the treaty limit and consistent with not exceeding this treaty. This administration has decided that we should tighten up this uncertainty, perhaps by finding some way to get some calibration data that has meaning and to get better geophysical data or better calibration of the seismic nets.

This would require discussion and renegotiating, to provide more technical data of some consequence. Hal's example of his scientific discussions with the Soviets 15 years ago reminds us they will have to be very careful, because if they came to a conclusion that the data they might give to the U.S. shows that they were cheating, they are not going to agree to providing such data.

If the U.S. says yes, the correct data does show that you have been cheating, you could imagine what kind of a long-term discussion that would be. However, the Soviets have refused to come to the table at all, which may be the best solution of the problem for the moment. This situation illustrates how the political perception of what's adequate verification for one treaty sets precedent for the next treaty. TTBT only took a few months to negotiate once we decided to do it and it was agreed that 150 kilotons would be the limit. However, the Soviets had a large peaceful nuclear explosion program by which they hoped to dig a large canal which was to move the water from a north-flowing river to the south; sounds like California's version of rerouting the Columbia River. They had to cut through a few mountain ranges, which they were going to do with nuclear explosives, and they wanted some way around the limit of 150 kilotons. The Peaceful Nuclear Explosions Treaty, which Warren Hechrotte helped to write in Moscow, was probably the most complicated technical treaty we have ever negotiated. It discusses considerable technical detail, including much geophysical data, and a complicated operational plan. As an example, taking pictures in the Soviet Union is a sensitive subject. Therefore, in order to get an agreement they would take the pictures with a double-lens polaroid camera and two pictures would come out with each side getting one, but we were never allowed to hold the camera. The question of measuring the yield of these large peaceful explosions which could be fired concurrently arose, thereupon a hydrodynamic-yield measuring scheme was put on the table for the Soviets. This involves using a coaxial cable it gives you a time *vs*. length history of the crushed cable which is related to the yield as long as the emplacement geometry is good without any big voids. Also, local seismic nets were going to be needed in the area to measure other special seismic phenomenon. As you can see, a lot of our specialties were involved there. From a political standpoint, we had a problem with the equipment required to make all of these measurements. Since the Soviets were sure that some of our equipment might be bugged, we agreed to bring two trailers so they could take one home and examine it while we used the other one. That's expensive. Anyway, the two treaties were signed and sent to the Senate for a hearing in the fall of 1976 and later they were set aside so as not to interfere with work on CTB when the Carter administration came in. They have been signed but never ratified, a point the Soviets keep

pressuring us on.

In the spring of 1977 I was involved in the president's review memorandum study which made it clear that we were going to attempt a negotiation. Some of us felt it was slightly steam-rollered, however. A review was put together which said yes in principal, that we could find some form of verification and here were some ideas, therefore a decision was made to start a negotiation. In the summer of 1977, the U.S. and the USSR met first and in the fall the UK joined us for all subsequent discussions. The U.S. and USSR started the treaty negotiations with two different views of the principal issues, however, the U.S. and the UK were basically in agreement on most parts. For us the duration was to be unlimited with a five year review and would continue unless it is decided to stop. The USSR wanted it to be 3 years and it would continue depending on joining by others, which meant France and China. They were not part of the negotiations and everyone felt that France and China would not join; therefore, some of us felt that the Soviets were asking for a 3 year moratorium with a legal way of walking out which the U.S. would not buy. We spent a lot of time that first fall arguing about the military benefits of peaceful nuclear explosions. There are two forms of benefits; one in the infrastructure; *i.e.*, your test and theoretical personnel, as well as your whole-laboratory structure, would have real experiments to do. There is something meaningful there to keep them going. Most of you know what it means to have experiments for your science. Well, the same is true of weapon design personnel. We felt that since we had no PNE program in the United States, as it had died a natural death from economic and environmental reasons, therefore, we could not agree to the Soviets being able to keep up their infrastructure and laboratory confidence. Secondly, the devices could contain within themselves technical experiments known only to the Soviets. However, some people ask why don't you open the device and examine it. A physical examination doesn't really tell you what's in a nuclear weapon, you have to find the scientist that did the original drawings. There really wasn't any given in the U.S. position and the Soviets finally understood it, so that in November they agreed on a moratorium on PNE's which would run as long as the treaty, provided we would agree to separate negotiations on finding a means to solve the PNE problem. We told them there was no solution but they said okay; we will agree anyway. Concerning on-site inspections, the U.S. wanted them to be mandatory; the Soviets wanted them voluntary. The question of seismic stations, numbers, kinds, locations, were at that point fairly open on both sides.

By December 1977, we came up with a couple of other problems. the first involved the question of so called "permitted experiments" or "what is the definition of a nuclear test?" This definition has eluded physicists,

lawyers, and politicians ever since it was first discussed. Any definition will be completely arbitrary. Remember, this is a multinational treaty; so define an experiment that doesn't legalize the other 150 nations to do something you don't want them to, however that you want to do yourself. What worried us most was what the U.S. would be permitted to do, rather than what it was the Soviets could do as we had no way of monitoring very small explosions.

The question of verifying large chemical explosions arose. The Soviets use very large chemical explosions (about a kiloton or larger) mostly for mining and we were concerned about the verification aspects of these. On the political side we decided to provide the treaty with two tracks— same as the CW (Chemical Warfare) treaty. Namely, a multinational treaty with arrangements for any parties to make private arrangements for extra verification measurements. We were also working on a three-sided arrangement with the Soviets and the UK. We now began a discussion on the question of the number of seismic stations, data retrieval and authentication. The signal coming from the stations would not be encrypted but authenticated. We started working groups at this point, which changed Hechrotte's life as he became chairman of the technical group, which continued for two years with endless discussions on various subjects. We also came up with the concept of the international seismic data exchange system which would be a worldwide open system for everybody. Whatever else that we would negotiate with the Soviets would be separate—it could be complementary, too, but it would be separate. The Soviets reminded us from time-to-time, as they still do today, that national technical means, *i.e.*, our own seismic net plus ISDE, were really all that was necessary for verification of a treaty. In the Soviet view on-site inspection was a political necessity only to the U.S.—they said we really don't need to do this, but we understand it's politically necessary. In January 1978, the U.S. shifted to voluntary OSI's. The Soviets then said that all these national seismic stations (NSS) had to be nationally manned. We were considering manning the stations internationally or bilaterally but they said no, it would be our own people. Warren's working group on OSI's were beginning to draw on the PNE treaty details for the rights of inspectors. The Soviets concern over black boxes came up constantly. Another interesting question arose; namely if you want to make an on-site request, it was agreed you would have to have some reason—you couldn't just say you would like to go. They were insisting that seismic data must be included.

They said no spy stories from the Washington Post it must include seismic data, however, we insisted it could be data from anywhere. These discussions highlight another Soviet way of doing business, which was to leave all these details on the on-site inspection activities to a joint consultive

commission that would work them out later. There is a counterpart to this idea in the Standing Consultive Commission for the ABM and SALT I treaties. The U.S. believes it is necessary to get most of the details worked out before the treaty is signed because it is tough going after that to ask for something that requires them to give very much.

In the summer of 1978, we finally came to understand the national security consequences of a CTB. Notice I haven't said anything about them until now. That is because they really weren't well understood. During the first year and a half of the negotiations, the weapons labs began to face the question of what would happen if we actually implemented a full CTB with no testing. They pointed out that inevitably you would lose confidence in the reliability of the nuclear stockpile. Can you imagine the reaction of the military who say, "Look, we break our backs to make the rockets work, the communications work, the targeting work, and you want us to agree that its alright to not be sure the weapon is going to work"? As you can see, this idea is not conducive to support by the armed forces. There ensued a debate in the U.S. over whether you can ensure reliability without testing. There are several letters to the President from weapons experts which said yes, and others from the lab directors, as well as other knowledgeable people, who said no, which was persuasive to the political authority in Washington. Therefore, the U.S. shifted to a fixed five-year treaty with the possibility of testing afterwards. You can understand what this might do to the nonproliferation regime if countries signed up for only five years. In my view this completely negates any nonproliferation benefits. There is no middle ground for this treaty. It's either black or white; you can't have it both ways even though we tried. We also tried to define a criteria for high explosives, *i.e.*, what is a reasonable size and rate of fire for high explosives activities that would require verification provisions. This is another example of political/technical interaction.

By this time, we had gotten to the point where we were trying to get the Soviets interested in the U.S. design of the NSS stations which Sandia Corporation had under development. Paul Stokes, who is in the audience today, came to Geneva and over a period of three or four days gave an extremely detailed set of briefings with stacks of documents to the Soviets. We then proposed a total of 15 single borehole stations, with a later upgrade to include arrays. Based on this number we gave them a layout in the Soviet Union based on assumed noise levels, which meant you had to eventually find out if the noise levels were correct. By this time, the U.S. proposed a three year treaty based on our concern for national security. It isn't well-known, but the U.S. has had stockpile failures, the most important being connected with the submarine fleet. People believe that if you have degradation in the stockpile, it will affect all systems. Not so. It's generic to only

one system. You can lose 50% of a system over a short interval of time, however you don't necessarily lose any other system. You don't have an overall degradation, rather you have a specific warhead degradation and that's important to understand, because if it's a strategic deterrent system like the submarine that is very important.

Returning to the question of monitoring chemical explosions, the Soviet Union, which utilizes chemical explosions in many government departments, stated they would have to create a new bureau; therefore, they were not interested in talking about verifying chemicals explosions. When the U.S. proposed ten stations in the Soviet Union in conjunction with a three year treaty the USSR said they would accept ten in the Soviet Union, ten in the U.S. and of course ten in the UK and their territories. Their position created a serious impasse. We had predicted that they wouldn't ask for any stations in the UK however, maybe one, not ten. After much consideration the UK, with U.S. support, agreed to accept only one. The Soviets then picked ten locations, several of which are no longer under UK control. They indicated that if we didn't want to agree to 10-10-10, then any other set of equal numbers would be of interest. They said equal participation required equal responsibilities. The Soviets also indicated they were not going to use any U.S. manufactured NSS's and would not discuss them in any detail until the British changed their position. The U.S. and UK viewed the Soviet position as pure politics with no technical justification.

The Soviets came to the U.S. in the summer of 1979 and spent a week with us. We took them to the operating seismic station at Tullahoma, Tennessee, then to Albuquerque where they spent 2 or 3 days with the Sandia Corporation to discuss in detail the NSS. This was followed by a visit to the Boston area and Alexandria, Virginia, to discuss data handling. Several discussions were held in Geneva concerning a possible joint cooperative program involving one of these NSS stations. The Soviets indicated a desire to purchase 2 sets of the main components of the NSS. However, that really didn't get anywhere because of their invasion of Afghanistan and our nonratification of SALT II. The negotiations were further influenced by the upcoming U.S. election resulting in no further progress.

As you know, the current administration has not agreed to resuming the trilateral negotiations even though the Soviets proposed them many times. Our present position is that until we have a deep and verifiable reductions in deterrent forces, nuclear testing is too important for national security. Also, there are several new carrier systems which require new warheads which are needed to counterbalance the Soviet threat. Furthermore, the safety and security of our device/weapons needs to be improved. There are many ideas to make a weapon extremely safe from fire and crash in an accident; or safe from terrorism. To make this improvement will

require rebuilding the primary which would require testing.

When the Limited Test Ban Treaty was ratified it was decided that the U.S. would have a four point safe-guard program: (1) vigorous labs; (2) vigorous underground testing; (3) standby testing capability for atmosphere; and (4) better verification. Number 4 is the source of much of the money that was for support of seismological community for a better understanding of detection and identification. There will have to be a counterpart safeguard program for CTB. The question of how you keep a lab active raised the issue of permitted experiments. Our experience with preparation for resumption of atmospheric testing (item 3) is an example of what happens to your budget when nothing is going on, it just disappears. However, in this situation I think that seismic verification might get added support. The U.S. government never did finish the CTB safeguard program because the treaty didn't get far enough along. The CTB safeguard program would be a collection of what is technically needed, and is politically accepted. We had many debates about how the safeguard programs would allow some permitted experiments. We considered the question of shutting down the Nevada test site completely, because if we were to have a drill rig running there, it might be a symbol of getting prepared to do a test and break out of the treaty.

I have tried to show you how science and politics came together to change the course of events during a treaty negotiation. This will apply to almost every treaty we are doing including START, INF, and especially a CW treaty which has the most difficult verification challenge I have ever seen.

VELA Overview: The Early Years of the Seismic Research Program

Carl F. Romney

On April 23, 1959, the President's Special Assistant for Science and Technology, Dr. Killian, met with Atomic Energy Commission Chairman McCone and Deputy Secretary of Defense Quarles to discuss the recommendations of the Berkner Panel (on seismic improvement) and the Panofsky Panel (on detection of high altitude nuclear explosions). At this meeting it was decided to implement the programs of research recommended by these panels for improving national capabilities to detect and identify foreign nuclear explosions conducted in the two difficult environments. The Department of Defense was assigned the primary responsibility for these national efforts, with support to be provided by the AEC and NASA. This was the key decision of 25 years ago that launched the "VELA Program", as it was named when the Secretary of Defense assigned responsibility to the Advanced Research Projects Agency.

The problems that set the initial directions for the program had their foundations in technical and international political events that occurred prior to 1959. Similarly, the subsequent course of the program was influenced by political developments — especially those associated with negotiations for nuclear test ban treaties — as well as by technical developments within the research program. I plan to recount some of those developments and events that were important in shaping the course of the VELA seismic program or its output of advice to policy levels of the government. These developments will often not be those that might be selected as the major technical highlights as gleaned from the technical journal literature, but rather reflect a view from within the government of some of the things that seemed to be important at the time. Because of the size and diversity of the program and the limited time available, I will be able to present only a few examples of the work that went on. Most of what I will cover has been taken from the official records and archives and from collections of technical documents that I assembled from time to time because they were useful reference materials in explaining the research (and justifying the budget) or advising policy-makers

associated with test ban treaty negotiations on capabilities and limitations of seismic methods.

I will concentrate on the early phases of the VELA seismic program with the expectation that these parts are least familiar to most of the audience, and that the topical state-of-the-art reports to follow will bring the main technical threads of the program up to date. Table 1 provides a chronology of some of the key events that led to the establishment of the research program.

Background

Early test ban discussions. Fundamental differences between the Soviet Union and the United States on verification of a possible nuclear test ban treaty were clearly evident as early as 1955-1956. U.S. proposals for a test ban included provisions for monitoring such a treaty. The Soviets, on the other hand, asserted that it was "possible to detect *any* explosion *wherever* it may be set off"* and consequently there was no need for special verification measures.

While this was probably an accurate perspective from the point of view of a closed society looking at an open society, the reverse was not true and prudence indicated that the U.S. would require highly sophisticated technical monitoring means to give it even approximate parity with the USSR's ability to monitor the U.S. from open sources.

RAINIER Explosion. Capabilities and limitations of methods for detecting atmospheric nuclear explosions were relatively well known and tested by the mid to late 1950s. Little was known about underground

Table 1. Background

1955-1956	Early test ban talks foreshadow research need
Sept 1957	RAINIER explosion: technical start
Jul-Aug 1958	Geneva Conference of Experts
Aug-Sept 1958	Johnston Island, ARGUS high altitude tests — subsequent Soviet tests
Oct 1958	HARDTACK II underground tests
Oct 31, 1958	Negotiations begin, moratorium on testing
Dec 1958	Berkner and Panofsky panels formed, report conclusions and recommendations in Mar 1959
Jan 1959	"New Seismic Data" (HARDTACK II) tabled in Geneva
Apr 23, 1959	Berkner, Panofsky research assigned to DoD
Sept 2, 1957	Assigned to ARPA, funded $9.6M

*Letter of September 11, 1956, from Premier Bulganin to President Eisenhower. Italics added.

and high altitude nuclear explosions. RAINIER, a 1.7 kiloton nuclear explosion in September 1957, produced the first direct experimental data on underground nuclear explosions. It was detected at about ⅔ of the seismic stations within 600 kilometers and at only three stations beyond 1000 kilometers. Its magnitude (M_L) was initially estimated as a 4.25 based on data from seven local stations equipped with Wood-Anderson seismographs. It looked like a normal earthquake (Fig. 1), with strong *SH* waves (a phenomenon still poorly understood) and no apparent indication of its explosive origin. RAINIER established that detection of low yield underground nuclear explosions at long ranges could be difficult, and that identification could be an even more serious problem.

Geneva Conference of Experts. Eight months later, in July of 1958, the "Conference of Experts" convened in Geneva to advise the governments of the eight participating nations on technical aspects of nuclear test detection and identification. By the end of August, the "Experts" had discussed and agreed on observables from nuclear explosions in the atmosphere, underground, and underwater. They defined apparatus for detection, and described and outlined the capabilities of one specific network of "Control Posts" for consideration by governments (Table 2). They did not propose the network for implementation, nor describe it as adequate. Methods for monitoring high altitude and near-space explosions were left as unfinished business. Evasive testing methods were not considered, by and large.

The RAINIER explosion played a large role in the experts' deliberations on monitoring underground explosions, as its specific applicability

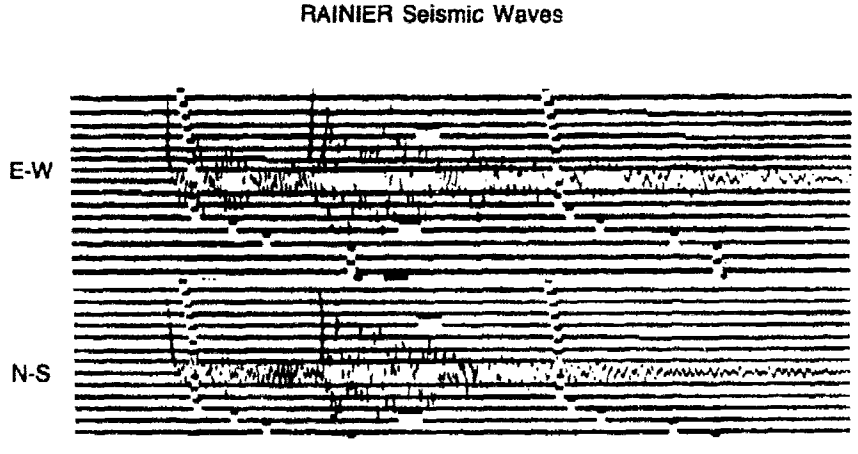

Fig. 1. Seismic waves from the RAINIER explosion recorded at Tinemaka, California, 180 km almost due west. Note large transverse motion.

Table 2. Conference of Experts

Discussed detection methods and defined capabilities of a network of 170-180 Control Posts, 10 ships and aircraft debris sampling

Atmospheric Tests:	1 kt at 0-10 km identified with good probability
Underwater Tests:	Detect 1 kt in deep open ocean; identification sometimes impossible
High Altitude Tests (above 30 km):	No conclusions; potential methods outlined
Underground Tests:	Most difficult; determines spacing of control posts; 10 element *SP* arrays in 3-km area; 3 component *LP, SP, BB* seismographs; detect (quiet sites) 1 kt under RAINIER coupling; identify 90% of quakes equivalent to 5 kt (first motion); on-site inspection may be required on 20-100 events per year; amplitude varies as $^2/_3$ power of yield

and uniqueness justified. Its magnitude became the most important basis for estimating the number of natural seismic events that would produce signals of equivalent size, and that would have to be identified as earthquakes as part of the monitoring activity. Published formulas were used to relate the local magnitude, M_L, (as measured from RAINIER), to the teleseismically determined "unified magnitude," m_b, (as used for the lower magnitude events in "Seismicity of the Earth," the source of seismicity data used by the U.S. delegation). These formulas implied that $m_b > M_L$.

It was agreed on theoretical grounds that the seismic amplitudes from explosions at other yields should vary as the $^2/_3$ power of the yield. Identification was to be based on the direction of first motion, and it was estimated that a signal-to-noise ratio of two would be required. Other potential identification methods were discussed, but there was insufficient information available to assess their applicability. It was agreed that not all events could be identified, and that 20-100 events per year might require on-site inspection. The fact that the Soviets had agreed to the need for on-site inspections was widely hailed as a breakthrough, establishing a precedent for other arms limitation agreements in the future.

Some members of the U.S. delegation had suggested that "decoupling" of underground explosions might be possible through packing rubble around the explosive device. Further analysis showed that that specific

method was flawed, however, and the U.S. presented a technical report at the conference showing that the method would not work and casting doubt on the general concept of decoupling.

It was concluded that underground tests would be more difficult to monitor than tests in other media and that seismic monitoring requirements would largely determine the locations and numbers of "Control Posts." These were to be spaced at 1000 km intervals in seismic areas, and at 1700 km intervals in aseismic areas. This was to insure that three or so stations would be within P_n range from most events, and that additional stations would be in the strong signal zone between about 1700-2500 km from the event where mantle P waves first emerge.

New Seismic Data. Two months later, well-calibrated seismic stations were deployed in the U.S. to record the underground nuclear explosions of the HARDTACK II series, which included two explosions substantially larger than RAINIER. The resulting data placed test detection seismology on a far firmer footing than had been the case at the time of the Experts Conference, but the net result was to expose greater detection and identification problems than had been previously estimated. One unexpected result was that the amplitudes of P_n decreased as the cube of the distance in the first 1000 km, implying greater detection difficulties than anticipated at representative distances within the detection network described by the Experts. The first motion decreased with distance even more rapidly and was, therefore, smaller than expected relative to the maximum amplitudes of P_n at the greater distances. Apparent rarefactions were observed. Long period Love waves were recorded as far away as Resolute Bay from the larger explosions. While the short period S waves could qualitatively be rationalized as resulting from scattering of P, the existence of earthquake-like long period shear waves suggested fundamental problems in seismic wave generation from explosions.

Two of the explosions, LOGAN and BLANCA, were large enough to permit measurements of magnitude, m_b, from directly observed teleseismic P waves, and M_L was measured at local stations. It was found that $m_b = M_L$, contrary to the published formulas used at the Experts Conference, as a basis for estimating the seismicity background problem. The consequence was to reduce the estimated m_b for a given yield, and hence to increase the estimated numbers of equivalent earthquakes. Further, based on the average M_L from the 10 stations equipped with Wood Andersons that recorded the larger explosions, the relative M_L measurements at seven common stations indicated that the value for RAINIER should be revised downward to $M_L = 4.1$. This was the first serious example of network magnitude bias caused by the use of only the larger (detectable) signals from events near enough to the detec-

tion threshold that the full range of amplitudes was not sampled — a problem that continued to plague the VELA program, producing many misleading results for many years. The predicted amplitude *versus* yield relationship ($A \propto Y^{2/3}$) was experimentally shown to be incorrect; the observed first power relationship between amplitude and yield (Fig. 2) implied that low yield tests would be more difficult to detect than previously predicted. In short, detection of explosions would be more difficult than anticipated; at a given yield the reduced magnitude implied that they would be mixed in with more earthquakes than previously estimated; and the principal known method for discriminating between earthquakes and explosions was less effective than anticipated by the Experts.

The Berkner Panel. One response to this information was a request by the Department of State to the Special Assistant to the President for Science and Technology, to review these conclusions and recommend a course of action. Dr. Killian formed the Panel on Seismic Improvement as a result of this request. The Panel, chaired by Lloyd Berkner:

- confirmed the HARDTACK II conclusions and endorsed them as a better basis for treaty negotiation than the Experts' conclusions;
- defined potential detection and identification methods that might improve nuclear test monitoring capabilities (including the foundation for the M_s:m_b criterion);
- reviewed and confirmed recent work which indicated that a nuclear explosion in a sufficiently large air-filled cavity would

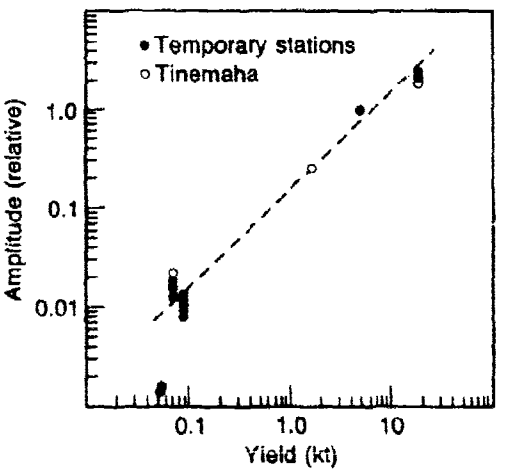

Fig. 2. Normalized *P* wave amplitude from HARDTACK II explosions and RAINIER. Dashed line shows amplitude increasing as first power of yield.

be decoupled by a factor of 100 or more relative to a tamped explosion like RAINIER;

- proposed a national program of research at about $25 million annually to address these problems (see Table 4).

The Berkner Panel report was published on 31 March 1959. A research charter was given to the Department of Defense as previously mentioned, and initial funding was made available to ARPA on 2 September 1959.

Early Effects of Test Ban Negotiations on VELA

Technical Working Group II. Meanwhile, in Geneva, trilateral negotiations (the U.K., U.S., USSR) on a comprehensive nuclear test ban treaty were proceeding, and the negotiating countries had pledged a moratorium on nuclear testing. The HARDTACK II data had been presented by the U.S., and the USSR had refused to consider them within the framework of the negotiations, stating that the report of the Experts' Conference constituted the *only* technical basis for the treaty. The Soviets finally realized that they must take the new data into consideration, and consequently "Technical Working Group II"* was convened on 22 November 1959 under a charter from the test ban treaty conference to report on "the use of objective instrumental readings" for monitoring a test ban treaty. See Table 3 for a chronology of events during this period.

Between 25 November and 18 December 1959, the TWG II scientists of the three countries reviewed the HARDTACK II data (the 19 kt BLANCA explosion, incidentally, had been detected at only three stations inside the USSR, according to the Soviet reports). The decoupling concept was presented, along with preliminary confirming experimental data from the U.K. (the U.S. COWBOY experiment was too late to affect the discussions — the first shot took place the day before TWG II adjourned), and various seismic identification criteria were presented and analyzed. No detailed agreements were reached, and each of the three scientific delegations of TWG II reported separately to the Conference.

However, it was clear that all recognized problems in discriminating between earthquakes and explosions, that improvements beyond the system described by the Conference of Experts were desirable, and that the decoupling concept was sound in principle. The feasibility of conducting decoupled explosions was strongly questioned on engineering grounds by the Soviets, and they also did not accept that the estimate of the

*Technical Working Group I had met in August to report on high altitude detection.

Table 3. Events in Early VELA Period

Aug 1959	TWG I (h. alt.) report
Nov-Dec 1959	TWG II (seismic) report - HARDTACK II data - Identification criteria - Decoupling - Improvements
Dec 1959	ORPHEUS, COWBOY decoupling tests
Mar 1960	Agreement on M 4.75 threshold - Moratorium below M 4.75 - Research program
May 1960	Seismic Research Programme Advisory Group - Summit meeting collapse, repudiation
Jun 1960	Soviets "consent" to U.S. research, veto power
Jul 1960	Soviets agree to 15 Control Posts in USSR

number of earthquakes equivalent to an explosion of given yield should be revised upward as a result of the HARDTACK II data. The U.S. revision downward of the RAINIER magnitude estimate was a particularly contentious issue, and elaborate arguments were presented by the Soviets purporting to show that the teleseismic magnitudes of all shots were larger than the U.S. interpretation implied. The failure to detect BLANCA, $m_b = 4.8$ by the U.S. estimate, at more than three Soviet stations did not seem to dampen these arguments. All parties agreed that, in principle, identification criteria based on focal depth and the occurrence of foreshocks and aftershocks could be formulated, although specific identification criteria could not be agreed to at the time.

In spite of the inability of the three nations to reach detailed technical agreement, all understood that there were significant seismic verification problems. This led to agreement in principle in March of 1960 to a treaty providing for a magnitude 4.75 threshold on underground nuclear testing, a moratorium on tests below that level, and a joint program of research on detection and identification of underground explosions.

Seismic Research Programme Advisory Group. As a consequence of the latter point, the "Seismic Research Programme Advisory Group" met in Geneva between 3 May and 30 May 1960. Scientists of the U.S., U.K. and USSR presented proposed programs of research, including underground nuclear and chemical explosions. The developing VELA program was described in detail, as were suggested programs by the other countries. While Ambassador Tsarapkin had previously declared that the USSR had no objection to a "strictly limited" number of underground

nuclear explosions for research, the Soviet scientists made it clear that none would be conducted by or on the territory of the USSR.

After several days of interaction and joint planning, the three scientific groups were in essential agreement on a set of coordinated research programs. As an example of the give-and-take that occurred, the Soviet scientists criticized the U.S. explosion program for having too few mobile seismic recording stations; the U.S. took this advice and the consequence was that VELA's "Long Range Seismic Measurements" (LRSM) program increased the number of stations from 20 to 40. A report on the coordinated programs reached an advanced draft stage, and there was general optimism among the scientists that an important joint research program would actually result from their recommendations. However, as an aftermath of the recent collapse of the summit meeting (Eisenhower and Khruschev) the Soviet scientists were abruptly instructed to withdraw. They appealed unsuccessfully.

Two weeks later the conclusions and recommendations of the Soviet scientists were repudiated by Ambassador Tsarapkin. He also "consented" to the U.S./U.K. research, but insisted that it must be agreed to by the USSR. He served notice that the number and type of explosions, and the manner in which they were conducted, must be approved or the USSR would resume nuclear testing. Decoupling tests would be vetoed.

Early VELA Results

Initial goals. The VELA program, reshaped and sharpened as a result of interaction with our scientific colleagues of the U.K. and USSR, was off to a good start, with well-defined objectives and approaches. Initial major goals were to lower the detection threshold, develop effective identification criteria, and develop on-site inspection techniques. The third of these goals included an associated goal of improving seismic location accuracy. The specific task organization and funding to meet these goals are given in Table 4, which compares the Berkner Panel recommendations with the ARPA program, as modified during the Seismic Research Programme Advisory Group meetings. Details of the planned explosion programs are shown in Table 5. A chronology of events that influenced the program during this period is given in Table 6.

Fundamental research. Although the explosion program and the development of new detection and analysis systems were the major items in the VELA underground program (Table 4), it was known from the outset that a strong and sustained fundamental research program would be required. The Berkner Panel was particularly clear on this point, noting that the seismic monitoring problems that had been exposed stemmed

Table 4. Research program (2 years)

	Berkner Panel 30 March 1959	AkPA (SPRAG) 11 May 1960
World-Wide Standard Seismological Network	$ 2,250 K	$ 3,375 K
Generation and propagation of seismic waves	8,700 K	8,550 K
Detection methods	3,600 K	4,850 K
Systems development	13,200 K	10,050 K
Large nuclear and H.E. detonations	24,000 K	45,000 K
On-site inspection	-	2,100 K
	≈$52,000 K	≈$74,500 K

from the lack of fundamental knowledge of seismic wave generation, propagation and detection — in short, the classical problem of seismology. Consequently, even before the program was funded and assigned to ARPA, AFTAC had notified the University community on the Berkner Panel recommendations and the decision of DoD to implement the program. Most of the major institutions involved in seismology had responded with proposals and were provided with funds soon after the formal administrative and management structure of VELA was established. The increased funding available for seismology seeded and matured what became a major expansion of seismology and a continuing source of new ideas and new understanding of nuclear test detection and identification.

New seismic measurement capabilities. Much of the initial effort under VELA went into the construction and deployment of new seismic measurement systems and networks. Perhaps the most notable of these programs was the development of the Worldwide Standard Seismic Network (WWSSN) — an ambitious program, well-executed by the U.S. Coast and Geodetic Survey, for establishing 125 new high quality seismic stations. Forty of these stations were operating by 1962, giving seismologists the ability, for the first time, to study seismic events recorded globally by calibrated instruments with common, known response characteristics. Major effort was also going into development of a U.S. network of "Geneva arrays" to experimentally test systems of the type recommended by the Conference of Experts. Forty mobile recording systems of the Long Range Seismic Measurements (LRSM) program were rapidly constructed to keep pace with the largest VELA program of all: the explosion program (Table 5). Both the Geneva arrays and the

LRSM systems included magnetic tape recording capability — a first on such a scale. All of these seismic measurement systems were soon to produce data providing greatly improved understanding of long range seismic effects of explosions. But, with one exception, *not* from the explosion program as planned.

Testing resumes. On 30 August 1961 the USSR abruptly announced that it would no longer adhere to the moratorium on testing that began at the start of the nuclear test ban treaty negotiations, and immediately began the largest atmospheric nuclear weapons testing series that had ever taken place. The U.S. responded with a token explosion of its own two weeks later (ANTLER, an underground explosion of 2.6 kt, 15 Sept 1961), followed by other low yield underground tests leading up to full scale testing during the next year. Underground testing also

Table 5. The DoD/AEC nuclear-chemical explosion program

NO. OF EVENTS	NAME	TYPE	YIELD	MEDIUM	DEPTH (FT)	SITE
SHADE						
1	ORCHID	NUCLEAR	5 KT	TUFF	1350	NTS
1	CRYSTAL		1 KT			
1	LOLLIPOP		5 KT	GRANITE	1500	
1	LINEN	HE		TUFF	1250	
1	STINGRAY	NUCLEAR	25-50 KT		2000+	
1	MUSLIN		¼ KT		1350	
1	SHOAL		5 KT	GRANITE	—	—
1	PORPOISE			GRANITE	7500	NTS
DRIBBLE						
1	RECORD	NUCLEAR	100 T	SALT	2500	TATUM DOME
1	HAYRIDE		500 T			
1	HERMIT		100 T			
1	GAUCHO		5 KT			
1	GREENBEAN		25 KT			
1	TIPSY		5 KT			
GROUNDHOG						
1	GH I	HE	100 T	SALT	2500	TATUM DOME
1	GH II				240	
1	GH III		30 T	HARD	[illegible]	—
1	GH IV				900	
3	GH V-VII		50-100 T	—	50	CALIFORNIA
3	GH VIII-X				350	NEVADA
11	GH XI - XXI		½ T	VARIOUS	110-1100	—

Table 6. Events in early VELA period

Aug 1961	Propose 3 O.S.I., veto powers
Aug 30, 1961	Soviets resume nuclear testing
Dec 1961	GNOME, FISHER explosions
Feb 1962	Semipalatinsk explosion
May 1962	Sahara explosion
Jun 1962	Revised seismicity estimate for USSR
Dec 1962	Soviets propose 3 "black boxes," quota 2-3 O.S.I.
Jul 1963	LTBT signed in Moscow Safeguard D

began in the USSR in October and, in November, France conducted its first underground test in the Sahara. Data from these and especially the larger nuclear explosions that followed, as recorded by the new seismic systems, were prompt and dramatic.

GNOME. Perhaps the most geophysically revealing explosion was the GNOME shot in December of 1961. GNOME, a part of the U.S. Plowshare* program, was an explosion of 3.5 kilotons in salt near Carlsbad, New Mexico. It was announced well in advance and numerous "volunteer" stations obtained recordings that supplemented the LRSM recordings (Fig. 3).

The observed travel times showed unexpectedly large regionally correlated departures from the standard Jeffreys-Bullen tables. There were corresponding effects on the amplitude of P_n and L_g; for example, P_n amplitudes decayed inversely as the third power of the distance to the west, and as the square of the distance to the east. These measurements established in an unequivocal way major upper mantle differences between the eastern platform region of North America, and the tectonic region west of the Rocky Mountain front (Fig. 4) — a notion that continues to color our thinking today.

Alluvium coupling. FISHER, a 13 kiloton shot in alluvium at the Nevada Test Site (NTS) occurred one week earlier and was recorded by the same LRSM stations that recorded GNOME. Pre-shot predictions were of unknown reliability, but included predictions that an explosion in a low strength material would be better coupled than an explosion in relatively strong salt. A direct comparison of GNOME and FISHER

*Nuclear explosions detonated for peaceful purposes.

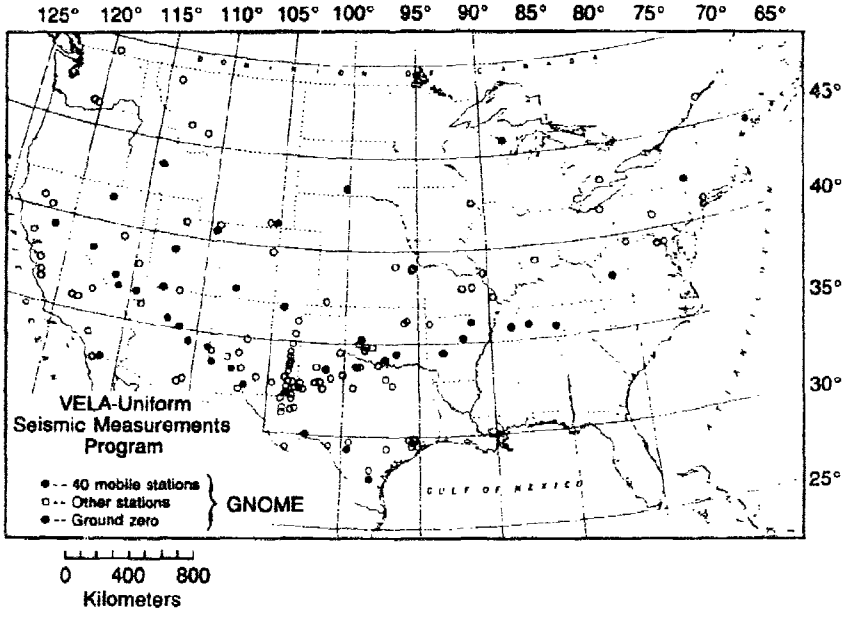

Fig. 3. Deployment of seismic stations for the GNOME explosion, 3.5 kt in salt near Carlsbad, N.M. Solid circles show locations of LRSM stations.

P_n amplitudes at identical stations along the GNOME-NTS profile (Fig. 5) could be made to measure the alluvium/salt coupling ratio. P_n exhibited the same travel times and inverse third power amplitude fall-off rate with distance as did GNOME, but when adjusted for the yield difference, the alluvium shot produced signals ***40 times smaller*** than the shot in salt!

It was an unexpected and disturbing result. The implications for evasive testing seemed obvious and were of concern to those conducting or guiding the test ban treaty negotiations. The capabilities described by the Experts in Geneva clearly needed redefining, but any attempt to do so could be extremely disruptive to the negotiations. Our ability to understand seismic coupling was shown to be primitive, if not unsoundly based. Quite evidently the measurement and analysis of seismic data from underground nuclear explosions would need to remain a major part of the VELA program for some time to come.

As more data accumulated, a general picture of seismic coupling began to emerge. By early 1983, Rainier Mesa and Yucca Flats were experimentally differentiated on the basis of coupling (Fig. 6), and "hard-rock" coupling (granite, salt) seemed even stronger than coupling in alluvium or tuff. The observed differences were known to be correlated with strength

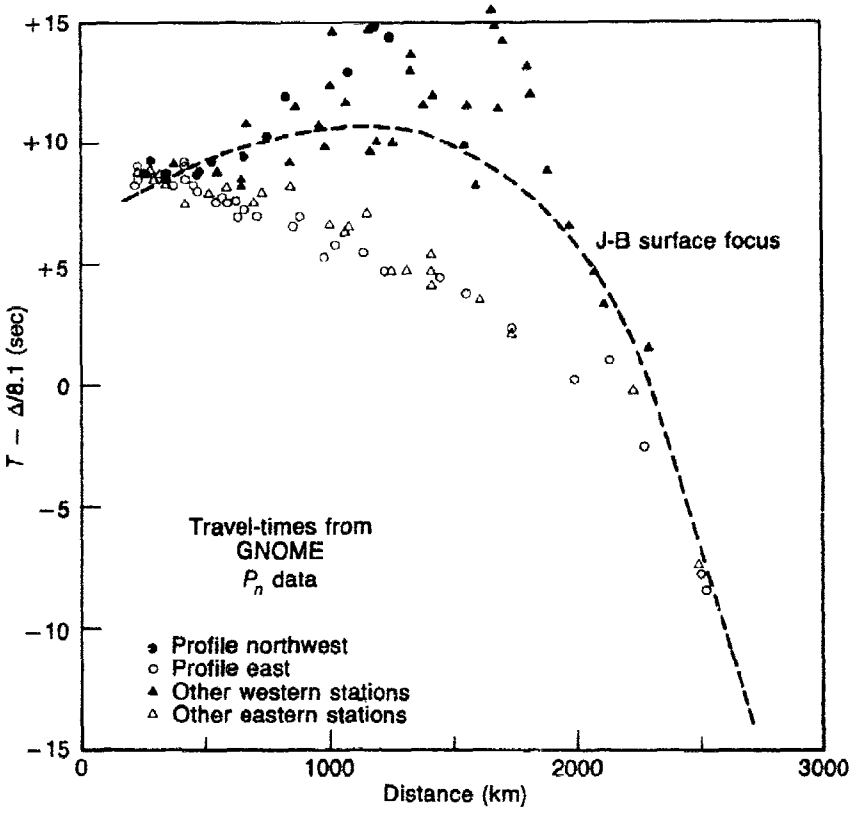

Fig. 4. Travel times for GNOME clearly show profound difference in propagation east and west of the Rocky Mountains Front.

and seismic velocities. The roles of porosity and water had not been established because there had been no shots large enough to require emplacement below the water table in Yucca Flats where these effects subsequently became apparent. Very little teleseismic data was available at the time Fig. 6 was prepared because of the low yields and low coupling of most of the tests, and the time required for assembling and analyzing the seismic data. Consequently, the magnitude scale on Fig. 6 was inferred from the measured magnitude of BLANCA (4.8 based on a handful of measurements) and an assumption that magnitudes for lower yield shots would scale as the average P_n amplitude normalized to 500 km. The picture was to change for the better very shortly.

m_b / yield relationship. Data from U.S. higher yield short, starting with HAYMAKER on 27 June 1962, were collected from WWSSN and

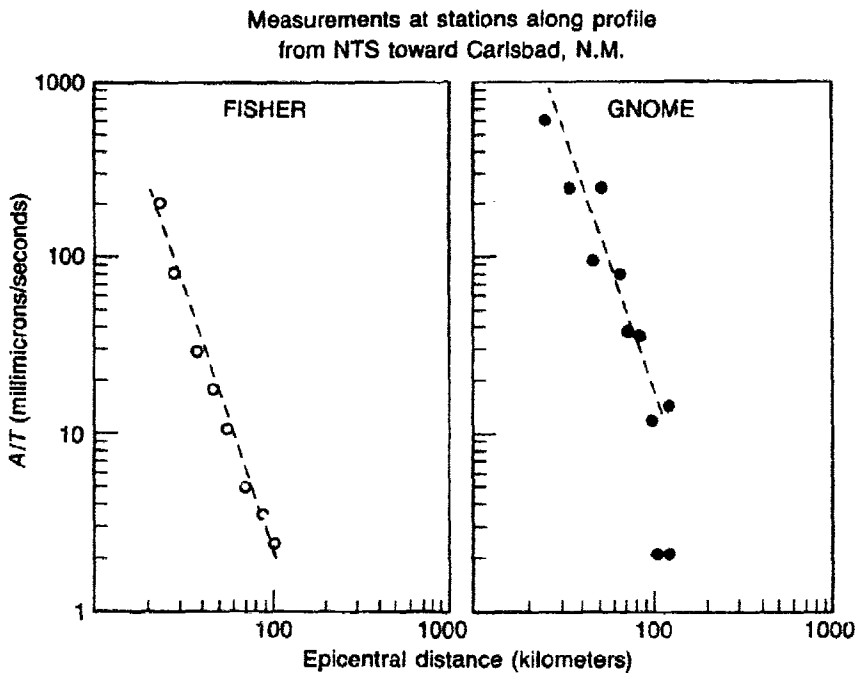

Fig. 5. P_n **amplitudes at the same stations for GNOME (3.5 kt) and FISHER (13 kt in dry alluvium). Relative amplitudes adjusted for yield show a coupling factor for dry alluvium 30 times smaller than for salt.**

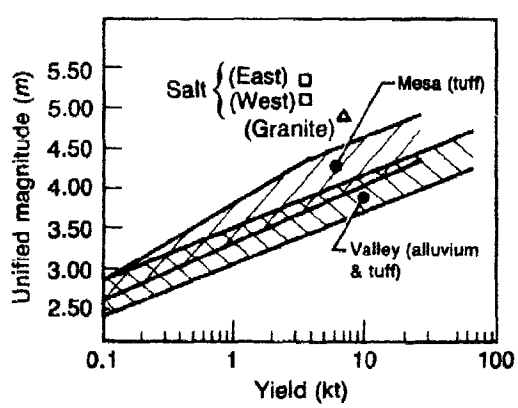

Fig. 6. Early version of the magnitude *vs* **yield curve. Average amplitude of** P_n, **corrected to 500 km by the observed amplitude** *vs* **distance curve, were plotted as a function of yield. Magnitudes were then inferred from the measured magnitude (4.75) and yield (19 kt) of the BLANCA explosion, since most of the other events were too small to produce well-detected teleseismic signals.**

LRSM stations and analyzed as they became available. MISSISSIPPI, 100 + kt on 5 October 1962 was particularly important; although its P_n and teleseismic P wave amplitudes were essentially the same as BLANCA's, it was recorded teleseismically by many more recently installed stations and the data put the m_b/yield relationship on a relatively firm basis (confirming, incidentally, the prior U.S. estimate of m_b for BLANCA). Similar relationships between yield and both M_s and the amplitude of L_g were developed at the same time. Contaminating effects on surface waves, now attributed to tectonic release, were noted early on (Fig. 7 shows an example, although recorded much later). These effects, together with the relatively poor M_s detection threshold, made the M_s *vs* yield data a rather questionable basis for yield estimation. The fact that the scatter in L_g amplitudes was less than for P was also noted.

Seismicity estimate revised. Seismicity statistics for Asia and other parts of the world, based on methods for P wave amplitude measurement and magnitude estimation that were identical to those used on the explosions, had also been accumulated. Of equal importance was the fact that both the earthquakes and the explosions were recorded by a network of stations having identical response curves and known calibration constants. Large explosions near Semipalatinsk (February 1962) and in the Sahara (May 1962) were important in showing that the corrections for distance in the magnitude formula (the so-called "B-factor") applied to surface focus events as well as to the deeper earthquakes from which they had been derived. For the first time, reliable numbers of earthquakes

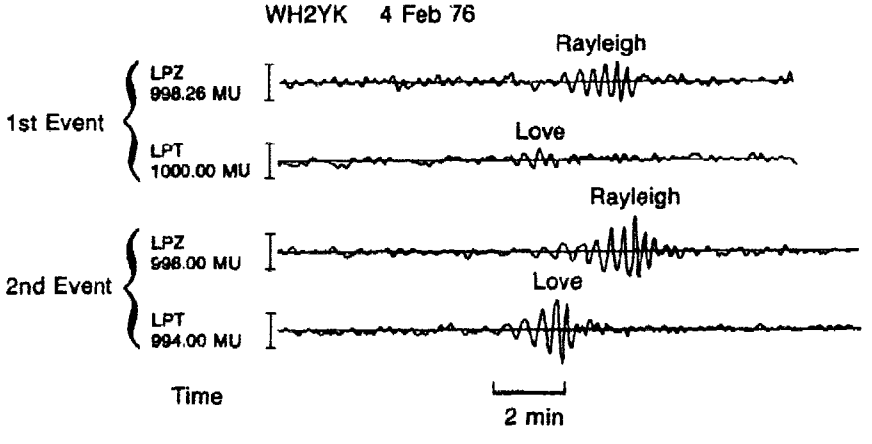

Fig. 7. Large differences in the excitation of Love and Rayleigh waves from two explosions of essentially the same yield and within a few km of one another were recorded on 4 February 1976. Vertical and transverse components at Whitehorse.

as a function of m_b could be compared directly with explosions of known yield without using conversion formulas relating m_b to M_s or M_L. (In fact, measurements of M_s and M_L for the same events failed to corroborate the published conversion formulas except at high magnitude). The result was that the estimated number of earthquakes equivalent to an explosion of given yield was reduced by about a factor of 2. From the standpoint of numbers of on-site inspections, this was highly significant and the result was greeted as a breakthrough by those involved in test ban treaty negotiations.

Epicenter location accuracy. Although results will not be described here, on-site inspection research was an important part of the early VELA program. This work had a strong impact on the seismological research since it was evident that the effectiveness of most on-site inspection techniques depends critically on the size of the area that would have to be inspected. Accordingly, research on hypocentral location accuracy became an important part of VELA. The Geiger method was soon extended to include a calculation of the 3-dimensional confidence ellipsoid around the focus. These calcuations were experimentally evaluated by applying them to precisely located explosions (Fig. 8) and as a result, indications of location bias apparently associated with the source region, as well as systematic effects of particular recording networks, were soon apparent. Several explosions off the Nevada Test Site (SHOAL, SALMON, LONGSHOT*) were conducted, in large part, to investigate location accuracy. LONGSHOT demonstrated that biases of about 25 kilometers attributable to deep crustal or mantle velocity structure were possible in teleseismically determined epicenters. The research also demonstrated that small networks of detecting stations would be unable to provide location precisions of 10 km or so (Fig. 9), independent of biases, in regions uncalibrated by explosions at independently known locations. Another result of this research was a greatly improved travel-time table for P, which has largely supplanted the traditional Jeffreys-Bullen table. Research on location accuracy gradually faded from importance after the signing of the Limited Test Ban Treaty in 1963, but it is clear that problems stemming from unknown regional bias, or poor location precision for events recorded at only a few stations, remain for any future monitoring system.

Detection methods and systems. One of the largest of the early VELA projects included the establishment of a network of five seismic observatories with short period arrays and other equipment as described

*Unfortunately for later research, the yield of LONGSHOT was never determined because the stated objectives did not require it.

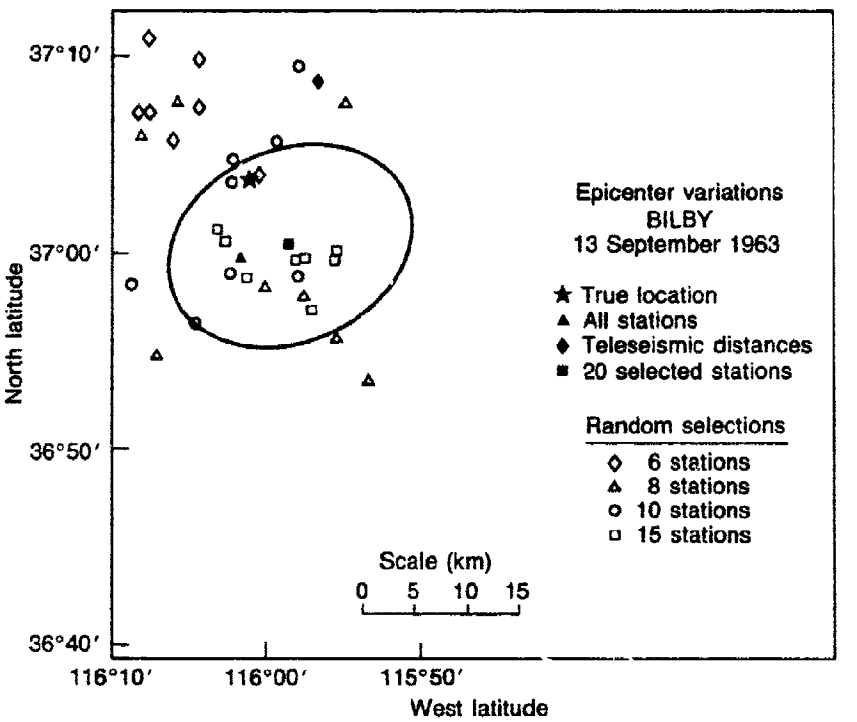

Fig. 8. Calculated epicenters for NTS explosion BILBY. Confidence ellipse applies to network of 20 stations selected to give good azimuthal and distance distribution. Locations based on larger network suggest a systematic epicentral bias.

Fig. 9. Radius of circle having the same area as the confidence ellipse about epicenters, calculated from network subset of various numbers of stations recording BILBY.

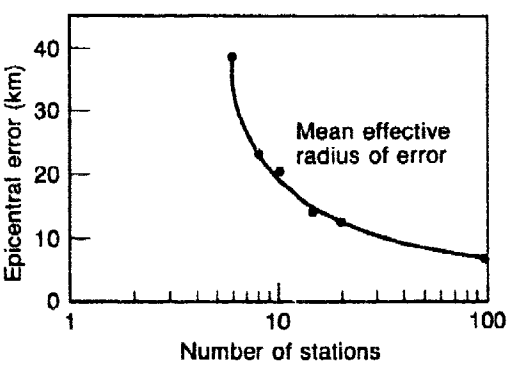

by the Geneva Experts. The objective was to model and evaluate a part of the network as agreed by the Experts. In July of 1960 the USSR agreed to permit 15 Control Posts inside the Soviet Union, and the VELA project to establish a network of array stations took on added importance as an urgent effort to develop a prototype for deployment inside the USSR and elsewhere. Key characteristics of these observatories were:

- stations to be separated by about 1000 km in seismic areas and 1700 km in aseismic areas
- equipment to include a 10 element short period array of vertical sensors distributed over about 3 km
- equipment to include 3-component short period, long period and broad-band sensors.

The resulting network and array geometries are shown in Fig. 10. Two of the observatories, Tonto Forest Seismological Observatory

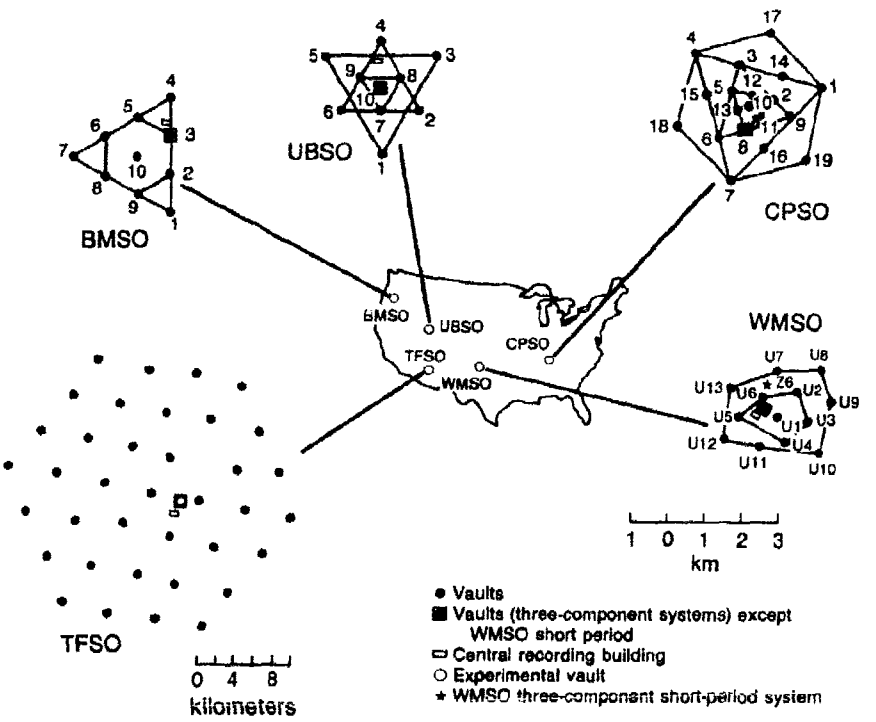

Fig. 10. Configurations of various seismometer arrays at observatories constructed to evaluate detection capabilities of stations similar to those recommended by the Conference of Experts.

(TFSO) and Columbia Plateau Seismological Observatory (CPSO), had larger arrays than the nominal 10-element array to support research on array design. Several array geometries and processing schemes (including Weiner filtering and adaptive processing) were tested. Analysis showed that the signal-to-noise gain was relatively insensitive to array design or processing method, and that simple delay-and-sum processing was about as good as could be done, provided that the sensors were far enough apart that the noise was essentially uncorrelated. Signal-to-noise improvements were about equal to the square root of the numbers of sensors. At smaller separations noise correlation reduced the effectiveness of the array.

Methods to eliminate noise caused by bouyancy effects on long period seismometers were developed and tested as part of this project. Borehole installation techniques for optimizing short period array performance were also demonstrated. The observatories operated for several years, producing much high-quality data on earthquakes and explosions for discrimination research. Of greatest significance, the program provided a sound basis for estimating capabilities of monitoring systems of the kind discussed in test ban treaty negotiations, and the U.S. gained the experience required to specify seismic characteristics of Control Posts inside the USSR.

An associated program resulted in measurements of signal and noise at various depths in a number of deep wells. The hope was that the short period noise propagated predominantly as Rayleigh waves, and that quiet conditions for detecting *P* waves would be found at depth because of Rayleigh wave attenuation. Some of the early results were highly favorable; signal-to-noise improvements of 20:1 were found at Grapevine, Texas, for example (Fig. 11). However, in localities where the surface noise level was relatively low (Elko, Nevada, for instance) there was little noise reduction at depth. These experiments, together with the studies of array performance, led to the concept that short period noise consists of an irreduceable ambient component consisting of high velocity, or "mantle *P* wave" noise, and a Rayleigh wave component confined to the surficial layers and often having far larger amplitudes. In regions where the Rayleigh component predominates a borehole installation may out-perform a very large surface array.

Another technique for improving signal-to-noise ratios was based on combining the outputs of a strain- and pendulum-seismograph. Various combinations of horizontal and vertical sensors can be devised, in principle, to enhance selected wave types. For instance, theory predicts that combined horizontal instruments should have directional discrimination capabilities for propagating surface waves comparable to a large long-

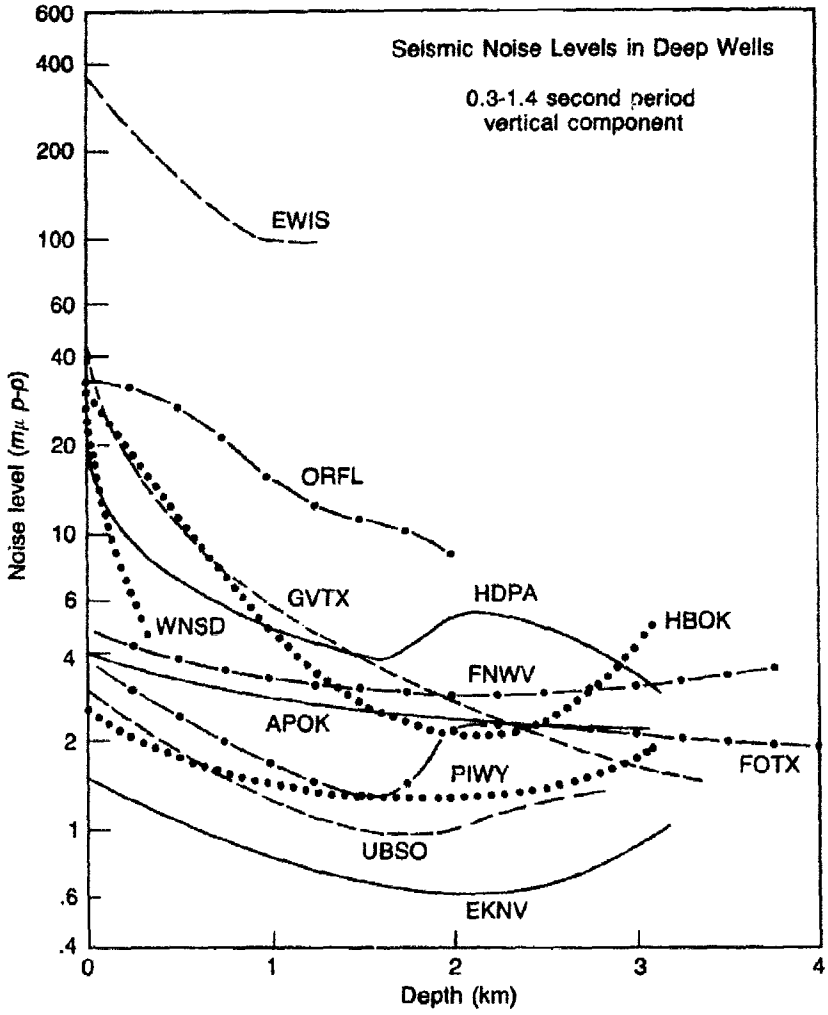

Fig. 11. Short period noise as a function of depth in boreholes. At noisy sites employment of seismometers at depths of 0.5-1.0 km gives a signal-to-noise improvement equivalent to a rather large array. More than 20 dB signal-to-noise increase was observed at Grapevine, Texas, (GVTX) at 10,000 ft depth. At quiet sites like Elko, Nevada, (EKNV) there was little signal-to-noise increase with depth.

period array (Fig. 12), and experimental data on large events seems to confirm this. The technique has not been useful at interesting amplitudes, however, because instrumentation and installation noise problems have not been solved. Both this technique and the deep well technique could

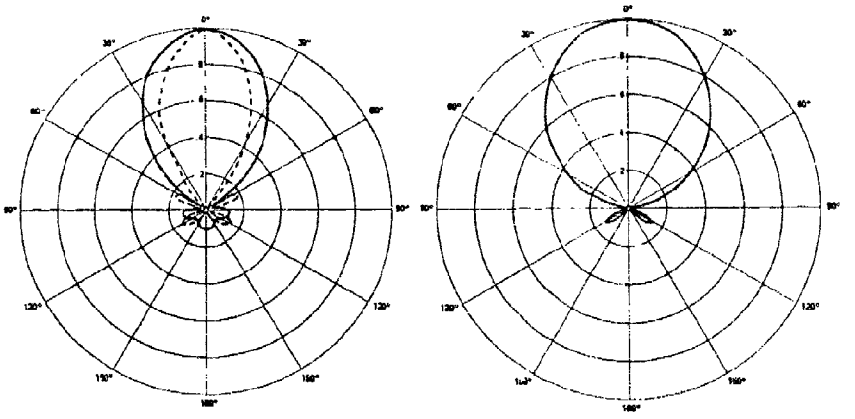

Azimuthal Beam Pattern
19-Element Filled Hexagonal Array
20 km separation
— 0.04 CPS waves at 3.5 km/sec
--- 0.06 CPS waves at 3.5 km/sec

Azimuthal Beam Pattern
Combined Horizontal Strain and
Pendulum Seismographs Steered
for Surface Waves
(Pattern applies at all frequencies)

Fig. 12. Comparison of beam patterns of a long period seismometer array and a combined pendulum and strain seismometer. Strain/pendulum pair has theoretical azimuthal resolution and noise rejection characteristics comparable to those of a large seismometer array. Strain seismographs have, to date, suffered from noise problems that have prevented the achievement of this capability except on an experimental basis.

be of high value in places where the intrusiveness of a station must be minimized.

Treaty negotiations in the early 1960's rather soon bogged down in issues relating to verification — primarily of underground nuclear tests. Although the USSR had agreed to 15 Control Posts on their territory, they insisted that they would operate them. Although the need for on-site inspection was agreed, the annual numbers to be permitted and the objectivity and technical adequacy of such inspections, under conditions that could be negotiated with the USSR, were unsatisfactory to the U.S. and U.K. By December of 1962 the situation had deteriorated to the point that the USSR proposed that underground nuclear test monitoring should be based on three unmanned seismic stations, or "black boxes" as they were called, and a quota of two or three annual on-site inspections. Even on this offer, attending conditions left grave doubt as to the objectivity of any resulting data. Much effort was applied to developing unmanned seismic stations, on analyses of how they could be "spoofed," and on how to make them secure. More importantly, the VELA program began

The most elaborate station of all, directed almost exclusively to teleseismic detection, was the Large Aperture Seismic Array (LASA) in Montana. This program was proposed in March, 1964, and its proponents advocated a design consisting of 21 subarrays of 25 sensors with *small* spacing — about 0.5 km — in spite of the experience with the Geneva arrays. It was claimed that this array would be able to exploit the coherence of the short period noise to achieve a gain of more than the square root of the number of sensors. The selected location for the array was not particularly quiet insofar as naturally generated noise was concerned, but man-made noise was not a problem and, anyway, the large number of sensors and hoped-for performance were expected to make LASA the world's best station. The subarrays were distributed over an area having a 200-km diameter for relatively high beam resolution. Each subarray contained a 3-component long period set and short period horizontals in addition to the vertical array sensors.

LASA was given a very high priority. Work started in October of 1964 and by the end of the next May the entire array was complete! The data were in digital form — a first on a large-scale within the VELA program. Highly sophisticated signal processing methods were applied to the data in the attempt to improve the signal to noise ratio.

Initial claims of signal-to-noise improvements beyond $\sqrt{n}$ were made, but it was soon found that these estimates included the signal-to-noise improvement normally accomplished by band-pass filtering to eliminate storm microseisms, as well as the array gain *per se*. In short, the reported gain was based on a band-pass filtered output relative to a broad band input. When comparisons were made with identical before and after frequency filtering, the true array gain was found to be less than $\sqrt{n}$ because the noise was not reduced as expected and there was signal decorrelation over the large distances between subarrays. The net result was that LASA's detection threshold (Fig. 13) was only comparable to that of a small array in a carefully selected quiet location. Thus one of the major goals of the LASA was not met, and the subarrays were subsequently decimated of seismometers in recognition that the noise coherency at small sensor separation could not be effectively exploited. The removed seismometers were subsequently used for the NORSAR array. The expected high beam resolution, however, was verified and found to be useful in providing an initial estimate of epicentral location.

Identification criteria. By early 1962 it had been demonstrated that *pP* could be used reliably to establish the focal depth of many earthquakes. Research was aided by the recently acquired ability to calculate error ellipsoids, and used together, it was shown that these methods could establish focal depths of a large fraction of events occurring in Asia.

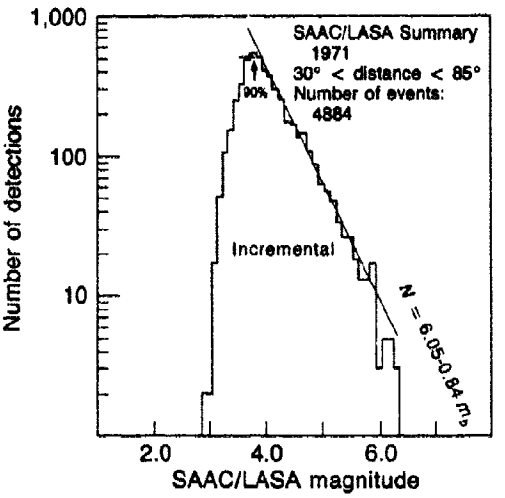

Fig. 13. Earthquake recurrence curve observed at the Large Aperature Seismic Array (LASA). A detection threshold of about m_b = 3.8 may be inferred from this data.

The determination of depth of focus became — and remains — the most effective and physically satisfying means for discrimination. It identifies earthquakes only, of course, so other discriminates were required to discriminate shallow seismic events.

Experience with explosions continued to show that the direction of first motion was an unreliable discriminate except at very high signal to noise ratio. Furthermore, analyses of earthquakes occurring in the USSR showed that they tended to be on thrust faults, radiating compressional first motion into the part of the focal sphere observable teleseismically. This method thus identifies few of the seismic events of interest to the U.S.

A measure of *P*-wave "complexity" (energy in the *P* coda relative to that of the initial pulse) was developed by colleagues in the U.K. Initial favorable empirical results as a discriminant were promptly passed *via* high level political channels to the U.S. and caused a great flurry of excitement among the test ban negotiating community. This also stimulated several investigations within the VELA program. As a result, it was found that the method worked well in cases where focal depth could be established by *pP* (and hence was redundant), but was mostly ineffective when applied to apparently shallow events (Fig. 14). Furthermore, when the highly complex explosion occurred in Novaya Zemlya in September 1964, ideas about the cause of complexity had to be drastically revised. It was apparent that the observed effect was not a primary property of the source but rather of the region in which it was located. The experience with complexity taught a very important lesson, however:

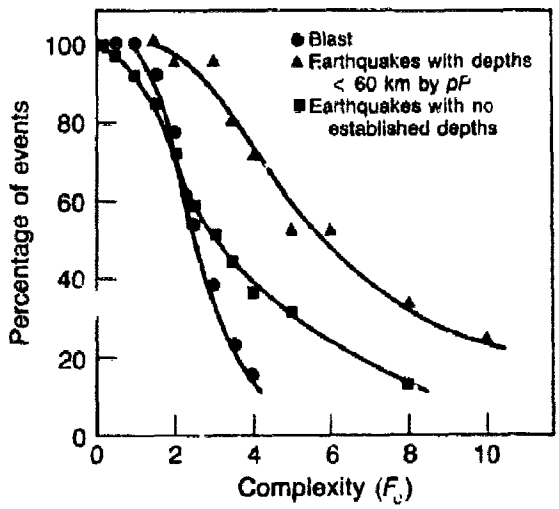

Fig. 14. "Complexity" of earthquakes and explosions. This measure of the ratio of energy in the coda of *P* to that of the main *P* pulse is a fairly effective discriminant between earthquakes and explosions for events with detectable *pP*, but much less so for events whose depth cannot be determined. It is thus redundant (and less satisfying physically than establishing a deep origin) in most cases.

a completely believable criterion must have a sound physical basis. A corollary is that a strictly empirical basis is insufficient.

Suggestions were made at the Expert's Conference that the relative excitation of long period and short period waves might be a means of discriminating between earthquakes and explosions. An empirical criterion was developed early in the VELA program based on the ratio of the area of the envelope of the long period Rayleigh waves to the amplitude of short period *P* waves (the "*AR*" criterion). It was soon shown that M_s was an equally good measure, and work concentrated on M_s:m_b. An apparent "breakthrough," based on East Coast observations of explosions at NTS as compared with earthquakes at various locations, was that an M_s estimate based on 40-50 second waves rather than 20 second waves greatly enhanced discrimination. This was soon shown to be a path effect, rather than a source effect, by comparing waveforms from the explosions along different paths (Fig. 15). Comparing earthquakes and explosions along the same path (Fig. 16) showed no particular increased effectiveness at the longer period. Once again, the need for a firm physical

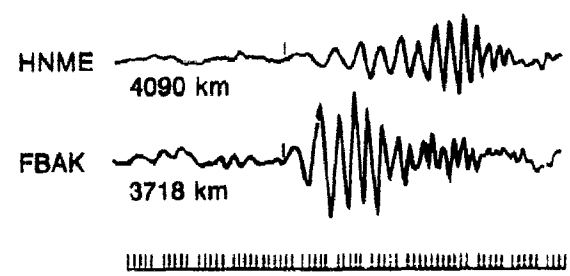

Fig. 15. NTS explosion PURSE recorded at Houlton, Maine and Fairbanks, Alaska. Relative amplitudes of 40-50 second and 20 second Rayleigh waves shown to be a path effect rather than a source effect. Time marks at 10 second intervals, skips at selected minutes.

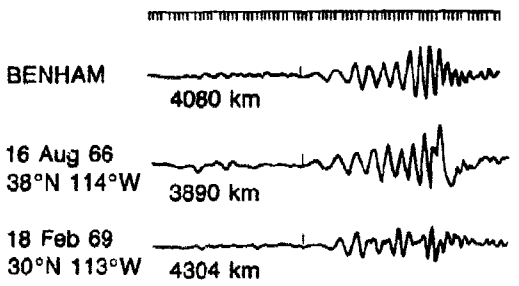

Fig. 16. NTS explosion BENHAM compared with Nevada and Gulf of California earthquakes as recorded at Houlton, Maine. When observed after traveling similar paths, relative amplitude of 40- 50-second Rayleigh waves are similar for earthquakes and explosions. Time marks at 10 second intervals, skips at selected minutes.

basis for a discriminant was emphasized. Although M_s:m_b remains as a highly regarded discriminant, it is disturbing that it is not fully understood — particularly so since it is also known that tectonic effects can perturb Rayleigh wave generation from explosions in a significant way and that propagation effects can perturb both *P* and Rayleigh waves in uncorrelated ways.

Evasion research. VELA was tasked to determine whether a nation could conceal a nuclear explosion from detection systems and to develop countermeasures to evasive testing techniques that appeared to be effective. The initial U.S. work on cavity decoupling, undertaken by the AEC, had shown a reduction of about a factor of 100 in the low frequency signals relative to tamped high explosive charges. Several technical questions could not be answered by H.E. explosions, however, and VELA prepared for a nuclear program. This was to consist of SALMON, a 5 kt tamped shot in salt (conducted in 1964), a low yield nuclear tamped shot and a shot of the same low yield conducted in a mined cavity in salt. Plans for the latter two shots were abandoned because of difficulties caused by leakage of water while constructing the shaft needed for the mined cavity.

STERLING, a 380 ton nuclear shot in the SALMON cavity, was subsequently detonated in 1966. Although the cavity was too small for optimal decoupling of 380 tons, there was substantial decoupling at low frequencies (about a factor of 50-70 by most estimates) and the relative SALMON/STERLING spectral shapes seemed to agree with theory (Fig. 17). Additional explosions at the Nevada Test Site investigated ways to further enhance decoupling by adding energy absorbing material in the cavity, with some success.

Supporting work on the feasibility of constructing large cavities indicated that holes of sufficient size to decouple 10 kt were feasible. Even

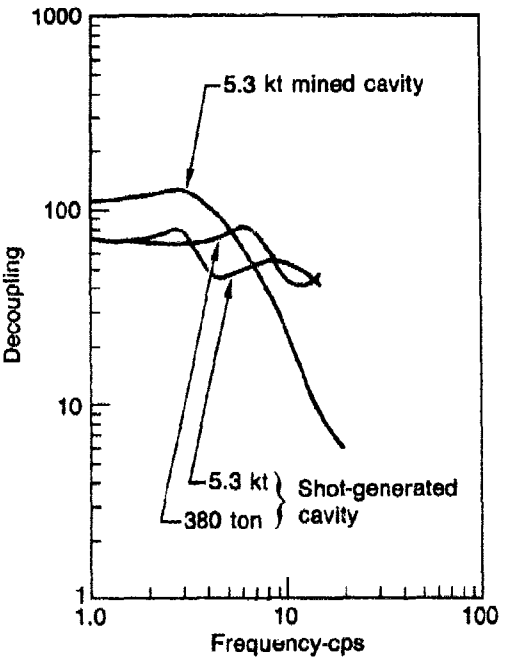

Fig. 17. Partial decoupling of 380 ton and 5.3 kiloton shots, as inferred from STERLING and SALMON data. Also shown is the estimated decoupling for a 5.3 kiloton shot in a mined cavity.

larger cavities exist, although none are spherical. Although many questions remain, as a result of this work decoupling is generally accepted to be a feasible means for reducing seismic signals by about two orders of magnitude for explosions up to several tens of kilotons.

Laboratory simulations, as well as a few fortuitously timed nuclear explosions, showed that an explosion conducted shortly after a major earthquake might not be detected. There are difficult operational problems associated with testing in this mode, and the yield that could be concealed by an earthquake of a given magnitude is strongly dependent on the characteristics of the monitoring network.

Similarly, carefully timed multiple explosions — perhaps also conducted in the coda after a large earthquake — could complicate or prevent identification of the events. Simple scenarios of this type have been shown to be ineffective, but a well-designed series of shots would appear to be capable of spoofing a monitoring network, based on currently validated identification criteria.

Summary Comments

Most of the problems for underground nuclear test monitoring that remain today were known by the mid-to-late 1960's. This is not a reflection on the quality or vigor of the program since that time, but rather of the

fundamental nature and great complexity of seismic sources and the earth itself that cause the problems.

There were major technical accomplishments during the early VELA period. Landmarks that I would cite are establishing the WWSSN, the development of borehole technology to protect both short and long period sensors from environmental noise, the development (and continuing proliferation) of digital technology, and the development of effective seismic discriminants. Equally important — even if less satisfactorily concluded — major efforts were in array technology (a bit disappointing in that only $\sqrt{n}$ improvement in S/N was achieved) and evasion research (still arguable quantitatively, and probably will remain so without nuclear experiments).

Perhaps the most important accomplishments have been the development of a strong technology base and the continuing support given to test ban treaty policy making and negotiations. Manifestations of the strength of the technology base are visible in terms of the increased numbers of students, researchers and institutions involved in seismology, as well as in the ability of the participants in the program to turn quickly to new problems as they arise. A case in point was the ability to support the Threshold Test Ban Treaty negotiations in 1974, even though research on yield estimation had been neglected because prior U.S. policies had explicitly rejected consideration of threshold treaties. Throughout the entire period of test ban negotiations, VELA workers and the DARPA staff have been the primary source of technical advice, as well as participants in the negotiations themselves. I believe that these latter points are attributable in large measure to three characteristics of the VELA program:

- It has remained a national program — not a Department of Defense program — focusing on problems of interest to all agencies of the government concerned with test ban policy. The program has never been pressured by senior DoD officials to support any narrow agency viewpoint.
- With few exceptions, program managers have established high standards of proof and required thorough backup prior to supplying technical advice to policy levels of government. While this careful approach is slow at times, it has been essential in resolving opposing points of view among the federal agencies concerned with test ban policy, and the reliability of the advice has been crucial to the continuing support of the program.
- Program managers, by and large, have resisted the temptation to assume policy roles, confining their advice during the policy formulation process to technical matters within their competence.

Twenty-Five Years of Source Theory

Bernard J. Minster

1. Introduction

In the past twenty-five years the earth sciences in general and seismology in particular have undergone more vigorous development than at any time in the past. Our perception of the earth and of geological processes has been greatly modified by the advent of plate tectonics which offers a global framework for the study of the planet. Naturally, the study of seismic sources, a rather specialized discipline of geophysics, has also progressed considerably during that period.

Twenty-five years ago, the underlying causes for seismic activity, the reasons behind the geographical distribution of earthquakes, and the mechanics of failure during an earthquake were by and large mysteries yet to be uncovered. Today, we worry about rather subtle features of seismograms, complicated rupture histories, and detailed simultaneous modeling of near-field and teleseismic waveforms.

Twenty-five years ago, there was considerable debate on whether an equivalent point source should be taken as a single-couple or a double-couple. Today, a complete description of the source requires typically six functions of space and time, namely the components of a moment rate tensor density.

The reasons for this progress are many, but they can mostly be traced to the requirements of a nuclear test-ban treaty monitoring capability. It is primarily in response to this need since the early 60's that many of the technological and theoretical tools we enjoy today have been developed.

(1) Underground nuclear testing has provided accurate, well located and controlled sources of sufficient size for the signals to be recorded everywhere at the surface of the Earth.

(2) The deployment of the World Wide Network of Standard Seismometers, and the installation of several large aperture seismic arrays have provided seismologists with a wealth of high-quality observations with much improved

areal and azimuthal coverage. More recently, digital networks have yielded even better data, well suited for modern computer-based data processing (SRO, ASRO, IDA).

(3) Advances in seismometry and the development of digital recording techniques have greatly increased the information content of seismograms, particularly at long periods.

(4) The advent of digital computers, which have been used early on in geophysical modeling and research, opened the door for the analysis of large data sets, the generation of ever more realistic earth models, the calculation of synthetic seismograms, and the numerical modeling of complex phenomena which cannot be studied analytically.

(5) Considerably increased support in fundamental research in the earth sciences was fueled by the needs for treaty verification, discrimination and yield estimation. It permitted continued development and expansion of theoretical geophysics. Many scientists, who a decade earlier would have undoubtedly been attracted to other fields of physics, became seismologists instead.

Thus, theoretical geophysics as we know it today could really be considered to be a creation of the 60's. In many ways, this is also true of source theory. The VELA program has been instrumental in this; many of the workers in the field have been supported directly or indirectly through this program, often starting from their graduate career.

Source theory is a generic term which covers many endeavors of fundamental research in seismology, from the study and understanding of the failure of rocks in the earth and earthquake mechanics, to the examination of detailed processes in the vicinity of underground nuclear explosions. It pertains to the study of microcracks in laboratory rock samples or of the detonation of gram-size explosive charges embedded in such samples, to the study of the 1960 Chilean earthquake; these sources span twenty-five orders of magnitude in moment.

Although it is often customary to organize seismological work into the study of sources, wave propagation, and receiver properties, the distinction between these various areas is blurred. For instance, it is not possible to ignore wave propagation effects when one attempts to retrieve source parameters by inversion of seismic observations. This separation is often made for convenience. Unfortunately, it leads to the concept of a "source region", a phrase commonly used in the literature, which takes on a different meaning depending on the context. In this paper, I shall use this phrase, for lack of a better term, to indicate the volume

of the earth within which source phenomena *per se* are confined. The source region should at least include all material subjected to brittle or ductile failure; if one includes the domain in which the material does not fail, but is subjected to high enough strains that its rheology is inelastic (nonlinear), then the source region could conceivably be much larger. Wave propagation inside the source region should really be analyzed as part of the source mechanism; this includes scattered and diffracted waves (*e.g.*, Das, 1980; Stevens, 1980b), strong acoustic fields (Melosh, 1979), spall phenomena near an underground explosion (Day *et al.*, 1983) and generally any propagating disturbances which interact with the material so as to affect the outgoing wavefield. Such phenomena are the object of on-going research in source theory.

A comprehensive review of source studies would be a monumental task requiring considerable time and resources. Fortunately, a number of excellent reviews of the subject are available (*e.g.*, Honda, 1962; Dahlman and Israelson, 1977; Rice, 1980; Masse, 1981; Bache, 1982; Boore, 1983). In addition, a tutorial presentation of the theory and supporting observations is found in three separate chapters of Aki and Richards's text (1980) and a more esoteric mathematical presentation is given by Ben-Menahem and Singh (1981). The reader who is seriously interested in the details of source theory is urged to turn to these works; I shall not provide in this paper the tools needed to actually understand the source mechanism; instead I shall attempt to describe some of the ideas on the subject which at one time have held the attention of seismologists.

If one measures the vigor of a discipline by the amount of debate that it generates in the community, then source theory is indeed a young and growing field. Over the past twenty-five years, virtually all aspects of source theory have been the object of considerable argument, and sometimes lively controversy. Some of these arguments have been resolved to everyone's satisfaction, others are still with us today, and new ones arise as the field progresses. It would be presumptuous to claim good enough understanding of all points of view and robust enough objectivity to provide a lasting historical perspective, particularly when it comes to those topics which are still debated today.

I have tried to organize the material into various sections in an attempt to simplify the characterization of the arguments. However, the reader should be aware that each topic was not actually debated separately in its own context. As can be expected, and as any reader would quickly notice by perusing the literature, the arguments are often intertwined in complex ways, so that there is some danger of losing in accuracy what is gained in simplicity of presentation.

2. Single- and Double-Couples

Since the early work of Reid (1910), who demonstrated that the 1906 San Francisco earthquake was associated with faulting along the San Andreas fault and formulated the elastic rebound theory, seismologists have been very interested in the rupture mechanism of earthquakes. Although the various disciplines of seismology did undergo vigorous expansion in the few decades that followed, especially in Japan, it was not until the 50's that the modern ideas about seismic source models started appearing in the literature.

Nevertheless, from the extensive review by Honda (1962)—who compiled as many as 278 references on the subject—one cannot but be impressed with the remarkable variety of fundamental solutions which have been available to seismologists for a very long time. In addition, in spite of the general sparseness of seismic stations installed at the time, a very large number of observational studies were undertaken successfully, particularly concerning the distribution of first motions as an indication of the faulting mechanism. Among others, I should mention the series of publications by Hodgson and co-workers who developed to a remarkable extent the art of determining fault-plane solutions using stereographic projections originally introduced by Byerly (1938). Many of their solutions are still used on occasion in the literature. Coulomb and Jobert (1973) credit T. Shida with the first observations (*circa* 1927) of the quadrantal distribution of first motions from a shallow earthquake. The connection of this distribution with the theory of elastic rebound was made by Gutenberg (1956).

A major conceptual advance was achieved by Vvedenskaya (1956). In a series of papers between 1956 and 1961, she and her co-workers introduced dislocation theory as a systematic tool to model earthquake sources, compute the associated displacements, and determine the orientation of stresses active near the focus from seismological observations. She demonstrated the double-couple equivalence of point sources of slip (Vvedenskaya, 1956). Other investigators did use dislocation theory very early on; for example, Knopoff and Gilbert (1959, 1960) studied the radiation field from a strike-slip fault and derived the distribution of first motions from such models. It seems that the main debate was in fact centered on the problem of defining an equivalent point source, rather than on the appropriateness of the dislocation model *per se*.

In retrospect, it seems a bit puzzling that one of the great subjects of debate during that time was whether an earthquake source is equivalent to a single-couple with moment, or to a pair of couples with equal and opposite moments. As late as 1962, Honda felt a need to distinguish between type I and type II source models, which he equated respectively

to these two alternatives. Knopoff and Gilbert (1959, 1960) actually went to considerable lengths to contrive a combination of two parallel dislocations with opposite Burgers's vectors in order to achieve a tie between dislocation theory and a single-couple source.

There were several reasons for this lasting debate: The first one is that *P*-wave first motions alone are not sufficient to distinguish between the two models. Consequently, one must examine the radiation pattern for *S*-waves in order to choose between the two hypotheses (*e.g.*, Byerly and Stauder, 1958) and such data are more difficult to obtain reliably—although Honda (1962) argues that at least in some cases, *S*-polarity observations could be made unambiguously. Another reason—pointed out by Kostrov (1970)—why the single-couple proponents remained unconvinced is that Vvedenskaya's treatment somehow lacked sufficient rigor in the derivation.

The use of dislocations and of double-couples to describe the kinematics of earthquakes, as well as the static deformations associated with faulting, gained ground steadily through the late 50's and early 60's. Steketee (1958) used Volterra's dislocation theory to compute displacements produced by faulting and to analyze the strain energy of faulting. Chinnery (1961, 1963) applied the model to the study of ground deformation around vertical transcurrent faults. Dislocation and double-couple models of the source were also used in surface wave studies of the earthquake mechanism (Aki, 1960; Brune, 1960) and in the early work on free oscillations (Benioff *et al.*, 1961). Aki (1960) showed that Love-wave radiation from the 1956 Kern county earthquake was consistent with a double-couple.

The theory remained relatively incomplete until Maruyama (1963) built on the static work of Steketee, and showed that the displacement field due to a dynamic dislocation is exactly equivalent to a distribution of double forces. In 1964, Maruyama tabulated for the first time all the components of the Green's tensors for static dislocations in an infinite space and in a half-space. Finally, Burridge and Knopoff (1964) produced a comprehensive and rigorous analysis of the body-force equivalents to a dislocation source under general assumptions (general inhomogeneous anisotropic medium). The orientations of equivalent double-couples and double forces without moment are related to the directions of the Burgers vector and the normal to the fault only if the medium is isotropic. A simple argument given by Benioff (1964) provides the missing link by relating the double-couple force system to the theory of elastic rebound. Thus, I would place the "death" of the single-couple point source around 1964.

By that time, the dislocation model had gained fairly general acceptance as a kinematical representation of earthquake faulting, and its

double-couple equivalent point source gradually became somewhat of a standard. However, perhaps for reasons of convenience, perhaps for purposes of completeness, the use of single-couples persisted in the literature well into the end of the decade. For example, Kanamori (1970) demonstrated that the double-couple source matches long-period surface wave radiation pattern, whereas the single-couple does not. Archambeau (1968) argued that, in a multipolar expansion of the radiation field, the dipolar component cannot exist by itself, but must be always present in combination with higher order multipoles in order to satisfy conservation of angular momentum. In other words, systems of double forces with net moment are precluded.

Other advances in the theory of seismic sources accomplished during the early part of the decade were less controversial. Important contributions include the analysis Ben-Menahem (1961), who examined the radiated energy and excitation of surface-waves by moving sources of finite dimensions. He formally introduced the finiteness factor, and the directivity of surface wave radiation patterns, a concept subsequently used in many source studies involving long-period observations.

During that same period, the study of seismic waves generated by underground nuclear explosions began in earnest; we shall return to that subject in a later section.

The greatest success of the equivalent point source model is indubitably the determination and interpretation of fault-plane solutions. I have already mentioned the early work, dominated by the contributions of Hodgson and his co-workers; since then, countless determinations of focal solutions have been made for all types of events, deep and shallow, local and teleseismic. The principles are well-known and will not be repeated here. However, it must be pointed out that it is the tool that was used by Sykes (1967) to demonstrate the nature of oceanic transform faults and thus contribute powerfully to the acceptance of plate tectonics by the geophysical community. Since then, focal solutions have been used to resolve a remarkable number of important tectonic questions, and to constrain global plate motion models. The determination of a focal solution remains essentially the first order of business (after location) in the analysis of any seismic event, as well as one of the few unambiguous discriminants between earthquakes and underground nuclear explosions, whenever a well-determined mechanism can be obtained.

3. From Kinematic Dislocations to Dynamic Crack Models

One observation which cannot fail to impress anyone who attempts a review of the evolution of source theory over the past two decades

is the systematic evolution of the models from purely kinematical dislocations to more and more sophisticated models which incorporate an increasing number of dynamical characteristics.

In this section, I shall try to outline this evolution, by focusing primarily on those source models which involve a thin faulting surface, starting from the now classical planar dislocations and ending with some of the most recent numerical simulations of dynamic cracks.

3.1 Kinematic Source Models. The establishment of dislocation models as a powerful tool for studying the kinematics of earthquake sources was consolidated by the work of N. Haskell in the mid- to late 60's (Haskell, 1964, 1966, 1969). This work was seminal in the sense that it has been and continues to be the basis for many source studies.

What has come to be known as "Haskell's model" is described in detail by Aki and Richards (1980); it is a planar dislocation model for a long and narrow fault swept by a dislocation line, parameterized by:

(1) the fault length, typically taken along the strike
(2) the fault width, (usually the depth)
(3) the rupture velocity
(4) the final slip offset
(5) the rise time

Instead the final-slip and rise-time one could specify a so-called *source function*, the time derivative of which can be shown to control the far-field waveforms. In addition, it is usually assumed that the fault slip never reverses its direction—that is, the source function is *unipolar*— and that the rupture is unilateral, that is, the rupture front propagates along a single direction.

This five-parameter model offers considerable flexibility in that it is capable of representing a wide variety of faulting situations, and is amenable to both analytical and numerical treatment. As a result it has been used extensively in various forms for body-wave, surface-wave, free-oscillation, and near-field studies.

Note that a physical parameter which is not formally included as part of the specification of Haskell's model is the stress, or more specifically the *stress drop* associated with the faulting. This emphasizes the kinematical character of the model. Once the geometry of the fault has been determined, information about the stress drop can be retrieved by comparing the results with those obtained from another model with similar geometry, for instance a crack model.

One method, applied for the first time by Aki (1966), uses simultaneous estimates of the seismic moment and of the energy released. However, as discussed by Wyss (1970a,b), there remains the problem of relating the true energy released during faulting to that which is radiated in the form of seismic waves; in other words, one needs an estimate of the seismic efficiency.

Brune (1970) proposed a simple earthquake model in which both sides of the fault are accelerated by an "effective stress", applied instantaneously over the fault surface. Although this model was quite primitive compared to later quasi-dynamic crack models, it gained some degree of popularity as an interpretive tool, mostly because the simple parameterization of the spectrum predicted from it allowed convenient processing of body-wave observations by spectral analysis (*e.g.*, Hanks and Wyss, 1972; Hanks and Thatcher, 1972; Tucker and Brune, 1973).

In spite of the considerable attention paid to Haskell's model in the late 60's and through the 70's, it was not until 1978 that Madariaga (1978) obtained an exact analytical solution for the wavefield generated by a Haskell source at any point of a uniform elastic infinite space. For a rectangular fault, he showed the wave field to be the superposition of cylindrical waves generated by the sudden start and stop of the dislocation line and spherical waves emanating from the corners of the rectangle.

Variations on the basic dislocation model have been devised, usually for the purpose of studying particular phenomenological aspects of the source. An early model was the one proposed by Savage (1966), in which the phenomenon includes three stages; it nucleates from a point, spreads radially until it fills some area of prescribed shape, and stops. However, Savage assumed the slip function to be identical at all points on the fault. This somewhat unrealistic circumstance was corrected by Sato and Hirasawa (1973), who assumed the distribution of slip over a growing circular fault to be identical at all time with the static equilibrium distribution derived by Eshelby (1957). Another modification was suggested by Molnar *et al.* (1973), who assumed that the rupture spreading phase is followed by a healing phase propagating inwards from the periphery of the final fault at a velocity equal to the rupture velocity, and thus avoided the peculiarities associated with a rupture which stops simultaneously at all points on the fault.

Yet another model was examined in some detail by Dahlen (1974); he considered a growing elliptical fault, with a constant aspect ratio, and used the exact slip function derived earlier by Burridge and Willis (1969) for a growing elliptic crack with constant stress drop. He avoided some of the difficulties attached to stopping the crack growth by assuming a

gradual slowing down of the growth after a certain fault dimension has been reached.

Although dislocation models with spatially uniform slip function and a simple time dependence have proved useful for studying low frequency (less than 1 Hz) radiation (*e.g.*, Aki, 1968; Haskell, 1969; Anderson and Richards, 1975; Bouchon, 1979), the high-frequency wavefield (1 to 20 Hz) is much more sensitive to details of the faulting process, particularly in the near-field. For instance, the analysis of Madariaga (1978), shows that uniform-slip models are usually inadequate for modeling near-field ground motions with wavelengths much shorter than the fault width (see for instance, Day, 1982a).

More complicated models can be invoked, which rely on a statistical representation of a complex faulting process. This approach was first adopted by Haskell (1966), who suggested that the statistical properties of slip distribution along a single fault can be related to ensemble averages of the properties of many events, similar to the "ergodic" assumption of time series analysis. Hanks (1979) invoked a statistical model in an attempt to explain the apparent randomness of ground accelerations, and recently, Andrews (1980, 1981) examined both static and time-dependent stochastic fault models, which he describes as "fractal objects" (Mandelbrot, 1977), and showed that such a description is phenomenologically compatible with a variety of observations.

However, by the late 70's it had become increasingly evident that further refinements of the models should take into account considerations about the physics of rupture and rely on dynamical rather than kinematical calculations.

3.2 Quasi-Dynamic and Dynamic Models of Earthquake Rupture. The transition from the 60's to the 70's was characterized by a marked increase in the investigation of quasi-dynamic and dynamic source models. The qualifier "dynamic", as applied to a source model implies that the growth history (fault size, rupture velocity) and slip history is a result of the modeling, as opposed to an input. However, much has been learned about the mechanics of fracture as applied to earthquake sources by specifying the growth history and the stress drop in advance and examining the consequences of this choice on the "dynamic" (as opposed to "static") stresses near the fault and on the slip history on the fault. I shall call the latter class of models "quasi-dynamic", since the slip history is dynamically consistent with the prescribed stress drop associated with fault growth, even though this fault growth itself is kinematically specified.

Much of this work draws heavily from crack theory; a comprehensive review of the topic and applications to the mechanics of earthquake

rupture is given by Rice (1980) and will not be repeated here.

Kostrov (1964, 1966) was the first to recognize the applicability of crack theory to the problem. His pioneering work on the self-similar growth of circular shear cracks, and the unsteady propagation of longitudinal shear cracks has withstood the test of time and remains the basis for many current studies. He later extended the theory to in-plane shear cracks as well (Kostrov, 1975). Kostrov (1970) reviewed the application of the theory to the modeling of seismic sources; he is also credited with the introduction of the seismic moment tensor, which I shall discuss in a later section.

Useful insight is offered by analytical solutions which can be obtained for special two-dimensional geometries, in particular for the anti-plane problem for which the relationship between slip and shear stress on a fault with prescribed rupture velocity is simple. Freund (1972) produced a simple and elegant formalism for the energetics near a crack tip, from which it can be shown that for a cohesionless crack, the energy flow at the tip vanishes when the rupture velocity is equal to the shear velocity for anti-plane problem, and to the Rayleigh velocity for in-plane problems.

In a series of papers, Burridge (1969, 1973), Burridge and Willis (1969) and Burridge and Halliday (1971) examined increasingly complicated crack problems using a combination of analytical and numerical techniques. More recently, Burridge and Moon (1981) presented numerical solutions for slipping on a three-dimensional frictional crack, using an integral equation technique proposed by Burridge (1969), for the case of pre-specified rupture velocity equal to the wave speed. A related numerical algorithm was introduced by Hamano (1974), and refined by Das and Aki (1977a), Richards (1979), and Das (1981).

The prominent difficulty encountered in dynamical modeling has to do with how to stop crack propagation (Aki and Richards, 1980). Because of this, numerical techniques are necessary, particularly in three dimensions, although analytical solutions are known in two dimensions (*e.g.*, Kostrov, 1966; Freund, 1979). Quasi-dynamic models, in the sense defined above, have been calculated for circular faults (Madariaga, 1976; Das, 1980), semi-circular faults (Archuleta and Frazier, 1978), and rectangular faults (Madariaga, 1977, 1979; Archuleta and Day, 1980; Day, 1982a). Dynamic models, involving *spontaneous* failure, have been presented in two dimensions by Das and Aki (1977a), Knopoff and Chatterjee (1982), Chatterjee and Knopoff (1983), and in three dimensions by Das (1981), Day (1982b), and Virieux and Madariaga (1982).

One essential ingredient of these models is the presence of a "cohesive zone" just ahead of the crack tip, which eliminates the stress singularity predicted on the basis of linear elastic models. This concept,

originally due to Barenblatt (1959) as an improvement on the classical Griffith criterion for the stability of cracks, was further refined by Willis (1967). It was introduced in earthquake source modeling by Ida (1972), and further analyzed by Andrews (1976a, b).

The energy balance at the crack tip is usually analyzed in terms of a "specific fracture energy" which must be greater than the specific surface energy on the rocks themselves, because of the inelastic processes involved, and because of the finite thickness of the fault zone (see Husseini *et al.*, 1975). Archambeau and Minster (1978) examined in detail the conservation equations in a medium with a propagating failure boundary, and derived general jump conditions which must be satisfied across the failure boundary. Husseini and Randall (1976) stated that the concept of a specific fracture energy is but a two-dimensional idealization of these jump conditions, although to my knowledge the equivalence of the two treatments has not been formally worked out, in the sense of one being a limiting case of the other.

This class of investigations almost forms a separate discipline, and many of the conclusions reached so far are still the object of current research and debate, especially with the continuing acquisition of laboratory data on the behavior of simulated fault zones (*e.g.*, Scholz *et al.*, 1972; Dieterich *et al.* 1978; Dieterich, 1980, 1981).

Among the various conclusions reached from such studies, several appear to have acquired fairly general acceptance:

(1) For a rupture surface with inhomogeneous prestress or inhomogeneous strength, the rupture velocity may vary abruptly as the rupture front impinges upon one of these inhomogeneities.

(2) Peak slip velocity is strongly coupled with rupture velocity, at least for situations in which cohesion is uniform along the fault. Sub-shear rupture velocity is predicted for predominantly anti-plane crack motion, but super-shear rupture velocity is observed for in-plane crack motion if the cohesive zone is sufficiently weak. However, the average rupture velocity remains sub-shear, at least for the types of models studied so far (Day, 1982b).

(3) A fault plane with distributed barriers of greater strength may explain some of the complexities of faulting inferred from near-field observations. Depending on the initial stress load and the relative strength of the barrier, a barrier may

- be broken immediately as the crack tip impinges on it

- be left behind as an unbroken asperity
- break later in the phenomenon, due to dynamic loading behind the crack tip.

As discussed by Das and Aki (1977a), and by Aki (1980), a barrier model provides a satisfactory explanation for the well-known complexity of the faulting in great earthquakes.

The alternative point of view to the barrier model is the asperity model, in which seismic faulting occurs when a strong patch of the fault fails, while weaker patches may slip aseismically. Of course, an asperity could be associated with an unbroken ligament left by an earlier event which failed according to the barrier model. The barrier model and the asperity model have been compared by Rudnicki and Kanamori (1981), who show that inhomogeneities of fault strength can bias estimates of moment, stress drop and strain energy release, albeit in slightly different ways. Their results are compatible with those of Madariaga (1979), who examined the effects of both strength and stress heterogeneities on the relation between seismic moment and stress drop. The effects of rupture complexity on source size estimates of the aftershocks of the 1975 Oroville, California, earthquake have been reviewed from an observational and theoretical point of view by Boatwright (1984). Using a simple and intuitive model, he shows that ignoring rupture complexity can lead to large systematic errors in the estimates of source dimension and stress drop.

Das and Scholz (1981) investigated the complete time-dependent process of rupture in the earth, from nucleation to catastrophic failure, from the point of view of fracture mechanics, including sub-critical crack growth due to stress corrosion and triggering of multiple events. Finally, the rupture of a single circular asperity of constant strength was recently treated by Das and Kostrov (1983); this problem presents interesting characteristics insofar as the rupture front progresses in a rather complicated fashion, first encircling the asperity, and then propagating inward toward the center.

Boore (1983) considers the documentation of the complexity of earthquake rupture to be one of the most important recent developments in the understanding of the earthquake source. It is a feature of large earthquakes (*e.g.* Wyss and Brune, 1967; Kanamori and Stewart, 1978, 1982; Stewart and Kanamori, 1982) and of smaller events as well (*e.g.* Strelitz, 1975; Hartzell and Helmberger, 1982; Olson and Apsel, 1982). Especially interesting is the documentation of localized fault patches breaking with near-compressional rupture velocity by Olson and Apsel (1982); this provides strong support for the numerical models discussed above.

4. Relaxation Source Models

An alternative to the dislocation model and its variants is the stress relaxation model developed by Archambeau (1964, 1968), and by Randall (1964a, b, 1966). Although the approaches developed independently by these two authors differ significantly in the details the underlying philosophies are rather similar.

4.1 Modeling Concepts. Honda (1960) recognized early on that an earthquake can be viewed as a relaxation phenomenon of pre-existing tectonic stresses. Based on this general concept both Randall and Archambeau argue that failure of the medium corresponds to a sudden (or progressive) change in material properties inside a "failure zone". As a result of this change, the static equilibrium configuration of the medium in the presence of the failure zone is modified; the evolution toward the new equilibrium state is then achieved dynamically and generates a transient elastodynamic wave field. The natural mathematical treatment of the problem requires therefore the solution of an initial value problem, or in the case of a gradually growing source region, a generalized initial value problem, requiring only the calculation of a sequence of static equilibrium states (Archambeau, 1968; Randall, 1971; Minster, 1973).

Randall (1964b) considered the case of a sudden volume change inside the failure zone, and later (Randall, 1966) examined the case of a sudden phase transition. Archambeau (1964, 1968) addressed the more general problem of a growing and propagating failure zone in a pure shear field. [Note that Archambeau's initial solution, and also the work of Minster (1973) used a particular potential representation of the radiated fields which cannot be used in the case of pure compressional prestress. This was corrected by Stevens (1980a).]

In terms of the general Green's tensor solution, the radiation field is expressed as the sum of a volume integral over the whole space—or at least the whole earth—and surface integrals over the various boundaries, including the boundary of the failure zone itself. The general representation theorem was reviewed in detail by Archambeau and Minster (1978), including the set of boundary conditions appropriate for the case of a moving failure boundary. The volume integral represents the contribution of body forces and of the initial values, and the surface integrals contain the scattered fields. Solutions which ignore the latter have been dubbed "transparent solutions" since they allow waves to be transmitted undisturbed through the failure zone.

The solution is usually given in terms of a multipolar expansion of fields (*e.g.* Archambeau, 1964, 1968; Randall and Knopoff, 1970; Randall, 1971, 1972), of which the monopole represents the isotropic, and the quadrupole the double-couple component of the field. [Harkrider

(1976) suggests that the term "mixed quadrupole" be used since P and S waves have different source histories, as opposed to the point shear dislocation model.] Higher multipoles are excited in the case of a propagating source or in the presence of inhomogeneous prestress (Stevens, 1980b) but, as discussed by Archambeau (1968), their complex amplitudes must combine in such a way as to preserve angular momentum. The manipulation of multipolar expansions in that context and their transformations under changes of coordinate system have been reviewed by Minster (1976).

4.2 A Debate in Source Theory. Comparison of dislocation and relaxation models of the earthquake source generated a lively debate from the beginning, and this debate lasted well into the 70's. One of the main sources of controversy arose from the need to reconcile the predictions of the relaxation theory with those of the more intuitively satisfying kinematic dislocation models. Although I do not recall that there ever was much argument about stress relaxation being the correct phenomenon to model, there was considerable controversy about the correctness of details of the model as implemented by Archambeau and his coworkers, and about features of the radiation fields predicted by the model.

Criticisms of Archambeau's model focused on

(1) The geometry and boundary conditions used in specific applications of the theory.

(2) The approximations made in the calculations, some of which were later shown to be invalid, which cast doubt on some of the inference drawn from simulations which used this model.

Mainly for reasons of algebraic convenience, the relaxation model was only computed in detail for the case of a spherical failure zone with total loss of rigidity. In contrast that of a typical dislocation model, this geometry is certainly far removed from that of typical fault zones observed at the surface of the earth, and was unpalatable to many. Furthermore, at a time when attempts were being made to incorporate the concepts of static and dynamic friction and of partial stress drop in dislocation models, a model with total loss of shear strength within the failure zone was considered unrealistic.

Randall (1966) argued that a spherical failure zone might be appropriate for some deep earthquakes presumably associated with sudden phase changes, and comparable arguments were made by Archambeau (1968). Archambeau (1972) suggested that the model might also apply to volcanic events. In addition, this geometry is clearly appropriate for

the study of the anomalous radiation from an explosion detonated in a prestressed material, one of the main applications of the model to which I shall return later. Archambeau did try to achieve more realistic geometries for the modeling of earthquakes by considering a growing and propagating spherical failure zone, but as discussed by Minster (1973), this begged the difficult question of material healing after failure. Furthermore, the sequence of static equilibria used in Archambeau's initial treatment did not account for the static fields generated by the portion of the failure zone which had already healed. [Archambeau (1964), and later Minster (1973) attempted to treat the case of an ellipsoidal rupture, but found the evaluation of the initial value fields extremely difficult. The recent work of Stevens (1980b, 1982) would greatly simplify the problem.]

However, these models served to illustrate, at least in the far-field, first order features of the radiation field, such as the effect of source growth and propagation on spectral shapes and radiation patterns as a function of frequency, and asymptotic scaling laws incorporating the effects of prestress, size of the failure zone, and rupture velocity. The far-field "equivalence" between a growing spherical relaxation source and a dislocation source with same growth history was shown by Minster and Suteau (1977); they showed that different equivalent dislocations are required for transsonic growth of the failure zone, and that the spherical relaxation model differs from the corresponding dislocation by a factor of 3.6 in moment.

A fair amount of confusion arose from the fact that the early implementations of Archambeau's theory used several approximations, the main ones being:

(1) The transparent source approximation, in which the boundary conditions on the failure zone boundary are not satisfied by the dynamic field.

(2) The attempt to model localized prestress by truncation of the volume integral at a finite distance from the failure zone.

The first approximation could be shown to be a defensible one by comparison with exact solutions. Hirasawa and Sato (1963) produced an exact solution for the sudden creation of a spherical cavity in a pure shear stress field; Burridge and Alterman (1972) treated a uniformly growing spherical cavity, and Burridge (1975) used the results to test the transparent source approximation. Koyama, Horiuchi and Hirasawa (1973) gave an exact treatment of the sudden creation of a fluid-filled cavity.

These solutions have been reviewed by Stevens (1980b), who showed the equivalence of the transparent solution with a stress pulse applied on the cavity wall. The main difference between exact and transparent solutions is that the latter predicts a waveform with an abrupt termination, whereas the former predicts a broader pulse with damped oscillations due to scattered fields. Interestingly, the amplitude spectra are much simpler looking for the exact solution than for the transparent approximation, in the sense that they are much smoother at high frequencies. Stevens points out that most of the high-frequency structure seen in the approximate spectra is due to interference between waves which are allowed to propagate through the "transparent" source, instead of being diffracted.

More controversial was the attempt to account for the finiteness of prestressed regions in the earth. Archambeau (1968) obtained a transparent solution for a spherical cavity under pure shear, but approximated a localized prestress field by simply truncating the initial value volume integral at some distance from the source. This led to the prediction of a low frequency spectral peak, in conflict with the flat long period spectra predicted from dislocation models. This discrepancy was a source of great puzzlement, and much effort was spent to try and identify its cause. Molnar *et al.*, (1973) showed that a spectral peak could arise from a dislocation model only (1) if different parts of the fault, but on the same side of the fault, slip in opposite directions or (2) if the fault slips back after exceeding the maximum displacement. On that basis, they suggested that the spectral peak predicted by Archambeau's model was due to lack of frictional damping.

Randall (1973) was the first to recognize that simple truncation of the volume integral does not provide a valid approximation of localized prestress; this was further discussed by Minster (1973), and later by Snoke (1976), who argued that truncation simply removed long-period energy from the outgoing radiation fields. Snoke (1976) and Harkrider (1976) pointed out that, in the time domain, this leads to an acausal arrival generated by the discontinuity in the initial value fields artificially introduced at the truncation radius. The basic problem with a truncated initial value field is that is violates one of the basic tenets of the theory, since it does not satisfy the equations of static equilibrium in the absence of body forces.

It was not until recently that Stevens (1980a, b, 1982) produced correct solutions which account for prestress inhomogeneities. He summarizes his conclusions as follows:

(1) Localized stress concentrations increase the amount of

energy radiated at high frequencies, and may cause a sizable increase of the corner frequency.

(2) Far-field spectral peaks may be present, near the nodes of the quadrupole radiation pattern for slight inhomogeneities, and at all azimuths for strong stress concentrations. However, these are high-frequency peaks, quite different from those discussed earlier. In particular, the moment is not reduced by stress concentrations.

(3) Radiated amplitudes do not vanish at the quadrupole nodes.

(4) A scattered wave travels around the cavity.

(5) The radiation pattern may be affected, but less so than the spectra and waveforms.

(6) The waveform generated near the stress concentration is sharp, but the waveform emitted in the opposite direction is more complex.

The effects of cavity growth have been reviewed by Stevens (1982). He concludes that a finite growth rate results in lower amplitude, longer waveforms (at constant moment), with diffraction effects reduced compared to the instantaneous source.

Another problem debated in the context of relaxation versus dislocation models pertains to the source of radiated seismic energy: In a relaxation model the source of energy is the prestressed medium surrounding the failure zone; even in an infinite space, the whole medium participates in the phenomenon. On the other hand, for a dislocation model, the source of radiated energy is the fault plane itself.

I think it is somewhat of a semantic debate: ultimately the only source of available energy is clearly the strain energy stored in the medium before the event; at the same time it is just as clear that seismic waves are emitted from the source region itself, otherwise kinematic models would fail to predict observed seismograms.

A satisfactory answer was again given by Stevens (1980b, 1982) who demonstrated that the stress relaxation problem could be reduced to a stress pulse problem, both for approximate and exact solutions.

5. Shape and Scaling Laws of the Seismic Spectrum

From the mid-60's to the present, discussions of earthquake source modeling have become more and more oriented toward the retrieval of physical source parameters from seismic observations. Although the tendency since the early 70's has been increasingly to compare observed and synthetic seismograms in the time domain, many of the arguments

about the source itself are more easily cast in terms of the displacement spectrum predicted by the source model.

This is mostly due to the fact that these arguments center around the amplitude spectrum, which can often be characterized in terms of relatively few parameters, while time domain information depends heavily on the phase spectrum, for which simple scaling laws are not available. Furthermore, complications associated with the propagation of waves tend to modify the phase spectrum rather severely and in non-intuitive ways, whereas they typically modulate the amplitude spectrum, without changing its general shape.

5.1 Shape of the Seismic Spectrum. The proliferation of kinematic dislocation models in the past two decades stemmed in large part from the need to predict correctly the shape of the seismic spectrum. There were two principal purposes for this: (1) to determine physical parameters of the faulting from seismic measurements, and (2) to uncover and explain differences between earthquakes and underground explosions (*e.g.*, Wyss *et al.*, 1971). Seismic observations at teleseismic distance are contaminated by path effects, attenuation, and scattering. Separation of source contributions from propagation effects requires that a parameterized model of the source be constructed, and constrained by additional observations, such as aftershock distribution, near-field recordings, *etc.*

Unfortunately, as discussed in detail by Aki and Richards (1980), by suitable adjustment of the parameters of a kinematic model, it is possible to change significantly the shape of the corresponding spectrum. The corresponding variety of predicted far-field waveforms is even greater.

[The far-field regime is defined as the regime where the frequencies of interest are high enough that the source is many wavelengths away. If the observer is also many source dimensions away, then a point-source approximation is often appropriate. Requiring that these two conditions be met simultaneously is best expressed in terms of the classical Fraunhofer diffraction condition (Aki and Richards, 1980).]

Discussion of the far-field spectral shape is usually in terms of three parameters, as suggested by Brune (1970); they are

(1) The long-period spectral level.
(2) The high frequency asymptote, usually described by its logarithmic slope.
(3) The position of the corner frequency, defined by the intersection of the long-period and high frequency asymptotes.

At sufficiently long periods, such that the wavelength is long compared to the source dimensions, (yet short enough that the far-field approximation holds), the source can be approximated by a point source with delta-function time history. This holds, for instance, for the analysis of long-period surface-waves at large distances from the source, or for free-oscillation studies. As a result, we expect the corresponding portion of the displacement spectrum to approach a constant level, proportional to the seismic moment. If, in addition, we assume that the slip does not show an overshoot, the far-field pulse is unipolar (Molnar *et al.*, 1973), and the amplitude spectrum is a maximum at zero frequency.

At sufficiently high frequencies, the spectrum becomes sensitive to fault geometry and slip history:

(1) Rupture propagation over a fault of finite length has a smoothing effect which contributes a logarithmic slope of -1 at high frequency.

(2) A finite rise time increases the slope to -2.

(3) If one takes finite width into account, the slope becomes -3.

As summarized by Aki and Richards, a number of additional factors can affect the high frequency slope. However, the main one pertains to the existence of "stopping phases", a term introduced by Savage (1966). The meaning of the term can be generalized to include any source phenomenon which generates a large high-frequency contribution to the displacement spectrum. Such is the case, for example, if the rupture velocity changes abruptly (*e.g.* drops to zero), or if the slip is frozen instantaneously over a large fraction of the fault surface. The contribution to the high-frequency displacement spectrum depends on the singularity generated in the far-field time function. For example, a square-root singularity subtracts ½ from the spectral slope, while a step-function subtracts 1 from it. Ultimately, it is the strongest singularity in the time function which determines the high-frequency spectral slope. Geometrical factors also come into play: in the circular fault model of Molnar *et al.*, (1973), the spectral slope varies from -3 to -2 depending on the azimuth of observation relative to the normal to the fault plane. (A similar behavior was discussed by Minster and Suteau (1977)). In contrast, models which are designed not to generate stopping phases typically yield a high-frequency slope of -3 (*e.g.*, Dahlen, 1974).

An important aspect of stopping phases is that they contain information about the size of the fault at the time when they are generated. Intuitively, a late stopping phase is generated by a large source and produces a large amount of radiated energy, so that its contribution dominates

the high-frequency spectrum. On the other hand, the spectrum produced by a model without a stopping phase produces a high-frequency asymptote which does not depend on source size. For instance, in the self-similar fault model investigated by Dahlen (1974), the rupture is allowed to stop smoothly and the high-frequency asymptote depends on rupture velocity and particle velocity (rise time) but not on the final source dimension.

For relaxation models, the shape of the seismic spectrum depends primarily on two parameters, namely the rupture velocity and the distribution of prestress (Archambeau, 1968, 1972; Minster, 1973; Stevens, 1980a, b). For subsonic growth of the failure zone, the high-frequency slope is -3 for both *P*-wave and *S*-wave spectra; for trans-sonic rupture velocity the *S*-spectrum has a slope of -2; for supersonic rupture velocity, such as might be expected for the cavity created by an explosion, both spectra exhibit a slope of -2. In addition to these general results, the analysis of Stevens (1980b) shows that spectral peaks may, in fact, exist at some or all azimuths if the prestress field is sufficiently inhomogeneous. For a weakly inhomogeneous prestress, a spectral peak appears only near the nodes of the quadrupole, where most of the radiation is contributed by higher order multipoles; for a strongly inhomogeneous prestress, the spectra may be peaked at all azimuths.

Recent numerical modeling of complex earthquake ruptures, which I have reviewed earlier, also leads to variations in the spectral shape. This is mostly due to abrupt changes in rupture velocity, associated either with strength inhomogeneities (*e.g.*, Das and Aki, 1977b) or with stress variations along the fault (*e.g.*, Day, 1982b). These abrupt changes lead to stronger high-frequency radiation than in the case of a smooth rupture, and can affect significantly the spectral shape at individual azimuths. However, Das and Aki (1977b) conclude that if the barriers on the fault remain unbroken, the corner frequency averaged over all azimuths is essentially unaffected; it is decreased slightly if the breakage of these barriers is merely delayed.

5.2 Scaling Laws and Stress Drops. Aki (1967) was the first to try and systematize the scaling laws of the seismic spectrum, based on two models which he called the "omega-square" and "omega-cube" models, based on their respective high-frequency asymptotic behavior. Since then the problem has been revisited by a number of investigators, who used the various source models discussed in the preceding sections.

The basic scaling of the spectrum is due to the fact that, at constant stress drop, the long-period level is proportional to the third power of the nominal fault dimension, while the corner frequency is inversely proportional to that dimension. Thus, for a self-similar family of models, the

locus of the corner itself is a straight line with slope -3 (see Hanks and Thatcher, 1972). As a result, if the high-frequency spectral slope is -3, the spectral amplitude at a given frequency does not exceed a maximum value as the fault size increases; any magnitude scale which is based on measurements made at a particular frequency ultimately saturates. On the contrary, if the high-frequency spectral slope is -2, no such saturation occurs, since the spectral level at any frequency can increase without bounds with increasing fault dimension. Based on the data then available, Aki (1967) preferred the second alternative, but Hanlas (1979) showed that this type of argument, based on spectral amplitude, does not necessarily carry over to time-domain magnitudes, unless all the energy contributing to the relevant frequency band arrives at a single instant of time. However as we shall see, things have become somewhat more complicated as better and more numerous data have been collected.

For relaxation models, the scaling laws are very similar (Archambeau, 1968; Minster, 1973). The high-frequency spectral slope depends on the relative values of the rupture velocity and the wave speed and, for the models calculated, the spectral level is directly proportional to the prestress level. For subsonic rupture velocities, these models predict saturation of magnitude scales (Minster, 1973).

That the long-period spectral level should scale linearly with moment is a common feature to all models. More controversial are (1) the position of the corner frequency, and (2) the high-frequency spectral slope, which I have discussed earlier.

A difficulty raised by some kinematic fault models, is that they predict a higher corner frequency for *S*-waves than for *P*-waves (*e.g.*, Savage, 1972; Dahlen, 1974). In contrast, other models, such as that of Molnar *et al.*, (1973), or the relaxation models (Archambeau, 1968; Minster, 1973) predict just the opposite. Point sources endowed with a single time function predict the same corner frequency for both *P*- and *S*-spectra. In many cases, observations show the dominant period of *S*-waves to be longer than the dominant period of *P*-waves, by 30% to 50% (*e.g.*, Furuya, 1969; Hanks, 1981). This led Hanks (1981) to challenge the validity of earthquake modeling *via* waveform matching by synthetic seismograms calculated from a point source or a superposition of point sources, as performed by Burdick and Mellman (1976) or by Langston (1978), as well as the estimate of attenuation by Burdick (1978). On the other hand, Langston (1978) showed that surface reflections such as *pP* and *sP* could have a severe effect on measured far-field spectra, possibly result in peaked spectra, and thus jeopardize the correctness of spectral estimates of moment and corner frequency from teleseismic observations such as those of Hanks and Wyss (1972). I believe that the ensuing polemic has

not been resolved to the satisfaction of all involved, and appeared at times to be conducted at cross purposes. In a way, it points to the dangers involved in trying to characterize complex phenomena in terms of simplified models; although this is obviously the first thing to try, better and more numerous data will invariably result in a need for more realistic treatments, incorporating all known aspects of the phenomenology.

A recent discussion of the corner frequency shift from a novel point of view is given by Silver (1983). He uses a spatio-temporal moment tensor expansion of degree two to define a new characteristic radiation frequency for both *P*- and *S*-waves, in the same manner as Silver and Jordan (1983), and compares it to the classical definition of corner frequency in terms of intersecting asymptotes. Interestingly his definition yields a higher *P*- wave corner frequency for *any* dislocation model of a finite source, so that the "corner frequency shift" cannot be used to discriminate between models. He further argues that corner frequencies actually measured from far-field body wave data should in fact be compared to the characteristic frequency defined from the second temporal moment, rather than to the intersection of low- and high-frequency asymptotes. I shall return to moment tensors in a later section.

One of the most interesting discoveries about seismic sources is the near constancy of apparent average stress drop over a large range of event sizes, measured by moment and source dimension. Brune (1970) devised a simple method for estimating stress drop from the corner frequency and seismic moment using a circular crack model. This method has been used systematically by Hanks and Thatcher (1972) for small to medium size earthquakes, and the results have been summarized by Hanks (1977). They show a systematic trend between the logarithms of moment and source radius over nearly ten orders of magnitudes in moment, with inferred stress drops confined between 1 and 100 bars.

Kanamori and Anderson (1975) showed that the same relationship holds for great earthquakes as well, for which moment is determined from long period observations (surface waves and free oscillations) and source dimension from a variety of observations ranging from aftershock distribution to static deformations and tsunami source area. They then used the Haskell model and simple geometric considerations to provide a theoretical basis for a variety of empirical scaling relations, including magnitude *vs.* moment, energy and fault area, as well as the well-known magnitude-frequency distribution of earthquakes.

The constancy of stress drop with earthquake size was reviewed by Aki (1980), who also presents additional results obtained for small earthquakes by the coda method developed by Aki and Chouet (1975). The key conclusion reached by Aki is that the observed scaling of the

seismic spectrum does not quite satisfy the laws predicted on the basis of a simple, smooth rupture model. For example, within a given region, there is evidence that stress drop increases with earthquake size at small magnitude, and that the high frequency slope increases with magnitude at larger magnitudes, two effects which tend to limit the variations of corner frequency with magnitude. This is supported by observations made by Johnson and McEvilly (1974) on central California events with magnitudes 4 to 5.

As discussed by Aki (1980), a barrier model of the source is capable of explaining these observations, if the barriers have a characteristic separation distance. Furthermore, the inferred local stress drops can be an order of magnitude larger if a barrier model is invoked, and thus be comparable with the stresses needed to fracture rocks in the laboratory ($\sim$1000 bars). Similar conclusions, based on comparable arguments, have been reached by Madariaga (1978), Rice (1980) and Rudnicki and Kanamori (1981).

Further evidence bearing on the problem is provided by the work of Sykes and Sbar (1973) who showed that intraplate earthquakes point to the presence of large (100 bars) horizontal compressive stresses in the interior of plates. For mid-plate earthquakes, Liu and Kanamori (1980), found stress drops of a few hundred bars; such variations have been confirmed by a number of recent investigations. Very large observed stress drops, inferred from near-source high frequency observations are reported more and more frequently in the literature. A recent instance is the work of Munguia and Brune (1984), who find stress drops ranging from as low as 1 bar to as high as 2.5 kbars for a swarm of events on Baja California. comparison with earlier stress drop estimates for events in the same region (*e.g.*, Thatcher and Hanks, 1973) make it increasingly clear that significant tradeoffs between inferred source properties and path effects (attenuation) must be sorted out carefully. This raises of course important questions for discrimination, yield estimation, and for the release of tectonic prestress by underground explosions.

The existence of very high stress drop events in regions where conventional wisdom would only allow low stress drops tends to support the asperity model. This model was applied to the study of large subduction zone earthquakes by Lay *et al.*, (1982), who show enormous variability of the mode of failure from region to region, from strong coupling in the form of large asperities, to practically complete decoupling. Additional supporting evidence is found in the work of Ebel and Helmberger (1982), who reanalyzed the 1968, April 9, Borrego Mountain earthquake, and modeled it in terms of two short-period sources with stress drops of several hundred bars. Furthermore, they argue that the absence of

aftershock activity or post-seismic creep near the probable location of these sources is consistent with the hypothesis that the event was triggered by the failure of an asperity.

Additional support for the asperity model is provided by an increasing number of instances where small earthquakes yield almost identical recordings, indicating that they all have practically identical source regions (Geller and Mueller, 1980).

The general question of asperity versus barrier models of complex earthquake sources is the focus of a considerable amount of current research. It is clear that simple scaling laws of the seismic spectrum do not accommodate easily this type of complications, and must be considered only as a rather crude approximation. This does not mean, however, that simple scaling laws are useless. Indeed, the body of high quality near-field observations is still relatively limited; they are totally lacking in most seismic regions, where we only have access to teleseismic observations, for which use of the scaling laws is probably justified.

The effect of spectral scaling on the distribution of magnitudes and more specifically on the relation between body wave and surface wave magnitudes was reconsidered by Geller (1976). He used a self-similar family of Haskell-type models, with a high frequency slope of -3 to account for fault width, and argued that it satisfies the body wave and surface wave data of Evernden (1975) better than the "omega-square" model preferred by Aki (1967). As a result, he finds that both types of magnitudes should be bounded, with a maximum value of about 6 for body waves, and about 8.2 for surface waves. A similar conclusion had been reached on the basis of scaling laws for the spherical relaxation source model by Minster (1973), although in that case, the bounds are linearly proportional to prestress. However, this argument has been challenged by Hanks (1979), on the basis that magnitudes are measured in the time domain, and that spectral amplitudes can be misleading for extended sources, since the energy at, say, 1 Hz may be distributed over a finite time window.

Saturation of the conventional magnitude scales with increasing source size (when the source dimension exceeds the wavelength of the waves used in magnitude measurements) leads to serious underestimation of the energy released in great earthquakes. This led Kanamori (1977, 1978) to quantify such events by using the moment—a static concept—to measure the sizes of very large events. For convenience in comparing this new magnitude measure based on moment and the magnitude-energy relation. Accordingly, the 1960 Chilean earthquake, with a classical surface wave magnitude of 8.3, is now assigned an equivalent magnitude of 9.5. The concept of a moment-magnitude scale was extended by Hanks and Kanamori (1979), but some pitfalls were subsequently discussed by

Boore (1983), in particular the fact that spectra from different types of earthquakes do not necessarily scale with moment in the same way.

It is clear that since the early work of Aki (1967), we have grown to perceive the earthquake phenomenon as being infinitely more complex and varied than simple models can account for. It is probable that continuing work will only enhance that perception, unless general laws can be formulated which have sufficient predictive power that they lead to a reduction of the problems to fewer, but more fundamental physical questions.

6. Explosion Sources

Underground nuclear testing naturally led to considerable research on the elastodynamic radiation associated with buried explosions. The subject can be logically separated into the study of the simple, isotropic spherical waves generated by a simple model of the explosion itself, and that of the "anomalous radiation", by which is meant any wavefield demonstrably generated in the near vicinity of the shot point at or near the time of the detonation. The importance of the problem stems from its consequences for discrimination between earthquakes and explosions, and for the estimation of explosion yields from seismic observations.

Recent reviews of these topics are given by Masse (1981) and by Bache (1982); I shall only touch on the highlights.

6.1 The Spherically Symmetric Explosion Source. Perhaps the simplest kind of seismic source to study analytically is the explosive (or implosive) source in a uniform, homogeneous, isotropic elastic medium. One of the early solutions is that of Jeffreys (1931) who considered the wave field generated from a pressurized spherical cavity. a more detailed treatment is that of Sharpe (1942). For most purposes, the problem is greatly simplified: since seismic wavelengths are usually longer than the so-called "elastic" radius, one can retain good accuracy by reducing the source to a point of dilatation, which is then entirely characterized by a source time function. Furthermore, as long as spherical symmetry holds and anelastic effects near the source can be neglected, the wave field can be represented near the source in terms of a scalar "reduced displacement potential" or, by suitable differentiation, a scalar "reduced velocity potential" valid in the elastic region around the source (*e.g.*, Hudson, 1969).

A direct but rather complicated analytical treatment of a spherical source in a half-space was given by Ben-Menahem and Cisternas (1963). This solution has not been used very much, because cases where the free surface must be taken into account as part of the source region

surrounding a buried explosion can either be treated using standard wave propagation techniques (*e.g.*, Burdick and Helmberger, 1979), or else involve nonlinear interactions such as spalling (see Day *et al.*, 1983).

A variety of different models have been proposed in the literature (*e.g.* Toksoz *et al.*, 1964; Haskell, 1967; von Seggern and Blandford, 1972). A commonly used one was derived empirically by Mueller and Murphy (1971) and Murphy and Mueller (1971) who account in a simple way for departures from the classical "cube-root-yield" scaling of the seismic spectrum by including the effects of depth of burial, and of the containing medium. The corresponding seismic spectra typically show a slope of -2 at high frequency.

The choice of time function appropriate for underground explosions has been re-examined by Burdick and Helmberger (1979), who show that it is possible to explain teleseismic short- and long-period body wave seismograms without recourse to aspherical nonlinear processes in the source region, provided that the time function exhibits substantial overshoot. They use the parameterization proposed by von Seggern and Blandford (1972) because of its simplicity, which makes it attractive for inversion purposes.

Although the pressurized cavity model is, in principle, sufficient to represent the "free field" from a spherically symmetric source, there remains a number of unresolved questions about the radius of the cavity and the pressure history, and their dependence on source setting. These problems are usually described under the generic term of "*source coupling*". Source coupling has been reviewed recently by Bache (1982); the bulk of current research on theoretical modeling of near-source phenomena relies on nonlinear one- and multi-dimensional numerical calculations, which depend in turn on parameterized rheological models for the confining medium. Some of the important effects which are included in recent modeling efforts include:

(1) The material strength: coupling increases as material strength decreases.
(2) The porosity: coupling decreases rapidly with increasing air-filled porosity.
(3) Tension failure: tension cracks are produced as a result of hoop stresses associated with the spherically expanding stress wave, and spallation results from interactions with the free surface.

Furthermore, material strength may drop sharply if some fluid-filled porosity remains after the air-filled porosity has been crushed out by shock

loading, although this effect is more controversial and has not been demonstrated unambiguously. As discussed by Bache (1982), there remain puzzling difficulties in reconciling models with observations. Perhaps the one which has offered the most resistance to the modelers' efforts is the discrepancy between U.S. granite explosions at NTS and French granite explosions in the Sahara. After they have been scaled to a common yield, cavity volumes reported for the French tests (*e.g.*, Duclaux and Michaud, 1970) remain about a factor of 3 smaller than those observed for U.S. tests, although the material strengths are comparable, based on laboratory samples and available near-field measurements. The observed body wave magnitude for the French test SAPHIR is then larger, by 0.3 to 0.5 magnitude units, than the PILEDRIVER magnitude would be if PILEDRIVER were scaled to the same cavity size. This points to the possibility of strong path effects which cancel the source coupling differences, or to shortcomings of the source models (Bache, 1982).

Another phenomenon, which has not yet been incorporated systematically in the source models, is near-field, amplitude-dependent, and thus nonlinear attenuation in the region surrounding the cracked zone, where strains are still large. Although this effect could be properly considered a wave propagation phenomenon, it is confined to the near-source region, and can be incorporated in a model of an effective source (Minster, 1982). Larson (1982) reviewed near-field data for explosions in salt, and illustrated the validity of cube-root scaling over ten orders of magnitude in yield for this material, from gram-size laboratory tests, to the COWBOY chemical explosions and the SALMON nuclear test. He compared detailed near-field waveforms recorded in the laboratory and concluded that

(1) Apparent attenuation is amplitude (and frequency) dependent, and thus nonlinear well beyond the radius where the material fails, and

(2) Linear superposition of waveforms seems to hold in that region.

These two apparently contradictory statements have not yet been satisfactorily reconciled. Preliminary results indicate that the decay of peak velocity and peak displacement with scaled radius observed for the COWBOY shot sequence are consistent with laboratory measurements of amplitude dependent attenuation in salt (Tittman, 1983; Minster and Day, 1984). However, a realistic and physically correct source model which accounts for these effects has not yet been produced, partly because numerical schemes which account for a realistic absorption band have not been available until recently (Day and Minster, 1984).

6.2 Departures from Spherical Symmetry. From the very beginning, it was noticed that the surface waves excited by underground nuclear explosions could not be explained by a simple spherically symmetric source (*e.g.*, Oliver *et al.*, 1960). This observation has led to one of the most enduring problems of explosion source theory, which has not been completely resolved yet. It pertains to the generation of *SH* and Love waves and to the anomalous excitation of Rayleigh waves by explosions. The question has obvious importance for discrimination between earthquakes and explosions, since those explosions which excite significant anomalous radiation exhibit earthquake-like character; it is also important for yield estimation, since the question must be answered of whether the nonisotropic component increases or decreases magnitude estimates.

Various hypotheses advanced to explain this phenomenon have been reviewed by Aki and Tsai (1972), Archambeau (1972), Masse (1981), and Bache (1982). They are:

(1) Mode conversion due to heterogeneities near the source and along the wave path.

(2) Direct effects of the explosion, due to anisotropy near the source, crack formation, block motions, or due to the initial shape of the cavity.

(3) Release of tectonic stress, either through the triggering of motion along a preexisting fault, or through tectonic release permitted by the introduction of the cavity and the surrounding crushed zone into a prestressed medium.

The first class of explanations invokes mode conversion due to inhomogeneities near the source and along the path. The work of Brune and Pomeroy (1963) and Aki (1964) eliminated this hypothesis. The latter showed that Love and Rayleigh wave arrivals were consistent with a common source location and time, and the former observed that while the explosion itself could generate both Rayleigh and Love waves the subsequent cavity collapse did not.

An alternate explanation calls for direct effects in the immediate neighborhood of the shot point.

Asymmetry of the radiation pattern due to near-source phenomena such as formation of new cracks or block motion was first advanced by Kisslinger *et al.*, (1961) who showed that *SH* waves were generated by small explosions detonated in soil. This hypothesis is an interesting one because it does not require the presence of tectonic prestress. It remained of secondary interest until the mid-70's, when observations of the MIGHTY EPIC and DIABLO HAWK tests showed significant displacements at depth along preexisting faults and joints (Bache and

Lambert, 1976). A simple analytical model of a slipping joint triggered by a nearby explosion was proposed by Salvado and Minster (1980), and extended to more realistic boundary conditions by large scale three-dimensional numerical modeling by Stevens *et al.*, (1982). Although the question is far from resolved, preliminary results indicate that significant perturbations to the *long-period* radiation field can be generated by this mechanism through conversion of incident *P*-waves into *S*-waves, provided that slip on the joint is not axisymmetric, due either to the proximity of the free surface or to a small amount of prestress.

A somewhat similar mechanism was simulated numerically in two dimensions by Andrews (1973); he required relatively large stresses on the preexisting fault, however. In a similar vein, Masse (1981) suggested that explosion-induced thrust faulting around the shot point may contribute a significant component of anomalous radiation.

Another possibility which has apparently not been examined in detail has to do with anisotropy of the medium in the neighborhood of the shot point. An organized system of weak joints with preferential orientation can lead to gross anisotropy of the medium (*e.g.*, Morland, 1974a,b). Further, Kisslinger *et al.*, (1961) report a preferential orientation of the cracking pattern in response to explosions in soil. Analysis of dislocation sources in an anisotropic medium by Kawasaki and Tanimoto (1981) shows that the moment tensor always has a nonzero trace in that case, and the radiation pattern can be quite different from that of a double-couple. It is reasonable to conjecture that the converse is true, and that an explosion detonated in an anisotropic material will result in nonisotropic radiation, although the magnitude of the effect is a matter of speculation at this stage.

By far the best studied mechanism, relaxation of tectonic stress as the source of anomalous radiation from underground explosions, remains a subject of current research. Two competing models have been proposed in the literature, namely

(1) Release of tectonic stress caused by the introduction of the cavity in a prestressed medium (Press and Archambeau, 1962; Archambeau, 1964, 1968, 1972, 1973; Archambeau and Sammis, 1970; Smith *et al.* 1969; Harkrider, 1977), and

(2) Triggering of an earthquake quasi-synchronous with the explosion (Brune and Pomeroy, 1963; Aki, 1964; Aki *et al.*, 1969; Aki and Tsai, 1972).

If the prestress is purely deviatoric and uniform in the neighborhood of the shot point, either type of explanation leads to the superposition of a quadrupolar (double-couple) field on the intrinsic explosion monopole. The relative strengths of the two contributions is measured by the

so-called F-factor, introduced by Toksoz, *et al.*, (1965) as the ratio of the double-couple and explosion energies.

Quantitative estimates of F-factors for U.S. explosions were obtained by Toksoz and Kehrer (1972a, b), under the assumption that the double-couple has a strike-slip orientation. They found values generally less than 1, with some exceptions, notably the granite explosions PILEDRIVER and HARDHAT, with F-factors near 3.

Arguments against tectonic relaxation, and in favor of triggered faulting, have been presented by Aki and Tsai (1972) and may be summarized as follows:

- The triggered event model can explain the Love wave observations for several NTS explosions, assuming a strike slip dislocation model with dimensions comparable to the extent of the aftershock distribution—particularly for BENHAM (Hamilton and Healy, 1969)—, and a low stress drop of order 10 bars, consistent with comparable estimates for earthquakes.
- In contrast, at least in some cases, the strain relaxation model may require large prestress levels (on the order of 1000 bars), and the strain energy release calculated using Honda's (1960) cavity model is much larger than the total seismic energy estimated from the body wave magnitude.

Counter-arguments have been presented by Archambeau (1972, 1973), and Lambert *et al.*, (1972), who performed a detailed analysis of the surface waves generated by BILBY and SHOAL, and compared these explosions with a nearby earthquake (July 20, 1962, near Fallon, Nevada).

- Although the earthquake surface waves can be explained in terms of a double-couple source at long periods, fault propagation effects cause asymmetries in the radiation pattern at short periods.
- On the other hand, surface waves from the explosions do not exhibit asymmetries attributable to fault propagation in the same period range.
- Both the radiation pattern and the amplitudes of the Love waves generated by BILBY can be explained by the model of Archambeau and Sammis (1970) for reasonable values of prestress (70 bars) and cavity radius (420 m). Furthermore, the source dimension inferred for the anomalous radiation from BILBY from surface wave spectra is much smaller than the dimension required for a fault which would give the required total energy release.

They conclude that the surface wave observations for these events are consistent with tectonic energy release due to the explosion-created shatter zone, and not with triggered faulting. (An interesting modeling experiment was performed by Day *et al.* (1982), who showed that a nonlinear numerical calculation of the stress relaxation phenomenon yield results in good agreement with the linearized theory formulated by Archambeau and his co-workers. Additional work is required, however, before it can be concluded that this should be generally the case.)

Masse (1981) offered a critique in which he summarized difficulties encountered with both types of models, among which:

- Surface faulting associated with underground explosions often involves significant vertical displacements, and smaller horizontal displacements, in disaccord with the hypothesis of a strike-slip triggered event.
- It is difficult to correlate the distribution of tectonic aftershocks following the BENHAM explosion with surface ground fractures in spite of the shallowness of the hypocenters.
- Not only are Rayleigh wave trains often similar from explosion to explosion in a given source area, but the Rayleigh waves generated by the cavity collapse are often phase-reversed and scaled-down copies of those generated by the explosion itself. Whenever this is true, it argues against significant tectonic release or large-scale faulting. (There are, however, conspicuous exceptions discussed below.)
- As recognized by Aki and Tsai (1972), the left-lateral surface motion observed along the Boxcar fault after BOXCAR, is inconsistent with the Rayleigh-wave radiation pattern. In addition, the BOXCAR aftershock sequence may have been the result of stresses generated by the explosion itself, rather than by tectonic prestress, based on the historic seismicity of the area. Finally, the decay of strain after BENHAM is difficult to explain if large scale faulting is associated with the explosion.

Based on these and other arguments, Masse advocates a mechanism analogous to the block motions discussed earlier, with explosion-induced thrust faulting around the explosion; to my knowledge, this hypothesis has not been tested extensively.

Fairly recently, the excitation of Rayleigh waves by nuclear underground explosions became the object of renewed attention, following the observation of phase-reversed Rayleigh waves from some East Kazakh

tests (*e.g.* Rygg, 1979). North and Fitch (1984) confirmed that such an occurrence is not uncommon, and that for some events Rayleigh waves are phase-reversed at all observed azimuths. As discussed by Bache (1982), an additional clue lies in the significant delay (up to several seconds) associated with the anomalous surface waves. Viecelli (1973) formulated a theoretical argument favoring spall slap-down as a possible mechanism for the anomalous surface wave excitation, and Murphy (1977) noted that the slap-down model might explain apparently anomalous surface wave amplitudes observed for high-yield explosions. However, Bache *et al.* (1982), examined the nonlinear free surface interaction for two-dimensional numerical simulations and concluded that spall effects could not affect Rayleigh wave amplitudes significantly. Their analysis was generalized by the work of Day *et al.* (1983), who demonstrated that the early models were flawed and did not conserve momentum.

On the other hand, these conclusions only hold at long-enough periods. For body waves, and for short period surface waves, nonlinear interactions with the free surface could well be significant (Day *et al.* 1983). In addition, Burdick and Helmberger (1979) found that they needed to lower the *P*-wave velocity in the shallow layers above the CANNIKIN shot point in order to explain the timing of the *pP* phase. They suggested that velocities in the crushed zone above the shot point might be lowered by as much as 25% in that case.

North and Fitch (1984) showed that a thrust-oriented double-couple superposed on the explosion monopole can explain the anomalous Rayleigh waves; this particular orientation is the most efficient one for teleseismic *P*-waves as well. On the other hand, Bache (1976) demonstrated that the tectonic release contributes negligibly to the *P*-wave signature if the prestress is uniform pure shear. As shown by Stevens (1980b) this is not necessarily true if prestress concentrations exist near the source; in that case, anomalous *P*-waves could be produced for selected directions, although it might well be difficult to untangle source effects from wave propagation effects due to near-source structural complications.

Scott and Helmberger (1983) used the Kirchhoff-Helmholtz integral technique to study near-source wave propagation above the shot point of an underground explosion in the spall zone. Based on a simplified model—a gap in the free surface—they find that the free surface reflection coefficient can be affected in a way compatible with the observations of Helmberger and Hadley (1981). They can also explain delays in the *pP* phase comparable to those described above (see also Shumway and Blandford, 1980). These results are preliminary, however.

By and large, perturbations of the body-waves by near-source complications is an unresolved observational and theoretical problem, in the

sense that it is difficult to separate unambiguously source and path effects, since we need a much more detailed knowledge of both sources and earth structure at short wavelengths.

7. Moment Tensor Representations

The 60's might be characterized as the decade of the double-couple, the dislocation and relaxation source models, and the scalar moment. The 70's, on the other hand, might be characterized as the decade of numerical models, and of moment tensors. The moment tensor representation of a seismic source is a particularly useful one since the displacement field can be shown to depend linearly on the components of the moment tensor, so that the inverse problem is greatly simplified, and automated source parameter retrieval made possible. This explains the steady growth in popularity of this particular representation over the past 10 to 15 years.

In this representation, a seismic event is described by ten parameters: its origin time, spatial location, and moment tensor, the latter accounting for six parameters. A fully specified moment tensor includes an isotropic component, which permits the representation of explosive sources or volumetric sources with volume change (*e.g.* sudden phase transitions). If one assumes *a priori* that the source is a dislocation, then only four components of the moment tensor are needed; they are merely another representation of the three parameters required to describe the fault plane geometry, plus the scalar seismic moment.

7.1 Moment Tensors and Source Theory. The earliest mention of a spatial moment expansion of the source I have been able to find was made by Archambeau (1964, 1968), who also recognized the tensorial character of the coefficients, and related them to multipole moments. However, the introduction of "the" moment tensor as used in the seismological literature is usually credited to Kostrov (1970), although Randall (1970) arrived at the conclusion (apparently independently) that the "seismic moment is properly a tensor". The latter author also related the concept to the multipole representation (harmonics of degrees zero and two) used previously by Knopoff and Randall (1970) and Randall and Knopoff (1970). Any mechanism in which only the monopole and quadrupole are excited can be specified in terms of a symmetric, second order moment tensor, equivalent to a linear combination of couples with no net torque.

Gilbert (1971, 1973) recognized the power of moment tensor equivalent point sources as applied to the excitation of free oscillations of the earth; the linear dependence of the displacement field on the components of the moment tensor further allowed him to formulate a linear

inverse problem for the retrieval of source parameters from very low frequency observations, for which the point source approximation is obviously valid, and for which the time function may be approximated by a step.

Gilbert argued that the moment tensor could be considered as the volume integral (over the whole earth) of the static stress drop associated with the event. This was criticized by Backus and Mulcahy (1976a, b) who argued that the moment tensor density, whose divergence yields the equivalent body forces, is not uniquely defined, and that the stress drop is not an appropriate moment tensor density, since it ignores gravitational changes. They introduced the "stress glut" as the difference between actual stress in the earth and that calculated from the displacement field using an assumed rheology (the "model" stress), and argued that stress gluts are the most appropriate moment tensor densities to use in seismological applications. Stress gluts can be related to the "stress-free strain", a concept used by Eshelby (1957) to study static inclusion problems, and present the advantage that they vanish outside the source region.

Backus and Mulcahy (1976a) further proposed a general formalism for polynomial moment expansions, both in space (see also Archambeau, 1968) and in time. They showed that the only moments of seismological interest are those of the equivalent forces. Such expansions are useful for the description of sources which can be considered to be localized in space and time, namely:

(1) For the wavelengths of interest, the spatial expansion can be truncated to a few moments of low degree
(2) For the periods of interest, the Fourier spectrum of the moment rate tensor varies slowly with frequency

In such cases, the source may be represented adequately by the first few terms of a moment expansion about its spatio-temporal centroid. Through use of singular generalized functions, the theory was then extended to the case of sources with displacement discontinuities (Backus and Mulcahy, 1976b), and used by Backus (1977a, b) for a detailed treatment of sources with moments of degree two.

Jobert (1977) used the concept of "stress glut" to demonstrate that a continuous medium cannot sustain the action of a dipole source without faulting (creation of a displacement discontinuity), and further that a dislocation is in fact equivalent to a continuous infinity of sets of three dipoles. The classical equivalence with a distribution of orthogonal dipoles is thus only a special case without physical significance.

As a phenomenological or kinematical representation of the source, the moment tensor has been very successful indeed, as we shall see. However, more work is needed to relate it to the dynamics of the failure process, since the true stresses and displacements are not known in the earth, and since estimates of the "model" stress depend both on the approximation made for the displacement and on the assumed rheology (*e.g.* Archambeau and Scales, 1984).

7.2 Applications. The contributions of Gilbert (1971, 1973) triggered a series of investigations of the source mechanism which used the moment tensor formalism (*e.g.* Dziewonski and Gilbert, 1974; Gilbert and Dziewonski, 1975; Gilbert and Buland, 1976; McCowan, 1976; McCowan and Dziewonski, 1977; Stump and Johnson, 1977; Mendiguren, 1977; Strelitz, 1978, 1980; Okal and Geller, 1979; Patton and Aki, 1979; Ward, 1980a, b; Deschamps *et al.*, 1980; Patton, 1980; Kanamori and Given, 1981; Dziewonski *et al.*, 1981; Silver and Jordan, 1982, 1983; Doornbos, 1982; Dziewonski and Woodhouse, 1983).

Among the advances described in these papers, I shall mention three:

(1) Evidence for an isotropic component of radiation for some earthquakes
(2) Evidence for the existence of "slow" earthquakes
(3) Development of fast, automated source mechanism determination techniques

Dziewonski and Gilbert (1974) and Gilbert and Dziewonski (1975) detected a slow compressive, perhaps precursive, component of the rupture process for two deep events. On the other hand, Okal and Geller (1979) pointed out the inherent difficulties in trying to detect an isotropic source component based on fundamental mode observations. More recently, Silver and Jordan (1982) developed optimal estimations techniques for scalar invariants of the moment rate tensor. The estimates are optimized by minimization of a positive semi-definite quadratic form which accounts for the bias introduced by lateral inhomogeneities (Patton and Aki, 1979) and by ambient noise. Since the method also yields an estimate of the variance of the solution, they can formulate statistical tests of various hypotheses about the source mechanism. Furthermore, their treatment permits the use of prior information about the source mechanism in the form of prior probability densities on the solution, which allows them to eliminate the negative bias in moment estimates caused by the degeneracy of the problem for shallow sources (Kanamori and Given, 1981). Direct estimation of the scalar invariants of the moment tensor is also a superior approach since it can be shown that the values calculated by inversion

for the moment tensor itself are biased estimators (Silver and Jordan, 1982).

Silver and Jordan (1982) applied their method to two earthquakes, a deep one (1978 March 7, Honshu), and a shallow one (1978 November 29, Oaxaca). In the first case, they tentatively conclude that an isotropic component is indeed resolvable, based on data dominated by overtones, which circumvents the misgivings of Okal and Geller (1979). Dziewonski and Woodhouse (1983) examined the deviation from a double-couple mechanism for a large number of events, using automated analysis techniques described by Dziewonski *et al.* (1981), in which it is assumed that the moment tensor is traceless, that is, purely deviatoric. Deviations from a pure double-couple mechanism are rather common, for both shallow and deep-focus events, although their significance has not yet been established. (I have mentioned earlier some of the proposed mechanisms for this behavior; they range from postulated catastrophic phase transitions, to the effects of anisotropy in the source region).

Rapid and automated data processing techniques for the retrieval of source parameters have been described by Kanamori and Given (1981) and by Dziewonski *et al.* (1981). Such techniques are made possible by the deployment of high-quality digital networks (SRO, ASRO, IDA), and are very likely to revolutionize source theory as the number of stations increases. One question which can be addressed by sophisticated processing of the long-period seismograms recorded at such stations is that of "slow" earthquakes, a concept introduced by Kanamori and Cipar (1974), Kanamori and Stewart (1976, 1979), and Sacks *et al.* (1978, 1981). Kanamori and Anderson (1975) also argued for a slow precursor to the Chilean earthquake of 1960.

A recent examination of the problem was conducted by Silver and Jordan (1983) who applied the techniques of Silver and Jordan (1982) to the determination of total-moment spectra for fourteen large earthquakes. [They suggest that a convenient unit for measuring seismic moment is 10^{20} Nm = 1 A, after the first investigator to measure this quantity (Aki, 1966)]. They find some shallow events to be "fast", and others to be "slow", with a tentative correlation with depth of rupture: slow events may be associated with ruptures propagating through the more ductile lower lithosphere. Interestingly, the five deep events they examined were all found to be "slow"; these include those events for which a slow compressive component had been suggested by Gilbert and Dziewonski (1975) and Silver and Jordan (1982).

The treatments of Silver and Jordan (1982, 1983), and Dziewonski *et al.* (1981), pertain to the spatio-temporal centroidal representation of the source, a concept introduced by Backus (1977a). [The effects of the

finite spatio-temporal dimensions of the source have been examined theoretically by Doornbos (1982)]. While a low-order moment expansion is clearly well-suited for global studies based on long- to intermediate-period data (*e.g.*, Dziewonski and Woodhouse, 1983), an alternate representation will be required to model high-frequency and near-field data (see, however, Stump and Johnson, 1982). For such purposes, the classical fault-plane models will probably be used for some time to come.

These problems are, of course, the focus of a vigorous on-going research effort.

A noteworthy application of moment tensor inversion of long-period Rayleigh waves is described by Romanowicz (1981). She examined the residuals associated with the solutions from the point of view of event-depth resolution and analyzed the effects of phase velocity variations for Eurasian paths. She later refined the method (Romanowicz, 1982), and concluded that if phase velocities calculated from a well constrained event are used as regional path corrections near the source, then the depths of neighboring events could be constrained to ± 5 km, and their source mechanisms to ± 5° in fault orientation.

Source representations in terms of low order moments is naturally most appropriate for the analysis of long period signals. Moment tensor sources are obviously just as applicable to the study of body-waves (*e.g.* Ward, 1980a, b; Fitch *et al.*, 1980; Fitch, 1981; Fitch *et al.*, 1981). However, Stump and Johnson (1982) demonstrated that higher order moments are important at higher frequencies, and required in order to account for source finiteness and rupture propagation. They point out that inclusion of the higher moments can in principle resolve the fault plane ambiguity and the tradeoff between rise time and rupture time, a conclusion reached earlier by Backus (1977a, b). They find that the seismic spectra of the higher moments are strongly peaked, and dominate at certain azimuths. This is in accord with Stevens's analogous conclusion for higher multipoles excited by prestress concentrations.

Although the systematic use of moment tensors in modeling the kinematic properties of the source (both forward and inverse problems) represents a significant advance, because it provides a very convenient formalism, appropriate for all types of seismic observations, the use of other models, such as dislocation models, is likely to persist in the future because these models entail a geometrical description of the fault which appeals to the intuition. The relationships between moment tensors and physical characterizations of the source phenomenon have not been completely sorted out. It is relatively easy to start from some physical model and compute the corresponding moment rate tensor density; the converse is much more difficult. Furthermore, the relationships between

moment tensor densities, stress drops, "true" and "model" stresses, stress gluts, and nonlinear failure processes are still a matter of controversy (Archambeau and Scales, 1984).

8. Comments and Conclusions

It is, of course, not possible to predict what the future holds for source theory, but, based on the recent trends, I shall risk a few conjectures:

From a theoretical point of view, we have not yet used the complete arsenal of tools available to us now. Because seismic activity takes place in response to stress accumulation in the earth due to tectonic deformation, it is clear to me that stress relaxation is ultimately the correct point of view one should adopt to investigate the seismic phenomenon. The same holds for anomalous radiation from explosions. The specific mode of relaxation, aseismic or catastrophic, depends on local physical conditions, and on the history of the medium. In view of the complexity of geological materials and geological settings, a satisfactory treatment will involve statistical and deterministic features which are found today in individual models, but are rarely combined. Thus, I consider it likely that for realistic initial conditions (inhomogeneous prestress, variable material properties), relaxation models and crack propagation models will eventually merge into a general treatment of failure. This requires, of course, that we learn to solve relaxation problems for arbitrary geometries, since geometry should not be pre-specified in a fully dynamical treatment.

It is also clear to me that the most important recent advances are driven by the collection and analysis of large, high-quality data sets. This includes teleseismic observations, near-field recordings, and laboratory data. Digital recording, and automated digital processing have brought to us a wealth of information which we have hardly begun to exploit. To date, only in a few instances have we been able to produce a detailed description of a seismic event with all the complications associated with variable conditions along the fault. In the future, with the acquisition of very complete data sets, one could envisage the formulation and solution of ever larger inverse problems aimed at retrieving three-dimensional details of the source mechanism. This would tell us what the models should simulate and ultimately predict.

The phenomenological descriptions of sources must, of course, be on a par with the level of detail one tries to represent. In practice, this probably means that descriptions based on a few low-order moments will not be adequate; moment expansions do not converge fast enough to be very useful at short wavelengths and in the analysis of near-field data. Perhaps alternate expansions, capable of representing source details in

space and time can be devised, starting with moment tensor densities ("stress gluts"). In any case, I suspect that such developments will be "data driven".

This review of source theory has not done justice to the enormous amount of work which has characterized the last twenty-five years. It is heavily biased toward the more theoretical aspects of source modeling, and touches on the problems of retrieval of source parameters from seismic observations only in a peripheral way. In particular, I have not touched on a great many subjects which are of obvious and tremendous importance, such as

(1) The retrieval of source parameters by waveform modeling [*e.g.* Burdick and Mellman, (1976)]. This topic is intimately related to wave propagation, which is reviewed elsewhere in this volume.

(2) Anomalous seismic sources which are not explosive, nor earthquake-like, but can be represented by single forces, such as volcanic sources (*e.g.* Kanamori and Given, 1982), or impacts.

(3) Sources of seismic noise, volcanic tremor, etc.

(4) Phenomenological aspects of the seismic source which may have precursory character.

In fact, there are probably many more aspects of the available theoretical baggage which I simply have not thought of.

My hope is that my selection of material did convey the impression of a continually growing field, which branches out into many others, such as fracture and crack mechanics, mathematical theory of stability of nonlinear systems, etc.

Great progress has been achieved in the past decades, and we can expect further discoveries in the future. The most likely source of progress is the installation of numerous recording instruments which represent state-of-the-art in modern seismometry, and the automated processing of large data sets. This holds for dense local and regional arrays, of strong-motion instrumentation, and for global networks. The study of seismic sources is in fact one of the most prominent arguments for the deployment of a digital Global Seismic Network (IRIS, 1984). The new data acquisition systems and processing techniques will help answer some of the questions we are facing today.

They will surely raise new ones.

Acknowledgements

Steven Day has spent many hours reading portions of the manuscript, and has guided me through some of the literature. He had also pointed out some errors and misinterpretations which I have attempted to correct. His friendly and patient advice are gratefully acknowledged; any remaining errors or omissions are, of course, my responsibility. I also thank Jeffry Stevens, Thomas Jordan and Thomas Hanks for their helpful comments and suggestions.

This work was supported by the Advanced Research Projects Agency of the Department of Defense, while the author was a consultant for Science Applications International Corporation.

References

Aki, K., "Study of earthquake mechanism by a method of phase equalization applied to Rayleigh and Love waves," *J. Geophys. Res.*, **65**, p. 729, 1960.

Aki, K., "Study of Love and Rayleigh waves from earthquakes with fault plane solutions or with known faulting Part 1. A phase difference method based on a new model of earthquake source," *Bull. Seismol. Soc. Amer.*, **54**, pp. 511-527, 1964a.

Aki, K., "Study of Love and Rayleigh waves from earthquakes with fault plane solutions or with known faulting Part 2. Application of the phase difference method," *Bull. Seismol. Soc. Amer.*, **54**, pp. 529-558, 1964b.

Aki, K., "A note on surface waves generated from the HARDHAT nuclear explosion," *J. Geophys. Res.*, **69**, pp. 1131-1134, 1964c.

Aki, K., "Generation and propagation of *G* waves from the Niigata earthquake of June 16, 1964, parts 1 and 2," *Bull. Earthq. Res. Inst. Tokyo Univ.*, **44**, pp.23-88, 1966.

Aki, K., "Scaling law of seismic spectrum," *J. Geophys. Res.*, **72**, pp. 1217-1231, 1967.

Aki, K., "Seismic displacements near a fault," *J. Geophys. Res.*, **73**, pp. 5359-5376, 1968.

Aki, K., "Characterization of barriers on an earthquake fault," *J. Geophys. Res.*, **84**, pp. 6140-6148, 1979.

Aki, K., "Re-evaluation of stress drop and seismic energy using a new model of earthquake faulting," *Mechanism and Earthquake Prediction*, (Coulomb volume), ed. C.J. Allegre, pp. 23-50, editions C.N.R.S., Paris, 1980.

Aki, K., M. Bouchon, and P. Reasenberg, "Seismic source function of an underground nuclear explosion," *Bull. Seismol. Soc. Amer.*, **64**, pp. 131-148, 1974.

Aki, K., and B. Chouet, "Origin of coda waves: source, attenuation, and scattering effects," *J. Geophys. Res.*, **80**, pp. 3322-3342, 1975.

Aki, K., P. Reasenberg, T. De Fazio, and Y.-B. Tsai, "Near-field and far-field seismic evidences for triggering an earthquake by the BENHAM explosion," *Bull. Seismol. Soc. Amer.*, **59**, pp. 2197-2207, 1969.

Aki, K., and P.G. Richards, *Quantitative Seismology, Theory and Methods, I and II*, W.H. Freeman, San Francisco, California, 1980.

Aki, K. and Y.B. Tsai, "Mechanism of Love-wave excitation by explosive sources," *J. Geophys. Res.*, **77**, pp. 1452-1475, 1972.

Anderson, J.G. and P.G. Richards, "Comparison of strong ground motion from several dislocation models," *Geophys. J. R. Astr. Soc.*, **42**, pp. 347-373, 1975.

Andrews, D.J., "A numerical study of tectonic stress release by underground explosions," *Bull. Seismol. Soc. Amer.*, **63**, pp. 1376-1391, 1973.

Andrews, D.J., "Rupture velocity of plane strain shear cracks," *J. Geophys. Res.*, **81**, pp. 5679-5687, 1976b.

Andrews, D.J., "A stochastic fault model 1. Static case," *J. Geophys. Res.*, **85**, pp. 3867-3877, 1980.

Andrews, D.J., "A stochastic fault model 2. Time dependent case," *J. Geophys. Res.*, **86**, pp. 10821-10834, 1981.

Archambeau, C.B., *Elastodynamic Source Theory*. Ph.D. Thesis, California Institute of Technology, Pasadena, California, 1964.

Archambeau, C.B., "General theory of elastodynamic source fields," *Rev. Geophys.*, **16**, pp. 241-288, 1968.

Archambeau, C.B., "The theory of stress wave radiation from explosions in prestressed media," *Geophys. J. R. Astr. Soc.*, **29**, pp. 329-363, 1973.

Archambeau, C.B. and J.B. Minster, "Dynamics in prestressed media with moving phase boundaries: a continuum theory of failure in solids," *Geophys. J. R. Astr. Soc.*, **52**, pp. 65-96, 1978.

Archambeau, C.B. and C. Sammis, "Seismic radiation from explosions in prestressed media and the measurement of tectonic stress in the earth," *Rev. Geophys. Space Phys.*, **8**, pp. 473-500, 1970.

Archambeau, C.B. and J. Scales, "The physical significance of seismic moment tensor representations," in preparation, 1984.

Archuleta, R.J. and S.M. Day, "Dynamic rupture in a layered medium: the 1966 Parkfield earthquake," *Bull. Seismol. Soc. Amer.*, **70**, pp. 671-689, 1980.

Archuleta, R.J. and G.A. Frazier, "Three-dimensional numerical simulations of dynamic faulting in a half-space," *Bull. Seismol. Soc. Amer.*, **68**, pp. 573-598, 1978.

Bache, T.C., "The effect of tectonic stress release on explosion *P*-wave signatures," *Bull. Seismol. Soc. Amer.*, **66**, pp. 1441-1447, 1976.

Bache, T.C., "Estimating the yield of underground nuclear explosions," *Bull. Seismol. Soc. Amer.*, **72**, pp. S131-S168, 1982.

Bache, T.C., S.M. Day, and H.J. Swanger, "Rayleigh wave synthetic seismograms from multi-dimensional simulations of underground explosions," *Bull. Seismol. Soc. Amer.*, **72**, pp. 15-28, 1982.

Bache, T.C. and D.G. Lambert, "The seismological evidence for the triggering of block motion by large explosions," *S-Cubed Technical Report, DNA4323T*, La Jolla, California, 1976.

Backus, G., "Interpreting the seismic glut moments of total degree of two or less," *Geophys. J. R. Astr. Soc.*, **51**, pp. 1-25, 1977a.

Backus, G., "Seismic sources with observable glut moments of spatial degree two," *Geophys. J. R. Astr. Soc.*, **51**, pp. 27-45, 1977b.

Backus, G., and M. Mulcahy, "Moment tensors and other phenomenological descriptions of seismic sources, I, Continuous displacements," *Geophys. J. R. Astr. Soc.*, **46**, pp. 341-361, 1976a

Backus, G., and M. Mulcahy, "Moment tensors and other phenomenological descriptions of seismic sources, II, Discontinuous displacements," *Geophys. J. R. Astr. Soc.*, **47**, pp. 301-329, 1976b.

Barenblatt, G.I., "The formation of equilibrium cracks during brittle fracture: General ideas and hypotheses, axially symmetric cracks," *J. Appl. Math. Mech.*, **23**, pp. 434-444, 1959.

Barker, J.S. and C.A. Langston, "Moment tensor inversion of complex earthquakes," *Geophys. J. R. Astr. Soc.*, **68**, pp. 777-803, 1982.

Ben-Menahem, A., "Radiation of Seismic surface waves from finite moving sources," *Bull. Seismol. Soc. Amer.*, **51**, pp. 401-435, 1961.

Ben-Menahem, A. and A. Cisternas, "The dynamic response of an elastic half-space to an explosion in a spherical cavity," *J. Math. Phys.*, **42**, pp. 112-125, 1963.

Ben-Menahem, A and S.J. Singh, *Seismic Waves and Sources*, Springer-Verlag, New York, 1981.

Benioff, H., "Earthquake source mechanisms," *Science*, **143**, pp. 1399-1406, 1964.

Benioff, H., F. Press, and S. Smith, "Excitation of the free oscillations of the earth by earthquakes," *J. Geophys. Res.*, **66**, pp. 605-619, 1961.

Boatwright, J., "The effect of rupture complexity on estimates of source size," *J. Geophys. Res.*, **89**, pp. 1132-1146, 1984.

Boore, D.M., "Strong motion seismology," *Rev. Geophys. Space Phys.*, **21**, pp. 1308-1317, 1983.

Bouchon, M., "Predictability of ground displacement and velocity near an earthquake fault: An example: The Parkfield earthquake of 1966," *J. Geophys. Res.*, **84**, pp. 6149-6159, 1979.

Brune, J.N., "Tectonic Stress and the spectra of seismic shear waves from earthquakes," *J. Geophys. Res.*, **75**, pp. 4997-5009, 1970.

Brune, J.N. and P.W. Pomeroy, "Surface wave radiation patterns for underground nuclear explosions and small magnitude earthquakes," *J. Geophys. Res.*, **68**, pp. 5005-5028, 1963.

Burdick, L.J., "t^* for S waves with a continental ray path," *Bull. Seismol. Soc. Amer.*, **68**, pp. 1013-1030, 1978.

Burdick, L.J., "Comments on 'The corner frequency shift, earthquake source models, and Q' by T.C. Hanks," *Bull. Seismol. Soc. Amer.*, **72**, pp. 1419-1426, 1982.

Burdick, L. J. and D. V. Helmberger, "Time functions appropriate for nuclear explosions," *Bull. Seismol. Soc. Amer.*, **69**, pp. 957-973, 1979.

Burdick, L.J. and G.R. Mellman, "Inversion of the body waves of the Borrego Mountain earthquake to the source mechanism," *Bull. Seismol. Soc. Amer.*, **66**, pp. 1485-1499, 1976.

Burridge, R., "Numerical solution of certain integral equations with nonintegrable kernels arising in the theory of crack propagation and elastic wave diffraction," *Phil. Trans. Roy. Soc. London Ser. A.*, **265**, pp. 353-381, 1969.

Burridge, R., "The pulse shapes and spectra of elastic waves generated when a cavity expands in an initial shear field," *J. Geophys. Res.*, **80**, pp. 2606-2607, 1975.

Burridge, R. and Z. Alterman, "The elastic radiation from an expanding spherical cavity," *Geophys. J. R. Astr. Soc.*, **30**, pp. 451-477, 1972.

Burridge, R., G. Conn, and L.B. Freund, "The stability of a plane-strain shear crack with finite cohesive traction," *J. Geophys. Res.*, **84**, pp. 2210- 2222, 1978.

Burridge, R. and G.S. Halliday, "Dynamic shear cracks with friction as a model for shallow focus earthquakes," *Geophys. J. R. Astr. Soc.*, **24**, pp. 261-283, 1971.

Burridge, R. and L. Knopoff, "Body force equivalents for seismic dislocations," *Bull. Seismol. Soc. Amer.*, **54**, pp. 1875-1888, 1964.

Burridge, R. and R. Moon, "Slipping on a frictional fault plane in three-dimensions: A numerical simulation of a scalar analogue," *Geophys. J. R. Astr. Soc.*, **67**, pp 325-342, 1981.

Burridge, R. and J.R. Willis, "The self-similar problem of an expanding eliptical crack in an anisotropic solid," *Proc. Camb. Phil. Soc.*, **66**, 443-468, 1969.

Byerly, P., "The earthquake of July 6, 1934: Amplitudes and first motion," *Bull. Seismol. Soc. Amer.*, **28**, pp. 1-13, 1938.

Byerly, P. and W. Stauder, "The mechanism at the focus of an earthquake," *Earthquake Notes*, **29**, pp. 17-23, 1958.

Chatterjee, A.K. and L. Knopoff, "Bilateral propagation of a spontaneous two-dimensional anti-plane shear crack under the influence of cohesion," *Geophys. J. R. Astr. Soc.*, **73**, pp. 449-473, 1983.

Chinnery, M.A., "The deformation of the ground around surface faults," *Bull. Seismol. Soc. Amer.*, **51**, 355-372, 1961.

Chinnery, M.A., "The stress changes that accompany strike-slip faulting," *Bull. Seismol. Soc. Amer.*, **53**, pp. 921-932, 1963.

Coulomb, J. and G. Jobert, *Traite de Geophysique*, Masson, Paris, 1973.

Dahlen, F.A., "On the ratio of *P*-wave to *S*-wave corner frequencies for shallow earthquake sources," *Bull. Seismol. Soc. Amer.*, **64**, pp. 1159-1180, 1974.

Dahlman, O. and H. Israelson, *Monitoring Underground Nuclear Explosions*, Elsevier Scientific Publishing Co., Amsterdam, 1977. 440 pp.

Das, S., "A numerical method for determination of source time functions for general three-dimensional rupture propagation," *Geophys. J. R. Astr. Soc.*, **62**, pp. 591-604, 1980.

Das, S., "Three-dimensional spontaneous rupture propagation and implications for the earthquake source mechanism," *Geophys. J. R. Astr. Soc.*, **67**, pp. 375-393, 1981.

Das, S. and K. Aki, "A Numerical study of two-dimensional spontaneous rupture propagation," *Geophys. J. R. Astr. Soc.*, **50**, pp. 643-668, 1977a.

Das, S. and K. Aki, "Fault plane with barriers: a versatile earthquake model," *J. Geophys. Res.*, **82**, pp. 5658-5670, 1977b.

Das, S. and B.V. Kostrov, "Breaking of a single asperity: Rupture process and seismic radiation," *J. Geophys. Res.*, **88**, pp. 4277-4288, 1983.

Das, S. and C.H. Scholz, "Theory of time-dependent rupture in the earth," *J. Geophys. Res.*, **86**, pp. 6039-6051, 1981.

Day, S.M., "Three-dimensional finite difference simulation of fault dynamics: rectangular faults with fixed rupture velocity," *Bull. Seismol. Soc. Amer.*, **72**, pp. 705-727, 1982a.

Day, S.M., "Three-dimensional simulation of spontaneous rupture: the effect of nonuniform prestress," *Bull. Seismol. Soc. Amer.*, **72**, pp. 1881- 1902, 1982b.

Day, S.M. and J.B. Minster, "Numerical simulation of attenuated wavefields using a Pade approximant method," *Geophys. J. R. Astr. Soc.*, **78**, 1984. (in press)

Day, S.M., N. Rimer, and J.T. Cherry, "Surface waves from underground explosions with spall: analysis of elastic and nonlinear source models," *Bull. Seismol. Soc. Amer.*, **73**, pp. 247-264, 1983.

Day, S.M., N. Rimer, J.T. Cherry, and J.L. Stevens, "Nonlinear modeling of tectonic release from underground explosions." *S-Cubed report SSS-R-82-5555*, La Jolla, California, 1982.

Deschamps, A., H. Lyon-Caen, and R. Madariaga, "Mise au point sur les methodes de calcul de sismogrammes synthetiques de longue periode," *Ann. Geophys.*, **36**, pp. 167-178, 1980.

Dieterich, J.H., "Experimental and model study of fault constitutive properties," *Solid Earth Geophysics and Geotechnology*, AMD-vol.42, ed. S. Nemat Nasser, Amer. Soc. Mech. Eng., N.Y., 1980.

Dieterich, J.H., *Constitutive properties of faults with simulated gouge*, AGU Geophysical Monograph Series (J. Handin Festschrift), 1981.

Dieterich, J.H., D.W. Barber, G. Conrad, and Q.A. Gordon, "Preseismic slip in a large scale friction experiment," *Proc. 19th US Rock Mech. Symp.*, Mackay School of Mines, Univ. Nevada, Reno., 1978.

Doornbos, D.J., "Seismic source spectra and moment tensors," *Phys. Earth Planet. Inter.*, **30**, pp. 214-227, 1982.

Duclaux, F. and L. Michaud, "Conditions experimentales des tirs nucleaires souterrains francais au Sahara," *R. Acad. Sc. Paris Ser.B*, **270**, pp. 189- 192, 1970.

Dziewonski, A.M., T.A. Chou, and J.H. Woodhouse, "Determination of earthquake source parameters from waveform data for studies of global and regional seismicity," *J. Geophys. Res.*, **86**, pp. 2825-2852, 1981.

Dziewonski, A.M. and F. Gilbert, "Temporal variation of the seismic moment tensor and the evidence of precursive compression for two deep earthquakes," *Nature*, **247**, pp. 185-188, 1974.

Dziewonski, A.M. and J.H. Woodhouse, "An experiment in systematic study of global seismicity: Centroid-moment tensor solutions for 201 moderate and large earthquakes of 1981," *J. Geophys. Res.*, **88**, pp. 3247-3272, 1983.

Ebel, J.E. and D.V. Helmberger, "*P*-wave complexity and fault asperities: the Borrego Mountain, California, earthquake of 1968," *Bull. Seismol. Soc. Amer.*, **72**, pp. 413-437, 1982.

Eshelby, J.D., "The determination of the elastic field of an ellipsoidal inclusion, and related problems," *Proc. Roy. Soc. London, Sect.A*, **241**, pp. 376-396, 1957.

Evernden, J.F., "Further studies on seismic discrimination," *Bull. Seismol. Soc. Amer.*, **65**, pp. 359-391, 1957.

Fitch, T.J., "Correction and addition to 'Estimation of the seismic moment tensor from teleseismic body wave data with applications to intraplate and mantle earthquakes' by T.J. Fitch, D.W. McCowan, and M.W. Shields," *J. Geophys. Res.*, **86**, pp. 9375-9376, 1981.

Fitch, T.J., D.W. McCowan, and M.W. Shields, "Estimation of the seismic moment tensor from teleseismic body wave data with applications to intraplate and mantle earthquakes," *J. Geophys. Res.*, **85**, pp. 3817-3828, 1980.

Fitch, T.J., R.G. North, and M.W. Shields, "Focal depth and moment tensor representations of shallow earthquakes associated with the Great Sumba earthquake," *J. Geophys. Res.*, **86**, pp. 9357-9374, 1981.

Freund, L.B., "Energy flux into the tip of an extending crack in an elastic solid," *J. Elasticity*, **2**, pp. 341-349, 1972.

Freund, L.B., "The mechanics of dynamic shear crack propagation," *J. Geophys. Res.*, **84**, pp. 2199-2209, 1979.

Furuya, I., "Predominant period and magnitude," *J. Phys. Earth*, **17**, pp. 119-126, 1969.

Geller, R.G., "Scaling relations for earthquake source parameters and magnitudes," *Bull. Seismol. Soc. Amer.*, **66**, pp. 1501-1523, 1976a.

Geller, R.J., "Body-force equivalents for stress-drop seismic sources," *Bull. Seismol. Soc. Amer.*, **66**, pp. 1801-1804, 1976b.

Geller, R.J. and C.S. Mueller, "Four similar earthquakes in central California," *Geophys. Res. Lett.*, **7**, pp. 821-824, 1980.

Gilbert, F., "Excitation of normal modes of the earth by earthquake sources," *Geophys. J. R. Astr. Soc.*, **22**, pp. 223-226, 1971.

Gilbert, F., "Derivation of source parameters from low-frequency spectra," *Phil. Trans. R. Soc. London Ser.A*, **274**, pp. 369-371, 1973.

Gilbert, F., "The relative efficiency of earthquakes and explosions in exciting surface waves and body waves," *Geophys. J. R. Astr. Soc.*, **33**, pp. 487-488, 1973.

Gilbert, F. and R. Buland, "An enhanced deconvolution procedure for retrieving the seismic moment tensor from a sparse network," *Geophys. J. R. Astr. Soc.*, **50**, pp. 251-255, 1976.

Gilbert, F. and A.M. Dziewonski, "An application of normal mode theory to the retrieval of stru tural parameters and source mechanisms from seismic spectra," *Phil. Trans. R. Soc. London Ser.A*, **278**, pp. 187-269, 1975.

Gutenberg, B., "The energy of earthquakes," *Quart. J. Geol. Soc. London*, **62**, pp. 1-14, 1956.

Hamano, Y., "Dependence of rputure time history on the heterogeneous distribution of stress and strength on the fault plane (abstract)," *EOS, Trans. Amer. Geophys. Union*, **55**, p. 352, 1974.

Hamilton, R.M. and J.H. Healy, "Aftershocks of the BENHAM nuclear explosion," *Bull. Seismol. Soc. Amer.*, **59**, pp. 2271-2282, 1969.

Hanks, T.C., "Earthquake stress drops, ambient tectonic stress and stresses that drive plate motions," *Pageoph.*, **115**, pp. 441-458, 1977.

Hanks, T.C., "*b* values and $\omega^{-\gamma}$ seismic source models: implications for tectonic stress variations along active crustal fault zones and the estimation of high frequency strong ground motion," *J. Geophys. Res.*, **84**, pp. 2235-2241, 1979.

Hanks, T.C., "The corner frequency shift, earthquake source models, and *Q*," *Bull. Seismol. Soc. Amer.*, **71**, pp. 597-612, 1981.

Hanks, T.C., "'Reply to "Comments on 'The corner frequency shift, earthquake source models, and *Q*' "'," *Bull. Seismol. Soc. Amer.*, **72**, pp. 1433-1447, 1982.

Hanks, T.C. and H. Kanamori, "A moment magnitude scale," *J. Geophys. Res.*, **84**, pp. 2348-2350, 1979.

Hanks, T.C. and W. Thatcher, "A graphical representation of seismic source parameters," *J. Geophys. Res.*, **77**, pp. 4393-4405, 1972.

Harkrider, D.G., "Potentials and displacements for two theoretical seismic sources," *Geophys. J. R. Astr. Soc.*, **47**, pp. 97-113, 1976.

Harkrider, D.G., "Elastic relaxation coefficients for a spherical cavity in a prestressed medium of arbitrary orientation," *Geophys. J. R. Astr. Soc.*, **50**, pp. 487-491, 1977.

Hartzell, S. and D.V. Helmberger, "Strong-motion modeling of the Imperial Valley earthquake of 1979," *Bull. Seismol. Soc. Amer.*, **72**, pp. 571-596, 1982.

Haskell, N.A., "Total energy and energy spectral density of elastic wave radiation from propagating faults," *Bull. Seismol. Soc. Amer.*, **54**, pp. 1811-1842, 1964.

Haskell, N.A., "Total energy and energy spectral density of elastic wave radiation from popagating faults, 2, A statistical source model," *Bull. Seismol. Soc. Amer.*, **56**, pp. 125-140, 1966.

Haskell, N.A., "Analytic approximation for the elastic radiation from a contained underground explosion," *J. Geophys. Res.*, **72**, pp. 2583-2587, 1967.

Haskell, N.A., "Elastic displacement in the near-field of a propagating fault," *Bull. Seismol. Soc. Amer.*, **59**, pp. 865-908, 1969.

Helmberger, D.V. and D.M. Hadley, "Seismic source functions and attenuation from local and teleseismic observations of the NTS events JORUM and HANDLEY," *Bull. Seismol. Soc. Amer.*, **71**, pp. 51-67, 1981.

Hirasawa, T., "Radiation patterns of *S* waves from underground nuclear explosions," *J. Geophys. Res.*, **76**, pp. 6440-6454, 1971.

Hirasawa, T. and R. Sato, "Propagation of elastic waves from a spherical origin: parts 1 and 2," *Zisin*, **16**, pp. 52-77, 1963.

Honda, H., *The generation of seismic waves*, Publ. Dominion Obs., Ottawa, 24, 1960.

Honda, H., "Earthquake mechanism and seismic waves," *Geophys Notes Tokyo Univ.*, **15** (suppl.), pp. 1-97, 1962.

Husseini, M.I., "The far-field spectrum of the displacement generated by a sudden *SH* crack," *Bull. Seismol. Soc. Amer.*, **66**, pp. 1427-1439, 1976.

Husseini, M.I., D.B. Jovanovich, M.J. Randall, and L.B. Freund, "The fracture energy of earthquakes," *Geophys. J. R. Astr. Soc.*, **43**, pp. 367-386, 1975.

Husseini, M.I. and M.J. Randall, "Rupture velocity and radiation efficiency," *Bull. Seismol. Soc. Amer.*, **66**, 1173-1187, 1976.

Ida, Y., "Cohesive forces across the tip of a longitudinal-shear crack and Griffith's specific surface energy," *J. Geophys. Res.*, **77**, pp. 3796-3805, 1972.

IRIS, (Incorporated Research Institutions for Seismology), *Science plan for a new Global Seismographic Network*, 1984. 130 p.

Jeffreys, H., "On the cause of oscillatory movements in seismograms," *Monthly Notices R. Astr. Soc. Geophys. Suppl.*, **2**, pp. 407-416, 1931.

Jobert, G., "On equivalent models of seismic source," *J. Geophys.*, **43**, pp. 329-339, 1977.

Johnson, L.R. and T.V. McEvilly, "Near-field observations and source parameters of central California earthquakes," *Bull. Seismol. Soc. Amer.*, **64**, pp. 1855-1886, 1974.

Kanamori, H., "Synthesis of long-period surface waves and its application to earthquake source studies—Kurile Islands earthquake of October 13, 1963," *J. Geophys. Res.*, **75**, pp. 5011-5027, 1970.

Kanamori, H., "The energy release in great earthquakes," *J. Geophys. Res.*, **82**, pp. 2981-2987, 1977.
Kanamori, H., "Quantification of great earthquakes," *Tectonophysics*, **49**, pp. 207-212, 1978.
Kanamori, H. and D.L. Anderson, "Theoretical basis of some empirical relations in seismology," *Bull. Seismol. Soc. Amer.*, **65**, pp. 1073-1095, 1975.
Kanamori, H. and J.J. Cipar, "Focal process of the great Chilean earthquake, May 22, 1960," *Phys. Earth Planet. Inter.*, **9**, pp. 128-136, 1974.
Kanamori, H. and J.W. Given, "Use of long-period surface waves for rapid determination of earthquake-source parameters," *Phys. Earth Plant. Inter.*, **27**, pp. 8-31, 1981.
Kanamori, H. and J.W. Given, "Analysis of long-period seismic waves excited by the May 18, 1980, eruption of Mount St. Helens—A terrestrial monopole?," *J. Geophys. Res.*, **87**, pp. 5422-5432, 1982.
Kanamori, H. and G.S. Stewart, "Mode of the strain release along the Gibbs fracture zone, mid-Atlantic ridge," *Phys. Earth Plant. Inter.*, **11**, pp. 312-332, 1976.
Kanamori, H. and G.S. Stewart, "A slow earthquake," *Phys. Earth Plant. Inter.*, **18**, pp. 167-175, 1979.
Kawasaki, I., "A method for the near-source anisotropy by the pair-event inversion of Rayleigh-wave radiation patterns," *Geophys. J. R. Astr. Soc.*, **71**, pp. 395-424, 1982.
Kawasaki, I. and T. Tanimoto, "Radiation patterns of body waves due to the seismic dislocation occuring in an anisotropic source medium," *Bull. Seismol. Soc. Amer.*, **71**, pp. 37-50, 1981.
Kisslinger, C.E., E.J. Mateker, Jr., and T.V. McEvilly, "*SH* motion from explosions in soil," *J. Geophys. Res.*, **66**, pp. 3487-3496, 1961.
Knopoff, L. and A.K. Chatterjee, "Unilateral extension of a two-dimensional shear crack under the influence of cohesive forces," *Geophys. J. R. Astr. Soc.*, **68**, pp. 7-25, 1982.
Knopoff, L. and F. Gilbert, "Radiation from a strike-slip fault," *Bull. Seismol. Soc. Amer.*, **49**, pp. 163-178, 1959.
Knopoff, L. and F. Gilbert, "First motions from seismic sources," *Bull. Seismol. Soc. Amer.*, **50**, pp. 117-134, 1960.
Knopoff, L. and M.J. Randall, "The compressed linear-vector dipole: A possible mechanism for deep earthquakes," *J. Geophys. Res.*, **75**, pp. 4957-4963, 1970.
Kostrov, B.V., "Self-similar problems on the propagation of tangential shear fractures," *J. Appl. Math. Mech.*, **28**, pp. 1077-1087, 1964.
Kostrov, B.V., "The inverse problem of the theory of earthquake foci," *Izvestia, Earth Physics*, pp. 84-101, 1970.
Kostrov, B.V., "The theory of the focus for tectonic earthquakes," *Izvestia, Earth Physics*, pp. 18-29, 1968.
Kostrov, B.V., "Seismic moment and energy of earthquakes and seismic flow of rock," *Izvestia, Earth Phys.*, pp. 23-40, 1974.
Kostrov, B.V., "On the crack propagation with variable velocity," *Intern. J. of Fracture*, **11**, pp. 47-56, 1975.
Kostrov, B.V., "Unsteady propagation of longitudinal shear cracks," *J. Appl. Math. Mech.*, **30**, pp. 1241-1248, 1966.
Koyama, J., S.E. Horiuchi, and T. Hirasawa, "Elastic waves generated from sudden vanishing of rigidity in a spherical region," *J. Phys. Earth*, **21**, pp. 213-226, 1973.
Lambert, D.G., E.A. Flinn, and C.B. Archambeau, "A comparative study of the elastic wave radiation from earthquakes and underground explosions," Geophys. J. R. Astr. Soc., **29**, pp. 403-432, 1972.
Langston, C.A., "Moments, corner frequencies, and the free surface," *J. Geophys. Res.*, **83**, pp. 3422-3426, 1978.
Langston, C.A., "Comments on 'The corner frequency shift, earthquake source models, and *Q*' by T.C. Hanks," *Bull. Seismol. Soc. Amer.*, **72**, pp. 1427-1432, 1982.

Larson, D.B., "Inelastic wave propagation in sodium chloride," *Bull. Seismol. Soc. Amer.*, **72**, pp. 2107-2130, 1982.

Lay, T., H. Kanamori, and L. Ruff, "The asperity model and the nature of large subduction zone earthquakes," *Earthquake Prediction Res.*, **1**, pp. 3-71, 1982.

Liu, H.-L. and H. Kanamori, "Determination of source parameters of mid-plate earthquakes from the waveforms of body waves," *Bull. Seismol. Soc. Amer.*, **70**, pp. 1989-2004, 1980.

Madariaga, R., "Dynamics of an expanding circular fault," *Bull. Seismol. Soc. Amer.*, **66**, pp. 639-666, 1976.

Madariaga, R., "High-frequency radiation from crack (stress drop) models of earthquake faulting," *Geophys. J. R. Astr. Soc.*, **51**, pp. 625-651, 1977.

Madariaga, R., "The dynamic field of Haskell's rectangular dislocation fault model," *Bull. Seismol. Soc. Amer.*, **68**, pp. 869-887, 1978.

Madariaga, R., "On the relation between seismic moment and drop in the presence of stress and strength heterogeneity," *J. Geophys. Res.*, **84**, pp. 2243-2250, 1979.

Mandelbrot, B. *Fractals*, W.H. Freeman, San Francisco, Calif., 1977.

Maruyama, T., "On the force equivalents of dynamic elastic dislocations with reference to the earthquake mechanism," *Bull. Earthquake Res. Inst. Tokyo Univ.*, **41**, pp. 467-486, 1963.

Maruyama, T., "Statical elastic dislocations in an infinite and semi-infinite medium" *Bull. Earthquake Res. Inst. Univ. Tokyo*, **42**, pp. 289-368, 1964.

Masse, R.P., "Review of seismic source models for underground nuclear explosions," *Bull. Seismol. Soc. Amer.*, **71**, pp. 1249-1268, 1981.

McCowan, D.W., "Moment tensor representations on surface waves," *Geophys. J. R. Astr. Soc.*, **44**, pp. 595-599, 1976.

McCowan, D.W. and A.M. Dziewonski, "An application of the energy-moment tensor relation to estimation of seismic energy radiated by point and line sources," *Geophys. J. R. Astr. Soc.*, **51**, pp. 531-544, 1977.

Melosh, H.J., "Acoustic fluidization: A new geologic process?," *J. Geophys. Res.*, **84**, pp. 7513-7520, 1979.

Mendiguren, J.A., "Inversion of surface wave data in source mechanism studies," *J. Geophys. Res.*, **82**, pp. 889-894, 1977.

Minster, J.B., *Elastodynamics of failure in a continuum*, Ph.D. Thesis, Seismological Laboratory, California Institute of Technology, Pasadena, California, 1973.

Minster, J.B., "Transformation of multipolar source fields under a change of reference frame," *Geophys. J. R. Astr. Soc.*, **47**, pp. 397-410, 1976.

Minster, J.B., "Near-field waveforms from an arbitrarily expanding transparent spherical cavity in a prestressed medium," *Geophys. J. R. Astr. Soc.*, **56**, pp. 81-96, 1979.

Minster, J.B., "Effects of near-field, nonlinear attenuation on outgoing seismic wavefields," *Terra Cognita*, **2**, p. 153, 1982.

Minster, J.B. and S.M. Day, "Decay of wavefields near an explosive source due to high-strain, nonlinear attenuation," *Geophys. J. R. Astr. Soc.*, 1984. (in preparation)

Minster, J.B. and A. Suteau, "Far-field waveforms from an arbitrarily expanding spherical cavity in a prestressed medium," *Geophys. J. R. Astr. Soc.*, **50**, pp. 215-233, 1977.

Molnar, P., K.H. Jacob, and K. McCamy, "Implications of Archambeau's earthquake source theory for slip on faults," *Bull. Seismol. Soc. Amer.*, **63**, pp. 101-104, 1973.

Molnar, P., B.E. Tucker, and J.N. Brune, "Corner frequencies of *P* and *S* waves and models fo earthquake sources," *Bull. Seismol. Soc. Amer.*, **63**, pp. 2091-2104, 1973.

Morland, L.W., "Continuum model of regularly jointed mediums," *J. Geophys. Res.*, **79**, pp. 357-362, 1974.

Morland, L.W., "Elastic reponse of regularly jointed media," *Geophys. J. R. Astr. Soc.*, **37**, pp. 435-446, 1974.

Mueller, R.A. and J.R. Murphy, "Seismic characteristics of underground nuclear detonations Part I. Seismic spectrum scaling," *Bull. Seismol. Soc. Amer.*, **61**, pp. 1675-1692, 1971.

Munguia, L. and J.N. Brune, "High stress drop events in the Victoria, Baja California earthquake swarm of 1978 March," *Geophys. J. R. Astr. Soc.*, **76**, pp. 725-752, 1984.

Murphy, J.R., "Seismic source functions and magnitude determination for underground nuclear detonations," *Bull. Seismol. Soc. Amer.*, **67**, pp. 135-158, 1977.

Murphy, J.R. and R.A. Mueller, "Seismic characteristics of underground nuclear detonations Part II. Elastic energy and magnitude determinations," *Bull. Seismol. Soc. Amer.*, **61**, pp. 1693-1704, 1971.

North, R. and T. Fitch, "Anomalous surface wave excitation by underground nuclear explosions," *J. Geophys. Res.*, 1984. (pre-print).

Okal, E.A. and R.J. Geller, "On the observability of isotropic seismic sources: The July 31, 1970 Colombian earthquake," *Phys. Earth Plant. Inter.*, **27**, pp. 393-446, 1979.

Oliver, J., P. Pomeroy, and M. Ewing, "Long-period surface waves from nuclear explosions in various environments," *Science*, **131**, pp. 1804-1805, 1960.

Olson, A.H. and R.J. Apsel, "Finite faults and inverse theory with applications to 1979 Imperial Valley earthquake," *Bull. Seismol. Soc. Amer.*, **72**, pp. 1969-2001, 1982.

Patton, P. and K. Aki, "Bias in the estimate of seismic moment tensor by the linear inversion method," *Geophys. J. R. Astr. Soc.*, **59**, pp. 479-495, 1979.

Press, F. and C.B. Archambeau, "Release of tectonic strain by underground nuclear explosions," *J. Geophys. Res.*, **67**, pp. 337-343, 1962.

Randall, M.J., "On the mechanism of earthquakes," *Bull. Seismol. Soc. Amer.*, **54**, pp. 1283-1289, 1964.

Randall, M.J., "Seismic energy generated by a sudden volume change," *Bull. Seismol. Soc. Amer.*, **54**, pp. 1291-1298, 1964.

Randall, M.J., "Seismic radiation from a sudden phase transition," *J. Geophys. Res.*, **71**, pp. 5297-5302, 1966.

Randall, M.J., "Elastic multipole theory and seismic moment," *Bull. Seismol. Soc. Amer.*, **61**, pp. 1321-1326, 1971.

Randall, M.J., "Stress drop and the ratio of seismic energy to moment," *J. Geophys. Res.*, **77**, pp. 969-970, 1972.

Randall, M.J., "Spectral peaks and earthquakes source dimension," *J. Geophys. Res.*, **78**, pp. 2609-2611, 1973.

Randall, M.J. and L. Knopoff, "The mechanism at the focus of deep earthquakes," *J. Geophys. Res.*, **75**, pp. 4965-4976, 1970.

Reid, H.F., "The mechanics of the earthquake," *The California Earthquake of April 18, 1906, Report of the State Investigation Commission, vol. 2*, Carnegie Institute of Washington, Washington, DC, 1910.

Rice, J.R., "The mechanics of earthquake rupture," in *Physics of the Earth's Interior*, ed. A. M. Dziewonski and E. Boschi, pp. 555-668, *Proceedings of the International School of Physics "Enrico Fermi"*, 1980.

Richards, P.G., "The dynamic field of a growing plane elliptical shear crack," *Intern. J. Solids Struct.*, **9**, pp. 843-861, 1973.

Richards P.G., "Dynamic motions near an earthquake fault: a three-dimensional solution," *Bull. Seismol. Soc. Amer.*, **66**, pp. 1-32, 1976.

Richards, P.G., "Elementary solutions of Lamb's problem for a point source and their relevance to three-dimensional studies in spontaneous crack propagation," *Bull. Seismol. Soc. Amer.*, **69**, pp. 947-956, 1979.

Romanowicz, B., "Depth resolution of earthquakes in central Asia by moment tensor inversion of long-period Rayleigh waves: Effects of phase velocity variations across Eurasia and their calibration," *J. Geophys. Res.*, **86**, pp. 5963-5984, 1981.

Romanowicz, B., "Moment tensor inversion of long-period Rayleigh waves: A new approach," *J. Geophys. Res.*, **87**, pp. 5395-5408, 1982.

Rudnicki, J.W. and L.B. Freund, "On energy radiation from seismic sources," Bull. Seismol. Soc. Amer., **71**, pp. 583-595, 1981.

Rudnicki, J.W. and H. Kanamori, "Effects of fault interaction on moment, stress drop, and strain energy release," *J. Geophys. Res.*, **86**, pp. 1786-1793, 1981.

Rygg, E., "Anomalous surface waves from underground explosions," *Bull. Seismol. Soc. Amer.*, **69**, pp. 1995-2002, 1979.

Sacks, I.S., A.T. Linde, J.A. Snoke, and S. Suyehiro, "Slow earthquake sequence following the Izo-Oshima earthquake of 1978," *in Earthquake Prediction: An International Review, Maurice Ewing Ser.*, vol. 4, ed. D. W. Simpson and P. G. Richards, pp. 617-628, AGU, Washington, DC, 1981.

Sacks, I.S., S. Suyehiro, A.T. Linde, and J.A. Snoke, "Slow earthquakes and stress redistribution," *Nature*, **275**, pp. 599-602, 1978.

Salvado, C. and J.B. Minster, "Slipping interfaces: A possible source of *S* radiation from explosive sources," *Bull. Seismol. Soc. Amer.*, **70**, pp. 659-670, 1980.

Sato, T. and T. Hirasawa, "Body wave spectra from propagating shear cracks," *J. Phys. Earth*, **21**, 415-431, 1973.

Savage, J.C., "Radiation from a realistic model of faulting," *Bull. Seismol. Soc. Amer.*, **56**, pp. 3788-3795, 1972.

Savage, J.C., "The relation of corner frequency to fault dimensions," *J. Geophys. Res.*, **27**, pp. 577-592, 1966.

Scholz, C.H., P. Molnar, and T. Johnson, "Detailed studies of frictional sliding of granite and implications for the earthquake mechanism," *J. Geophys. Res.*, **77**, pp. 6392-6406, 1972.

Scott, P. and D.V. Helmberger, "Applications of the Kirchoff-Helmholtz integral to problems in seismology," *Geophys. J. R. Astr. Soc.*, **72**, pp. 237-254, 1983.

Sharpe, J.A., "The production of elastic waves by explosive pressures, 1, Theory and empirical field observations," *Geophysics*, **7**, pp. 144-154, 1942.

Shumway, R.H. and R. Blandford, "On detecting and estimating multiple arrivals from underground nuclear explosions," *Earthq. Notes*, **50**, p. 34, 1980.

Silver, P., "Retrieval of source-extent parameters and the interpretation of corner frequency," *Bull. Seismol. Soc. Amer.*, **73** pp. 1499-1511, 1983.

Silver, P.G. and T.H. Jordan, "Optimal estimation of scalar seismic moment," *Geophys. J. R. Astr. Soc.*, **70**, pp. 755-787, 1982.

Silver, P.G. and T.H. Jordan, "Total-moment spectra of fourteen large earthquakes," *J. Geophys. Res.*, **88**, pp. 3273-3293, 1983.

Smith, S.W., C.B. Archambeau, and W. Gile, "Transient and residual strains from large underground explosions," *Bull. Seismol. Soc. Amer.*, **59**, 2185-2196, 1969.

Snoke, J.A., "Archambeau's elastodynamical source-model solution and low-frequency spectral peaks in the far-field displacement amplitude," *Geophys. J. R. Astr. Soc.*, **44**, pp. 27-44, 1976.

Steketee, J.A., "Some geophysical applications of the elasticity theory of dislocations," *Can. J. Phys.*, **36**, pp. 1168-1198, 1958.

Stevens, J.L., *Seismic stress relaxation phenomena in an inhomogeneously prestressed medium*. Ph.D. Thesis, University of Colorado, Boulder, Colorado, 1980a.

Stevens, J.L., "Seismic radiation from the sudden creation of a spherical cavity in an arbitrarily prestressed elastic medium," *Geophys. J. R. Astr. Soc.*, **61**, pp. 303-328, 1980b.

Stevens, J.L., "The growing spherical seismic source," *Geophys. J. R. Astr. Soc.*, **69**, pp. 121-135, 1982.

Stevens, J.L., S.M. Day, H.J. Swanger, T.G. Barker, B. Shkoller, E.J. Halda, and J.B. Minster, *Modeling of block motions due to a buried explosion*. S-cubed Technical report SSS-R-82-5376, 1982.

Stewart, G.S. and H. Kanamori, "Complexity of rupture in large strike-slip earthquakes in Turkey," *Phys. Earth Plant. Inter.*, **28**, pp. 70-84, 1982.

Strelitz, R.A., "The September 5, 1970 Sea of Okhotsk earthquake: A multiple event with evidence of triggering," *Geophys. Res. Lett.*, **2**, pp. 124-127, 1975.

Strelitz, R.A., "Moment tensor inversions and source models," *Geophys. J. R. Astr. Soc.*, **52**, pp. 359-364, 1978.

Strelitz, R.A., "The fate of the downgoing slab: a study of the moment tensors from body waves of complex deep-focus earthquakes," *Phys. Earth Plant. Inter.*, **21**, pp. 83-96, 1980.

Stump, B.W. and L.R. Johnson, "The determination of source properties by the linear inversion of seismograms," *Bull. Seismol. Soc. Amer.*, **67**, pp. 1489-1502, 1977.

Stump, B.W. and L.R. Johnson, "Higher degree moment tensors—the importance of source finiteness and rupture propagation on seismograms," Geophys. J. R. Astr. Soc., **69**, pp. 721-743, 1982.

Sykes, L.R., "Mechanism of earthquakes and nature of faulting on the mid-oceanic ridges," *J. Geophys. Res.*, **72**, pp. 2131-2153, 1967.

Sykes, L.R. and M.L. Sbar, "Intraplate earthquakes, lithospheric stresses and the driving mechanisms of plate tectonics," *Nature*, **245**, pp. 298-302, 1973.

Thatcher, W.R., "Regional variation of seismic source parameters in the northern Baja California area," *J. Geophys. Res.*, **77**, pp. 1549-1565, 1972.

Thatcher, W.R. and T.C. Hanks, "Source parameters of southern California earthquakes," *J. Geophys. Res.*, **78**, pp. 8547-8576, 1973.

Tittman, B.R., *Studies of absorption in salt, 1983*. Final report, contract no. F49620-82-C-0015, Rockwell International Science Center.

Toksöz, M.N., A. Ben-Menahem, and D.B. Harkrider, "Determination of source parameters of explosions and earthquakes by amplitude equalization of surface waves: Part I, Underground nuclear explosions," *J. Geophys. Res.*, **69**, pp. 4355-4366, 1964.

Toksöz, M.N. and H.H. Kehrer, "Tectonic strain release by underground nuclear explosions and its effect on seismic discrimination," *Geophys. J. R. Astr. Soc.*, **31**, pp. 141-161, 1972a.

Viecelli, J.A., "Spallation and the generation of surface waves by an underground explosion," *J. Geophys. Res.*, **78**, pp. 2475-2487, 1973.

Virieux, J. and R. Madariaga, "Dynamic faulting studied by a finite difference method," *Bull. Seismol. Soc. Amer.*, **72**, pp. 345-369, 1982.

von Seggern, D.H. and R.R. Blandford, "Source time functions and spectra for underground nuclear explosions," *Geophys. J. R. Astr. Soc.*, **31**, pp. 83-97, 1972.

Vvedenskaya, A.V., "Determination of displacements fields for earthquakes by means of the dislocation theory," *Izv. Acad. Sci. USSR Geophys. Ser.*, **3**, pp. 277-284, 1956.

Ward, S.N., "Body wave calculations using moment tensor sources in spherically symmetric, inhomogeneous media," *Geophys. J. R. Astr. Soc.*, **60**, pp. 53-66, 1980a.

Willis, J.R., "A comparison of the fracture criteria of Griffith and Barenblatt," *J. Mech. Phys. Solids*, **15**, pp. 151-162, 1967.

Wyss, M., "Stress estimates for South American shallow and deep earthquakes," *J. Geophys. Res.*, **75**, pp. 1529-1544, 1970.

Wyss, M. and J.N. Brune, "The Alaska earthquake of 28 March, 1964: A complex multiple rupture," *Bull. Seismol. Soc. Amer.*, **57**, pp. 1017-1023, 1967.

Wyss, M., T.C. Hanks and R.C. Liebermann, "Comparison of *P*-Wave spectra of underground explosions and earthquakes," *J. Geophys. Res.*, **76**, pp. 2716-2729, 1971.

Elastic Wave Attenuation in Rock and the Transition Zone from Linearity to Nonlinearity*

J.R. Bulau, B.R. Tittmann, and M. Abdel-Gawad

Summary

In this paper we discuss the use of laboratory measurements of attenuation to (1) define the amplitude of transition from linear behavior to nonlinear behavior in various rock types under controlled environmental conditions and (2) examine the functional dependence of attenuation on strain amplitude.

Conclusions and Recommendations

On the basis of laboratory measurements of Q as a function of strain amplitude we find that the transition from linear behavior to nonlinear behavior depends on a number of factors including the strength of intergranular bonding in the rock, effective pressure, and the condition of the rock with respect to adsorbed moisture. Transition amplitudes can be small, in some cases significantly less than 10^{-6}, corresponding to stresses of about 1 bar. Improved techniques are being developed which will enable us to better delineate the linear to nonlinear transition amplitude and provide the most reliable and accurate measurements of material response to applied stresses over the widest and most useful range of amplitudes and frequencies.

Abstract

The coupling efficiency between a source explosion and the resulting seismic waves is well known to depend on differences existing between various rock types. In order to account for these differences and relate them quantitatively to the mineralogy and microstructure of various rocks, it is necessary to (1) define the radius of transition from the near field, which exhibits nonlinear behavior, and the far field, which exhibits true linear behavior; and (2) evaluate the nonlinear processes which occur in

*Work sponsored by Advanced Research Projects Agency (DOD), ARPA order number 4400, monitored by NP under contract #F49620-83-C-0065.

materials as an explosive shock front passes through them in the near field at high nonlinear amplitudes. There are two major objectives to our program: (1) use laboratory measurements to define the amplitude of transition from linear to nonlinear behavior in various rock types under controlled environmental conditions of pressure, temperature, and composition; and (2) examine the functional dependence of attenuation of strain amplitude and relate laboratory measurements to theoretical models. These measurements are especially relevant to interpretive studies of the observed decay of peak particle velocity and displacement with scaled distance from explosions.

A number of different approaches have been used by us in the laboratory to measure the attenuation of elastic waves in rock under controlled conditions. The forced resonance technique has been found useful for measuring the Q of vibrating beams under linear conditions, and for defining the amplitude of transition from the linear seismic regime to the nonlinear near field regime. Typically rocks show a linear regime at low strain amplitudes where Q is independent of strain amplitude, and a transition to the nonlinear regime at high strain amplitude where Q becomes amplitude dependent.

The amplitude of transition from the linear regime to the nonlinear regime is not the same for all rock types and depends upon the strength of intergranular bonding, confining pressure, and the amount of water contained within the rock. We have documented these observations with experimental measurements. These results suggest that the mechanism for nonlinear attenuation involves internal friction between grains. For sandstone and poly-crystalline salt. Our experimental evidence also demonstrates that the presence of even small amounts of moisture in the form of surface adsorbed water can significantly reduce the transition amplitude. The water evidently has the effect of reducing the coefficient of friction along intergranular contacts, resulting in a decrease in the frictional stress required for intergranular shear.

Whereas most of our measurements have been acquired with the forced swept resonance technique, we have begun data acquisition with two other complementing techniques for measurements at high amplitudes and low frequencies. First, at relatively high frequencies (>10 Hz) a modified resonance type of measurement can be performed. The resonant vibration is excited very quickly and the vibration amplitude is monitored as a function of time during the free decay. The second technique, which is most useful at relatively low frequencies (0.01-5 Hz), requires simultaneous measurements of stress and strain in a specimen which is subjected to cyclic loading. The Q can then be obtained from an analysis of the time functions of stress and strain.

Introduction

It is well known that the efficiency of coupling between a source explosion and resulting seismic waves depends upon various factors, including the source rock type, whether the explosion was tamped or detonated in a cavity, and the condition of water saturation in the source rock. When interpreting seismic signals it is useful to consider the near field source regime independently of the far field seismic regime. The boundary between these two regimes is often described in terms of how the material responds to the stresses associated with the seismic pulse. In the near source regime material response is nonlinear, inelastic, and amplitude dependent. In the far field the material behavior is linear anelastic, and independent of amplitude.

The usual approach to a quantitative description of the seismic source involves measurements of particle motions at distances which are relatively close to the source. These free-field particle motion measurements generally show that peak displacement, velocity, and acceleration decay more quickly with increasing scaled distance than that predicted from simple geometric spreading in a perfectly linear elastic medium. Laboratory studies have shown that the amplitude of transition from the linear anelastic seismic regime to the nonlinear near source regime can occur at very low amplitudes. In some cases, as shown below, nonlinear effects have been observed at strains significantly lower than 10^{-6}, which corresponds to a stress of approximately 1 bar. On the basis of these measurements it must be concluded that the free field particle motion measurements which are frequently used for calculating the reduced displacement potentials were not obtained at linear amplitudes, and therefore may not be suitable for defining the seismic source. We have found (Tittmann, 1983) that measurements of Q as a function of vibration amplitude can be used as a very sensitive indicator of the transition amplitude from linearity to nonlinearity. It is, therefore, our objective to (1) shed light on this problem by using laboratory measurements to define the amplitude of transition from the seismic regime to the near source regime in various rock types under controlled conditions of pressure, temperature, and rock type, and (2) examine the functional dependence of attenuation on strain amplitudes up to 10^{-4}, and compare these measurements to theoretical models.

Available experimental results indicate that the amplitude of transition can depend upon a number of factors, including pressure and the strength of intergranular bonding. In a compilation of experimental results Stewart *et al.*, (1983) have shown that relatively well bonded materials exhibit a higher amplitude of transition than relatively poorly cemented materials. The measurements on quartzite and proxenite presented by

Gordon and Davis (1968) indicate a transition amplitude near strains of 10^{-5}. The measurements on limestone by Peselnick and Outerbridge (1961) show a transition amplitude greater than 10^{-5}. These contrast with measurements by Johnston and Toksöz (1980) and Winkler *et al.*, (1979) on various sandstones, which show significant nonlinearity at strains below 10^{-6}. In a more recent experimental study Tittmann *et al.*, (1981) examined the effects of strain amplitude and confining pressure on attenuation in Berea and Boise sandstones. They demonstrate that while the porosity and permeability of these two sandstones are similar, the Boise sandstone exhibits strong intergranular bonding due to silica overgrowths, while the Berea sandstone exhibits relatively weak intergranular bonding with clay. Contrasting with Berea sandstone, the Boise sandstone exhibits relatively high compressive strength and modulus, a relatively small effect of strain amplitude on attenuation, and a relatively high amplitude of transition from near linearity to significant nonlinearity. Attenuation in Berea sandstone is also relatively more sensitive to confining pressure. Tittmann (1983) has examined the effects of confining pressure on attenuation in natural dome salt. He clearly demonstrated that the amplitude of transition in this material increases with increasing confining pressure. These results are consistent with the arguments of Mavko (1979) and Stewart *et al* (1983) that nonlinear attenuation can be explained by frictional sliding along intergranular surfaces. Increasing the confining pressure on the rock increases the forces normal to intergranular surfaces, resulting in increased frictional stress and an increase in the strain amplitude required to exceed the elastic limit.

In the remainder of this paper we will present some experimental results which complement the above mentioned studies, and show that small amounts of water in the form of a surface adsorbed layer can also affect the transition amplitude. Finally, we will discuss briefly some of the issues which must be considered prior to applying measurements of nonlinear Q, using small specimens in the laboratory, to free-field seismic data.

Effects of Moisture on Attenuation in Berea Sandstone

1. **Experimental Methods:** A cylindrical sample of Berea sandstone 1.42 cm in diameter and 12.34 cm long was suspended in the resonating bar apparatus, which is illustrated schematically in Fig. 1. The apparatus was contained in a controlled atmosphere chamber, and attenuation values were obtained using both torsional and flexural modes of vibration, at various ambient humidity levels between 0% *RH* and 93% *RH*.

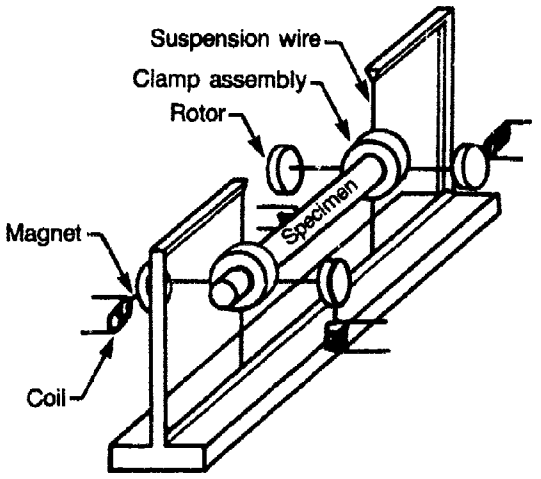

Fig. 1. Schematic illustration of the resonating bar apparatus.

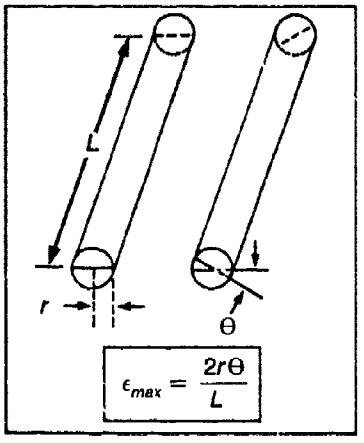

Fig. 2. Definition of strain amplitude in torsion.

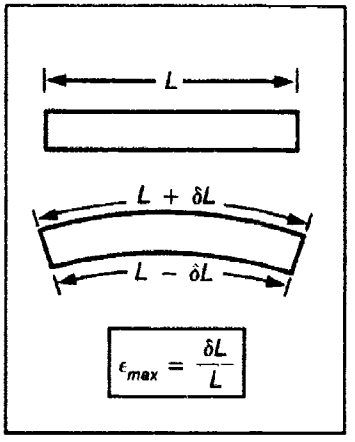

Fig. 3. Definition of strain amplitude in flexure.

Q was calculated by taking the ratio of the resonant frequency to the bandwidth of the forced resonance peak. Maximum strain amplitude is defined in Figs. 2 and 3.

2. **Experimental Results:** At all humidities up to 31% *RH* the results, which are illustrated in Figs. 4 and 5, indicate the existence of a linear, strain independent Q at relatively low amplitudes, with a transition to a nonlinear, amplitude dependent Q at relatively high amplitudes. The magnitude of the linear attenuation increases with increasing humidity, and the amplitude of transition decreases with increasing humidity.

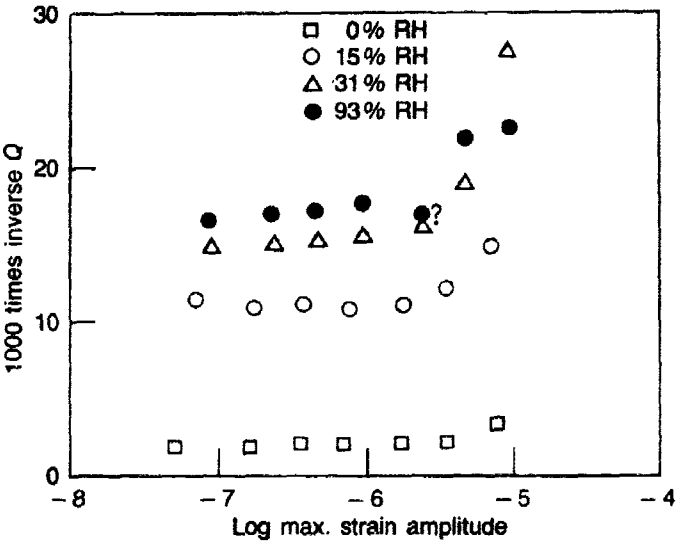

Fig. 4. Attenuation *vs* strain amplitude for Berea sandstone resonating (200 Hz) in flexure at several different ambient humidity levels.

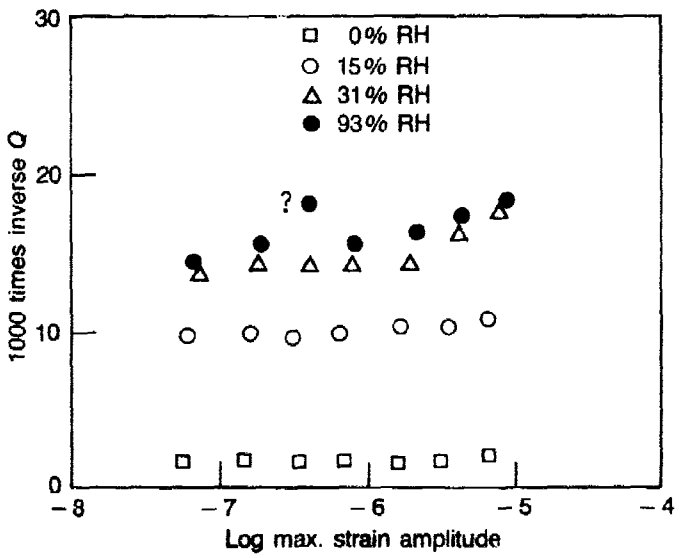

Fig. 5. Attenuation *vs* strain amplitude for Berea sandstone resonating (210 Hz) in torsion at several different ambient humidity levels.

Tittmann (1983) presents similar results for hydrostatically pressed salt specimens. These results indicate that the most important linear anelastic attenuation mechanism involves the relaxation of stresses within the hydrous layer located on intergranular crack surfaces and grain boundaries. We also observe that the amplitude of transition deceases with increasing humidity. In the context of the frictional attenuation model (Mavko, 1979; Stewart *et al.*, 1983) this would indicate a reduction with increasing humidity in the coefficient of friction between opposing crack faces.

Nonlinear Q Measurements

Although the resonant bar-type measurements are well-suited for measuring attenuation and modulus in the linear anelastic regime, and for defining the transition amplitude from linear to nonlinear behavior, several other issues need to be considered before one can apply the high amplitude nonlinear Q measurements to studies of high amplitude seismic pulse propagation in the near field.

1. **Forced Resonant Vibrations:** Q is frequently calculated from the ratio of the resonant frequency to the bandwidth of the resonance peak measured at half power amplitude. It is well established (cf. Nowick and Berry, 1982) that this is a sound technique for measuring Q in a material with linear response. However, this may not be a particularly satisfactory technique for measuring energy dissipation in a material with properties that depend on vibration amplitude. In most rocks, when vibrations exceed the elastic limit the modulus decreases with increasing vibration amplitude, probably due to frictional sliding along microcracks (Mavko, 1979; Tittmann *et al.*, 1982; Tittmann, 1983). The shape of the resonance peak at low amplitude is nearly symmetrical. At high amplitudes the peak becomes severely skewed toward the high frequency side. We have observed this effect at high amplitude in all but the most tightly consolidated rock types. The observation is illustrated in Fig. 6 for natural dome salt at 0.689 MPa effective pressure. This result casts suspicion on the usefulness of the swept forced resonance technique for obtaining reliable measurements of Q and modulus at high nonlinear amplitudes.

2. **Definition of Strain Amplitude:** Another problem with measuring nonlinear Q involves the definition of strain amplitude. Strain amplitude is usually calculated for a position of maximum strain in the specimen, as in Figs. 2 and 3. Using this convention first-order strains vary from zero to the maximum value reported, depending on location within the specimen. Since the attenuation measurements reported do not represent values for incremental units of volume exposed to homogeneous train, as would be the case for free field vibrations, it is felt that a careful analysis of the stress field within the specimen is necessary.

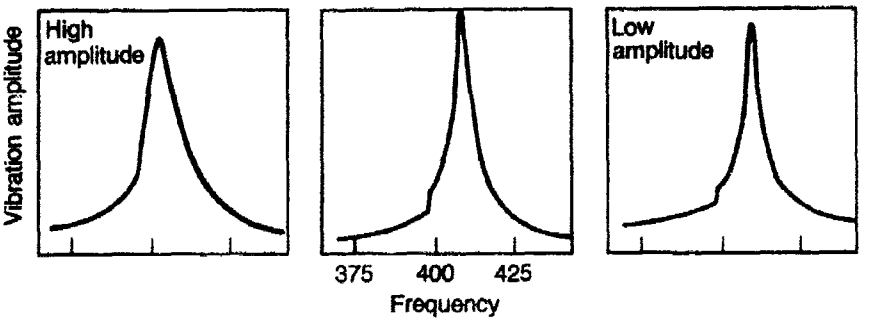

Fig. 6. Illustration of the shape of swept resonance peaks. Low amplitude vibrations within the linear regime are generally nearly symmetric, as shown in the lower frame (2.9×10^{-8} maximum strain), while skewness is apparent at higher strains (2.2×10^{-7}, center; and 1.0×10^{-6}, top).

3. **Memory Effect:** Another problem, which is somewhat more subtle involves the response of the specimen to repeated cycles of vibration at very high nonlinear amplitudes. The test specimens appear to have a memory, such that the first elastic pulse propagates through a material which has come to equilibrium with a more or less static environment over a relatively long time period. Each subsequent pulse passing through the material sees the accumulated changes resulting from exposure to previous pulses, while causing changes itself.

The forced resonance technique measures modulus and attenuation in a specimen which has come to equilibrium after exposure to a long train of high amplitude pulses. The accumulated effects of repeated cycles at high amplitude is demonstrated in Fig. 7. The test specimen was a piece of natural dome salt vibrating in torsion at an effective pressure of 0.7 MPa. The amplitude of forced resonant vibration was monitored as a function of time with constant driving power. Peak vibration amplitude was controlled using a lock-in amplifier. The decrease in vibration amplitude increases with repeated exposure to high stress levels. (The effects are reversed in a comparable period of time.)

Preferred Techniques for Nonlinear Measurements

It is apparent that if the results of high amplitude Q measurements are to be applicable to seismic pulse propagation in the near field environment the number of high amplitude pulses should be minimized. The procedures outlined below are being developed for the purpose of measuring linear and nonlinear attenuation and modulus on granite and natural dome salt.

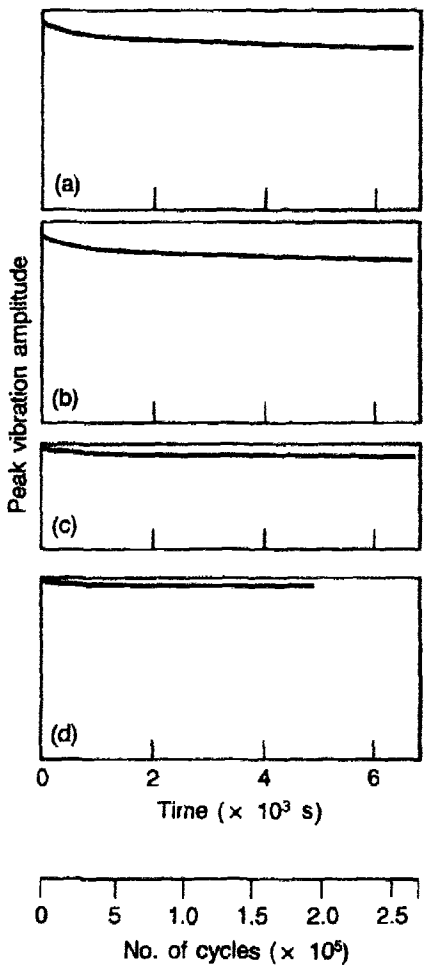

Fig. 7. Demonstration of accumulated damage caused by repeated exposure of dome salt sample to high amplitude torsional vibrations. Sequence (a) to (d) corresponds to decreasing vibration amplitude. (Strains: (a) 1.1×10^{-6}, (b) 7.6×10^{-7}, (c) 3.5×10^{-7}, (d) 1.0×10^{-7}.) See text for complete details.

1. **Modified Resonance Technique:** One possible technique for measuring Q at high nonlinear amplitude involves monitoring the free decay of vibration amplitude in a test bar which is rapidly accelerated to high initial nonlinear vibration amplitude. A preliminary version of this experiment has not been tested in the laboratory. Representative results are shown in Fig. 8. The sample of natural dome salt was accelerated to high amplitude using a 22 cycle sinusoidal wave train at the resonant frequency of 410 Hz. A non-contact coil and magnet-type transducer was used to couple the electrical signal to the sample. Vibration amplitude was monitored with a second transducer of the same type. The signal from this transducer was amplified, digitized, and stored for analysis. In future

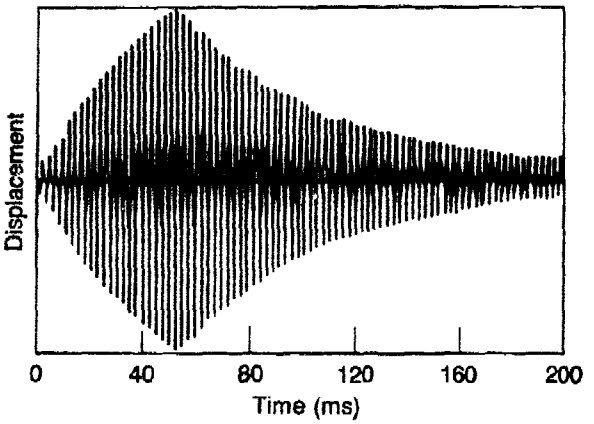

Fig. 8. Graph of vibration amplitude *vs* time for natural dome salt at 0.7 MPa effective pressure vibrating in torsion. Sample was driven at the 410 Hz resonant frequency for 22 cycles, followed by a period of free decay.

experiments a mechanical impact technique may be used in order to excite vibrations at even higher amplitudes than can be obtained using electromagnetic transducers.

For a liner solid the envelope of free decay of vibration amplitude with time is given by

$$A(t) = A_o \exp(-\tfrac{1}{2}\omega t\, Q^{-1}) \tag{1}$$

where A_o is vibration amplitude at time t_o, $A(t)$ is vibration amplitude at time t,ω is angular frequency, and Q^{-1} is attenuation. For nonlinear materials Mavko (1979) proposed an amplitude dependent frictional attenuation model in which the attenuation is a linear function of strain, ϵ,

$$Q^{-1}(\epsilon) = Q_o^{-1} + \alpha\epsilon \tag{2}$$

where Q_o^{-1} is a value of anelastic attenuation taken at low strain, and may depend on frequency. Minster (1982) and Minster and Archambeau (1983) used this relationship to explain the decay of peak displacements and velocities measured as a function of scaled distance in the COWBOY series of explosions in dome salt. In our experiments we will fit the decay envelope to a decay function similar to Eq. (1), but expanded to include an amplitude dependent Q function, as in Eq. (2).

2. **Stress-Strain Measurement Apparatus:** Rockwell has funded a program to build an apparatus for measuring complex modulus through analysis of the stress and strain time functions. The apparatus is modeled

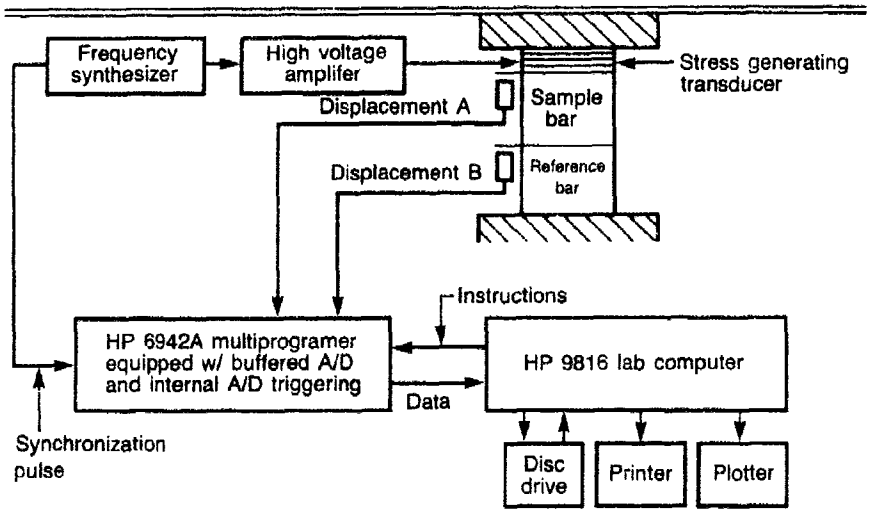

Fig. 9. Schematic illustration of the low-frequency complex modulus appartus.

after the design of Liu and Peselnick (1983). It is illustrated schematically in Fig. 9. A test sample bar and a high Q linear elastic reference bar are oriented in series with a piezoelectric stress generating transducer. Displacement is measured using non-contact capacitive transducers at two locations, one at the top of the reference bar and one at the top of the sample-reference assembly. the displacement on the reference bar can be translated into stress provided that the spring constant is known. The difference between the two displacements corresponds to sample strain. The amplitude and shape of the loading curve can be controlled by modulating the voltage on the piezoelectric transducer. An operating range from below 0.01 up to about 5 Hz is expected. For very low amplitude measurements with poor signal to noise ratio the system is designed for extensive signal averaging.

For a linear material

$$Q^{-1} = \phi = \frac{\Delta E}{4\pi E} \tag{3}$$

where ϕ is the phase angle between the sinusoidal stress applied to the sample and the resulting sinusoidal strain, ΔE is the area of the elliptical hysteresis loop, and E is the energy of one full loading cycle. For a nonlinear material, a sinusoidal load function does not result in a sinusoidal displacement function, and it is best to calculate Q from measurements of both

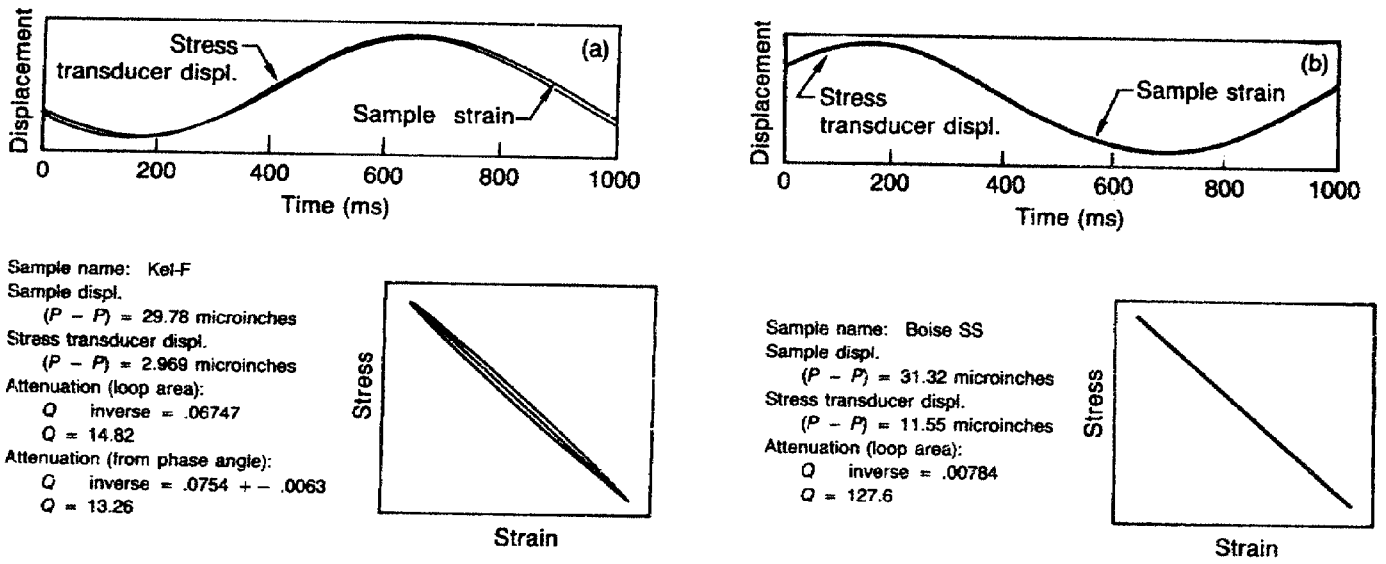

Fig. 10. Preliminary results of attenuation measurements at 1 Hz taken with the low-frequency complex modulus apparatus illustrated in Fig. 9. Test specimens were Kel-F teflon (a) and Boise sandstone (b).

the area under the loading curve and the area of the hysteresis loop. Nonlinearity manifests itself as harmonic distortion when the results are recast into the frequency domain.

Some preliminary results of measurements on Boise sandstone and Kel-F teflon are presented in Fig. 10. Both sets of measurements were made at 1 Hz. An open hysteresis loop is clearly evident in the low Q Kel-F specimen. The loop is relatively small in the high Q Boise sandstone specimen. The area of the loop is, however, measured reproducibly provided that sample signal to noise ratio is reasonably high, as illustrated in the figure.

References

1. Gordon, R.B. and L.A. Davis (1968) "Velocity and Attenuation of Seismic Waves in Imperfectly Elastic Rock," *J. Geophys. Res.*, **73**, 3917-3935.
2. Johnston, D.H. and M.N. Toksoz (1980) "Thermal Cracking and Amplitude Dependent Attenuation," *J. Geophys. Res.*, **84**, 937-942.
3. Liu, H.-P, and L. Peselnick (1983) "Investigation of Internal Friction in Fused Quartz Steel, Plexiglass, and Westerly Granite from 0.01 to 1.00 Hertz at 10^{-8} to 10^{-7} Strain Amplitude," *J. Geophys. Res.*, **88**, 2367-2379.
4. Mavko, G.M. (1979) "Frictional Attenuation: An Inherent Amplitude Dependence," *J. Geophys. Res.*, **84**, 4769-4776.
5. Minster, J.B. (1982) "Effects of Near-Field Nonlinear Attenuation on Outgoing Seismic Wavefields (abstr.)," *Terra Cognita*, **2**, 153.
6. Minster, J.B. and C.B. Archambeau (1983) "High Strain Nonlinear Attenuationin Salt and its Effects on Near-Source Outgoing Seismic Wavefields, presented at the Fifth Annual DARPA/AFOSR Symposium on Seismic Detection, Analysis, Discrimination, and Yield Determination," Orcas Island, East Sound, Washington, 16-18 May, 1983.
7. Nowick, A.S. and B.S. Berry, "Anelastic Relaxation in Crystalline Solids," Academic Press, New York, 1972, 677 pp.
8. Peselnick, L. and W.F. Outerbridge (1961) "Internal Friction and Rigidity Modulus of Solenhofen Limestone Over a Wide Frequency Range," *U.S. Geol. Surv. Prof. Pap.*, **400B**.
9. Stewart, R.R., M.N, Toksöz, and A. Timur (1983) "Strain Amp · Attenuation: Observations and a Proposed Mechanism," *J. Geophys. Res.*, ' 6-5[illegible].
10. Tittmann, B.R. (1983) "Studies of Absorption in Salt, Final Repo[illegible] Period Dec. 1, 1981 through Nov. 30, 1982 " Prepared for Air Force Office of [illegible]ific Research under contract number F49620-82-C-0015.
11. Tittmann, B.R., M. Abdel-Gawad, C. Salvado, J. Bulau, L. Ahlberg, and [illegible] Spencer (1982) "A Brief Note on the Effect of Interface Bonding on Seismic Dissipation," *Proc. Lunar and Planet. Sci. Conf.*, **12th**, 1737-1745.
12. Winkler, K., A. Nur, and M. Gladwin (1979) "Friction and Seismic Attenuation in Rocks," *Nature*, **227**, 528-531.

Linear Elastic Waveform Modeling in the Inelastic Region of Underground Nuclear Explosions

L.J. Burdick, J.S. Barker, D.V. Helmberger and D.G. Harkrider

Summary

In an attempt to characterize the way in which linear elastic theory breaks down within the inelastic region near underground nuclear explosions, we have compared the observed velocity waveforms from the inelastic region with predictions of ordinary elastic generalized ray theory. In earlier studies, models for events at both Pahute Mesa and Amchitka were developed using ground motion recordings from the 5 to 20 km distance range. The models consisted of a source time function and a source strength, ψ_∞, for a point source in a layered elastic crust. In this study the predictions of the models were evaluated at ranges from 0 to 5 km. Surprisingly, the elastic models predict the observed peak vertical velocity very accurately even in the spall zone. They also predict the rise times of the velocity pulses into surface zero. The elastic synthetic seismograms match the observed velocities up until the time when the spalled material begins to decelerate. The observed radial motions are much more poorly modeled. Nevertheless, the results suggest that only low-order corrections to elastic theory may be required to explain some of the phenomena within the inelastic region of contained nuclear explosions.

Vertical velocity waveforms within the spall zones of Amchitka and Pahute Mesa events are well modeled by linear elastic theory during the compressive pulse prior to spall. We introduce the definition of the "compressive elastic radius."

The inelastic region of an underground nuclear explosion is generally considered to include not only the zone of high deformation and high strain immediately surrounding the explosion, but also that portion of the subsurface that undergoes spall. Eisler and Chilton (1964) and Chilton, *et al.*, (1966) have defined spall as rock failure that occurs when the downgoing tensional stress wave that results from a reflection at the free surface exceeds the sum of the upward compressional stress, the lithostatic stress

and the tensile strength of the rock. Previous computations of the motions within the spall zone have involved numerical approximations to the full non-linear problem (*e.g.*, Viscelli, 1973; Day *et al.*, 1983, 1983). Due to the extreme deformations, spalling is certainly an inelastic process, but is may be reasonable to assume that in the period of upward compression immediately preceding spall, the material behavior is only mildly nonlinear. This paper reports an attempt to characterize the degree to which linear elastic theory breaks down within the spall zone of underground nuclear explosions.

In previous studies, detailed crustal structure models and source function representations have been developed for events at Amchitka (Burdick *et al.*, 1984) and Pahute Mesa (Hartzell *et al.*, 1983) by modeling waveforms at 5-20 km epicentral distance. These results from well-within the elastic region have been used to compute synthetic seismograms for comparison with the first compressional pulse recorded within the spall zone. Ordinary elastic generalized ray theory is used, along with the Helmberger and Hadley (1981) source representation. Both upgoing and diving P waves are considered.

Results for the Amchitka event, CANNIKIN, are presented in Fig. 1. In the left panel are the observed vertical velocity waveforms (solid traces) and the elastic synthetic seismograms (dotted lines) plotted with a common origin time. the excellent agreement in arrival times indicates that lateral variations in P wave velocities are negligible. The onset of spall is indicated by a constant, $-1g$ slope in the observed velocities. The fit of the synthetics to the first rise, which is equivalent to modeling the first peak in vertical acceleration, is quite good throughout the spall zone. In particular, that the initial slope is well predicted by the elastic model indicates that inelastic effects in the direct P wave not already accounted for by the source representation are minor. The right panel of Fig. 1 summarizes the decay of peak velocities with epicentral distance. The predictions of the Burdick *et al.*, (1984) source model (solid line) match the vertical observations (circles) into ranges less than 1 km distance. The radial peak velocities (crosses) are overpredicted by the model (dashed line) by a factor of about two, indicating that radial velocities may be more sensitive to inelastic processes or variations in the structure model.

Similar results for another Amchitka event, MILROW, are presented in Fig. 2. Once again, excellent predictions of arrival times and initial slopes indicate that the crustal structure model and source representation determined by Burdick *et al.*, (1984) for waveforms recorded at 7-12 km range yield excellent predictions of the compressional pulse into surface zero. The model somewhat overpredicts the peak vertical velocities. The synthetic seismogram for the surface zero station (S-0), however, reflects

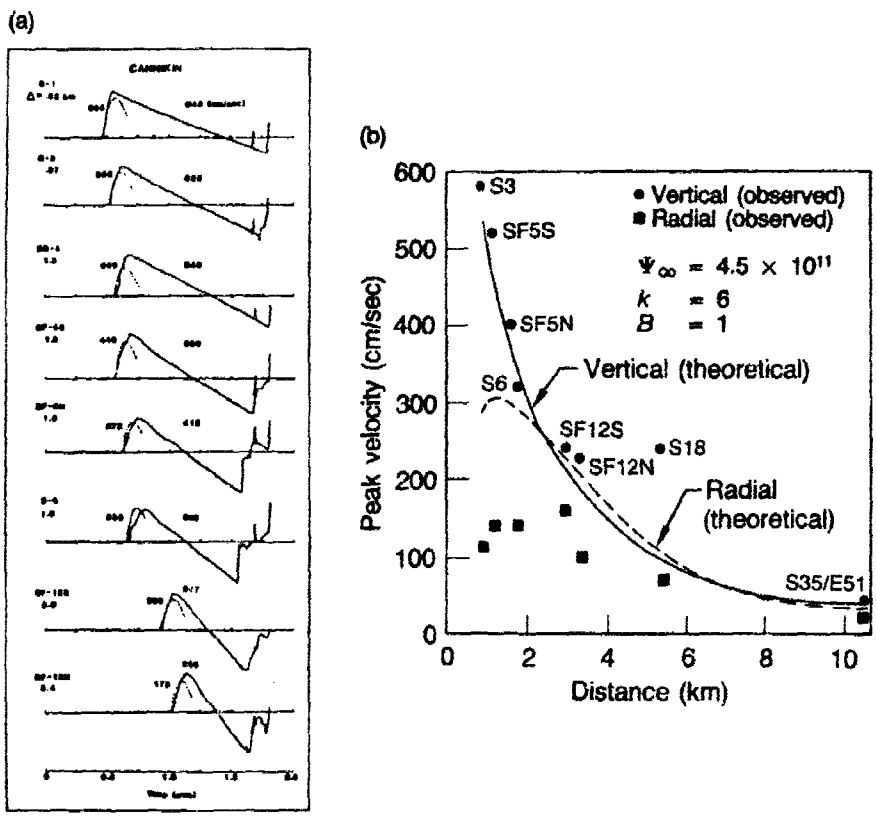

Figure 1. A comparison of the observed velocity data from within the spall zone of CANNIKAN with elastic predictions based on data from the elastic region. (a) Observed vertical velocity waveforms (solid lines) and generalized ray synthetics (dotted lines) computed for the compressional pulse prior to spall and plotted on a common scale. (b) Observed peak vertical (circles) and radial (squares) velocities and elastic model predictions (solid and dashed lines) plotted as a function of epicentral distance.

the proximity of a branch point singularity in generalized ray theory for vertical incidence. Once again the radial peak velocities are notably overpredicted.

For comparison, we now turn our attention to the Pahute Mesa event, BOXCAR, which had a yield and depth of burial similar to that of MILROW (BOXCAR: 1300 kt, 1160 m; MILROW: 1000 kt, 1219 m). Hartzell *et al.*, (1983) developed a structure model for Pahute Mesa and a source representation for BOXCAR based on waveform modeling in the distance range 4–11 km. Figure 3 presents the results into surface zero. Once again, the observed vertical velocity waveforms are plotted on the left as solid

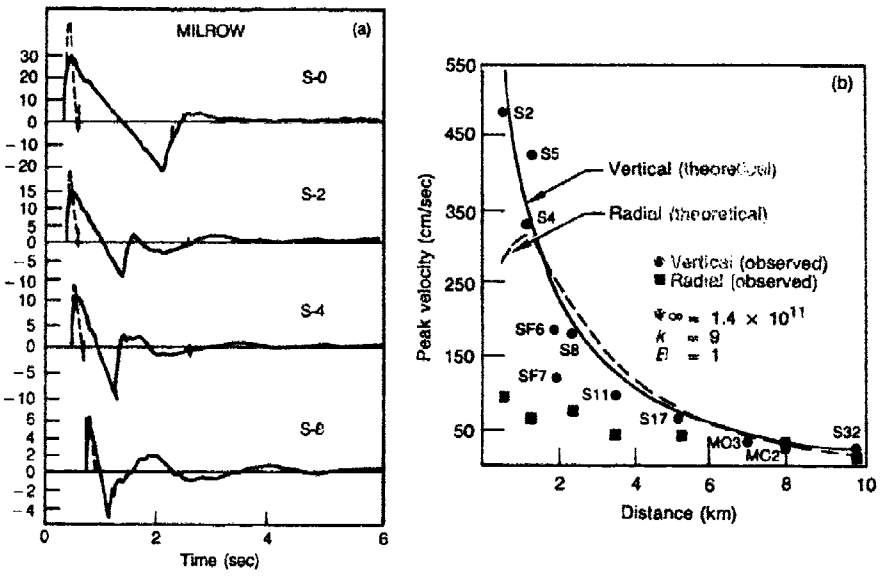

Figure 2. A comparison of observed velocity data and elastic model predictions for MILROW. (a) Observed vertical velocity waveforms (solid lines) and generalized ray synthetics (dotted lines) computed for the compressional pulse prior to spall and plotted on a common scale. (b) Observed peak vertical (circles) and radial (squares) velocities and elastic model predictions (solid and dashed lines) plotted as a function of epicentral distance.

lines and the synthetic predictions are dotted lines. The spall zone extends to just beneath station S-12; a radial distance of 3.8 km. Arrival times are not matched as well as in the Amchitka events, suggesting that lateral crustal structure variations are more prevalent at Pahute Mesa. No correction for station elevation has been made. With a slight time shift, the slope and rise time at stations S-16 and S-24 are well matched. This is to be expected, since these waveforms were used by Hartzell *et al.*, (1983) in obtaining the source model. The fit to the velocity rise times, and by implication, the peak accelerations, degrades toward surface zero, with the observed pulses significantly broader than the predictions. However, the peak vertical velocities, plotted on the right side of Fig. 3 as a function of slant range, are quite well predicted into surface zero. Radial peak velocities are, once again, overpredicted. In comparing the elastic source representation for BOXCAR and MILROW, we find that BOXCAR has a longer rise time (parameterized as a lower K value in the Helmberger and Hadley (1981) representation) than MILROW. This indicates differences in inelastic processes and coupling between Amchitka and Pahute Mesa which are included in the elastic source representations. In addition, we find that BOXCAR observed velocities include variations in

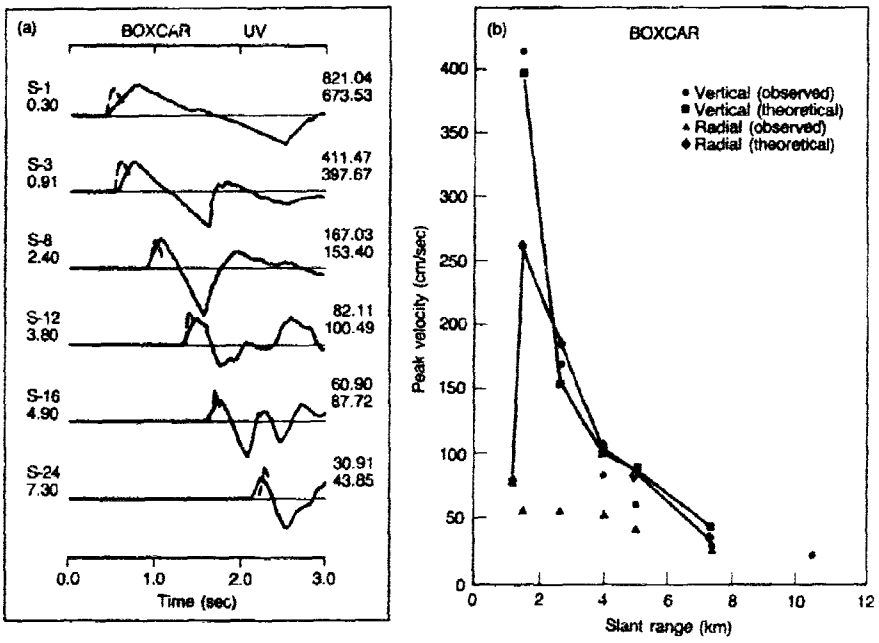

Fig. 3. A comparison of observed velocity data and elastic model predictions for BOXCAR. (a) Observed vertical velocity waveforms (solid lines) and generalized ray synthetics (dashed lines) plotted on a common scale. Noted to the right of each trace are the peak velocities in cm/s for the observed (upper) and synthetic (lower) compressional pulses. (b) Observed peak vertical (circles) and radial (triangles) velocities and elastic model predictions (boxes and diamonds, connected by lines) plotted as a function of slant range.

inelastic effects or unmodeled source or propagation effects as the direct P wave incidence angle approaches vertical.

By contrast, the Pahute Mesa event, INLET, presented in Fig. 4, shows little variation in the quality of fit into surface zero. Arrival times are not well matched, particularly where the P wave take-off angle is nearly horizontal. With slight time shifts, however, the slope, rise time and peak velocity of the compressional arrival are quite well predicted by the elastic model into surface zero.

Some justification of our approach may be obtained from measurements of peak radial stress measurements for various geological media near small underground nuclear explosions (Fig. 5, modified from Rodean, 1981, from a study by Holzer, 1966). These are effectively wholespace measurements. The radius of rock vaporization for these materials is about 2 m/kt$^{1/3}$ (Butkovich, 1967). Outside of this all materials cluster about a common strong-shock solution. At about 10 m/kt$^{1/3}$, the strong, non-porous rocks

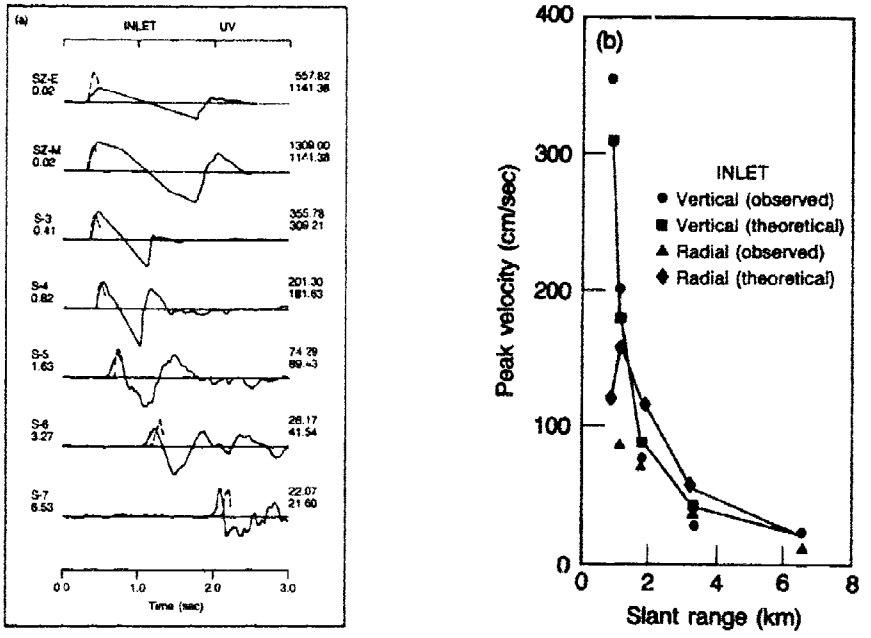

Figure 4. A comparison of observed veolcity data and elastic model predictions for INLET. (a) Observed vertical velocity waveforms (solid lines) and generalized ray synthetics (dotted lines) plotted on a common scale. Noted to the right o each trace are the peak velocities in cm/s for the observed (upper) and synthetic (lower) compressional pulses. (b) Observed peak vertical (circles) and radial (triangles) velocities and elastic model predictions (boxes and diamonds, connected by lines) plotted as a function of slant range.

begin to approximate an elastic wave solution. For the weaker, more porous materials, this change occurs at approximately 35 m/kt$^{1/3}$. Indicated by bars on the plot are the scaled slant ranges used in this study for CANNIKIN, MILROW, BOXCAR and INLET. The basalts and pillow lavas of Amchitka are probably very similar to the granite and sale measurements, and would be expected to fall on the upper elastic curve. The tuffs and rhyolites of Pahute Mesa, on the other hand, would plot on the lower curve with tuff and alluvium. Continuing the analogy, we see that all of the surface recordings used in this study fall outside of the wholespace elastic radius for their respective media, and that the radius for Pahute Mesa should be larger than for Amchitka.

Returning to the more realistic case of a layered half-space, we may define the "compressive elastic radius" as the radius beyond which the material response is elastic while under compression. The concept is illustrated in the upper panel of Fig. 6, in which the "compressive elastic radii" for MILROW and BOXCAR are displayed. The effects of inelastic

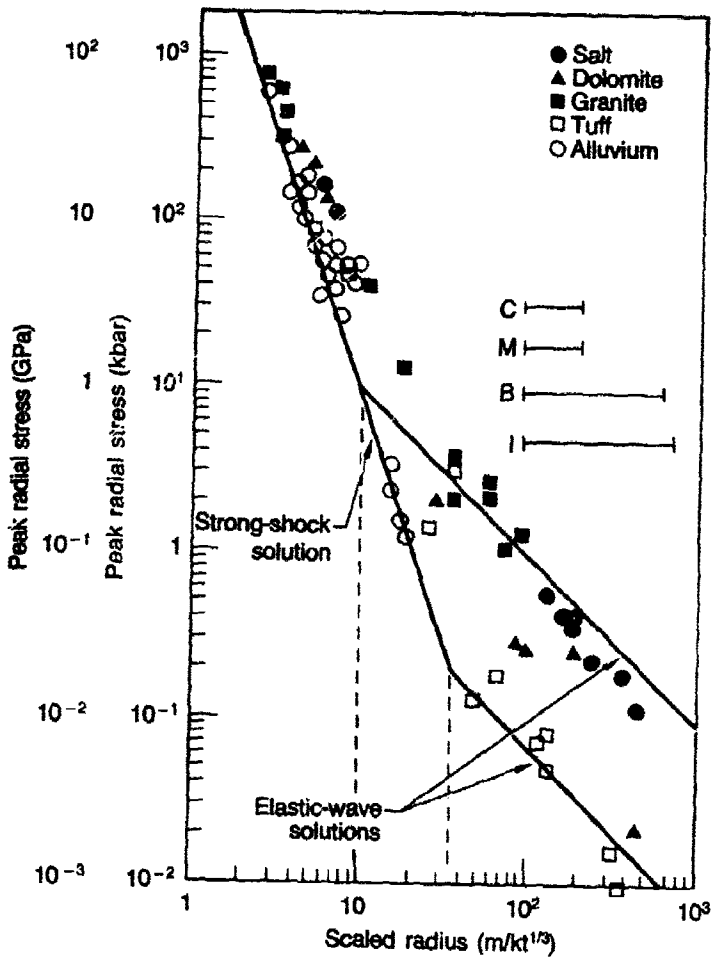

Figure 5. Measurements and theoretical solutions for peak radial stress produced by small underground nuclear explosions for a variety of geological materials. Dashed lines indicate the wholespace elastic radii for strong, nonporous media and weak, porous media. Bars indicate the scaled slant ranges of the surface velocity data used in this study. C = CANNIKAN, M = MILROW, B = BOXCAR, I = INLET. (Modified from Rodean, 1982; measurements by Holzer, 1966.)

processes within these radii are taken into account by the elastic source representations. Pahute Mesa events demonstrate greater inelastic absorption than Amchitka events due to the greater "compressive elastic radius." The variation in apparent absorption of BOXCAR waveforms into surface zero is indicative of the "compressive elastic radius" reaching near the surface. This may be attributed to a number of effects, including

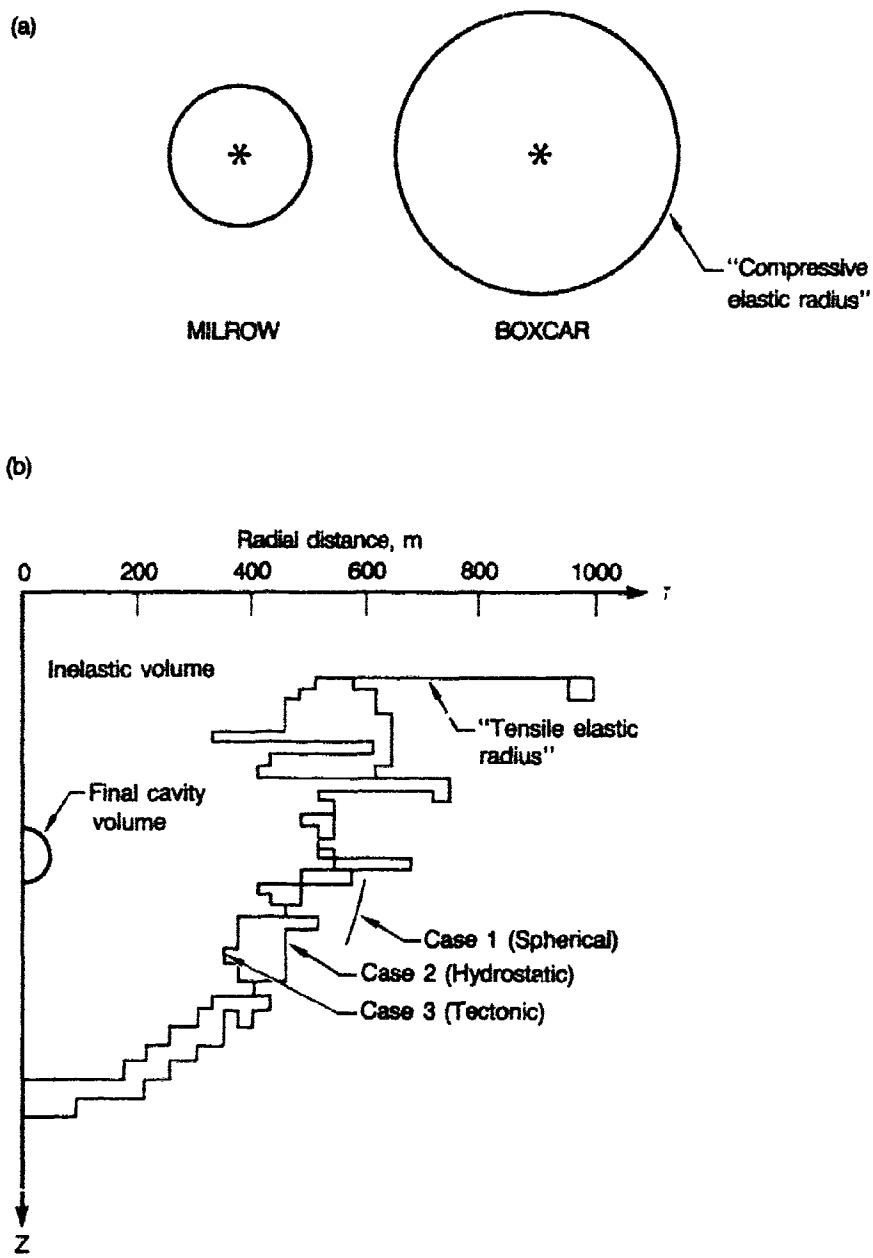

Fig. 6. (a) A schematic representation of the "compressional elastic radii" for MILROW and BOXCAR. Both events had similar yields and depths of burial, but the elastic radius under compression is greater for the Pahute Mesa event, BOXCAR, than for the Amchitka event, MILROW. (b) An example of the "tensile elastic radius" in effect after the onset of spall from a numerical approximation to the full non-linear problem by Day, *et al.*, (1982).

multiple spall openings, initiation of cavity collapse, or inelastic propagation through a "chimney" of crushed rock above the source. With the onset of spall, the "tensile elastic radius" replaces the "compressive elastic radius," encompassing the portion of the surface within the spall zone. An example from the numerical models of Day *et al.*, (1982) is shown in the lower panel of Fig. 6.

References

1. Burdick, L.J., T.C. Wallace, and T. Lay (1984), "Modeling Near Field and Teleseismic Observations from the Amchitka Test Site," *J. Geophys. Res.*, (in press).
2. Butkovich, T.R. (1967), "The Gas Equation of State for Natural Materials", Lawrence Radiation Laboratory, Report UCRL-14729, Livermore, California.
3. Chilton, F., J.D. Eisler and H.G. Heubach (1966), "Dynamics of Spalling of the Earth's Surface Caused by Underground Explosions," *J. Geophys. Res.*, **71**, 5911-5919.
4. Day, S.M., J.T. Cherry, N. Rimer and J.L. Stevens (1982), "Nonlinear Modeling of Tectonic Release from Underground Explosions, S-Cubed," Report VSC-TR-83-3, La Jolla, California.
5. Day, S.M., N. Rimer and J.T. Cherry (1983), "Surface Waves from Underground Explosions with Spall: Analysis of Elastic and Nonlinear Source Models," *Bull. Seism. Soc. Am.*, **73**, 247-264.
6. Eisler, J.D. and F. Chilton (1964), "Spalling of the Earth's Surface by Underground Nuclear Explosions," *J. Geophys. Res.*, **69**, 5285-5293.
7. Hartzell, S.H., L.J. Burdick and T. Lay (1983), "Effective Source Functions for Pahute Mesa Nuclear Tests," Woodward-Clyde Consultants, Report WCCP-R-83-3, Pasadena, California.
8. Helmberger, D.V. and D.M. Hadley (1981, "Seismic Source Functions and Attenuation from Local and Teleseismic Observations of NTS Events JORUM and HANDLEY," *Bull. Seism. Soc. Am.*, **71**, 51-68.
9. Holzer, F. (1966), "Calculation of Seismic Source Mechanisms," *Proc. Roy.Soc., London*, Ser. A, **290**, 408-429.
10. Rodean, H.C. (1981), "Inelastic Processes in Seismic Wave Generation by Underground Explosions", in "Identification of Seismic Sources—Earthquake or Underground Explosion," *Proc. of NATO ASI*, E.S. Husebye and S. Mykkeltveit, Eds., Reidel Publishing Co., Dordrecht, Holland.
11. Viscelli, J.A. (1973), "Spallation and the Generation of Surface Waves by an Underground Explosion," *J. Geophys. Res.*, **78**, 2475-2487.

Spall Contribution to Local Seismograms

Roy J. Greenfield

Summary

The contribution of spall to seismograms at local distances (tens of km) is investigated. Numerous teleseismic observations have shown spall effects. Thus, it is reasonable to expect that it will affect the local waves. We concentrate on the short period (.25 to 2. Hz) surface waves at local ranges. Understanding these local records may be useful in characterizing the source and thus how spall will affect near regional seismograms. The spall-generated local waves are also important to the extent that scattering from them contributes to wave complexity and the coda on regional and teleseismic records.

Seismograms are modeled using a numerical wave number integration program. In addition to the normal explosion ssource, the spall is included by a surface distribution of vertical point sources added with proper delay. At each point on the surface the point source is given the time function suggested by Day et al. (1983); a numerical superposition is made of the surface contributions. The synthetics may be verified by comparison to local CANNIKIN and MILROW records, because the spall extend of these explosions is well documented.

Introduction

The phenomenon of spall may have important effects on the seismic signals from underground nuclear explosions. To improve estimates of the size of explosions it is important to understand the effect of spall on the signal. This paper considers the generation, by spall, of Rayleigh waves observed at local distances. A method is developed to use source area measurements of spall extent to predict the local Rayleigh wave amplitude. The method is similar in conception to that used by Viecelli (1973). The method is applied to the surface waves observed for the CANNIKIN event. This event was used because free-field measurements were available to generally determine spall extent and several stations in the 10 to 20 km distance range recorded clear surface waves. The purpose of the calculation is to show if the spall effects the one to four second period surface waves or if they are mainly due to the direct blast wave.

Method of Computing the Spall Wave

The spall at any point is included as a vertical force time function applied at the surface. Early work (*e.g.*, Viecelli, 1973) simply used a vertical downward time impulsive force applied at the time of spall landing. The form of this impulse, per unit area of surface, is

$$F_I(T) = V_0 \cdot H \cdot \rho \cdot \delta(t_L)$$

where V_0 is the initial spall velocity, H is the spall layer thickness, ρ is the density and $\delta(t_L)$ is the delta function at the landing time.

Recent work (Bache *et al.*, 1982; Day *et al.*, 1983) gives persuasive theoretical and computational evidence that suggests that the spall force time function should not be modeled as a single downward force but rather one that does not impart a net momentum to the Earth. This model is represented by the time function of a downward impulsive force of the magnitude $V_0H\rho$ at spall launch time, a second equal downward force at the time of landing, and a constant upward force, due to the removal of the spall mass of $2V_0H\rho/T_s = 2H\rho g$ where T_s is the time extent of the spall and g is the gravity force. This force time function, denoted by $F_c(t)$, applies no net momentum to the Earth. The majority of the computations use $F_c(t)$. Though, results show that the spall component of the Rayleigh wave is not greatly different if the single impulse $F_I(t)$ is used instead.

Let $G(R,\tau)$ be the Green's Function for a vertical time impulsive point source at the distance R from the receiver. The spall force depends only on time and r, the horizontal distance from the sources to the spall; θ is the azimuth angle around the source. Then the total spall ground motion is given by a convolution over the surface and over time.

$$q_i(t) = \iint \left[F(t,r)^* G_i(R,t)\right] dr\, d\theta \qquad (1)$$

Here $q_i(t)$ is the horizontal or vertical ground velocity at the receiver $G_i(R,\tau)$ is the Green's Function for ground velocity, including the instrument and * indicates convolution.

For computational convenience the convolution in (1) was reordered as

$$q_i(t) = \int dR\left[G_i(R,t) * S(R,t)\right] \qquad (2)$$

where $S(R,t)$ is the total force time function acting at R from the source.

The integral in (2) was approximated by a sum. The $S(R,t)$ was computed using .5 km increments in both R, and r. The $G_i(R,t)$ were evaluated by the wave number integration method used by Baag (1984).

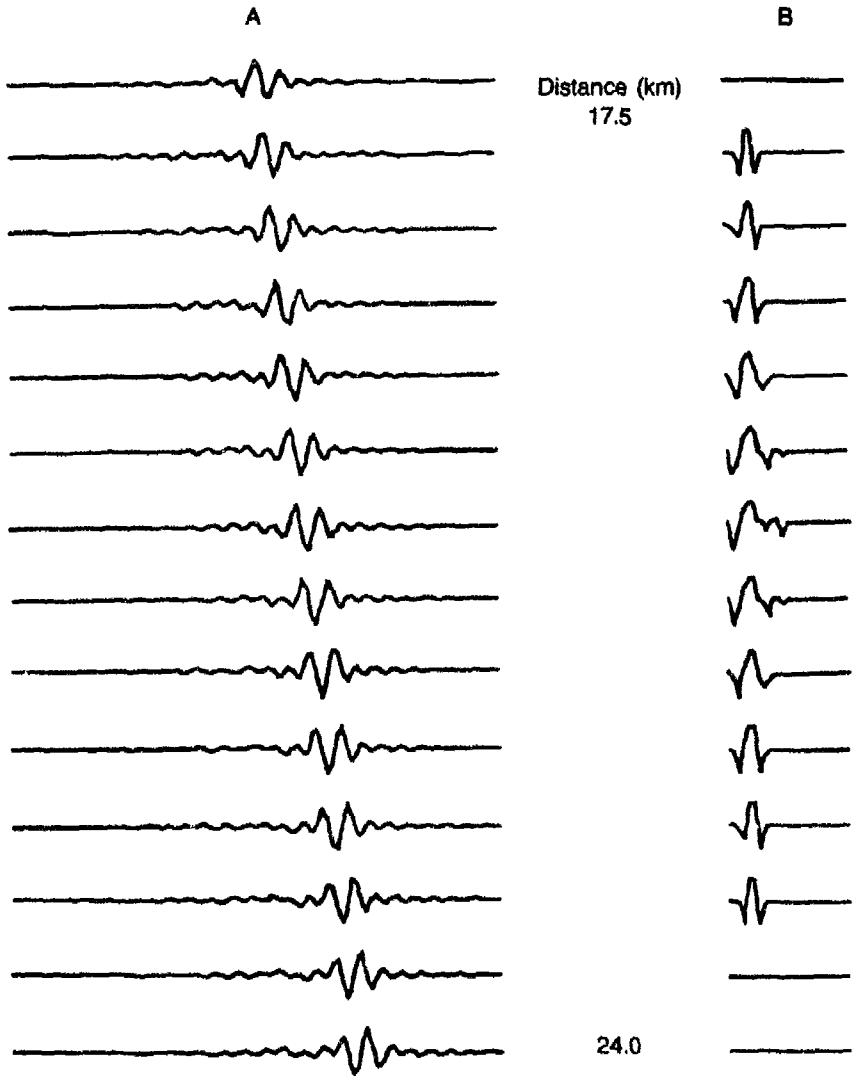

Fig. 1. A) Green's Function. B) Source Functions S(R,t). For r_m = 2.5 km, $F_c(t)$ type source.

The earth model used was Model 1 of Burdick *et al.*, 1981. Figure 1 shows the resulting vertical velocity Green's Functions, $G\ (R,t)$ for an impulsive force and the $S\ (R,t)$.

The Spall Model

Data from Perret (1973) was used to develop the spall model. Figure 2 gives the V_0 and spall arrival time curve used in the calculation of the spall

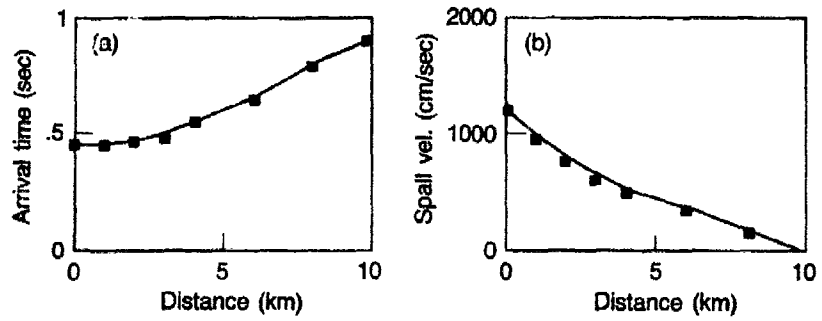

Fig. 2. Spall parameters. (a) Arrival times. (b) Spall takeoff velocity.

force time functions. T_s was calculated as $2V_0/g$. The total extent, r_m, of the spall is not known precisely but the appearance of surface records indicates at least some spall occurred to r of 6 km. A spall thickness of 9,144. cm was used in the calculations, following the analysis of Perret (1973). However, this may well be an underestimation by a factor of 2. The thickness would be on the order of 20,000 cm if the curve given by Viecelli (1973) had been used.

Results for the Spall-Generated Surface Wave

Figure 1 shows the functions $S\ (R,t)$. It should be noted that the time extent of the S is largest for the R that included the explosion point. Here the time function of $S\ (R,t)$ is approximately 2.5 seconds. This is slightly longer than the maximum spall time, T_s, of 2.3 seconds directly above the source.

Figure 3 gives the total vertical velocity response for a receiver at 20 km from the source. Synthetics are shown for assumed spall extents, r_m, of 2.5 and 4.5 km for the $F_c\ (t)$ time function. Also shown is a synthetic for a $F_I\ (t)$ source. As would be expected, the signal is more extended in time and thus, the frequency content is lower than for the individual Green's functions. The amplitude is, however, only about 3.0 cm/sec peak to peak. Figure 4 shows data at 20.0 km from CANNIKIN. The observed vertical surface wave amplitude was 20. cm/sec. thus, the theoretical spall generated surface wave amplitude was 20. cm/sec. thus, the theoretical spall generated surface wave was close to an order of magnitude lower than observed. There is no major difference for the $F_c\ (t)$ and $F_I\ (t)$ force time functions.

Figure 4 also shows velocity synthetics computed for the explosive source without spall. Results are given for a reduced displacement potential (RDP) close to that used by Burdick *et al.*, (1981). These synthetics match the amplitude of the observed 2.5 second period Rayleigh waves.

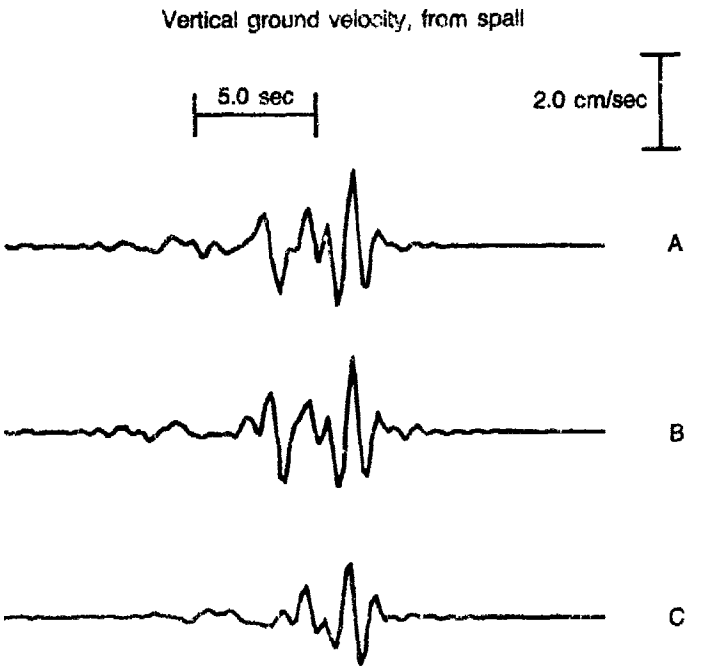

Fig. 3. Velocity synthetics for spall alone. The explosion is not included. Low pass filtered at 1.2 Hz.

A) r_m = 2.5 km, $F_c(t)$ source.
B) r_m = 4.5 km, $F_c(t)$ source.
C) r_m = 4.5 km, $F_1(t)$ Source.

However, they also have some large later arriving 1.7 second Rayleigh waves. These waves do not appear in either the CANNIKIN data nor in the MILROW synthetics given by Lay *et al.*, (1983). When we computed synthetics using a homogeneous halfspace, these higher frequency Rayleigh waves were not present. Thus, they result from the lower velocity surface material in Burdick (1981) model. Synthetics were computed using a RDP with a smaller overshoot. As shown on the figure, this reduced the amplitude of the higher frequency Rayleigh waves. It is more likely, however, that the 1.7-second waves are not in the observed data because of the lack of lateral continuity of the low-velocity surface layers.

Conclusion

The surface wave from CANNIKIN can be modeled by the explosive source alone. The size of the spall contribution is an order of magnitude

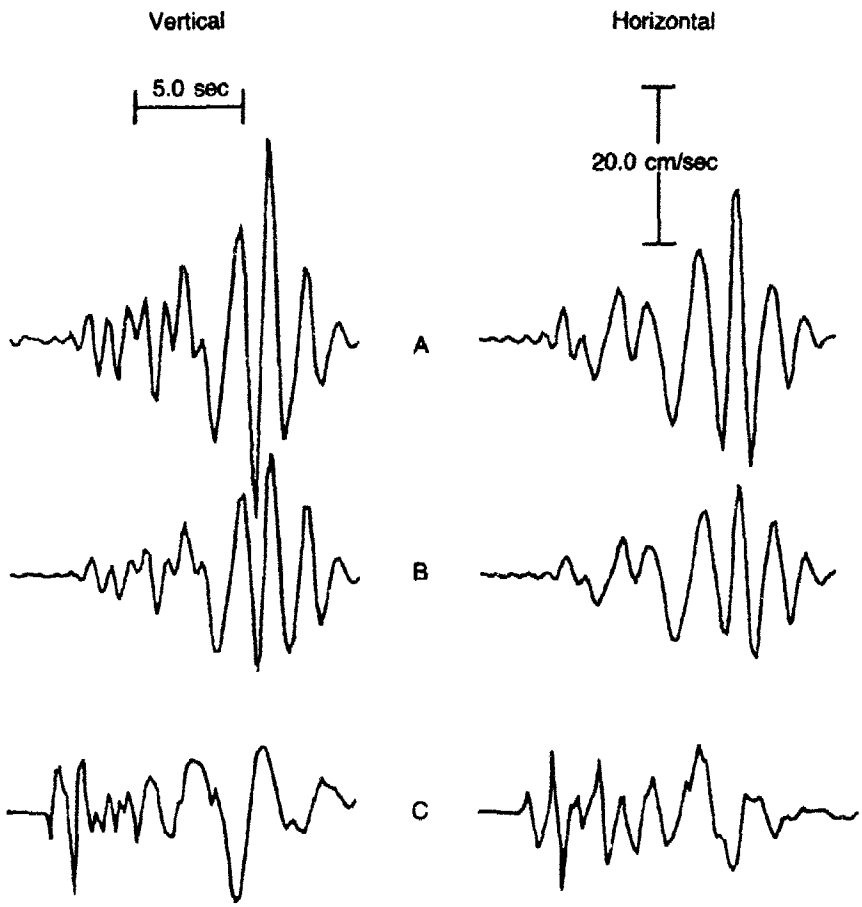

Fig. 4. Velocity Seismograms. A) Synthetic at 20 km, CANNIKIN source function. B) Synthetic at 20 km for a reduced source overshoot. C) Data for station MO7 distance = 20.7 km.

lower than the observed Rayleigh wave. The wave amplitude would however be larger if the spall thickness were greater than the 9000 cm value used. The amplitude of the .25 Hz Rayleigh wave due to the spall is not sensitive to the use of the single downward impulse time function, F_I, rather than the momentum conserving force time function, F_c. It is important to consider the spall parameter of other events to see if the spall component can be discounted, in general, as a source of short-period Rayleigh waves.

References

1. Baag, C. (1984), "Computation of the Shear-Coupled *PL* Wave." Annual Technical Report of AFOSR Contract No. F49620-83-K-0019, *Calculation of Source and Structure Parameters at Regional and Teleseismic Distances*.
2. Bache, T.C., S.M. Day, and H.J. Swanger (1982), "Rayleigh Wave Synthetic Seismograms from Multi-Dimensional Simulations of Underground Explosions," *Bull. Seis. Soc. Am.*, **72**, 15-28.
3. Burdick, L.P., D.M. Cole, D.V. Helmberger, T. Lay, and T. Wallace (1981), *Effective Source Functions from Local Surface Measurements*, Woodward-Clyde Consultants, WCCP-R-82-01, Pasadena, California.
4. Day, S.M., N. Rimer, J.T. Cherry (1983), "Surface Waves from Underground Explosions with Spall: Analysis of Elastic and Nonlinear Source Models," *Bull. Seis. Soc. Am.*, **73**, 247-264.
5. Lay, T., L.J. Burdick, D.V. Helmberger, and C.G. Arvesen (1983), *Estimating Seismic Yield and Defining Distinct Test Sites Using Complete Waveform Information*, Woodward-Clyde Consultants, WCCP-R-84-01, Pasadena, California.
6. Perret, W.R. (1973), *Ground Motion in the Vicinity of CANNIKIN Nuclear Explosion*, Sandia Labs, Report SLA-73-43. Albuquerque, New Mexico.
7. Viecelli, J.A. (1973), "Spallation and the Generation of Surface Waves by an Underground Explosion," *Jour. Geophys. Res.*, **78**, 2475-2578.

Regional Studies with Broadband Data

Lane R. Johnson and Thomas V. McEvilly

Summary

Considerable effort has been invested in obtaining high-quality broadband ground motion data that samples as much as possible of the focal sphere. A total of 13 NTS events have been recorded with up to 11 three-component stations located in the distance range of 0.5 to 10 km. Station distributions have included both networks surrounding the source and small dense arrays. The individual elements of the first-degree force moment tensor have been estimated for some of the explosions. Through frequency-wavenumber analysis, shear waves have been identified at near distances which appear to be coming from the immediate source region of the explosion. Coherency studies have been used to investigate the importance of scattering upon the records. Phase-matched filtering has been applied to regional surface wave data from NTS, providing accurate group velocity and attenuation estimates for Love and Rayleigh waves in the period range of 3 to 50 sec.

Introduction

VELA-sponsored research at Berkeley began around 1960 with the program of Dr. Don Tocher and Prof. Perry Byerly to expand their central California network of the UC Seismographic Stations, and to link for the first time such a network by FM telemetry to a central recording site (see Fig. 1). Their purpose was to improve research capabilities for studying the mechanisms of local earthquakes. Shortly thereafter, with AFOSR support, the BKS WWSSN station was installed, and a three-component, broadband (flat velocity response, 0.03–10 Hz, dual gains) station was installed at BRK with continuous slow-speed (0.06 ips) FM recording on magnetic tape. In 1964 the tape recording system was expanded to handle also six of the short-period telemetered stations.

During the subsequent two decades leading to today, the AFOSR-supported research program has concentrated on investigations into the source mechanisms of earthquakes and explosions, along with techniques for discriminating between them. From the start, the research was based largely upon the new broadband data being acquired by the network from local earthquakes and from underground explosions at the nearby Nevada

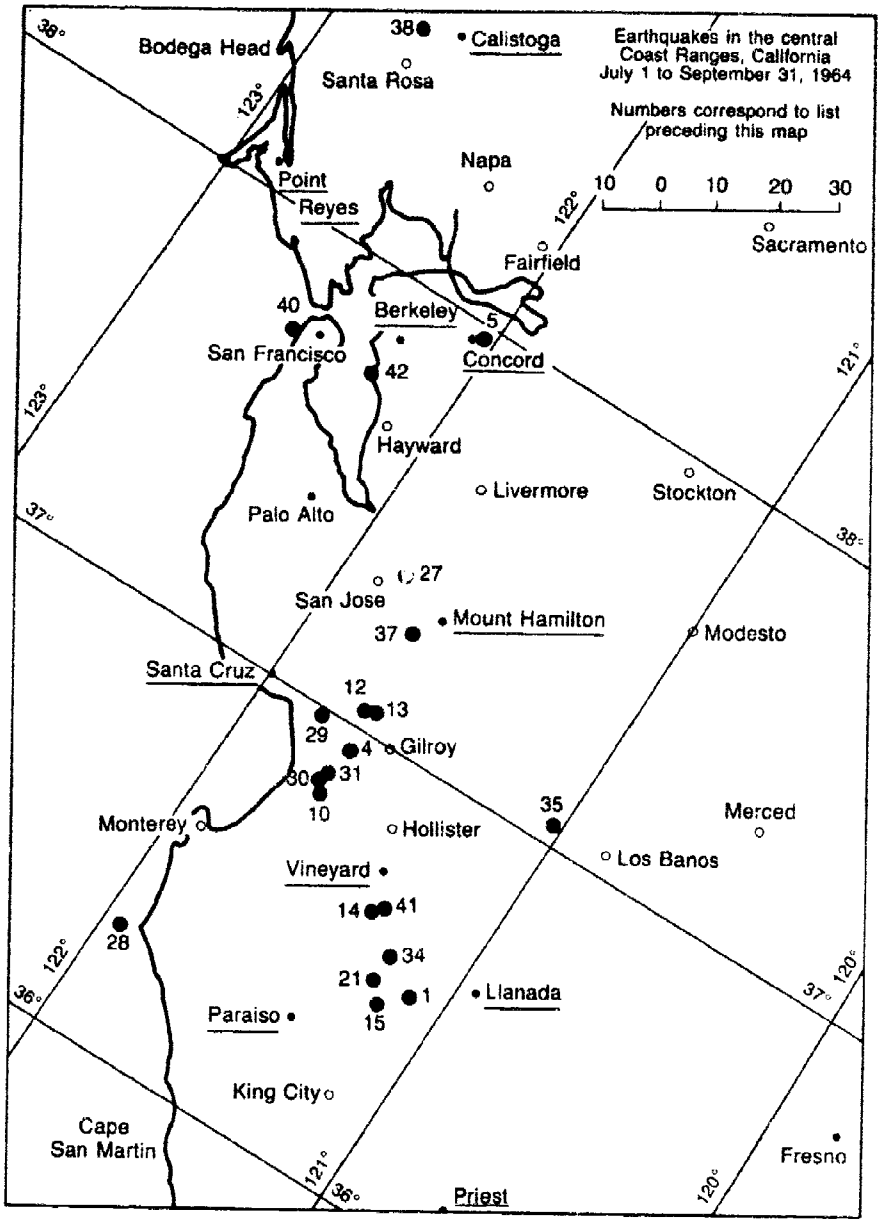

Introduction

Fig. 1. UC seismographic stations network in 1964 with third-quarter seismicity. Stations of AFOSR-supported telemetered network are underlined.

Test Site (NTS), although some studies used teleseismic data. Promising results of early discrimination studies with NTS data, along with source studies of moderate-size central California earthquakes, led to further expansion of the broadband stations to BKS, JAS, WDC and SAO (see Fig. 2). Early work on near-field observations of earthquakes, at Berkeley and elsewhere, led to initiation in the early seventies of the AFOSR "Near Field Program," a multi-institution co-operative study of the Bear Valley-Stone Canyon seismogenic zone along the San Andreas fault. Methods for inverting near-field seismograms for moment tensor components were developed, and much was learned about the characteristics of seismicity in that zone.

Scientific interest in AFOSR-related problems has in recent years moved toward the development of better understanding of the earthquake source. Using high-quality near-field data from selected NTS explosions, techniques have been developed to extract the explosion and non-isotropic components of the source function, in an attempt to better define the role of

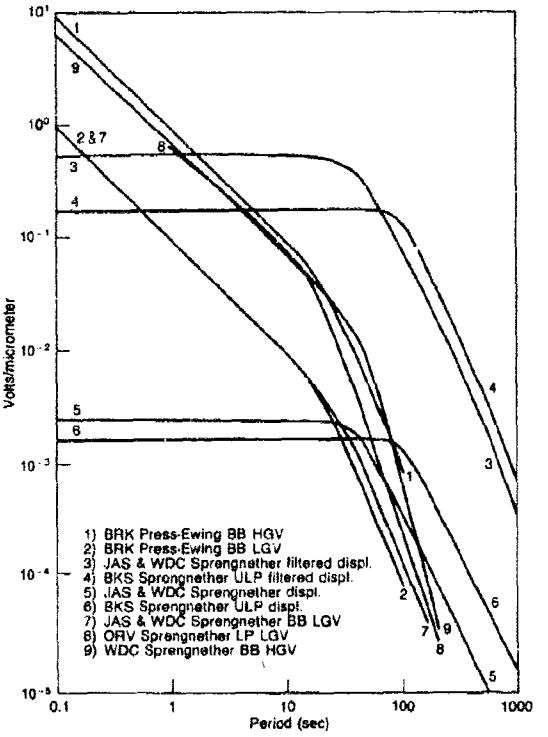

Introduction

Fig. 2. Response curves for broadband seismographs recorded on slow-speed FM magnetic tape at BRK. Displacement sensitivity (magnification) in volt/micrometer when reproduced on Honeywell LAR 7400 system (± 4 volts output).

tectonic stress release and source medium heterogeneity in shaping the elastic radiation, and thus to improve techniques for explosive yield estimation. A highly portable network of digital event recorders has been developed for these studies. In related research, the broadband data available from Lawrence Livermore National Laboratory (LLNL) for their four-station network have been used for discrimination research and, more recently, for improving crustal structure models needed in explosion source studies using regional data.

In this paper we present short reviews of several of the research studies in the AFOSR program, in an attempt to give a general overview of the Berkeley research efforts through the years. The following sections, with their figures, are self-contained. Many co-authors are represented in these selected reviews, and many other studies exist but cannot be covered in the available space. We acknowledge with warm appreciation the contributions of our colleagues at Berkeley throughout the program.

Spectral Evidence for Fault Rupture Parameters

The M_L 5.5 1966 Parkfield earthquake was well-recorded on the BRK broadband system, providing data for many investigations since. In one study the Love wave spectra were analyzed for propagation of the rupturing fault surface. This early application of directivity effects compared Love wave spectra for five of the larger earthquakes in the sequence, shown in Fig. 1. The spectra, seen in Fig. 2, reveal clear notches at periods consistent with

Spectral Evidence for Fault Rupture Parameters

FIG. 1. Love waves of the five Parkfield earthquakes used in this study.

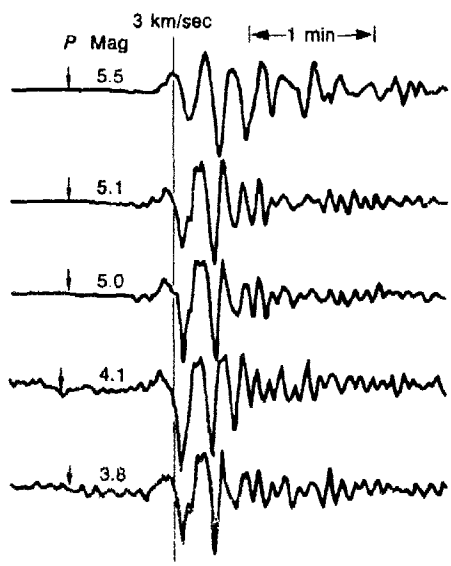

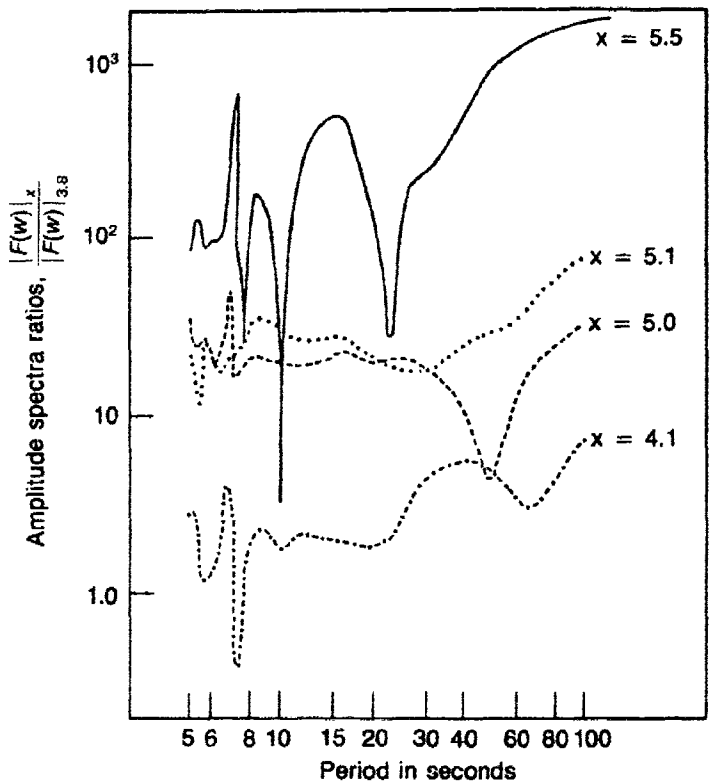

Spectral Evidence for Fault Rupture Parameters

FIG. 2. Ratios of the amplitude spectra normalized to the smallest earthquake used in this study.

a fault rupture length of about 30 km and a rupture velocity of 2.2 km/sec. The four smaller events (M_L 3.8 to 5.1) are quite similar, scaling at 10–20 sec periods closely with M_L. The 5.5 M_L main shock at these periods scales to a much larger value than its measured M_L, as seen in Fig. 2, which represents an early demonstration of the M_L saturation phenomenon.

Short Period Discriminant at Regional Distances

A spectral ratio method was shown to successfully discriminate between underground explosions and natural earthquakes when applied to the P_g phase at regional distances. The data set included 69 events recorded at the Berkeley network station JAS in the distance range 250 to 500 km and the magnitude range 2.8 to 4.5 (Table 1). The P_g spectral ratio (0.6-1.25 Hz)/1.35-2.0 Hz) shows explosions and natural earthquakes to

Table 1

Event characteristics

No.	Type	Date	OT (GMT)	Lat. (N)	Long. (W)	Δ (km) from JAS	$M^{(1)}$	Spectral ratio (P_g)	Comments
1	a	1966 February 3	18 17 37·1	37° 07′ 34″·7	116° 04′ 10″·1	380	4·2	1·00	PLAID (Y), in alluvium[4]
2	a	1966 April 1	18 40 00	37 06 09 ·7	116 01 11 ·8	395	3·6	1·90	LIME (Y), in tuff[2]
3	a	1966 April 6	13 57 17·1	37 08 22 ·3	116 08 27 ·1	385	4·1	—	STUTZ (Y), in tuff[2]
4	b	1966 April 6	17 56 31·7	37·3	115·4	450	3·6	4·60	[3]
5	d	1966 May 19	15 37 18	37 06 40 ·1	116 03 28 ·5	390	3·8	2·43	DUMONT Collapse (Y) [2]
6	d	1966 July 1	01 33 40	37 18 56 ·9	116 17 56 ·3	390	4·0	1·99	HALFBEAK Collapse (Y)[2]
7	a	1966 September 12	15 30 00·5	36 52 37 ·0	115 57 02 ·2	410	3·9	1·04	DERRINGER, in alluvium[2]
8	e	1967 January 5	12 15 23·1	37·3	116·5	360	3·6	1·15	[3]
9	d	1967 February 23	21 11 35	37 07 36 ·7	116 03 59 ·0	390	3·6	7·17	AGILE Collapse (Y)[2]
10	a	1967 March 2	15 00 00	37 09 57	116 02 55	395	3·6	1·49	RIVET III (Y), in alluvium[2]
11	e	1967 March 3	15 19 02	(37·3)	(116·4)	(360)	3·4	0·98	[4]
12	a	1967 April 7	15 00 00	37 03 15 ·8	116 01 20	400	3·8	1·91	FAWN (Y), in alluvium[2]
13	a	1967 April 21	15 09 00	37 01 09 ·4	116 02 14 ·7	400	3·7	1·28	CHOCOLATE (Y), in alluxium[2]
14	a	1967 April 27	15 45 00	37 08 19 ·6	116 03 47 ·5	395	4·0	0·69	EFFENDI (Y), in alluvium[2]
15*	e	1967 April 28	12 22 58	37·1	116·0	(390)	2·9	0·91	[4]
16	b	1967 May 7	18 01 36·1	37·0	115·0	490	4·5	7·22	[3]
17	b	1967 May 9	00 42 25·9	37·0	115·0	490	3·3	3·01	[3]
18	e	1967 May 23	15 37 47	(37·2)	(116·4)	(360)	3·4	5·34	Assume hypocentre of event No. 21
19	e	1967 May 23	16 22 08	(37·2)	(116·4)	(360)	2·8	3·07	Assume hypocentre of event No. 21
20	e	1967 May 23	17 52 04·1	37·2	116·4	360	3·3	3·26	[3]
21	e	1967 May 23	20 14 06·3	37·2	116·4	360	3·7	4·88	[3]
22	a	1967 June 22	13 10 00	37 07 32	116 01 32 ·2	400	3·8	2·34	SWITCH (Y), in tuff[2]
23	a	1967 June 29	11 25 00·4	37 01 43	116 01 21	400	3·8	1·08	UMBER (Y), in alluvium[2]
24	a	1967 July 27	13 00 00	37 08 55 ·4	116 02 54 ·7	395	4·3	—	STANLEY (Y), in tuff[2]
25	e	1967 August 8	17 52 13·8	37·2	116·5	360	3·3	1·24	[3]

Table 1 (*continued*)

No.	Type	Date	OT (GMT)	Lat. (N)	Long. (W)	Δ (km) from JAS	M[4]	Spectral ratio (P_g)	Comments
26	e	1967 August 9	06 45 05·3	37·2	116·7	340	3·4	1·24	[3]
27	a	1967 August 10	14 10 00	37 09 24 ·1	116 02 50 ·2	395	3·9	1·23	WASHER (Y), in tuff[2]
28	e	1967 August 24	13 30 00	(37·3)	(116·4)	(360)	3·9	0·70	[4]
29	d	1967 September 7	14 24 18	37 09 11 ·4	116 03 10 ·0	390	3·6	9·37	YARD Collapse (Y)[2]
30	b	1967 October 27	01 42 26	(37·2)	(17·7)	(260)	2·8	0·31	White Mountains Earthquake
31	a	1968 January 18	16 30 00	37 08 44 ·1	116 03 56 ·4	395	4·2	0·55	HUPMOBILE (Y)[2]
32	a	1968 January 26	16 00 00	37 16 51 ·1	116 30 52	350	3·8	1·80	CABRIOLET (P), in rhyolite[2]
33	e	1968 January 31	15 30 00	(37·3)	(116·4)	(360)	3·7	1·92	[4]
34	a	1968 March 12	17 04 00·1	37 00 27	116 22 11 ·9	350	4·1	0·66	BUGGY (R), in basalt[2]
35	a	1968 March 14	15 19 00·1	37 02 51 ·8	116 00 38 ·9	400	3·4	1·15	POMMARD (Y), in alluvium[2]
36	a	1968 April 23	17 01 30	37 20 15 ·8	116 22 32 ·1	345	4·1	0·54	SCROLL (P), in tuff[2]
37	c	1968 April 26	15 14 52	37·1	116·2	(360)	4·0	0·82	[3]—BOXCAR 'Afterevent' in Rayleigh wave
38	c	1968 April 26	15 24 00	(37·2)	(116·4)	(360)	4·0	0·78	BOXCAR 'Afterevent'
39	c	1968 April 26	15 32 21	37·2	116·5	360	4·3	0·93	[3]—BOXCAR 'Afterevent' (collapse?)
40	c	1968 April 26	16 08 00	(37·2)	(116·4)	(360)	3·5	0·93	BOXCAR 'Afterevent'
41	c	1968 April 26	16 12 50	(37·2)	(116·4)	(360)	3·4	0·65	BOXCAR 'Afterevent'
42	c	1968 April 26	16 35 17	37·2	116·4	360	4·1	1·77	[3]—BOXCAR 'Afterevent'
43	d	1968 April 26	16 45 30	(37·2)	(116·4)	(360)	4·0	1·35	BOXCAR Collapse
44	c	1968 April 26	20 42 19	37·2	116·4	360	3·4	0·63	[3]—BOXCAR 'Afterevent'
45	c	1968 April 26	21 50 15	(37·2)	(116·4)	(360)	3·3	0·37	BOXCAR 'Afterevent'
46	c	1968 April 27	09 06 33	(37·2)	(116·4)	(360)	3·8	0·66	BOXCAR 'Afterevent'
47	e	1968 May 4	23 28 45	37·2	116·4	360	3·1	0·35	[3]
48	e	1968 May 15	16 01 11	37·2	116·3	360	3·3	0·63	[3]
49	e	1968 June 30	21 21 22	37·2	116·6	360	3·1	0·93	[3]
50	a	1968 July 30	13 00 00	37 08 00	116 04 56	390	4·1	0·46	TANYA (B)[2]
51	e	1968 November 15	15 30 00	(37·1)	(116·0)	(390)	3·6	2·09	[4]
52	a	1968 November 15	15 45 00·4	37 01 34	116 02 00	400	3·8	1·27	KNIFE B (Y)[2]
53	a	1968 November 22	16 19 00	37 08 24	116 02 32	395	4·1	1·35	TINDERBOX (Y)[2]

Table 1 (*continued*)

No.	Type	Date	OT (GMT)	Lat. (N)	Long. (W)	Δ (km) from JAS	M[4]	Spectral ratio (P_g)	Comments
54	e	1968 December 12	15 20 00	(37·1)	(116·0)	(390)	3·8	1·36	[4]
55	c	1968 December 19	17 30 22·8	37·2	116·5	360	3·4	1·24	[3]—BENHAM 'Afterevent'
56	c	1968 December 19	19 18 19·6	37·3	116·4	360	3·5	0·48	[3]—BENHAM 'Afterevent'
57	c	1968 December 19	19 54 01·2	37·2	116·5	360	3·4	0·39	[3]—BENHAM 'Afterevent'
58	c	1968 December 19	22 23 26·3	37·2	116·5	360	3·6	1·06	[3]—BENHAM 'Afterevent' (collapse?
59	c	1968 December 20	20 08 20·4	37·2	116·5	360	3·8	0·61	[3]—BENHAM 'Afterevent'
60	c	1968 December 21	00 14 25·2	37·3	116·5	360	4·3	—	[3]—BENHAM 'Afterevent)
61	c	1969 January 6	06 34 14·5	37·3	116·5	360	4·2	—	[3]—BENHAM 'Afterevent'
62	c	1969 January 10	09 41 21·5	37·2	116·5	360	3·9	1·72	[3]—BENHAM 'Afterevent'
63	c	1969 January 10	17 01 44·5	37·2	116·5	360	3·8	2·82	[3]—BENHAM 'Afterevent'
64	c	1969 January 10	17 14 17·2	37·2	116·5	360	3·8	0·88	[3]—BENHAM 'Afterevent'
65	c	1969 March 18	14 40 02·7	37·2	116·0	400	3·8	0·69	[3]
66	c	1969 September 16	15 43 49·2	37·2	116·5	360	3·8	2·38	[3]—JORUM 'Afterevent'
67	c	1969 September 16	16 23 53·8	37·3	116·5	360	3·9	1·39	[3]—JORUM 'Afterevent'
68	c	1969 September 16	17 31 14·7	37·3	116·5	360	4·0	3·44	[3]—JORUM 'Afterevent'
69	c	1969 September 16	18 15 39·3	37·3	116·5	360	3·8	1·52	[3]—JORUM 'Afterevent'

[1] Magnitudes based on P_n and P_g amplitudes at JAS. The scale is based on Wood–Anderson magnitudes at BRK for larger events.

[2] Personal communication, Don Springer, 1970. The letter designations (Y) and (P) indicate the test areas Yucca Flat and Pahute Mesa, respectively; (R) indicates an elongated explosive charge was detonated as a 'row shot' at Buckboard Mesa. The origin times of collapses may be uncertain by a few seconds.

[3] U.S.C.G.S. hypocentre.

[4] Arrival times at the Berkeley net indicate NTS hypocentre. Δ = 360 or 390 km is assumed for purposes of attentuation and magnitude calculations.

* Arrival times available for this event are inconsistent so that the epicentral distance is uncertain. The magnitude thus may be as large as 3·2 if the epicentre is 500 km from JAS. The error in the attenuation correction due to the epicentral uncertainty is not significant.

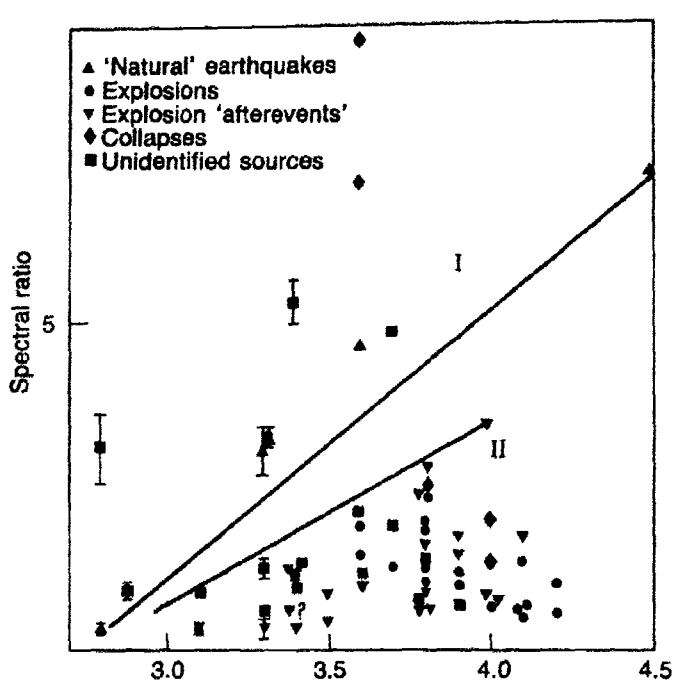

Short Period Discriminant at Regional Distances

Fig. 1. P_g spectral ratio of vertical surface displacement, corrected for attenuation with $Q = 400$, at JAS for events within 100 km of NTS. I and II denote the earthquake and explosion fields, respectively.

separate into distinct sets for magnitude greater than 3.2, with explosions relatively richer in the high frequency band. An interesting result was that the spectra of afterevents of large explosions resemble the spectra of explosions more than that of natural earthquakes. However, these afterevents appear to be more like natural earthquakes when the m_b:M_s discriminant is applied.

Deconvolution of Teleseismic *P* Waves from Explosions

Teleseismic *P* waves from the Amchitka Island explosions MILROW and CANNIKIN were used to study the effect of the free surface on shallow explosions. Homomorphic deconvolution was applied to short-period waveforms at 6 LRSM stations and 2 stations of the Berkeley network (Table 1). Figures 1 and 2 show that the first 3 seconds can be interpreted in terms of a direct *P*-wave, the surface reflection *pP*, and a slapdown phase associated

Table 1

Seismographic stations

Station	Type of instrument	Location	Epicentral dist. from MILROW (deg)	Azimuth from MILROW (deg)
Belleview, Florida (BEFL)	Geotech 18300 (CANNIKIN)	28° 54′ 19″ N; 82 03 52 W	73·1	64·8
Berkeley, California (BRK)	Press Ewing LP (CANNIKIN)	37 52 ·4N; 122 15 ·6W	42·7	84·8
Houlton, Maine (HNME)	Portable Benioff (MILROW) Geotech 18300 (CANNIKIN)	46 09 43 N; 67 59 09 W	66·9	44·0
Kanab, Utah (KNUT)	Large Benioff (MILROW) Geotech 18300 (CANNIKIN)	37 01 22 N; 112 49 39 W	49·1	79·1
Las Cruces, New Mexico (LCNM)	Portable Benioff (MILROW)	32 24 08 N; 106 35 58 W	56·0	79·1
Priest, California (PRI)	Portable Benioff (CANNIKIN)	36 08 ·5N; 120 39 ·9W	44·8	85·6
Red Lake, Ontario (RKON)	Portable Benioff (MILROW) Geotech 18300 (CANNIKIN)	50 50 20 N; 93 40 20 W	51·5	54·0
San Jose, Texas (SJTX)	Geotech 18300 (MILROW) Geotech 18300 (CANNIKIN)	27 36 43 N; 98 18 46 W	64·4	77·2

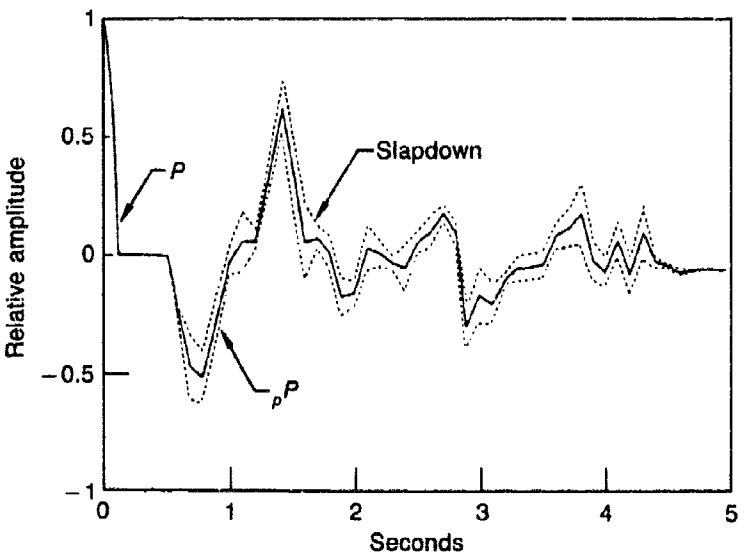

Deconvolution of Teleseismic *P* Waves from Explosions

Fig. 1. Mean impluse train (solid line) ± its standard deviation (dashed line) for MILROW. Impluse trains from KNUT, HNME, LCNM and RKON were used to compute the mean.

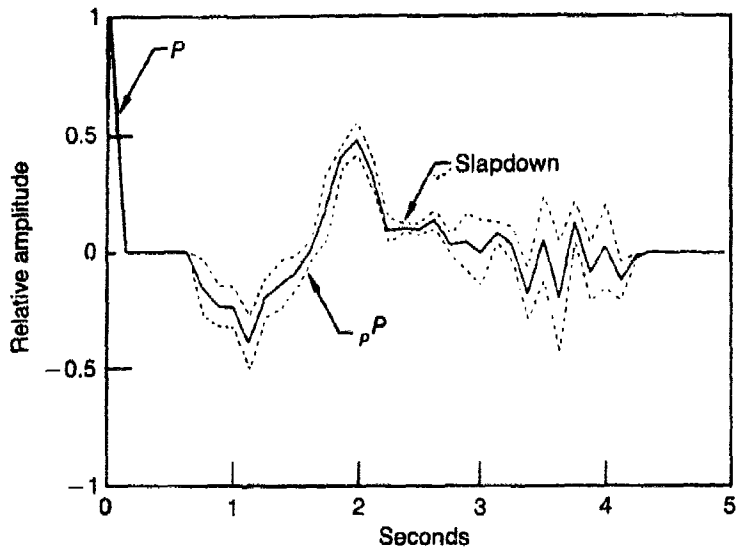

Deconvolution of Teleseismic *P* Waves from Explosions

Fig. 2. Mean impulse train (solid line) ± its standard deviation (dashed line) for CANNIKIN. Impulse trains from HNME, KNUT, SJTX and BRK were used to compute the mean.

with surface spallation. The amplitude of the pP phase is only about half that predicted by simple theory.

Surface Wave—Body Wave Discriminants for NTS Events

Broadband data for NTS explosions, afterevents, and collapses were compared with similar data for earthquakes in a study of relative excitation of Rayleigh and P_n waves for a large set of events recorded at BRK (Table 1), and a second set (Table 2) of events recorded on the LLNL four-station broadband network around NTS. Stations are shown in Fig. 1. In an early test of M_S:m_b convergence at small magnitudes, and an investigation of the effects of tectonic stress release, these studies demonstrated that, at least for NTS events, the surface wave—body wave discriminant persists to events as small as M_L 3.5 with no indication of convergence (Figs. 2 and 3). Furthermore, the data suggest strongly that the non-isotropic (non-explosion) part of the source, whether due to tectonic stress release or to medium heterogeneity, involves processes acting very near to the explosion and coincident with it in time, at all yields studied (up to around 1 MT).

Table 1

Data on events used in this study

Event	Location	Time	Date	Amplitude Rayleigh	Amplitude P_n	M_L
Explosions						
PINSTRIPE	NTS	1838	1966 April 25	4·0	0·8	4·5
CYCLAMEN	NTS	1400	1966 May 5	1·0	0·4	4·2
DUMONT	NTS	1356	1966 May 19	100·0	18·0	5·5
DISCUS THROWER	NTS	2000	1966 May 27	7·5	4·0	4·7
PUCE	NTS	1430	1966 June 10	2·0	0·7	4·3
KANAKEE	NTS	1803	1966 June 15	2·5	0·8	4·8
VULCAN	NTS	1713	1966 June 25	2·0	1·0	4·5
HALFBEAK	NTS	2215	1966 June 30	500·0	30·0	5·9
NEWPOINT	NTS	1750	1966 December 13	1·0	0·3	4·5
GREELEY	NTS	1530	1966 December 20	1440 0	60·0	6·2
AGILE	NTS	1850	1967 February 23	80·0	12·0	5·5
MICKEY	NTS	1340	1967 May 10	6·5	1·5	4·6
COMMODORE	NTS	1500	1967 May 20	180·0	20·0	5·6
SCOTCH	NTS	1400	1967 May 23	240·0	14·5	5·6
KNICKERBOCKER	NTS	1500	1967 May 26	124·0	9·0	5·2
MIDI MIST	NTS	1600	1967 June 26	5·5	2·0	4·7
UMBER	NTS	1125	1967 June 29	1·0	0·6	4·6
YARD	NTS	1345	1967 September 7	12·5	3·5	5·0
KNOX	NTS	1530	1968 February 21	70·0	19·0	5·6
DORSAL FIN	NTS	1708	1968 February 29	6·0	3·0	4·6
NCOR	NTS	1400	1968 April 10	2·0	1·0	4·3
SHUFFLE	NTS	1405	1968 April 18	8·0	4·0	5·2
SCROLL	NTS	1702	1968 April 23	2·5	0·5	4·5
BOXCAR	NTS	1500	1968 April 26	1960·0	80·0	6·3
DIANA MOON	NTS	1630	1968 August 27	1·0	0·5	4·0
NOGGIN	NTS	1400	1968 September 6	82·0	17·0	5·5
HUDSON SEAL	NTS	1705	1968 September 24	5·5	3·5	4·6
CREW	NTS	1515	1968 November 4	4·0	3·0	4·6
SCHOONER	NTS	1600	1968 December 8	12·0	2·3	5·1
BENHAM	NTS	1530	1968 December 19	2720·0	48·0	6·2
WINESKIN	NTS	1930	1969 January 15	26·0	6·0	5·0
BLENTON-THISTLE	NTS	1700	1969 April 30	30·0	5·0	5·0
JORUM	NTS	1430	1969 September 16	1240·0	100·0	6·2
PIPKIN	NTS	1430	1969 October 8	112·0	12·5	5·5
CRUET	NTS	1930	1969 October 29	1·0	0·7	4·4
CYATHUS	NTS	1424	1970 March 6	0·5	1·0	4·2
SHAPER	NTS	2305	1970 March 23	54·0	8·0	5·4
HANDLEY	NTS	1900	1970 March 26	1360·0	120·0	6·2
CORNICE	NTS	1330	1970 May 15	20·0	8·0	5·0
MORRONES	NTS	1415	1970 May 21	11·2	1·7	5·0
HUDSON MOON	NTS	1416	1970 May 26	2·5	1·2	4·2
FLASK	NTS	1500	1970 May 26	30·0	14·5	5·2
BANEBERRY	NTS	1530	1970 December 18	7·0	4·5	4·9
EMBUDD	NTS	1450	1971 June 16	2·0	0·5	4·2
LAGUNA	NTS	1530	1971 June 23	2·4	1·1	4·5
HAREBELL	NTS	1400	1971 June 24	8·3	3·5	4·9
Unidentified*	NTS	1830	1971 June 29	4·7	2·7	4·4
Unidentified*	NTS	1400	1971 September 22	0·5	0·6	3·9
PEDERNAL	NTS	1400	1971 September 29	1·5	0·5	4·1
CATHAY	NTS	1430	1971 October 8	1·5	0·5	4·7
Unidentified*	NTS	1430	1971 October 14	1·0	0·3	4·0
Explosion Collapses						
DUMONT	NTS	1537	1966 May 19	14·0	0·4	4·5
HALFBEAK	NTS	0133	1966 July 1	21·0	0·5	4·2
AGILE	NTS	2111	1967 February 23	10·0	0·3	4·3
YARD	NTS	1425	1967 September 7	7·5	0·2	4·1
KNOX	NTS	1634	1968 February 21	15·0	0·3	4·4
BOXCAR	NTS	1635	1968 April 26	15·0	0·5	5·0

Table 1 (*continued*)

BOXCAR	NTS	1645	1968 April 26	21·0	0·2	4·8
BENHAM	NTS	2224	1968 December 19	47·0	0·3	4·6
JORUM	NTS	1544	1969 September 16	4·0	0·6	3·8
JORUM	NTS	1623	1969 September 16	6·0	0·4	3·7
JORUM	NTS	1731	1969 September 16	13·0	0·5	4·3
JORUM	NTS	1815	1969 September 16	15·0	0·3	4·2
SHAPER	NTS	0115	1970 March 24	6·4	0·2	4·2
HAREBELL	NTS	1441	1971 June 24	5·5	0·3	3·8
Explosion Aftershocks						
SCOTCH	NTS	2014	1967 May 23	2·5	0·3	3·8
BOXCAR	NTS	1532	1968 April 26	112·0	2·5	5·3
BENHAM	NTS	0014	1968 December 21	26·0	1·3	4·8
BENHAM	NTS	1810	1968 December 22	7·0	0·5	4·2
BENHAM	NTS	0634	1969 January 06	11·0	0·8	4·6
BENHAM	NTS	0941	1969 January 10	10·0	0·4	4·6
BENHAM	NTS	1701	1969 January 10	6·0	0·2	4·4
BENHAM	NTS	1714	1969 January 10	6·0	0·3	4·5
Earthquakes						
CENTRAL NEVADA	38·6 N 116·2 W	1321	1968 May 22	36·0	0·8	4·9
ADEL, OREGON	42·2 N 119·8 W	1255	1968 May 28	3·5	0·3	3·8
ADEL, OREGON	42·3 N 119·8 W	0037	1968 May 30	22·0	0·5	4·7
SANTA BARBARA	34·3 N 119·7 W	1912	1968 June 29	148·0	4·0	4·9
SANTA BARBARA	34·2 N 119·6 W	2036	1968 June 29	9·0	0·3	3·8
SANTA BARBARA	34·2 N 119·7 W	0036	1968 July 5	22·0	0·5	4·2
SANTA BARBARA	34·1 N 119·7 W	0045	1968 July 5	720·0	14·0	5·5
NORTHERN NEVADA	41·0 N 117·4 W	1402	1968 June 16	62·0	2·0	5·2
SANTA BARBARA	34·2 N 119·8 W	1433	1968 July 7	60·0	2·0	4·5
SAN FERNANDO	34·4 N 118·4 W	1401	1971 February 9	7520·0	10·0	6·5
SAN FERNANDO	34·4 N 118·4 W	0517	1971 February 10	18·0	0·8	4·6
NTS	36·9 N 116·0 W	1753	1971 August 5	10·0	0·7	4·2

* Unidentified NTS events listed with explosions on basis of Rayleigh-P_n ratios.

Surface-Body Wave Discriminants for NTS Events

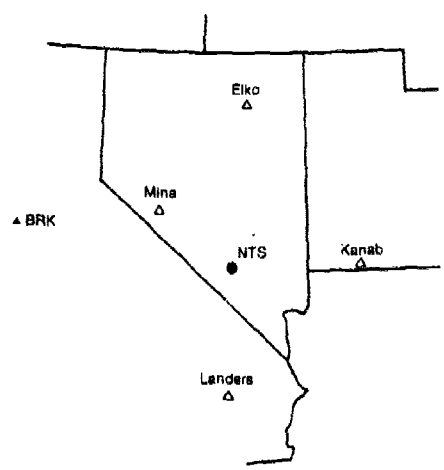

Fig. 1. Stations of the LLL network (open triangles) and the Berkeley (BRK) observatory.

Table 2

Data on events used

Event No.	Date		Type	T_0 (GMT)	Lat. (N)	Long. (W)	Depth (km)	Amplitudes ELKO R	ELKO PNMAX	KANAB R	KANAB PNMAX	LANDERS R	LANDERS PNMAX	MINA R	MINA PNMAX	M_L	Source
1*	1969 Sept. 16	JORUM	EX	14 30 00	37°18·9′	116°27·6′	1·2					41000	18000	95000	40000	6·2	(1)
2	1969 Oct. 29	CRUET	EX	19 30 00	37°07·4′	116°07·7′	0·2			46	208	30	74	44	328	4·4	(1)
3	1969 Oct. 29	POD	EX	20 00 00	37°08·1′	116°08·1′	0·3			105	320	60	240	175	460	4·6	(1)
4	1969 Oct. 29	CALABASH	EX	22 01 52	37°08·6′	116°03·8′	0·9					2800	1920			5·5	(1)
5	1970 Feb. 25	CUMARIN	EX	14 28 38	37°02·2′	116°00·0′	0·4			750	1200			850	1360	4·6	(1)
6	1970 Feb. 26	YANNIGAN	EX	15 30 00	37°07·0′	116°03·7′	0·4			350	800			600	1400	4·8	(1)
7	1970 Mar. 06	CYATHUS	EX	14 24 01	37°01·4′	116°05·5′	0·3			17	60	40	70	105	180	4·2	(1)
8	1970 Mar. 06	ARABIS	EX	15 00 00	37°08·4′	116°02·2′	0·2			7	26	<25	35	<15	140	4·1	(1)
9	1970 Mar. 19	JAL	EX	14 03 30	37°00·1′	116 01·4′	0·3			<30	150			70	168	4·1	(1)
10	1970 Mar. 23	SHAPER	EX	23 05 00	37°05·2′	116°01·3′	0·5			2700	4200	2500	1500	2800	6000	5·4	(1)
11*	1970 Mar. 26	HANDLEY	EX	19 00 00	37°18·0′	116°32·0′	1·2			90000	25400	68000	27200	110000	50000	6·2	(1)
12	1970 May 15	CORNICE	EX	13 30 00	37°09·7′	116°02·3′	0·4			1200	840	950	440	1200	4880	5·0	(1)
13	1970 May 21	MANZANAS	EX	14 00 00	37°01·7′	115°59·5′	0·3			30	198			13	64	3·6	(1)
14	1970 May 21	MORRONES	EX	14 15 00	37°04·3′	116°00·7′	0·4	400	850	900	1600	600	550	800	1700	5·0	(1)
15	1970 May 26	HUDSON MOON	EX	14 16 00	37°11·0′	116°12·8′	0·4			29	140	62	116	150	560	4·2	(1)
16	1970 May 26	FLASK	EX	15 00 00	37°06·8′	116°03·7′	0·5					1700	550	2200	4800	5·2	(1)
17‡	1970 May 28		EX	12 00 03	37·2°	116·0°	<1			30	105	<24	38	<15	70	3·9	(3)
18	1971 June 16	EMBUDD	EX	14 50 00	37°02·0′	116°00·8′	<1			60	220	80	100			4·2	(2)
19	1971 June 23	LAGUNA	EX	15 30 00	37°01·3′	116°01·4′	<1	220	320	190	1300	300	480	600	1250	4·5	(2)
20	1971 June 24	HAREBELL	EX	14 00 00	37°08·8′	116°04·0′	<1	350	760	500	760	450	380	560	1240	4·9	(2)
21‡	1971 June 29		EX	18 30 00	37°	116°	<1			300	1720			400	1160	4·4	(3)
22‡	1971 Sept. 22		EX	14 00 00	37°	116°	<1			<20	65	25	38	<15	68	3·9	(3)
23	1971 Sept. 29	PEDERNAL	EX	14 00 00	37°00·6′	116°00·4′	<1			100	400			156	720	4·1	(2)
24	1971 Oct. 08	CATHAY	EX	14 30 00	37°06·8′	116°02·3′	<1	110	200	126	640	90	180	124	400	4·7	(2)
25‡	1971 Oct. 14		EX	14 30 00	37·2°	116·1°	<1							110	530	3·9	(3)
26‡	1971 Nov. 30		EX	15 45 00	37·1°	116·1°	<1	<180	184	80	144	<100	88	80	192	4·3	(3)
27	1972 Apr. 19	LONGCHAMPS	EX	16 32 00	37°07·3′	116 05·0′	<1	70	280	20	72	70	112	100	350	4·2	(2)
28‡	1972 July 25		EX	13 30 00	36·9°	116·0°	<1	<10	24	<40	104	<10	40	56	216	4·0	(3)
29	1972 Sept. 26	DELPHINIUM	EX	14 30 00	37°07·3′	116°05·1′	<1	75	240							4·4	(2)
30	1971 Aug. 05		EQ	17 58 18	36°54·9′	115°59·4′	4·6	1040	60	800	160	1400	76	1300	192	4·2	(4)
31	1971 Aug. 05		EQ	22 20 03	36°53·6′	115°56·3′	9·0	<2	7	34	44	48	25	62	15	3·3	(4)
32	1973 Feb. 18		EQ	18 05	36·9°	116·0°	?			76	60			120	40	3·8	(3)
33	1973 Feb. 19		EQ	11 15	36°49·0′	115°53·5′	4·7	92	45			80	40			3·9	(5)
34	1973 Feb. 19		EQ	13 43	36·9°	116·0°	?					80	28			3·5	(3)
35	1968 Dec. 20		EXA	20 08 19	37°13·0′	116°30·7′	4·1							144	40	4·1	(6)
36	1968 Dec. 21		EXA	00 14 25	37°15·8′	116 29·3′	3·5			320	136	592	136	800	296	4·8	(6)
37	1968 Dec. 22		EXA	18 10 52	37°14·2′	116 30·6′	4·3			80	56	90	69	320	104	4·2	(6)
38	1969 Jan. 06		EXA	06 34 15	37°14·7′	116°30·5′	4·2			800	300	208	88	800	216	4·6	(6)
39	1969 Jan. 10		EXA	08 08 41	37°10·8′	116°30·8′	2·8					26	7	120	20	3·6	(6)

Table 2 (*continued*)

Event No.	Date	Type	T_0 (GMT)	Lat. (N)	Long. (W)	Depth (km)	Amplitudes ELKO R	ELKO PNMAX	KANAB R	KANAB PNMAX	LANDERS R	LANDERS PNMAX	MINA R	MINA PNMAX	M_L	Source
40	1969 Jan. 10	EXA	09 41 22	37°10·8′	116°30·9′	2·7										
41	1969 Jan. 10	EXA	17 01 45	37°10·6′	116°30·9′	2·8					120	48	880	128	4·6	(6)
42	1969 Jan. 10	EXA	17 14 17	37°11·1′	116°30·7′	3·0					128	40	640	56	4·4	(6)
43	1970 Mar. 27	EXA	15 45 06	37°18·4′	116°32·8′	3·6					80	32	320	116	4·5	(6)
									20	7					3·5	(6)
44	1969 Sept. 16	C	15 43 39	37°18·8′	116°27·4′	0·6(R)†										
45	1969 Sept. 16	C	16 23 53	37°18·7′	116°27·3′	0·6(R)							52	34	3·8	(6)
46	1969 Sept. 16	C	17 31 14	37°19·0′	116°27·6′	0·6(R)					96	12	140	29	3·7	(6)
47	1969 Sept. 16	C	18 15 39·1	37°19·0′	116°27·3′	0·6(R)					140	26	230	32	4·3	(6)
48	1970 Mar. 24	C	01 15	(SHAPER)							190	20	246	35	4·2	(6)
									82	4	160	8	100	20	4·2	(3)
49	1970 Mar. 27	C	05 51	(HANDLEY)					240	44						
50	1970 Mar. 27	C	16 42	(HANDLEY)					440	57	360	49	620	70	4·1	(3)
51	1970 Mar. 27	C	18 08	(HANDLEY)					1880	64	1400	56	960	88	4·2	(3)
52	1970 Mar. 27	C	18 18	(HANDLEY)					3200	320	3600	300	1440	800	4·9	(3)
53	1970 May 15	C	15 20	(CORNICE)							280	10	280	112	3·6	(3)
54	1971 Oct. 08	C	15 33	(CATHAY)			160	40	140	80	90	35	90	164	4·3	(3)
55	1972 July 25	C	13 56				32	8	21	32					3·2	(3)
56	1972 Sept. 26	C	15 25	(DELPHINIUM)					27	< 3					2·8	(3)

Notes:
* Events not plotted in Figs 3–6
† Restrained depth
‡ Presumed explosion

Data sources
1. Springer & Kinnaman (1971);
2. PDE cards;
3. Berkeley data;
4. Fischer, Papanek, Hamilton (1972);
5. Fischer (1973, private communication);
6. Hamilton, Fischer & Papanek (1971).

Event type
EX = explosion;
EQ = earthquake;
EXA = explosion aftershock;
C = collapse.

Surface-Body Wave Discriminants for NTS Events

Fig. 2. Rayleigh to P_n amplitude relations.

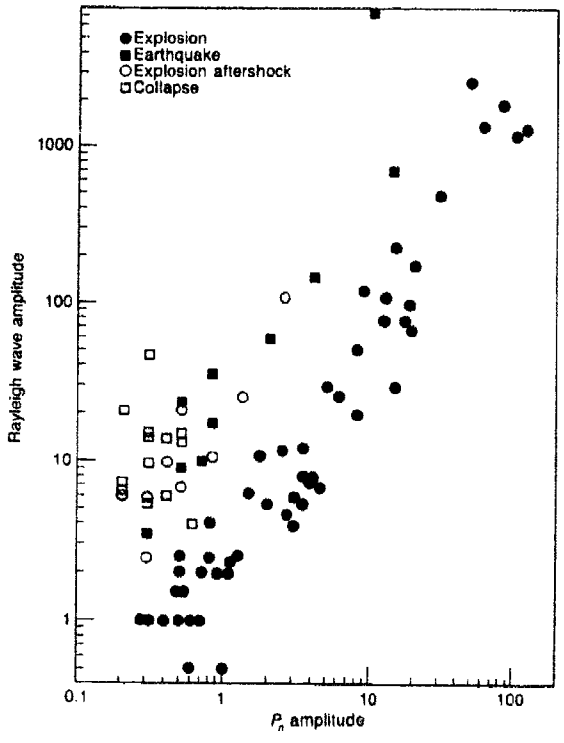

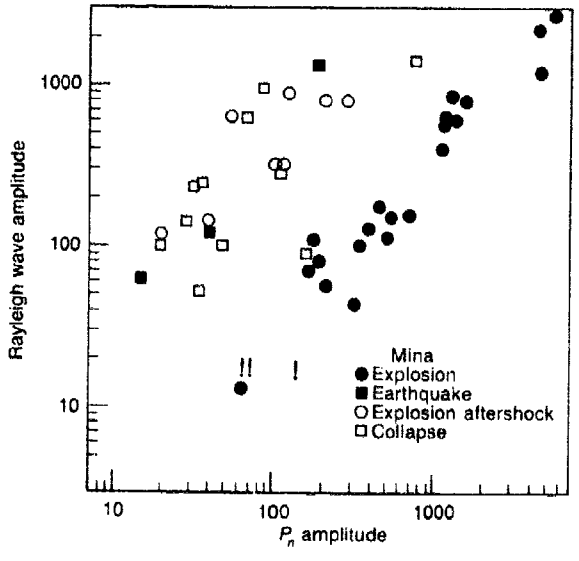

Surface-Body Wave Discriminants for NTS Events

Fig. 3. Rayleigh *vs* P_n amplitudes for events recorded at Mina, Nevada. Cuniforms denote upper limit readings.

Broadband Studies of Earthquakes in the Near Field

Broadband recordings (0.03 to 10 Hz) in the near field (2 to 40 km) were used to study a series of earthquakes along the San Andreas fault in central California. Special broadband instruments were operated on both sides of the fault at the San Andreas Geophysical Observatory (SAGO). The 13 earthquakes used in the study are listed in Table 1 and plotted in Fig. 1. Spectra were used to estimate scalar moments (Fig. 2) and establish a relationship between moment and local magnitude (Fig. 3). The near field terms of the elastic displacement field caused by an earthquake were clearly present on the seismograms (Fig. 5) and at near stations could be reasonably well modeled by a point dislocation source in a homogeneous halfspace (Figs. 4 and 5), although the effects of tilt on the seismometers also had to be included.

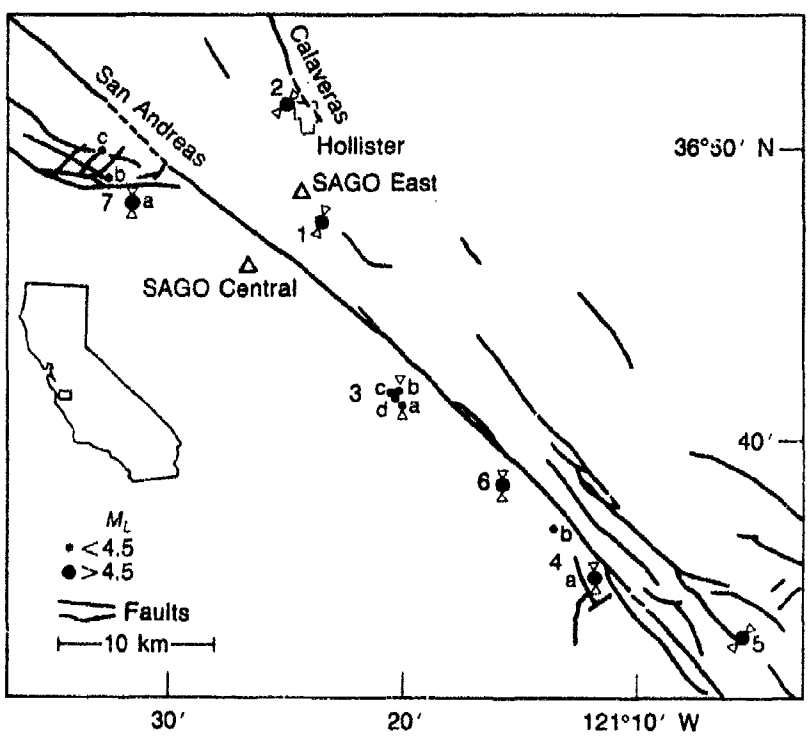

Broadband Studies of Earthquakes in the Near Field

Fig. 1. A map of part of central California showing the primary mapped fault traces, the locations of the seismographic stations at SAGO-Central and SAGO-East, and the epicenters of the 13 earthquakes studied. The identification numbers key the earthquakes to Table 1. The open triangles associated with the larger earthquakes denote the directions of principal compression as determined from fault-plane solutions (Fig. 2).

TABLE 1

DATA SUMMARY FOR EARTHQUAKES

Event No	Location	Date	Origin Time h m s	M_L	Coordinates d m	Depth (km)	SAGO-C Dist. (km)	SAGO-C Az. (deg)	SAGO-E Dist. (km)	SAGO-E Az (deg)	Strike Princ comp.	Strike Fault plane
1	Harris Ranch	27 Oct. 69	10 59 42.8	4.6	36 47.4 N 121 23.6 W	12.5	5.5	240	2.3	274	N13E	N32W
2	Hollister	13 Mar. 70	07 02 28.6	4.7	36 51.5 N 121 25.1 W	10.2	10.6	194	5.7	170	N39E	N06W
3a	Limekiln Road	29 Dec. 71	00 25 35.7	4.0	36 41.2 N 121 20.1 W	3.7	13.2	311	14.8	334	N06W	N49W
3b			01 06 30.7	2.6	36 41.7 N 121 20.2 W	4.6	12.5	308	14.0	333		
3c			01 37 13.7	3.7	36 41.6 N 121 20.6 W	4.0	12.2	311	13.9	336		
3d			01 55 47.7	2.4	36 41.4 N 121 20.4 W	3.6	12.6	311	14.3	335		
4a	Melendy Ranch	24 Feb. 72	15 56 51.3	5.1	36 35.3 N 121 11.8 W	6.4	29.7	311	30.7	322	N09W	N55W
4b			20 21 48.7	3.6	36 37.0 N 121 13.6 W	7.6	25.6	310	26.6	323		
5	San Benito	27 Feb. 72	22 13 08.6	4.7	36 33.3 N 121 05.6 W	10.6	39.3	306	39.7	315	N39E	N05W N95W(?)
6	Stone Canyon	04 Sept. 72	18 04 40.9	4.7	36 38.5 N 121 15.8 W	5.1	21.3	310	22.4	325	N01E	N45W
7a	San Juan Bautista	03 Oct. 72	06 30 02.0	4.9	36 48.1 N 121 31.7 W	5.2	8.3	120	10.8	87	N01E	N80W
7b			11 10 13.3	4.1	36 48.9 N 121 32.7 W	5.1	10.4	122	12.3	94		
7c		04 Oct. 72	08 41 05.6	3.0	36 49.9 N 121 33.1 W	4.3	12.0	128	13.2	102		

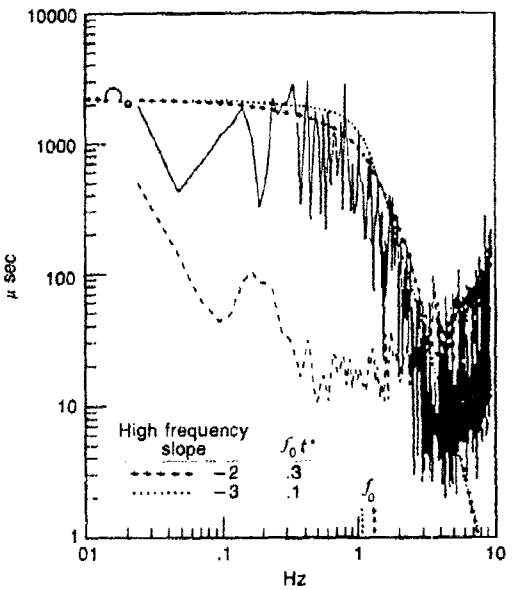

Broadband Studies of Earthquakes in the Near Field

Fig. 2. Example illustrating two different estimates of the low-frequency level Ω_0 and the corner frequency f_0 of the spectrum from the NS component at SAGO-East from event 6 (Table 1).

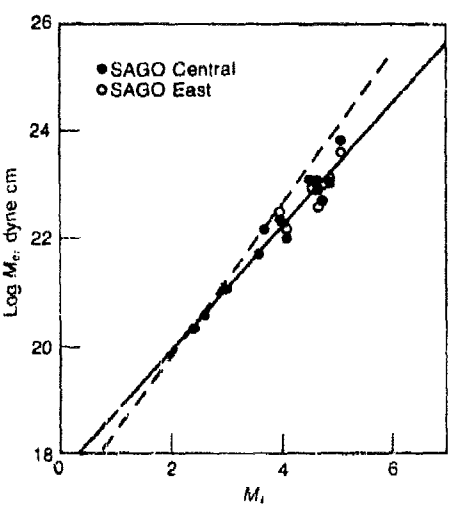

Broadband Studies of Earthquakes in the Near Field

Fig. 3. Relation between seismic moment and magnitude. The solid line was fit to the data points by linear regression and the dashed line is from Wyss and Brune (1968). The SAGO-East values have been divided by a factor of 3 to remove an amplification effect.

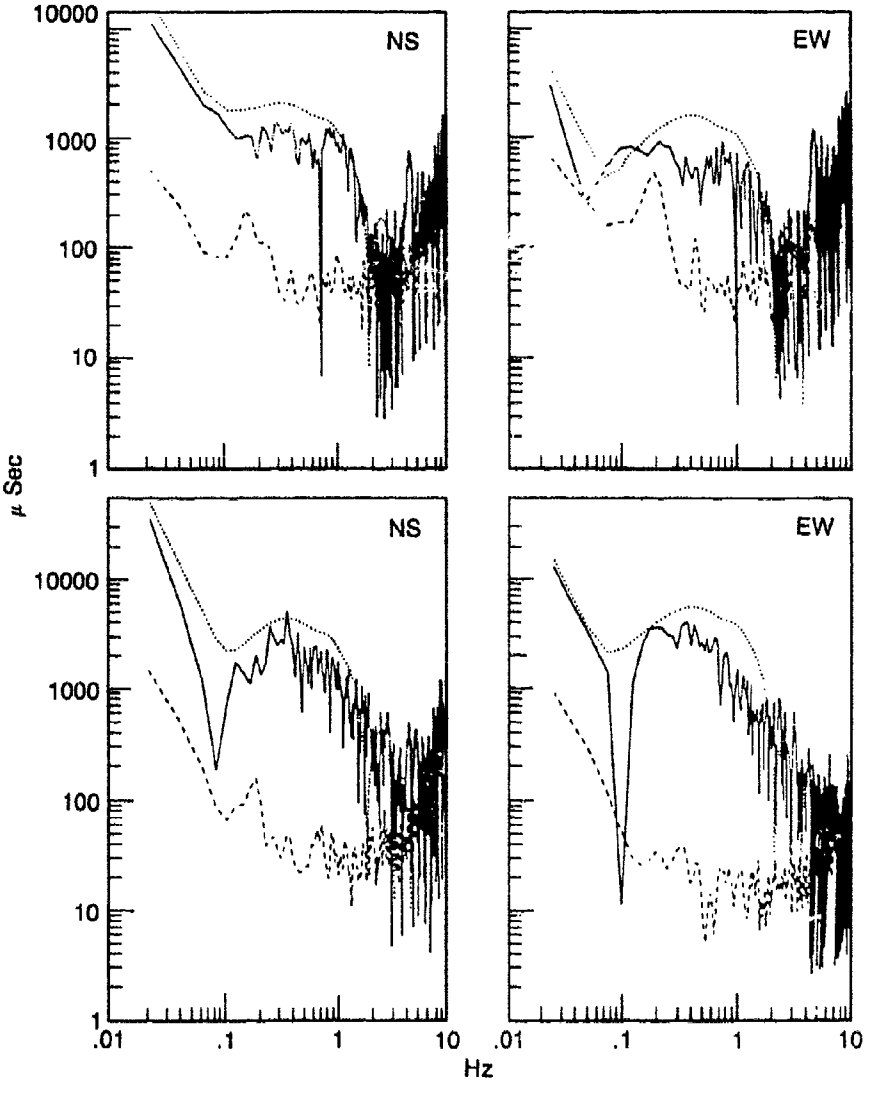

Broadband Studies of Earthquakes in the Near Field

Fig. 4. Amplitude density spectra calculated for event 1 (Table 1) from seismograms recorded at SAGO-Central (*top 2 spectra*) and at SAGO-East (*bottom 2 spectra*). The solid lines are calculated from the observed seismograms, the dashed lines are estimates of the noise, and the dotted lines are calculated from the synthetic seismograms.

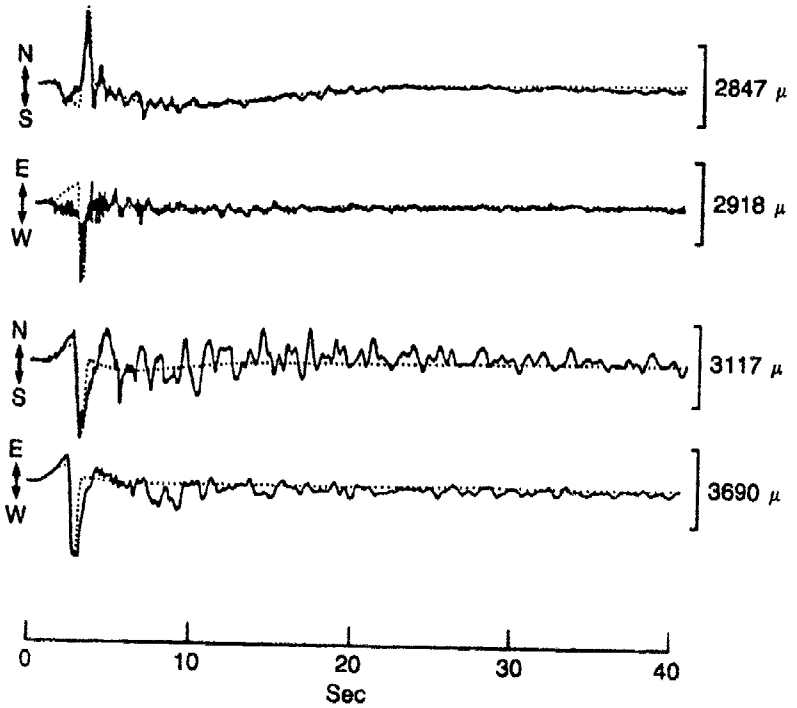

Broadband Studies of Earthquakes in the Near Field

Fig. 5. The displacement seismograms from event 1 (Table 1) recorded at SAGO-Central (*top 2 traces*) and at SAGO-East (*bottom 2 traces*). The dotted lines are the synthetic seismograms with an additional negative impulse in tilt at the arrival time of the *S* wave.

Near Field Project

The "Near Field Project" grew out of some of the problems that became apparent at the Woods Hole meeting on seismic discrimination in 1970. Because the type of high quality data necessary to test various theoretical models of an earthquake was not available at that time, a cooperative experiment was designed to trap a moderate size earthquake within a network of stations designed to provide data over a large range of frequency, azimuth, and distance. The Stone Canyon-Bear Valley section of the San Andreas fault in central California was selected as the target area, and U.C. Berkeley had the responsibility of developing and installing a network of three-component broadband seismographs. Both acceleration and displacement were recorded and an effective bandwidth of 0.02 to 50 Hz was achieved (Fig. 2).

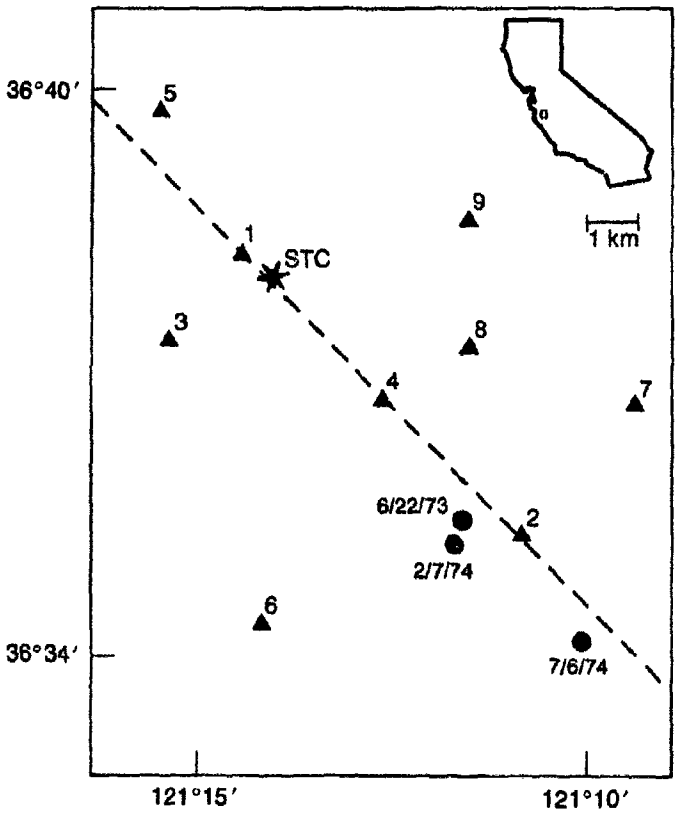

Near Field Project

Fig. 1. Map of a part of central California showing the locations of the stations of the near-field network (solid triangles) and the epicenter of the recorded earthquakes (solid circles) STC is Stone Canyon Observatory. The dashed line is the surface trace of the San Andreas fault.

The 9 stations of the network were installed in early 1973 and remained operational until early 1977. Figure 1 shows the locations of the stations and the epicenters of 3 earthquakes which provided useable data. Figure 3 shows the recordings of ground acceleration from the magnitude 3.3 event on July 6, 1974, obtained at an epicentral distance of 2 km. The clear separation of *P* and S waves, the short duration of the phases, the high frequencies, and the rather large accelerations for an event of this size are all of interest. Figure 4 shows the recordings of ground displacement at the same station from the same event. Here we see the large effect which can be introduced by ground tilt at stations in the near field.

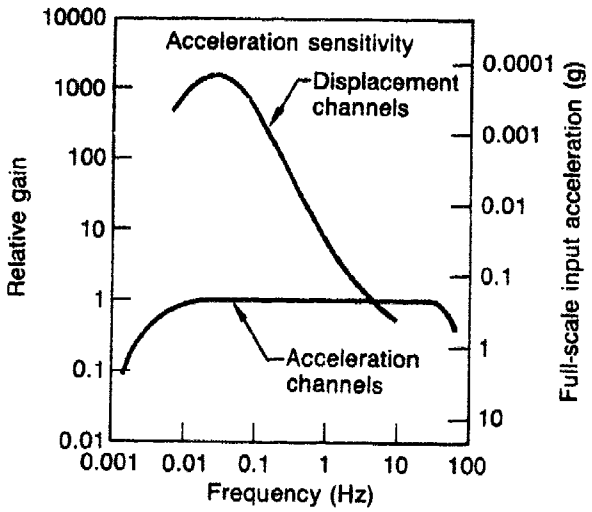

Near Field Project

Fig. 2. The system response functions of the acceleration and displacement.

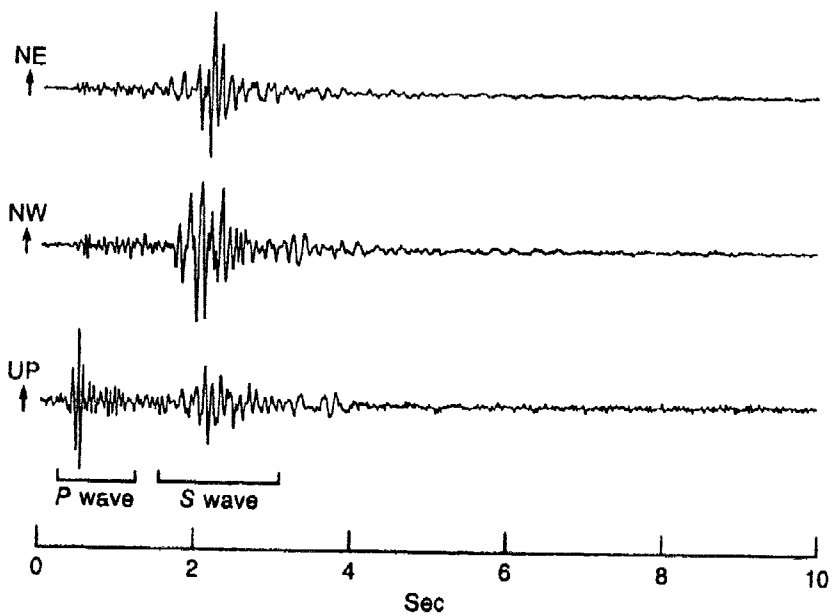

Near Field Project

Fig. 3. The outputs of the acceleration channels at station 2 for the earthquake of 6 July 1974. The maximum accelerations on the NE, NW, and Z channels are 19.4%g, 11.6%g, and 12.5%g, respectively.

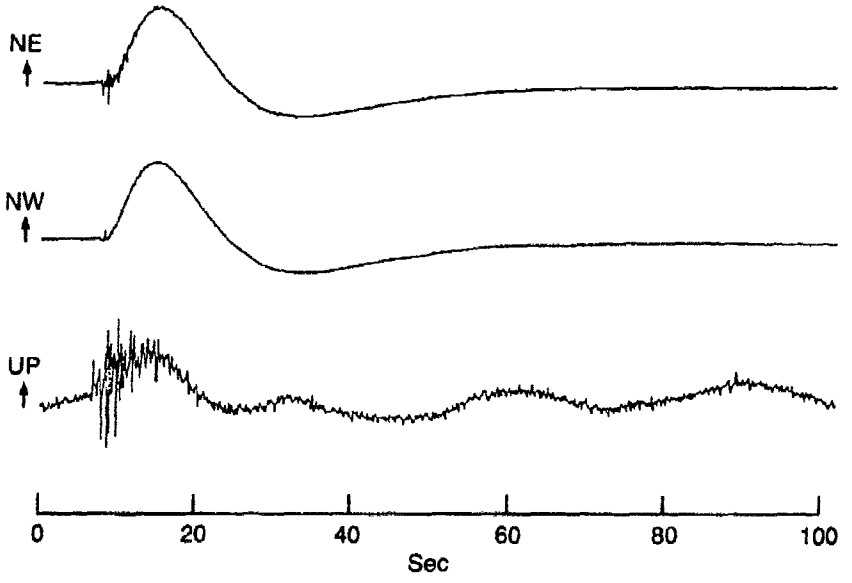

Near Field Project

Fig. 4. The outputs of the displacement channels at station 2 for the earthquake of 6 July 1974 after being passed through a four-pole low-pass filter with a corner frequency at 4 Hz. The maximum displacements on the NE, NW and Z channels are 3220 μ, 7720 μ and 340 μ respectively.

Fault Zone Properties from Near Field Observations

Precise monitoring of seismicity in the Bear Valley—Stone Canyon area of the Near Field Project led to improved resolution in epicenters (Fig. 1), focal depths (Fig. 2), and fault plane orientations (Fig. 3). In addition, careful analysis of the *P*-wave nodal planes for well-located events revealed a pervasive distortion (Fig. 4). This effect, interpreted in terms of a lateral velocity change across the fault zone in the focal region, led to estimates of 20% or more for the velocity jump on some patches of the fault plane.

Near Field Experiments at the Nevada Test Site

Beginning in 1969, U.C. Berkeley has conducted an experimental program of recording explosions at the Nevada Test Site. Table 1 lists the 13 events which have been recorded so far. These experiments have included events in both Yucca Valley and Pahute Mesa. They have also included a variety of recording arrangements, ranging from arcs at a single

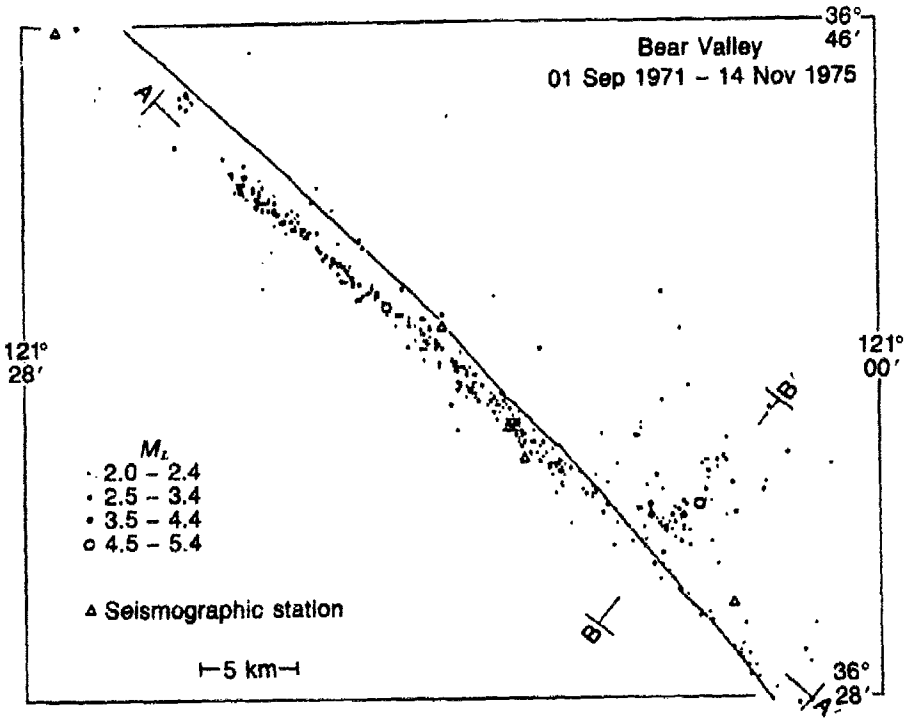

Fault Zone Properties from Near Field Observations

Fig. 1. Seismicity of Bear Valley/Stone Canyon study region, 1971 – 1975.

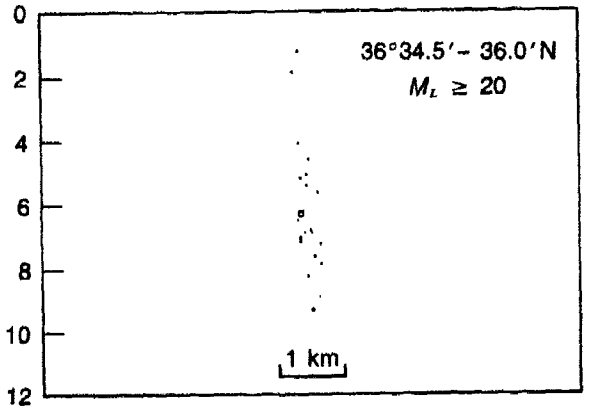

Fault Zone Properties from Near Field Observations

Fig. 2. Cross section across fault at 36°34.5′ to 36.0′, showing narrow vertical fault plane.

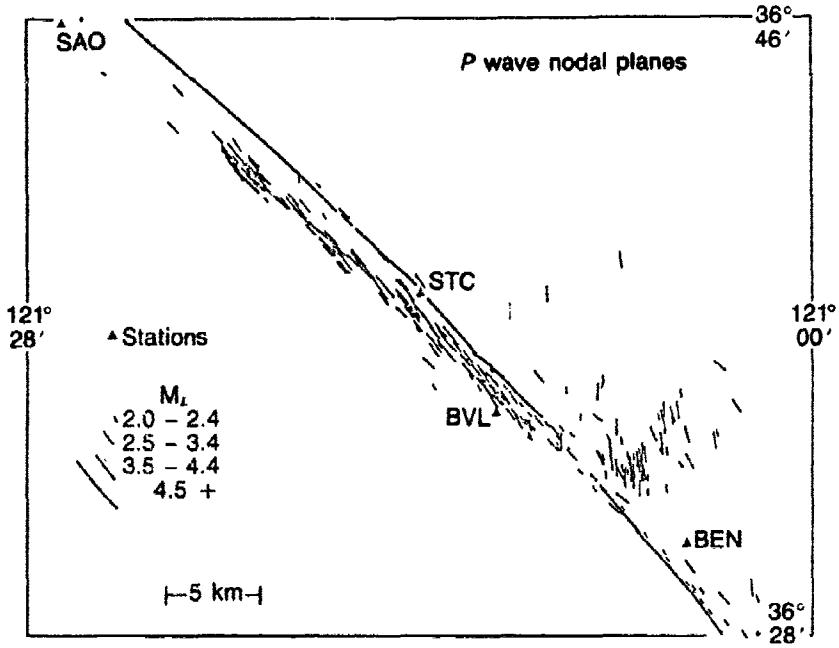

Fault Zone Properties from Near Field Observations

Fig. 3. Orientations of right-lateral strike-slip fault planes (nodal planes) from the *P*-wave focal mechanism solutions.

Fault Zone Properties from Near Field Observations

Fig. 4. Examples of distorted nodal plane patterns in "flat" display.

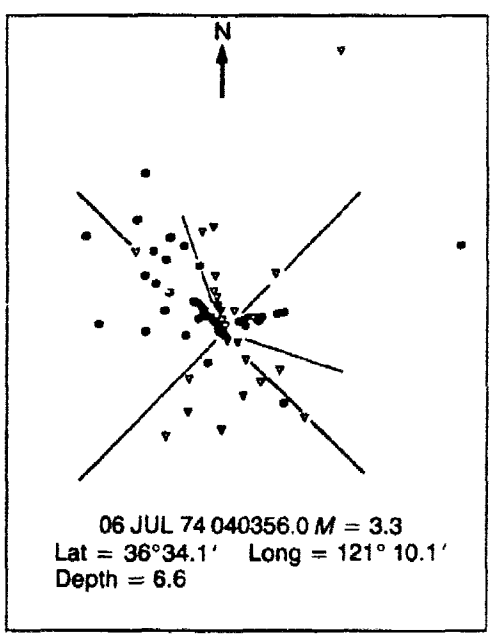

Table 1. NEAR FIELD RECORDINGS OF NTS EVENTS

Event	Date	Region	M_L	h (km)	no. sta	range (km)	azimuth (deg)	station distribution
JORUM	9/16/69	Pahute	6.2		3	8.0	45	arc
PIPKIN	10/8/69	Pahute	5.5	0.62	5	5.6-23.6	55	network
HANDLEY	3/26/70	Pahute	6.3	1.20	4	8.0	100	arc
EMMENTHAL	11/2/78	Pahute	4.3	0.58	4	0.6-1.7	150	network
FARM	12/16/78	Pahute	5.5	0.69	4	4.2-9.7	120	network
AZOUL	12/12/79	Yucca	4.7	0.42	0	3.5	7	400 m 2D array
LIPTAUER	4/3/80	Yucca	4.7	0.42	8	1.9	12	400 m 2D array
COLWICK	4/26/80	Pahute	5.6	0.63	8	6.0	4	400 m 2D array
SERPA	12/17/80	Pahute	5.0	0.57	7	9.3	0	720 m 1D array
BASEBALL	1/15/81	Yucca	5.5	0.56	9	8.0-9.0	110	arc
HARZER	6/6/81	Pahute	5.4	0.64	8	3.5-6.6	360	network
COALORA	2/11/83	Yucca	3.8	0.28	10	0.7-5.4	150	network
CHANCELLOR	9/1/83	Pahute	5.3		11	1.8-9.7	360	network

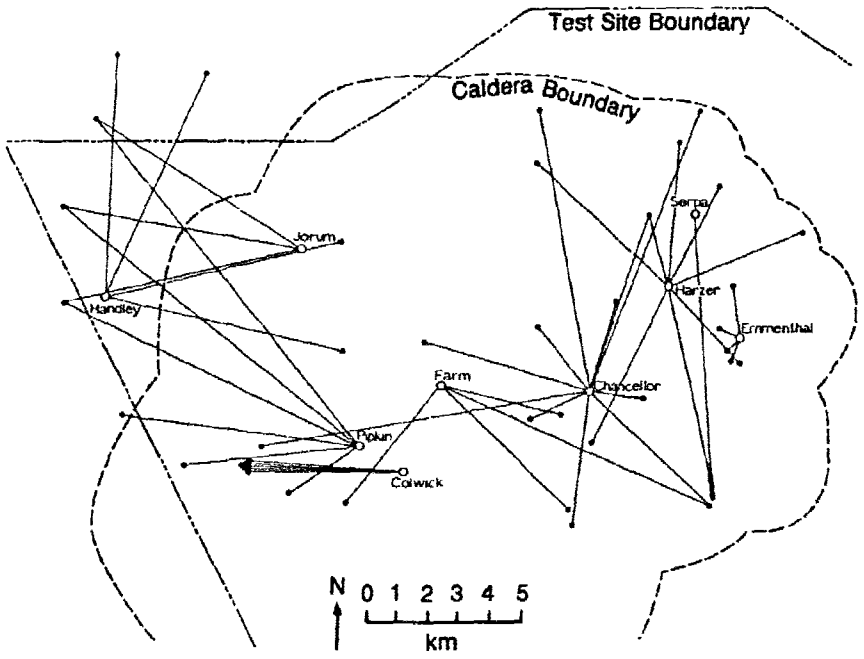

Near Field Experiments at the Nevada Test Site

Fig. 1. Explosion sites (open circles with names) and respective recording sites (filled circles) for near field data acquisition at Pahute Mesa.

distance, networks containing stations at a variety of azimuths and distances, one-dimensional arrays, and two-dimensional arrays. Figure 1 shows the events and stations for the experiments at Pahute Mesa. The combined data set from this series of experiments is now large enough to permit systematic studies of propagation and site effects, particularly for the Pahute Mesa region.

Small Array Studies of Wave Propagation Effects

Seismic arrays with dimensions of a few hundred meters have been useful in helping to understand wave propagation effects at close distances to both explosions and earthquakes. Figure 1 shows the array geometry used to record the explosion COLWICK in Pahute Mesa and Fig. 2 shows the records of ground acceleration. Through frequency-wavenumber processing of these data it was possible to show that the large transverse pulse arriving 1.3 sec after the P wave (Fig. 3) is coming from the direction of the explosion and arrives at a time consistent with cogeneration with the P wave. These array experiments have also permitted studies of wave

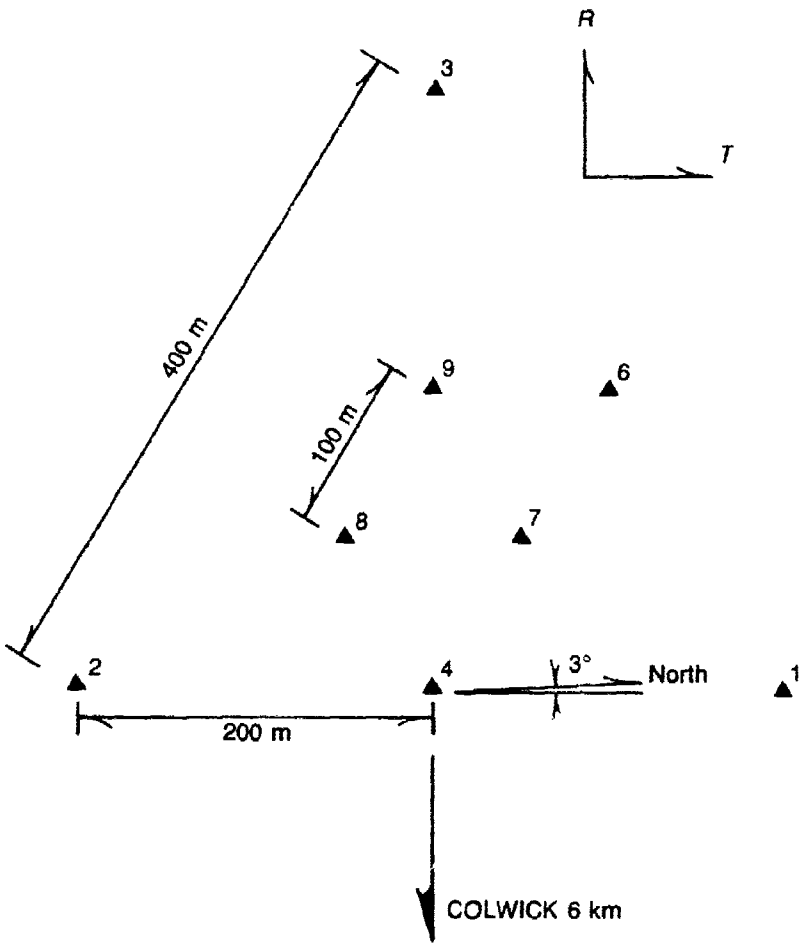

Small Array Studies of Wave Propagation Effects

Fig. 1. The eight stations of the COLWICK array arranged in nested triangles of 400, 200 and 100 m. Each station consisted of a three-component accelerometer package and a digital event recorder. Vertical is up, radial is away, and transverse is clockwise from radial. COLWICK was 6 km 93° E of N from the array.

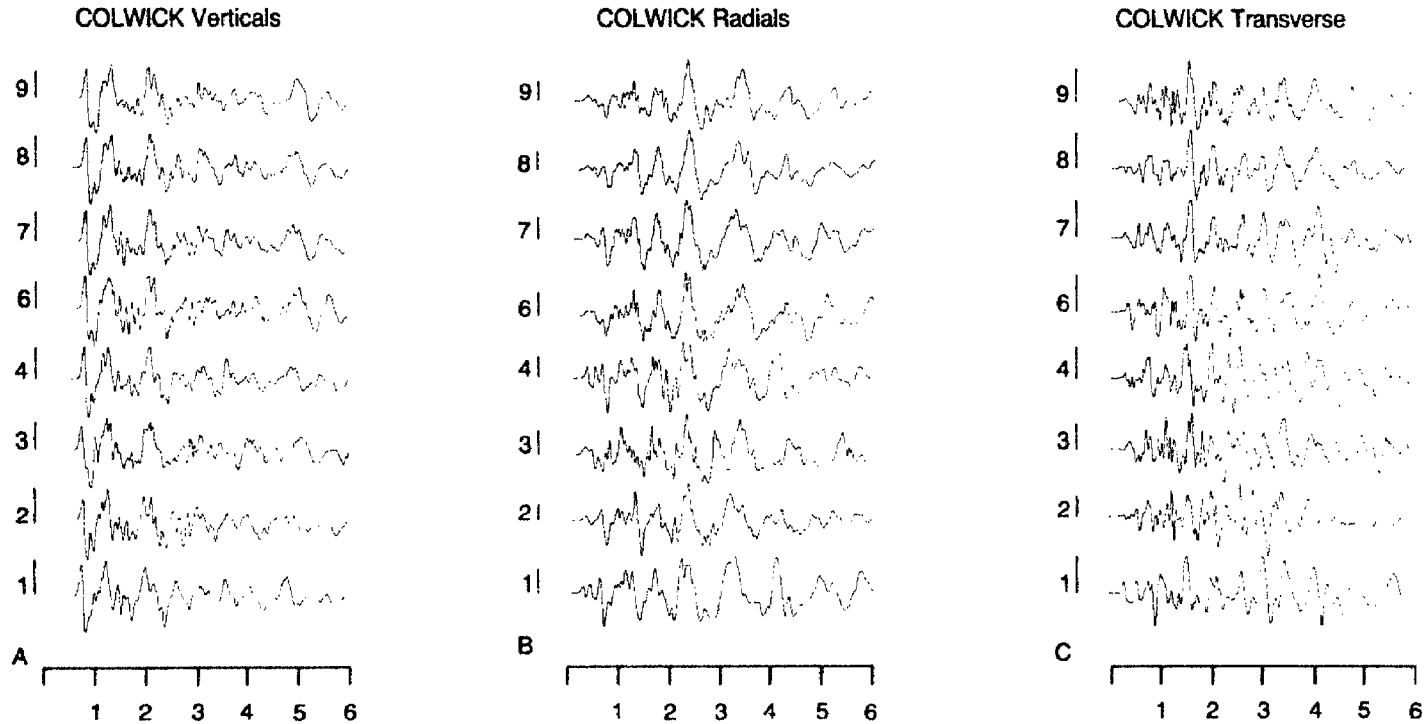

Fig. 2. (A) to (C). The first 6 sec of the acceleration records. The bars to the *left* are 0.1 g and the tic marks at the bottom are seconds. The numbers to the *left* of the traces identify the station numbers.

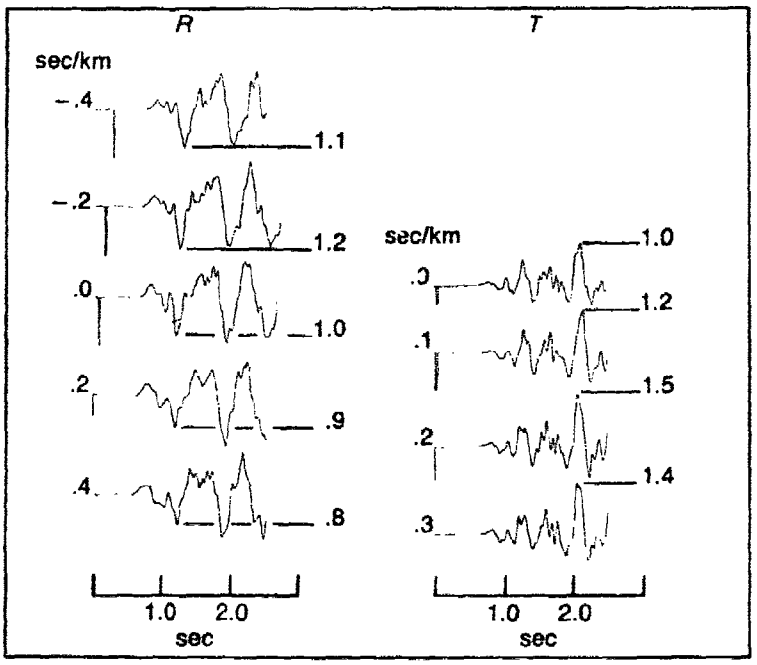

Small Array Studies of Wave Propagation Effects

Fig. 3. Eight-station stacked *R* and *T* acceleration records. Radial records are shown at −0.4, −0.2, 0.0, 0.2 and 0.4 sec/km relative to the *P* wave at the source azimuth (negative slownesses are faster than the *P* wave). The strong radial *P*-to-*SV* converted phase is apparent 0.4 sec after the *P* wave and with slowness 0.0 to −0.2 sec/km with respect to the *P*. The amplitudes shown are normalized to the amplitudes of the stacked 0.0 sec/km seismogram. Transverse records are shown at 0.0, 0.1, 0.2 and 0.3 sec/km relative to the *P* wave at source azimuth. The large pulse 1.3 sec after the *P* is between 0.2 and 0.3 sec/km slower than the incident *P* wave, as suggested by the *f*–*k* spectra.

coherency. Figure 4 shows that for distances of a few hundred meters, there is a considerable loss of coherency for frequencies above 5 Hz.

NTS Area Crustal Velocity and *Q* Structure from Broadband Surface Waves

An application of the phase-matched filtering process to multimode Rayleigh and Love waves from NTS explosions recorded at the four LLNL broadband stations (Fig. 1, Table 1) proved surprisingly effective in extracting pure-path group velocities. Fundamental mode Love and Rayleigh waves and first shear mode of the Rayleigh wave were observed, yielding data in the period range 2 to 50 seconds. Data for the Landers station are

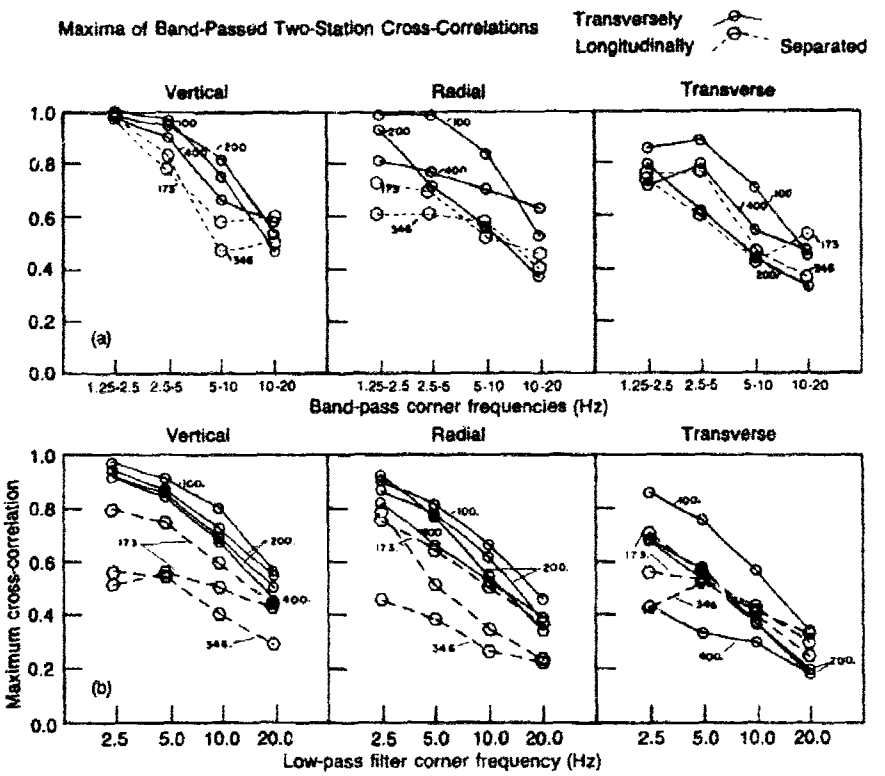

Small Array Studies of Wave Propagation Effects

Fig. 4 (a) and (b). Bandpassed and lowpassed cross-correlation function maxima for station pairs (1,2), (1,4), (2,4), (7,8), (3,9), (3,4) and (4,9). The interstation distances are 400, 200, 200, 100, 173, 173 and 346 m apart, respectively and indicated on the figure. Station pairs (1,2), (1,4), (2,4) and (7,8) are separated transversely, or across the wave front, and are generally better correlated. Station pairs (3,9), (4,9) and (3,4) are longitudinally separated. Bandpass filters were selected at octaves 1.25 to 2.5, 2.5 to 5.0, 5.0 to 10.0 and 10.5 to 20.0 Hz. Lowpass filters were selected at 1.25, 2.5, 5.0, 10.0 and 20.0 Hz. All station pairs show a fall-off of correlation with increasing frequency content above 5 Hz. Window $P+S$ (b) includes P and S waves while window P (a) encompasses only the P wave and its coda.

shown in Fig. 2, in which observations are given as dots. These velocities are the lowest found for the Basin-Range, apparently because they represent the shortest observation paths ever used, thus avoiding upward bias of true velocities inherent in the averaging process which is involved in using long paths. Inversion for structure yields the NTS-Landers model of Fig. 3, and the calculated dispersion curves are shown as solid curves in Fig. 2. Statistically significant differences in models for the four paths are

Table 1: Seismic Source Information

	Origin Time		Location			Magnitude
Event	Date	h:m:s	Lat.(N)	Long.(W)	Depth(m)	m_L*
Escaboss	7/10/74	16 00 00.1	37.075	116.032	640	5.7
Collapse*	7/10/74	21 09 4.22	37.075	116.032		
Stanyan	9/26/74	15 05 00.2	37.133	116.068		5.6
Collapse	9/26/74	15 54 35.2	37.133	116.068		3.7
Topgallant	2/28/75	15 15 00.1	37.106	116.056	713	5.7
Collapse	2/29/75	01 19 26.3	37.106	116.056		4.0
Stilton	6/3/75	14 20 00.0	37.340	116.523	731	5.9
Mizzen	6/3/75	14 40 00.1	37.095	116.036	637	5.7
Kasseri	10/28/75	14 30 00.0	37.290	116.412	1265	6.4
Inlet	11/20/75	15 00 00.1	37.225	116.368	817	6.0
Chiberta	12/20/75	20 00 00.2	37.128	116.062	716	5.7
Muenster	1/3/76	19 15 00.2	37.300	116.330	1451	6.4
Fontina	2/12/76	14 45 00.2	37.271	116.488	1219	6.3
Cheshire	2/14/76	11 30 00.2	37.243	116.420	1167	6.0
Estuary	3/9/76	14 00 00.1	37.310	116.364	889	6.0
Collapse	3/9/76	16 55 03.4	37.310	116.364		4.1
Colby	3/14/76	12 30 00.2	37.310	116.470	1273	6.3
Collapse	3/14/76	14 09 52.0	37.310	116.470		4.1
Collapse	3/14/76	14 18 15.0	37.310	116.470		4.3
Pool	3/17/76	14 15 00.1	37.256	116.312	879	6.1
Strait	3/17/76	14 45 00.1	37.107	116.052	780	5.8
Rudder	12/28/76	18 00 00.08	37.100	116.036	640	5.5
Collapse	12/28/76	20 29 26.0	37.100	116.036		4.4
Marsilly	4/5/77	15 00 00.17	37.120	116.062	690	5.5
Collapse	4/5/77	16 57 10.3	37.120	116.062		4.4
Scantling	8/19/77	17 55 00.08	37.110	116.055	701	5.5
Farallones	12/14/77	15 30 00.10	37.136	116.086		5.6
Panir	8/31/78	14 00 00.16	37.276	116.357	681	5.5
Collapse	8/31/78	23 56 16.5	37.276	116.357		4.0
Rummy	9/27/78	17 20 00.08	37.080	116.051	640	5.5
Collapse	9/27/78	19 10 22.2	37.080	116.051		4.5
Farm	12/16/78	15 30 00.16	37.273	116.410		5.5

*Local magnitudes are from the Bulletins of the University of California Berkeley Seismographic Station.

seen, apparently correlating with the regional variations in heat flow. Pure-path amplitudes are also extracted by the phase-matched filtering, and they allow estimation of a regional Q structure which, while highly uncertain, indicates Q values greater than 100 in the upper 5-10 km, and less than 50 below that depth. These new data on Basin-Range structure will be used to improve Greens Functions for explosion source inversion from regional data sets.

NTS Area Crustal Velocity and Q Structure from Broadband Surface Waves

Fig. 1. LLNL network.

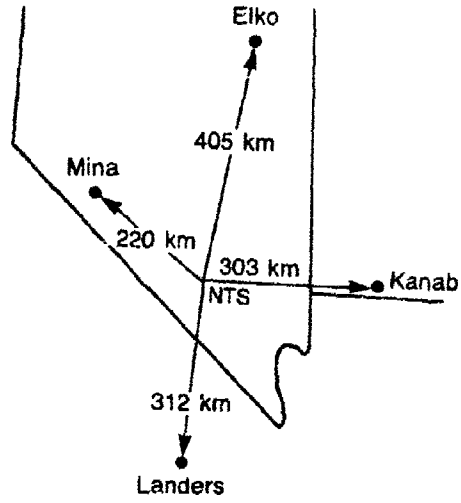

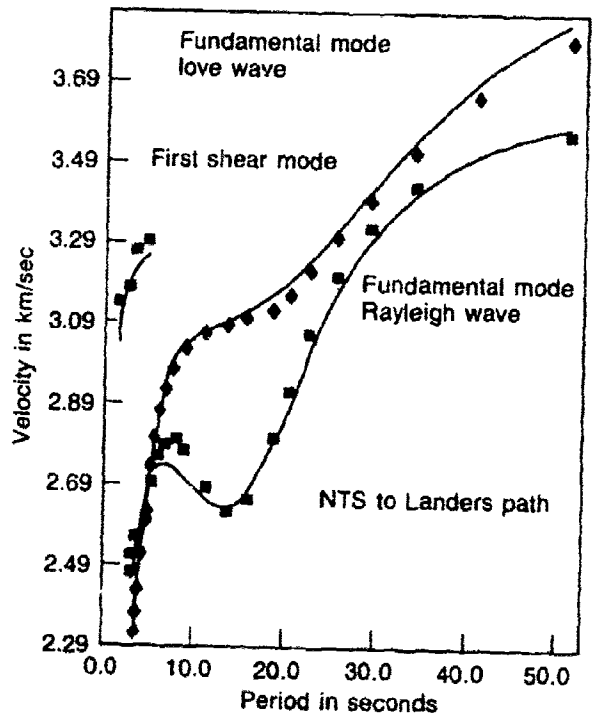

NTS Area Crustal Velocity and Q Structure from Broadband Surface Waves

Fig. 2. Observed (dots) and calculated dispersion.

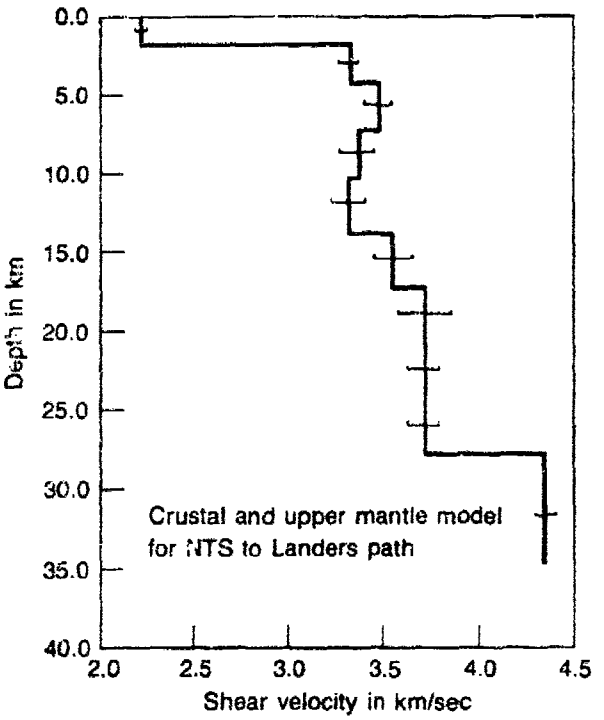

NTS Area Crustal Velocity and *Q* Structure from Broadband Surface Waves

Fig. 3. NTS – Landers model based upon inversion of data in Fig. 2.

Source Studies Through Moment Tensor Inversion

One approach to the study of both explosion and earthquake sources is to characterize the source in terms of the seismic moment tensor. This is a linear inverse problem, and given sufficient recording coverage in distance, azimuth, and bandwidth plus the capability to generate realistic Green Functions, useful results can be obtained. This procedure was applied to the first 5 sec of data from 24 channels of acceleration recorded from the explosion HARZER in the distance range 2.2 to 6.8 km. Figure 1 is a comparison at one station between observed accelerations and those predicted by the estimated moment tensor. Figure 2 shows the 6 elements of the moment tensor which emerged from the estimation procedure. The source is dominated by the isotropic part of the moment tensor which is shown in Fig. 3. The deviatoric part of the moment tensor can also be analyzed in terms of its eigenvalues and eigenvectors. This leads to a result which is predominantly east-west extension and vertical compression, and this appears to be consistent with the faulting pattern in Pahute Mesa.

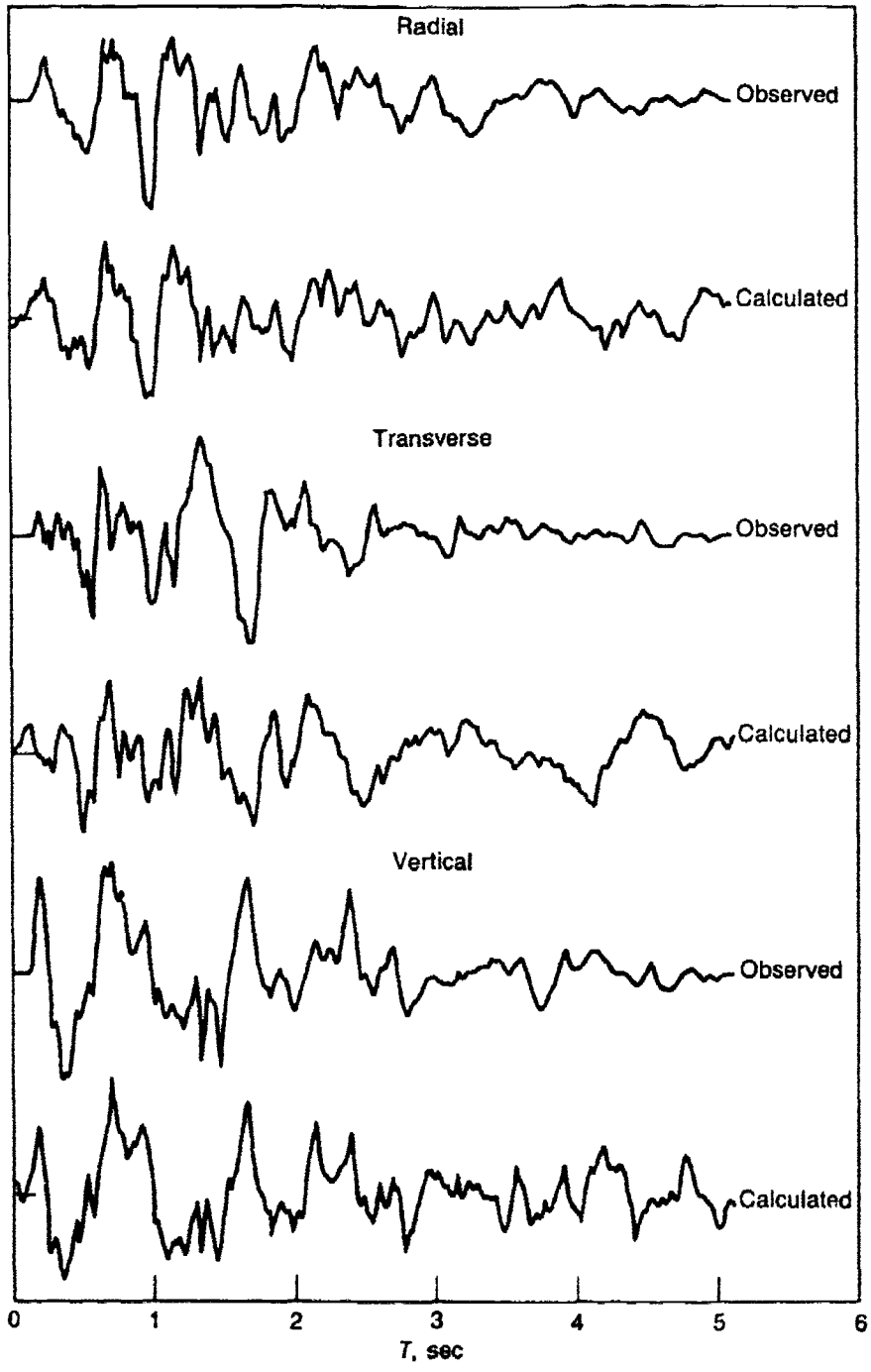

Source Studies Through Moment Tensor Inversion

Fig. 1. Observed and calculated accelerations for station H9 of HARZER.

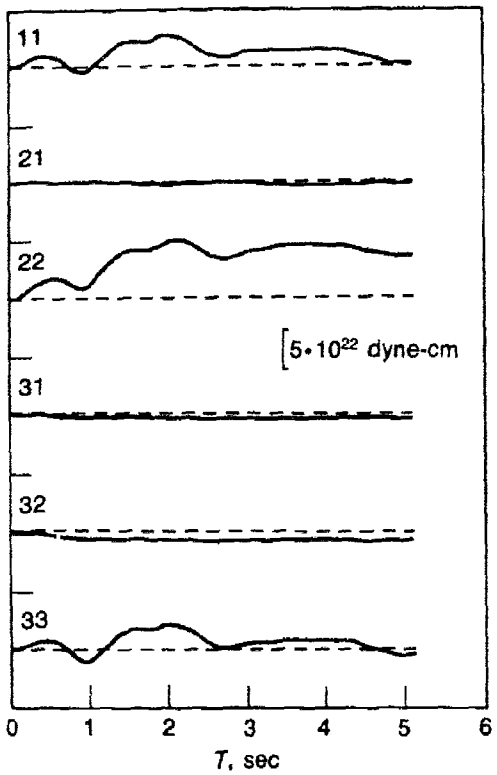

Source Studies Through Moment Tensor Inversion

Fig. 2. Estimates of the elements of the first-degree moment tensor of the explosion HARZER.

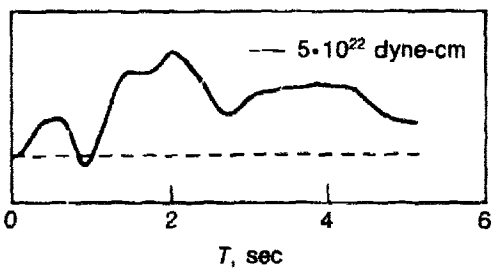

Source Studies Through Moment Tensor Inversion

Fig. 3. Estimate of the isotropic part of the first-degree moment tensor of the explosion HARZER.

Seismic Wave Propagation Effects — Development of Theory and Numerical Modeling

Paul G. Richards

Abstract

I discuss methods applied to the detailed interpretation of seismograms, emphasizing what has been learned about Earth structure (rather than the seismic source). The theory and practice of working with synthetic seismograms is described in broad terms. The main idea is to work with the sum (or integral) over wave solutions in separated variables. The sum is taken over horizontal wavenumber (or ray parameter), and frequency. The terminology of normal modes, surface waves, and body waves, supplies three somewhat different perspectives. Some detailed examples are given of the opportunities and problems of seismic wave analysis, where there is influence from structure in the crust, and/or mantle, and/or core. At periods (T) greater than about twenty seconds, there is now, in general terms, a fairly complete understanding of seismograms, apart from certain effects due to lateral variation in Earth structure. For $1 < T < 20$ seconds, only limited portions of a teleseismic record (e.g., about 15 seconds following a P-arrival, or 30 seconds after SH) may be well understood. At the short-period end of this range there is debate about trade-offs between the seismic source (for a particular event, is it strong or weak?) and attenuation in the Earth (strong, or weak).

For methods based on spherically symmetric Earth models, and particularly clean data sets (why are they clean?), excellent agreement between waveform synthetics and data is often possible. But of course this is not enough, particularly in deciding the trade-off between source spectrum and attenuation; and sometimes the agreement is less than excellent. This paper will give a case for interpreting body wave observations in terms of Earth models with quite low intrinsic friction for teleseismic short-period phases, and will criticize certain use of absorption band models in which pulse broadening is linked to properties of pulse amplitude spectra. Scattering, either by thin layering in the mantle or by lateral and vertical heterogeneities, may play an important role. The success of future analysis may lie in separating the deterministic component of the Earth's profile (i.e., a standard model in which there is smooth variation of velocity with depth, plus a few discontinuities), from a superimposed statistical component. As we

face the complications of an Earth which internally may be inhomogeneous on all spatial scales, with evidence too for some anisotropy in the upper mantle, it is clear that our science is now restrained by inadequacy of our data.

Introduction

The detailed interpretation of seismograms has become, in the last fifteen years, a sophisticated exercise in modeling. A recorded motion of the ground may be given to an analyst, who seeks to match it purely by computation of what happens in the model. His model must have a description of the source, an appropriate theory of wave propagation, and a description of the Earth's internal structure. And these three components must be developed in a computational package that takes the assumptions the analyst makes and translates them into a synthetic seismogram more or less like the data.

Synthetic seismograms now do indeed quite often look remarkably like the data. Figure 1 gives some examples, and they represent a very considerable achievement. They indicate in general terms that seismologists are now working with quite good models of the source; that we have developed an appropriate theory of wave propagation; and that we have reasonably accurate models of Earth structure. It appears too that computational packages for generating synthetics are now effective and trustworthy. Note that for the different examples of Fig. 1, computation of synthetics was developed quite independently and successfully by many people.

For the broad purposes of the VELA program, it is most important to appreciate and to acknowledge the general success of modern seismology as demonstrated in Fig 1. Seismograms are now being used and understood in detail in ways not possible ten years ago. I emphasize this, because experts do disagree in some important areas of seismogram interpretation. Later sections of this paper emphasize some of these disagreements, but the broad picture is one of solid progress.

The intent in what follows is to review the use of synthetic seismograms, as applied to learning about the Earth's internal structure. Well before the use of synthetics, knowledge of deep Earth structure (determined from travel time curves) was intensively developed in terms of velocity models for *P*-waves and *S*-waves. Thus, by 1939 the independent efforts of Beno Gutenberg and Harold Jeffreys in applying ray theory had led to velocity models of the whole Earth which differ from each other by only a few percent. In the depth range 800-2800 km, there is less than 1% difference between their two *P*-velocity models, and less than

Event of 11/08/80, 10:27:34.0, Lat 41.12, Long −124.25, Depth 19.0

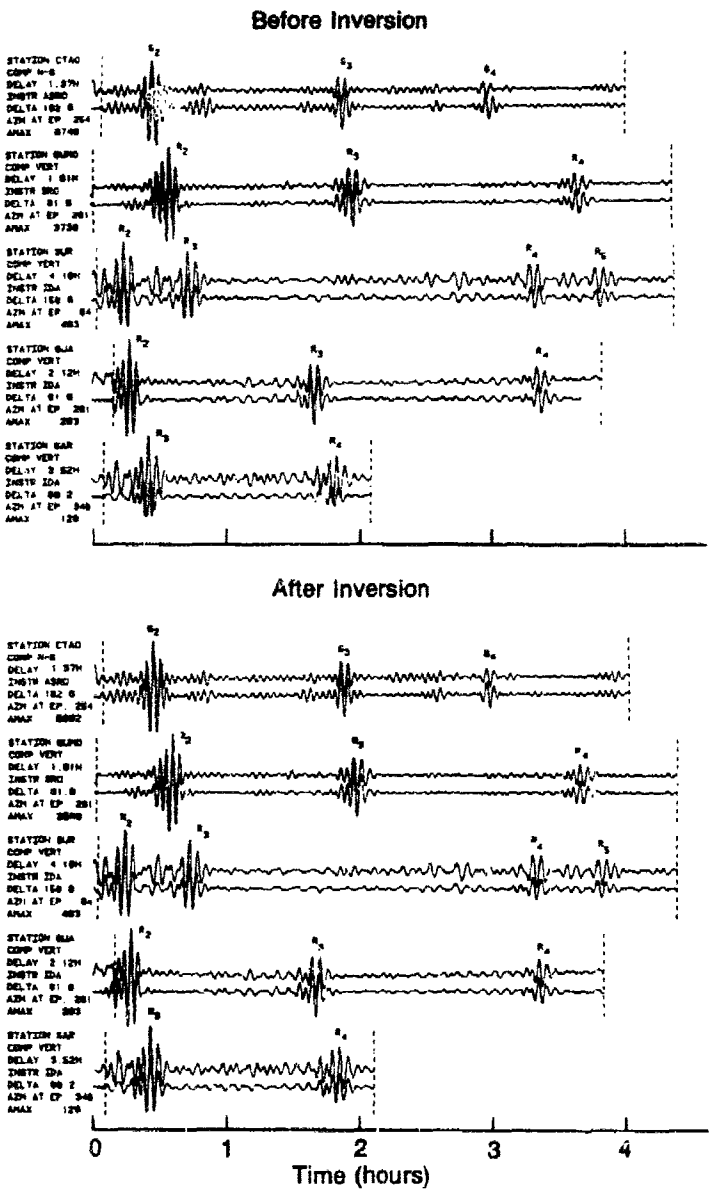

Fig. 1a. A comparison of data (top trace in each pair) with synthetic seismograms for a shallow earthquake. The upper panel shows the result of a centroid-moment tensor inversion in the Preliminary Reference Earth Model (PREM) of Dziewonski and Anderson [1981], and the lower panel shows the improved result after path corrections (controlled by lateral heterogeneity) have been determined. From Woodhouse and Dziewonski [1984].

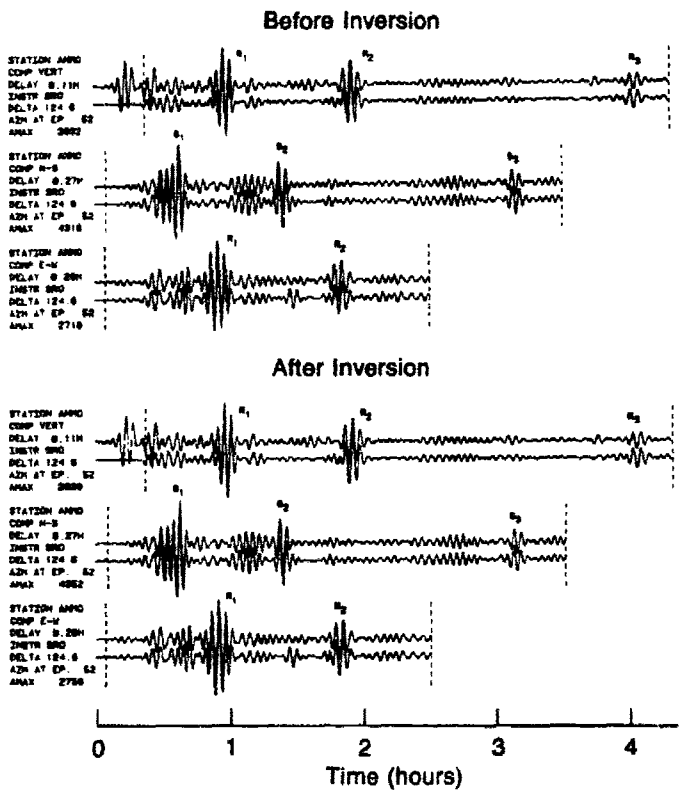

Fig. 1b. Same as Fig. 1a, but for a deep event. From Woodhouse and Dziewonski [1984].

1% too between Jeffreys' model and the model 1066B of Gilbert and Dziewonski [1975].

Accurate estimates of crustal thickness had begun with Mohorovičić in 1909; Gutenberg in 1913 gave the depth to the core-mantle boundary as 2900 km; and the existence of an inner core was recognized by Inge Lehmann in 1936. What then has been added, by use of synthetics (*i.e.*, the ability to work with whole waveforms in the data)?

It is generally recognized that the upper mantle contains two depth ranges (around 400 km and 650 km) within which the velocity gradient is anomalously large. But this was convincingly demonstrated by Johnson [1967] again using travel time analysis (with an array), not synthetics. Note too that the oil industry has in the 1980's been spending about $4 billion per year on the acquisition and processing of geophysical data

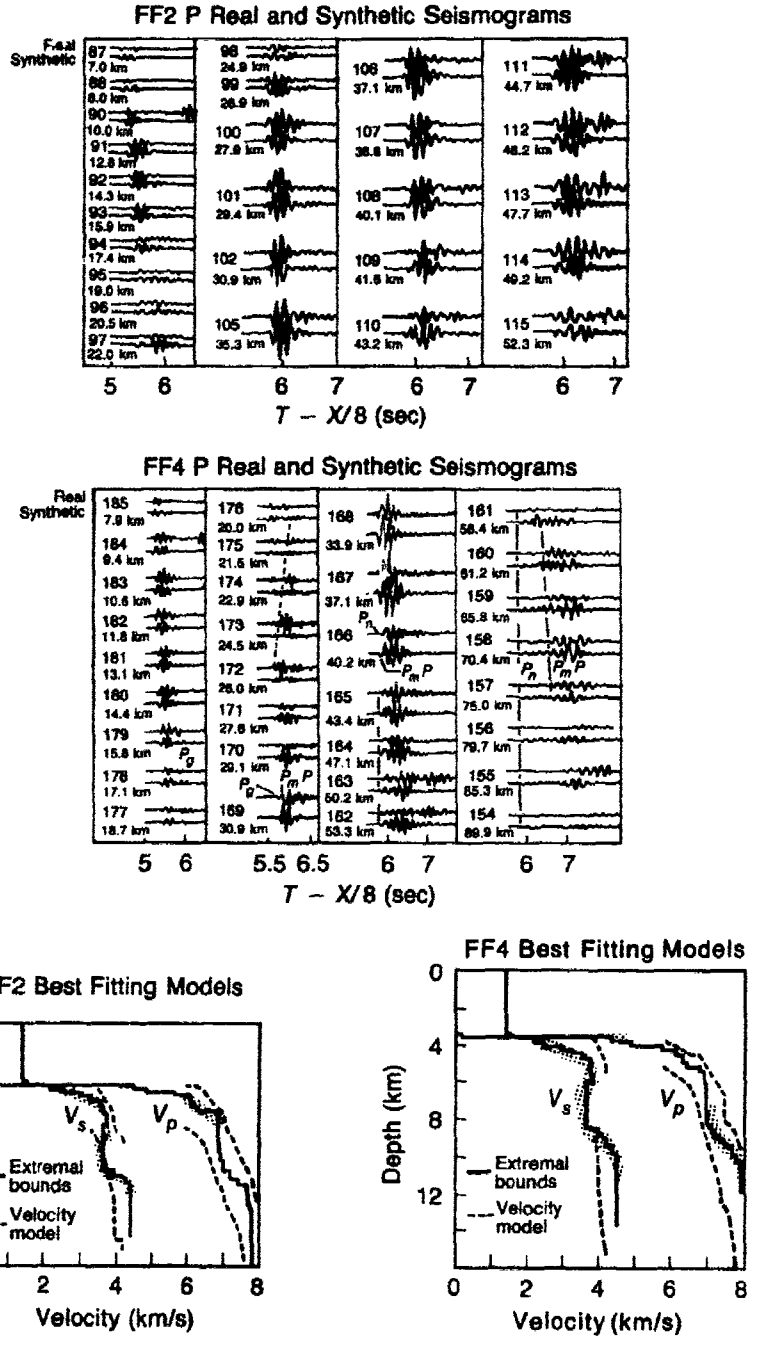

Fig. 1c. Comparison between observed hydrophone records and synthetics using the reflectivity method in the oceanic crustal models shown on the bottom. From Spudich and Orcutt [1980].

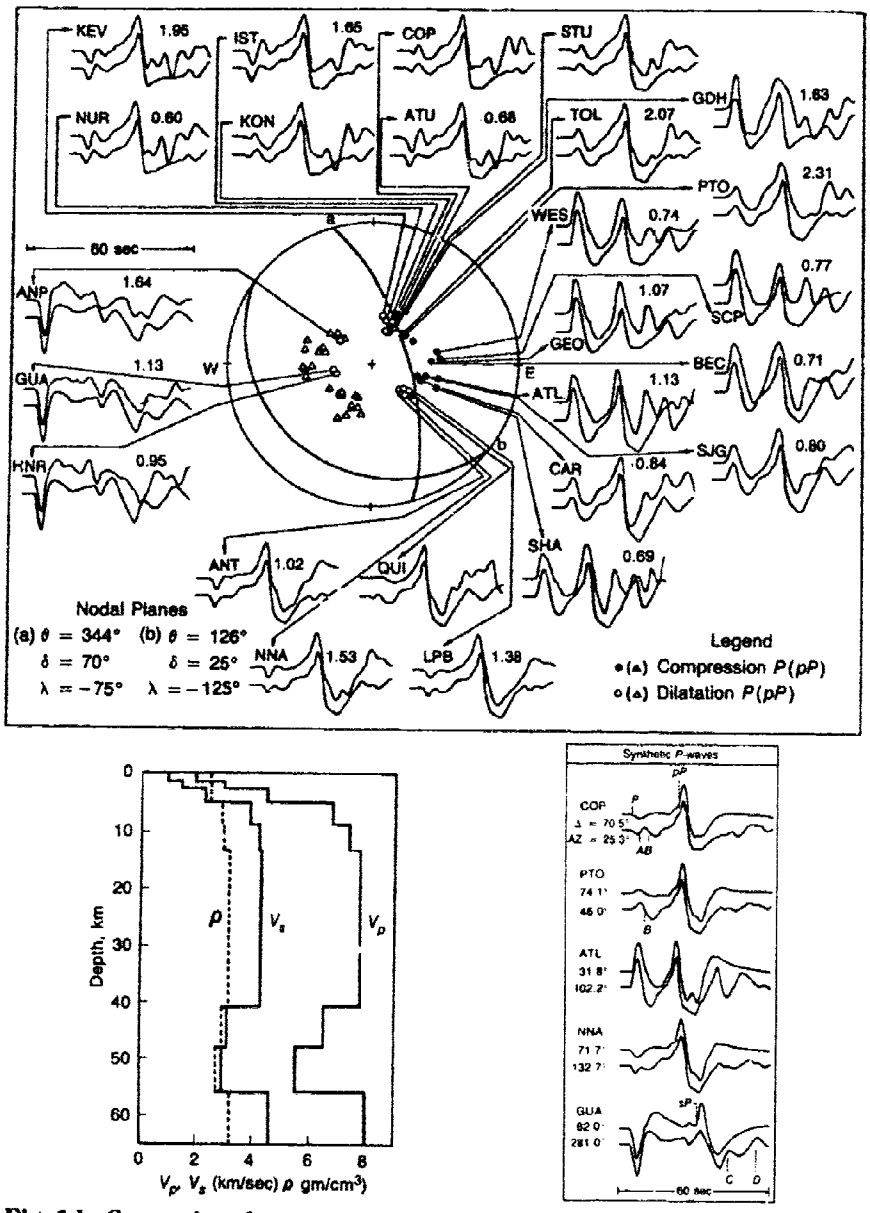

Fig. 1d. Comparison between observed (top) and synthetic (below) *P* waves for the 29 April 1965 Puget Sound earthquake. The *P* waveforms were simultaneously modeled for source and structure parameters. Arrivals between *P* and *pP* were interpreted as reflections from interfaces above the source. The inferred crustal structure is shown on the lower left. On the lower right, is a display to indicate the effect of the low velocity zone. In each pair, the synthetic for a one layer crust lies above, and the synthetic for a crust with low velocity zone lies below. Other studies in the region have also found evidence for a low velocity zone. From Langston and Blum [1977].

(almost all of it multi-channel seismics), and little of this goes for synthetics, in an industry dedicated to getting results.

From this brief history, it is not simple to make the case that use of synthetics is essential, purely for elucidating the Earth's velocity structure. However, there *is* a good case. It lies first in the ambiguity of interpreting imperfect travel time data [Backus and Gilbert, 1969]. For the ensemble of Earth models that fit a given set of travel times, synthetics impose constraints that act to reduce the ensemble, limiting it to Earth models for which amplitude and waveform data are fit, too. (For study of complex crustal structures, the oil industry has taken the route of hugely expanding the travel time set.) Another reason for using synthetics, in global seismology, is linked to the averaging properties of long period data, which permit accurate estimation of velocity structure averaged over tens of vertical kilometers, and over hundreds or thousands of horizontal kilometers (see Fig. 1ab).

If our interest includes not only velocity profiles, but attenuation within the Earth, then travel time analysis is inadequate, and use of synthetics (or, at least, study of spectral amplitudes) is essential. However, the vast literature on seismic attenuation does not yet indicate that agreement has been reached among different groups of seismologist, on acceptable profiles of attenuation. Because of its importance for studies of the seismic source (and yield estimation in particular), research on attenuation is very active. Some topics in this field are reviewed below, intended to make two points. First, that body wave pulses that have traversed both upper and lower mantle should probably be interpreted with an average Q that rises with frequency, having values of Q_S of 1 Hz that are 4 or 5 times higher than values at 0.01 Hz. Second, that attenuation of seismic waves may partly be caused by scattering from small-scale heterogeneities.

The following section gives a brief review of the theory. Later sections describe: some numerical experiments that compare different methods for computing synthetics; some particular examples of Earth structure that have been proposed on the basis of comparison between synthetic and observed waveforms; and a description of problems that arise in interpreting the attenuation of body waves.

Theory

To quantify the seismic waves excited by a given source, it is useful to replace the source by an equivalent body force, and to develop a way of computing the seismic waves set up by such an equivalent source. The most widely used equivalent body force for a point source is the second order moment tensor **M**, characterizing nine possible couples from

which can be constructed the radiation for an explosion or, in the case of a natural earthquake, for a generally oriented displacement discontinuity. Conservation of angular momentum requires that **M** be symmetric, and thus have only six independent components. The text by Aki and Richards (1980), hereinafter cited as AR, gives an extended presentation of the theory.

If **M** is known, for a particular point source, what is the resulting seismic motion?

This question can be answered, by giving explicit formulas for the excitation of seismic waves such as *P*, *S*, Rayleigh waves, Love waves, or normal modes, by the given source. It is particularly simple to do this for normal modes, as Gilbert (1971) showed by using ideas from Rayleigh's classic text on the theory of sound. If ${}_j\mathbf{u}(\mathbf{x})\cos\omega_j t\, e^{-\omega_j t/2Q_j}$ is the jth normal mode of the Earth, with frequency ω_j and temporal attenuation Q_j^{-1}, then a seismogram is just a sum over j with excitation coefficients given by the moment tensor. In fact, the result for ground displacement is

$$\mathbf{u}(\mathbf{x},t) = \sum \left({}_j\bar{\mathbf{e}}(x_s) : \dot{\mathbf{M}}(t)\right) *_j \mathbf{u}(\mathbf{x}) \frac{1-\exp(-\omega_j t/2Q_j)\cos\omega_j t}{\omega_j^2} \quad . \quad (1)$$

Here, ${}_j\mathbf{e}(\mathbf{x}_s)$ is the Earth strain (at the source) in the jth mode; an overbar indicates a complex conjugate; an overdot is a time derivative; an asterisk indicates convolution; and $\mathbf{e}:\mathbf{M} = e_{pq}M_{pq}$.

Equation 1 is one of the most important starting points for modern seismology. From it, one can go in the direction of Woodhouse (1982) and Woodhouse and Dziewonski (1984) who generalized to allow aspherical perturbations and subsequently developed an inverse scheme to obtain global patterns of heterogeneity [see also Tanimoto (1984)]. Or, Eqn. 1 can be used to study the excitation of surface waves, by developing a "traveling wave" interpretation of the "standing wave" Legendre functions for normal modes in a spherical Earth (AR; Section 8.3). That is, we can find an expression for the Rayleigh wave or Love wave motion at $\mathbf{x}$ due to a moment tensor characterization of a point source at $\mathbf{x}_s$ [Mendiguren (1977); and AR equations 7.147-7.150]. [Of course, there had been earlier successes in finding workable expressions for the surface waves set up by a given point source. Keilis-Borok and Yanovskaya (1962) did this for Love waves; Harkrider and Anderson (1966), for Rayleigh waves. Papers by Ben-Menahem and Toksöz (1963), Haskell (1964) and Ben-Menahem *et al.* (1965) derived the basic radiation patterns for surface waves from point sources, but their expressions did not lead naturally to a method for synthesizing wave trains.] Another

development gives the body waves due to a moment tensor source. This was done by McCowan (1977) in the context of ray theory; and Aki and Richards (1980; Box 9.10) and Langston (1981) give details for generalized rays. Although these authors did not start from the normal mode perspective, their results could have been obtained from Eqn. 1. Finally, if the seismic source is effectively of finite extent, then moment tensor concepts can be extended using, for example, a moment density tensor; or, using point source moment tensors with order higher than two.

Therefore, in order to obtain a general understanding of how synthetics may be computed, and whether seismic motions of interest will be large or small, one can go back to see what general features emerge from Eqn. 1. The first term describes the radiation pattern and time dependence of the source. This is convolved with the rest of the expression, describing the possible waves that can indeed propagate in the Earth model for which one is computing synthetics. And, most important of all, for practical details that differ radically between different methods of obtaining synthetics; there is a sum over j. The normal mode sum, for a spherical Earth, would take j as discrete, systematically indexing modes that individually are naturally described by a triplet of integers (ℓ, m, n), say. Here, ℓ and m are the angular and azimuthal order numbers associated with surface harmonics, *e.g.*, $P_\ell^m(\cos\theta)e^{im\phi}$, and n is the overtone number for the radial eigenfunction. The symbolic "sum over j" is thus a triple sum, over ℓ and m and n. The sum over m is small, being at most over the range $-2 \le m \le 2$ (unless we use higher order moment tensors), because of the simple, broad-lobed, azimuthal radiation patterns for seismic sources.

We therefore factorize Eqn. 1 and can think of the synthetic as a sum over ℓ and over n, of an expression where the dependence on source, Earth structure, and receiver are relegated to different factors:

$$\mathbf{u}(\mathbf{x},t) = \sum_{\ell} \sum_{n} \sum_{m=-2}^{2} f(\text{details of the source})\, e^{im\phi}$$
$$\times\, g(\text{receiver depth, and details of the Earth model})$$
$$\times\, \mathbf{h}(\text{horizontal separation of source and receiver}). \quad (2)$$

Each of the functions, f, g, and $\mathbf{h}$ depend on ℓ and n. But, for a laterally homogeneous Earth, g is independent of m.

Equation 2 gives another view of the basic procedure for computing synthetics. Closer examination of the sum over m, and the m-dependent

function f, shows in practice that the synthetic depends only on a very few linear combinations of moment tensor elements. Thus, with a cartesian coordinate system at the source in which x is north, y is east, and z is down, it is simple to get the following results:

(a) for all synthetics where we are interested only in P-waves leaving the source, we need only work with three basic synthetics, and combine them as

$$\mathbf{u}(\mathbf{x},t) \text{ for } P\text{-wave source } = \dot{M}_{zz} * \sum_{\ell} \sum_{n} f_1(\ell,n)\, g\mathbf{h}$$

$$+ (\cos^2\phi \dot{M}_{xx} + \sin 2\phi \dot{M}_{xy} + \sin^2\phi \dot{M}_{yy} - \dot{M}_{zz}) * \sum_{\ell} \sum_{n} f_2(\ell,n) g\mathbf{h}$$

$$+ (\cos\phi \dot{M}_{xz} + \sin\phi \dot{M}_{yz}) * \sum_{\ell} \sum_{n} f_3(\ell,n) g\mathbf{h} \; ; \qquad (3)$$

(b) for all synthetics where we are interested only in SV-waves leaving the source, we need only work with two basic synthetics, and combine them as

$\mathbf{u}(\mathbf{x},t)$ for SV-wave source

$$= (\cos^2\phi \dot{M}_{xx} + \sin 2\phi \dot{M}_{xy} + \sin^2\phi \dot{M}_{yy} - \dot{M}_{zz}) * \sum_{\ell} \sum_{n} f_4(\ell,n) g\mathbf{h}$$

$$+ (\cos\phi \dot{M}_{xz} + \sin\phi \dot{M}_{yz}) * \sum_{\ell} \sum_{n} f_5(\ell,n) g\mathbf{h} \; ; \qquad (4)$$

(c) for all synthetics where we are interested only in SH-waves leaving the source, we need only work with two basic synthetics, and combine them as

$\mathbf{u}(\mathbf{x},t)$ for SH-wave source

$$= (\tfrac{1}{2}\sin 2\phi [\dot{M}_{yy} - \dot{M}_{xx}) + \cos 2\phi \dot{M}_{xy}) * \sum_{\ell} \sum_{n} f_6(\ell,n) g\mathbf{h}$$

$$+ (\cos\phi \dot{M}_{yz} - \sin\phi \dot{M}_{xz}) * \sum_{\ell} \sum_{n} f_7(\ell,n) g\mathbf{h} \; . \qquad (5)$$

Thus, by "basic synthetic" we mean one of the sums over (ℓ n) in Eqns. 3-5, where each term has a factor (f, in the above) depending on the source depth; a factor (g) depending on the vertical wave function, and a factor (h) depending on the vector surface harmonic.

The angle ϕ in Eqns. 3-5 is azimuth from source to receiver measured (as usual) clockwise round from north. There are many different ways to rearrange terms in these three equations. With the choice above, an explosion radiating P-waves symmetrically in all directions out of the focal sphere is described merely by the first of the three P-wave expressions.

For a point dislocation, characterized by its strike (ϕ_s), dip (δ), rake (λ), and seismic moment $M_o(t)$, the moment tensor has components

$$M_{xx} = -M_o(\sin\delta\ \cos\lambda\ \sin 2\phi_s + \sin 2\delta\ \sin\lambda\ \sin^2\phi_s)\ ,$$

$$M_{xy} = M_o(\sin\delta\ \cos\lambda\ \cos 2\phi_s + \tfrac{1}{2}\sin 2\delta\ \sin\lambda\ \sin 2\phi_s) = M_{yx}\ ,$$

$$M_{xz} = -M_o(\cos\delta\ \cos\lambda\ \cos\phi_s + \cos 2\delta\ \sin\lambda\ \sin\phi_s) = M_{zx}\ ,$$

$$M_{yy} = M_o(\sin\delta\ \cos\lambda\ \sin 2\phi_s - \sin 2\delta\ \sin\lambda\ \cos^2\phi_s)\ ,$$

$$M_{yz} = -M_o(\cos\delta\ \cos\lambda\ \sin\phi_s - \cos 2\delta\ \sin\lambda\ \cos\phi_s) = M_{zy}\ ,$$

$$M_{zz} = M_o \sin 2\delta\ \sin\lambda\ . \qquad (6)$$

For an explosion source, seismologists associated with the VELA program usually work with a reduced displacement potential (RDP), $\psi = \psi(t)$, such that radial displacement at distance r is $(\partial/\partial r)\,[\psi(t - r/\alpha)/r]$ in a homogeneous region with P-wave speed α. Such a source, symmetrically radiating P-waves alone, has moment tensor components given by

$$M_{ij} = M_1(t)\ \delta_{ij} \qquad (7)$$

with M_1 related to the RDP *via* $M_1 = 4\pi(\lambda + 2\mu)\mathrm{RDP} = 4\pi\rho\alpha^2$ (λ and μ are the Lamé constants, ρ is the density).

Müller (1973) pointed out that the scalar moments M_o and M_1, associated respectively with earthquakes and explosions, have similar properties when interpreted in terms of displacement across surfaces associated with the source. Thus, for an earthquake, $M_o(t) = \mu < u > A$ where A is the area of faulting, and $< u(t) >$ is the average displacement discontinuity across A at time t. For an explosion, $M_1(t) =$

$(\lambda + 2\mu)u_r A$ where A is the area of a sphere centered on the explosion, and u_r is the radial displacement (outward) on A.

Equations 3-7 are the basic formulas used for computation of synthetics, for earthquakes or explosions, for surface waves and body waves on/in a laterally homogeneous Earth. In practice, they can also be used for normal modes (except for very low values of ℓ). Though the generality of these equations is obvious from their basis in normal mode theory, it is not generally recognized that the multitude of different methods for computing body waves, surface waves, leaking modes, head waves, *etc.* are all special examples of Eqns. 3-5. Let us continue to explore the structure of these equations, in particular the summations over ℓ and n.

We know that angular order number ℓ is related simply to horizontal wavenumber (k), and to ray parameter (p) via

$$\ell + \tfrac{1}{2} = k = \omega p$$

(often called Jean's relation; see AR, pages 356 and 415). For cases where we prefer to work with a continuum of wavenumbers or ray parameters, we can therefore replace the summation operation $\sum_{\ell}$ by integration as $\int dk$ or $\omega \int dp$.

At fixed ℓ (or k), the overtone number n increases with frequency ω. For cases where we prefer to work with a continuum of frequencies, we can replace the summation operation $\sum_{n}$ by integration as $\int d\omega$.

The literature on theoretical seismic wave propagation is vast, because (i) the details of going from sums over (ℓ, n) to integrals over (k, ω) or (p, ω), are not trivial, and occasionally take one into laborious exercises that call upon wide knowledge of Legendre functions, Bessel functions, and properties of functions defined by integrals; (ii) there are many alternate routes to the particular answer in which one is interested; and (iii) there are many ways, in practice, that different seismologists have developed for obtaining the integrands and for actually carrying out the integrals over (k, ω) [or, over (p, ω), or, sums over (p, n)]. Chapman (1978a, b) has advocated carrying out the frequency integral first, for synthesizing body wave seismograms, so that intermediate results are found as a function of ray parameter, before the final integration over p. He calls this sequence a slowness method. Synthetics that are produced by first integrating over p, to obtain intermediate results in the frequency domain, are obtained by a spectral method, requiring a final integration over frequency components. Cagniard-de Hoop methods are a particularly elegant series of procedures that allow the outcome of (p, ω) integrations to be recognized without actually having to carry

out either integration. In many of these methods, the integral over p is taken into the complex p-plane. In some cases, there is merit in working with complex frequencies.

The question of which method for computing synthetics is most appropriate for interpreting a particular set of waveform data, is not amenable to a simple answer.

If the data contain long periods (> 60 s) with signal lasting several minutes, then it is natural to work with normal modes, or with a surface wave method if one can avoid the problems of interference between waves that have traveled on minor arc, major arc, and global great circles between source and receiver.

If the data is recorded in the near field or at "regional distances", and composed of wavelengths short enough to be unaffected by gravitation, then many seismologists have found it natural to work with a continuum of horizontal wavenumbers. In recent years, direct integration over (k, ω) has become practical in these cases. The reflectivity method originated by Fuchs takes this route. In practice it depends heavily on the ability to compute all plane-wave multiples in a stack of homogeneous elastic layers — an ability pioneered by Haskell (1953, 1960, 1962). Fuchs and Müller (1971) assessed this method for crustal structures; Kind (1976) gave a fast program for obtaining the integrand as a function of (k, ω); and the method has been extended to find wide application even at teleseismic distances [*e.g.*, Grand and Helmberger (1984) use it to validate another method for examining *SH* waves out to about $\Delta = 100°$, which may be influenced by structure at the base of the lower mantle]. If the "reflectivity method" [an inadequate but widely used phrase, referring to direct integration over real (k, ω) values] is applied to include surface waves as well as body waves, then numerical complications arise in that the real-axis path of k-integration includes singularities (poles) requiring special treatment. Bouchon (1981), Apsel and Luco (1983) and Luco and Apsel (1983) show how such surface wave contributions can be assessed. And Harvey (1981) developed a "locked-mode" approach in which the set of "surface waves" (discrete modes) was made to provide a complete basis for seismic motions within a finite time window. More recent procedures, for computing synthetics in layered structures that allow body wave multiples and all surface wave modes to be included, permit individual layers to be inhomogeneous. [Kennett's (1983) textbook reviews his own research contributions; see also Cormier (1980)].

It must be acknowledged that programs for synthesizing all multiples and all surface waves, in realistic structures, are viewed as quite cumbersome and expensive to run, if they are to sample (k, ω) space sufficiently well to produce long-duration broad-band time series that match the

signal-length and band-width of modern digital data. It has therefore been necessary in practice to develop methods for synthesizing isolated portions of a seismogram, usually body wave pulses, that one presumes are modulated only by restricted regions of the Earth's interior. This is the subject of generalized ray theory. There are many such theories, *i.e.*, there are many different approximations proposed, for choosing the integrands for (p, ω) integration, and for executing the integrals. Helmberger (1968) took a major practical step, when he showed how Cagniard-de Hoop methods could be used, with appropriate approximations, to get the generalized reflection response (head wave, wide angle reflection) of a single interface below a stack of layers. He applied this to marine refraction (hydrophone) waveforms in the Bering Sea, and by trial and error with layered Earth models was able to study the transition from oceanic crust to mantle across the Moho. This moved seismology to a new level of analysis, since it stimulated our need to know detailed source time functions, Earth attenuation, and instrument characteristics, before even a start could be made on getting at the potential Earth structure information in recorded waveforms.

Unfortunately, the Earth is not made very well (John Ewing, personal communication). This is stated from the perspective of one who sets out to obtain a reasonably complete description of Earth structure using the details of seismic arrivals and waveforms (*i.e.*, reasonably complete for purposes of answering fundamental questions in petrology, and other branches of Earth science). From structures at depth (*e.g.*, the "Lehmann discontinuity" at about 200 km depth; velocity gradient anomalies (at about 400 and 650 km); anomalous velocities at the bottom of the lower mantle and top of the inner core), there is tantalizing evidence from possible reflections that we can state new properties of the Earth. But, in light of subsequent work, it turns out broadly that three problems arise. (a) Non-uniqueness. Instead of an observed waveform being interpreted by the modulating effect of some newly proposed deep structure, it may turn out that shallow structure under certain of the receivers recording the data can have the same effect. Also the trade-off between source spectrum and attenuation is notorious. (b) Various effects arising from lateral variation in Earth structure. For example, some of the earliest observations of short-period core-diffracted *P*-waves indicated arrivals with frequency content up to 1 Hz even out to 125°. But, for other source-receiver pairs, diffracted *P* is seen only at much longer period. Inversion of sub-sets of the data give different structure. (c) For complicated models of Earth structure, it may not always be certain that we know how to solve the forward problem, *i.e.*, to generate synthetics. Certainly, this is the case for many three-dimensional structures, and

anisotropy introduces new levels of non-uniqueness and problems in forward modeling.

Since a companion paper by D. L. Anderson discusses three-dimensional modeling of the Earth, I shall in what follows emphasize one-dimensional modeling, *i.e.*, in structures that vary only in depth.

Computation of Synthetics in Depth-Dependent Structures

One of the best ways to build confidence in one's ability to compute synthetics, is to check that essentially the same synthetic is reproduced by two different methods.

Thus, Fig. 2 compares two computations of the ground motion at 80° for the *P*-wave group (*P* plus *pP* plus *sP*), using a point shear dislocation at depth 15 km and specified values of $[\phi_s, \delta, \lambda, M_o(t)]$. Though these computations are merely the outcome of geometrical ray theory, they are executed somewhat differently. In the first computation, an elastic Earth model is assumed. Then the motion at distance Δ_o,

$$u(\Delta_o, t) = \sum_t \sum_n f g h$$

is manipulated into the form

$$u(\Delta_o, t) = \int ds\, e^{+st} \int F(p,s)\, e^{-s[T(p)-p\Delta(p)+p\Delta_o]}\, dp$$

where $T(p)$ and $\Delta(p)$ are respectively the time and distance of emergence of the ray with ray parameter p; and s is the independent Laplace transform variable. For an elastic Earth model, $F(p,s)$ can be factorized in the above integrand, and a Cagniard method (*i.e.*, one that directly recognizes the outcome of the pair of integrations, without the need to execute each explicitly) is applied. For the final synthetic, the effects of attenuation, source-time function, and summation as in Eqns. 3-5 are accounted for. In this computation, a frequency-independent Q was used with a t^* value of 1 s ($t^* = \int Q^{-1}\, dt$ along the ray), applying a Carpenter [1967] operator that gives a small amount of body wave dispersion. Details are given in Langston and Helmberger [1975] and Langston [1981].

In the second computation of Fig. 2, an anelastic model is assumed, with complex values of *P* and *S* velocity. The motion at distance Δ_o is manipulated into the form

$$u(\Delta_o, t) = \int d\omega e^{-i\omega t} \int G(p, \omega) e^{i\omega[T(p)-p\Delta(p)+p\Delta_o]} dp\ .$$

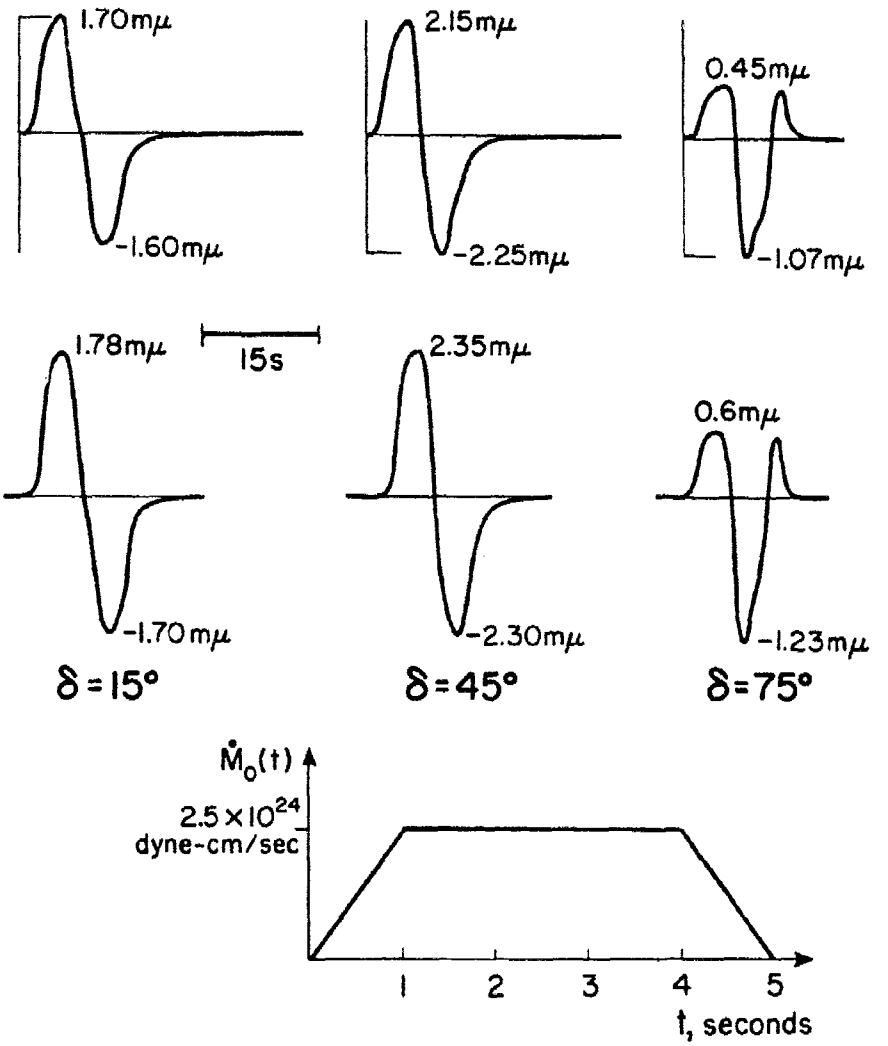

Fig. 2. Each pulse gives the *P*-wave group ($P+pP+sp$) at distance 80°, and 30° off the strike direction, from a point source 15 km deep. Rake is 90°, and results are given for three different dips. These are displacements in the upward vertical direction (after a free surface correction). t^* is taken as 1 second, and the time dependence of the source is given at the bottom of the figure.

The upper row uses a Cagniard first motion approximation [Langston and Helmberger, 1975]. The lower row (which has the same time scale but is displayed with a slightly different amplitude scale) uses the complex saddle point spectral method reviewed in the text, with model PEM-C and a Q structure that gives $t^* = 1$ at 80°.

Numbers displayed are displacement in $m\mu$. The two methods, each of which is basically geometrical ray theory adapted to an attenuating medium, agree to within about 10%.

Having sampled the integrand in real p at fixed ω, the vicinity of a stationary value of $T(p)-p\Delta+p\Delta_o$ is easily identified. By fitting a parabola one obtains the constant T_o, p_o, and $(\partial\Delta/\partial p)$ in

$$T(p)-p\Delta(p)+p\Delta_o = T_o + \frac{(p-p_o)^2}{2}\frac{-\partial\Delta}{\partial p} .$$

Just these three constants are all that is needed to obtain the "first-motion" approximation, though here it is interesting that T_o is complex (with imaginary part equal to 0.5 t^*), and the method is unchanged if Q (and hence t^*) is frequency dependent.

The main point from Fig. 2 is that agreement in amplitude and waveform appears very good. For isolated body-wave pulse shapes it can be presumed that synthetics are trustworthy in the distance range 30°-90° (apart from interference from core phases). It is from body-wave data in this distance range, that much has been learned about seismic sources.

However, using synthetics to learn about Earth structure usually necessitates more than just the geometrical ray examples of Fig. 2. With multiple arrivals, and effects coming from velocity gradients in the model, can we still be sure that synthetics are accurately computed? Burdick and Orcutt [1979] explore comparisons between generalized ray and reflectivity methods of synthesis. They give a rare, and very useful, summary of some of the difficulties encountered in computing synthetics for upper mantle structures. Figure 3 describes some of their results. Though they conclude that "the reflectivity and generalized ray methods.... yield essentially the same results", they did point out special cases where it was not obvious how to truncate the set of generalized rays.

In order to build up complicated depth-dependent profiles, it is common to show layered structures as here in Fig. 3a. But generalized ray and reflectivity methods are applied typically after an Earth flattening transformation has been applied. In the context of spherical layers, such velocities should therefore be shown increasing in value with radius (AR, pages 463-465). However, instead of building up a profile from tens or hundreds of component layers (for example, in order to simulate a gradual increase of velocity with depth), it is possible instead to work directly with a few inhomogeneous layers. The penalty lies in not being able to use plane wave theory for the equivalent flat Earth model. Rather, vertical eigenfunctions become the subject of special methods of computation. A uniformly asymptotic method is often still accurate, and was employed by Cormier and Choy [1981] again to study body wave interactions with upper mantle structure. Called a "full wave" method, their

Fig. 3a. Upper mantle model T7.

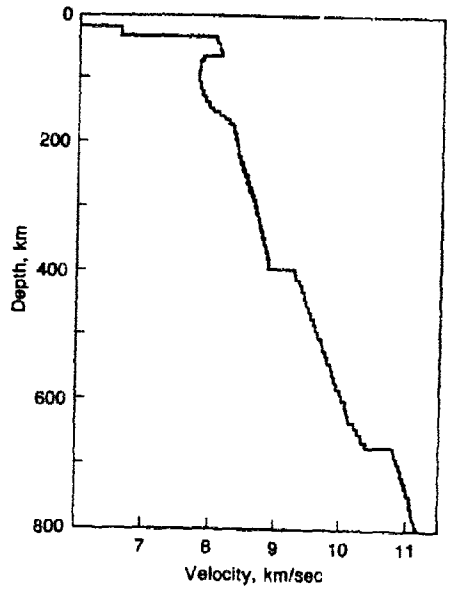

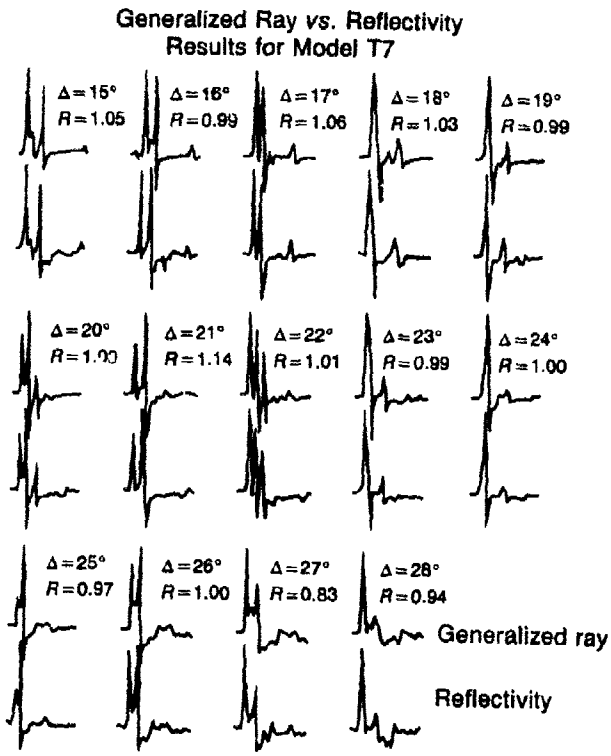

Fig. 3b. Comparison of Cagniard (generalized ray) and reflectivity synthetics in T7. From Orcutt and Burdick [1979].

synthetics are compared in Fig. 4 with those of Burdick and Orcutt [1979]. Again, there is good agreement. Cormier and Choy state that differences "between the methods do exist but are most evident at high frequencies, where the planar layer methods suffer from numerical limitations on layer thickness and the number of layers needed to approximate the earth model."

Such differences become more apparent for computation of core phases. Choy *et al.* [1980] synthesized diffracted *SV* plus *SKS* and *SmKS* in model 1066B, using reflectivity and hundreds of layers; and also using a full wave method and eight inhomogeneous layers. Results are shown in Fig. 5. Comparison of the Green functions does not look promising (Fig. 5ab). Comparison after convolution with the typical long-period WWSSN response looks much better — although pulse shapes between the two methods still differ (Fig. 5cd). However, after additional convolution to simulate a source function with a few seconds duration, there is excellent agreement (Fig. 5ef). Note that both these methods were applied in ways that retained the infinite multiples associated with "whispering galleries" such as $SKS+SKKS+S3KS+....+SmKS+.....$

An example where a finite ray series leads to inaccurate synthetics is demonstrated by Grand and Helmberger [1983], shown here on the right of Fig. 6. This gives *SH* synthetics for the upper mantle, comparing a Cagniard (generalized ray) method and the WKJB method of Chapman [1978a]. The latter has not been developed in a form that quantifies tunnelling through the high velocity "lid" of the shield model SNA. Note, however, that the WKBJ synthetics, which often provide the most

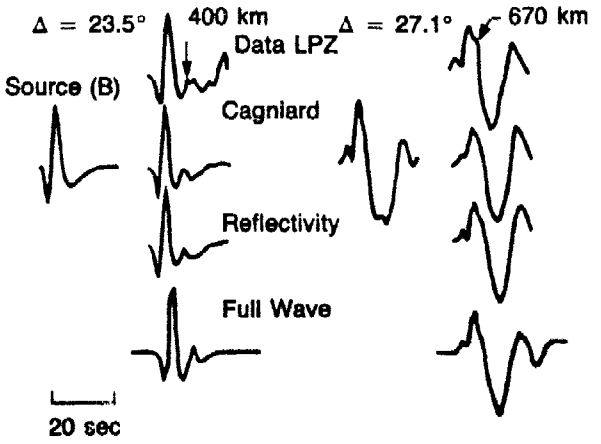

Fig. 4. Comparison of data and three different methods of waveform synthesis for the T7 model. From Cormier and Choy [1981].

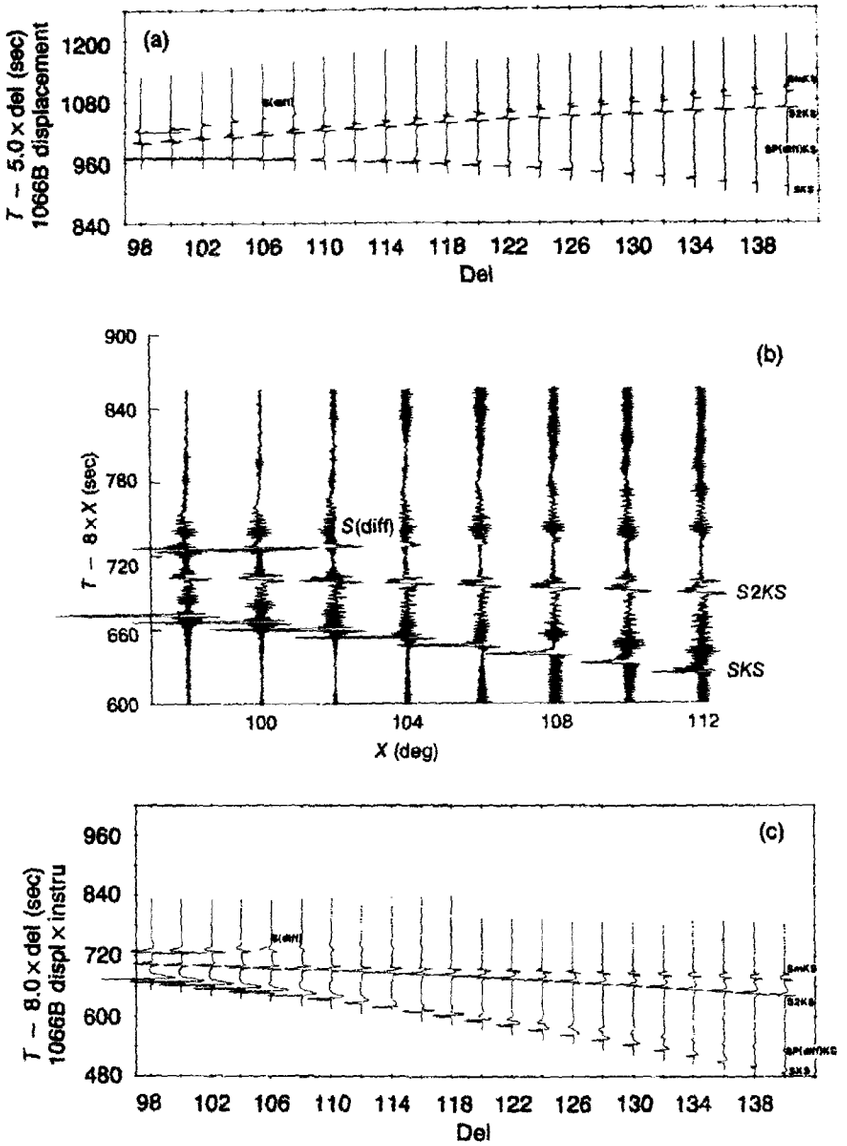

Fig. 5. (a). Synthetic seismograms computed by the full wave theory for the horizontal radial component of displacement for *SV* waves interacting with the Earth's outer core. The computation used model 1066B without attenuation, a point double-couple source with one nodal plane oriented vertically, and surface depth for both source and receiver. The sampling interval is 1 s. (b). The displacement for distances in (a) as computed by the reflectivity method. The sampling interval is also 1 s. (c). Synthetic seismograms as in (a), computed by the full wave theory, after introducing the effect of the instrument response of a 15-100 s seismograph.

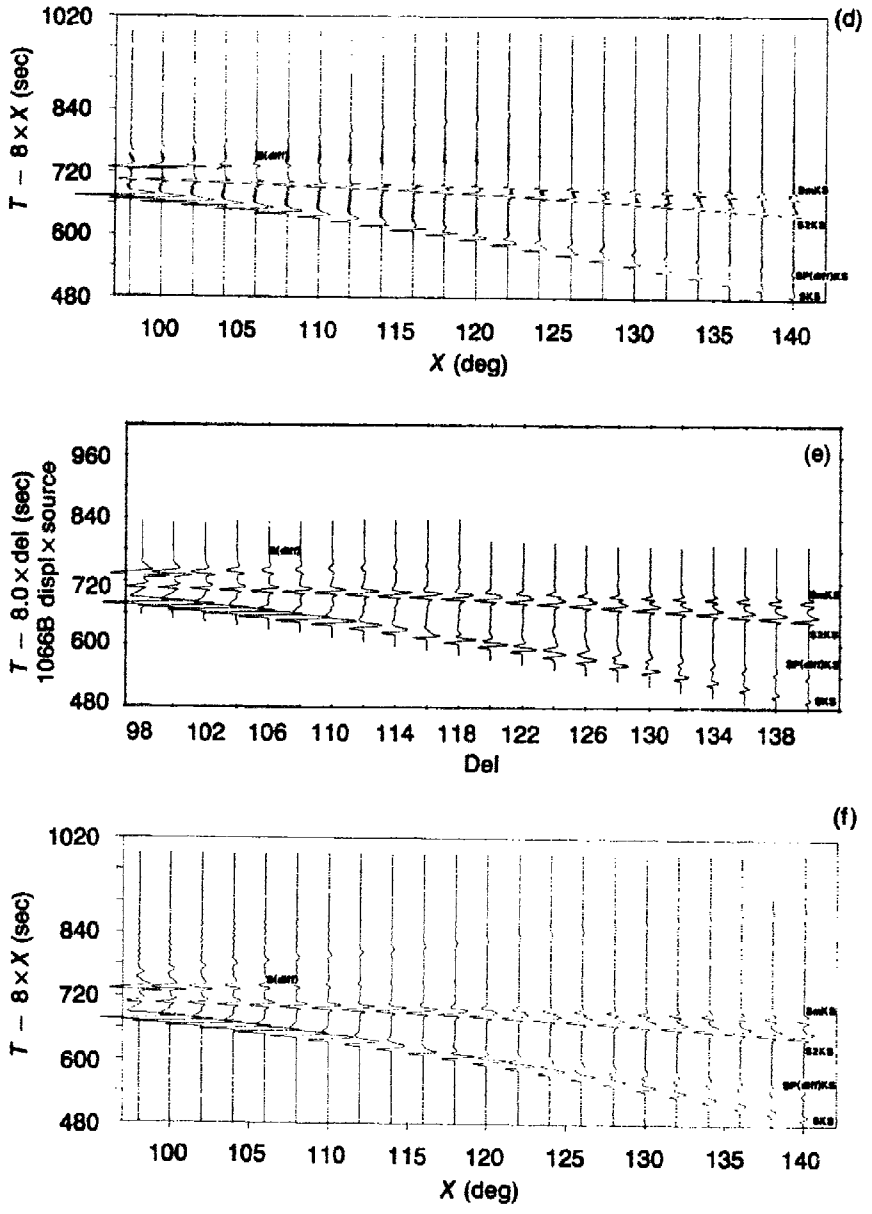

Fig. 5. (d). The reflectivity records for the same distances. This set of seismograms is normalized with part (c) such that at 98° the amplitudes of *SKS* measured from baseline to the first peak is the same for both sets of records. (e). The same synthetic seismograms, computed by the full wave theory, after convolution with a source function and the instrument response. (f). The reflectivity records for the same distances as in part (e). Again, the record sets are normalized to the baseline-to-peak amplitude of *SKS* at 98°. From Choy *et al.* [1980].

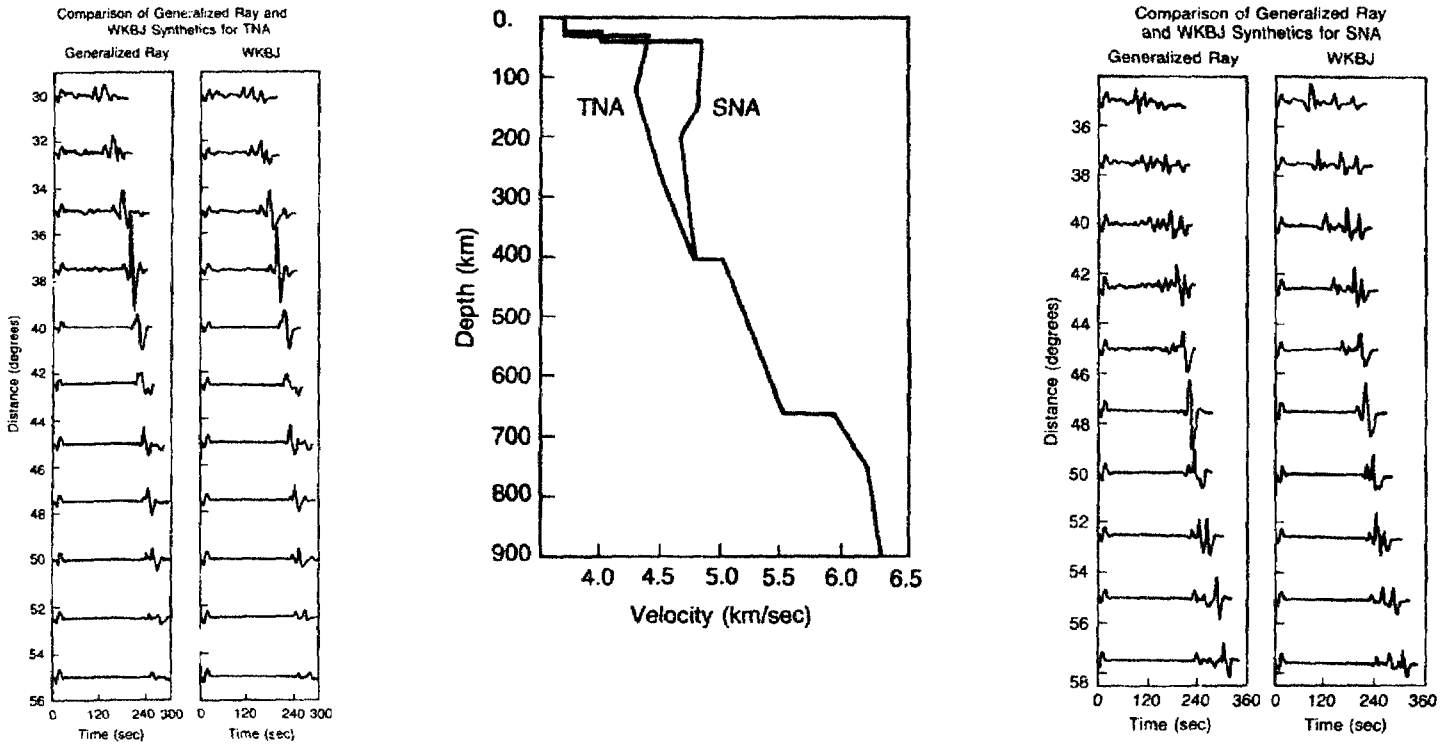

Fig. 6. Tectonic (TNA) and shield (SNA) models of the shear wave velocity in the upper mantle.
On the left is shown a comparison between generalized ray and WKBJ synthetics giving good agreement for model TNA.
A similar comparison, on the right, is less successful for model SNA, which does not have a turning ray at depths somewhat above 200 km. From Grand and Helmberger [1984].

efficient way to compute a record section, give very good comparison with the Cagniard record section on the left of Fig. 6.

The outcome of such comparisons [see also, Stephen, 1983; Apsel and Luco, 1983; and Luco and Apsel, 1983] generates confidence that after many years of development, computation of synthetics has for many purposes become reliable. Given a structure in which velocities mainly increase with depth, with perhaps a low velocity zone and/or a few discontinuities, we can compute seismograms relevant to the bandwidth of our data. Because of this development, which comes after many man-years of effort, it would be an aid to scientific progress if the most successful programs were documented and generally available. However, at present it appears that access to programs is arranged only on an informal basis. It would also be most helpful if, in publishing synthetics, enough information were supplied to enable other seismologists to reproduce the computation.

Earth Structure, from Analysis of Seismic Waveforms: Selected Studies

It was pointed out above that major sub-divisions of the Earth's structure (crust, mantle, fluid core, solid core) were identified decades before synthetics came into routine quantitative use. However, in a qualitative fashion, synthetics have played an influential role since Lamb's [1904] classic paper showed how body wave and surface wave pulses would appear for a point source in an elastic half-space. Lamb's work, and developments by Nakano, Pekeris and Lapwood for simple structures, led to synthetic seismograms consisting essentially of a few isolated pulses. The puzzle facing observational seismologist was that ground motion in a seismogram is commonly oscillatory for many minutes. Jeffreys [1931] examined and rejected many explanations, concluding that "the only suggestion which survives is that the oscillations are due to reflections of the original pulse within the surface layers." That this is basically a satisfactory explanation is now confirmed by many numerical studies of the past decade, in which the computation of all body wave multiples and/or all surface wave modes has been undertaken in structures with many layers. (The most notable example of surprisingly long-lasting oscillations occurs in the oceanic P_n and S_n phases, which can be modeled as reverberations in a few crustal layers and the water column; see Gettrust and Frazer [1981].)

As seismology developed in the 50's and 60's, with better instrumentation and a more complete understanding of wave propagation, the first part of a seismogram to be thoroughly understood (apart from simple arrival times) was the dispersion in surface waves. The wish to study

deeper and deeper structures by this method led naturally to efforts in instrumentation at longer periods, and led also to efforts in understanding wave propagation that promoted working with discrete normal modes of the whole Earth. It is interesting that in their paper entitled "Preliminary Reference Earth Model", Dziewonski and Anderson [1981] did not work with synthetics. Rather, they used about "1000 normal mode periods, 500 summary travel time observations, 100 normal mode Q values, mass and moment of inertia." They also used a set of about 1.75 million travel times for P and S indicating significant lateral heterogeneity (which they sought to average). Their PREM model is shown in Fig. 7, with upper mantle discontinuities at about 400 km and 650 km depth.

There is now an extensive literature on these proposed discontinuities. The natural questions to ask are: how thick is each of these two regions? (A discontinuity has zero thickness.) How big is the jump in velocity across each anomalous region? And what velocity gradients are present just above and just below 400 and 650 km? Good answers are available, using synthetics for depth dependent structures, only if there is also available a good data set, for sources and receivers within

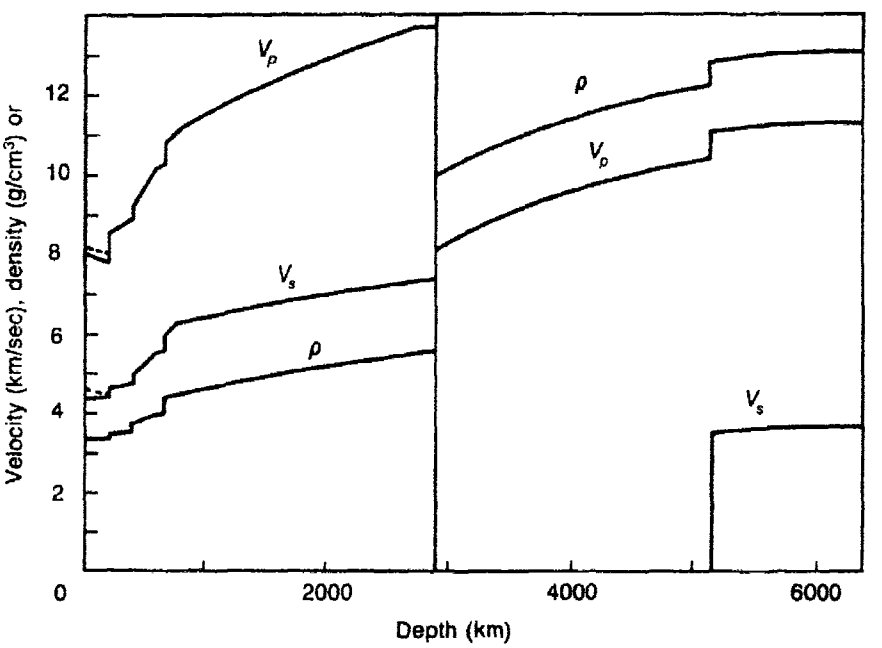

Fig. 7. The Preliminary Reference Earth Model (PREM). Dashed lines are for horizontal velocities in a transversely isotropic layer. From Dziewonski and Anderson [1981].

a region about 3000 km across, that indeed does not vary laterally. Walck [1984] used more than 1400 short-period digital seismograms from earthquakes in Mexico and Central America, recorded by the Southern California Seismic Network. From travel-time analysis and inversion of $dT/d\Delta$ observations, she obtained a starting model for the P-velocity profile that was subjected to more than 100 trial-and-error iterations, resulting in the final model, GCA, shown in Fig. 8. Some waveform data and synthetics relevant to the three questions just asked are shown in Fig. 9. Reflections from 390 and 660 km are wide angle, so, although this is short-period data, she stated it was not possible to distinguish between discontinuities (as shown in Fig. 8) and equivalent high gradients over 10-20 km. The jumps in velocity were found to be quite small (only 2.8% at 660 km), but were associated with large gradients just above 390 and 660 km, and just below 660 km.

Upper mantle structure, from analysis of *SH* and *SV* Waveforms. Grand and Helmberger (1983) have studied triplications in S and SS for SH waves in the range 10° to 60°. From waveforms recorded in western North America for earthquakes on the East Pacific Rise they have proposed a tectonic upper mantle model having a zone of slightly low velocities centered on a depth of 120 km. From waveforms for events northwest of North America they have proposed a shield model with a more pronounced low velocity zone centered on about 200 km depth,

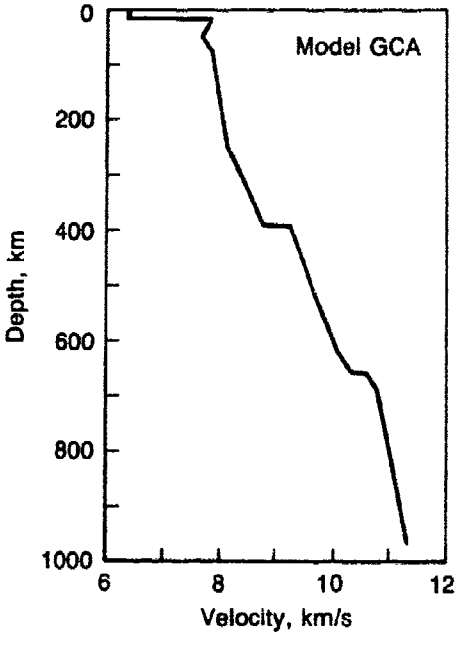

Fig. 8. Upper mantle P-velocity model GCA. Developed for the Gulf of California spreading region, GCA has a 20 km crust and velocities that in general are low in value down to 350 km depth, with an unusually large gradient from 225 to 390 km. Velocity discontinuities are 4.7 per cent at 390 km and 2.8 per cent at 660 km. From Walck [1984].

above which is a thick zone (50-150 km depth) of high and almost constant velocity. The models are the same below 405 km and have velocity jumps at 450 km and 660 km. These models are shown in the center of Fig. 6. Associated synthetics and waveform data, are shown in Fig. 10.

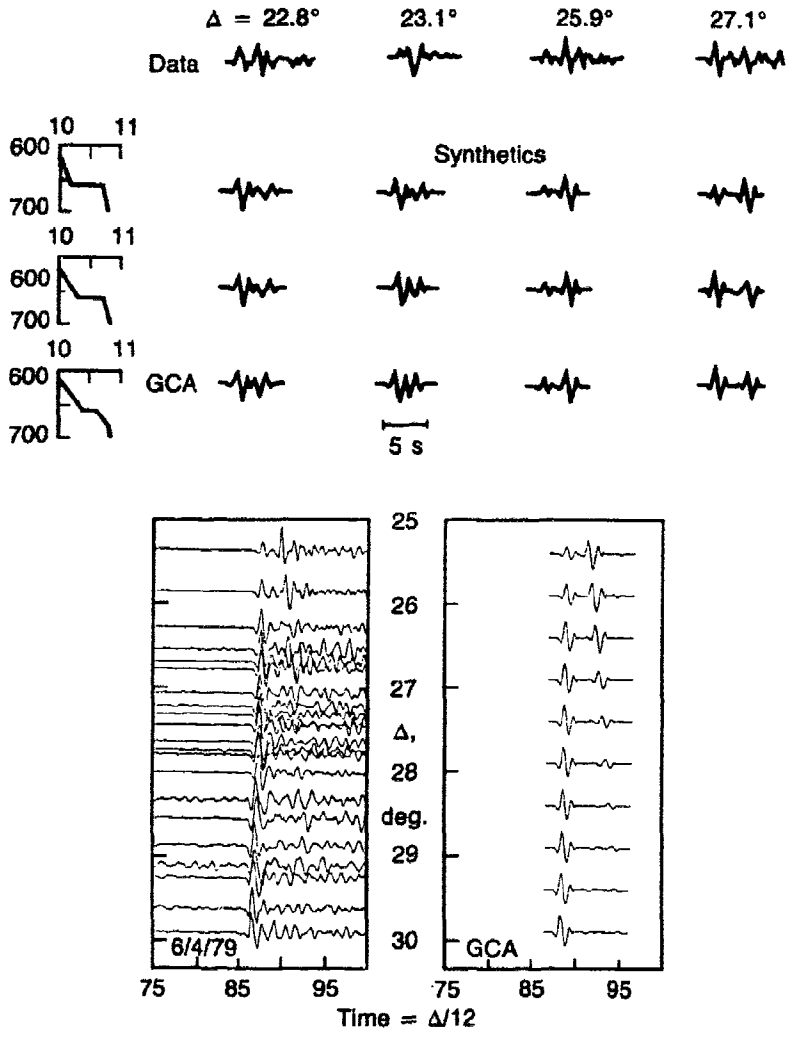

Fig. 9. Detailed analysis of the 660 km discontinuity. (a) The synthetics are calculated for model GCA with differing gradients above and below 660 km, from a simple step (top row) to large gradients above and below (bottom row). (b) Data (left panel) and synthetics for GCA (right panel) for part of the triplication due to structure at 660 km. Relative amplitudes change from a weak first arrival near 26° to a simple pulse near 28°. From Walck [1984].

Waveform data for *P-SV* pertinent to this region of the Earth appear to be intrinsically more complicated than *SH*, yet Priestley *et al.* [1980] had considerable success fitting synthetics to data. Lerner-Lam and Jordan (1983) tackled *P-SV* data using an inversion method based on improving the fit between higher-mode surface waves in synthetics and observed seismograms. They derived upper mantle models of *SV*

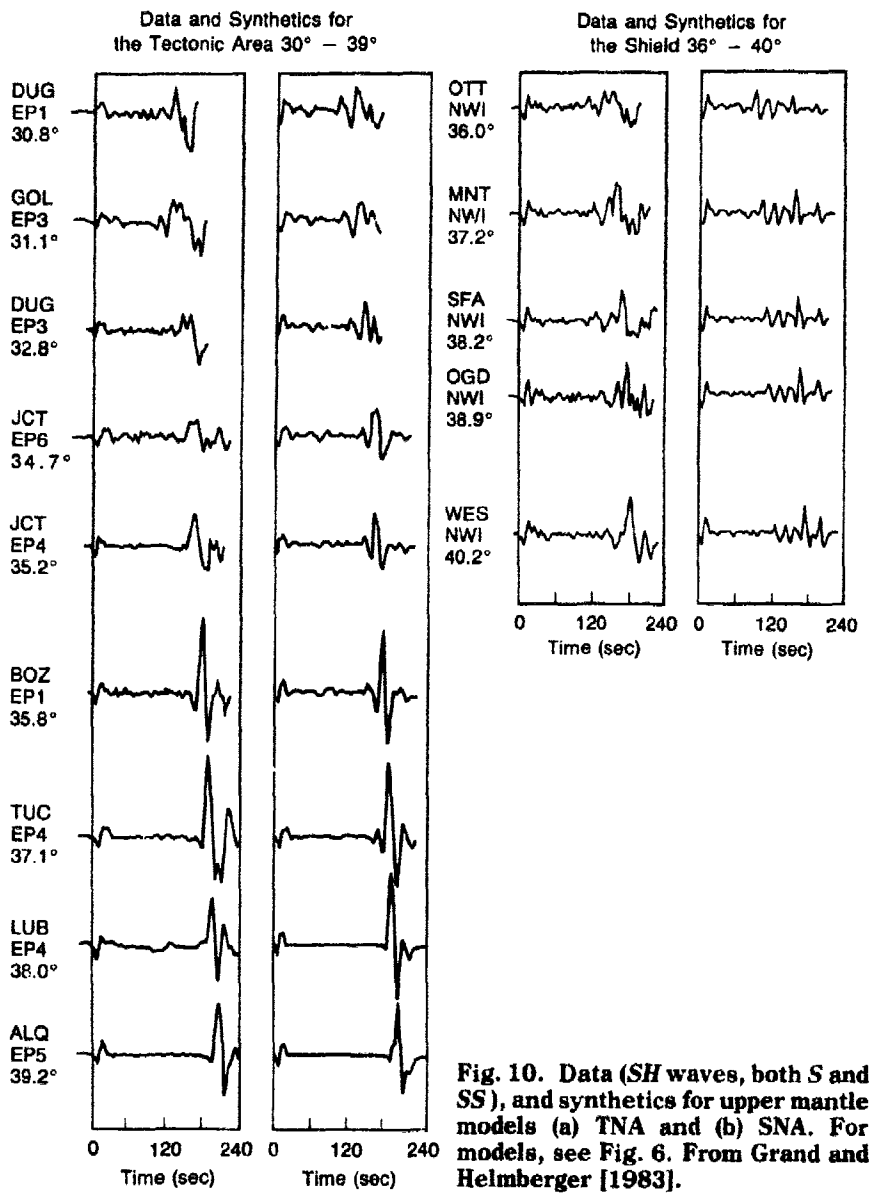

Fig. 10. Data (*SH* waves, both *S* and *SS*), and synthetics for upper mantle models (a) TNA and (b) SNA. For models, see Fig. 6. From Grand and Helmberger [1983].

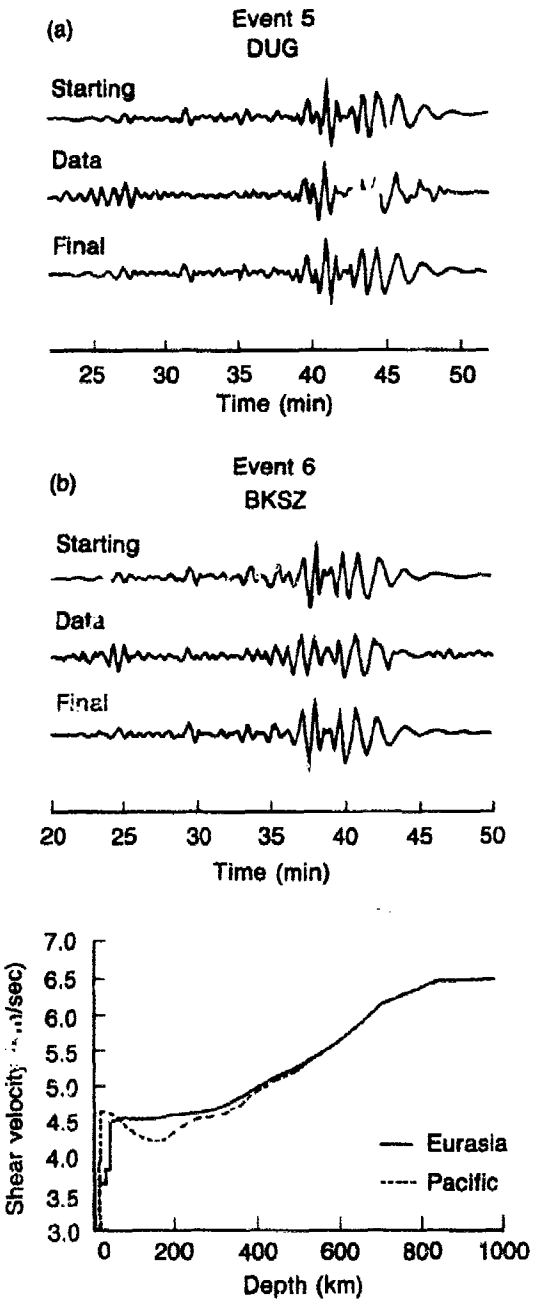

Fig. 11. Data and synthetics for *SV* upper mantle. From Lerner-Lam and Jordan [1983].

velocity for Eurasia and for the Pacific that show substantial differences below 200 km. Examples of their data and synthetics, and their models, are shown in Fig. 11. These upper mantle models do not display velocity gradient anomalies (let alone discontinuities) near 400 and 650 km depth. Comparison of models in Fig. 6 (for *SH*) and Fig. 11 (for *SV*), for velocities averaged over about 600–650 km depth, might indicate that *SV* is faster than *SH*. The possibility of anisotropy is directly addressed by Dziewonski and Anderson [1981] and Anderson and Regan [1983], but emphasizing upper mantle low velocity zones. With the Graefenberg array of Wielandt instruments in Germany, Choy [1982] identified clearly earlier arrivals of *SH* as compared to *SV*, from a deep earthquake in the Kuriles.

Clearly, the extent of anisotropy in the upper mantle is at present speculative. The best hope for a definitive statement will, as usual, rest with an analysis of long period signals (*e.g.*, the classic "discrepancy" in Rayleigh and Love wave dispersion for isotropic models — see Dziewonski and Anderson [1981]). As pointed out by Backus [1962], the explanation may be horizontal isotropic layering. An analogue experiment by Melia and Carlson [1984] confirms that isotropic layers can lead to apparent anisotropy.

Core studies. The two qualities of the data that make detailed study of the upper mantle so difficult (lateral variability of the data, and hence of the structure; and the difficulty in seeing reflections at near vertical incidence), are less of a problem for the core. Narrow angle reflections give such strong evidence for discontinuity between lower mantle and fluid core, and between fluid and solid cores, that the range of possible core structures can be investigated relatively simply in terms of velocity gradients just above and below the interfaces. Thus, Choy [1977] compared data and synthetics for $SKS+SKKS+....+SmKS+$ to conclude that the velocity gradient in the outer fluid core was very close to that expected for an adiabatic gradient. Choy and Cormier [1983] found properties of the BC branch of PKP near 155° to be very sensitive to velocity gradient at the base of the fluid core (see Fig. 12). And for the DF branch of PKP, their synthetics fit waveform observations near 130° only for models that had strong gradients in the outer 200 km of the solid core.

Attenuation

During transmission through the Earth, a seismic wave loses amplitude as a result of a variety of anelastic and scattering processes. The emphasis in this section will be on body waves, and the effects of propagation on a waveform that initially is impulsive. An excellent review of body wave attenuation is given by Cormier [1982]. I shall focus on a particular issue, on which seismologists appear to be divided. Namely,

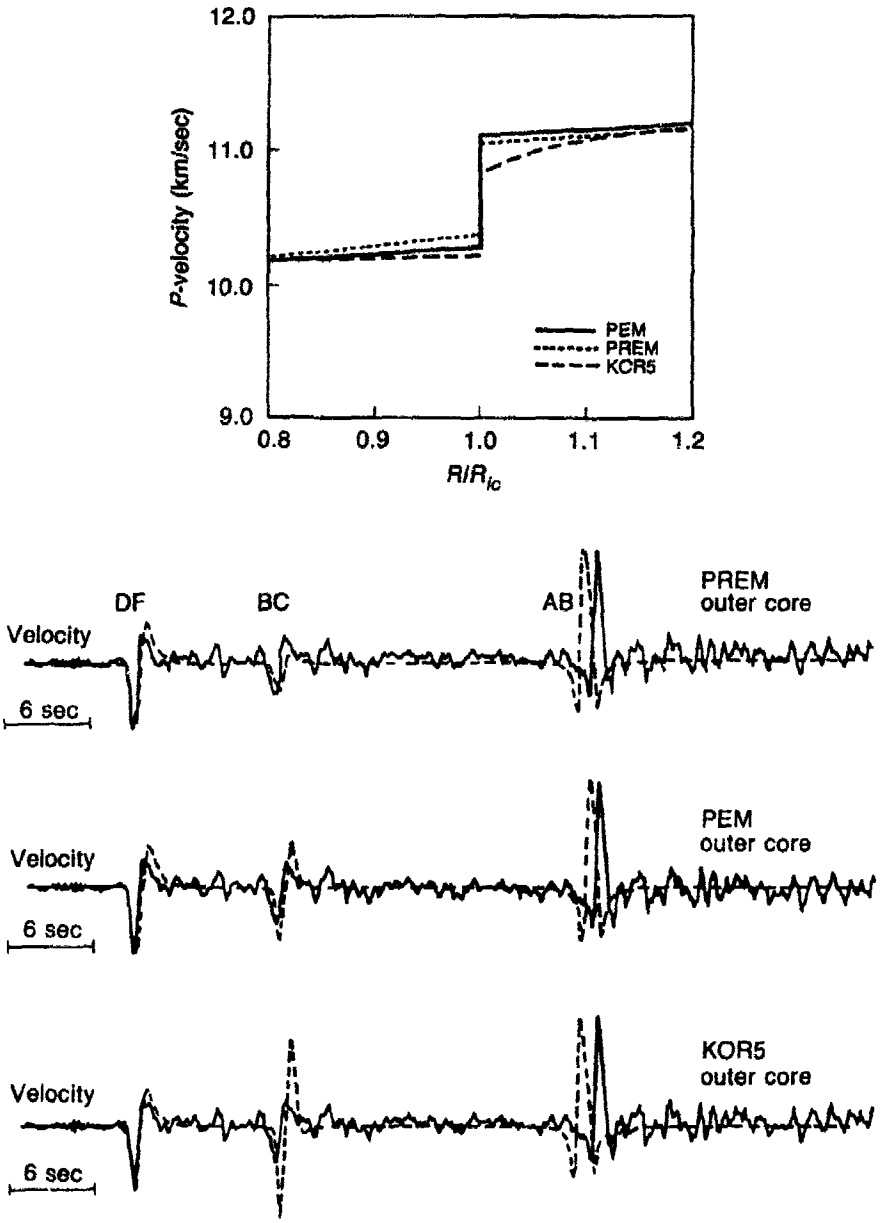

Fig. 12. (a) The *P*-velocity profile in the vicinity of the inner core/outer core boundary, normalized to the radius of the inner core, for three Earth models. (b) *PKP* velocity waveform data from SHIO ($\Delta = 156.3°$); and synthetic (dashed line) for the three different outer core structures shown in Fig. 12a. The synthetic BC amplitude varies considerably. It appears that in the lowest part of the fluid core, a velocity gradient between that of PEM and PREM is indicated. From Choy and Cormier [1983].

the attenuation and associated frequency-dependent phase delay (if any) imparted by the Earth to pulse shapes observed teleseismically.

Basic definitions can first be stated for a wave propagating in a homogeneous medium for which (at a given frequency ω) stress and strain are proportional to each other, but related by a complex modulus. Thus, for a plane wave $p(x,\omega)$ with both attenuation and phase delay increasing in the x-direction, the amplitude and phase are given by

$$p(x,\omega) = \exp\left(\frac{-|\omega|x}{2cQ}\right)\exp\left[i\omega\left(\frac{x}{c}-t\right)\right] = \exp i(Kx-\omega t) .$$

Here $c = c(\omega)$ is the (real) phase velocity; attenuation is described by Q^{-1}, where $Q = Q(\omega)$; and $K = (\omega/c)+i\alpha$ is the complex wavenumber. It follows that the spatial attenuation rate is $\alpha = |\omega|/(2cQ)$, and Gutenberg [1958] found evidence from teleseismic P-waves to suggest that α is roughly independent of frequency. Since c varies only slightly with frequency, it would then follow that Q is roughly proportional to frequency. But, in recent years, hundreds of studies have been published that are based on the premise that Q is constant, to within a few percent, over the frequency range 0.02-1.5 Hz. In order to concentrate the debate, I shall focus on analyses of *ScS* waves.

Continuing with the basic properties of $p(x,\omega)$, we shall assume there exists a finite value c_∞ for $c(\omega)$ in the limit as $\omega\to\infty$, and give a summary of results in Aki and Richards [1980, pages 167-185]. If the wave has zero amplitude in the time domain, prior to an "arrival time" x/c_∞, we say it displays "causality". It is an elementary exercise then to show that c must vary with frequency (if $Q^{-1} \neq 0$), and that this dispersion is completely determined if the behavior of α is known at all frequencies. The rule is

$$\frac{\omega}{c(\omega)} = \frac{\omega}{c_\infty} + H(\alpha(\omega))$$

where H denotes a Hilbert transform.

The transform of $\alpha(\omega)$ can be explicitly or numerically derived for a variety of cases corresponding to Q being roughly constant over the bandwidth of seismic waves. Commonly, but not invariably, one finds the following practical rule for assessing body wave dispersion:

$$c(\omega) = c(\omega_o)\left(1 + \frac{1}{\pi Q}\ln\frac{\omega}{\omega_o}\right)$$

in which ω_o is taken as a point of reference, often 1 Hz (*i.e.*, $\omega_o = 2\pi$). Many authors have derived this logarithmic rule [*e.g.*, Futterman, 1962; Carpenter, 1967; Azimi *et al.*, 1968], and it was given a physical basis by Liu *et al.* [1976]. A more general analysis was carefully developed by Minster [1978a, b]. The main idea, following Anderson *et al.* [1977], is to work with a seismic absorption band, regarded as a spectrum of independent relaxation mechanisms for a standard linear solid. In Minster's model, an important role is played by a parameter τ (the reciprocal of the high frequency cut-off of the relaxation spectrum). Thus, phase velocity departs from the logarithmic rule at sufficiently high frequency, becoming constant for ω well above τ^{-1}. The Q factor is effectively constant at lower seismic frequencies but begins to rise as ω approaches τ^{-1}. At frequencies above τ^{-1}, Q is roughly proportional to frequency. Thus, in this model, a tendency for Q to show an increase with frequency is interpreted as an effect of the sharp cut-off in the relaxation spectrum at high frequencies.

Figure 13 shows the characteristic features of the time-domain pulse $p(x, t)$, associated with constant Q and the logarithmic rule for phase delay. High frequencies have been selectively removed, and the pulse shape is broadened with an asymmetric rise and fall.

Early work on *ScS* waves concentrated on taking spectral ratios, *i.e.*, on the determination of Q from the amplitude spectrum. Anderson's [1967b] review indicates that several studies are in fair agreement with conclusions of the spectral ratio method used by Kovach and Anderson

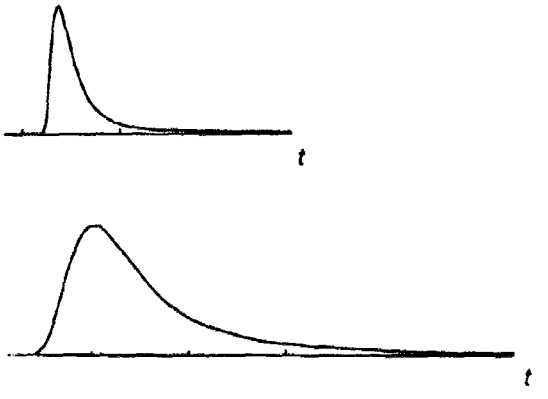

Fig. 13. The attenuated/dispersed impulse associated with constant Q and the logarithmic rule for phase delay.

These two examples correspond to *P*-arrivals from a deep event at $\Delta = 48°$, with $t^* = 0.21$ s (upper) and $t^* = 0.72$ (lower). Tick marks are seconds.

[1964] for multiple *ScS* and *sScS*. They obtained Q_S values of 600, 200 and 2200, as averages for the whole mantle, the upper 600 km, and the lower mantle respectively. Jordan and Sipkin [1977] studied multiple *ScS* phases for events in the western Pacific using HGLP data, and from spectral ratios concluded that the path average for $1/Q$ yields Q_{ScS} constant, having a value 156 ± 13 over the range 0.006-0.06 Hz. Sipkin and Jordan [1979] extended this study to higher frequencies using three deep-focus earthquakes in Tonga/Fiji, but with WWSSN long-period and short-period instruments on Guam and Hawaii. Attenuation is sufficiently strong to remove frequencies above about 0.1 Hz from the multiple *ScS* arrivals, so in this frequency range they worked with a model of the source spectrum, assuming it to fall off as ω^{-2} at sufficiently high frequencies. They did conclude that Q_{ScS} increases with frequency above 0.1 Hz, and they suggested this is associated with a value of τ (in Minster's model) in the range $0.2 \leq \tau \leq 1$ s. They pointed out that Q_{ScS} values below 200 would make *ScS* unobservable on short-period records. The fact that they had good observations at short-period led them to estimate Q_{ScS} as greater than 400, at frequencies above 1 Hz. However, it remained to find a way to reach such a conclusion without having to make any assumption about the source spectrum.

To this end, Burdick [1981b, 1983] worked with some excellent short-period *ScS* data, using the data for *ScP* as a way to avoid assumptions about the source. Figure 14 shows results from an earlier experiment of this type, published by Kanamori [1967]. Effectively the same pulse shapes leave the focal sphere for both *ScP* and *ScS*. But Fig. 15 shows a very clear example in which *ScS* has some high frequency loss compared to *ScP*, and *ScS* is a relatively broader pulse, perhaps twice as broad. Burdick showed that if this pulse broadening is interpreted *via* Minster's [1978a, b] extension of the usual logarithmic rule of phase dispersion, he required a significantly lower value of the τ parameter than had been suggested by Sipkin and Jordan [1979]. The effect (on pulse broadening) of varying τ is shown in Fig. 16. For the *ScP*, *ScS* data of Fig. 15, pulse broadening with the τ model required a very low value to reproduce *ScS* characteristics from filtering *ScP*. This is apparent in Fig. 17a, where $\tau = 0.01$ s is used.

A low value of τ in turn gives a low value of Q out at the high frequencies of this *ScS* data. And then the term

$$\frac{1}{\pi Q} ln\left(\frac{\omega}{\omega_o}\right)$$

in the logarithmic rule encourages pulse broadening, because different frequency components (over the bandwidth of the data) travel at different

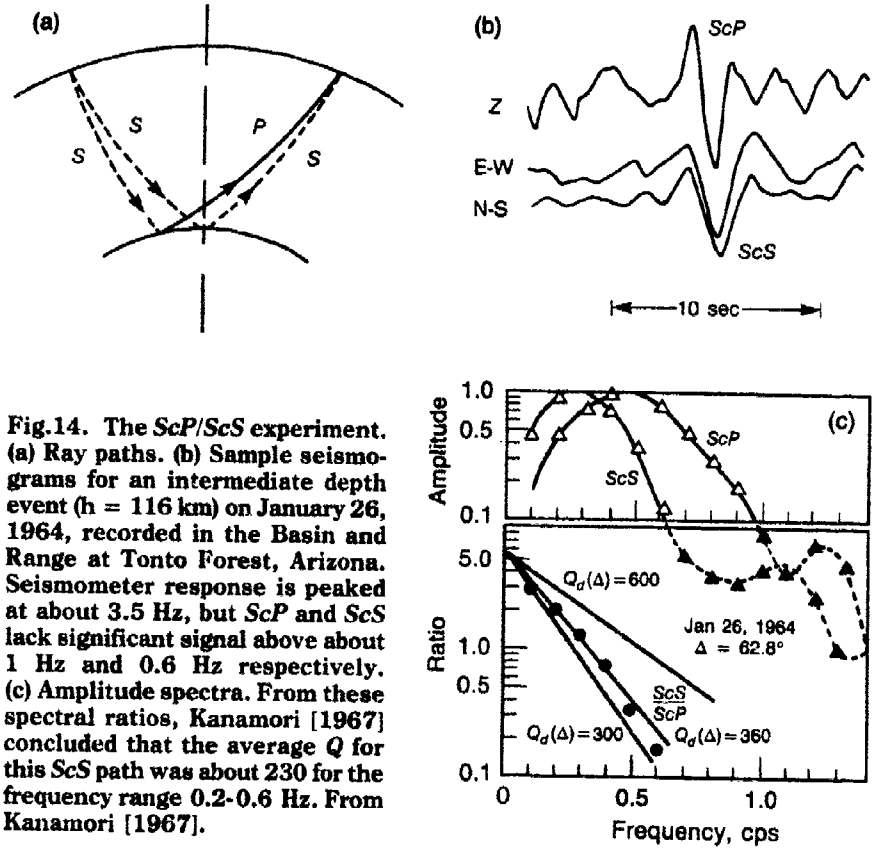

Fig.14. The *ScP*/*ScS* experiment. (a) Ray paths. (b) Sample seismograms for an intermediate depth event (h = 116 km) on January 26, 1964, recorded in the Basin and Range at Tonto Forest, Arizona. Seismometer response is peaked at about 3.5 Hz, but *ScP* and *ScS* lack significant signal above about 1 Hz and 0.6 Hz respectively. (c) Amplitude spectra. From these spectral ratios, Kanamori [1967] concluded that the average *Q* for this *ScS* path was about 230 for the frequency range 0.2-0.6 Hz. From Kanamori [1967].

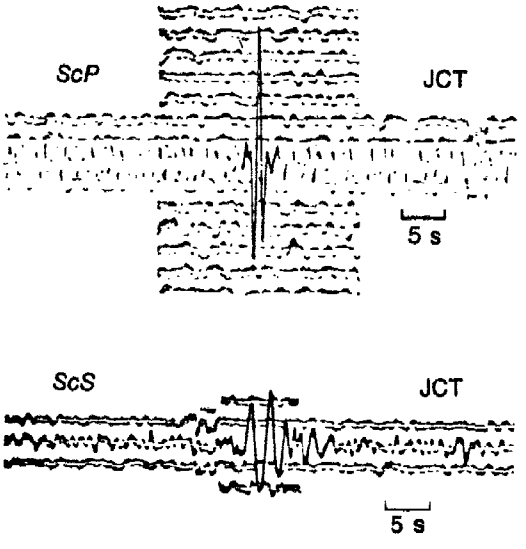

Fig. 15. WWSSN short-period records from Junction City, Texas, for the deep South American event of March 27, 1967. *ScS* here contains signal up to about 1.5 Hz. From Burdick [1981b].

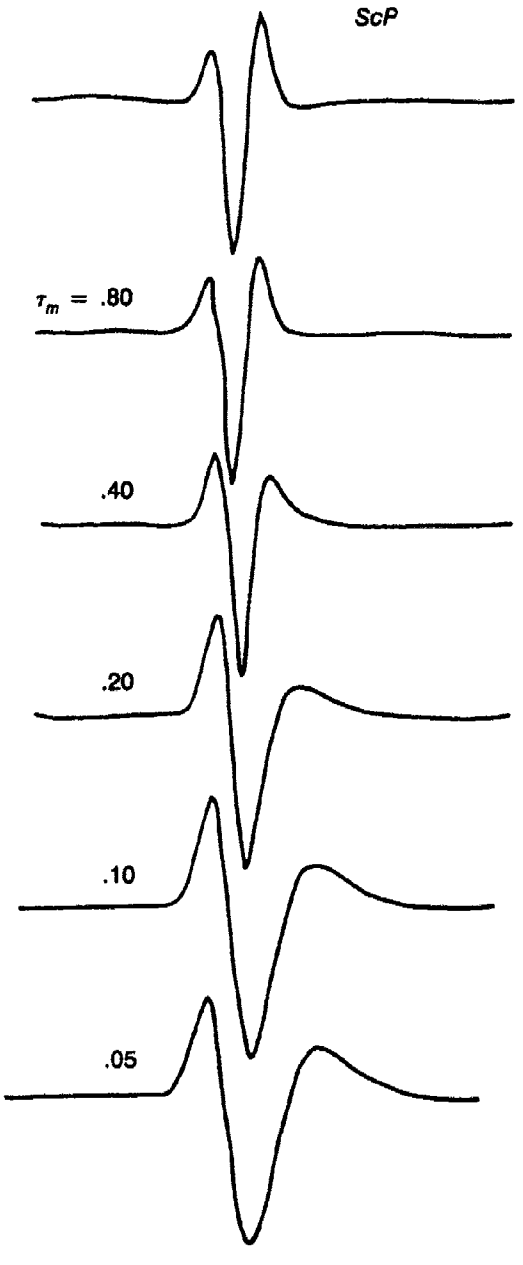

Fig. 16. The effect of filtering on *ScP* signal is shown for various τ values. Pulse-broadening does not become significant until $\tau \leq 0.2$ s. From Burdick [1981b].

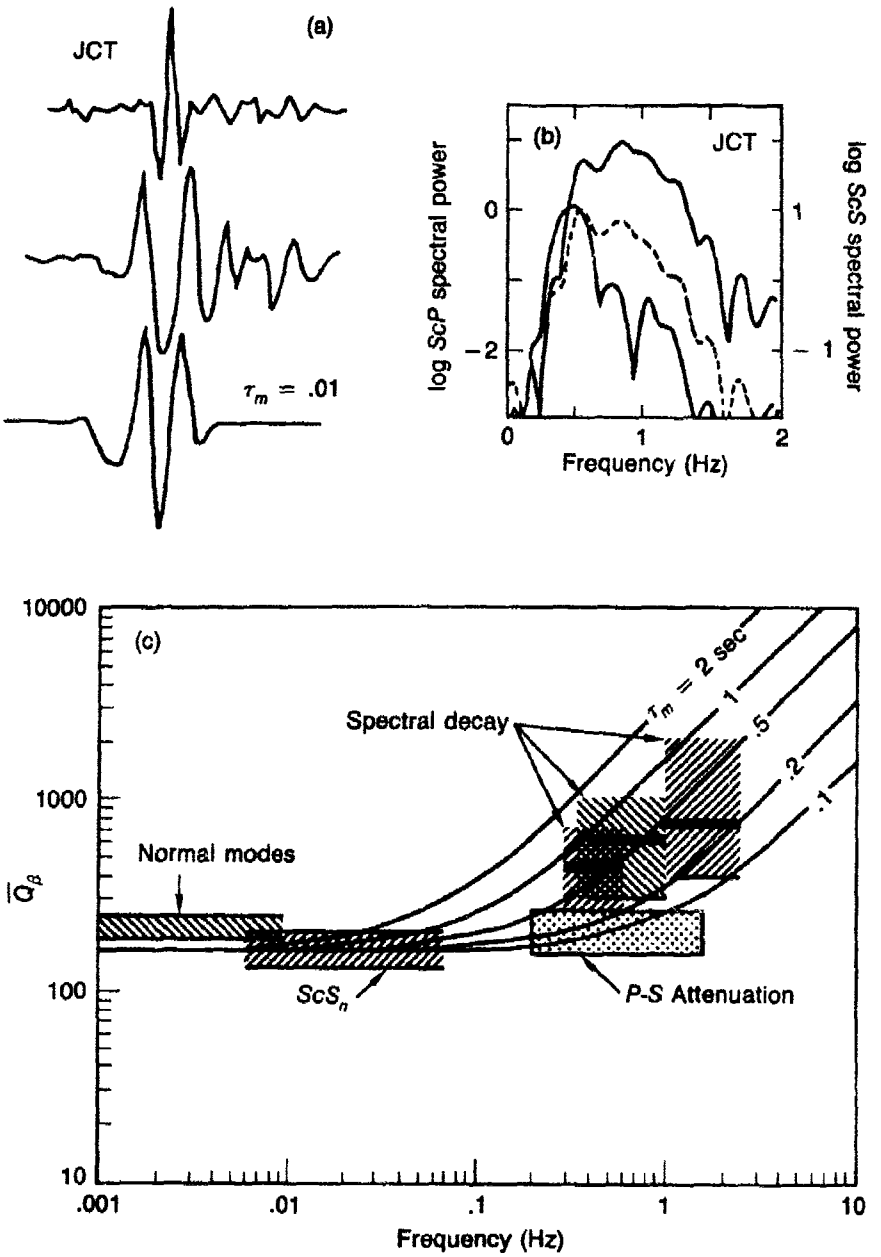

Fig. 17. The first and second traces are the *ScP* and *ScS* signals shown in Fig. 15. The last trace is the result of filtering *ScP* by assuming a τ-value of 0.01 s. (b) Power spectra for *ScP (top solid line, left-hand scale) and ScS* (lower solid line, right-hand scale), and for *ScP* filtered with $\tau = 0.2$ s (dashed line). Filtered *ScP* does vary with frequency roughly like *ScS*. (c) Reciprocal of average $1/Q_\beta$. From Burdick [1983].

speeds. (Note that some pulse broadening will occur in the presence of attenuation, even if there is no dispersion.) Because τ is so low, Burdick (1983) concluded that Q_{ScS} stays down at a low value, around 250, out to 1.5 Hz.

However, it seems that a different conclusion must be reached if we look again at this data and emphasize properties of the amplitude spectra rather than just the pulse broadening. Using now the label Q_β for the Q of S-waves traveling a path such as ScS from the core-mantle boundary right up to the Earth's surface, and Q_α for P-waves on a similar path, the spectral ratio of ScS/ScP is dominated by the factor

$$R(\omega) = exp\left\{ -\frac{\omega}{2}\left(\frac{T_\beta}{Q_\beta} - \frac{T_\alpha}{Q_\alpha}\right)\right\}.$$

Here, T_β and T_α are the S- and P-travel times for the upward portions of ScS and ScP, throughout the whole mantle and crust. It is instructive to evaluate $R(\omega)$ with different Q_β, using representative values of T_β (say, 500 s) and T_α (say, 300 s), and the usual approximation $Q_\alpha = (3\alpha^2/4\beta^2]Q_\beta \approx 2Q_\beta$.

If $Q_\beta = 250$, then $R(\omega)$ is about 0.1, 0.01, and 0.001, at 0.5 Hz, 1 Hz, and 1.5 Hz respectively. These low values are not indicated by a direct assessment of spectral ratios in the data. Although ScS has lost high frequencies compared to ScP, ScS does contain significant signal at 1 Hz. It thus seems that Q as estimated from pulse broadening (using the standard linear solid; a sharp cutoff in the relaxation spectrum at high frequencies; and the logarithmic dispersion rule over the frequency range where Q is constant) is, in this example, significantly lower than the Q inferred from spectral ratios. To make the case for this conclusion in another way, Fig. 17b gives power spectra (albeit with different scales) for ScP and ScS, and indicates in a general way that τ around 0.2 is a fair estimate from the spectral ratio. Figure 17c summarizes the work of Burdick, Jordan, and Sipkin on Q_{ScS}, and also displays the relation between τ values and the rise of Q at high frequencies.

Faced with this level of inconsistency in the attenuation model, seismologists have made different choices. Some have continued to work with low Q estimates, but some work with relatively high Q such as proposed by Archambeau, Flinn and Lambert [1969]. If these two choices are pursued to the extent of applying the logarithmic dispersion rule in each case (*i.e.*, Q constant in each case), they lead to pulse shapes that are substantially different, as shown in Fig. 18. Especially, if one is using synthetics to study details of a seismic source, this figure indicates

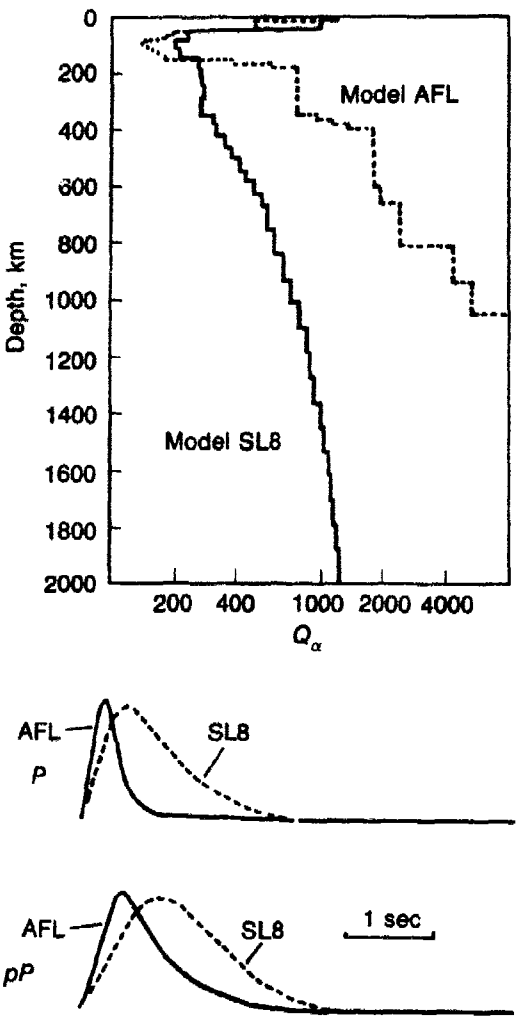

Fig. 18. (a) Two models (SL8, and AFL) of Q as a function of depth. (b) The pulse broadening of P, and pP, for propagation to $\Delta = 48°$ from a deep event, if Q is frequency-independent. From Choy and Boatwright [1981].

that a fundamental problem in modern seismology is as yet unresolved. Another choice, favored by this author, is to question the practical applicability of the Hilbert transform relation between phase delay and attenuation spectrum. We should recognize that linear theory of wave propagation is a fair approximation, for seismology, but is pushed to extremes in the slowly converging Hilbert transform corresponding to nearly constant Q. If scattering has a significant role in attenuation [*e.g.*, Dainty, 1981; Aki, 1982; Richards and Menke, 1983], then one's mind

set can change to the view that the Earth may be far more complicated than is generally supposed by geophysicists working with smoothly varying structures. The question of whether scattering or anelasticity controls attenuation is most actively under debate by exploration geophysicists studying the upper crust (see Anstey [1984] for the basic ideas). But petrologists are claiming great complexity of structure also in the upper mantle. In view of such three-dimensional complexity, research on Earth structure is now quite naturally developing along two different but complementary lines. The first, entails a normal mode/long-period surface wave analysis, exemplified in Fig. 1a, that accurately estimates smoothed structure. The second, which is more in the tradition of the oil industry in working with large amounts of short-period travel time data, or with surface-wave phase velocities, entails tomography rather than synthetics. Both of these approaches are yielding new results about Earth structure. And both of them indicate there is more to be learned, if they can be applied to much larger data sets. The chief restriction on our knowledge of three-dimensional structure now appears to be the limitations of the present global data base.

Acknowledgements

I thank Gerardo Suarez and Shamita Das for reviews; and George Choy, Chuck Langston, John Orcutt, Dean Witte, and John Woodhouse for their help with some of the figures. My research in wave propagation has been supported in recent years by contract NOOO14-80-C-0654 with the Office of Naval Research. Lamont-Doherty Geological Observatory Contribution Number 3890.

References

Note: The list below includes many more titles than have been cited in the text. As well as research papers, it includes reviews and major summaries by Chapman and Orcutt [1985], Cormier [1982], Dziewonski and Anderson [1981], Harkrider [1983] and Richards [1975, 1979], and textbooks by Aki and Richards [1980], Ben-Menahem and Singh [1981], Kennett [1983] and Hudson [1980].

Aki, K., "Source and Scattering Effects on the Spectra of Small Local Earthquakes, *Bull. Seismol. Soc. Am.*, **71**. 1687-1700, 1981.

Aki, K., "Scattering and Attenuation," *Bull. Seismol. Soc. Am.*, **72**, S319-S330, 1982.

Aki, K., "Three-Dimensional Seismic Inhomogeneities in the Lithosphere and Asthenosphere: Evidence for Decoupling in the Lithosphere and Flow in the Asthenosphere," *Rev. Geophys. Space Phys.*, **20**, 161-170, 1982.

Aki, K., and P.G. Richards, *Quantitative Seismology: Theory and Methods*, W.H. Freeman and Co., San Francisco, Calif., 2 volumes, 1980.

Anderson, D.L., "The Anelasticity of the Mantle," *Geophys. J.R. Astr. Soc.*, **14**, 135-164, 1967a.

Anderson, D.L., "Latest Information from Seismic Observations," in *The Earth's Mantle*, pp. 355-420, Academic Press., Inc. London, 1967b.

Anderson, D.L., "Bulk Attenuation in the Earth and Viscosity of the Core," *Nature*, **285**, 204-207, 1980.

Anderson, D.L., and C.B. Archambeau, "The Anelasticity of the Earth," *J.Geophys. Res.*, **69**, 2071-2084, 1964.

Anderson, D.L., and R.S. Hart, "*Q* of the Earth," *J. Geophys. Res.*, **83**, 5869-5882, 1978.

Anderson, D.L., and J. Regan, "Upper Mantle Anistrophy and the Oceanic Lithosphere," *Geophys. Res. Lett.*, 841-844, 1983.

Anderson, D.L., A. Ben-Menahem, and C.B. Archambeau, "Attenuation of Seismic Energy in the Upper Mantle," *J. Geophys. Res.*, **709**, 1441-1448, 1965.

Anstey, N.A., "Seismic Interpretation: The Physical Aspects," *Internat. Human Resources Development Corp.*, 1984.

Apsel, R.J., and J.E. Luco, "On the Green's Functions for a Layered Half-Space, Part II," *Bull. Seismol. Soc. Am.*, **73**, 931-952, 1983.

Archambeau, C.B., E.A. Flinn, and D.G. Lambert, "Fine Structure of the Upper Mantle," *J. Geophys. Res.*, **74**, 5825- 5866, 1966.

Backus, G., and F. Gilbert, "Constructing *P*-Velocity Models to Fit Restricted Sets of Travel-Time Data," *Bull. Seismol. Soc. Am.*," **59**, 1415-1418, 1969.

Ben-Menahem, A., and S.J. Singh, *Seismic Waves and Sources*, Springer Verlag, New York, 1981.

Ben-Menahem, A., and M.N. Toksöz, "Source Mechanism from Spectra of Long Period Surface Waves," *J. Geophys. Res.*, **68**, 5207-5222, 1963.

Ben-Menahem, A., S.W. Smith, and T.L. Teng, "A Procedure for Source Studies from Spectrums of Long-Period Seismic Body Waves," *Bull. Seismol. Soc. Am.*, **55**, 203-235, 1965.

Bouchon, M., "A Simple Method to Calculate Green's Functions for Elastic Layered Media," *Bull. Seismol. Soc. Am.*, **71**, 959-972, 1981.

Brennan, B.J., "Pulse Propagation in Media with Frequency- Dependent *Q*," *Geophys. Res. Lett.*, **7**, 211-213, 1980.

Budiansky, B., E.E. Sumner, Jr., and R.J. O'Connell, "Bulk Thermoelastic Attenuation of Composite Materials," *J. Geophys. Res.*, **88**, 10343-10348, 1983.

Bungum, H., "NORESS Noise and Signal Characteristics," *NORSAR Semi-Annual Technical Summary*, April-September 1982.

Burdick, L.J., "A Comparison of the Upper Mantle Structure Beneath North America and Europe," *J. Geophys. Res.*, **86**, 5926-5936, 1981a.

Burdick, L.J., "Waveform Studies of the Velocity and *Q* Structure of the Mantle," Annual Rept. of AFOSR Contract F4920- 79-C-0021, 1981b.

Burdick, L.J., Comments on "The Corner Frequency Shift, Earthquake Source Models, and *Q*," by T.C. Hanks, *Bull. Seismol. Soc. Am.*, **72**, 1492-1426, 1982.

Burdick, L.J., "Estimation of the Frequency Dependence of *Q* From *ScP* and *ScS* phases, *DARPA Semi-Annual Technical Report WCCP-R-83-06*, 15 November 1982 - 15 June 1983, 1983. Also, *Geophys. J. R. Astr. Soc.*, **80**, 33-55, 1985.

Burdick, L.J., and J.A. Orcutt, *A Comparison of the Generalized Ray and Reflectivity Methods of Waveform Synthesis*," *Geophys., J. R. Astro. Soc.*, **58**, 261-278, 1979.

Butler, R., "Azimuth, Energy, *Q*, and Temperature: Variations on *P* Wave Amplitudes in the United States," *Rev. Geophys. Space Phys.*, **22**, 1-36, 1984.

Cara, M., A. Nercessian, and G. Nolet, "New Inferences from Higher Mode Data in Western Europe and Northern Eurasia," *Geophys. J. R. Astro. Soc.*, **61**, 459-478, 1980.

Carpenter, E.W., "Teleseismic Signals Calculated for Underground, Underwater, and Atmospheric Explosions," *Geophysics*, **32**, 17-32, 1967.

Chapman, C.H., "A New Method for Computing Seismograms," *Geophys. J. R. Astr. Soc.*, **54**, 481-518, 1978a.

Chapman, C.H., Body Waves in Seismology, in *Modern Problems in Elastic Wave Propagation*, edited by J. Miklowitz and J.D. Achenbach, Wiley, New York, 1978b.

Chapman, C.H., and R. Drummond, "Body-Wave Seismograms in Inhomogeneous Media Using Maslov Asymptotic Theory," *Bull. Seismol. Soc. Am.*, **72**, S277-S318, 1982.

Chapman, C.H., and J.A. Orcutt, "The Computation of Body Wave Synthetic Seismograms in Laterally Homogeneous Media," *Rev. Geophys.*, **23**, 105-163, 1985.

Choy, G.L., "Experiments with SRO and GRF-Array Data," *U.S. Geol. Surv. Open-File Rpt. 82-216*, 1982.

Choy, G.L., and V.F. Cormier, "The Structure of the Inner Core Inferred from Short-Period and Broadband GDSN Data," *Geophys. J.R. Astr. Soc.*, **72**, 1-22, 1983.

Choy, G.L., V.F. Cormier, R. Kind, G. Müller, and P.G. Richards, "A Comparison of Synthetic Seismograms of Core Phases Generated by the Full Wave Theory and by the Reflectivity Method," *Geophys. J. R. Astr. soc.*, **61**, 21-39, 1980. (See **62**, 733-735 for corrigendum.)

Cormier, V.F., "Synthesis of Complete Seismograms in an Earth Model Specified by Radially Inhomogeneous Layers," *Bull. Seismol. Soc. Am.*, **70**, 691-716, 1980.

Cormier, V.F., "The Effect of Attenuation on Seismic Body Waves," *Bull. Seismol. Soc. Am.*, **72**, S169-S200, 1982.

Cormier, V.F., "The Trade-offs between Explosion Source Parameters and Anelasticity," Lincoln Laboratory Semi-Annual Technical Summary, Seismic Discrimination, pp. 21-29, 31 March, 1982.

Cormier, V.F., "Deep Earth Structure," *Rev. Geophys. Space Phys.*, **21**, 1277-1284, 1983.

Cormier, V.F., and G.L. Choy, "Theoretical Body Wave Interactions with Upper Mantle Structure," *J. Geophys. Res.*, **86**, 1673-1678, 1981.

Cormier, V.Fl., and P.G. Richards, "Full Wave Theory Applied To a Discontinuous Velocity increase: The Inner Core Boundary," *J. Geophys.*, **43**, 3-31, 1977.

Dainty, A.M., "A Scattering Model to Explain Seismic Q Observations in the Lithosphere Between 1 and 30 Hz," *Geophys. Res. Lett.*, **8**, 1126-1128, 1981.

Der, Z.A., and T.W. McElfresh, "Short-Period P-Wave Attenuation Along Various Paths in North America as Determined from P-Wave Spectra of the SALMON Nuclear Explosion," *Bull. Seismol. Soc. Am.*, **66**, 1609-1622, 1976.

Douglas, A., and J.A. Hudson, Comments on "Time Functions Appropriate for Nuclear Explosions," by L.J. Burdick and D.V. Helmberger, and "Seismic Source Functions and Attenuation from Local and Teleseismic Observations of the NTS Events Jorum and Handley," by D.V. Helmberger and D.M. Hadley, *Bull. Seismol. Soc. Am.*, **73**, 1255-1264, 1983.

Dziewonski, A.M., "Elastic and Anelastic Structure of the Earth," *Rev. Geophys. Space Phys.*, **17**, 303-311, 1979.

Dziewonski, A.M., and D.L. Anderson, "Preliminary Reference Earth Model," *Phys. Earth Planet. Int.*, 297-356, 1981.

Frasier, C.W., and J. Filson, "A Direct Measurement of the Earth's Short-Period Attenuation Along a Teleseismic Ray Path," *J. Geophys. Res.*, **77**, 3782-3787, 1972.

Futterman, W.I., "Dispersive Body Waves," *J. Geophys. Res.*, **67**, 5279-5291, 1962.

Gettrust, J.F., and L.N. Frazer, "A Computer Model Study of the Propagation of Long Range P_n," *Geophys. Res. Lett.*, **8**, 749-752, 1981.

Gilbert, F., "Excitation of the Normal Modes of the Earth by Earthquake Sources," *Geophys. J. R. Astr. Soc.*, **22**, 223- 226, 1971.

Gilbert, F., and A.M. Dziewonski, "An Application of Normal Mode Theory to the Retrieval of Structural Parameters and Source Mechanisms from Seismic Spectra," *Phil. Trans. R. Soc. London*, **278**, 187-269, 1975.

Gladwin, M.T., and F.D. Stacey, "Anelastic Degradation of Acoustic Pulses in Rock," *Phys. Earth Planet. Int.*, **8**, 332- 336, 1974.

Grand, S.P., and D.V. Helmberger, "Upper Mantle Shear Structure of North America," *Geophys. J. R. Astr. Soc.*, **76**, 399-438, 1984.

Gutenberg, B., "Attenuation of Seismic Waves in the Earth's Mantle," *Bull. Seismol. Soc. Am.*, **48**, 269-282, 1958.

Hanks, T.C., "The Corner Frequency Shift, Earthquake Source Models, and Q," *Bull. Seismol. Soc. Am.*, **71**, 597-612, 1981.

Hanks, T.C., "'Reply to "Comments on 'The Source Corner Frequency Shift, Earthquake Source Models, and Q,' " " " *Bull. Seismol. Soc. Am.*, **72**, 1433-1445, 1982.

Harkrider, D.G., "Synthetics and Theoretical Seismology," *Rev. Geophys. Space Phys.*, **21**, 1299-1308, 1983.

Harkrider, D.G., and D.L. Anderson, "Surface Wave Energy from Point Sources in Plane Layered Earth Models," *J. Geophys. Res.*, **71**, 2967-2980, 1966.

Harvey, D.J., "Seismogram Synthesis Using Normal Mode Superposition: The Locked Mode Approximation," *Geophys. J. R. Astro. Soc.*, **66**, 37-69, 1981.

Haskell, N.A., "The Dispersion of Surface Waves in Multilayered Media, *Bull. Seismol. Soc. Am.*, **43**, 17-34, 1953.

Haskell, N.A., "Crustal Reflection of Plane *SH* Waves," *J. Geophys. Res.*, **65**, 4147-4150, 1960.

Haskell, N.A., "Crustal Reflection of Plane *P* and *SV* Waves," *J. Geophys. Res.*, **67**, 4751-4767, 1962.

Haskell, N.A., "Radiation Pattern of Surface Waves from Point Sources in a Multi-layered Medium," *Bull. Seismol. Soc. Am.*, **54**, 377-394, 1964.

Helmberger, D.V., "On the Structure of the Low Velocity Zone," *Geophys. J. R. Astr. Soc.*, **34**, 251-263, 1973.

Helmberger, D.V., and L.J. Burdick, "Synthetic Seismograms," *Ann. Rev. Earth Planet. Sci.*, **7**, 417-442, 1979.

Helmberger, D.V. and G.R. Engen, "Upper Mantle Shear Structure," *J. Geophys. Res.*, **79**, 4017-4028, 1974.

Helmberger, D.V., and D.M. Hadley, "Seismic Source Functions and Attenuation from Local and Teleseismic Observations of NTS Events, JORUM and HANDLEY," *Bull. Seismol. Soc. Am.*, **71**, 51-68, 1981.

Helmberger, D.V. and R.A. Wiggins, "Upper Mantle Structure of Mid-Western United States," *J. Geophys. Res.*, **76**, 3229- 3245, 1971.

Hudson, J.A., *The Excitation and Propagation of Seismic Waves*, Cambridge University Press, 1980.

Jeffreys, H., "On the Cause of Oscillatory Movement in Seismogra[m] *Monthly Notices of the Royal Astronomical Society, Geophysical Supplement*, **2**, [4]16, 931.

Johnson, L.R., "Array Measurements of *P* Velocities in the Upp[er] [M]le," *Geophys. Res.*, **72**, 6309-6325, 1967.

Kanamori, H., "Spectrum of Short-Period Core Phases in Relation [to] Attenuation in the Mantle," *J. Geophys. Res.*, **72**, 2181-2186, 1967.

Keilis-Borok, V.I., and T.B. Yanovskaya, "Dependence of the Spectrum of [Sur]face Waves on the Depth of the Focus within the Earth's Crust," *Bull. Acad. of Sci., U.S.S.R., Geophys. Ser.* (English translation), **11**, 1532-1539, 1962.

Kennett, B.L.N., *Seismic Wave Propagation in Stratified Media*, Cambridge University Press, 1983.

Kovach, R.L., and D.L. Anderson, "Attenuation of Shear Waves in the Upper and Lower Mantle," *Bull. Seismol. Soc. Am.*, **54**, 1855-1864, 1964.

Lamb, H., "On the Propegation of Tremors over the Surface of an Elastic Solid," *Phil. Trans. Roy. Soc. Lond.*, **A203**, 1- 42, 1904.

Langston, C.A., "Source Inversion of Seismic Waveforms: The Koyna, India Earthquake of 14 September 1967," *Bull. Seismol. Soc. Am.*, **71**, 1-24, 1981.

Langston, C.A., and D.E. Blum, "The April 29, 1965, Puget Sound Earthquake and the Crustal and Upper Mantle Structure of Western Washington," *Bull. Seismol. Soc. Am.*, **67**, 693-711, 1977.

Langston, C.A., and D.V. Helmberger, "A Procedure for Modeling Shallow Dislocation Sources," *Geophys. J.R. Astr. Soc.*, **42**, 117-130, 1975.

Langston, C.A., and J.-J. Lee, "Effect of Structure Geometry on Strong Ground Motions: The Duwamisk River Valley, Seattle, Washington," *Bull. Seismol. Soc. Am.*, 73, Pt. A, 1851-1864, 1983.

Lay, T., and D.V. Helmberger, "A Lower Mantle *S*-Wave Triplication and the Shear Velocity Structure of *D*''", *Geophys. J. R. Astr. Soc.*, **75**, 799-838, 1983.

Lerner-Lam, A.L., and T.H. Jordan, "Earth Structure from Fundamental and Higher-Mode Waveform Analysis," *Geophys. J. R. Astr. Soc.*, **75**, 759-798, 1983.

Liu, H.-P., D.L. Anderson, and H. Kanamori, "Velocity Dispersion Due to Anelasticity: Implications for Seismology and Mantle Composition," *Geophys. J. R. Astr. Soc.*", **47**, 41-58, 1976.

Luco, J. E., and R. J. Apsel, "On the Green's Functions for a Layered Half-Space," Part I, *Bull. Seismol. Soc. Am.*, **73**, 909-930, 1983.

Masters, G., and F. Gilbert, "Attenuation in the Earth at Low Frequencies," *Phil. Trans. R. Soc. Lond.*, **A308**, 479-522, 1983.

Masters, G., J. Park, and F. Gilbert, "Observations of Coupled Spheroidal and Toroidal Modes," *J. Geophys. Res.*, **88**, 10, 285-298, 1983.

McCowan, D.W., "A Moment-Tensor Representation of Body-Wave Displacement Vectors on the Focal Sphere," *Semi-Annual Technical Summary, Seismic Discrimination*, Lincoln Laboratory, pp. 9-13, 1977.

McKenzie, D., "A Possible Mechanism for Epeirogenic Uplift," *Nature*, **307**, 616-618, 1984.

Melia, P.J., and R.L. Carlson, "An Experimental Test of *P*-Wave Anisotropy in Stratified Media," *Geophysics*, **49**, 374- 378, 1984.

Mellman, G.R., and D.V. Helmberger, "A Modified First-Motion Approximation for the Synthesis of Body-Wave Seismograms," *Geophys. J. R. Astr. Soc.*, **54**, 129-140, 1978.

Mendiguren, J., "Inversion of Surface Wave Data in Source Mechanism Studies," *J. Geophys. Res.*, **82**, 889-894, 1977.

Menke, W., "A Formula for the Apparent Attenuation of Acoustic Waves in Randomly Layered Media," *Geophys. J. R. Astr. Soc.*, **75**, 541-544, 1983.

Minster, J.B., "Transient and Impulse Responses of a One- Dimensional Linearly Attenuating Medium—I. Analytical Results," *Geophys. J.R. Astr. Soc.*, **52**, 497-502, 1978.

Minster, J.B., "Transient and Impulse Responses of a One- Dimensional Linearly Attenuating Medium—II. A Parametric Study," *Geophys. J. R. Astr. Soc.*, **52**, 503-524, 1978.

Müller, G., "Seismic Moment and Long-Period Radiation of Underground Nuclear Explosions," *Bull. Seismol. Soc. Am.*, **63**, 847-857, 1973.

Müller, G., "Rheological Properties and Velocity Dispersion of a Medium with Power-Law Dependence of *Q* on Frequency," *J. Geophys.*, **54**, 20-29, 1983.

O'Doherty, R.F., and N.A. Anstey, "Reflections on Amplitudes," *Geophys. Prospecting*, **19**, 430-458, 1971.

Olson, P., D.A. Yuen, and D. Balseger, "Mixing of Passive Heterogeneities by Mantle Convection," *J. Geophys. Res.*, **89**, 425-436, 1984.

Priestley, K., J. Orcutt, and J. Brune, "Higher-Mode Surface Waves and the Structure of the Great Basin of Nevada and Western Utah," *J. Geophys. Res.*, **85**, 7166-7174, 1980.

Richards, P.G., "Theoretical Seismology," *Rev. Geophys. Space Phys.*, **13**, 295-298 and 313-316, 1975.

Richards, P.G., "Theoretical Seismic Wave Propagation," *Rev. Geophys. Space Phys.*, **17**, 312-327, 1979.

Richards, P.G., and W. Menke, "The Apparent Attenuation of a Scattering Medium," *Bull. Seismol. Soc. Am.*, **73**, 1005-1021, 1983.

Sacks, S.I., "*Q*s of the Lower Mantle—A Body Wave Determination," in *Anelasticity*

in the Earth, Geodynamics Series, **4**, pp. 55-58, edited by F.D. Stacey, M.S. Paterson, and A. Nicholas, AGU, GSA, 1981.

Saito, M., "Excitation of Free Oscillations and Surface Waves by a Point Source in a Vertically Heterogeneous Earth," *J. Geophys. Res.*, **72**, 3689-3699, 1967.

Sato, H., "Attenuation and Envelope Formation of Three-Component Seismograms of Small Local Earthquakes in Randomly Inhomogeneous Lithosphere," *J. Geophys. Res.*, **89**, 1221-1241, 1984.

Schoenberger, M., and F.K. Levin, "Apparent Attenuation Due to Intrabed Multiples," *Geophysics*, **39**, 278-291, 1974.

Schoenberger, M., and F.K. Levin, "Apparent Attenuation Due to Intrabed Multiples, II," *Geophysics*, **43**, 730-737, 1978.

Schoenberger, M., and F.K. Levin, "The Effect of Subsurface Sampling on One-Dimensional Synthetic Seismograms," *Geophysics*, **44**, 1813-1829, 1979.

Sipkin, S.A., and T.H. Jordan, "Frequency Dependence of Q_{ScS}," *Bull. Seismol. Soc. Am.*, **69**, 1055-1080, 1979.

Sleep, N.N., R.J. Geller, and S. Stein, "A Constraint of the Earth's Lateral Heterogeneity from the Scattering of Spheroidal Model Q^{-1} Measurements," *Bull. Seismol. Soc. Am.*, **71**, 183-198, 1981.

Solomon, S.C., "On Q and Seismic Discrimination," *Geophys. J.R. Astr. Soc.*, **31**, 163-178, 1972.

Spencer, T.R., J.R. Sonnad, and T.M. Butler, "Seismic Q — Stratigraphy or Dissipation," *J. Geophysics*, **47**, 16- 24, 1982.

Spudich, P., and J. Orcutt, "Petrology and Porosity of an Oceanic Crustal Site: Results from Waveform Modeling of Seismic Refraction Data," *J. Geophys. Res.*, **85**, 1409-1434, 1980.

Spudich, P., and U. Ascher, "Calculation of Complete Theoretical Seismograms in Vertically Varying Media Using Collocation Methods," *Geophys., J. R. Astr. Soc.*, **75**, 101-124, 1983.

Stephen, R.A., "A Comparison of Finite Difference and Reflectivity Seismograms of Marine Models," *Geophys. J. R. Astr. Soc.*, **72**, 39-58, 1983.

Stewart, R.C., "Q and the Rise and Fall of a Seismic Pulse," *Geophys. J. R. Astr. Soc.*, **76**, 793-806, 1984.

Strick, E., "Implications of Jeffreys-Lomnitz Transient Creep," *J. Geophys. Res.*, **89**, 437-452, 1984.

Tanimoto, T., "A Simple Derivation of the Formula to Calculate Synthetic Long-Period Seismograms in a Heterogeneous Earth by Normal Mode Summation," *Geophys. J. R. Astro. Soc.*, **77**, 275- 278, 1984.

Vinnik, L.P., R.A. Avetisjan, and N.G. Mikhailova, "Heterogeneities in the Mantle Transition Zone from Observations of *P*-to-*SV* Converted Waves," *Phys. Earth. Planet. Int.*, **33**, 149-163, 1983.

Walck, M.C., "The *P*-Wave Upper Mantle Structure Beneath an Active Spreading Centre: The Gulf of California," *Geophys. J. R. Astr. Soc.*, **76**, 697-724, 1984.

Wiggins, R.A., and D. Helmberger, "Upper Mantle Structure of Western United States," *J. Geophys. Res.*, **78**, 1870-1880, 1973.

Woodhouse, J.H., "The Joint Inversion of Seismic Waveforms for Lateral Variations in Earth Structure and Earthquake Source Parameters," *Lecture Notes for the Enrico Fermi School on Earthquakes: Observations, Theory and Interpretation*, 1982.

Woodhouse, J.H., and A.M. Dziewonski, "Mapping the Upper Mantle: Three Dimensional Modeling of Earth Structure by Inversion of Seismic Waveforms," *J. Geophys. Res.*, **89**, 5953-5986, 1984.

Seismic Wave Propagation Effects — Development of Theory and Numerical Modeling

Text of Oral Presentation

Editor's note: The following is the text of the oral presentation delivered to the VELA 25th Anniversary Conference in Santa Fe, New Mexico, in May, 1984. It is intended to convey the basic material of the preceding paper in a different and complementary way. Figures identified by numbers refer to figures which appear in the preceding paper.

The central exercise in seismology is understanding seismograms. What you do with the answer is sometimes politics, sometimes finding oil, sometimes a discovery about the Earth. But, again, the central exercise is understanding seismograms.

Every generation of seismologists, for the last 100 years, has pushed for quantitative results, and in the 1980's this means that we try to interpret seismograms essentially by reproducing or modeling the waveform data. Our model has to have a description of the seismic source; an appropriate theory of wave propagation; and of course a description of the Earth's internal structure. One can expect that in decades to come, all of these components of our modeling will continue to improve.

We heard yesterday from Bernard Minster about progress in the study of the source, and today I am asked to review seismic wave *propagation*, and how we have come by our present-day understanding of Earth structure. I suppose the subject includes the theory of wave propagation, and a description of the relevant data. It should include inverse theory, and it would have to include a description of the answer, Earth structure as we currently perceive it. However, an orderly presentation of all these good things is obviously not possible in one session. Instead, I'll try and make, overall, perhaps three main points.

First, I think it is true to say that synthetics, as now computed, do indeed often look very much like the data.

The second point, which is related is that if we work with Earth models that are elastic, with structure that varies more or less smoothly

with depth, perhaps with a handful of discontinuities, then we do have a variety of trustworthy ways of computing the synthetics.

The third point I want to make takes us in another direction. We see attenuation effects in the waveform data that require us to go well beyond simply an elastic model of the Earth. We have to work with an anelastic model of the Earth, and, I do believe, with an Earth model that scatters waves. It is my belief that we don't really yet have a very good understanding of those processes, anelasticity and scattering, simply because in the scattering context the Earth is inhomogeneous on all spatial scales.

The first slide (Fig. 1d, upper) is intended to make my first point. It is from work of Langston and Blum and shows that synthetics really do look very much like the data. In this work we are also taught something new about the structure. The data here are WWSSN *P*-wave arrivals plus surface reflections and perhaps other crustal effects. As you scan over this (the data above and the synthetic below), I think you can see there is a remarkable agreement in this case. The way in which this agreement was obtained was essentially trial and error, fitting for the crustal structure above an earthquake source in the Puget Sound area. And in fact the structure that emerged, in synthetics fitting the data, had a low velocity zone. The overall details that emerged in developing synthetics you can look at here (Fig. 1d, lower right). One of those pairs of synthetics in each case had just a single layer of crust with no low velocity zone. The other synthetic had that low velocity zone. My goal here (and, as I am talking, you can look at these two synthetics, one with the low velocity zone in the crust above the earthquake, and one with just a single layer crust) is to convey a sense of the slight differences that you see in those two synthetics. The synthetic in each of those pairs that better fits the waveform data between *P* and *pP*, led Langston and Blum to say that this crustal structure had a low velocity zone. The conclusion here is confirmed by other kinds of data, refraction data, for example, in the area.

In this talk I'll come back several times to the point that synthetics really do look like the data in many cases. But Ann did put the word "theory" in the title of my talk, so I'll briefly review the theory to see how synthetics like this are computed.

(Figure A) I haven't put in an equation yet. This is all symbolic. We first describe the normal modes of the Earth in an orderly way. Then one can simply add those normal modes up to synthesize the way the ground moves — a seismogram. In a very schematic way, I want to march on here with that basic method of solving the relevant partial differential equations, the method of separation of variables. In this way, the sum

If the jth normal mode of the Earth is

$$_j\mathbf{u}(\mathbf{x}) \cos \omega_j t \exp[-\omega_j t/2Q_j]$$

then a seismogram is just a sum over j with excitation coefficients given by the moment tensor. $j = (l,m,n)$, a triplet of integers.

Fig. A.

of normal modes breaks down into a sum over angular order number ℓ, a sum over radial order number n, and in seismology, fortunately, the sum over azimuthal order number m is relatively simple (Fig. B). So one finds from the method of separation of variables this type of factorization. This typical presentation concentrates on *SH* waves. The representations that everyone uses have this kind of structure. The first factor is effectively the details of a point source. I used here some detailed terminology in notations of the seismic moment tensor. The basic synthetic that one works with is the sum over ℓ and over overtone number n, of separate factors. One can work away at rearranging this, recognizing, if one chooses to do it, that one can go to a continuum of horizontal wave numbers and overtone numbers (Fig. C). Then n simply counts up in

$$\mathbf{u}(\mathbf{x},t) = \sum_{\ell} \sum_{n} \sum_{m=-2}^{2} f(\text{source})\, e^{im\phi}$$

$$\times\, g(\text{receiver depth, and Earth model})$$

$$\times\, h(\Delta)$$

$\mathbf{u}(\mathbf{x},t)$ for *SH*-wave source

$$= \left[\tfrac{1}{2}\sin 2\phi[\dot{M}_{yy} - \dot{M}_{xx}) + \cos 2\phi \dot{M}_{xy}\right]$$

$$\times \sum_{\ell} \sum_{n} f_1(\ell,n)\, g\, h$$

$$+ (\cos\phi \dot{M}_{yz} - \sin\phi \dot{M}_{xz})$$

$$\times \sum_{\ell} \sum_{n} f_2(\ell,n)\, g\, h$$

Fig. B.

Basic synthetic, by mode summation:

$$u(x,t) = \sum_{\ell} \sum_{n} [\text{separate factors describing source Earth model, receiver depth source-receiver separation } (\Delta)$$

Continuum: $\sum \rightarrow \int$

$\ell + \frac{1}{2}$ = horizontal wavenumber = $k = \omega p$

n = overtone number (increasing frequency at fixed ℓ)

Basic synthetic

$$= \int dk \int d\omega \text{ separate factors for source, etc.}$$
$$= \omega \int dp \int d\omega \ldots\ldots\ldots$$

Fig. C.

frequency, but one has exactly the same structure in many cases, working with a basic synthetic that is now an integration over horizontal wavenumber and frequency.

Because of various choices in the way integrands and integrations here can be approximated, there are dozens of different ways to get the answer. Someone in the audience may recognize this (Fig. D). It appeared in a review of a paper I had submitted. So if you are out there I thank you and note that I and many others in this audience have spent years picking our way over the details of various choices here. There is the choice about how to handle layers — should one use a few inhomogeneous layers or should one work with hundreds of homogeneous layers? What order should one do the integration in? Should one use a slowness method or a spectral method, and so on.

It turns out that programs for synthesizing all body wave multiples, and surface waves, in realistic structures, are quite cumbersome and expensive if they are to be broadband, and last many minutes. So, it has been necessary in practice to develop special and quick methods for isolated portions of the seismogram. This is the subject of generalized ray theory, and Don Helmberger took a major practical step in 1968 when he showed how to use Cagniard-de Hoop methods to get the generalized response of a single interface within a stack of layers. Before that time, synthetics had been used only a qualitative way. Since 1968, synthetics have been used to get quite detailed information about Earth structure.

The Basic Choices for $\omega - k$ Integration
(not including Cagniard-de Hoop)

1. Earth flattening to cylindrical coordinates
2. No earth flattening. Use spherical coordinates

Integrand ×
1. WKBJ or Langer approximation with appropriate Debye expansions at discontinuities
2. Layer matrices with homogeneous layers
3. Layer matrices with inhomogeneous layers
4. Direct numerical integration of an arbitrary velocity profile

Integration ×
1. Spectral method with contour for the p integral along the $Re\,(p)$ axis
2. Spectral method with part of the contour for the p-integral off the $Re\,(p)$ axis
3. Slowness method. (Chapman 1978)

Fig. D.

Before turning to some of these studies of structure, let me emphasize that the various methods for getting synthetics all seem fairly trustworthy. Several papers have come out in recent years making this point, simply comparing different methods of computation in the same Earth model. Larry Burdick and John Orcutt, working with a upper mantle model that had this (Fig. E) travel time curve, compare a generalized ray method with the reflectivity method (Fig. 3b). We can look at this for a while, and basically the question is, do these two different methods give the same results? You can form your own conclusions about that.

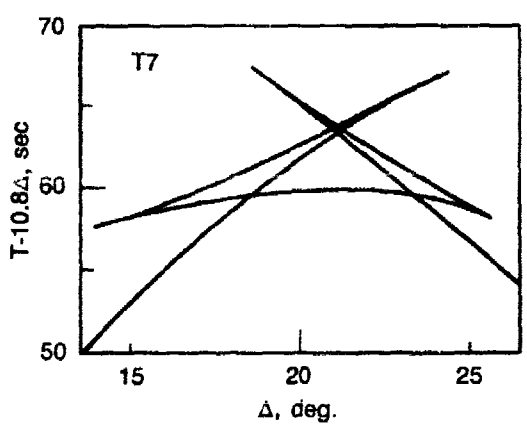

Fig. E. From Orcutt and Burdick [1977].

I claim that at most of these distances they really do seem to give the same detail, "wiggle for wiggle." One can be picky and point to a few places where they don't, and one can get into a morass of question about why there are various strange features that are due to how the phase velocity integration is cut off, of how the generalized ray sum is truncated. The point is that in the hands of the expert who is developing these synthetics, the methods are effective. If it's a question of whether computed synthetics are now being carried out accurately, I think the answer now is: "usually, yes."

Another exercise of comparing synthetics in the context of waves that go really deep down into the Earth, brings up the problem of doing the calculation by methods that require very many (hundreds of) layers in the Earth model (Fig. F). In this case I'm going to show some examples of the reflectivity method, executed by Gerhard Mueller (Fig. 5f); compared with work of George Choy (Fig. 5e, overlayed on Fig. 5f), who used an Earth model with a few inhomogeneous layers. In practice when the Green function describing propagation (through these two different ways of handling the Earth's velocity increase with depth) is

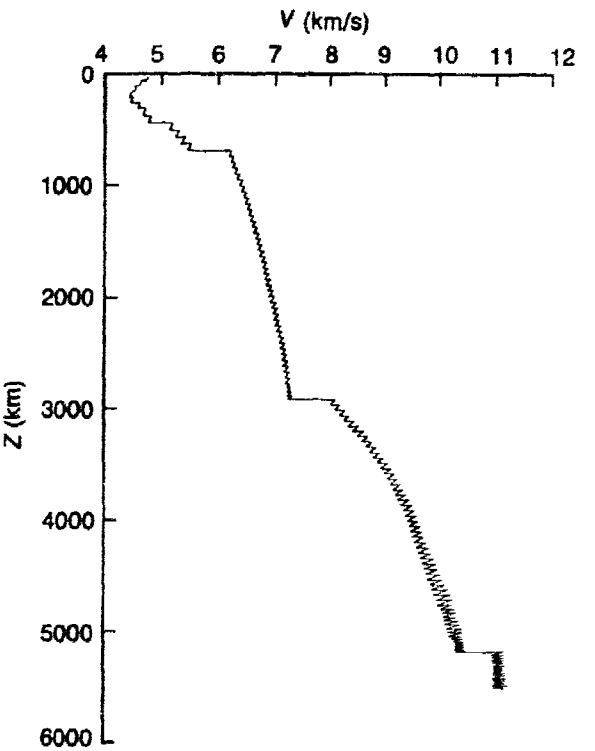

Fig. F. Earth model for reflectivity computations of *SV* (including *SKS*). From Choy *et al.* (1980).

convolved with a typical source and instrument response, then we see that there is basically very good agreement.

There are going to be some pitfalls still. Pitfalls, however, that are recognized by practitioners. One of the best methods (it's the cheapest) is called the WKBJ method, pioneered and advocated by Chris Chapman, and Grand and Helmberger recently reported an interesting comparison of *SH* synthetics calculated by two different methods in a couple of upper mantle structures — tectonic North America and shield North America (Fig. G). To see how cheaply we can compute seismograms, for example, in the TNA model, we can look at the right half of the panel (Fig. H) compared with a more expensive, but more general method on the left, and you can form again you own opinions about the agreement of those two methods, but I think it's pretty darn good; they basically do very well. But yet, if one goes through the same exercise, as Grand and Helmberger show, for the other upper mantle structure, the structure that they call shield North America, then on the right hand side of this panel (Fig. I) is the WKBJ computation, and on the left, the generalized ray computation. I would say, as Grand and Helmberger have pointed out, there are clearly some significant differences in this forward computation of synthetics.

Why does it work out that in TNA the computation can effectively be done accurately by the WKBJ method, but not so for the SNA structure? It has to do with what actually is the worst velocity gradient in

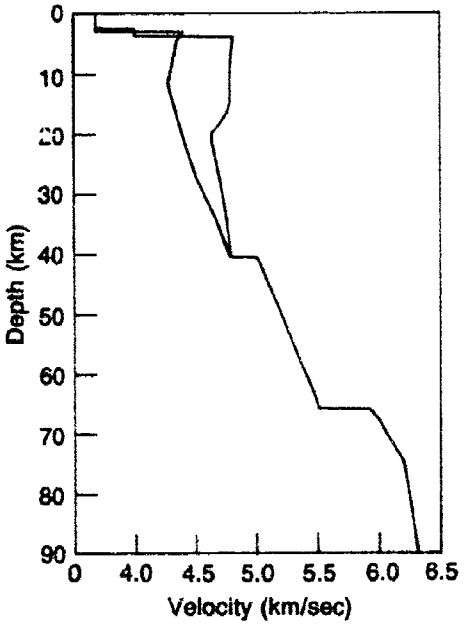

Fig. G. Mantle models for tectonic North America (TNA) and shield North America (SNA). From Grand and Helmberger [1984].

Fig. H. From Grand and Helmberger [1984].

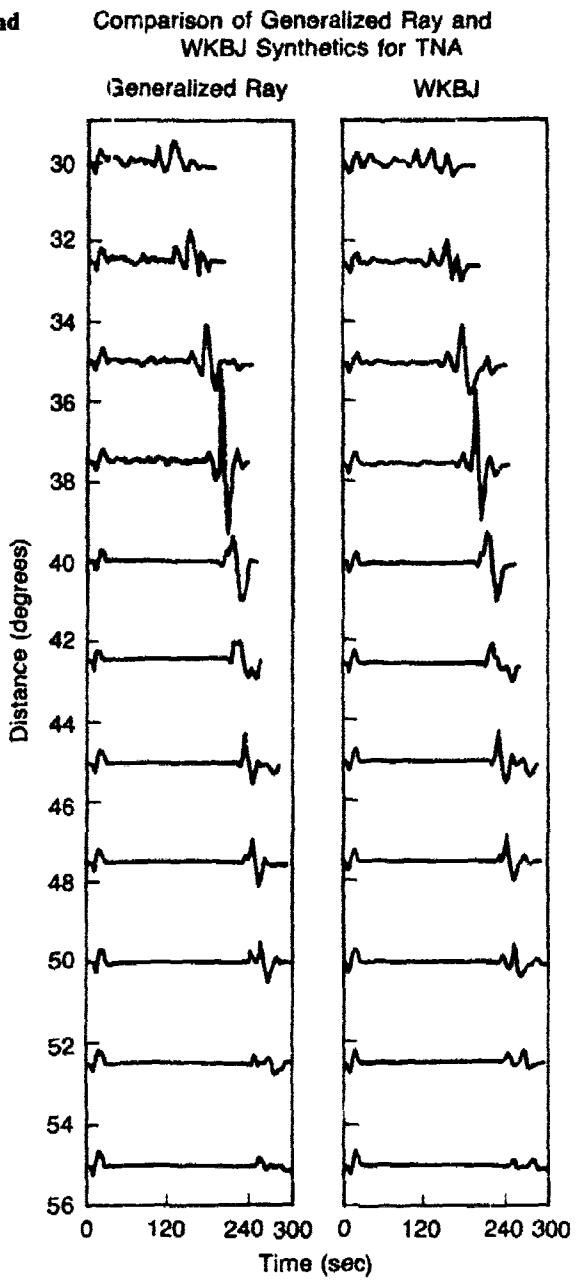

those two upper mantle models. What is shown here (Fig. J) superimposed on the TNA is a series of steps (layers) having the critical velocity gradient required in a typical layer approximation to the model. That is, in these layers the velocity gradient, dv/dr, equals v/r. As it happens,

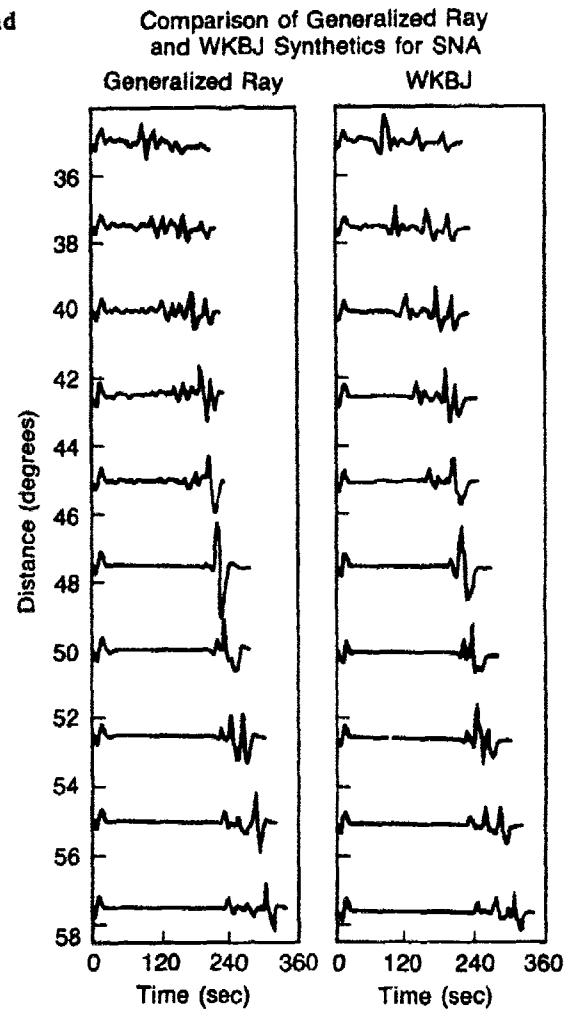

Fig. I. From Grand and Helmberger [1984].

TNA although it has a low velocity zone and a region with $dv/dr > 0$, never attains values of dv/dr as great as v/r. But SNA does. In technical terms, this means that TNA has a turning point radius that is single valued and varies continuously with ray parameter, but SNA does not. In this case, an important feature of the wave propagation in SNA is the tunneling of energy through the high velocity region about the low velocity zone. And this can be handled by generalized ray methods, but not with relatively simple WKBJ procedures.

It is pitfalls such as this that make it difficult to develop computational synthetics packages that are both foolproof and efficient. But the

Fig. J.

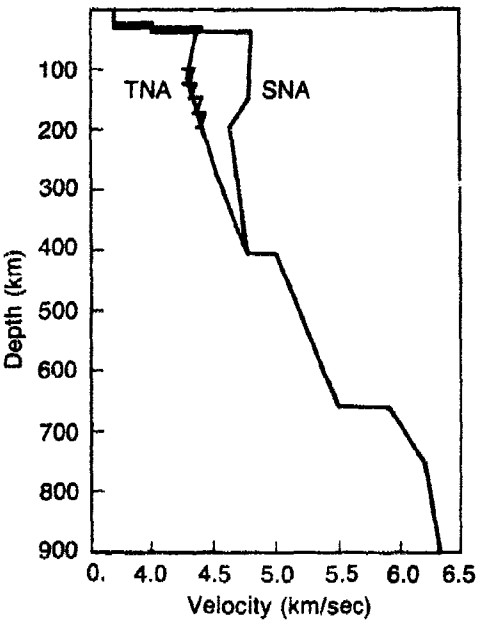

main point is that successful methods at last do exist for accurate seismogram modeling.

Now let's look again at what has been learned about structure. The next slide (Fig. 7) is the Preliminary Reference Earth Model published by Dziewonski and Anderson in 1981. I remind you — I'm supposed to be making the case for using synthetics to learn about Earth structure. But I don't want to do violence to history here, because remember Mohorovičić in 1909 began to develop ideas about a crust of the Earth, and began to investigate the thickness of that crust. He did it without using synthetics. In 1913, Beno Gutenberg, standing on the shoulders of Oldham and Wiechert, gave a very accurate estimate of the depth to the Earth's core. In 1936, Lehmann recognized the existence of an inner core. In the 1940's, Maurice Ewing began to study the oceanic crust and found out how thin it was. These early studies go beyond just the major discontinuities, because in 1967 Lane Johnson published convincing evidence for two regions of very high velocity gradients in the Earth's upper mantle.

So all of this good work was done without using synthetics. In fact this model itself (PREM) was published without using synthetics. So, here I am, I'm supposed to make a case for synthetics, but I simply want to try and be fair, not just to say "everything depends on synthetics these days." Because that's not the case. What in fact does one learn with

synthetics, then? I would have to say they can be exceedingly useful. They can be used to sharpen details of our knowledge of structures. In this context, I think it's very interesting to see what the oil industry does. The oil industry has been spending about four billion dollars a year to acquire and process geophysical data. Almost all of that is seismic data. But they don't spend much on synthetics! The oil industry typically works with massive travel time sets, and that might be a crude way to summarize reflection data, but that's all it is. It's largely kinematic data. Of course there are appeals to amplitudes in that data, and I know about studies with bright spot analysis and so on, but largely, I think it's still true to say that synthetics are not very much used in that industry. So what are we doing using synthetics in our kind of seismology? It's mainly an exercise to try and get the maximum information out of the data that we do have available, because we don't have four billion dollars a year, and even if we did, it would be hard to go . . . well, we could do a better job, of course! But I'm simply asking that you think what would one really do if one really had to get the answer as, in practical terms, the people working in the oil industry have to. That is an industry dedicated to getting results. They just haven't gone this route of working with synthetics, because of two reasons, I suppose: the kinds of depth-dependent structures, with the kinds of wavelengths they are using, are indeed very complicated; and they have to work with three dimensional structures. As I'm sure Don Anderson and Adam Dziewonski will show us, the direction to go for us too is indeed going to lead us into complicated structures of a three dimensional Earth. However, having made this digression, I'm going to accept a restriction. I'm supposed to talk about one dimensional structures of the Earth, and using waveform data. Don and Adam will take off from there.

So, synthetics, how are they used? The principal use is still trial and error fits to data in an effort to maximize the extraction of information. In fact, most of the practitioners don't use formal inverse theory. Most of the practitioners don't even have the opportunity to work with reversed record sections. But still, let's not deny that a great deal is still to be learned. Let's look again at this PREM model, noting in particular that the upper mantle discontinuities are present at around 400 and 650 km depth. It's natural to go in this direction of synthetics, trying to check out detailed structures around those two discontinuities, or regions of high velocity gradients in the upper mantle.

A recent major attempt has been published by Walck who worked with digital data, short period data largely, from the Southern California Network. 1400 short-period digital records, I understand, went into this work. She developed this detailed conclusion (Fig. 8). about upper mantle

structure, south and east of the array. When it comes down to details, and use of synthetics, the main interest is to look here and see how big is the velocity jump of these transitions. In this case it's a little less than 3% at the deeper discontinuity and about 4% at the upper one. The details are not just the magnitude of that discontinuity, but what kinds of gradients are found just above and below the discontinuities. I can't do justice to this extensive study, but simply to give a flavor of it I'll show some figures from a recent paper of hers in the *Geophysical Journal* to study the effect of structure around whatever is going on, a discontinuity perhaps, at 660 km depth (Fig. 9, top). The top row is some short period data, and the next row is synthetics for a relatively large jump in velocities. In the subsequent two rows she reduced that discontinuity, but added regions of anomalously high gradients, in one case just above, in the other case above and below. It is by hundreds of attempts of trial and error fitting in this way that one finds what is the power of data actually to resolve details.

On the lower left is her final choice for the structure around 660 km depth. On the next slide (Fig. 9, bottom), on the left is shown a small amount of the data intended to bring out the clear first arrival. Following that first arrival, is a second branch, which begins to fade out around 28 or 29 degrees. This is present in the data on the left and in the synthetic on the right. It is interesting that in her paper, the author still says the question about thickness of transition zones is unresolved. She could not tell whether, indeed, there was a discontinuity at that depth, or whether the velocities might have increased over a zone perhaps as thick as 20 km. The data and the synthetics would look about the same in this case.

Although this is relatively short period data, this is still fairly wide angle incidence at that interface. It turns out that the key data on the question of transition zone thickness, which is of great importance petrologically in our understanding and appreciation of Earth history and so on, is the data from nearly vertical incidence. An important consideration here has to do with what kind of reflection coefficient results from transition zones of various thickness. If you'll accept the idea here (Fig. K) of having some kind of hyperbolic tangent, some kind of continuous increase of velocity with depth, where most of the action takes place over a transition thickness marked as lowercase d, and if one asks the question for near vertical incidence, "How does the reflection coefficient behave?" what is shown here is that the reflection coefficient is strongly dependent on frequency. This example has a total 10% change in impedance, so the biggest coefficient possible is 5%, at long period. (The wavelength is lambda, incident from below. Transition thickness 1

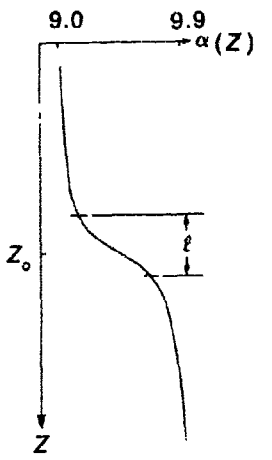

$$\frac{\alpha(Z)}{\alpha(Z_o)} = \left\{ 1 - 0.095 \tanh \left[\frac{1.76}{\ell} (Z - Z_o) \right] \right\}^{-\frac{1}{2}}$$

ℓ/λ	R
0.1	4.5×10^{-2}
0.2	2.5×10^{-2}
0.5	1.8×10^{-3}
1	1.0×10^{-5}
2	3.2×10^{-10}

Fig. K. Reflection coefficient (R), tabulated for different ratios of transition thickness to wavelength.

encompasses 75% of the total impedance change.) The best way to summarize is to say that if the transition gets spread out over more than about a quarter of a wavelength, then the reflection coefficient very rapidly falls to zero. So, the exercise of trying to get detailed information about transition zones in the upper mantle is still a very active research field. The pertinent data has to be short period data as near to vertical incidence as one can get. I was delighted to see a contribution on this subject in the current issue of, again, the *Geophysical Journal* that reached me just two days before I flew out here. This is from the work of Bock and Ha, and maybe Anton Hales can comment on it.

What we're looking at here (Fig. L) are some short period arrivals at the Warrumunga array, in Australia, from deep earthquakes in Tonga. Shown here is the *P*-wave, and there's a phase marked *X*. Each trace here is for a different deep earthquake and the *X* phase is by these authors given the interpretation of an *S*-wave which goes down from the source, is reflected/converted from an upper mantle discontinuity around 650 km, and propagates up as *P*. These are vertical components, and again there are more observations of that *X* phase here on the right hand panel. This is a talk about synthetics, and the authors showed the results of a forward computation (Fig. M). On the upper panel, again here is the first arriving *P*-wave, and their *X* phase is shown as having a noticeable magnitude if they do the calculation with a very sharp transition zone. However, if the same computation is done as on the lower panel, with a different focal mechanism, it turns out that the *X* phase is hardly

G. Bock and J. Ha

S—P Conversion Near 700 km

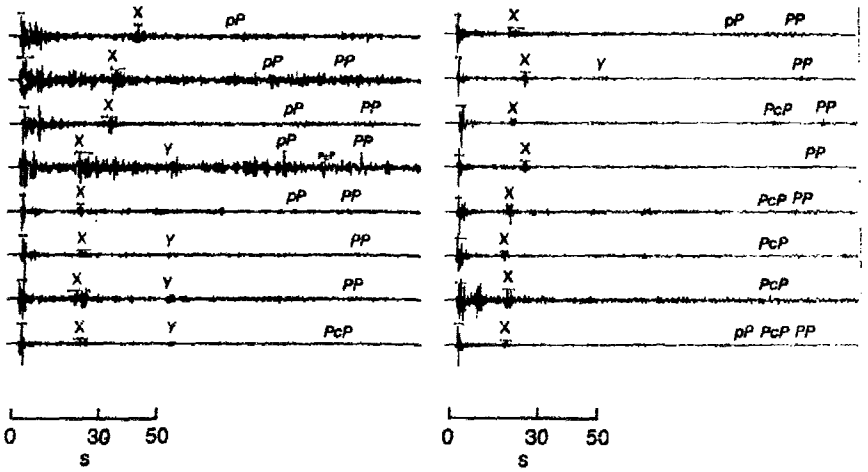

Fig. L. From Bock and Ha [*Geophysical Journal R.A.S.*, May 1984].

present at all in the waveforms. These authors were able to explain their observations in terms of the focal mechanism for departing *S*-waves.

Moving down lower in the Earth, I'd like to describe an example of synthetics used to study the core of the Earth. Let me remind you (Fig. N) of what the travel time curve for PKP looks like. This slide includes the reflection from the inner core (branch *CD*), and the transmission through the inner core (branch *DF*). Again, the framework of analysis in which synthetics have been used is to study the effect of velocity gradients just above and just below the major interfaces. One searches in the data to find phases that are known, because of experience with synthetics, to be sensitive to details of structure. It turns out that the *BC* branch, just near the point *C*, is a place where amplitudes are exceedingly sensitive to structure at the base of the fluid core (*i.e.*, just above the inner core/outer core boundary). Near the point *D*, where there is a mixture of PKiKP and PKIKP, there is sensitivity to velocity gradient in the outer part of the solid inner core. Going back to the *BC* branch again (Fig. 12b), near 156°, this is a study by Choy and Cormier intended to show synthetics resulting from three slightly different models near the inner core/outer core boundary. In each case the synthetic is superimposed on the same observed seismic waveform. At this distance, there is little sensitivity in the *DF* and *AB* arrivals. But *BC* is quite variable. (This is broad band data reconstructed from short and long period SRO data.) The indication from this comparison of *BC* synthetics is that

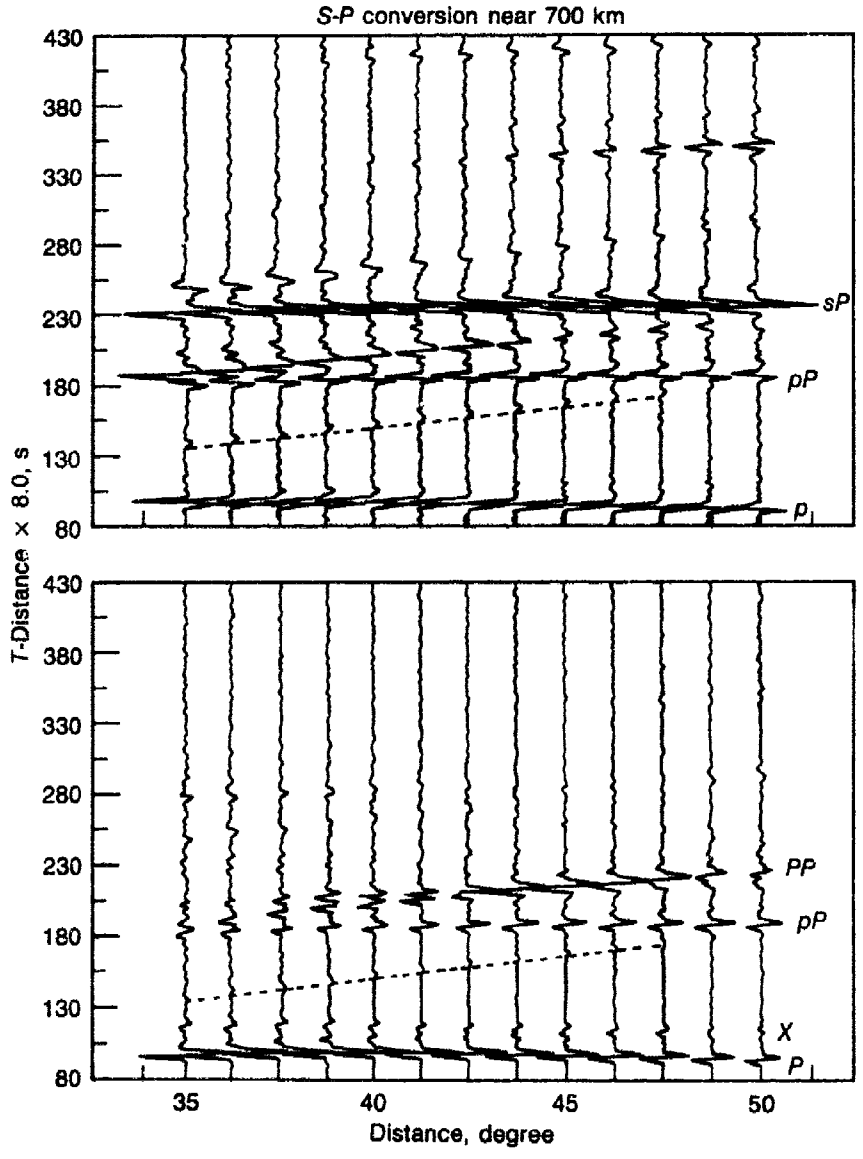

Fig. M. From Bock and Ha [*Geophysical Journal R.A.S.*, May 1984].

Fig. N. Travel time curve for *PKP*.

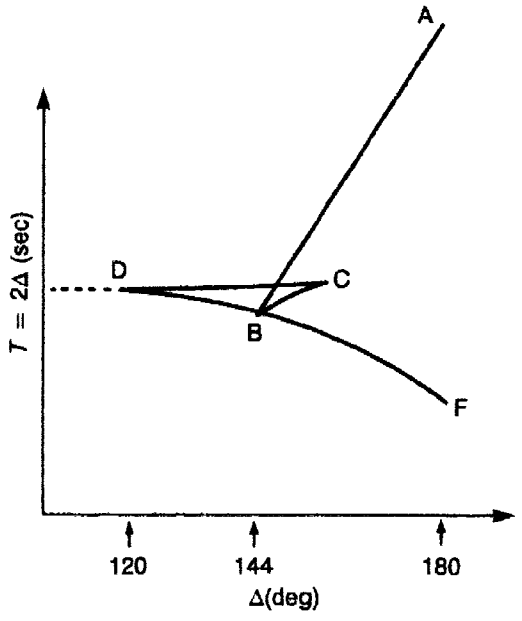

a velocity gradient between that of models PEM and PREM is appropriate, for the lowest part of the fluid outer core.

Well: so far, so good. Treating the Earth as a medium that varies smoothly with depth alone, and having just a few discontinuities, we seem to be doing a good job now of generating synthetics and fitting data, especially long period body wave data.

But now we come to another property of the Earth, namely attenuation, which I don't believe is so well understood. We have to say a little here (Fig. O) about the theory. First, for a plane wave in a homogeneous elastic medium, we work with real wavenumber k and real frequency omega. If the wave attenuates as it travels I will take the route of wavenumber being complex, frequency still real. Breaking the wavenumber into real and imaginary parts, alpha is the spatial amplitude decay rate, and is often characterized equivalently in terms of Q; c is the phase velocity. Thus Q describes the effect on the amplitudes spectrum, as the wave propagates. If we want the effect of all this in the time domain (Fig. P), we just integrate over all frequencies. I remind you that if one works with constant Q and constant c then if we start out with an impulse propagated through a homogeneous anelastic medium, the pulse subsequently loses its high frequencies and broadens symmetrically. But a detailed examination of such a pulse shape shows it to have completely unphysical characteristics. It begins to grow far too early in time, and is said to be non-causal. So it turns out we have to do more

Brief review of attenuation by { internal friction / anelasticity / true dissipation

---

Consider a very simple wave in an *elastic* medium:

$e^{i(kx - \omega t)}$ $\quad k = \omega/c$. Homogeneous

Generalize for anelasticity to:

$e^{i(Kx - \omega t)}$ with complex $K = k + i\alpha$

$e^{i(kx - \omega t)} e^{-\alpha x}$

$\alpha = \dfrac{\omega}{2cQ}$ Affects amplitude spectrum

Fig. O.

than this. And for about 20 years this has been recognized in seismology. The fix is to "impose causality," which effectively requires slight frequency dependence in the phase velocity. The most commonly used description that emerges is one in which there is a small logarithmic dependence. After integrating over all frequencies, the resulting pulse has physically plausible features, such as a clear onset, and this asymmetrical shape (see last part of Fig. P).

Now, I'm sure you won't expect me to review all the main studies of Q in the Earth. Instead I want to focus on one issue, which is why quite high values of t^* are sometimes promoted, and why there is argument about this. It seems to me that until this issue is resolved, the use of body wave synthetics is under a cloud.

To make my point I want to focus on one particular experiment, involving *ScS* waves, for which the data is relatively good. *ScS* attenuation was first studied by Frank Press and subsequently many others in the 1960's. But in 1967 Kanamori published an interesting comparison of *ScS* and *ScP* waves (Fig. 14a), in which he was able to ratio out our ignorance of the source spectrum. And here (Fig. 14b) is an example of his data, showing the vertical component for *ScP* on top, and horizontal components for *ScS* below. These are from Johnson-Matheson instruments peaked at around 3 Hz, and you can see there is no signal in these seismograms at 3 Hz. He took amplitude spectra (Fig. 14c), and a spectral ratio is shown by the dots fit with a line in the lower part of the slide, and he summarized his experiment as indicating a Q of around

Integrate over all frequencies $\int_{-\infty}^{\infty} [\ ] \frac{d\omega}{2\pi}$.

to get result in the time domain:

Impose causality:

$$\frac{c(\omega_1)}{c(\omega_2)} = 1 + \frac{1}{\pi Q} \log\left(\frac{\omega_1}{\omega_2}\right)$$

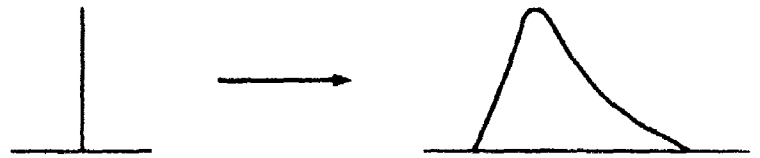

Fig. P.

230, over the frequency range 0.2-0.6 Hz, for *S* waves making a single passage from core-mantle boundary to the Earth's surface. His data also indicated pulse broadening of *ScS* relative to *ScP*, but his analysis concentrated on spectral ratios.

The next slide (Fig. 15) is again a comparison of *ScS* and *ScP*, from the WWSSN short-period station at Junction, Texas. This is excellent data, and has been discussed by Larry Burdick. Relative to the Kanamori study, it is high-frequency data, and Burdick concluded this data required the *S*-wave *Q* to stay low (around 250) out to frequencies as high as 1.5 Hz. He reached that conclusion by studying not the spectral ratio but by discussing another property of the data, a very important property, which is the pulse broadening. We can see that the *ScS* pulse lasts longer

than *ScP*. The next slide (Fig. 17a) shows at the top *ScP* and in the middle *ScS* data. The lowest trace shows the effect on *ScP*, of filtering it as appropriate for passage up through the mantle again as *S* (rather than *P*). So, this lowest trace is an *ScS* synthetic, and Burdick showed that with constant *Q* and an absorption band model, it was necessary to keep *Q* low right out to high frequency (1.5 Hz) in order to achieve the observed pulse broadening of *ScS*.

I am focussing on this data, because it may illustrate a problem with the absorption band model in which *Q* is constant out to a cut-off in the spectrum of relaxation times, and then *Q* rises (proportional to frequency) at higher frequencies. For, in this case, the low value of *Q* at 1.5 Hz that results from a pulse-broadening analysis does not seem to fit with the basic observation that high-frequency components are present in the *ScS* waveform. One notes that it takes about 500 seconds for an *S* wave to travel from the core-mantle boundary up to Texas. At 1.5 Hz this is 750 wavelengths, and so the power spectral ratio between *ScP* and *ScS*

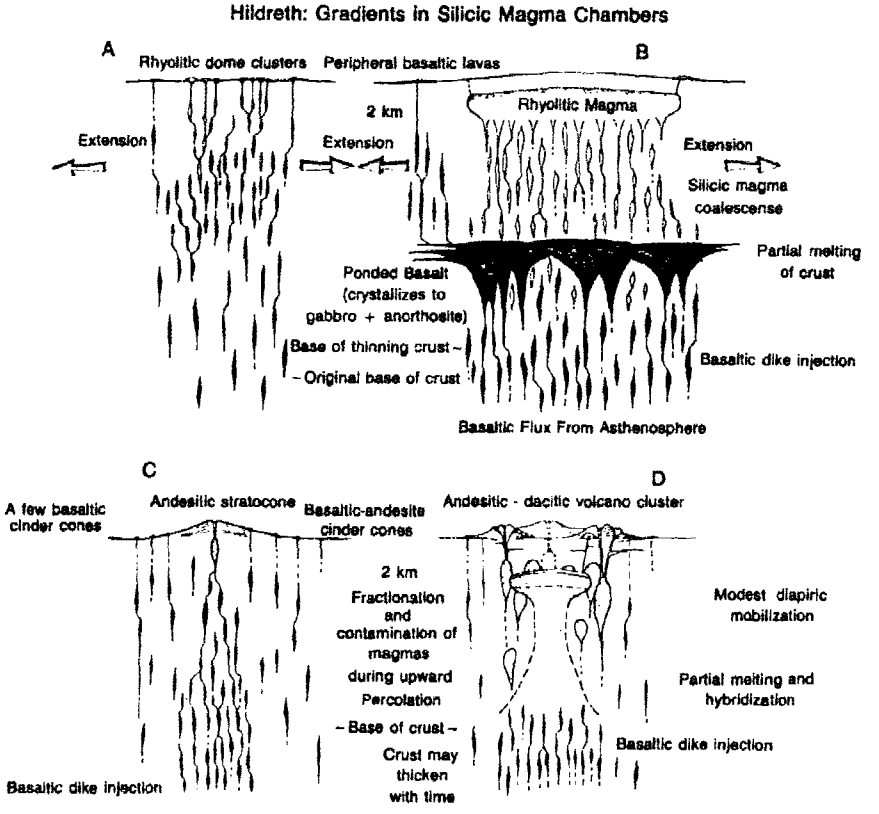

Fig. Q. From Hildreth [*J. Geophys. Res.*, Nov. 10, 1981].

would be about 105 or 106. Yet looking directly at the power spectrum for these pulses (Fig. 17b), the power spectral ratio might be more like 102 at 1.5 Hz.

It therefore seems that we should consider possibilities other than anelasticity, when we try to interpret observed loss of high frequencies, plus observed pulse broadening, of body wave pulse shapes in the Earth. In this connection it is perhaps interesting to be reminded of what Earth scientists who are not seismologists now consider as candidate structures. Here are three, that extend into the upper mantle (Figs. Q, R, and S). I therefore suggest that we turn our attention to the effects of highly heterogeneous structures, to see what scattering can do. The subject is most highly developed in the context of crustal layering, and here (Fig. T) on the left hand side is shown a well log measured in a drill hole. This is not the Earth model, smoothy varying with depth, that has been associated with synthetics described so far in this talk. On the right, is shown an idealization of the well log, using 40 crustal layers. Bill Menke and I went through an exercise of propagating a plane wave impulse through complicated structures such as these (albeit still not as complicated as the Earth itself). We found (Fig. U) that various features reminiscent of attentuation arise; the loss of high frequencies in the most prominent part of the transmitted pulse; the pulse broadening; and, of course, coda is present too.

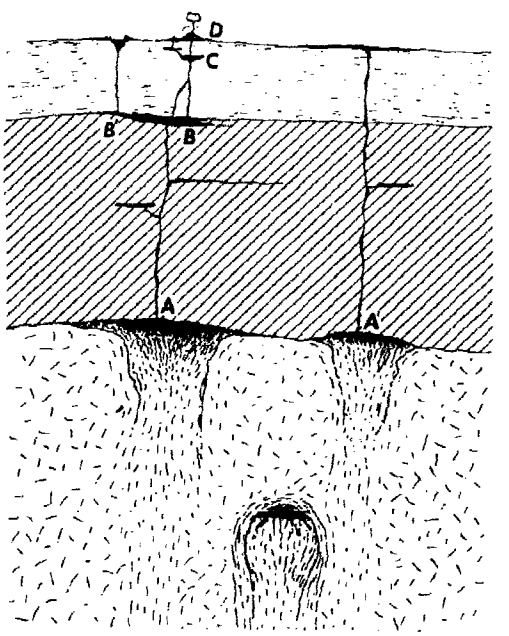

Fig. R. From Basaltic-Volcanism Study Project, [*Basaltic-Volcanism of the Terrestrial Planets*, Pergamom, New York 1981].

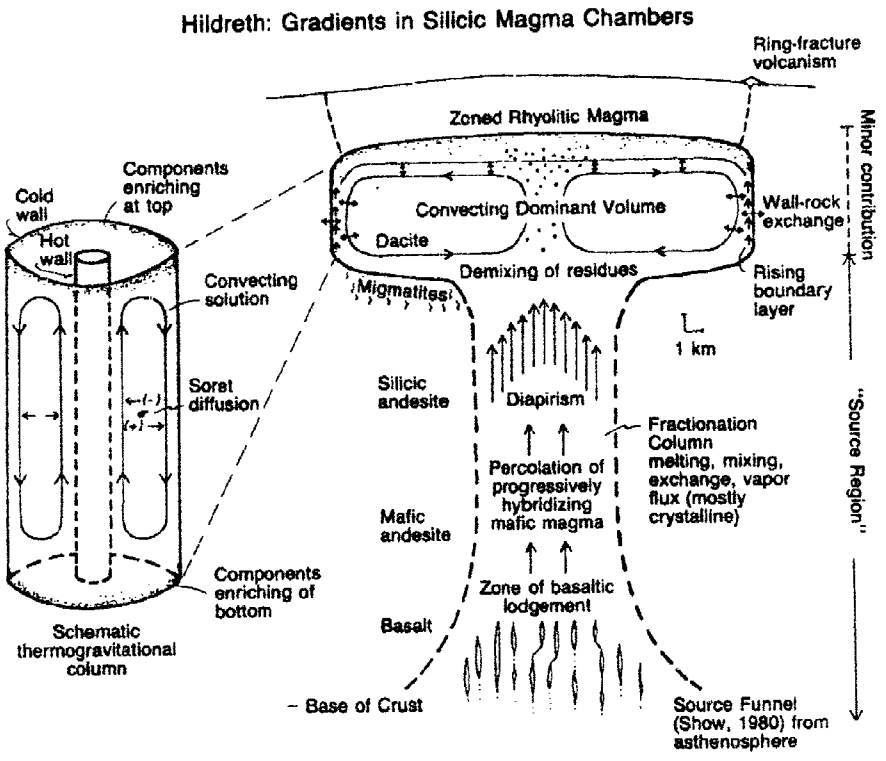

Fig. S. From Hildreth [*J. Geophys. Res.*, Nov. 10, 1981].

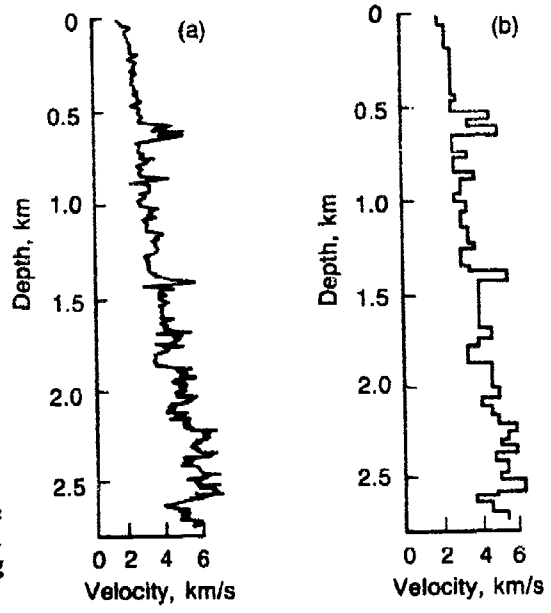

Fig. T. (a) Typical acoustic velocity log from borehole. (b) Idealization of log using about 40 plane layers.

Fig. U.

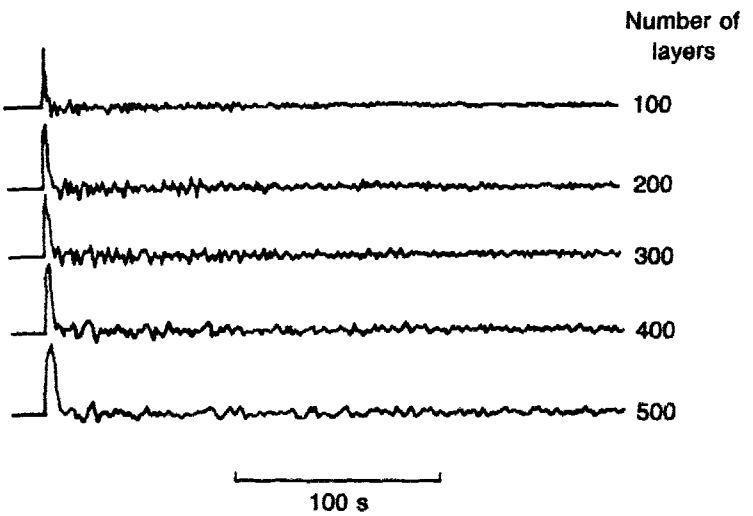

The exercise of computing synthetics such as these, can lead to a change in one's whole mindset about the Earth's internal structure. The relatively simple first arriving pulses here (Fig. U) are in fact composed of forward-scattered multiples. I find it disconcerting, to have spent half of my professional life studying the Earth on the basis of generalized ray theory, which is supposed to get simpler at high frequency, and now to find it isn't much use in assessing scattering and coda, which are such prominent features of short period seismograms. It's important then to look again, carefully, and see what might help in a diagnostic way to decide on whether scattering is important in removing high frequencies. I will simply say that high frequencies do show up in this signal, because this is an elastic calculation and if one looks (Fig. V) at the power spectrum in an early window one finds as shown on the left that the signal is losing power at high frequencies. But on the right is shown the power spectrum for part of the coda, and this rises with frequency. So at least in an elastic calculation the high frequency is pushed later into the coda.

I began this talk by saying that our main job as seismologists is interpreting seismograms. So I'd like to show you an example that has high frequencies in the coda. I asked the people here from Teledyne Geotech if I might show a couple of transparencies made from a short paper they submitted for this meeting, and here (Fig. W) is some indication of high frequencies arriving after the first few seconds. This can be shown (Fig. X) with the data run through various narrow bandpass filters, and systematically it is evident that higher frequencies are coming in later.

What then are we going to do about this?

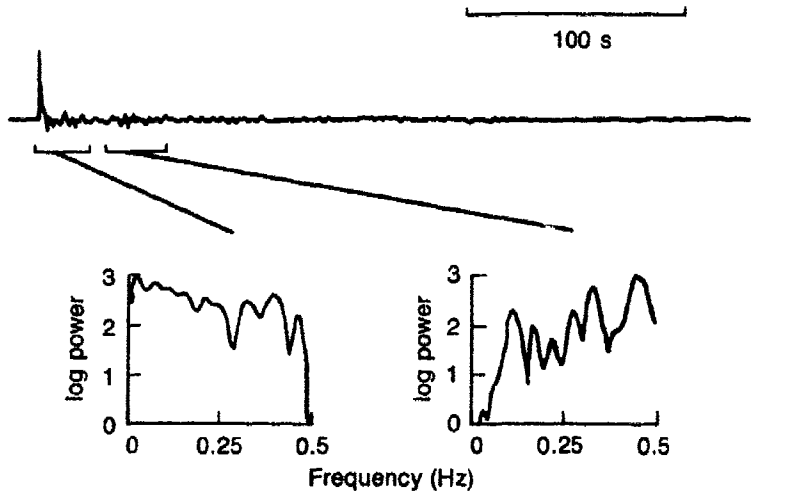

Fig. V. *Top* **Transmission response of upper 100 layers of log used in Fig. T.** *Bottom* **Power spectra of initial portion of pulse and later coda. Note loss of higher frequencies from initial pulse.**

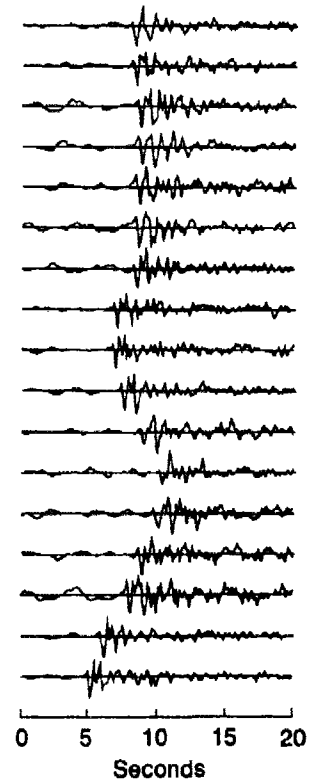

Fig. W. NORSAR seismograms for an East Kazakh explosion. Variation of the *P* amplitude, *P* waveform, and initial *P* coda is considerable in the first 5 seconds. The initial coda (5 to 6 seconds) possesses higher frequency content than the initial (first 2 seconds) *P* wave pulse. From Teledyne Geotech.

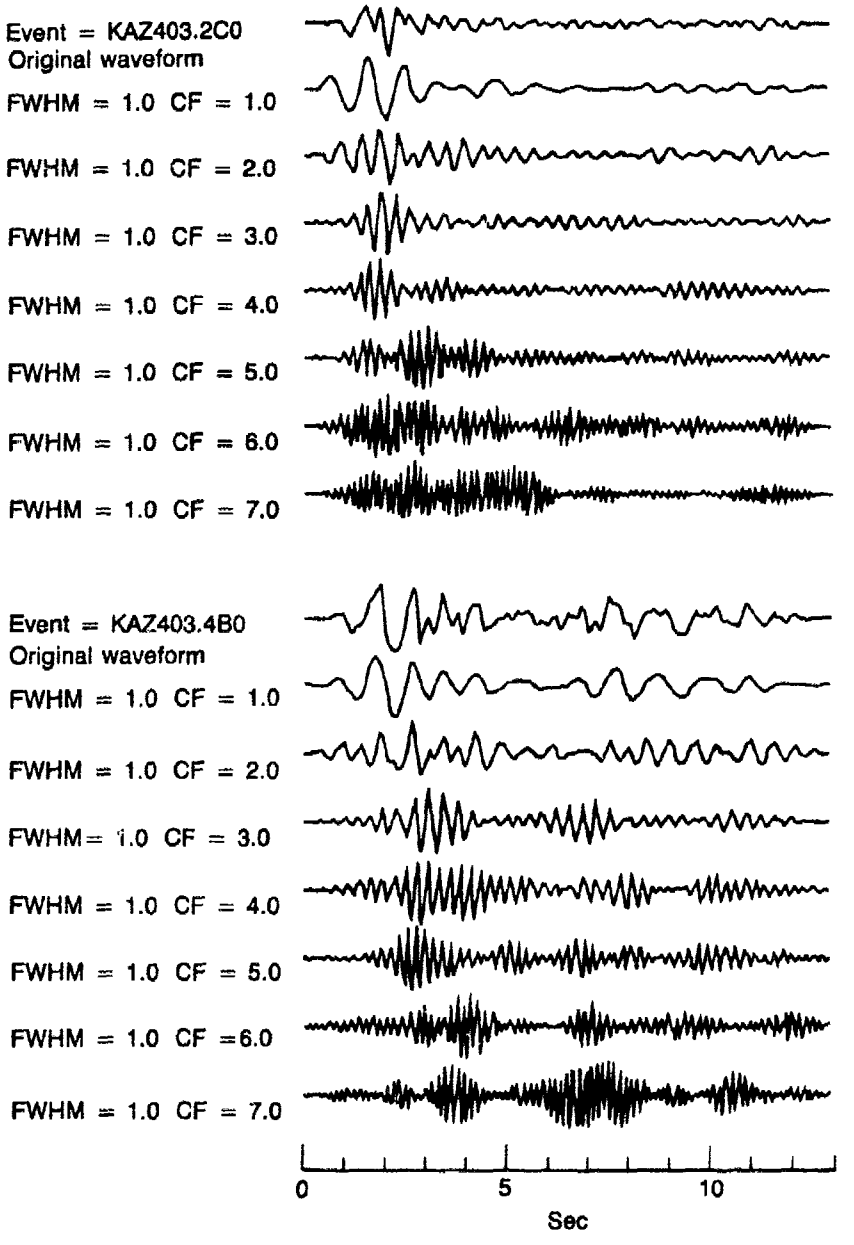

Fig. X. Band-pass filtered seismograms of two NOFSAR stations using zero-phase-shift Gaussian filters with center frequencies of 1, 2, 3, 4, 5, 6, and 7 Hz. Each filter has a half-width-half-maximum of 0.5 Hz. From Teledyne Geotech.

Certainly, one way to go is to work with longer periods that average out such fine scale scattering structures. As I hope I indicated in the earlier part of my talk, I think such uses of data, and associated synthetics, are in relatively good shape. However, when it comes to detailed studies of pulse shape, where attenuation and dispersion are noticeable, I am reluctant to see casuality relations (such as Krämers-Krönig) applied unthinkingly. Seismology is a branch of material science, and our wave equation is not a fundamental equation of physics, like, say the Maxwell equations. We observe, teleseismically, waves over a frequency range of about 10^4 (from roughly 0.001 Hz to 10 Hz), and at different wavelengths we must presume that seismic waves average Earth structure in slightly different ways. We thus need to search more directly for evidence of body wave dispersion, rather than assuming we know what dispersion is because of inferences from observed attenuation. When it comes to analysis of short period signals, and the statistics of coda, we must attempt the difficult transition from Earth models described deterministically (*i.e.*, velocities that smoothly vary with depth), to Earth models that have fine-scale inhomogeneities described statistically.

Although I began this talk claiming that synthetics do look like the data, and that we do know at last how to compute synthetics appropriately for smoothly varying Earth models that may also have a few discontinuities, I am concluding that for short-period data there are still some important unsolved problems.

The Effect of Q on Teleseismic P Waves

Thomas C. Bache

Background and Objective

Understanding the effect of regional attenuation variations on P wave signals in the 0.5 to 3.0 Hz band is important for accurate yield estimates and for event identification methods that rely on earthquake/explosion spectral differences. Key issues remain unresolved because (1) there are strong tradeoffs between source and attenuation variations in this band; (2) there are large variations in published t^* estimates for key regions; (3) the (necessarily indirect) inference of amplitude variations from inferred attenuation differences is not well supported by empirical observation; and (4) synthetic seismograms incorporating proposed regional differences fail to match important characteristics of observed data.

The objective of this study is to determine a Q model consistent with time and frequency domain observations of P waves from nuclear explosions at the major test sites. The Q effect can then be accounted for and source differences determined. The technique is to analyse the spectra of very short time windows chosen to isolate the initial P wave pulse. Thus, we are estimating the attenuation that controls amplitudes used to measure quantities like m_b.

Data

The four 20-element UK arrays (Table 1) provide a uniform data base spanning almost the entire history of underground testing. Because of the array's small size and the instrument response (Fig. 1), the data are uniquely suited to high frequency spectral analysis. A large data base including recordings of Soviet, French (Sahara and Pacific) and US (including Amchitka) explosions has been collected and carefully vetted to delete channels that are clipped or otherwise faulty.

To estimate the P wave spectrum, each element of the array is processed separately. Energy density spectra are computed for very short (typically 2.2 to 2.7 seconds) time windows, and the power spectrum of a noise window just before the signal is subtracted. The final event spectrum is then computed by averaging these (corrected) energy density spectra over the array. As seen in the example in Fig. 2, these array spectra are much simpler than single sensor spectra, suggesting that

TABLE 1

United Kingdom Arrays

Station	Code	Location	Element Spacing (km)	Maximum Element Spacing (km)	Date Operational	Date of Digital Recording
Eskdalemuir Scotland	EKA	55°19'59"N 3°09'33"W	0.9	9.8	17 May 1962	14 Nov 1983
Yellowknife Canada	YKA	62°29'34"N 114°36'17"W	2.5	22.5	26 Nov 1962	-
Gauribidanur India	GBA	13°36'15"N 77°26'10"E	2.5	32.0	1 Feb 1966*	4 Mar 1979
Warramunga Australia	WRA	19°56'39"S 134°20'27"E	2.5	26.3	1 Mar 1966*	7 Jun 1977

much of the complexity of the latter is associated with near receiver effects. In Fig. 3 the spectra are plotted for GBA recordings of thirteen explosions in the southwest portion of the Shagan River test site. The variations are of the kind expected from differing depths of burial, source geology and prompt secondary source radiation due to tectonic release. Since these seem to be largely uncorrelated, the spectra from events in the same area are stacked to obtain for each station a smooth teleseismic P wave spectrum $|\mathbf{F}(\omega)|$ for events in that area. At any frequency f the source spectrum is proportional to f^{-n} and $\log |\mathbf{F}(\omega)| \approx -n \log f - 1.36\, t^* f$. The objective is then to simultaneously estimate n and t^*, recognizing that both may depend on frequency.

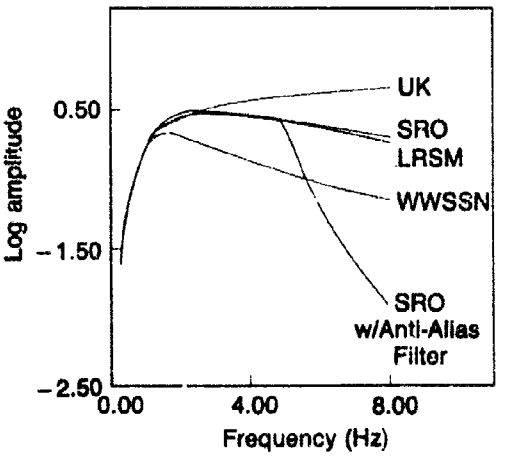

Fig. 1. The instrument amplitude response for the UK arrays is compared to the response for several other short period systems.

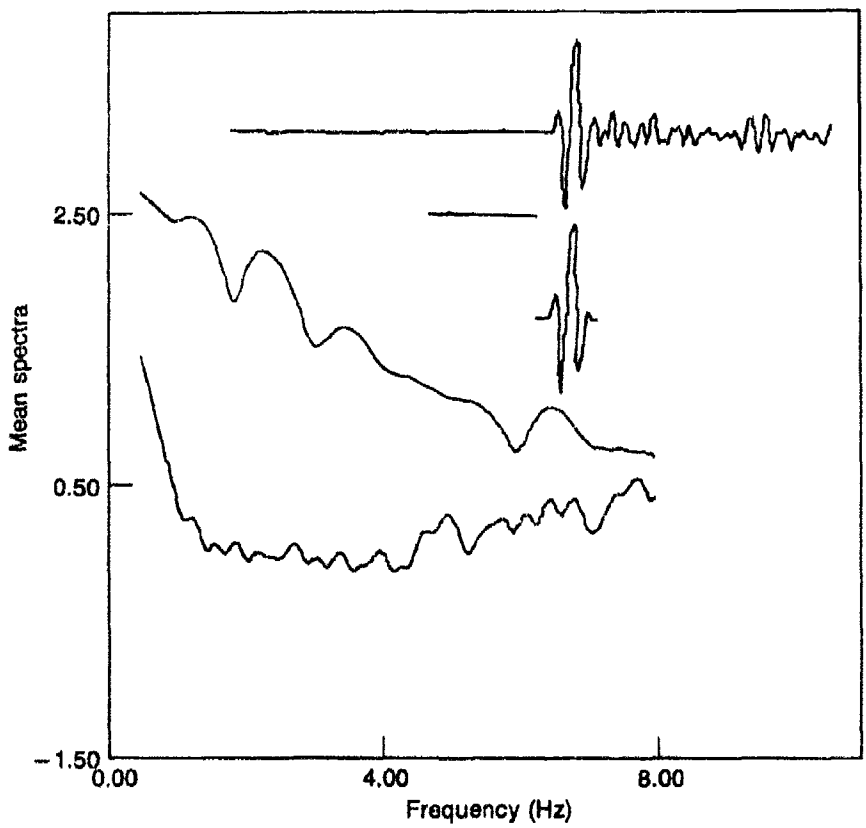

Fig. 2. The computed spectrum is plotted for the GBA recordings of the 27 December 1981 Shagan River explosion (ISC m_b = 6.2). Also shown is the spectrum computed from the average noise power for the twelve channels processed. Both have been multiplied by f^2 for frequencies (f) greater than 1 Hz, which approximately corrects the signal spectrum for the source. At the top is shown a typical channel and the signal and noise windows used for the calculation.

Attenuation from East Kazakh to UK Array Stations

The "stacked" spectrum for GBA recordings of southwest Shagan River events is plotted in Fig. 4. Above 2.5 Hz the spectrum is remarkably close to the straight line fit and the simplest interpretation is that the average source is indeed proportional to f^{-2} and t^* is independent of frequency. If there is frequency dependence, it is neatly cancelled by source spectrum effects averaged over many events. Below 2.5 Hz there is a distinct change of slope which must be due to frequency-dependence of Q.

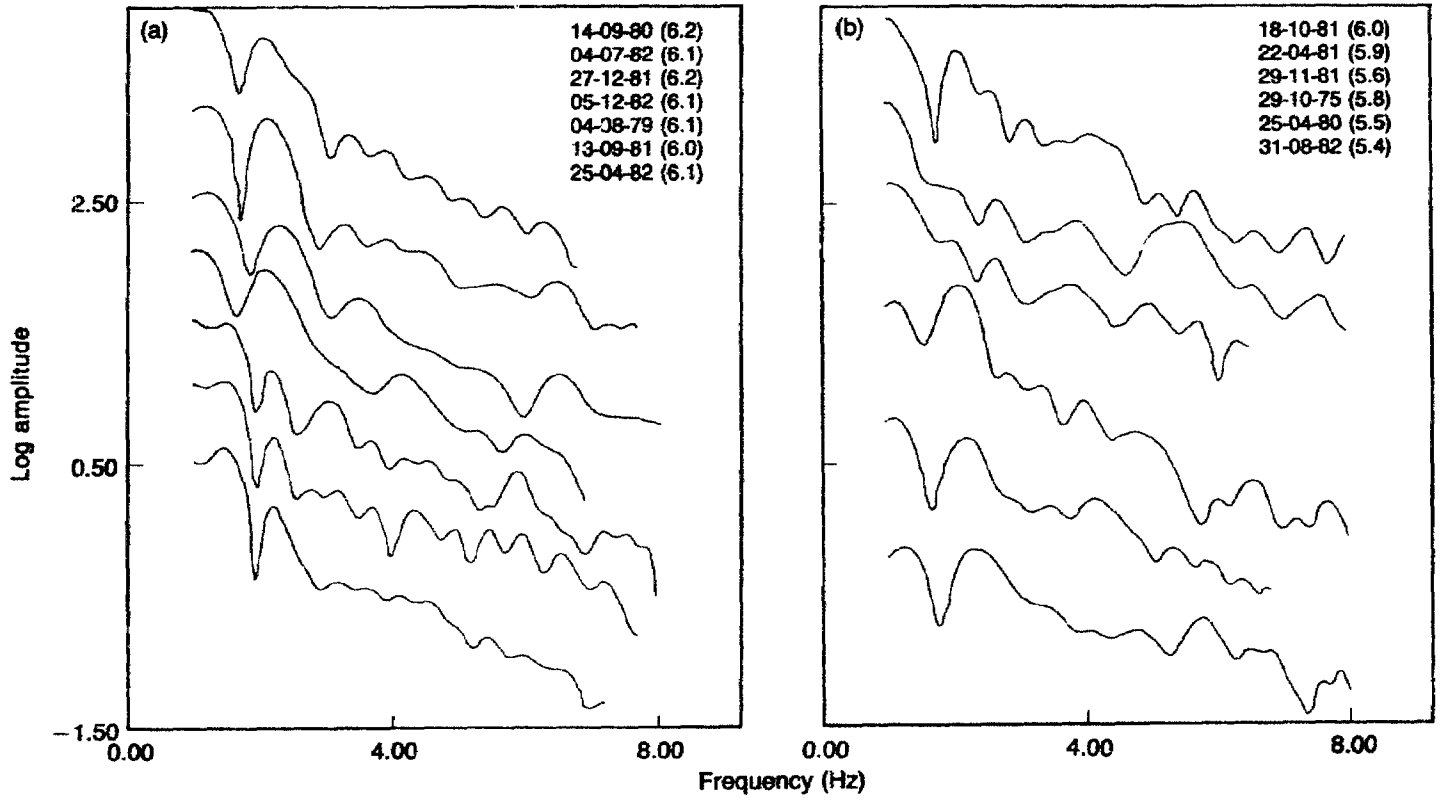

Fig. 3(a),(b). The spectra are plotted for thirteen events (listed with their ISC m_b) in the southwest portion of the Shagan River test site. Each has been multiplied by f^2. The amplitude scale is arbitrary since the spectra have been shifted for convenient display.

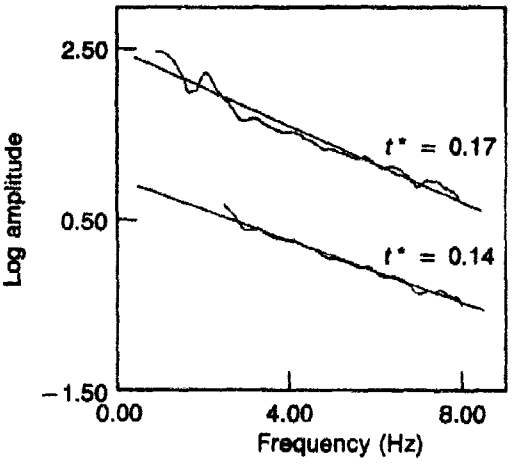

Fig. 4. The stacked spectrum derived from the event spectra in Fig. 3 is plotted over the 1.0 – 8.0 and 2.5 – 8.0 Hz bands. A least squares linear fit and the t^* derived from the slope of that line are shown.

Details of the source spectrum have a strong influence on the spectrum below 2.5 Hz. This is seen in Fig. 5 where composite spectra are plotted for all four UK arrays. Except for YKA where the data are sparse because the clipping threshold is about m_b 5.5, the East Kazakh events are divided into three populations. The bisection of the Shagan River site is along a line trending 45° west of north and is based on consistent waveform differences that distinguish events on either side of the line.

The three populations of events are characterised by differences that are consistent from station-to-station, and are best explained by attributing them to systematic differences in the source corner frequency. That is, it appears that the assumption of an f^{-2} source is reasonable above 1 Hz for the SW Shagan events, but that the corner frequency is almost certainly greater than 1 Hz for the Degelen events, with the NE Shagan events intermediate between the two. The SALMON spectrum is included as an extreme example of a high corner frequency event (the yield is about 5 kt). Certainly we expect the Degelen events to have higher corner frequencies due to differences in yield. The differences between the mean m_b for the SW Shagan and Degelen populations is 0.64 at GBA, 0.54 at WRA, and 0.43 at EKA. In the simplest interpretation, assuming yield proportional to m_b and corner frequency to cube-root of yield, this translates to a corner frequency shift of 40-60% (evidence of a yield related corner frequency shift is also seen in the event spectra in Fig. 3). But there must also be some source material property contribution to the corner frequency shift. This is seen in several ways. First, for YKA the Degelen population actually has a larger average m_b than the Shagan population, yet a perceptible difference still remains. More interesting,

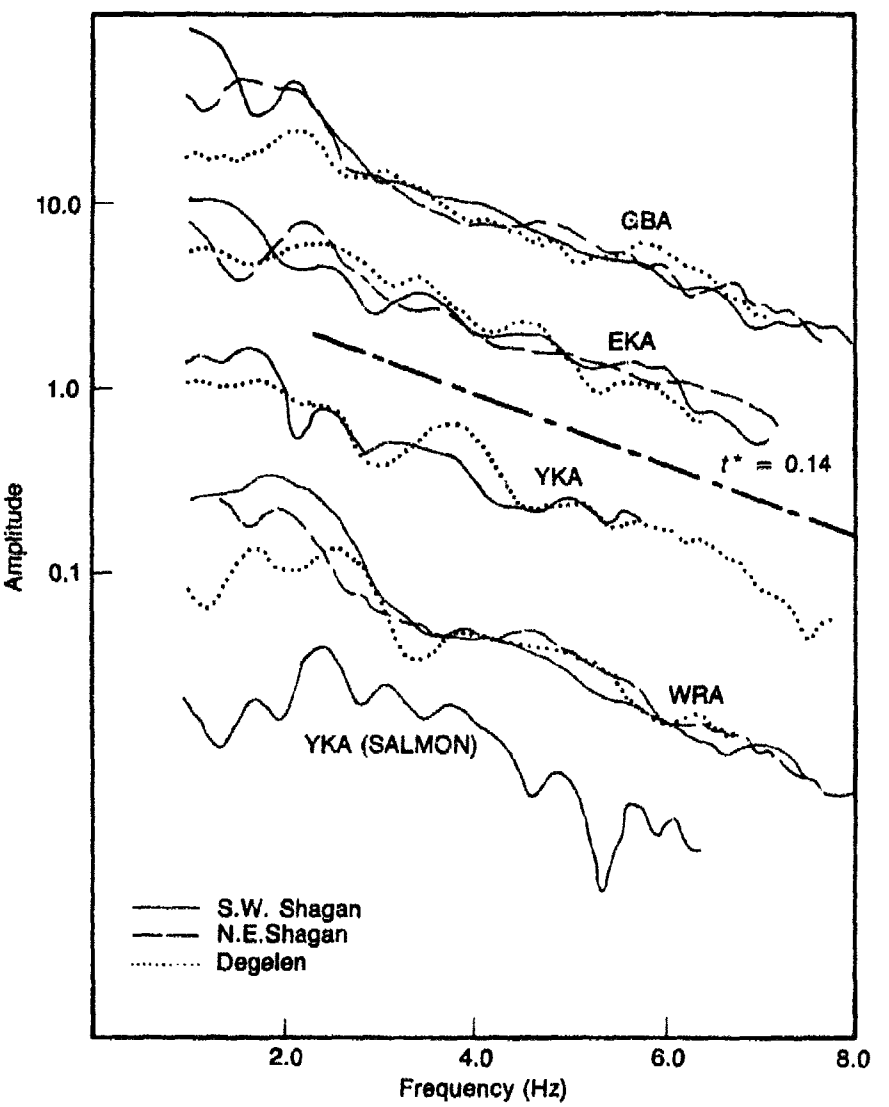

Fig. 5. The stacked spectra are shown for E Kazakh explosions recorded at the UK arrays. The total number of events spectra included are 36 at GBA, 38 at EKA, 16 at YKA and 28 at WRA. The events are divided into three populations, except at YKA where unclipped data were available for only five Shagan River events. At each station the stacked spectra were superimposed so that the least squares linear fit in the 2.5 – 8.0 Hz band passes through the same value at 5 Hz. Also shown is the spectrum for SALMON at YKA and a line with slope corresponding to $t^* = 0.14$.

the difference between NE and SW Shagan River events is best explained by the latter having a lower corner frequency since the difference persists even when the event populations have the same mean m_b.

Above 2.5 Hz all the spectra for East Kazakh events are fit very well by a frequency-independent t^* of 0.14 seconds. This is seen in Fig. 5 and is confirmed by computing the best (least squares) fitting lines to these spectra. The small differences that do occur are well within the range expected for minor deviations of the average source from the assumed f^{-2} behaviour. Of course, the average source could have a steeper falloff, and this would lead to a lower t^* estimate. It is also interesting to note that there appear to be no significant differences in the attenuation (for $f > 2.5$ Hz) for these four travel paths.

Over the whole band the spectra are best modelled with an absorption band Q (Liu *et al.*, 1976; Minster, 1978) that includes two bands, one to fit the decreasing t^* between 1 and 2.5 hz, and a second that keeps the apparent t^* nearly constant from 2.5 to 8.0 Hz. To minimize contamination by source effects at the low frequency end, we fit only the lowest corner frequency events, which are large m_b explosions at SW Shagan River. We also need some constraint at long periods. Most long period t^* estimates are near 1 second (*e.g.*, Anderson and Given, 1982), but are based on global or broad regional averages, so smaller values are likely for paths like these. Values like 0.5 or 0.6 seconds seem reasonable, but this remains a subject for investigation.

In Fig. 6 a double absorption band model is fit to the best estimate for the GBA spectrum. Three models are shown to illustrate the tradeoffs among the controlling parameters. The best is Model 2, which has a long period t^* of 0.6 seconds and a τ_M of 0.05 seconds. Models 1 and 3 indicate the sensitivity to t_0^* and τ_M. Other models fitting as well as model 2 must have $t_0^* < 0.6$ and $\tau_M < 0.05$ or $t_0^* > 0.6$ and $\tau_M > 0.05$. If we impose the reasonable constraint that $0.5 < t_0^* < 1.0$, then an estimate for the bounds is $0.04 < \tau_M < 0.08$. The second (lower t^*) absorption band is relatively well constrained to have an almost frequency-independent Q that gives a t^* of about 0.1 seconds, so the spectrum has a nearly constant slope over the 2.5 to 8.0 Hz band.

Similar double absorption band models can be fit to WRA and EKA spectra for large m_b events in the SW Shagan River Area, and several examples are shown in Fig. 7. The WRA spectrum is unusual in the way it decreases below 2 Hz. This may be a pP effect that is especially strong for this particular set of events (the three 5-event populations differ; there are no events in common between GBA and EKA and only two in common for GBA-WRA and EKA-WRA). Assuming this to be the case, there appears to be no significant difference in the attenuation along the paths

to GBA and WRA. Comparison of stacked spectra for sets of common events also indicates no difference. On the other hand, for EKA the effects of frequency-dependent Q appear to be less than for GBA and WRA over the frequency band plotted, suggesting a larger τ_M. If t_0^* is fixed

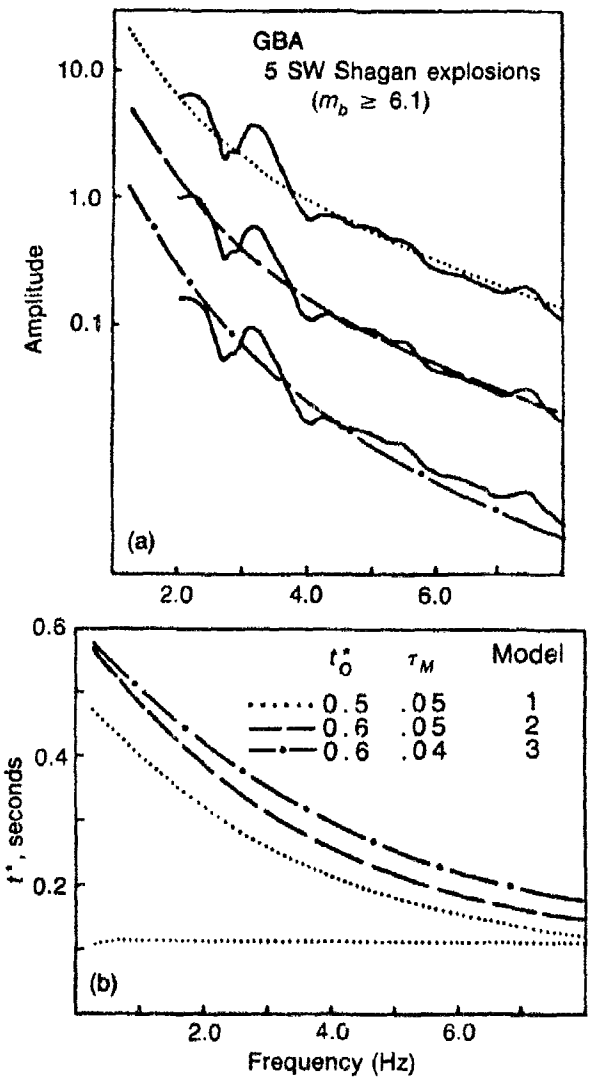

Fig. 6. (a) The GBA stacked spectrum for large SW Shagan explosions is fit with several double absorption band Q models. (b) The models are shown with the key parameters listed. The t_0^* is the t^* in the flat part of the upper band and τ_M is the short period half amplitude point. All three models have a second absorption band with t^* essentially constant at 0.11 seconds over the range plotted.

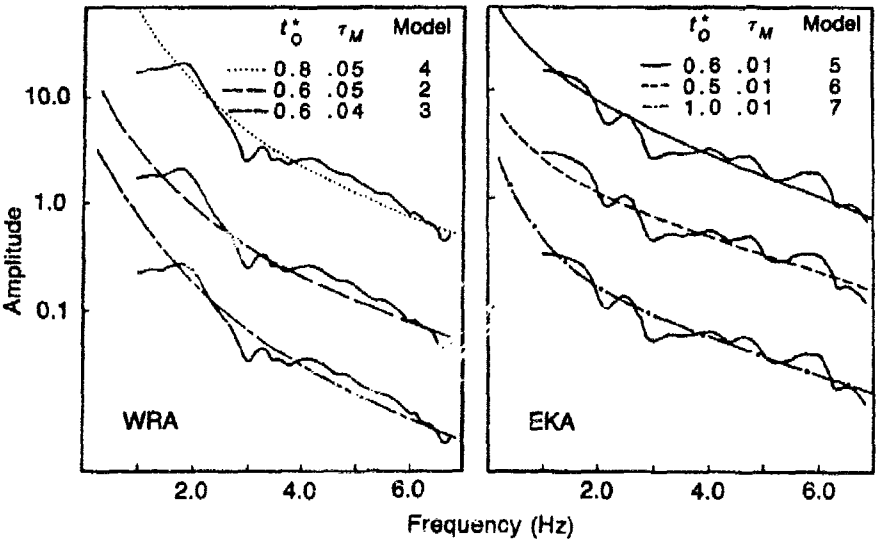

Fig. 7. WRA and EKA stacked spectra for five large ($m_b > 6.0$) SW Shagan explosions are fit with double absorption band Q models. The models are similar to those in Fig. 6 and the key parameters are listed. The second (lower t^*) absorption band is the same as in Fig. 6 except Model 5 for which this band has a somewhat larger (0.14 sec) constant t^* level.

at 0.6 sec, the best τ_M is about 0.1 sec. The large event data are not available for a similar analysis of the path to YKA, but comparing spectra for Degelen events (Fig. 5), it can be seen that the attenuation on the YKA path is at least as strong as on the GBA and WRA paths, and there is some indication that the frequency dependence is greater at low frequencies. This suggests τ_M slightly less or t_0^* slightly more than for the GBA and WRA paths, but the differences are small.

The interpretation of the two absorption bands is that one represents mainly intrinsic attenuation, and the other is mainly due to scattering (thus it is not really an "absorption band"). Richards and Menke (1983) point out that scattering due to many weak inhomogeneities has the effect of a frequency-independent Q, just like the lower t^* part of the model. Since some scattering will always occur, there must be a minimum level for the total t^*, and perhaps the t^* of 0.1 seconds for the lower band is near that minimum. Where scattering is the predominant mechanism, we expect the coda to contain relatively more high frequency energy than the initial pulse. Comparison of our short time window spectra with spectra computed for windows including some of the P coda (Fig. 8) shows that this is indeed the case. Thus, the lower t^* must be due almost entirely to scattering. The mechanism for the attenuation represented by the larger

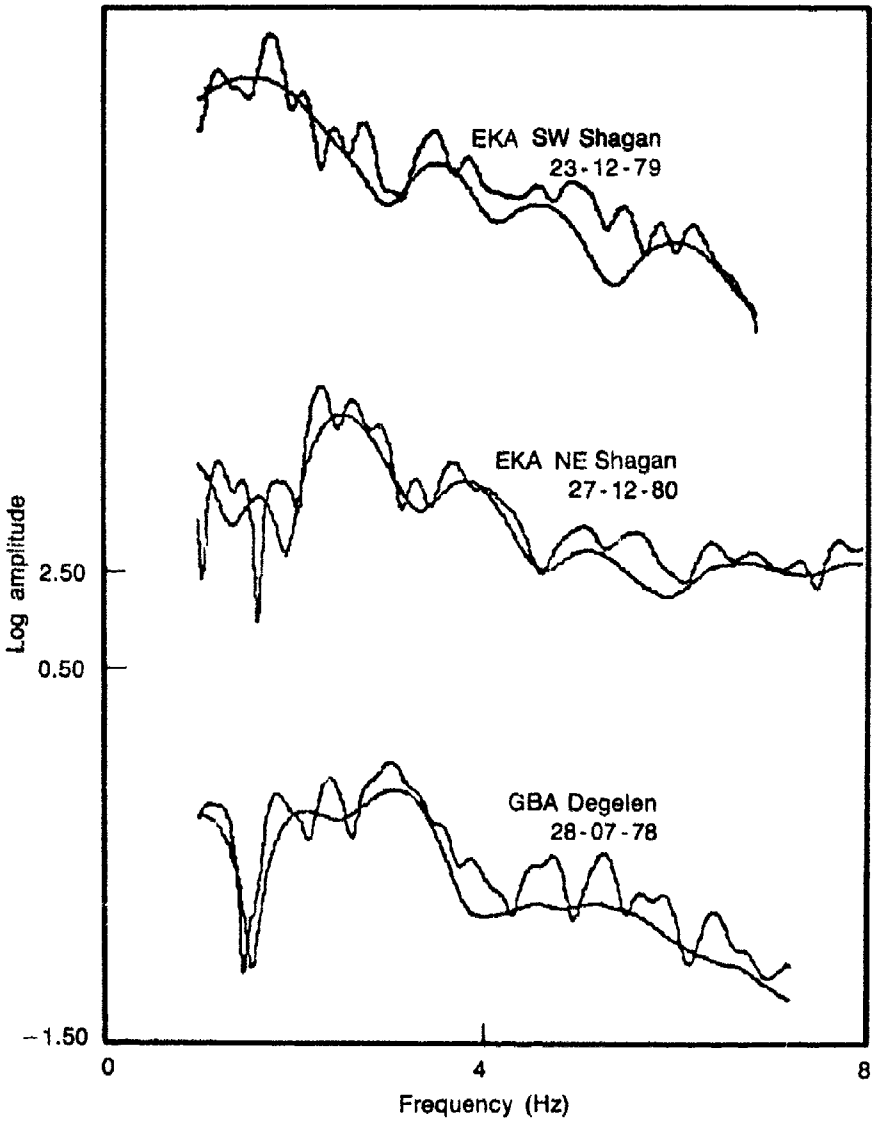

Fig. 8. Several comparisons are made between event spectra computed for different time windows. In each case the window length is 5 seconds for the less-smooth of the two. The short window length is 2.4 seconds for the middle comparison and 2.2 seconds for the others.

t^* absorption band remains a subject for speculation, but the effect seems to be intrinsic absorption. Our conclusion that τ_M is 0.05 to 0.1 seconds for this band is consistent with earlier work to define the frequency dependence of t^* near 1 Hz. For example, Der *et al.*, (1982) suggest $\tau_M = 0.08$ sec for shield-to-shield paths.

Excellent recordings of *PcP* are obtained at GBA for large East Kazakh explosions, and these can be used to further define the Q model. The results are shown in Fig. 9. Differences in the attenuation for P and *PcP* are difficult to resolve, but if there is a difference, it is toward somewhat greater attenuation of *PcP*. This means slightly lower τ_M or greater t_o^*. A model between those in the figure (*e.g.*, $t_o^* = 0.7$, $\tau_M = .05$) provides a good fit.

In summary, our preferred t^* is given by Model 2 (Fig. 6) for GBA and WRA, slightly lower t^* for EKA and slightly higher t^* for YKA, while the GBA *PcP* seems to be somewhat more attenuated than any of the P waves. These five ray paths are spaced to sample the mantle quite evenly, as seen in Fig. 10. Thus, the t^* can be inverted for a Q model. However, the preferred values cannot be fit by a smooth azimuthally symmetric model; differences between stations must be due to azimuthal effects. But to see the kind of Q model implied by these t^*, we can assume

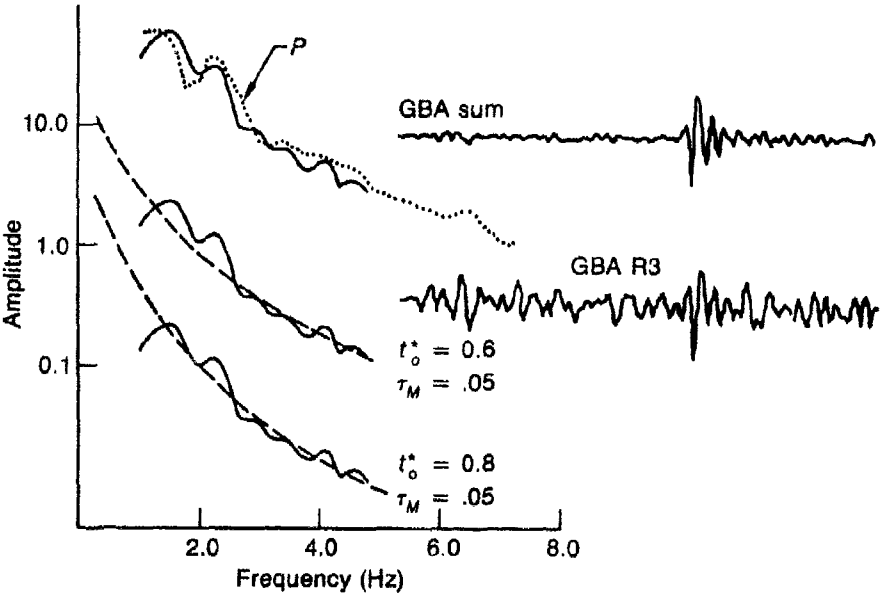

Fig. 9. The stacked spectra for GBA recordings of P_cP for 5 large SW Shagan River events is compared to the P spectrum (Fig. 6) for the same events and is fit with two double absorption band Q models. At the right is shown a typical single channel and beam sum P_cP recording.

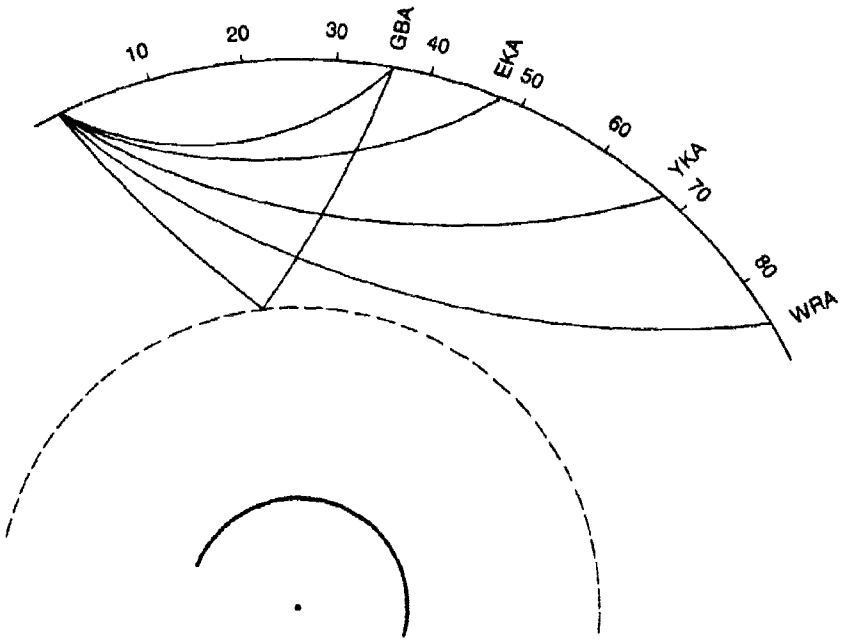

Fig. 10. The ray paths for the UK array stations are plotted for a Jeffreys-Bullen earth model. The plot is drawn to scale and the depth to the outer core is 2890 km. The source-station azimuths (measured clockwise) are 6° for YKA, 129° for WRA, 182° for GBA and 309° for EKA.

the Model 2 also represents the EKA and YKA paths. This would be entirely appropriate if the differences are caused by the receiver half of the patch, and the Q model would then represent Central Asia.

The Q model from the inversion is plotted in Fig. 11 for 1 and 5 Hz and is compared to the Q at 1 Hz from the Anderson and Given (1982) model which is based on worldwide average data over the entire band from normal mode periods to 1 Hz. Our Q model at 1 Hz is essentially the same as this model. The only significant difference is near the core-mantle boundary, but this depends entirely on our PcP t^* which is not very well constrained. Also shown in the figure is the model resulting from assuming $t^* = 0.14$ sec for the four P waves and 0.19 sec for GBA PcP. This t^* is a good fit to the data above 2.5 Hz (Figs 5 and 9) if a frequency-independent Q is assumed. This shows that large errors in Q result if frequency dependence is present, but not included in the model.

Synthetic Seismograms

It is one thing to show that the spectra of East Kazakh explosions are consistent with a Q model like that in Fig. 11. It is quite another

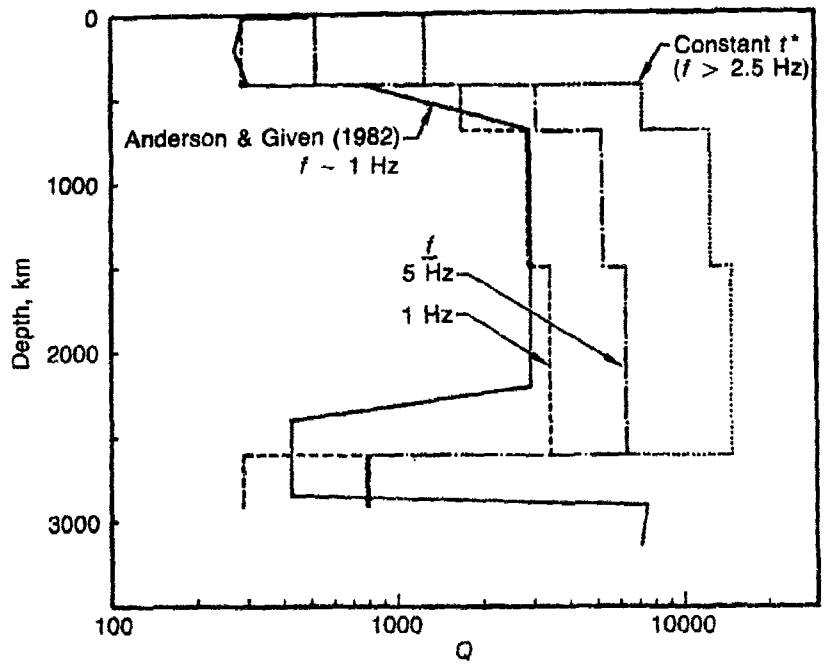

Fig. 11. A Q model for central Asia derived from UK array observations of E Kazakh explosions is plotted for 1 and 5 Hz. Also shown is a Q model derived by assuming a frequency-independent t^* and using the value that best fits the spectral falloff for $f > 2.5$ Hz.

to fit this into a complete model for P-wave signals from explosions, for this requires consideration of the phase spectrum of the Q and source, as well as proper representation of the pP phase. Computing synthetic seismograms with currently available models, we can see that some important issues remain unsolved.

In Fig. 12 typical single sensor GBA recordings of two large SW Shagan River explosions are compared to several synthetic seismograms. The synthetic seismograms were computed with a program based on Douglas *et al.*, (1972) and include reasonable models for the crystal structure at the source and receiver and the Carpenter (1966) geometric spreading factor. The Mueller and Murphy (1971) source model was used and the yield was fixed at 150 kt. The first synthetic seismogram is for a frequency independent t^* of 0.2 seconds and the source depth (corresponding to a $P-pP$ lag time of 0.44 sec) was chosen so the period T_c (twice the first trough to second peak time) would be about the same as observed. At first glance, the waveform comparison may not seem too bad, but there are some important discrepancies. In particular, the

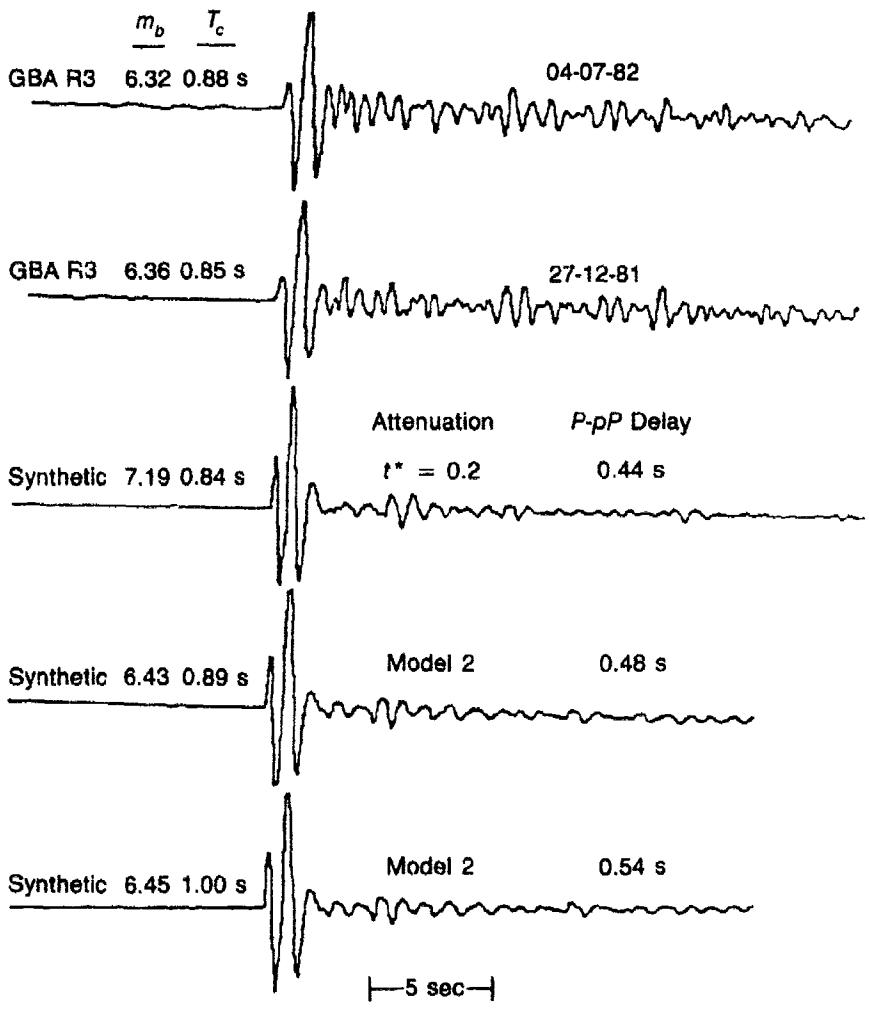

Fig. 12. Single sensor recordings of two typical SW Shagan River explosions are compared to several synthetic seismograms. For the observations the m_b is for this element; the PDE m_b are 6.1 (04-07-82) and 6.2. The T_c is twice the first trough to second peak and is used to calculate the m_b. The key parameters for the synthetics are the attenuation model and P-pP delay time, and these are indicated.

onset is too abrupt, the first peak is too large and the T_b period (twice the first trough to first peak time) is about 0.2 seconds too small. Further, looking back at Fig. 3, we see a robust spectral hole at frequencies no larger than 2.0 Hz for the $m_b > 6.0$ events, suggesting $P-pP$ lag times of 0.5 - 0.6 sec for these events. But the most significant discrepancy is in the m_b, for the amplitude of the synthetic seismogram is nearly

an order of magnitude too large. This discrepancy, in itself, is a strong indication that there must be rapid shift to greater attenuation in the 1 - 2 Hz band which controls the amplitude.

Our preferred model for attenuation along the GBA East Kazakh path is Model 2 in Fig. 6, and the other two synthetics were computed with it (the Doornbos, 1983, formulation was used for the computations). The first has T_b and T_c periods very near those observed and an m_b that is also in reasonable agreement.

However, the P--pP lag time is too short to be consistent with the major spectral hole, and the final synthetic was computed with a $P-pP$ lag time consistent with the spectral evidence. These synthetics clearly represent a step in the right direction, and the major discrepancies are what we should expect. The most obvious is the shape and relative amplitude of the first peak, which is sensitive to the high frequency portion of the Q model. But we have concluded that scattering is the dominant attenuation mechanism at high frequencies, and expect an absorption band model derived from the amplitude spectrum to under predict the dispersion and pulse-broadening associated with scattering (Richards and Menke, 1983). Thus, a correct representation of the phase spectrum for a Q due to scattering will clearly change the appearance of the first peak toward that seen in the observed seismograms.

The second major problem with the synthetics is that elastic theory is used to compute pP, and there is ample evidence from previous work (*e.g.*, Bache, 1982) and from these data to conclude that this cannot be correct. Synthetic and observed amplitude spectra are compared in Fig. 13. The first trough in the observed spectra can reasonably be assumed to be due to $P-pP$ interference, but there is no more than a hint of higher frequency peaks. This is about what one should expect for a pP reflection coefficient that is smaller than the elastic and strongly dependent on frequency. The next generation of synthetic seismograms must include such a coefficient along with the proper phase spectrum for a Q due to scattering, and is expected to closely resemble the observations in all important respects. These improvements may change the m_b of the synthetics by several tenths, so we must be cautious about interpreting the attenuation effect on m_b until they are included.

SALMON and the Amchitka Events

The one available spectrum (YKA) for the SALMON event ($\sim$ 5 kt in a Mississippi salt dome; $m_b \sim 4.5$) was plotted in Fig. 5 as an example of an event for which the corner frequency must be over 1 Hz. This means that we cannot infer much at t^* below 3 -4 Hz without correcting for the source, with all the uncertainty that entails. However, comparison

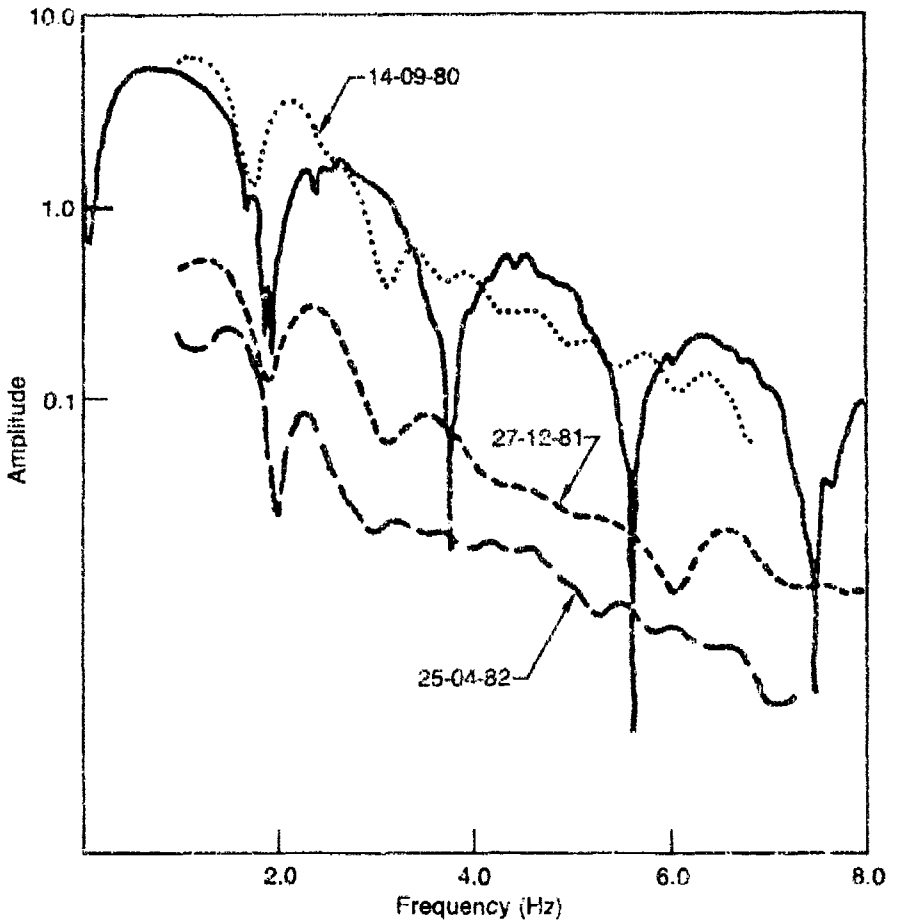

Fig. 13. The amplitude spectrum of the synthetic seismogram computed with attenuation Model 2 and a P–pP delay of 0.54 seconds is compared to the GBA spectra for three typical SW Shagan events.

with YKA spectra from the smallest East Kazakh events is enlightening (Fig. 14). At high frequencies (> 3 Hz) there is not much difference, though it appears that the SALMON spectrum falls off slightly more rapidly. The low frequency behavior is consistent with the expectation that SALMON has a higher corner frequency.

The available spectra for the Amchitka events are plotted in Fig. 15. Array spectra are only available for LONGSHOT. At EKA this suggests strong frequency-dependence of attenuation, but the effect is not seen in the single element spectra for the other events. The CANNIKIN spectrum decays faster, but for this huge event ($\simeq$ 5000 kt), we should be

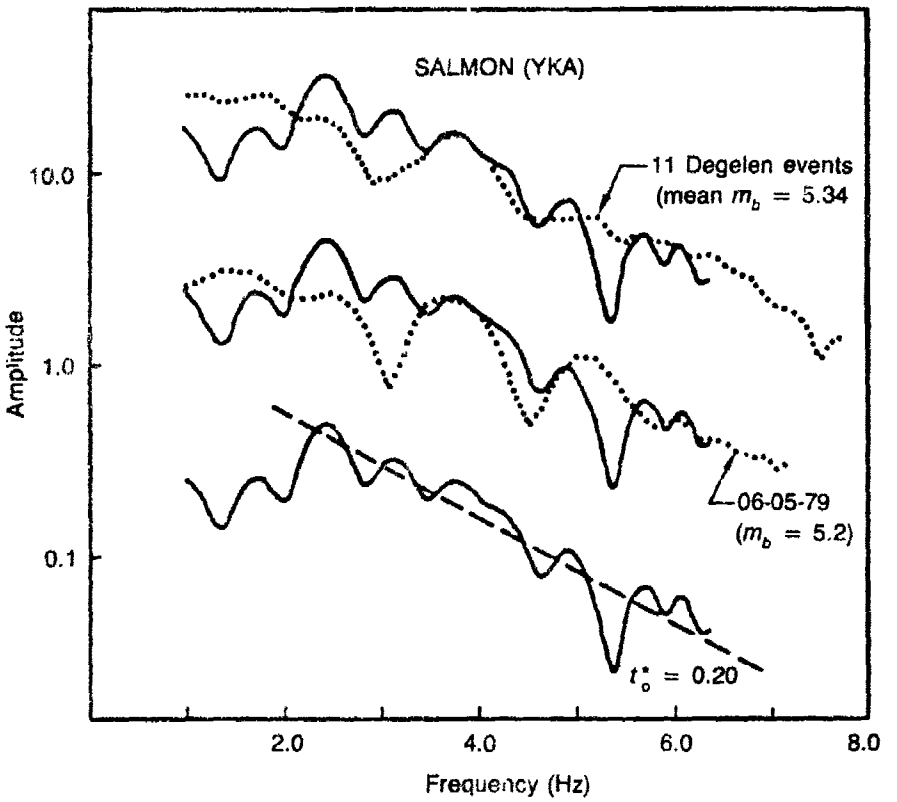

Fig. 14. The YKA SALMON spectrum is compared to the YKA stacked Degelen spectrum from Fig. 5 and the spectrum for one of the smallest Degelen events. At the bottom it is shown with a line corresponding to a frequency-independent t^* of 0.2 seconds.

so far beyond the corner frequency that the source decay may be more rapid. At YKA and EKA the attenuation above 2 Hz seems little different than for SALMON (or the East Kazakh events). The similarity to the East Kazakh paths is also seen in comparing long and short window spectra; the results for LONGSHOT at YKA and EKA look much like Fig. 8. At WRA the spectral decay is greater and long and short window spectra plot together over the whole band; thus, there seems to be more intrinsic attenuation on this path.

Developing a more quantitative model for the Q for $f < 2$ Hz, the band of importance for m_b, will require correction for the source. Analysis of the spectral nulls in Fig. 15 shows some of the difficulties that must be faced in doing so. The first null is at frequencies corresponding to a $P-pP$ lag time of 0.55 sec for LONGSHOT and 0.85 sec for

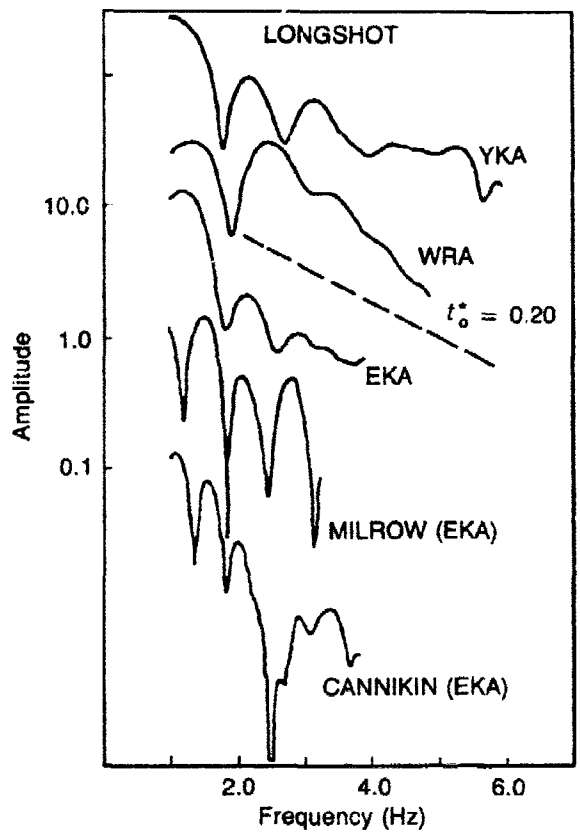

Fig. 15. The available spectra are plotted for the Amchitka events.

MILROW, values consistent with previous work (*e.g.* King *et al.*, 1974). The first CANNIKIN null corresponds to 0.75 sec, much too early to be *pP*. But there are actually several nulls at regular intervals and these appear to be multiples of 0.9 Hz for LONGSHOT, 0.6 Hz for MILROW and 0.6 Hz for CANNIKIN. These suggest lag times (1.1 sec and 1.6 sec) that cannot be right for *pP*. Thus, it appears that a phase later than *pP* (spall slapdown?) is an important contributor to the spectrum for these events and interpretation is that much more difficult.

French Sahara Events

The well-determined spectra for French tests in the Sahara are plotted in Fig. 16. The best data are from EKA and they show a consistent pattern, assuming that SAPHIR (~ 120 kt) is the largest corner frequency event. The preferred model for East Kazakh-GBA fits these data rather

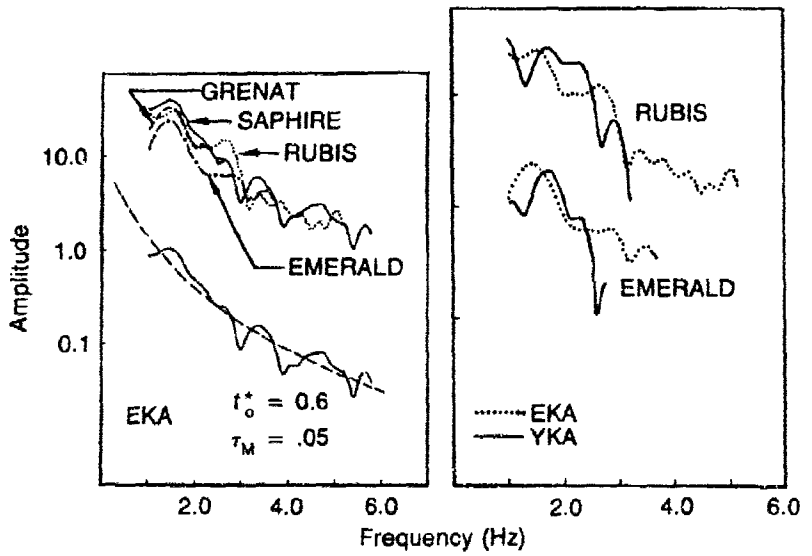

Fig. 16. The spectra for French Sahara explosions are plotted and the EKA SAPHIR spectrum is fit with Model 2 from Fig. 6.

well, so one can only argue that attenuation on the French Sahara-EKA path is greater than from East Kazakh by assuming that the SAPHIR spectrum is contaminated by some source effect (*e.g.*, the corner frequency may be greater than for the SW Shagan events). However, an indication that the attenuation is different than on the East Kazakh-GBA path is that short time window SAPHIR spectra have more high frequency energy than long time window spectra. Thus, the attenuation has apparently not reached the level where scattering predominates.

There is strong evidence that there is greater attenuation on the French Sahara-YKA path, though it is troublesome to note the large differences in the low frequency character of the spectra for the same event at these two stations. Again, as for SALMON and the Amchitka events, a quantitative estimate for the attenuation will require a confident correction for the source.

Conclusions

The key conclusion is that the effect of regional attenuation variations on magnitude is not represented very well by differences in the frequency— independent t^* that fit explosion P wave spectra in the 0.5 to 3.0 Hz band. Source spectrum variations can have a large biasing effect, and there must be frequency dependence in this band. These contributions are potentially resolvable with the smooth spectral estimates

we have computed from the UK array data, together with spectrum and waveform modelling using absorption-band models for Q.

A detailed understanding of the attenuation along the paths from the East Kazakh test site to the UK arrays is emerging. Comparing spectra from different events, we can see the effects of varying source corner frequency due to yield and, apparently, varying source material properties. Thus, we can select events where the source effect is minimized, and so isolate the effect of attenuation. We find that we are able to separate intrinsic attenuation, which is strongly dependent on frequency, from attenuation due to scattering, which is not. The two kinds of Q imply different dispersion, but both must be properly represented in synthetic seismograms to clarify the relationship of attenuation to m_b in this situation. It will also be necessary to include the pP phase, and we can see that a reflection is required. But the tools to handle these Q and pP effects are available, and there is reason for optimism about the prospects to explain in detail the P wave signals from East Kazakh explosions.

We have the data to apply the same techniques to explosions from other areas. Here we have shown only the spectra for a few sites for which the data are sparse and interpretation difficult. The major point is again that it is necessary to accurately account for the source to understand the effect of attenuation. For SALMON and two of the three teleseismic paths from Amchitka there is no obvious evidence for significant attenuation differences with respect to East Kazakh; for one path (Amchitka to WRA) the attenuation is clearly greater. For French Sahara events a similar mixed picture emerges, with some indications of greater attenuation, but other evidence that it is not much different than for East Kazakh.

The next step is to study spectra for NTS events, which are numerous enough that we can hope to separate source and attenuation effects. Certainly the NTS spectra appear to be quite different on initial review. Perhaps the insight gained in interpreting them will also help fit the Amchitka and French Sahara spectra into a coherent picture of regional attenuation variations and their effect on body wave magnitude.

References

Anderson, D.L. and J.W. Given (1982). "Absorption Band Q Model for the Earth," *J. Geophy Res.*, **81**, 3893-3904.

Bache, T.C. (1982). "Estimating the Yield of Underground Nuclear Explosions," *Bull. Seism. Soc. Am.*, **72**, 5131-5168.

Carpenter, E.W. (1966). "A Quantitative Evaluation of Teleseismic Explosion Records," *Proc R Soc Lond A*, **290**, 396-407.

Der, Z.A., T.W. McElfresh, and A. O'Donnell (1982). "An Investigation of the Regional Variations and Frequency Dependence of Anelastic Attenuation in the United States in the 0.5-4.0 Hz Band," *Geophys. J. R. Astr. Soc.*, **69** 67-99.

Douglas A., J.A. Hudson, and C. Blamey (1982). "A Quantitative Evaluation of Seismic Signals at Teleseismic Distances - III. Computed *P* and Rayleigh-Wave Seismograms," *Geophys. J*, **28**, 385-410.

Doornbos, D.J. (1983). "Observable Effects of the Seismic Absorption Band in the Earth," *Geophys. J. R. Astr. Soc.*, **75**, 693-711.

King, C.Y., A.M. Abo-Zena (1974). "Teleseismic Source Parameters of the LONGSHOT, MILROW and CANNIKIN Nuclear Explosions," *J. Geophys. Res.*, **79**, 712-718.

Liu, H.R. D.L. Anderson, and H.K. Kanamori (1976). "Velocity Dispersion Due to Anelasticity: Implications for Seismology and Mantle Composition," *Geophys. J.R. Astr. Soc.*, **47**, 41-58.

Minster, J.B. (1978). "Transient and Impulse Responses of a One-Dimensional Linearity Attenuating Medium - II. A Parametric Study," *Geophys. J.R. Astr. Soc*, **52**, 503-524.

Mueller, R.A. and J.R. Murphy (1971). "Seismic Characteristics of Underground Nuclear Detonations," *Bull. Seism. Soc. Am.*, **65**, 1675-1692.

Richards, P.G. and W. Menke (1983). "The Apparent Attenuation of a Scattering Medium," *Bull. Seism. Soc. Am.*, **73**, 1005-1021.

Investigation of Q and Backscattering in Codas

Anton M. Dainty

Summary

The coda of two earthquakes in the Mammoth Lakes, California, region have been analyzed to determine Q and the backscattering turbidity for the purpose of determining the effect of scattering on attenuation.

The backscattering turbidity and the Q are not consistent with each other at low frequencies if single scattering is assumed to be occurring. The backscattering turbidity implies that the Q should be lower than it is. This potentially casts doubt on the use of parameters derived from the coda. Further research should be undertaken to determine whether this situation occurs in other regions, and what the cause is.

Introduction

There are (at least) two causes for the observed phenomenon of the attenuation of body wave pulses in the earth, usually parameterized as Q: imperfect elasticity leading to the conversion of seismic energy to heat, and scattering of energy out of the pulse by heterogeneity. In this paper the codas of two earthquakes that occurred near Mammoth Lakes, California, on May 26, 1980, at 19:01 and May 29, 1980, at 7:52 (Archuleta *et al.*, 1982; Fig. 1) are analyzed to obtain estimates of Q, describing total attenuation, and the backscattering turbidity, or backscattering cross-section per unit volume, partially describing scattering. From the backscattering turbidity, an estimate may be made of the intensity of scattering to try and determine the relative contribution of scattering and imperfect elasticity to Q.

Theory and Analysis Methods

The coda of local earthquakes consists of a train of waves arriving after the body wave and surface wave phases have passed. Aki (1980) has presented a theory of the coda as singly backscattered S waves. According to this theory, the power spectrum of the coda between t and $t+\Delta t$ after origin time is

$$P_c(\omega,t) = At^{-2} \exp[-\omega t/Q] \qquad (1)$$

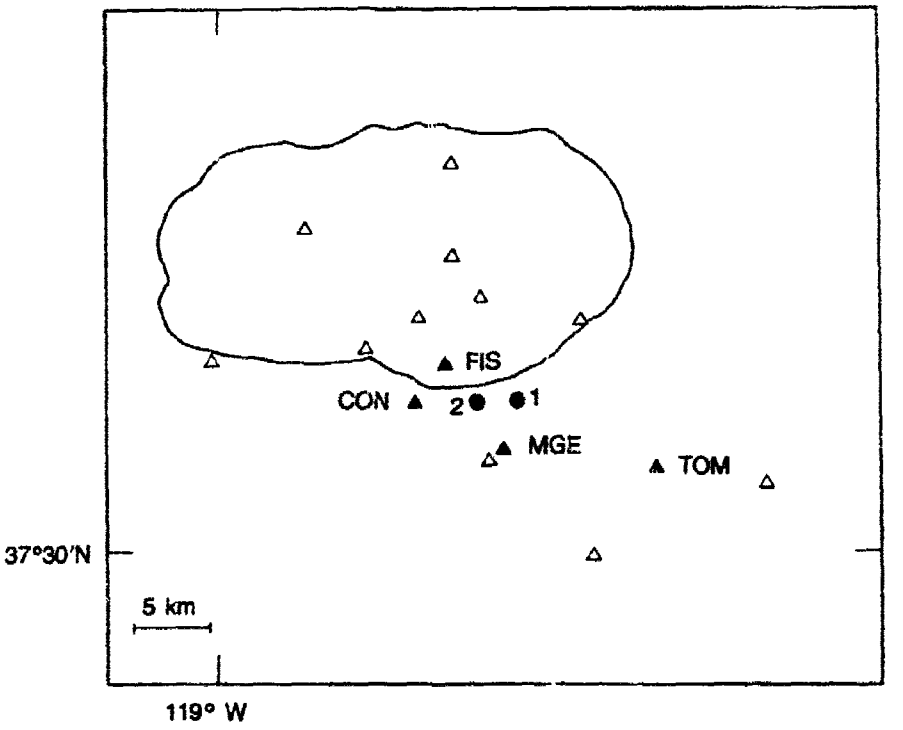

Fig. 1. Recording stations (triangles) and epicenters (circles) at Mammoth Lakes, California. Closed triangle - stations used in this study. 1 - event at 148:19:01. 2 - event at 151:07:52.

where

$$A(\omega) = P_s(\omega)\ exp\ [\omega t_s/Q] \cdot 8\pi \cdot V \cdot g(\pi,\omega) \cdot t_s^2 \qquad (2)$$

$P_s(\omega)$ is the square of the magnitude of the Fourier transform of the S wave pulse, t_s is the S wave travel time, V is the S-wave velocity, and $g(\pi,\omega)$ is the backscattering turbidity. For the two earthquakes considered in this study, the parameters $A(\omega)$ and $Q(\omega)$ are determined by fitting Eqn. (1) to values of $P_c(\omega,t)$ calculated in a moving window 0.64 sec long and averaged over an octave. This is done for three vertical seismograms from each earthquake. $P_s(\omega)$ is determined as the average of the squared magnitude of the Fourier transform in the two nearest windows to the S wave arrival time. The backscattering turbidity $g(\pi,\omega)$ may then be calculated from (2) since t_s is known, assuming V = 3.2 km/sec.

To further analyze $Q(\omega)$, Dainty (1981) shows that for attenuation due to both imperfect elasticity and single scattering,

$$1/Q = 1/Q_i + g_t(\omega)\, V/\omega \tag{3}$$

Q_i is the intrinsic Q, representing the effect of imperfect elasticity, and $g_t(\omega)$ is the total turbidity, or total cross-section per unit volume. Since the total turbidity includes the combined effect of backscattering, sidescattering, and forward scattering, $g_t(\omega)$ must always be greater than $g(\pi,\omega)$. Typically, Q_i is relatively constant with frequency (Knopoff, 1964); Dainty (1981) suggests that $g_t(\omega)$ is relatively constant with frequency above 1 Hz (the geometrical scattering approximation). From (3)

$$g_t(\omega) = [\omega/V] \cdot [1/Q - 1/Q_i] \tag{4}$$

For purposes of comparison with $g(\pi,\omega)$, the apparent total turbidity has been calculated from

$$g_a(\omega) = [\omega/V] \cdot [1/Q] \tag{5}$$

Then

$$g_a(\omega) \geq g_t(\omega) \geq g(\pi,\omega) \tag{6}$$

The relationship between $g(\pi,\omega)$ and $g_t(\omega)$ depends on the nature of the scattering medium. For isotropic scattering,

$$g_t(\omega) = 4\pi\, g(\pi,\omega) \tag{7}$$

For high frequency scattering from an acoustic random medium with velocity fluctuations (Dainty, 1984):

$$g_t(\omega) = 56\pi g(\pi,\omega) \tag{8}$$

Note that both (7) and (8), as well as the results of Wu and Aki (1984) for a random elastic medium, indicate that $g(\pi,\omega)$ and $g_t(\omega)$ should have the same frequency dependence at high frequencies, *i.e.*, approximately independent of frequency.

Results and Discussion

Figure 2 shows the average values of $g_a(\omega)$ determined from (5) and $g(\pi,\omega)$ determined from (1) and (2). Note that $g(\pi,\omega)$ is approximately constant at high frequencies and has values roughly consistent with (8),

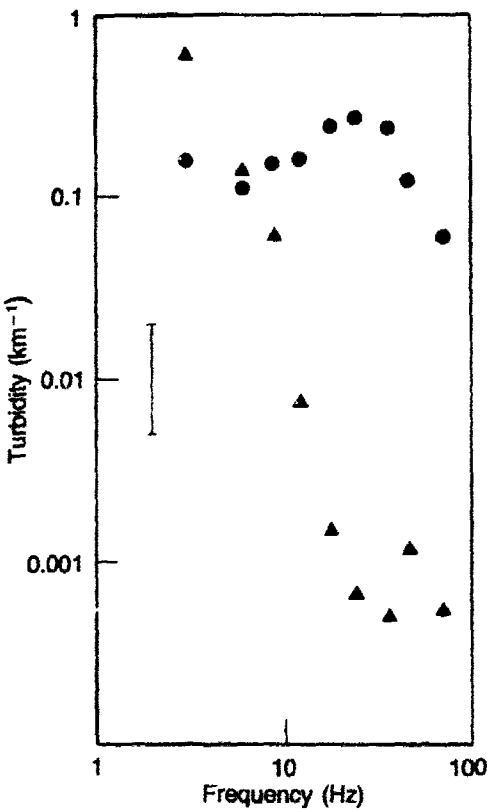

Fig. 2. Turbidity as a function of frequency, average results. Triangles - backscattering turbidity. Circles - apparent total turbidity. Error bar indicates a factor of two error, probably typical.

suggesting that high frequency scattering is occurring. At frequencies below 20 Hz, however, $g(\pi,\omega)$ increases by over two orders of magnitude as frequency decreases, until at 3 Hz $g(\pi,\omega)$ is actually larger than $g_a(\omega)$, which by (6) is theoretically impossible (Andrews, 1982). This discrepancy requires an explanation.

Several possibilities have been considered. The measurement of $P_s(\omega)$ and hence $g(\pi,\omega)$ may be incorrect if the window length is either too short or too long, as suggested by Aki (1980). However, the results presented here show the opposite effect to that seen by Aki, *i.e.*, $g(\pi,\omega)$ is high at low frequencies rather than high frequencies, as was the case in Aki's investigation. Further, it seems difficult to explain a frequency dependent effect that spans over two orders of magnitude by this mechanism. Another possibility is the Q in (3) is in fact mainly due to

Q_i, and not to scattering. In fact, $Q(\omega)$ for one of the events is quite constant with frequency between 5 and 30 Hz, as might be expected if this were true. In the context of single scattering theory, however, note that (4) and (5) indicate that $g_s(\omega)$ should be much larger than $g_i(\omega)$ if this were the case, and certainly larger than $g(\pi,\omega)$, in contradiction to the results presented here. Another possible explanation within the context of single scattering theory is that fluctuations of different material properties are primarily responsible for backscattering and total scattering, as suggested by Wu and Aki (1984). However, (6) must still hold, and it seemingly does not.

The result of attempting explanations which retain the concept of single scattering in the coda, such as those above, seems to be that single scattering cannot in fact be retained. It appears that for the two earthquakes examined here, we must conclude that multiple scattering is occurring in the coda. Under these conditions, Q will tend to Q_i, and not to the result given in (3) (Dainty and Toksoz, 1981); this may be important in investigations which rely on coda measurements of Q. In fact, the constancy of Q between 5 and 30 Hz mentioned above for one of the earthquakes suggests that Q_i is being measured. Obviously, the results presented here must be checked for other regions and other earthquakes.

References

1. Aki, K. (1980), "Scattering and Attenuation of Shear Waves in the Lithosphere," *Jour. Geophys. Res.*, **85**, 6496.
2. Andrews, D.J. (1982), "Shear Wave and Coda Attenuation of Two Aftershocks at Mammoth Lakes, California," *EOS*, **63**, 1029.
3. Archuleta, R.J., E. Cranswick, C. Mueller, and P. Spudich (1982), "Source Parameters of the 1980 Mammoth Lakes, California, Earthquake Sequence," *Jour. Geophys. Res.*, **87**, 4595.
4. Dainty, A.M. (1981), "A Scattering Model to Explain Seismic Q Observations in the Lithosphere Between 1 and 30 Hz," *Geophys. Res. Lett.*, **8**, 1126.
5. Dainty, A.M. (1984), "High Frequency Acoustic Backscattering and Seismic Attenuation," *Jour. Geophys. Res.*, **89**, 3172.
6. Dainty, A.M., and M.N. Toksoz (1981), "Seismic Codas on the Earth and the Moon: A Comparison," *Phys. Earth Planet. Int.*, **26**, 250.
7. Knopoff, L. (1964), "Q", *Rev. Geophys.*, **2**, 625.
8. Wu, R.S., and K. Aki (1984), "Scattering of Elastic Waves by a Random Medium and the Small Scale Inhomogeneities in the Lithosphere," *Jour. Geophys. Res.*, submitted.

Anelastic Behavior of Tuff

M. D. Denny

Summary

We have used Achenbach and Chao's (1962) 3-parameter model to study Larson's free-field particle motion data taken in small scale experiments on Mt. Helen tuff. This model behaves very much like a Standard Linear Solid (Pound et al., 1982) but is much easier to handle. It did an excellent job of describing the propagation over the available range of data, which were measured well outside of the non-linear region where compaction takes place. Since the strains were on the order of 10^{-3}, we cannot assert that our data was strictly linear. Nevertheless, we believe that these results demonstrate the feasibility of inverting free-field data to obtain a material's creep function, and ultimately its apparent source function. Preliminary results indicate that the 'effective source radius' is approximately three times the size of the chemical explosive which would make it only slightly larger than a nuclear cavity.

Since this model contains a characteristic frequency which is not scalable, we find that for the same scaled distance the particle motions suffer increased attenuation with increased yield.

Anelastic Behavior in Free Field Data

Liu, Anderson, and Kanamori, 1976, demonstrated that a series of closely spaced relaxation mechanisms can explain a nearly constant Q behavior over a wide band of frequencies. The resulting linear anelastic theory is consistent with observations of constant Q over the seismic band. We believe that viscoelastic mechanisms, (with very different relaxation times) can explain the observed behavior of free-field particle velocity from both nuclear and small scale chemical explosions, (CE).

Blake, 1974, derived the asymptotic solution for a standard linear solid and found that at large distances, r, from a source whose time history was a step function, the peak velocities and peak displacements decay

*Work performed under the auspices of the U.S. Department of Energy by the Lawrence Livermore National Laboratory under contract Number W-7405-ENG-48.

as r^{-2} and $r^{-1.5}$, respectively, while at a given distance the peak velocity was proportional to energy (or yield). In a second paper (Blake and Dienes 1976), the authors tried to apply this asymptotic solution to data taken by DNA in dry tuff during a chemical explosion experiment dubbed Minedust. They were not successful in matching the data, thereby contributing to the skepticism about the utility of free-field experiments.

We believe, however, that Blake and Dienes failed because they attempted to apply the asymptotic solution of an anelastic phenomenon to data which were taken in the pore compaction region. The basis for our position is given in Fig. 1 where we have compared the peak velocity data for Minedust with data from Larson's small scale CE experiments in Mt. Helen tuff and with data from five nuclear explosions in Rainier Mesa tuff, Perret 1975. The Minedust data have the same slope, $r^{-2.5}$, as does the Mt. Helen tuff in its pore compaction region. Assuming that Blake and Dienes were applying this theory in an inappropriate region, it is understandable that their results were not good.

In Fig. 1 we also show the results of extrapolating Achenbach's and Chao's, 1962, three-parameter anelastic model to large scaled ranges. We note that in the region of the data used to obtain our rough estimates of the three parameters the slope is $r^{-1.3}$ but that the extrapolated

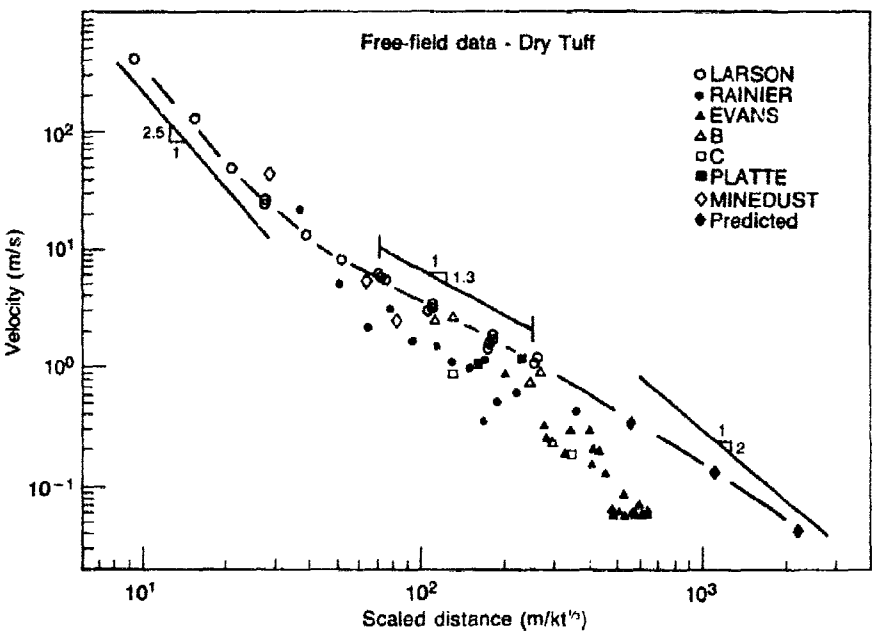

Fig. 1.

curve asymptotically approaches a decay of $r^{-2.0}$ at large distances.* Figure 2 also highlights the shortcomings of almost all of the experimental programs. Any one experiment typically does not cover a large enough range to show a definitive behavior. The measurements from RAINIER, for example, show the transition from pore compaction to anelastic behavior but were not taken at great enough distances to show the r^{-2} behavior. On the other hand, all of the measurements made on event EVANS appears to be in the r^{-2} anelastic region.** In addition, the early nuclear and chemical experiments are characterized by very large scatter in the measurements.

The sandstone, granite, and dolomite data, Fig. 2, all appear to show similar behavior. In each of these figures, the small scale CE data postfixed "LDN" in the legend seem to be asymptotically approaching a slope of $r^{-2.0}$. The nuclear data in granite and dolomite, in comparison to the small scale CE experiments, have so much scatter in them that no such trend can be observed. However they fall below the $r^{-2.0}$ line of the small scale CE experiments. This is primarily due to the difference in the equation of state between the nuclear explosive and the chemical one. But it could also be due, in some part, to the anelastic behavior of the material.

The following formulation for the Laplace transform of the particle velocity, $v(\tau)$, at any distance, r, due to a step in pressure, P_0, at a distance R_0, was taken from Tsay, 1972:

$$L[v(\tau)] = \frac{-\left(\frac{1}{r} + \frac{s}{\bar{c}(s)}\right) R_0 P_0 \exp\left[-s(r-R_0)\left(\frac{1}{\bar{c}(s)} - \frac{1}{c_\infty}\right)\right]}{r\rho\left(\frac{4\bar{\mu}(s)}{R_0^2\rho} + \frac{4\bar{\mu}(s)s}{R_0\rho\,\bar{c}(s)} + s^2\right)} \tag{1}$$

and rewritten in reduced time, τ, where $\tau = t - (r-R_0)/c_\infty$ and c_∞ is the instantaneous or "unrelaxed" velocity of propagation. $c(s)$ and $\mu(s)$ are the complex phase velocity and shear modulus, respectively, and ρ is the density. In the elastic case $\mu(s) = \mu$, a constant, $c(s) = c_\infty$, and the exponential disappears.

---

*Since the meeting at Santa Fe, we have modeled the same data with an absorption band model. With this model the asymptotic limit on the slope is reached by 2000 m/kt$^{1/3}$ and is -2.5, not -2.0, implying that the apparent applied stress should be represented as decaying exponentially instead by a step function. The extrapolated curve for Larson's data with the model is just offset from that of RAINIER and EVANS.

**Or $r^{-2.5}$.

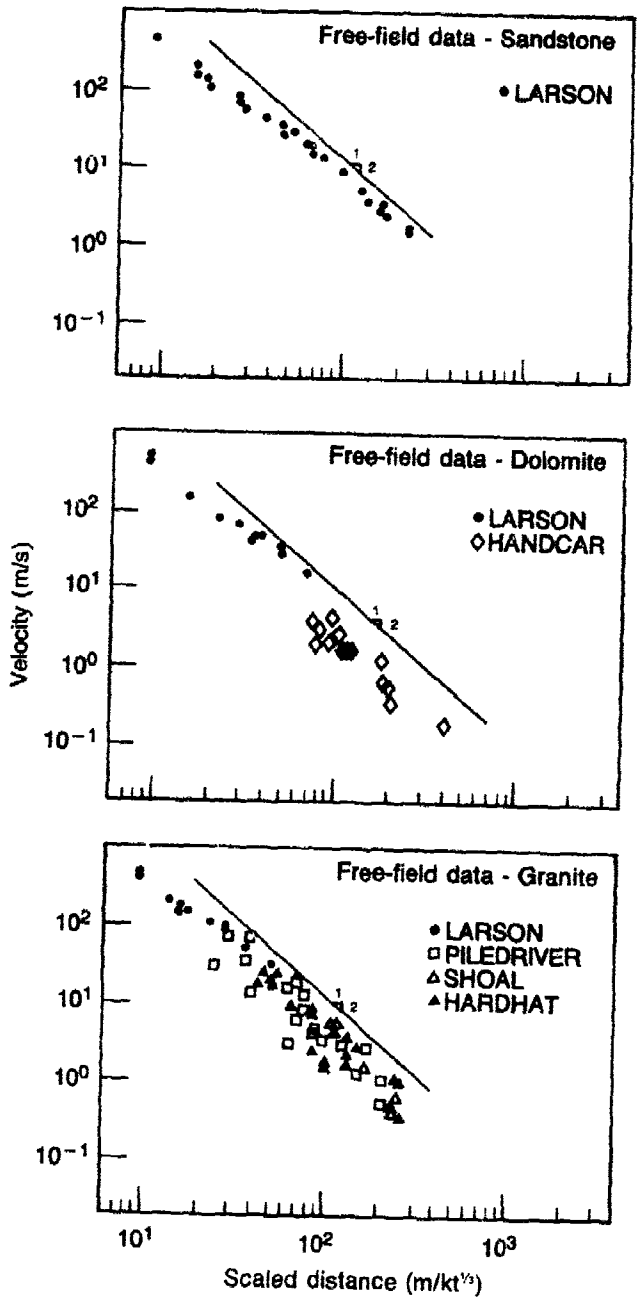
Free-field data - Sandstone
• LARSON
Free-field data - Dolomite
• LARSON
◇ HANDCAR
Free-field data - Granite
• LARSON
□ PILEDRIVER
△ SHOAL
▲ HARDHAT
Velocity (m/s)
Scaled distance (m/kt^1/3)

Fig. 2.

The following discussion is simplified if we identify the three elements of Eqn. 1 by name. Thus Eqn. 1 consists of a geometrical spreading term:

$$\frac{1}{r}\left(\frac{1}{r}+\frac{s}{\bar{c}(s)}\right) \tag{1.a}$$

an apparent boundary condition term:

$$\frac{R_0 P_0}{\rho\left(\frac{4\bar{\mu}(s)}{R_0^2\rho}+\frac{4\bar{\mu}(s)s}{R_0\rho\,\bar{c}(s)}+s^2\right)} \tag{1.b}$$

and an attenuation term:

$$\exp\left[-s(r-R_0)\left(\frac{1}{\bar{c}(s)}-\frac{1}{c_\infty}\right)\right] \tag{1.c}$$

The phase velocity, $c(s)$, in a viscoelastic model is assumed to have a modulus $c(\omega)$, which varies smoothly from some value, c_0, at $\omega = 0$ to another value, c_∞, at $\omega = \infty$ and where c_0 is less than c_∞. Thus the transient outward propagating velocity pulse defined by Eqn. 1 has an onset time which is determined by c_∞. Close to the source, the attenuation term 1.c has little effect on the high frequency components so that the arrival time is clearly determined by c_∞. However, at large distances the attenuation term suppresses the high frequency components and the pulse becomes emergent.

In elastic theory R_0 is known as the elastic radius. This, obviously, is inappropriate in anelastic theory and a better name might be the "effective source radius". For a given P_0 and yield, W, R_0 scales as the cube root of the explosive energy or yield, W, or $R_0 = kW^{1/3}$ so that Eqn. 1 becomes

$$L[r,t)] = \frac{\frac{1}{\bar{c}(s)}\left(\frac{\bar{c}(s)}{W^{1/3}(r/W^{1/3})}+s\right)kP_0\exp\left[-sW^{1/3}\left(\frac{r}{W^{1/3}}-k\right)\left(\frac{1}{\bar{c}(s)}-\frac{1}{c_\infty}\right)\right]}{\frac{r}{W^{1/3}}\rho\left(\frac{4\mu(s)}{k^2W^{2/3}\rho}+\frac{4\bar{\mu}(s)s}{kW^{1/3}\rho\bar{c}(s)}+s^2\right)} \tag{2}$$

If $\mu(s)$ and $c(s)$ are weakly dependent on frequency. Then we see that at the same scaled range, $r/W^{1/3}$, the frequencies in the boundary condition term and the geometrical spreading term will approximately scale

but that the exponential attentuation term will not scale. In fact, as the yield increases, $v(\tau)$ loses high frequencies more rapidly with increasing yields for the same scaled distance. This, of course, is not the case for elasticity. The degree to which this systematic bias is significant depends on both the magnitude of the departure of $c(s)$ from c_∞ and the frequency at which it occurs. Thus Eqn. 2 could explain both the change in the slopes from something less than r^{-2} at small scaled ranges to r^{-2} and the bias between the small scale CE and nuclear explosions seen in Figs. 1 and 2.*

The possibility exists, of course, that we are comparing attenuation due to different mechanisms, since we do not know the similarities or differences between Mt. Helen tuff and Rainier Mesa tuff, or between Blair dolomite and Climax stock dolomite, or between Westerly granite and Climax stock granite. On the other hand, the fact that a simple model can explain two prominent features of the free-field data is promising enough to justify additional work to remove these uncertainties.

Our estimates of the three parameters in the Achenbach and Chao (1962) model for Mt. Helen tuff were obtained by trial and error and there is room for improvement in the application of this model and even for the use of a different model. Our chief motive in choosing the Achenbach and Chao three-parameter model was its simplicity in form which in turn made the solution of Eqn. 1. easy to handle.

The Achenbach and Chao model is

$$\bar{c}(s) = c_\infty \left(\frac{s + a^2 b}{s + ab} \right) \quad \text{where } 0 \leq a \leq 1 \tag{3}$$

so that

$$\lim_{s \to \infty} s \left(\frac{1}{\bar{c}(s)} - \frac{1}{c_\infty} \right) \to \frac{ab\,(1-a)}{c_\infty} \text{, a constant.} \tag{4}$$

Hence as $s \to \infty$ the spectral amplitude ratio of the particle velocities at two different ranges becomes a constant. In order to find the spectral ratios we used the four signals shown in Fig. 5 labeled "Original Data". We then found the transfer function between the largest signal and each of the smaller ones using a signal identification algorithm which we obtained from Dennis Goodman, of LLNL's Engineering Research Department. From these transfer functions we estimated the ratio $ab\,(1\text{-}a)/c_\infty$ to be 25 from the three values of the transfer function at the

*Or $r^{-2.5}$.

Nyquist frequency. We assumed c_∞ could be estimated from the relative onset times, which gave a value of 2660 m/s. To complete the parameter estimation process we simply calculated $v(\tau)$ for each of the three smaller signals using the largest as the input and for a range of values of a. A good match was obtained as shown in Fig. 3 for $a = .95$. In this figure, we see that the anelastic model, $a = .95$, more closely estimates the correct peak amplitudes and the times to the peak amplitudes than does the elastic model, $a = 1.0$. In the elastic case all the peaks occur at the same reduced time.

In order to find these transfer functions, we first fit each of the four signals with a high order rational polynomial to approximate Eqn. 1. It turned out that most of the energy was concentrated in three of four terms and that the term which contributed the most energy consisted

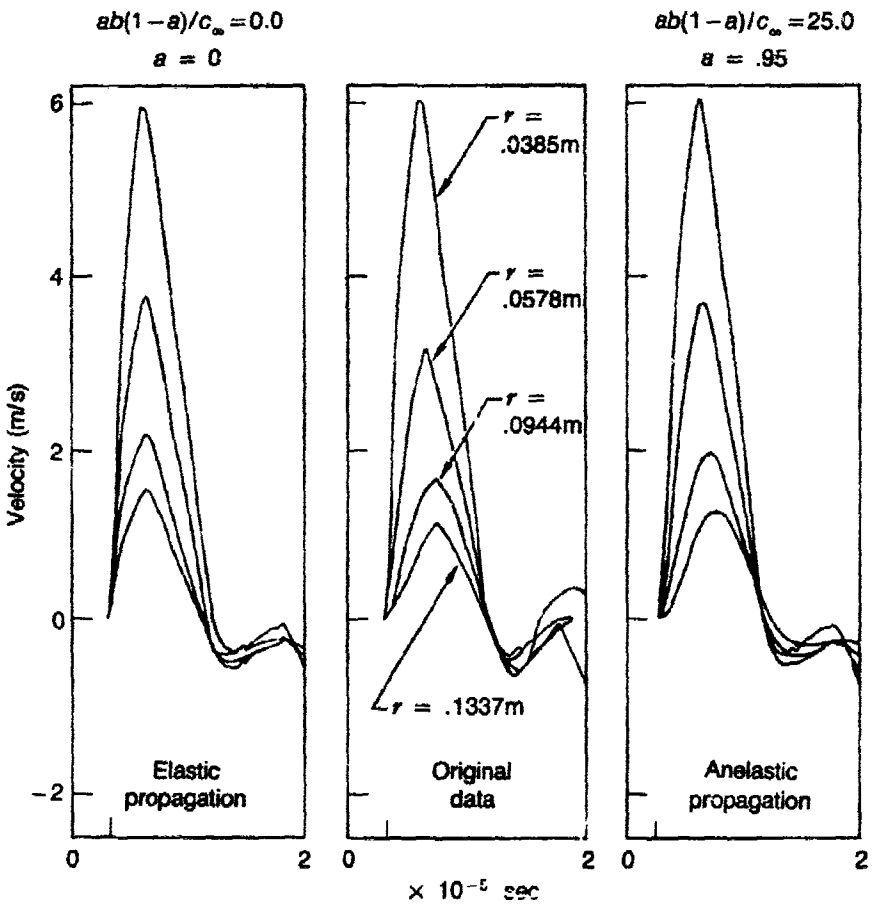

Fig. 3.

of a complex pair whose frequency, 0.444×10^6 Hz, was very nearly independent of distance but whose damping was dependent on distance. We therefore speculate that this frequency is the frequency of the boundary condition term and that the damping value is obscured by the attenuation term. With this assumption, (to validate this we shall have to implement a rigorous inversion procedure), we calculated the instantaneous source radius R_0 using Poisson's ratio as determined from the work of Heard *et al*,. (1973) and from the observation that the boundary condition term for $a = .95$ is nearly identical to the elastic case. From this procedure we found $R_0 = 7.55$ mm from an explosive 2.5 mm in radius with a yield of 1.59×10^{-10} kt. For a one kiloton explosion, the fundamental frequency would be 38 Hz and R_0 would be 14 m.

The Need for a Linearity Experiment

A major criticism of all past free-field measurement programs has been that all the measurements have been made at relatively large strains, that is 10^{-4} or greater. Many investigators believe that this is a nonlinear region. Gordon and Davis (1968), Johnston (1978), and Winkler and Nur (1970) suggest that the upper limit on strain for linearity is between 10^{-5} and 10^{-6}. However, Larson (1981) demonstrated that superposition, the ultimate test for linearity, holds in pressed salt at a strain of 7×10^{-4} under no confining pressure.

This question of linearity is fundamental to any modeling effort, therefore, we propose to conduct a linearity experiment. In our experiment we will construct models and instrument them at distances corresponding to strains of 10^{-3}, 10^{-4}, 10^{-5}, and 10^{-6}. Within each range we propose to uniformly space 4 or 5 gauges so that we can evaluate the "creep function" at each of these levels. Since the creep function, $J(t)$, is dependent only on time, we can assert that linearity holds at whatever range (strain level) the creep function becomes independent of range.

To summarize, the theory of linear anelasticity is highly developed (see for example Chin and Thigpen (1978), Minster (1978), and Anderson (1982)) and we believe that its use in interpreting the data from model experiments will allow us to accurately describe the behavior of the material under test. This in turn will enable us to provide accurate source models for explosions.

Short-Period Amplitude Patterns from Pahute Mesa, Tectonic or Propagation

Donald V. Helmberger, Thorne Lay, Patricia Scott, and Terry Wallace

Summary

Pahute Mesa underground nuclear tests produce teleseismic short-period P waves with a systematic azimuthal amplitude variation. It is possible to account for this azimuthal variation by interference between the explosion and tectonic release P waves, where the parameters of the tectonic release are constrained to be those indicated by long-period studies. Nearly vertical, high stress drop, strike slip faulting is required by long-period P waves from Pahute Mesa events. This predicts a factor of 2.0-3.0 amplitude variation with a sin(2φ) azimuthal distribution for short-period teleseismic P waves, if the tectonic release is driven by the explosion. While it is shown that tectonic release could affect teleseismic short-period signals significantly, and may contribute to the Pahute Mesa amplitude pattern, other possible explanations are considered.

Introduction and Discussion

The first cycle (*ab* amplitude) of teleseismic short-period *P* waves from underground nuclear explosions at Pahute Mesa (NTS) show a systematic azimuthal amplitude pattern that can possibly be explained by tectonic release or perhaps lower crustal structure. The amplitudes vary by a factor of three, with diminished amplitudes being recorded at azimuths around N25°E. This azimuthal pattern has a strong $\sin(2\varphi)$ component and is observed, to varying degree, for 25 Pahute Mesa events, but not for events at other sites within the NTS, see Fig. 1. The *bc* measure of amplitude yields similar ratios to those given in Fig. 1. A comparison of the observed waveforms for FAULTLESS *vs.* GREELEY from 30° to 100° is displayed in Fig. 2, where the waveforms are quite similar for the two events at most stations.

Evidence for teleseismic radiation of high frequency energy from tectonic release was presented by Wallace *et al.* (1983). They demonstrated that long-period *P* waves (with dominant periods of 2 to 3 sec) at upper mantle distances from Pahute Mesa explosions have clear *sP* arrivals.

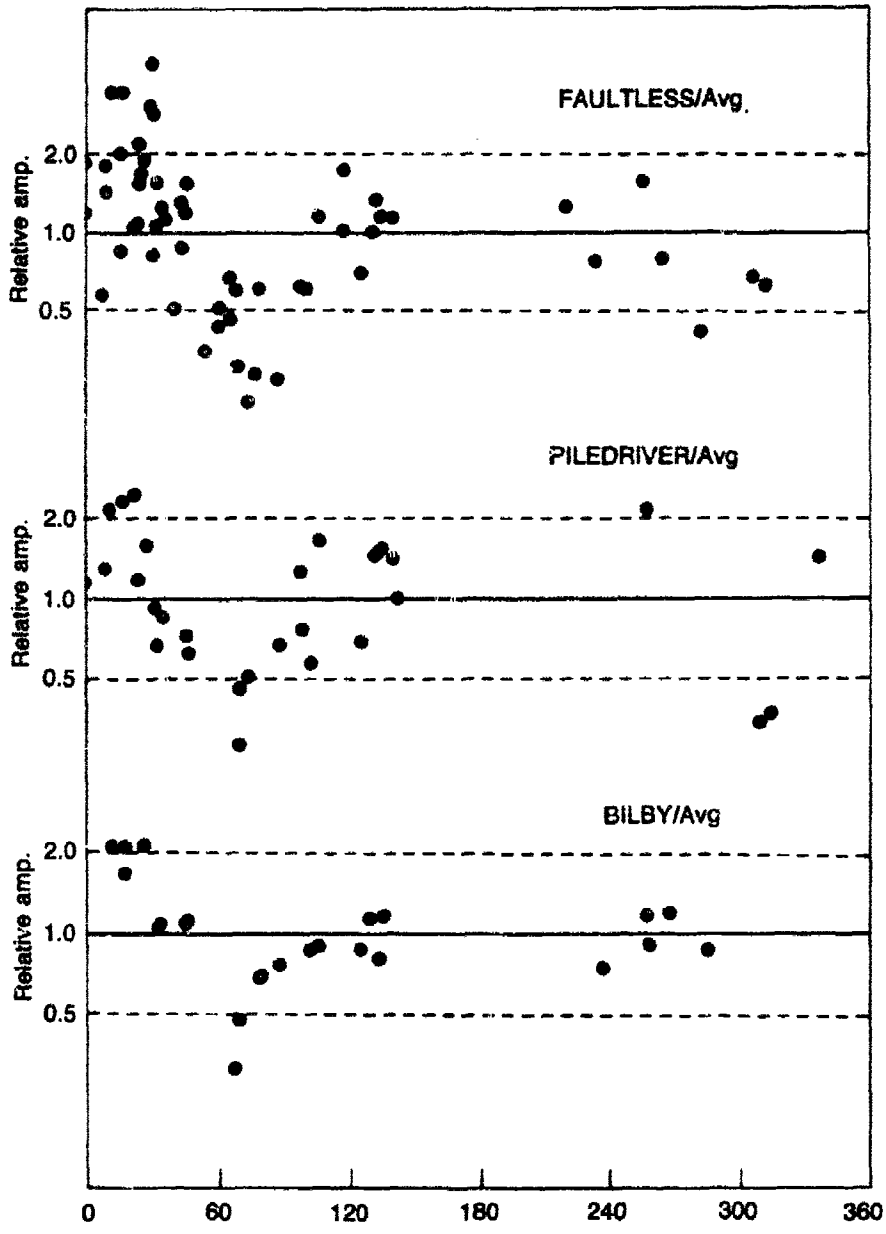

Fig. 1. Ratios of the short period *P* wave *ab* amplitudes measured from FAULTLESS, PILEDRIVER and BILBY divided by the Pahute average. Pahute events appear to have small amplitudes near 20° and large amplitudes near 80°.

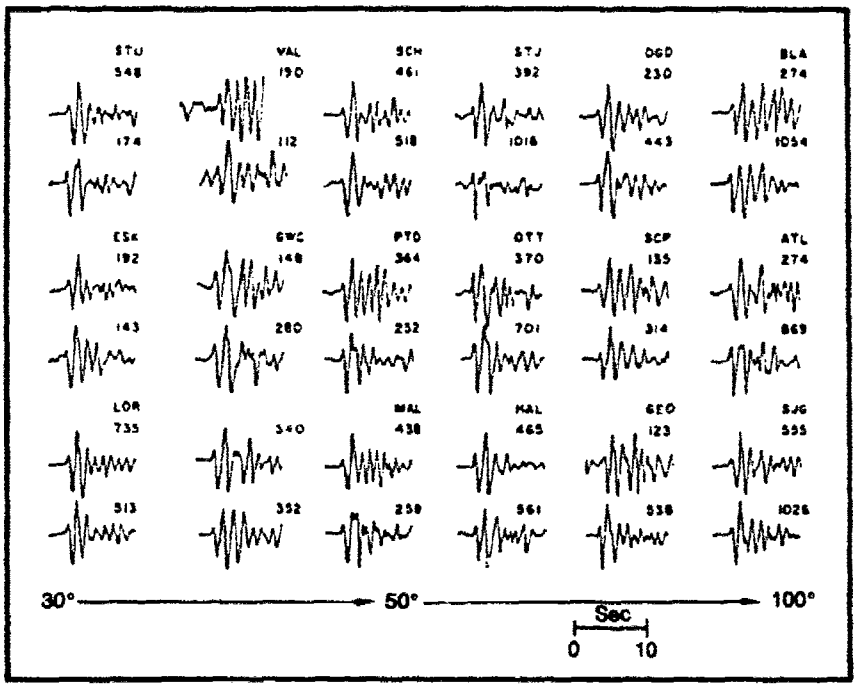

Fig. 2. Comparison of waveforms between FAULTLESS (upper trace) and GREELEY (lower trace). The numbers indicate relative amplitudes. Note the similarity between the two events at each station but with different amplitudes.

Events which are within 4 km of a previous explosion usually have a substantially reduced *sP* arrival. Analysis of *SH* waves and regional P_{nl} signals indicates that the tectonic release orientation is predominantly strike slip, through up to a 10% dip slip contribution cannot be ruled out, see Wallace *et al.* (1984). For example, the best fitting strike direction for the GREELEY event is N25°E. This orientation predicts that the direct *P* wave from the tectonic release is opposite in polarity to the *P* arrival from then explosion which appears to be quite compatible with Fig. 1. Because of this association, we choose to fit a $\sin(2\varphi)$ curve to the amplitude patterns of 25 Pahute Mesa events. For each event, the mean *ab* amplitude, $\vec{A}_{ww}$, of the WWSSN stations was determined, and the amplitudes divided by $\vec{A}_{ww}$. A curve was fit to the zero-mean ratios with the form:

$$A/A_{ww} - 1 = a \sin 2 (\varphi - \varphi_0)$$

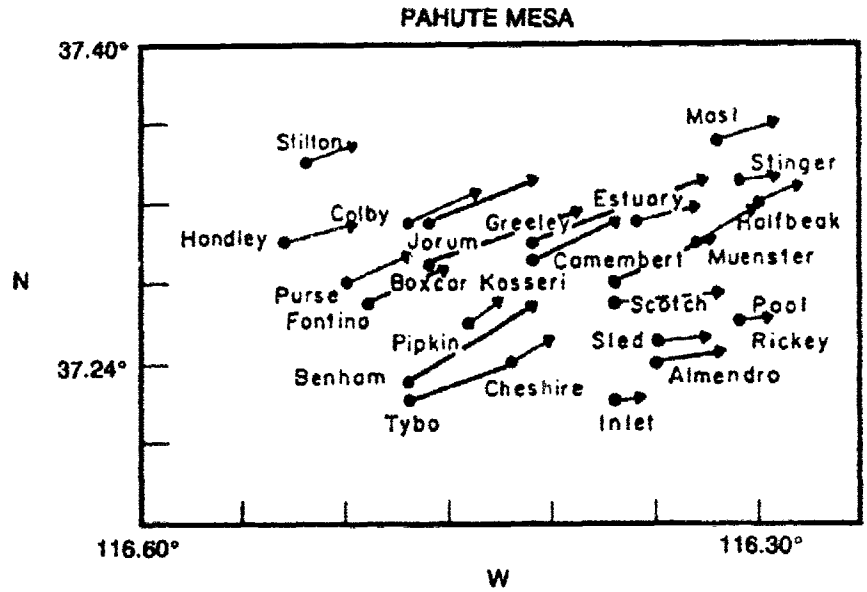

Fig. 3. For each of the events an arrow is shown for which the width and length are proportional to the *f*-ratio, and the azimuth is given by φ_0 for that event. The *f*-ratio is large for those events for which a $\sin(2\varphi)$ curve significantly reduces the variance.

The two parameters a and φ_0 were inverted for by least squares and tested for significance by applying the *f*-test, see Lay *et al.* (1984). For the Pahute Mesa events only 5 events of the 25 events fail the *f*-test at the 99% confidence level. Those events with large *SH* and Love waves yield higher confidence levels as displayed in Fig. 3. However, all four non-Pahute mesa events fail the *f*-test at the 95% confidence level while only two Pahute events fail at similar values.

Given the lack of obvious waveform variations for events such as GREELEY versus FAULTLESS, see Fig. 2, it becomes important to consider whether the amplitude effects predicted by Fig. 3 are accompanied by waveform variations. Figure 4 presents the synthetic waveforms for the explosion alone, and the vertical strike slip dislocation models. The first column indicates the explosion signal and the tectonic release signals in the loop directions for the point source and finite source. Note that the *ab* amplitudes are comparable. The next two columns show the explosion plus double couple waveforms in the positive and negative loop directions. The finite source synthetics because the downward directivity produces destructive interference for the *sP* arrival. Thus, the finite source produces less waveform variation with azimuth. Even for the point

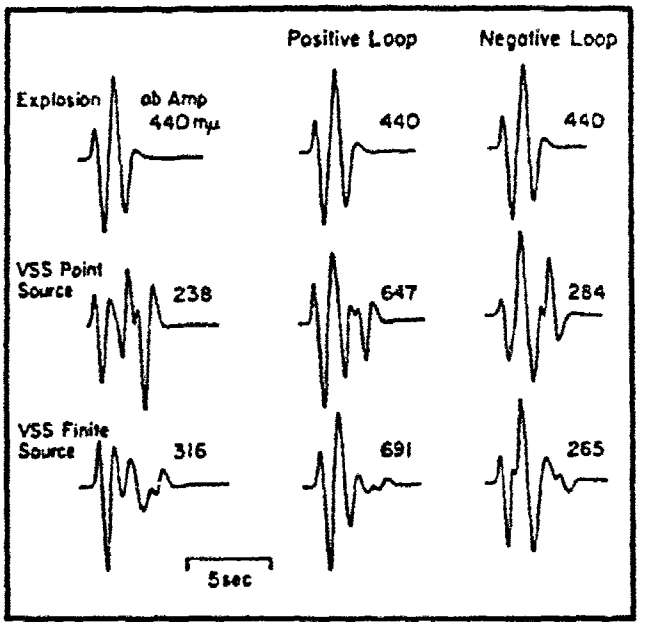

Fig. 4. Short-period synthetic waveforms for the GREELEY synthetics. The top row shows the explosion synthetic alone. The middle row shows the vertical strike slip point source synthetic, and the sum of the bomb plus point source in the positive loop and negative loop directions of the double couple radiation pattern. The bottom row is similar to the middle row, only it shows the downward rupturing finite source synthetic results.

source model, though, the azimuthal variation is quite subtle, and the first order effect is the amplitude variation. Referring to Fig. 2, it is unlikely that such variations could be resolved given the additional path, receiver, and near source contributions to the coda. Note that the finite source produces nearly uniform suppression of the explosion waveform, thus the *bc* amplitudes show the same pattern as the *ab* amplitude, which is what is actually observed.

Another possible explanation of the azimuthal pattern suggested in Fig. 1, can be given in terms of structure. In particular, Scott and Helmberger (1984), show that the .25 to .4 sec time anomalies associated with Pahute events, as discussed by Minster *et al.*, (1981) can be used to constrain a up-warped crust-mantle boundary that can produce this type of pattern.

Synthetics for various types of interface distortions are given in Fig. 5 where the source is centered above the structure. These responses are the result of a numerical evaluation of the Kirchhoff-Helmholtz integral. The method calculates the response of a wave transmitted through

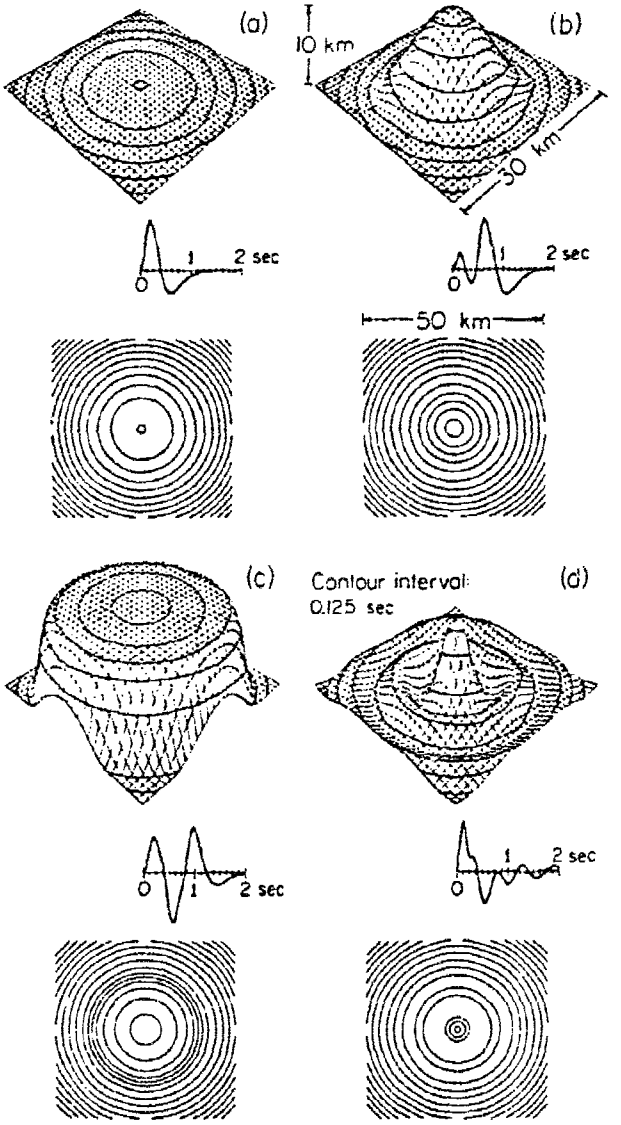

Fig. 5. Here we display four synthetics and their two-way travel-time functions contoured in intervals of .125 seconds. The functions are projected onto the actual topographies (top figure) and a horizontal 50 × 50 km grid (bottom figure). The synthetics are calculated for receivers 20,000 km below the source. We see how each topography perturbs the travel-time function relative to a flat interface and causes complexity in the synthetic.

a warped boundary and is similar to the formalism discussed by Scott and Helmberger (1983). The effects of off-center positioning of the source is displayed in Fig. 6 where we see a change in overall complexity of the synthetics as a function of azimuth. The waveforms from the group at $\Theta = 0°$ are simple and impulsive with relatively high amplitudes. Only the stations at nearly vertical incidence have multiple arrivals. As we rotate counter-clockwise around the structure, we see a greater percentage of the synthetics in each group which have multiple arrivals, and, as a consequence, low amplitudes. Synthetics at $\Theta = 135°$ and 180° all have multiple arrivals. The reason for this trend is the same as in the previous modeling study. When the sources move in the direction of a line along $\Theta = 0°$, a greater proportion of the elements which constitute the planar part of the grid contribute to the potentials calculated in the direction of this line. Hence, synthetics of this line become more impulsive as the source migrated from position A to position D. By contrast, the synthetics at $\Theta = 135°$ and 180° remain complex. The elements which contribute to these potentials are largely from the perturbed part of the boundary.

In Fig. 7 we include the (*pP*) interference, WWSSN short period response, and two choices of t^*. Note that considerable azimuthal amplitude patterns develop for source positions at the edge of the upwarped structure.

We have succeeded in producing the order of magnitude of variation of first amplitudes as displayed in Fig. 1; however, this variation is created at the cost of considerable distortion of the waveform. This feature of low-amplitude waveforms with complex or broadened pulses and high amplitude waveforms with simple narrow pulses has not been particularly noted.

Conclusions and Recommendations

The numerical experiments on effects of warped boundaries show a clear correlation between travel time residuals and amplitudes. This correlation may be diagnostic of structure since we would not expect tectonic release to produce travel time anomalies. The question, then, is such a correlation observed? Unfortunately, the data sets of amplitude and travel time measurements do not have a one-to-one correspondence. Lay *et al.*, (1984) measures the *ab* amplitudes of short period WWSSN instruments while Minster and Spence use culled travel time measurements from the ISC catalogs. We clearly need a study which compares the travel time and amplitude from the same seismogram. Such a study, though, requires good accuracy in travel time measurements. In addition, such studies should involve both events within the mesa and events outside the mesa.

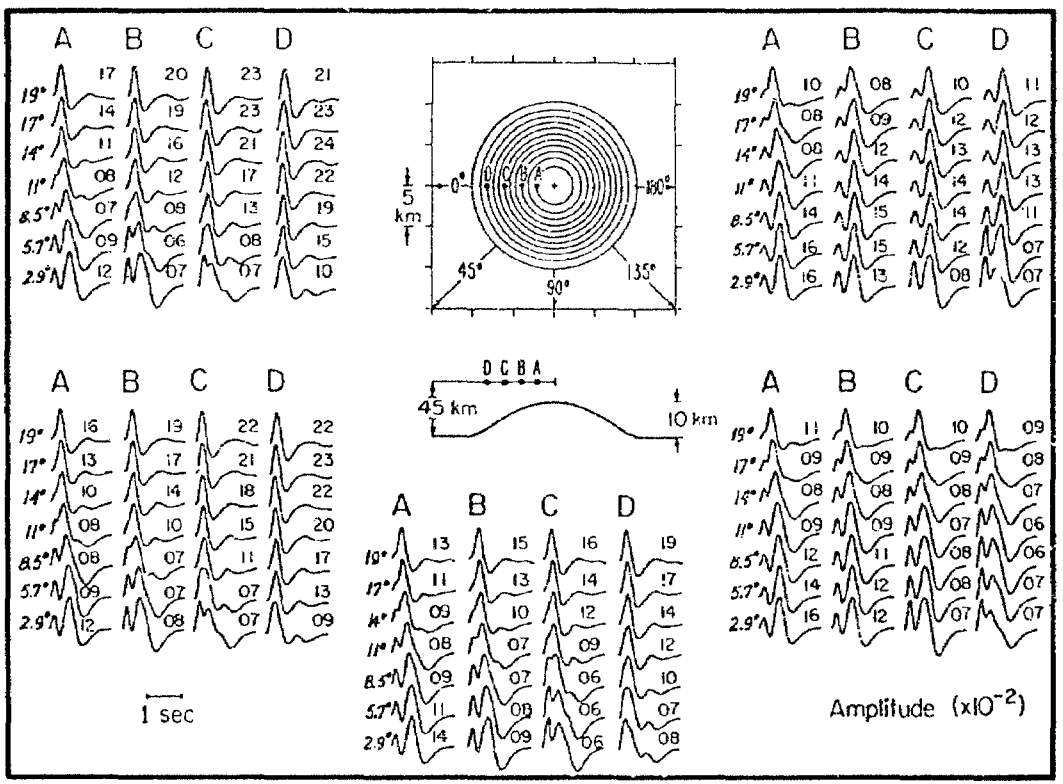

Fig. 6. Synthetics (*P*) from the topographic upwarp calculated for 4 source positions, 5 azimuths, and 7 angles of incidence. The topographic map of the upwarp is shown in the center of the plot.

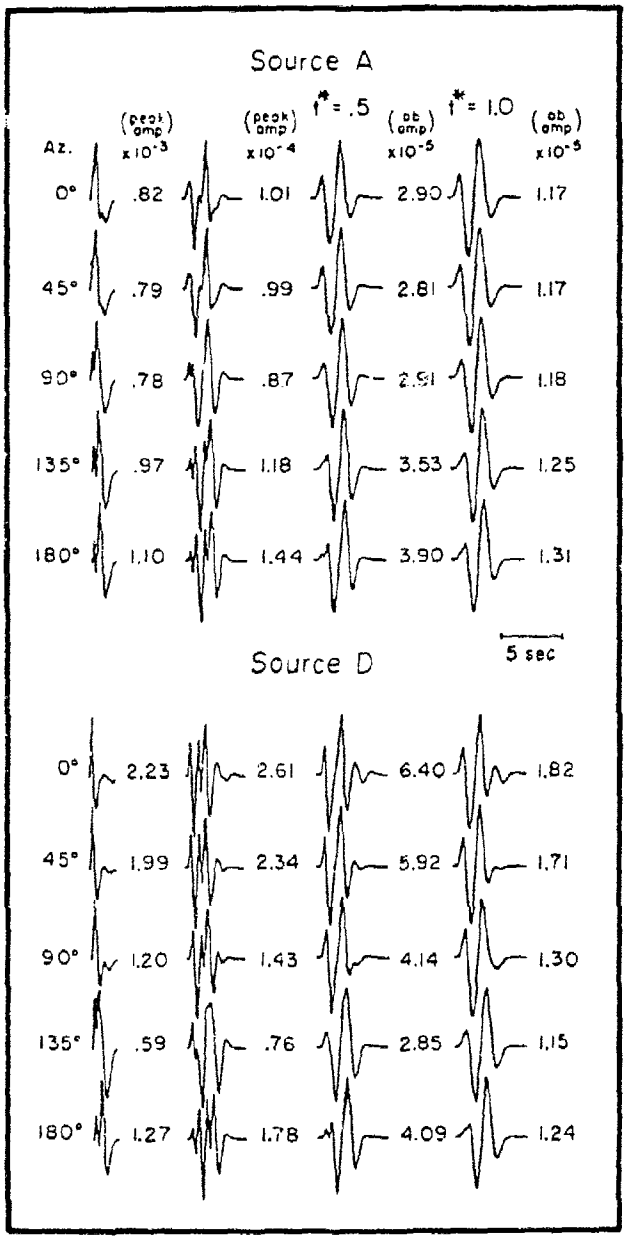

Fig. 7. Synthetic short period responses are displayed for source positions A and D appropriate for teleseismic distances. The columns on the left display the behavior before and after the addition of *pP*. The columns on the right contain the instrument response and *Q*-operators.

On the other hand, if the teleseismic short period amplitude is controlled by tectonic release we would expect to see amplitude effects in the near-field before any propagational distortions occur. Thus, complete model compatibility at all ranges is recommended if we are to make significant progress in our understanding of seismic signals generated by explosions.

References

Lay, T., T. C. Wallace, and D.V. Helmberger (1984). "The Effects of Tectonic Release on Short-Period *P* Waves from NTS Explosions," *Bull. Seism. Soc. Am.*, **74**, 819-842.

Minster, J.B., J.M. Savino, W.L. Rodi, T.H. Jordan, and J.F. Masso (1981). "Three-Dimensional Velocity Structure of the Crust and Upper Mantle Beneath the Nevada Test Site, " Final Technical Report, SSS-R-81-5138, S-Cubed, La Jolla, California.

Scott, P., and D.V. Helmberger (1983). "Applications of the Kirchhoff-Helmholtz Integral to Problems in Seismology," *Geophys. J.R. Astr. Soc.*, **72**, 237-254.

Scott, P., and D.V. Helmberger (1984). "Applications of the Kirchhoff-Helmholtz Method to Transmitted Body Waves," *Bull Seism. Soc. Am.*, **75**, 131-156.

Wallace, T.C., D.V. Helmberger, and G.R. Engen (1983). "Evidence of Tectonic Release from Underground Nuclear Explosions in Long-Period *P* Waves." *Bull. Seism. Soc. Am.*, **73**, 593-613.

Wallace, T.C., D.V. Helmberger, and G.R. Engen (1984). "Evidence of Tectonic Release from Underground Nuclear Explosions in Long-Period *S* Waves," *Bull. Seism. Soc. Am.* **75**, 157-174.

Propagation of Teleseismic *SV* Waves

Charles A. Langston

Summary

Theoretical developments in the analysis of teleseismic body waves from earthquakes and explosions are reviewed. The theoretical treatment of teleseismic SV wave forms is a logical and useful extension of the current program of source parameterization and analysis of large scale crust and mantle structure.

Discriminating explosions from earthquakes and estimating explosion yield are basically problems in source inversion. Given a data set consisting of analog or digital seismograms recorded at scattered locations throughout the world, one is required to determine a set of parameters which describe the type of source and its size in space and time. A major part of the author's program supported by AFOSR/DARPA has been concerned with developing the theoretical tools needed to parameterize a seismic source, the computation of the necessary wave propagation from source to receiver, and implementing inversion procedures to extract source parameters from the wave form data.

An implied assumption in this work is that it is possible to usefully extract source parameters from the amplitude data. Experience has shown that this assumption is valid only when the distorting effects of earth structure are known. Historically, this has meant that progress has usually been made only in the longer-period bands where body or surface wave wavelengths are sufficiently long (typically ~ 50 km) to average over major crustal heterogeneities or where the wave propagation effects are relatively simple (as for body waves turning in the lower mantle).

The study of teleseismic *P* and *SH* waves has proved useful in source inversion since wave propagation effects are usually limited to reverberations and reflections occurring near the source, if it is shallow. Propagation through the lower mantle is relatively simple consisting of a geometric turning ray with anelasticity included in a linear attenuation operator. Receiver effects are usually not important for long-period vertical *P* waves and tangential *S* waves, although severe receiver-induced distortions can occur. Langston and Helmberger (1975), among others, suggest a method of modeling shallow earthquakes as shear dislocation sources imbedded

in layered elastic structure. Parameterizing the source in terms of dislocation orientation, depth, and far-field time function, synthetic seismograms may be computed and compared to the body wave data using trial-and-error or a formal generalized inverse.

A number of earthquake studies have been performed using these techniques. For example, Fig. 1 displays the results of a study of the 1967 Koyna, India, earthquake (Langston, 1976) using a generalized inversion procedure. If source parameters are reasonably well known then the problem can be turned around to one of estimating near-source crustal

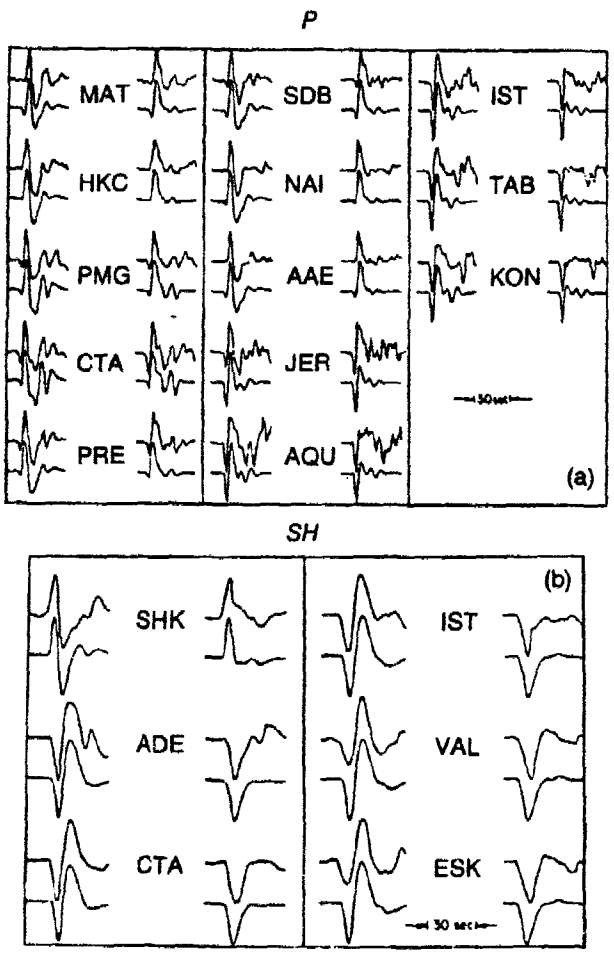

Fig. 1. Comparison of observed and calculated *P* waves (a) and *SH* waves (b) for the 10 Dec. 1967 Koyna earthquake. At each station the observed is on top with the synthetic below. To the left of the station letters are the observed and calculated with the instrument response included and to the right the instrument response is not included.

structure. An example of this is shown in Fig. 2. Here, P wave forms from the relatively deep 1965 Puget Sound earthquake (Langston and Blum, 1977) were simultaneously modeled for structure and source parameters. Arrivals between P and pP were interpreted to be reflections from interfaces above the source. The source crustal structure inferred from this exercise is shown in Fig. 3. Although the absolute value of velocity is largely unconstrained in this model, the general feature of the low velocity zone has been confirmed by other studies in the region.

The source information contained in long-period body waves is considerable. Langston (1979, 1981, 1982) showed that simple relative amplitude measurements coupled with a systematic trial-and-error ("grid") model testing procedure can put significant constraints on fault mechanisms. Occasionally, for some source orientations, it is possible to obtain a well constrained focal mechanism from data recorded at a single station. Figure 4 shows example results for the 1980 Sharpsburg, Kentucky earthquake and Fig. 5 displays the short-period vertical P wave used in the relative amplitude measurement. The ability to extract source

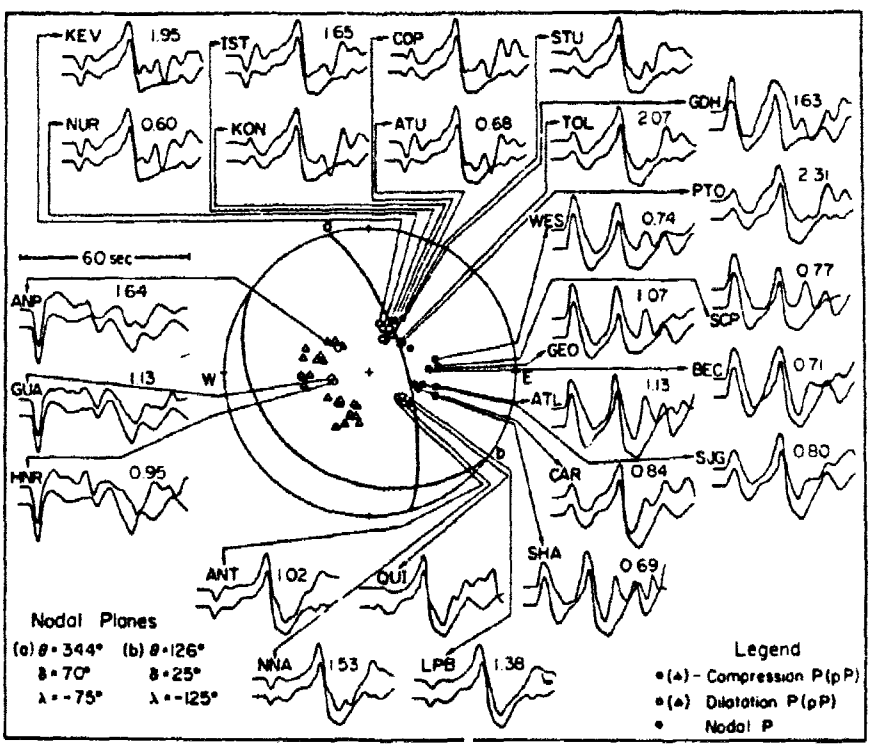

Fig. 2. Comparison of observed (top) and synthetic (below) P waves for the 29 April 1965 Puget Sound earthquake.

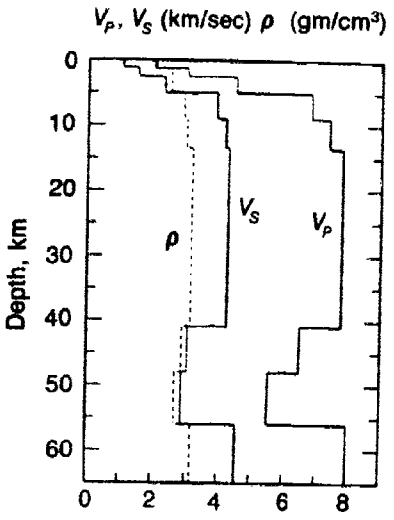

Fig. 3. PS-9 earth model for Puget Sound.

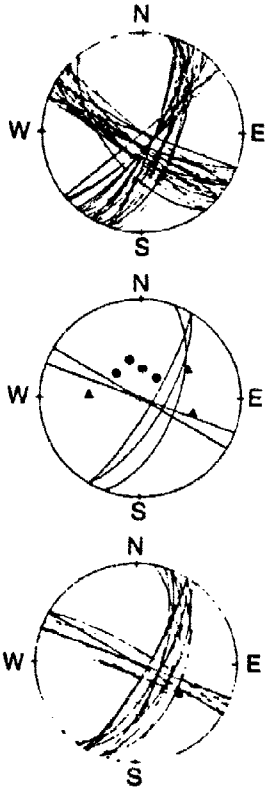

Fig. 4. Acceptable fault plane solutions for the body wave data from the Sharpsburg earthquake under various assumptions concerning the input data. All solutions are right-lateral on the NE-trending planes. All possible solutions were tested with an increment angle of 5° in strike, dip, and rake.

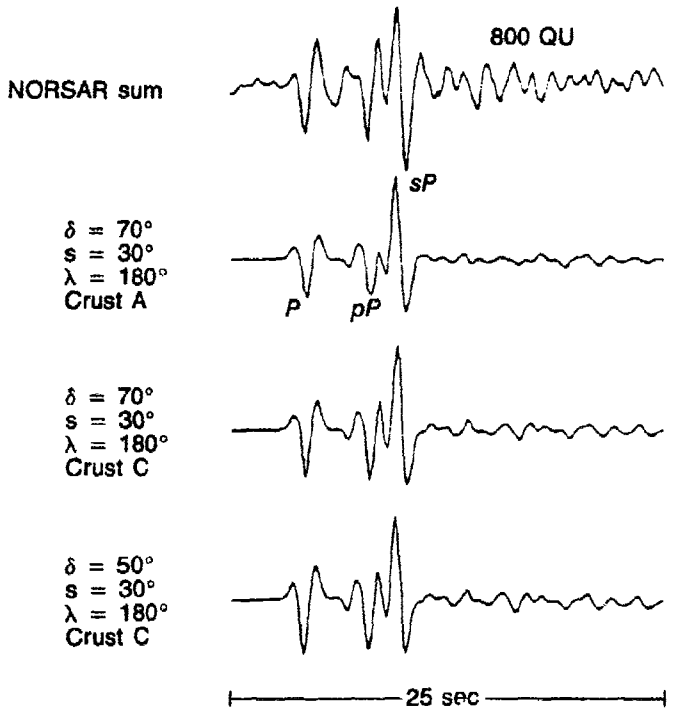

Fig. 5. Observed (top) *P* waveform at NORSAR for the Sharpsburg earthquake with synthetic waveforms (below). δ, s, and λ are fault dip, strike and rake, respectively. The zero-to-peak maximum amplitudes of the NORSAR sum is given in quantized units (QU). For single sensors at NORSAR, 1 QU = 0.0427 nm at 1-sec period.

parameters from small data sets is important in the problem of discriminating small earthquakes from explosions. These results suggest that it is advantageous to learn as much as possible about wave propagation effects in other phases of the seismogram so that these too may be incorporated into source studies.

Parameterizing the source as a second rank moment tensor is increasingly becoming popular because of linearity of the inversion problem and because the response to a number of seismic sources can be constructed quite easily, given the basic Green's functions for the earth response. Langston (1981) and Langston *et al.*, (1982) describe a method of inverting wave form data using a moment tensor source description. Earthquake models have been developed by Langston (1981), Barker and Langston (1981), Pavlin and Langston (1983), and Barker and

Langston (1983). The effect of improper source and structure assumptions on moment tensor inversions has been studied by Langston (1981), Barker and Langston (1982), Langston and Arnold (1982), and Johnston and Langston (1984). Figure 6 shows some results from Barker and Langston (1983) of a moment tensor inversion of the fourth major Mammoth Lakes, California, earthquake. The use of a moment tensor source description in explosion studies is natural since the isotropic and deviatoric components of the source can be separated and examined separately.

In virtually all of the previously mentioned studies, teleseismic waveform data have been restricted to *P* and *SH* waves. *SV* waves have been ignored because of the complicating effects of *Sp* conversions at the receiver and the "leaky-mode" phase *SPL*. Indeed, *SV* waves have largely been ignored in most standard seismological studies as well (*e.g.*, travel time studies) because of these problems. The variability of the *SV* waveform with range, receiver, and source type suggests that there is considerable source and structure information contained within it.

In order to incorporate the *SV* wave form into the previously mentioned inversion procedures and to use it in crust and mantle structure studies, we have undertaken a program to develop theory for the computation of teleseismic *SV* wave forms from a general point source.

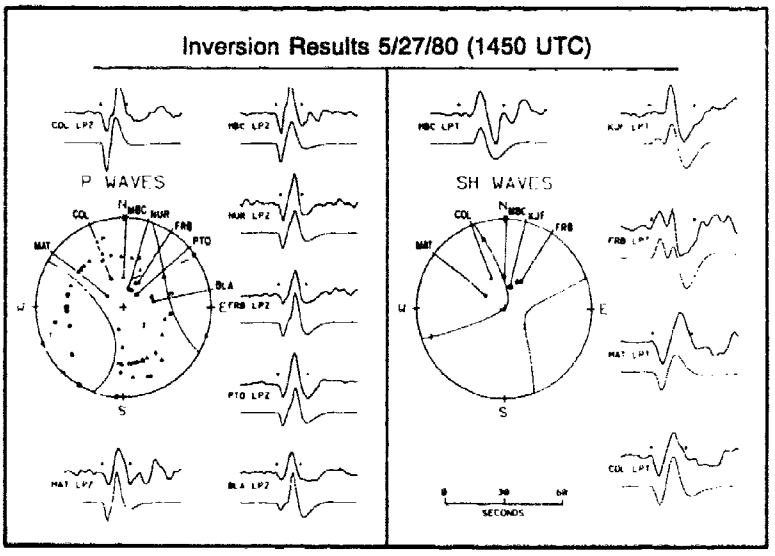

Fig. 6. Observed (top) and synthetic (below) waveforms for a Mammoth Lakes, California, earthquake found using the moment tensor inversion method. The moment tensor nodal surfaces for the model are shown for *P* and *SH* waves as lower hemisphere projections of the focal sphere.

Figure 7 outlines the approach described in Baag and Langston (1984a) for computing teleseismic *SV* waves. In the method, a large part of mantle model is represented by a continuous velocity structure. The *SV* wave in this region is treated as a turning wave using the WKBJ approximation. Crustal and uppermost mantle structure near the source and near the receiver is treated using the Thomson-Haskell propagator matrix method. For example, a shallow point source is introduced in the layered structure as jump conditions in displacement and stress at the source depth (Harkrider, 1964). The potential coefficient for the down-going *SV* wave is evaluated at the inhomogeneous halfspace boundary and transformed into WKBJ form. The potential is propagated to the receiver structure using the WKBJ approximation for a turning ray. This up-coming wave impinges at the base of the layered receiver structure and is used to calculate displacement coefficients at the free surface. Spectral displacement is found through a wave number integration. The response to spherical earth structure is obtained using an earth stretching transformation.

Figure 8 shows a comparison of synthetic seismograms computed using the WKBJ technique and Kind's (1978) reflectivity method for a shallow source in the Gutenberg-Bullen earth model. Inclusion of the WKBJ approximation in this problem decreases computation time by an order of magnitude but does not sacrifice accuracy.

The method has been used to study the excitation of *SPL* by deep and shallow sources (Baag and Langston, 1984b). Figures 9 and 10 show

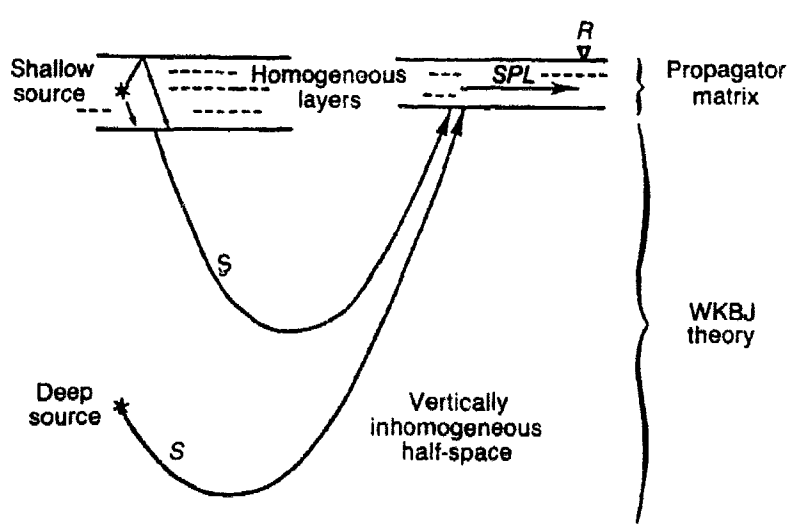

Fig. 7. Schematic representation of the WKBJ spectral method used to compute teleseismic *SV* waves.

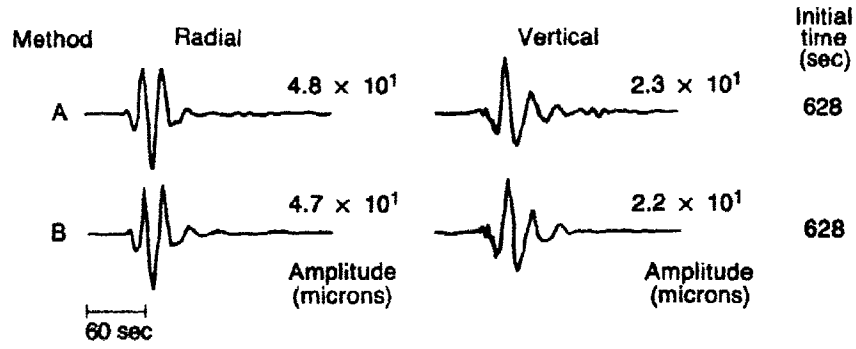

Fig. 8. Comparison of synthetic *SV* waves computed using the extended reflectivity method of Kind (1978) (top) and the WKBJ spectral method (below). The source is a shallow strike-slip dislocation.

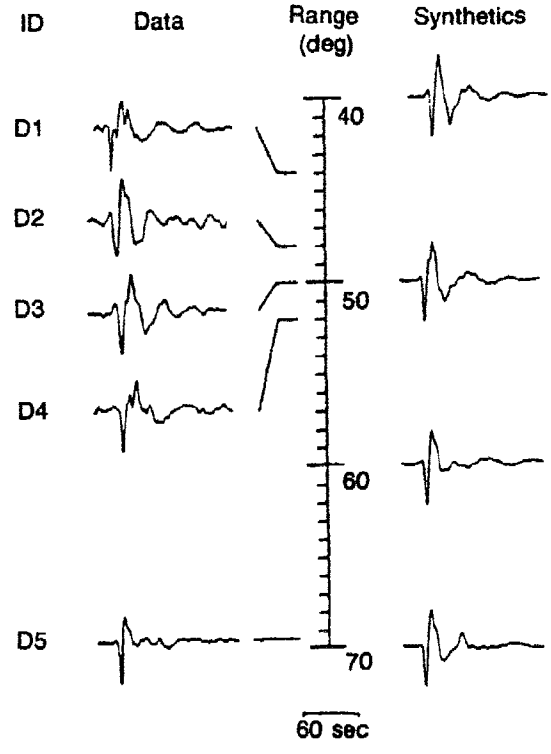

Fig. 9. Comparison of observed and synthetic *SV* waves for deep earthquakes recorded in North America. The *SPL* wave is relatively unimportant in these waveforms and occurs as the small sinusoid following the initial *SV* pulse.

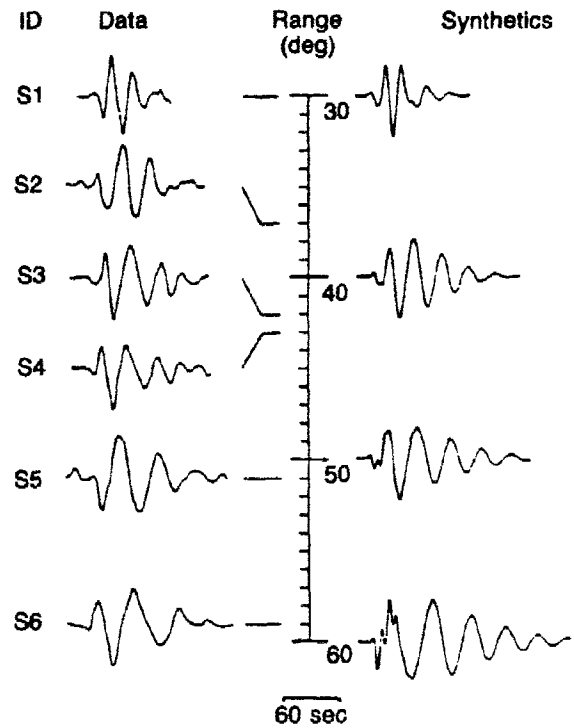

Fig. 10. Comparison of observed and synthetic *SV* waves for shallow earthquakes recorded in North America. Unlike in deep event *SV* waves, the *SPL* wave is a large long-period sinusoid which masks the direct *SV* wave. The data in this figure and in Fig. 9 are from several separate events. No attempt has been made to model source parameters.

that the *SPL* wave is seen to be excited preferentially by a crustal source relative to a deep source. This is in accordance with the observations and is due to large source area reverberations which leak into the mantle as *SV* waves. This dependence on source area structure suggests that the *SV* wave form from earthquakes or explosions may be used to estimate the velocity structure near the source, once the receiver structure is calibrated.

Conclusions and Recommendations

A method has been developed to incorporate *SV* waves into studies of the source and in studies of earth structure. The ability to calculate accurate *SV* synthetic seismograms allows the inclusion of *SV* data in moment tensor inversions and can augment sparse data sets of small events where each piece of data is very important in constraining source parameters. The method is also useful for modeling large scale crust and

mantle structure. For example, the simultaneous study of *SV* and *SH* wave forms and travel times may yield information on mantle anisotropy. The analysis of teleseismic *SV* wave forms appears capable of yielding estimates of both receiver structure and source structure. Current work involves theoretical comparison of ray theory approximations for *SV* with the spectral calculation, the modeling of specific source and receiver structure using *SPL* and diffracted *Sp*, and the inclusion of the *SV* wave in moment tensor inversions of explosion and earthquake data.

References

Baag, Chang-eob and C.A. Langston (1984a). "A WKBJ Spectral Method for Computation of *SV* Synthetic Seismograms in Cylindrically Symmetric Media," submitted to *Geophys. J. R. Astr. Soc.*

Baag, Chang-eob and C.A. Langston (1984b). "Shear-Coupled *PL*," submitted to *Geophys. J. R. Astr. Soc.*

Barker, J.S. and C.A. Langston (1982). "Moment Tensor Inversion of Complex Earthquakes," *Geophys. J. R. Astr. Soc.*, **68**, 777-803.

Barker, J.S. and C.A. Langston (1981). "Inversion of Teleseismic Body Waves for the Moment Tensor of the 1978 Thessaloniki, Greece, Earthquake," *Bull. Seism. Soc. Am.*, **71**, 1423-1444.

Barker J.S. and C.A. Langston (1983). "A Teleseismic Body-Wave Analysis of the May 1980 Mammoth Lakes, California, Earthquake," *Bull. Seis. Soc. Am.*, **73**, 419-434.

Harkrider, D.G. (1964). "Surface Waves in Multi-Layered Elastic Media, Part I. Rayleigh and Love Waves from Buried Sources in a Multilayered Elastic Halfspace," *Bull. Seism. Soc. Am.*, **54**, 627-679.

Johnston, D.E. and C.A. Langston (1984). "The Effect of Assumed Source Structure on Inversion for Earthquake Source Parameters: The Eastern Hispaniola Earthquake of 14 September 1981," submitted to *Bull. Seism. Soc. Am.*

Kind, R. (1978). "The Reflectivity Method for a Buried Source," *J. Geophys.*, **44**, 603-612.

Langston, C.A. (1976). "A Body Wave Inversion of the Koyna, India, Earthquake of December 10, 1967, and Some Implications for Body Wave Focal Mechanisms," *Jour. Geophys. Res.*, **81**, 2517-2529.

Langston, C.A. (1979). "A Single-Station Fault-Plane Solution Method," *Geophys. Res. Letters*, **6**, 41-44.

Langston, C.A. (1981). "Source Inversion of Seismic Waveforms: the Koyna, India, Earthquakes of 13 September 1967," *Bull. Seism. Soc. Am.*, **71**, 1-24.

Langston, C.A. (1982). "Single-Station Fault Plane Solutions," *Bull. Seism. Soc. Am.*, **72**, 729-744.

Langston, C.A. and W.A. Arnold (1982). "Moment Tensor Inversions and Dipping Slabs," *Geophys. Res. Letters*, **9**, 1290-1293.

Langston, C.A., J.S. Barker, and G.B. Pavlin (1982). "Point-Source Inversion Techniques," *Phys. Earth Planet. Int.*, **30**, 228-241.

Langston, C.A. and D.E. Blum (1977). "The April 29, 1965, Puget Sound Earthquake and the Crustal and Upper Mantle Structure of Western Washington," *Seism. Soc. Am.*, **67**, 693-711.

Langston, C.A. and D.V. Helmberger (1975). "A Procedure for Modelling Shallow Dislocation Sources," *Geophys. J.R. Astr. Soc.*, **42**, 117-130.

Pavlin, G.B. and C.A. Langston (1983). "Source Parameter Inversion of a Reservoir-Induced Seismic Sequence: Lake Kariba, Africa (1863 September)," *Geophys. J.R. Astr. Soc.*, **74**, 819-841.

Attenuation of Fundamental- and Higher-Mode Surface Waves at Intermediate Periods

Brian J. Mitchell, J.J. Chen and B. Mandal

Summary

Apparent Q_β in the crust, as well as its frequency dependence, exhibit strong regional variations. In studies to date, both Q_β and its degree of frequency dependence have been found to be smaller in regions which have undergone recent tectonic activity than they are in more stable regions.

Conclusions and Recommendations

Surface waves at intermediate periods, from about 5 to 100 s, have been used extensively to determine the anelastic properties of the crust and upper mantle. In order to obtain realistic models of shear wave Q (Q_β), it is important to have reliable attenuation data in which the effects of source complexities and lateral variations in Q structure have been minimized. The two most commonly used methods for obtaining attenuation data are (1) the two-station method in which spectral amplitudes are measured at two seismographs which lie on a common great circle path through an earthquake epicenter, and (2) a method in which theoretical amplitudes for known sources are compared to spectral amplitudes observed at several seismographs surrounding an earthquake or explosion source. In the two-station method, it is usually assumed that source effects are removed by taking comparative measurements at two stations. In complex regions, such as the western United States, however, lateral refraction of surface waves, especially at shorter periods, is a commonly observed phenomenon. When that happens the spectral amplitudes observed at two stations do not correspond to waves which left the same portion of the radiation pattern of the earthquake. For earthquakes with a large strike-slip component, a difference of only a few degrees in azimuth can sometimes cause amplitudes to vary by nearly an order to magnitude. It is important therefore in using the two-station method to determine the particle motion of the waves of interest; fundamental-mode Rayleigh waves should, for instance, be retrograde elliptical and the plane of the

ellipse should lie along the path of propagation. Large deviations from predicted particle motion should indicate that the data are suspect. An example of a particle motion diagram which we routinely use appears in Fig. 1 where Love (transverse) and Rayleigh (elliptical) motion are clearly apparent.

The second method, that of matching observed and theoretical amplitude radiation patterns must be used with caution in regions across which Q varies laterally. In such cases, attenuation coefficient values may be either underestimated or overestimated, depending on the station configuration with respect to the source location and the lateral Q distribution.

A more recently developed method uses data recorded at a single station from a source with a known focal mechanism. This method avoids some of the difficulties described above, but assumes that the shape of the event source spectrum is approximately known.

Inversions of attenuation data at intermediate periods have yielded models of Q_β as a function of depth for several regions of the world (Osagie and Mitchell, 1983). The most recent inversions have been done for South America. Our work to date indicates that models for the stable and tectonically active portions of that continent can be taken to be typical for other stable and active regions. Figure 2 presents models for the stable portion of eastern South America and the tectonically active portion of western South America on the same diagram. The crust of the tectonically active region has much lower Q_β values than the stable region. This same result was found earlier for North America and appears to also be the case for the Indian sub-continent. The model for western South America also includes a zone of low Q values in the upper mantle, whereas the model for eastern South America does not. The differences in the models for the stable and tectonic regions of South America, both in the crust and mantle, are clearly required by the data. The same differences were found to occur beneath the stable and active regions of North America in earlier studies.

The surface wave attenuation data used for the determination of Q_β models are usually fundamental-mode data at periods between about 5 and 60-80 seconds. Using those data alone, it is not possible to determine whether or not Q_β varies with frequency in the crust or mantle. However, we can determine whether or not the models obtained from fundamental-mode data can produce the proper attenuation of higher-mode surface waves at short periods. There are compilations of Q for 1-Hz L_g waves in several regions of the world. It is now possible to routinely compute synthetic seismograms for the models described above at several distances and to measure the fall-off of amplitudes with distance to obtain Q for theoretically produced L_g in exactly the same way that Q is

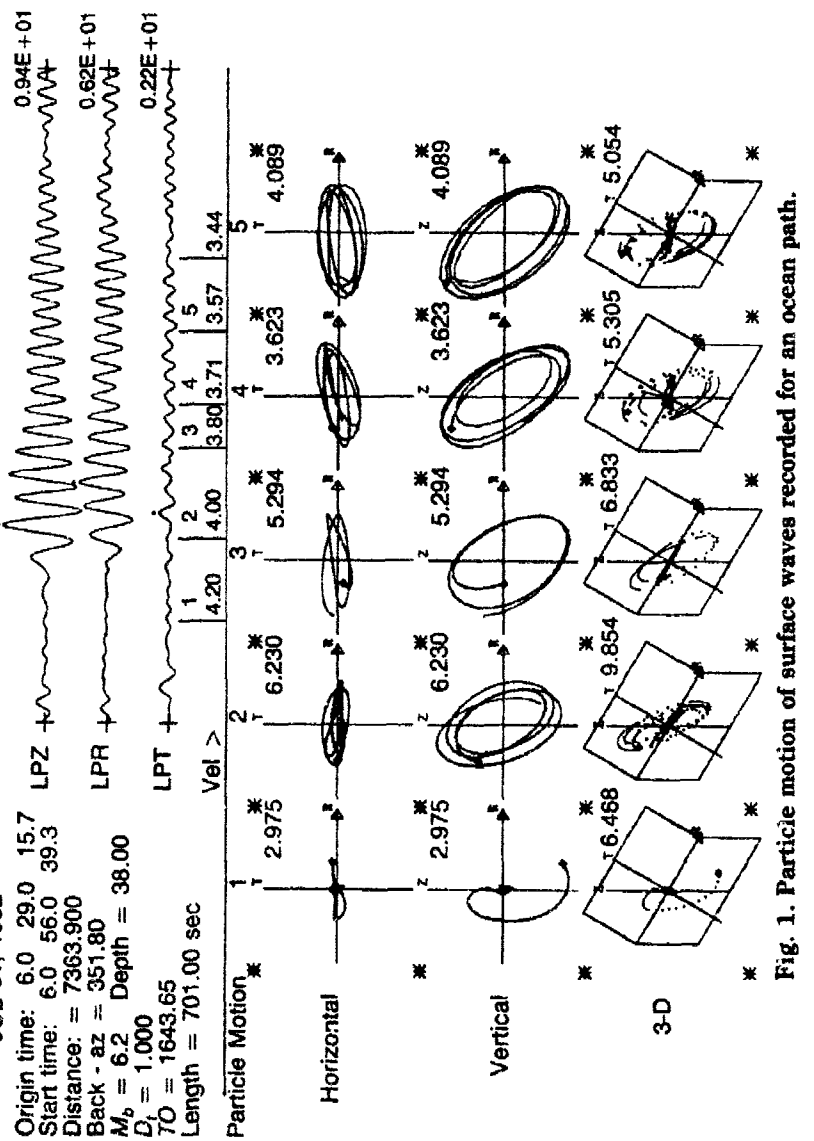

Fig. 1. Particle motion of surface waves recorded for an ocean path.

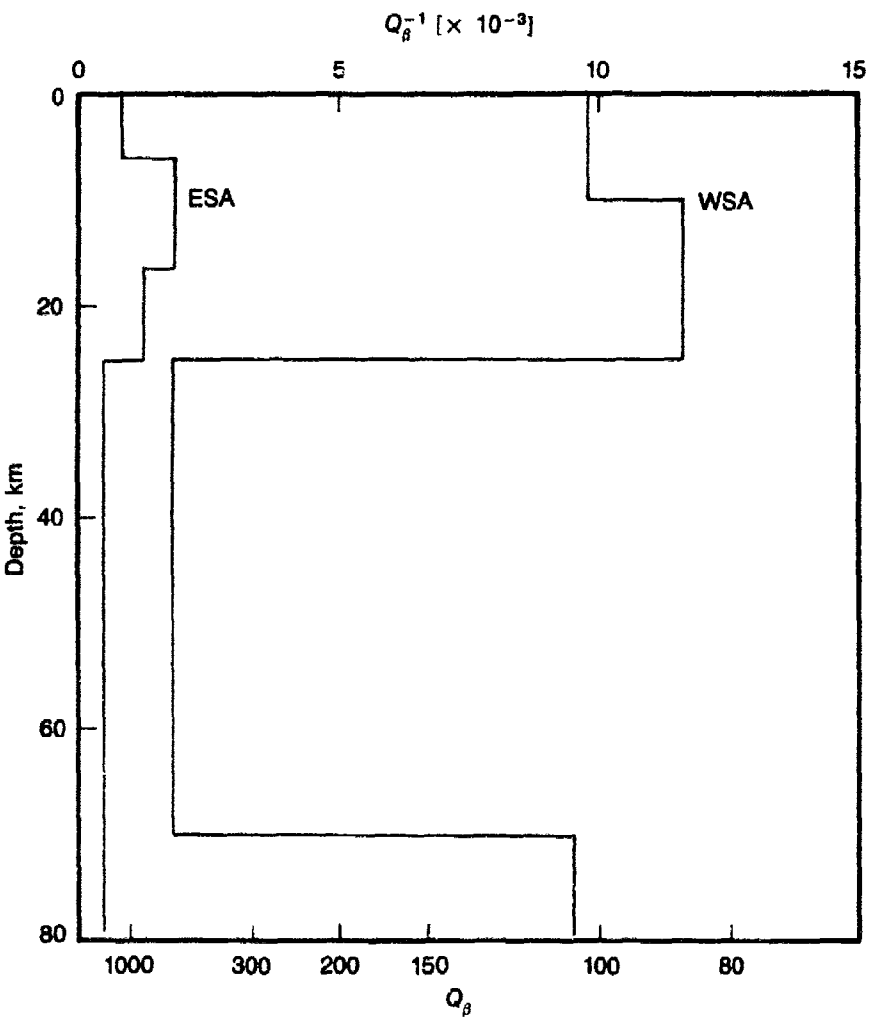

Fig. 2. Models of anelasticity for eastern and western South America. From Osagie and Mitchell (1983).

obtained from observed L_g waves. The Q value obtained from the synthetic seismograms for the model of eastern South America is given in Fig. 3 along with synthetics computed at five distances. That value (480) can be compared with an average observed value of about 800 for that region. In order to obtain a Q_β value of 800 from the computed L_g waves to agree with observed values, we would have to increase Q_β in the crust at a frequency of 1-Hz compared to what it is at the lower frequencies used to obtain the model of eastern South America in Fig. 2. Thus Q_β

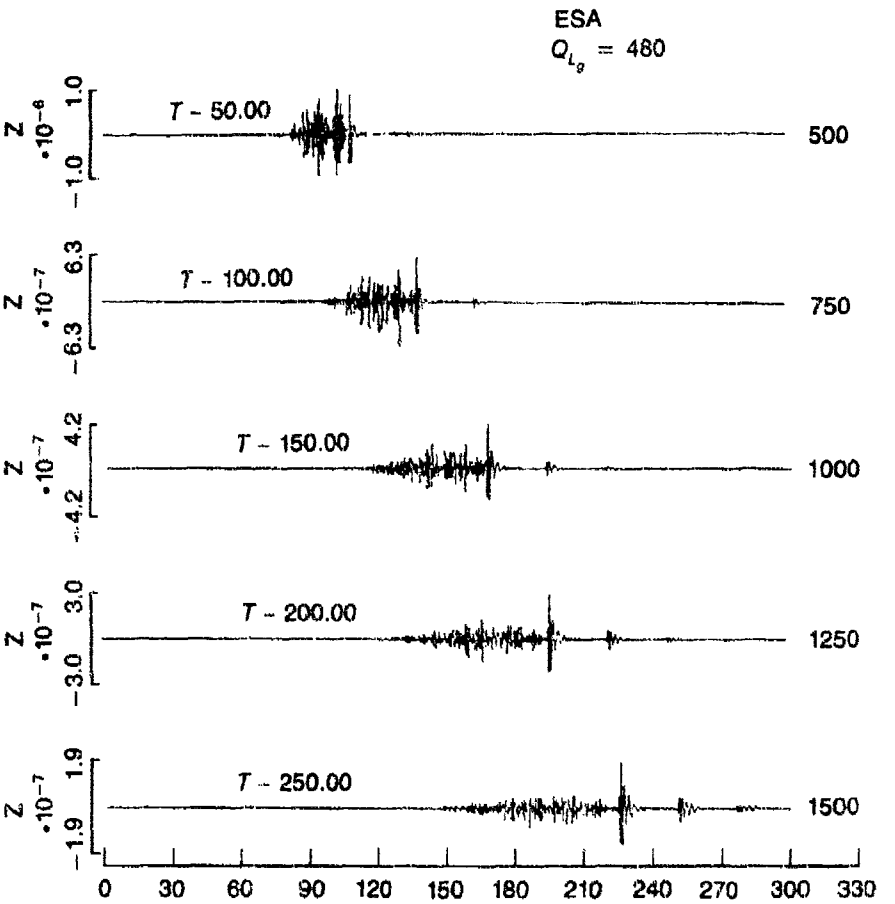

Fig. 3. Synthetic seismograms for paths across eastern South America for the phase L_g as recorded on short-period WWSSN seismographs.

appears to depend on frequency in eastern South America, at least at frequencies near 1-Hz.

In western South America, however, the Q values obtained from the fall-off of amplitudes of theoretical seismograms (290) is nearly the same as the average Q value observed there for L_g (200-340). This similarity indicates that the frequency dependence of Q_β observed in the crust of eastern South America either does not occur or is too small to measure in western South America. A similar result was found previously for the stable and tectonically active portions of North America.

The frequency dependence of Q_β in the crust and its regional variation are well-documented in only a few regions of the world and only at frequencies near 1-Hz. There is little precise knowledge of the degree

of frequency dependence of Q_β in the crust or of the manner in which it changes with frequency. For instance, in eastern North America, Q_β might vary as $\omega^{0.3}$ for all periods between 1 and 50 s or it might be independent of frequency at periods greater than 4 or 5 seconds and vary as $\omega^{0.5}$ at shorter periods; either situation would explain observed surface wave attenuation (Mitchell, 1980). In order to obtain the necessary data to study the frequency-dependence of Q_β in detail it will be important in future studies to obtain high-quality broad-band higher-mode data in several different tectonic settings. In this way we may perhaps be able to relate Q_β to the tectonic evolution of the crust in different regions. We should then be able to predict Q values in any region which can be reliably applied to yield estimation.

References

Mitchell, B.J., "Frequency Dependence of Shear Wave Internal Friction in the Continental Crust of Eastern North America," *J. Geophys. Res.*, **85**, 5212-5218, 1980.

Osagie, E. O., and B.J. Mitchell, "Regional Variation of Q_β and Its Frequency Dependence in the Crust of South America," in Semi-Annual Report, DARPA/AFOSR, 30 Nov. 1983, *Attenuation of Seismic Waves at Regional Distances*, 30-45, 1983.

Techniques for Modeling of L_g Propagation Across Regional Transition Zones Using Finite Elements and the Representation Theorem

Janice Regan and David G. Harkrider

Summary

Using a finite element form of the Seismic Representation Theorem, SH waves or L_g mode sums are inputted into and propagated across a 2-D grid model of transition zones. The input is the SH displacement history at depth over two consecutive vertical rows of grid elements. The input histories are calculated from either theoretical solutions or from an overlapping finite element grid closer to the source. The latter form of input allows "boot-strapping" of overlapping grids across the transition zone. This reduces the lateral number of grid elements and reflections from the far edge of the grid.

Introduction

The modeling of surface waves crossing regional transition zones such as ocean-continent margins has been done in the past with finite difference or element codes in terms of the effect of these margins on individual modes. That is, a single mode is input into the code and the resultant wave on the other side of the margin is interpreted in terms of the conversion into other modes. This may be informative in a modal sense but it is not particularly relevant to the propagation of L_g waves across these regions since the L_g wave train is probably a composite of many higher modes. Using a Finite-Element code (FE) coupled by the Representation Theorem (RT) to modal surface wave propagation codes, we propose to determine the mechanism for annihilation or enhancement of L_g waves as they cross crust and upper mantle modals of regional transition zones.

Previous studies, using finite difference or element codes, have concentrated on mode conversion, both reflection and transmission, for normal incidence across crust and upper mantle models of transition regions as complicated as down-going slabs. The input to these code calculations were single incident modes and the output waves were analyzed in terms of mode conversion.

For our purposes, the decomposition of the FE calculation into modes is an unnecessary step. What we are primarily interested in is the effect of the transition region on the sum of modes representing the L_g wave. This can be accomplished using the Representation Theorem and its finite element equivalent. For the finite element code the RT surface integral can be replaced by specifying the time step displacement history on two consecutive nodes normal to and spanning the original surface. This double surface eliminates the need for inputting the normal stress histories over the RT surface. As with other investigations involving finite transition zones, we will restrict ourselves to normal incidence and use the 2-D finite difference code SWIS. The input will be determined from the displacement field at depth obtained from mode sum calculations. The resulting displacement stress field on the other side of the grid will then be propagated using 2-D Green's functions approximate for that side of the propagation path. The Green's functions with their weighting as specified by the RT algorithm are themselves modal sums.

The use of the RT not only allows one to look at the effect of one transition zone but also to investigate propagation across a sequence of transition zones such as continent ocean then ocean continent. It also can be used to isolate the effect on individual modes by using a single mode Green's function on the FE output.

Accomplishments

An option to enable seismograms to be used as input, constraining the motion of specified nodes with time, has been added to SWIS code. This option has two main uses. First, it can be used to simulate a grid larger than the grid being used. Second, it can be used to couple energy from a source distant from the edge of the grid, to the starting edge of the finite element grid.

Figure 1 shows how a grid of a given size can be used to simulate a larger grid by using seismogram input. In the upper drawing a 50 × 50 node grid is illustrated. A line force, normal to the plane of the figure, is applied to the first node in the nth row of nodes. Its location is denoted in the figure as a crossed circle. The two adjacent vertical lines within the grid represent the sixteenth and seventeenth columns of nodes where intermediate seismograms are recorded for later use as input in the second step of the procedure. The single vertical line represents the thirty-first column of nodes where final seismograms representing results for a 50 × 50 grid are recorded. The lower drawing shows a second 50 × 50 grid used for the second step of the procedure. For this step the intermediate seismograms recorded in step 1 are used as input to columns one and two of the grid. The completeness of the representation

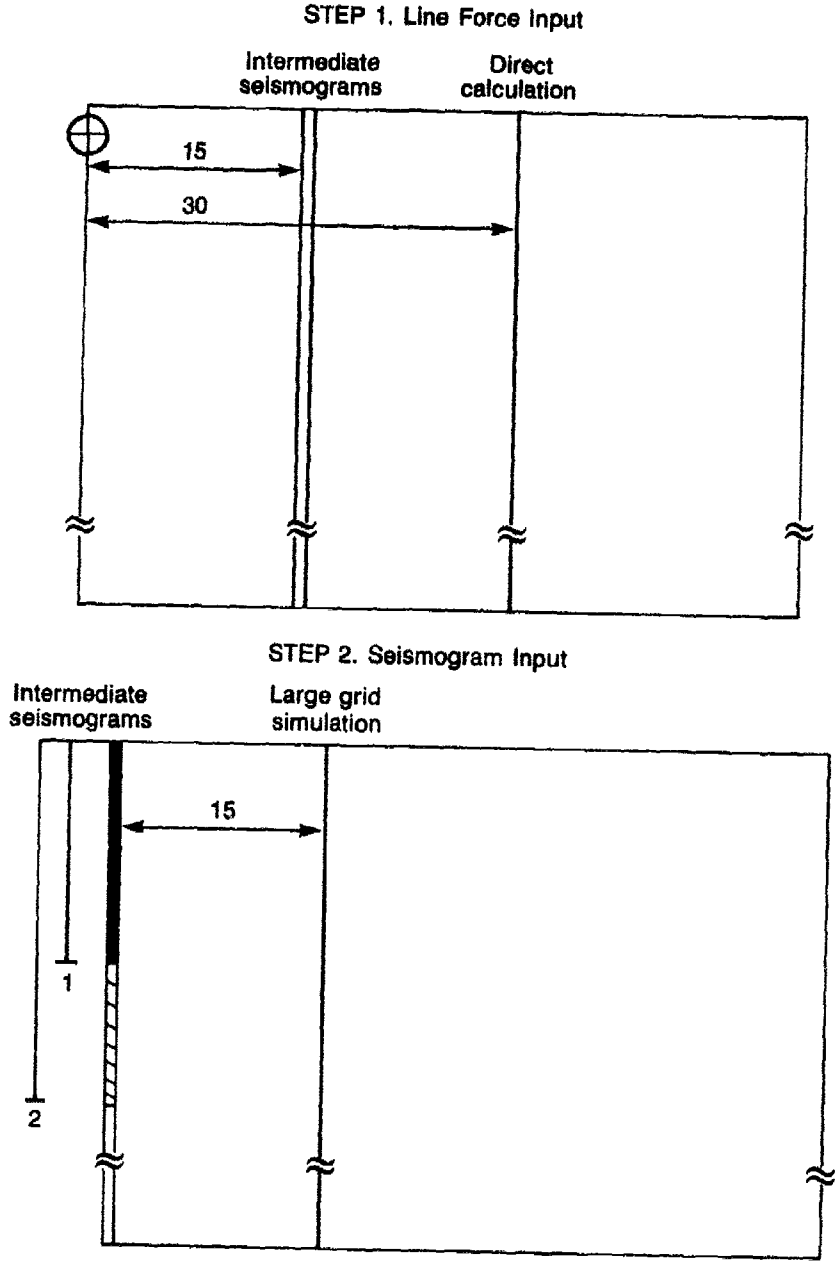
STEP 1. Line Force Input
Intermediate seismograms
Direct calculation
15
30
STEP 2. Seismogram Input
Intermediate seismograms
Large grid simulation
15
1
2

Fig. 1.

of the original source is based on the representation theorem. The single vertical line within the grid represents column sixteen, where final seismograms for the large grid simulation are recorded. The total propagation distance for the large grid simulation, summed over both steps, is equal to the distance propagated in the direct calculation.

Figure 2 shows a comparison of the seismograms generated by a direct calculation and by a large grid simulation. The monitor number increases with depth. The initial waveforms are almost identical, but a second pulse resulting from reflection off the end of the grid is seen for the direct calculation only. The reflection is not seen on the large grid

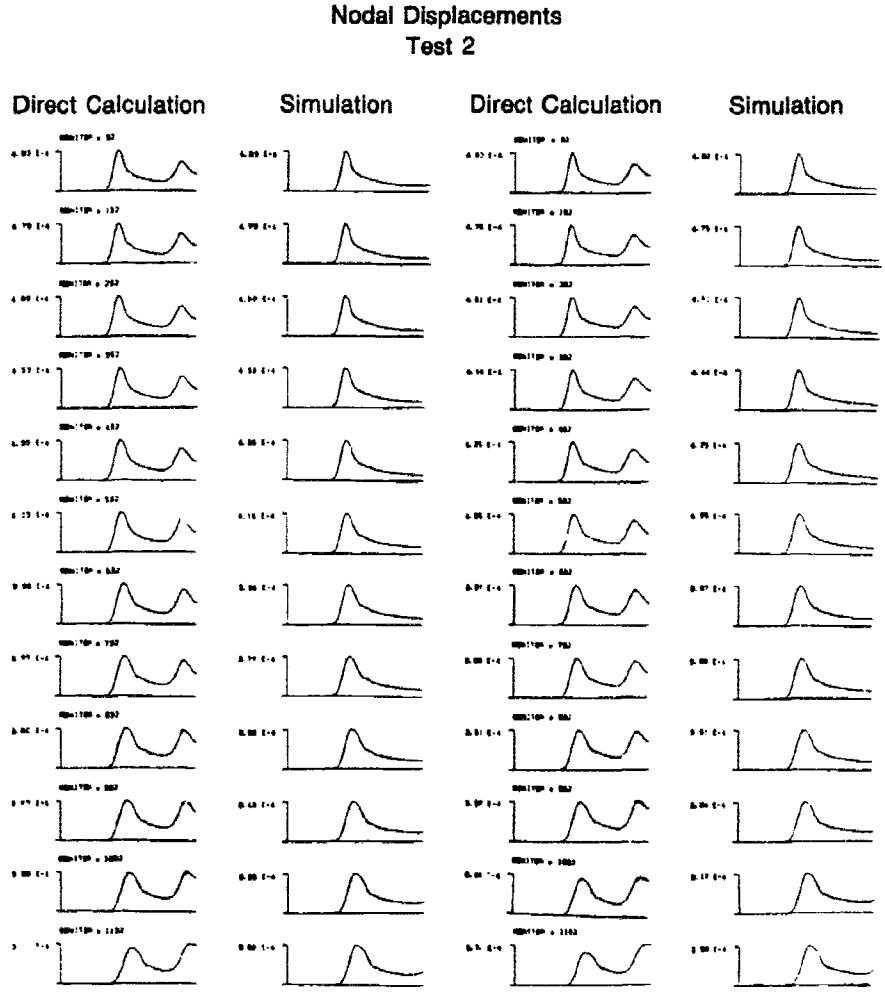

Fig. 2.

simulation because the grid has been extended fifteen element widths moving the reflection to a time later than the end of the seismogram. It should be possible to shift at least half the width of the grid without worrying about reflections from the end of the grid. In that case two small grid runs of the finite element would be faster than one run with an expanded grid. Thus, the large grid simulation would be worthwhile.

In order to avoid contamination by reflection from the bottom of the grid, and to minimize the number of seismograms input, not all of the intermediate seismograms were used in the large grid simulation. Two tests of the accuracy of this truncation were made. TEST 1 used the uppermost fifteen pairs of nodes, and TEST 2 used the uppermost twenty-five pairs of nodes. The amplitude ratios for each of the tests as a function of the row in the finite element grid are plotted in Fig. 3. The amplitude ratio, A, is defined as

$$A(\text{node } i) = \frac{\textit{AMPLITUDE OF DIRECT CALCULATION (node } i)}{\textit{AMPLITUDE OF LARGE GRID SIMULATION (node } i)}$$

As expected the amplitude correspondence is better when more complete input is used. Considering Fig. 3, it is reasonable to assume that if results for n rows are desired, input of $n + 5$ rows of nodes would be adequate to produce amplitude correspondence within, at worst, a couple of percent.

Figure 4(a) shows how seismogram input can be used to couple energy from a distant source into the grid. Seismograms for an event one kilometer deep at a distance of fifteen kilometers from the edge of the grid were determined using a numerical calculation for the analytic 2-D half-space solution. The complete set of input seismograms contained a seismogram for each mode in columns one and two of the grid. Solution for sets of seismograms (direct solutions) at distances from the source corresponding to rows sixteen and thirty-one of the grid were also determined using this method. Using the input seismograms finite element solutions were calculated for all nodes in columns sixteen and thirty-one. Thus, the direct solutions can be compared to the finite element solutions.

If one wishes the direct solutions to correspond well to the finite element solutions the frequency content of the input and the damping coefficient used in the finite element calculation become important. To investigate the effects of these parameters the procedure above was completed for two sets of input seismograms. Both sets had triangular time functions, the first with a duration of .15 seconds, the second with a duration of .45 seconds. For each of these input sets the finite element code was use t damping. The following results were observed. First, if the

input seismograms contain frequencies higher than those that can be propagated through the finite element grid, then the grid acts as a low pass filter reducing the finite element solution's amplitude significantly. The correspondence of amplitudes and waveforms between the direct solution and the finite element solution for this situation is poor. Low pass filtering the direct solution will improve the waveform fit enormously and bring the amplitude ratios much closer to one (Fig's 4b and 5). Amplitudes and waveforms both correspond well when the input has no significant high frequency component. Secondly, if the finite element is run without damping the amplitudes produced are much too large, and in addition if high frequencies are present in the input spurious high frequency oscillations appear in the finite element solution. To remedy these problems

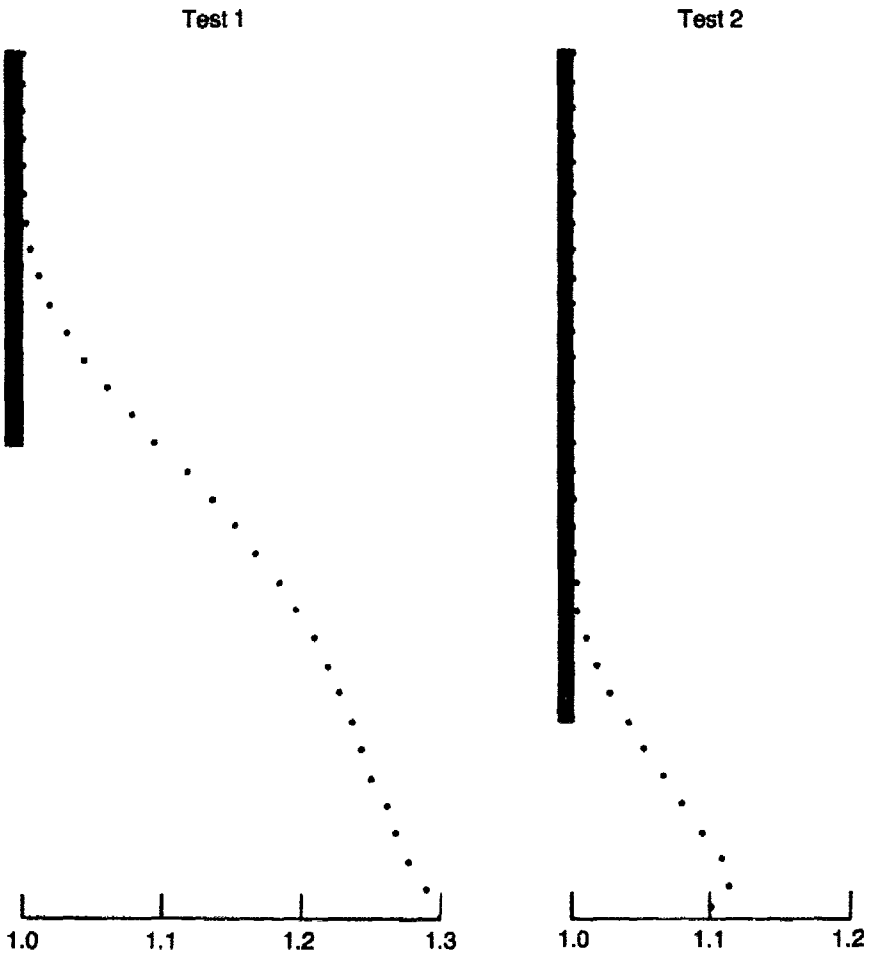

Fig. 3.

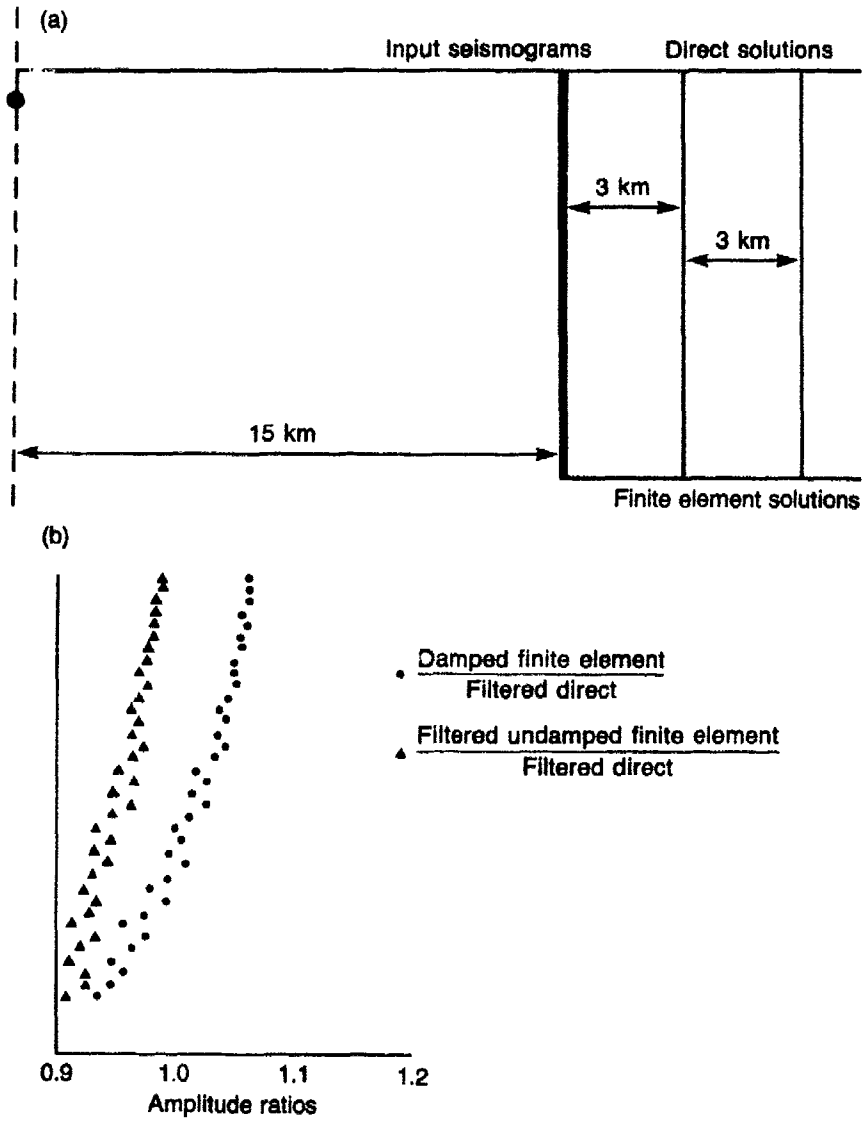

Fig. 4.

undamped finite element solution must be low pass filtered. The cutoff frequency should be at most the highest frequency that the grid can propagate. The amplitude and waveform correspondence of the filtered undamped finite element solution to the filtered direct solution is then excellent. Finally, the damping coefficient used in the finite element code is dependent on distance. Therefore, a single damping coefficient cannot produce correct amplitudes at a variety of distances. At the distance

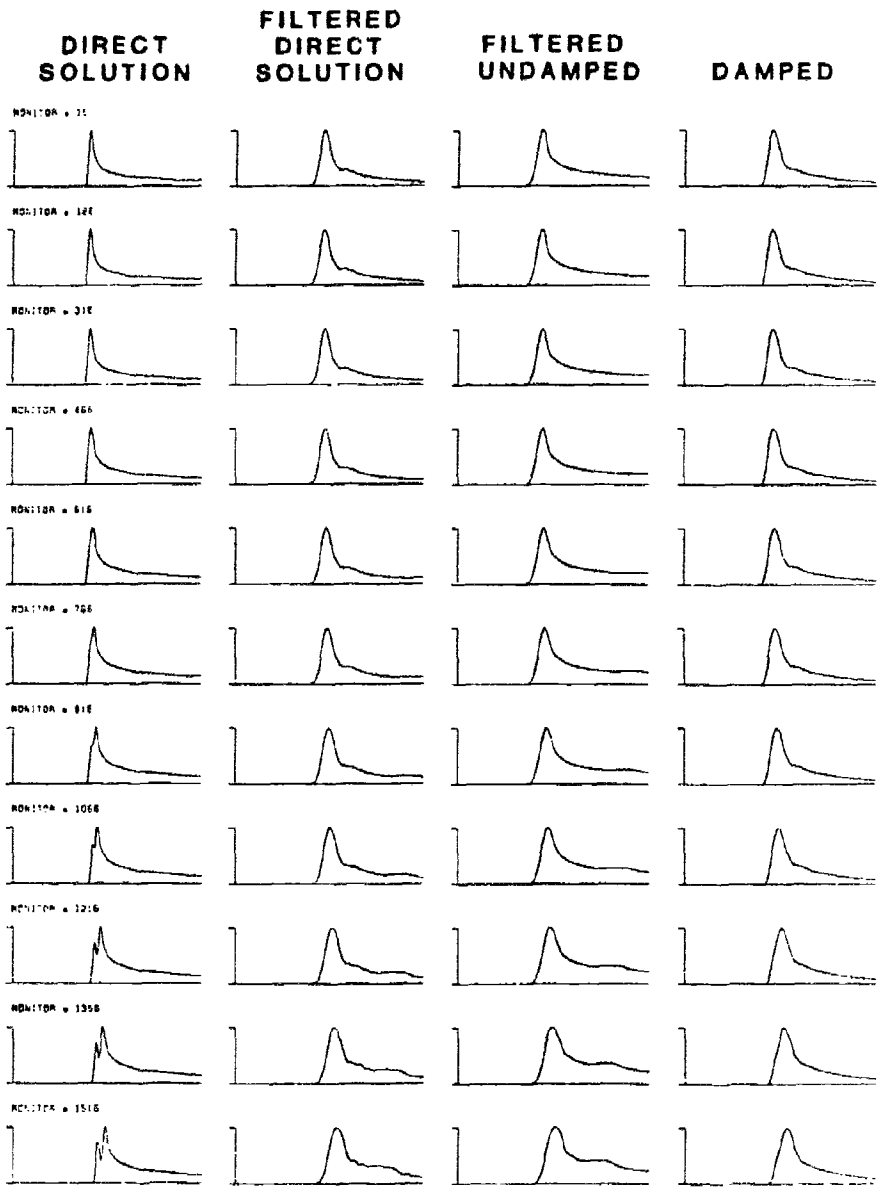
DIRECT SOLUTION
FILTERED DIRECT SOLUTION
FILTERED UNDAMPED
DAMPED

Fig. 5.

for which the coefficient is calculated, and within a few grid spacings of that distance, the coefficient produces finite element results that correspond very well with the direct solution. If the direct solution contains high frequencies the results correspond to the filtered direct results. However, as distance from the point at which the coefficient is calculated increases the amplitude ratios depart from one. Considering these effects the best combination of filtering and damping when a range of distances is to be used is to filter an undamped finite element solution. If theoretical results are available the filtered undamped solutions should be compared directly to them. If the theoretical results contain high frequencies they should be low pass filtered before being compared to the filtered undamped solutions. This approach should give the best correspondence to the theoretical results.

Conclusion

The modeling experiments described above indicate that this coupling technique will be successful in modeling realistic regions transition zones in the crust and upper mantle. We are proceeding with modal sum L_g wave synthetics input for a source 1000 km from the grid. The grid is being extended from a 50 × 50 to a 100 × 100 nodes. The size of the grid in the direction of propagation will be extended by the "bootstrapping" procedure when back reflections are primarily due to the grid boundaries and not the transition structure.

The Resolution of Free Surface Interactions from Near Source Seismograms

Brian W. Stump

Summary

Spall models which conserve momentum are quantified by near source observations and found to contribute ½ of near source peak velocities. Relative excitation of compressive and Rayleigh waves, near source, for varying source burial depths is determined.

Introduction

The material property free surface above an explosive source can change the radiated energy in at least three ways. The first is the simple reflection of the *P* wave. The second, a subset of the first, occurs when the compressive wave leaving the source interacts with the tractionless free surface and reflects back into the half space as a tension wave. This reflection may fail the material if the overburden stress, tensile strength, and upgoing compressive wave tail are overcome. This tensile failure then imparts momentum to near surface layers which execute ballistic free fall until reimpacting with the parent body. This process takes energy out of the spherical explosion which may be minimum phase, delays it in time, and reradiates the energy with at least cylindrical symmetry.

The third effect of the free surface proximity to an explosive source is the coupling of the explosion into elastic radiation and the partitioning of this radiation into body and surface waves.

Both of the latter two effects have been studied utilizing near source observations and synthetic seismograms. In order to obtain a robust data set for the study, the focus here is upon a set of chemical explosions detonated in alluvium. The geometrical relation of these tests to the free surface is given in Fig. 1. For reference the CHEAT explosion, 115 kg, is the fully contained event at 11.5 m depth of burial. The instrumental array close in to these shots is typified by the array for CHEAT in Fig. 2. In addition to these gages three component accelerometers were fielded out to beyond 200 m for all tests.

Spall

Previous models designed to quantify the effect of near surface tensile failure as a source of elastic radiation have replicated the process

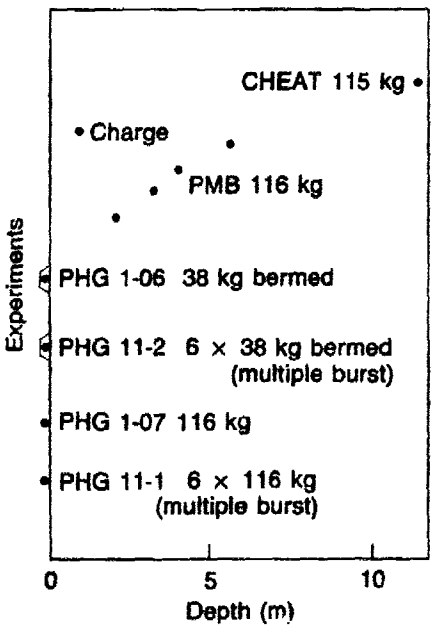

Fig. 1. Charge geometry for the PMB, PHG and CHEAT tests.

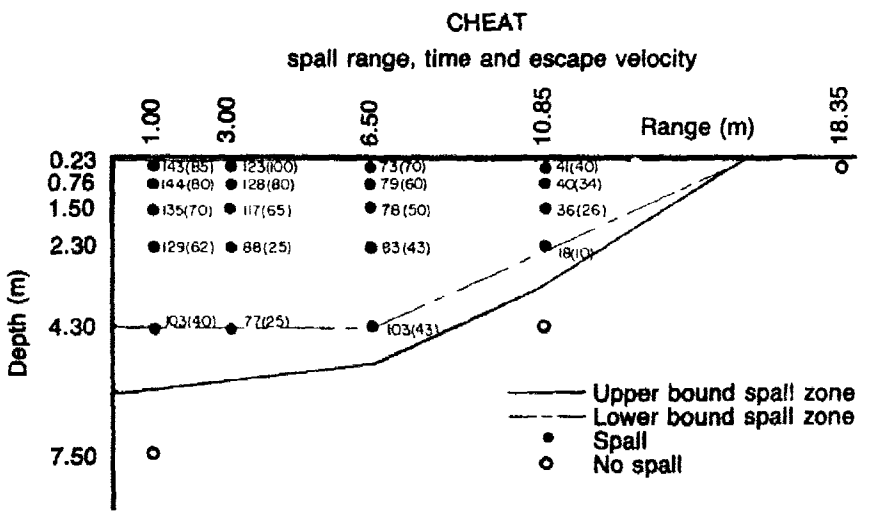

Fig. 2. The close-in instrument array for the CHEAT experiment. The spalled gages are marked. Spall dwell time in ms and escape velocity in cm/sec (parenthesis) is given for each gage.

as a vertical point force which failed to conserve momentum (Viecelli, 1973; Springer, 1974; and Sobel, 1978). Recently, point force models which include spall initiation, gravitational rebound, and spall slapdown have been developed which conserve momentum (Day *et al.*, 1983). We have taken this conservative vertical point force model and modified it to include the temporal variation of spall initiation and slapdown as determined from the observational data in the nonlinear regime (Fig. 2).

Constrained by the propagation of spall initiation quantified in Fig. 2 we introduce a smooth time function to replicate the finite time required for the total mass to spall. Since we wish to model accelerograms which are observationally smooth, we impose a continuous first and second order derivative on the spall mass time function:

$$M_s(t) = M_T \left(\frac{6t^5}{T_{sr}^5} - \frac{15t^4}{T_{sr}^4} + \frac{10t^3}{T_{sr}^3} \right) \left(H(t) - H(t - T_{sr}) \right) \quad (1)$$

where $M_s(t)$ is the spall mass, M_T is the maximum spall mass, and T_{sr} is the spall rise time constrained by the observational data. Spall slapdown is assumed to follow the same time function to yield a symmetric source pulse. Once spall has occurred the material is in ballistic free fall for a time $T_s = 2\,V_o/g$ where V_o is the initiation velocity of spall (Fig. 2) and g is the acceleration of gravity. The total vertical point force model of spall for $T_s = 108$ ms and $T_{sr} = 56$, 108 ms is given in Fig. 3 ●. The integral of the point force ○ illustrates that total momentum is conserved by this smooth model. The equivalent vertical body force when convolved with the Green's function for the material of interest will give the motion from spall.

$$U_k(\mathbf{x}'; t') = G_{k3}(\mathbf{x}'; t', x_3, t) \otimes f_3(x_3, t) \quad (2)$$

$f_3(x_3,t)$ can be calculated if $M_s(t)$ is known from near source nonlinear motion observations (forward calculation). Given a set of observed seismograms, $U_k(\mathbf{x}', t')$, and the propagation path effects, $G_{k3}(\mathbf{x}', t'; x_3,t)$, a set of linear equations such as (2) can be solved for $f_3(x_3,t)$ (inverse solution). Both the forward and inverse determination of $f_3(x_3,t)$ has been completed for the PHGI-06 explosion in Fig. 1. Comparison of the two sources is given in Fig. 4. The two determinations agree very well in phase and amplitude beyond 40 ms. Prior to this time the directly coupled energy from the explosion is important and not included in the spall forward model.

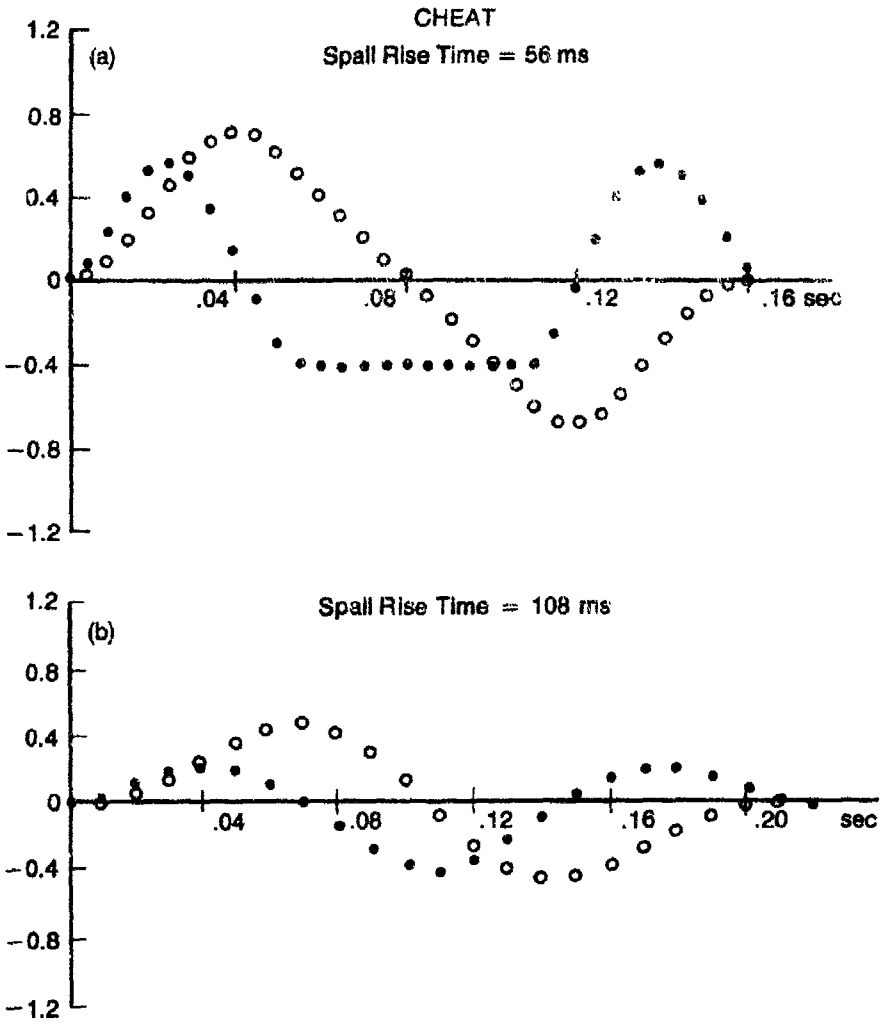

Fig. 3(a), (b). CHEAT spall model for equivalent body force (solid circles × 10^{13} dynes) and their integrals (open circles × 10^{11} dyne-sec) for rise times of (a) 56 ms and (b) 108 ms.

Based on the agreement between the forward and inverse sources for PHGI-06 which was a surface burst covered with a beam of sand, the spall model was used to calculate synthetics from the contained explosion CHEAT. In order to complete a total seismogram a Mueller-Murphy spherical explosion source was calculated in the form of a moment tensor. The complete motion becomes:

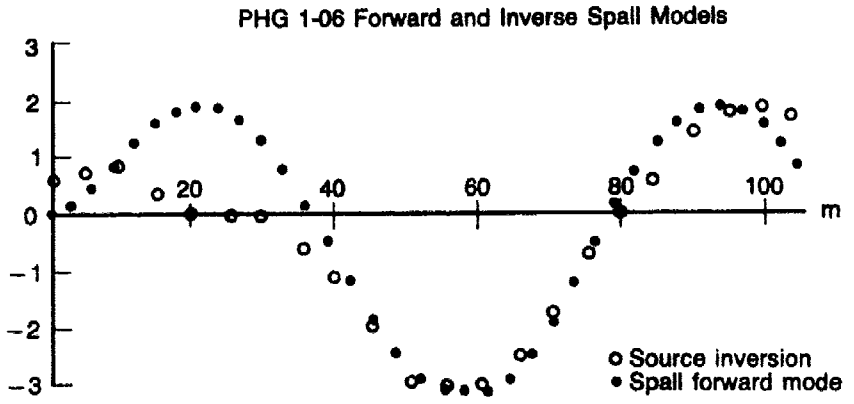

Fig. 4. The integral of the vertical source function for PHG1-06 (open circles) and the spall model prediction for PHG1-06 (closed circles). All values need to be multiplied by 10^{11} to yield dyne-sec.

$$U_k(\mathbf{x}';\, t') \;=\; G_{k3}\,(\mathbf{x}';\, t';\, x_3,t) \otimes f_3(x_3,t)$$
$$+\; G_{kij}\,(\mathbf{x}';\, t';\, \mathbf{0},\, o) \otimes M_{ij}\,(\mathbf{0},t) \qquad (3)$$

Comparison of near source velocity waveforms from the first and second terms of Eqn. 3 indicate that the two contributions are approximately equal. One reason for this equivalence is that the spall source is much shallower than the spherical explosion and thus at near source distances a source rich in Rayleigh energy.

Comparison of the forward model synthetics with observational data from CHEAT (Figs. 1 and 2) is given in Fig. 5. Although the phasing and amplitudes from this simple model (elastic half-space propagation) are not in exact agreement with the observations, the fit with no interactions is good. The body waves are matched by the spherical explosion while the late arriving, large amplitude surface waves result from the vertical point force spall source.

Source Coupling

Utilizing the PMB depth of burial data we have attempted to quantify source coupling and relative generation of body and surface waves from these sources in the near source region. The basis of this study has been a set of velocity waveforms from the explosions.

To date, work has focused on the relative and absolute size of body and surface waves from these sources at ranges varying from 10's of meters to a few tenths of a kilometer. A summary of the data at the 73 m

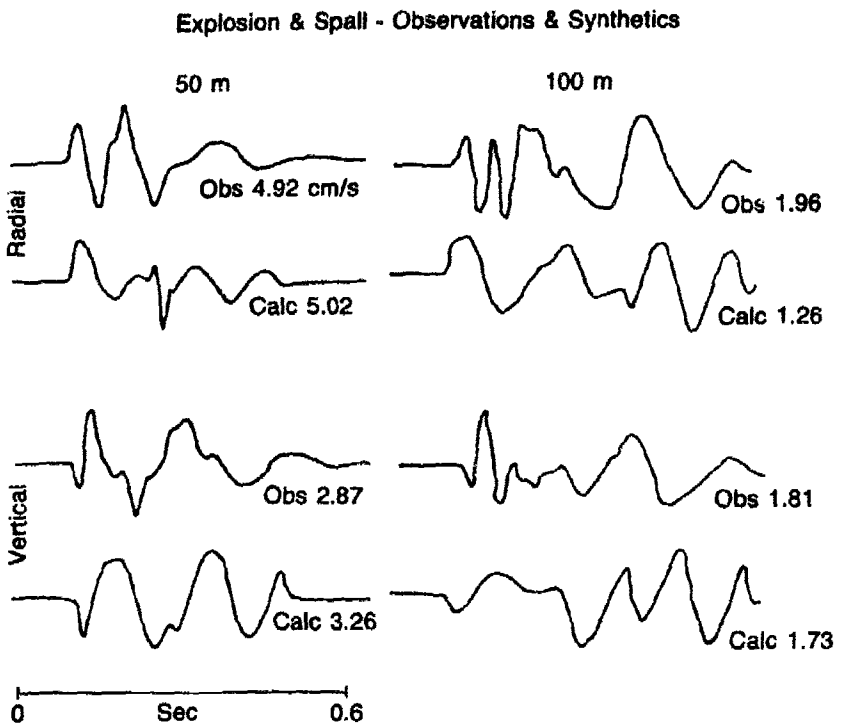

Fig. 5. Two characteristic observations from the CHEAT experiment at 50 and 100 m. Synthetic seismograms consisting of the explosion and spall sources are also given.

range is given in Fig. 6. The P wave amplitudes increase by a factor of four for the range of source depths, Rayleigh wave amplitudes increase over the first couple meters of source depth and then decrease beyond this point. The geometry of the source with respect to the Rayleigh wave excitation function seems to dominate over the increased coupling with burial depth.

Conclusions

Both forward and inverse models of spall in the near source region indicate that the process can be quantified by simple conservative vertical point force models. Extension of these models to buried sources yield spall velocity waveforms which are comparable in size to the purely spherical source records. The reason for this equivalence is the large amplitude Rayleigh waves from the shallow spall source.

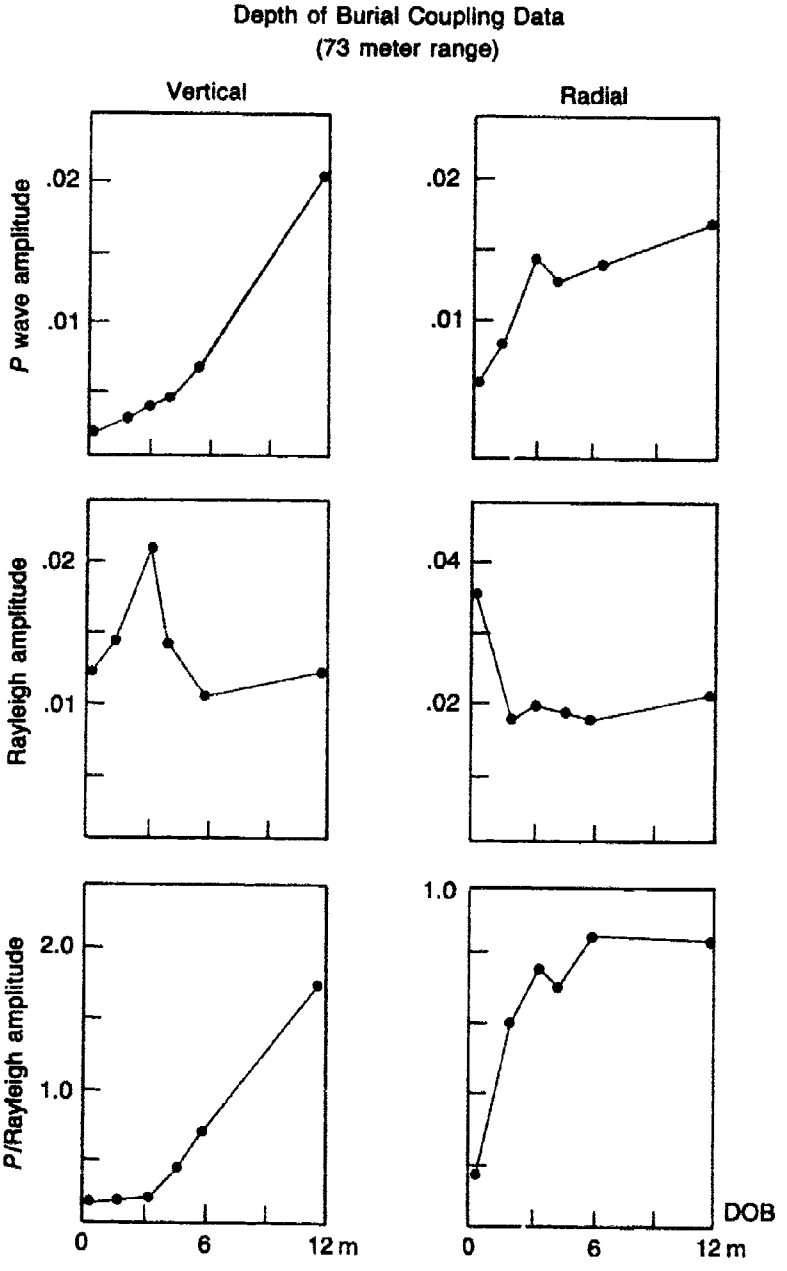
Depth of Burial Coupling Data
(73 meter range)
Vertical
Radial
P wave amplitude
.02
.01
.02
.01
Rayleigh amplitude
.02
.01
.04
.02
P/Rayleigh amplitude
2.0
1.0
1.0
0
6
12 m
0
6
12 m
DOB

The effect of source burial depth on coupling is most dramatically observed on near source body waves where a four fold increase in velocity is observed. Surface waves on the other hand appear to be controlled by the free surface boundary condition and thus decay as the source is buried more deeply.

References

Day, S.D., N. Rimer, and J.T. Cherry, 1983. "Surface Waves from Underground Explosions with Spall, Analysis of Elastic and Nonlinear Source Models," *Bull. Seism. Soc. Am.*, **73**, 247-264.

Sobel, P.A., 1978. "The Effect of Spall on m_b and M_s, Teledyne Geotech Report SDAC-TR-77-12, Dallas, Texas.

Springer, D., 1974. "Secondary Sources of Seismic Waves from Underground Nuclear Explosion," *Bull. Seism. Soc. Am.*, **64**, 581.

Viecelli, J.A., 1973. "Spallation and the Generation of Surface Waves by an Underground Explosion," *J. Geophys. Res.*, **78**, 2475-2487.

Three-Dimensional Ultrasonic Modeling of Rayleigh Wave Scattering

M. Nafi Toksöz and J.T. Bullitt

Abstract

The effects of topographic features on Rayleigh wave propagation and scattering are investigated in the laboratory using ultrasonic models. Starting from simple steps, different topographic features are modeled. The effects of these features on Rayleigh wave transmission and scattering are examined as a function of wavelength and as a function of angle of incidence. In general, backscattered or reflected Rayleigh waves are small, compared to transmitted waves. However, a significant fraction of the Rayleigh wave energy is scattered into body waves. At oblique incidence angles transmission coefficients (transmitted energy/incident energy) computed from spectral ratios vary strongly with incidence angle; at wavelengths equal to twice the step height the transmission coefficient ranges from approximately 5% at normal (90°) incidence to 50% at 15° incidence, for the case of a vertical step. The balance of the energy is distributed among the scattered phases. At each angle transmission coefficients strongly vary with frequency. Because of phase shifts, the wave train is distorted. Significant waveform distortion occurs also in the case of a tapered step. Converted and reflected phases generated at the upper edge of the step are suppressed when the upper edge is rounded. The effect of the steps on the apparent dispersion of Rayleigh waves is demonstrated by convolving synthetic dispersed wavetrains with the model seismograms. Some features of crustal Rayleigh waves commonly attributed to multipathing in the Earth may be due to scattering effects.

Introduction

The problem of Rayleigh wave scattering in two dimensions by simple structural discontinuities has been examined in the last two decades using a variety of experimental techniques (*e.g.*, Knopoff and Gangi, 1960; Lewis and Dally, 1970). The problem of Rayleigh wave scattering in three-dimensional structure has not, however, received the same systematic study. Complex scale models of realistic three-dimensional structures have been used in ultrasonic experiments to investigate gross features

of the effects of surface topography on Rayleigh wave propagation (*e.g.*, Chamuel, 1982). Because of the complexity of such models, however, subtle features in the waveforms are easily obscured. It is difficult to make meaningful quantitative measurements of scattering phenomena in such complex (*i.e.*, realistic) models, in which particular features of the waveforms cannot be readily associated with corresponding structural features. An important first step towards an understanding of scattering in three-dimensional models is therefore the investigation of wave propagation in simple models of canonical form. This report describes observations of Rayleigh wave propagation across simple step and ramp structures in a three-dimensional model.

Experimental Method and Results

The model used in this study consists of a solid block ($8 \times 8 \times 4''$) cut from 6061T6 aluminum plate. Steps of various height and geometry are milled into one of the large faces (Fig. 1).

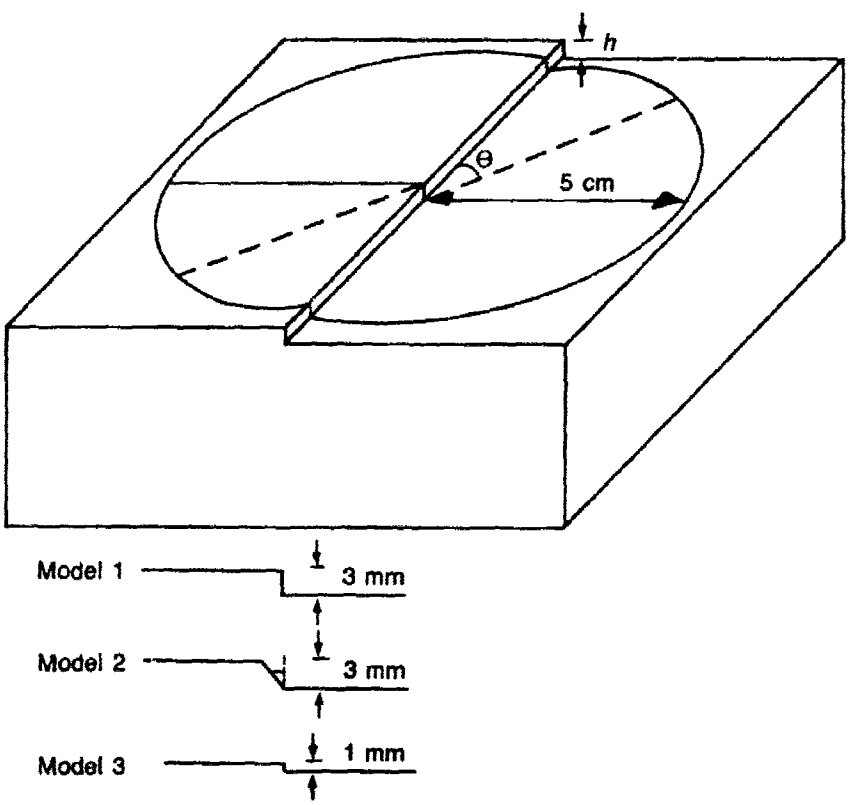

Figure 1. Geometry of the models used in this study. The inset shows cross sections of the steps used in the models.

The model used in this study consists of a solid block (8x8x4") cut from 6061T6 aluminum plate. Steps of various height and geometry are milled into one of the large faces (Fig. 1).

The ultrasonic source and receiver each consist of a 2.25 MHz *P* wave transducer coupled to a lucite wedge. The geometry of the wedges is such that *P* waves generated by the transducer are critically refracted upon entering the aluminum block, thereby exciting Rayleigh waves in the aluminum with great efficiency. The radiation pattern of the transducer-wedge combination is highly directional—at an angle of 10° from the axis of the central lobe, peak energy is reduced to 25% the central peak energy. The combination of these features makes the transducer-wedge combination especially useful when working with a low-loss medium such as aluminum; attenuation can be neglected in the analysis of Rayleigh wave propagation, and the observed Rayleigh waves are uncontaminated by body waves multiplely reflected at the edges or bottom of the model.

Figure 2 (a) shows the signal recorded for a Rayleigh wave propagating across the smooth aluminum surface. Because a halfspace is non-dispersive to Rayleigh waves, this represents the response of the transducer-wedge source and receiver. Figure 2(b) shows the Fourier amplitude spectrum of the Rayleigh wave. Peak energy of Rayleigh waves traveling on the aluminum block (V_P = 6.4 km/sec; V_s = 3.2 km/sec; C_R = 3.0 km/sec) lies in the range 0.2-2.0 MHz. We consider this to be the usable bandwidth for the modeling experiments.

Three models have been used in these experiments:

Model 1: 3 mm vertical step;

Model 2: Tapered step, 60° slope, 3 mm height;

Model 3: 1 mm vertical step.

Seismograms of Rayleigh waves crossing the step in each model over a range of incidence angles were recorded and digitized. Incidence angle is measured from the direction of the strike of the step (Θ in Fig. 1).

Energy Transmission and Reflection

When the Rayleigh wave encounters the step some of the incident energy is transmitted through the step, some is reflected from the step, and some is converted to body waves. The fraction of incident energy which emerges from the step as reflected and transmitted energy was measured as a function of incidence angle. In general the efficiency of transmission through or reflection from a step depends on the length of a wavelength relative to the step height. In order to facilitate comparison of models with different step heights, therefore, wavelengths are normalized to the step height. The "normalized frequency," $\hat{f}$, is obtained

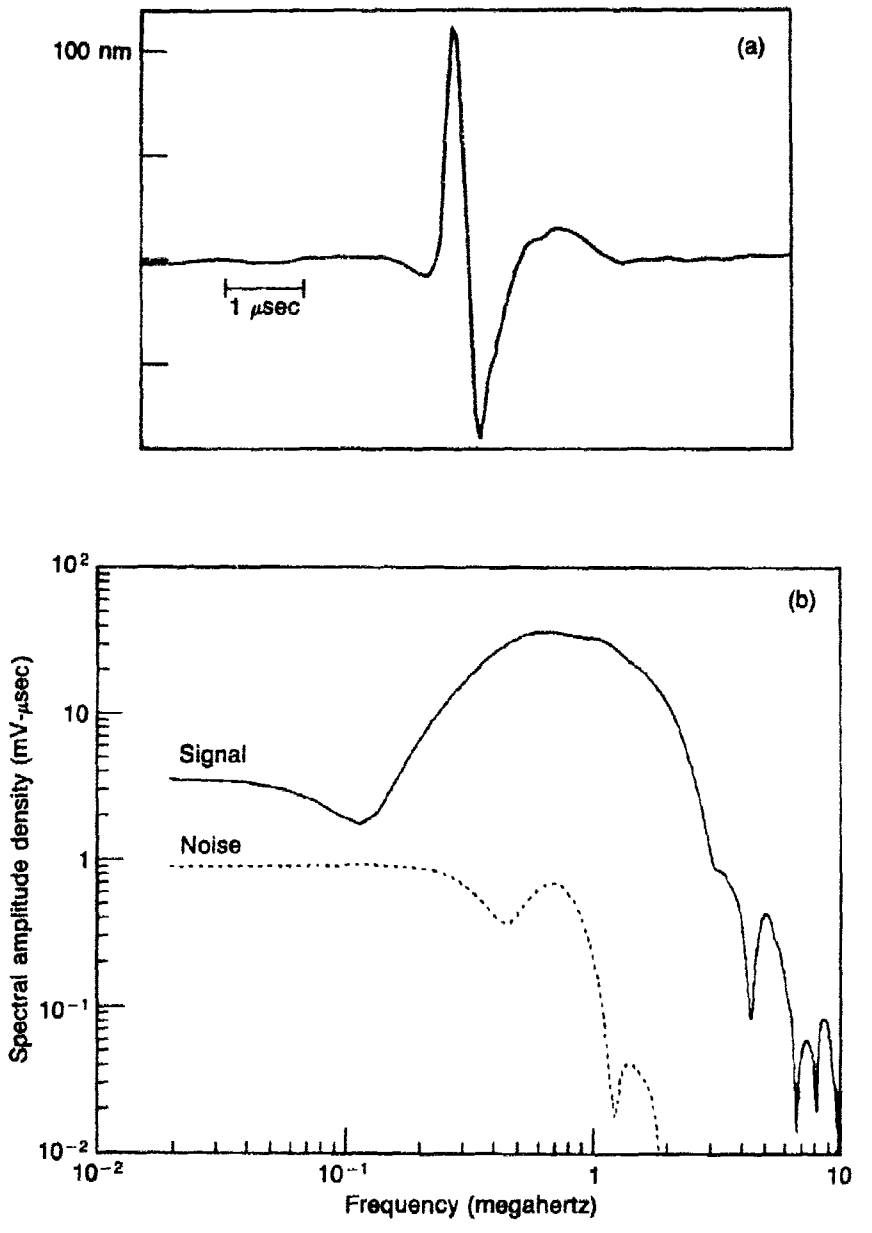

Fig. 2. (a) Rayleigh wave propagating across the aluminum surface in the absence of a step. (b). Amplitude spectrum of the Rayleigh wave shown in (a).

from the relation

$$\hat{f} = \frac{hf}{c} = \frac{h}{\lambda} \quad ,$$

where f is the frequency, c is the phase velocity, λ is the wavelength, and h is the step height.

The energy transmission coefficient, E_T, is defined here as

$$E_T(\hat{f}) = \left[\frac{A_T(\hat{f})}{A_0(\hat{f})}\right]^2 \quad ,$$

where $A_T(\hat{f})$ is the Fourier amplitude spectrum of the transmitted Rayleigh wave, and $A_c(\hat{f})$ is the amplitude spectrum of the Rayleigh wave propagating across the aluminum halfspace. The energy reflection coefficient, E_R, is defined in an exactly analogous way:

$$E_R(\hat{f}) = \left[\frac{A_R(f)}{A_0(\hat{f})}\right]^2 \quad ,$$

where $A_R(\hat{f})$ is the amplitude spectrum of the reflected Rayleigh wave.

Transmitted Rayleigh waves are recorded by keeping source and receiver at opposite points on a circle centered on the step (see Fig. 1). Reflected waves are recorded by placing source and receiver at equal angles from the normal to the strike of the step.

Model 1

Figure 3(a) shows seismograms of Rayleigh waves transmitted across the step in Model 1 for incidence angles ranging from 15° through 90° (normal incidence) in 15° increments. The small signal arriving about 1 μsec before the Rayleigh wave is an S wave excited at the step. Frequency-dependent scattering and phase shift are obvious at all angles of incidence. Figure 3(b) shows transmission coefficients for Rayleigh waves propagating in Model 1. At normal incidence ($\Theta = 90°$) the transmission coefficient agrees well with that obtained for a two-dimensional step using finite-difference calculations (Martel *et al.*, 1977). Near normal incidence E_T is less than 0.2 except when $\hat{f}$ is less than 0.2. This represents a loss of over 80% of the incident Rayleigh wave energy to converted body waves and reflected surface waves. The energy minimum near $\hat{f} = 0.5$ at normal incidence deepens and moves to higher frequency as the incidence angle decreases. In fact, while the curve is

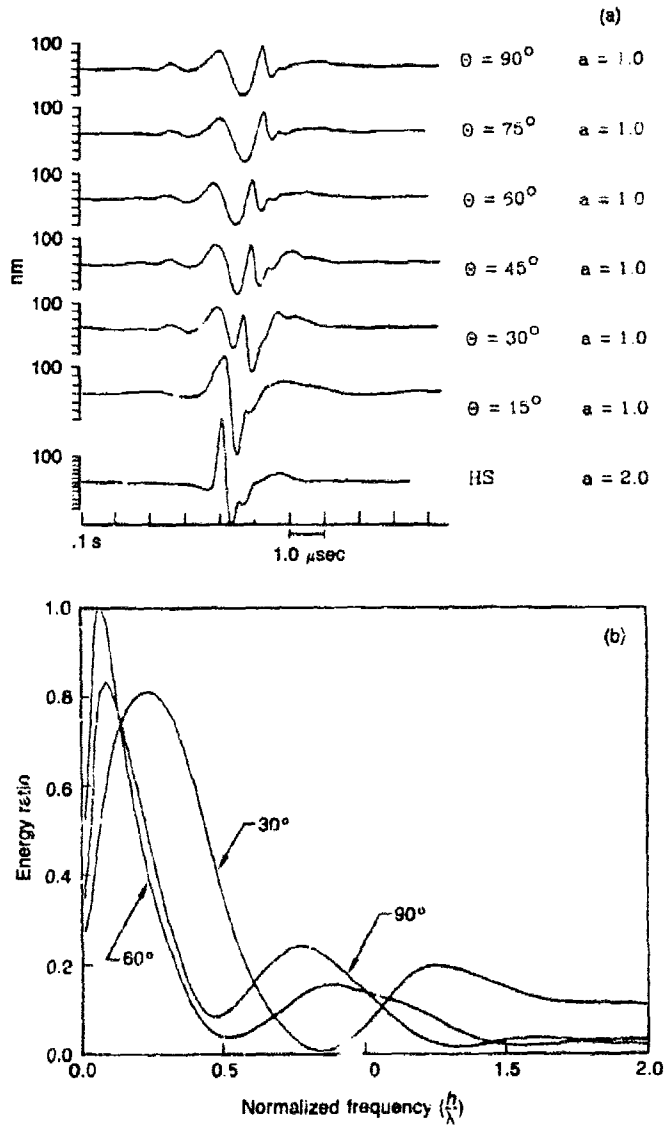

Fig. 3. (a) Waveforms of Rayleigh waves transmitted across the step in Model 1 (3 mm vertical step). Transmission is in the upstep direction. The small pulse arriving about 1.0 μsec before the Rayleigh wave is an *S* wave excited at the step. The bottom trace corresponds to the "normal path" path. The factor 'a' is the scaling factor by which the displays have been compressed vertically. Tick marks on the left indicate intervals of 10 or 50 mV, according to the number shown above the amplitude scale. (b) Transmission coefficients for the Rayleigh waves in (a). The horizontal axis is normalized frequency ($\bar{f} = \frac{h}{\lambda}$), where h is the step height and λ is the wavelength. Curves are shown for three angles of incidence.

similar in shape at each incidence angle, it tends to be pushed to higher frequencies as the incidence angle decreases. Thus, at shallow incidence angles the transmission coefficient is affected in the same way it would be were the step height increased. To grazing or near-grazing Rayleigh waves, then, the step appears higher than at steeper angles.

Figure 4(a) shows seismograms of Rayleigh waves reflected from the step, incident from the depressed side of the step. The seismograms are complicated by the existence of double reflections, the first from the lower edge of the step, the second from the upper edge. This double reflection has been observed in two-dimensional modeling experiments (*e.g.*, Nathman, 1980).

Figure 4(b) shows reflection coefficients at three incidence angles for Rayleigh waves traveling in the upstep direction. At normal incidence very little energy is reflected from the step. As the incidence angle becomes more grazing the reflected energy increases rapidly, especially for wavelengths approximately equal to three times the step height ($\hat{f} = 0.3$).

Figure 5(a) shows seismograms of Rayleigh waves reflected from the step, incident from the elevated side of the step. Reflection coefficients obtained from these seismograms are presented in Fig. 5(b). These reflections are generally stronger than the upstep reflections, but do not exhibit the same rapid increase with incidence angle.

In all the cases considered above, the character of the transmitted and reflected waveforms changes rapidly as the incidence angle decreases below about 30°. It is in the range 0° to 30° that the Rayleigh waves are observed to depart most strikingly from the waveforms predicted by finite-difference or other two-dimensional methods.

Model 2

Rarely in the Earth do we find structural discontinuities as severe as the one modeled in Model 1. To investigate the effect of a more gradual change of elevation the step was tapered to a slope of 60° from the horizontal (see Fig. 1). Seismograms and transmission coefficients of Rayleigh waves traveling across the ramp are shown in Figs. 6(a) and 6(b). Note the strong interference of phases, particularly at normal incidence [top trace, Fig. 6(a)]. The transmission coefficients for this model [Fig. 6(b)] are generally higher than those in the step model [Fig. 3(b)] at frequencies below $\hat{f} \approx 0.5$. The energy minimum near $\hat{f} \approx 0.9$ at normal incidence is considerably smaller than the corresponding minimum for the step model. Note that here the frequencies have been normalized to a step height of $h = 3.0$ mm; in fact, this normalization is arbitrary, as the slope of the ramp will also affect the scaling

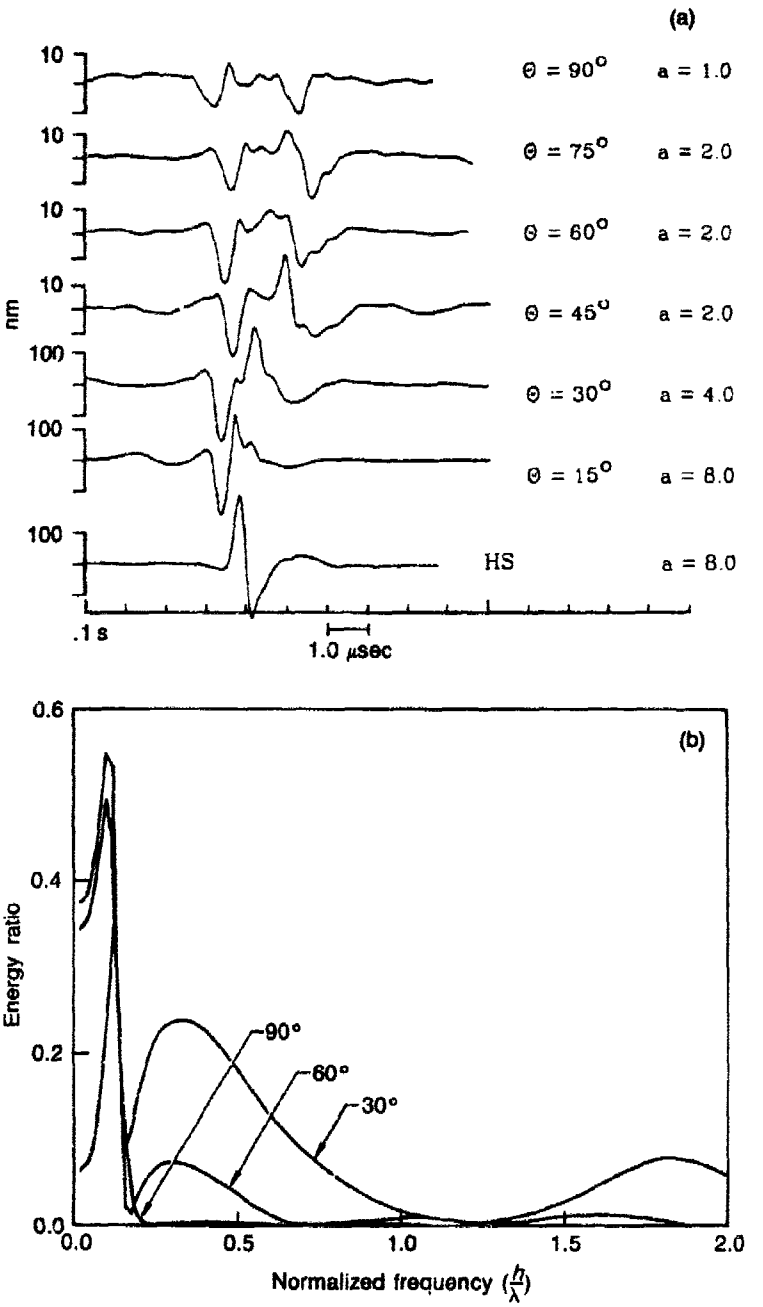

Fig. 4. (a) Seismograms of reflected Rayleigh waves directed in the upstep direction, Model 1, Note the secondary reflection corresponding to a reflection from the *upper* edge of the step. (b) Reflection coefficients (energy ratios) for the Rayleigh waves in (a). Note the change of vertical scale from Fig. 3b.

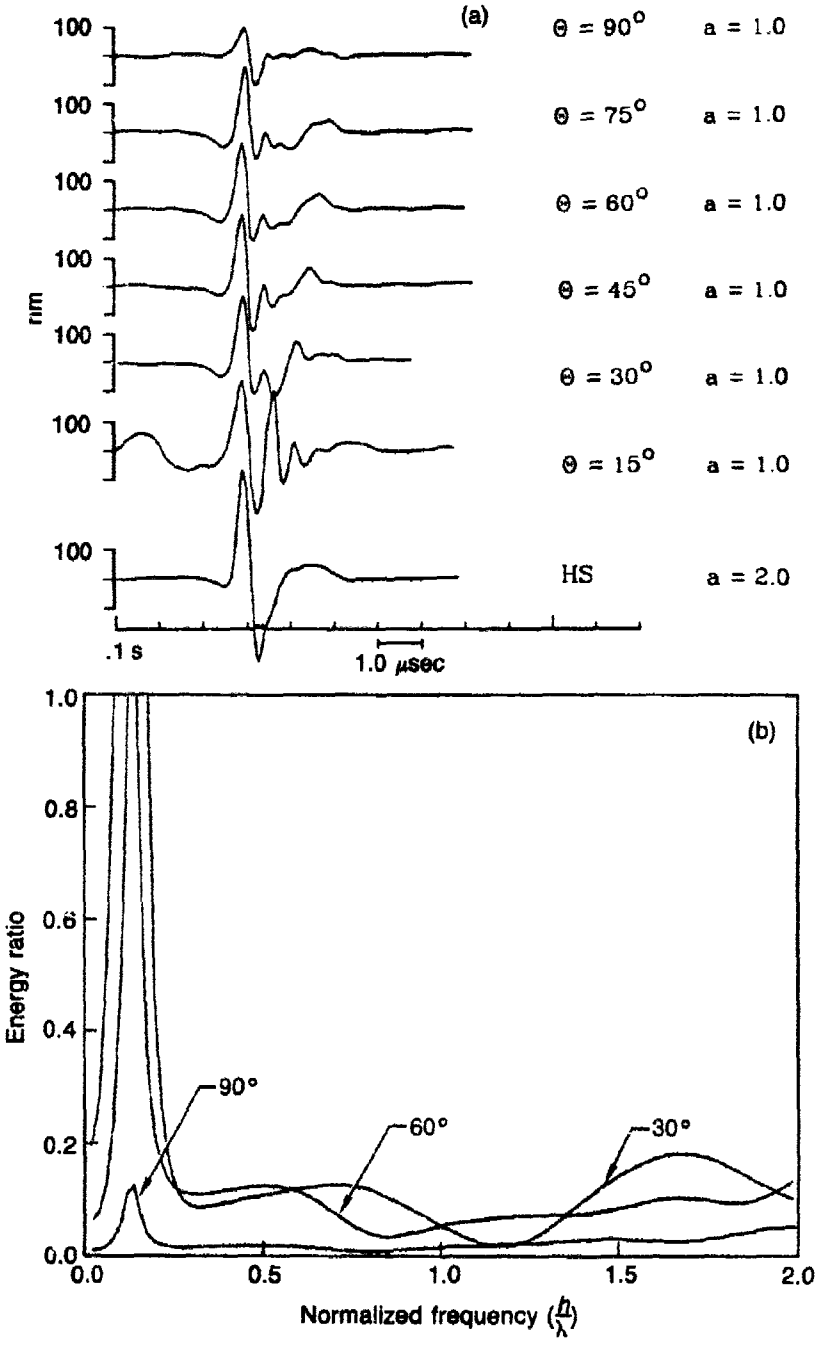

Fig. 5. (a) Seismograms of reflected Rayleigh waves directed in the downstep direction, Model 1. (b) Reflection coefficients (energy ratios) for the Rayleigh waves in (a).

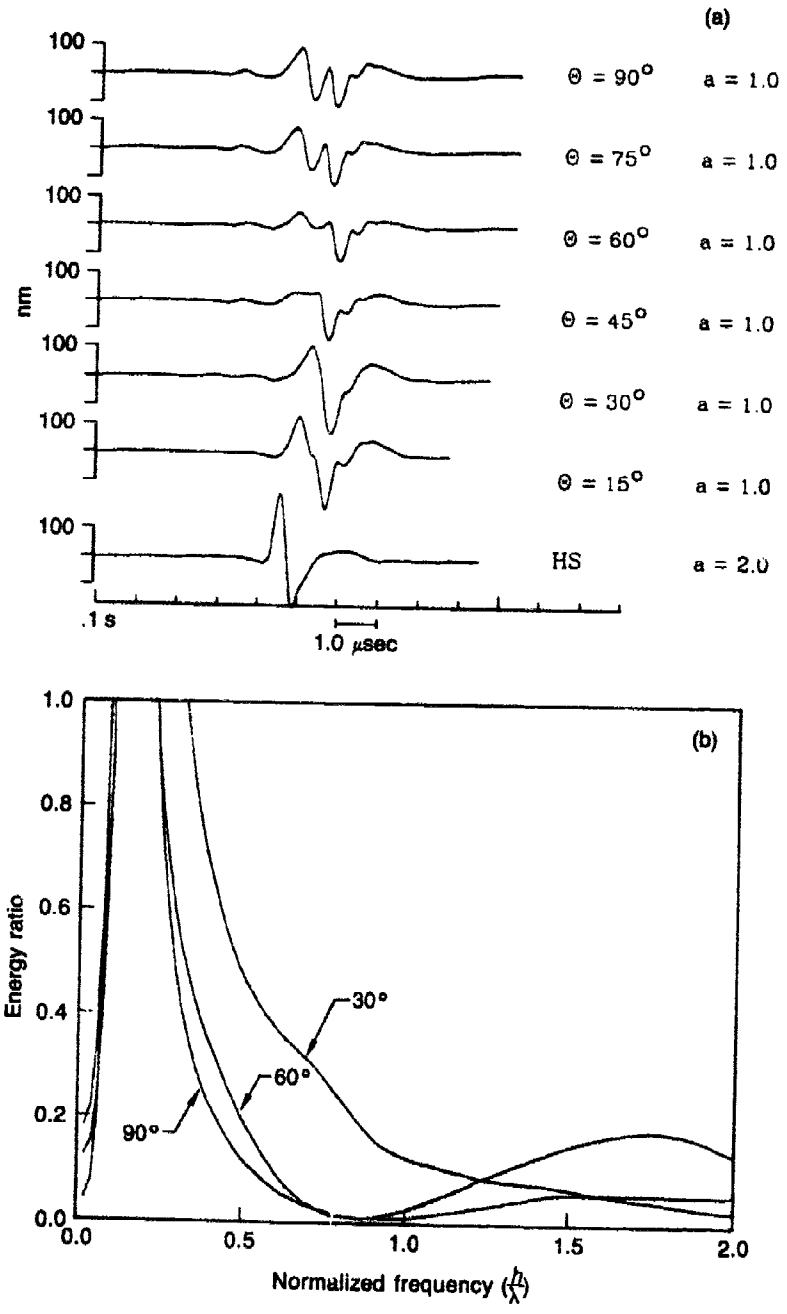

Fig. 6. (a) Seismograms of transmitted Rayleigh waves directed in the upstep direction, Model 2. (b) Transmission coefficients (energy ratios) for the Rayleigh waves in (a).

relations. Direct comparisons between step and ramp transmission and reflection coefficients may not, therefore, be appropriate.

Figure 7(a) shows seismograms of Rayleigh waves reflected from the ramp. The source is aimed in the upstep direction. Figure 7(b) shows the corresponding reflection coefficients. The reflected waves are considerably smaller than in the case of the vertical step. The double reflection is, however, still visible at all angles.

Model 3

As a check on the linearity of the scaling relations and to study the effect of steps of reduced size, Rayleigh waves were recorded propagating across a 1mm vertical step. Figures 8(a) and 8(b) show seismograms and transmission coefficients, respectively, for Rayleigh waves propagating across the 1mm step. The effect of this step on the seismograms is generally much less pronounced than the 3 mm step. The transmission coefficients show nearly identical behavior over the usable frequency band to those computed from the 3 mm step model, suggesting that linearity of the scaling relations is conserved between the two models.

The Effect of a Step on Dispersed Wavetrains

To determine the effect of a step on long, dispersed wavetrains we calculated synthetic examples using the impulse response derived from the models. The transfer functions of the step model for different angles of incidence are obtained from spectra of the halfspace and transmitted wave seismograms. In particular, we have for the model transfer function $\hat{M}_1(\omega)$:

$$\hat{M}_1(\omega) = \frac{\hat{X}_1(\omega)}{\hat{X}_0(\omega)} \quad ,$$

where $\hat{X}_1(\omega)$ and $\hat{X}_0(\omega)$ are the spectra of seismograms corresponding to the step and halfspace cases, respectively.

Figure 9 shows the convolution of a chirped sinusoid with the impulse response of Model 1 and Model 3. At some incidence angles and frequencies the envelope of the wavetrain drops to near zero, suggestive of the "beating" phenomenon frequently observed in seismograms of Rayleigh waves propagating across ocean basins. This beating is usually attributed to multipathing due to lateral heterogeneities along the propagation path. It is conceivable that at least part of the amplitude modulation of dispersed Rayleigh wave trains may be due to sharp structural

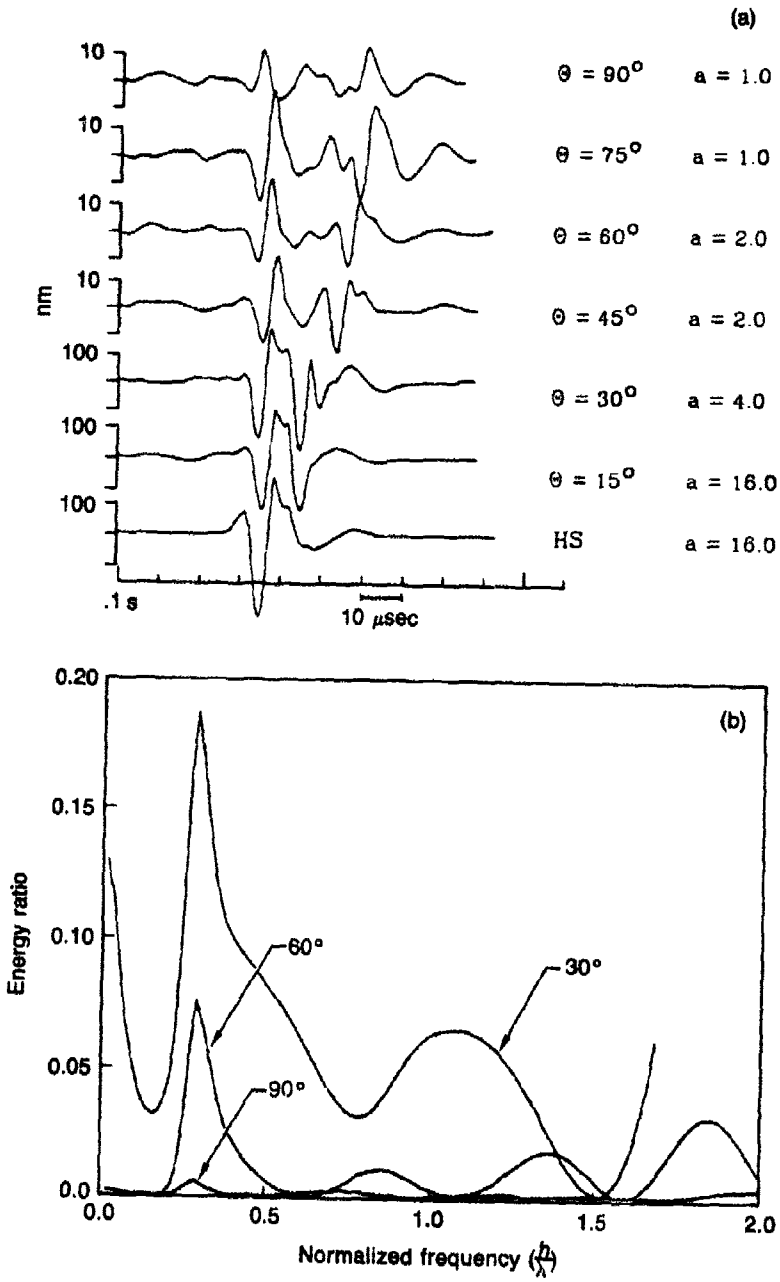

Fig. 7. (a) Seismograms of reflected Rayleigh waves directed in the upstep direction, Model 2. The seismograms were high-pass filtered at 0.3 MHz at the time of recording to enhance the signal-to-noise ratio. (b) Reflection coefficients (energy ratios) for the Rayleigh waves in (a). Note change of vertical scale.

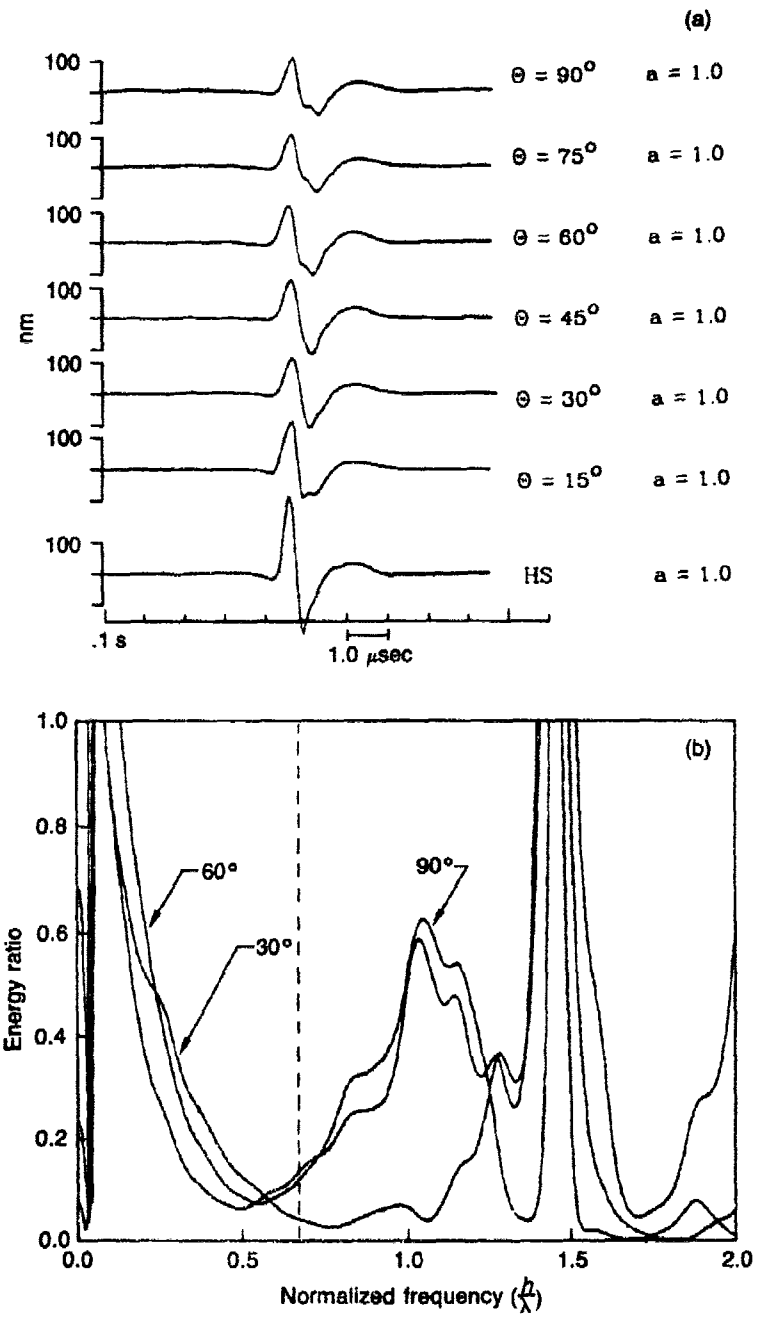

Fig. 8. (a) Seismograms of transmitted Rayleigh waves directed in the upstep direction, Model 3. (b) Transmission coefficients (energy ratios) for the Rayleigh waves in (a). Normalized frequencies greater than approximately 0.7 (dashed line) are outside the frequency band considered usable.

features such as those modeled here. The relatively abrupt transition from oceanic to continental crust along a surface wave propagation path may contribute to the observed amplitude modulation.

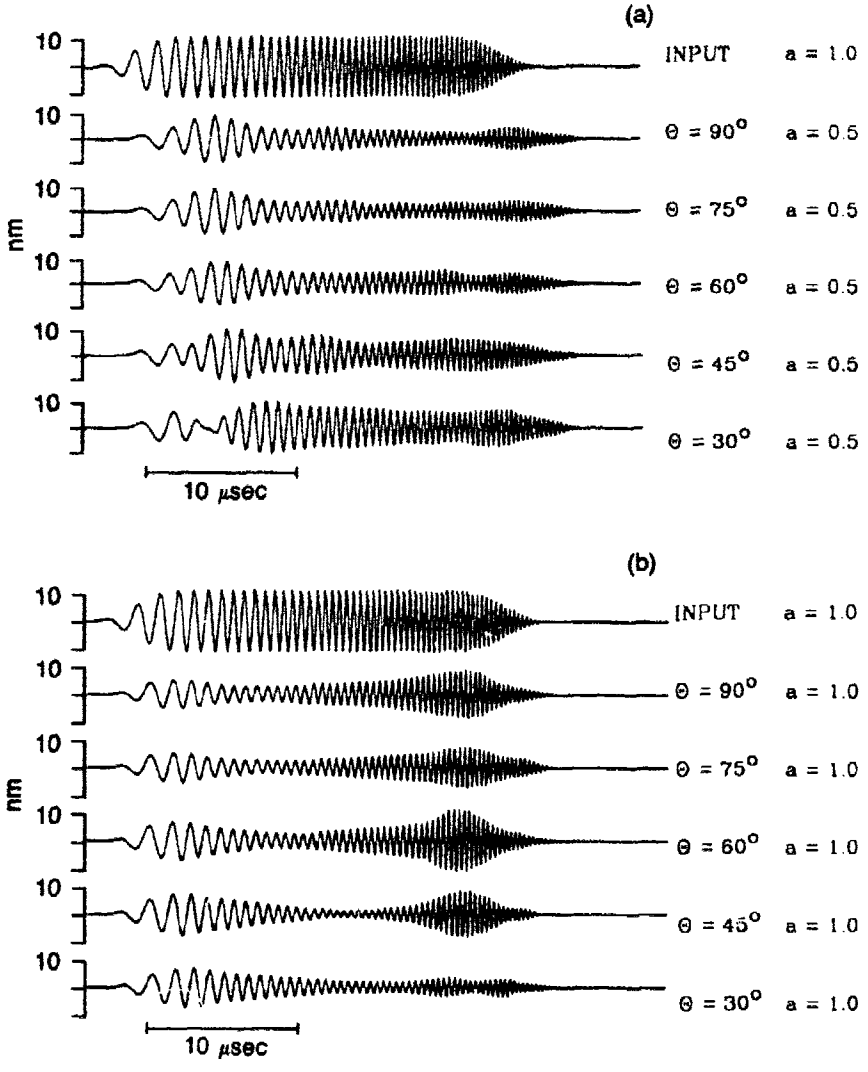

Fig. 9. The effect of the step on a dispersed wavetrain. (a) Model 1. (b) Model 3. The input signal (top trace in both cases) is a linear chirped sinusoid, whose frequency increases from 0.2 to 2.0 MHz in 30 μsec. The corresponding range of $\frac{h}{\lambda}$ is 0.2 to 2 (a) and 0.07 to 0.7 (b). The vertical scales of the transmitted waveforms in (a) have been expanded to show detail of the waveforms.

Conclusions

These experiments illustrate the high degree to which energy from a Rayleigh wave pulse encountering a sharp structural discontinuity is lost to converted body waves radiating into the medium. Moreover, the strong azimuthal dependence of transmission and reflection coefficients suggests that two-dimensional modeling is not adequate for studying effects of surface wave propagation in the three-dimensional Earth. The effects of sharp topographic features on Rayleigh wave propagation as modeled in the laboratory can play an important part in the propagation of surface waves in the Earth. In particular, estimates of source size based on surface wave amplitudes may be inaccurate when the measured amplitudes have been modulated by strong structural effects.

References

Chamuel, J.R. (1982). *Three Dimensional Seismic Ultrasonic Modeling Techniques and Experimental Results*, R-1569, CSDL, June 1982.

Knopoff, L. and A. Gangi (1960). "Transmission and Reflection of Rayleigh Waves by Wedges," *Geophysics*, **25**, pp. 1203-1214.

Lewis, D. and J.W. Dally (1970). "Photoelastic Analysis of Rayleigh Wave Propagation in Wedges," *Geophysics*, **75:17**, pp. 3387-3398.

Martel, L., M. Munasinghe, and G.W. Farnell, (1977). "Transmission and Reflection of Rayleigh Waves Through a Step," *Bull. Seis. Soc. Am.*, **67:5**, pp. 1277-1290.

Nathman, D.R. (1980). *Rayleigh Wave Scattering Across Step Discontinuities*, M.S. Thesis, Mass. Institute of Technology.

In-Situ Strain Paths and Stress Bounds, with Application to Desert Alluvium

John G. Trulio

Abstract

In the nearly-spherical field of a buried burst, material undergoes continuous radial compression and hoop stretch out to at least ten charge radii, almost to its time of peak displacement. For such deformation, all relevant stress-strain measurements known to us (e.g., uniaxial-strain tests) support two physically plausible hypotheses: i) Hoop stress is no greater than radial stress (compressive stress is > 0 here), and ii) until failure occurs in hoop tension, hoop stress will not increase when radial stress decreases. The first hypothesis and the equation for spherical continuum motion imply a rigorous lower bound on live radial stress in terms of material velocity. A rigorous upper bound is obtained by equating the material's hoop stress to its tensile strength, overburden included.

Radial-stress bounds were computed as functions of time from velocity pulses measured in the wholespace field of a 20-ton charge of CH_3NO_2, fired at a depth of 20 m in dry desert alluvium (Event MP2; 11/83). At the smallest ranges yielding credible velocity pulses (3⅓ and 4½ charge radii, where peak radial stresses run from ~ .10 to .02 Gpa), those bounds are tight enough to define radial-stress pulses, in situ, with useful accuracy. More pregnant, however, is a qualitative result implied by the measured data despite their scatter: After initial shock-like uniaxial strain at 3⅓ radii, a) radial stress decays severalfold, even though b) compressive radial strain more than doubles, c) causing volume to decrease despite growing hoop-stretch. Thus (hypothesis ii)) hoop stress drops unless its tensile limit is reached; so does mean stress, steady volume shrinkage notwithstanding.

The main cause of the behavior noted appears to be shear-induced pore collapse, like that remarked in connection with the Hudson Moon H.E. Experiment (1971).[1] Such stress relief is in basic conflict with the five material models used to make pre-shot calculations of MP2 motion. However, it was also deduced from earlier, if shakier, SCOOTER data (500 tons of TNT at a depth of 38 m; 1960).[2] Moreover, cylinders of MP2 soil have been tested in the laboratory along strain paths of almost the same shape as the MP2 paths, but at far lower strain rates, and at stress-amplitudes lower by a factor of ten.[3] Mean stress fell at first (despite

increasing axial and volumetric compression) on the shear-dominated path-leg that follows initial, almost uniaxial strain.

About eighteen months ago, we found a way to extract bounds on live stress from measured motion. For fields with approximate spherical symmetry, like those driven by buried nuclear explosive (NE) or chemical explosive (CE), the method yields upper and lower bounds on live radial stress if pulses of radial motion have been measured at two or more radii (as in the SCOOTER event, to which the method was first applied[2]). As usual with bounds, their value hinges on their closeness. In this case, of course, the bounds start from zero at any given radius, r_g, and, for purely geometric reasons (below), they must remain close while r_g is large compared to the distance $r_f - r_g$ that the wavefront has advanced beyond r_g. However, near a burst point ($r_g \leq \sim 10$ CE charge radii for a given yield), motion amplitudes at r_g are still sizable fractions of their peaks when $r_f - r_g$ is no longer small relative to r_g. Fortunately, the bounds in question often remain usefully close even then—and so they do for bursts in dry desert alluvium, on which attention is centered here. Such bounds have great value right now: Stress gauges are becoming operational, but there are few ways to fix their accuracy, especially in situ. At the same time, the constitutive equations used to compute free field motion in soils and rocks are fraught with unchecked assumptions and guesswork. Stress-strain curves measured along strain paths actually followed in explosively driven fields hold the key to correcting that situation and creating trustworthy material models.[4]

Continuous Fields from Discrete Pulses

To obtain strain paths and stress bounds from discrete velocity pulses, a continuous field must first be constructed from those pulses. One procedure for so doing is called "LASS";[5] another, developed at about the same time as LASS, is the method of nonlinear traveling waves.[6,7] Both amount to rules for interpolating spatially between the stations at which pulses have been measured, thereby obtaining a continuous field from those pulses on the space-time region of measurement.

The traveling-wave method was used in the present work. By that method, pulses are broken into such sections as can be seen to have separate and clearly defined amplitude, A, and width (duration), W, over the space-time region of measurement. For the SCOOTER and MP2 events [2,8] in alluvium, it suffices to divide velocity pulses into a low-amplitude precursor, a subsequent period of rapid rise to a maximum value, and then one of partial decay, as in Fig. 1. (Much motion occurred after that, but some key records were cut off by gauge failure before

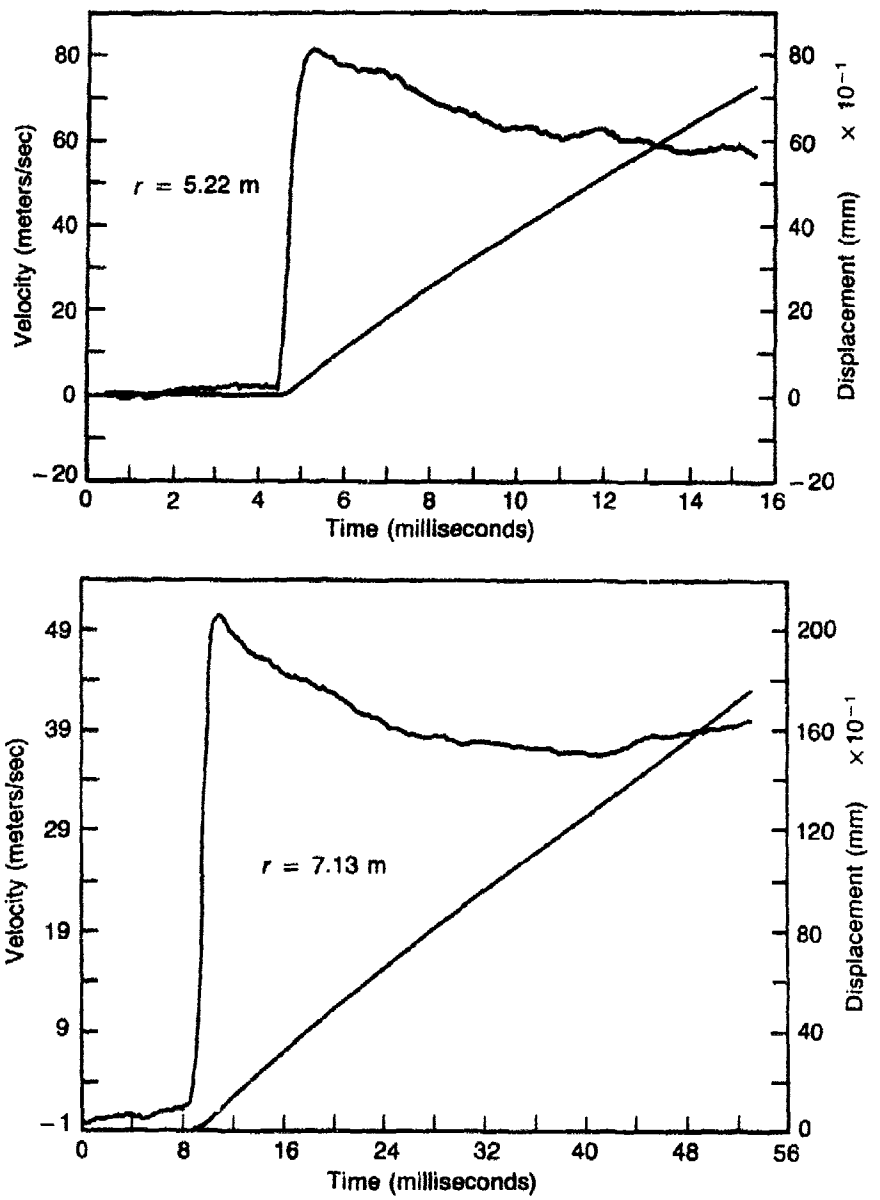

Fig. 1. Velocity Pulses at the Smallest Radius of Successful Motion-Measurement in Event MP2, and at the Next Farther Radius. The pulses came from accelerometers at shot depth (5.22 m) and on an upward-slanting line (7.13 m). Each consists of a low-amplitude precursor, a steep rise to peak, and then much slower decay. The precursors here are mainly artifacts of measurement.

velocity returned to zero, ending its main positive outward phase.) Each pulse-section is then expressed as the product of A (its amplitude) and a form-factor φ of unit amplitude.

The factor A varies with range; *e.g.*, for velocity-pulse-sections that meet at the time of peak, A refers to that peak (which often decays as as inverse power of radius). As for φ, it depends in simplest form only on a non-dimensional time-like variable, τ, which undergoes unit change across a pulse-section:

$$\tau = (t-t_a)/W \tag{1}$$

where t_a is the time a pulse-section arrives at a given gauge, and t is the time. A waveform $\varphi^j(\tau)$ then issues from each of the measured pulses ($j = 1, 2,\ldots$ in order of increasing radius); $\varphi(\tau)$ can be chosen as the most typical of the φ^j, or as an average of them all, and spline-fit. More generally, φ^j is accurately spline-fit for each j, and, between the ranges of pulses j and $j + 1$, φ is made a linear combination of φ^j and φ^{j+1}:

$$\varphi = \alpha\varphi^j(\tau) + \beta\varphi^{j+1}(\tau) \tag{2}$$

In Eq. (2), α goes smoothly from 1 to 0, and β from 0 to 1, on moving from range j to $j + 1$; also $\alpha + \beta = 1$. Eq. (2) was used in this work, but in any case a continuous field F is defined as follows:

$$F = \sum A\varphi(\tau) \tag{3}$$

where the sum extends over all pulse-sections.

From a field of the form given by Eq. (3), the derivatives and integrals of velocity needed to compute stress-bounds and strains can be found; to compute radial strain, for example, the spatial derivative of radial velocity must be taken and time-integrated. Traveling waves are especially convenient for that purpose because they describe the field in terms of simple algebraic formulas for such basic physical properties as rise time and arrival time (*vs.* slant range). Moreover, individual pulses are so combined that the continuous field they give will, if desired, reproduce their forms in complete and exact detail. Also, pulses can be broken into sections at any desired points (not just at their zeros and extremes) without sacrificing continuity of the resulting field[9]—but simplicity fades as the number of pulse-sections grows.

Stress Bounds in Spherical Fields

For spherical motion, stress is specified completely by its radial component σ_r and its hoop component σ_θ. Momentum and mass conservation link those two stresses to radial acceleration, $\dot{u}$, via the equation of motion:

$$\rho \dot{u} = -\partial\sigma_r/\partial r - 2(\sigma_r - \sigma_\theta)/r \tag{4}$$

where ρ is the density of material at radius r at any given time, and compressive stress is > 0.

The right-hand member of Eq. (4) increases monotonically with σ_θ, whence upper and lower bounds on σ_θ imply upper and lower bounds on $\dot{u}$. To obtain an upper bound on σ_θ, note that material is at first driven outward from the shot point, and therefore stretched in every hoop direction as it compresses radially. We assert that as long as increments in radial *strain* remain compressive while hoop-strain increments remain tensile, hoop stress will not be more compressive than radial stress ($\sigma_\theta \leq \sigma_r$)—a "hydrodynamic" bound on σ_θ since $\sigma_\theta = \sigma_r$ for fluids. Spring-and-ratchet hookups can be contrived as counterexamples (though not easily in a medium that admits spherical fields), but we know of no tests on soils that contradict the inequality $\sigma_\theta \leq \sigma_r$, and a large body of test data confirms it.[10] It also makes intuitive sense: To compress a cylinder of soil axially but not laterally, at least as much pressure must be applied to its planar end faces as to its curved surface.

With $\sigma_\theta \leq \sigma_r$, Eq. (4) implies that:

$$\rho\dot{u} \leq -\partial\sigma_r/\partial r \;;\; \partial\sigma_r/\partial r \leq -\rho\dot{u} \tag{5}$$

Integrating Eq. (5) at fixed time from a given radius r_g to radius r_f at the front of the outgoing wave (or just beyond), where live stress is zero, we find that:

$$-\sigma_r^g \leq -\int_{r_g}^{r_f} \rho\dot{u}\, dr \;;\; -\sigma_r^g \geq \int_{r_g}^{r_f} \rho\dot{u}\, dr \tag{6}$$

where σ_r^g is the live radial stress at r_g.

At the other extreme of behavior, live hoop stress cannot be more tensile than a material's tensile strength plus overburden ($\sigma_\theta \geq -T \leq 0$), whence [Eq. (4)]:

$$\rho\dot{u} \geq -\partial\sigma_r/\partial r - 2(\sigma_r + T)/r = -(1/r^2)\,\partial[r^2(\sigma_r + T)]/\partial r \tag{7}$$

Eq. (7) implies that

$$\sigma_r^g \leq T\,[(r_f/r_g)^2 - 1] + \int_{r_g}^{r_f} (r/r_g)^2\ \rho\dot{u}\,dr \tag{8}$$

The density ρ_i of a material element at some initial time t_i, divided by its density ρ at any later time t, follows rigorously from material motion alone ($\rho_i/\rho = 1+$ cubical dilation). To calculate ρ_i/ρ, it helps to view the element's current radius r as a function of t, and of its position ζ at time t_i; *i.e.*, $r = r(\zeta,t)$ where $\zeta = r(\zeta,t_i)$. The shell of material between radii ζ and $\zeta + d\zeta$ at time t_i then lies between radii r and $r + dr$ at a time t, and mass conservation requires that

$$\rho r^2\,dr = \rho_i \zeta^2 d\zeta \tag{9}$$

Thus, making use of the Lagrangian coordinate ζ (Lagrangian because its value never changes for a given material element), changes in density are readily computed. For that reason, and because ground-motion gauges are supposed to move with material velocity (*i.e.*, as Lagrangian points), field properties are calculated here (as in LASS) in terms of ζ and t. In particular, Eqs. (6), (8) and (9) yield the result that

$$\int_{\zeta_g}^{\zeta_f} \left(\frac{\zeta}{r}\right)^2 \rho_i \dot{u}\,d\zeta \leq \sigma_r^g \leq T\left[\left(\frac{r_f}{r_g}\right)^2 - 1\right] + \int_{\zeta_g}^{\zeta_f} \left(\frac{\zeta}{r_g}\right)^2 \rho_i \dot{u}\,d\zeta \tag{10}$$

To get the physical sense of Eq. (10), picture a right cone of small half-angle, ϵ, with its vertex at shot-point. Material surfaces of radius r_g and $r_f > r_g$ slice out the section of cone from r_g to r_f (section "CS"), leaving it with spherical end-caps. Live stress, and hence the component of force along the cone's axis, are zero on the outer end-cap. The axial force F_r on the inner cap is the product of the live radial stress σ_r^g and $\pi(r_g \sin\epsilon)^2$ (the projection of the inner cap's area on any plane normal to the cone's axis). If F_θ is the axial force on the conical surface of CS, then $F_r + F_\theta$ must equal $\dot{M}$, the rate of change of axial momentum within CS. The smallest physical value of F_θ is $-T$ times $\pi(r_f^2 - r_g^2)\sin^2\epsilon$, the area of the projection of CS's conical surface on any plane normal to the cone's axis. The largest value of $\sigma_r^g\,\pi(r_g \sin\epsilon)^2$ is therefore $\dot{M} + T\pi(r_f^2 - r_g^2)\sin^2\epsilon$, whence σ_r^g must be $\leq T[(r_f/r_g)^2 - 1] + \dot{M}/\pi r_g^2 \sin^2\epsilon$. The quantity $\dot{M}/\pi r_g^2 \sin^2\epsilon$ is just the integral on the right of Eq. (10), since the rate of change of axial momentum in the shell between material surfaces ζ and $\zeta + d\zeta$ [current radii $r(\zeta, t)$ and $r(\zeta + d\zeta, t)$] is equal to $\pi(\sin^2\epsilon)\dot{u}\rho_i\zeta^2\,d\zeta$. The rate of change of momentum of the shell, per unit area of either of its spherical surfaces,

is a vector of the same magnitude at all surface-points ($\dot{u}\rho\,dr$), but directed along the local outer normal; hence (as in computing F_r), its rate of change of axial momentum is the product of $\dot{u}\rho\,dr$ and $\pi(r \sin \epsilon)^2$, or [Eq. (9)] of $\dot{u}\rho_i d\zeta$ and $\pi(\zeta \sin \epsilon)^2$.] The left-hand member of the inequality [Eq.(10)] is a bit subtler; the change in σ_r^g that attends a slight change in r_g must be calculated, conserving momentum.

Generalizing Eq. (10) so that it holds for uniaxial, cylindrical-radial, and spherical fields is a simple task (Appendix A). Moreover (Appendix A), a separate upper bound on σ_θ issues from knowledge of a shear-strength limit as general as $f(\sigma_r, \sigma_\theta) \geq 0$ where f is some function of the two stresses. The resulting shear-strength bound on σ_r tends to fall between those of Eq. (10) because the shear stress on octahedral planes is $\frac{1}{3}\sqrt{2}\,(\sigma_r + T)$ at the tensile limit of σ_θ—and that value commonly exceeds shear strength.

In-Situ Stress Bounds: Bursts in Dry Alluvium

The bounds specified in Eq. (10) were first evaluated using measured pulses from the SCOOTER event in desert alluvium. A few months later they had also been computed from pulses measured in dome salt (SALMON event), and from radial velocity pulses measured in grout in the laboratory.[11] More recently, Eq. (10) was applied to data from a 20-ton burst 20 m below the ground surface in dry desert alluvium (Event MP2). The main MP2 results are shown in Figs. 2-4. All three refer to the smallest range of successful ground-motion measurement (5.22 m), but they reflect different treatments of the measured data. In each figure, bounding pulses of radial stress appear along with the strain path that goes with a given pair of bounds; the excess-compression pulse implied by that path also appears (excess compression $\equiv \mu \equiv \rho/\rho_i - 1$). The numbered points on the path (which makes no explicit reference to time) occur at times noted by like numbers on the lower part of the figure, where stress bounds and compression are plotted.

In Figs. 2-4, initial nearly-uniaxial strain with rapidly increasing compression turns abruptly to shear combined with slowly increasing compression. In each figure, excess compression (μ) oscillates somewhat during the shearing stage of deformation, but about an upward-slanting line; the increase in μ during shear amounts to $\sim .3$ of the μ-value reached in nearly-uniaxial strain. The radial-stress bounds are close enough in Figs. 2-4 to show that radial stress is decreasing in situ (becoming less compressive), even though both radial strain and volumetric compression are increasing; hoop stress must also be decreasing, since *a*) strain is growing ever more tensile in the hoop direction, and *b*) even compression in the radial direction does not suffice to prevent the decay

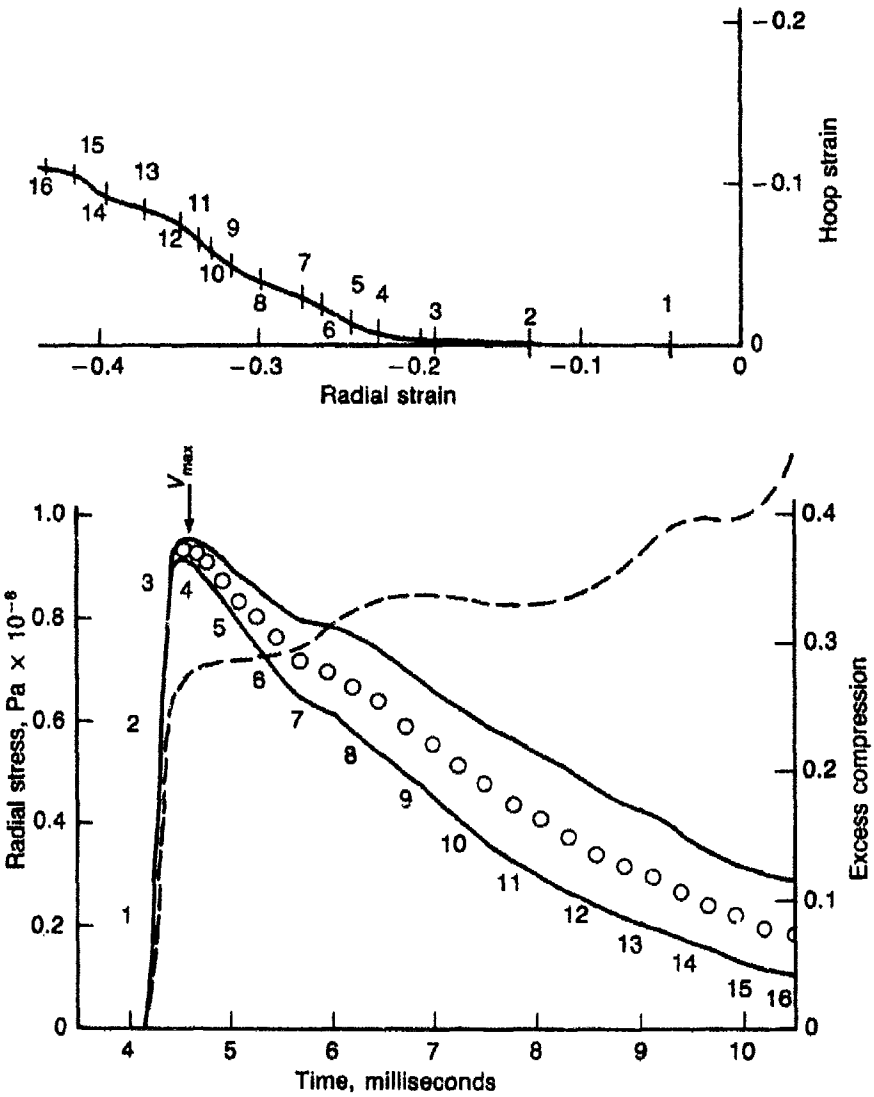

Fig. 2. Strain Path and Stress Bounds for Event MP2 at a Slant Range of 5.22 Meters. Excess compression (density divided by initial density, minus 1; dashed curve) is also shown *vs.* time. The waveforms used in generating the curves were those of velocity pulses measured at nominal slant-ranges of 5.3, 7.1 and 9.5 meters. Radial velocity has a peak outward value at the time denoted "V_{max}". Points 1-16 along the strain path are reached at the times shown by numbers 1-16 on the stress-bound plot. The upper, middle (○) and lower curves, respectively, are dictated by limits of tensile strength, shear strength and hydrodynamic behavior; the first two are upper bounds.

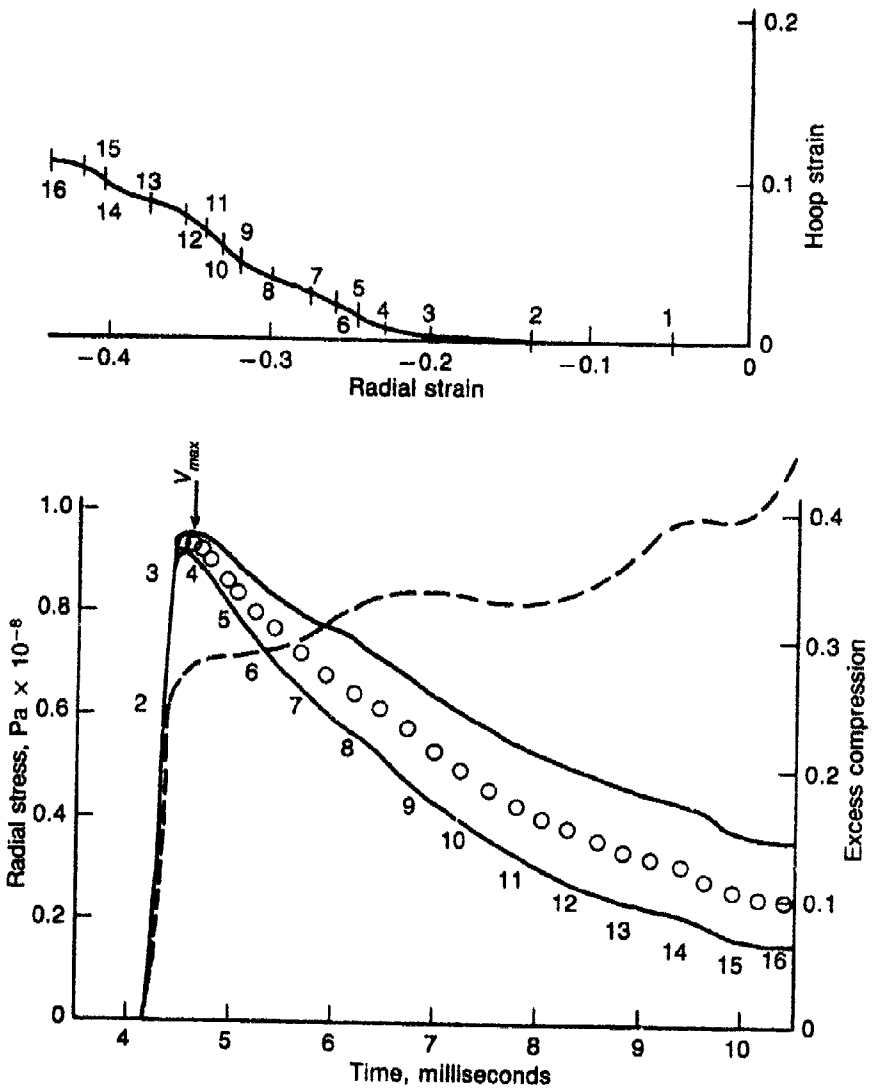

Fig. 3. Strain Path and Stress Bounds for Event MP2 at a Slant Range of 5.22 Meters. Excess compression (density divided by initial density, minus 1; dashed curve) is also shown *vs.* time. Except for use of a different waveform at a nominal range of 7.1 meters, the curves were obtained exactly as in Fig. 2. The format is that of Fig. 2.

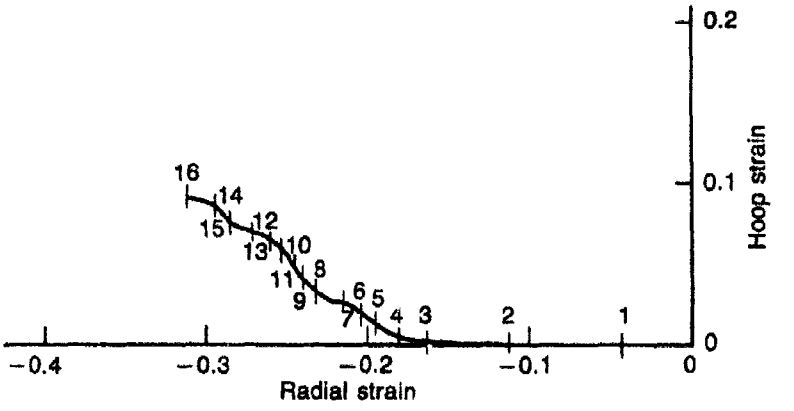

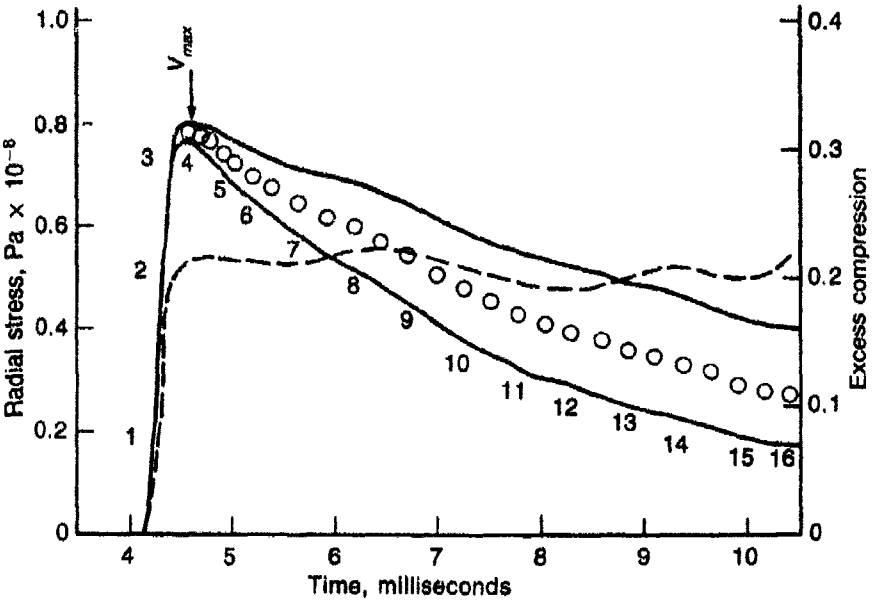

Fig. 4. Strain Path and Stress Bounds for Event MP2 at a Slant Range of 5.22 Meters. Excess compression (density divided by initial density, minus 1; dashed curve) is also shown *vs.* time. Except for the use of a quadratic least-squares fit to measured peak velocities, rather than a linear fit, the curves were obtained exactly as in Fig. 3. The format is that of Fig. 2.

of radial stress. The figures therefore imply that mean stress falls despite growing compression, being strongly dependent in that way upon shear strain. No such behavior is accounted for by the material models used to make pre-shot calculations of MP2 motion. Further, while models that embrace non-ideal plasticity (and perhaps some rate-dependent models) can reproduce it, none appears to do so at present—but then, the strain-path data available before Event MP2 did not require that behavior. Thus, to the extent that MP2 velocity pulses are reliable (below), a result with basic and sweeping model-implications has emerged from the radial-stress bounds implied by the MP2 pulses.

Of the MP2 velocity pulses from ~ 5.2 m, only one (Fig. 1) is free of serious artifacts, even before the early time of peak velocity. That record was used to define the waveform $\varphi_1(\tau)$ [Eq. (1)] on which Figs. 2-4 are based. Its precursor is not credible (arriving much sooner than measured seismic wavespeeds permit); a real precursor may be present, but at an amplitude so far below the rest of the pulse as to justify its omission in Figs. 2-4. Thus, the pulse as utilized consists of just two sections, namely, a steep rise to peak and gradual decay from it. Those two sections meet at the time of peak velocity, and hence share the same amplitude factor $A(\zeta)$ [Eqs. (2) and (3)].

In keeping with Eq. (2), the waveform at $\zeta \equiv \zeta_1 \approx 5.2$m is averaged with one at the next range of measurement ($\zeta \equiv \zeta_2 \approx 7.1$ m) to give the waveform at any intermediate range. However, as functions of ζ, the weighting factors α and β [Eq. (1)] have relative extrema at ζ_1 and ζ_2. As a result, the only waveform affecting the strains computed for Figs. 4-6 is $\varphi_1(\tau)$. In addition, the same amplitude factor $A(\zeta)$ was used in preparing Figs. 2 and 3. As a result, strains are identical in those two figures. Their stress-bounds nevertheless differ because the figures refer to different waveforms at $\zeta_2 \approx 7.1$ m; waveforms at and beyond ζ_2 affect the bounds computed for range ζ_1 [Eq. (10)].

To define A (ζ) for Figs. 2 and 3, each peak radial velocity not open to serious doubt (due mostly to obvious artifacts) was read from the MP2 gauge records. A least-squares straight line through all but one of the resulting (log A, log ζ)-points gave log $A(\zeta)$ and hence a power-law expression for $A(\zeta)$ itself. The excluded point, one of four from the farthest gauge-range (~ 30 m), had an A-value smaller by a factor of ~ 4 than any of the other three; all points are plotted in Fig. 5 along with the straight line in question. The corresponding least-squares quadratic defined $A(\zeta)$ for Fig. 4, whose curves were otherwise computed from the data used for Fig. 2. Variances in the quadratic's coefficients proved as large as the coefficients themselves (*vs.* variances of ~ 5% in the line's coefficients), and inclusion of the quadratic term did

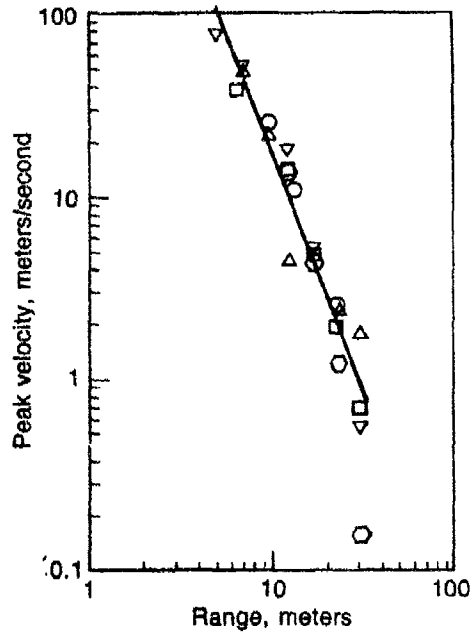

Fig. 5. Measured Peak Radial Velocity of Material, *vs.* Distance from Shot Point, for Event MP2. The straight line is a least-squares fit to all data-points but the one of lowest velocity.

not reduce the variance of data-points from the least-squares fit. The line is therefore much more plausible than the quadratic. Still, by presenting a rather extreme view of $A(\zeta)$, the quadratic helps to show how strain paths and stress bounds depend on the interpretation of measured data (at 5.22 m, the line and quadratic have respective A-values of 108.5 and 90 m/s, and slopes of -2.725 and -2.17). In addition, if the aberrant point at ~ 30 m is added to the set, the resulting least-squares line has a slope of -2.95 and an A-value (at 5.22 m) of 125 m/s. That line yields strains and stress-bounds qualitatively like those of Figs. 2 and 3, though excess compression (μ) eventually tops the measured value corresponding to removal of all air filled voids ($\mu = .37 \pm .07$)[12]—a matter discussed below.

At the next smallest gauge-range ($\sim$ 7.1 m), two very different waveforms are at hand. Whereas one of them has fallen smoothly to zero only 14 ms after reaching its peak, the other (Fig. 1; lower plot) is still at $\sim$ ¾ of its peak velocity 34 ms after the peak occurs. Taken with a more distant pulse (at 9.5 m, nominally), the two yield the respective strains and stress-bounds of Figs. 6 and 7. Understandably, strain paths in Figs. 6 and 7 differ widely after initial uniaxial strain, and some elastic recovery is evident in Fig. 6 (*e.g.*, μ reaches a maximum and then drops appreciably). Still, Fig. 6 contains a brief period of rising μ and falling σ_r, that comes into clear focus if shear strength is used to define the upper σ_r-bound. Indeed, the shear-strength bound reduces

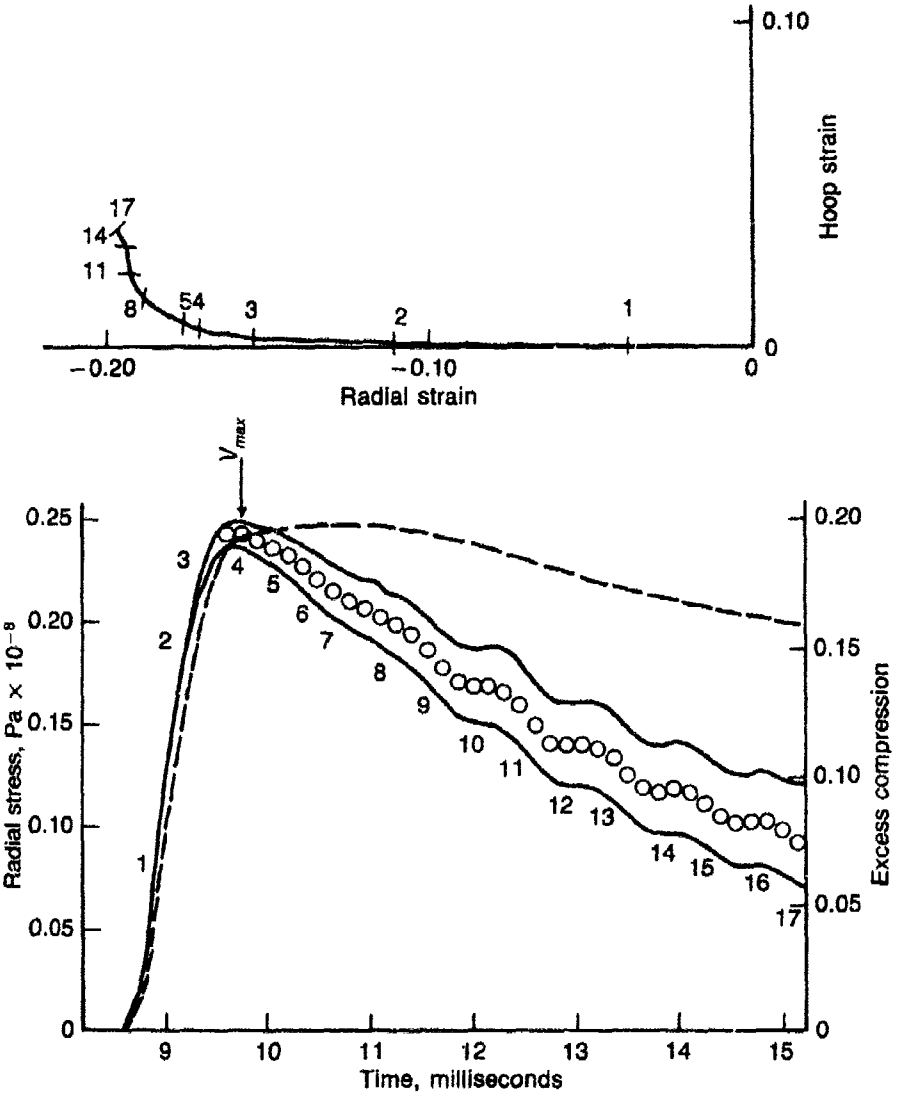

Fig. 6. Strain Path and Stress Bounds for Event MP2 at a Slant Range of 7.06 Meters. Excess compression (density divided by initial density, minus 1; dashed curve) is also shown *vs.* time. The curves were obtained from exactly the same data used for Fig. 2, except for omission of the waveform at 5.3 meters (since the nominal range here is 7.1 meters). The format is that of Fig. 2.

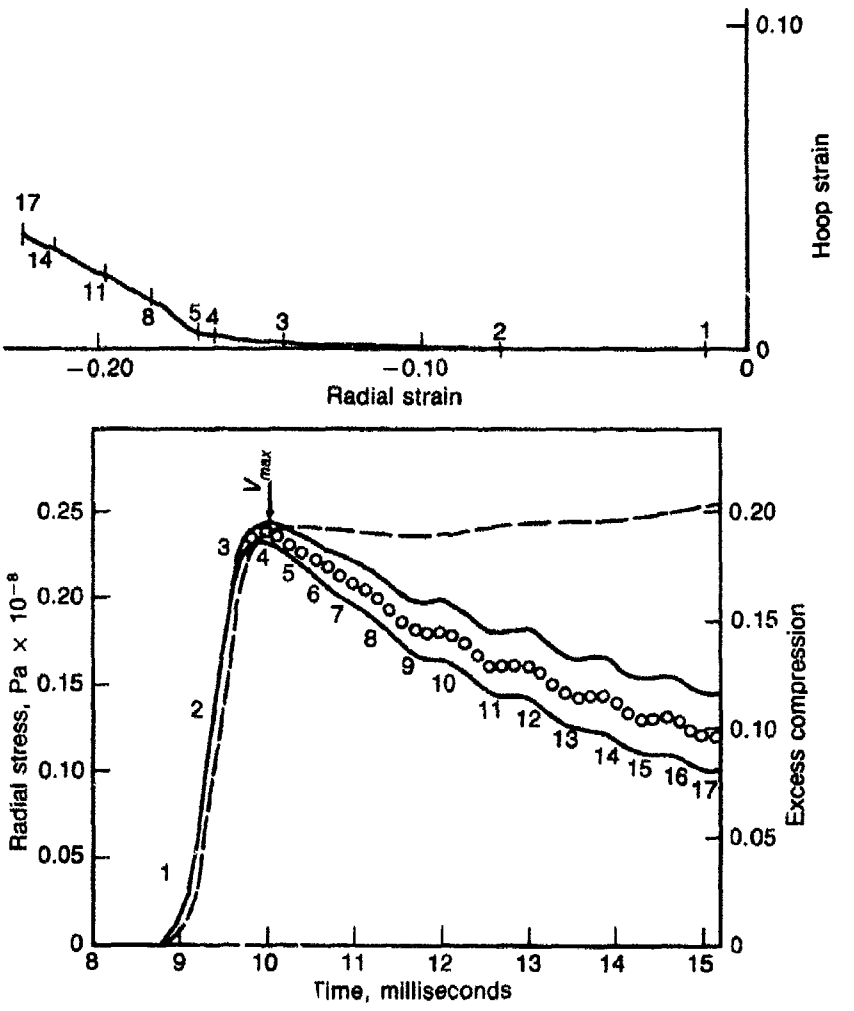

Fig. 7. Strain Path and Stress Bounds for Event MP2 at a Slant Range of 7.13 meters. Excess compression (density divided by initial density, minus 1; dashed curve) is also shown *vs.* time. Except for use of a different waveform (that of Fig. 3) at a nominal range of 7.1 meters, the curves were obtained exactly as in Fig. 6. The format is that of Fig. 2.

uncertainty in σ_r to gratifyingly low levels in all cases (generally $< 10\%$). However, much more information is needed to specify shear strength than tensile strength. Hence, though the failure envelope used here rests on a broad base of laboratory tests,[14] there is no ready answer to the kind of question that lab-test data always raise: Does shear strength lie within that envelope for the material in situ, on strain paths of the actual

event, and at actual loading rates? Unease on these points has been allayed somewhat by computing stress-bounds with other strengths than those measured: Setting T to 0 (rather than .5 MPa as in the figures) lowers the tensile upper bound in Fig. 2 or 3 by only about a line-width; increasing the tangent of the angle of internal friction from .68 (measured) to .79 raises the shear-strength bound by $< 3\%$.

None of this is meant to suggest that Fig. 6, with its brief interval of rising μ and falling σ_r, presents serious evidence for apparent bulk moduli < 0. In fact, the curves for 7.1 m are ambiguous on that score; μ rises slowly and steadily in Fig. 7 from about the time of peak σ_r onward, but it falls in Fig. 6 over most of that period. Rather, the main evidence for negative "bulk moduli" in MP2 comes from 5.22 m (above), as befits the general trend toward elastic behavior with increasing range.[4] At the reduced stress and motion amplitudes found at 7.1 m, elastic strain appears large enough as a fraction of total strain to assure that little or no shrinkage occurs while material unloads and comes to rest.

Critique of the Data and Results

The closeness of the bounds in each case (Figs. 2-4, 6 or 7) is due to the low speed S of the main outgoing wave (540 m/s at 5.22 m; 330 m/s at 7.1 m). For the main wave to advance from 5.22 to 7.1 m takes ~4.3 ms, or most of the time of motion covered by Figs. 2-4. At that point, the largest ratio of integrands in the two bounding integrals of Eq. (10) [*i.e.*, $(r_f/r_g)^2$ at 8.7 ms] is only about 5/3. Also, while main-wave speed S is subject to large error at 5.22 m (Fig. 8), even with $S = 980$ m/s the stress bounds dictate decay of σ_r less than ⅓ ms after velocity reaches its peak. As for 7.1 m, variations in S that the data might reasonably admit (Fig. 8) are too small to cause appreciable changes (much less qualitative ones) in Figs. 6 and 7.

In all likelihood, however, the compressions of Figs. 2 and 3 are too high. The material's measured air-filled porosity of $26.7 \pm 3.6\%$ implies cubical dilatations (Δ-values) no greater than $-.303$ ($= -.267 - .036$) at these low stresses. At the final time shown, $\Delta\ [\equiv -\mu/(1+\mu)]$ has very nearly reached that limiting value in Figs. 2 and 3; ~ 4 ms later (gauge-failure time) $\Delta \approx -.41$, a value at odds with the porosity limit. To help explain that fact, we recall that if the short rise to peak velocity A is neglected—*i.e.*, if the main wave is treated as a shock—then Δ is given by $-A/S$ at the peak. With $A = 108.5$ m/s (from the least-squares lines of Fig. 5), and with $S = 540$ m/s (from the free-form curve of Fig. 8), we obtain $\Delta = -.201$ for the shock; taking account of actual rise time (Figs. 2 and 3), Δ becomes .217 at the time of peak velocity.

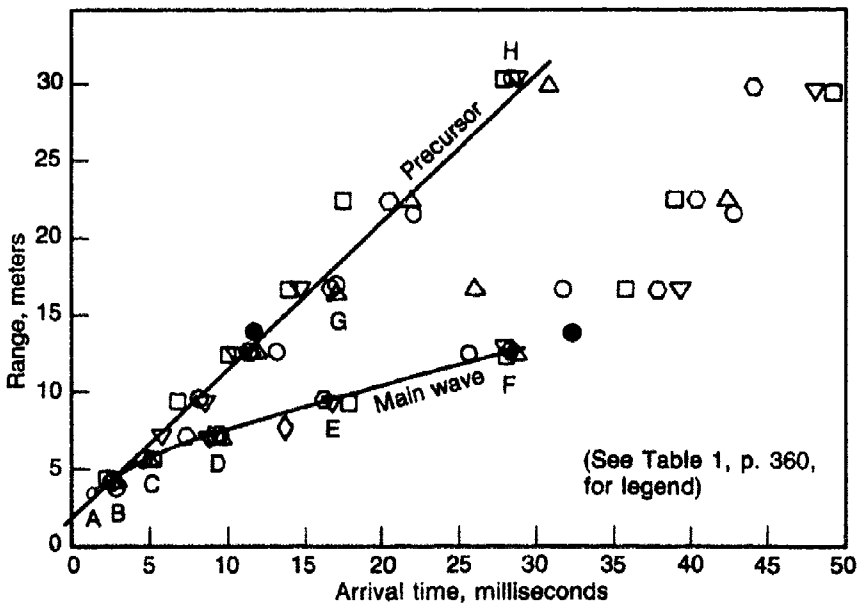

Fig 8. Times of Arrival of Precursor and Main Wave, *vs.* Distance from Shot Point, for Event MP2. Main-wave arrivals were defined as points of maximum curvature in the measured acceleration pulses. The main-wave curve was free-formed; the straight line for the precursor is a least-squares fit to the data shown, which include the inverted triangle (▽) and hexagon (○) at ~7.1 m, but no points at ~ 5.3 m. The point at ~3 m came from stress-gauge records.

However, values of S from 300 to 980 m/s are possible owing to uncertainties left by the gauge records as to how and where the main wave and precursor separate (Fig. 8). The value 540 m/s was obtained by fitting the points with a curve that allows S to fall about as gradually with range as the data permit; even so the fall is rapid—but no measurements suggest that S should drop discontinuously as peak loads decrease, and laboratory compression tests suggest that it should not.[15]

A near-discontinuity would be needed for S to be as low as 300 m/s at 5.22 m, and the Δ-value (−.36) reached in a shock would then lie outside the permissible Δ-range. On the other hand, 700 m/s is about the largest value S can have if the precursor and main wave separate at a range > 5.22 m (which is likely, since all four points at ~ 5.3 m fall below the precursor path; Fig. 8). With S = 700 m/s, the porosity limit is still exceeded at gauge-failure time (Δ = −.36), but Δ = −.26 at the final time of Figs. 2 and 3; indeed, over the period covered in those figures, an increase in S from 540 to 700 m/s does little else than lower all

Table 1. Legends for Fig. 8.

Group	Symbol	Arrival Time	Range
A	σ	0.9	3.01
B	□	1.685	4.13
	⊕	1.84	4.01
	△	2.01	4.01
	○	1.93	4.01
C	△	4.0375	5.42
	△	4.5250	5.42
	○	3.6125	5.25
	○	3.9500	5.25
	▽	4.4250	5.22
	▽	4.4250	5.22
	□	4.200	5.26
D	▽	8.2570	7.06
	△	8.5250	7.13
	□	8.8500	7.11
	○	8.8000	6.85
		9.0375	7.16
E	○	15.6625	9.50
	△	16.5250	9.51
	○	15.9625	9.54
F	▽	27.6875	12.56
	□	26.7250	12.55
	○	27.7500	12.64
	△	28.0000	12.61
G	○	15.8000	16.77
	○	15.8000	16.87
	△	16.2000	16.82
H	□	27.8000	30.00
	○	28.3000	30.05
	▽	28.4000	29.98

μ-values by .07-.08, without changing the shape of the compression curve (*e.g.*, μ-values at 5, 7 and 9 ms become .211, .260 and .297, respectively). Likewise, cutting $A(\zeta)$ by a mere numerical factor lowers all hoop and radial strains by that factor, and hence makes little change in the shape of the μ-curve. Using such a factor, peak radial velocity can be brought from its value on the least-squares line (108.5 m/s) to the observed value (79.6 m/s), but the least-squares figure is the more likely; there is at least as much reason to trust the points at $\sim$ 7.1 m in Fig. 5 as the point at 5.22 m, and a line drawn from the mean of the 7.1-m points to the one at 5.22 m would have the improbable slope of -1.72.

In sum, main-wave speed may have been set too low and peak velocity too high (mainly the former) in reading MP2 data for Figs. 2 and 3, making their final compressions too large. Yet such misreadings cannot—plausibly—have caused a) the μ-values of Figs. 2 and 3 to exceed the material's measured porosity, or b) the rise in μ after the time t_v of peak radial velocity. Further, on the available data, values of μ at time t_v are hard to alter much from those of Fig. 2 (or 3). We therefore note that, in every case, μ is lower at time t_v and the peak σ_r-value higher, than behind a shock of the same speed and peak radial velocity: At time t_v in Figs. 2-4, 6 and 7, respectively, $-\Delta$ is equal to .217, .217, .176, .162 and .159, while peak upper-bound values of σ_r are 95.3, 94.9, 80.0, 24.9 and 24.3 MPa; for shocks these Δ- and σ_r-figures become .201, .201, .166, .144, and.141, and 107.3, 107.3, 88.7, 28.8 and 28.0 MPa. Thus, the structure of the field, which has no effect on compression in a true shock (nor does shock heating here), is such as to augment shock compression over the short rise times of the pulses ($\sim$ ½ ms at 5.22 m). The field properties that govern changes in compression will now be made explicit.

At a given instant, material moving at radius r with velocity u forms the surface of a sphere whose volume is changing at the rate of $4\pi r^2 u$. Said material will be undergoing compression if and only if the volume of a slightly larger sphere is changing at a lower rate (*i.e.*, if and only if $r^2 u$ is a decreasing function of ζ). From Eq. (3) and the power-law decay of peak velocity implied by the line in Fig. 5, it follows that

$$r^2 u = Kr^2 \varphi/\zeta^n = K(r/\zeta)^2 \varphi/\zeta^{n-2} \tag{11}$$

where φ refers to whichever pulse-section (precursor, rise or decay) presents itself at radius r at the given instant, and $-n$ and $\log_{10} K$ are the line's slope and intercept. Also, since α and β [Eq. (2)] are stationary with respect to ζ at the ends of any range interval (above) the only pulse whose form enters Eq. (11) at ζ = 5.22 m is the one recorded at that

range (top half of Fig. 1). Thus, in ~ 10 ms, the decay-section of φ falls from 1 to ~.75, but has almost stopped falling by then (peak velocity drops by a factor of ~4 in that period, and keeps dropping). Therefore (and for simplicity), suppose first that φ is constant. In that case r^2u decreases with ζ—whence material becomes more and more compressed—if $r \geq 2$ (for, $r/\zeta = 1 + D/\zeta$, where displacement D decreases rapidly with ζ at any time during the always-outward motion of Fig. 1). Thus, the long rise in μ past the porosity limit (Figs. 2 and 3), is simply the result of steep decay in peak velocity with range ($n \gtrsim 2.7$), coupled with a velocity at 5.22 m that soon stops falling. And now comes the rub: Accelerometers of MP2 type often develop small, long-lasting offsets from their baselines that cause errors in velocity to grow; their output, as a result, is generally given less and less credence as time advances. Hence, we recomputed the strain path and stress bounds of Fig. 2, allowing the initial rate of decay of the pulse at that range (Fig. 1) to last forever. As Fig. 9 shows, $-\Delta$ [$=\mu/(1 + \mu)$] again rises after time t_v, but it reaches a reasonable peak (.262) and then drops.

To understand how the factor φ [Eq. (11)] affects compression, note that the farther we go in radius at a given time, the closer we come to the front of an outgoing wavetrain; the velocity seen at the larger of the two ranges thus occurs a shorter time after arrival of the pulse at that range. Hence, in the decay-section of a pulse of unchanging shape, φ increases with range. Of course (Fig. 1), pulse-shape does change with range here (as usual), the pulse spreading as it travels; the time in which φ falls from 1 to .9 (say) increases with range. On moving outward at a fixed time, φ therefore approaches 1 more rapidly than if pulse-shape were unchanging; on the decay-section of a pulse, the increase in φ with range at fixed time is thus enhanced (though not dominated) by pulse-spreading. In short, the decay of φ makes r^2u more positive, tending to cancel the compressive contribution of the other two factors in Eq. (11). The growth of that tendency, causing a downward curvature of μ with time, is also readily understood; for, Eq. (11) implies that

$$[\delta(r^2\mu)]/(r^2u) = 2(\delta\epsilon_\theta)/(1+\epsilon_\theta) - (n-2)(\delta\zeta)/\zeta + (\delta\varphi)/\varphi \qquad (12)$$

where $D/\zeta \equiv \epsilon_\theta \equiv$ hoop strain, and δ here is a variation in ζ at fixed time ($\delta\zeta$ is the arbitrary initial thickness of a spherical shell at location ζ). Since $0 \leq \epsilon_\theta \ll 1$ and $(\delta\zeta)/\zeta$ is time-independent, the only term on the right of Eq. (12) that can change much with time is $(\delta\varphi)/\varphi$. For a given $\delta\varphi > 0$, that term grows as φ decays, whence it adds ever more

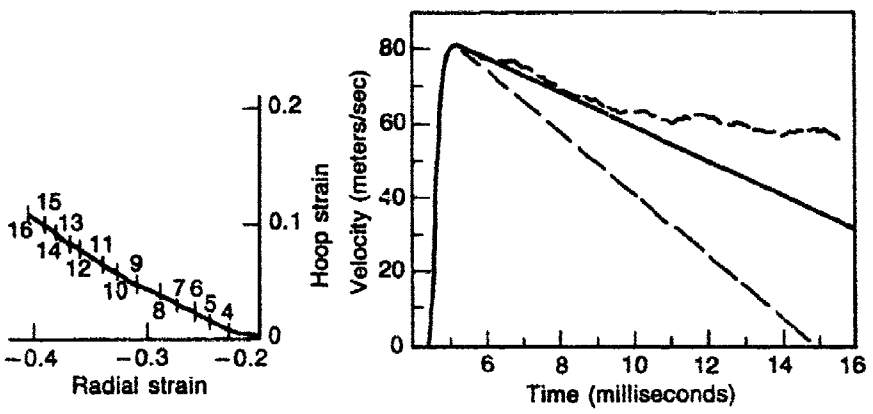

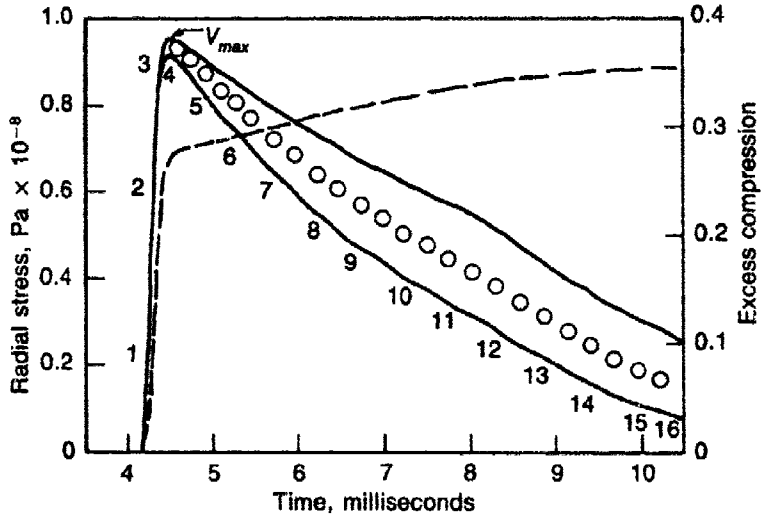

Fig. 9. Strain path and stress bounds of Fig. 2, but with velocity decaying at a constant rate (solid line). The format, and the strain path up to point "4", are those of Fig. 2. The measured pulse (top half of Fig. 1) is traced by the dashed curve at the upper right. The dashed straight line decays at the greatest fixed rate for which compression increases while radial stress decreases.

increments to changes in r^2u, and slows the rate of compression more and more (downward curvature).

Interplay of the terms of Eq. (12) is simplest in Fig. 9 because a linear $\varphi - \tau$ relation makes $\delta\varphi$ only weakly time-dependent [$\delta\tau/\delta\zeta$ depends on time; Eq. (1)]. As the decay rate is increased, both peak compression and its time of occurrence, t_c, decrease. At a critical decay rate,

t_c becomes equal to the time when σ_r, along its tensile upper bound, equals the peak lower-bound value of σ_r; if t_c exceeds that time, then σ_r itself must fall while μ is rising. The decay rate is critical on the dashed line of Fig. 9. In the same sense, if φ-decay is fixed, then n also has a critical value—2.24, for the solid line of Fig. 9.

One further point: Relative to Fig. 2, μ increases only slightly in Fig. 7 after peak-velocity-time t_v, even though the pulse-forms at 7.13 and 5.22 m are much alike (Fig. 1). That happens mainly because the pulse takes much longer to decay at 7.13 m than at 5.22 m. Thus Fig. 7 spans only the time of most rapid velocity decrease at 7.13 m in Fig. 1 (in which period φ falls ~ 3/5 as fast as on the solid line of Fig. 9). After time t_v, the compression curve of Fig. 7 is therefore relatively straight. Also, a smooth curve through all the pulse-width data [as in Fig. 5 for $A(\zeta)$] gave the function $W(\zeta)$ actually used; pulse decay at 7.13 m is somewhat hastened as a result, increasing the fraction 3/5 to ~ 5/6. With $1/\zeta$ and ϵ_θ smaller at 7.13 m than at 5.22 m, the sum of the first two terms on the right of Eq. (12) (which are compressive), shrinks relative to the third (which is expansive). The compression curve of Fig. 7 is therefore relatively flat after time t_v. At later times than in Fig. 7, the velocity pulse flattens and compression climbs above the porosity limit, as in Fig. 2; the gauge fails before probable gauge drift turns to certain drift, but radial velocity is plainly rising at the end.

Independent Data, Models and Conclusions

Data from the MP2 event firmly back the view that, on the strain paths followed in situ, all stress components depend strongly on shear strain. Each compression history deduced from the data at nominal ranges of 5.3 and 7.1 m, including sensitivity-study paths (Figs. 4 and 7), shows a sizable period of growing or constant compression, during which radial stress falls. No such behavior occurs in hydrostatic laboratory tests, nor is it observed for uniaxial strain, either in situ or in the laboratory. Over the years, those two kinds of test (hydrostatic and uniaxial strain) have provided most of the material properties data for calculating explosively driven soil motion; they differ in their ratios of shear strain to compression (the present strain paths differ from both in that same respect.) It was observed early on that the hydrostat for a porous tuff (~ 5% air-filled voids) was much softer in uniaxial strain than hydrostatic strain, a result deemed due to the breakdown of pores in shear.[1] With still more shear along present paths, we find hydrostats to be—at the least—a good deal softer yet. Indeed, at and near times of stationary compression, when

only shear strain occurs, radial stress appears to drop at about the same steady rate as at other times.

The message of the early tuff data has sunk into soil models, but not far. Modelers recognized that hydrostats derived from uniaxial strain tests could differ grossly from those of hydrostatic strain tests, and opted for the former as being better suited to fields with steep-fronted compression waves (a step in the direction of strain-path methods). However, mean stress P is still related to compression alone in most models. Typically, the models admit pore collapse by stating that P-μ curves are steeper on unloading than loading—far steeper for soils, as in Fig. 10.

Four of the five models used to calculate MP2 motion (preshot) had hydrostats resembling that of Fig. 10. The fifth has the rate-dependence of a standard linear solid; mean stress drops when the uniaxial leg of the strain path (Fig. 2) gives way to the shear leg—but it soon levels off, whereas (above) MP2 stresses steadily fall. Even at ~ 7.1 m the models' conflict with MP2 data is clear: If compression drops appreciably, as in Fig. 6, then (Fig. 10) the models have mean stress falling much more rapidly than Fig. 6 implies; if compression increases slightly, as in Fig. 7, then the models have mean stress rising—not falling steadily, as Fig. 7 implies.

The models collide most seriously with MP2 data at ~ 5.3 m. There mean stress decreases steadily despite a large increase in compression. That happens (Fig. 9) even if an overcorrection (probably) is made for gauge drift—drift being the most likely cause of the surplus compression seen at late times if the gauge record at 5.22 m is taken literally (above). The hydrostat of Fig. 10 fails to provide even a starting point for describing such behavior, whose physical burden is that mean stress is greatly relieved by shear strain (negative bulk moduli are not the answer). Softening of MP2 kind can be handled within the framework of non-ideal plasticity, which a few models of explosions embraced years ago. However, while capable of quite different behavior than the others, models that include non-ideal plasticity and/or rate effects have usually given stress-strain curves and motions much like the others'. Indeed, that fact is a major reason for the longevity of simpler models. Another is historical: The models are outgrowths of ideal elasto-plastic theory, which, in simplest form, has P proportional to Δ. Non-ideal plasticity was later invoked to control the excessive inelastic growth of porosity ("dilatancy") implied by the associated flow rule for some frictional materials in shear. Here we confront the opposite effect—a large inelastic loss of porosity for such materials in shear ("compactancy"?).

The effect in present form was first found on in-situ strain paths when those paths, and stress bounds, were deduced[2] from SCOOTER pulses.

In the SCOOTER event,[14] useful pulses were measured only at shot depth, without redundancy. By luck, the range of the SCOOTER pulse closest to shot point, when simply-scaled to MP2 yield, is very nearly 5.3 m. However, peak velocity in that pulse was much too high to fit

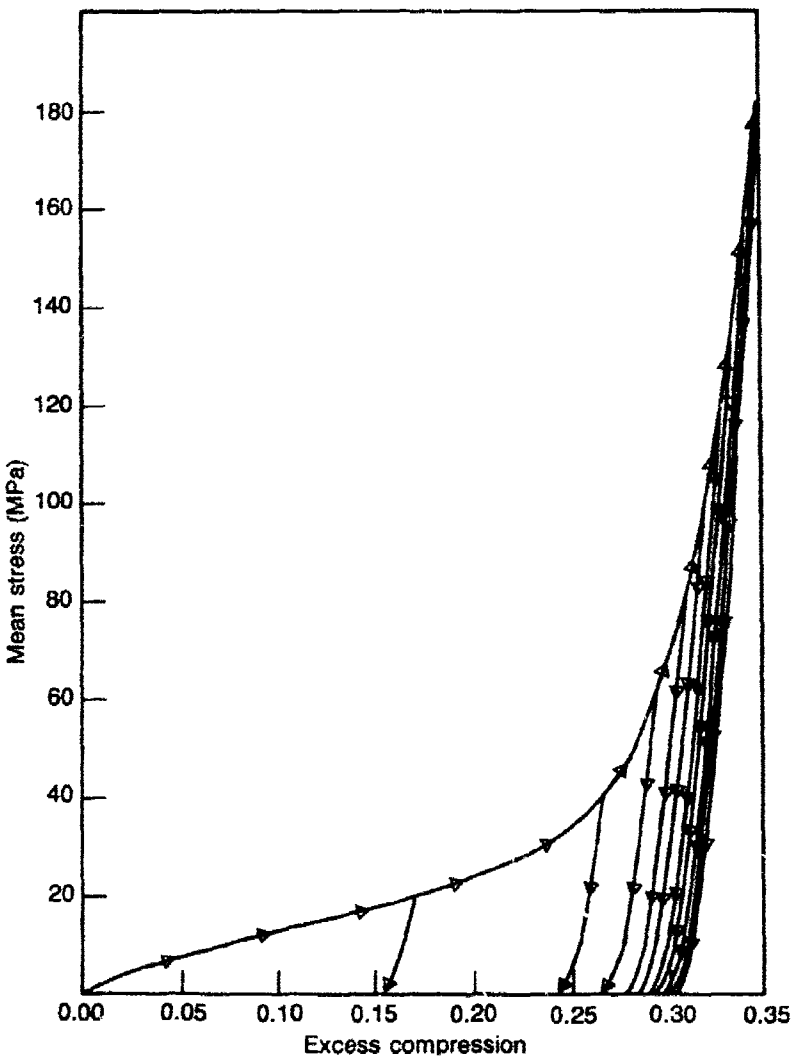

Fig. 10. Mean Stress *vs.* Excess Compression in a Model of MP2 Alluvium. The hysteretic relation pictured here fully defined mean stress in the preshot calculations made at Applied Theory, Inc. Mean stress was independent of shear strain in every model used for preshot calculations of the MP2 event.

with the rest, and was given little credence by its measurer.[15] Hence, while the pulse's form-factor φ was retained, its amplitude was set by a least-squares line through the other points (log A vs. log ζ). The resulting strain path and stress bounds appear in Fig. 11. Their early cutoff is due to failure of the gauge in question, but they last long enough to tell the same story as the curves of Figs. 2, *etc.*—with considerably less confidence.

Shortly before event MP2, stresses were also measured in the laboratory along strain paths like that of Fig. 2, using samples of MP2 soil. At the point where uniaxial strain gives way to nearly pure shear, radial stress starts to fall (Fig. 12). The drop is shallow and short-lived but becomes more pronounced in the laboratory P-μ curves (Fig. 12). Qualitatively, that result (μ rising, P falling) agrees with our MP2 and SCOOTER results, and is not compatible with Fig. 10. In quantitative terms, it differs greatly from the MP2 and SCOOTER results. Among the more likely explanations for that fact are far lower laboratory loading rates (by a factor $> 10^5$), differences between laboratory and in-situ properties, and lower laboratory stresses. As for interpreting MP2 data, the assumption of spherical symmetry, power-law decay of velocity, and broad trends in the waveforms, are all subject to error. Symmetry of the field is assured by the data, but only within its sizable scatter—and with a possible exception in Fig. 5: Peak velocity may fall faster with range along one gauge-line (downgoing; symbol ○) than on the others (measurements were made in five directions from shot point); however, the point at ~ 30-m radius is suspect (it would force faster falloff than r^{-7} at 30 m), and there are only three others. Otherwise, no significant directional differences are apparent— at least in peak velocity, and in precursor and main-wave arrival times.

Again, if peak velocity were considered exact at 5.22 m, and were coupled with the linear pulse-decay of Fig. 9, then $A(\zeta)$ would fall slowly enough at that range to undermine our main result there (μ rising, P falling). Such a procedure, however, is less reasonable than that adopted here, since peak velocity is a random variable. Besides, results that depend heavily on detailed data at the limit of a measurement's range, are innately less credible on that account (which would have been reason enough to vary the waveform at 5.22 m). Moreover, on testing the hypothesis of a quadratic (log A, log ζ) relation, we found it less probable than a linear one, and even the quadratic supports our broad conclusion (sensitivity of stress to shear strain; Fig. 4). Further, the models have a more severe problem *vis-a-vis* the data than their P-μ relations suggest: The fall of σ_r is clear. Yet, radial compression constantly increases, and its increments so far exceed hoop-stretch increments as

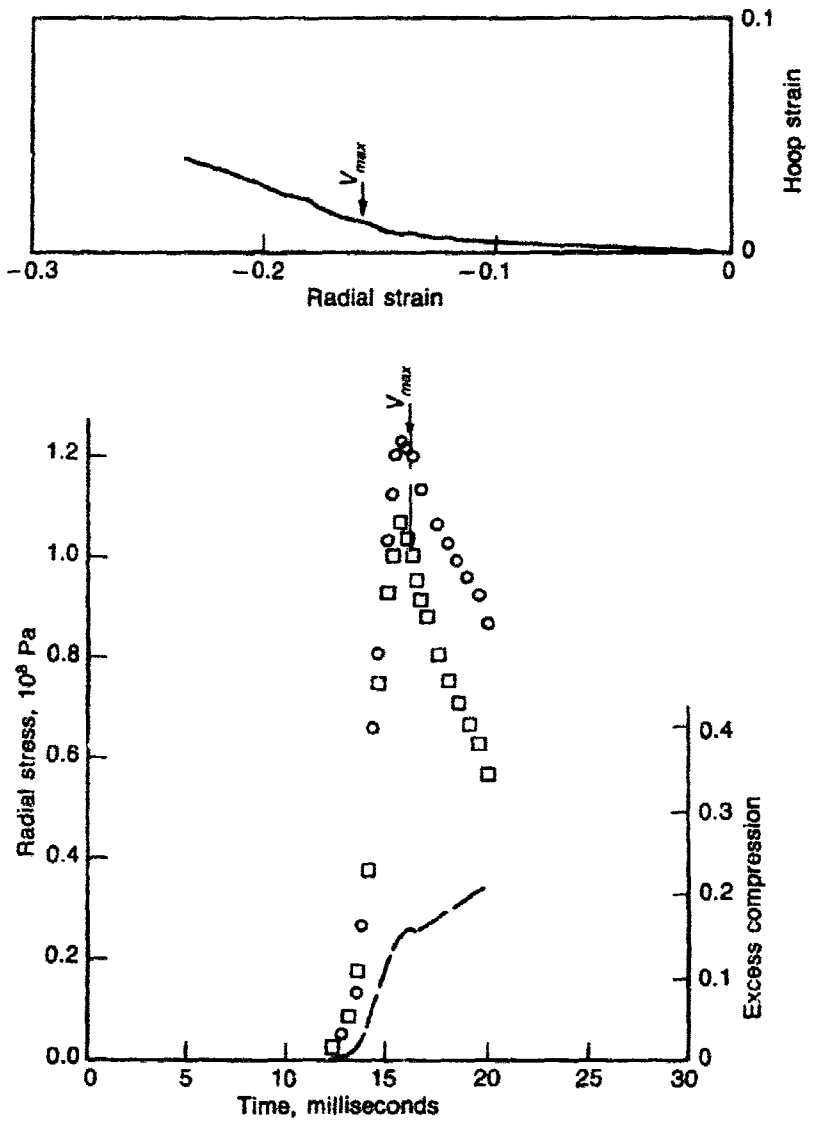

Fig. 11. Strain Path and Stress Bounds for the SCOOTER Event at a Slant Range of 15 Meters (5.3 Meters When Simply Scaled to MP2 Yield). The curves were computed from velocity pulses measured on a horizontal line through shot point, at ranges of 15, 30, 45 and 60 meters. The 15-m pulse was multiplied by the factor .3 to make it consistent with the motion amplitudes measured at the other SCOOTER ranges.

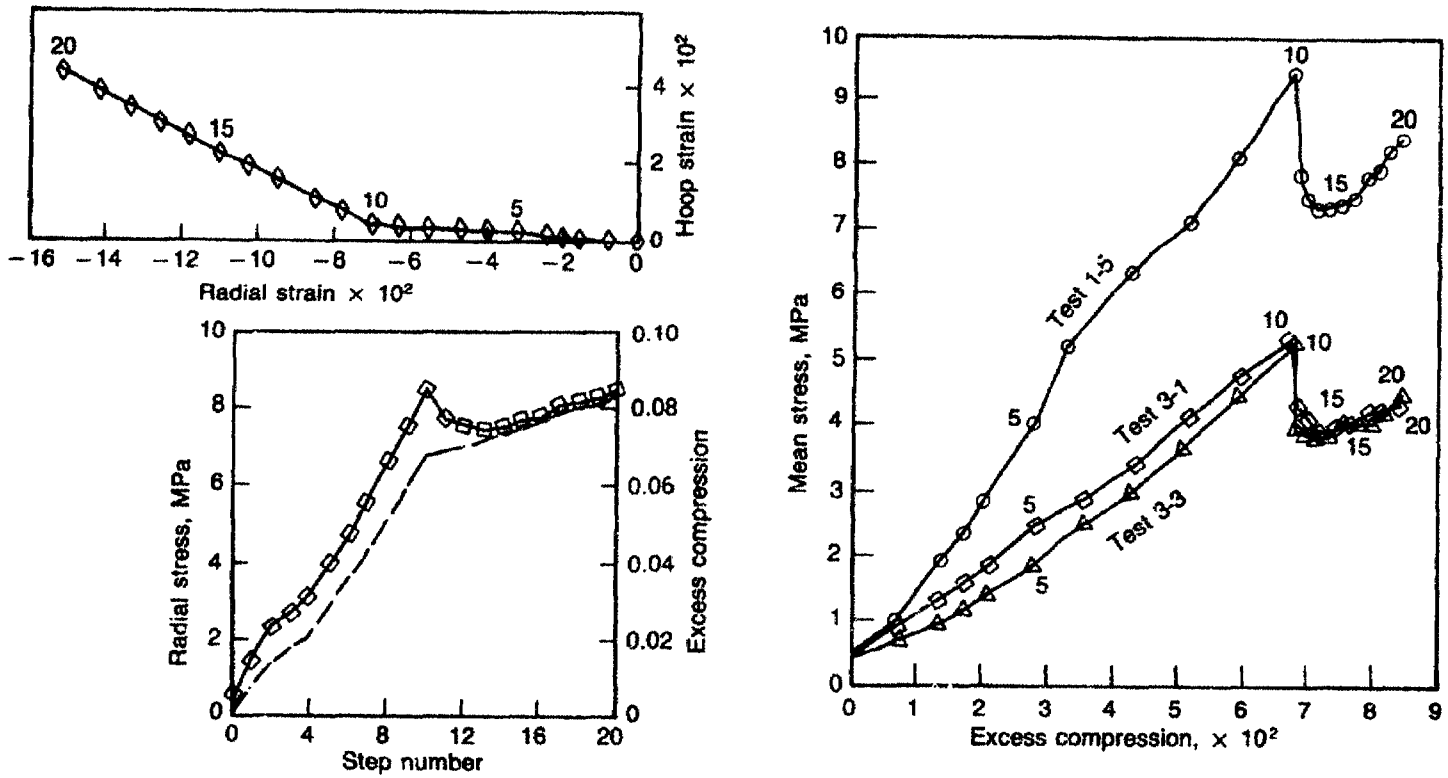

Fig. 12. Laboratory Stress-Strain Curves for MP2 Soil Along a Prescribed Strain Path.[3] The plot at the upper left gives the path; every fifth step taken in traversing it is numbered. The path was followed closely in the three tests whose resulting hydrostats appear in the right-hand plot. For Test 3-1 (◇), the logically-radial stress and the excess compression are plotted *vs.* step number.

to render volume either about constant or decreasing. No MP2 model is qualitatively compatible with such behavior.

In the order of declining confidence, the conclusions drawn from the data—especially MP2 data—are these:

i) The stress-strain curves generated in all calculations of MP2 motion go wrong after peak velocity is reached.
ii) All components of stress are greatly relieved by shear strain, on the strain paths actually followed in such events.
iii) The effect (ii) persists in the face of substantial decreases in volume.

The mechanism of shear-induced pore collapse, long recognized, will account for these findings. In any case, to dispute them is to argue with the measurements. Unfortunately the MP2 data are arguable, which is the main source of uncertainty in the conclusions stated. Still, their confirmation is likely when more consistent and complete measurements are made in future explosive events. That surmise calls forth our overriding conclusion: There must be more events like MP2 because conclusions i)-iii) are so basic. If they are borne out, then the models' impressive postdictions of explosively driven soil motion will come to little more than roundabout curve-fitting. The models will then become credible tools for extrapolation (*i.e.*, for predicting unfamiliar ground motions) only after fundamental revision.

Much can be learned from laboratory tests along the proper strain paths, which are known, but at present nothing can replace the measurement of stress-strain curves in situ. By making radial stress accessible through radial motion alone, the methods described here will, in part, furnish those curves. In so doing, they can also supply the independent data needed to fix the accuracy of stress gauges, whose improvement is the key to the problem of modeling explosions.

Appendix

With $n = 0$, 1 and 2, respectively, uniaxial, cylindrical-radial and spherical motions are governed by the equation

$$\rho \ddot{u} = - \partial \sigma_r / \partial r - n(\sigma_r - \sigma_\theta)/r \tag{11}$$

where r and σ_r denote distance and normal stress in the direction of motion; σ_θ is hoop stress. For motion that begins with compression of material in the r-direction, but not at right angles to that direction, we again have $\sigma_\theta \leq \sigma_r$; also, σ_θ remains $\leq \sigma_r$ as long as the principal strain

in the r-direction becomes increasingly compressive, and no compressive changes take place in the other two principal strains. During that time, Eq. (11) implies that

$$\rho \dot{u} \geq - \partial \sigma_r / \partial r \tag{12}$$

Thus, the lower σ_r-bound given by Eq. (8) flows from Eq. (11) for all n, and not just $n = 2$. As for the upper (tensile) bound, we find that

$$\rho \dot{u} = -\partial \sigma_r / \partial r - n(\sigma_r + T)/r = (1/r^n)\, \partial [r^n (\sigma_r + T)]/\partial r \tag{13}$$

or

$$\sigma_r^g \leq T[(r_f/r_g)^n - 1] + \int_{r_f}^{r_g} (r/r_g)^n \rho u \, dr \tag{14}$$

If ζ is the position of an arbitrary material element at some initial time t_i, then mass conservation is expressed for $n = 0$, 1 and 2 by the relation

$$\rho r^n dr = \rho_i \zeta^n d\zeta \tag{15}$$

where ρ_i and ρ again denote density at times t_i and t. Using Eq. (15) to eliminate $\rho r^n dr$ from Eqs. (8) and (14), we find that

$$\int_{\zeta_g}^{\zeta_f} \left(\frac{\zeta}{r}\right)^n \rho_i \dot{u} \, d\zeta \leq \sigma_r^g \leq T\left[\left(\frac{r_f}{r_g}\right)^n - 1\right] + \int_{\zeta_g}^{\zeta_f} \left(\frac{\zeta}{r_g}\right)^n \rho_i u \, d\zeta \tag{16}$$

With $n = 0$, the upper and lower bounds of Eq. (16) are the same; motion determines σ_r uniquely, since σ_r is the only stress component that affects $\dot{u}$ when $n = 0$ [Eq. (11)].

The limited ability of all materials to sustain shear stress means that $\sigma_r - \sigma_\theta$ has an upper bound other than the tensile limit $\sigma_r + T$. Thus, there exists a second upper bound on σ_r in terms of motion. That bound is readily derived for the case of a Mohr-Coulomb-von Mises material, *i.e.*, a material for which (if $\sigma_r \geq \sigma_\theta$)

$$\sigma_r - \sigma_\theta \geq \text{Min}(a + bP, y_{vm}) \; ; \; 3P \equiv \sigma_r + 2\,\sigma_\theta \tag{17}$$

where a, b, and y_{vm} (von Mises' limiting value of $\sigma_r - \sigma_\theta$) are material-specific constants, such that $a \leq y_{vm}$, $b \geq 0$. Besides the shear-strength limit [Eq. (17)] σ_θ is still constrained by the tensile-strength limit $\sigma_\theta \geq -T$. Thus the accessible region of the $(\sigma_r, \sigma_\theta)$-plane has a continuous lower boundary B comprised of three straight sections—straight because

equating $\sigma_r - \sigma_\theta$ to either $a + bP$, y_{vm} or $\sigma_r + T$ leads to a linear (σ_θ, σ_θ)-relation. The σ_r-range on which each straight line forms a part of B is set by the points at which the lines cross; accordingly, we find that

$$\sigma_\theta \geq \sigma_\theta^B \tag{18}$$

where

$$\sigma_\theta^B = \begin{cases} -T\,; & \sigma_r \leq \sigma_r^1 \\ [(1-\tfrac{1}{3}b)\sigma_r - a]/(1+2b/3)\,; & \sigma_r^1 < \sigma_r < \sigma_r^2 \\ \sigma_r - y_{vm}\,; & \sigma_r \geq \sigma_r^2 \end{cases} \tag{19}$$

and

$$\sigma_r^1 = [a-(1+2b/3)T]/(1-\tfrac{1}{3}b) \tag{20}$$

$$\sigma_r^2 = [(1+2b/3)y_{vm}-a]/b \tag{21}$$

It follows from Eqs. (11), (18) and (19) that

$$\begin{aligned} \rho\dot{u} &\geq -\partial\sigma_r/\partial r - n(\beta\sigma_r + K)/r \\ &= -nK/r - [\partial(r^{n\beta}\sigma_r)/\partial r]/r^{n\beta} \end{aligned} \tag{22}$$

where

$$\beta \text{ and } K = \begin{cases} 1 \text{ and } T\,; & \sigma_r \leq \sigma_r^1 \\ b/(1+2b/3) \text{ and } a/(1+2b/3)\,; & \sigma_r^1 < \sigma_r < \sigma_r^2 \\ 0 \text{ and } y_{vm}\,; & \sigma_r \geq \sigma_r^2 \end{cases} \tag{23}$$

Rearranging Eq. (22) and integrating [as in moving from Eq. (7) to Eq. (8)], we obtain the bound

$$\sigma_r^g \leq \int_{r_f}^{r_g} (r/r_g)^{n\beta}\,(\rho u + nK/r)\,\mathrm{d}r \tag{24}$$

Time is a fixed parameter of Eq. (24) just as in Eqs. (8) and (14). Now, however, on integrating from r_f to r_g, β and K change [Eq. (23)]

at whatever r-values mark the passage of σ_r from one to another of the regions $\sigma_r \leq \sigma_r^1$, $\sigma_r^1 < \sigma_r < \sigma_r^2$ and $\sigma_r \geq \sigma_r^2$. The changes can be made if we know how σ_r varies with r at any given time—but if that were known, there would be no need to bound σ_r in the first place. To break the deadlock, recall that the key to an upper bound on σ_r^g lies in bounding $\rho\dot{u}$ from below, which is achieved by bounding σ_θ from below. Strict use of curve B for that purpose leads to the bound σ_θ^B [Eq. (18)], whose sections cover specific σ_r-ranges. We don't know how to relate those ranges to the position r, but we can avoid the need to do so by observing that as σ_r increases, each successive section of B lies on a steeper line than the one before it. Hence, if we let a smaller stress than σ_r (σ_r^L, say) determine when each section of B is used, then the value of σ_θ found on B for a given σ_r (σ_θ^{BL} say) will be at least as low as σ_θ^B—and σ_θ^{BL} will also bound σ_θ from below. More precisely put:

If

$$\text{i) } \sigma_\theta^B \text{ is given by Eq. (19), and } \sigma_\theta^B \leq \sigma_\theta \text{ [Eq. (18)]}$$

$$\text{ii) } \sigma_r^L \leq \sigma_r \tag{25}$$

iii)

$$\sigma_\theta^{BL} = \begin{cases} -T\,; & \sigma_r^L \leq \sigma_r^1 \\ [(1-\tfrac{1}{3}b)\sigma_r - a]/(1+2b/3)\,; & \sigma_r^1 < \sigma_r^L < \sigma_r^2 \\ \sigma_r - y_{vm}\,; & \sigma_r^L \geq \sigma_r^2 \end{cases}$$

then

$$\sigma_\theta^{BL} \leq \sigma_\theta^B \leq \sigma_\theta$$

As proof, note that B consists of sections of three curves (straight lines here), namely $f_1(\sigma_r)$, $f_2(\sigma_r)$ and $f_3(\sigma_r)$, with the following vital property: $f_2 \geq f_1$ for all $\sigma_r \geq \sigma_r^1$, and $f_3 \geq f_2$ for all $\sigma_r \geq \sigma_r^2$. Now suppose that $\sigma_r \geq \sigma_r^2$. Then $\sigma_\theta^B = f_3(\sigma_r)$. Also, since $\sigma_r^L \leq \sigma_r$, either $\sigma_r^2 \leq \sigma_r^L$ ($\leq \sigma_r$) or $\sigma_r < \sigma_r^L < \sigma_r^2$ or $\sigma_r^L \leq \sigma_r^1$. In the first case $\sigma_\theta^{BL} = f_3(\sigma_r) = \sigma_\theta^B$; in the second $\sigma_\theta^{BL} = f_2(\sigma_r)$; in the third $\sigma_\theta^{BL} = f_1(\sigma_r)$. But $f_3(\sigma_r) \geq f_2(\sigma_r) \geq f_1(\sigma_r)$ [since $\sigma_r \geq \sigma_r^2 > \sigma_r^1$], whence $\sigma_\theta^{BL} \leq \sigma_\theta^B$. Similar reasoning tells us that $\sigma_\theta^{BL} \leq \sigma_\theta^B$ *if* $\sigma_r^1 < \sigma_r < \sigma_r^2$, and $\sigma_\theta^{BL} = \sigma_\theta^B$ if $\sigma_r \leq \sigma_r^1$; *q.e.d.* The lemma has obvious extension to any number of B-sections.[16]

To apply the lemma, we need a lower bound σ_r^L on σ_r, where σ_r^L is a known function of r. Such a bound appears on the left of Eq. (16), and we therefore write

$$\sigma_r^L = -\int_{\zeta_f}^{\zeta} \left(\frac{\xi}{r}\right)^2 \rho_i u \, d\xi \tag{26}$$

Integrating backwards from ζ_f [Eq. (26)] makes it easy to determine σ_r^L as a function of ζ, the upper limit of integration—and hence as a function of $r\,[= r(\zeta, t)]$. Since $\sigma_\theta \leq \sigma_\theta^{BL}$ we again obtain Eq. (24), except that

$$\beta \text{ and } K = \begin{cases} 1 \text{ and } T; & \sigma_r^L \leq \sigma_r^1 \\ b/(1+2b/3) \text{ and } a/(1+2b/3); & \sigma_r^1 < \sigma_r^L < \sigma_r^2 \\ 0 \text{ and } y_{vm}; & \sigma_r^L \geq \sigma_r^2 \end{cases}$$

In applying these formulas to MP2 data, T, a, b and y_{vm} were assigned the values .5 MPa, .5 MPa, .8 $\sqrt{3}$ and ∞, respectively.[12]

References and Notes

1. R. Bjork, *Computed Response of the Hudson Moon H.E. Experiment*, Systems, Science and Software Topical Report No. 3SIR-976 Feb. 7, 1972 (Contract DASA01-69-C-0165).
2. Summary of CARES Material Properties Program Meeting, February 3-4, 1983, AFWL, Kirtland AFB, NM, Distributed by Tech Reps., Inc. under cover of letter dated 29 March 1983.
3. P. Lade, *Strain Path Tests on Yuma Soil*, (final report; Subcontract ATS-55-1; Contract No. DNA001-80-C-0232).
4. J. Trulio, *Strain Path Modeling for Geo-Materials*, Defense Nuclear Agency Topical Report No. TR-84-105, Sections 1 and 4, June 1984 (to be published).
5. L. Seaman, "Lagrangian Analysis for Multiple Stress or Velocity Gauges in Attenuating Waves," *J. Appl. Phys*, 1974, p. 4303.
6. J. Trulio, *Ground Shock Deformation Fields*, Report No. ATR-77-48-6; 1977 (final report; Contract No. F04704-76-C-0031). Analytic use of the separation of fields into amplitude and waveform factors appears first to have been made by Dennis Grady ("In Situ Constitutive Relations of Soils and Rocks," Defense Nuclear Agency Report No. DNA 3671Z, p. 50-56, March 1974).
7. J. Workman, J. Trulio and E. Stokes, *Trajectory Analysis, an Aid in Defining the MX System Ground Motion*, Air Force Weapons Laboratory, Technical Report No. AFWL-TR-80-56, Vol. I, May 1981 (final report for Contract No. F29601-79-C-0065).
8. Air Force Weapons Laboratory Project Officer's Report on CARES Material Properties Test 2; to be published.
9. Ref. 6, Section 2.6.

10. See, for example, A.E. Jackson and R. Petersen, *Material Property Investigation for Pre-Dice Throw I and II: Results from the Laboratory Testing Programs*, issued by U.S. Army Engineer Waterways Experiment Station, November 1976 (work sponsored by Field Command, Defense Nuclear Agency and Headquarters, Defense Nuclear Agency).
11. N. Rimer and K. Lie, *Numerical Simulation of the Velocity Records from the SRI Grout Spheres Experiments*, Systems, Science and Software Topical Report No. SSS-82-R-5580, Sept. 1982 (Contract No. DNA001-82-C- 0043).
12. A.E. Jackson and J. Cargile, *Preliminary Material Property Estimates for Dry CARES*, distributed under cover of a letter from the Waterways Experiment Station dated 18 April 1983. 13. Ref. 12, Figs. 1 and 2.
14. W. Perret *et al.*, *Project SCOOTER*, Report No. SC-4602, October 1963 [Sandia Laboratory, Albuquerque; also issued in TID 4500 (23rd Ed.), *Nuclear Explosions-Peaceful Applications*.]
15. W. Perret, private discussions, 1983.
16. If section n lies on the curve $\sigma_\theta = f_n(\sigma_r)$ for some range of σ_r whose upper limit is σ_r^n, and if $f_{n+1} \geq f_n$ for all $\sigma_r \geq \sigma_r^n$, then the curves $f_1(\sigma_r)$, $f_2(\sigma_r)$, . . . need not be straight lines for the theorem to hold. That fact is not useful here because $\partial\sigma_r/\partial r + F(\sigma_r)/r$ has no integrating factor in r alone, unless $F(\sigma_r)$ is linear in σ_r .

Acknowledgement

This work was performed for the Defense Nuclear Agency under Contract DNA001-84-C-0128. It is a pleasure to acknowledge the support of Dr. George Ullrich throughout the program, and the able assistance of Mr. Neil Perl and Dr. James Workman with its performance.

Modeling L_g Codas of *P-SV* and *SH* by Vertical Boundaries

C.Y. Wang and R.B. Herrmann

Summary

We are attempting to model the effect of 2-D heterogeneities upon L_g wave excitation and propagation.

Conclusions and Recommendations

The mathematical theory developed works. The earth models considered are simplistic because

(1) no mode conversion is permitted
(2) no wavetype conversion (Love–Rayleigh–Love) is permitted
(3) the two-dimensional character of the model does not give correct geometric attenuation of the coda for comparison to real data.

On the other hand, we have been able to demonstrate the effect of vertical and horizontal layering on the shape and extent of the L_g arrivals. Future work will address the problem in a different manner by considering the effect of a three-dimensional distribution of point scatterers on L_g surface waves. This work will yield the correct geometrical spreading as well as conversion from Rayleigh to Love waves and back.

Introduction

Most current theories about the coda of L_g waves are concentrated on the seismic scattering from inhomogeneities in the crust and upper mantle. These models mostly assume stochastic processes and consider the average behavior of the waves interacting with randomly distributed particles (Aki and Chouet, 1975; Sato, 1984). This statistical nature, however, makes it difficult to isolate the individual factors which affect the coda. In this report, we try another approach to see if some kind of deterministic solution is still possible to describe the complicated ray path effect such as coda.

The basis of our approach is to find an analytic solution for a model more complex than just plane horizontal layers. Upon the horizontal layers we add several vertical cylindrical boundaries which are centered at the source (Fig. 1). These vertical boundaries describe some sort of lateral inhomogeneity, hence, they make the problem more two-dimensional. An analytic solution exists in such a model if the materials in each annulus satisfy the Higuchi conditions (Kazi and Niary, 1983), which keep the eigenfunctions unchanged when crossing a boundary; therefore, mode conversion does not occur. These restrictions, although extreme, make a close form of solution possible. To some extent, this model can be looked at as a limiting case describing lateral inhomogeneities. Our aims focus on the effect of multiple bouncing of waves among horizontal and vertical boundaries.

Theory

First, we assume the materials in each annulus of vertical cylindrical model satisfy the Higuchi's conditions:

$$\frac{\mu_{1L}}{\mu_{1R}} = \frac{\mu_{2L}}{\mu_{2R}} = \cdots\cdots = \frac{\lambda_{1L}}{\lambda_{1R}} = \frac{\lambda_{2L}}{\lambda_{2R}} = \cdots\cdots$$

$$\frac{1}{\beta_{1L}^2} - \frac{1}{\beta_{1R}^2} = \frac{1}{\beta_{2L}^2} - \frac{1}{\beta_{2R}^2} = \cdots\cdots = p\left(\frac{1}{c_L^2} - \frac{1}{c_R^2}\right)$$

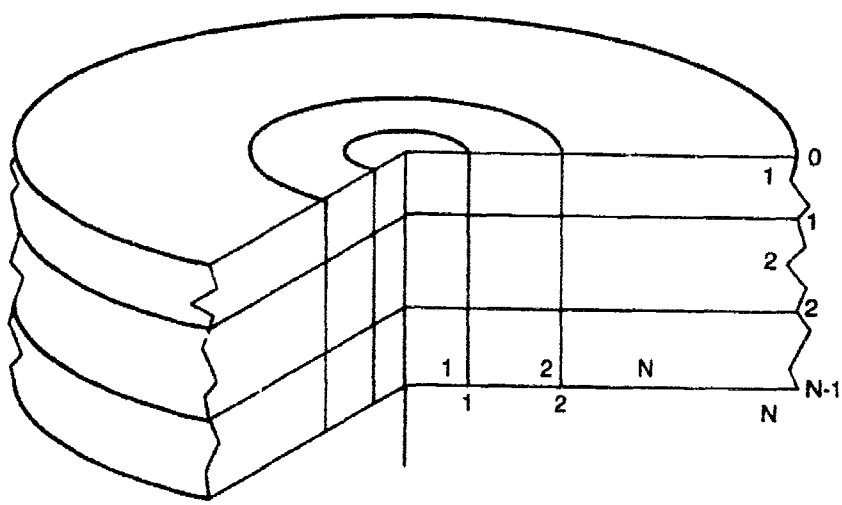

Fig. 1. Vertical cylindrical boundary model.

where the numbers indicate the layer numbers and L and R are for two medium on the left or right side of a vertical boundary. The value of p is unity for *SH* and higher mode *P-SV*, but for the fundamental mode *P-SV* wave this value is the solution of Rayleigh equation if λ/μ are constant for all layers. Under these conditions the eigenfunctions will have the same shapes in each medium, thus, there is no mode conversion (Alsop, 1966). These conditions can be verified by applying the differential equations for elastic wave propagation. Since the application to *P-SV* is proposed first time in the literature, some numerical tests are conducted (Fig. 2). Figure 2a shows the radial displacement eigenfunctions from two Higuchi media. These eigenfunctions match each other sufficiently well if some numerical error is allowed. Figure 2b displays the component $\partial c/\partial\beta$ which is calculated using the perturbation of energy

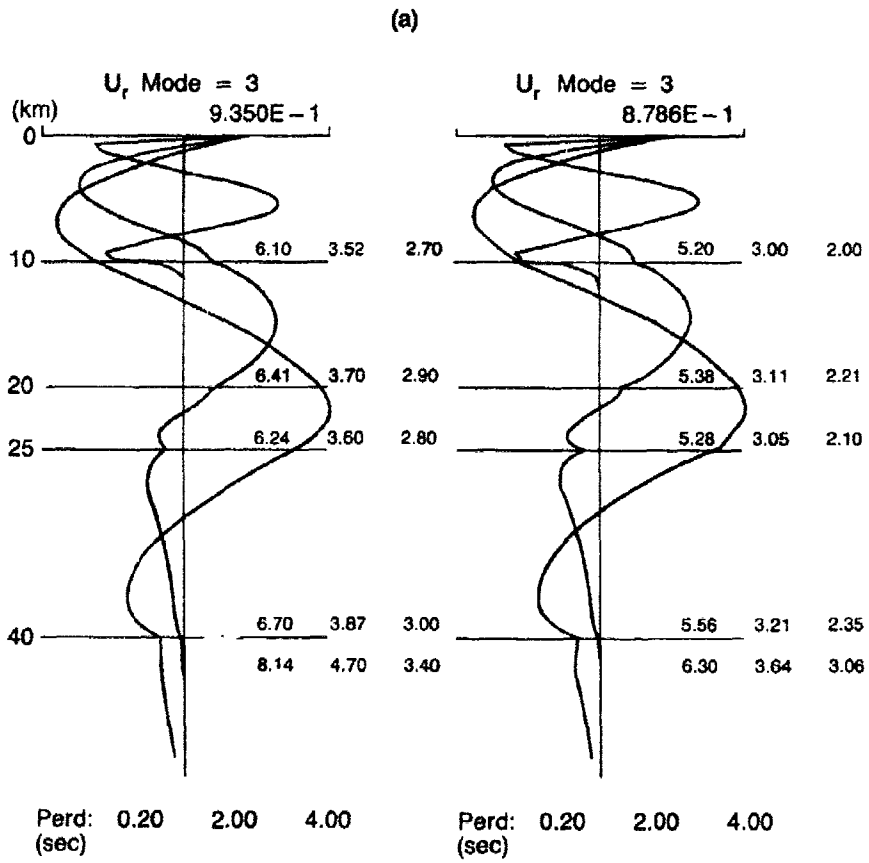

Fig. 2a. Radial displacement eigenfunctions from two models which satisfy the Higuchi's conditions.

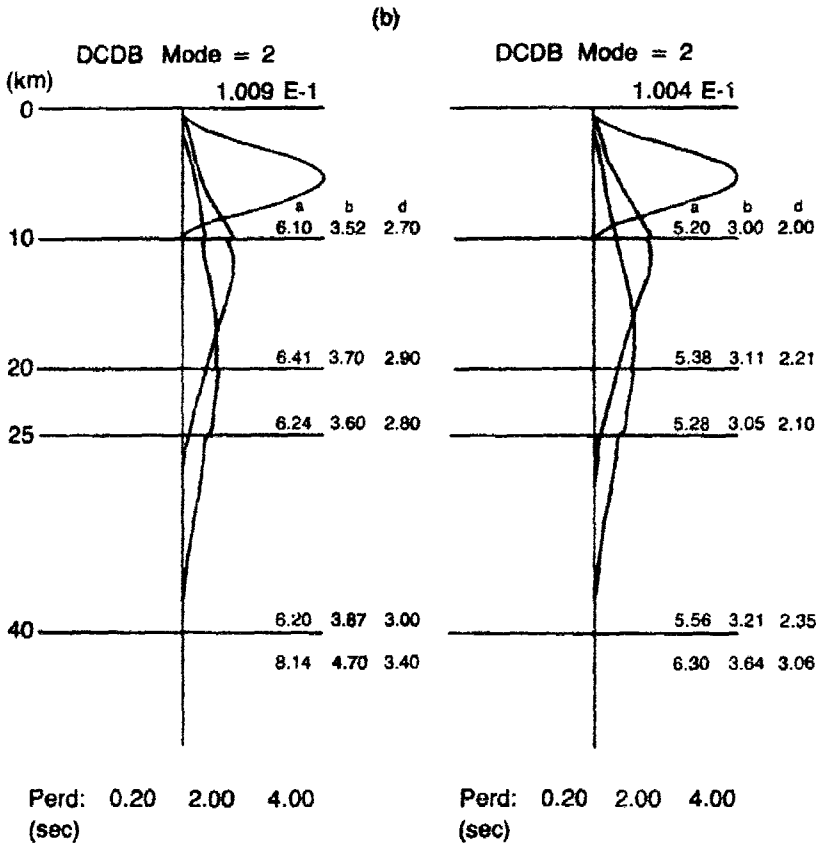

Fig. 2b. $\partial c/\partial\beta$ **varying with the depth from two models satisfying the Higuchi's conditions.**

integrals (Wang, 1981). The agreement of two curve sets in Fig. 2b further proves the correctness of the above Higuchi's conditions, and also shows the stability of our eigenfunction calculation. Note that there is a low velocity layer in the velocity model.

Assuming no mode conversion at the vertical boundaries, we set up the lateral cylindrical layer response by Haskell's matrix method. The boundary conditions to be satisfied are not vertical, and the wavefields are propagating in the horizontal direction. A similar mathematic expression of these wavefields can be found in Luco and Apsel (1983). The derivation is straight-forward but trivial as in the general Haskell's theory for layered medium. The effect of lateral layer boundaries can be summarized as

$$u(r,z,\omega) = \sum_{\text{mode}} F(k,\omega)\, S(k,\omega)\, H_n^{(2)}(kr)$$

In this expression, the $F(k,\omega)$ is the standard medium response to a point source, $S(k,\omega)$ is the effect of the lateral inhomogeneities. Every mode is scattered differently, then they are summed to form the final solution. In the *P-SV* case, the phase conversion between *P* and *SV* motions along the horizontal as well as the vertical boundaries are included.

To confirm the theory as well as the computer programs, a simple test is conducted. Figure 3a is the waveforms generated in a simple crust model which has a 40 km top layer. The source is at 10 km deep with dip-slip mechanism and the receiver is at 45° azimuth and 100 km away. The highest frequency used is 10 Hz. A higher mode wave of pulse shape followed by a low frequency fundamental mode can be seen in this figure. Upon this simple crust model we start to add on some vertical boundaries. In Fig. 3b, a vertical layer with 10 km width and 2 km/sec shear velocity sandwiched by two 12.5 km and 5 km/sec velocity layers are inserted in the middle between the source and the receiver. The horizontal two-way travel time in each vertical layer is 5 or 10 seconds. We can see that the reflected waves come in at 5 seconds apart, and their amplitudes are quite close to the values estimated by the simple reflection and transmission formula. In Fig. 3c, this vertical layer model is put outside the receiver. The backward reflected waves generated seem stronger than the forward transmitted waves as those in Fig. 3b. If the vertical layers are placed with the center at the receiver, *i.e.*, the receiver is surrounded by several reflection boundaries, more realistic coda shape waveforms are obtained as shown in Fig. 3d. The back and forth multiply bounced waves arrive as a decaying tail. Their polarities also show an interesting pattern as expected. The fundamental mode arrivals seem to act in a different way compared with the higher modes.

Test

With the success of the above example, we now try more complicated cases. On the simple crust model (Fig. 3a), we insert five small horizontal layers. Each is 1.2 km thick and has the shear velocity increasing evenly from 3.63 to 3.77 km/sec. A much complicated waveform results in this layered model as seen in Fig. 4a. Next, we create a lateral varying velocity model by fluctuating the basic velocity with 10%. In Fig. 4b, we put these random velocities in twenty 1 km layers around the receiver which is at 100 km from the source. A coda tail starts to grow as the waves are reflected back and forth among the boundaries. If these vertical layers

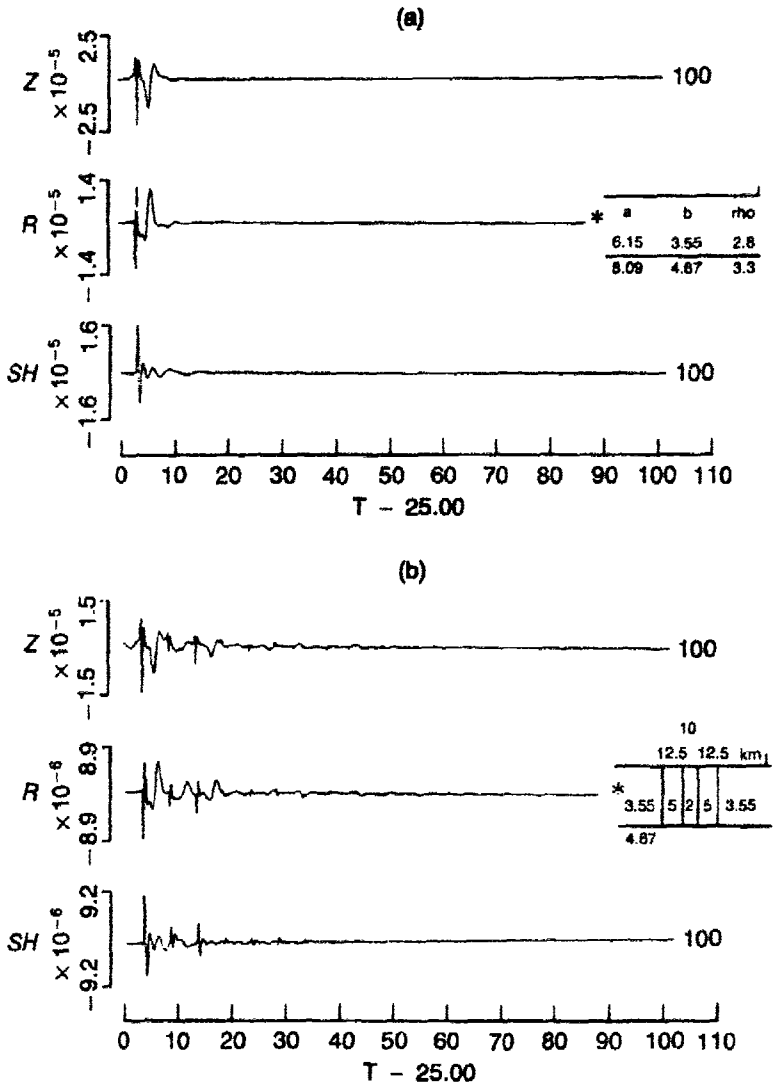

Fig. 3. Tests of vertical boundary effect on a simple crust model. Models are shown on the right side of each three componet set of seismograms.

are moved to the source side, the tail becomes weaker because of the smaller transmission coefficient than reflection coefficient (Fig. 4c). However, the case can be made more complex as that shown in Fig. 4d. Forty randomly-fluctuated velocity layers with 0.5 km thickness are distributed within 20 km width around the source. The coda tail is again well-developed. In this case, although the vertical boundary layer is so

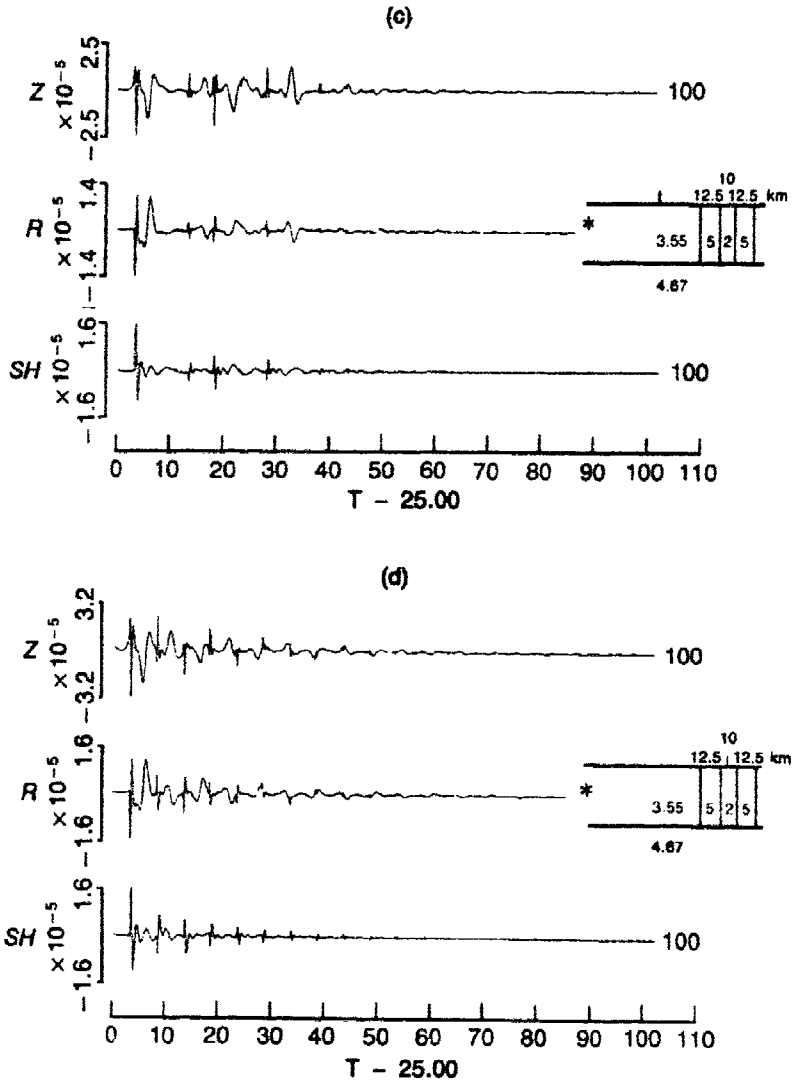

Fig. 3. (Continued.)

close to the source, the main L_g wave shape still keeps the same as that for the horizontal layer (Fig. 4a). Hence, if the horizontal layering is dominant in an area, the energy trapped in the layers may travel far without contamination by the local inhomogeneities.

Now we know that the vertical boundaries can be made complicated to generate stronger codas. Figures 4e and 4f are further examples. The

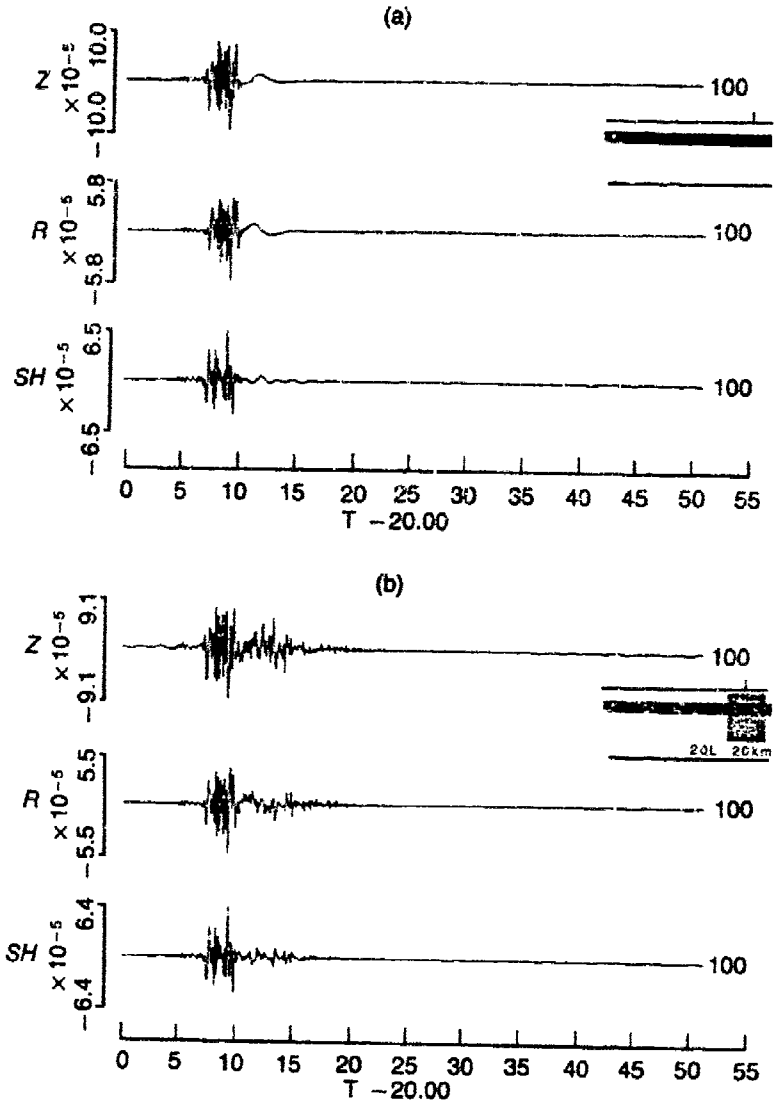

Fig. 4. Effect of horizontal and vertical boundary layering. Models are accompanied with each seismogram set. The receiver is at 100 km away as indicated by a small tick. The velocity fluctuation is 10%.

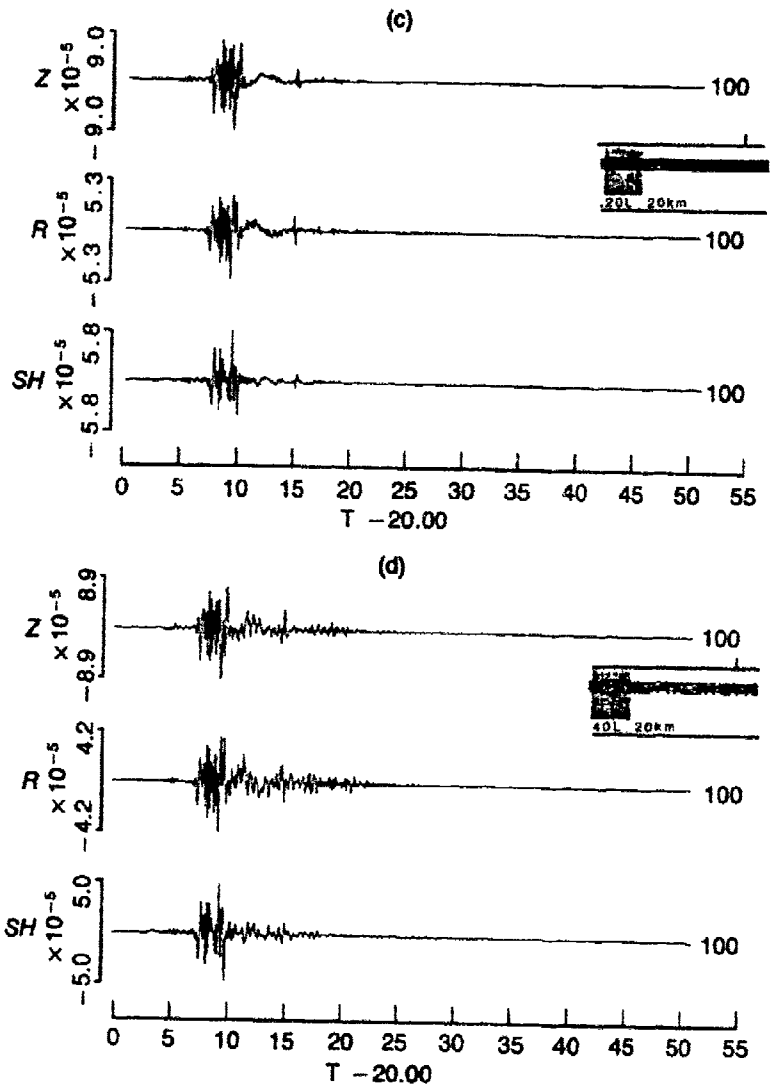

Fig. 4. (Continued.)

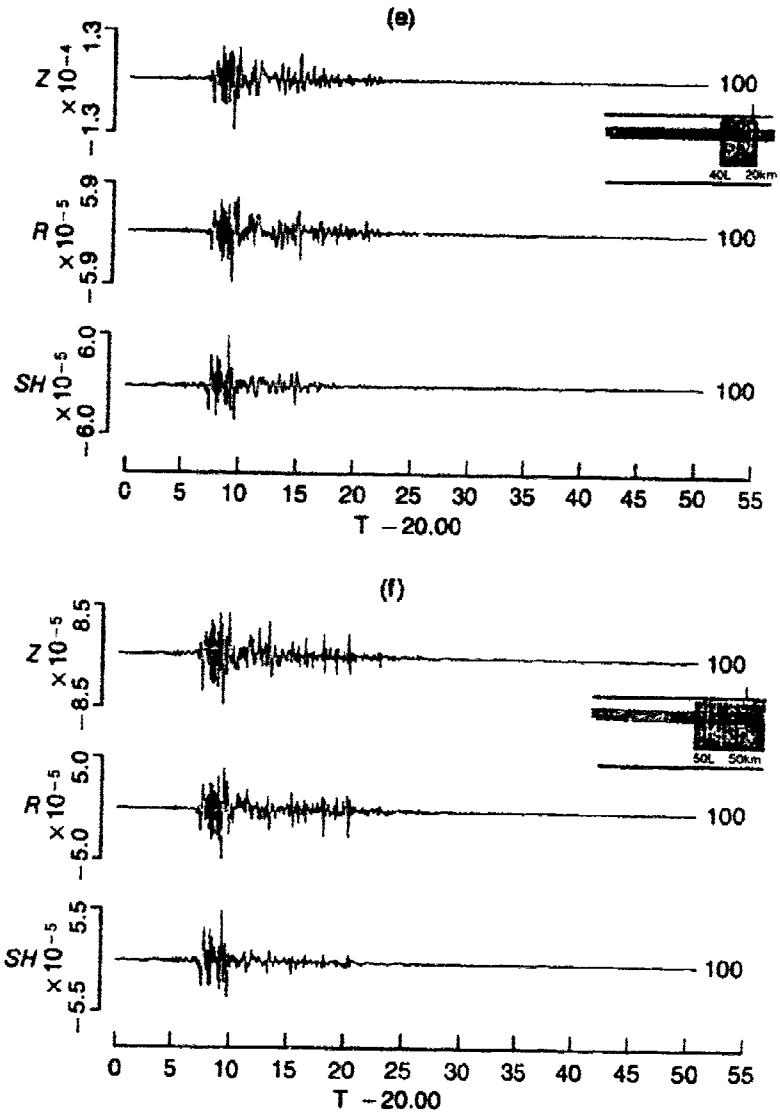

Fig. 4. (Continued.)

model contains more random and more thinner layers, the coda has better and longer tail. As the mean-free-path or turbidity are used to measure the strength of scattering, the randomness and density of vertical layers are required to explain the codas in our model.

In the last example we use a more realistic model which has a low velocity sedimental layer at the top. The lateral vertical layers used are 200 km wide distributed in 3000 km range, and the velocity fluctuation

is 2.5%. Figure 5a and 5b are the waveforms with and without lateral boundaries, respectively. We used 0.025 second as the sample rate, which is able to generate 20 Hz waves. Figures 5c and 5d are waveforms after the absorption of intrinsic attenuation. We can see the scattered energy

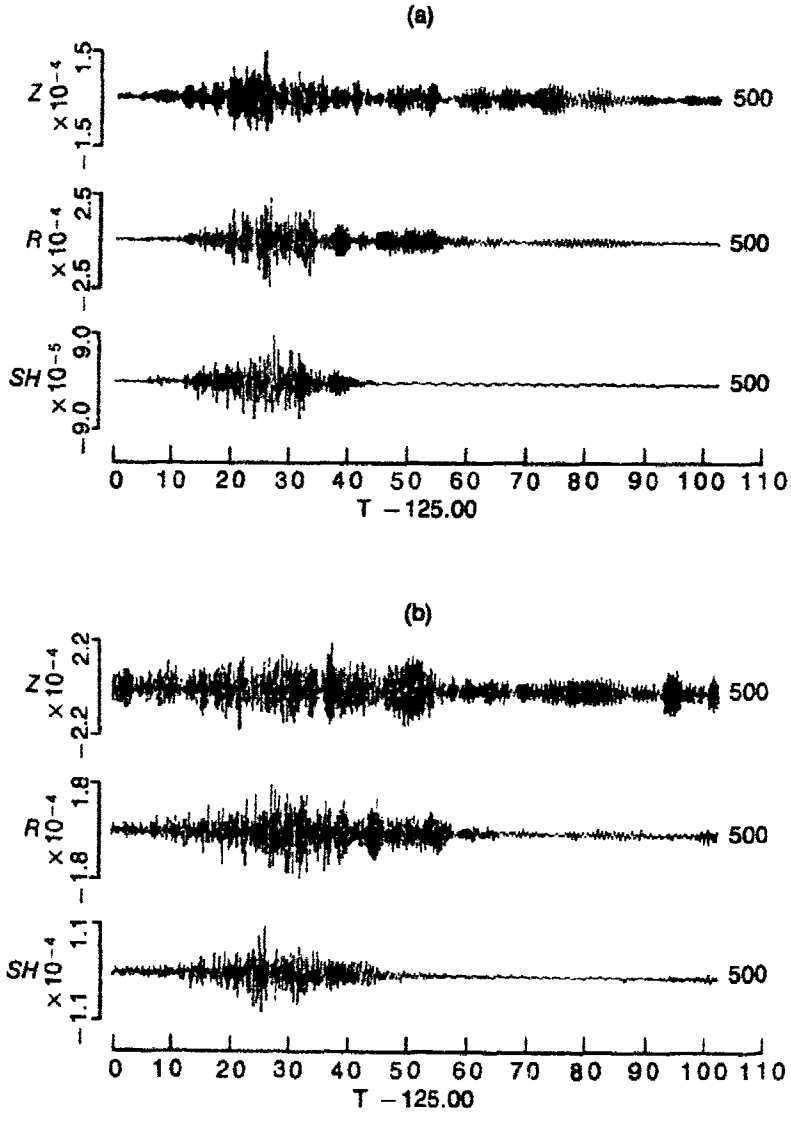

Fig. 5. High frequency synthetic seismograms from an east United States model. The vertical boundary model is a 200 km layer distributed within a 3000 km range. The velocity fluctuation is 2.5%. Figures 5c and 5d correspond to Figs. 5a and 5b after adding on the Q absorption.

(c)

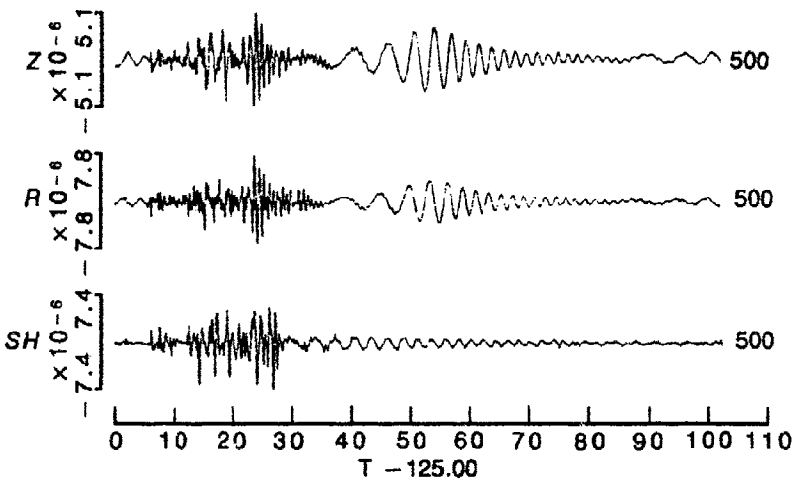

(d)

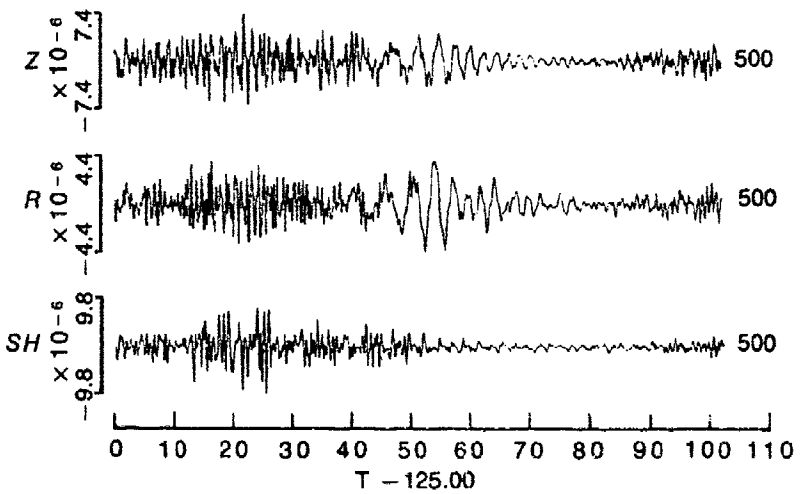

d	a	b	rho	Qa	Qb
0.25	2.305	1.295	2.30	300	150
0.75	4.824	2.710	2.67	1200	600
6.00	6.177	3.470	2.75	1500	750
18.0	6.533	3.670	2.90	2000	1000
18.0	7.084	3.980	3.00	2000	1000
	8.152	4.580	3.30	2000	1000

Fig. 5. (Continued.)

prevails in the high frequency range, especially after the absorption of attenuation (Fig. 5d). This implies that the scattering might affect the value of the apparent Q in the high frequency range.

References

Aki, K. and B. Chouet (1975). "Origin of Coda Waves: Source Attenuation and Scattering Effects," *J. Geophys. Res.*, **80**, 3322-3343.

Alsop, L.E. (1966). "Transmission and Reflection of Love Waves at Vertical Discontinuity," *J. Geophys. Res.*, **71**, 3969-3984.

Kazi, M.H. and A. Niazy (1983). "Generalization of Higuchi's Conditions for Love Waves Propagating Through Two Welded Quarter-Spaces With Two Surface Layers on Each," *Bull. Seism. Soc. Am.*, **73**, 1023-1030.

Luco, J.E. and R.J. Apsel (1983). "On the Green's Functions for a Layered Halfspace. Part I." *Bull. Seism. Soc. Am.*, **73**, 909-930.

Sato, H. (1984). "Attenuation and Envelope Formation of Three-Component Seismograms of Small Local Earthquakes in Randomly Inhomogeneous Lithosphere," *J. Geophys. Res.*, **89**, 1221-1241.

Wang, C.Y. (1981). *Wave Theory for Seismogram Synthesis*, Ph.D. Dissertation, Saint Louis University, St. Louis, Missouri.

Analytic Approaches to Linear and Nonlinear Attenuation

W.R. Wortman and G.D. McCartor

Summary

A review of near-field data from explosions indicates that nonlinear behavior extends well beyond a few hundred meters/kt$^{1/3}$. Frequency dependent contributions to Q, perhaps from scattering, can lead to underestimates of magnitudes using spectral ratio methods.

Introduction

Until recently it has been assumed that the behavior of rock beyond the radius of cracking ($\geq$ 100 m/kt$^{1/3}$) due to an explosive source shows a linear but perhaps inelastic character. Beyond 300 m/kt$^{1/3}$, the "elastic radius," seismic propagation has been taken as nearly elastic with mild attenuation due to anelasticity which is generally described in terms of Q or Q^{-1}, the "internal friction." As a result a major topic for study for seismic detection is that of the behavior of path integrated Q^{-1} as a function of path, frequency and possibly amplitude. The approach to the study of Q^{-1} has been largely phenomenological and experimental with only moderate consideration of physical mechanisms or use of analytic techniques.

In this paper we shall review the data from explosions at ranges from about 10 m/kt$^{1/3}$ to 3000 m/kt$^{1/3}$ in order to establish the extent to which the attenuation must be described as nonlinear and the extent to which Q^{-1} is dependent upon frequency. It will be found that these near-field data suggest a significant nonlinearity for which an empirical Q^{-1} is consistent with being linearly dependent upon amplitude at large strain but which becomes constant at small strains.

A. Near-Field Data and Nonlinear Attenuation

Near-field data from explosive sources in salt provides the best available information on the attenuation of pulses in the moderate strain regime. These data are from: Larson's work in pressed salt with scaled

ranges from 10 m/kt$^{1/3}$ (mean frequency 10^4 Hz); SALMON nuclear explosion in dome salt with ranges from 100 m/kt$^{1/3}$ to 400 m/kt$^{1/3}$ (mean frequency 5 Hz); and COWBOY series tamped chemical explosions in dome salt with ranges from 200 m/kt$^{1/3}$ to 3000 m/kt$^{1/3}$ (mean frequency 10 Hz or greater). A plot of peak velocity versus scaled range is shown in Fig. 1. This illustrates the well-known result that simple cube root scaling applies with remarkable accuracy to data from events with a yield variation of ten orders of magnitude (and thus a range of frequencies spanning more than three orders of magnitude). This result is all the more interesting because it takes place in a regime where the peak values of both velocity and displacement fall off much more rapidly than $1/r$. That is, for this spherical geometry, the behavior cannot be simple elastic since the decay exceeds that for geometrical divergence alone. The residual attenuation may result from linear but inelastic (*i.e.*, anelastic) behavior or from nonlinear attenuation. In either case, the existance of simple scaling demonstrates that the effective Q^{-1} must be nearly independent of frequency, at least for this frequency and strain regime. The peak strains

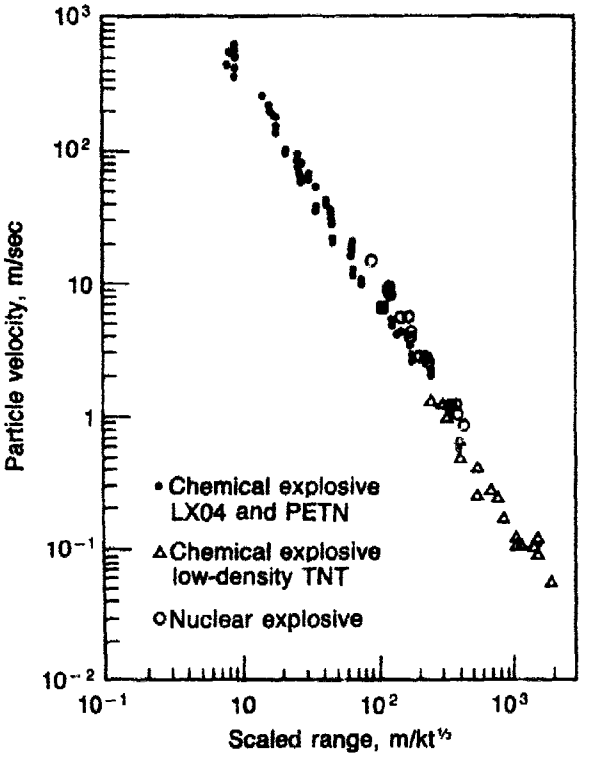

Fig. 1. Peak particle velocities from explosion in salt, from Larson (1982).

($\approx$ peak velocity/propagation speed) from Fig. 1 range from about 10^{-1} to 10^{-5}.

In order to address the question of linear or nonlinear attenuation, we now consider the implications for such possibilities. If a linear viscoelastic mechanism is to account for these data, the effect can be expressed in terms of a Q which is, at least approximately, independent of frequency over the frequency range of the experiments. This leaves some latitude in selection of an attenuation model but since the behavior in other frequency regimes has little effect, a reasonable attempt is to simply take Q to be completely independent of frequency. Such a model has been constructed by Kjartansson (1980) who provides rather simple expressions for attenuation and dispersion which can be written as a complex phase velocity

$$c(\omega) = e^{\frac{-i\pi\gamma}{2}\mathrm{sgn}(\omega)} \Big/ \left(\frac{\rho}{M_0} \left(\frac{\omega_0}{\omega} \right)^{2\gamma} \right)^{1/2}$$

where M_0 is a modulus, ρ the density, ω_0 an arbitrary frequency scale and γ is an arbitrary measure of the attenuation rate. In particular, $\gamma \approx Q^{-1}/\pi$ if $Q \gg 1/\pi$. For a spherical pulse with a velocity spectrum at radius a of $\tilde{V}(a,\omega)$ the velocity pulse at any time is given by

$$V(r,t) = \frac{1}{2\pi} \int d\omega\, \tilde{V}(a,\omega) \left(\frac{\frac{i\omega}{cr} - \frac{\alpha}{r} - \frac{1}{r^2}}{\frac{i\omega}{ca} - \frac{\alpha}{a} - \frac{1}{a^2}} \right) \exp\left(-\alpha(r-a) + i\omega \left(\frac{r-a}{c} - t \right) \right)$$

where

$$c = \left(\frac{M_0}{\rho} \right)^{1/2} \left| \frac{\omega}{\omega_0} \right|^{\gamma} \left(\cos(\pi\gamma/2) \right)^{-1}$$

is the phase velocity, and

$$\alpha = \omega\, c^{-1} \tan\left(\pi\gamma\, \mathrm{sgn}(\omega)/2\right)$$

is the spatial attenuation constant.

A velocity pulse from SALMON at a scaled range of 230 m/kt$^{1/3}$ is shown by Larson (1982) and this is used as the initial point for a study of effects of anelastic attenuation for constant Q. A sequence of pulses at increasing range is shown in Fig. 2 including frequency dependent attenuation (α is proportional to ω for constant Q) and the attendant dispersion. Attenuation and lengthening of the pulse are evident for this case using $Q = 10$. The corresponding decay of peak velocity as compared to the SALMON and COWBOY data is shown in Fig. 3. The value of Q was chosen to match approximately the slope of the SALMON data ($v_{max} \sim r^{-1.88}$) at the initial range and it is apparent that at larger ranges the decay is somewhat more rapid for constant Q. [It is easy to show that for sufficiently large ranges the peak velocity will fall off like r^{-2} if the spectrum is flat below the corner frequency. Smaller Q (greater attenuation) results in a more rapid onset of the r^{-2} behavior.] From this it seems that, in the absence of other constraints, a rather small $Q \sim 10$ from an anelastic model can give a rough fit to the SALMON and COWBOY data. However, recent work at Rockwell (Tittmann, 1983) indicates that for strains from 10^{-8} to 10^{-6}, the Q from dome salt is approximately 500 as measured at $\sim$ 500 Hz. Tittmann further notes that at strains greater than 10^{-6} Q^{-1} increases significantly at least up to strains of 10^{-5} which is the maximum available in the experiment. In short the experiments suggest that attenuation increases with amplitude (*i.e.*, it is nonlinear) for strains in excess of 10^{-6}. The magnitude of the measured Q at small strains is much different from that required to fit the explosion data suggesting that a linear mechanism cannot account for these data. Furthermore, the Rockwell data for nonlinear behavior indicate an onset at $\sim 10^{-6}$ suggesting that, since even the smallest strain from COWBOY is $\sim 10^{-5}$, nonlinear behavior is a vital element in accounting for the decay of the explosively generated pulses in the near-field. We intend to apply the spectral ratio method to SALMON and COWBOY data to verify nonlinearity as well as to explore any frequency dependence of Q.

Microscopic models of frictional attenuation due to sliding of crack surfaces such as Mavko (1980) and Steward *et al.*, (1982) generate at contribution to Q^{-1} which is proportional to the peak strain during a cycle but which is also independent of frequency. As a result it has been suggested that an approximate Q can be written as

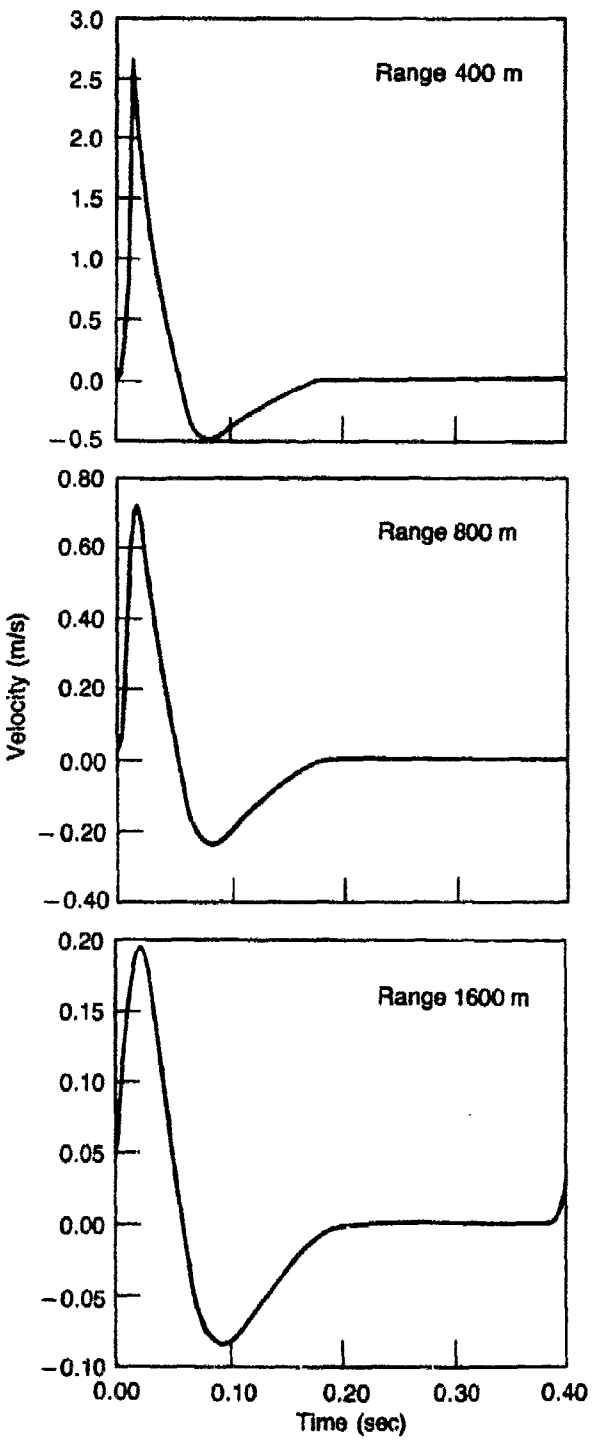

Fig. 2. Waveform of SALMON velocity pulse at three ranges for $Q = 10$.

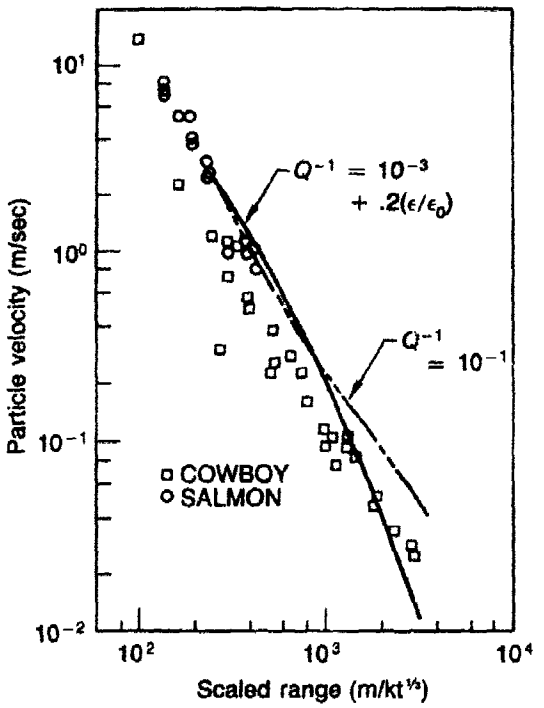

Fig. 3. SALMON and COWBOY velocity data compared to constant $Q = 10$ and nonlinear Q models (data from Trulio (1978)).

$$Q^{-1} \approx Q_0^{-1} + (\epsilon/\epsilon_0)\, Q_{\epsilon_0}^{-1}$$

where Q_0 is the "intrinsic" Q and the second term is the frictional Q which is linear in strain (and normalized at ϵ_0). Such a form has been considered by Minster and Archambeau (1983) in a fashion similar to that which follows here. The above form for a nonlinear Q ignores the fact that Q is inherently a linear concept. Here it is to be interpreted to mean that the spectral content will decay with range, r, according to a factor

$$\exp\left(-\frac{\omega r}{2cQ}\right)$$

where the strain ϵ which appears, is taken as the peak strain during the pulse. Using such a model for nonlinear behavior, we have found the attenuation of the SALMON velocity pulse by a closely spaced series of Fourier synthesis advancements in which Q^{-1} is taken to be constant

in each small step but altered (in fact decreased) according to the amplitude between steps. The limiting result for sufficiently small steps is shown in Fig. 3. In the example shown $Q_0 = 10^3$ and Q at the smallest range (230 m/kt$^{1/3}$) was 5. These variable Q parameters have been chosen both to give a reasonable fit to the SALMON data (which are always a bit above the COWBOY data) and to provide an onset of nonlinear behavior which is consistent with the Rockwell experiments. However, the result is rather insensitive to the value of Q_0 because the smallest strain in the explosion data is well above 10^{-6}.

It appears that a model of nonlinear Q^{-1} with a dominant term proportional to the strain gives a decay of the pulse from explosions in salt which is consistent with observation as well as consistent with small strain behavior of Q. However, the data are not adequate to fix the exponent of the strain in Q^{-1}. For example $Q^{-1} \propto \epsilon^{1/2}$ or ϵ^2 can also give a fair fit to the data although the transition to linear behavior is moved somewhat from the 10^{-6} value. The strongest statement we can make is that the assumed form of Q is consistent with the explosion and laboratory data but the particular form is not tightly constrained. Still a nonlinear mechanism appears to be necessary to account for the two types of data.

B. Implications of Q Behavior for Teleseismic Signals

Customary calculations of teleseismic propagation of signals from explosions and earthquakes often treat a near-source region as giving the initial conditions for a subsequent linear propagation. In the case of explosions this "elastic radius" is often taken as 300 m/kt$^{1/3}$ and it is assumed that all nonlinear behavior occurs inside this radius. It is now generally thought that nonlinear effects extend out to larger radii, perhaps out to $\sim 10^4$ m/kt$^{1/3}$. The behavior in this intermediate strain regime is a significant source of uncertainty in the ultimate problem of relating teleseismic signals to source characteristics.

From the point of view of linear calculations of seismic signals, nonlinear mechanisms provide anomolous attenuation which has the potential for altering the relation between teleseismic signals and the near-field pulse. However, mere existence of nonlinear attenuation does not necessarily negate spectral ratio methods unless the nonlinear aspect has a different frequency dependence that the assumed Q. This is due to the fact that spectral ratio methods depend upon finding a path-integrated Q^{-1}, which is generally expressed as t^*, which may or may not be as a function of frequency. If, for example, t^* is taken as independent of frequency and found by matching the high-frequency slope of the observed spectrum to an assumed source spectrum, the existence of a frequency

independent but nonlinear contribution to t^* would not alter the result except to raise the value of t^* which is proportional to the mean value of Q^{-1} along the path. On the other hand, if the nonlinear contribution to t^* has a frequency dependence different from the assumed one, use of a suitable slope connecting t^* to find a magnitude at the source may be in error. This question has been raised by Der (1983) in a slightly different context. This arises from use of spectral ***shape*** changes with propagation distance to deduce information about spectral ***amplitude*** changes. In particular it is noted that if the true t^*, which describes the amplitude change, is related to the spectral slope apparent t^* by

$$\bar{t}^* = t^* + \omega \frac{\partial t^*}{\partial \omega}$$

If t^* is independent of ω the two are identical but if t^* decreases with frequency $\bar{t}^* < t^*$. According to the work of Lundquist and Samowitz (1983), such is in fact the case although this remains a question for discussion. For example, Der and Lundquist, working with exactly the same data set, have found significantly different values for t^*. Using an absorption band model for Q (for which $Q \propto \omega$ at large ω) Lundquist has fit the data using as variables the low-frequency t^* and a period below which t^* rolls off. Der, on the other hand, has fit the data assuming $\bar{t}^*$ is constant in various frequency bands and then inverted the above relation to find t^*. At 2 Hz the difference between the fits at distant stations appear to be $\Delta t^* \sim .1$ to .2 sec so this translates into a source intensity ratio of ~ 10. That is attenuation will be underestimated if t^* is fit as constant and this will cause the magnitude of the source to be underestimated.

It should be noted that if Q^{-1} has a term which is proportional to ω^{-1} this will serve to provide an overall attenuation of the spectral amplitude but it will not alter the spectral shape so that the contribution to $\bar{t}^*$ will be zero. Thus, it is very important to include any such effects which, for example, occur at high frequency in the absorption band model. Observations and analysis by Aki and Chouet (1975) of coda attenuation indicate that at least some portions of the coda result from single scatterings of the main pulse by inhomogeneities in the lithosphere. Earthquake coda have been analyzed to find an effective Q which is frequency dependent giving Q increasing with frequency from 1 to 25 Hz. Dainty (1983) has looked at other earthquakes finding similar effects showing Q, apparently due to scattering, which is approximately proportional to frequency in the 3 to 50 Hz regime.

Dainty, in a theoretical analysis, has found the contribution of scattering to Q by considering the Born approximation in the presence of randomly distributed inhomogeneities in propagation speed in the medium. It is found that if the autocorrelation function of the inhomogeneities has a nonzero first derivative at zero lag, the contribution to Q is proportional to frequency. It is suggested that discontinuities at the scattering structure edge lead to this result. Basically, the Born scattering Q will be proportional to ω for wavelengths small compared to the overall dimensions of the structures but large compared to the thickness of the edges.

Independent of the exact nature of the physical mechanism which leads to the lithospheric contribution to Q, the fact that the observed character is $Q \propto \omega$ is of interest for application of spectral ratio methods to waves which pass through the lithosphere. Both Aki and Dainty indicate that the Q found from coda takes a value of ~ 200 at frequencies of a few Hertz. As was previously noted, a $Q^{-1} \propto \omega^{-1}$ will provide an overall attenuation of the amplitude of the pulse spectrum but it will not alter the shape. An underestimate of source magnitude will result from propagation through the lithosphere and the degree can be found, given a path length. For example, for a path of 100 km an additional Q^{-1} of 5×10^{-3} at 2 Hz will lead to an apparently decreased source magnitude at all frequencies of

$$\exp\left(\frac{2\pi fr}{cQ}\right) \approx 5$$

if the source of attenuation is not explicitly taken into account.

C. Conclusions and Recommendations

A preliminary study of the attenuation observed for explosively generated near-field pulses in salt indicates that the behavior is distinctly nonlinear for the strains for 10^{-1} to 10^{-5}. The observed behavior is consistent with a Q^{-1} which is the sum of a constant (Q at small strains are found in Rockwell experiments) and a term linear in the strain (which is as found in frictional crack models). It is recommended that dynamical models be formulated which conform to these near-field data for inclusion in calculations of waveforms out to a proper elastic radius.

A frequency-dependent Q will alter the relation between spectral amplitude and spectral shape leading possibly to substantial underestimates of source magnitudes using spectral ratio methods. This is especially true for lithospheric scattering which gives a contribution to Q which may not alter the spectral shape at all. It is important to establish the extent and

character of scattering contributions to Q in order to refine magnitude estimation methods.

References

Aki, K. and B. Chouet (1975), "Origin of Coda Waves: Source, Attenuation and Scattering Effects," *J. Geophys. Res.* **80**, 3322.

Dainty, A. (1983). "Coda Q in the Crust," 1983 DARPA/AFOSR Seismic Research Symposium.

Der, Z. *et al.* (1983). "Frequency Dependence of Q in the Mantle Underlying the Shield Areas of Eurasia," 1983 DARPA/AFOSR Seismic Research Symposium.

Kjartansson, E. (1980). "Constant Q-wave Propagation and Attenuation," *J. Geophys. Res.*, **84**, 4737.

Larson, D. (1982). "Inelastic Wave Propagation in Sodium Chloride," *Bull. Seism. Soc. Am.* **72**, 2107.

Lundquist, G. and I. Samowitz (1983). "t^* Estimates for the Global Array about the Eastern Kazakh Test Site," 1983 DARPA/AFOSR Seismic Research Symposium.

Mavko, G. (1979). "Frictional Attenuation: An Inherent Amplitude Dependence," *J. Geophys, Res.* **84**, 4769.

Minster, B. and C. Archambeau (1983). "High Strain Nonlinear Attenuation in Salt and its Effects on Near-Source Outgoing Seismic Wavefields," 1983 DARPA/AFOSR Seismic Research Symposium.

Stewart, R., M. Toksoz and A. Timur (1983). "Strain Dependent Attenuation: Observations and a Proposed Mechanism," *J. Geophys. Res.* **88**, 546.

Tittmann, B. (1983). *Non-Linear Wave Propagation Study*, Rockwell International Science Center, Report SC5361.3SAR.

Trulio, J. (1978). *Simple Scaling and Nuclear Monitoring*, Applied Theory, Inc., Report ATR-78-45-1, Los Angeles, California.

Evolution of Earth Structure and Future Directions of 3D Modeling

Asphericity, Anisotropy, and Anelasticity of the Mantle

Don L. Anderson

Summary

It is no longer adequate to treat the Earth as a nearly spherically symmetric body with simple receiver, source and attenuation corrections tacked on. The aspherical velocity structure is now being determined by surface wave and body wave tomographic techniques and it has been found that heterogeneities are present at all levels. In the upper mantle the lateral variations in velocity are as large as the variations across the radial discontinuities. There is good correlation of velocity with surface tectonic features in the upper 250 km but the correlation rapidly dimishes below this depth. The focusing and defocusing effect of these lateral variations can cause large amplitude anomalies and these effects can be more important than attenuation.

Velocity variations in the mantle can be caused by temperature, mineralogy and anisotropy, or crystal orientation. The largest variations are caused by anisotropy and relaxation phenomena such as partial melting and dislocation relaxation. There is increasing evidence for anisotropy in the upper mantle and this must be taken into account in Earth structure modeling. Both azimuthal and polarization effects are important. Layering or fabric having a scale length less than a wavelength will show the statistical properties of the small scale structure. Global maps of heterogeneity and anisotropy show that if anisotropy is ignored the data will be mapped into a false heterogeneity. Azimuthal anisotropy compounds the off-great-circle problem.

The absorption band concept predicts that Q should be higher at short periods than at long periods and that there should be large lateral and radial variations in Q. The t^* controversy is probably related to shifts in the absorption band. If velocity is anisotropic then Q should be as well. Evidence is starting to suggest that there is a Love wave, Rayleigh wave discrepancy in Q, suggestive of Q anisotropy.

Introduction

Rapid progress has been made in the past few years in understanding departures of the Earth from an idealized spherically symmetric, isotropic and perfectly elastic body. Although much can be learned about the Earth, and the propagation of seismic waves, by intensive study of energy in a few narrow spectral bands some phenomena in these bands cannot be understood without information from a broader band of frequencies. Understanding the amplitudes of seismic waves, for example, requires knowledge of focusing, scattering, anelastic dispersion and mode coupling and these in turn require information about the Earth that cannot be obtained by narrow band studies of single wave types.

There is increasing evidence that the Earth is laterally heterogenous on all scales and at all depths. This heterogeneity cannot be described with a standard set of travel time curves and station and source residuals. Station residuals are demonstrably affected by lower mantle as well as upper mantle heterogeneity. Station residuals, in fact, form the basis of recent tomographic studies of heterogeneity of the lower mantle and the upper mantle near sources and receivers. Surface waves provide a more uniform coverage of upper mantle heterogeneity, or asphericity, but with the present limited number of broad-band digital stations the lateral resolution is poor.

Evidence for upper mantle anisotropy is also increasing. Anisotropy introduces extra parameters into Earth structure studies and a large data base is required. It now appears, however, that some apparent structural complexity may be the result of attempting to satisfy data from the real Earth with isotropic models. Small scale structure, such as laminations, may also give rise to an apparent anisotropy, giving hope that even sub-wavelength complexities can be modeled.

The lateral heterogeneity of the upper mantle is such that significant off-great-circle propagation is expected. The resulting focusing and defocusing causes large amplitude anomalies.

The physics of anelasticity and the associated anelastic dispersion, *i.e.*, frequency dependence of velocity, is now fairly well understood. The shift of the absorption band with pressure, temperature and tectonic stress explains the large lateral and radial variations of Q and t^*. The anisotropy of anelasticity is one of the important problems to be resolved in understanding t^* and the amplitudes of seismic waves.

Asphericity of the Mantle

The large variation in P- and S-residuals, or station corrections, and surface wave velocities are the most obvious manifestations of lateral heterogeneity. P-wave station residuals are now available for about 1000

global sites, and many more if local and regional arrays are considered. Travel-time anomalies were the basis of the early study by Dziewonski, Hager and O'Connell of the long wavelength heterogeneity of the lower mantle. Dziewonski and Anderson published new average travel times and station residuals for about 1000 stations using ISC data. For many stations they were also able to derive the $\cos(2\theta)$ and $\cos(4\theta)$ azimuthal terms (see Figs. 1, 2 and 3). Dziewonski has recently published a spherical harmonic description of asphericity of the lower mantle. His results show that a significant portion of the static and azimuthal station effect is due to structure in the lower mantle. This result indicates that the use of average travel time curves with source and receiver corrections is no longer adequate and that travel time anomalies are not entirely due to upper mantle effects. The next quantum jump is epicenter location accuracy which will involve a three-dimensional description of velocity throughout the Earth combined with ray-tracing from source to receiver.

A variety of tomographic body-wave techniques has been developed by Robert Clayton and his colleagues at Caltech. They have successfully inverted 1.7×10^6 body wave arrival times to define the velocity in $5° \times 5° \times 200$ km cells in the mantle. The lower mantle results have been used by Brad Hager and his colleagues to explain the long wavelength part of the geoid. The Clayton group has also used the large, dense southern California array (SCARLET) to obtain a detailed three-dimensional structure under this region down to about 600 km. Global and regional body-wave tomography is making it possible to model and understand heterogeneity on both a global and regional scale. The body wave tomographic results to date show that the regions between 670 and 800 km depth and D'' are the most heterogeneous parts of the lower mantle. Velocity variations are of the order of several percent. The discovery of small scale velocity anomalies in the lower mantle explains the rapid lateral and directional dependence of station residuals and shows that detailed three-dimensional modeling of the mantle is required in order to improve epicentral locations. These small scale velocity anomalies may also help explain the variation of body wave amplitudes.

Surface Wave Tomography

Several groups have recently analyzed large numbers of long-period digital seismograms with the aim of mapping the large scale heterogeneity and anisotropy of the upper mantle. Nakanishi, Tanimoto and Anderson have derived phase and group velocities over many hundreds of paths, for both Rayleigh waves and Love waves. Tanimoto is currently investigating the resolving power and uniqueness of this type of data. Nataf, Nakanishi and Anderson have inverted this data for heterogeneity and

polarization anisotropy of the upper mantle. Their model, NNAG, is shown in a series of figures at the end of this report. Present data is adequate to expand the heterogeneity to $\ell = m = 6$ for all of the Earth, and $\ell = m = 10$ for some regions. The average half-wavelength of resolvable features is about 2500 km. With a greatly expanded global digital network it should be possible to map heterogeneities as small as 500-1000 km. Portable digital arrays can be used to map even smaller structures using body wave and surface wave tomography.

Woodhouse and Dziewonski have used waveform matching techniques to study the dispersion of surface waves, including higher modes, over about 800 paths. They have inverted this information to obtain average shear wave velocities to depths of 670 km. In most regions their results are similar to the Nataf, Nakanishi, Anderson model. The differences are primarily due to different treatments of the crustal correction, the neglect of anisotropy, different choice of parameterizations, and different data sets. These differences should be understood in the next year but higher resolution must await the expanded global digital network.

Tanimoto and Anderson have recently determined the azimuthal variation of Love and Rayleigh waves on a global basis. The fast directions of Rayleigh waves appears to correlate with flow directions in the mantle. The azimuthal dependence of surface wave velocity will considerably complicate the ray tracing problem, including focusing and defocusing. There is no reason to expect that body wave propagation is immune from these anisotropic effects.

Lay and Kanamori have ray traced through model NNA6, showing the effects of focusing and defocusing. The amplitude anomalies due to geometric effects are much greater than expected from Q effects. Even relatively mild, long wavelength asphericity gives appreciable amplitude and off great circle effects.

Anisotropy

The most studied effects of anisotropy include azimuthal variation of P_n and surface wave velocities, shear wave birefringence and polarization anisotropy. The minerals of the mantle are strongly anisotropic and are easily oriented by stress and flow. Variations in crystal orientation are more important than differences in temperature and composition in causing variation in velocity. Global data requires upper mantle anisotropy in order to explain Love and Rayleigh wave data and the $\cos(4\theta)$ terms in station residuals. In a few areas differences in arrival times of SH and SV have been documented. In general $SH > SV$ but this is reversed in regions of ascending and descending mantle flow as shown in studies by Regan, Anderson, Nataf and Nakanishi. This can be understood in

terms of orientation of olivine crystals. The large lateral variation in surface wave velocities are partly due to velocity variations caused by temperature and chemical differences and partly due to anisotropy. If anisotropy is ignored then erroneous velocity models will result.

If velocity is anisotropic then Q should be as well. There is some evidence that there is a Love-Rayleigh discrepancy in Q, just as there is in velocity. Physical mechanisms of attenuation, such as dislocation relaxation, are expected to be strongly anisotropic. If so, the commonly used expressions relating P-wave and S-wave Q are invalid.

Body Wave Heterogeneity

Detailed body wave models now exist for such diverse tectonic regions as shields, tectonic, rise and old ocean. Velocities differ by as much as 10% in the upper 200 km and 4% between 200 and 670 km. These differences are much greater than can be explained by temperature alone and partial melting, dislocation relaxation or anisotropy are implied. The variations are similar to those inferred from surface wave tomographic results. We now need detailed attenuation and anisotropy studies in the same areas.

The use of SS, PP, multiple ScS and $P'P'$ precursors promise to provide detailed velocity and structural information in regions inaccessible to other phases. The power of these phases has been demonstrated particularly by Don Helmberger and Stephen Grand and their colleagues.

Mineralogical modeling of the new velocity models has led to the surprising result that the transition region is mainly clinopyroxene and garnet, rather than olivine. The olivine-spinel transition gives much greater velocity jumps than observed at 400 km. On the basis of seismic velocities the shallower mantle can be either peridotite or eclogite. Ridges and tectonic regions seem to be partially molten to depth of at least 300 km.

Anelasticity

The effects of attenuation on velocity is now well understood and is incorporated into most recent seismic modeling. This effect reconciled body wave and free oscillation surface wave models. The frequency dependence of Q is still not understood. A frequency-independent Q is implausible but a mild frequency dependence over a narrow frequency range is permitted. Since absorption is likely to be a thermally activated relaxation phenomena the absorption band should shift with depth. High Q regions should have a strongly frequency dependent Q. Since temperature shifts the location of the band laterally variations in Q (or t^*) should be accompanied by a change in the frequency dependence. Observed Q, or t^*, over a given path is the result of superposition of

absorption bands with different center or corner frequencies. The low-Q parts of the path, of course, dominate. There should not be a single t^* or τ_m for all locations and depths and attempts to model waveforms with one or two parameter models are doomed to failure. Scattering and mode conversion can contribute to apparent attenuation. Both a laterally- and depth-dependent absorption band Q model has not yet been fully exploited. τ_m is exponentially dependent on temperature and therefore cannot be treated as a constant.

Figures

The figures give a series of maps at various depths and cross-sections of shear velocity (*VSV*) and shear wave anisotropy (*XI*). These parameters are combined in seismic flow maps and cross-sections. These maps and cross-sections are based on model NNA6 of Nataf, Nakanishi and Anderson (Geophysical Research Letters, 1984).

XI is the anisotropy parameter $(VSH)^2/(VSH)^2 - 1$ and is positive for horizontal flow (*a*-axis horizontal for olivine).

The azimuthal variation map is from Tanimoto and Anderson (Geophysical Research Letters, 1984) and is for 200 sec. Rayleigh waves. The lines are oriented in the fast direction. For comparison is the flow map of Hager and O'Connell.

The station residual maps are from a study by Dziewonski and Anderson.

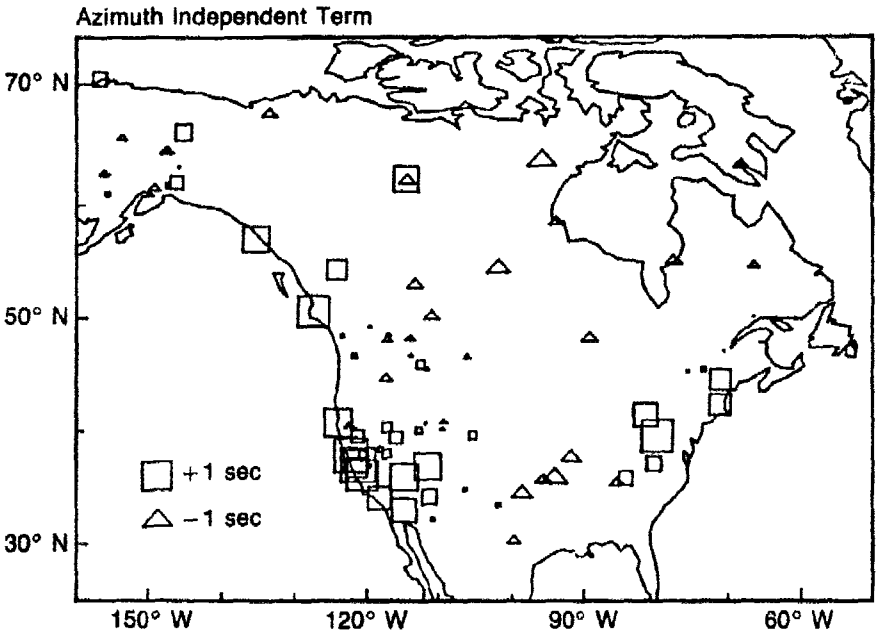
Azimuth Independent Term
70° N
50° N
30° N
150° W
120° W
90° W
60° W
+1 sec
−1 sec

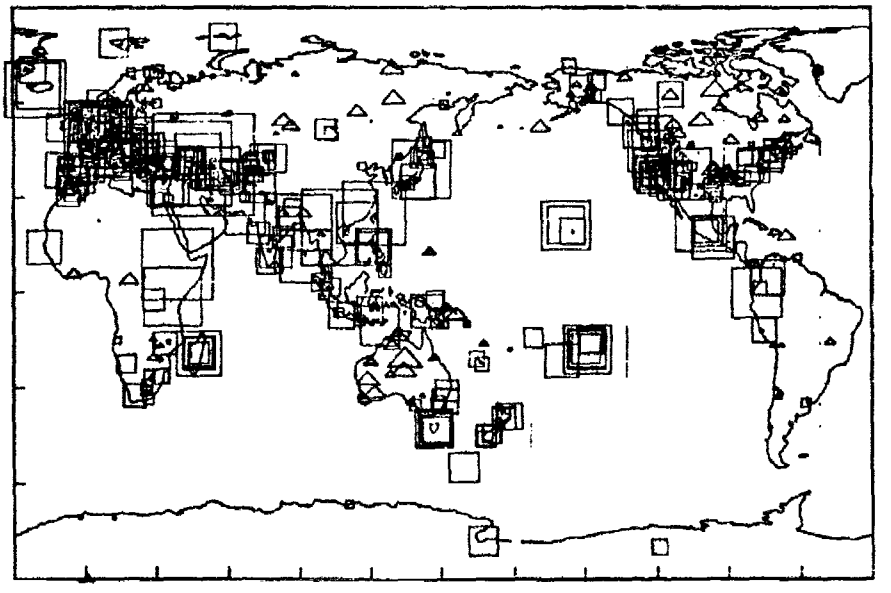

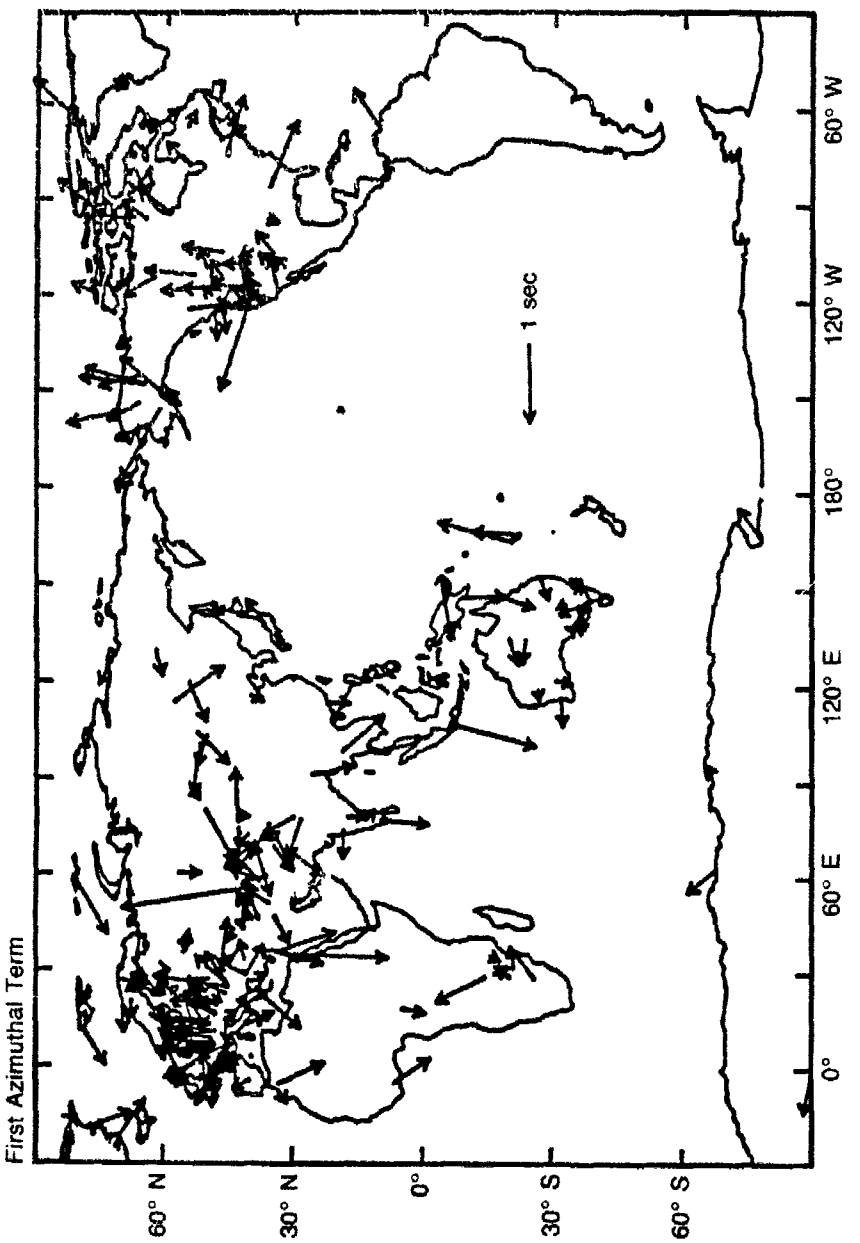
First Azimuthal Term
1 sec
60° N
30° N
0°
30° S
60° S
0°
60° E
120° E
180°
120° W
60° W

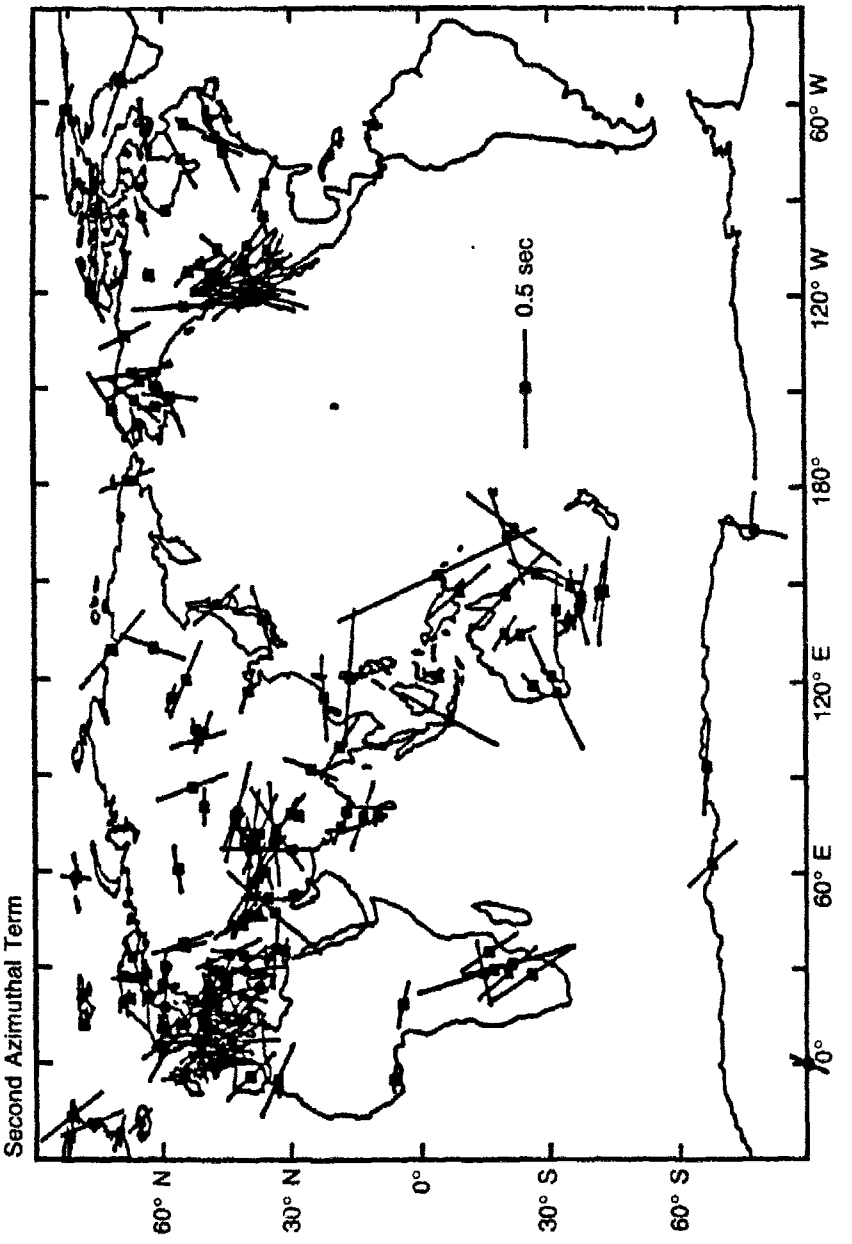
Second Azimuthal Term
0.5 sec
60° N
30° N
0°
30° S
60° S
0°
60° E
120° E
180°
120° W
60° W

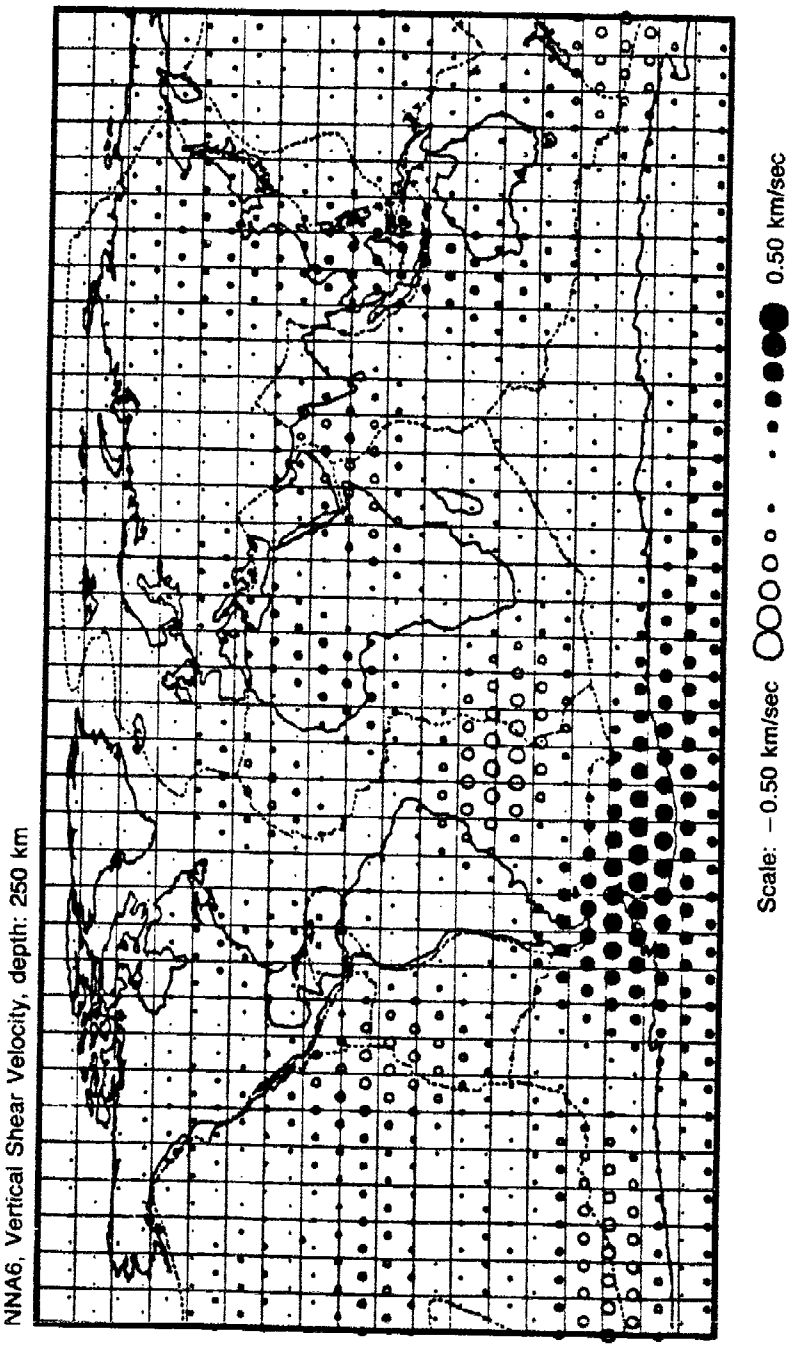
NNA6, Vertical Shear Velocity, depth: 250 km
Scale: −0.50 km/sec
0.50 km/sec

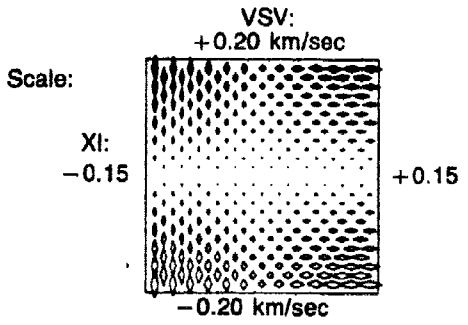

NNA6, Seismic Flow Map, depth: 100 km

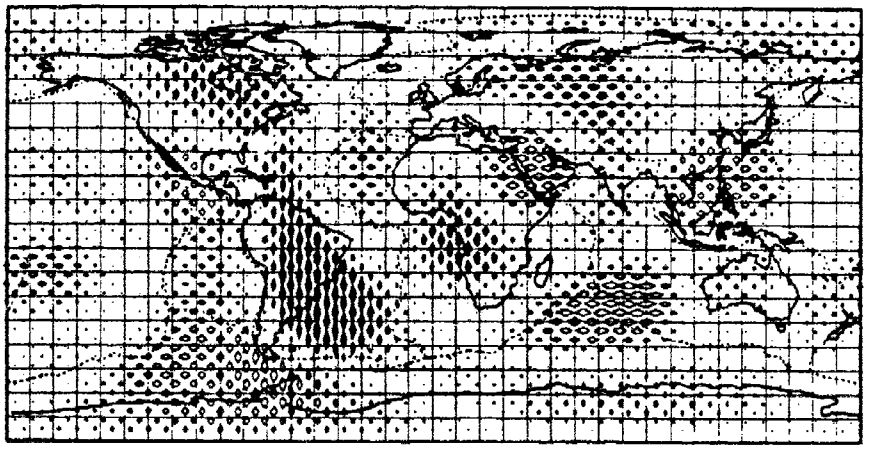

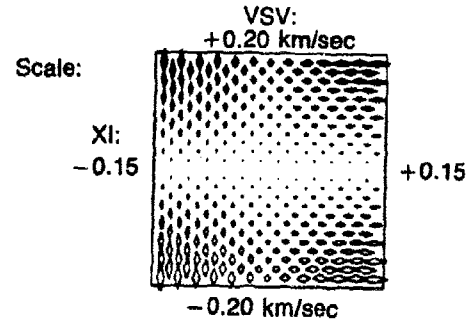

NNA6, Seismic Flow Map, depth: 160 km

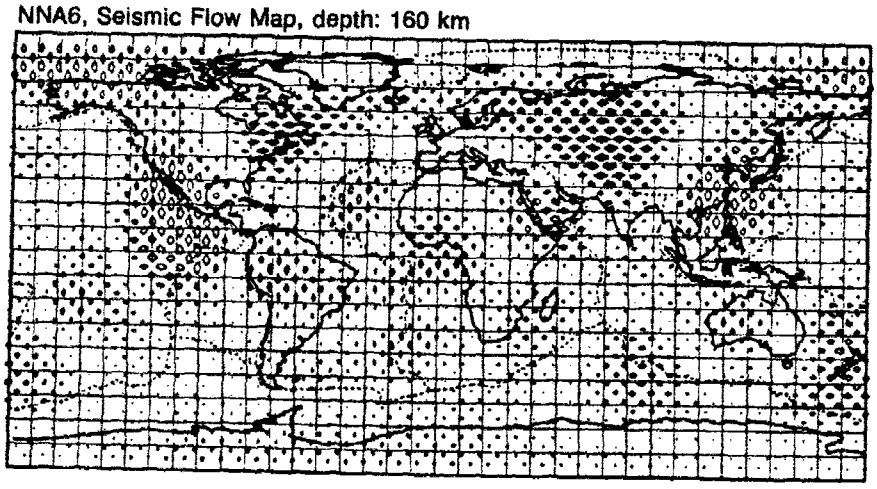

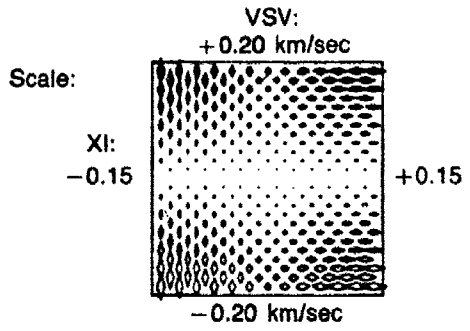

NNA6, Seismic Flow Map, depth: 340 km

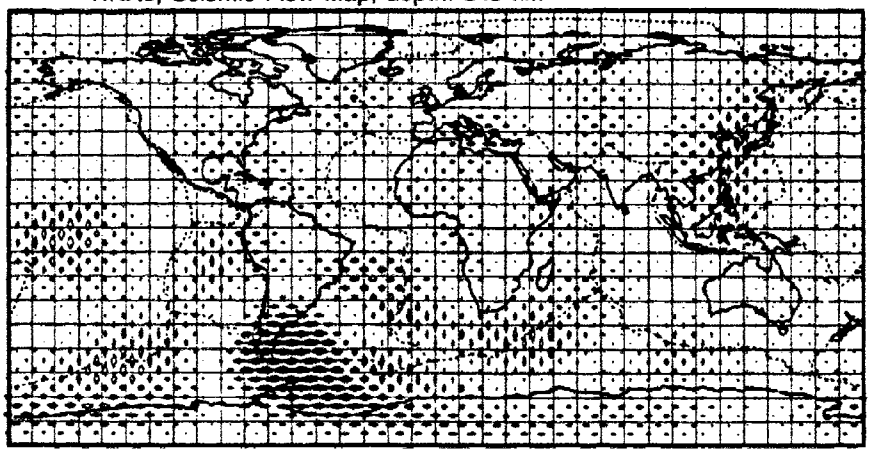

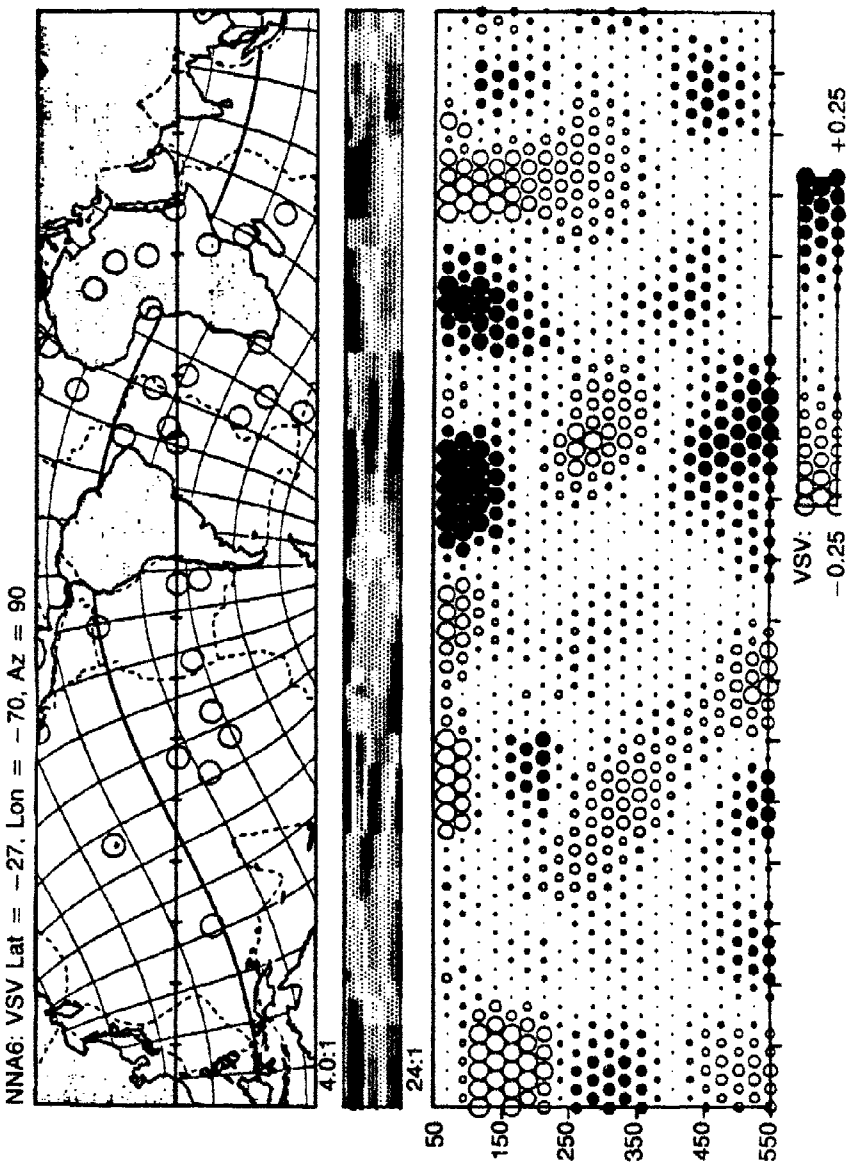
NNA6: VSV Lat = −27, Lon = −70, Az = 90
4.0:1
24:1
50
150
250
350
450
550
VSV:
−0.25
+0.25

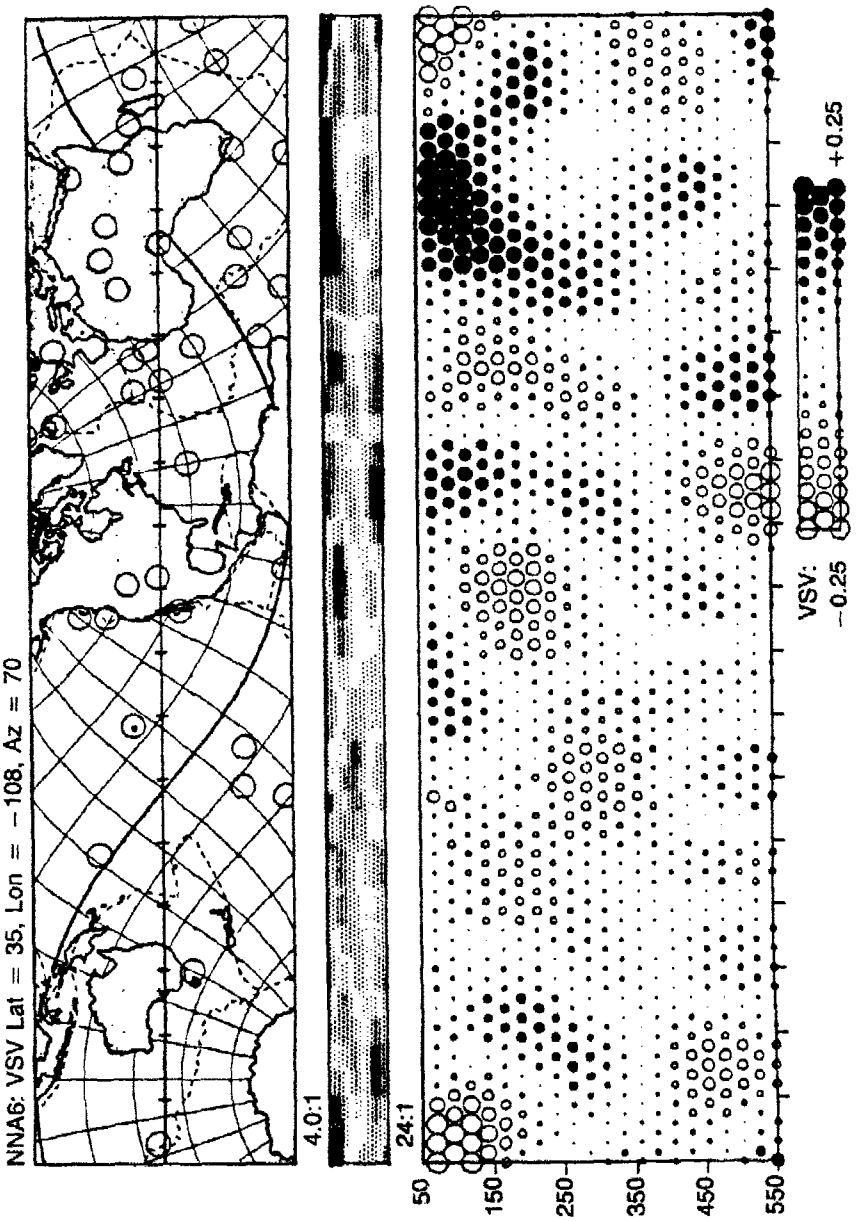
NNA6: VSV Lat = 35, Lon = −108, Az = 70
4.0:1
24:1
50
150
250
350
450
550
VSV:
−0.25
+0.25

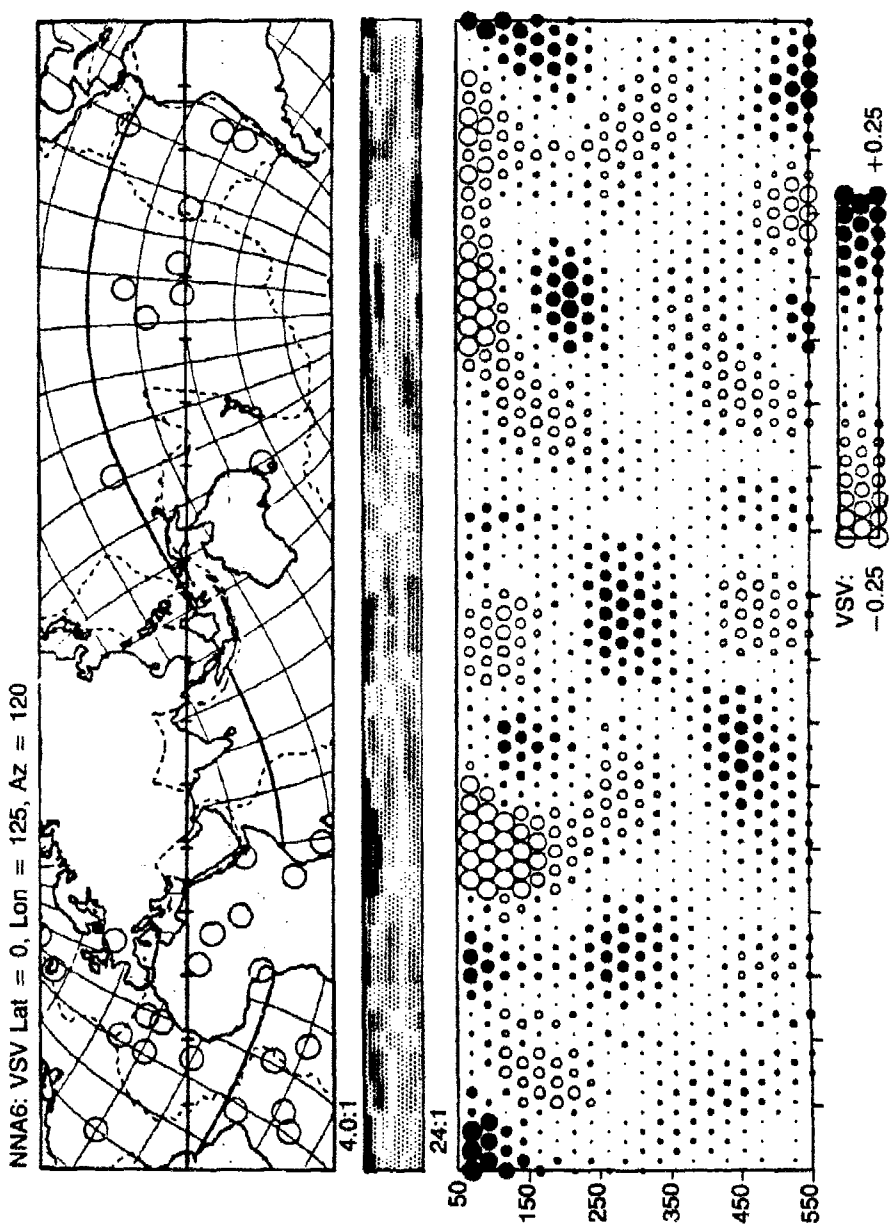
NNA6: VSV Lat = 0, Lon = 125, Az = 120
4.0:1
24:1
50
150
250
350
450
550
VSV:
−0.25
+0.25

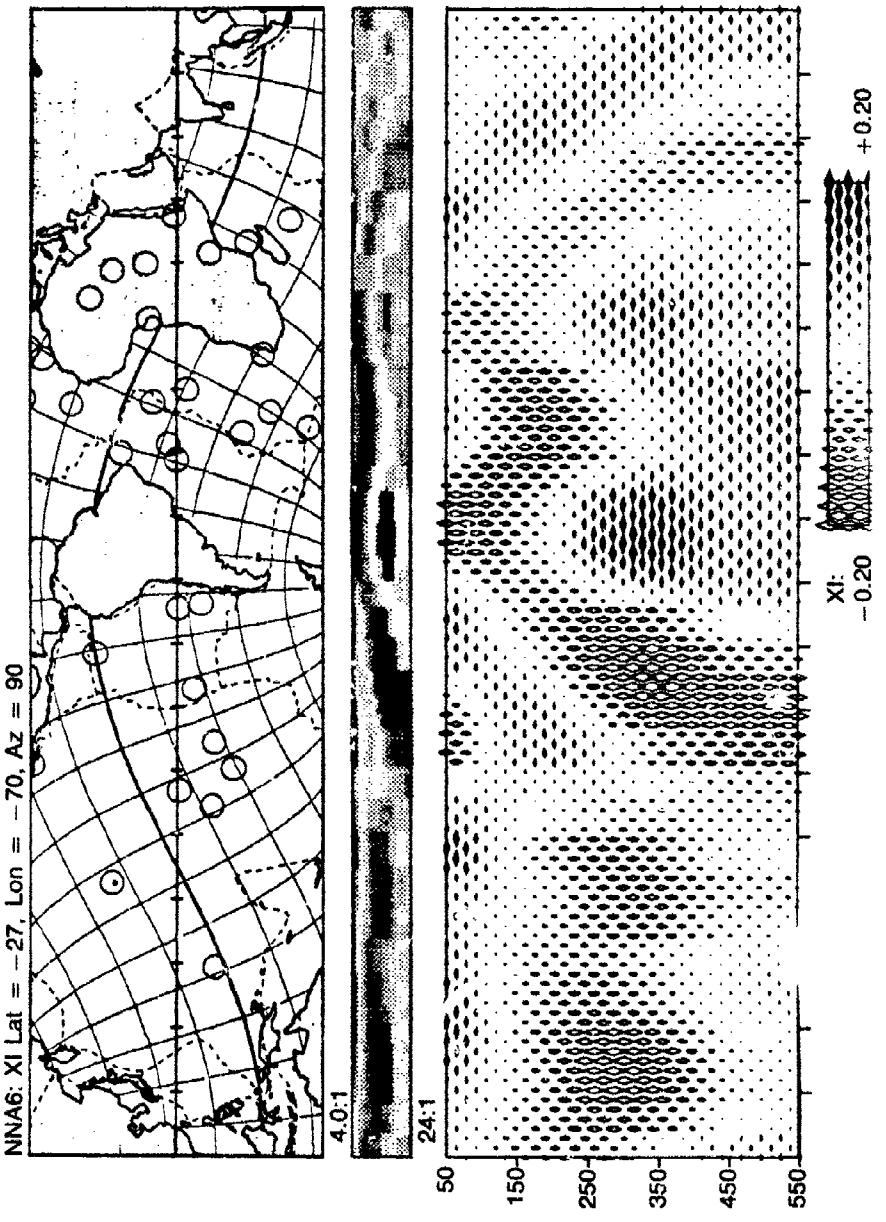
NNA6: XI Lat = −27, Lon = −70, Az = 90
4.0:1
24:1
50
150
250
350
450
550
XI:
−0.20
+0.20

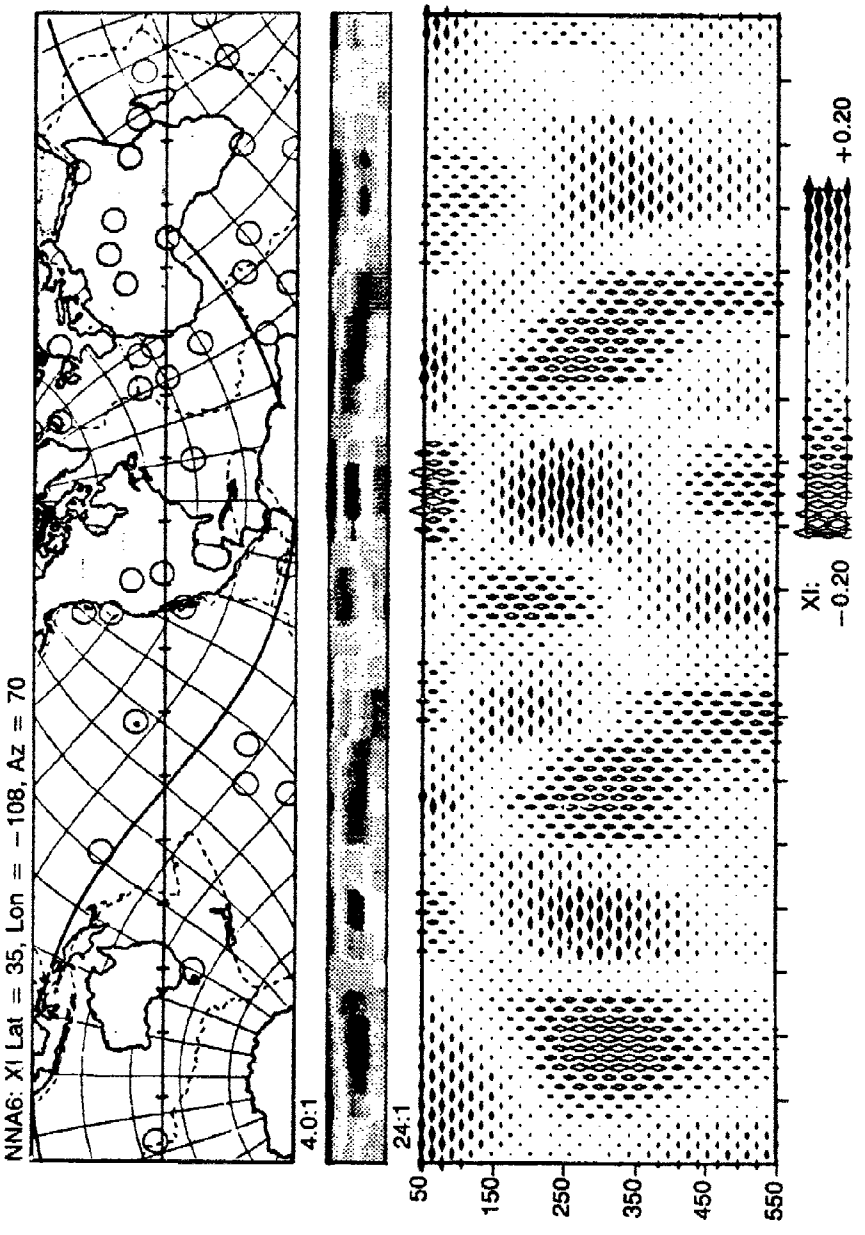
NNA6: XI Lat = 35, Lon = −108, Az = 70
4.0:1
24:1
50
150
250
350
450
550
XI:
−0.20
+0.20

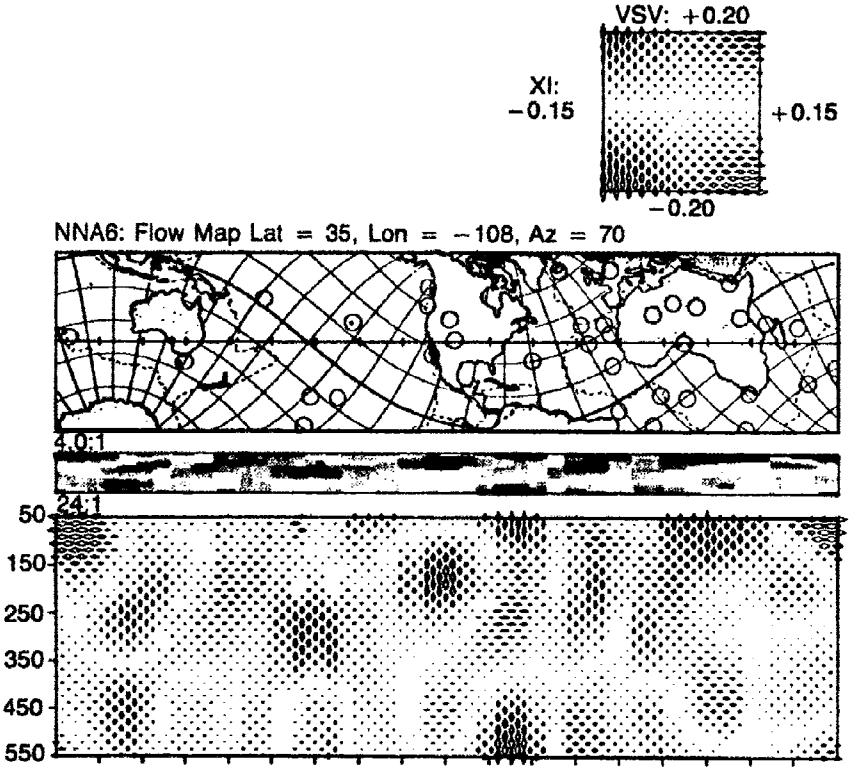
VSV: +0.20
XI:
−0.15
+0.15
−0.20
NNA6: Flow Map Lat = 35, Lon = −108, Az = 70
4.0:1
24:1
50
150
250
350
450
550

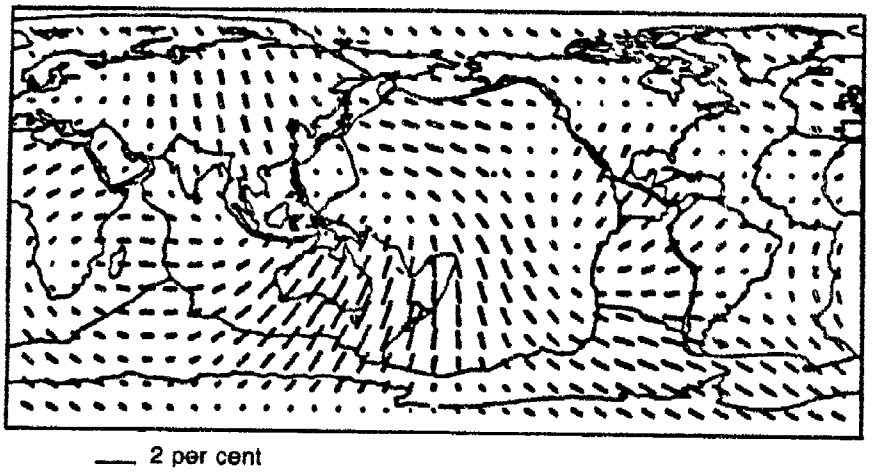

— 2 per cent

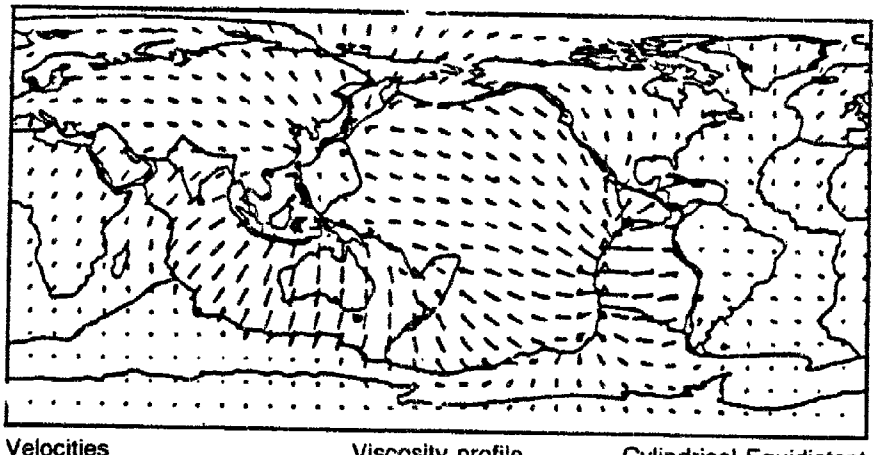

Velocities

260 km depth

Viscosity profile

z/s	η (noise)
.99 - 1.00	10^{23}
.98 - .99	10^{19}
.89 - .98	10^{22}
.55 - .89	10^{25}

Cylindrical Equidistant

Scale = 75 MY

▲- upgoing

▼- downgoing

Seismic Scattering and Lithospheric Heterogeneity

K. Aki, R. Wu, and R. Nowack

During the past year, we have continued our work on seismic scattering problems relevant to the identification of underground nuclear testing.

In the following, we summarize our results on (1) full elastic wave theory applied to forward and backscattering, (2) fluctuation of direct *P*-wave amplitude, and (3) formation of *P* coda.

(1) Coda waves in the local and regional distances contain information on heterogeneities near the source region which is important for the monitoring of a comprehensive (low-yield) test-ban treaty. The teleseismic *P* and *P*-coda, on the other hand, are important to yield estimations for the monitoring of a threshold test-ban treaty. To understand these waves, we need a theory of seismic scattering in the laterally inhomogeneous earth. In the past, the generation of coda waves and the phase and amplitude fluctuations of direct *P* waves have been studied by the use of a scalar wave theory. In our work, we have developed a full elastic-wave scattering theory for both discrete scatterers (Wu and Aki, 1984a) and random media (Wu and Aki, 1984b), using equivalent body force and the first Born approximation. We found that, in Rayleigh scattering (when the wavelength is much longer than the scale length of the inhomogeneities) and Mie scattering (when the wavelength is comparable to the scale length of the inhomogeneities) range, both the spatial scattering pattern and the frequency dependence of the total scattered power have some significant differences from the scalar case. In the forward direction the wave scattering is controlled primarily by the velocity inhomogeneities. The phase and amplitude fluctuation of direct *P* and the properties of teleseismic *P*-coda are basically forward scattering problems, and can be treated approximately by the scalar wave theory. On the other hand, the local or regional coda waves are mainly formed by backscattered and wide-angle scattered waves, which need a full elastic-wave treatment. For local coda, backscattering plays a major role, and is controlled by the impedance homogeneities.

Local and regional coda waves are more sensitive to small- and medium-scale inhomogeneities, while teleseismic *P* waves are only sensitive to large-scale velocity inhomogeneities. Analysis of both local and

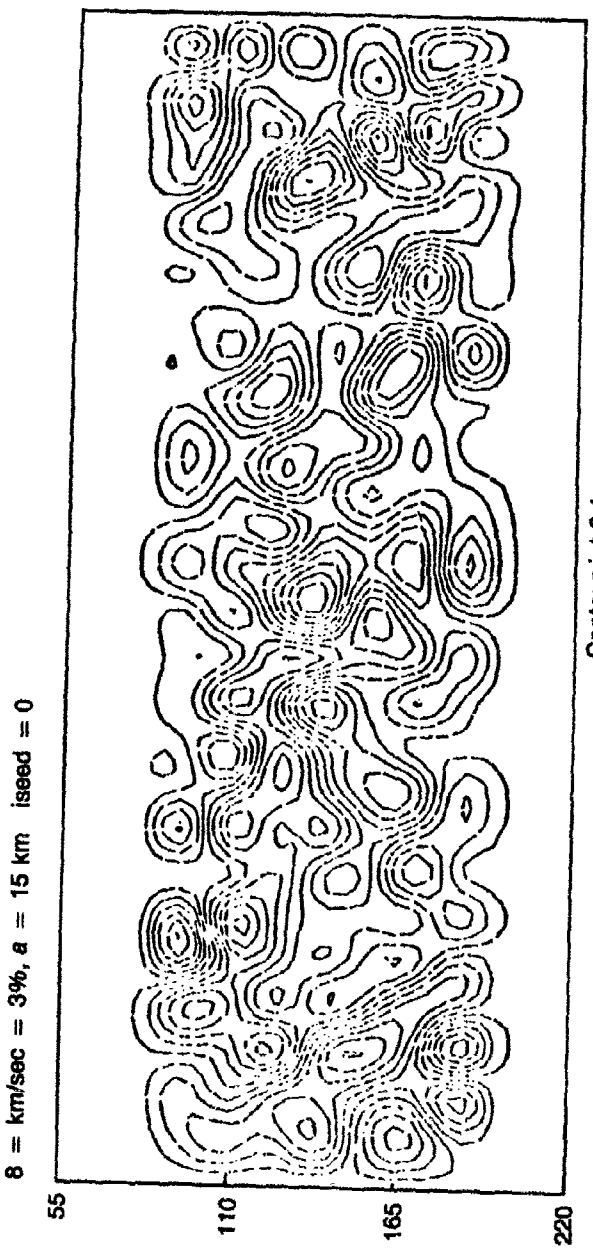

Fig. 1. The velocity structure of the random layer of thickness 120 km. The r.m.s. velocity perturbation is of 3%. The correlation length is 15 km.

teleseismic data (Aki, 1982; Wu and Aki, 1984b has indicated that besides the 10-20 km large-scale velocity inhomogeneities, the lithosphere may be rich in small-scale (less than 1 km) impedance inohomogeneities in tectonically active regions.

(2) The great variability of direct *P* and the stability of *P*-coda have been discussed and examined both theoretically and numerically in our work (Aki, 1982; Aki, Wu and Comer, 1982; Nowack and Aki, 1984). The travel-time and amplitude fluctuations have been attributed to the velocity and absorption variation between different ray paths or the focusing and defocusing effects. We examined the other possibility of multipath interference due to velocity inhomogeneities. The Gaussian beam method has been used to obtain the synthetic seismograms for a plane wave incident on a 120 km thick lithospheric layer having random velocity perturbation of 3% (r.m.s. perturbations) with correlation length of 15 km (Nowack and Aki, 1984). Figure 1 shows the velocity structure of the random layer. The perturbed wavefields after passing through the random layer are shown in Fig. 2 for both 1 Hz and 2 Hz plane waves. The great variabiiity of direct *P* waves can be seen easily. Figure 3 shows the correlation between the phase fluctuations and the log-amplitude fluctuations. The results agree in general with the observation in LASA. In the statistical treatment (Aki, Wu and Comer, 1982) the teleseismic *P* waves are assumed to be in the saturated region of scattering; then the theoretically predicted standard deviation of the magnitude estimation is 0.278, in agreement with the observations of 0.25-0.30 after regional calibrations. Therefore the multipath interference is a viable mechanism for the variability of direct *P*.

(3) The formation of *P*-coda has been tested by both theoretical and numerical methods. Assume a 60 km thick lithospheric layer having r.m.s. velocity perturbation of 4% and correlation length of 10 km. Using the Feynman path integral approach of scattering theory (Flatte *et al.*, 1979), we found that the wave scattering in the assumed medium is not strong enough to produce multiple arrivals, *i.e.*, coda waves (Aki, Wu and Comer, 1982). To check this, we did 3-D ray tracing for a specific region in California using the lithospheric velocity structure derived by 3-D *P*-time residual inversion (Aki, Wu and Comer, 1982). The Gaussian beam method is also used for this purpose (Nowack and Aki, 1984). In both cases, no noticeable coda was produced. Therefore we conclude that the 10-km size, 4% random velocity perturbations in the lithosphere alone may not be able to produce the observed *P*-coda. We need to consider some other inhomogeneities such as the small-scale impedance heterogeneities, the Moho, the irregular topography of surface and interface, *etc.*

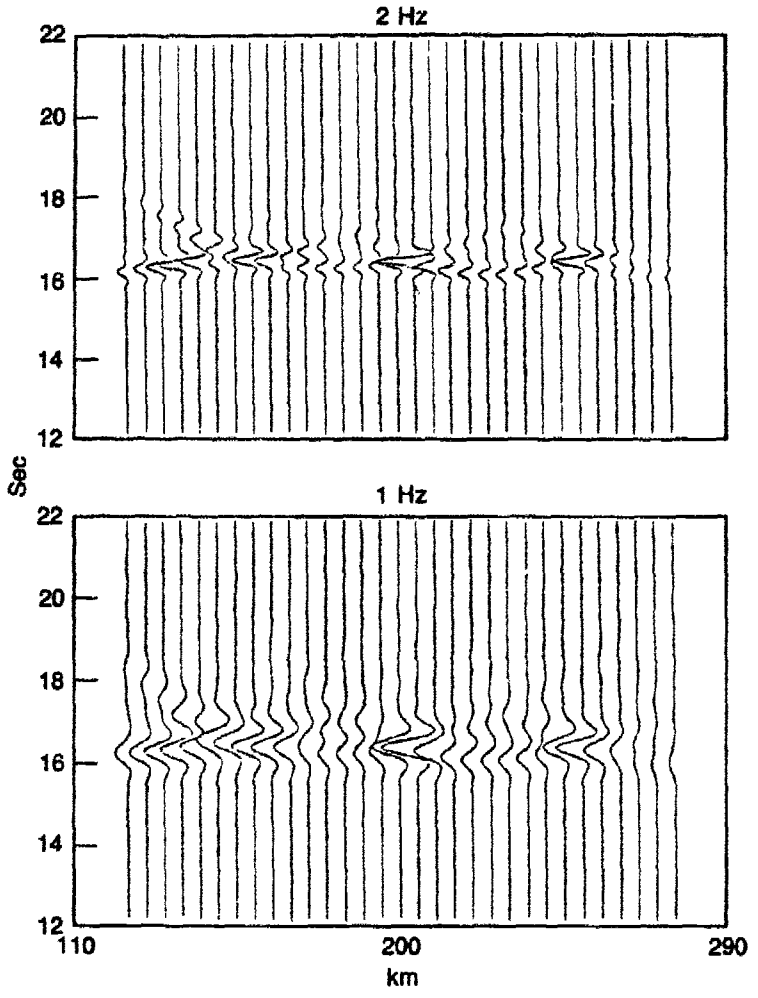

Fig. 2. The perturbed wavefield of a plane wave after passing through the random layer.

References

Aki. K. (1982). *Scattering and Attenuation*, Semi-Annual Technical Report, 1 Jan. 1982 - 30 June 1982. Also in *Bull. Seis. Soc. Am.*, **72**, 6, 5319-5330. 1982.

Aki, K., R.S. Wu and R.P. Comer (1982). *Variability of Direct P. Stability of P Coda and Heterogeneities of the Lithosphere*, Semi-Annual Technical Report. 1 Jan. 1982 - 30 June 1982.

Flatte, S.M., R. Dashen, W.H. Munk, K.M. Watson, and F. Zachariasen (1979). *Sound Transmission Through a Fluctuating Ocean*, Cambridge University Press, 1979.

Nowack, R. and K. Aki (1984). *The 2-D Gaussian Beam Synthetic Method: Testing and Applications*, Semi-Annual Technical Report, 1 Jan. 1983 - 30 June 1983. Submitted to *J. Geophys. Res.*, 1984.

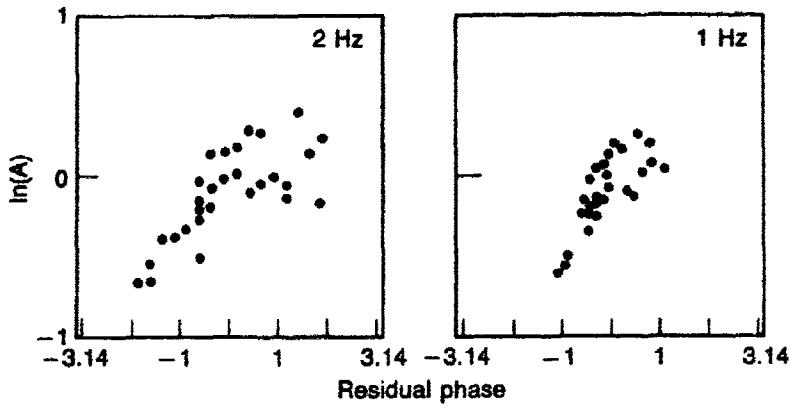

Fig. 3. The correlation between the phase and amplitude fluctuations of the wavefield shown in Fig. 2.

Wu, R.S. (1982). *The Scattering Pattern of A Single Scatterer in an Elastic Medium and Coda Waves*, Semi-Annual Technical Report, 1 Jan. 1982 - 30 June 1982.

Wu, R.S. and K. Aki (1984a). *Scattering Characteristics of Elastic Waves by An Elastic Inclusion*, Annual Technical Report, 1 Jan. 1982 - 31 Dec. 1982. Submitted to *Geophysics*, 1984.

Wu, R.S. and K. Aki (1984b). *Scattering of Elastic Waves by a Random Medium and the Small-Scale Inhomogeneities of the Lithosphere*, Annual Technical Report, 1 Jan. 1982 - 31 Dec. 1982. Submitted to *J. Geophs. Res.*, 1984.

Body Wave Propagation in Three-Dimensional Source and Receiver Structure

Charles A. Langston

In the analysis and inversion of body wave seismograms from earthquake or explosion sources, it is occasionally apparent that certain receivers are anomalous in that the underlying structure is complex enough to give rise to large secondary arrivals in vertical *P* waves and tangential *SH* waves. Recognizing these effects is important in the source inversion problem since structure-caused arrivals on the seismogram may be interpreted as a source effect. Closely related to receiver-induced waveform distortions is the well-known problem of short-period body wave amplitudes. It has been a common observation at major seismic arrays that very local receiver structure causes an order of magnitude variation in body wave amplitude. This is, of course, a major problem in yield assessment of underground explosions.

Closely allied with the receiver problem is the effect of near-source scattering, both in teleseismic body waves and in local- or near-field recordings of explosions. Near-source scattering may cause considerable amplitude variation in teleseismic body waves and it is conceivable that it may also give rise to apparent non-isotropic source effects. For example, it is common in near-source accelerometer recordings of explosions at NTS to observe distinct *SH* wave pulses. It is not clear whether these *SH* waves are caused by a non-isotropic source effect or an effect of scattering in 3D earth structure.

In an effort to analyze the scattering effect of 3D receiver and source structure, ray algorithms have been developed to compute synthetic seismograms for incident plane and spherical waves. Accurate numerical techniques, such as finite difference or finite element methods, are known to be expensive and difficult to implement for 3D geometry. While only an approximation, ray theory is relatively inexpensive and allows one to interpret model results in terms of physically intuitive ray paths. Ray theory results can be used to estimate the magnitude of a scattering effect and can also lend physical insight into results obtained by more rigorous methods, once they become available.

Theory and numerical results for structures involving planar dipping interfaces were presented by Langston (1977b). Problems involving incident plane P or S waves under receiver structure or point dislocation sources within the structure which radiate P and S waves to teleseismic distances were considered. It was found that simple dipping receiver structure induced off-azimuth particle motion in recorded P waves which could be used to infer velocity contrast and interface orientation. Results for radiated teleseismic P waves from sources in the structure indicated that amplitudes and waveshapes could be significantly changed from the plane-layer model results, particularly for strike-slip dislocation sources.

Complex and azimuthally dependent particle motion (*e.g.*, "tangential" P waves) has been observed at a number of receivers. These include LON (Longmire, Washington) (Langston, 1979), COR (Corvallis, Oregon), VIC (Victoria, British Columbia) (Langston, 1981), AAE (Addis Ababa, Ethiopia) (Herbert and Langston, 1984), PAS (Pasadena, California), TIN (Tinemaha, California)(Lee, 1983), TRN (Trinidad, West Indies) SJG (San Juan, Puerto Rico) (Burdick and Langston, 1976) and a number of Asian stations (Peseckis and Burdick, 1982). For example, Fig. 1 displays rotations of teleseismic P waves recorded at LON (Langston, 1979) showing large tangential components. In practice, the effective source time function and instrument response is removed from this kind of data by deconvolving the vertical component from the horizontals. Since the vertical component is not as severely affected by off-azimuth

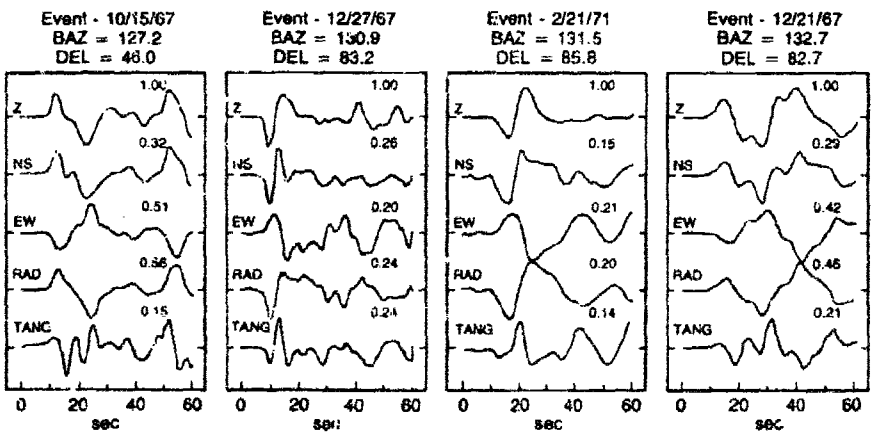

Fig. 1. Examples of observed vertical (Z), north-south (NS), and east-west (EW) P wave components recorded at LON for teleseismic earthquakes. The waveforms are vectorially rotated into radial (RAD) and tangential (TANG) motions with respect to the source backazimuth. Note the large tangential motions.

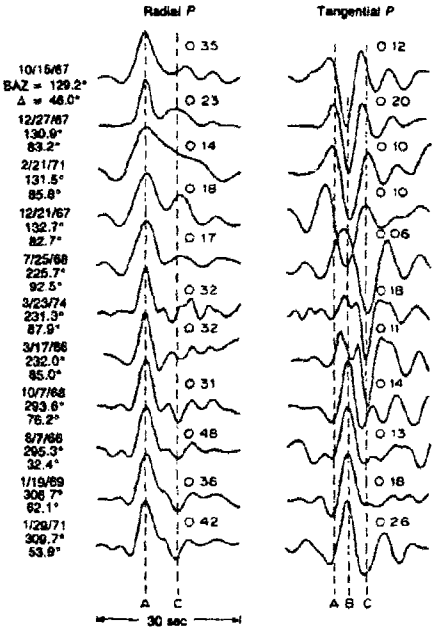

Fig. 2. Equalized radial and tangential *P* wave components for a number of events recorded at LON. Note the good correlation of waveforms for events of similar backazimuth (BAZ).

arrivals and *P* to *S* conversions as are the radial or tangential motions, this technique can be shown to be justified (Langston, 1979). Figure 2 shows the result of this source function equalization procedure for the data observed at LON. Note the agreement between tangential waveforms from sources with similar back azimuths. Figures 3 and 4 show equalized waveforms from a larger data set collected by Lee (1983) for PAS. In this case, there were a number of events at similar back azimuths such that waveform averages could be constructed to reduce the effect of processing noise.

The magnitude of the scattering effect seen in these data sets precludes an interpretation based solely on planar dipping interfaces. Lee and Langston (1983a) extended the ray method for incident plane waves by allowing interface curvature in three dimensions. Model studies carried out by Lee and Langston (1983a, 1983b) and Langston and Lee (1983), among others showed that 3D interface curvature can cause major focusing and defocusing effects in the response. Using this method, Lee (1983) performed a study of the data recorded at PAS (Fig. 3 and 4) to deduce a crustal model for the receiver. Figure 5 shows the waveform features modeled and Fig 6 is a sketch of the crustal model under the receiver. Figures 5 and 6 demonstrate that relatively minor and smooth variations in the velocity model can give rise to complex azimuthal variations in the wave response.

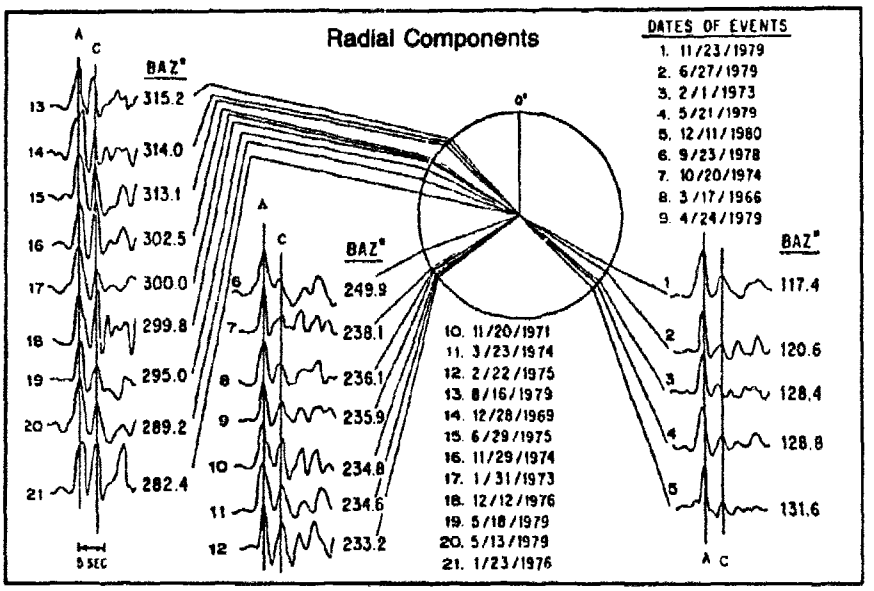

Fig. 3. Equalized radial *P* waves for earthquakes recorded at PAS. Note the variation in relative amplitude of phases A and C. A is the direct *P* wave and C is interpreted to be the Moho *P*-to-*S* conversion. This azimuthal variation is due to heterogeneous receiver structure.

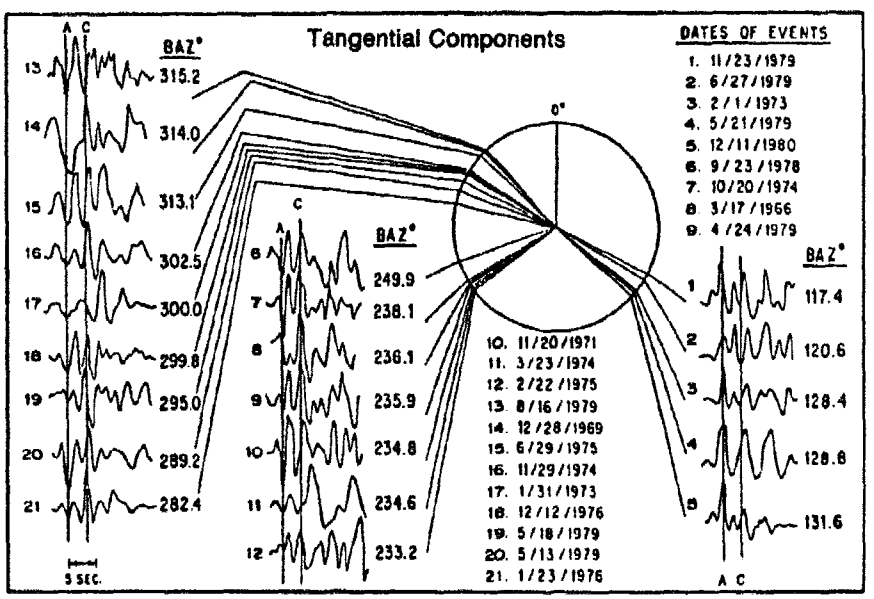

Fig. 4. Equalized tangential *P* waves for earthquakes recorded at PAS. The scatter in the data can be reduced by averaging waveforms from events of similar azimuth.

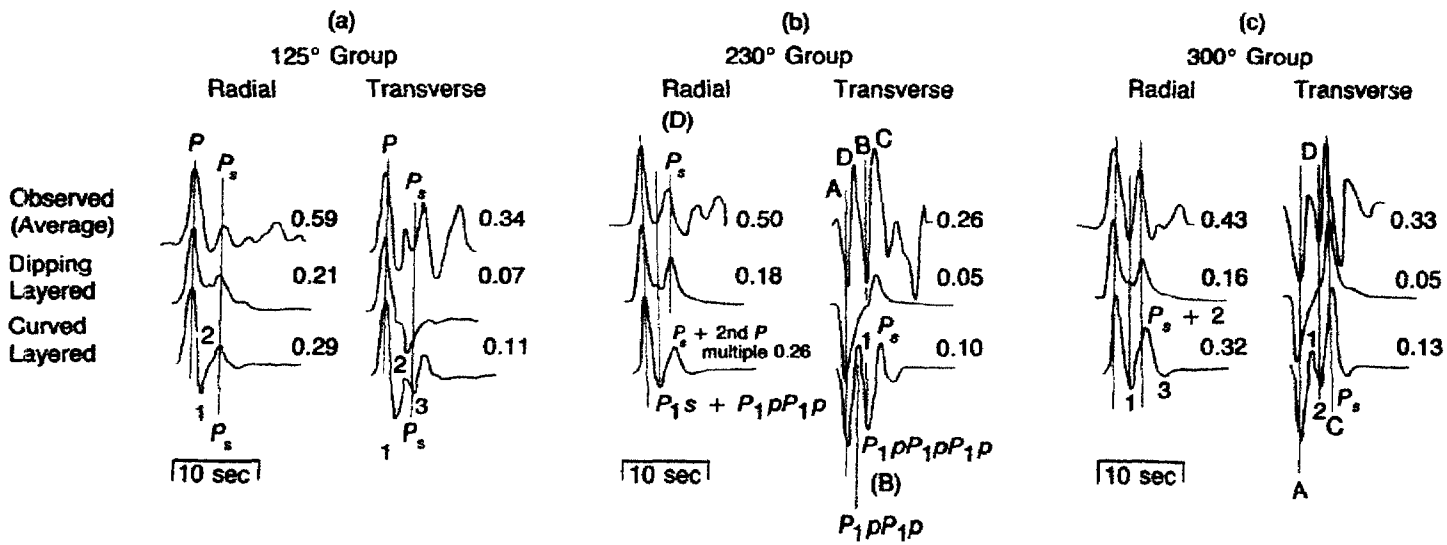

Fig. 5. Comparison of observed and synthetic waveforms for two models of PAS structure. The observed radial and transverse components were obtained by averaging individual event data at backazimuths near 125° (a), 230° (b), and 300° (c). The dipping layer model result incorporates planar dipping interfaces. The planar interfaces of this model were adjusted to fit polarities and relative amplitudes of phases seen in the data. Allowing interfaces to become curved ("curved layer" waveforms) results in a better match to major arrivals in the tangential waveforms.

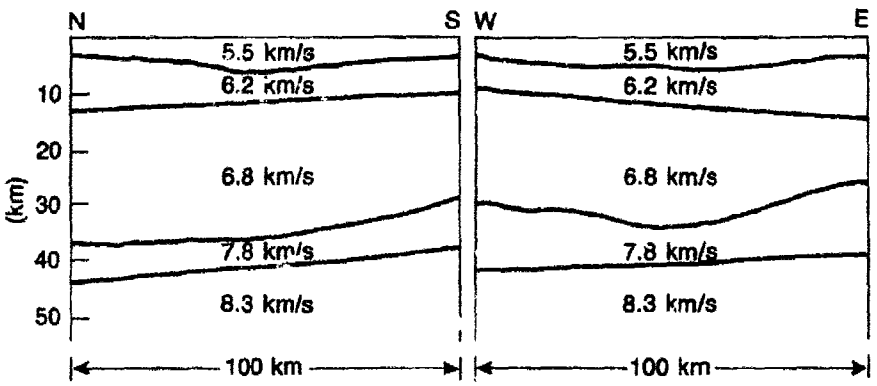

Fig. 6. Sketch of the structure inferred under PAS. Velocities and some dips of major boundaries were taken from previous geophysical studies.

Recently, the 3D ray algorithm has been modified to include point sources located in or near the 3D structure for the purpose of examining near-source scattering in locally recorded ground motions. In particular, we wish to examine the problem of alluvium geometry in the scattering of waves from buried explosions at NTS.

Figure 7 displays a comparison of the 3D ray tracing result (RT) with a Generalized Ray Theory (GRT) calculation for a point source in a plane layered model. Table 1 contains the model parameters. The 3D ray theory synthetic seismogram is a good representation of the response, particularly for the source under the layer (Model A). For a source in the layer (Models B and C), the ray theory synthetics fail to give several diffracted arrivals such as *P* head waves traveling under the free surface (phases a and b) associated with *S* and *sSS*. This is to be expected from ray theory, Note, however, that the character of the seismogram is relatively unaffected and that over-all amplitudes of major phases are consistent between GRT and RT synthetics.

Computation of *S* wave response from dislocation sources in simple curved 3D alluvium structures indicate that particle motions can become very complex, depending on source-receiver geometry. This is due to a combination of focusing of reverberations and distortions of the ray path from the vertical plane. These effects are as complex and significant as these seen in plane wave responses of simple structures and Langston; 1983a; 1983b). Current work involves the parameterization of NTS alluvium structure and computation of synthetic seismograms for explosion sources imbedded in the alluvium.

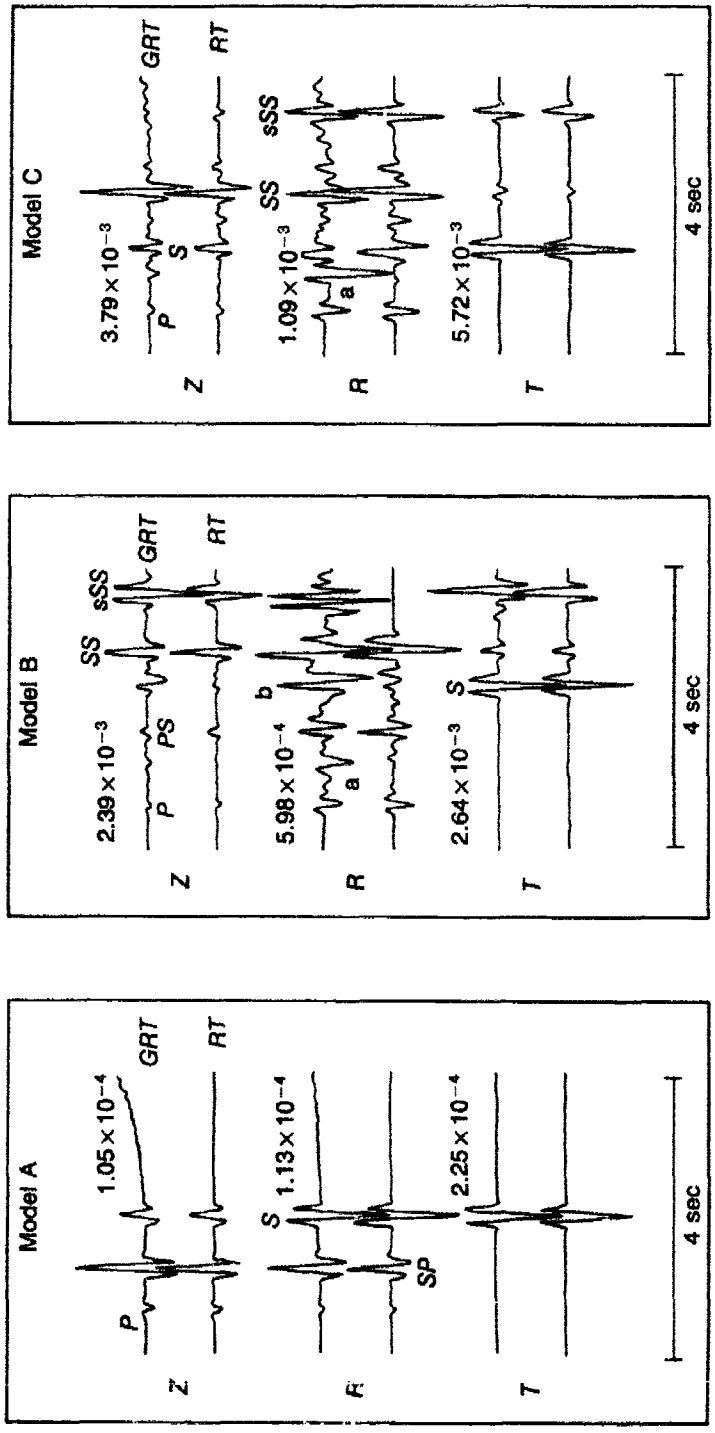

Fig. 7. Comparison of generalized ray (GRT) synthetic seismograms with 3D ray algorithm (RT) synthetics. Parameters for each model are listed in Table 1. The shape of the far-field time history assumed here is precisely shown in the tangential component of Model A. *Z*, *R*, and *T* are the vertical, radial, and tangential components of ground motion, respectively.

Table 1. Model parameters for ray theory verification.

Layer	V_p (km/sec)	V_s (km/sec)	Density (gm/cc)	Thickness (km)
1	3.0	1.5	2.0	2.0
2	6.0	3.5	2.7	—
Dislocation point source:			Dip = 35°, Rake = 60°, Strike = 15° Moment = 1×10^{20} dyne-cm	
Station azimuth:			90° (East)	
Cerveny time function parameters:			$f_m = 5, \gamma = 3, \nu = 0$	

Model	Source Depth (km)	Receiver Distance (km)
A	5	5
B	1	5
C	1	2.5

Conclusions and Recommendations

The effects of lateral heterogeniety in earth structure at the receiver and at the source appear to be major problems which affect many aspects of nuclear discrimination and yield assessment. A useful approach to evaluating 3D structure effects in an approximate way is to construct synthetic seismograms using ray theory. Ray theory is relatively inexpensive to implement and yields physical insight through the examination of ray paths and amplitudes. Problems amenable to this approach include the analysis of large scale crustal structure under receivers through particle motion studies of teleseismic *P* waves and the scattering of explosion body waves by 3D source structure, particularly where there are independent geophysical constraints on such structure.

References

Burdick, L.J. and C.A. Langston (1976). "Modeling Crustal Structure Through the Use of Converted Phases in Teleseismic Body Wave Forms," *Bull. Seism. Soc. Am.*, **67**, 677-691.

Herbert, L. and C.A. Langston (1984). "Crustal Thickness Estimate at AAE (Addis-Ababa, Ethiopia) and NAI (Nairobi, Kenya) Using Teleseismic *P*-Wave Conversions," submitted to *Tectonophysics*.

Langston, C.A. (1977a). "Corallis, Oregon, Crustal and Upper Mantle Receiver Structure from Teleseismic *P* and *S* waves," *Bull. Seism. Soc. Am.*, **67**, 713-724.

Langston, C.A. (1977b). "The Effect of Planar Dipping Structure on Source and Receiver Responses for Constant Ray Parameters," *Bull. Seism. Soc. Am.*, **67**, 1029-1050.

Langston, C.A. (1979). "Structure Under Mount Rainier, Washington, Inferred from Teleseismic Body Waves," *Jour. Geophys. Res.*, **84**, 4749-4762.

Langston, C.A. (1981). "Evidence for the Subducting Lithosphere Under Southern Vancouver Island and Western Oregon from Teleseismic *P* Wave Conversions," *Jour. Geophys. Res.*, **86**, 3857-3866.

Langston, C.A and Jia-Ju Lee (1983). "Effect of Structure Geometry on Strong Ground Motions: the Duwamish River Valley, Seattle, Washington," *Bull. Seism. Soc. Am.*, **73**, 1851-863.

Lee, Jia-Ju (1983). *A Three-Dimensional Ray Method and Its Application to the Study of Wave Propagation in Crustal Structure With Curved Layers*, Ph.D. Thesis, The Pennsylvania State University, University Park, PA 16802.

Lee, Jia-Ju and C.A. Langston (1983a). "Three-Dimensional Ray Tracing and the Method of Principal Curvature for Geometric Spreading," *Bull. Seism. Soc. Am.*, **73**, 765-780.

Lee, Jia-Ju and C.A. Langston (1983b). "Wave Propagation in a Three-Dimensional Circular Basin," *Bull. Seism. Soc. Am.*, **73**, 1637-1653.

Peseckis, L.L. and L.J. Burdick (1982). "Station Site Characteristics of WWSSN Stations in India and Southern Asia," *Bull. Seism. Soc. Am.*, **72**, 1207-1218.

P Wave Dispersion Due to Scattering and the Effects on Attenuation and Magnitude Determination

K.L. McLaughlin and L.M. Anderson

Summary

Short period P wave seismograms exhibit a number of characteristics diagnostic of scattering in a stochastic medium. Direct P wave arrivals systematically exhibit a longer period than would be predicted from examination of the frequency of P wave coda. High frequencies are systematically delayed in the P wave signal with respect to low frequencies. Spatial coherence is greatest in the initial portion of the waveform and decays with higher frequencies, and with elapsed time after the P wave arrival. These effects are an effective dispersion with a random component, stochastic dispersion.

This hypothesis predicts that time domain and frequency domain modeling techniques should result in systematic differences as a result of the delay of high frequencies and the decay of coherence. Time domain modeling emphasizes the initial coherent deterministic swing of the P wave. Frequency domain modeling averages the distribution of the signal energy over a window that combines the deterministic part of the waveform with the more random coda. Since the initial P waveform is not independent of the P coda multipathing we should expect a lower frequency initial pulse and a higher frequency coda. Lower rise-time estimates and greater t^* estimates will result from time domain modeling than from frequency domain modeling. This appears to be the case for recent determinations of attenuation.

Measurements of the stochastic dispersion for several source and receiver localities have been made. Comparison of the observed dispersion to theoretical models is under way. Some of these theories allow the determination of the statistics of the medium, and subsequent prediction of expected variances for P wave measurements. We wish to determine these statistics and test whether the discrepancies between time and frequency domain modeling can be reconciled with available theories of scattering.

Introduction

The inverse correlation between short period *P* amplitudes and seismogram complexity has been used as an argument that coda is a more

consistent measure of the source than the deterministic wave (see Aki, 1982 for a review). Douglas *et al.* (1973) concluded that the direct signal may experience defocussing or anomalous attenuation, but that multipathing is also a contributor to complexity. Such multipathing is virtually random, since adjacent receivers and sources exhibit different multipaths. The effects of multipathing are not just the simple modulation of the signal spectrum as would be expected if each multipath were a mimic of the direct signal. In reality, the direct signal is attenuated as a result of the removal of scattered energy along the ray path, and multipaths are not replications of the most direct signal; therefore multipathing is frequency dependent. Long wavelengths are less sensitive to heterogeneity and see a more homogeneous medium. Consequently, multipath arrivals are likely to be high-pass filtered versions of the original signal. The net effect is a pulse widening of the direct P wave and a delay of high frequencies.

In the past, considerable work has been expended on the analysis of time and amplitude fluctuations of P waves observed at large arrays. Such work has given us a great deal of information about the fine structure of amplitude and travel time statistics. Although deterministic modeling (Bertuessen, 1975a, 1975b; Aki *et al.* 1976) has been used, random scattering models have also contributed to our understanding of the short period wave field. The random scattering models (Aki, 1973; Capon, 1974; Bertuessen *et al.* 1975) have been for the most part been based on the work of Chernov (1960), and limited by the Rytov approximation. The theoretical limitations to simple geometries, weak scattering, and the Rytov approximation, have limited the analysis to low frequencies and to models of the lithosperc directly beneath the receivers. Higher frequencies (> 1 Hz) and refracted ray paths have been intractable because of the stronger scattering, and the curved geometry of teleseismic rays. Since the initial work of Chernov, considerable work has extended the theory of forward scattering from the realm of weakly perturbed plane waves to the effects of pulse broadening by multipathing and curved wavefronts. The analytic treatments of stochastic scalar wave theories for pulse broadening by Uscinski (1977), Ishimaru (1978), Dashen (1979), and McCoy (1980) are just a few. These treatises have in common the assumption that the parabolic wave equation is a good approximation of the wave field.

Furthermore, Monte-Carlo methods have been shown by Williamson (1975) to give the same answers for simple geometries of wave propagation as the analytic methods of Uscinski (1974). More complicated structures, such as gradient layer models with random components of velocity, remain intractable for analytic calculations of wave statistics.

Numerical simulations of these more complicated models are necessary to calculate the statistical variations of the waveform. One example of such numerical simulations are the calculations of Richards and Menke (1983) and Menke (1983) to examine the response of a random one dimensional stack of layers to plane P and S waves of different slownesses with P-SV coupling. Although Menke's results apply to small inhomogeneities (thin random layers) with respect to a wavelength, they also demonstrate the stochastic delay of high frequencies with respect to lower frequencies, by essentially Monte-Carlo techniques. Mereau

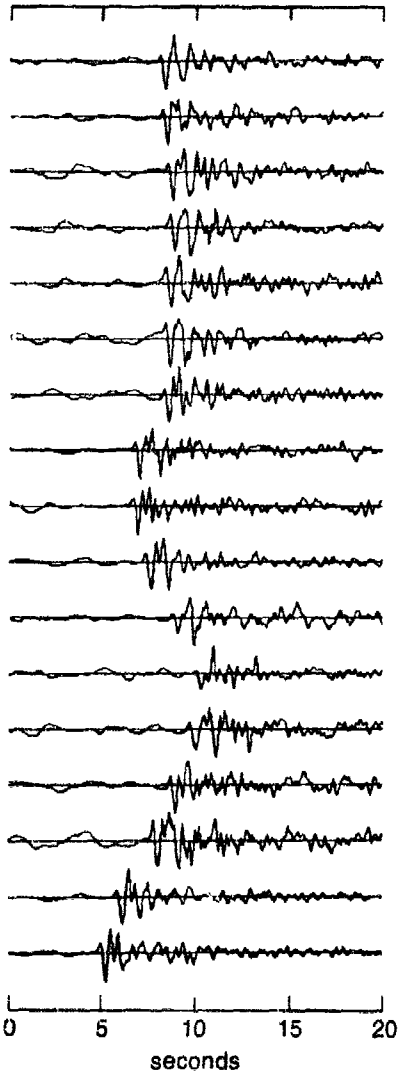

Fig. 1. NORSAR seismograms for an East Kazahk explosion. Variation of the P amplitude, P waveform, and initial P coda is considerable in the first 5 seconds. The initial coda (5 to 6 seconds) possesses higher frequency content than the initial (first 2 seconds) P wave pulse.

and Ojo (1981) used ray tracing through a random media to demonstrate that linear gradient models with small random perturbations exhibited travel time anomalies resembling a layered structure.

Observations of Some *P* Wave Statistics

Figure 1 shows seismograms of the NORSAR array for an explosion in East Kazahk. Apart from the variation of P wave amplitude, there is considerable variation in the P waveform and coda in the first 5 to 6 seconds. Visual observation shows that the initial coda (first 5 to 6 seconds) possesses higher frequency content than the initial pulse (first 1 to 2 seconds). To examine the effect of this dispersion, Fig. 2 shows bandpass filtered seismograms of two stations for a similar event. The filters are 1 Hz bandwidth zero-phase-shift Gaussian filters with center frequencies of 1, 2, 3, 4, 5, 6, and 7 Hz. The impulse responses of these filters are Gaussian shaped wave packets centered on the arriving impulse. The high frequencies are most prominent in the early P coda, and the secondary arrivals in the coda are often discrete high frequency pulses. To quantify these two effects in terms of a net dispersion, the signal energy temporal centroid was calculated for each band-passed seismogram. The signal energy temporal centroid is defined as

$$T = \int s(t)^2 \, t \, dt \Big/ \int s(t)^2 \, dt \tag{1}$$

where $s(t)^2$ is the square of the signal as a function of time. The temporal centroids show considerable scatter for any given source-receiver pair, but yield consistent averages for either a closely spaced array of sources or for a single source averaged over the array. These averages constitute an approximation of an ensemble of source-receiver paths with similar statistics. Figure 3 shows two plots of the scatter of temporal centroids as a function of frequency. The centroids have been reduced to the temporal centroid of the unfiltered seismogram. Figure 3(a) shows the scatter for ten stations and 6 sources where the integral of Eq. 1 has been taken over 3.2 seconds of signal. Figure 3(b) shows the results of averaging over the array for each source. The error bars shown are for the standard deviation of a single observation. The statistics of a single observation appear to be Gaussian. The results indicate that the temporal centroid is a stochastic quantity with a well defined ensemble average. Figure 4 shows that a longer window of 6 seconds has similarly delayed high frequency energy. A net average difference of 0.5 seconds is not uncommon between the centroid measured at 5 Hz with respect to the centroid measured at 1 Hz. Attempts to match the first arrival's

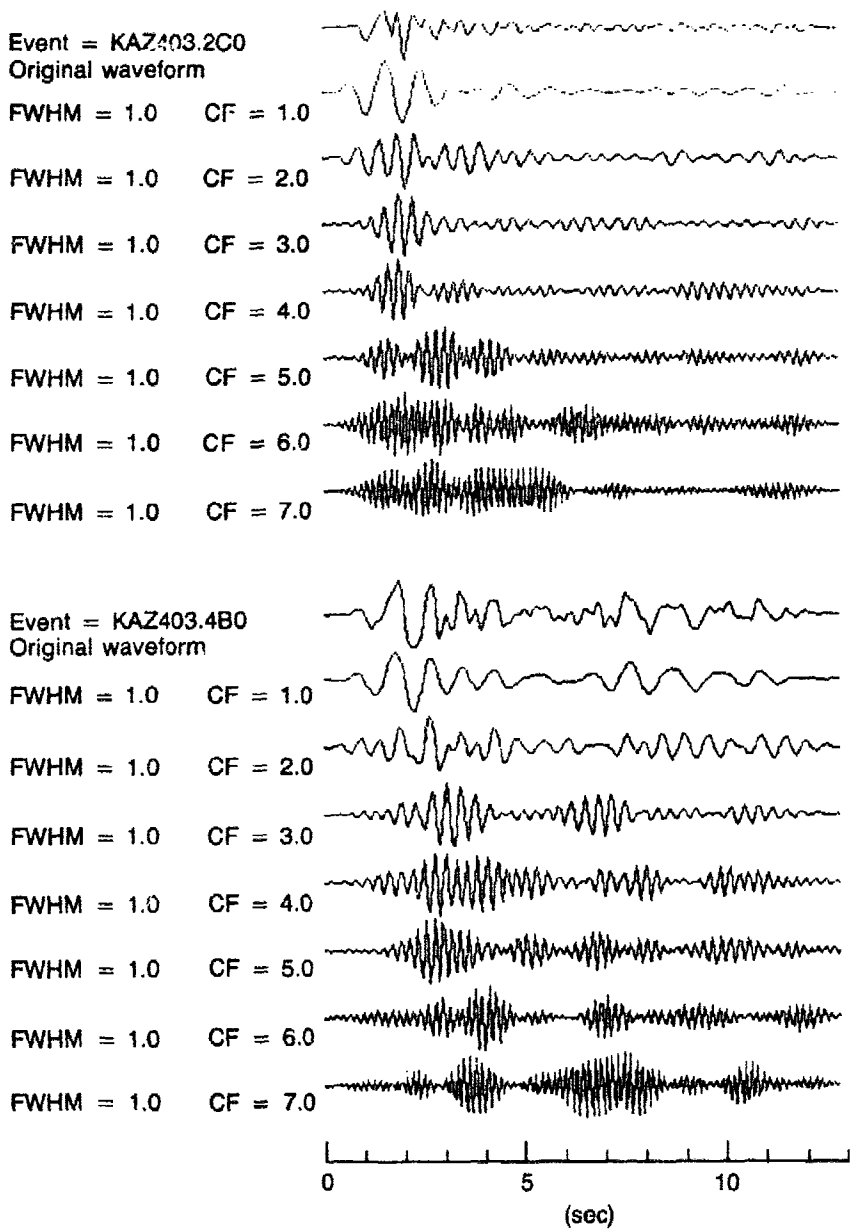

Fig. 2. Band-pass filtered seismograms of two NORSAR stations using zero-phase-shift Gaussian filters with center frequencies of 1, 2, 3, 4, 5, 6, and 7 Hz. Each filter has a half-width-half-maximum of 0.5 Hz.

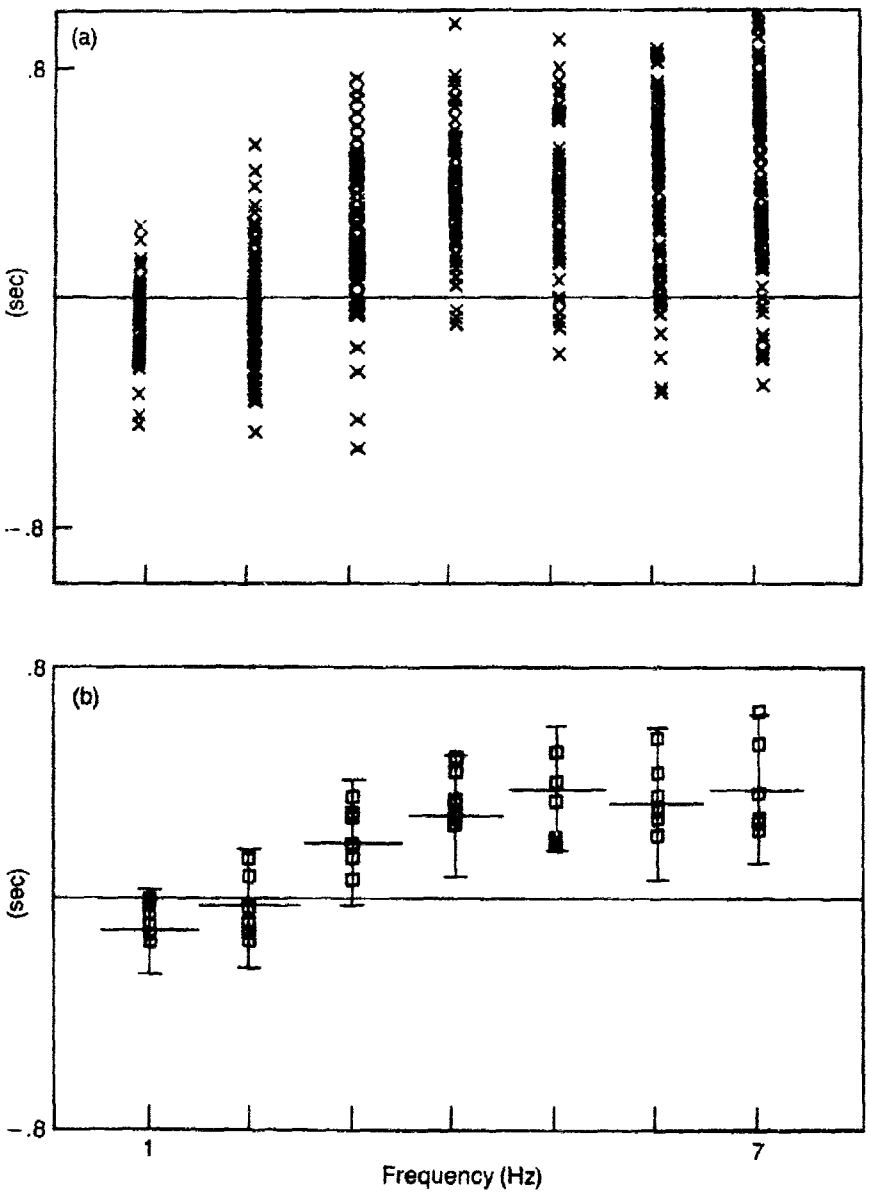

Fig. 3(a). Scatter of temporal energy centroids as a function of frequency. The centroids are calculated from the band-pass filtered seismograms at 1 Hz intervals with filter widths of 1 Hz. The zero baseline is the centroid of the unfiltered trace. Results for 10 stations and 6 events are shown. (b). Centroids are averaged by event. The vertical errors bars are standard deviations of a single observation. Horizontal error bars represent the full width at half maximum of each filter.

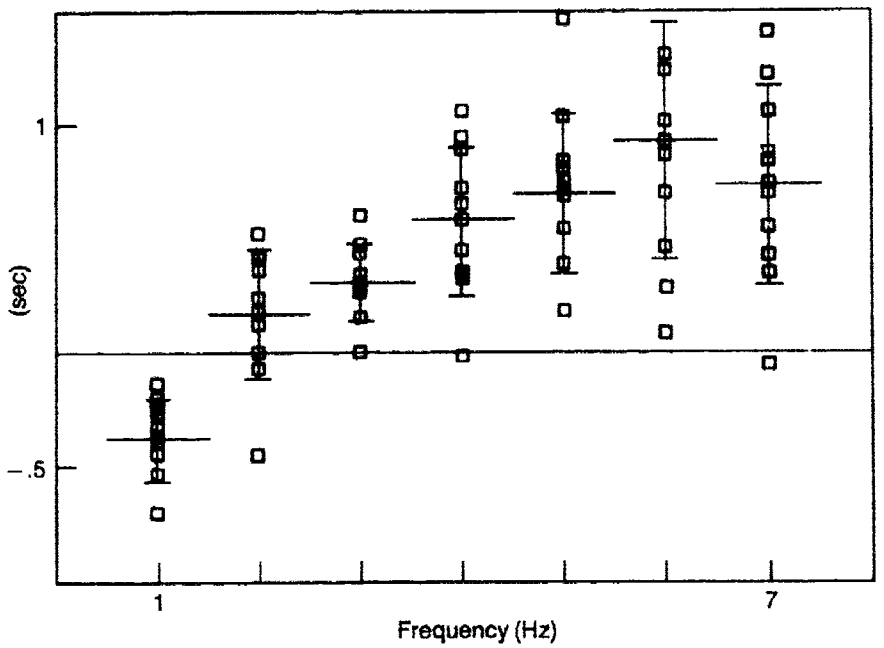

Fig. 4. Temporal energy centroids as a function of frequency for a 6 second time window. Standard deviations of a single measurement are shown by the vertical bars. Temporal centroids are all reduced to the centroid of the unfiltered trace. Horizontal bars represent the full width of the filter at half maximum.

characteristic frequency with time-domain modeling would not account for the delayed high frequency arrivals, while spectra calculated from a 6 second window do not indicate where the signal energy resides within the window. Attempts to model this effective group delay of the high frequencies due to instrument response, attenuation induced dispersion, minimum-phase source time functions have demonstrated that that average delay can not be modeled as minimum phase.

Only when a moderately large set of source and/or receivers is available can this kind of dispersion be characterized. Arrays such as NORSAR, LASA, and YKA will generally be required to approximate an ensemble average. However, we have shown that for the East Kazakh source area, that the dispersion statistics observed at NORSAR are the same for a suite of explosions at the same receiver as they are for a suite of NORSAR receivers for a fixed event. Furthermore, relative time delays of 0.1 or 0.2 seconds with narrow bandwidths at 1 or 2 Hz can not be measured on a single seismogram and require some sort of statistical averaging. Preliminary work at GRFO, ANTO and KONO indicate that

the same sort of dispersion is present at other sites for the East Kazakh test site explosions. Similarly, NTS events at NORSAR show some dispersion although the data has less bandwidth.

Some Simple Modeling

Following the simple approach of Williamson (1974), a simple Monte-Carlo calculation was performed for multipathing of scalar waves in a random medium. The calculation is intended to show the move-out of high frequencies with respect to lower frequencies. An initially plane scalar wave of specific frequency is incident on a space of constant velocity with random perturbations of zero mean. The random perturbations are described by their characteristic length, a, and rms velocity variation, η. The problem is reduced to two constants, β, and Γ,

$$\beta = \eta^2 k^2 a \tag{2}$$

and

$$\Gamma = ka \tag{3}$$

where k is the wavenumber. Figure 5 is a plot of cumulative energy from rays in an ensemble average of such media with fixed statistics. It constitutes a Monte-Carlo determination of the ensemble average of the energy envelopes. In this sense it is analogous to determination of the average energy envelope for a collection of independent band-passed seismograms. The temporal centroid of this envelope would correspond to the band-passed filtered temporal centroids in Figs. 2 through 4.

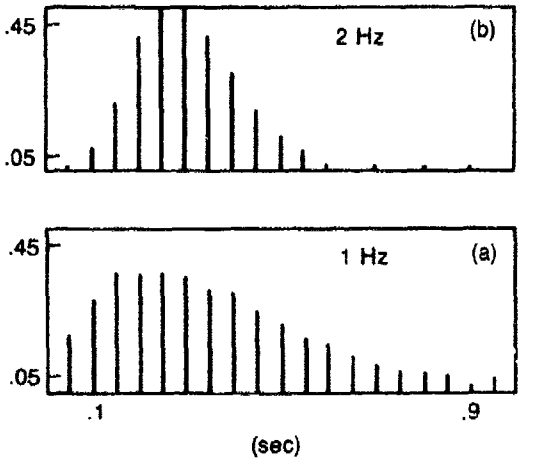

Fig. 5. Results of a Monte-Carlo calculation for 1 Hz (below) and 2 Hz (above) propagation through a medium with 5% rms velocity variation, and 50 km heterogeneity characteristic scale length. The bar graph is an ensemble average for such random media of the multipath energy arrivals as a function of time. Distance propagated is 500 km. There is a shift in the distribution peak between 1 Hz and 2 Hz of about 0.2 seconds.

Figures 5(a), and 5(b) are for two different wavenumber-heterogeneity scale length dimensionless constants. The shorter wavelength wave is delayed with respect to the longer wavelength wave for the same medium. This is a simple geometry, that illustrates the effective pulse broadening that might be expected for traveling through the upper mantle twice. Effects due to the refraction of rays by the spherically symmetric earth, are not modeled, and the heterogeneity of the earth is modeled as a single characteristic scale length. Also, the calculations are limited to the ensemble averaged signal energy as a function of time. Some of these limitations may be over come with calculations based on the more exact formulation of Gaussian beams (Cerveny *et al.* 1982). Ray shooting (Aric *et al.* 1980) is a relatively simple numerical process as opposed to two-point ray tracing, and random perturbations on the ray are easily introduced. Summation of beams can be used to model phase interference as well as the simple energy envelope.

Conclusions

These calculations are valid for $ka > 1$ (geometrical optics). It is also likely that stochastic dispersion effects described by Menke (1983), which are valid for $ka < 1$, are also at work. Additional mechanisms are likely to be active for the generation of *P* coda rich in high frequencies and delayed with respect to the initial wave. The linear finite difference calculations of an accompanying paper go a long way towards exploring the results of heterogeneity near the source and receiver. At this point, it is important to provide a model (or models) that explains all the stochastic features of the seismic field observed on the surface of the earth. These statistics include the spatial coherency, the attenuation, the dispersion, and the amplitude and arrival time delays associated with the scattering of seismic waves.

Whatever the mechanism for the observed stochastic dispersion of *P* waves from explosions, it is clear that the delay of high frequencies will result in a broadened first pulse and that time domain and frequency domain methods of intrinsic attenuation measurement will inevitably result in systematic differences. Only when we understand these systematic differences and the consequences of each can we correctly account for the correct proportion of intrinsic and scattering attenuation. Finally, from the point of view of magnitude yield determination, it seems that these are small but significant delays of high frequency with respect to low frequency.

References

Aki, K. (1973). "Scattering of *P* Waves Under the Montana LASA," *J. Geophys. Res.*,

78, pp 1334-1346.

Aki, K., A. Christoffersson, and E.S. Husebye (1976). "Three-Dimensional Seismic Structure of the Lithosphere Under Montana LASA," *Bull. Seism. Soc. Am.* **66**, 2, pp 501-524.

Aki, K. (1982). "Scattering and Attenuation," *Bull. Seism. Soc. Am.* **72**, B6, pp S319-330.

Aric, K. R. Gutdeutsch, and A. Sailer (1980). "Computation of Travel Times and Rays in a Medium of Two-Dimensional Velocity Distribution," *Pageoph*, **118**, pp 786-806.

Bolt. B.A. and R. Gutdeutsch (1982). "Re-Interpretation by Ray Tracing of a Transverse Refraction Seismic Profile Through the California Sierra Nevada," *Bull. Seism. Soc. Am.*, **72**, pp 889-900.

Bertuessen, K.A., A. Christoffersson, E.S. Husebye, and A. Dahle (1975). "Wave Scattering Theory in Analysis of *P* Wave Anomalies At NORSAR and LASA," *Geophys. J. Roy. Astr. Soc.*, **42**, pp 403-417.

Bertuessen, K.A. (1975a). "Crustal Structure and *P* Wave Travel Time Anomalies at NORSAR," *J. Geophys.*, **41**, pp 71-84.

Bertuessen, K.A. (1975b) "*P* Wave Amplitude Variability at NORSAR," *J. Geophys*, **41**, pp 595-613.

Capon, J. (1974). "Characterization of Crust and Upper Mantle Structure Under LASA as a Random Medium," *Bull. Seism. Soc. Am.*, **64**, 1 pp 235-266.

Cerveny, V., M.M. Popov and I. Psenick (1982). "Computation of Seismic Wave Fields in Inhomogeneous Media-Gaussian Beam Approach," *Geophys, J.* **70**, pp 109-128.

Chernov, L.A. (1960). *Wave Propagation in a Random Medium*, McGraw-Hill, 168 pages.

Dashen, R. (1979). "Path Integrals for Waves in Random Media," *J. Math Phys*, **20**, pp 894-920.

Douglas, A., P.D. Marshall, P.G. Gibbs, J.B. Young, and C. Blamey (1973). "*P* Signal Complexity Reexamined," *Geophys. J.*, **33**, pp 195-221.

Greenfield, R.J. (1971). "Short-Period *P* Wave Generation by Rayleigh Wave Scattering at Novaya Zemlya," *J. Geophys. Res.*, **76**, pp 7988-8002.

Ishimaru, A. (1978). *Wave Propagation and Scattering in Random Media, VII, Multiple Scattering, Turbulence, Rough Surfaces, and Remote Sensing*. Academic Press. 328 pages.

Menke, W. (1983). "On the Effect of *P-S* Coupling on the Apparent Attenuation of Elastic Waves in Randomly Layered Media," *Geophysical Research Letters*, **10**, 12, pp 1145-47.

McCoy, J.J. (1980). "Parabolic Wave Theories and Some Recent Applications," *Phys. Earth and Planet, Inter.*, **21**, pp 126-133.

Mueller, R.A. and J.R. Murphy (1977). "Seismic Characteristics of Underground Nuclear Detonations," *Bull. Seism. Soc. Am.*, **61**, pp 1675-1692.

Merea, R.F. and S.B. Ojo (1981). "The Scattering of Seismic Waves Through a Crust and Upper Mantle with Random Lateral and Vertical Inhomogeneities," *Phys. Earth and Planet, Inter.*, **26**, pp 233-240.

Richards, P.G. and W. Menke (1983). "The Apparent Attenuation of a Scattering Medium," *Bull. Seism. Soc. Am.* **73**, 4, pp 1005-1021. **3**, 4, pp 1005-1021.

Sato, H. (1982). "Amplitude Attenuation of Impulsive Waves in Random Media Based on Travel Time Corrected Mean Wave Formalism," *J. Acoustic Soc. Am.*, **71**, pp 559-564.

Uscinski, B.J. (1974). "The Propagation and Broadening of Pulses in Weakly Irregular Media," *Proc. R. Soc. Land*, **A336**, pp 379-392.

Uscinski, B.J. (1977). *The Elements of Wave Propagation in a Random Medium*, McGraw Hill.

Von Seggern, D.H. and R.R. Blandford (1972). "Source Time Functions and Spectra for Underground Nuclear Explosions," *Geophys. J.* pp 83-97.

Williamson, I.P. (1975). "The Broadening of Pulses Due to Multipath Propagation of Radiation," *Proc. R. Soc. Land.* **A342**, pp 131-147.

Linear Finite Difference Methods Applied to Scattering of Seismic Waves

K.L. McLaughlin, Z.A. Der, and L.M. Anderson

Summary

Numerous wave propagation problems involving heterogeneity near the source or receiver directly affect magnitude yield determinations. These include focussing/defocussing of short period body waves, multipathing, scattering attenuation and dispersion, generation of pP from a non-planar free surface, and P coda generation from crustal heterogeneity. Few of these problems may be solved analytically. We have begun to approach a number of these problems using a 2-D linear finite difference code with several boundary and initial conditions. Optional initial conditions include incident plane waves of P or S type, as well as cylindrical sources of P or S type. Optional boundary conditions include free surface, symmetric, and the Clayton and Engquist (1977) absorbing boundary conditions. We present in this paper, examples of some of our work in progress. First we show the effects of random heterogeneity in a half space upon planar incident P waves. Second, we show the effects of random heterogeneity on displacement amplitudes for a cylindrical source in a whole space. These constitute very general problems of elastodynamics with applications to the interpretation of array data, as well as near-field displacement measurements.

Linear Finite Difference Methods Applied to Scattering of Seismic Waves

Several theories of scalar wave propagation in heterogeneous media have been formulated over the years. However, no general scattering theory exists for the less tractable elastodynamic problems that we are faced with in the real earth. At high frequencies, it is commonly argued that scalar theories should apply, however, no tests have been made to compare the high frequency scalar approximations to more exact calculations. Heterogeneity in the earth is due to variations of the elastic modulii, as well as density. In our current study we are limiting heterogeneity to variations of P wave velocity, S wave velocity, and density. Additional complications due to anisotropic heterogeneity have been left for future

studies. S wave velocities are assumed to vary with the P wave velocities; the Poisson ratio is assumed to be a function of P wave velocity. This assumption, although based on physical intuition, will be relaxed at a later date.

Apart from approximations that rely on de-coupled scalar representations of the P and S wave fields, many specific problems of wave propagation are untractable without a complete 2-D or 3-D solution of the elastodynamic equations. Our research program encompasses a wide range of problems including both deterministic and stochastic models of the earth. We have recently completed several general studies of propagation in stochastic media for comparison with other methods for wave field calculation. The first of these problems is an array of stations with incident plane P waves on a randomly heterogeneous elastic half space. This example has obvious applications to the diagnostics of beam loss at seismic arrays and the systematic study of spatial coherency. In fact, the synthetics generated in this way can be used to test various adaptive beaming methods that attempt to compensate for the effects of signal incoherency. Because the heterogeneity scale lengths are often on the same order as the wavelength and because the dilatational and rotational fields are coupled, these results include diffraction and conversion. The second of these problems is a cylindrical source in a randomly heterogeneous medium. The same comments apply to this problem as the one of a plane wave except that the diffraction effects of a cylindrical wave are expected to differ from those of a plane wave. We are studying the attenuation, dispersion, and spatial incoherency of the waveforms due to scattering by the heterogeneous medium.

Plane Wave in a Heterogeneous Half Space

An array of seismograms recorded at the free surface is shown in Fig. 1, as the result of an incident 5.0 km wavelength plane wave on a layer of heterogeneity 14 km thick with a heterogeneity scale length of 2.5 km and a 10% variation in the P and S wave velocities. The seismograms are taken from points 2.0 km apart. By performing several of these numerical experiments we have compiled the dependence of certain statistics of this array on the wavelength of the incident wave. Figure 2 shows the average amplitudes observed at the free surface for various planar P waves that have propagated through a Gaussian random media with a constant rms P wave velocity variation of 10% superimposed on a constant velocity of 5 km/sec and a characteristic heterogeneity scale length of 2.5 km. Amplitudes are shown normalized to the value for a homogeneous half-space while the propagation distance has been scaled to $\beta = \eta^2 k^2 az$, where η is the rms velocity variation of 10%, a is the

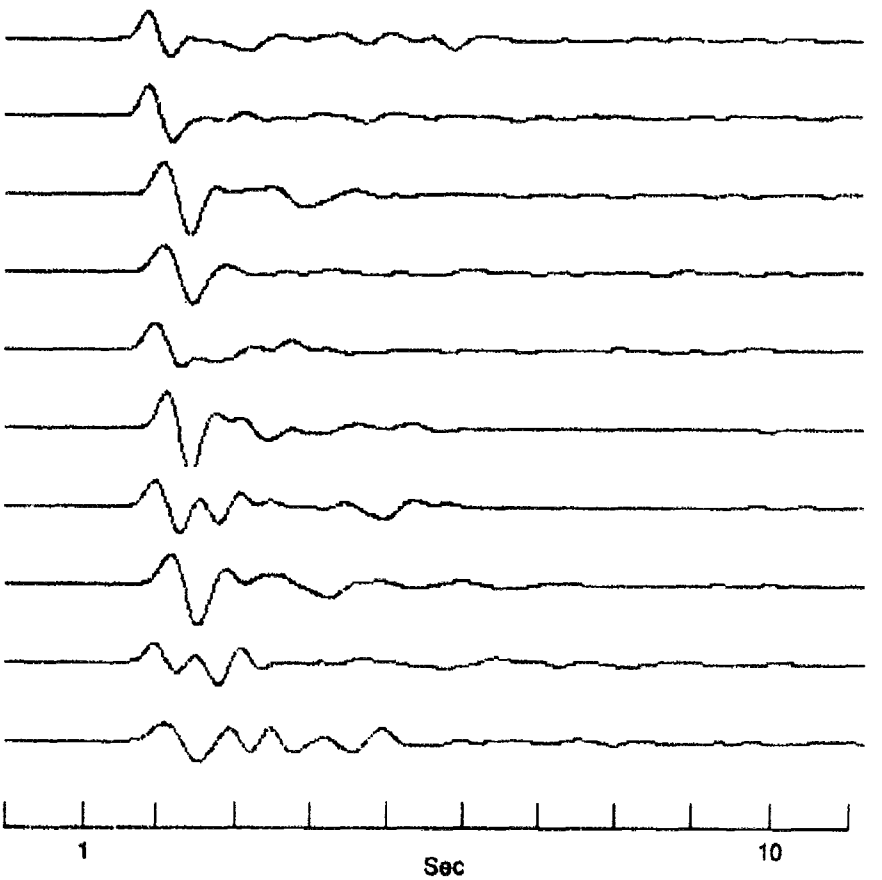

Fig. 1. Synthetic seismograms for an array of stations spaced 2.0 km apart. A plane P wave (wavelength of 5.0 km) has propagated 14 km through a Gaussian random medium with a 2.5 km scale length and 10% P and S wave velocity variation.

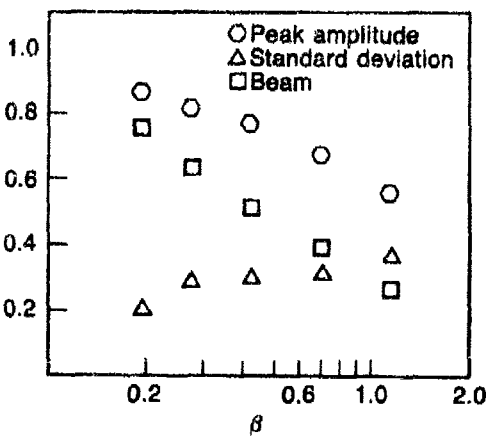

Fig. 2. Compilation of some amplitude statistics for numerical experiments such as shown in Fig. 1. The average peak displacement, (hexagon) and the peak displacement (square) of the beam both decline with scattering parameter β. The relative decline of the beam peak amplitude to the average peak amplitude is a measure of the beam loss. The standard deviation of the individual station peak amplitudes is shown as a triangle.

characteristic heterogeneity scale length of 2.5 km, k is the wavenumber, and z is the distance traveled. The wavelengths considered vary from 3 to 7 km. The average displacement peak amplitude for each station at the surface declines with increasing β, while the standard deviation of the peak amplitude across the array increases with β. In addition to the attenuation of the peak amplitude, variation of the waveform across the array creates "beam loss" and the peak amplitude of an array beam shows even steeper decline with increasing β than the average peak amplitude across the array. The dimensionless parameter β is proportional to the number of wave lengths traveled times the number of scale lengths per wavelength. The actual distance traveled was nearly constant for each frequency component of the signal, so it is clearly seen that attenuation, spatial incoherence and beam loss all rapidly increase with increasing frequency.

Cylindrical Source in a Heterogeneous Whole Space

Figure 3 shows the decline of peak displacement amplitude for a cylindrical source as a function of distance in another Gaussian random medium.

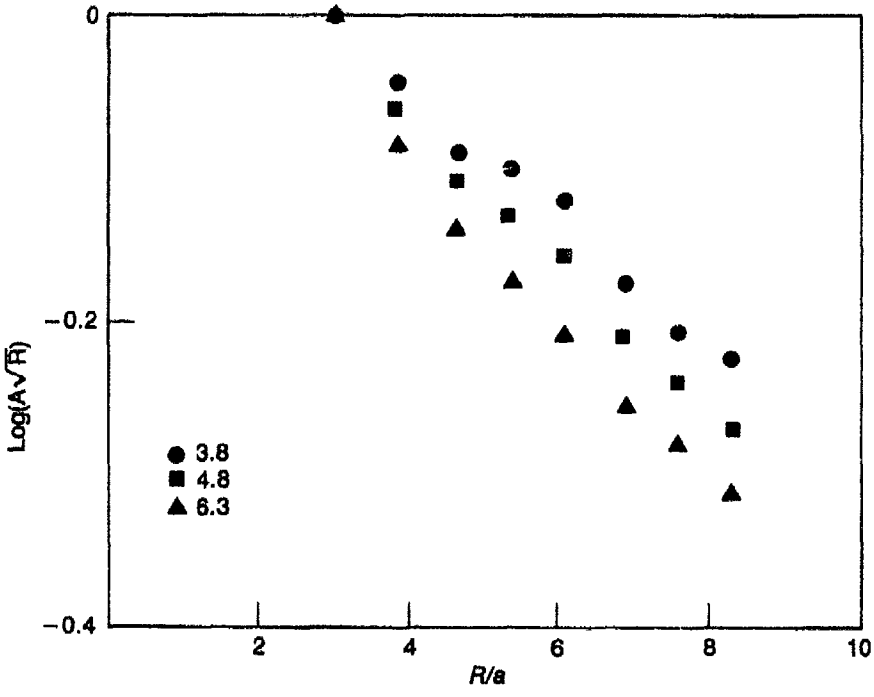

Fig. 3. Scaled amplitude versus scaled distance for a cylindrical source at three different values of $ka = (2\pi/\lambda) = 3.8, 4.8$ and 6.3. Medium is a whole space with a rms 10% variation in the P and S wave velocities.

Again, the rms velocity variation is 10% superimposed on a uniform velocity field. The propagation distance has been normalized to the heterogeneity scale length and the amplitudes have been scales to reflect cylindrical spreading. Three values of normalized wavenumber ka have been shown, ka = 3.8, 4.8, and 6.3. For comparison, to a cylindrical source in a medium of 5 km/sec with a heterogeneous scale length of 1.5 meters, and a 10% rms P and S wave velocity variation, we would expect a 2 Hz wave to be attenuated by a factor of 0.5 within 13 km. Results from the previous example with plane waves indicate that a plane wave would be attenuated by a similar factor of about 0.5. Since the degree of apparent attenuation that results from heterogeneity is not linear with the amplitude of the heterogeneity variation, these results should only serve as an indication of the extreme nature of the possible attenuation of peak amplitudes due to scattering. Furthermore, since a great deal of the energy is simply transferred to the coda of the direct wave, spectral measures would measure less attenuation of the seismic pulse.

References

Clayton, R. and B. Engquist (1977). "Absorbing Boundary Conditions for Acoustic and Elastic Waves Equations," *Bull. Soc. Seis. Am.*, **67**, 1529-1540.

Three-Dimensional Images of the Earth's Interior

J.H. Woodhouse and A.M. Dziewonski

Introduction

Even though the surface expression of the earth dynamics is known in great detail, and this overall pattern is well explained by the theory of plate tectonics, our understanding of the processes involved decreases rapidly with depth. The inaccessibility of the medium below some 10 km necessitates the inference of the conditions in the deep interior of the earth from observations at the surface. Of all methods available in earth sciences, seismological techniques have potentially the greatest resolution for the remote sensing of *in situ* material properties.

Knowledge of the lateral heterogeneity has also important practical applications in imaging the seismic source. The distortion of a lens from spherical symmetry may give a false image of the position and brightness (source mechanism, moment) of an event. An important part of our motivation to undertake this study was to obtain the means for a refined estimation of seismic source parameters.

Regional studies of crustal structure have been carried out for several decades. For depths less than, say, 150 km it was possible to use surface wave data from a particular region (Canadian Shield, Brune and Dorman, 1963; various provinces of the Pacific Ocean, Forsyth, 1975; Leeds, 1975, for example). Attempts to understand the pattern of regional variations in the upper mantle at greater depths began in the 1960's (Toksöz and Anderson, 1966) but these involved the important assumption that the structure is defined at all depths by the tectonic expression at the surface (shields, young or old oceans). This is so called 'pure path' analysis or the regionalization approach. Its weakness is that the initial assumptions cannot be tested: for example, it is impossible to find out in this way whether the Siberian and Canadian shields are different at depth, because all shields are constrained to be the same. The first papers in which the assumption of regionalization was avoided are recent (Masters *et al.*, 1982; Nakanishi and Anderson, 1982) and these were made possible by the availability of a large volume of high quality digital data from a global network of IDA instruments (International Deployment of Accelerometers; Agnew *et al.*, 1976).

The accumulation of data from the IDA network as well as the GDSN (Global Digital Seismograph Network; primarily its SRO/ASRO component; Peterson *et al.*, 1976) over the last six years makes it possible to sample the globe very densely with surface wave observations. Full utilization of these data has required the development of new techniques of analysis. In the present study we describe an approach involving the iterative refinement of the earth model by matching the observed and synthetic waveforms. This method allows us to use all information contained in a seismic recording, rather than just the fundamental mode dispersion characteristics, which have formed the basis of previous studies.

Global investigations of lateral heterogeneities in the lower mantle have been very few and have suffered from either poor spatial resolution (Dziewonski *et al.*, 1977) or instability (Sengupta and Toksöz, 1976). Travel times of body waves has been used to study the lower mantle structure. The uneven distribution of seismic sources and receivers leaves unsampled large areas of the world, and imposes a severe limitation on the scale of features that can be resolved globally. However, in the present study, we have found it possible to resolve lower mantle features up to degree and order 6 in spherical harmonics. This is achieved by making use of a very large data set compiled by ISC (International Seismological Centre), careful selection of data, and by formulating the inverse problem directly in terms of expansion coefficient of spherical harmonics.

The combination of the results obtained using these two very different data sets and techniques allows us, for the first time, to map in three dimensions the structure of the entire mantle.

Methods

Lateral variations both in the upper and lower mantle will be described by a spherical harmonic expansion with coefficients varying as polynomials in radius:

$$\delta m(r,\theta,\phi) = \sum_{k=0}^{K} \sum_{\ell=0}^{L} \sum_{m=-\ell}^{\ell} {}_k c_\ell^m f_k(r)\, Y_\ell^m(\theta,\phi) \,. \qquad (1)$$

In the upper mantle observations are powerfully sensitive to shear velocity, v_s; for technical reasons we use $\delta m = \delta v_s^2$ in expanding mantle structure in the interval $r_{670} < r < r_{\text{moho}}$. The functions $f_k(r)$ are Legendre polynomials defined on this interval. In the lower mantle the data are P-wave arrival times and $\delta m = \delta v_p$. The functions

$f_k(r)$ are again Legendre polynomials defined in the interval $r_{CMB} < r < r_{670}$, where CMB stands for the core-mantle boundary.

(a) Upper mantle. The data used in this study for the determination of upper mantle structure consist of seismic waveforms at period greater than 135 s, and the technique we adopt is that of adjusting the global structural parameters in an iterative least squares procedure to best match the observed traces. The records typically are from 4 to 9 hours in duration. The principal seismic phases contained in such data are fundamental mode Rayleigh and Love waves and (to a lesser extent) their first few overtones. Records of this length contain several orbits of these surface wave phases, so that a single record contains information about the entire great circle path defined by a particular source-receiver pair.

The theoretical seismogram corresponding to each data seismogram is calculated by model superposition (Dziewonski *et al.*, 1981), initially for the spherically symmetric reference model (model PREM; Dziewonski and Anderson, 1981), but in subsequent iterations for the adjusted aspherical model. To calculate the theoretical seismograms in an aspherical model we employ an asymptotic approximation to the phase of each mode, which depends upon the path averages of the model along the minor and major arcs of the path. This approximation also makes feasible the calculation of the partial derivatives of each synthetic seismogram with respect to the expansion coefficients of the model; these partial derivative seismograms are needed in the formulation of the inverse problem for structural parameters.

In order to apply this procedure we require a good representation of each earthquake source. The long period radiation of a source is characterized by its moment tensor, and while estimation of moment tensors has become somewhat routine (Dziewonski and Woodhouse, 1983), it is important in this study to minimize the effect of lateral heterogeneity on the moment tensor estimates. For this purpose we iteratively adjust average earth structure for each path, independently of other paths, and repeatedly determine the source parameters. At this stage both the 'mantle wave' data described above ($f < 1/135$ Hz) and long period body wave data ($f < 1/45$ Hz) are used, and the structure for each path is found by using simultaneously the body wave and mantle wave data for all available components (vertical, N-S, E-W).

The events used in this study were chosen to achieve good global coverage. Dividing the globe into $10° \times 10°$ cells, we have selected at least one, and often two, earthquakes in each cell for which a sufficiently large event was available. We are limited to earthquakes which have occurred in recent years since an adequate digital data set has been available

only since 1977. A total of 53 events was selected, ranging in moment from 4×10^{18} Nm to 3.6×10^{21} Nm. Data from the IDA and GDSN digital networks yielded some 2,000 mantle wave seismograms corresponding to 870 paths.

Using this data set we have found it possible to resolve the distribution of shear wave velocity up to degree and order 8 in spherical harmonics, with coefficients described by cubic polynomials in radius. Thus in Equation (1) $L = 8$, $K = 3$; the model is described by 324 parameters ${}_k c_l^m$.

Using the procedure outlined here, we have constructed two upper mantle models, M84A and M84C. The parameters of these models and a more complete description of the method are given in Woodhouse and Dziewonski (1984). For model M84A no *a priori* information was incorporated, and for model M84C a simple model of the distribution of continental and oceanic crust was specified. The effect of the crustal structure is significant but the two models do not differ greatly in qualitative terms. While the model M84A (without crustal correction) provides a valuable test of our ability to resolve known, large scale features near the surface—such as shields and mid-oceanic ridges—we regard the model M84C (with crustal correction) as the better representation of heterogeneity in the upper mantle, and only this model will be discussed here.

The introduction of corrections for laterally heterogeneous structure helps to achieve significantly better match between the observed and synthetic seismograms. An example is shown in Fig. 1; these records were not used in the derivation of the model.

(b) Lower mantle. The 'time term' approach to the analysis of travel times of seismic waves (Willmore and Bancroft, 1960) has been first used in the analysis of teleseismic ($\Delta \geq 25°$) data by Cleary and Hales (1966). A travel time anomaly, δt_{ij}, observed for the i-th station and j-th earthquake is assumed to be the sum of the source term, b_j, receiver term, d_i, and the effect of the anomaly associated with the structure of the medium, a_{ij}:

$$\delta t_{ij} = a_{ij} + b_j + d_i + \epsilon_{ij} ; \qquad (2)$$

where ϵ_{ij} is the error term. The methods of treating such observational equations in analyses involving several thousands of sources and nearly 1,000 stations have been discussed recently by Dziewonski and Anderson (1983). Here we assume that the receiver term absorbs the effect of anomalous upper mantle structure, and the source term is removed

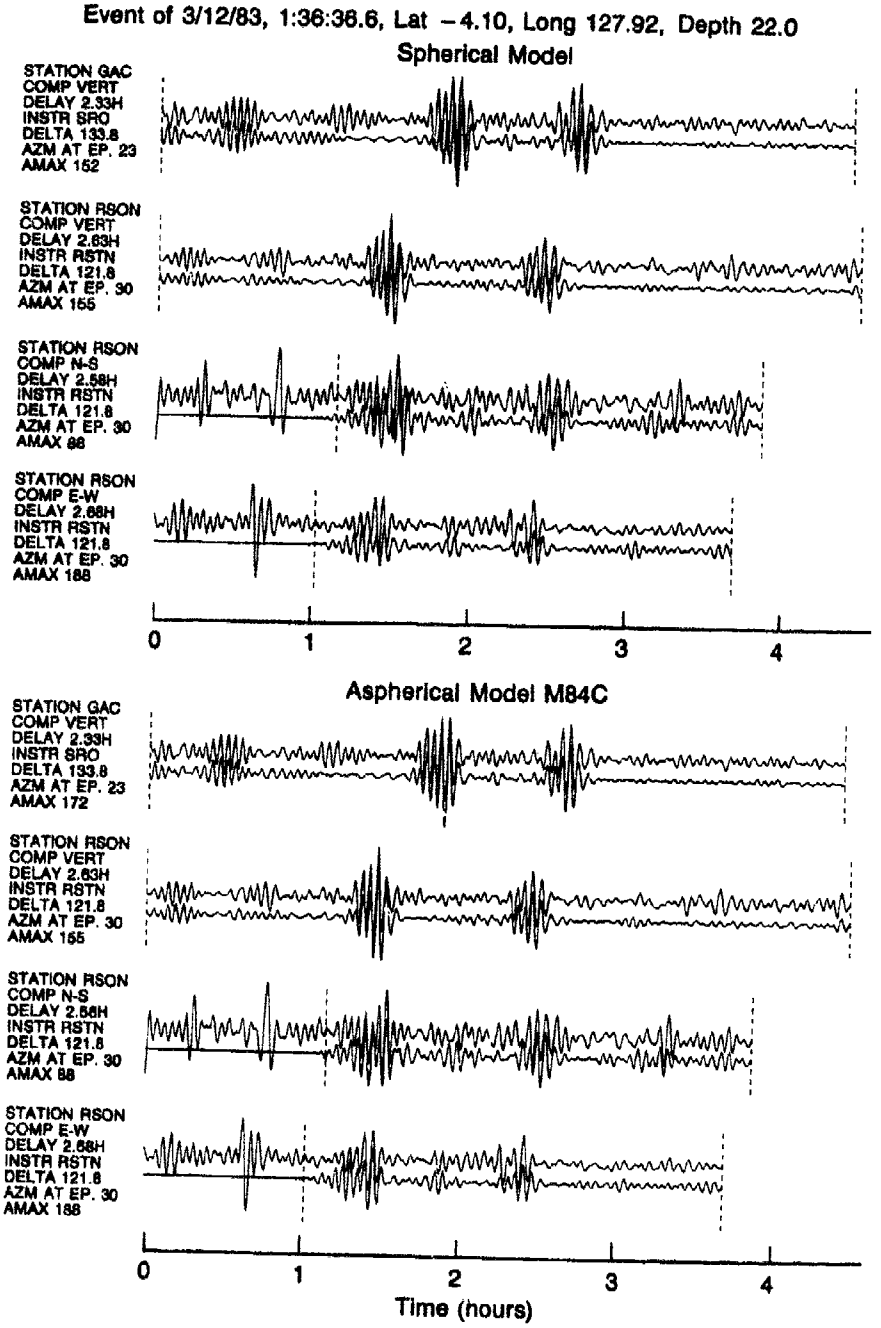

Fig. 1. Event of 3/12/83, 1:36:36.6, Lat −4.10, Long 127.92, Depth 22.0.

by spatio-temporal relocation of the event. The medium term a_{ij} depends on the laterally heterogeneous structure of the lower mantle:

$$a_{ij} = \int_{\mathbf{x}_j}^{\mathbf{x}_i} G(\xi) \cdot \delta v(\mathbf{x})\, d\xi\ ; \tag{3}$$

where ξ is the running arc distance, G is the differential kernel for the spherically symmetric reference model, and $\mathbf{x}(\mathbf{x}_i, \mathbf{x}_j, \xi)$ is the coordinate of the points along the ray path. Substituting our form of the velocity expansion, we have

$$a_{ij} = \sum_{k,\ell,m} {}_kc_\ell^m \int_{\mathbf{x}_j}^{\mathbf{x}_i} G(\xi)\, f_k(\xi)\, Y_\ell^m(\mathbf{x})\, d\xi\ . \tag{4}$$

The integral above can be evaluated numerically, and the equation of condition for δt_{ij} is now defined as a linear combination of the source and receiver terms as well as the coefficients ${}_kc_\ell^m$. The appropriate system of normal equation is solved using iterative methods; for details see Dziewonski (1984).

The ISC Bulletins for the years 1964-1979 list arrival times of body wave phases for over 100,000 earthquakes. The data on the *P*-wave arrivals are the most numerous and accurate: there are some 3 million readings contributed by over 1,000 globally distributed stations. The ISC data have been used recently by Dziewonski and Anderson (1983) to derive improved travel times for the *P*-waves and to determine the station correction terms. Several years ago, Dziewonski *et al.* (1977) used the data of 1964-1970 in the initial attempt to recover large scale velocity anomalies in the lower mantle.

Most of the earthquakes listed by ISC have inadequate station coverage in distance and azimuth to constrain well the source location: only 8,000 events passed our selection criteria. The distribution of events is uneven: using a 5° × 5° cell as a unit of geographical coverage, 75 percent of the cells are empty while the highest count for a single cell is nearly 500 or, roughly, 6 percent of all selected events (Fig. 2). Distribution of the receivers is also nonuniform, with a large concentration of stations in Europe and North America. To prevent aliasing by this uneven distribution of stations and receivers, we have established a weighting scheme in which contribution from each non-empty source-receiver pair of cells is treated with equal weight, regardless of the actual number of observations.

The dimensions of areas with no sources or receivers impose limits on the maximum angular, L, and radial, N, order number of the solution. Experiments indicate that beyond $L = 6$ and $N = 4$ the solutions are unstable; Dziewonski (1984) tabulates the coefficients ${}_k c_\ell^m$ for several models.

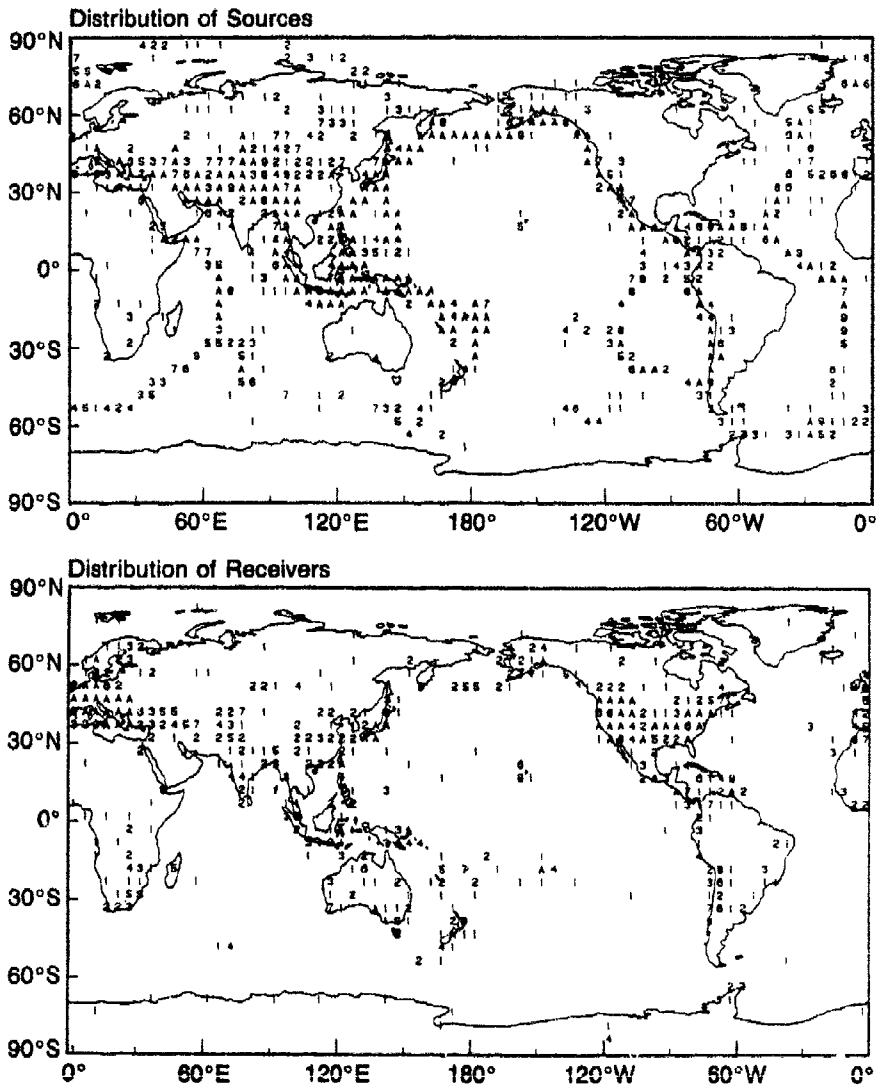

Fig. 2. Geometry of the experiment.

Maps of the Earth Interior

Representation of velocity anomalies by Eq. (1) allows us to calculate the perturbations at any point within the mantle. We shall show here several maps of the anomalies at fixed depth and cross-sections through the mantle along selected great circles.

Figure 3 shows anomalies in shear velocity at depths of 150 km and 550 km; shaded regions indicate positive deviations. At shallow depths well known tectonic features are apparent. All major shield areas—Baltic-Siberian, Canadian, Australian, South African, Brazilian and Antarctic—show high velocity anomalies. Low velocity regions follow the ocean ridges and subduction zones of the West Pacific. Old ocean basins show positive anomalies. It is important to bear in mind that this pattern emerges purely from the seismic data without any prior assumptions with regard to surface tectonics. The introduction of the crustal correction only accentuates the overall difference between continents and oceans, but does not change the pattern conceptually.

Features which would not have been predicted on the basis of surface observations include a velocity low off the west coast of North America, a bridge of high velocities connecting South Africa with Antarctica and relatively high velocities near the equator on the mid-Atlantic ridge.

The close correlation with the known surface features begins to diminish below 200 km. At 250 km many portions of ridges are underlain by high velocities; notable in this respect is the South East Indian Rise south of Australia. The back-arc regions of the west Pacific are fast at this depth. At 300-400 km ridges disappear, except for those of the southern Pacific, and the low velocity anomalies tend to localize in the neighborhood of major hotspots: Red Sea, Kerguelen, Hawaii, Iceland, Tristan da Cunha, together with a low velocity anomaly centered on New Zealand. One of the few linear features remaining at this depth is approximately aligned with the Emperor seamount chain of the north Pacific.

The map at 550 km depth (Fig. 3b) shows little or no resemblance to surface features, and is dominated instead by two large plateaus of high velocity—one encompassing South America, much of the south and central Atlantic and parts of west Africa, and the other extending from 50° N to 65° S in the west Pacific. The entire Pacific basin east of the 180° meridian, together with North America, is a region of low velocities, as is the Eurasian continent. The Red Sea remains a strong localized anomaly slightly shifted to the northeast. At this depth there is a strong degree 2 component, consistent with the transition zone model of Masters *et al.* (1982).

Figure 4 shows two maps of the lower mantle P-wave velocity anomalies. These maps are synthesized using expansion up to degree 6 in spherical harmonics rather than degree 8 used for the upper mantle. Figure 4a is for 1000 km depth. The maximum level of anomalies

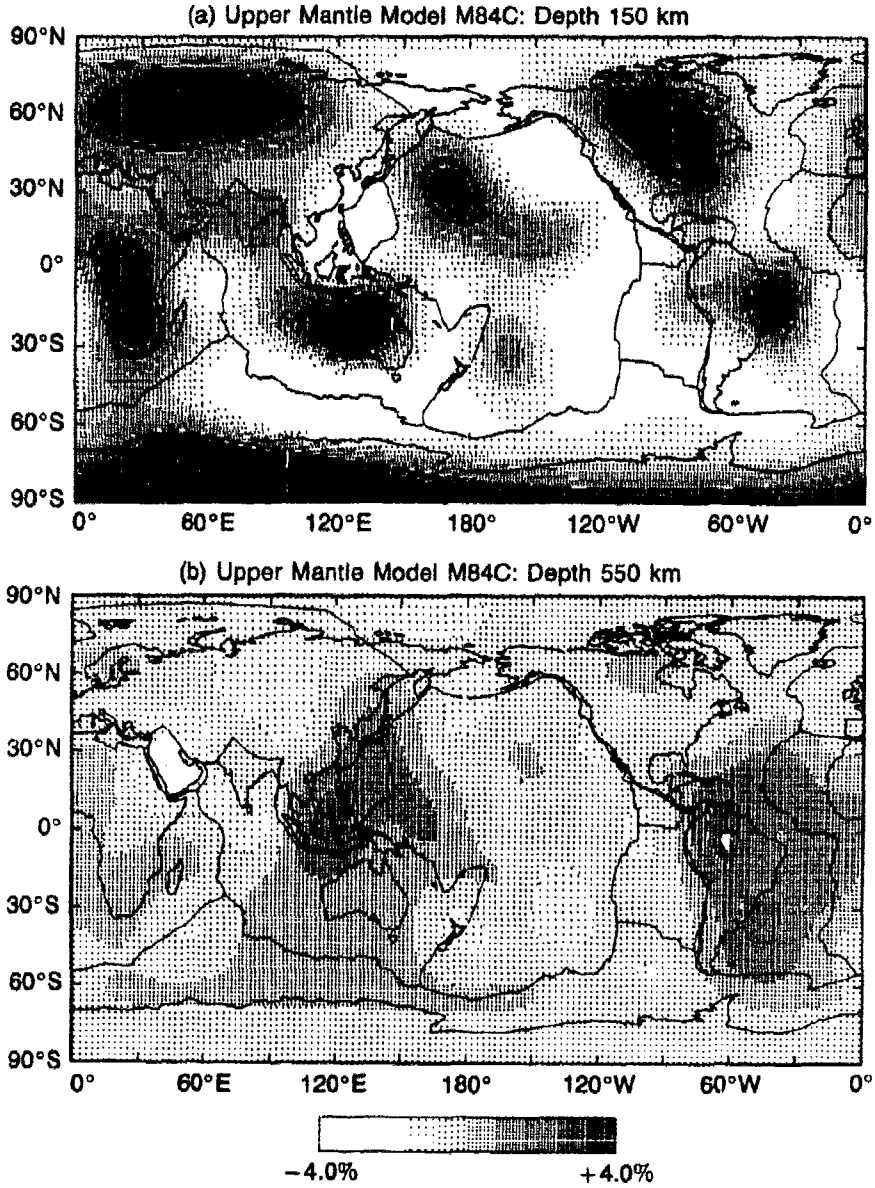

Fig. 3. Upper mantle model M84C. (a) Depth 150 km. (b) Depth 550 km.

exceeds only slightly 0.5 percent, significantly less than variations found for the upper mantle. One of the prominent features is a low velocity region south of Hawaii; there is also a high velocity zone near the southern tip of Africa. There seems to be very little correlation between the pattern for deeper regions of the upper mantle and the structure near the

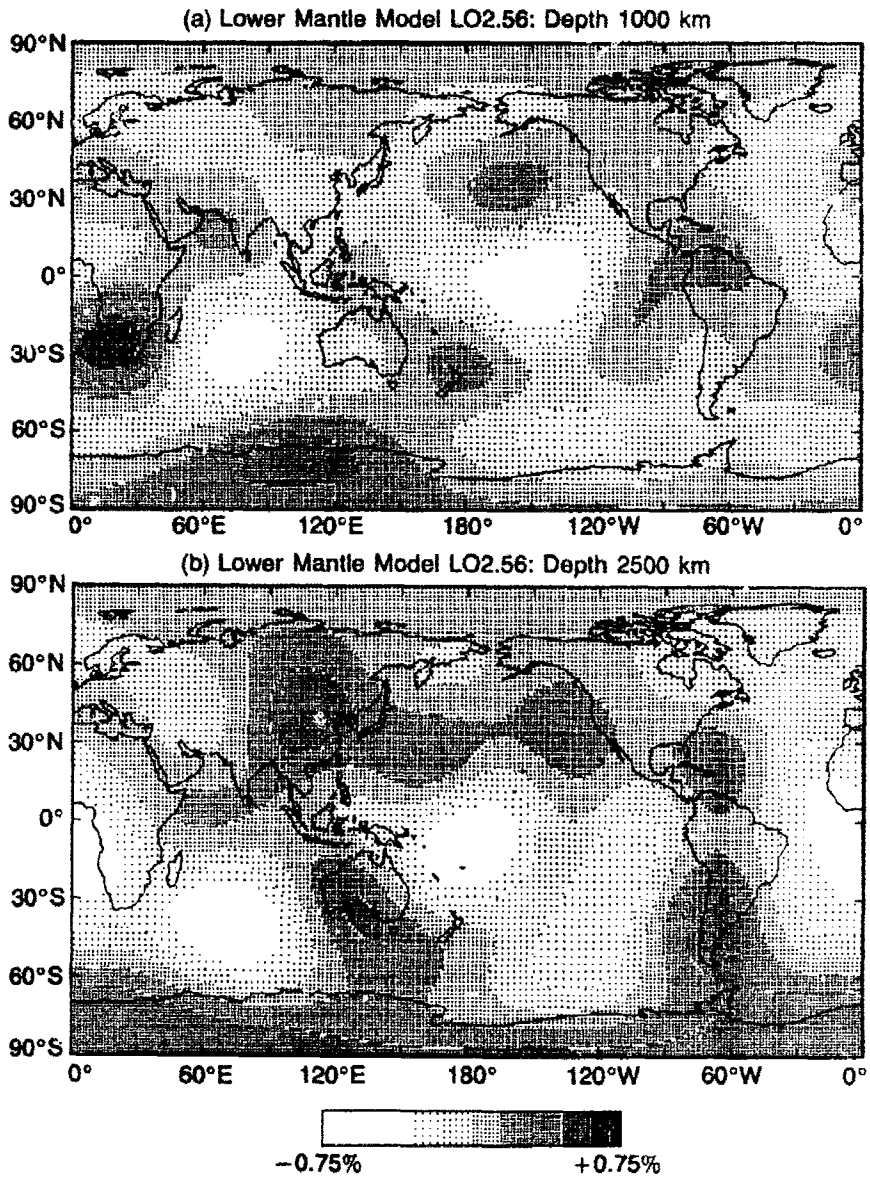

Fig. 4. Lower mantle model LO2.56. (a) Depth 1000 km. (b) Depth 2500 km.

top of the lower mantle. We shall show later, however, that there are a number of upper mantle features that continue obliquely into the lower mantle.

The most striking feature of the map at 2500 km depth is a ring of high velocities circumscribing the entire Pacific basin. Bottoming points of rays at this depth must be at least 40° away from the source region and, therefore, we do not expect this to be an artifact of the high velocity anomalies associated with subduction zones. The interior of the Pacific basin is slow and this is consistent with the pattern in the upper mantle.

The overall level of heterogeneity is high just below the 670 km discontinuity and just above the core-mantle boundary with variations being minimum at 2000 km depth. While one must consider the possibility that the structure at 670 km is poorly resolved, the high level of perturbations near the core-mantle boundary is well documented by the increase in the size of travel time anomalies in the distance range from 80° to 100° (see Fig. 10 in Dziewonski, 1984).

Figure 5 shows four cross-sections through the entire mantle. The center line in the accompanying map is the complete great circle along which the section is taken. The upper mantle (depth 25-670 km; vertical exaggeration 8:1) shows relative *S*-velocity perturbations, and the lower mantle (depth 670-2891 km; vertical exaggeration 4:1) shows relative *P*-velocity perturbations. Since resolution of both methods is poorest near the 670 km discontinuity, the details in this region should be regarded with caution.

Figure 5a is a section along the equator. Among the features of interest in this figure are the downward extensions of high velocity anomalies associated with the Brazilian shield and central Africa; these merge below 400 km, to form the broad plateau of high velocities noted in relation to Fig. 3b. The mid Atlantic ridge separates the two anomalies near the surface. The shallow dip of the African 'root' could possibly indicate shear deformation across the upper mantle. This structure appears to continue into the lower mantle at a somewhat steeper angle. Low velocities associated with the Carlsberg ridge extend throughout the upper mantle and into the uppermost portion of the lower mantle, merging with other low velocity anomalies, which continue obliquely to the core-mantle boundary. The back arc regions in the neighborhood of Borneo have low velocities at depths less than 200 km, underlain by a high velocity zone which may be associated with subduction in that region. This anomaly also appears to continue, at an oblique angle, through the 670 km discontinuity. Both upper and lower parts of the mantle show low velocities across the Pacific basin.

The central part of Fig. 5b shows a cross-section across the Pacific,

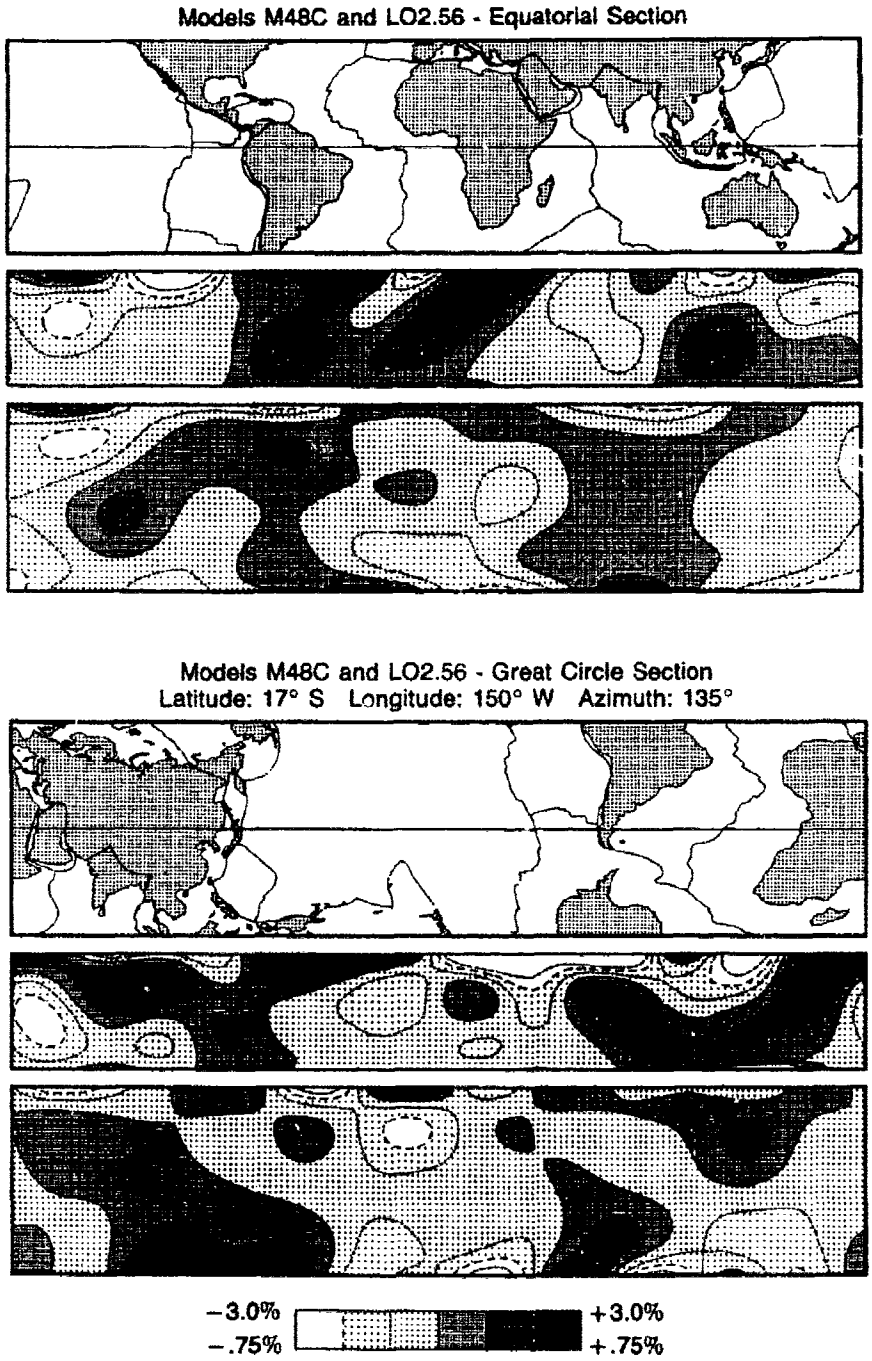

Fig. 5. Models M84C and LO2.56—equatorial and great circle sections.

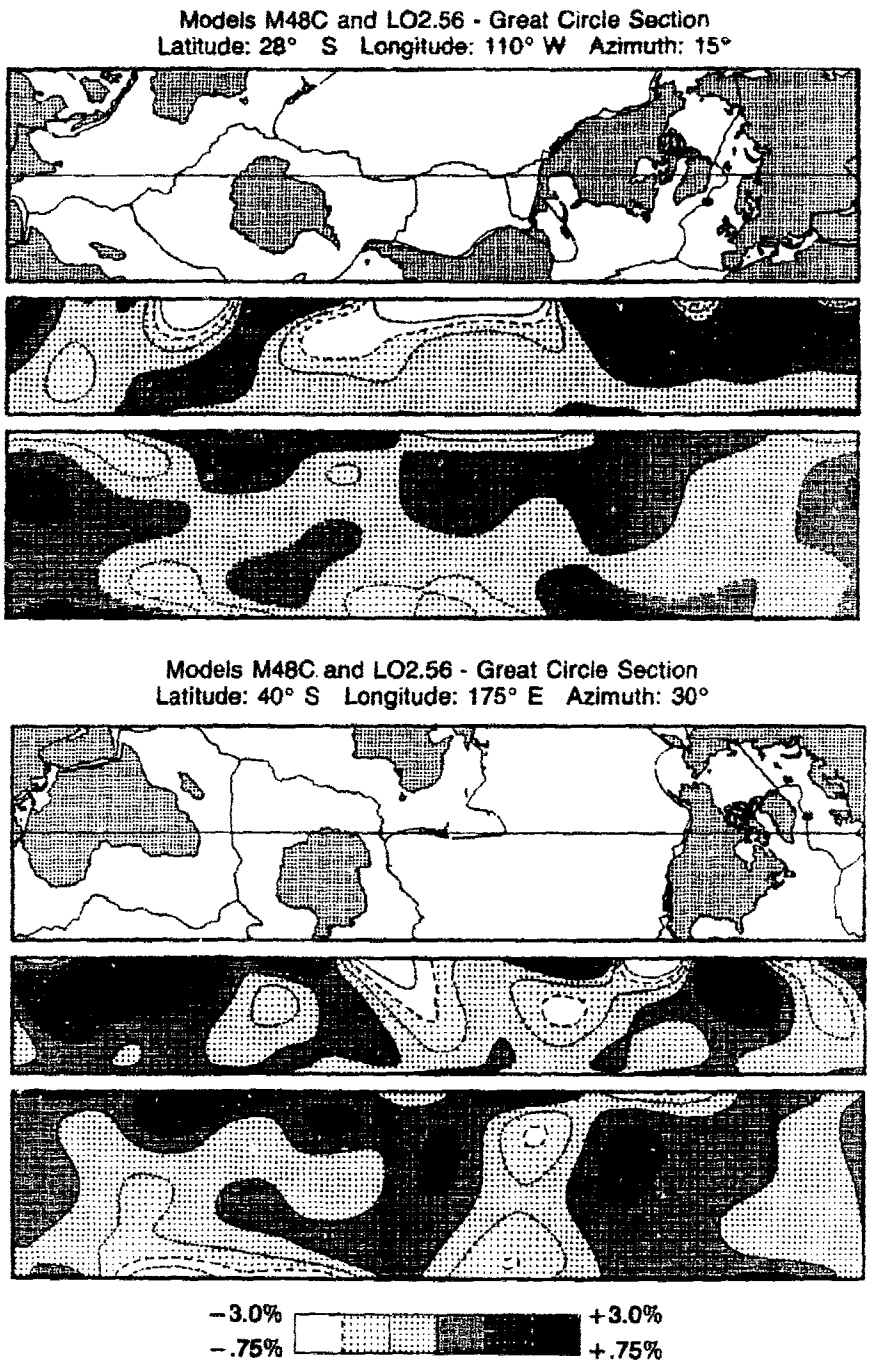

Fig. 5. (Continued.)

roughly parallel to the spreading direction. Lithospheric velocities (depth < 150 km) increase with age, as has been inferred from shorter period surface wave studies (this behavior could also be modelled by thickening of the lithosphere; Leeds *et al.*, 1973). At the edge of the Eurasian continent fast material occurs at depth, as may be expected from subduction, merging with the high velocity 'root' of Eurasia. It is of interest to note that the high velocities associated with subduction in Japan appear to continue into the lower mantle (Jordan, 1977; Creager and Jordan, 1983); one of the largest positive anomalies at the core-mantle boundary is also directly beneath this region. This cross-section cuts, at a different angle, the Atlantic anomaly in the lowermost upper mantle, and also shows the convergence at depth of the anomalies associated with South American and Africa. The pronounced low velocity anomaly beneath the Red Sea can be seen on the left, and also appears to continue into the lower mantle.

Figure 5c is centered on the ridges of the eastern and southern Pacific, and illustrates well the variability of the depth extent of the low velocity anomalies associated with ridges. The North American and Eurasian roots appear to persist to about 400 km depth, and are separated only near the surface by the spreading center. Low velocities behind the Himalayan front may be symptomatic of the Indian-Eurasian collision.

Figure 5d intersects the low velocity anomaly south of Hawaii, and shows it to be continuous with a feature which extends to the core-mantle boundary. The Tonga-Kermadec subduction zone is exceptional in that it does not express itself as a high velocity region in the lowermost upper mantle, but is underlain by a column of high velocities in the lower mantle. The African 'root' extends to great depths in the north, in contrast to North America, which appears in this section as a comparatively shallow anomaly.

Discussion

The studies reported here have produced the first three dimensional representation of the structure of the Earth's mantle. It is to be expected that further improvements in resolution and accuracy will follow, though this is, to a large extent, dependent on the improvements and expansion of the global digital network. We anticipate that the interpretations we have placed upon the observed patterns will be added to by future studies; our aim has been to present the observations, rather than to draw all of the possible conclusions. The following general conclusions may, however, be made.

The hypothesis of continental roots, extending deeper than the lithosphere (Jordan, 1975, 1978) appears to be largely confirmed by our

results. Typical depths of roots are of order 400 km, though Africa extends to greater depths.

Ridges are very variable in their depth extent, many terminating above a depth of 200 km, but other, particularly those of the south Pacific, extending to depths as great as 400 km.

At 350-450 km depth some hotspots represent well-defined negative anomalies. Otherwise, at depths greater than 400 km we find no apparent correlation with surface tectonic features. The transition zone is dominated by a degree 2 pattern, and the range of perturbations is of order ± 2.5%; this is comparable to the velocity contrast across the 400 km discontinuity, and should be taken into account when considering the global properties of this boundary.

Soon after the publication of the results of Masters *et al.* it was suggested that their strong degree 2 pattern for Rayleigh waves was not in conflict with a regionalized earth model. Our results indicate that regionalization would be justified for the upper 200 km, but that the nature of the transition zone is quite unrelated to surface tectonics, and our model of that region is rather similar to that of Masters *et al.*, except for some added detail.

While the distribution of velocities in the lower mantle bears no relation to surface tectonics, a number of upper mantle features appear to extend continuously into the lower mantle: *e.g.* the low velocity column south of Hawaii (Fig. 5d) which extends form the core-mantle boundary to a depth of 100 km.

One of the most regular features of the lower mantle model is a ring of high velocities around the Pacific, which can be traced from a depth of 1500 km to the core-mantle boundary. The level of perturbations increases significantly near the core-mantle boundary and the rms level of perturbations there is 3 to 4 times greater than at 2000 km.

Under the assumption that density perturbations are proportional to velocity perturbations it is possible to investigate the correlation of the velocity models with the geoid. The calculation is particularly simple if one treats the earth as a rigid body. In this case we find like Masters *et al.* (1982) that the velocity anomalies in the transition zone are strongly correlated with the geoid for degree 2. For degrees 4-7 we find a systematically negative correlation, in agreement with recent results of Nakanishi and Anderson (1983) who have correlated the geoid with the local phase velocities of Rayleigh waves. For the lower mantle strong negative correlation is found for degrees 2 and 3.

The earth is not, however, a rigid body, and the true geoid predictions of these models depend upon the response to internal loading of a viscous earth. Richards and Hager (1984) have developed a theoretical

framework for this calculation, and its application to models such as those described here, should follow soon.

Some improvements in the resolution of heterogeneous structures could be achieved by the use of currently available body wave data. However, because the distribution of major seismogenic zones is fixed, major progress will require a substantial increase in the number of high quality digital stations. We would hope that the current initiative of the seismological community, in the United States (IRIS) and abroad, to develop a global network of 100 very-broad-band stations will be strongly supported.

References

Agnew, D., J. Berger, R. Buland, W. Farrell and F. Gilbert, "International Deployment of Accelerometers: A Network of Very-Long-Period Seismology," *Trans. Am. Geophys. Un.*, **57**, 180-188, 1976.

Brune, J. and J. Dorman, "Seismic Waves and Earth Structure in the Canadian Shield," *Bull. Seismol. Soc. Am.*, **53**, 167-210, 1963.

Cleary, J. and A. L. Hales, "An Analysis of the Travel Times of *P* Waves to North American Stations in the Distance Range 30° to 100°," *Bull. Seismol. Soc. Am.*, **56**, 467-489, 1966.

Creager, K.C. and T.H. Jordan, "Slab Penetration into the Lower Mantle," *J. Geophys. Res.*, **89**, 3031-3049, 1984.

Dziewonski, A.M., "Mapping the Lower Mantle: Determination of Lateral Heterogeneity in *P* Velocity Up to Degree an Order 6," *J. Geophys. Res.*, **89**, 5929-5952, 1984.

Dziewonski A.M. and D.L. Anderson, "Preliminary Reference Earth Model (PREM)," *Phys. Earth Planet. Inter.*, **25**, 297-356. 1981.

Dziewonski, A.M. and D.L. Anderson, "Travel Times and Station Corrections for *P* Waves at Teleseismic Distances," *J. Geophys. Res.*, **88**, 3295-3314, 1983.

Dziewonski, A.M. and J.H. Woodhouse, "An Experiment in Systematic Study of Global Seismicity: Centroid-Moment Tensor Solutions for 201 Moderate and Large Earthquakes of 1981," *J. Geophys. Res.*, **88**, 3247-3271, 1983.

Dziewonski, A.M., B.H. Hager and R.J. O'Connell, "Large-Scale Heterogeneities in the Lower Mantle," *J. Geophys. Res.*, **82**, 239-255, 1977.

Dziewonski, A.M., T.-A. Chou and J.H. Woodhouse, "Determination of Earthquake Source Parameters from Waveform Data for Studies of Global and Regional Seismicity," *J. Geophys. Res.*, **86**, 2825-2852, 1981.

Forsyth, D.W., "A New Method for the Analysis of Multi-Mode Surface Wave Dispersion: Application to Love-Wave Propagation in the East Pacific," *Bull. Seismol. Soc. Am.*, **65**, 323-342, 1975.

Jordan, T.H., "Lithospheric Slab Penetration into the Lower Mantle Beneath the Sea of Okhotsk," *J. Geophys. Res.*, **43**, 473-496, 1977.

Jordan, T.H., "Composition and Development of the Continental Tectosphere," *Nature*, **274**, 544-548, 1978.

Jordan, T.H., "The Continental Tectosphere." *Rev. Geophys. Space Phys.*, **13**, 1-12, 1975.

Leeds, A.R., "Lithospheric Thickness in the Western Pacific," *Phys. Earth Planet. Inter.*, **11**, 61-64, 1975.

Leeds, A.R., L. Knopoff and E.G. Kausel, "Variations of Upper Mantle Structure Under the Pacific Ocean," *Science*, **186**, 141-143, 1974.

Masters, G., T.H. Jordan, P.G. Silver and F. Gilbert, "Aspherical Earth Structure from Fundamental Spheroidal-Mode Data," *Nature*, **298**, 609-613, 1982.

Nakanishi, I. and D.L. Anderson, "Worldwide Distribution of Group Velocity of Mantle Rayleigh Waves as Determined by Spherical Harmonic Inversion," *Bull. Seismol. Soc. Am.*, **72**, 1185-1194, 1982.

Nakanishi, I. and D.L. Anderson, "Measurements of Mantle Wave Velocities and Inversion for Lateral Heterogeneity and Anisotropy, 1, Analysis of Great Circle Phase Velocities," *J. Geophys. Res.*, **88**, 10267-10283, 1983.

Peterson, J., H.M. Butler, L.G. Holcomb and C.R. Hutt, "The Seismic Research Observatory," *Bull. Seismol. Soc. Am.*, **66**, 2049-2068, 1976.

Richards, M.A. and B.H. Hager, Geoid Anomalies in Dynamic Earth," *J. Geophys. Res.*, **89**, 5987-6002, 1984.

Sengupta, M.K. and M.N. Toksöz, "Three-Dimensional Model of Seismic Velocity Variation in the Earth's Mantle," *Geophys. Res. Lett.*, **3**, 84-86, 1976.

Toksöz, M.N. and D.L. Anderson, "Phase Velocities of Long-Period Surface Waves and Structure of the Upper Mantle, 1, Great Circle Love and Rayleigh Wave Data," *J. Geophys. Res.*, **71**, 1649-1658, 1966.

Willmore, P.L. and A.M. Bancroft, "The Time Term Approach to Refraction Seismology," *Geophys. J. R. Astro. Soc.*, **3**, 419-432, 1960.

Woodhouse, J.H. and A.M. Dziewonski, "Mapping the Upper Mantle: Three-Dimensional Modeling of Earth Structure by Inversion of Seismic Waveforms," *J. Geophys. Res.*, **89**, 5953-5986, 1984.

Sensors, Systems and Arrays: Seismic Instrumentation under VELA-Uniform

W.E. Farrell

1. Historical Overview

The VELA-Uniform program was inaugurated a quarter of a century ago to improve the seismic detection and identification of underground nuclear explosions. It has been a major sponsor of seismic research ever since. A key element in the program has been the development of improved seismic instruments and seismic systems. It was realized at the very inception that major advances could be expected to accrue from work in these areas, and instrumentation, signal processing and data management figured prominently in the Berkner report (Berkner, 1958) which formed the basis of VELA-Uniform. A dramatic visualization of the progress fostered by VELA-Uniform is seen by comparing photographs of a vintage 1960 WWSSN seismic observatory (Fig. 8) and a mid 1970's SRO seismic observatory (Figs. 6 and 7). Today we have moved even further, for the RSTN seismic system runs unattended and transmits data globally *via* real-time satellite telemetry.

The developments in instrumentation have been a response to two somewhat overlapping requirements for seismic identification of underground explosions. The first of these has been to understand the excitation and propagation of elastic waves in the earth. The response to this requirement has been the development of a succession of seismometer systems and the programs (LRSM, SDCS, SRO) for their deployment. The second general requirement might be called the monitoring requirement. Among the instrument systems sponsored to meet this requirement would be included the small (5 km aperture) Geneva-type arrays, the large (LASA, NORSAR) arrays, the ocean bottom seismology effort and the deep-well effort. To simplify even further, the objective of this latter work has been to eliminate noise, whereas the objective of the first has been to model signal.

The scale of effort required to build and operate the seismic systems, with respect to both data collection and data storage, has been so large

that from the beginning, industry has played a much larger role than academe in the instrumentation side of VELA-Uniform. Among the industries, Geotech (a division of Teledyne since 1965) stands first today, just as it did in the pre-VELA 1950's under its former names Beers and Heroy and the Geotechnical Corporation. Sensors, recording systems and field operations have always been the forte of Geotech.

During the first one and one-half decades of VELA-Uniform there were several other organizations which made important contributions. Notable among these are Texas Instruments, United Electro Dynamics (purchased by Teledyne in 1964, renamed Earth Sciences Division in 1965, and merged into the Geotech Division to form the Alexandria, Virginia, operation in 1968), and MIT Lincoln Laboratory. Texas Instruments, (represented, along with the Geotechnical Corporation, on the Berkner panel), played a major role in underwater seismology and real-time seismic array processing. They also installed the first two of the LASA sub-arrays, and participated in the operation of the Geneva arrays. United Electro Dynamics, in its various guises, has operated the seismic data centers, both for the fixed Geneva array data and the movable LRSM/SDCS array data. The MIT Lincoln Laboratories contribution to the VELA-Uniform instrumentation program was the design of the LASA telemetry and data-processing system.

The universities played a subordinate but valuable role in VELA-Uniform instrumentation. Columbia University's HGLP global seismic array still partially functions as the ASRO (Abbreviated Seismic Research Observatory) stations of the Global Digital Seismic Network (GDSN), run by the United States Geological Survey. Both Columbia and the Scripps Institution of Oceanography participated in ocean-bottom seismology, and Columbia operated a deep sea observatory off Cape Mendicino for several years. At the University of California, Berkeley, VELA-Uniform supported the establishment of several generations of moderate aperture seismic arrays, which utilized radio telemetry and portable recorders for data acquistion. These arrays were used to study earthquakes in California, and explosions at the Nevada Test Site (NTS). At Caltech, Benioff led numerous instrumentation projects including strain-pendulum combination seismographs, tiltmeters and "rotational" seismometers, and the group was an early practitioner of direct digital recording.

Many novel ideas for seismic sensors were developed and tested for VELA-Uniform, but most of the unconventional approaches have proved futile. Today, as in the past, vertical earth-motion is best sensed with a mass-spring transducer, and horizontal earth-motion is best sensed with a swinging boom transducer. Enormous progress in seismic systems

has taken place, however, even if the physics of the sensors is unchanged. Transducers are lighter (by more than an order of magnitude), smaller, more rugged, and better isolated from environmental disturbance. Electronic design is nowadays as important as mechanical design, and telemetry and data recording are vastly more sophisticated, as a consequence of the micro-electronics revolution.

The VELA Seismic Information Analysis Center (VESIAC) was established at the University of Michigan to collect and disseminate the findings of VELA-sponsored research. The coverage of this research by VESAIC is complete for the period, slightly longer than a decade, during which the center was in operation. The center was closed in 1971.

VESAIC organized and reported on topical meetings (*e.g.* VESIAC 1962a, 1964a, 1964b), prepared special review reports (*e.g.* VESAIC, 1962b, Carder, 1963), and maintained a complete bibliography. The final revision of the bibliography of articles published in the journal literature is given in VESIAC, 1971b. The entire bibliography, including unpublished contractor reports, was issued in two volumes. VESAIC, 1965 contains approximately 2000 abstracts of reports and articles. The bibliography for the second half of the period monitored by VESAIC is presented in VESAIC, 1971a. The final report for the entire VESAIC project is given in VESAIC, 1971c.

The heyday of the VELA-Uniform instrumentation program lasted from 1959 to 1975, the date when the last of the Geneva arrays (TFO) was closed, and the first SRO system was installed at the Albuquerque Seismological Laboratory of the United States Geological Survey. By this year the deep-hole research had terminated, all the Geneva arrays had been abandoned and the earth-strain and ocean-bottom seismology programs were greatly curtailed. Three years later LASA also ceased operations.

2. Seismic Sensors

The expression seismic sensor is used here to connote the mechanical or electromechanical assembly which converts earth-motion into a voltage. Sensors are distinguished from systems, in that the latter consist of multiple combinations of the former (*e.g.*, strain-inertial combinations) or consist of sensors coupled to recording apparatus. This division is somewhat artificial, but helps to organize the material.

Melton (1981a, 1981b) has given a more extensive history of recent seismograph developments. His comprehensive review article (Melton, 1976) describes the theoretical principles that have guided seismograph design. The current state-of-the-art has been described by Herrin (1982).

The usual division of sensors into long-period sensors and short-period sensors has been retained, but this concept, to the extent it alludes to the free period of a second order mechanical system, is now quite obsolete. The separation of seismic motion into surface waves and body waves, the nature of seismic noise, and technical limitations all dictated that, in the past, instruments of long free period were utilized to measure surface waves and instruments of short free period were utilized to measure body waves. The widespread application of force feedback has changed this. Designers today favor broadband (from near zero frequency to, perhaps, 20 Hz) feedback instrument for most applications, but the mechanical sensor can have either a short free period or a long free period. Sensors with short free period are especially advantageous for borehole systems because of their compactness.

2.1. Short-period sensors. The VELA-Uniform era opened with the massive Benioff instrument as the premier short-period seismometer. This was perhaps the last of the earth-powered seismometers. With its great inertial mass (100 kg), the Benioff was designed to be connected to a galvanometer for direct photographic recording. There was both a vertical and a horizontal instrument and the horizontal sensor had a somewhat more symmetrical arrangement of the parts than the vertical. First developed at Caltech, the Benioff design with its distinctive triangular case had been transformed into a mass-producible instrument by the Geotechnical Corporation in the late 1950's, in response to the needs of the seismic monitoring program. Each sensor weighed over 200 kg, and a hoist was required to place them in position. The Benioff instrument was the natural choice for the short-period sensors of the WWSSN network, the first major seismological project sponsored by VELA-Uniform. It continued to be used in most of the mobile LRSM observatories during the 1960's.

When connected to a phototube amplifier, the big Benioff could resolve earth motions as small as 0.1 nm at a frequency of 1 Hz, (Gudzin and Hamilton, 1961). This level is less than earth noise at this period, even at a quiet site.

Under the *aegis* of the LRSM program Geotech initiated work on short-period sensor technology to meet two main requirements: a more transportable sensor for field use, and a borehole sensor to support research in deep-hole seismology. By 1961 Geotech had developed the "portable" Benioff seismometers, models 6102 (horizontal) and 4681 (vertical). Gradually, over the next decade, these replaced the original "big" Benioff seismometers, models 1101 and 1051, respectively. The lighter sensors were much appreciated by the field crews, but they were still massive devices and awkward to install.

The next advance in short-period sensor technology was the Geotech 18300 moving-coil seismometer. Although not the fruit of VELA-Uniform research, it saw widespread use within the program from 1965 onwards. The same basic instrument was found in the Geneva arrays, the deep hole instrument systems and the portable seismic observatories. Like the Ranger seismometer of the same era, one sensor, with a minor mechanical adjustment, could function as either a vertical or horizontal seismometer. The entire instrument (5 kg inertial mass) weighs just over 15 kg, and is contained within a sealed case so that it may be buried directly in the earth. This sensor, known as the model S-13, is still manufactured today.

With the portable Benioff and the model 18300 proving satisfactory, sponsored research on traditional short-period sensors effectively ceased before 1970. By this date the triaxial seismometer was available in both short-period (Der, 1969) and long-period (Geotech, 1970b) versions and it could be fitted easily inside a borehole package. Subsequently, the KS36000 borehole system was developed in which force feedback was used in order to broaden the bandwidth of a long period sensor. Thus, advances in electronics, along with a requirement for three-component borehole operation (to reduce earth noise disturbances on the horizontal sensors) lead to other means for recording earth motion in the frequency band between 1 and 10 Hz.

2.2. Long-period sensors. Some of the most dramatic accomplishments of the VELA-Uniform work on seismic instrumentation may be seen in the history of the development of improved sensors for long-period seismic signals. Whereas short-period sensors mostly needed to be reduced in size, there were fundamental problems with long-period seismic systems, primarily associated with mechanical stability, and susceptibility to thermal and atmospheric pressure disturbance. Not only have these problems been largely eliminated, but simultaneously the sensor size has been so shrunken, that the modern Model 44000 will fit inside a 4 inch borehole.

2.2.1. *Early Geotech instruments*. The WWSSN and original LRSM mobile observatories used Sprengnether model 100 (vertical) and 201 (horizontal) long-period seismometers. As with the big Benioff, these sensors were designed for direct coupling to a galvanometer to provide earth-powered recording. The long-period Sprengnethers were relatively fragile, drifted, and tended to corrode in the field. They also were susceptible to thermal and pressure disturbance.

The Geotech model 7505A and 8700C (vertical and horizontal, respectively), instruments were developed to meet the VELA-Uniform requirement for a sensitive and portable long-period seismometer (Geotech,

1966a). The Geotech seismometers could be shipped fully assembled (except for the inertial mass) but they were not much more compact than the Sprengnethers, and with a weight of over 70 kg were clumsy to handle. Improved pressure seals and a massive case reduced the sensitivity of the vertical instrument to pressure fluctuations. Remotely-operated centering and free-period selection permitted adjustment in the field without the necessity of physical access and its concomitant thermal upset. This instrument remained the workhorse of the LRSM and SDCS projects.

For a while there was a need for a lighter and more portable long-period seismometer, and Geotech continued to test new concepts. These culminated in the model 28280 (vertical) / 28700 (horizontal) long period portable seismometers (Geotech, 1969). By the time these sensors were available, however, the LRSM field-measurements program was waning and the attention of the seismic identification program was turning towards borehole systems. Thus, the 28700/28280 sensors saw little field use, and, as happened with the short-period sensors, research into improved sensors of traditional design had effectively ceased by 1970.

2.2.2. *Triaxial sensors.* The triaxial seismometer of Melton represented a radically new approach to the problem of seismometer design. A ten year development program resulted in the testing of at least three sensors embodying this concept, and culminated in their selection for field installation in long period arrays in Alaska (ALPA) and Korea (KSRS). Yet analysts never fully became comfortable with the data from these instruments, and when ALPA was closed in 1970, the seismometers were retired, and the project terminated. The progress of this effort may be found in Hamilton *et al.*, (1961), Hamilton (1964), Kirkpatrick (1968), Simmons (1969), and, best of all, Melton and Kirkpatrick (1970). A brief summary is given in Melton (1981a). Although the triaxial sensor has been abandoned, to judge from photographs, the experience gained from putting this sensor in a borehole package influenced the design of its successor, the KS36000.

The triaxial seismometer was a three-component instrument, in which the sensing elements were all identical. This is in clear contrast to the practice, before and since, in which there is a fundamental asymmetry between the transducer used to sense vertical motion, and the transducer used to sense the two horizontal components of motion. The symmetrical arrangement was achieved by using the well known La Coste "zero-length" suspension system. Unlike a gravity meter, however, for which it is critical that the boom remain horizontal, in the triaxial seismometer the boom is intentionally tilted so that it is oriented at an angle of about 35 degrees above (or below) the horizontal. With three such devices

arranged symmetrically about the vertical, three orthogonal components of earth-motion are detected, but the coordinate system is skewed with respect to the vertical-horizontal system. The conventional up-north-east components of motion are recovered by a simple transformation. This may be accomplished by analog means, in real time, or as a step in the analysis of digital data.

A unique "triflexure" hinge provided control over the free period (Weinstein, 1965), but in the ALPA installation this was supplemented by an electronic period-adjustment, accomplished by a force feedback circuit. In the early devices, Geotech models 11550 and 15560 (Simmons, 1969), the three inertial masses lay in the same horizontal plane. This arrangement gave a diameter too large to permit borehole operation. The final model, Geotech 26310, had the sensors placed one above the other, resulting in a borehole package 10 inches in diameter and 2½ meters long. This package weighed over 400 pounds.

2.2.3. ***HGLP instruments.*** Starting with the work of Pomeroy *et al.*, (1969, but see also Sutton and Oliver, 1959 and Alsop *et al.*, 1961), researchers at Columbia's Lamont-Doherty Geological Observatory developed an improved long-period seismic system. By 1971 (Murphy *et al.*, 1971) a global network of High-Gain Long-Period instruments had been installed at sites in Alaska, Australia, Israel, Spain, and Thailand.

A major impetus behind this work was the collection of better data to assess the $m_b : M_s$ seismic discriminant. A major discovery of the work was the ubiquity of the seismic noise minimum (when measured in displacement units) at a frequency of about .03 Hz (Savino *et al.*, 1972). The technical description of these instruments is given in an anonymous Columbia University report (Lamont-Doherty, 1971). The vertical instrument was a Geotech model S-11 and the two horizontal instruments were Geotech model S-12's. These sensors were the commercial versions of the 7505 and 8700 described previously.

An important feature of the design was the massive hemispherical dome which covered each of the three sensors, and sealed them from barometric pressure changes (see Fig. 1). Three distinct transducers were used to sense the motion of the inertial mass. Two of these were velocity transducers of the moving-coil, fixed-magnet type, that were standard features of the Geotech instrument. In addition, a displacement sensor, using capacitor plates and a voltage-controlled oscillator, was added. One of the velocity pickoffs was coupled through a 100 second galvanometer to a phototube amplifier, the output of which was recorded on photographic film. This channel was called the "high-gain" channel. The second velocity pickoff drove another 100 second galvanometer which wrote on film directly. This was called the "low-gain" channel. The

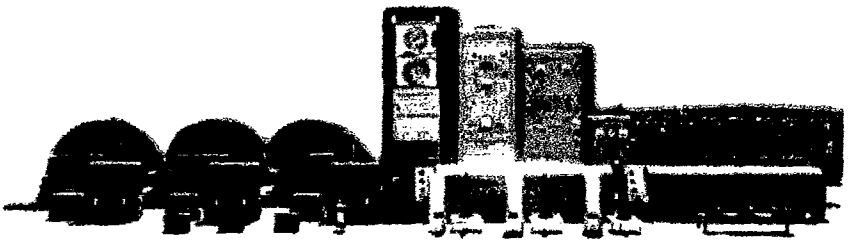

Fig. 1. The instrumentation for an HGLP observatory. The thick hemispherical instrument covers are seen at the left. Both photographic and digital magnetic tape recording was used in these systems.

output of the displacement channel, and the high-gain channel were both recorded digitally as well, and all quantitative analysis of HGLP data was made from these magnetic tapes.

When operation of the HGLP stations was transferred to the Albuquerque Seismological Laboratory, the recording systems were totally replaced with SRO-type digital recorders, and these stations remain in service as the ASRO (Abbreviated Seismic Research Observatory) stations of the Global Digital Seismic Network (GDSN).

2.2.4. ***Quartz (Block & Moore) accelerometer.*** From approximately 1965 until 1973, Block and Moore, working first at the University of Maryland, then at the University of California, San Diego, constructed a number of seismometers designed to measure long-period earth motion. All of their instruments utilized the force-balance principle, which had received sporadic attention previously, but more for the purpose of automatic drift compensation than as an intrinsic design technique. At first LaCoste and Romberg gravity meters were used as sensors, and this followed work by Weber at Princeton and Maryland as part of the NASA Apollo Program. He had developed a modified LaCoste gravity meter which was placed (unsuccessfully) on the moon for the purpose of testing gravitation theories. These modified instruments were the first sensors in which the instrumental noise was indubitably less than the very long period (>100 seconds) earth noise.

The seismological applications were apparent, and further work was sponsored by VELA-Uniform. By this time the desirability of borehole emplacement was recognized, and since the LaCoste instruments were difficult to obtain, were bulky, and were unable to function as horizontal sensors, a radically new design was conceived. In some respects, their instrument was reminiscent of the classic Wood-Anderson seismometer,

for the quartz accelerometer utilized an eccentric inertial mass attached to a torsion element.

For compactness, the inertial element in the quartz accelerometer was small. This raised the spectre of thermal fluctuations (Brownian motion) exceeding the seismic motions, and to ameliorate this problem, the instruments were evacuated. This caused difficulties from the start, for to reduce the gas damping enough a hard vacuum was required. This called for the use of stainless steel, and a lengthy bake-out. Damping, of course, has no effect on the rms Brownian motion; it simply shifts the power more and more into a narrow band at the resonant frequency, typically one hertz. For long-period measurements, these quasi-resonant oscillations could have been filtered out, so long as the sensing system remained linear, but the goal was to achieve a relatively broad band response, so another solution was sought. This solution was to employ feedback damping (Kittel, 1958, p. 152). Melton (1981a), recounts the early confusion about thermal noise amongst seismologists and notes that O.D. Starkey at Geotech was working along similar lines. See also Melton (1976). In fact, the principle of feedback damping never worked satisfactorily for the quartz accelerometer. Internal magnets were added to suppress the resonant oscillations, and virtually all published data from these instruments were obtained from open-loop sensors.

The most complete description of the quartz accelerometer may be found in the thesis of Dratler (1971), and briefer accounts are given by Block and Moore (1970), Dratler and Block (1972), and Block and Dratler (1972, 1973). A few commercial versions of this instrument were manufactured by the Diax Corporation, but a critical assessment of its manufacturability, cost, and reliability (Sherwin and Moore, 1973) resulted in the decision to terminate work on these instruments. Many of the lessons from this project, however, strongly influenced the design of the IDA long-period seismic system (Moore and Farrell, 1970; Agnew *et al.*, 1976), and the technique of feedback damping is central to Geotech's Model 44000.

2.2.5. *KS36000 (SRO) sensor.* The main issue of the VELA-Uniform research into seismometry is the SRO array of KS36000 (KS for Kirkpatrick and Starkey) seismometers. The initial design and experimentation on this sensor was conducted as an internal research project at Geotech. As the advantages of the new instrument became clear, the VELA program then sponsored advanced development and testing of a borehole configuration (Douze and Sherwin, 1975). The tests showed the performance of the KS36000 to be earth noise limited in the long-period band. On this basis it was selected for the Seismic Research

Observatory (SRO) program. The first SRO station was installed at the Albuquerque Seismological Observatory of the Geological Survey in 1975. By 1978 the full network of nearly twenty stations had been deployed worldwide.

The KS36000 (Fig. 2) is a compact, three-component seismometer, in which magnetic force feedback is utilized to shorten dramatically the natural period. In the absence of feedback, the sensors would have a free period of approximately 5 seconds, but in closed-loop operation the

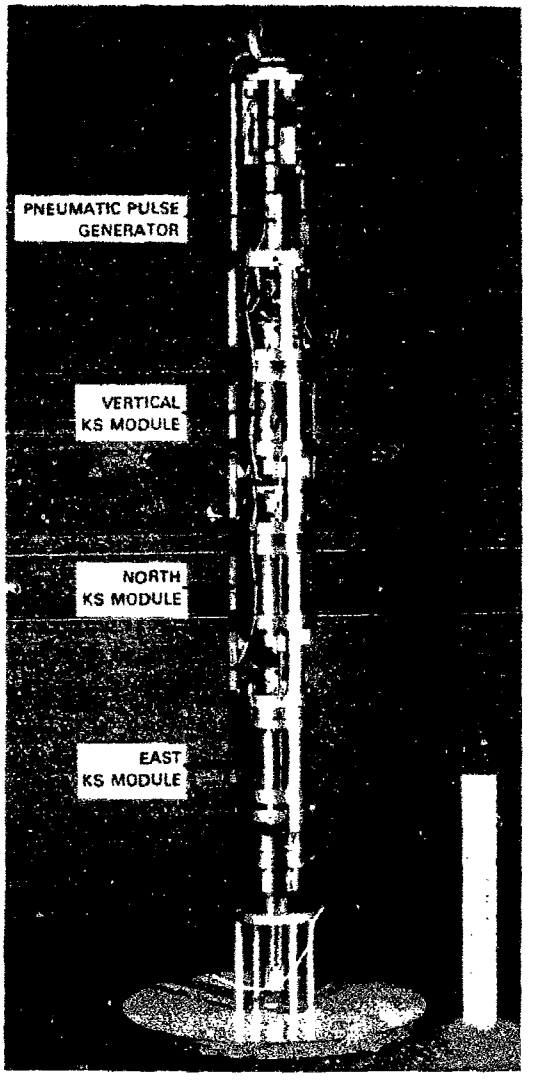

Fig. 2. The KS36000 seismometer module.

effective resonant frequency is approximately one hertz. Farrell and Berger (1979) describe the KS36000 feedback control system, and Peterson *et al.* (1980) provide a more general description, particularly emphasizing the frequency-response function and the calibration method.

Besides the remarkable achievement of adapting such a sensitive device to borehole operation, with the problems of locking in place, leveling, and remote control, the KS36000 is notable in that the vertical sensor has no provision for mechanical centering. This requires that the electronic force-balance circuitry be able to handle the full geographic variation in the acceleration of gravity (0.5 m/s^2), and yet have an rms noise level less than 10^{-9} m/s^2 around the earth-noise minimum at 20 seconds. This was achieved with a sophisticated modulation-demodulation arrangement within the feedback loop.

The KS36000 was originally designed to monitor the three components of long-period earth motion. For the SRO system an extra filter was attached to the vertical channel to provide one short-period output. This has not proved entirely satisfactory, for the short-period channel distorts, in a very subtle way, many teleseismic body waves from magnitude 6 and larger events. Also, certain details of the response functions of the several analog filters proved unsatisfactory, and although these have been and are being changed, the result is an extremely complicated calibration history. Further, experience in the field has shown that lightning-induced voltage pulses have caused the signal multiplexers to assign the wrong channel identifications in some instances.

Geotech has continued work on the KS line of seismometers and at least three versions of the KS36000 have been manufactured. Of interest for seismic identification research are the five units built in 1982 for the Department of Energy's Regional Seismic Test Network (RSTN). An even smaller system, the Model 44000, is being developed to fit within a 3¾ inch borehole (Geotech, 1984b). An engineering prototype is now operating at the Sandia Laboratory's seismic test facility in Albuquerque.

2.3. Strain sensors. Research on instrumentation to measure earth strain was initiated very early in the VELA-Uniform program, and continues to this day. Activity in this field peaked around 1970, when Shopland, Fix and others were reporting on experimental results obtained with the first generation of instruments. Developments since 1973 have been less publicized, and have been confined entirely to the problem of perfecting a short (1 m) borehole strainmeter.

The major impetus behind the persistent attention to strain sensors has been the possibility that signals from a single 3-axis seismometer and a strainmeter could be jointly processed to form directional beams and to improve the signal-to-noise ratio. If this could be successfully done,

then such a system might have performance comparable to a typical small aperture (~5 km) seismic array, but occupy just a fraction of the territory. This is the same rationale which motivated much of the early borehole seismometer work. Unlike the deep-hole seismometer arrays, which did not live up to their promise because of the complex composition of the seismic noise field with respect to vertical wavenumber and frequency, the development of strain-seismometer complexes has not proceeded far enough to test adequately the theoretical predictions.

Benioff (1962) and Romney (1964) presented the basic concepts behind the idea of combining strain data with seismometer data. The results of applying these ideas in practice were presented by Shopland and Kirklin (1969c, 1970). A complete review of the subject may be found in Fix (1973a), and a later analysis is given in Sorrells and Starkey (1980). Figure 3 shows a contemporary system.

The first results of the VELA-Uniform research in strain seismometry came from experiments conducted in the Ogdensburg observatory of Columbia University (Major *et al.*, 1964). The instruments used in this study were of the Benioff design, which uses quartz rods as the reference member, and capacitive position sensors. Three horizontal instruments approximately 200 ft. long, and a 50 ft. vertical sensor were built. These were basically long-period instruments, and most attention was paid to secular variations and the earth tides, although a few seismic surface waves were studied. Thus, these instruments did not address the possibilities of strainmeters in the 1 Hz frequency band.

Excepting a single, short (1 m) laser interferometer (Van Veen *et al.*, 1966), the quartz (or metal) bar technology has stayed with us. The reason for this has been that, until the 1970's, frequency drift in the available lasers was so large it generated instrument noise greater than intrinsic earth noise.

The VELA-Uniform research on strainmeters has been conducted almost entirely by Teledyne Geotech (but see Moore *et al.*, 1974), and has followed three distinct paths. These are (1) vertical instruments suitable for borehole use, (2) horizontal instruments and, (3) portable instruments. Today just the vertical borehole instrument is under active development (Geotech, 1984a).

Attempts to detect weak teleseismic body-waves by combining strain data with seismometer data are marginally successful (processor gain 6 dB) when the background microseismic (6 sec) noise is high (Woolson, 1971; Woolson and Sax, 1971; Woolson, 1972; Der, 1972). The method works under these circumstances because large amplitude microseisms are predominantly single-mode Rayleigh waves generated by ocean wave action. When the microseisms are low, and under all circumstances for

frequencies higher than 1 Hz, strain data seems to add no new information to that carried by the velocity (or displacement) field. This probably reflects the fact that for teleseismic body waves the signal-to-noise ratio for earth strain is less than for earth displacement.

2.3.1. ***Vertical (borehole) instruments.*** The vertical strainmeter developed by Geotech, model 14936 (Shopland and Kirklin, 1969a) was operated for some time at the Wichita Mountains Observatory (WMO), at a site near Garland, Texas, and at Houlton, Maine. Most of the 18 meter instrument package is taken up by the steel reference member, which is anchored at the top. A sensing assembly extends upwards from

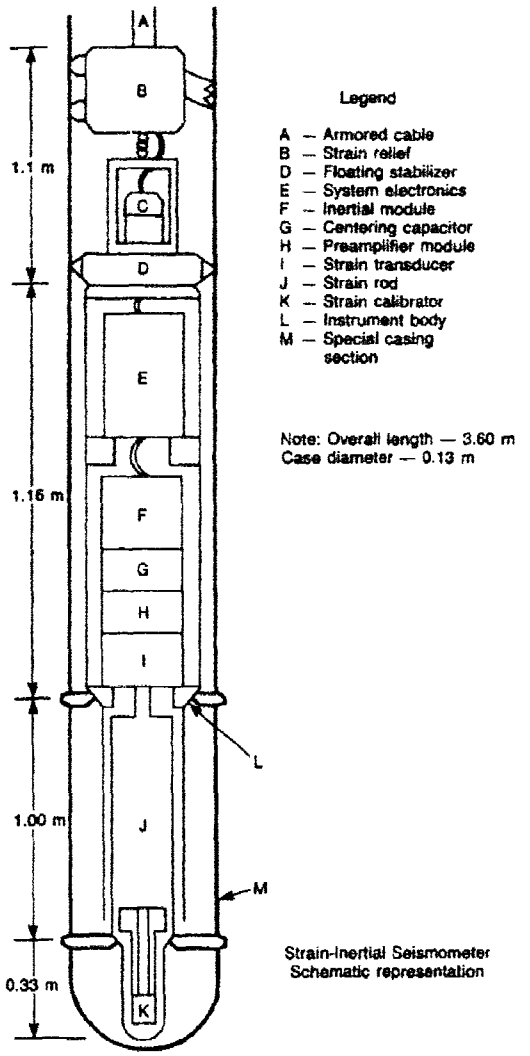

Fig. 3. A schematic representation of the borehole strain-inertial seismometer.

a lower anchor. Both a moving-coil and capacitive detector monitor the motion of the bottom of the reference member. The upper and lower anchors also serve to seal the hole, and the space between is filled with oil to damp transverse motion of the rod. A translating mechanism of high resolution is located in the sensing package, to allow the detectors to be adjusted after installation. A magnetostrictive calibration rod presses against the upper end of the reference member. An earlier report from this project is Geotech (1963b), and latest developments may be found in Geotech (1984a).

2.3.2. ***Portable instruments.*** Between 1963 and 1970, Shopland and his colleagues constructed a number of horizontal strainmeters at the Wichita Mountain Observatory (WMO) and the Nevada Test Site. These have been called "portable instruments", but the phrase is something of a misnomer for an instrument many meters long, buried in a 4 meter trench cut into rock. The strainmeters installed at WMO used 18 meter quartz rods, and contained both a displacement and a velocity transducer (Shopland, 1966, 1968; Shopland and Kirklin, 1969b, 1969c). Four separate instruments spanning an arc of 135 degrees radiated out from the central vault in which the transducers were located (Shopland and Kirklin, 1969c Fig. 1). The bandwidth of the system extended in frequency from .01 to 10 Hz.

The NTS installation used shorter rods (6 meters), and employed only a capacitive displacement transducer. Six instruments were constructed at the Nevada Test site (Shopland, 1970a, 1970b, 1971).

2.3.3. ***The Queen Creek instruments.*** The third major line of research in strainmeter technology was the observatory established at Queen Creek, Arizona, 40 km southwest of Phoenix (Fix, 1973a, 1973b; Fix and Sherwin, 1970, 1972). The last cited report by Fix and Sherwin describes the entire project, which lasted from mid-1968 until mid-1972. Two horizontal strainmeters 40 m long, and a vertical strainmeter 12 m long were installed in a mine, along with a variety of conventional seismometers. To isolate the instruments from non-seismic disturbances they were thermally insulated, and pressure-tight bulkhead doors were used to seal the tunnel. Invar, rather than quartz, was used for the rods, and both moving coil velocity sensors, and capacitance displacement sensors were attached to the rods. Across the two sensor channels the useful frequency range extended from 0 to 10 Hz.

The data obtained from the Queen Creek experiment greatly extended the understanding of the strain-noise spectrum, for no investigators before had made so many measurements with such good instruments. Numerous seismic signals, both short-period and long-period were recorded at this observatory.

3. Seismic Systems

3.1. Borehole instrumentation. The Berkner report recommended that the pre-VELA work in deep-hole seismometry (see, for example, Melton, 1981) be continued and expanded. This was done, and the initial focus of the effort was to devise low-noise short-period systems which could operate at depths in excess of 3 km. Later, the possibilities of vertical arrays of short-period sensors were investigated. Finally, as technical advances made it possible to fabricate small sensors with adequate sensitivity to long-period earth motion, these too were placed in boreholes.

Two considerations have motivated this work. The first has been the search for techniques to increase the signal-to-noise ratio of teleseismic body-waves on individual sensors. The second consideration has been the desire to combine multiple borehole sensors to form vertical arrays, giving the capability both of beamforming and increasing further signal-to-noise ratio. Neither of these ideas worked as well in practice as had been hoped, however, and the early flurry of activity had practically stopped by 1970.

The major legacy of this research has been the rather complete understanding of wind and pressure-generated earth-noise and its attenuation with depth (Sorrells, 1971; Sorrells *et al.*, 1971. Sorrells and Goforth, 1973) and the technology of borehole seismometer operation (*e.g.*, Van Sandt and Levin, 1963; Mack, 1966). Most of the advantages of borehole noise reduction are gained in the first hundred meters, and this determined the design of the SRO and RSTN seismic systems.

Although it was always found that the background earth-noise decreased with depth, so did the signal because of destructive interference between the up-going and down-going waves. For single-sensor systems, the signal-to-noise ratio for body-waves remained essentially constant down to depths of 2 km. At the bottoms of some of the deepest holes (3 km), however, the signal-to-noise ratio was often ten times its surface value (Douze, 1964).

Attempts to perform array processing on vertical seismometer strings were not successful because practical holes were not deep enough (<3 km) to give enough wavenumber resolution. Although computer studies indicated that multiple-mode noise fields could be filtered out (Shumway and Dean, 1968), the processing failed when applied to real data because of instability in the filter coefficients.

There were basically four instrument systems which were developed to support deep-hole research, but generally their novelty lies more in the packaging and provision for remote operation under hostile conditions than in the sensor systems. At the start, the big Benioff variable-

reluctance seismometer was adapted to fit in a deep, 7" hole. The packaged sensor was the Geotech 11167, and the entire borehole system was known as model 22625 (Geotech, 1963a, 1964).

The Geotech model 20171 shallow-hole seismometer was a moving-coil, short-period sensor with characteristics similar to the 18300/S-13, but it was contained within a 9.5 cm (3.75 in.) sonde 1 meter long (Andrew, 1965). The entire borehole system fabricated around this sensor was known as the 21540. The 20171 had a maximum operating depth of 300 m, only a tenth the depth of interest for the vertical array studies. Thus, the 20171 shallow-hole instrument was adapted for deep-hole (3 km) application (Andrew, 1965). The new instrument was designated as the model 23900 deep hole seismometer, and the entire system incorporating six of these into a vertical array was the model 248116 (Geotech, 1966a).

The fourth main branch of the borehole seismometry effort was the work focused around Melton's triaxial seismometer. This work may be divided into two subjects. First there were projects based on the borehole version of the short-period sensor, in which it was used in long vertical arrays (Shappee and Douze, 1967; Der *et al.*, 1968, Der, 1969). Secondly there was the borehole long-period sensor (McMillan, 1964; Melton, and Kirkpatrick, 1970), which was deployed in the ALPA and KSRS arrays and was the predecessor of the KS36000 seismometer.

One of the first vertical arrays was that described by Andrew (1965). This was a 6 element system 9000 feet long which utilized a modified 20171 (later designated model 23900) moving-coil instrument. Later work with the 6 element array was reported by Shappee and Douze (1967). Their measurements were taken at Grapevine, Texas, as previously, as well as sites in Oklahoma, West Virginia, Utah, and Pennsylvania. Further work with this short-period array at UBO (Kelley, 1968) gave a 9 dB improvement in signal-to-noise ratio.

Shappee and Douze also reported on measurements made in the Oklahoma well with another instrument package, a 4 element array of short-period triaxial sensors. This same array was later used by Der (Der *et al.*, 1968, Der, 1969) for further measurements at Grapevine, the deepest triaxial being placed nearly 3 km below the surface.

A long-period instrument was operated in a shallow borehole by Rector (1965), and we noted above the long-period triaxial system. Douze and Sherwin (1975), in one of the last reports concerning borehole seismometry, ran a KS36000 as deep as 1 km at Pinedale, Wyoming. The Wyoming work indicated that at long periods there was not a great advantage in going much deeper than 50 meters, at least at hard-rock sites.

The most exotic borehole work was the three dimensional array of

Broding *et al.* (1964) which operated briefly near Tyron, Oklahoma. Down 5 holes, they placed three sensors each (HS-10, the LASA instrument) at depths of approximately 1200, 2400, and 3600 feet.

3.2. Ocean-bottom instrumentation. There have been two main approaches to placing seismometers on the sea bottom; the self-contained free-falling capsule and the tethered system in which the recorder is located some distance away from the seismometer. The challenge is to make the instrument work at sea and to get it back afterwards. With so much of the earth unaccessible to conventional instruments, it is natural that the VELA-Uniform Program supported underwater seismometry from the beginning, and continued to do so almost until the present. Reviews of ocean-bottom seismometer applications and technology may be found in Philips and McCowan, 1978 and Prothero, 1984.

Considering the problems of attaching the instrument to the ocean floor, and keeping the power consumption small, it is not surprising that off-the-shelf seismic sensors have been used in all the instruments. Free-fall, or pop-up, capsules were developed by groups at the University of California, San Diego (Bradner, 1964; Bradner *et al.*, 1965a, Bradner *et al.*, 1965b), and at Texas Instruments (Arnett and Newhouse, 1965; Texas Instruments, 1968). The several instruments developed by both groups contained three-component, short-period sensors. Bradner *et al.* utilized a symmetrical three-axis sensor (a modified lunar seismometer, designed at the Caltech Jet Propulsion Laboratory and made commercially by United Electro Dynamics). This arrangement does not require careful leveling, just the recording of the orientation of the vertical and a compass bearing. The final Texas Instruments capsule used the Hall Sears HS-10, and *in situ* leveling was necessary. Data collected with both these systems showed that the seismic noise on the seafloor at high frequencies was about 30 dB greater than was typically found on land.

Approximately two dozen of the Texas Instrument systems were manufactured. Two major crustal refraction experiments were conducted with these capsules. Linville *et al.* (1968a) and Linville *et al.* (1968b) describe a three phase experiment across the Rat Islands on the extremity of the Aleutians. A total of 1000 km of data were acquired along a line centered on the island of Semisopochnoi and oriented in a northeasterly direction. Shots as large as five tons were employed. The other major experiment, conducted off the Kuriles, is reported in McDermott *et al.* (1967). The last study, apparently the end of the Texas Instruments ocean bottom seismometer work, is a description of measurements in the Gulf of Mexico by BeAbout *et al.* (1968).

The tethered approach to underwater seismometry was pioneered at Lamont (Sutton *et al.*, 1965). A complete observatory was established

100 miles off Cape Mendocino in 4 km of water. This observatory, after two unsuccessful deployments, ran for 6½ years (Nowroozi *et al.*, 1966; Latham and Nowroozi, 1968; Sutton *et al.*, 1970). The instruments, contained within three aluminum alloy spheres, were connected by cable to a shore installation, at which the data were recorded and from which commands were issued. Both long-period and short-period sensors were used in Lamont's OBS. The three-component long-period instrument was a modified version of the triaxial which had been developed at Lamont for NASA. A commercial (Electrotech EV17, EV17H) short-period seismometer was used.

The Columbia group also made a series of seismic measurements off Bermuda before the Point Arena observatory was installed. The use of acoustic telemetry makes the instrumentation of these experiments notable (Latham and Sutton, 1966; Thanos, 1966; Thanos and Hubbard, 1966).

The tethered approach to seafloor seismometry was recently selected for the DARPA/Navy Marine Seismic System (MSS) project (Fig. 4). The purpose behind this project was to place a seismometer

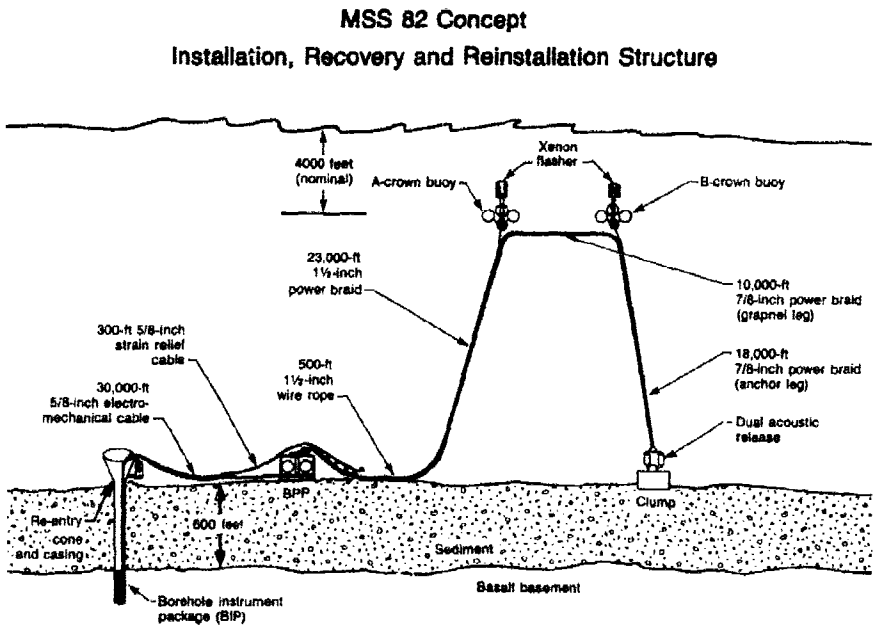

Fig. 4 The arrangement of the marine seismic system (MSS) shows the seismometer emplaced in a borehole, with the recording package located on the seafloor nearby. The loop of cable rising near to the surface is utilized for instrument recovery.

system in a hole, in order to obtain quieter conditions. A variety of designs was considered but the final selection had three Geotech short-period sensors configured in a tube, which itself was attached to a carrier and lowered to the seafloor. The carrier mated with the reentry coupling of the Deep Sea Drilling Project hole. Attached to the instrument package by 20,000 feet of wire was the recorder package, which also contained the battery system. The recorder package could be released from its anchor upon command from the support ship, so that the data could be recovered and the batteries changed without disturbing the instrument. The MSS has been deployed once in the Atlantic and twice in the Pacific oceans, but the project is now terminated.

3.3. LRSM mobile and portable systems. Two distinct systems were utilized in the LRSM program, the mobile observatories which formed the nucleus of the program, and the portable systems which were developed for the second half of the project (Wolfe, 1966; Geotech 1966b, 1970a). The mobile observatories (Fig. 5) required a small semitrailer to transport the equipment, which was basically an augmented WWSSN instrument system. This trailer was turned into the recording structure at the field site. The portable system was packed in field containers (Geotech, 1969, Fig. 2) and was transported by pickup truck. The mobile

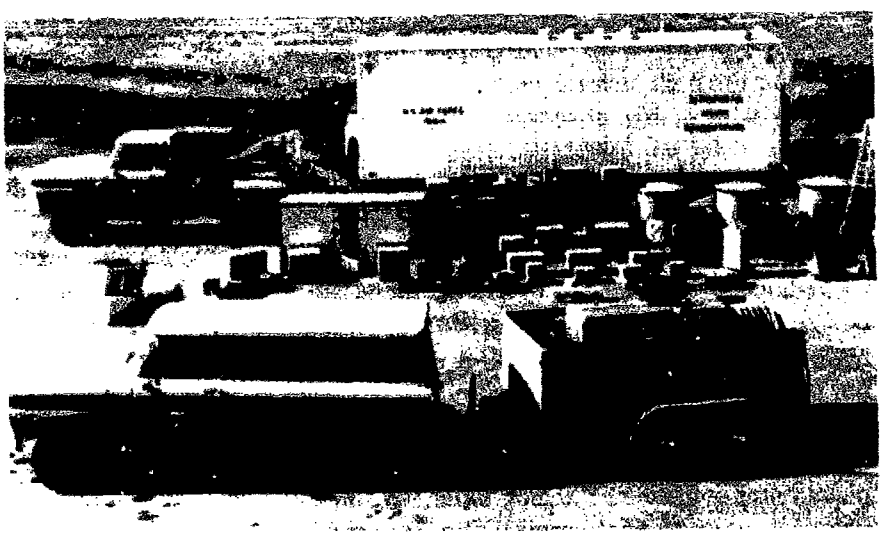

Fig. 5. The instrumentation used for the LRSM mobile observatories filled a semitrailer. The trailer served as the observatory headquarters after deployment. The Benioff short period instruments in their distinctive triangular case are located to the right. The box in the left midground is the shelter for the phototube amplifiers. Forty of these systems were acquired.

observatories required commercial power at the station, while the portable systems were operated from thermoelectric generators, and thus had much greater freedom of location.

Shallow surface vaults were fabricated to hold the three long-period and three short-period sensors for both systems. The compact Geotech 18300 short-period seismometer was utilized with the portable system so that the three sensors were established in a single vault rather than the three separate ones needed to hold the big Benioffs. The simplicity of the portable systems may be attributed to several factors: the sensors were smaller, FM magnetic tape rather than photographic film was used for recording data, and active electronic amplifiers supplanted the passive galvanometer amplifiers. In the mobile observatory a separate bunker was needed just to house the galvanometers. The portable systems could be set up by one person in less than a fifth of the time required for the mobile observatory: 70 man hours *vs.* 400 according to Geotech (1966a).

The mobile observatories were similar in many respects to the WWSSN instrument system of the late 1950's. Benioff short-period sensors (Geotech Model numbers 1101 and 1051) and Sprengnether long-period sensors (Models 101 and 201) were used for the seismometers. In the beginning, both the long-period and short-period systems in the mobile observatories utilized earth-powered recording (Geotech, 1961). There were no active amplifiers in this method, and the passive transducers were connected directly to a galvanometer, the deflection of which moved a light beam on photographic film.

Over the next several years, photocell amplifiers were incorporated into the older mobile observatories and designed into the new portable systems. (Melton, 1981b describes the history and technology of the photocell amplifier). The photocell amplifier was needed to make use of analog (frequency modulation) magnetic tape recording, and gave added flexibility in data filtering. This transformation in amplifier/recorder technology was completed by the middle of the decade. Advances in the design and performance of transistorized amplifiers were so rapid, that by 1966 (Geotech, 1966, p. 100) it was clear that these should be incorporated in future systems.

The period 1965-1967 saw the introduction of FM tape recording to both the mobile observatories and the portable systems. Analysis techniques still emphasized analog plots, so the FM tapes were generally played back on to photographic film. By the end of the LRSM program over 140,000 feet of film had been written. Although the FM tapes were considered the primary archive data, digital transcription became more and more prevalent during the concluding phases of the LRSM program, and transcription laboratories were established both in the Garland

(Geotech, 1968 Figs. 33, 34, 35) and Alexandria operations.

3.4. SRO system. The SRO seismic system (Peterson *et al.*, 1976) consists of a KS36000 borehole seismometer package (Fig. 6) and a data recording system (Fig. 7). The borehole assembly holds the three orthogonal sensors, the feedback electronics for each sensor, data filters and the sensor leveling mechanism. Multiconductor cable brings the seismic data uphole, and passes power and control signals downhole. The borehole assembly is wired directly to the recording system, except at the one station where radio telemetry is used.

The SRO recording system has visual recorders to display the three channels of long-period data and the single channel of vertical component short-period data. Two digital tape recorders are provided, and a 2400 foot tape lasts about a week. The long period data are recorded continuously with a 1 second sample interval. The short period data are passed through a signal detection algorithm. Then the detector triggers a short length of 20 sample/second data is recorded. The detector is adjusted to give approximately one false alarm each hour.

3.5. DWWSS system. The Digital World-Wide Standardized Seismograph (DWWSS) system was conceived in 1976 as an upgrade of selected WWSSN stations to direct, digital recording. The system was designed and assembled at the USGS Albuquerque Seismological Laboratory, and installation began in 1980. Approximately 15 stations have been modified to date.

A brief description of the DWWSS System has been written by Peterson and Hutt (1982). As with the SRO System, only the vertical component of short-period earth motion is recorded, and this takes place only for time windows in which an event detector is triggered. This channel is derived from the original Benioff seismometer.

The long-period Sprengnether seismometers were modifed with different pickup coils in order to support the DWWSS System. The amplified signals from all three orthogonal sensors are passed through both a long-period and an intermediate-period filter before digitization and recording. These signals are recorded continuously.

4. Seismic Arrays

4.1. WWSSN. Even after almost twenty years of operation, the World Wide Standardized Seismography Network remains, perhaps, "the finest, general-purpose, global system of seismic monitoring stations ever operated" (Oliver and Murphy, 1971). In the view of many, it is the premier accomplishment of the VELA-Uniform instrumentation program, and yet the instrumentation is almost medieval, by modern standards. Although set up as a research tool for studying fundamental problems

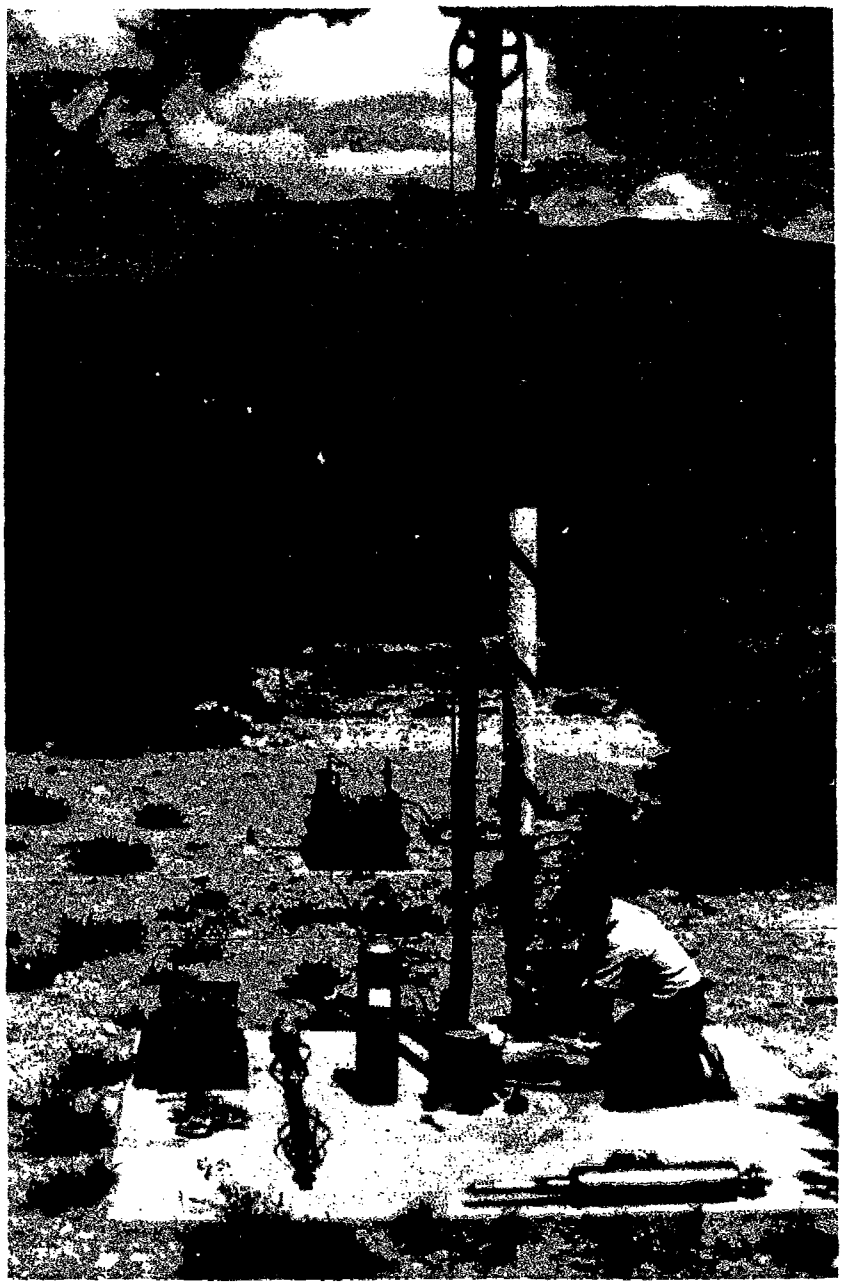

Fig. 6. The SRO sensor system is contained within a borehole sonde approximately 3 meters long. The emplacement depth is typically 100 m. Three sensors as well as all sensor electronics are contained within the module.

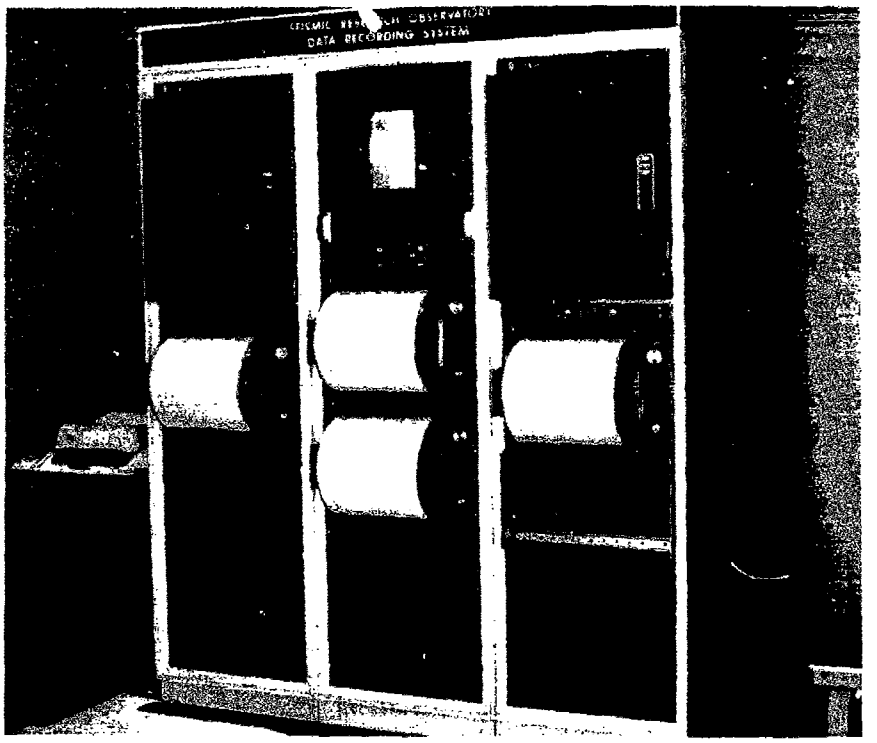

Fig. 7. The SRO recording system uses direct digital recording on magnetic tape. Long-period data are recorded continuously, but short-period data are recorded only when an "event" has been detected. The data recording and calibration are performed by the small computer located immediately below the right-most drum recorder.

in seismology, it can be argued that studies conducted on data from this single network have been comparable in importance to that provided by all other seismic systems for the problem of source identification and yield estimation.

The WWSSN has had a perilous history, and the support difficulties noted by Oliver and Murphy in 1971 have continued to this day. The WWSSN network has three fundamental weaknesses from the point of view of the requirements of monitoring underground nuclear explosions. The sites themselves, and the long-period sensors in particular, are noisy, the data are recorded on photographic film with limited dynamic range, and it usually takes many months for all stations to submit their data. The recent upgrade of selected WWSSN station to direct, digital recording (see Section 3.5) has not been completely successful. Despite these limitations, data from the WWSSN continues to be intensively analyzed,

and results of importance to nuclear monitoring problems continue to accrue.

For studying small underground explosions, the WWSSN is clearly inadequate. It is difficult to judge precisely the yield threshold below which the network detects less than half the actual number of events worldwide. A general impression can be gained from the study by North (1977) of the catalog produced by the International Seismological Center (ISC). A large fraction of the stations reporting to the ISC are WWSSN stations, and North found that most events with magnitude 5 or above were reported by 15 or more stations, and most events with magnitude greater than 4.5 were reported by 3 or more stations. Noting that there have been few presumed underground explosions with magnitude greater than 6.0 since the threshold limitation of 150 kt yield has been in effect, it appears that the WWSSN yield threshold is around 5 kt. Based on published data from the Lajitas site in Texas (Li, 1981, Fig. 20, Li *et al.*, 1984) contemporary, digital instrument systems installed at quiet sites would be capable of a tenfold reduction in this limit.

James T. Wilson was chairman of a committee formed to advise on the design and installation of the network. The strategy they devised was to concentrate on the traditional seismic frequency span (.01 to 10 Hz) and to use two separate 3-axis instrument systems. They called for proven instruments which would require no extensive development. To accomplish this the Geotechnical Corporation, working for the Coast and Geodetic Survey, designed and constructed the 3 component, Benioff short-period sensors, and the 3 component, Sprengnether long-period sensors. Direct light-beam recording on photographic film was employed, using galvanometers with periods of .75 and 100 seconds, respectively, for the two seismic bands. Thus, the WWSSN is a totally earth-powered seismic system. Figure 8 is a photograph of the equipment at a WWSSN station.

A critical part of the WWSSN station is the crystal controlled clock developed by Geotech (Melton, 1981b, Fig. 38). This gives accurate short-duration, time-interval measurements and the radio time codes impressed on the records establish absolute time at all stations. A unique feature, for the time, was the standardized response. Simple sensitivity adjustment was provided, which did not interact with the shape of the system transfer function. During normal operations calibration pulses are written each day. This is another noteworthy feature which allows seismologists to compare all records, quantitatively. The WWSSN project has undoubtedly delivered more seismograms to seismologists than all other research networks combined. This may be attributed to the efficient data-management organization and the established practice of

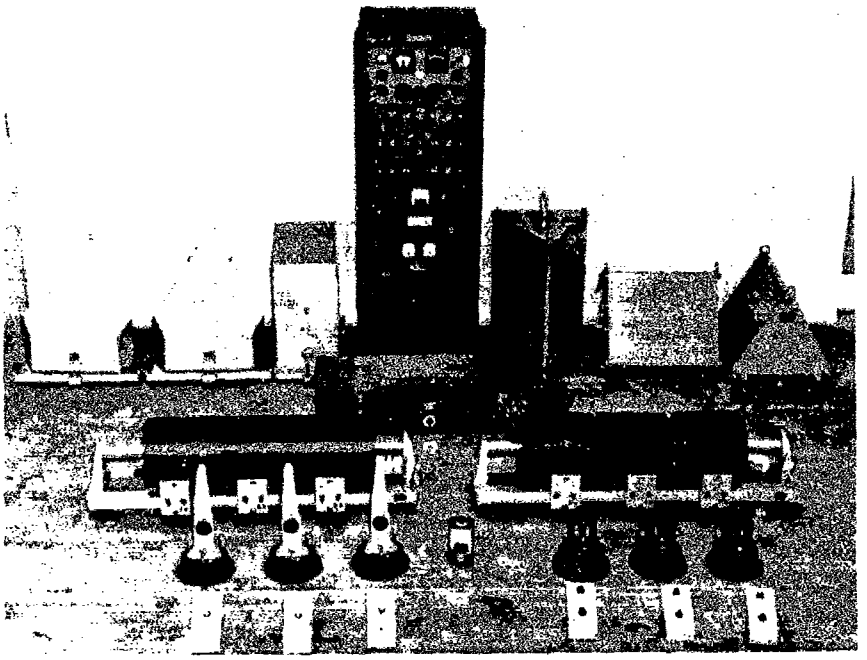

Fig. 8. The WWSSN instrumentation system shown here uses photographic recording exclusively and is earth-powered. The three Sprengnether long-period seismometers are displayed to the left of the cabinet that holds the timing and calibration apparatus. The three massive Benioff short-period seismometers are shown to the right.

copying every field record onto film "chips", photographic negatives slightly larger than a 3×5 index card. Despite years of effort, it is not yet possible for seismologists to browse digital data so effectively.

4.2. LRSM. The LRSM (Long Range Seismic Measurements) program began in June, 1960 and continued for most of the decade (see Geotech, 1969, for a brief history of the project and also Alsup and Guyton, 1964). The LRSM project continued a long-standing program to record seismic signals from tests in Nevada (Geotech, 1959) and it was succeeded by the Special Data Collection System, a field measurement effort of much smaller scope. The major purpose behind the LRSM program was to maintain a network of mobile seismological observatories at which high-quality film and magnetic tape (fm) recordings were to be obtained of signals from explosions at NTS and earthquakes. A vast quantity of data was obtained under the LRSM program. An inventory of the Seismic Data Analysis Center (SDAC) in 1981 (Dean, 1981) indicated that the combined LRSM and Geneva array data collection amounted to

37,000 analog tapes out of a facility total in excess of 83,000. During one project period, a total of fifty station-years of data were obtained during a twenty month period (Geotech, 1966b, Fig. 2). A map showing the principal LRSM observation points is given in Fig. 9.

The LRSM measurement program was conducted out of the Geotech Garland facility, and was rather distinct from the LRSM analysis program which was conducted through the Alexandria data center, originally known as the Seismic Data Laboratory (SDL). However, both of these activities, the collection of the data and the support of a dedicated data facility, followed directly from the recommendations of the Berkner panel.

A variety of special projects was accomplished within the LRSM program in addition to the basic observation program. Among these may be noted (Geotech 1966b; Geotech, 1970a):

(1) Site surveys for the LASA experiment
(2) Support of deep-hole seismography development
(3) Crustal studies near Tonto Forest Observatory, and participation in the TFO extended array telemetry program.
(4) Support of the strainmeter program.
(5) Support of the triaxial seismometer project.

The LRSM program began with 19, two-man observer teams who were fruitlessly sent out to record LOLLIPOP, an NTS shot which never occurred (Geotech, 1961). The number of observatories varied throughout the program, with about 40 mobile vans in operation by 1963 (Geotech, 1968). Shortly thereafter, concurrently with the growth of LASA, the LRSM program was scaled down, and the mobile observatories were

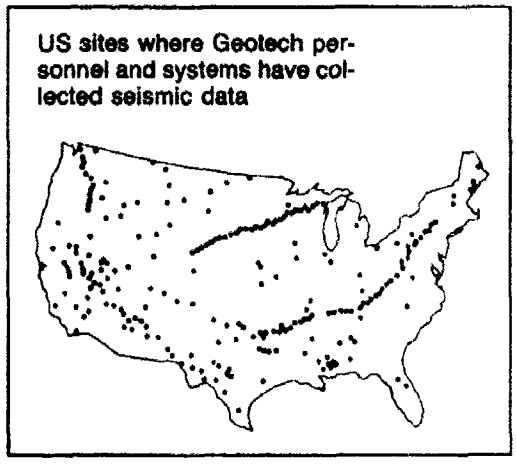

Fig. 9. The LRSM program spanned much of the United States. Several overseas stations (not shown) were operated as well.

transferred *in toto* to other organizations. By the end of the decade only 9 mobile observatories remained attached to the VELA-Uniform program (Geotech, 1970a). Two unique recording efforts, which were not actually part of the LRSM program but which had similar objectives, were the volunteer observers marshalled for the shots GNOME (Westhusing, 1963), and SHOAL (Weisbrich, 1965).

4.3. The Geneva arrays. In contrast to the WWSSN, which was a global network conceived to meet the data requirements for fundamental research in seismology, the Geneva arrays were installed specifically to study the application of multiple element seismic antennas to seismic monitoring of underground explosions. As with almost all the work conducted throughout the 1960's, the establishment of these arrays had been recommended in the Berkner report. Five arrays were installed between 1960 and 1963 (Fig. 10), and they ran continuously until 1970 at which time all except the Tonto Forest array were closed. Tonto Forest itself was shut down in 1975.

The early background of the arrays is summarized by Carpenter (1965). Wichita Mountains Seismological Observatory (WMO) in Oklahoma became operational in October, 1960, under the management of the Geotechnical Corporation. By the end of 1962 three additional arrays were built and opened by Texas Instruments. They were Blue Mountains (BMO) in Oregon, Uinta Basin (UBO) in Utah, and Cumberland Plateau (CPO) in Tennessee. Although the geometric arrangement of the sensors at these four arrays varied (see Fig. 11), the apertures were all about 4 km. CPO had 19 sensors, with only ten elements being utilized in the other three.

The Tonto Forest Observatory (TFO) in central Arizona was the principal research station. With respect to the other Geneva arrays, its aperture was bigger, the sensor spacing was denser, and it employed

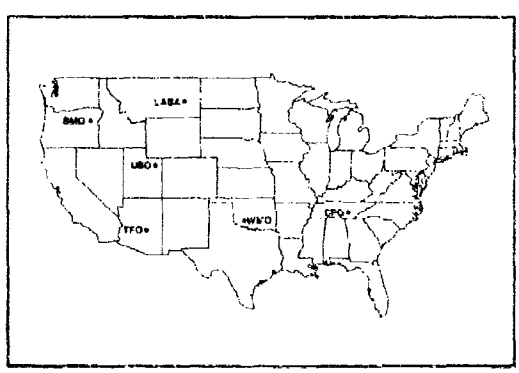

Fig. 10. The five Geneva seismic arrays were located in the western and southern states. The large LASA array was located in Montana. CPO is now the site of an RSTN station.

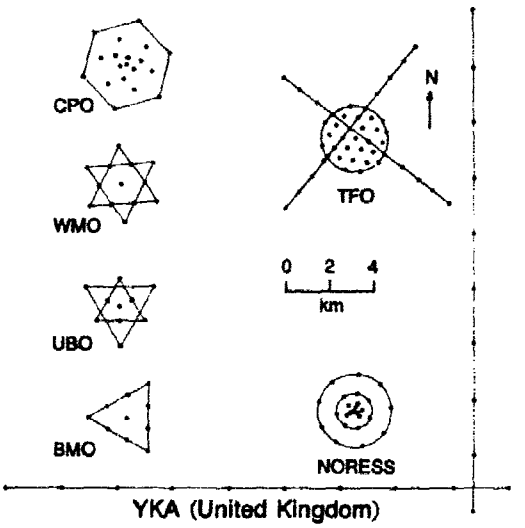

Fig. 11. The regular Geneva arrays (left column) had apertures of about 4 km. TFO was the experimental Geneva array. Also shown, for comparison, is NORESS and a typical United Kingdom array, but we have taken the liberty of moving the intersection point of the two crossed arms (Carpenter, 1965, Fig. 2).

more three-component sensors. Flinn and Dean designed TFO during 1960 and 1961, and it became operational under the management of United Electro Dynamics in August, 1962. Throughout its lifetime, TFO was the site of a number of special array studies, the most noteworthy being the extended-array work just prior to LASA's creation, and the long period array studies. The extended array configuration was achieved by siting a number of LRSM mobile observatories at offsets as great as 300 km from the array center.

The Geneva arrays produced data of the highest quality. This reflected the first class instrumentation, the care exercised over array location and sensor installation, and the interest of the full-time staff who monitored operations 24 hours a day.

Numerous sensors were utilized at the five Geneva arrays. Vertical-component Benioffs were originally installed for the array elements (Gudzin and Hamilton, 1961). The standard photocell arrangement was used for signal amplification, and recording was done on both photographic film and magnetic tape.

Over the years the big Benioff was supplanted by the JM seismometer (Johnson and Matheson, 1962), but the amplification, and recording systems were unchanged. In addition to the short-period sensors comprising the array elements, there was a variety of other instrumentation, including short-period horizontals, three-component long-period sensors, and shallow borehole verticals. All these data, including the individual elements of the array, were recorded on analog tape, and many studies of array seismology were based upon the records.

The Geneva arrays were installed to detect *P*-waves from weak events at teleseismic distances. These waves have phase velocities greater than 10 km/s. Since the arrays had apertures of order 3 km, and the greatest signal-to-noise ratio for *P*-waves is at a frequency near 1 Hz, a simple algebraic sum of the sensor voltages was used for the array output. Thus, there was no "steering" of the beam (by delay and sum processing, for example) away from the vertical.

The advantages of steering (or beaming) the array, and one technical approach for accomplishing this (passive, lumped-constant tapped delay lines) were described in one of the first Texas Instruments analyses of seismic arrays (Texas Instruments, 1961). Texas Instruments later built a dedicated processor which formed beams and performed event detection on the beams in real time (Texas Instruments, 1967). These processors were installed at CPO (Edwards *et al.*, 1967) and TFO (Clark, 1968). A discussion of the performance of the Texas Instruments processor at TFO may be found in Blandford (1974). We note that this addition of a dedicated beam-forming processor to the two Geneva arrays happened after the successful application of the method at LASA.

4.4. LASA. The Large Aperture Seismic Array in Montana was the grandest project of VELA-Uniform. It dominated DARPA seismological research from the mid 1960's almost until it was closed in 1978. As is clearly explained by Green *et al.* (1965, p. 1823), the major objective behind LASA was to obtain better seismograms with less interfering noise and not merely to make a seismicity bulletin with more complete coverage of small events. The principles behind the LASA array, and the details of its design and installation are given in some detail in the special issue of the *Proceedings of the IEEE*, Vol. 53, Number 12, published in December, 1965 (Briscoe and Fleck, 1965; Forbes *et al.*, 1965; Frosch and Green, 1965; Green *et al.*, 1965; Wood *et al.*, 1965). The story of how United Electro Dynamics built LASA in six months during the most severe winter (1964-1965) of the decade is fascinating, and demonstrates technical and project-management achievements of the highest order.

LASA (Fig. 12) may be looked upon as an array of arrays. It consisted of 525 seismometers distributed over an aperture of 200 km, but these instruments were grouped into 21 clusters, each comprising a subarray of 25 sensors with an aperture of 7 km. The considerations behind the concept of the sub-arrays have been summarized by Green *et al.* (1965, p. 1869). The sensors were vertical-component, short-period geophones, Hall-Sears model HS-10-1 (ARPA), which were modified versions of a standard refraction geophone. The sensitivity of these sensors was greatest at a frequency of 3 Hz.

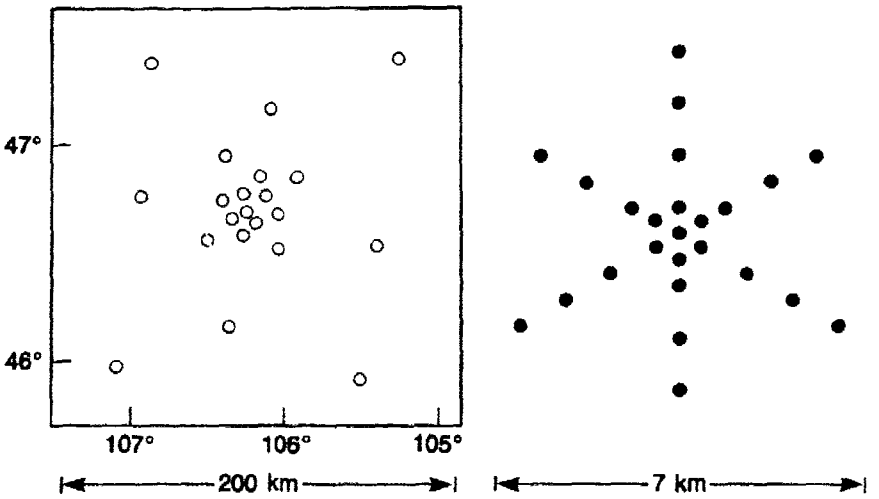

Fig. 12. The LASA array was composed of 21 subarrays, each with an aperture of about 7 km. The positions of the subarrays are shown on the left. The plan of seismometer locations for a typical 25-sensor subarray is drawn on the right.

The seismometers, within their water-tight housings, were installed on short posts at the bottom of a 200 ft. hole. The holes were all cased and cemented to be water-tight. At the ground surface, a small vault contained the Texas Instruments parametric amplifiers (RA-5) used for signal conditioning, as well as a calibration network (used to allow remote calibration of each individual sensor) and the lightning protectors. Subarray signals were sent by buried cables to a Central Terminal Housing, whence a mixture of land lines and microwave circuits carried the data to the main field facility at Billings, Montana.

At the Billings data facility, several computer systems managed array operations. Multiple beams were formed; these beams, as well as individual sensor-channels, were recorded on digital magnetic tape; real-time event detection codes monitored the received signals; and, finally, a reduced data-stream was transmitted to the MIT Lincoln Laboratories in Boston.

Shortly after LASA began operating, a three component, long-period seismic system was installed in the vicinity of the Central Telemetry Housing (CTH) of each of the 21 subarrays (Gudzin and Hennen, 1967). Subsurface vaults of reinforced concrete were built, with three sealed seismometer tank assemblies encased in the floor. The sensors installed in the tanks were the Geotech 7505B (vertical) and 8700D (horizontal). These sensors were only slightly different from the sensors with

similar model number discussed previously. Signal amplification and conditioning was accomplished in the CTH with a Texas Instruments parametric amplifier and associated filters.

Several additional equipment changes were made through the years. Among these were the installation of a microbarograph array, reduction from 25 to 16 in the number of short-period sensors in each sub-array, and reduction from 21 to 16 in the number of three-component sensors. The surplus short-period sensors were used to build the NORSAR array in 1970.

4.5. ALPA and other long-period arrays. The Alaskan long-period array (ALPA) operated near Fairbanks, Alaska, from 1968 until October, 1970 (Geotech 1970b). It was a highly symmetrical, 19 element array, with an aperture of 80 km and a sensor spacing of 20 km. Each of the three-component sensors was placed in a 15 m borehole. The sensors utilized were the Geotech Model 31300 triaxials, designed by Melton. The instrument package was designed to fit within a 12 5/8 inch cased and dry borehole, and accessories permitted the instrument to be unlocked and leveled after emplacement. Remote control of period and damping was also possible. This capability of parametric variation is a well recognized application of feedback technology, it is quite distinct from true forcebalance feedback, as employed, for instance, in the KS36000 seismometer.

The ALPA utilized digital radio transmission to send data and commands back and forth from the Monitor and Maintenance Center (MMC) at Pedro Dome, Alaska, and the separate sensor locations. On-site analog-to-digital conversion took place in the wellhead enclosure which contained the radio systems and the seismic amplifier and filter systems. A gain-ranging converter was used in order to maintain a wide dynamic range, and data was only transmitted following a request from the MMC, which was issued once each second to every station in the network. Primary power for each of the remote sites was obtained from a propane-fueled thermo-electric generator.

The ALPA telemetry system was improved in 1975 when the Long Period Data Acquisition Recording and Transmission System (LPDARTS) was installed (Geotech, 1974; 1976). This system utilized, at the field sites, autonomous clocks and digitizers which could be synchronized over the radio link. Also, the data recording system was significantly changed.

The Korean Seismic Research Station (KSRS) was installed in the early 1970's. Both a short-period array (using the Geotech 18300 sensor) and a long-period array (using the Melton triaxial sensor, Geotech model 31300) were constructed. The KSRS long-period array utilized the same LPDARTS telemetry and recording system which had been

developed for ALPA. Very little has been written about the two KSRS arrays, but the configuration of the short-period array may be found in Prahl *et al.*, 1975 and Shen, 1978. A seismological evaluation of the short-period array, conducted shortly after installation, is given by Blaik and Der, 1976. Somewhat later Texas Instruments installed the Iranian Long Period Array (ILPA), an array of seven KS36000 seismometers (Texas Instruments, 1977).

4.6. NORSAR and NORESS. The best references for the NORSAR seismic array are Bungum *et al.* (1971), and Ringdal and Husebye (1982). The design of NORSAR, which became operational in 1971, was strongly influenced by the LASA experience. Indeed, the original HS-10-1 (ARPA) seismometers and the Texas Instruments RA-5 parametric amplifiers were extracted from LASA to build NORSAR when the former array was reduced in density. The original NORSAR aperture of 100 km (see Fig. 13) was about half that of LASA, and the same concept of clustering the sensors into sub-arrays was utilized. In their original configuration there were slightly fewer (22 compared to 24) sub-arrays at NORSAR than at LASA.

The sub-arrays contain one long-period, three component seismic system (Geotech Model 8700C and 7505B), in addition to the 6 short period array elements. The sub-arrays have apertures of approximately 10 km, comparable to the LASA sub-array aperture, but the reduced number of array elements meant that the inter-sensor spacing at NORSAR was 3 km, rather than 1 km or less as was the case at LASA. Instruments are installed in vaults or shallow (3 to 15 m) boreholes.

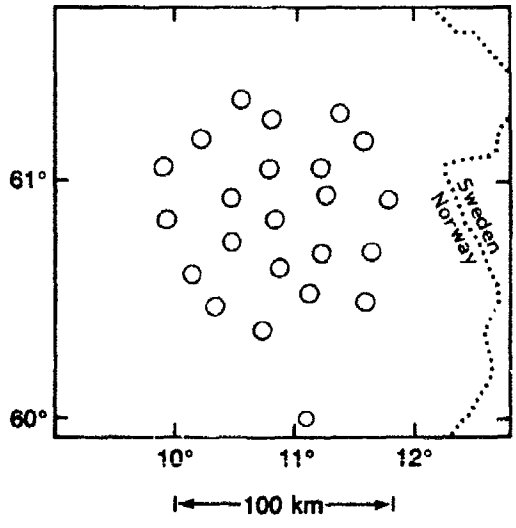

Fig. 13. The NORSAR array, like LASA, was composed of subarrays. The NORSAR subarrays utilized fewer sensors yet had a larger aperture.

NORSAR is supported by a data and operations center at Kjeller which conducts the same activities as the LASA Billings Center. Sensor signals are formed into beams, automatic detectors are used to scan the beam outputs, both single-sensor and beam outputs are recorded on digital magnetic tape, and a bulletin of seismic activity is produced.

As knowledge of the spatial characteristics of earth noise and seismic signals has grown, the sophistication of the array processing algorithms has increased. At NORSAR, the beam calculations made allowance for anomalous station-dependent time delays. Such anomalies are caused by structural inhomogeneities beneath the sensors.

In October, 1976, the size of the NORSAR array was reduced by half by removing from the south and west portions 15 out of the original 22 subarrays. This reduced array, with an aperture of 50 km, remains in operation today.

In 1979 the first version of a small-aperture experimental array (NORESS) was installed around the 02 sensor position of the 6C NORSAR sub-array (Mykkeltveit and Ringdal, 1981). Initially, the six existing NORSAR short-period sensors were repositioned from the original 9 km diameter arrangement, to a tight 2 km diameter arrangement. Additional HS-10 sensors were then added to densify the NORESS array (Mykkeltveit and Bungum, 1984). From studies of signal and noise correlations in data acquired from this experimental array, the final NORESS array was designed. With an aperture of 3 km, and sensor separations ranging from less than 100 m up to 1000 m (see Fig. 11) this is one of the densest arrays in operation.

Instrumentation for the final NORESS array was designed and installed by Sandia National Laboratory, for the Department of Energy. There are 24 elements in the array with three-component sensors located at 4 positions, and only vertical components located at the rest. Geotech GS-13 sensors are used. They are placed in shallow boreholes, at each of which is a well-head communications and control module. Fiber-optic cables bring the sensor signals to the array center. Also located at NORESS is a RSTN installation based upon the KS36000 seismic system. Data from NORESS is telemetered back from Europe to several sites in the United States. The on-line processing system for NORESS data has been described by Mykkeltveit and Bungum (1984).

4.7. SDCS. The SDCS (Special Data Collection System) was a continuation of the LRSM program, but utilized both analog and digital recording techniques. The project, which was initiated in 1970 (Geotech, 1972) and lasted until 1979, was directed towards understanding the cause of the observed difference in body-wave amplitudes between eastern U.S. and western U.S. stations (Der *et al.*, 1980; Der *et al.*, 1981). The

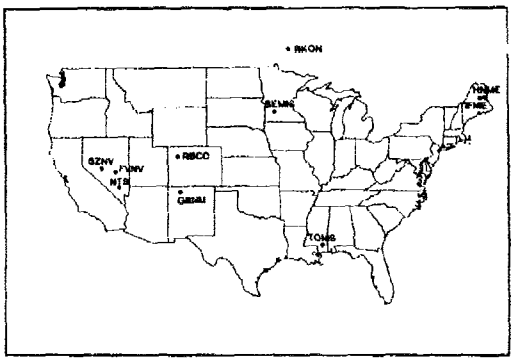

Fig. 14. The SDCS recording station used the portable observatories which had been developed under the LRSM program. Most SDCS observations were obtained at the sites of underground explosions, and the numerous positions occupied at NTS have not been distinguished on this map.

principle recording locations are shown in Fig. 14.

The majority of the sensing and recording systems used in the initial phases of the SDCS program was inherited from the LRSM program, but by this time most of the mobile observatory vans had been retired, and it was the eleven portable systems that formed the primary instrumentation. The three-component short-period data and three-component long-period data were recorded on FM tape recorders at two different gain levels, 20 dB apart. The dual-gain setting was used to overcome the limited dynamic range (40 dB, typically) inherent in the frequency modulation recording method. Since the SDCS recording system was an analog system it was not possible to use dynamic gain-ranging. Two special systems with even greater dynamic range were produced. The units (Geotech, 1972) utilized a greater number of fixed gain amplifiers, and generated 22 data channels. This required use of two 14 channel FM tape recorders.

About half of the SDCS data were collected on digital field-tapes which were added in the last two years of the program. The response functions of the SDCS short-period systems had a somewhat narrower band width than the LRSM response functions, but both peaked at about 4 Hz, significantly higher in frequency than the maximum at 1 Hz in the sensitivity of the WWSSN instruments.

Acknowledgements

I thank R. Blandford, W. Dean, W. Helterbrand, F. Ringdal, C. Romney, O.D. Starkey, R. Van Nostrand and J. Whalen for patiently answering my questions. I hope they enjoyed telling me the stories of VELA-Uniform as much as I enjoyed listening to them. This work was partially supported by the Cecil H. and Ida M. Green Foundation for Earth Sciences during my tenure as a Green Scholar.

References

Agnew, D., J. Berger, R. Buland, W. Farrell, and F. Gilbert (1976), "International Deployment of Accelerometers: A Network for Very Long Period Seismology," *EOS Trans. A.G.U.*, **57**, 180-188.

Alsop, L.E., G.H. Sutton, and M. Ewing (1961), "Free Oscillations of the Earth Observed on Strain and Pendulum Seismographs," *J. Geophys. Res.*, **66**, 631-641.

Alsup, S.A., and J.W. Guyton (1964), "Operational Magnification and Physical Environment of Seismograph Stations," *Geophysics*, **29**, 188-196.

Andrew, D.B., (1965), *Six-Element Vertical Array System Design*, Technical Report No. 65-132, Teledyne Industries, Geotech Div., Garland.

Arnett, R.A., and T.W. Newhouse (1965), "Ocean-Bottom Seismograph," *Proc. IEEE*, **53**, 1899-1905.

BeAbout, E.G., H.K. Harris, R.F. Howard, B.F. Kimmler, and W.A. Johnson (1968), *Final Report Ocean-Bottom Seismograph Production and Gulf of Mexico Data Analysis*, Contract No. F33657-68-C-0242, Texas Instruments, Dallas.

Berkner, L.V. (1959), *Report of the Panel on Seismic Improvement, the Need for Fundamental Research in Seismology*, Department of State, Washington, D.C.

Benioff, H. (1962), "The Characteristics of Strain and Pendulum Seismograph Combinations," in *Proceedings of the Colloquim on Detection of Underground Nuclear Explosions*, VESIAC Special Report 4410-36-x, Ann Arbor, Institute of Science and Technology, University of Michigan.

Blaik, M. and Z. Der (1976), *Evaluation of the Korean Short Period Array*, Technical Report No. SDAC-TR-76-5, Teledyne Geotech, Alexandria.

Blandford, R.R. (1974) "An Automatic Event Detector at the Tonto Forest Seismic Observatory," *Geophysics*, **39**, 633-643.

Block, B., and R.D. Moore (1970), "Tidal to Seismic Frequency Investigations with a Quartz Accelerometer of New Geometry," *J. Geophys. Res.*, **75**, 1493-1505.

Block, B., and J. Dratler, Jr. (1972), "Improvements in the Wide-Band Vertical Quartz Torsion Accelerometer," *J. Geophys. Res.*, **77**, 3678-3689.

Block, B., and J. Dratler, Jr. (1973), "Quartz Fibre Accelerometers," *Phil. Trans. R. Soc., London*, **A 274**, 231-243.

Bradner, H. (1964), "Seismic Measurements on the Ocean Bottom," *Science*, **146**, 208-216.

Bradner, H., J.G. Dodds, and R. Foulks (1965a), "Coherence Measurements with Time Sampling Ocean-Bottom Seismometers," *Proc. IEEE*, **53**, 1906-1908.

Bradner, H., L.G. De Jerphanion and R. Langlois (1965b), "Ocean Microseism Measurements with a Neutral Buoyancy Free-Floating Midwater Seismometer," *Bull. Seism. Soc. Am.*, **60**, 1139-1150.

Briscoe, H.W., and P.L. Fleck (1965), "Data Recording and Processing for the Experimental Large Aperture Seismic Array," *Proc. IEEE*, **53**, 1852-1859.

Broding, R.A., N.J. Bentley-Llewellyn and D.P. Hearn (1964), "A Study of a Three-Dimensional Seismic Detection System," *Geophysics*, **29**, 221-249.

Bungum, H., E.S. Huseby, and F. Ringdal (1971), "The NORSAR Array and Preliminary Results of Data Analysis," *Geophys. J. R. Astr. Soc.*, **25**, 115-126.

Carder, D.S. (1963), *The Requirements of a High-Sensitivity Seismograph Station, State-of-the-Art*, Report 4410-63-X, Geophysics Laboratory, Willow Run Laboratories, Institute of Science and Technology, University of Michigan, Ann Arbor.

Carpenter, E.W. (1965), "An Historical Review of Seismometer Array Development," *Proc. IEEE*, **53**, 1816-1821.

Cawood, J.L. and R.F. McMurray (1969), *The Selection of Seismic Preamplifiers for the ALPA*, Technical Note 1/69, Teledyne Geotech, Garland.

Clark, D. (1968), *Preliminary Beamforming Study of the TFO-37 Array*, Seismic Data Laboratory Report No. 216, Teledyne Geotech, Alexandria.

Dean, W.C. (1981), *An Evaluation of Data Management R&D in VELA Uniform*, Technical Report No. AL-81-2, Teledyne Geotech, Alexandria.

Der, Z.A. (1969), "Surface Wave Components in Microseisms," *Bull. Seism. Soc. Am.*, **59**, 665-672.

Der, Z.A. (1972), *Investigation of the Signal Enhancement and Discrimination Capabilities of the Intermediate Period Strain-Pendulum Seismograph Combination at HNME (Houlton, Maine)*, Technical Report 294, contract F33657-72-C-0009, Teledyne Geotech, Alexandria.

Der, Z.A., E. J. Douze, and A.W. Simmons (1968), *Deep Well Array Operations*, Technical Report No. 68-24, Geotech, A Teledyne Company, Garland.

Der, Z.A., T.W. McElfresh, C.P. Mrazek, D.P.J. Racine, B.W. Barker, and A.H. Sproules (1980), *Results of the NTS Experiment, Phase II*, Technical Report No. SDAC-TR-78-4, Teledyne Geotech, Alexandria.

Der, Z.A., T.W. McElfresh, and A. O'Donnell (1981), *Results of the SDCS (Special Data Collection System) Attenuation Experiment*, Technical Report No. SDAC-TR-80-4 (VSC-TR-81-14), Teledyne Geotech, Alexandria.

Douze, E.J. (1964), "Signal and Noise in Deep Wells," *Geophysics*, **29**, 721-732.

Douze, E.J., and J.R. Sherwin (1975), *Deep Borehole Operation of the Borehole Seismometer System, Model 36000*, Technical Report No. 75-2, Teledyne Industries, Geotech Division, Garland.

Dratler, J., Jr. (1971), *Quartz Fiber Accelerometers and Some Geophysical Applications*. Thesis, University of California, San Diego.

Dratler, J., Jr. and B. Block (1972), "A Wide Band Horizontal Accelerometer with Preliminary Earth Normal Mode and Seismic Investigations," *Geophys. J. R. Astr. Soc.*, **27**, 337-367.

Edwards, J.P., S.A. Benno and G. Creesy (1967), *Evaluation of the CPO Auxillary Processor*, CPO Special Report No. 5, Texas Instruments Science Services Division, Dallas.

Farrell, W.E., and J. Berger (1979), "Seismic System Calibration: 1. Parametric Models," *Bull. Seism. Soc. Am.*, **69**, 251-270.

Fix, J.E. (1973a), *Strain/Inertial Seismograph Complexes*, Technical Report No. 73-16, Teledyne Geotech, Garland.

Fix, J.E. (1973b), "Theoretical and Observed Noise in a High Sensitivity, Long-Period Seismograph," *Bull. Seism. Soc. Am.*, **63**, 1979-1998.

Fix, J.E., and J. Sherwin (1970), "A High Sensitivity Strain/Inertial Seismograph Installation," *Bull. Seism. Soc. Am.*, *60*, 1803-1822.

Fix, J.E., and J. Sherwin (1972), *Development of LP Wave Discrimination Capability Using LP Strain Instruments*, Technical Report No. 72-3, Teledyne Geotech, Garland.

Forbes, C.B., R. Obenchain, and R.J. Swain (1965), "The LASA Sensing System Design, Installation and Operation," *Proc. IEEE*, **53**, 1834-1843.

Frosch, R.A., and P.E. Green (1966), "The Concept of a Large Aperture Seismic Array," *Roy. Soc. London Proc., Ser. A.*, **290**, 368-384.

Geotech (1959), *Field Measurements during Hardtack II*, Technical Report No. 59-16, Geotechnical Corp., Garland.

Geotech (1961), *Final Report on Phases I, II, and III Long-Range Seismic Measurement Program, Project VT/074*, Technical Report No. 61-3, The Geotechnical Corp., Garland.

Geotech (1963a), *Design and Recommendations for Deep Hole Installation of Bore Hole Seismometer*, Technical Report No. 63-61, Geotechnical Corp., Garland.

Geotech (1963b), *Final Report on Vertical Strain Seismograph, Project T/2029*, Technical Report No. 63-98, The Geotechnical Corp., Garland.

Geotech (1964), *Deep-Hole Seismometer (Variable Reluctance Type)*, Technical Report No. 64-108, The Geotechnical Corp. Garland, Texas.

Geotech (1966a), *Field Evaluation of the Protype Vertical Array Model 24811*, Technical Report No. 66-33, Teledyne Industries, Geotech Division, Garland.
Geotech (1966b), *Interim Report No. 3, Project VT/4051*, Technical Report No. 66-92, Teledyne Industries, Geotech Division, Garland.
Geotech (1968), *Final Report, Long Range Seismic Measurements (LRSM)*, Technical Report No. 68-19, Geotech, A Teledyne Co., Garland.
Geotech (1969), *Final Report, Project VT/8703*, Technical Report No. 69-7, Geotech, A Teledyne Co., Garland.
Geotech (1970a), *Final Report, Project VT/8703*, Technical Report No. 70-4, Teledyne Geotech, Garland.
Geotech (1970b), *Final Report, Project VT/8707, Alaska Long-Period Array*, Technical Report No. 70-39, Teledyne Geotech, Garland.
Geotech (1972), *Final Report, Project T/1703*, Technical Report No. 72-21, Teledyne Geotech, Garland.
Geotech (1974), *Project T/4107 Semi-Annual Report for the Period 15 March 1974 - 15 September 1974*,Technical Report No. 74-13, Teledyne Geotech, Garland.
Geotech (1976), *Project T/4107 Semi-Annual Report for the Period 1 March 1976 - 30 September 1976*, Technical Report No. 76-17, Teledyne Geotech, Garland.
Geotech (1977), *Special Data Collection Systems*, Technical Report No. 77-8, Teledyne Geotech, Garland.
Geotech (1984a), *Development of the Model 52500 Strain-Inertial Seismometer System (Prototype)*, Technical Report No. 83-9, Teledyne Geotech, Garland.
Geotech (1984b), *Final Report on the Model 44000 Seismometer System Development*, Technical Report No. 84-3, Teledyne Geotech, Garland.
Green, P.E., R.A. Frosch, and C.F. Romney (1965), "Principles of an Experimental Large Aperture Seismic Array (LASA)," *Proc. IEEE*, **53**, 1821-1833.
Gudzin, M.G., and J.H. Hamilton (1961), "Wichita Mountains Seismological Observatory," *Geophysics*, **26**, 359-373.
Gudzin, M.G., and E.G. Holle (1962), "Seismological Observatories," *Proc. Inst. Radio Eng.*, **50**, 2216-2224.
Gudzin, M.G., and F.M. Hennen (1967), *Final Report, Project VT/6701, LASA LP System*, Technical Report No. 67-17, Geotech, A Teledyne Co., Garland.
Hamilton, J.H. (1964), *Summary of Long-Period Seismograph Work at Geotech*, Technical Report No. 64-121, The Geotechnical Corporation, Garland.
Hamilton, J.H., and E. Stephens, Jr. (1961), "New Developments in Seismological Instruments," in *Proceedings of the Colloquium on Detection of Underground Nuclear Explosions*, edited by VESIAC staff, Report 4410-36-X, Geophysics Laboratory, Willow Run Laboratories, Institute of Science and Technology, Univ. of Michigan, Ann Arbor.
Herrin, E.T. (1982), "Resolution of Seismic Instruments Used in Treaty Verification Research," *Bull. Seism. Soc. Am.*, **72**, S61-S67.
Johnson, D.P., and H. Matheson (1962), *An Analysis of Inertial Seismometer-Galvanometer Combinations*, National Bureau of Standards, Report 7454.
Kelley, D.S. (1968), *Preliminary Evaluation of The UBSO Vertical Array*. Technical Report No. 68-51, Geotech, A Teledyne Company.
Kirkpatrick, B.M. (1968), *Long-Period Triaxial Seismograph Development*, Technical Report No. 68-20, Geotech, A Teledyne Co., Garland.
Kittel, C. (1958), *Elementary Statistical Physics*, John Wiley, New York.
Lamont-Doherty Geological Observatory (1971), *High-Gain, Long-Period Seismograph Station Instrumentation, Volume 1*, Advanced Research Projects Agency, ARPA Order 1513.
Latham, G.V. and G.H. Sutton (1966), "Seismic Measurements on the Ocean Floor 1, Bermuda Area," *J. Geophys. Res.*, **71**, 2545-2573.
Latham, G.V. and A.A. Nowroozi (1968), "Waves, Weather, and Ocean-Bottom Microseisms," *J. Geophys. Res.*, **73**, 3945-3956.

Li, T.M. (1981), *Lajitas Quiet Site Noise Study*, Technical Report No. 81-10, Teledyne Geotech, Garland.

Li, T.M., J.F. Furguson, E. Herrin, and H. Durham (1984), "High Frequency Seismic Noise at Lajitas, Texas," *Bull. Seism. Soc. Am.*, **74**, 2015-2033.

Linville, A.F., R.F. Howard, and G.D. McNeedy (1968a), *Signal and Noise Analysis Report, Aleutian Islands Experiment, Ocean-Bottom Seismographs Experiments*, Contract No. F33657-67-C-1341, Texas Instruments, Dallas.

Linville, A.F., G.D. McNeely, R.D. Bauer, R.F. Howard, and A.R. Mendina (1968b), *Final Analysis Report Aleutian Islands Experiment Ocean-Bottom Seismographic Experiments*, Contract No. F33657-67-C1341, Texas Instruments, Dallas.

Mack, H. (1966), "Attenuation of Controlled Wave Seismograph Signals Observed in Cased Boreholes," *Geophysics*, **31**, 243-252.

Major, M.W., G.H. Sutton, J. Oliver, and R. Metsger (1964), "On Elastic Strain of The Earth in The Period Range 5 Seconds to 100 Hours," *Bull. Seism. Soc. Am.*, **54**, 295-346.

McDermott, J.G., A.F. Linville, and T.W. Harley (1967), *Final Report, Kurile Islands Experiment, Ocean-Bottom Seismographic Experiments*, Contract No. F33657-67-C-0105-P002, Texas Instruments, Dallas.

McMillan, R.E. (1964), *Melton Long-Period Borehole Triaxial Seismometer*, Technical Report No. 64-89, Geotechnical Corp.,Garland.

Melton, B.S. (1976), "The Sensitivity and Dynamic Range of Inertial Seismographs," *Rev. Geophys. and Space Phys.*, **14**, 93-116.

Melton, B.S. (1981a), "Earthquake Seismograph Development: A Modern History — Part 1," *EOS Trans. A.G.U.*, **62**, 505-510.

Melton, B.S. (1981b), "Earthquake Seismograph Development: A Modern History — Part 2," *EOS Trans. A.G.U.*, **62**, 545-548.

Melton, B.S., and B.M. Kirkpatrick (1970), "The Symmetrical Triaxial Seismometer — Its Design for Application to Long-Period Seismometry," *Bull. Seism. Soc. Am.*, **60**, 717-739.

Moore, R.D., and W.E. Farrell (1970), "Linearization and Calibration of Electrostatically Fedback Gravity Meters," *J. Geophys. Res.*, **75**, 928-932.

Moore, T.C., L.H. Rorden, R.L. Kovach, and S.W. Smith (1974), *Deep Borehole Strainmeter to Measure Earth Strain*, Technical Report 428-740930, Develeo, Inc., Mountain View.

Murphy, A.L., G.P. Hade, Jr., J.M.W. Rynn and P.L. Ward (1971), "An Improved High-Gain, Long-Period Seismograph System, 1, Design and Installation at Six Sites Around the World," paper presented at 52nd Annual Meeting, American Geophysical Union.

Mykkeltveit, S. and F. Ringdal (1981), "Phase Identification and Event Location at Regional Distances using Small-Aperture Array Data," in *Identification of Seismic Sources — Earthquakes or Underground Explosions*, E.S. Husebye and S. Mykkeltveit, editors, D. Reidel Publishing Co., Dordrecht, Holland, p. 467-481.

Mykkeltveit, S. and H. Bungum (1984), "Processing of Regional Seismic Events using Data from Small-Aperture Arrays," *Bull. Seism. Soc. Am.*, **74**, 2313-2333.

North, R.G. (1977), *Station Magnitude Bias — Its Determination, Causes, and Effects*, Technical Note ESD-TR-77-85, MIT Lincoln Laboratories, Lexington.

Nowroozi, A., G.H. Sutton, and B. Auld (1966), "Ocean Tides Recorded on the Sea Floor," *Ann. Geophysics.*, **22**, 512-517.

Oliver, J., and L. Murphy (1971), "WWNSS: Seismology's Global Network of Observing Stations," *Science*, **174**, 254-261.

Peterson, J. H.M. Butler, L.G. Holcomb, and C.R. Hutt (1976), "Seismic Research Observatory," *Bull. Seis. Soc. Am.*, **66**, 2049-2068.

Peterson, J., C.R. Hutt, and L.G. Holcomb (1980), *Test and Calibration of the Seismic Research Observatory*, U.S. Geological Survey Open-File Report 80-187, 86pp.

Peterson, J., and C.R. Hutt (1982), *Test and Calibration of the Digital World-Wide Standardized Seismograph*, U.S. Geological Survey Open-File Report 82-1087, 170pp.

Phillips, J.D. and D.W. McCowan (1978), *Ocean-Bottom Seismometers for Research: A Reassessment*, Technical Note ESD-TR-78-255, Lincoln Laboratory, Massachusetts Institue of Technology, Lexington.

Pomeroy, P.W., G. Hade, J.M. Savino, R. Chander (1969), "Preliminary Results from High-Gain, Wide-Band, Long-Period Electro-Magnetic Seismograph System," *J. Geophys. Res.*, **74**, 3295-3298.

Prahl, S.R., W. Shen and R.L. Whitelaw (1975), *Preliminary Evaluation of the Korean Seismological Research Station Short-Period Array*, Technical Report No. ALEX (01)-TR-75-05, Texas Instruments, Dallas.

Prothero, W.A. (1984), "Ocean Bottom Seismometer Technology," *EOS Trans. A.G.U.*, **65**, 113-116.

Rector, R.E. (1965), *Shallow-Hole Test of Long-Period Horizontal Seismometer*, Technical Report No. 65-30, The Geotechnical Corp., Garland.

Ringdal, F., and E.S. Husebye (1982), "Application of Arrays in the Detection, Location, and Identification of Seismic Events," *Bull. Seism. Soc. Am.*, **72**, S201-S224.

Romney, C. (1964), "Combinations of Strain and Pendulum Seismographs for Increasing the Detectibility of *P*," *Bull. Seism. Soc. Am.*, **54**, 2165-2174.

Savino, J, K. McKamy and G. Hade (1972), "Structures in Earth Noise Beyond Twenty Seconds - a Window for Earthquakes," *Bull. Seism. Soc. Am.*, **62**, 141-176.

Shappee, R.M., and E.J. Douze (1967), *Deep-Well Research*, Technical Report No. 67-3, Teledyne Industries, Geotech Division, Garland.

Shen, W. (1978), "Feasibility Study of Mixed-Signal Separation Techniques," *Technical Report No. ALEX (01)-TR-78-07*, Texas Instruments, Dallas.

Sherwin, J.R., and R.D. Moore (1973), *Evaluation of Block & Moore Quartz Fiber Accelerometers*, Technical Report No. 73-2, Teledyne Geotech, Garland.

Shopland, R.C. (1966), "Shallow Strain Seismograph Installation at the Wichita Mountains Seismological Observatory," *Bull. Seism. Soc. Am.*, **56**, 337-360.

Shopland, R.C. (1968), *Multicomponent Strain Seismograph*, Technical Report No. 68-3, Geotech, A Teledyne Company, Garland.

Shopland, R.C. (1970a), *Design of Portable Strainmeter System*, Technical Report No. 70-6, Teledyne Geotech, Garland.

Shopland, R.C. (1970b), *Evaluation of Field Operational Characteristics of the Portable Strainmeter System*, Technical Report No. 70-10, Teledyne Geotech, Garland.

Shopland, R.C. (1971), *Analysis of Data from Six Portable Strainmeters in Southern Nevada*, Technical Report No. 71-20, Teledyne Geotech, Garland.

Shopland, R.C. and R.H. Kirklin (1969a), *Application of A Vertical Strain Seismograph to the Enhancement of P Waves*, Technical Report No. 69-9, Geotech, A Teledyne Company, Garland.

Shopland, R.C. and R.H. Kirklin (1969b), *Short-Period Multicomponent Strain System*, Technical Report 69-11, Geotech, A Teledyne Company, Garland.

Shopland, R.C., and R.H. Kirklin (1969c), "Application of Strain Seismographs to the Discrimination of Seismic Waves," *Bull. Seism. Soc. Am.*, **59**, 673-689.

Shopland, R.C., and R.H. Kirklin (1970), "Application of a Vertical Strain Seismograph to the Enhancement of *P* Waves," *Bull. Seism. Soc. Am.*, **60**, 105-124.

Shumway, R.H., and W.C. Dean (1968), "Best Linear Unbiased Estimation for Multivariate Stationary Processes," *Technometrics*, **10**, 523-534.

Simmons, A.W. (1969), *Long Period Triaxial Seismograph Development*, Technical Report No. 69-17, Geotech, A Teledyne Company, Garland.

Sorrells, G.G. (1971), "A Preliminary Investigation Into the Relationship Between Long-Period Seismic Noise and Local Fluctuations in the Atmospheric Pressure Field," *Geophys. J. R. Astr. Soc.*, **26**, 71-82.

Sorrells, G.G., J.A. McDonald, Z.A. Der, and E.T. Herrin (1971),"Earth Motion Caused by Local Atmospheric Pressure Changes," *Geophys. J. R. Astr. Soc.*, **26**, 83-98.

Sorrells, G.G. and T.T. Goforth (1973), "Low-Frequency Earth Motion Generated by Slowly Propagating Partially Organized Pressure Fields," *Bull. Seism. Soc. Am.*, **63**, 1583-1601.

Sorrells, G.G., and O.D. Starkey (1980), *An Assessment of the Use of Strain and Inertial Seismographs to Enhance Seismic Signal-To-Noise Ratio*, Technical Report No. 80-6, Teledyne Geotech, Garland.

Sutton, G.H., and J. Oliver (1959), "Seismographs of High Magnification at Long Period," *Annal. Geophys.*, **T15**, 424-433.

Sutton, G.H., W.O. McDonald, D.D. Prentiss, and S.N. Thanos (1965), "Ocean Bottom Seismic Observatories," *Proc. IEEE*, **53**, 1909-1920.

Sutton, G.H., M.C. Odegard, N. Mark and N.J. LeTourneau (1970), *Research in Seismology related to the Columbia Ocean-Bottom Seismograph*, Final Report H16-70-12, Hawaii Institute Geophysics.

Texas Instruments (1961), *Seismometer Array and Data Processing Systems*, Contract AF 33(600)-41840, Geoscience Division, Dallas.

Texas Instruments (1967), *Array Research Final Report*, Contract No. AF33(657)-14648, Texas Instruments, Dallas.

Texas Instruments (1968), *Operation Manual for 30-Day Ocean Bottom Seismograph*, prepared for Air Force Technical Applications Center under Contract No. F3365-68-C-0242, Sciences Services Division, Dallas, Texas.

Texas Instruments (1977), *Iranian Long Period Array Final Report*, Report No. U1-703604-F, prepared for United States Geological Survey under Contract 14-08-0001-14031, Texas Instruments Group, Dallas.

Thanos, S.N. (1966), OBS Calibration Manual, Technical Report Submitted to Office of Naval Research, Lamont Geological Observatory, Palisades, N.Y.

Thanos, S.N. and A.C. Hubbard (1966), "Two-way Hydroacoustic Communication Link for an Ocean-Bottom Seismograph," *IEEE Trans. Geosc. Elect.*, **GE4**, 17-24.

Van Sandt, D.R. and F.K. Levin, (1963) "A Study of Cased and Open Holes for Deephole Seismic Detection," *Geophysics*, **28**, 8-13.

Van Veen, H.J., J. Savino, and L.E. Alsop (1966), "An Optical Laser Strainmeter," *J. Geophys. Res.*, **71**, 5478-5479.

VESIAC (1962a), *Proceedings of the Colloquium on Detection of Underground Nuclear Explosions*, Report 4410-36-X Geophysics Laboratory, Willow Run Laboratories, Institute of Science and Technology, University of Michigan, Ann Arbor.

VESIAC (1962b), *Deep-Borehole Seismic Research*, Report 4410-16-X, Acoustics and Seismics Laboratory, Institute of Science and Technology, University of Michigan, Ann Arbor.

VESIAC (1964a), *Washington Conference Proceedings: A Review of Broad Band Seismographs to Include Digital Seismographs*, Institute of Science and Technology, University of Michigan, Ann Arbor.

VESIAC (1964b), *VESIAC Conference Proceedings: Progress of VELA Uniform Borehole Research*, Report 4410-83-X, Geophysics Laboratory, Institute of Science and Technology, University of Michigan, Ann Arbor.

VESIAC (1965) *A Bibliography of Seismology for the VELA Uniform Program*, Report 4410-81-B, Geophysics Laboratory, Willow Run Laboratories, Institute of Science and Technology, University of Michigan, Ann Arbor.

VESIAC (1971a), *A Bibliography of Seismology for Project VELA*, Report 78850-50-B, Geophysics Laboratory, Willow Run Laboratories, Institute of Science and Technology, University of Michigan, Ann Arbor.

VESIAC (1971b), *VELA Uniform Sponsored Research Publications in Seismology*, Report 78850-5-X9, Geophysics Laboratory, Willow Run Laboratories, Institute of Science and Technology, University of Michigan, Ann Arbor.

VESIAC (1971c), *VELA Seismic Information Analysis Center (VESIAC)*, Report 78850-51-F, Geophysics Laboratory, Willow Run Laboratories, Institute of Science and Technology, University of Michigan, Ann Arbor.

Weinstein, W.D. (1965), "Flexure Pivot Bearings," *Machine Design*, **37**, 150-157.

Weisbrich, R.A. (1965), "Project SHOAL Volunteer Team Program," *Geophysics*, **30**, 262-278.

Westhusing, K. (1963), "Project GNOME Volunteer Seismological Teams," *Geophysics*, **28**, 20-45.

Wolfe, R. (1966), *The LRSM Mobile Seismological Lab.*, Technical Report No. 66-27, Teledyne Geotech, Garland.

Wood, R.V., Jr., R.G. Enticknap, C.S. Lin, and R.M. Martinson (1965), "Large Aperture Seismic Array Signal Handling System," *Proc. IEEE*. **53**, 1844-1851.

Woolson, J.R. (1971), *Preliminary Analysis of the Queen Creek, Arizona (QCAZ) Strain System, Including Comparison with the TFO Long-Period Array*, Technical Report No. 271, Teledyne Geotech, Alexandria.

Woolson, J.R. (1972), *Combinations of Strain and Pendulum Seismographs to Enhance Long Period P and Rayleigh waves at Queen Creek, Arizona*, Technical Report No. 290, Teledyne Geotech, Alexandria.

Woolson, J.R., and R.L. Sax (1971), *Comparison of Teleseismic Signals Using a Vertical Pendulum and Strain System at HNME, Technical Report No 265., Teledyne Geotech, Alexandria.*

Design Criteria for Sizing Regional Arrays

John P. Claassen

Summary

A network of small arrays for in-country monitoring of a CTBT has been advocated for well-known reasons. To date, experience with regional signals and arrays has, however, been limited in comparison to teleseismic monitoring. In view of the significant differences between teleseismic and regional signals, careful consideration must be given to designing seismic arrays for monitoring at regional distances.

Considerations from detection and estimation theory have identified three criteria for sizing a regional array. The first criterion indicates that the array diameter must satisy

$$D \geq 5\lambda$$

for minimal velocity filtering and estimation. The second criterion states that accurate bearing estimates, using high or low resolution methods, require an array diameter of three or more kilometers. The third consideration states that the diameter should not exceed the signal correlation distance. As a result of these criteria, the array size is bounded above and below.

The bases for these criteria are established and discussed. The effects of wavefront distortion, receiver perturbations and signal decorrelation on array performance in light of these criteria are illustrated. The application of these design criteria is hampered by inadequate knowledge of the signal characteristics of regional events in different geologies.

Introduction

In view of the provisions of the Limited Test Ban Treaty of 1963, a Comprehensive Test Ban Treaty (CTBT) focuses on the detection, characterization and identification of underground nuclear explosions. A network of small seismic arrays for in-country monitoring at regional distances has been proposed as a method of verifying conformance to a CTBT at an acceptable level. To date, experience in evaluating seismic verification has largely been limited to events monitored at teleseismic distances. In view of the significant differences between teleseismic and

regional signals, careful consideration must be given to designing regional arrays.

The design of a seismic array entails defining such factors as size, geometry, number of sensors and the mixture of vertical and horizontal sensors. Identification of these factors requires knowledge of the signal characteristics and considerations arising from detection and estimation theory. These elements are combined to particularly address the matter of array diameter/size. The sizing of an array is important to specifying the performance of an array, defining suitable detection and estimation algorithms and allocating real estate in the treaty negotiations.

Notions from velocity estimation, bearing estimation and detection theory are integrated with known signal characteristics to establish bounds on the array size. It is shown that velocity and bearing estimation dictate arrays many wavelengths across for accurate performance. In particular, the array size is established for three bearing estimators to overcome residual phase perturbations introduced by wavefront distortions and variations in receiver characteristics. Good detection performance also dictates large arrays appropriately filled with receivers.

Although detection and estimation both dictate large arrays, the size of regional arrays is ultimately limited by the distance over which seismic signals remain coherent. To establish the available spatial coherence, prior efforts are reviewed and applied to estimate array size for the L_g phase. It is also shown that current empirical evidence isn't sufficiently consistent to specify array size for the P_g and P_n phases. Extrapolations of NORESS data (Ref. 6) suggest spatial correlation for P_g much larger than previously reported (Ref. 4). New evidence also suggests useful spatial coherence above 5 Hz for these phases.

Sizing Criteria

Results from Velocity Estimation. From Nyquist sampling theory, the spatial resolution of an array in cycles/km is given by

$$\frac{k}{2\pi} = \frac{1}{D} \tag{1}$$

where D is the array diameter. When it is recognized that $k/2\pi = f/v$, where f is the frequency and v is the velocity resolution criterion

$$\frac{\Delta v}{v} \geq \frac{\lambda}{D} \tag{2}$$

can be established at a constant frequency. To resolve velocity with 20% accuracy requires an array diameter satisfying $D \geq 5\,\lambda$. For wavelengths near 8 kilometers, the above constraint specifies an array diameter larger than 40 kilometers. This same result implies that two nearly concurrent events differing in velocity by 20% can just be separated with velocity filtering. The above results assume conventional beamforming.

Results from Bearing Estimation. Although bearing estimates haven't played a dominant role in locating seismic sources at teleseismic distances, it is conceivable that at regional distances their role may be more significant since the receivers are closer to the source. Accurate bearing estimation, on the other hand, is extremely important to high resolution beamforming for detection and signal recovery purposes. Pointing errors simply degrade the performance of high resolution algorithms.

The significance in minimizing bearing error for accurate location is evident in the graphs of Fig. 1. There it is shown that a 1° error translates into a positional error of 3 to 40 kilometers depending on the range Δ. The graphs are only intended to be meaningful if the bearing biases introduced by the medium have been removed and if position is estimated from a single array.

The ability to estimate bearing accurately depends on the estimator, the time-band width product (TB) of the signal, the signal to noise ratio

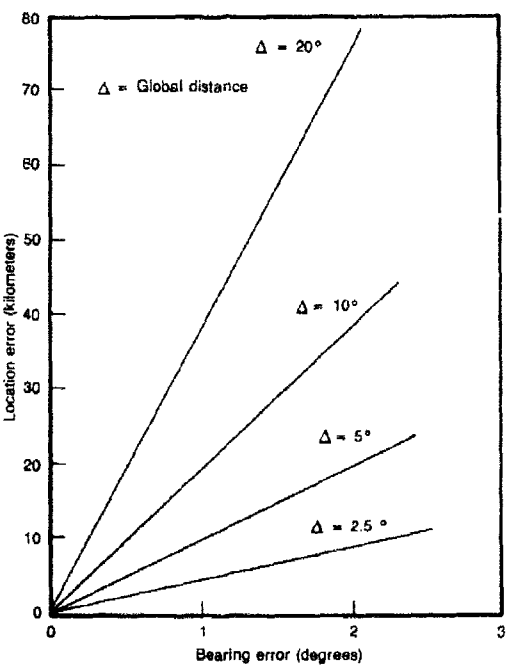

Fig. 1. The relationship between bearing error and location error.

(S/N), and anomalous amplitude and phase errors introduced by the receivers and medium in which the array is located. The designer can select an optimal estimator and size the array to abate the effect of phase errors.

To evaluate the influence of the choice of algorithm and array size on bearing estimates, Monte Carlo simulations were conducted using the concentric ring array proposed by LLL (Ref. 1) for use at NORESS. See Fig. 2 for the array geometry. The simulations estimated bearing errors for three algorithms, *viz*, 1) conventional, 2) minimum energy (Ref. 2), and 3) MUSIC (Ref. 3), when phase errors are introduced. The bearing error performance for all three algorithms was identical as shown in Fig. 3

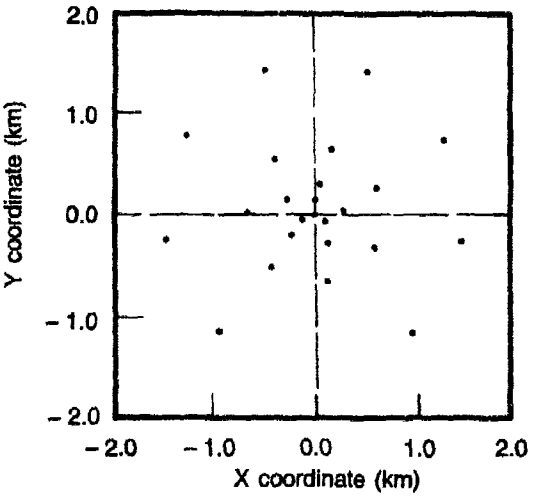

Fig. 2. Geometry of a small regional array.

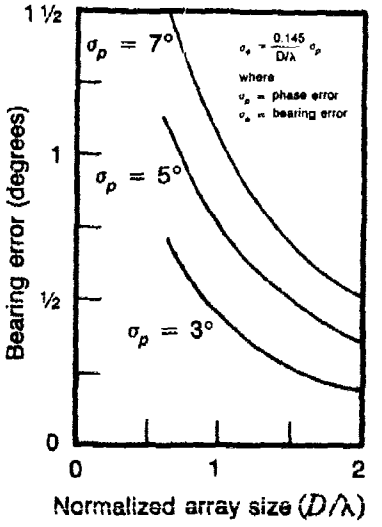

Fig. 3. Dependence of bearing error on array size and sensor phase error.

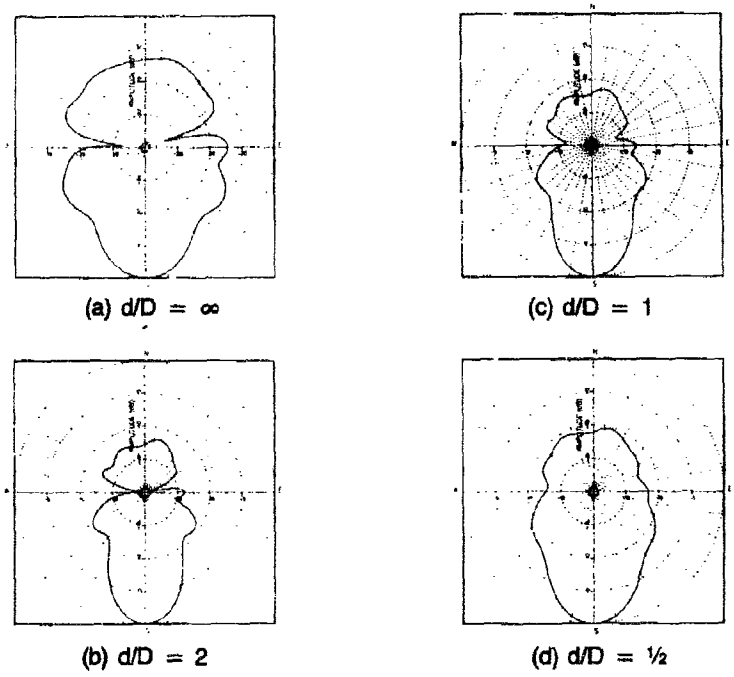

Fig. 4. Influence of spatial decorrelation on conventional beampatterns.

for the three rms phase errors ϕ_p indicated. The simulations used exact covariance matrices except as perturbed by random phase error. The errors are thought to be representative of the residual errors to which the receivers can be corrected.

The graphs reflect that the error for all three algorithms is dependent on D/λ as one would expect from elementary consid[illegible]. The empirical performance fit indicated on the figure shows t[illegible]ence on D/λ. It is apparent from these graphs that the array a[illegible]r should satisfy $D/\lambda \geq 1$.

Results from Detection Theory. Array detection and es[illegible]ation may be viewed as a spatial matched filtering process. As a consequence, when the signal field exhibits limited spatial coherence, the matched filter cannot be extended in space indefinitely in hopes of improv[illegible] performance. It is well known that the array size should not exceed the signal decorrelation distance to prevent deterioration of array performance.

The deterioration in array performance may be readily observed in the beampatterns and array gain when the decorrelation distance d is altered with respect to array size D. The decorrelation distance is defined as the distance where the signal decorrelates to 37% of its maximum.

The effect of spatial decorrelation on the conventional beampatterns of the proposed NORESS array is illustrated in the sequence of patterns of Fig. 4. As d/D decreases, the mainlobe broadens, the sidelobes rise and the nulls fill. The corresponding deteriorations in array gain appears in the graph of Fig. 5. From these results, it is evident that the constraint $d/D \geq 1$ must be imposed.

Current Evidence on Spatial Decorrelation

Since regional signals primarily propagate in the earth's crust, they are subject to scattering, multipathing, and mode conversion. As a consequence, the spatial coherence of regional phases is much less than perfect. An early effort to document the spatial coherence of regional phases was made by Mraseh, *et al.* (Ref. 4). They showed that mode theory predicts high coherence of regional signals across distances up to 10 kilometers. However, their measured coherence was lower than that predicted. In particular, they observed an anisotropic character in the L_g phase with the coherence across the direction of propagation lower than that along the direction of propagation. In contrast, P_n and P_g exhibited an isotropic coherence characteristic. The entries of Table 1 indicate their observed average decorrelation distances at 1 Hz. The investigators emphasize that the coherence of a specific event may deviate

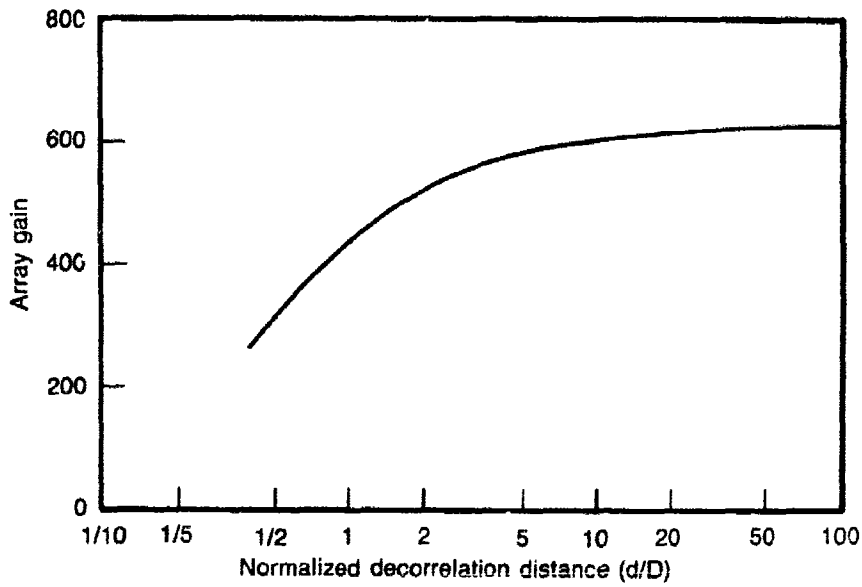

Fig. 5. Dependence of array gain on spatial decorrelation.

significantly from the average coherence. The estimates were constructed from high S/N data observed at CPO, LASA, and NORSAR.

Table 1. Decorrelation Distances Observed by Mraseh (Ref. 2) at 1 Hz

Seismic Phase	$d_{\parallel}^{*}$ (km)	$d_{\perp}^{*}$ (km)
P_n	6	6
P_g	10	10
L_g	4	3

* $d_{\parallel}$ = decorrelation distance parallel to propagation direction
$d_{\perp}$ = decorrelation distance perpendicular to propagation direction

A recent follow-on effort by Der, *et al.* (Ref. 5) has developed a deeper insight into the spatial coherence associated with L_g. At 1 Hz their YKA observations indicate decorrelation distance of $d_{\perp}$ = 5 km and $d_{\parallel}$ = 7.5 km. The same data indicates correlation distances better than 2.5 km up to 3.5 Hz. Within the same work an F statistic was used as a measure of the beamforming ability on L_g at various stations. They ranked the beamforming ability as shown in Table 2. The influence of geology on these rankings is clearly evident.

Table 2. L_g Beamforming Ability

Station	F Statistic
CPO	12
LASA	22
YKA	37
NORESS	High

Recent efforts by Mykkeltveit, *et al.* (Ref. 6) have also empirically inferred coherence at the NORESS site. Rather than estimating coherence

in narrow frequency bands, their estimates were formed over relatively wide bands throughout the lower *SP* frequency band. To more closely examine the correlation characteristics, exponential functions were fit to their measurements to estimate the decorrelation distance for P_n, P_g and L_g phases. These estimates appear in the graphs of Fig. 6 as a function of the center frequency in each band. The reader should note that the large correlation distances inferred from these data actually represent extrapolations of measurements from more closely spaced sensors. If these extrapolations are valid, then L_g exhibits a coherence characteristic similar to that reported by Der *et al.* (Ref. 5) at YKA where the geology is similar to that of NORESS. The correlation trends of P_g and P_n with frequency are, however, suspect since the correlations should decrease with frequency. The potential for large correlation distances for P_g, however, is apparent in these extrapolations.

Conclusions

Considerations from estimation theory have indicated that arrays should be many wavelengths in diameter. This translates into array diameters larger than 20 kilometers for L_g and 40 kilometers for P_n. It is clear, however, that such large diameters are prohibited by the spatial decorrelation of the regional signal fields. On the evidence in the previous section, there appears to be agreement on the decorrelation distance for L_g in shield formations. As a consequence, array diameters are limited to 7.5 to 10 kilometers at 1 Hz in such formations. The signal fields at higher frequencies exhibit smaller decorrelation lengths. Again

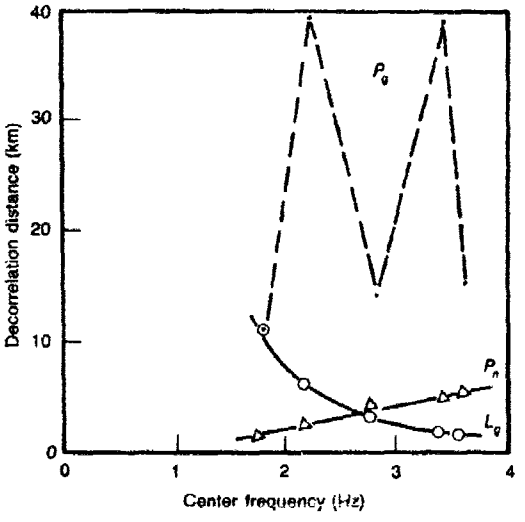

Fig. 6. Decorrelation trends with frequency as observed in Mykkeltveit's data (Ref. 6).

based on the evidence in the previous section, decorrelation distances in the vicinity of 3.5 Hz appear to be bounded between 2 and 3 kilometers. It is also apparent from the beamforming F statistic that the useable array dimension will be further restricted in more complex geologies such as found at CPO and LASA.

If a 7.5 to 10 kilometer array is installed and if processing is to emphasize the L_g phase (as it may have to in Russia (Ref. 7)), then it is clear that the array should consist of 6 to 25 sub-arrays to provided sub-optimal detection at high frequencies. The NORESS regional array under installation appears to be well-suited to high frequency L_g components.

Currently size limitations imposed on P_n and P_g phases by spatial decorrelation is not clear. Results from Mraseh (Ref. 4) and Mykkeltveit (Ref. 6) seem to indicate decorrelation distances of 10 kilometers or more for P_g and 6 kilometers for P_n at 1 Hz. The smaller distance for P_n may be attributable to the low S/N associated with this arrival rather than the actual signal coherence. The influence of geology on these two phases is not yet discernable.

If there is any potential for high frequency beamforming, the likelihood is thought to be better for P_n and P_g. Analyses of the NORSAR bulletin, for example, indicate first arrivals spanning the ½ to 5 Hz band for regional events. Analysis of higher frequency data from a 5 element NORESS array indicates P_g spectral components above 5 Hz exhibiting strong coherence between sensors separated by 1.7 kilometers. A spectral coherence estimate for this separation is shown in Fig. 7 where a coherence estimate near unity is observed at 9 Hz. The beamforming ability on this line is illustrated in the F-K spectrum of Fig. 8 for the 5-element array.

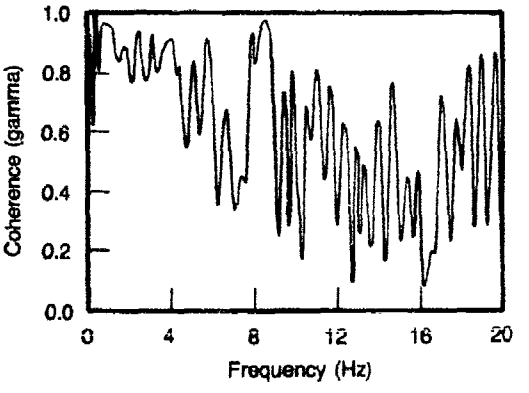

Fig. 7. Spectral coherence estimate for two sensors separated 1.7 km at NOKESS.

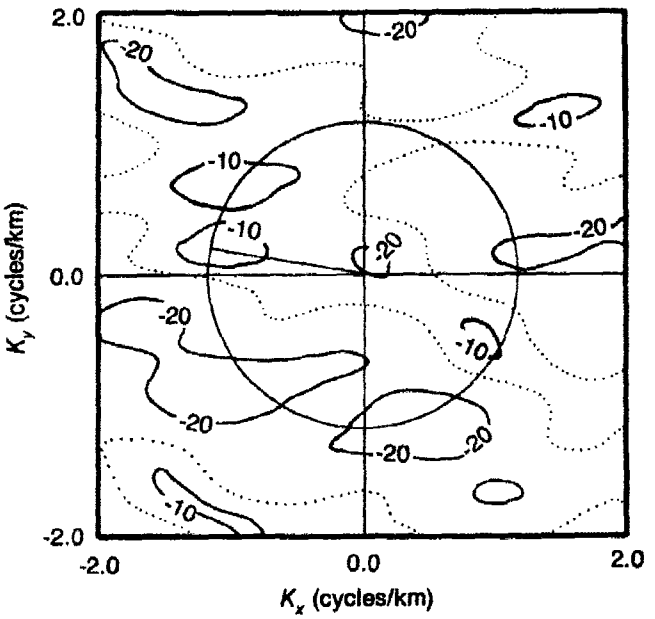

Fig. 8. F-K spectrum at 9 Hz for a 5 element array at NORESS.

The above evidence indicates the importance of estimating the spatial coherence characteristics of P_n and P_g arrivals at both high and low frequencies. A physical rationale should also be included in this kind of study so as to be able to model the coherence in different geologies and to infer array size in these geologies.

References

1. Followill, F. and D.B. Harris, *Comments on Small Aperture Array Design*, Lawrence Livermore National Laboratory, Livermore CA, 1983.
2. Capon, J., R.J. Greenfield and R.J. Kolker, "Multidimensional Maximum-Likelihood Processing of a Large Aperture Seismic Array," *Proc. of IEEE*, **55**, pp 192-211, Feb. 67.
3. Schmidt, R.O., *A Multiple Subspace Approach to Multiple Emitter Location and Spectral Estimation*, PhD Dissertation, Stanford University, 1982.
4. Mraseh, C.P., Z.A. Der, B.W. Barker, and A. O'Donnell, "Seismic Array Design for Regional Phases," *Geotech-Teledyne Report AL80-1*, Alexandria, VA 1980.
5. Der, Z.A., M.E. Marshall, A. O'Donnell, and T.W. McElfresh, "Spatial Coherence Structure and Attenuation of the L_g Phase Site Effects and Interpretation of the L_g Coda," Geotech-Teledyne, Alexandria, VA 1984 (Submitted to *BSSA*).
6. Mykkeltveit, S., K. Astebol, P.J. Doornbos and E.S. Husebye, "Seismic Array Configuration Optimization," *BSSA*, **73**, No. 1, pp 600-616, Feb. 83.
7. Hannah, W.J., Private Communication, Lawrence Livermore National Laboratory, Livermore, CA 1984.

Regional Seismic Array Program and High Frequency Instrumentation

H. B. Durham

Introduction

The RSAS (Regional Seismic Array System) is a joint DARPA/DOE development program initiated in early 1983. Like the ongoing RSTN (Regional Seismic Test Network) program, the RSAS program is intended to contribute to our knowledge and capabilities in the general area of underground nuclear test treaty compliance verification by means of seismic monitoring. General program objectives include:

1. Develop and evaluate array signal processing techniques to detect, locate and identify seismic events.
2. Develop operational concepts and techniques required to support continuous real-time array operations.
3. Develop and evaluate array system elements.

When operating, the RSAS will include the following elements:

1. Seismic Array
2. Satellite Communications Link
3. Monitoring and Recording Station
4. Data Analysis Centers

A brief description of the pertinent characteristics and functions of each of the elements follows:

Seismic Array. The array consists of 25 elements deployed at the NORSAR 06C sub-array region currently containing the NORESS experimental short-period array. Like NORESS, the RSAS will be a small aperture, short-period array. The array geometry consists of a central point plus 24 additional elements deployed on concentric rings as follows:

Ring Diameter 300 meters—3 elements
Ring Diameter 600 meters—5 elements
Ring Diameter 1400 meters—7 elements
Ring Diameter 3000 meters—9 elements

The logarithmic nature of the ring spacing is intended to provide a "broad band" capability within the constraints imposed by the maximum aperture and the limited number of elements.

All points within the array will provide short-period, vertical-axis data. To evaluate the potential utility of three-axis data, the central point and three additional points will provide two-axis horizontal data resulting in three-axis short-period data from four points in the array. The short-period data will be digitized at each array point, at a 40-sample per second rate, and transmitted via a fiber optics digital link to the array central point.

At the central point, and co-located with the three-axis short-period seismometers, a broad band system will be deployed. The broad band system will provide three-axis long-period data comparable to the SRO and RSTN long-period channels. Also, three-axis intermediate-period data will be acquired at ten samples per second providing data in the 50-second to 2-Hz region. The individual channel responses are shown in Fig. 1.

The seismometers at the central point are deployed in co-located 60-meter deep boreholes. The three-axis broad band seismometer is a Teledyne-Geotech KS36000-04 as used in the RSTN system. The three-

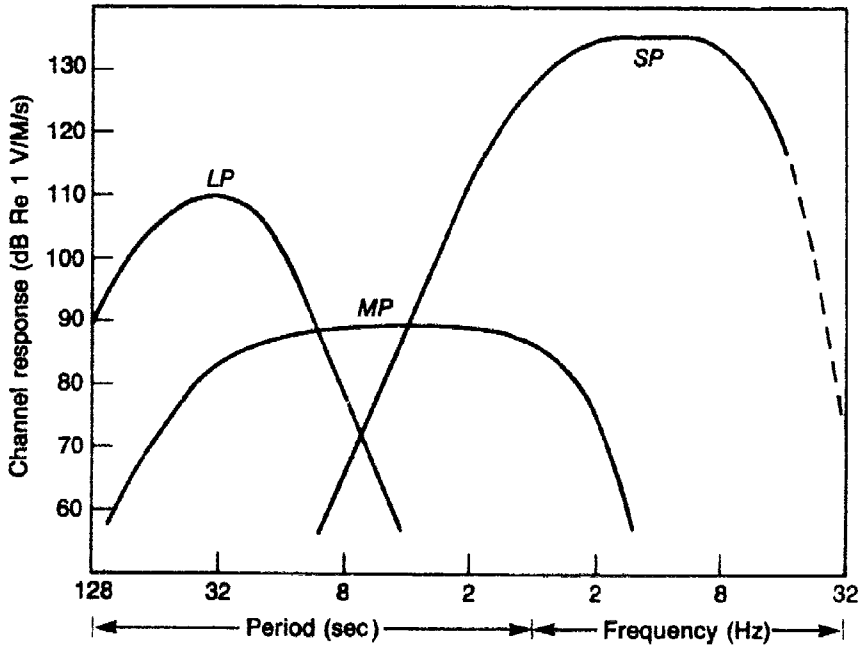

Fig. 1. RSAS channel responses.

axis short-period data at the central point is derived from a Teledyne-Geotech S3 seismometer. The S3 is a new development which incorporates three improved Model 18300 (S13) seismometers in a borehole three-axis package.

The remaining short-period seismometers are Teledyne-Geotech Model GS13s deployed in surface vaults. The GS13 is capable of either vertical or horizontal operation and is functionally equivalent to the individual S3 modules. (Specific characteristics of the GS13 and S3 modules are discussed in a subsequent section.)

Satellite Communications Link. Data from the individual array points are transmitted via a fiber optic digital data link to the central point. Data are generated at the rate of 500 bits/second/short-period channel. The broad band system and the central point state-of-health data are each equivalent to a single short-period channel. Counting all data channels and redundancy transmissions, the equivalent of 40 data channels are transmitted resulting in a data rate of 20,000 bits/second.

Data are transmitted from the array central point directly to the Atlantic Intelast satellite and returned via the down link to the U.S. East Coast. At this point, the data are transferred to a U.S. domestic satellite ground terminal and then transmitted to the domestic satellite. Data can be received from the domestic satellite at any compatible ground terminal within the U.S.

Monitoring and Recording Station. The overall status and performance of the array and associated elements will be monitored, on a real-time basis, at the monitoring and recording station. System status will be assessed by examination of state-of-health data generated at each array point and at the array central point. These data will provide a detailed definition of the system status and will also provide data required to identify potential failures or diagnose system malfunctions.

The status of each of the 39 seismic data channels will be assessed on a routine basis by examining calibration data, time series data and background spectrum data. An automatic calibration sequence will be programmed into the central point array control unit which, in turn, generates calibration commands and transmits these commands to the individual array points via a fiber optic digital data link. This data link also provides time synchronization for all array point digitizers.

In addition to monitoring and analyzing system performance data, the seismic data received from the satellite link must be de-commutated, formatted, recorded and archived for future use by the seismic community. These functions will be performed at the monitoring and recording station which will be co-located with the RSTN control and receiving station at Sandia National Laboratories in Albuquerque, New Mexico.

Data Analysis Centers. Current plans provide for real-time RSAS data links to a data center at NORSAR in Norway and, in the U.S., to data centers at the Center for Seismic Studies (Arlington, VA), Lawrence Livermore National Laboratories (Livermore, CA) and the station at Sandia National Laboratories (Albuquerque, NM). The work at NORSAR will include a continuation of current activities related to an automated, real time, detection and location capability.

High Frequency Seismic Instrumentation

During the course of the development programs for the Regional Seismic Test Network (RSTN) and the Regional Seismic Array System (RSAS), there has been a continuing effort to improve seismic instrumentation in terms of detection thresholds. This has been a joint effort involving Teledyne Geotech, the Department of Energy and the Defense Advanced Research Projects Agency. As a result of these activities, there are several instruments in existence today to support continuing studies related to the utility of high frequency (10-100 Hz) energy in detecting, locating and identifying decoupled nuclear explosions. This brief paper is intended to identify these instruments and to define their capabilities in the high frequency region.

Table I identifies the instruments that have been developed or tested in conjunction with the RSTN and RSAS programs. Figure 2 defines

Table 1
High Frequency Instruments

Designation	Description/Comments
• GS13	Surface mounting - conventional spring-mass-coil-magnet. Improved S13/18300.
• S3	Three axis borehole system using elements like GS13.
• GS21	Vertical axis borehole system. Conventional spring-mass-coil-magnet. Improved 20171/23900.
• S750	Small accelerometer using ceramic charge generators. Can be used in any axis. Surface or borehole deployment.

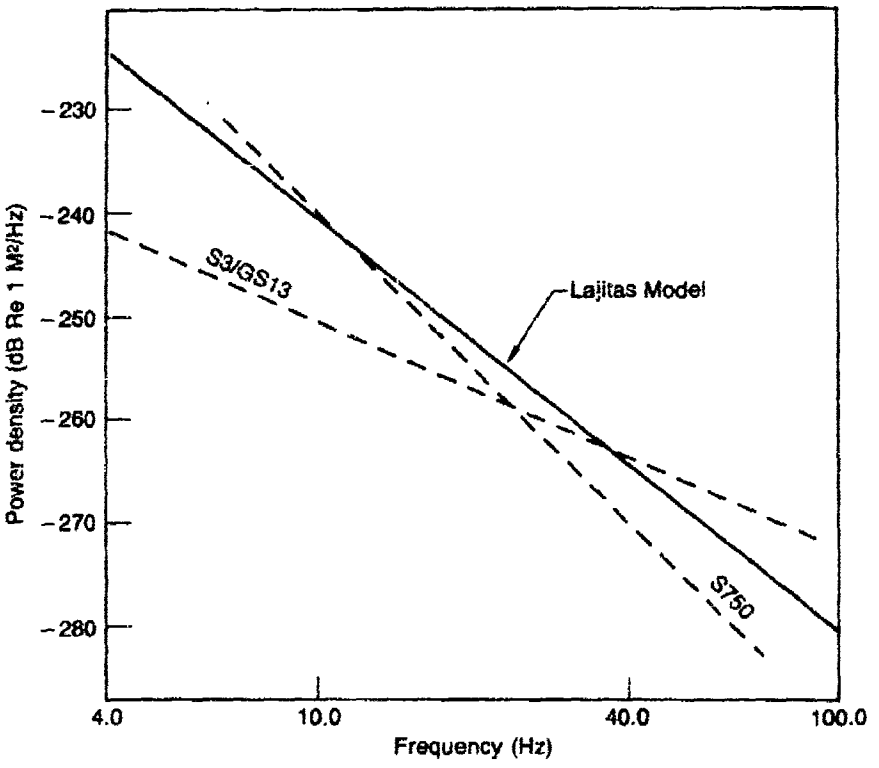

Fig. 2. System equivalent noise estimates.

system noise power density estimates, or system resolution estimates, in displacement power density (DBS-dB re 1 Meter^2/Hertz). Figure 1 also depicts an estimate of the Lajitas, Texas, quiet background spectrum in the high frequency region.

Studies at the Lajitas Station

Eugene Herrin

The character of the background noise at the Lajitas site in far West Texas has been well determined from data collected independently by our group, by Teledyne-Geotech and by Sandia. The results of studies by all three groups are summarized in Fig. 1 (from Li, Todd, J. Ferguson, E. Herrin and H. B. Durham (1984), "High-Frequency Seismic Noise at Lajitas, Texas," *Bull. Seismol. Soc. Amer.*, in press) which shows ambient noise displacement spectra for a three-component element just below the surface at Lajitas during a low-wind period. (Also see Herrin, E. (1982), "The Resolution of Seismic Instruments Used in Treaty Verification Research," *Bull. Seismol. Soc. Amer.*, **72(6)**, S61-S67). Several characteristics of the noise spectra for all components are as follows:

1. Above about 2 Hz the background displacement spectra fall of at a rate of about 40 dB/decade (12 dB/oct). Above 20 Hz system noise begins to dominate the spectra. There is no reason to believe that this fall-off in ambient noise with increasing frequency does not continue beyond 20 Hz; in fact, independent observations at Lajitas and other quiet sites using other instruments strongly suggest that the fall-off does continue to higher frequencies.

2. The ambient, low-wind background noise on all three components at Lajitas is about 10^{-24} m^2/Hz (−240 dBs) at 10 Hz. We suggest that this low spectral level is characteristic of an ultra-quiet site.

3. The origin of the spectral peaks seen between 1 and 20 Hz some of which change rapidly as a function of time, is still unknown. These peaks are very time-stationary in frequency but not in amplitude. It has been determined that the peaks below 20 Hz are seismic in nature; that is, they do not result from noise in the system.

Now that the noise at Lajitas has been extensively investigated, we have begun to examine the character of the signals seen there and the detection capability of the site particularly for regional signals. Analyses of P_n and L_g arrivals at the Lajitas site on a helicorder record were made in order to make a preliminary estimate for detection capability. Figure 2 shows the signal-to-noise observed for P_n (dots) and L_g (squares) as a

function of distance and normalized to magnitude 2.0. Based on NTS data, magnitude 2.0 is equivalent to tamped yields in saturated rock of 3 to 10 tons (nuclear). From Fig. 2 it can be seen that a signal-to-noise ratio of about one (zero dB) is seen at a distance of 600 km on the helicorder records with their limited frequency response. The analysis methods used to obtain these results are discussed in our last semi-annual report.

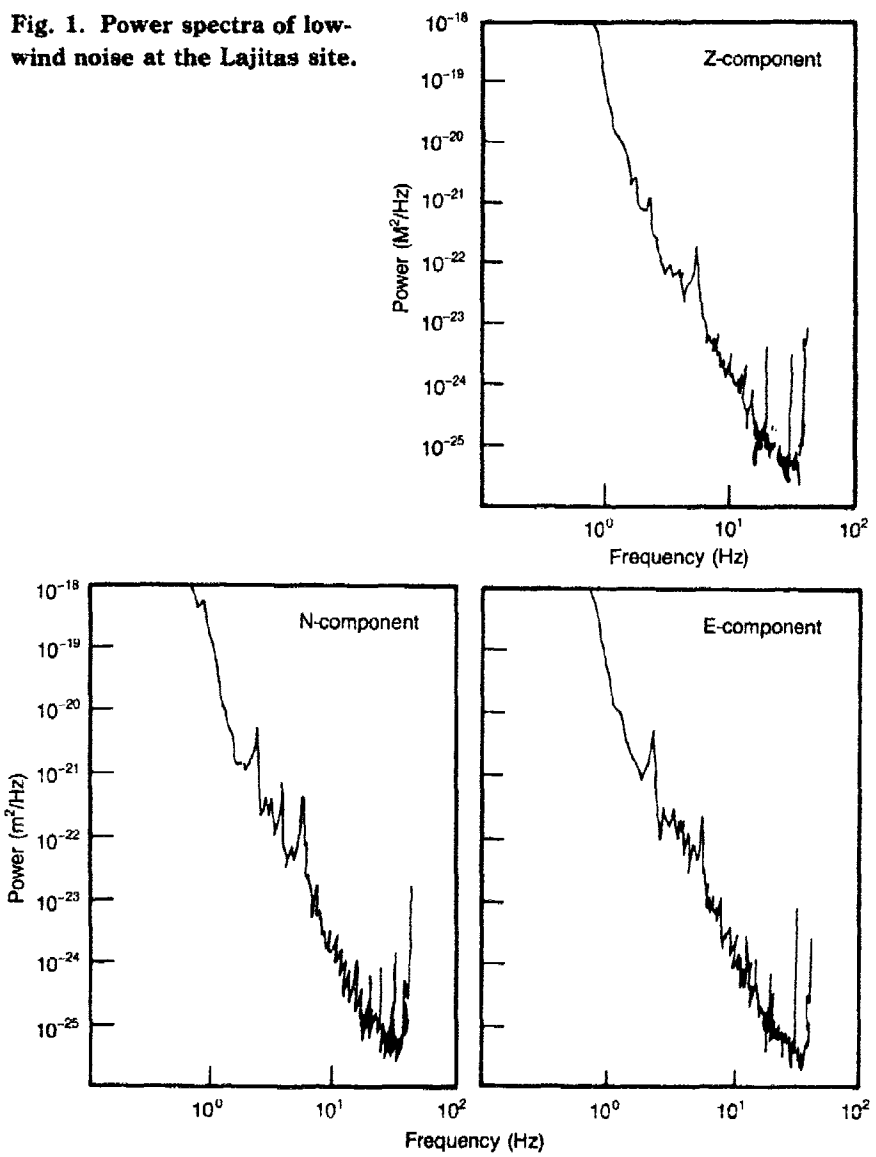

Fig. 1. Power spectra of low-wind noise at the Lajitas site.

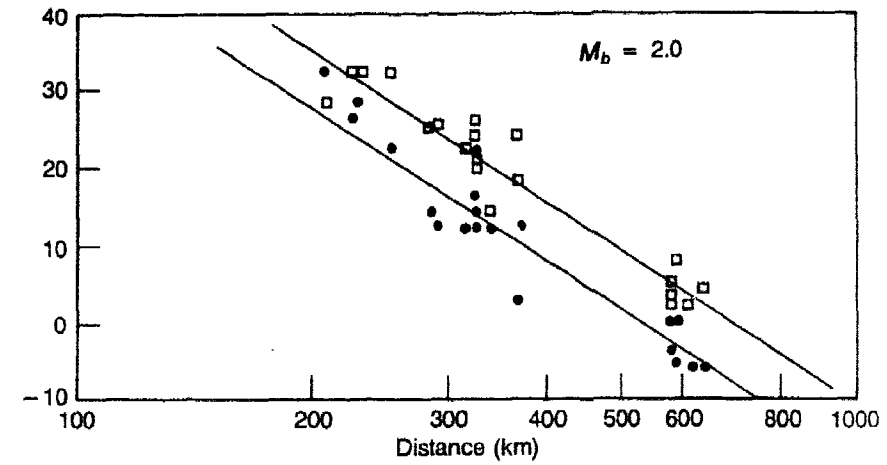

Fig. 2. Regional events seen at Lajitas.

More pertinent data on detection capability are obtained from digital recordings of regional arrivals from explosions. Figure 3 shows the first arrival from Direct Course, a 600 ton ANFO surface explosion at White Sands Missile Range about 500 miles NNW of Lajitas. The first arrival is P_n; all subsequent arrivals, such as P_g and L_g, were very strongly clipped. Using a scaling law provided by Brian Stump, we calculated that P_n from a surface HE shot of 5 to 10 tons at the same site might just be detected on the vertical component at Lajitas (s/n 0.5 to 1.0).

Figure 4 shows the vertical component of the P_n arrival time for a 5 ton HEST shot at Kirkland AFB about 725 km from Lajitas. About 1/5 of the way into the record we picked the P_n arrival. Although the signal-to-noise level is probably less than 1.0, the arrival is easily detected by the Walsh auto-detector. Figure 5 shows this digital signal after hi-pass filtering (3 pole Butterworth, corner at 2.5 Hz) and Fig. 6, after hi-pass

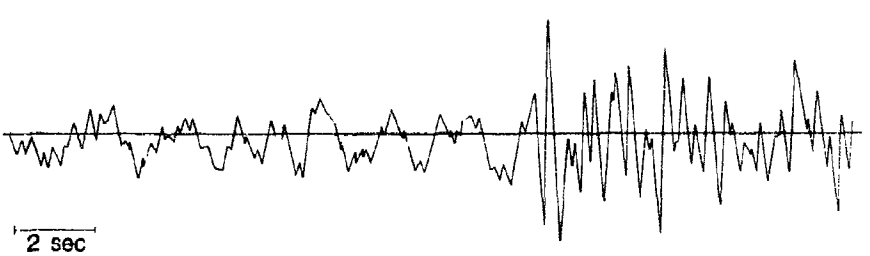

Fig. 3. First arrival from event Direct Course seen on the vertical component, short period instrument at Lajitas.

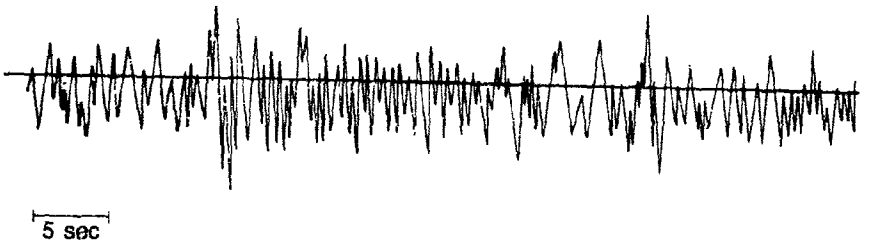

Fig. 4. P_n arrival from Albuquerque shot seen on Z-component at Lajitas.

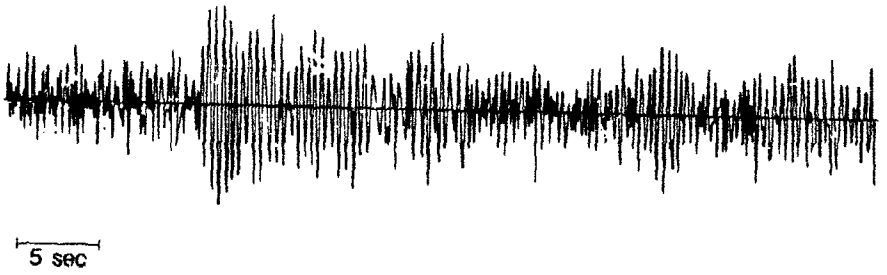

Fig. 5. Signal from Fig. 4 hi-passed filtered, corner at 2.5 Hz.

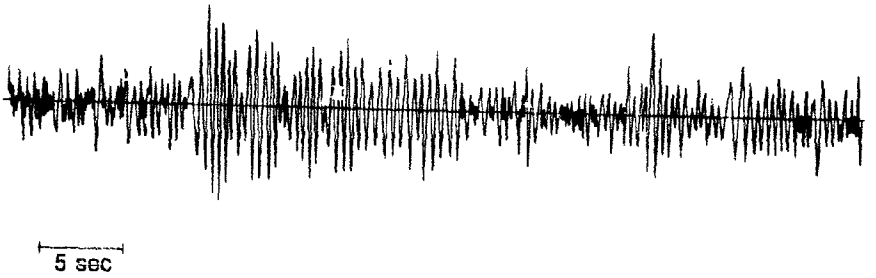

Fig. 6. Signal from Fig. 5 hi-passed filtered, corner at 1.5 Hz.

filtering (3 pole Butterworth, corner at 1.5 Hz). The signal-to-noise ratio is one or greater on either filtered record.

Following a scaling law given by Brian Stump, this HEST shot represents a seismic source equivalent to a fully tamped explosion with a yield of 1 to 1.5 tons. At the peak frequencies recorded for the HEST shot, the ratio for complete decoupling determined from the SALMON-STERLING events is a factor of 50 or less. Taking the upper value, we would predict that a single, bore-hole, vertical seismometer at Lajitas could detect a fully decoupled explosion of about 100 tons (HE) or a fully decoupled nuclear explosion with a yield of about 0.2 kt at distances of the order of 750 to 1000 km. Processing of three component data and array data at Lajitas could be expected to lower this threshold.

The path from Lajitas to Albuquerque is not one we would pick to be especially efficient for P_n propagation, because a substantial part of it lies in the Basin and Range province. For a more efficient path to the northeast from Lajitas which might be more representative of paths in the Soviet Union, we are led to speculate that a short period, state-of-the-art, three-component bore hole system at Lajitas might be expected to detect automatically the signal from a fully decoupled nuclear explosion of 0.2 kt yield at a distance of 1000 km. The consequences of such a speculation are extremely important to CTBT verification studies and, therefore, we have initiated a comprehensive research program to determine the regional detection capability at Lajitas with high confidence.

Seismic Arrays for Everyone

E.S. Husebye, S.F. Ingate, and E. Thoresen

Abstract

Seismic arrays have proved indispensible for research and otherwise proved very useful for monitoring earthquake and nuclear explosion occurrence both on local and global scales. There are generally two cost-oriented drawbacks with arrays, the modern, computerized ones like NORSAR are relatively costly to build, maintain and operate and thus not affordable for most academic research institutions. On the other hand, technically simple arrays without an integrated time basis and nondigital recording produce data which are extremely difficult to handle and analyze efficiently. In this article we discuss hardware and software requirements for automated miniarrays (comprising say eight short period seismometers) the realization of which should make such systems affordable for most research groups.

The basic concept here is that of the Remote Seismic Terminal Enhanced (RSTE), a field unit whose tasks comprise analog/digital conversion of data streams, real-time event detection processing, creation of event logs/seismic bulletins as a background processing task and finally temporary storage of original event data of significance. The software base for the RSTE is a real-time multitasking operating system, Polyforth II, and the languages are FORTH and Assembler which makes it possible to write very compact and efficient ROMable codes.

The field unit is operated by an RST which may be a much simpler device, say based on a personal computer with graphics installed in a study at home. The major tasks of the RST are to retrieve data from the field, download new operational instructions for the RSTE, redefine operational parameters, etc.

The RST/RSTE communication link may either be via the switched telephone network, satellites or other convenient means. Details on hardware, software and operation principles of the miniarray system we have in mind are given in the text. The hardware cost for a compact RSTE (excluding seismometers) field unit is estimated to roughly $5000 while an RST (personal computer type with graphics) is also estimated to roughly $5000.

Introduction-The Seismic Array Concept

The primary objectives of seismic arrays are to detect low-magnitude events and to provide a data base for further research. In the latter case the array design reflects the desire through 2-D sampling of the seismic wave field to achieve phase identification, to suppress interfering signals, and by beamforming to reduce waveform distortion caused by source/receiver scattering effects. It may be said that the concept of arrays was formally introduced to the seismological community in July/August 1958, when a committee of experts met in Geneva to consider the design of an inspection system for underground nuclear testing. Phased seismic arrays, in the sense of spatial arrangements of seismometers with a common time base, were recommended by the panel as the only effective means of monitoring underground nuclear explosions. Research programs immediately began in the U.S. and UK, and a number of seismic arrays of varying designs were built between 1959 and 1963 (for a comprehensive review, see Douglas, 1981). Under the VELA Uniform program, arrays with apertures of a few kilometers were stressed: in 1962, the UK group began to build a series of arrays with apertures almost an order of magnitude greater than the VELA arrays. The next increase in array size, both in aperture and in the number of sensors with a concomittant increase in gain by an order of magnitude, came in 1965 when LASA in Montana began operation, the NORSAR array in Norway in 1970 and the ALPA array in Alaska in 1971. The truly unique feature of the LASA and NORSAR arrays was their dedicated data centers, which permitted automated array operations comprising real-time signal detection processing, off-line signal parameter extraction (including a seismic bulletin), and remotely conducted testing and calibration of the field instrumentation.

The large research arrays were in full operation for a period of approximately 5 years, during which a large volume of high quality data was accumulated. Only NORSAR now remains in operation, although in a reduced configuration (7 subarrays out of the original 22), reflecting relatively high operational and maintenance overheads. Over the years medium-sized arrays have been operated in several countries; the most well-known appear to be Warramunga (Australia), Yellowknife (Canada), Brazilian Seismic Array (Brazil), Garibindinaur (India), Eskdalemuir (Scotland), Hagfors (Sweden) and Grafenberg (Fed. Rep. of Germany). The literature contains a vast number of contributions relating to the design principals and data processing methodologies of arrays and microearthquake networks—useful sources of references might be Husebye and Mykkeltveit (1981), Lee and Stewart (1981) and Ringdal and Husebye (1982).

Advances in array seismology remained fairly static until recently. As of today, however, the interest in array design has shifted back to small-sized arrays, primarily because of the cost considerations arising from the formidable logistics and difficulty in detecting regional and local events on large arrays. Another factor of significance is that recent and likely future advances in microcomputer technology and digital data transmission will significantly influence digital seismometry developments, *e.g.*, see Husebye and Thoresen (1984), probably to such an extent that deployment and operation of small arrays will become affordable for academic institutions with relatively low budgets. The topic of this article is to present our own attempts in designing an automated microcomputer-based miniarray system, incorporating the unique operational features of the above-mentioned large arrays while maintaining operational and manual analysis costs at a minimum. Such a field system will in the following be denoted a Remote Seismic Terminal Enhanced (RSTE) which may be operated/controlled by a personal computer (PC) serving as a host (RST). The 'seismic arrays for everyone' scenario we are attempting to realize in practice is sketched in Fig. 1. The RSTE/RST concepts were introduced by Ann Kerr of DARPA and her colleagues while a prototyped demonstration of basic operational principles was given by Husebye and Thoresen in Geneva in 1982 (see also Sec. 'Practical Experience').

As a prelude to this presentation we describe briefly and illustrate the rationale behind the NORSAR on-line and off-line processing systems, as principally similar tasks have to be incorporated into the miniarray system. We will also forward comments on desirable modifications for the design of presumably affordable RSTE systems aimed at providing observational data principally for seismological research purposes.

System Design Principles

Array operation as seen today or in the past comprises five major tasks, which naturally must be incorporated in a remotely located miniarray system. These tasks are:

i) Data transmission from seismometer to computer
ii) Real-time event detection processing
iii) Event analysis; signal parameter extraction and event log (bulletin) creation
iv) External hardware testing and operational software modifications
v) Communication, data storage and exchange.

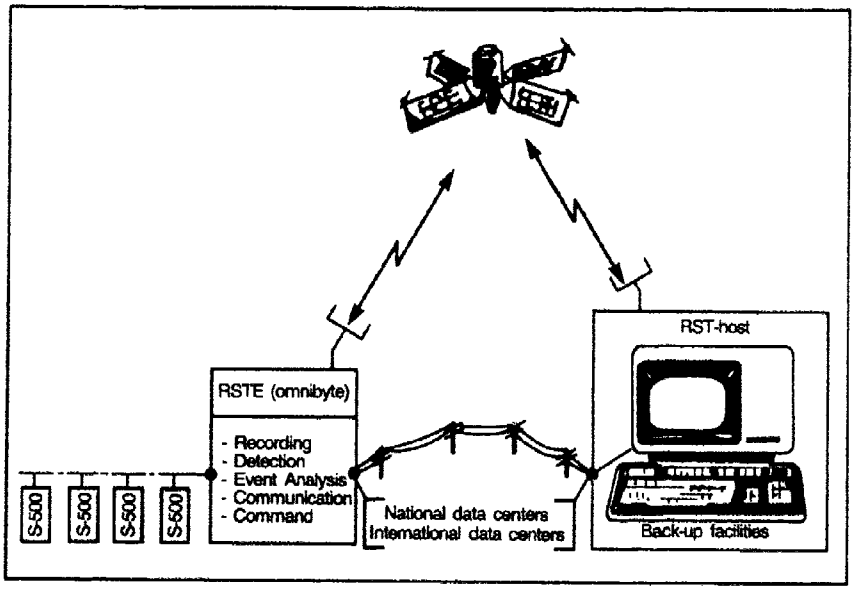

Fig. 1. Illustration of the RSTE/RST concept (Remote Seismic Terminal (Enhanced)). The RSTE is a specialized minicomputer system in the field whose main tasks are to sample, control and analyze outputs from an array of seismometers. It is remotely controlled, including options for software modifications, from an RST or host computer which even may be of the 'personal computer' type. Back-up facilities may comprise a printer and extra data storage on disk or tape. The only similarities between the RSTE and RST are the communications protocols for transfer of selected "raw" data and analysis results from field to host, and down-loading commands in the RSTE system from the RST. National and international seismological data centers may be granted permission to independently extract data and/or analysis results from the RSTE or RST.

Data Transmission from Seismometer to Computer

For the large-aperture arrays the seismometers are clustered in subarrays (see Fig. 2), the hub of which is a central terminal vault (CTV). Data transmission from the individual seismometers to the CTV is *via* trenched cables in an analog form. Here the analog signals are converted to digital form, multiplexed and transmitted *via* ordinary telephone lines (2400 baud transmission rate) to a computer center, which may be located hundreds of kilometers away from the field installations. *All* data processing is performed at the computer center.

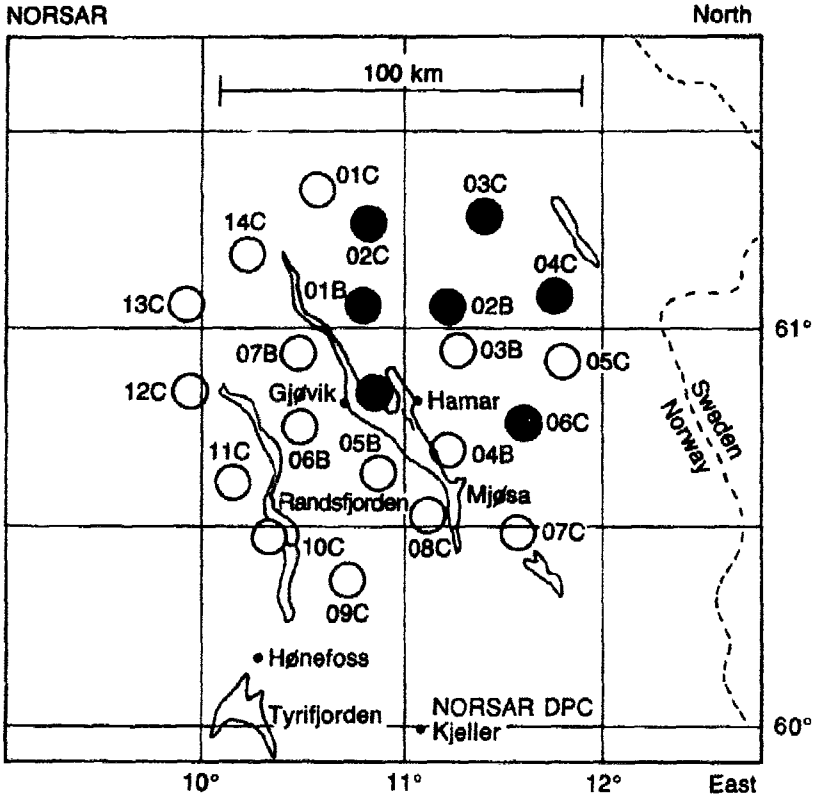

Fig. 2. The NORSAR array configuration. Each circle represents one subarray consisting of 6 short-period seismometers and one 3-component long-period seismometer. All 22 subarrays were in operation from 1971 to 1976, where a subset of 7 subarrays (filled circles) have been kept in operation since then.

Comments. For a research array it is essential that most of the data processing takes place in the field, *i.e.*, close to the field installations in order to save on costly transmission fees charged by local telecommunications utilities. The point is simply on average the recorded signal data of interest may amount to about 15 minutes/day, and there is obviously no need for a permanent line to transmit such a moderate data volume.

Real-Time Event Detection Processing

This is a 3-step process, which comprises noise suppression, detector design per se and determining an acceptable false alarm rate. The following comments apply:

Noise suppression. This is achieved in two independent ways, namely, through simple bandpass filtering (recursive Butterworth filters are widely used) and beamforming/stacking. In the latter case the (approximately valid) assumptions are that signals are identical and noise uncorrelated, so a $\sqrt{N}$ (N = number of sensors) signal-to-noise improvement is achieved. The NORSAR beam deployment is shown in Fig. 3; notice that beamforming is a computer-costly operation, as very many beams must be formed to ensure an adequate coverage of seismic zones of interest.

Detector design. The purpose here is simply to detect potential signals in ambient noise, and such a search is usually performed almost

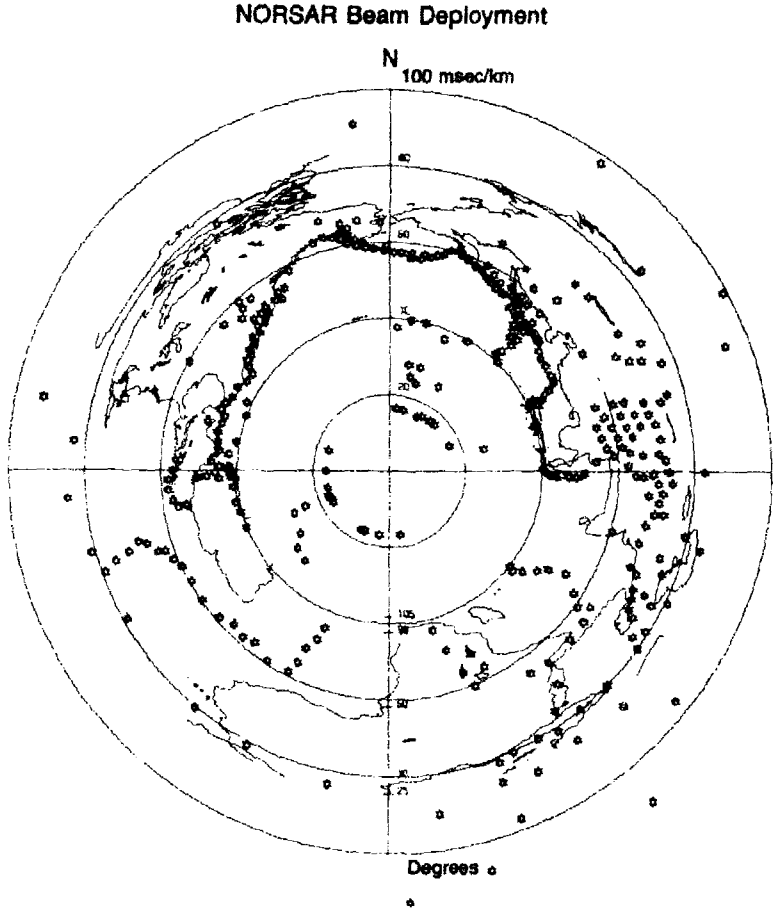

Fig. 3. The NORSAR full beam deployment in inverse-velocity space for real-time event detection. The highest density of beams corresponds to the most active seismic regions.

continuously in real time on the beam trace or individual sensor traces. The type of detector most commonly used in seismology is tied to comparing average signal power (or rectified amplitudes) in a short term window (STA) with a similar one estimated over a long term window (LTA). Whenever the STA/LTA-ratio exceeds a preset threshold, a detection is declared as illustrated in Fig. 4. Over the years many types of detectors have been suggested in the seismological literature (*e.g.*, see Ringdal and Husebye, 1982 for references), but few if any seem to perform significantly better than the STA/LTA. In addition, STA/LTA remains attractive due to its simplicity of real-time implementation.

False alarm rate. As mentioned above when STA/LTA exceeds a threshold a detection is declared which might be either a noise wavelet

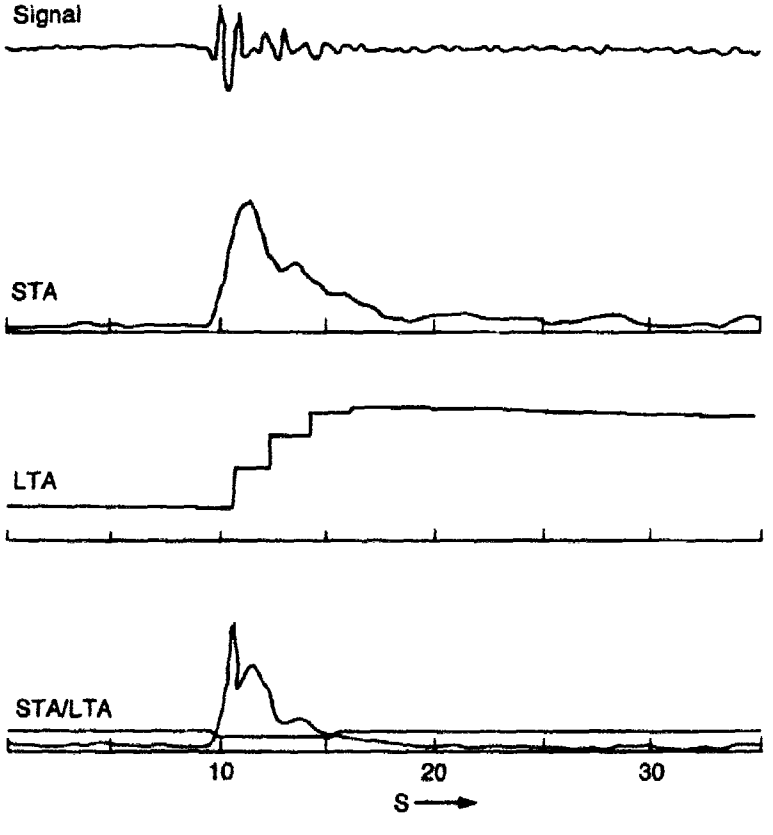

Fig. 4. NORSAR beam, STA, LTA and STA/LTA traces from an earthquake in Tsinghai, China, 27 Jan 1970. STA integration time is 1.8 seconds and LTA updating rate 5/9 Hz. The short line above the STA/LTA curve indicates detection state, and the line crossing the curve is the threshold.

or a seismic signal generated by an earthquake or underground explosion. If the threshold is lowered, the number of false alarms per unit time increases much faster than those tied to the likely occurrence of seismic signals, as illustrated in Fig. 5. In other words, to avoid overloading the array processing system, the threshold may be set such that the average false alarm rate amounts to 1 to 2 per hour. It should be added that the false alarm rate is not only dependent on number of tests performed but also on noise whiteness; in the latter case the observed increase in false

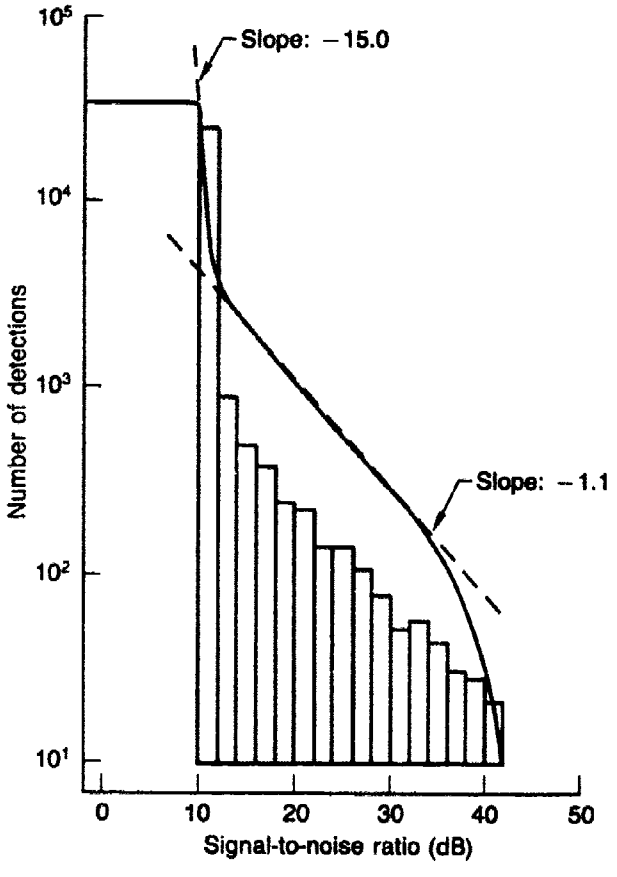

Fig. 5. Number of NORSAR detections as a function of STA/LTA ratio for the period July-December 1972. For decreasing "threshold" values, particularly below 12 dB, the number of detections increases sharply. Most of these are false alarms as the line with slope −1.1 indicates the number of occurring earthquakes to be expected on the basis of earthquake recurrence relationship ($\log N = a + bM$).

alarms during night time has been credited to a decrease in relatively high-frequency cultural noise (Steinert *et al*, 1977).

Comments. For an array aimed at recording seismic events for use in a research context which requires a reasonable signal-to-noise ratio, the NORSAR detection processing scheme can be simplified and thus perform with less computing requirements. The essential feature is to abandon the beamforming process, and instead run STA/LTA threshold tests on individual sensor traces. Detection declaration might then be a voting process, *i.e.*, event detection is declared when, for example, half of the sensors exceed threshold tests within a time window corresponding to the propagation time for L_g across the array. In short, a 'beamforming' detector optimizes event detectability in specific regions, while a 'voting' detector has a relatively lower but uniform global detectability, as implicitly demonstrated in Veith's (1981) Walsh-detector experiment. An example here might be illustrative; a miniarray of 10-15 sensors may give a beamforming gain of 10-12 dB at best, while the net difference *vis-a-vis* for a voting detector threshold would be around 4 dB (*e.g.*, see Ingate *et al.*, 1985). This is equivalent to a detection threshold difference of 0.2 m_b units, which is insignificant in a research context.

Event Analysis

On the basis of declared detections and associated original sensor recordings, event analysis is aimed at extracting signal parameters like phase arrival times, amplitude and period (Level 1 data), create an event log or seismic bulletin and finally store relevant parts of the signal wave train (Level 2 data). In the NORSAR system this process is automated but analyst intervention is needed in about 70% of events identified as real signals. Practical problems often arise from sidelobe detections; secondary phases may be detected on other beams and classed as a *P*-wave from a separate event, *etc*. However, most of these intricacies are easily handled by an experienced analyst.

Comments. In our RSTE system the event analysis would be performed in the field, that is, without any analyst intervention. The small aperture of such arrays permits the use of frequency-wavenumber (f-k) analysis (*e.g.*, see Fig. 6), the outcome of which, in combination with dominant signal frequency should suffice for a rather unique phase identification, *i.e.*, differentiate between P_g, P_n, S_n, L_g (local and regional phases) and teleseismic *P*. As regards epicenter locations small-aperture arrays would have a rather poor performance for teleseismic events ($\Delta > 30°$) unless seismicity information is incorporated. For example, epicenter location can be tied to an event's azimuth bearing intersecting

a seismicity zone like those of mid-oceanic ridges. As regards picking onset times new techniques have been proposed recently which seem to work remarkably well; reading accuracy to the nearest 0.1 second (Allen, 1982). The most important task of the event analysis is nevertheless to ensure that significant signal (Level 2) data are not lost.

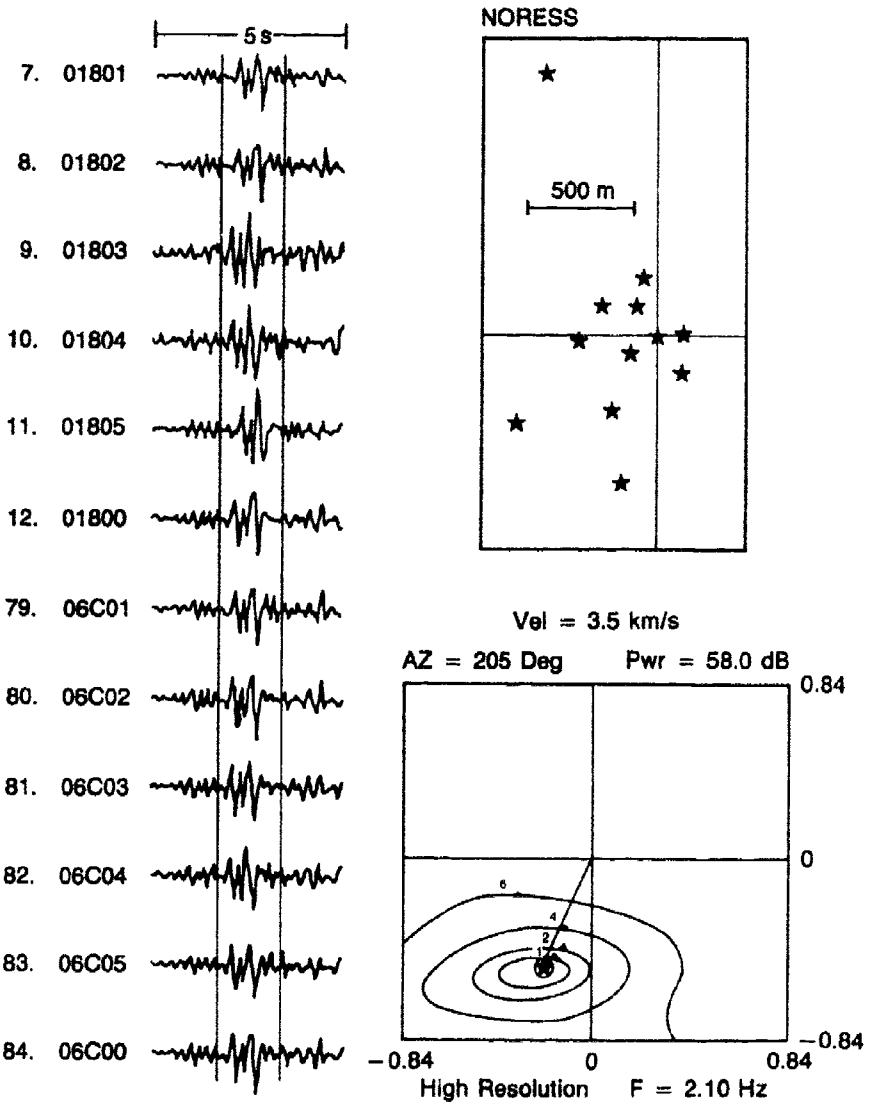

Fig. 6. Frequency-wavenumber analysis results for an L_g-recording by the NORESS miniarray temporarily installed within the NORSAR subarray 06C. The numbers to the left reflect the original sensor notations.

External Hardware Calibration and Software Modification

From the NORSAR data center at Kjeller seismometer response tests are performed by subjecting instruments to steady-state sine pulses or multifrequency signals. The long-period instruments can even be calibrated by activating small electromotors in the instrument vault. Software modifications are performed directly in the data center as no computer handling is performed in the field.

Comments. A mini-array would probably be equipped with modern, stable short-period seismometers for which simple response test should suffice. Malfunctioning instruments can easily be replaced by new ones or actually a double set of instruments may be used. As regards software modifications, such an option must be available and moreover be simple to implement through an RST (host) which can, in turn, download operational parameters to the field computer (RSTE).

RSTE/Miniarray System Design

Many of the portable seismic instrument systems developed in recent years make use of digital recording on magnetic tape. The digital method produces records of high quality, but suffers from the inherent disadvantage that recording time with standard tapes is limited to a few days or weeks; the problem is especially pronounced with systems recording on compact cassettes. Other drawbacks of such systems are the manual aspect of operation, mini-tape conversion to computer-readable tapes is slow and finally the long time lags involved from the recordings in the field until the data are available to the seismologists.

The miniarray system we are now designing may be termed a second-generation RSTE/RST system, as our first generation, tied to a small North Star minicomputer, already has been demonstrated to work satisfactorily (*e.g.*, see Husebye and Thoresen, 1984.). Design considerations here are to:

- take advantage of recent improvements in communication systems and advances in microcomputer technology
- to produce a presumably affordable seismological recording system that can retrieve, process and transfer data in automated and semi-automated modes from an array remotely located
- to produce continuous/detected data from an unattended array that is immediately available to the user, thereby severing links with slow and cumbersome centralized data centers. Adding a color graphic display option to the host computer entails that waveform displays and

associated analysis results can easily be visually assessed by the user even if the RST is based on a personal computer set-up

- to produce a mobile and interactive system that allows the user ultimate flexibility in creating his own data base.

Hardware Configuration

The hardware system, schematically shown in Fig. 6, is segmented into three parts: i) field installation, ii) host computer, and iii) field/host communication linkage. The necessary details here are as follows:

i) Field instrumentation prototype.

- Omnibyte 68K1A Multibus CPU
- 1 megabyte random access memory (RAM)
- 8 channels 16 bit analog-to-digital (A/D) converter
- 20 megabyte Winchester disk
- 1.2 megabyte floppy disk
- 8 Teledyne-Geotech S-500 seismometers including field amplifiers

Under consideration:

- Marinco APB-3024 array processor board. The arithmetic section can deliver up to eight million 24-bit floating-point operations per second. A FFT on a 128 sample data series takes 4 ms.

Comments. The Omnibyte minicomputer is powerful and consequently relatively expensive. Its choice was motivated by flexibility in software development for a prototype system. Adding a multiplexer to the A/D converter, it can handle up to 32 channels (differential inputs or 64 single-ended channels), although A/D conversion and multiplexing 8 channels of 16 bits requires 4 ms. We are considering a double input from each seismometer; one unfiltered and one analog bandpass filtered channel. The S-500 seismometer is inexpensive and completely portable without the need for a mass lock. It can be operated as either a vertical or horizontal instrument in a variety of environmental conditions. Peaked at 1 Hz, the instrument response is virtually flat to 100 Hz.

ii) RST computer configuration.

- Personal computer (PC, IBM compatible) with the Polyforth operating system and language
- Color graphics option required for waveform display.

Comments. Any reasonable computer may serve as host, although use of a PC is to emphasize the personal seismometry aspect.

iii) RSTE/RST communication linkage.

- Data exchange and communication between field installation and host computer can be achieved in many ways: via the switched telephone network, radio telemetry, dedicated data links and satellite communications. Many options are available (*e.g.*, see Kirstein (1974) and Anonymous (1983)), but here we refer to probably the simplest means available, *i.e.*, the switched telephone network, which is accessible by use of appropriate modems.

Comments. An advantage in using the telephone network is that the host also can easily communicate with other centers locally and/or abroad and vice versa. Also, no costly extra hardware is needed, and with the data processing in the field, transmission loads are kept at a minimum.

Miniarray Software System

The software base for this system (illustrated in Fig. 7) is a real-time multitasking operating system, Polyforth II from Forth Inc. (Whitney and Conrad, 1983). The languages are FORTH and Assembler, which makes it possible to write very compact and efficient ROMable code. This is a very important point, since we plan to build a complete solid-state field version. Multitasking capability enables simultaneous data collection, detection processing, temporary data storage, communication, *etc.* It also allows for built-in 'watch dog' functions in the unattended field unit, *e.g.*, restarting the system in case of an uncontrolled abort. Important, typical scientific languages like Fortran, Pascal and PL/I are relatively inefficient for handling real-time multitasking jobs. FORTH is considerably more compact than these languages as it is built on functions that are like subroutine calls. Time-critical routines may be coded in Assembly language.

The operating system itself, complete with virtual disk I/O, Assembler, compiler and screen editor, occupies less than 16 kilobyte of the system's 1024 kilobyte of memory. The application software code is estimated to occupy another 16 kilobyte, leaving almost a full megabyte for buffers and event storage. Expanding RAM to the maximum 16 megabyte, using 256 kilobyte chips, may be done using only 4 standard memory cards; the current system uses only 2 cards of 512 kilobytes each.

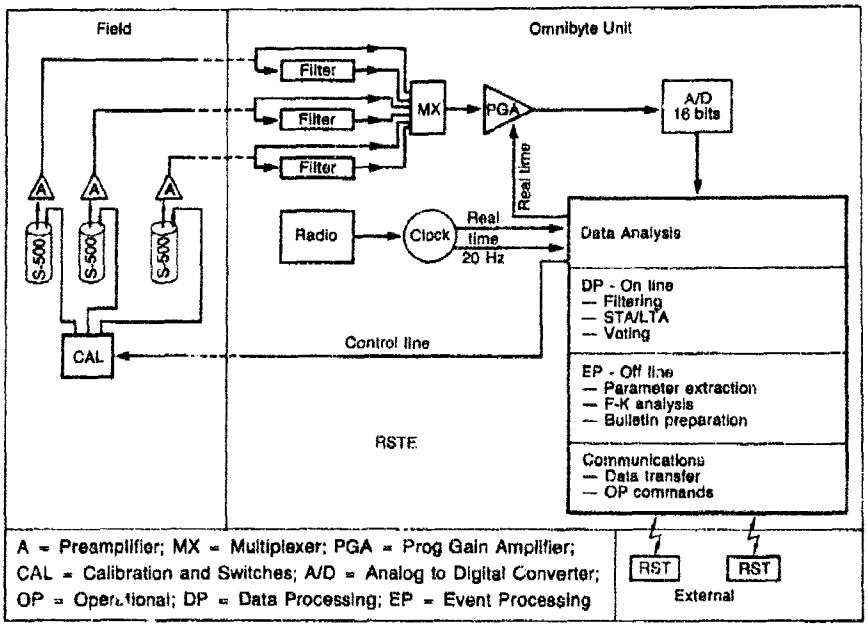

Fig. 7. The RSTE hardware configuration as detailed in test plus the essential steps involved in the data analysis centered on the powerful Omnibyte minicomputer. Using a multiplexer the A/D converter can handle up to 32 channels, which, if desired, permits seismometer inputs to be split in two, for example, an unfiltered and an analog-filtered channel. Such an option would reduce the CPU-load during the on-line detection processing.

In time, of course, a low-power unit will be adapted for use. Such a unit will obviate the need for high-power consumption disk drives through use of very large RAMs, bubble memories or other types of low-power mass storage devices. Such a system will be able to operate independently in very remote regions for several months using only solar cells and/or batteries. Polyforth's ability to generate complete ROM-able applications is of major importance in this context.

Present Field Array Software Functions

The following functions/tasks are now operative

- Analog seismic data collection, A/D conversion, filtering, and real-time event detection processing.
- Detected event cataloging and relevant data storage.
- Demand and automatic digital seismic data transfer over the switched telephone network.

- Demand and automatic control of the conversion, filtering and detection processes.

Software for extended analysis of detected events (functions described in a previous section) are now under development and implementation.

RST (host) Computer Software Functions

The major task of the host (PC) is to serve as the terminal emulator for data extraction, control and status testing of the field recording system as illustrated in Fig. 8. Available functions via modems are:

- A/D converter gain and speed settings, and channel selection
- Filter parameter setting
- Detection algorithm(s) and parameter selection

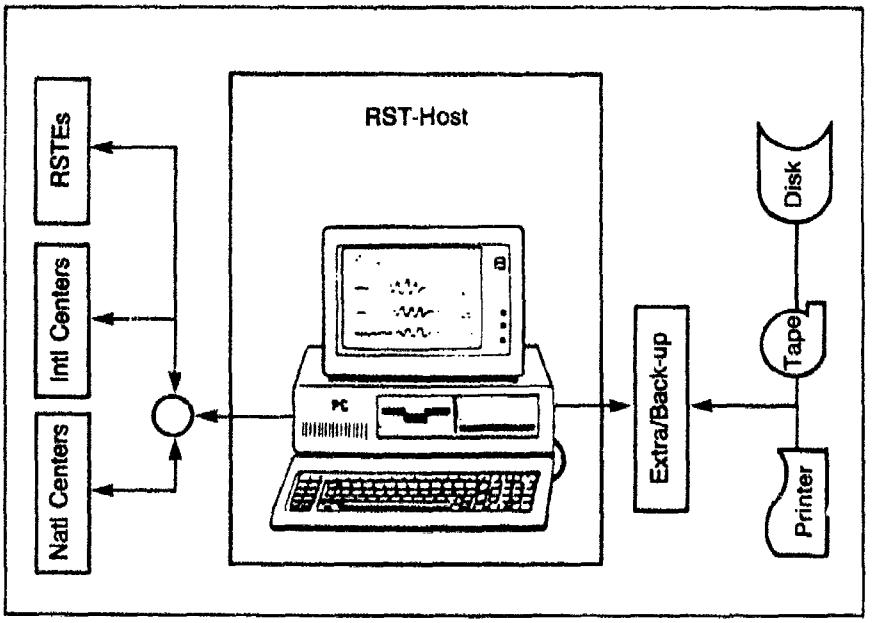

Fig. 8. The RST (host) system configuration built around a personal computer (PC), preferably IBM-compatible. This is a minimum configuration, intentionally displayed in order to emphasize the personal aspect of 'seismic arrays for everyone'. As mentioned in the text any reasonable computer installation can serve as a host for several RSTE's and otherwise communicate with a multitude of RST's, national and international data centers.

- Directory display of detection log and stored events detection log (Level I data)
- Transmission of selected event waveform (Level 2) data
- Downloading new programs and operational parameters
- Exchange of data files stored on the RSTE's optional disk.

Other more generalized tasks under development are:

- Data base and receiving station for remote RSTE's
- Data base and network node for the exchange of waveform files, bulletins and messages
- Graphic work station for analyzing waveform data using the graphic display, light pen and plotter.

The latter task relates to interactive operations, which might provide an analyst considerable flexibility in seismogram analysis work if such use is deemed desirable.

RST/RSTE Computer Communication-the SAFT Protocol

Computer-to-computer linkage via switched telephone networks, data links or satellites was established already in the early 1960s and is in widespread use today. An outstanding example here is the so-called ARPANET linking together major computer centers in the USA, and also with a line to Europe (NORSAR) (*e.g.*, see Kirstein, 1975). The protocols in common use here like HDLC, SDLC, DDCMP, *etc.*, for handling the data transfers require special hardware and software at a substantial cost, and therefore make themselves unsuitable for personal computer usage. A viable alternative here is the SAFT protocol (a simple ASCII File Transfer system—Fink *et al.*, 1981) specially designed for utilizing a standard RS 232 port, cheap modems and dial-up telephone lines. Moreover, the SAFT software, available for most types of computers, appears to be implemented on very many academic research computers. In our RST/RSTE experiments SAFT has been exclusively used for data transfers and the only problems encountered have been tied to mismatch of modems. For example, the European standard modems differ from the US standards, so special-purpose ones have to be used for intercontinental data transfer. However, European standard CC ITT V23 modems are compatible with US BELL 212J at 1200 baud. Finally, to be fair it must be stated that we do not believe that SAFT is the answer to all communication problems, but for transfer of modest amounts of

data, messages, meeting abstracts, *etc.*, it has some distinct advantages compared to the mentioned 'network' protocols.

Recently data transfer via satellites whose operations are not controlled by national telecommunications authorities have attracted the interest of geoscientists. For example, Level 1 data are transmitted to international seismological centers via the WMO/GTS (World Meteorological Organization) communication network; data collected by oceanographic buoys in remote seas are transmitted via orbiting ARGOS satellites and the same applies to seismometers monitoring Etna's volcanic activity (Dr. Pouppinet, Grenoble, pers. comm.). Geophysical observatories in Antarctica communicate via the geo-stationary INMARSAT satellites (special permission) using their own ground stations.

Cost Breakdown

It may be of interest to provide a cost breakdown of the separate units constituting the 'second-generation' prototype RSTE; Host or RST and a stripped RSTE version. The prices quoted are in U.S. dollars approximate, and may vary considerably according to country and with time.

RSTE Field Installation

Omnibyte 68k 1A multibus CPU	$13,000
16 bits A/D converter	1,500
20 M-byte Winchester disk and 1.2 M-byte floppy disk	2,000
1 M-byte RAM modem	1,500
8 S-500 seismometers	6,500
Cables, preamplifiers, etc.	1,500
Total	$26,500

Number crunching in the field is feasible using, for example, Marinco APB-3024 array processor board with a unit cost of approx. $4,500.

Stripped RSTE Version (Excluding Seismometers)

CPU card	$1,000
A/D converter	1,500
4 M-byte RAM	3,000
Modem	500
Total	$6,000

RST Computer	
PC (IBM compatible)	$2,500
Graphics software plus color monitor	1,000
Modem	500
Total	$4,000

Comments. Software development costs are excluded in the above price estimates. Otherwise, we remark that the very strong competition in the computer electronics field is likely to ensure falling hardware prices in the years to come or alternatively more computing power and disk storage for the dollar. Also, the RST functions may be handled by the institute computer with hardly any extra cost.

Practical Experience—the Geneva Experiment

The science of seismology is of political interest in the sense that underground nuclear explosions only can be detected by seismic means (*e.g.*, see Husebye and Mykkeltveit, 1981). International disarmament negotiations in United Nations' regi are largely delegated to the Conference of Disarmament (CD) whose member states regularly convene in Geneva. The political grouping has established an Ad Hoc Group (not resricted to CD member states) for providing technical (seismological) advice on a monitoring system for underground nuclear tests. As part of the Norwegian contribution to the Ad Hoc Group's work, the 'first-generation' RST/RSTE functions were demonstrated from the top floor restaurant in the UN headquarters for an audience of scientific experts and diplomats. The installation of the RST, comprising a North Star microcomputer, terminal, printer, graphic display and modems (SAFT communication protocols used) was uneventful and took only 30 minutes. The actual experiment was essentially a 3-step process, namely:

- Step 1. RST to RST communication. Automatic dialing (using Bell 212 modems) and log-in on a PDP 11/44 in USA (DARPA data center in Rosslyn, VA) for transfer and subsequent display of waveform (Level II) data and bulletins (Level I data).
- Step 2. RST to RSTE communication. This involved dialing and log in on a PDP 11/34 at NORSAR, Kjeller, Norway, extracting real-time information on the status of the seismic network in southern Norway. The detection log was used to select a few events for display and analysis.

- Step 3. This involved calling a Northstar 'sister' RSTE with seismometer installed in a private study in Trondheim, Norway. After establishing the modem link, we were able to demonstrate most of the RSTE functions described in the previous section.

Ad hoc demonstration: After the above experiments had been completed, a delegate from Australia asked us whether we could log-in on 'his' computer in Canberra. Given the telephone number and password we managed on the first try to extract and display local bulletin files, *etc.* Further details on this experiment in Husebye and Thoresen (1984).

Concluding Remarks

Recent advances within the fields of microprocessor technology and telecommunications already have had a great impact on industrialized societies and we consider the time ripe for seeing a similar impact on the ways and means by which seismological data are collected in the field. In this article we have tried to document and demonstrate how the indispensible research tool a seismic array represents can be made affordable even for small academic research institutions. For the seismological community as a whole, the present and future digital seismometry developments should prove most beneficial; seismological data exchange, bulletin transfer and naturally abstracts for meetings should be transferable on an individual basis and not necessarily routed via the postal system and/or complex data centers. The future in seismology as we now see the contours is that of digital seismometry for everyone.

Acknowledgement

Many free and frank discussions with Professor A. Christoffersson, Uppsala, and Mr. J.A. Mathiesen, Trondheim, on array processing schemes and corresponding software implementation are much appreciated. The continuous interest and encouragement from Mr. S. Lundbo, Ministry of Foreign Affairs, Oslo, are also much appreciated. Our RSTE/RST development project is supported by grants from the Royal Norwegian Council for Scientific and Industrial Development (NTNF) and the Ministry of Foreign Affairs, Norway. One of us (SFI) acknowledges a Postdoctoral Fellowship from NTNF.

References

Allen, R. (1982), "Automatic Phase Pickers, Their Present Use and Future Prospects," *Bull. Seism. Soc. Am.*, **72**, 5225-5242.

Anonymous (1983), "Satellite Systems for Mobile Communications and Navigation," *Conf. Publ. no. 222, IEE*, Savoy Place, London WC2, UK.

Douglas, A. (1981), "Seismic Source Identification, a Review of Past and Present Research Efforts," *Identification of Seismic Sources-Earthquake or Underground Explosions*, E.S. Husebye and S. Mykkeltveit, eds., D. Reidel Publ. Co., Dordrecht, Holland.

Fink, R.L., O. Lerine and H. Nilsson (1981), "SAFT: a Simple ASCII File Transfer System; User and Implementation Documentation," *Special Rep. of Stockholm University Computing Cent.*, QZ, FACK, S-10450 Stockholm, Sweden.

Husebye, E.S. and S. Mykkeltveit (Eds.) (1981), "Identification of Seismic Sources—Earthquake or Underground Explosions," *Proceedings NATO Advanced Study Institute Series*, D. Reidel Publ. Co., Dordrecht, Holland.

Ingate, S.F., E.S. Husbye and A. Christoffersson (1985) "Regional Arrays and Optimum Data Processing Schemes," *Bull. Seism. Soc. Am.*, **75**, Aug. 85.

Kirstein, P.T. (1975), "UK experiences with the ARPA Computer Network," *Exploitation of Seismograph Networks*, K.G. Beauchamp (ed.), Nordhoff-Leiden, Holland, 55-80.

Lee, W.H.K. and S.W. Stewart (1981), "Principles and Applications of Microearthquake Networks," *Academic Press*, New York, 293 pp.

Ringdal, F. and E.S. Husebye (1982), "Application of Arrays in the Detection, Location and Identification of Seismic Events," *Bull. Seism. Soc. Am.*, **72**, S201-S224.

Steinert, O., E.S. Husebye and H. Gjoystdal (1975), "Noise Variance Fluctuations and Earthquake Detectability," *J. Geophys.*, **41**, 289-302.

Veith, K.F. (1981), *Seismic Signals Detection Algorithms*," Teledyne-Geotech Tech. Rep. No. 81-12, Alexandria, Va, USA.

Whitney, A. and M.C. Conrad (1983), "Call FORTH for Realtime Control Programming," *Computer Design*, April 1983, 81-84.

A New Regional Array in Norway: Design Work and Results from Analysis of Data from a Provisional Installation

S. Mykkeltveit

Summary

The subject of this paper is a new experimental regional array, which is to be installed in Norway during the summer of 1984. A review is given of the design work for the new array and results from analysis of data from a provisional installation are presented.

Introduction

An experimental regional array will be installed in Norway during the summer of 1984. The array will comprise 25 short period elements, 4 of which will be 3-component deployments with the remaining 21 elements consisting of vertical motion seismometers only. In addition, there will be a broad-band three-component system. Sampling rates will be 40 Hz for the short period channels and 10 Hz (intermediate period) and 1 Hz (long period) for the broad-band system.

The geometry of the new NORESS array is shown in Fig. 1. The short period central element will be a three-component borehole system.

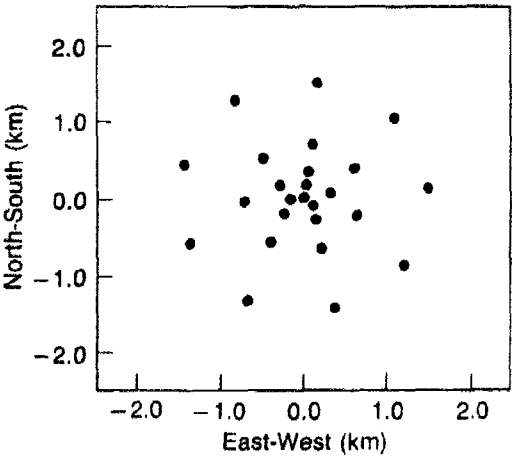

Fig. 1. Geometry of the new NORESS array to be installed during the summer of 1984. All 25 sites will have a vertical seismometer; 4 out of the 25 will, in addition, be equipped with horizontals.

The three remaining three-component elements will be located on the third ring from the center (diameter 1400 m). The broad-band system will also be a borehole deployment at the central site. The remaining 24 sites will be deployments in shallow vaults. Data will be transmitted within the array using fiber optic cables. This makes the array flexible in terms of future reconfiguration experiments. It will, for example, be possible to reconfigure the array into an 11- or 12-element array of three-component stations.

The subject of this contribution is the scientific objectives and design criteria for the new array. In addition, results from analysis of data from a provisional installation which comes close to the geometry of Fig. 1 are presented and discussed.

Design Work for the New NORESS Array

We have previously devised a method for array configuration optimization with respect to SNR gain by beamforming (Mykkeltveit *et al.*, 1983). We have demonstrated optimized geometries leading to theoretical gains well in excess of the standard $\sqrt{N}$ gain by utilizing negative minima in the observed noise correlation curves. Such optimum geometries, however, tended to be rather "peaked" in their frequency response, *i.e.*, a very high gain at one particular frequency was generally accompanied by low gains at other (relevant) frequencies. The optimized geometries were characterized by one particular intersensor spacing being represented as many times as possible in the geometry. This distance reflects the separation for which the noise correlation has its minimum, for a given frequency interval. For optimization explicitly taking several frequency bands into consideration (*e.g.*, giving equal weight to each of five different frequency bands in the gain expression), again one single intermediate frequency "dominated" the geometry. For on-line processing of regional events on the new array, signal frequencies in the range 1.5 to above 5.0 Hz will be of importance. In this range the distance corresponding to the noise correlation minimum varies by as much as a factor of 3 or more and optimum geometries for different frequencies within this range would be vastly different. At this stage of the design work it was clear that the configuration to be finally deployed would have to contain many combinations of sensor pairs at nearly optimum separation for any frequency within a fairly wide range.

From the foregoing discussion it follows that we have not been able to make much use of our optimization procedure during the more recent stages of planning for the new array. Rather, a design idea set forth by

Followill and Harris of LLNL (Followill and Harris, 1983) has been pursued. They have proposed a geometry based on concentric rings spaced at log-periodic intervals in radius R, according to the relation:

$$R = R_{\min} \bullet \alpha^n, \qquad n = 0,1,2, \ldots \tag{1}$$

Their design includes the deployment of an odd number of elements symmetrically distributed in azimuth, and it has the following attractive features:

- With an odd number of elements in each ring, the corresponding coarray (defined as the set of all intersensor separations, in vector space) pattern has no overlap among its points, *i.e.*, it samples the wavefield in the best possible way, in this respect.

- Designs based on (1) comprise comprehensive subsets of sensors with very different typical intersensor separations, implying that both high-frequency and low-frequency phases could be well-enhanced by appropriate subsets of the array.

- The beam patterns for the above designs are favorable, with narrow main lobe yielding good resolution in phase velocity and azimuth and absence of cumbersome side lobes.

The configuration in Fig. 1 is the realization of (1), with $R_{\min}$ = 150 m, α = 2.15, n = 0,1,2,3 and with 3,5,7 and 9 elements in each ring, plus one in the center. This gives an array of aperture about 2.98 km.

The location and phase identification capability of an array depend on the wavenumber resolution offered by the geometry of the array. The width of the beam pattern main lobe is a measure of the uncertainty in the estimation of the direction of approach of a recorded signal. Standard beam pattern computations,however, assume identical signals over the array. In order to assess the role of the aperture in a wavenumber resolution context, response patterns incorporating realistic signal correlations were computed. It was found that the resolution capability of the array was generally degraded as a consequence of a widening of the beam pattern main lobe. It is possible, in effect, to estimate a maximum aperture, for which there is no longer an improvement in wavenumber resolution by increasing the aperture further.

The detection capability of an array is controlled by its SNR improvement by beamforming. Theoretical SNR gains by beamforming for the

proposed design and subgeometries of it were checked using correlation curves for signals and noise based on recordings on previous versions of the NORESS array (Mykkeltveit *et al.*, 1983). Signal and noise correlations for the two frequency bands 1-3 and 3-5 Hz were used and theoretical gains were computed for a range of values of R_{min} in (1) and shown in Fig. 2 for different weighing of frequency bands and different sensor masking schemes. It is found that for the proposed value of 150 m for R_{min}, it does not pay to delete the outer ring of 9 elements for the frequency band 3-5 Hz. For the lower frequency range, however, gain improvement is achieved by masking the inner two rings. A general impression from this figure is that one should be able to improve the gain

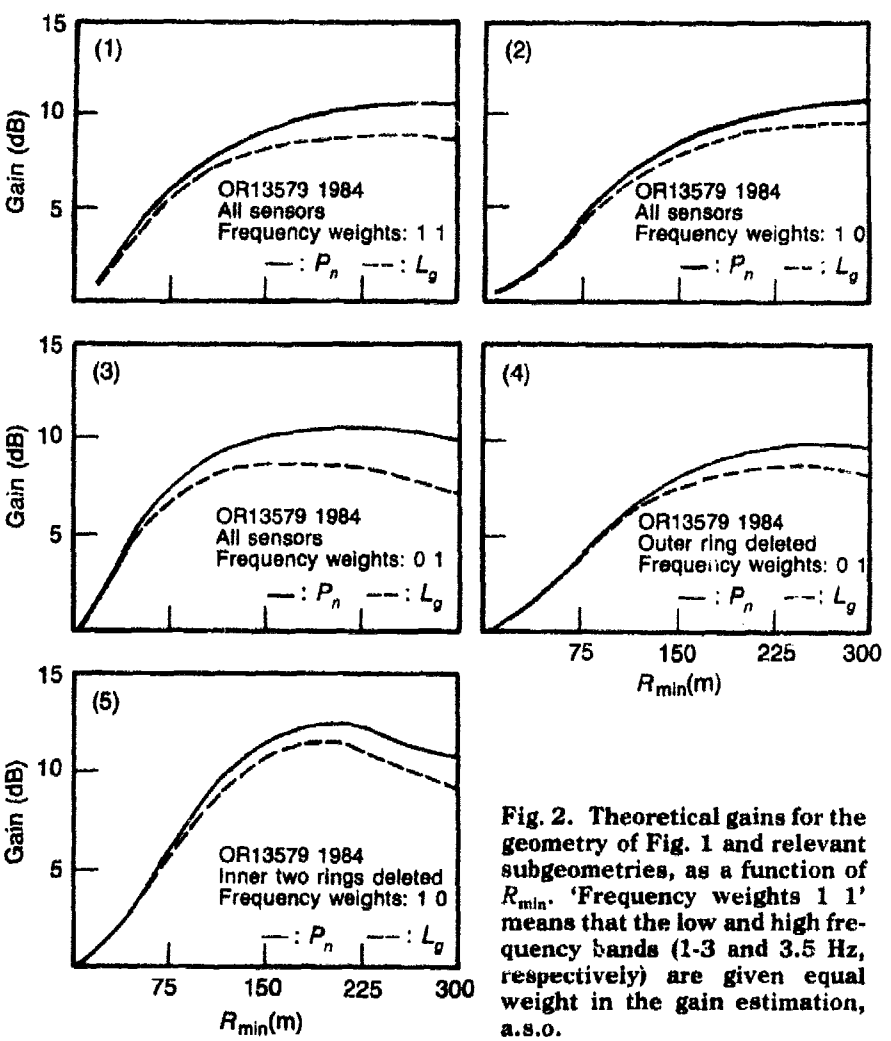

Fig. 2. Theoretical gains for the geometry of Fig. 1 and relevant subgeometries, as a function of R_{min}. 'Frequency weights 1 1' means that the low and high frequency bands (1-3 and 3.5 Hz, respectively) are given equal weight in the gain estimation, a.s.o.

by a slight increase of R_{min} and a corresponding increase in the aperture to close to 4 km, but the net gain from this would amount to less than 1 dB, which is of minor importance compared to logistic implications and the above concern on array resolution.

Other geometrical patterns, both previous array realizations and new concepts, have been investigated along the same lines as above. None of these, however, produced both a beam pattern, a coarray pattern and theoretical gains equal to or better than the Followill and Harris odd-ring designs.

Analysis of Data from a Provisional Installation

In order to have an experimental check on our design ideas for the new NORESS array, a provisional 21-element array was installed during the summer of 1983, which comes close to a realization of the geometry proposed for the new NORESS array. The provisional array comprises all elements in Fig. 1, except 4 stations in the outer ring (nos. 3, 6, 8 and 9 in the outer ring, counted clockwise from due north). Correlation curves of signals and noise on which the proposed geometry was based have been confirmed by the new data, providing a much denser sampling and broader range of intersensor spacings than available before. Figure 3 shows noise correlation curves for the two frequency bands 1-3 Hz and 3-5 Hz. The curves closely resemble Bessel functions, suggesting the importance of propagating noise at Rayleigh wave velocities (Mykkeltveit *et al.*, 1983).

The on-line processing of data from the new NORESS array will be based on a new program package (Mykkeltveit and Bungum, 1984). The performance of frequency-wavenumber analysis for detected signals will be of crucial importance to the location capability, because it provides estimates of phase velocity and arrival azimuths for the phase arrivals. An example of the performance of the new regional array processing package for data from the provisional 21-element array is given in Fig. 4. The detection algorithm part of the package has found four phase arrivals, which have been subjected to f-k analysis and results in terms of estimated signal frequencies, phase velocities and arrival azimuths are given. The phase association and location part of the processing package has produced a final event location as shown, after having identified the strongest secondary arrival and assigned to it the role of *Lg* (group velocity 3.50 km/s) in the estimation of epicentral distance.

For the event shown in Fig. 4 and several other events the exact epicenter geographical coordinates are known. These events thus represent an important data base for the estimation of location errors. Processing of these events indicates that station-to-epicenter azimuths can

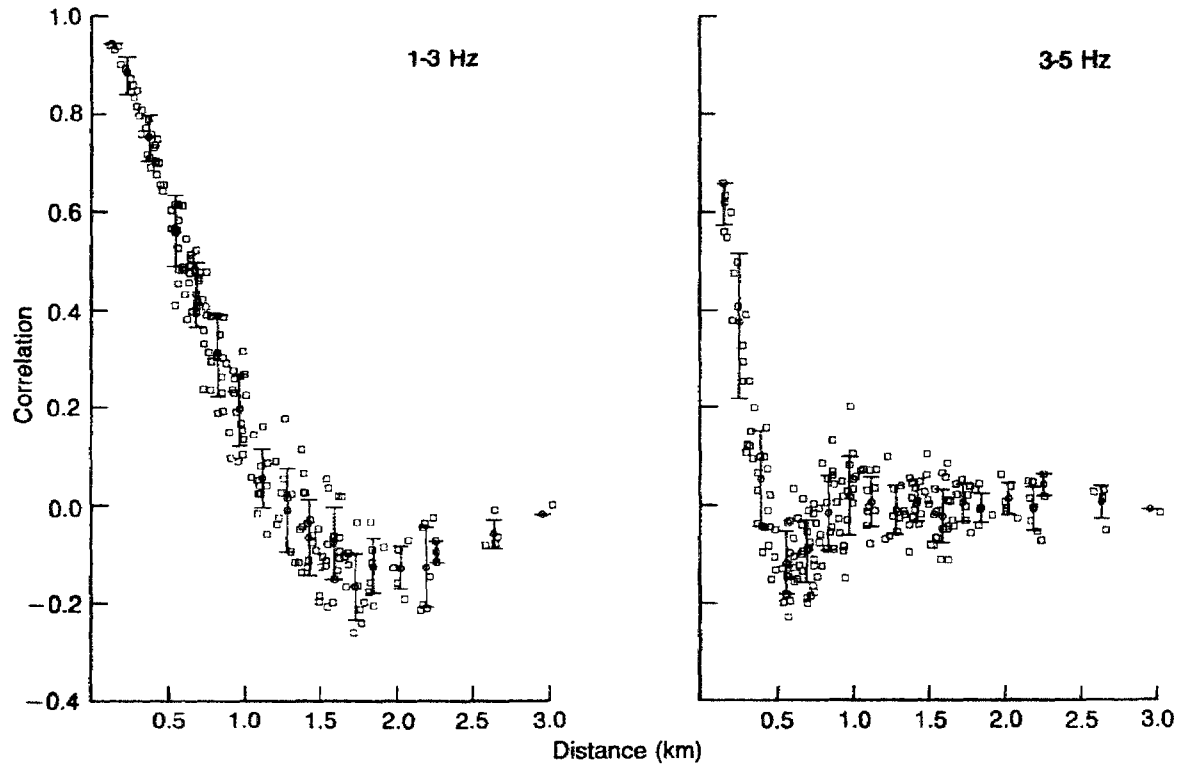

Fig. 3. Noise correlation curves for the frequency bands 1-3 Hz and 3-5 Hz for the 21-element array. The data interval is 102.4 sec long. Mean values and standard deviations within separation intervals of 150 m are given by special symbols.

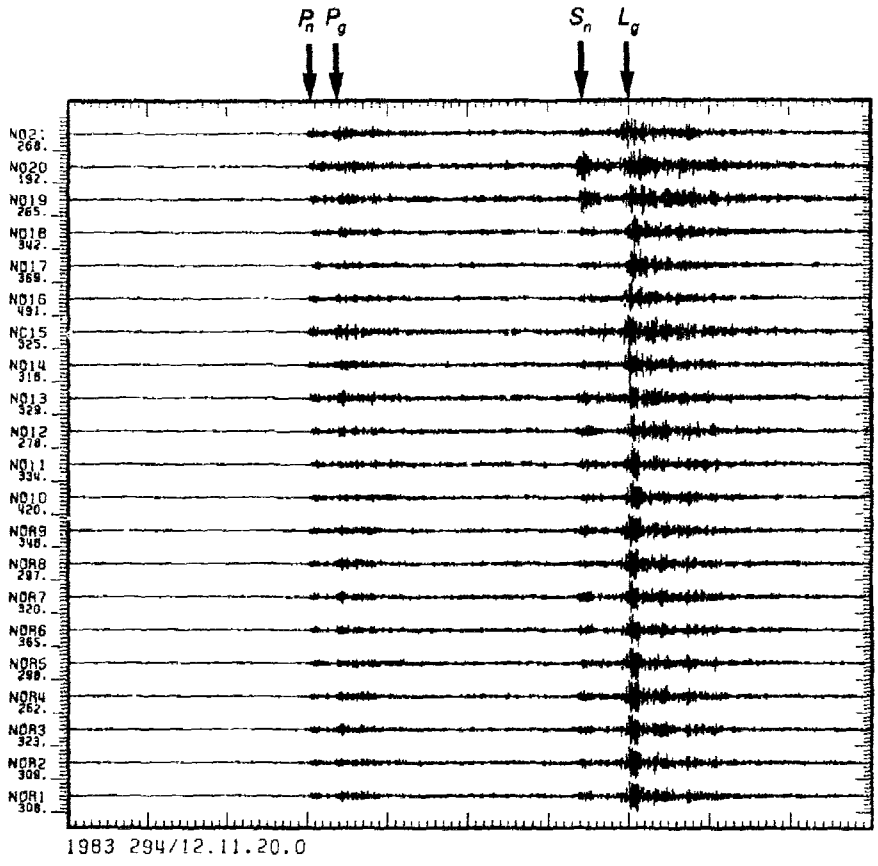

YEAR	DOY	TIME OF DAY	FN	AMPL	SNR	PER	FREQ	VEL	AZI	PWR	STA
1983	294	12 11 50 3	15	54.	4.94	0.17	5.90	7.45	243.4	12.6	20.5
1983	294	12 11 53 7	15	62.	4.73	0.12	6.60	6.20	240.3	21.8	28.3
1983	294	12 12 24 1	14	68.	4.71	0.31	3.20	5.30	238.0	31.4	30.1
1983	294	12 12 29 9	14	207.	4.82	0.29	3.30	3.99	241.4	37.1	108.9

```
Lg type phase detected at      1983  294  12 12 24 1
Associated with P arrival at   1983  294  12 11 50 3
Event located at                                    Lat, Lon = 59.475   7.751

'g type phase detected at      1983  294  12 12 29 9
Associated with P arrival at   1983  294  12 11 50 3
Overriding earlier solution                         Lat, Lon = 59.416   7.071
```

Fig. 4. Event detected and automatically located by the new processing package for regional array data. The event is an explosion associated with hydroelectric power plant construction activities and the data are from the provisional 21-element array. The data window is 100 sec long.

be determined with an accuracy of a few degrees, without entering regional corrections. Distance is adequately estimated even for the simple travel time tables incorporated in the processing package at its present stage of development.

Conclusions

Design objectives and criteria for the new NORESS array in Norway have been reviewed. Several partly conflicting demands have been made on array performance, and the geometry in Fig. 1 represents a compromise between such demands. This geometry has, however, provided the best overall response to the design requirements. The design objectives and actions taken to satisfy actual requirements can be summarized as follows:

(a) **Detection:** The array should provide optimum SNR gain by beamforming. This has been achieved through use of actually observed correlations for signals and noise.

(b) **Location:** The array should have a narrow main lobe and small side lobes. Beam patterns have been computed for realistic signal correlations.

(c) **Performance of array:** The array performance should be good or at least reasonable for a wide range of frequencies, typical of regional wave propagation. This aspect is well taken care of by the proposed geometry as it contains several useful subgeometries, which are close to optimum for different frequencies.

(d) **Research:** The array should have an optimum coarray pattern for unique spatial sampling. The odd number of elements in each ring for the proposed design ensures this.

Results from the present provisional array installation have basically confirmed the projected capabilities of the new array.

References

Followill, F. and D. Harris (1983): *Commentss on Small Aperture Array Designs*. Informal report, Lawrence Livermore National Laboratory.

Mykkeltveit, S., K. Astebol, D.J. Doornbos and E.S. Husebye (1983): "Seismic Array Configuration Optimization" *Bull. Seism. Soc. Am.* **73**, 173-186.

Mykkeltveit, S. and H. Bungham (1984): "Processing of Regional Seismic Events Using Data from Small-Aperture Arrays. *Bull. Seism. Soc. Am.* **74**, 2313-2333.

Seismic Array Processing: Past, Present, and Future

Edward A. Flinn

In this paper we discuss the past and probable future evolution of methods for processing and management of data from seismic arrays. Even after twenty-five years of intensive research, optimum methods have not yet been developed by analyzing and managing the large quantities of data produced by these arrays.

Seismic array data analysis and management can be divided into several categories, which will be discussed in order:

(1) Signal detection. The combination of array elements in space and time, to detect seismic signals and determine their waveform characteristics, direction of arrival, and phase velocity. Past developments include simple beamforming, optimum filtering, and frequency-wavenumber domain detection. Promising new developments include adaptive beamforming and further development of f-k detection.

(2) Signal association. Grouping together the detected phases from a given seismic event, frequently in the presence of overlapping events. A human analyst still appears to be an essential part of this process.

(3) Event location and characterization. The combination of information from individual arrays, to determine the location, depth, magnitude, and focal mechanism of a detected event. New developments include allowance for correlation of time residuals between stations, magnitude calculations taking focal mechanism into consideration, and the use of a general linear model for magnitude estimation.

(4) Identification of a seismic event as an explosion or an earthquake. New developments include ratios of energy in different spectral bands from broad-band instruments.

(5) Archiving and retrieval of data. These are problems of great complexity, the effective solution of which depends heavily on technological improvements in mass storage devices, data communication, and on-line computer systems designed with human factors taken into account.

The sheer quantity of data, the similarity of signals produced by earthquakes and underground explosions, the inhomogeneities in the real earth (which vitiate the simple past assumptions of signal coherence across the arrays), and the need to drastically improve signal/noise ratios: all these factors have affected, and continue to affect, the frontiers of many fields of science and engineering. Among these are seismology, digital signal analysis, optimum filter theory, and parallel processing. While the program has maintained a clear focus on the basic problem of detection and identification of underground explosions, its scientific contributions also have been highly significant. Advances in geophysics—especially the development of plate tectonics—and study of the problem of detection and identification of underground explosions have maintained a symbiotic relationship for the past quarter-century.

The Canadian Seismic Verification Research Program

P.W. Basham and R.G. North

Historical Perspective

Canada has been active in seismic verification issues since 1959 with a participant in the Geneva meeting of experts. In 1962, Canada agreed to accept the installation at Yellowknife of a medium aperture array designed by the UK. Canada took over operation of the array in 1964, and in subsequent years much of the Canadian research on teleseismic detection was undertaken using Yellowknife data. By 1974, the Yellowknife array was refurbished with radio telemetry from the outstations and automatic digital detection processing, and it has operated in a stable configuration since that year.

The most active years of Canadian research were the decade 1964-1974, with studies of body and surface wave detection, complexity and $M_s - m_b$ discrimination, theoretical work on crust and mantle transfer functions, magnitude-yield, and simulation of multiple explosion evasion scenarios. Much of the early work in this period was presented as Canada's contribution to the 1968 SIPRI conference. In 1969, Canada sponsored a resolution in the U.N. General Assembly which asked all countries to submit information on their seismograph stations, and subsequently undertook to analyse these data to estimate the current global detection and discrimination thresholds. In the early 1970's, these research results were employed in support of Canada's position at informal meetings of the Conference of the Committee on Disarmament (CCD) in Geneva.

Since 1976, most of Canada's seismological effort in this area has been used in support of the Group of Scientific Experts (GSE) in Geneva, who were given their first mandate in that year by CCD to consider matters related to International Seismic Data Exchange (ISDE) under a comprehensive test ban treaty. In 1982, Canada announced new initiatives in arms control and disarmament that included more active participation in experiments sponsored by the GSE, and a new focus for seismic verification research.

International Seismic Data Exchange

Canada's view of ISDE as described by the GSE in its three reports is very similar to that of other western countries: much useful groundwork

has been laid, but much useful work remains to be done. The next important step in the work of the GSE will be the data exchange "Technical Test" in late 1984. Canada will participate in this test by contributing data from three stations, and by attempting to intercept messages from all other participants as part of the evaluation of the WMO communication channels. A very important part of this test, however, will be an evaluation of the ability of experimental data centres to derive similar and timely seismic event bulletins for redistribution to participants.

We place a great deal of importance on facilities for rapid exchange of waveform data, and have initiated contact with digital waveform exchanges using "switched analog", "circuit switched" and "packet switched" telephone connections. Some emphasis in the GSE has been put on satellite circuits for rapid waveform exchange. Telephone exchange may be more valuable under an operational ISDE as it can be put into effect in virtually any country.

Seismic Verification Research Plans

It has been recognized that North America, and in particular parts of Canada, has geologic conditions that provide a useful analog of parts of the Soviet Union. This has been utilized in the experimental deployment of the Regional Seismic Test Network which has two stations on the Canadian Shield. The central craton of the shield is virtually surrounded by earthquake source zones in Precambrian, Paleozoic and young tectonic terrains. There are interesting shallow seismic sources in the magnitudes 3-4 range such as rockbursts in the shield of Quebec and Ontario and earthquakes induced by potash mining activity in Saskatchewan. Many of the earthquake source parameters in southeastern and southwestern Canada are well defined by dense networks of stations.

The principal focus of continuing seismic verification research will take advantage of these situations to attempt to make a contribution to a number of regional problems. High quality data from the RSTN, Yellowknife and the rest of the Canadian network (about 80 analog and digital station) will be used to assess regional crustal wave attenuation, event location with small numbers of regional stations (with independent control from dense networks); focal depth estimates (with independent control from dense networks or knowledge of rockbursts or induced earthquakes); and compilation of potential discrimination characteristics for seismic events in many environments. We welcome suggestions related to this research from all others engaged in similar work.

Automatic Association

R. R. Blandford and J. H. Goncz

Summary

The automatic production of a seismic bulletin from a list of signal arrivals is a problem that has been completely solved in that operational programs exist. Yet it seems that state-of-the-art capabilities of existing Automatic Association (AA) programs never do quite as well as an experienced human analyst. So the thrust of continued work in this field is to try to put more intelligence into these computer programs and to devise algorithms that make more effective use of the information in the signal arrival queue.

Work done with a signal arrival queue containing a mixture of automatic detections and analyst-picked detections indicates that it is necessary to give more weight to the analyst detections than to the automatic detections, for the latter contain more false alarms and are less reliable. We use a program unit call SCREEN to accomplish this, and the weights assigned therein are based completely on empirical rules.

This report describes some of the more recent enhancements incorporated into AA during 1983. The capabilities of these procedures as well as short comings are described.

As more algorithms are added to get better results, the processing time gets longer: about 10 hours cpu time for a few thousand arrivals. Further improvements comes about by repetitious processing; techniques are needed to make AA programs computationally more efficient.

Introduction

The general concept of Automatic Association programs is to reduce, or eliminate if possible, the tasks performed by a human analyst in deducing the seismic events, earthquakes and explosions, that have caused a series of seismic arrivals to be detected at a network of seismic observatories.

To date, it has been found impossible to completely eliminate the need for human intervention in the preparation of a seismic event bulletin; indeed, human judgement and experience seem to be necessary components of a good seismic bulletin. Even the most extensive computerized seismic data analysis system under development today relies on analyst to review most of the stages of event generation.

Recent Improvements in Automatic Association

In 1983 the Automatic Association (AA) program was extensively tested with the synthetic arrival data created for use in the International Data Exchange Exercise. The idea was to develop and implement certain features into the version of AA at the Seismic Research Center (SRC), at Teledyne Geotech, and to compare its performance to the version existing at Center for Seismic Studies (CSS) as well as the Swedish version.

However, a good comparison was not possible to achieve because of the lack of a mutually readable data set common to both the UNIX operating system at CSS and to the VAX/VMS operating system at SRC. The following list of items illustrates the features that were investigated at this time using the SRC AA. These items will be described in the body of this paper showing how successful they were and where further improvement is considered necessary.

- Kinematic/dynamic use of amplitude data.
- Use of *pP* and *sP* to automatically constrain depth.
- Two array event location.
- Slowness check of all later phases (in addition to PKP).
- Unassociated arrivals shown in final summary bulletin.
- Confidence ellipse in summary bulletin.

Kinematic/Dynamic Use of Amplitude

Theoretical basis for this work lies in an unpublished memorandum by R.R. Blandford dated 14 July 1982. The maximum likelihood estimate of magnitude is computed using an efficient Newton-Raphson procedure for computational improvement.

A subset of the full network of reporting stations is chosen to compute the maximum likelihood estimate. In general, the most reliable stations will be used. It is also desirable that these stations exhibit low seismic noise levels. It would be an additional improvement to have diurnal and seasonal seismic noise levels rather than a single average value. Station bias values for magnitude are included, if available. These quantities should exist in the station coordinates and information file in the computing center where the AA program is being executed. Unfortunately in most Centers this is not true and the values have to be entered via separate file thereby restricting the flexibility of this method. It is clearly essential that a station be removed from the maximum likelihood calculation if it is in a not-reporting condition.

There are three cases to consider regarding detections recorded by the network of magnitude estimating stations:

(1) A station does not report a detection event though the m_b estimate indicates that it should have detected.

(2) A station reports a detection whose amplitude is extraordinarily high or low according to the estimated m_b. This amplitude is computed to have a probability of less than .01.

(3) The station reports a detection but the noise level of the station and the estimated m_b indicate that it should not have detected.

These special cases are handled by adjusting the number of points accumulated by that station in the SCREEN algorithm according to Figs. 1 and 2. The SCREEN algorithm requires that a certain number of points be totaled up by the stations making the event before the event is declared. Additional points are awarded if an S detection is present for the station, if azimuthal information is present, *etc.* The values of the constants in SCREEN have been established by experience and empirical observations; they are unquestionably network dependent.

- Select "reliable stations," get detection thresholds
- Compute Ringdal m_b
- If a station did not detect but should have, subtract points, *i.e.*:
  If P(det) > .95: −1.0
  P(det) > .99: −2.0
- If a station did detect and reports an 'unusual' amplitude, A_0, discard that amplitude for this event:
  If P(amp > A_0) < .01 or
  P(amp < A_0) < .01 then reject A_0, start screen over
- If a station did detect but should not have, discard all points due to that station, *i.e.*:
  If P(det) < .01, − (all points due to station)

Fig. 1. Amplitude modifications to screen.

Automatic detection:	+0.82
If (θ) and $\Delta < 90°$:	+1.02
If (R) and $\Delta < 7°$:	+0.85
Analyst — certified detections:	+0.98
If (θ) and $\Delta < 90°$:	+1.18
If (p) and $\Delta < 90°$:	+0.89
If (R) and $\Delta < 7°$:	+1.10
If in shadow zone:	−0.65
If S phase:	+1.10
If in coda:	−0.20
If slowness error large:	−1.07
If no later phases:	−0.50
5 points required for declaration	
10 points in a-seismic zone	

Fig. 2. SCREEN points.

Depth Constraint With *pP* and *sP*

Our experience with analyst-picked phases indicates a tendency to label the teleseismic phase that arrives next after *P* as *pP*. In fact, the next arriving phase may not be *pP*, but it may be *sP*, *PcP* or some unidentified phase. Restraining depth to the analyst's *pP-P* time observation could lead to difficulties in correct event location and association of phases.

These considerations lead to the "soft" treatment of *pP* and *sP* labeled phases that is described here.

The list of *P* arrivals about to be input to the HYPO location program is examined in time order, and the arrival queue is searched for each station for a detection at the same station that is labeled *pP* or *sP*. If *sP* is found the search terminates and the depth for *sp-P* time is uses as an ***unrestrained*** starting depth for HYPO. The idea here is not to constrain the HYPO solution but rather to start the iteration process as an optimum point in event parameter space. If no *sP* is found, the smallest *pP-P* time, if any *pP* detections are found, is used to establish the input starting depth to HYPO in the same way. Previously, the input starting depth in HYPO had been set to zero because of the lack of any better

depth, and this method is believed to be better, although it has been rather difficult to establish that it is.

Once the event has been fixed and later phases associated an attempt to constrain the depth by a labeled depth phases is made. The arrivals are examined to see if there is a station reporting both *P* and *sP* for this event, and also if the analyst's label agrees with the AA label. If this is so, the *sP-P* depth is used to constrain the HYPO solution to this depth and the event is relocated and reassociated. Again, if no *sP-P* pair is found, the same algorithm is applied using the shortest *pP-P* time,

$$\delta P_x^1 = \frac{\partial P_x^1}{\partial \theta} d\theta + \frac{\partial P_x^1}{\partial \psi} d\psi + \frac{\partial P_x^1}{\partial h} dh$$

Array 1 $$\delta P_y^1 = \frac{\partial P_y^1}{\partial \theta} d\theta + \ldots$$

$$\delta T^1 = \frac{\partial T^1}{\partial \theta} d\theta + \ldots + \delta T_0$$

$$\delta P_x^2 = \frac{\partial P_x^2}{\partial \theta} d\theta + \ldots$$

Array 2 $$\delta P_y^2 = \frac{\partial P_y^2}{\partial \theta} d\theta + \ldots$$

$$\delta T^2 = \frac{\partial T^2}{\partial \theta} d\theta + \ldots + \delta T_0$$

or

$$\boldsymbol{\delta} = B\, d\mathbf{x}$$

$$d\mathbf{x} = (B^T \Sigma^{-1} B)^{-1} B^T \Sigma^{-1} \boldsymbol{\delta}$$

Σ contains travel time and slowness error variance estimates down the diagonal.

Fig. 3. Two-array location.

if any. This algorithm seems to work very well with the synthetic data because the analyst-labeled *sP* is always "honest". More work should be done on this algorithm to expand its usefulness to real data.

Other AA Improvements

In addition to the previous two major improvements described above, some continuing effort at enhancing the capabilities of AA was performed. The check on signal slowness has been extended to include all phases recognized by AA, and not limited to just *P* and *PKPDF*. Since the travel times for the remaining later phases are computed by polynomial approximation rather than by table lookup, it was necessary to create a complete new program section in which there is duplication of several of the computational modules used in travel time determinations during location.

Formation of trial epicenters by two arrays has been added, based on the intersection of their confidence ellipses. Since SRC's AA uses this kind of trial epicenter search for the last pass through the signal arrival queue, very few events are started this way. It has been added to be compatible with other AA programs. Equations for the two array computation are shown in Fig. 3.

The major and minor axes of the location confidence ellipse have been added to the summary bulletin in accordance with standard practice.

The format of the summary bulletin has been expanded so that "left overs", or unassociated, detections are printed adjacent to the declared events and their associations. This printing is a great help in reviewing the bulletin and in analyzing the performance of AA. Various printing highlights are used to make the unassociated detections different from the associated detections.

References

Goncz, J.H, (1980). *Present Status and Dynamic Planning for Automatic Association Programs*, SDAC-TR-80-2, Seismic Data Analysis Center, Teledyne Geotech, Alexandria, Virginia.

Teledyne Geotech Staff (1982). *Seismic Research Information System (SARSI), Vol. 1, Functional Descriptions*, Teledyne Geotech, Alexandria, Virginia.

Three-Component Array Processing

C. Esmersoy, V.F. Cormier, and M.N. Toksöz

Introduction

The monitoring of a comprehensive test ban treaty may require the processing of regional data from many multi-element arrays. Event location and association of small events benefits from the use of as much information as possible that can be extracted from seismograms, including wavevector, polarization, and ellipticity. In this paper, we outline a technique of processing seismograms recorded by three-component arrays to retrieve this information in moving time windows. The objectives of this research are to provide a robust technique of beam forming and parameter extraction from three-component arrays and also to identify modes of body and surface wave scattering in real data.

Estimation of wave parameters from the observations at spatially separated sensors has been an area of interest particularly in radar, sonar, physical oceanography and seismic signal processing literature. With the development of maximum likelihood array processing (Levin, 1964; Kelly and Levin, 1964, Capon *et al.*, 1965) and maximum likelihood frequency-wavenumber (f-k) analysis (Capon, 1969), the usual method of azimuth estimation has been to estimate the f-k spectrum and to find the wavenumber which maximizes the estimate. This and other similar techniques represent the ***beamforming*** approach to the problem. Various applications exist in literature (Lacoss *et. al.*, 1969, Rikiishi, 1978, Bienvenu, 1979). Estimation errors for the optimum processor has been derived for some array geometries and simple noise structures (Seidman, 1971; Cox, 1973; MacGarthy, 1974; Altes, 1979; Schultheiss and Ianello, 1980).

Another approach to the azimuth estimation problem is to estimate the ***time delays*** between the sensor couples. Hahn (1975) shows that optimum bearing estimation can be obtained by a weighted linear combination of the delays in the case of incoherent noise. Knapp and Carter (1976) derive the maximum likelihood estimator and compare it with several other proposed estimators. Another comparative analysis is given by Hassab and Boucher (1979). Chan *et. al.* (1978) investigate the least square estimation of time delay obtaining an asymptotically optimum estimate for incoherent noise. They also note the disadvantage of phase unwrapping requirement of this technique.

Some other techniques such as split-beam tracker which combines the beamforming and cross-correlation approaches have also been considered. MacDonald and Schultheiss (1969) show that a slightly modified version of the conventional split-beam tracker yield an rms error at or close to the lower bound for most practically interesting array configurations assuming incoherent noise. Shensa and Black (1978) provide an algorithm to remove the 2π uncertainties of split-beam trackers.

Interest in dispersive propagation has been limited. Fidler and Carlton (1981), discuss a technique which performs a bearing estimate for each frequency and sensor pair separately, then averages the estimates over the frequency and smooths it over the bearing. Hamon and Hannan (1974) examine the time delay estimation in dispersive media. They present a parametric approach by assuming a model for the dispersion function and estimating the model parameters.

When the wavefield of interest is vectoral, such as seismic waves, coherency between the wave components on perpendicular axes may be used to estimate the propagation direction. There has been relatively little work on 3-component array data processing. Harris (1982) examines the Cramer-Rao error bounds in estimating compressional wave direction with a 3-component uncorrelated noise with identical power densities in channels.

In many applications an array of 3-component sensors are used to observe the wavefield. One possible way to handle this data would be to process each 3-component sensor separately and then to combine the results. However, a better way is to formulate the problem as a whole thus utilizing all available polarization and propagation information optimally. Here, the 3-component array processing problem is presented as a generalization of the 1-component beamforming approach.

Our primary objective is to decompose an observed data set into different wave types and estimate the propagation direction and phase velocity of each component. In general, a wavefield consists of a finite number of components each characterized by a propagation direction and a phase velocity. One difficulty in velocity estimation is that observations are usually made along a line (*e.g.*, borehole) or on a plane (*e.g.*, earth surface) providing no information about the wavevector component perpendicular to the observation space. Since the propagation direction of the wave is also unknown, it seems that there is no way of estimating the direction and the velocity simultaneously. However, relationships between the particle motion and propagation direction of the seismic waves makes this simultaneous estimation possible from 3-component observations along a line or in a plane.

Parametric Signal Model

Particle Motion Model. Seismic waves in laterally homogeneous

isotropic media are usually examined by decomposing the wave into three components, namely *P*, *SV* and *SH*. *SH* is the horizontal particle motion component of the shear wave and it obeys the scalar wave equation. *P* is the compressional wave with the particle motion along the propagation direction and *SV* is the other component of the shear wave which represents the particle motion perpendicular to both *P* and *SH* wave. Since *P* and *SV* waves interact at the boundaries they are examined together. In the case of horizontally layered media surface waves exhibit two modes of propagation. Rayleigh wave results from the *P* and *SV* wave interaction at the surface and posses particle motion in vertical and radial (direction of propagation) components. Love wave is the *SH* component and has only the transversal particle motion.

From the particle motion properties summarized above different types of seismic waves may be modeled. For body waves and Love waves angles ψ and ϑ represent the direction of propagation measured from the vertical and x-axis respectively. For Rayleigh waves $\psi = \tan^{-1}e$, where e is the ellipticity (Boore and Toksöz, 1969), and ϑ is the back azimuth measured from the x-axis. Three-component observations of the particle displacement, at a given frequency and at one point in space can be written as follows

P waves:

$$\mathbf{r}(\omega) = \begin{bmatrix} -\sin\psi\cos\vartheta \\ -\sin\psi\sin\vartheta \\ \cos\psi \end{bmatrix} \quad s(\omega) \equiv \mathbf{h}_p\, s(\omega)$$

SH waves and Love waves:

$$\mathbf{r}(\omega) = \begin{bmatrix} -\sin\vartheta \\ \cos\vartheta \\ 0 \end{bmatrix} \quad \mathbf{s}(\omega) \equiv \mathbf{h}_{SH}\, s(\omega) \tag{1}$$

SV waves:

$$\mathbf{r}(\omega) = \begin{bmatrix} \cos\psi\cos\vartheta \\ \cos\psi\sin\vartheta \\ \sin\psi \end{bmatrix} \quad \mathbf{s}(\omega) \equiv \mathbf{h}_{SV}\, s(\omega)$$

Rayleigh waves:

$$\mathbf{r}(\omega) = \begin{bmatrix} -j\sin\psi\cos\vartheta \\ -j\sin\psi\sin\vartheta \\ \cos\psi \end{bmatrix} s(\omega) \equiv \mathbf{h}_R\, s(\omega)$$

where j in the Rayleigh model represents a 90° phase shift between the horizontals and the vertical and $s(\omega)$ is the Fourier component of the waveform. To be more precise, the $-j$ term in the horizontal components should be replaced by $-j\,\mathrm{sgn}(\omega)$ where the sign function is

$$\mathrm{sgn}(\omega) = \begin{cases} +1; & \omega > 0 \\ -1; & \omega < 0 \end{cases}$$

Note also that the Rayleigh model represents retrograde particle motion, which is usually the case for fundamental modes. The model for the prograde case is obtained by changing the signs of the horizontal components.

Particle motion models given in this section represent amplitude and phase relations between Cartesian components of various type of waves.

Propagation Model. In many applications an array of 3-component seismometers are used to observe the wavefield. In such cases the phase relations between the sensors may be exploited as well as the phase relations between the components. In this section, definition of the focusing or steering phase shifts for different wave types are given.

The propagation model at one frequency may be written in terms of phase shifts at a given set of sensor locations. The phase delay (due to propagation) at sensor m may be represented by the complex exponential

$$d_m = e^{j\varphi_m} \tag{2}$$

where φ_m is the corresponding phase shift.

For plane wave front, phase shifts for different wave types are as follows:

Table 1.

	Sensor location	
Wave type	along a vertical line	on the surface
P	$\varphi_m = -\frac{\omega}{v_P}\,\rho_m \cos\psi$	$\varphi_m = -\frac{\omega}{v_P}\,\rho_m \cos(\vartheta_m - \vartheta)\sin\psi$
SH	$\varphi_m = -\frac{\omega}{v_S}\,\rho_m \cos\psi$	$\varphi_m = -\frac{\omega}{v_S}\,\rho_m \cos(\vartheta_m - \vartheta)\sin\psi$
Rayleigh, Love	$\varphi_m = 0$	$\varphi_m = \frac{\omega}{v_{R,L}}\,\rho_m \cos(\vartheta_m - \vartheta)$

where v is the phase velocity at frequency ω, (ρ_m, ϑ_m) are the polar coordinates of sensor m and (ψ, ϑ) are the propagation direction angles.

Combined Model. Combining the particle motion and propagation, each wave type can be modeled by a $3M$ vector (M is the number of sensors)

$$\mathbf{r}(\omega) = \begin{bmatrix} d_1\mathbf{h} \\ d_2\mathbf{h} \\ \vdots \\ d_M\mathbf{h} \end{bmatrix} \qquad s(\omega) \equiv \mathbf{a}(\omega)s(\omega) \tag{3}$$

where

$$d_m = d_m(\omega, v, \psi, \vartheta)$$

$$\mathbf{h} = \mathbf{h}(\psi, \vartheta)$$

Equation (3) corresponds to the noise-free observation of a particular wave type with given parameters.

Three-Component Array Processing

Stochastic Case. First consider the case where the time waveform may be regarded as a jointly stationary stochastic process. An example of this is microseismic noise. Using the model given by Eqn. 3 observed data at frequency ω may be written as

$$\mathbf{r}(\omega) = \sum_{l=1}^{L} \mathbf{a}_l(\omega) s_l(\omega) \tag{4}$$

where $s_l(\omega)$ is the Fourier coefficient of the wave l. Zero mean, uncorrelated signal components are assumed, *i.e.*

$$E\{\mathbf{s}_i \mathbf{s}_j^*\} = P_i \delta_{ij} \tag{5}$$

For a given wave type (*P*, *SH*, *SV*, Love or Rayleigh) the model vector **a** is represented by three parameters v, ψ, and ϑ. Each set of parameters corresponds to a wave propagating with velocity v along the direction defined by ψ and ϑ. In the case of Rayleigh waves, ellipticity is given by $\tan\psi$ and the back azimuth is ϑ. If the signal power corresponding to each candidate wave (v,ψ,ϑ) is computed, then the maximum or the local maxima correspond to the waves of one particular type propagating across the array. Accuracy and resolution of the estimated parameters are determined by the same properties of the signal power estimate.

The most straightforward way to estimate the signal power is to perform a project-delay-sum process. This may be written as

$$P(v,\psi,\vartheta) = E\left\{\int_{\omega_a}^{\omega_b} d\omega |\mathbf{a}^H(\omega,v,\psi,\vartheta)\mathbf{r}(\omega)|^2\right\} = \int_{\omega_a}^{\omega_b} d\omega\ \mathbf{a}^H R\mathbf{a} \tag{6}$$

where $R = E\{\mathbf{r}(\omega)\mathbf{r}^H(\omega)\}$ is the data spectral correlation matrix, $[\omega_a : \omega_b]$, is the frequency band of analysis. Eqn. 6 corresponds to the conventional Bartlett estimate of the power spectrum or the delay and sum beamforming of one component array processing.

A high resolution estimate of the power has been used in array processing and applied to the direction estimation of microseismic noise. Derivation of the maximum likelihood power estimate can be found in the literature

(Capon, 1969; Baggeroer, 1974). The problem consists of finding an optimum spatial weighting at each frequency and for each direction. A similar derivation can be made for a more general parameter estimation problem leading to an equation of the same form (Esmersoy, 1985). Applied to the foregoing problem the high resolution estimate is given by

$$P(v,\psi,\vartheta) = \int_{\omega_a}^{\omega_b} \frac{1}{\mathbf{a}^H R^{-1} \mathbf{a}} \, d\omega \tag{7}$$

The spectral correlation matrix $R\,(3M \times 3M)$ is obtained by

$$R = \sum_{l=0}^{L} \mathbf{r}_l \, \mathbf{r}_l^H \tag{8}$$

where $\mathbf{r}_l(\omega)$ is $3M$ vector of segment l in Fourier domain. Note that due to the form of Eqn. 8, $R(\omega)$ is guaranteed to be positive semidefinite. Therefore, the estimated power in Eqns. 6 and 7 is nonnegative. From a computation point of view the number of segments must be $L \geq 3M$. Otherwise the rank of R is L and it is not invertible. Moreover, to have a stable estimate L should be much larger than stated above. However, it is limited by the time-bandwidth product of the available data.

Transient Wave Case. In many applications, signal waveforms of interest are relatively short duration pulses, therefore, they cannot be treated as stationary signals. Using the model given by Eqn. 3 observed data at frequency ω may be written as

$$\mathbf{r}(\omega) = \sum_{l=1}^{L} \mathbf{a}_l(\omega) \, s_l(\omega) + \mathbf{w}(\omega) \tag{9}$$

where $\mathbf{w}$ is the noise vector, s_l is the Fourier coefficient of the wave l. Zero means and uncorrelated signal components and noise are assumed, *i.e.*

$$E\{s_i s_j^*\} = P_i \, \delta_{ij} \qquad E\{s_l \, \mathbf{w}^*\} = \mathbf{0} \tag{10}$$

There are several ways to formulate the estimation problem depending on how much is known about the noise characteristics, signal waveform

and parameters to be estimated. In cases where signal to noise ratio is low, the noise characteristics may be estimated in a time segment prior to the first arrival. Then, the estimated noise spectral matrix can be used to minimize the noise interference effects. Formulation for this processing will not be discussed further in this paper. It is assumed in the following that no *a priori* knowledge is available except an estimate of the signal frequency band.

In one-component array processing problem, transient signals are handled by windowing the data in time, and analysing each set of windowed data separately. One approach to the problem is, for each set of windows, to calculate a coherency measure. The set of parameters corresponding to the maximum coherency are the desired estimates. Neidell and Taner (1971) give a comparative analysis of this technique and apply in determination of stacking velocities from multiple ground coverage seismic data. Instead of computing normalized cross correlations between channels, an array processing based technique, similar to the stochastic case, may be used. The major difference in the nonstationary signal case is the way that the spectral correlation matrix R is computed. Usually R is computed by averaging over a narrow frequency band around the frequency sample of analysis. However, when the number of array elements are large averaging over a narrow frequency band does not produce a stable matrix. In such cases, a small positive number is added to the diagonal elements to assure invertibility of the matrix. Some examples of the applications of this technique are given by Baggeroer and Falconer (1982) and Duckworth *et. al* (1982). In 3-component arrays the matrix dimensions are 3 times larger. Therefore, the stability problem becomes more important.

Considered here is another technique for the transient wave case. The spectral matrix is computed by averaging over a range of velocities. This is done by shifting the time windows at each sensor appropriately and averaging the resultant spectral matrices. This operation may be formulated as

$$R(\omega) = \int_{v_a}^{v_b} dv\ \mathbf{r}(v,\omega)\mathbf{r}^H(v,\omega) \tag{11}$$

where

$$[\mathbf{r}(v,\omega)]_m = \int_{t_m(v)}^{t_m(v)+T} \mathbf{r}_m(t)\, e^{-j\omega t}\, dt \tag{12}$$

where $\mathbf{r}_m$ is the 3-component observations at sensor m and T is the length of the time window. The amount of window shift t_m is determined by the array geometry. Performance of this technique is currently under investigation. Satisfactory results have been obtained in applications to various data sets. Some examples are given in the next section.

Applications

Figure 1 shows data recorded by the Lajitas, Texas, array from the underground nuclear test TURQUOISE at NTS on April 14, 1983. This event has reported magnitudes of 5.7 m_b by U.S.G.S and 5.5 M_L by BRK. It is 12.8° from the Lajitas array and its back azimuth is 309°. The instrumentation consists of four three-component stations deployed in a Y-shaped array, having a 150 m station spacing (H[illegible]n and Goforth, 1983). Each component is broadband to ground velocity in the 1 to 30 Hz band. The complete array, consisting of all components and sites, was processed using the techniques outlined in the previous sections. The results of processing a waveform

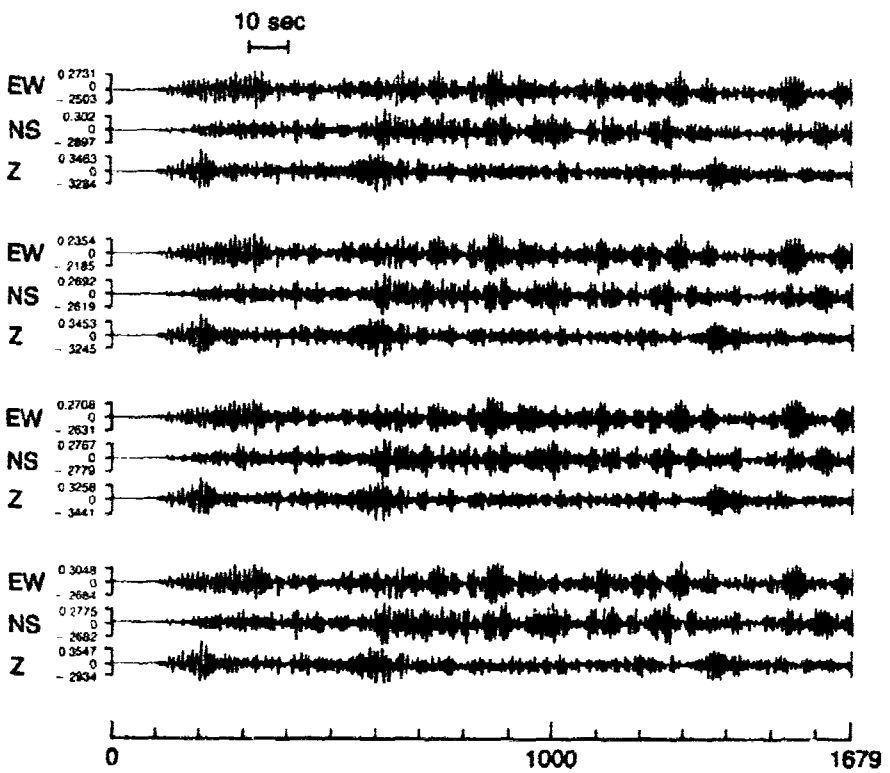

Fig. 1. Seismograms recorded by the Lajitas, Texas array of a 5.5 m_b underground nuclear test ("TURQUOISE", 14 April 1983). (Data provided by T. Li, Teledyne-Geotech).

3.5 km/sec averaged over a wavelength of a 0.8 Hz. body wave. These attributes are compatible with those expected of a P_n phase.

The records contain two more linearly polarized phases with particle motion predominantly in the plane of the wavefront (Fig. 3), having both *SH* and *SV* components. These can also be processed for back azimuth. Figures 4a and 4b show an example of processing for Rayleigh waves on a waveform segment recorded by the NORSAR array from a deep focus earthquake beneath the Sea of Japan. The array elements consist of standard, three-component long period instruments. Azimuth, ellipticity, and surface phase velocity are estimated by the processing. The true back azimuth of the event was 46°. The estimated azimuth is 58°. Figures 5 a and 5b show the results of processing for *S* waves on an earlier waveform segment of the same event. Several *S* phases (*S*, *sS*, *ScS*, *etc.*) have been included in the analyzed segment. For the *S* waves, the predicted azimuth of 45° agrees well with the true azimuth of 46°. The deviation of the Rayleigh wave from true azimuth may be more a reflection of lateral heterogeneity in the upper mantle than a measure of the performance of the processing

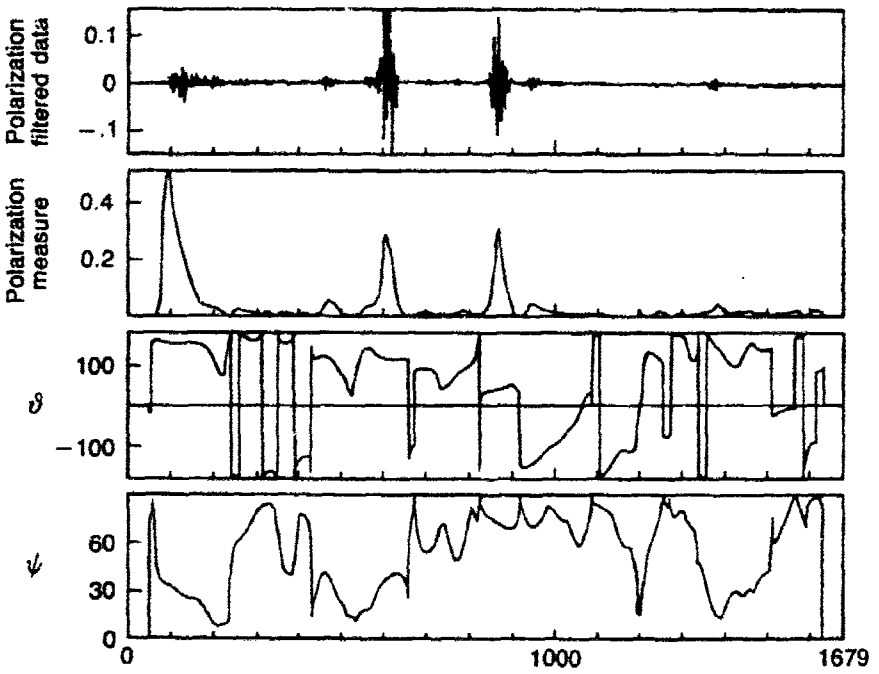

Fig. 3. Example of a single Lajitas site polarization filtered to pass linearly-polarized waves. Plots of polarization measure, azimuthal angle, and vertical angle of particle motion. Time scale same as in Fig. 1.

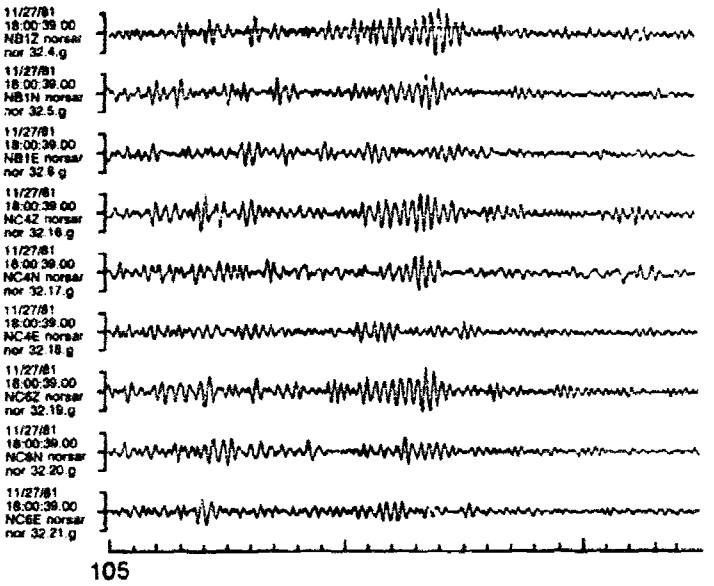

Fig. 4a. Waveform segments (surface wave window) at three 3-component elements of NORSAR from a deep focus event in the Sea of Japan.

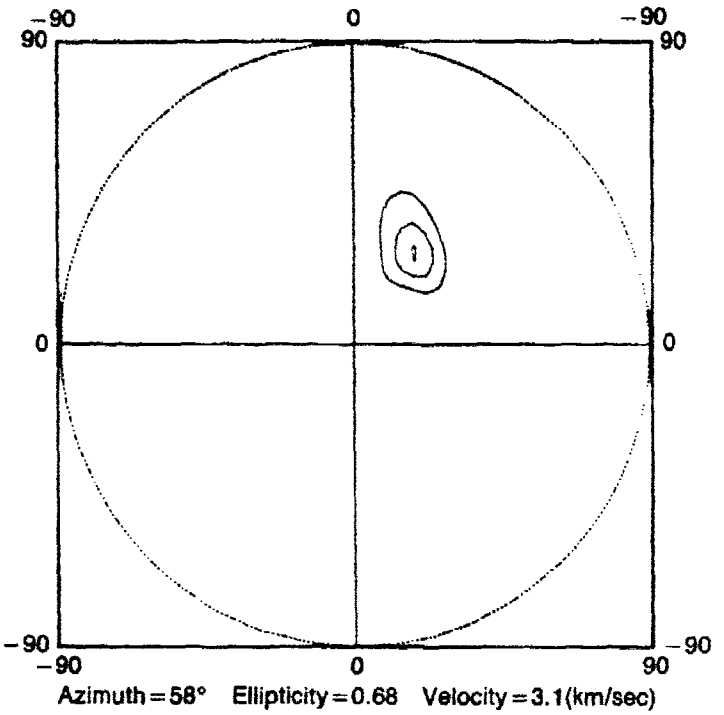

Fig. 4b. Results of Rayleigh wave wave processing.

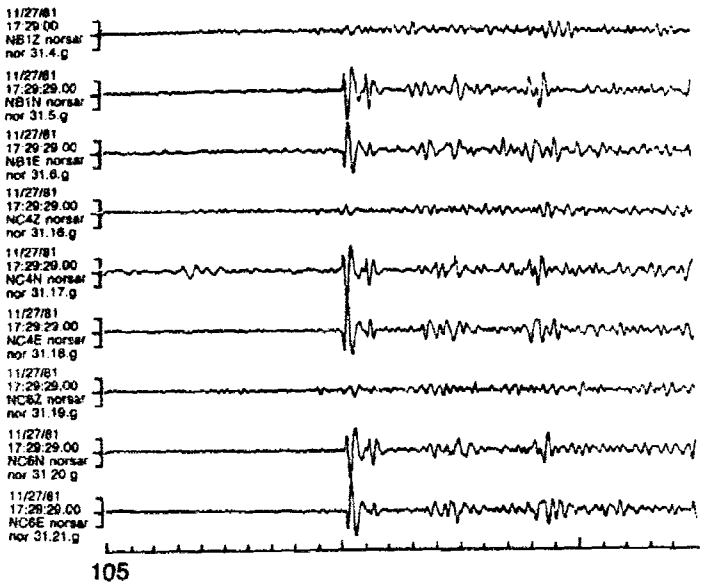

Fig. 5a. Waveform segments (body wave window) at three 3-component elements of NORSAR from a deep focus event in the Sea of Japan.

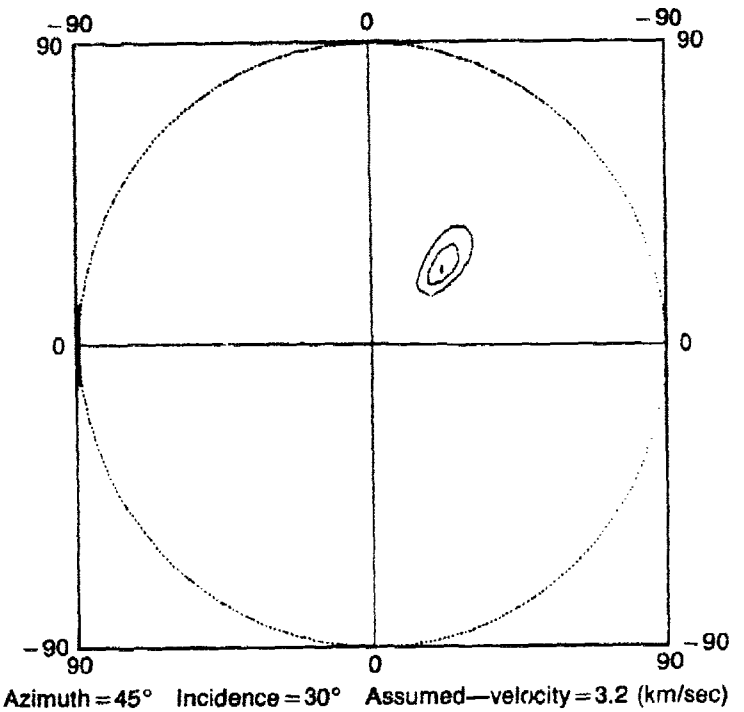

Fig. 5b. Results of *S* wave processing.

segment surrounding the first arrival are shown in Figs. 2a and 2b. From these a back azimuth (295°) and apparent slowness along the ray (1/3.5 sec/km) are estimated. An apparent angle with respect to the vertical is also estimated. This angle can be used together with the slowness along the ray to estimate a horizontal slowness of 1/8.3 sec/km. The slowness estimates are compatible with a velocity of 8.3 km/sec at the turning point of rays comprising the phase and suggest a surficial velocity of about

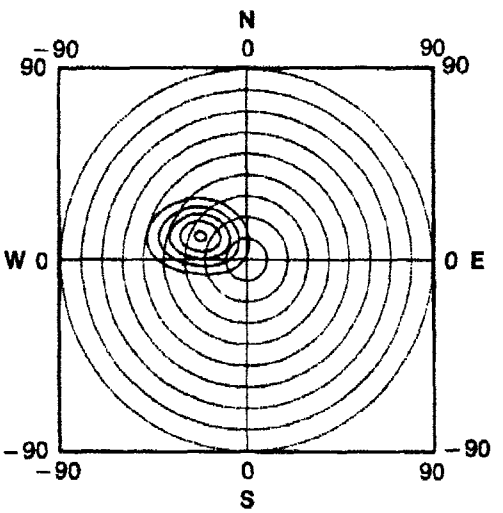

Fig. 2(a). Azimuth-elevation contours obtained from processing Lajitas, Texas, data from Fig. 1. Concentric circles spaced at 10° intervals from the vertical.

Azimuth-elevation plot—peak at −25° and 295°

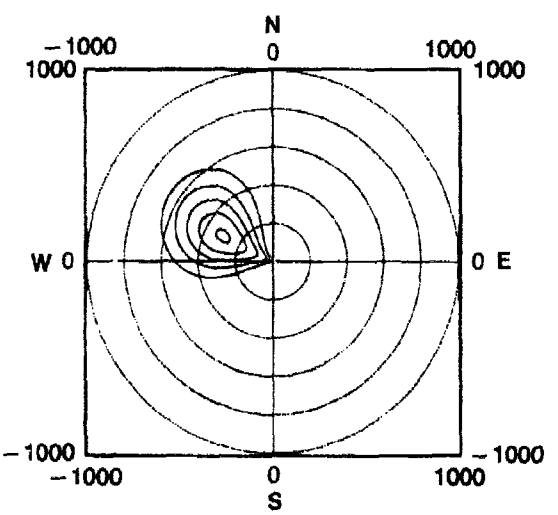

Fig. 2(b). Slowness (along ray direction)-azimuth contours obtained from processing Lajitas, Texas, data. Concentric circles spaced at 0.2 sec/km slowness intervals.

Slowness plot—peak at −1/3.5 sec/km and 155°

algorithm. Indeed, it is encouraging that any Rayleigh wave was found at all because the excitation of the fundamental Rayleigh mode for an event this deep should be small.

References

1. Altes, R.A, "Detection, Estimation, and Classification with Spectograms," *J. Acoust. Soc. Am.*, **67**. 4 April 1980.
2. Baggeroer, A.B. and R. Falconer, "Array Refraction Profiles and Crustal Models of Canada Basin," *J. Geophys. Res.*, **87** B7, 1982.
3. Bienvenu, G., "Underwater Passive Detection and Spatial Coherence Testing," *J. Acoust. Soc. Am.* **65** 2, February 1979.
4. Boore, D.M. and M.N. Toksoz, "Rayleigh Wave Particle Motion and Crustal Structure," *Bull. Seis. Soc. Am.* **59**, February 1969.
5. Capon, J., "High-Resolution Frequency-Wavenumber Spectral Analysis," *Proc. IEEE*, **57** 8, August 1969.
6. Capon, J., R.J. Greenfield and R.J. Kolker, "Multidimensional Maximum Likelihood Processing of a Large Aperture Seismic Array," *Proc. IEEE*, **53**, December 1965.
7. Chan, Y.T., R.V. Hattin and J.B. Plant, "The Least Squares Estimation of Time Delay and its Use in Signal Detection," *IEEE*, 1978.
8. Duckworth, G., A.B. Baggeroer and H.R. Jackson, "Crustal Structure Measurements Near FRAM II in the Pole Abyssal Plain," *Tectonophysics*, **89** 173-215, 1982.
9. Esmersoy, C., "Signal Power Upper Bound in Parameter Estimation," *IEEE Trans. ASSP* **33**, 1, February 1985.
10. Fidler, R.W., and P.N. Carlton, "Locating Seismic Sources Passively," *CASAD*, August 1981.
11. Hamon, B.V. and E.J. Hannon, "Spectral Estimation of Time Delay for Dispersive and Non-Dispersive Systems." *Appl. Statist.*, **23** 2, p. 134, 1974.
12. Hassab, J.C. and R.E. Boucher, "Optimum Estimation of Time Delay by a Generalized Correlator," *IEEE Trans. ASSP* **27** 4, August 1979.
13. McGarty, T.P., "The Effect of Interfering Signals on the Performance of Angle of Arrival Estimates," *IEEE Trans. AES*, **10** 1 January 1974.
14. Neidell, N.S. and M.T. Taner, 'Semblance and Other Coherency Measures for Multichannel Data," *Geophysics*, **36** 3 June 1971.
15. Rikiishi, K., "A New Method for Measuring the Directional Wave Spectrum, Part 1: Description," *J. Phys. Ocean.*, **8** 508, May 1978.
16. Schultheiss, P.M. and J.P. Ianniello, "Optimum Range and Bearing Estimation with Randomly Perturbed Arrays," *J. Acoust. Soc. Am.* **68** 1 July 1980.
17. Seidman, L.P. "Bearing Estimation Error with a Linear Array," *IEEE Trans. AU*, **19** 2, June 1971.
18. Shensa, M. and C. Black, "Passive Bearing Estimation: The Removal of Bias and Two-π Ambiguities," *J. Acoust. Soc. Am.* **63** 1 January, 1978.

Signal Detection by Pattern Recognition Methods

H.P. Harjes and M. Joswig

Summary

The efficiency of a network of high-gain seismic stations largely depends on the ability to automize signal detection and classification for further analysis. In a first step events have to be classified as local, regional, or teleseismic which is conventionally achieved by STA/LTA-detectors operating in different frequency bands. The decision process of a human analyst is much more complex using experience from long observation intervals. This experience can be included in a pattern recognition procedure comparing the instantaneous seismic trace with a set of masks adapted to typical waveforms. A short-term spectral analysis is used to establish a parameter set which is in a wide sense invariant to changes in phase clarity or magnitude for events from a specific region. A practical application in Germany uses a M-68000 microcomputer which can handle up to 50 templates in real time on single channel (100 Hz) data. The detector output from all sites is transmitted to a central station and further evaluated in a second-stage coincidence detector. In a one-month test-run the automatic process approached the performance of a skilled analyst.

I. Introduction

Event detection by automated methods has been an essential element of data processing schemes ever since local or regional seismic networks have been established. Its implementation is, however, heavily influenced by technical constraints. In early networks data were transmitted as analogue signals to a central station before they could be converted to digital format appropriate for further computerized processing. The main disadvantage of this concept was the limited bandwidth of the telemetry — usually about 40 to 50 dB, *i.e.* only a range of two magnitude units between system noise and clipping. In the next step a/d-conversion was shifted to the remote seismometer site thereby improving the dynamic range of data acquisition. The Graefenberg (GRF) broadband array (Ref. 1) uses this technique, but in real time operation there is a limitation with regard to the product of number of channels, sampling rate, and word length, defined by the capacity of the transmission line.

Typically in Germany 2400 baud lines are available which are already saturated by 1 seismometer a/d-converted with 16 bit and digitized at 120 Hertz.

Communication networds with automatic computer controlled switching (× .25, in Germany DATEX-P) introduces new possibilities for local or regional seismic systems because data transmission can be handled pseudo-offline, if each station is equipped with an event detector implemented in a local microprocessor. Transmission rates are thus governed by the seismicity level and the available amount of local storage capacity. To avoid disintegration of the network into a set of isolated single stations an automated dialogue between remote stations and a central facility can be implemented. Initially all stations store their data locally and send a message to the center each time an event is detected. The central processor decides from a number of criteria including coincidence and other measures either to accept these messages or to reject them as false alarms. In case of acceptance all stations including those which did not report a detection are automatically requested to send data; otherwise, all stations get the message to release stored data.

By separating event decision (short communication) and data transmission the network operates quite efficiently even with high false alarm rates at single stations.

II. Detection By Pattern Recognition

The detector design is critical to the effectiveness of the seismic network as outlined in the previous paragraph. Fig. 1 shows the basic elements of two typical single channel detectors (Refs. 2 and 3). In a first step the seismic data pass a frequency filter usually adapted to the optimum s/n-band at the station. It may include more than one passband to separate local and teleseismic events. Subsequently, the detector

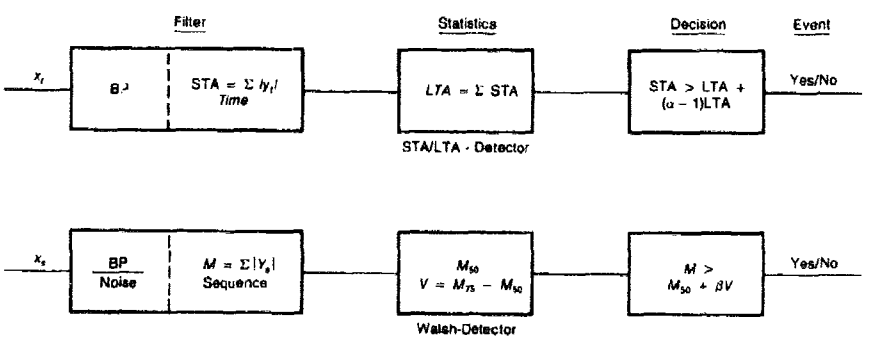

Fig. 1. Logical structure of single-channel detectors.

algorithms include a transformation of the time series which represents short-term changes in the waveform. This transformation may be simply taking the absolute value of the input data or rather complex operations like Fourier or Walsh transforms. In the past the choice of the algorithm was mainly determined by the computational power of the microprocessor, but this is now made less important with the new generation of 16/32 bit microprocessors. Now the trade-off between sophistication and robustness of the algorithm is the ultimate obstacle (Ref. 4).

The next block includes the estimation of the long-term behavior of the time series which is usually derived from second order statistics and recursively calculated from the short-term function. A detection is declared whenever the short-term function exceeds a threshold defined as some multiple of the long-term expression, where this multiple is a function of the variance of the STA/LTA-ratio during noise conditions. This decision is independent of the future developments of the signal, thus it does not take into account later phases which might have higher s/n-ratio especially on local or regional seismograms. It is the knowledge of this overall picture which makes the human analyst superior to an automated single phase detector.

Several attempts were made to reconstruct the time-frequency behavior of seismograms with a low order parameter model and this resulted in a short-term spectral analysis using FFT.

The interpretational disadvantages of the Walsh transform were compared against its computational advantages which became less attractive in the light of 16/32 bit cpu's.

The computational procedure transforming the time series into a 'sonogram' is shown in Fig. 2. Segments of 2.56 s length (sampling rate is 100 Hz) are windowed by a cosine function and Fourier transformed. The short-term power spectrum is plotted on a logarithmic frequency scale every 1.25 s using overlapping windows.

In Fig. 3 (upper part) a seismogram of a local earth quake ($m_l = 2.0$, epicentral distance = 35 km) is compared to a sonogram of the same event (lower part) which clearly shows the frequency shift between *P*-phase and *S*-phase and even gives some indication of surface wave dispersion.

These spectral representations of typical regional events were used to establish a set of templates which were then implemented in an automated detector. One of these masks taken from the master event plotted in the previous graph is shown on top of Fig. 4.

This mask is compared with the sonogram (lower part of Fig. 4) from a smaller event of the same region by calculating the coincidence at several power levels of the spectrum in exponentially increasing steps starting from the noise background. The reference value is set to one within the

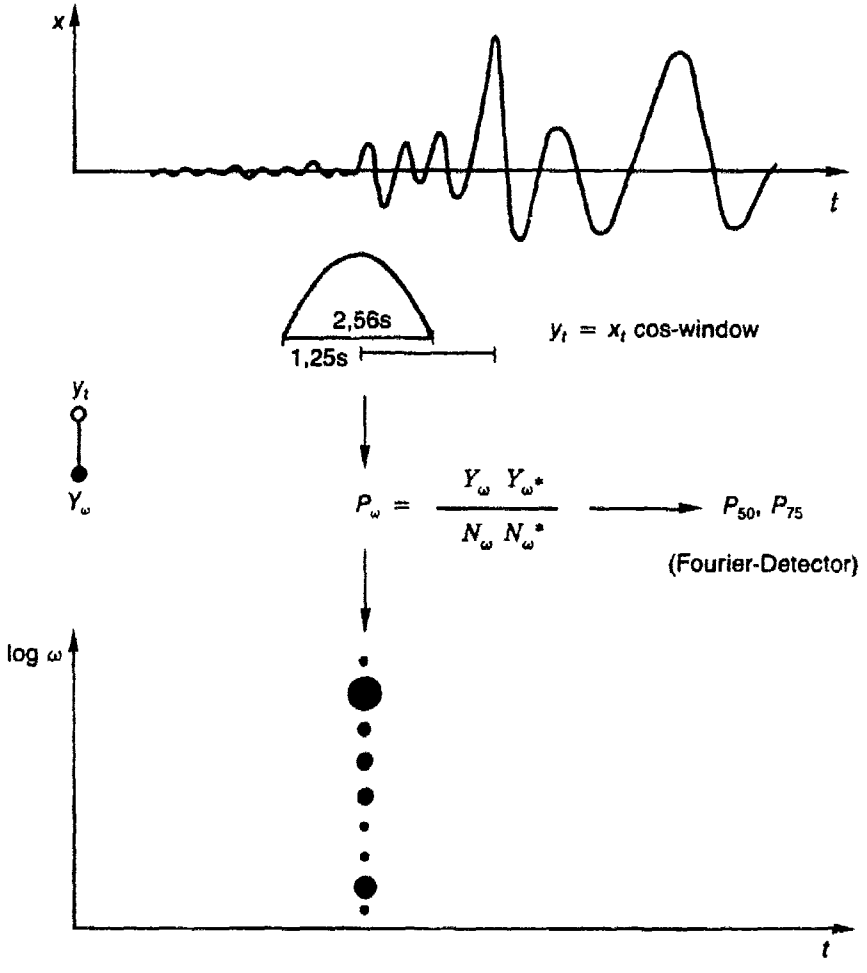

Fig. 2. Computational procedure for sonograms.

template and to zero outside. Furthermore, to enhance the contrast to the noise background the edge of the template is inverted (value -1).

The comparison is performed in 13 frequency bands at each intensity level every 1.25 seconds. Stations are equipped with M68000 microprocessors which can handle up to 50 masks in realtime. This number is sufficient to include all known local sources and, additionally, some templates are used for typical noise sources as well as teleseismic events. Fortunately, events from the same region are very stable in their spectral picture, so the templates are robust to changes in phase clarity and magnitude.

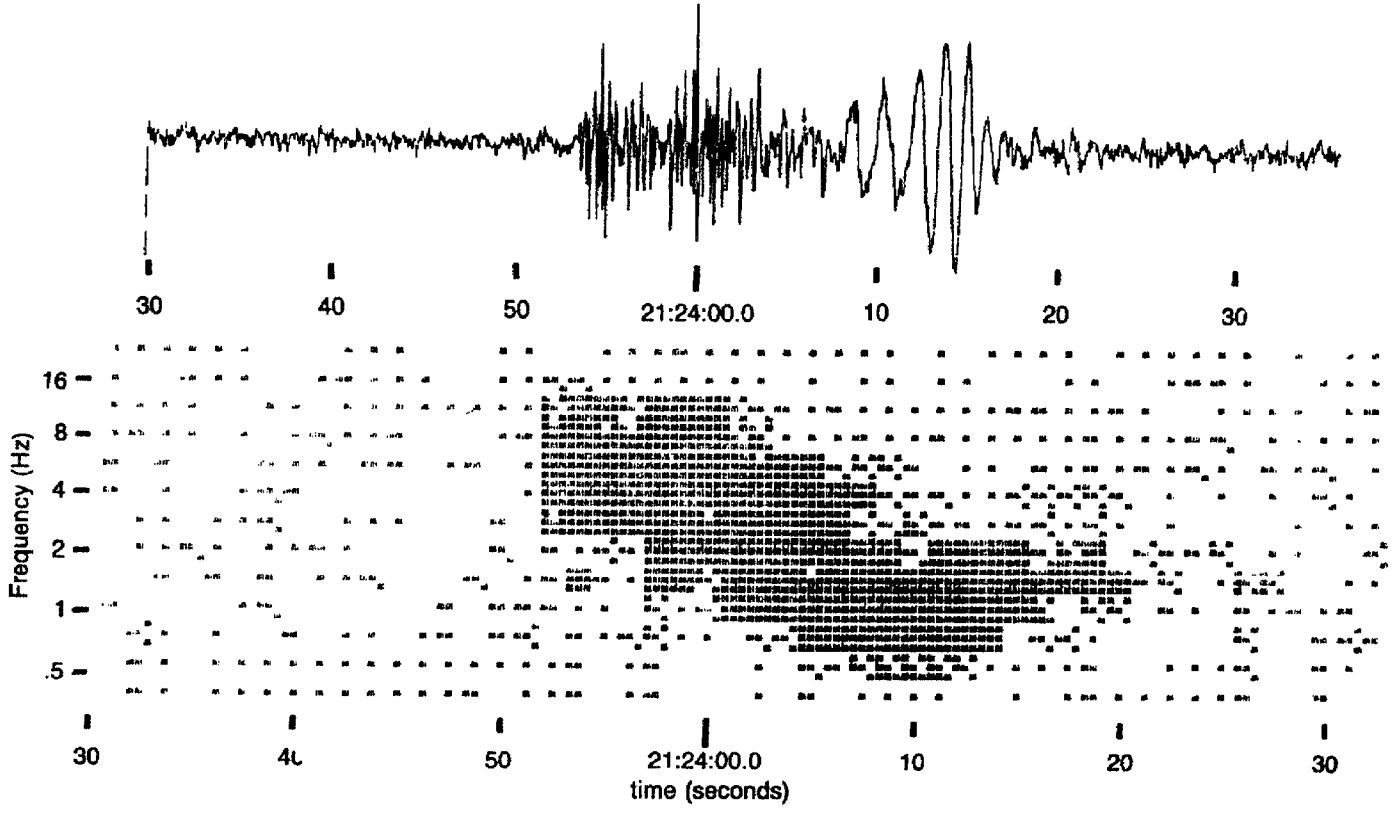

Fig. 3 Time series and sonogram of a local earthquake.

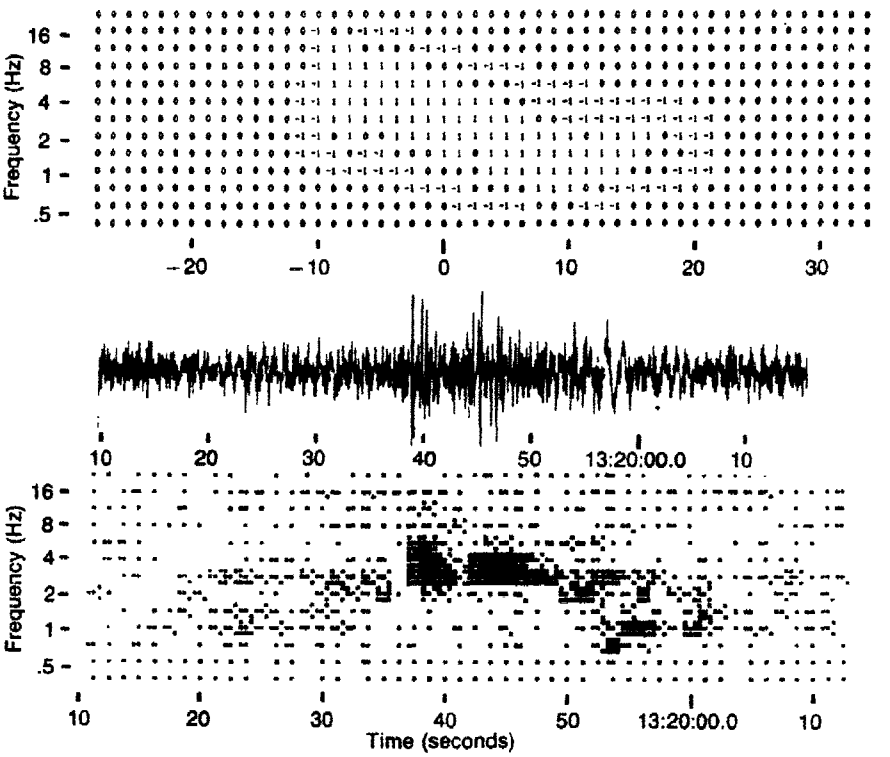

Fig. 4. Mask from master event (Fig. 3) compared to sonogram with lower s/n ratio.

Coherence values for templates at single stations can easily be transmitted to the central computer to be compared in the coincidence detector. Furthermore the center can transfer new templates to specific sites or update old ones by using the communication facilities within the network.

Preliminary results from a one month test-run have shown that the automated detector easily approaches the performance of a skilled analyst. It allows a cost-effective operation of a seismic network even in areas of high seismic noise level.

References

1. Ferber, R. and H.P. Harjes, "Adaptive Processing of Digital Broadband Data", *IEEE-GE*, 1984 (in press).
2. Goforth, T. and E. Herrin, "An Automatic Seismic Signal Detection Algorithm Based on the Walsh Transformer", *BSSA*, **71**, 1351-1360. 1981.
3. Harjes, H.P. and D. Seidl, "Digital Recording and Analysis of Broadband Seismic Data at the Graefenberg (GRF) Array", *J. Geophys.*, **44**, 511-523, 1978.
4. Lee, W.H.K. and S.W. Stewart, *Principles and Applications of Microearthquake Networks*, Academic Press, 50-60, 1981.

Digital Data: How Good Is It?

Robert Kemerait

Summary

This paper discusses the procedures currently being performed by ENSCO on collecting existing digital and hand-digitized seismic data. The emphasis is on quality control and formats.

The recent increase in availability of digital seismic data has resulted in a proliferation in the use of these data as part of basic research. As a direct result, a host of new research areas are now becoming available to seismologists. Examples include the maximum likelihood to event magnitude estimation, improved magnitude yield estimate procedures, path and attenuation studies, source studies (including focal mechanisms, radiation patterns, depth, etc.), and first motion detection, to name a few.

As these data have become more accessible to the researchers and more sophisticated processing techniques are applied, new demands are necessarily placed on these data. Common demands are for more accurate system response information, better network coverage (i.e. more data), better instruments (i.e. more bandwidth), more accurately calibrated data, and additional instrumentation (typically arrays and three-component long and short period data).

ENSCO has been heavily involved in the collection of existing digital data, the transformation of analog data (existing in several forms) to digital data, and the quality control of the data so that it will support this increased activity. This paper attempts to cover the major area of research and their direct relationship to improvements and limitations of the data. Our history of data collection has made us cognizant of the quality and character of these data.

I. Introduction

The recent shift of emphasis to digital data by the seismic community has opened many opportunities for basic research. This shift has been somewhat complicated by several factors such as:

- Limited number of Worldwide Digital Stations for networks such as the SRO and WWSSN,

- Remaining extensive networks of analog stations (WWSSN),
- Operating time frames such that many key events exist only in analog form,
- Limited number of arrays which are extremely valuable when processed digitally,
- Majority of analog data with very limited dynamic range, and
- System response functions which are in many cases, a problem area.

This paper indicates how several sources of data have been handled by ENSCO and where additional research is needed. A much needed result is a quantification of the effects each data shortcoming has on the results obtained from a specific processing tool.

The specific data sources which will be addressed in this paper are the World Wide Standard Seismograph Network (WWSSN), the Seismic Research Observatory (SRO), the Canadian Network Data, classified data, and other data such as NORSAR.

II. Technical Discussion

This section discusses a number of the problems/peculiarities associated with the seismic digital data. Unfortunately, more questions seem to be raised than answered. The single most important quantity that digital data makes available is the spectrum. Unfortunately, the teleseismic short period spectrum is in an extremely narrow band which causes complex problems in its use and interpretation (see Fig. 1). Signal processing techniques which are routinely applied to broadband signals are much more difficult to apply on these data. The remainder of this section treats those situations of most concern to the seismologist.

1. Instrument (Systems) Response and its Removal. Contrary to situations using analog data, digital data lends itself to correcting (removing) both the attenuation or amplification of the amplitude spectrum as well as modifications to the phase spectrum. Several problems which occur with much of the seismic data at this point are:

a) Calibration (yielding amplitude and phase information) is not satisfactory much of the time,

b) The system was not designed so that the phase response is easily removed (typical problem areas are the design of analog and digital filters),

c) The large dynamic range in frequency (extremely small values

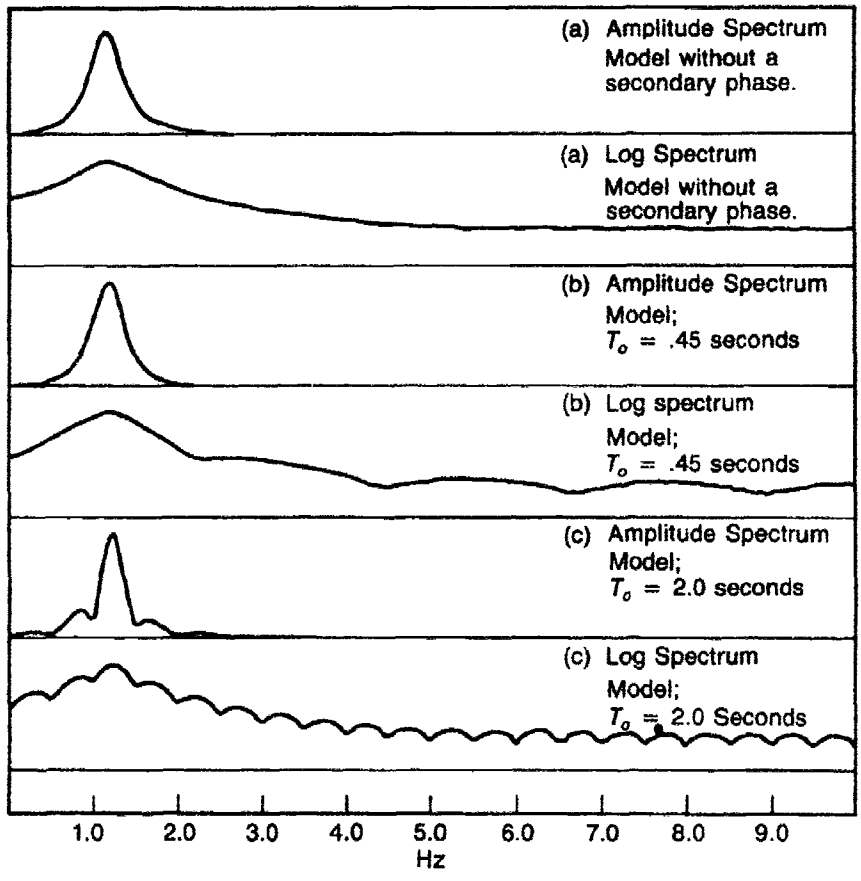

Fig. 1. Berlage model spectra; (a) basic model, (b) simulation of a shallow event, and (c) simulation of a deep event. (Reproduced from the chapter by Kemerait and Sutton, 1982).

at higher frequency can cause gross errors when removing the system response at these higher frequencies), and

d) The required data spans a considerable length of time so that the precise system configuration (response) may not be known at any one time.

2. Noise Sources. In addition to the seismic noise and the additive system noise, there are additional sources inherent in the digitization process and the subsequent processing. These include the following:

a) *Quantization noise* which is reduced by increasing the number of bits per sample,

b) *Aliasing noise* which is reduced by increasing the complexity of the analog prefilter,

c) *Gain-ranging* techniques which are usually employed for increasing the dynamic range of the data. Figure 2 is a simple example which illustrates the difference in spectral content obtained from the same system with a change in its dynamic range,

d) *Interpolation of the data* which is usually required since the samplers do not sample exactly at 20 and/or 1 sample per second (Fig. 3 shows spectral effects of interpolated sampling at different times), and

e) *Uncertainties associated with spectral processing*, examples of which are spectral leakage, main lobe smoothing, *etc.*

Within reason all of these noise contributions (except the seismic noise) are negligible in the vicinity of 0.5-2.0 Hertz which roughly corresponds to the frequency range of the analog data previously used for manual operations such as amplitude and period measurements. Above the 2 to 3 Hertz range, these noise sources most probably are not negligible and therefore should be accounted for in any process using these higher frequencies. Their importance is directly related to the specific signal process being applied to the digital data.

3. Diverse Origins of the Digital Data. When processing a specific event (earthquake or explosion), the seismologist may encounter digital data from several sources. Typical sources are:

a) Digital data digitized at or near the seismometer output in a real time mode. This method should yield the best possible data assuming uniform sampler, anti-aliasing filters, *etc.*

b) Digital data converted from analog data originally recorded on magnetic tape. Here we are faced with additional noise sources and a probable loss of overall dynamic range.

c) Digital data created by some form of operator controlled mechanical digitization, from analog data recorded on film or paper media. The method addressed here is the hand-digitizing process which, of course, adds additional sources of noise.

One of the basic questions addressed here is whether data from more than one of these sources should be combined in some of the more sophisticated signal processing now available. Should SRO and WWSSN data, for example, be combined in spectral studies for t^* or depth analysis, *etc.*

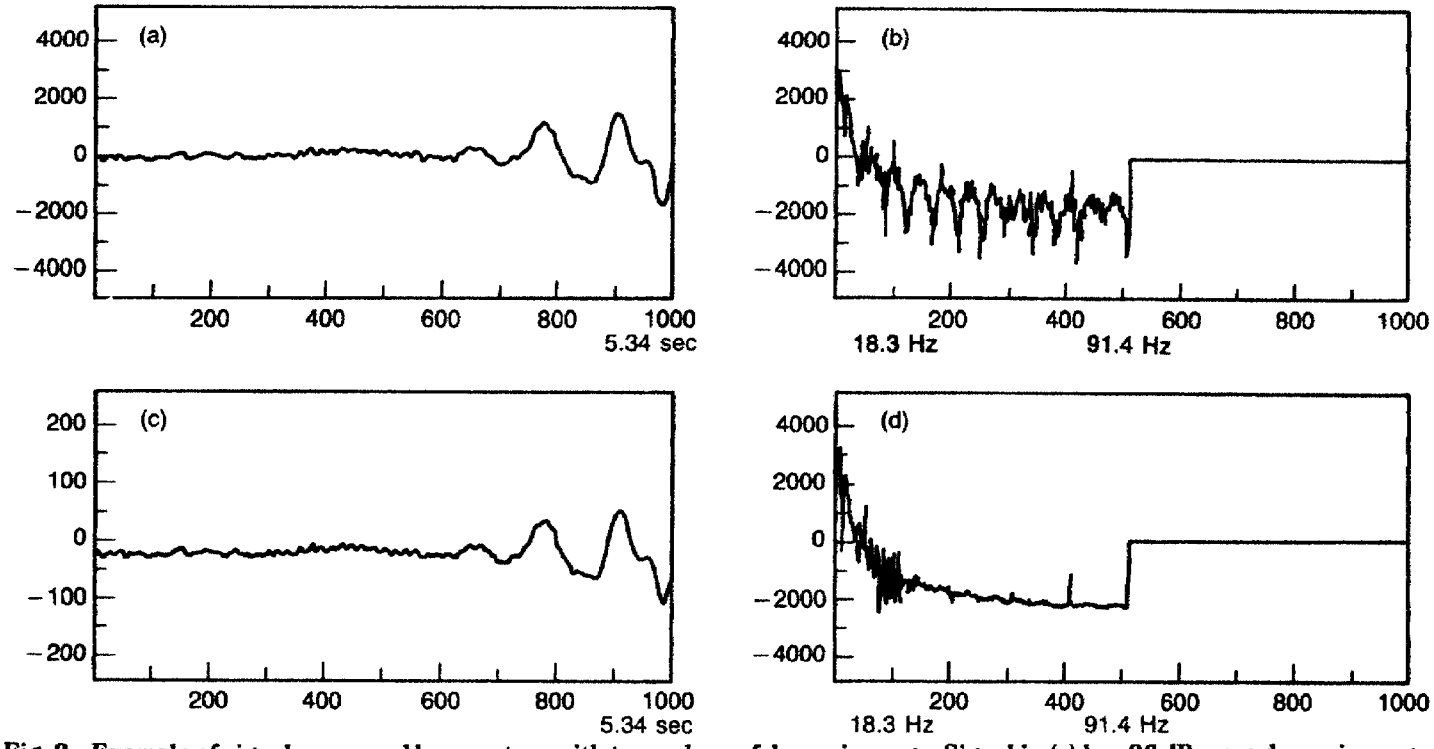

Fig. 2. Example of signal processed by a system with two values of dynamic range. Signal in (a) has 26 dB more dynamic range than signal in (c). 2(b) and 2(c) are the respective computed spectrums.

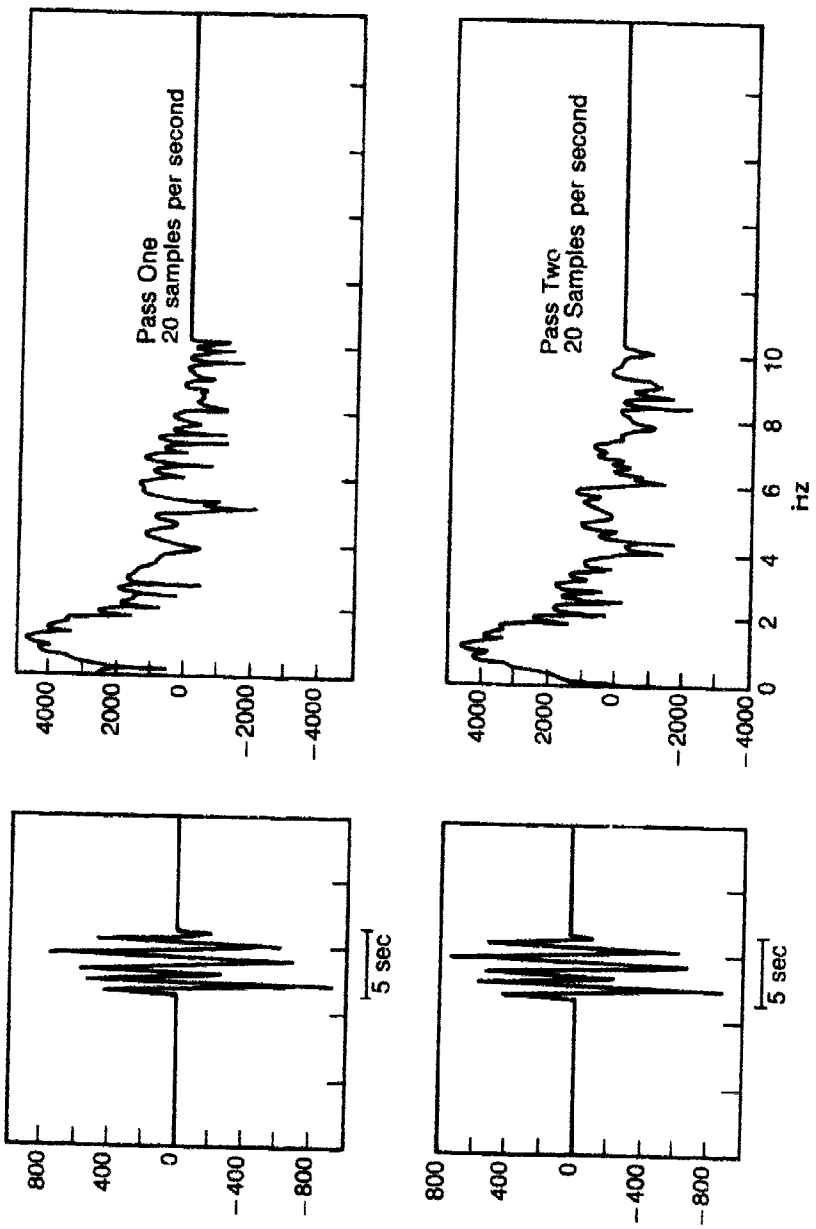

Fig. 3. Comparison of signal and spectrum from two different digital samplings of the same signal.

The method for collecting and organizing digital data currently employed by ENSCO is portrayed in Fig. 4. The procedure is basically to collect all usable digital data, machine digitize all usable analog tape

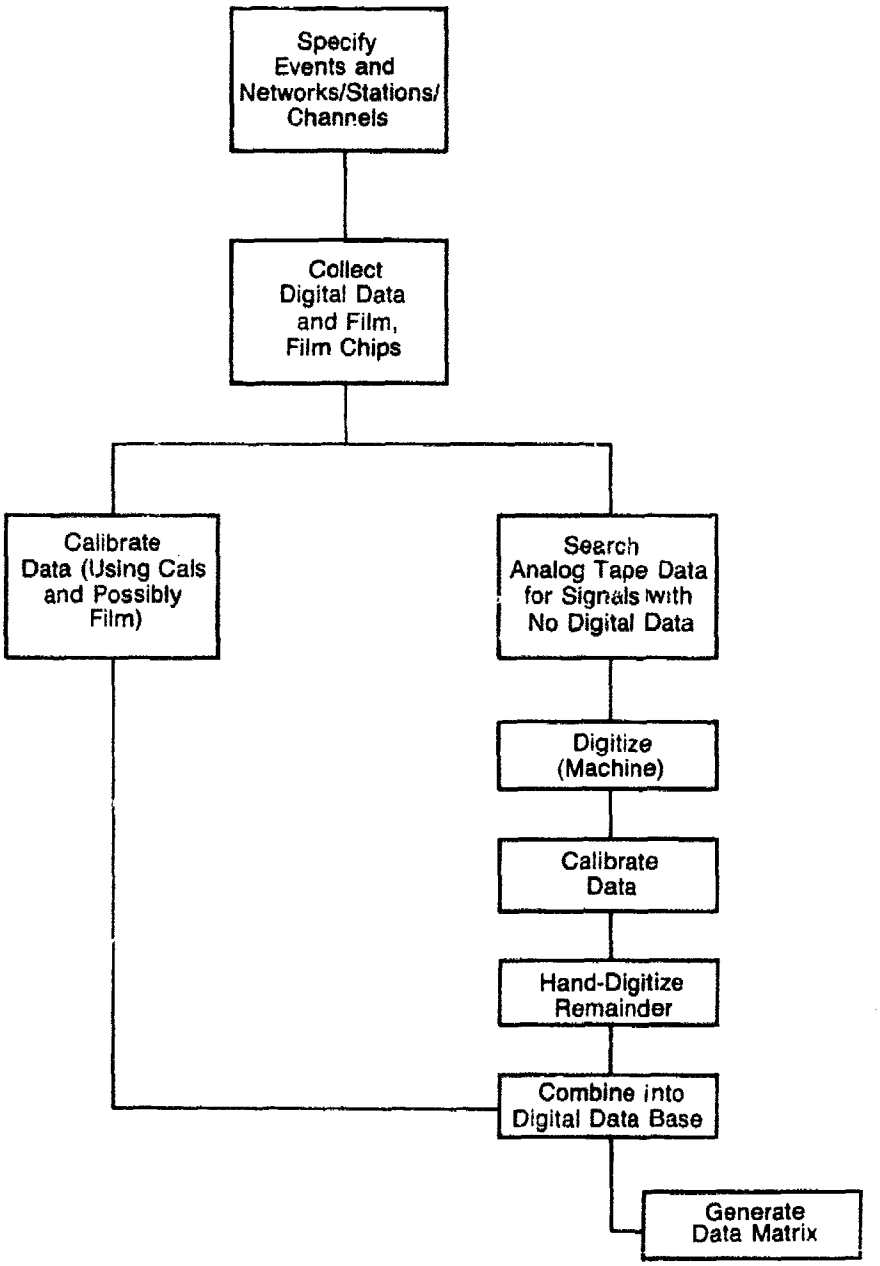

Fig. 4. ENSCO data flow for generating EVENT oriented digital data.

recorded data and digitize any remaining sources of film or paper recorded analog data. We have considered optical methods of digitizing this data and believe them to be of marginal use for most of the data we are currently handling (see Fig. 5).

For any data sources offering both digital and film or paper recorded analog data, we use analog data as a check on digitally recorded earth motion. The rationale is that the analog recorded data is much more visible and therefore less prone to error in magnification assignments. Obviously, periodic amplitude and phase calibrations are much more desirable and are given priority utilization, when available.

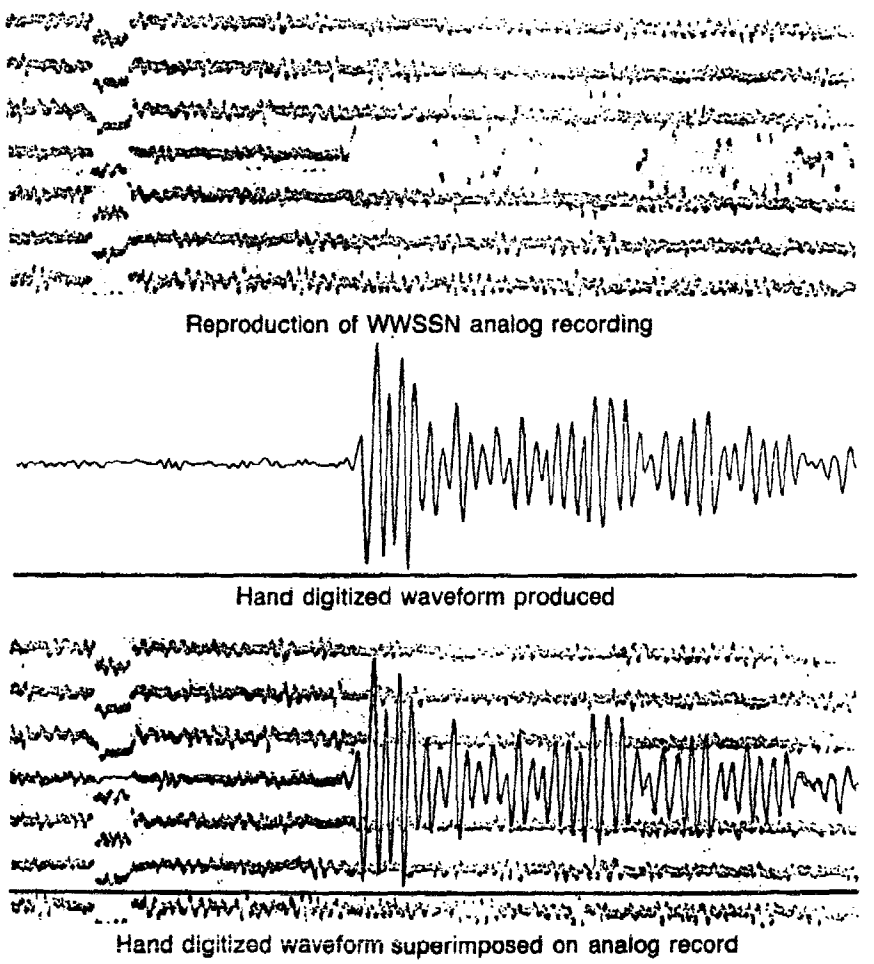

Fig. 5. Hand digitized signal produced from a marginal recording.

4. World Wide Seismic Data (WWSSN). The procedure developed by ENSCO during the past four years in the conversion of WWSSN analog data to digital data bears some detailed discussion.

A Minolta reader/printer is used to produce enlarged hard copy prints from the USGS-provided analog microform. (70mm chip or 32× reduction microfiche). The hard copy is then positioned on a TALOS 30″×40″ digitizing tablet and traced using a hand-held cursor. Both continuous point-to-point modes are used depending on signal amplitude and complexity. The distance between *x-y* coordinates, output from the tablet, is selectable in 0.001 inch increments starting at 0.005 inches.

The output from the TALOS tablet, in combination with associated SMART firmware, is then processed by ENSCO's HP-1000/45 computer system. The software features:

- Several options for removal of waveform "tilt" caused by helical recording media or mechanical misalignment.
- Hermite-Wiggins interpolation method.
- Numerous automatic checks on items such as time intervals and alphanumeric header information.
- Numerous interpolated segments can be concatenated and stored in 1000-point formatted waveform records.
- Emphasis on quality control with routine production of transparent digital waveform plots at the exact scale of the hard copy print used for digitizing. This step is accomplished while the hard copy is still positioned on the tablet, allowing easy editing of any waveform portions not exactly corresponding to the print. See Figs. 5 and 6 for examples of the hand digitizing results.

5. Data Formats. All data, regardless of source, is currently supplied by ENSCO in a standard format illustrated by Fig. 7. Additionally, we supply plots, scaled to a maximum peak-to-peak amplitude of one inch, for all hand digitized waveforms and a single page data matrix for each event. A summary of collected data is automatically entered into the matrix, including coded waveform lengths, channels and source. Additional information is hand entered and normally includes reasons for data exclusions. Standard examples are station inoperative, data unusable, *etc.*

III. Results, Conclusions and Recommendations

This paper has attempted to explain the peculiarities associated with the several data sources ENSCO has been collecting as well as to stimulate

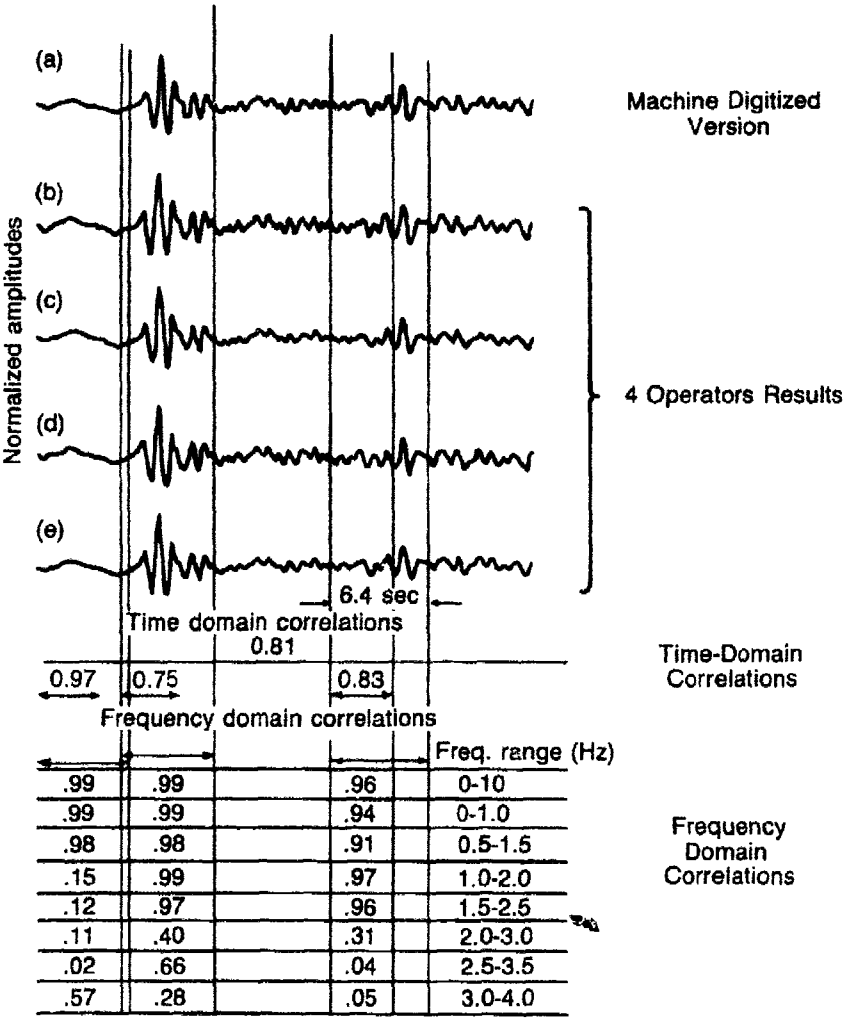

Fig. 6. Effects obtained from different operators hand digitizing identical signals.

interest in the problems/limitations of these data, especially those collected at teleseismic distances. Considering the purposes for which the several systems were designed and the length of time that they have been operational, the quality and quantity of the digital data now available and being made available is a major feat in itself.

Conversely, we believe that the researcher should be cautious in the processing of these data without regarding those limitations mentioned in this paper. One example is the validity of the spectral content in the 5 to 10 Hertz range. One should question the quality below 5 Hertz

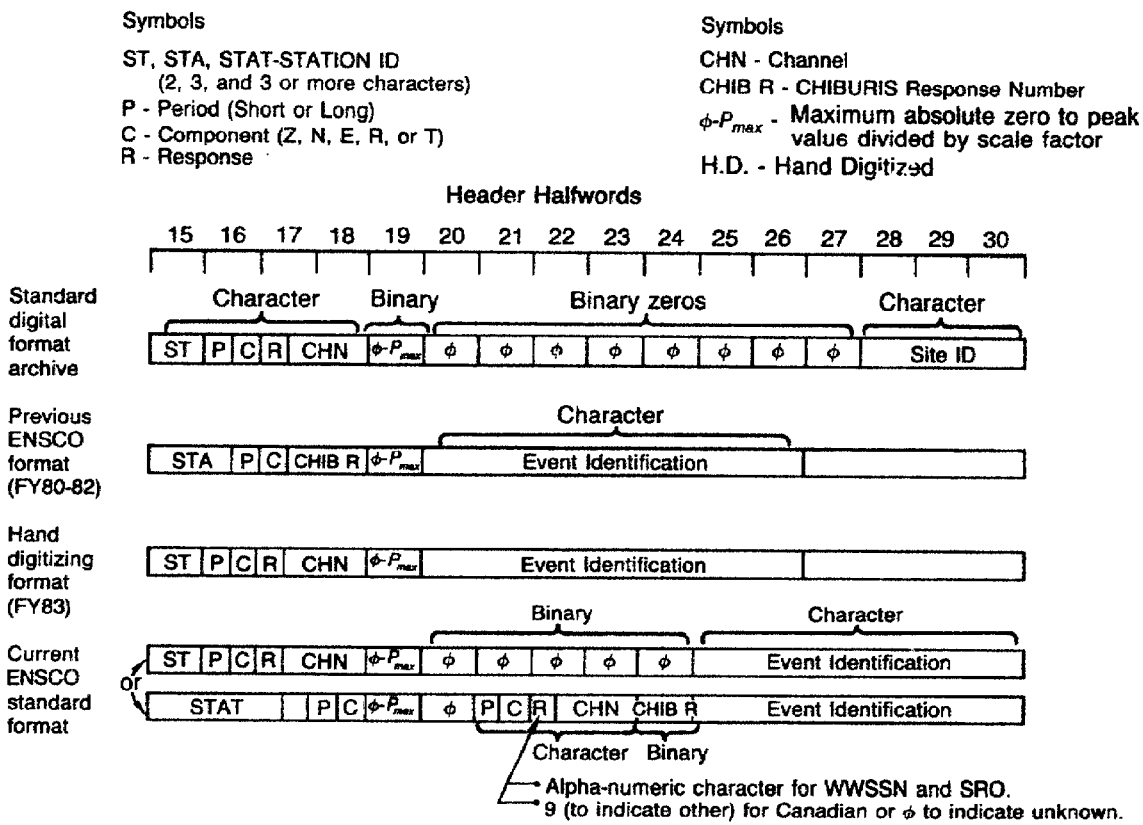

Fig. 7. Digital waveform header formats previously used and currently in use by ENSCO.

as well. Also, since in many applications all available data for a specific event is used, the researcher should take into account the differences in seismometers and systems (dynamic ranges, for example) as they directly relate to the processing and results that he is expecting.

Since many of these data exist for "one of a kind" events, we suggest that some level of research be undertaken to explain and quantify noise sources, such as those discussed. Particularly, the effects that they have on the various techniques being investigated in areas such as depth estimation, magnitude/yield estimation, *etc.* These investigations, we believe, should be run concurrent with the basic research required to develop new broadband instrumentation which should minimize most or all problems of this type.

Estimating Seismic Yield and Defining Distinct Test Sites Using Complete Waveform Information

Thorne Lay, L.J. Burdick, D.V. Helmberger and C.G. Arvesen

Summary

A new method for estimating the yields of events at a nuclear test site, and for identifying anomalous events and distinct subsites, is introduced and tested using Amchitka and NTS events. The intercorrelation method is an analytic relative waveform comparison technique, which involves convolution of the first few seconds of each short-period P wave recorded at a given station for two events with estimates of the effective source function (including pP) for the other event. This procedure accounts for common path and receiver effects as well as differences in time functions and near-source surface interactions. If the source parameters for a master event are determined independently, the assumed source parameters for a second event can be adjusted to minimize the residual differences in the intercorrelated signal pairs for a large number of stations simultaneously. Yield estimates can then be made using empirical relations between the source parameters and yield.

Introduction

The current procedure for estimating the size of nuclear events from seismic data is to infer yield from an m_b-yield calibration curve. The calibration curve is based on events of known yield from a few sites, but it is applied to events all over the world. This approach has several well-recognized shortcomings. One of these is the fact that the observations used to establish the calibration curves exhibit substantial scatter; moreover, it is a difficult type of scatter to deal with. Most events fall into a normal population on the m_b yield plane, but there are occasional outlyers that clearly belong to a different population. These events may have anomalous coupling, be overburied, or be strongly affected by tectonic release, but they obviously need to be analyzed separately from the rest of the events. A second shortcoming is that m_b is an overly simplified measure of a seismic signal. Since m_b is strongly influenced

in the period range spanned by both the teleseismic and the near-field data, as is shown by Lay *et al.* (1984). In applying the intercorrelation technique we will use Eq. (1) to allow comparison with the near-field results of Paper 1.

The intercorrelation procedure is presented in Fig. 1, where the observations from the two Amchitka events LONGSHOT [$O_L(t)$] and MILROW [$O_M(t)$] are displayed. If we have an effective source function for MILROW, $M(t)$, we can estimate the LONGSHOT source, $L(t)$, by noting that, if the Green's functions, anelastic attenuation filters, and instrument response are the same,

$$M(t) * O_L(t) = L(t) * O_M(t) \tag{3}$$

Actually, for this to work in the Amchitka case, where the depths vary substantially, the effect of pP must be included in the source function rather than in the propagation Green's function. That is, in this expression we assume the following:

$$O_M(t) = [E(t) + R_{pP}E(t + \Delta t)] * [S_M(t) * I(t) * Q(t)] \tag{4}$$

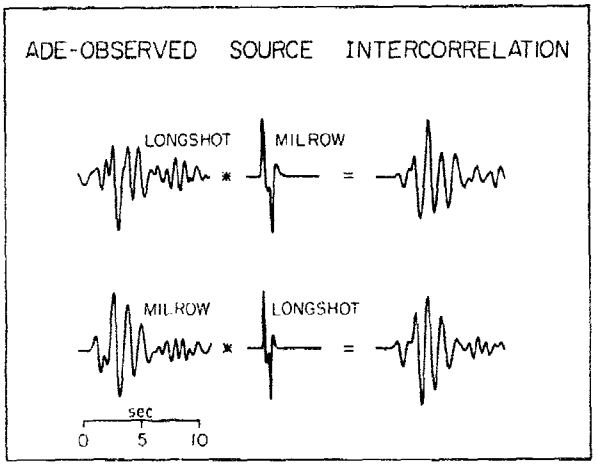

Fig. 1. An illustration of how the intercorrelation procedure accounts for waveform differences produced by the source. In the top row the LONGSHOT observation at station ADE is convolved with the expected MILROW source function, which includes the pP arrival and the source time function. The bottom row shows convolution of the MILROW observations at ADE with the LONGSHOT source function. The resulting signals are compared using equations (9) and (10). The waveform norm is minimized by adjusting the pP parameters, and the amplitude norm gives the ψ_m values. In practice this procedure is applied to many stations simultaneously.

by propagation and receiver effects it is necessary to rely on large numbers of azimuthally distributed measurements to obtain a 'representative' average. Much information about the nuclear source than can easily be determined from the seismic data is neglected if m_b is the sole measurement used. A third problem with current practice in yield estimation is that curves developed in one test site must be translated to new test sites with no proof that this procedure is valid. In fact, it is suspected that yield scaling behavior does vary from place to place. It has been suggested in negotiations that it would be useful to prescribe regions of the earth that are "distinct test sites". By definition, yield scaling relations are constant within these sites.

It is reasonable to expect that a technique utilizing the complete amplitude and waveform information contained in teleseismic P waves should provide more robust yield estimation than attainable using m_b alone, particularly if a limited number of observations is available. Since in most cases it is necessary to rely on data from high gain, narrowband short-period instruments, it is very desirable to adopt a procedure that explicitly accounts for the complex short-period propagation and receiver effects. One such technique was proposed by Mellman and Kaufman (1981), who developed a relative waveform inversion method that compares the P waves of two nuclear events recorded at a given station. Differences in the two observations are mapped into a simple parameterization of the transfer function that differs between the events. For explosions that are similar in size and close enough in location that the path and receiver properties are the same, the transfer function for each event can be idealized as a spike train consisting of P and pP arrivals. and Kaufman (1981). Because events of very different size are analyzed, the transfer functions we use include the source time functions as well as the P and pP arrivals, and the procedure is applied to many stations at the same time. This generalized procedure is called "intercorrelation." To overcome the inherent trade-offs of the relative waveform analysis, the results from near-field modeling are used to establish the absolute baselines needed to completely describe the effective seismic source functions.

The Intercorrelation Procedure and Analysis of Amchitka Events

Since the primary purpose of this report is to appraise the use of complete time domain waveform information for estimating seismic yield, it is desirable to apply such analysis to events that have been extensively studied, essentially as a test case. The three nuclear tests on Amchitka Island (LONGSHOT, MILROW AND CANNIKIN) are an obvious choice.

These events span a large range in yield and burial depth and were detonated at nearby sites. They have also been the subjects of many seismological studies, several of which have emphasized the source characteristics of the events (*e.g.* von Seggern and Blandford, 1972; King *et al.*, 1974; Burdick *et al.*, 1982). The most complete analysis was performed by Burdick, Wallace, and Lay (1984) (hereafter referred to as Paper 1), who performed forward modeling of near-field and teleseismic data for the Amchitka events. The difficulties encountered in extracting source parameters by forward modeling of the teleseismic data motivated the development of the method presented here.

Paper 1 presented modeling of near-field P and Rayleigh wave signals for MILROW and CANNIKIN, using a modified Haskell source model given by:

$$\psi(t) = \psi_\infty \{1 - e^{-Kt} [1 + Kt + (Kt)^2/ 2 - B(Kt)^3]\} \quad (1)$$

where ψ_∞ is the DC level source strength, K is the rise time parameter, and B governs the time function overshoot. Values of K and ψ_∞ (with B set equal to 1) were determined. The parameters B and ψ_∞ trade off inversely in the high frequency near-field data, so the ψ_∞ values found are not necessarily the actual DC source strength. A similar trade-off exists for narrowband short-period teleseismic data. However, for a given value of B there is a unique value of ψ_∞ that will give the correct source spectral amplitude in the passband of the data used. To emphasize that this is not necessarily the true DC source level, we will call the resulting parameter $\psi_\infty{}'$ where the superscript indicates the trade-off with B. To overcome this uncertainty, long-period surface wave signals must be analyzed simultaneously with short-period data (Lay *et al.*, 1984). However, it is shown below that for the Amchitka test site there is a simple power law relation between yield and $\psi_\infty{}'$ which suggest that accurate yield estimation is possible even using narrowband data alone.

Paper 1 also showed that for the larger Amchitka events the corner frequency parameter, K, scales with burial depth, h, and yield, Y, as predicted by the Mueller-Murphy (1971) relation:

$$K = C_1 h^{0.42} / Y^{1/3} \quad (2)$$

where C_1 is a constant for a given test site. While the latter relation was developed in the context of a source model for which the high frequency asymptote fall-off is proportional to ω^2, it is not surprising that it also holds for the ω^3 model given by (1). This is because the yield-scaling of the corner frequency is more important than the spectral decay rate

where:

$S_M(t)$ is the actual MILROW source time function.

$E(t)$ is the real earth response to a delta function source for the direct P phase.

$R_{pP}E(t + \Delta t)$ is the real earth response to a delta function for the reflected pP phase, where R_{pP} is the effective reflection coefficient (approximately -1) from the free surface.

Δt is time lag representing propagation to the free surface.

$*$ denotes temporal convolution.

Next, we arrange these operators to obtain

$$[E(t)+R_{pP}E(t+\Delta t)]*S_M(t) = E(t)*[S_M(t)+R_{pP}S_M(t+\Delta t)] \ . \quad (5)$$

We redefine the effective MILROW source $M(t)$ as

$$M(t) = S_M(t) + R_{pP}S_M(t + \Delta t) \quad (6)$$

so that

$$O_M(t) = E(t) * M(t * I(t) * Q(t) \quad (7)$$

and similarly,

$$O_L(t) = E(t) * L(t) * I(t) * Q(t) \ . \quad (8)$$

This assumes that the real earth respond $E(t)$ does not vary between the LONGSHOT and MILROW sites. Thus, by convolving the LONGSHOT observation with the modified MILROW source, $M(t)$, and the MILROW observation with the modified LONGSHOT source, $L(t)$, we should obtain the same time series.

To appraise the intercorrelation results, two norms are used. The first is a waveform norm given by

$$N_w = \frac{1}{n}\sum_{i}^{n} (1 - ccc_i) \quad (9)$$

where n is the number of stations and ccc_i is the optimal lag normalized cross-correlation coefficient for the i th station intercorrelation. This norm is most sensitive to the agreement in zero crossing times between signals

and is often used in waveform inversion techniques (*e.g.* Burdick and Mellman, 1976; Wallace *et al.*, 1981). The second norm retains the absolute amplitude information and is given by

$$N_a = \frac{1}{n}\sum_{i}^{n} w_i \int_t [I_i(t)^2 - J_i(t)]^2 \, dt \qquad (10)$$

where $I_i(t)$ is the convolution of the seismogram recorded at station i for the first event with the source function of the second event, and $J_i(t)$ is the convolution of the seismogram recorded at station i for the second event with the source function for the first event. The w_i are weights applied to give uniform contribution for each station, and the integral is performed for the optimal cross-correlation lag time. If $I_i(t)$ and $J_i(t)$ have unit squared area, and $w_i = 1$, $N_a = 2 \times N_w$. Minimization of the waveform norm gives the preferred pP parameters for each source model and the amplitude norm is minimized for optimal values of $\psi_\infty{}'$.

Results for Amchitka

The results of the MILROW:CANNIKIN intercorrelation are shown in Fig. 2. An interesting result is that the optimal pP-P and $|pP| / |P|$

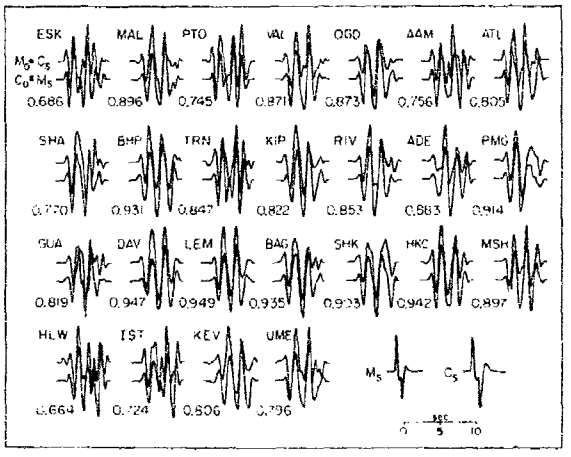

Fig. 2. The waveforms for the optimal MILROW:CANNIKIN intercorrelation. The top trace in each pair is the MILROW observation, M_o, convolved with the CANNIKIN source, C_s, and the second trace is the CANNIKIN observation, C_o, convolved with the MILROW source, M_s. The traces are ordered with increasing azimuth from Amchitka. The pP parameters for the case shown are $pP - p$ = 0.89 sec., $|pP| / |P|$ = 0.7 for MILROW; and $pP - p$ = 1.20 sec., $|pP| / |P|$ = 1.0 for CANNIKIN. The numbers are the normalized cross-correlation coefficients for each pair. The effective source functions for MILROW and CANNIKIN are shown at the bottom.

parameters for CANNIKIN are nearly independent of the values assumed for MILROW. The estimate of $\psi_\infty{}'$ for CANNIKIN decreases as the assumed $|pP| / |P|$ ratio for MILROW decreases. The waveform norm does not change substantially between these models, so it is not clear which *pP* parameters for MILROW are most appropriate, though the ranges are bracketed between pP-P = 0.8 to 0.85 sec and $|pP| / |P|$ = 0.7 to 0.9. With $pP-P$ = 1.2 sec and $|pP|/|P|$ = 1.0 for CANNIKIN the minimum N_w is obtained with $pP=P$ = 0.85 sec and $|pP|/|P|$ = 0.7 for MILROW; thus it could be argued that this is the optimal parameter selection for both events for the given source parameterization. Note that the individual normalized cross-correlation coefficients are generally larger than 0.8 in Fig. 2. This indicates that both source representatives are quite accurate, and that to first order most of the waveform differences are accounted for by the differences in source time functions and *pP* interference. This is because the events are very close together and the ray paths are similar. The results of the intercorrelation of MILROW and LONGSHOT and CANNIKIN and LONGSHOT are comparable to those shown in Fig. 2.

Conclusions for Amchitka

Utilizing complete time domain waveform information to estimate seismic yield appears to be a viable approach. Through a simple parameterization of the explosion source time functions and *pP* interference, it is possible to accurately map observations of an 80 kt event (LONGSHOT) into a 5000 kt event (CANNIKIN). The relative source strengths are estimated using the complete *P* wave signal with emphasis on the common frequency band. Using MILROW as a reference event, and keeping the amount of RDP overshoot the same, the source strength of CANNIKIN is estimated as $4.0 \pm 0.6 \times 10^{11}$ cm^3, compared with $4.5 \pm 0.5 \times 10^{11}$ cm^3 determined by near-field modeling. The source strength of LONGSHOT is found to be $2.0 \pm 0.3 \times 10^{10}$ cm^3. The yield estimates obtained by waveform intercorrelation are not strongly biased by late crustal or slapdown arrivals. It appears that relative waveform comparison gives a less biased estimate of the yield for LONGSHOT than that obtained by standard amplitude analysis.

Intercorrelations for Pahute Mesa

In order to provide a thorough investigation of the intercorrelation procedure, a very large data set of WWSSN and CSN (Canadian Seismic Network) short-period *P* wave recordings for NTS explosions was analyzed. Data sets were collected for the 25 Pahute Mesa explosions shown in Fig. 3 as well as for explosions FAULTLESS (150 km north of Pahute

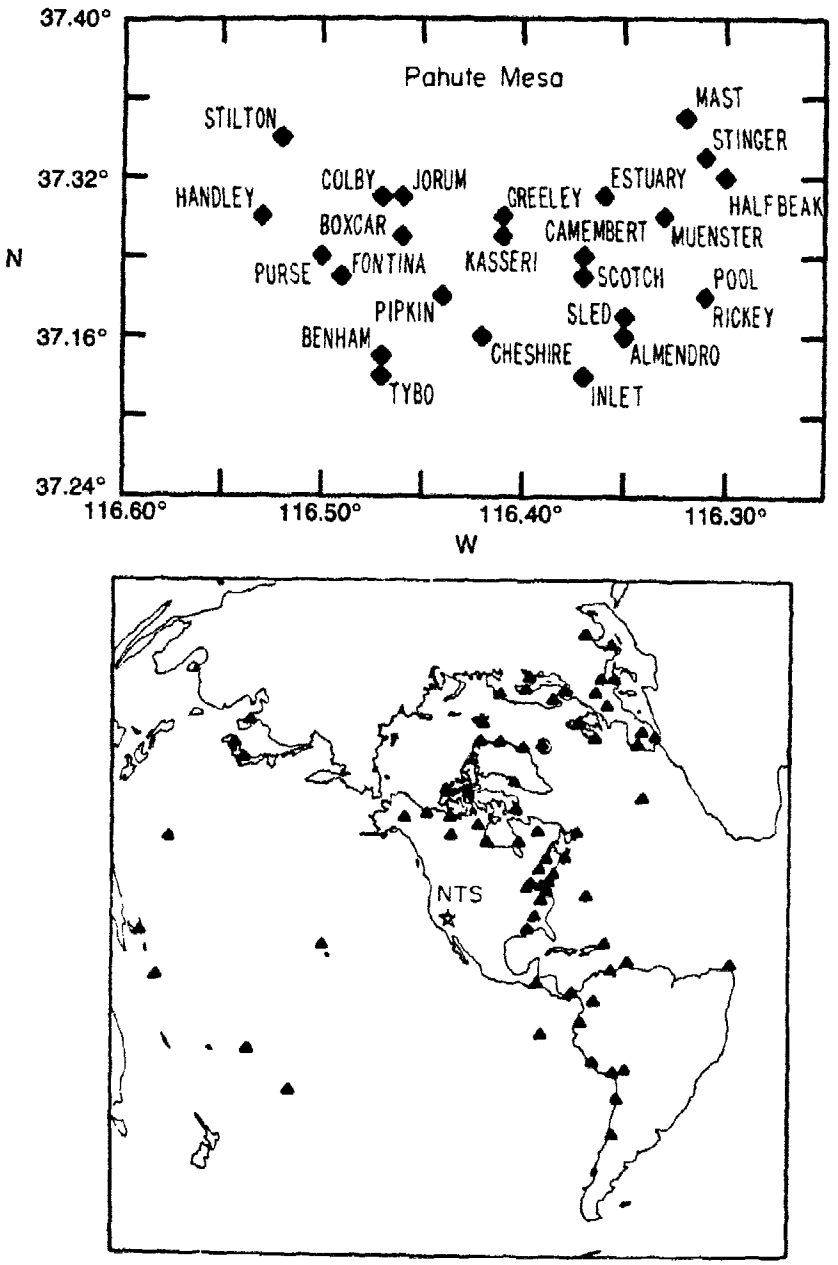

Fig. 3. Top: Base map showing the locations of the 25 Pahuta Mesa explosions for which teleseismic short-period *P* waves have been measured and digitized. Bottom: The distribution of the 74 WWSSN and CSN stations in the distance range 25° to 95° from the NTS from which data were collected.

Mesa), COMMODORE (Yucca Flats), BILBY (Yucca Flats), and PILEDRIVER (Climax Stock). The amplitudes were measured at each of the 74 stations shown in Fig. 3 whenever possible, giving 1284 amplitudes for the 29 events, and the waveforms were manually digitized whenever possible, yielding 1256 signals for 28 events (BILBY was not digitized). Because all of the events considered occurred prior to 1976, relatively little digital data was available for teleseismic stations, though we have found that the intercorrelation procedure can readily be applied to LRSM recordings from several of these events. The motivations for analyzing large data sets for each event are clear. Short-period *P* waves are notorious for rapid amplitude fluctuations and variable coda complexity, thus large data bases are required to provide stable results. It is also very desirable to inspect azimuthal and distance-dependent patterns in amplitudes and waveforms. These hold the key to understanding source effects, including tectonic release, near source velocity structure, and *pP* and slapdown interactions.

The results of the Amchitka intercorrelation study depended on a study of the Amchitka near field data (Paper 1) to establish some of the source parameters. An analogous near field study was performed for Pahute Mesa by Hartzell *et al.* (1983). This study provides enough information about some of the Pahute Mesa tests to allow intercorrelation to be accurate. Events whose properties are constrained by near field data are called "master events." The source parameters of an unknown event are only constrained relative to the master event. The four master events considered in the Pahute Mesa study were SCOTCH, BOXCAR, INLET and MAST.

The results of the Pahute Mesa yield estimation study are presented in Table 1. Since we wish to establish our technique as a superior for yield estimation, we estimated the yields of the events we st d both using amplitude information alone and using intercorrelatic e amplitude measure we adopted for use in our analysis was the first to-first-trough or *ab* amplitude. For all of the events considered the a parent *pP* delay times are 0.7 sec or greater, and thus the *ab* amplitude is generally a measure of direct *P* alone. We began by correcting each of the 1284 amplitude measurements for geometric spreading and station gain. Because different sets of stations were available for each event, it was necessary to develop station correction factors. We did so following the procedure given in Butler and Ruff (1980). The observed amplitude at each station for a given event was multiplied by the appropriate correction factor and the results averaged to obtain the mean amplitude *A* for that event. To obtain yield estimates from these averages, the announced yields for four Pahute Mesa events SCOTCH (155 kt),

Table 1. Yield Estimates

	Announced	From *ab* Amplitudes	Dahlman and Israelson	Master Event				
				SCOTCH	BOXCAR	INLET	MAST	Combined
PIP		113	82	63	85	100	86	82
STIN		126	160	98	112	120	126	113
SCO	155	152	140	152	153	150	149	151
PUR		193	150	137	162	175	153	156
RIC		265	300	152	198	250	203	199
STIL		276	275	173	212	223	222	206
EST		332	350	231	348	342	349	316
INL		387	500	294	285	480	315	340
SLE		404	260	245	279	299	252	267
CHE		448	350	269	324	333	340	316
POO		467	500	336	462	479	409	420
TYB		467	380	441	460	481	386	440
MAS		502	520	508	384	454	579	479
HAL		504	450	438	443	452	421	436
ALM		804	570	697	674	770	690	705
CAM		949	750	783	830	961	1003	896
GRE	870	958	830	928	948	1001	1069	987
MUE		1138	600	976	894	1157	1133	1040
JOR		1144	700	1118	1244	1180	1097	1160
KAS		1144	1200	1006	1033	1244	1272	1143
BOX	1300	1162	1000	1086	1216	1044	1131	1120
BEN	1150	1192	1000	1315	1146	1285	1116	1205
FON		1257	900	775	1106	1180	968	1018
COL		1492	900	938	1262	1250	1087	1141
HAN		1806	1900	1858	1753	1952	1766	1831
FAU	1200	1437		1093	1240	983	1207	
COM	250	282		142	296	245	238	
PIL	56	185		59	95	106	91	

GREELEY (870 kt), BENHAM (1150 kt), and BOXCAR (1300 kt) were used to determine a linear relation between log A and log Y. The yield estimates resulting from this procedure are listed in Table 1 along with those presented by Dahlman and Israelson (1976).

Yield estimation through intercorrelation analysis was accomplished at Pahute in much the same way that it was at Amchitka. Each of the 4 master events studied by Hartzell *et al.* (1983) was used to estimate relative values of the pP parameters and $\psi_\infty{}'$ of all of the events under consideration. The value of B in Eq. (1) was fixed at 1.0 and values for K were estimated from an empirical relationship between near-field measurements of K and the average teleseismic amplitude A. The waveform norm was used to define the optimal pP parameters and the amplitude norm was used to define $\psi_\infty{}'$. Typical results from the intercorrelations are shown in Figs. 4 through 7. Final yield estimates were obtained by regressing the $\psi_\infty{}'$ estimates on the Pahute events with

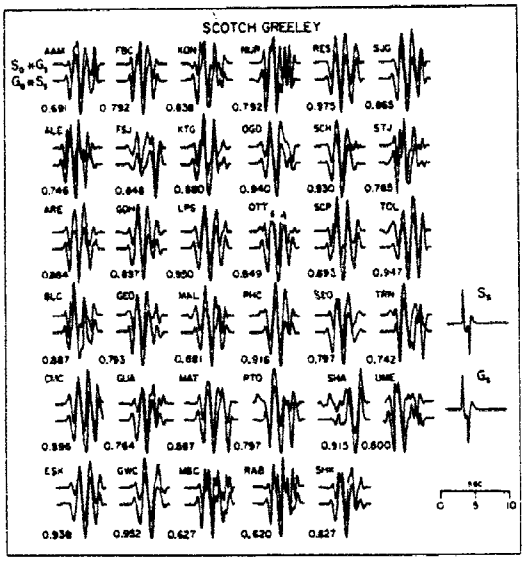

Fig. 4. Intercorrelation of SCOTCH and GREELEY. K = 10 for SCOTCH and 7.5 for GREELEY. The normalized cross-correlation coefficients for each station are shown below each trace pair. The effective source functions are shown on the right.

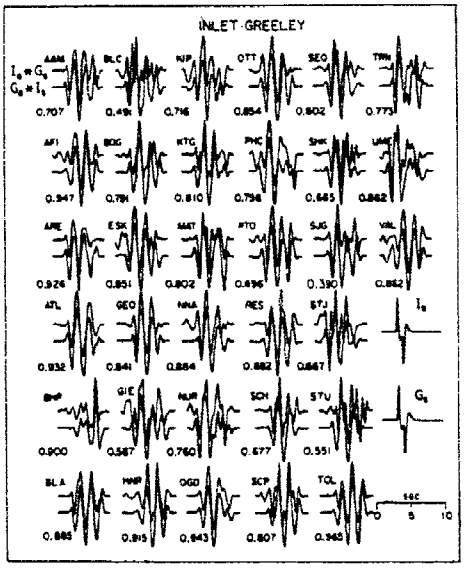

Fig. 5. Intercorrelation of INLET and GREELEY. K = 9 for INLET and 7.5 for GREELEY. The normalized cross-correlation coefficients for each station are shown below each trace pair. The effective source functions are shown on the right.

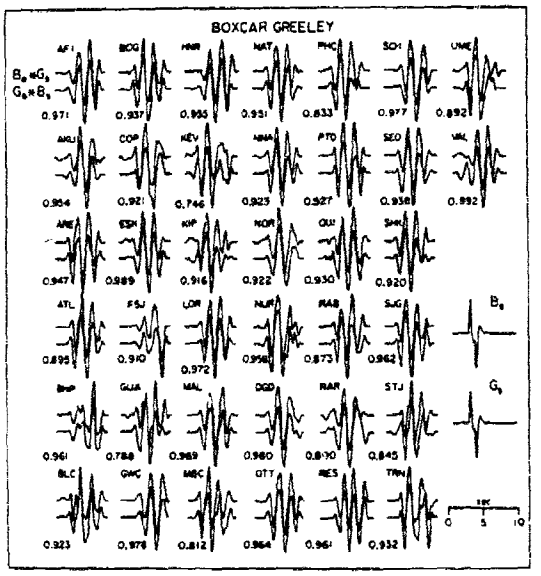

Fig. 6. Intercorrelation of BOXCAR and GREELEY. $K = 7$ for BOXCAR and 7.5 for GREELEY. The normalized cross-correlation coefficients for each station are shown below each trace pair. The effective source functions are shown on the right.

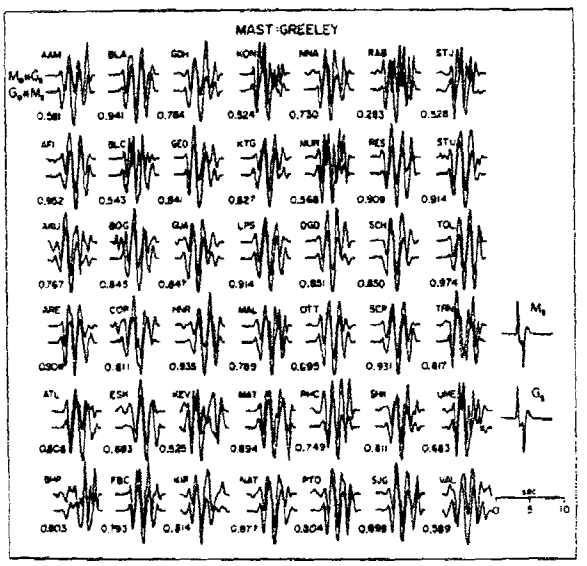

Fig. 7. Intercorrelation of MAST and GREELEY. $K = 6$ for MAST and 7.5 for GREELEY. The normalized cross-correlation coefficients for each station are shown below each trace pair. The effective source functions are shown on the right.

announced yields. This was done separately for each master event and for a combined data set. The results are given in Table 1.

Pahute Mesa as a Distinct Test Site

Up to this point we have emphasized the Pahute Mesa results, since 90% of our data is for those events. In both the amplitude and intercorrelation analyses, we treated FAULTLESS, PILEDRIVER, COMMODORE, and BILBY as though they were additional Pahute Mesa events, just as you would initially treat Soviet events close to but outside a well-studied test site. We found that the intercorrelation results gave large residual waveform mismatches for COMMODORE and PILEDRIVER and anomalous *pP* amplitudes for COMMODORE. FAULTLESS generally intercorrelated well, and the yields were pretty successfully predicted for all three events, despite these problems. The latter result appears to be rather fortuitous, for very large amplitude scatter was found for each intercorrelation. The waveform variations accompanying these amplitude patterns are also quite dramatic. The poor correlations obtained when intercorrelating Pahute Mesa events and PILEDRIVER and COMMODORE result from the clear waveform differences which appear at certain azimuths.

Conclusions

This project has been concerned with developing the intercorrelation technique to provide a means for estimating yield and identifying anomalous events and distinct test sites. A fundamental question is whether or not teleseismic, narrowband short-period recordings contain more useful information than just an amplitude sample. Clearly, scattering and receiver effects are dramatic, but the two studies presented in this report indicate that if a reasonable approach is adopted there is much information to be gleaned from using complete waveform information. Establishing exactly what is deterministic and what is not in these signals is difficult, and this report probably represents the biggest effort to date to address this question. An encouraging outcome is that when the intercorrelation process has worked poorly, indicating an anomalous event, there have been readily apparent waveform anomalies in the original data. Results with different master events have proved relatively consistent and stable.

This study is in many ways a preliminary investigation and as additional near-field modeling is performed additional master event analyses will be possible. Detailed consideration of the azimuthal and distance dependence of the individual station intercorrelations shows promise of increasing our understanding of *pP* and spall behavior as well as possible

contamination by tectonic release. The latter possibility has increased in plausibility given the recent demonstrations of high stress drop tectonic release.

The ψ_∞ estimates provided by the intercorrelation process can be used to predict yields, though a complete appraisal of their success is not possible with the few announced yields. Relative amplitudes that are free of *pP* contamination, as are the *ab* amplitudes for Pahute Mesa events, give similar relative estimates of event size. Further work is ongoing to appraise whether the intercorrelation estimates are superior to those obtained by m_b analysis of the same data set.

In summary, the use of the analytic comparisons of complete waveform information shows much promise for improving our understanding of underground explosion radiation and short-period wave propagation. The technique provides quantitative measures of the similarity of explosions and can be utilized to define anomalous events as well as distinct test sites.

References

Burdick, L.J., and G.R. Mellman, "Inversion of the Body Waves of the Borrego Mountain Earthquake to the Source Mechanism," *Bull. Seism. Soc. Amer.*, **66**, 1485-1499, 1976.

Burdick, L.J., D.M. Cole, D.V. Helmberger, T. Lay, and T. Wallace, *Effective Source Functions From Local Surface Observations*, Final Technical Report WCCP-R-82-01, Woodward-Clyde Consultants, Pasadena, California, 1982.

Burdick, L.J., T. Wallace, and T. Lay, "Modeling Nearfield and Teleseismic Observations From the Amchitka Test Site," *J. Geophys. Res.*, **89**, 4373-4388, 1984.

Hartzell, S.H., L.J. Burdick, and T. Lay, *Effective Source Functions for Pahute Mesa Nuclear Tests*, Final Report WCCP-R-83-3, Woodward-Clyde Consultants, Pasadena, California, 1983.

King, C.Y., A.M. Abo-Zena, and J.N. Murdock, "Teleseismic Source Parameters of the LONGSHOT, MILROW and CANNIKIN Nuclear Explosions," *J. Geophys. Res.*, **79**, 712-718, 1974.

Lay, T., D.V. Helmberger, and D.G. Harkrider, "Source Models and Yield-Scaling Relations for Underground Nuclear Explosions at Amchitka Island," *Bull. Seism. Soc. Amer.*, **74**, 181-200, 1984.

Mellman, G.R., and S.K. Kaufman, *Relative Waveform Inversion*, Semi-Annual Technical Report SGI-R-81-048, Sierra Geophysics, Seattle, Wash., 1981.

Mueller, R.A., and J.R. Murphy, "Seismic Characteristics of Underground Nuclear Detonations. Part I. Seismic Spectrum Scaling," *Bull. Seism. Soc. Amer.*, **61**, 1675-1692, 1971.

von Seggern, D., and R. Blandford, "Source Time Functions and Spectra for Underground Nuclear Explosions." *Geophys. J. R. astron. Soc.*, **31**, 83-97, 1972.

Wallace, T.C., D.V. Helmberger, and G.R. Mellman, "A Technique for the Inversion of Regional Data in Source Parameter Studies," *J. Geophys. Res.*, **86**, 1679-1685, 1981.

Study of Magnitudes, Seismicity and Earthquake Detectability Using a Global Network

Frode Ringdal

Summary

Based on 10 years of observations reported in the ISC bulletins (1971-1980), m_b magnitudes for about 70000 earthquakes have been recomputed using a maximum-likelihood estimation technique. Reportings from a network of 115 globally distributed stations were used in these calculations. Comparison to conventional m_b estimates show that the network magnitude bias problem is quite significant at low and intermediate magnitudes. Recurrence statistics based on the revised m_b estimates give b-values consistent with those obtained from LASA and NORSAR data, and indicate that the number of earthquakes worldwide of $m_b \geq 4.0$ averages about 7500 annually. The teleseismic detection capability of the network (requiring at least four detecting stations) has been estimated based on recurrence statistics. The estimated 90% incremental m_b threshold ranges from 3.9–4.5 in the northern hemisphere, and from 4.2–4.8 in the southern hemisphere. This is consistent with results obtained by the "Networth" approach.

Introduction

The problem of bias in magnitudes estimated by a network of stations has been addressed in a number of investigations, *e.g.*, Husebye *et al.* (1974), Ringdal (1976), Evernden and Kohler (1976), Chinnery (1978), Christoffersson (1980), Elvers (1980) and Clark (1983). Most of these studies have concluded that the bias problem is indeed significant, especially at low magnitudes. The maximum-likelihood estimation technique described by Ringdal (1976) and Christoffersson (1980) has been shown to reduce the bias significantly. In this paper, this method is adapted to a global network of the type reporting to the International Seismological Centre (ISC), and is applied to 10 years of ISC data (1971-1980). The revised magnitudes thus obtained are compared to those obtained through conventional estimation techniques, and are also used to develop seismicity recurrence relations and to estimate network detection capability.

Method

The basic model used in this paper has previously been described in detail by Ringdal (1976) and Christoffersson (1980). For a seismic network of N stations, let g_i ($i=1,2,\ldots, N$) denote the P-wave detection threshold in terms of log (A/T) of the ith station. Furthermore, for a set of M seismic events of unknown "true" body wave magnitudes ($\mu_j = 1,2\ldots, M$) let y_{ij} denote the P-wave signal level in terms of log (A/T) at the ith station for the jth event. Here, as customary, A/T denotes zero-to-peak amplitude (nanometers) divided by signal period (seconds).

We assume that g_i and y_{ij} can be considered as sampled from normal (Gaussian) distributions as follows:

$$g_i \sim N(G_i, \gamma_i^2) \tag{1}$$

$$y_{ij} \sim N(\mu_j - Q_{ij} + B_i, \sigma_i^2) \tag{2}$$

Here:

G_i is the average station detection threshold in terms of log (A/T),
Q_{ij} is the Gutenberg-Richter (1956) distance-depth correction factor,
B_i is the average station magnitude bias,
γ_i and σ_i are standard deviations within the distributions.

For the jth event we will, for the purpose of magnitude estimation, consider only the subset of stations within the distance range 21-100 degrees. This is in accordance with procedures employed by the ISC. Based on actual ISC reportings, the stations are then further classified into three groups:

A_j : Stations reporting a P-detection with an associated log (A/T) value (y_{ij}),
B_j : Stations reporting a P-detection with no associated log (A/T),
C_j : Stations not reporting a P-detection for the event.

For group C_j, the reasons for not reporting at all could be either that the signal was too weak to be detected, or that the station was inoperative at the particular time. Since we do not have access to the station operations records, it is necessary to treat this problem statistically, as was also done by Ringdal *et al.* (1977). Thus, we will denote by P_{ij} the probability that the ith station was inoperative for the jth event, given nondetection at that station.

Using a procedure similar to that described by Ringdal (1976), we can now derive a likelihood function $L(\mu_j)$ corresponding to the actually observed pattern of detections, nondetections and reported log (A/T) values for the jth event, given that its true magnitude is μ_j:

$$L(\mu_j) = \prod_{i \epsilon A_j} f_{ij}(\mu_j) \prod_{i \epsilon B_j} h_{ij}(\mu_j) \prod_{i \epsilon C_j} [1 - P_{ij}][1 - h_{ij}(\mu_j)] \qquad (3)$$

where

$$f_{ij}(\mu_j) = \frac{1}{\sigma_i} \varphi \left(\frac{\mu_j - (y_{ij} + Q_{ij} - B_i)}{\sigma_i} \right) \qquad (4)$$

$$h_{ij}(\mu_j) = \Phi \left(\frac{\mu_j - (G_i + Q_{ij} - B_i)}{\sqrt{\sigma_i^2 + \gamma_i^2}} \right) \qquad (5)$$

Here, φ and Φ denote the standard normal probability density and cumulative distribution functions, respectively.

The maximum likelihood estimate of the event magnitude μ_j is obtained through numerically maximizing the likelihood function (3). However, before applying this procedure it is necessary to estimate the station parameters G_i, B_i, σ_i, γ_i as well as the probability P_{ij}.

Estimates of G_i and γ_i for each station can be obtained through the procedure developed by Kelly and Lacoss (1969). The parameters B_i and σ_i will be estimated using the procedure of North (1977).

In order to estimate the probabilities P_{ij}, it is necessary to introduce some simplifying assumptions. Thus, we will assume that the *a priori* probability of any station being inoperative is a constant value P. Furthermore, for the jth event, we will assume that all nondetecting stations have the same probability of being inoperative, *i.e.* $P_{ij} = P_j$. Let us for the jth event denote by N_j the total number of network stations (within 21-100°) and by K_j the number of these that did not report. We then set:

$$P_{ij} = P_j = \begin{cases} N_j P / K_j & \text{if } N_j P < K_j \\ 1 & \text{otherwise} \end{cases} \qquad (6)$$

Note that the larger the event, (*i.e.*, the more stations that report), the more likely it becomes that a given nonreporting station is actually

inoperative. The above procedure has the effect of adjusting the probability P_j so that the *conditional* expectation of the number of inoperative stations ($K_j P_j$) matches as closely as possible the *a priori* expectation ($N_j P$).

Station Data

The data base for this study consisted of the ISC reportings for the 10 year period 1971-1980. At any given time in this period, a typical number of about 1000 seismic stations reported observations to the ISC. An investigation of the station reports confirmed the conclusions of North (1977), who analyzed similar data for the period 1964-1973. Thus, the large majority of stations contribute very few observations, in particular of $\log(A/T)$, and would thus be of little use in this study.

For the purpose of magnitude estimation, we found it desirable to select a sub-network of about 100 globally distributed stations. The following basic criteria were applied:

(a) Consistent reporting, preferably over the entire 10 year period

(b) High detectability, *i.e.*, a large number of teleseismic reports

(c) A sufficient number of $\log (A/T)$ reports to estimate station parameters

(d) Adequate geographical distribution.

Clearly, these criteria were sometimes in conflict. For example, several very sensitive stations, *e.g.*, the large LASA array and some VELA arrays, were only operational for part of the time period, but they were, nevertheless, selected. Also, the requirements were made less strict for stations in the southern hemisphere in order to improve geographical coverage. Still, only a few useful stations could be found in Africa and South America. In the end, a total of 115 stations were selected, as listed in Table 1. At any time during the 10 years, about 100 of these were in actual operation.

Table 1 also summarizes estimates of the parameters G_i, γ_i, B_i and σ_i based on the procedures mentioned in the previous section. We note that in applying the Kelly-Lacoss (1969) procedure, a constrained value of $\beta = 2.0$ was used. As shown by Chinnery and Lacoss (1976) such a constraint will have little effect on the estimated thresholds, but it serves to reduce the number of variables in the estimation procedure.

We further note that some stations reported $\log(A/T)$ for a low proportion of their detections. It is clearly possible that their detection threshold

Station Code	Parameters				Station Code	Parameters			
	G	γ	B	σ		G	γ	B	σ
ADK	1.73	0.23	0.22	0.42	KRP	1.71	0.18	0.43	0.36
ALE	0.80	0.21	-0.10	0.30	KTG	1.00	0.25	-0.07	0.29
ALQ	0.76	0.24	-0.20	0.33	LAO	0.43	0.25	0.04	0.35
ARE	1.33	0.15	0.17	0.32	LEM	1.46	0.15	0.11	0.39
ASP	1.34	0.31	0.09	0.39	LOR	0.89	0.25	-0.08	0.33
BAG	1.71	0.17	0.26	0.32	LPB	1.17	0.21	0.18	0.35
BDF	1.07	0.16	0.11	0.35	LPS	1.16	0.16	0.12	0.38
BDW	0.71	0.22	-0.15	0.35	MAIO	0.87	0.16	-0.11	0.37
BHA	0.76	0.08	-0.25	0.32	MAT	1.15	0.19	-0.01	0.38
BJI	1.24	0.18	0.06	0.34	MAW	1.18	0.27	0.04	0.31
BKR	1.29	0.19	0.38	0.33	MBC	0.75	0.26	0.09	0.35
BLC	1.02	0.21	0.21	0.29	MIR	1.48	0.15	0.22	0.33
BMO	0.30	0.17	-0.28	0.35	MNG	1.44	0.22	0.11	0.39
BNG	0.75	0.18	0.01	0.41	MOX	0.98	0.12	0.07	0.25
BOD	1.01	0.12	-0.02	0.34	MOY	1.22	0.14	0.12	0.29
BUL	0.83	0.10	-0.05	0.29	MSO	0.97	0.22	-0.06	0.44
CAN	1.52	0.22	0.11	0.31	MTD	0.82	0.08	-0.12	0.30
CAR	1.45	0.13	0.14	0.40	MTN	1.26	0.24	-0.08	0.38
CHG	1.00	0.23	-0.06	0.36	MUN	1.69	0.24	0.19	0.36
CIR	0.77	0.07	-0.24	0.30	NAO	0.37	0.24	-0.10	0.33
CLK	0.81	0.08	-0.24	0.29	NDI	1.57	0.24	0.30	0.38
CLL	0.97	0.10	0.16	0.28	NEW	0.94	0.23	-0.07	0.39
COL	0.87	0.12	0.07	0.34	NUR	0.98	0.17	0.11	0.46
CPO	0.82	0.16	-0.02	0.35	NVL	1.47	0.30	0.23	0.35
CTA	1.23	0.20	0.07	0.39	OBN	1.33	0.17	0.39	0.33
DAG	0.92	0.15	0.06	0.32	PET	1.61	0.22	0.24	0.36
DUG	0.95	0.26	-0.04	0.31	PMG	1.70	0.16	0.27	0.38
EDM	1.25	0.11	0.43	0.28	PMR	0.97	0.25	-0.11	0.39
EKA	1.04	0.26	0.	0.29	PNS	1.15	0.23	0.11	0.50
ELT	1.16	0.20	0.15	0.34	POO	1.50	0.16	0.19	0.35
EUR	0.54	0.29	-0.36	0.47	PPI	1.48	0.18	0.08	0.41
FFC	0.91	0.23	0.09	0.30	PRE	0.93	0.09	-0.08	0.40
FRB	1.26	0.14	0.37	0.29	PSI	1.14	0.11	-0.02	0.38
FRU	1.39	0.13	0.35	0.33	QUE	1.13	0.18	0.21	0.46
FVM	1.23	0.29	0.25	0.43	RAB	1.90	0.21	0.37	0.43
GBA	1.03	0.29	-0.07	0.42	RES	0.81	0.15	0.04	0.33
GDH	1.26	0.29	-0.05	0.30	SCH	1.48	0.28	0.27	0.34
GRF	1.20	0.26	0.25	0.28	SES	1.31	0.13	0.42	0.28
GRR	1.06	0.22	0.04	0.26	SHL	1.48	0.13	0.22	0.33
GUA	2.18	0.25	0.43	0.40	SJG	1.50	0.18	0.19	0.35
HFS	0.80	0.22	0.13	0.35	SPA	1.21	0.31	0.16	0.37
HYB	1.37	0.17	0.26	0.32	STK	1.55	0.22	0.27	0.38
ILT	1.09	0.17	0.08	0.32	SVE	1.37	0.19	0.37	0.31
IMA	0.93	0.24	-0.16	0.36	TIK	0.99	0.20	0.03	0.37
INK	1.08	0.10	0.25	0.29	TOO	1.50	0.23	0.13	0.35
IPM	1.34	0.13	0.10	0.36	TPT	1.60	0.24	0.09	0.34
IRK	1.17	0.19	-0.03	0.31	TUC	0.92	0.27	-0.17	0.32
JAY	1.70	0.07	0.15	0.41	TUL	1.03	0.23	0.21	0.34
KBL	1.09	0.16	0.15	0.30	TUP	0.76	0.12	-0.35	0.40
KBS	1.35	0.14	0.12	0.32	TVO	1.80	0.22	0.19	0.29
KEV	1.01	0.11	0.05	0.31	UBO	0.42	0.25	-0.13	0.38
KHC	0.88	0.20	0.03	0.26	UPP	1.36	0.09	0.60	0.33
KHE	1.53	0.21	0.37	0.31	WRA	0.71	0.28	-0.20	0.44
KHO	1.69	0.23	0.59	0.35	YAK	1.63	0.20	0.43	0.34
KIR	1.36	0.09	0.61	0.25	YKC	0.99	0.18	0.08	0.34
KJP	0.92	0.10	0.16	0.28	YSS	1.40	0.19	0.20	0.41
KOD	1.33	0.19	0.18	0.35	ZAK	0.86	0.18	-0.11	0.33
KRA	1.34	0.13	0.32	0.29					

Table 1. Estimates of the parameters G_i, γ_i, B_i, and σ_i as defined in the text for the 115 seismic stations selected for this study. Each station is identified by its station code as used by the ISC.

thus is significantly lower than their threshold for reporting log (A/T). This possibility was investigated for each station by comparing the average ISC event m_b for the total set of reported detections with the average m_b for the subset for which log (A/T) was reported. As a first order approximation, we then adjusted the estimated threshold according to the difference between these m_b values.

It should be observed that for some of the most sensitive stations, in particular some arrays, many of their reported detections are not associated with detected events in the ISC bulletin. Thus, the thresholds of Table 1 will be too high in these cases. In practice, this will make little difference in the maximum likelihood procedure since non-detections by these stations for ISC-reported events is usually due to the stations being inoperative. For array stations, we also note that reportings by subarrays, or associated stations, in some cases replaced the full array reporting.

Magnitude Estimation Results

The previously described method and station network was applied to obtain maximum likelihood m_b estimates for ISC-reported events during 1971-1980. Known and presumed explosions were removed from the data set so as not to bias the seismicity estimates. Furthermore, we restricted the data base to only those events which were reported by at least 4 stations of the 115 station network, and which had at least one detection in the distance range 21-100 degrees.

Since our network included most of the better stations reporting to the ISC, the resulting total of about 70,000 events comprised nearly all those events for which any teleseismic reports were included in the ISC bulletins. However, it should be noted that these bulletins also include a large number of events reported by local stations only.

To simplify the calculations, we used in (3) constant values of $\sigma_i = 0.35$ and $\gamma_i = 0.20$, corresponding to the average values over all network stations (Table 1). Furthermore, based on reporting statistics for the largest events, we found a value of $P = 0.15$ to be typical of the average down time of the stations. Simulation experiments showed that a very accurate value of P was not critically important, thus there was no reason to introduce variable P-values, *e.g.*, depending upon year and epicentral region.

Figure 1 shows the resulting frequency-magnitude statistics for shallow events (depth < 60 km) globally. For comparison, similar statistics are also plotted using the magnitude estimation procedure currently employed by the ISC (*i.e.*, averaging observed station magnitudes for all events with at least one log(A/T) report). The large difference in b-values ($b = 0.90$ *vs.*

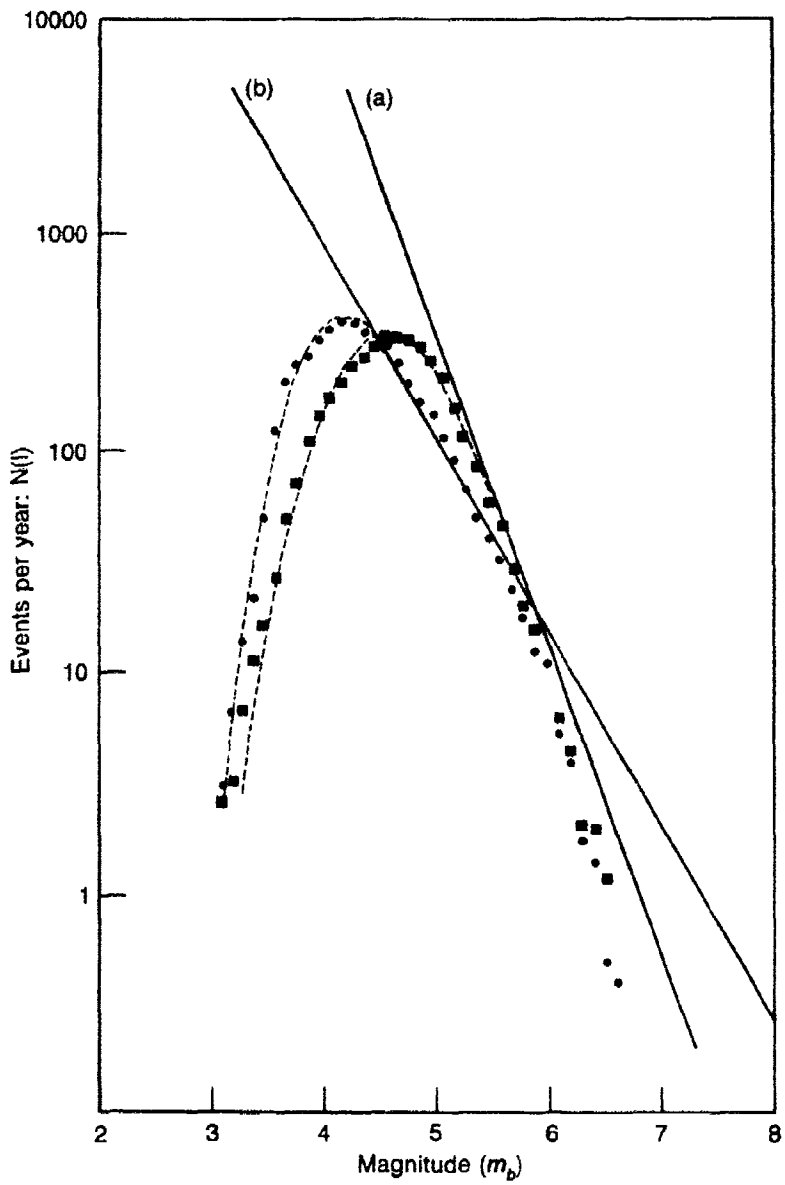

Fig. 1. Incremental recurrence statistics for shallow events (averaged per year), (a) using conventional m_b (one or more station observations) and (b) using maximum-likelihood m_b. The dotted lines indicate the fit of the Kelly-Lacoss model. Note the significant difference in slopes between the two cases.

$b = 1.40$) illustrates the statistical bias resulting from using conventional magnitude estimation.

Figure 1 is quite similar to those obtained when comparing ISC magnitudes to magnitudes reported by sensitive array stations . (Chinnery, 1978, Ringdal and Husebye, 1982). Average b-values obtained from array data for large epicentral regions are typically in the range 0.8-1.0, as demonstrated *e.g.*, for LASA, $b \sim 0.84$ (Dean, 1972), for NORSAR $b \sim 0.83$ (Bungum and Husebye, 1974) and for the VELA arrays, $b \sim 0.93$ (Chinnery, 1978). Thus, the results using maximum-likelihood estimation

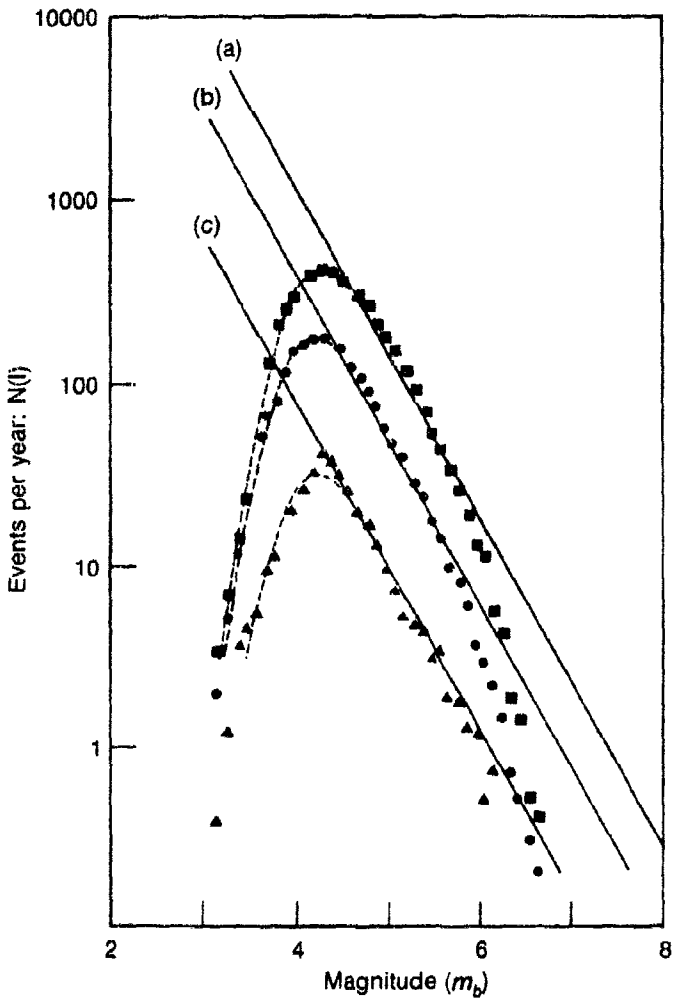

Fig. 2. Incremental recurrence statistics averaged annually for (a) shallow, (b) intermediate and (c) deep earthquakes globally, using maximum-likelihood m_b estimates.

are in good agreement with array studies. However, it must be realized that *b*-values can show significant regional variations (Evernden, 1970), and considerable caution in interpreting these data is therefore required.

Figures 2 and 3 show incremental and cumulative statistics, respectively, averaged annually for shallow, intermediate and deep earthquakes. The slopes are approximately parallel, and have in the plots been constrained to the same value. The best-fitting cumulative relationship can be expressed as follows:

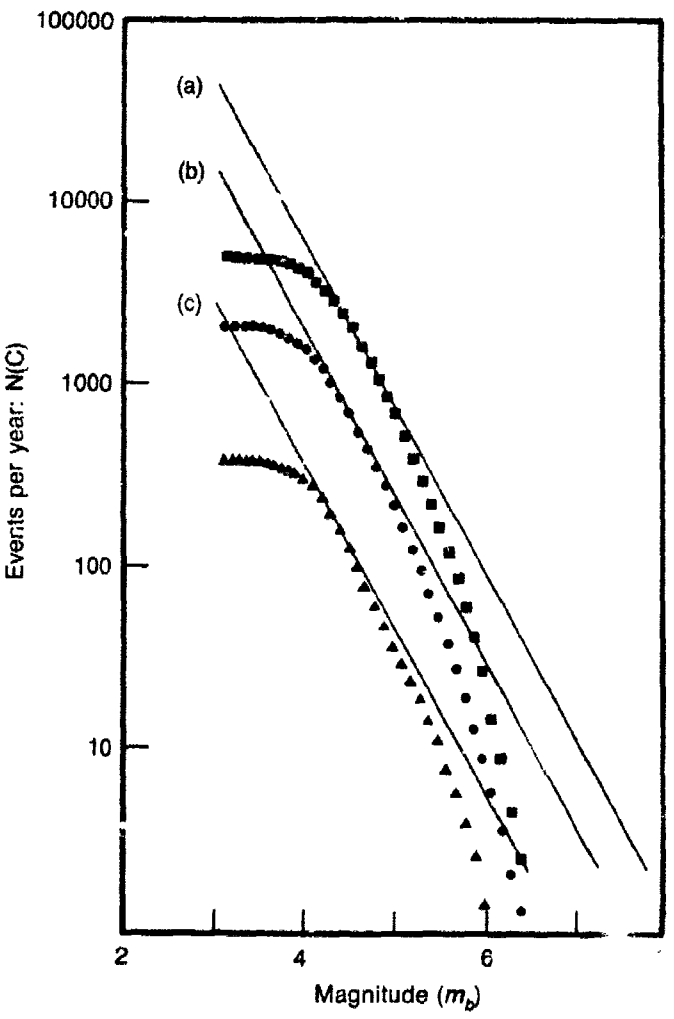

Fig. 3. Cumulative recurrence statistics averaged annually for (a) shallow, (b) intermediate and (c) deep earthquakes globally, using maximum-likelihood m_b estimates.

$$\log_{10}(N_c) = 7.33 - 0.90\, m_b \qquad D \leq 60 \text{ km} \tag{7}$$

$$\log_{10}(N_c) = 6.85 - 0.90\, m_b \qquad 60 \text{ km} < D \leq 300 \text{ km} \tag{8}$$

$$\log_{10}(N_c) = 6.13 - 0.90\, m_b \qquad D > 300 \text{ km} \tag{9}$$

Here, N_c denotes the cumulative number of earthquakes, and D denotes depth of focus as given by the ISC. Thus, about 70% of global earthquakes are shallow, 25% of intermediate depth and 5% deep. The estimated average annual number of earthquakes globally is about 7500 above $m_b = 4.0$, and the number ranges between 6000 and 9000 for individual years within the ten year period.

The distribution of estimated m_b bias values compared to conventional m_b estimation is illustrated in Figs. 4 and 5. In most cases , conventional m_b values are biased high by between 0.0 and 0.5 units. Figure 5 shows that the bias problem is most significant at intermediate magnitudes. As expected, the bias values decrease somewhat when three or more station reports are required for m_b determination, but are even then significant.

At high magnitudes, our approach gives essentially the same m_b values as those of the ISC. Thus, we have not taken into account the possibility of bias introduced by clipping of strong signals at some stations for such events (Chinnery, 1978, von Seggern and Rivers, 1978). While

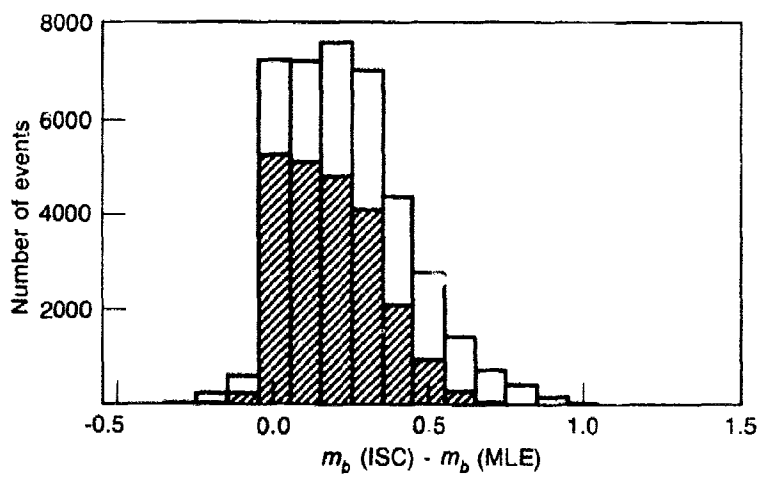

Fig. 4. Distribution of differences between conventional m_b and maximum-likelihood m_b. The filled columns correspond to requiring at least three observations in the conventional estimates.

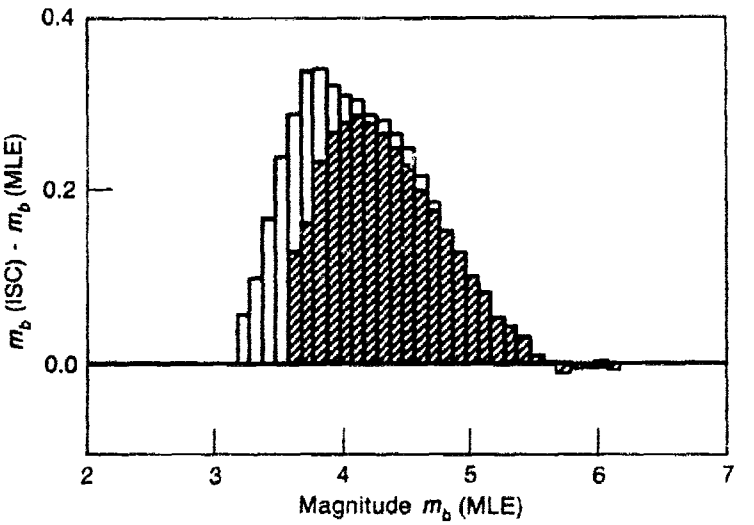

Fig. 5. Average m_b differences (as in Fig. 4) shown as a function of maximum-likelihood m_b. Note that the bias is most pronounced at intermediate magnitudes.

this problem is important in many contexts, it would not significantly influence the seismicity statistics and detectability estimates in this study.

Earthquake Detectability

Based on the estimated magnitude data, an attempt was made to estimate the global teleseismic detectability of shallow events for the 115 station network. For this purpose a regional subdivision of the earth in grids of 15 × 15 degrees was made, and recurrence statistics for observed shallow earthquakes were considered within each grid area. The method of Kelly and Lacoss (1969) was then used to obtain detectability estimates for regions with sufficient number of observations, and approximate contours were drawn corresponding to these estimates.

Figure 6 shows the results for 90% incremental probability of detection at at least four stations. It is seen that the threshold vary from better than m_b = 4.2 over much of the northern hemisphere to m_b = 4.6 or higher in parts of the southern hemisphere. It must be noted that a considerable amount of smoothing and interpolation was necessary in generating Fig. 6, and very detailed interpretation of these contours should therefore be avoided.

For comparison, the "Networth" approach (Wirth, 1970) was also applied to the network, using the threshold values of Table 1. The results

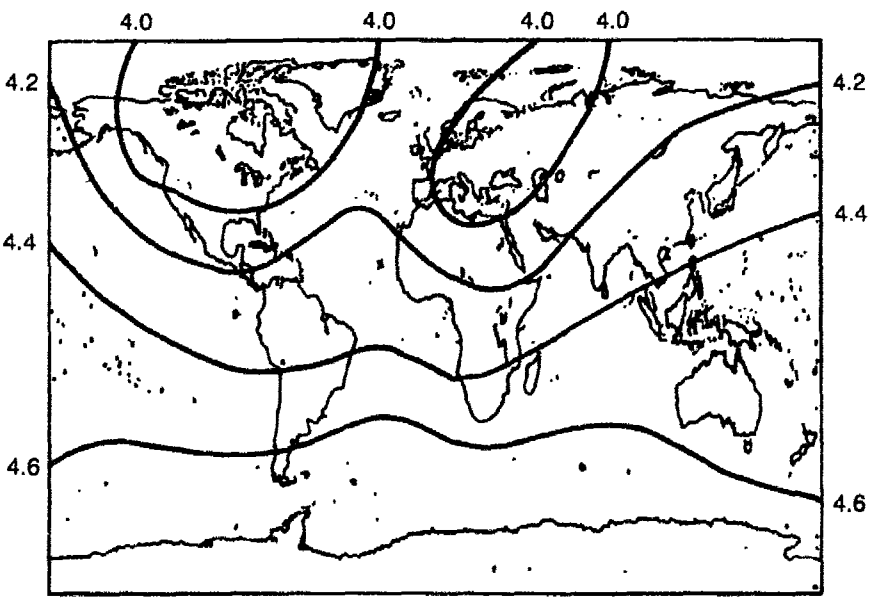

Fig. 6. Contours corresponding to 90% incremental probability of detection at at least 4 stations of the network, requiring at least 1 teleseismic detection. This figure is based on observed recurrence statistics using maximum-likelihood m_b.

are shown in Fig. 7, and can be seen to be in good agreement with those of Fig. 6. The actually observed differences are considered to be within the uncertainty limits of the estimation procedures employed. In some earlier studies, *e.g.*, the report CCD/558, theoretical detection capabilities of global networks were found to be inconsistent with actually reported magnitude data. It would appear that this inconsistency has been largely due to the network magnitude bias problem inherent in conventional magnitude estimation techniques.

The thresholds estimated in this paper relate to *average* operating conditions of the global network. Under special circumstances, the actual thresholds might be different, *e.g.*, the thresholds would be higher immediately after a large earthquake and during a major aftershock sequence. For this reason, the estimated seismicity levels must also be interpreted with some caution.

As expressed by Ringdal (1976), the maximum-likelihood procedure ideally requires actual measurements of threshold levels at all nondetecting stations for any given event. The statistical approach to thresholds and station downtimes used here, has been chosen for practical reasons. However, it has been found by Ringdal (1976) and Christoffersson (1980)

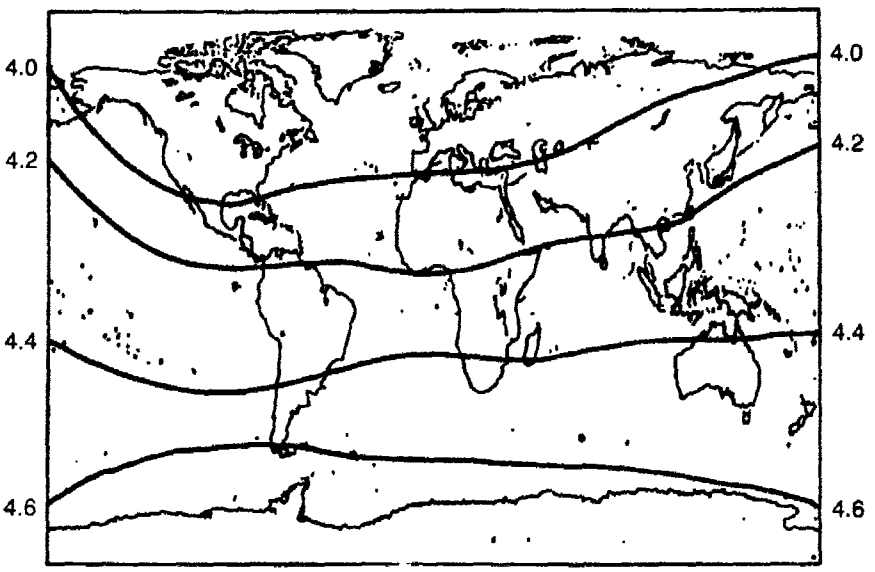

Fig. 7. Contours corresponding to 90% incremental probability of detection at at least 4 stations of the network, using the 'Networth' approach with threshold parameters as in Table 1.

that even under very unfavorable circumstances, *i.e.*, during a large aftershock sequence, the maximum likelihood procedure, using estimated thresholds, produces acceptable results. Thus, while some individual events, in particular those occuring closely after a large earthquake would be affected by occasional errors in the thresholds, the effect on the total earthquake statistics should be insignificant.

Acknowledgment

This research was carried out at the DARPA Center for Seismic Studies (CSS) in Rosslyn, Virginia. The support of Dr. Carl F. Romney and the entire staff at the CSS is gratefully acknowledged. The NORSAR project is supported by the Advanced Research Projects Agency of the Department of Defense, and monitored by AFTAC, Patrick AFB, FL 32925 under Contract FO8606-84-C0002.

References

1. Bungum, H. and E.S. Husbye (1974), *Bull. Seism. Soc. Am.*, **64**, 637-656.
2. CCD/558 (1978), Report to the Conference of the Committee on Disarmament, Geneva.
3. Chinnery, M.A. (1978), *Tectonophys.*, **49**, 139-144.
4. Chinnery, M.A. and R.T. Lacoss (1976), in Lincoln Lab. SATS, (30 June 1976).
5. Christoffersson, A.C. (1980), *Phys. Earth Planet Interiors*, **21**, 237-260.

6. Clark, R.A. (1983), *Geophys. J.* **75**, 545-553.
7. Dean, W.C. (1972), *Techn. Rep. No. 5*, Teledyne Geotech, Alexandria, Virginia.
8. Elvers, E. (1980), *FOA Report C 20368-T1*, Stockholm, Sweden.
9. Evernden, J.F. (1970) *Bull. Seism. Soc. Am.* **60**, 393-446.
10. Evernden, J.F. and W.M. Kohler (1976), *Bull. Seism. Soc. Am.* **66**, 1887-1904.
11. Gutenberg, B. and C. Richter (1956), *Annali Geofis.* **9**, 1-15.
12. Husebye, E.S.I, A. Dahle and K.A. Berteussen (1974), *JGR* **79**, 2967-2978.
13. Kelly, E.J. and R.T. Lacoss (1969), *Lincoln Lab. Techn. Note 1969* **41**.
14. North, R.G. (1977), *Lincoln Lab. Techn. Note 1977* **24**.
15. Ringdal, F. (1976), *Bull. Seism. Soc. Am.* **66**, 789-802.
16. Ringdal, F. and E.S. Husebye (1982), *Bull. Seism. Soc. Am.* **72**, S201-S224.
17. Ringdal, F., E.S. Husebye and J. Fyen (1977), *Phys. Earth Planet. Int.* **15**, P24-P32.
18. von Seggern, D. and D.W. Rivers (1978), *Bull. Seism. Soc. Am.* **68**, 1543-1546.
19. Wirth, M.H. (1970), *Research Memorandum*, Teledyne Geotech, Alexandria, Va.

An Adaptive ARMA TRAPS for Seismic Event Detection, Location and Classification

Bonnie Schnitta-Israel

Summary

TRAPS is a three-stage process. Stage One is a hybrid adaptive filter which is mathematically designed to achieve noise elimination on each phone. The output of Stage One is then beamformed and input into Stage Two, an adaptive process which performs signal enhancement. Stage Three of TRAPS calculates the range and bearing of the detected event. The main objective of the research effort was to develop extensions to TRAPS for the express purpose of improving TRAPS for nuclear monitoring applications.

The original TRAPS used a conventional beamformer. While the original TRAPS is superior to an adaptive beamformer (AB), an AB strategically placed between TRAPS' first two stages was analyzed for its differential gain over the original TRAPS. This was the first task of the contract.

The second task of the contract was to incorporate into TRAPS relevant background noise statistics. Consequently, a sophisticated slaved algorithm was built into Stage One of TRAPS so as to make it more capable of dealing with background noise while simultaneously preventing signal cancellation. Also, the original adaptive AR model of TRAPS was upgraded to an adaptive ARMA (AutoRegressive Moving Average) model to ascertain improved spectral estimation in a low SNR environment, while maintaining real time processing criteria. Additionally, the order and adaptation time of Stages One and Two of TRAPS were varied so that each stage was tailored to the statistics of either the noise or the signal.

The third task of the contract was to characterize the signal to facilitate automatic event identification. For this purpose the resultant parameters, innate to TRAPS and their related migration, were analyzed as an alternate mode of observing and detecting appropriate wave fronts.

Earth heterogeneities, scattering at the source, *etc.*, all contribute to difficulties in meeting the detection, location and classification objectives of the Comprehensive Test Ban Treaty. In combination with the quest for improved detection and classification capability is the need to develop an

automatic processing system which minimizes not only the false alarm rate of the system itself, but minimizes errors that result from various aspects of human intervention.

The blanket objective of the research described in this paper was to address the above stated issues by means of tailoring a 3-stage processing system, termed TRAPS, developed by Bonnie Schnitta-Israel (see Fig. 1 and Ref. 1) to the nuclear monitoring application. This broad statement was broken down into 4 specific Tasks. The work on these 4 Tasks for the past ¾ year and the conclusion to the work will be discussed in this paper.

The original TRAPS, which succeeded in doubling the range of detection in a previous seismic study (1), contained a conventional beamformer between Stage One and Stage Two of TRAPS. The first Task was thus to ascertain the most effective method of incorporating an adaptive beamformer into TRAPS and determining the processing gain achieved. Figure 2 presents the effectiveness of the original TRAPS, TRAPS with an adaptive beamformer and other conventional spectral estimators evaluated by means of a normalized frequency resolution procedure (2).

The goal of Task 2 was to analyze the environment within which TRAPS was to function. The knowledge of the relevant background noise statistics then gained by this study inspired the formulation of two algorithm

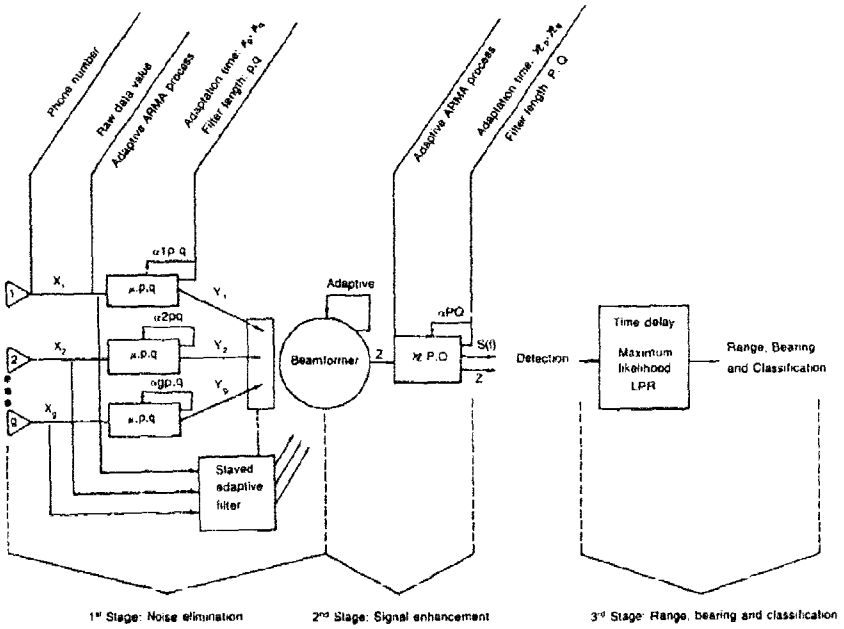

Fig. 1. TRAPS I TRansient Acoustic Processing System) Original and algorithm improvements resulting from (½ year) contract F49620-83-C-0137.

refinements. The first change to TRAPS was influenced by the knowledge that the ARMA (AutoRegressive Moving Average) model often provides better spectral estimates than the specialized AR model (3). Thus, the original adaptive AR model of TRAPS was transformed to an adaptive ARMA model, which could provide source parameterization improvement in a low SNR

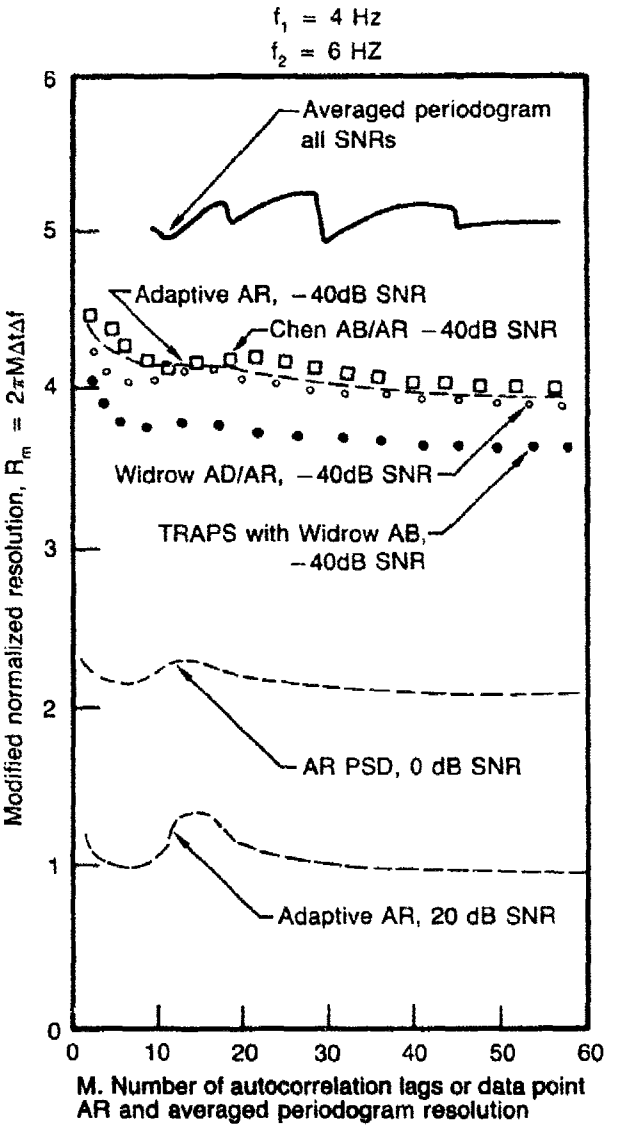

Fig. 2. Results of adaptive beamformer (AB) frequency resolution evaluation. Note that a smaller R denotes improved resolution.

environment, while maintaining real time processing criteria. To be able to meet such a criteria the following adaptive ARMA model was developed by the author. First the ARMA model is rewritten in two stages as follows:

$$\text{I:} \qquad e(n) \equiv x(n) - \sum_{i=0}^{p} a_i x(n-i) \tag{1}$$

and

$$\text{II:} \qquad \sum_{i=0}^{q} b_i W(n-i) = e(n) \tag{2}$$

in which $x(n)$ and $W(n)$ are taken to be the excitation and response time series, respectively.

An estimate, $\hat{e}(n)$, for the series $e(n)$ is initially provided, using an adaptive filter (1). This method cites that the coefficients of Eqn. 1 vary from one sample to the next at a rate, μ. The adaptive filter constructs a sequence of coefficient $\{a_j(n)\}$, which converge to the true coefficients as $n \rightarrow \infty$, such that

$$a_j(n) = a_j(n-1) - \mu \left[\sum_{j=1}^{p} a_j(n-1) x(n-1-j) \right] x(n-j-1) \tag{3}$$

This then allows $\hat{x}(n)$ to be calculated as

$$\hat{x}(n) = \sum_{j=1}^{p} a_j(n)\, x(n-j), \tag{4}$$

allowing the estimate, $\hat{e}(n)$, to be given by

$$\hat{e}(n) = x(n) - \hat{x}(n) \tag{5}$$

We now estimate b_i and $W(n)$ as those values $\hat{b}_i$, $\hat{W}(n)$ which minimize the total squared error:

$$G_n(\underline{b}, \underline{W}) = \sum \left[F_n(\underline{b}, \underline{W}) - \hat{e}(n) \right]^2 \tag{6}$$

Subject to the constraints

$$R_p(n) \sum_{i=0}^{m} W(n-i)W(m-p-i) \equiv \begin{cases} C & p=0 \\ 0 & 1 \le p \le s \le m \end{cases} \quad (7)$$

where C is an arbitrary constraint, and

$$F_n(b,W) \equiv \sum_{i=0}^{q} b_i W(n-i) \quad (8)$$

We now recast these equations into a form suitable for numerical treatment.

Suppose that at time $t_n = n\Delta t$ we have observed (estimate) $e(n)$. (We drop the "^"s for notational convenience.) We compute F from a backward sum

$$F_{n-k} = \sum_{i=0}^{q} b(i+1)W(n-k-i) \quad (9)$$

where $k = 0, \ldots, N \qquad (n > N)$
and $b\,(i + 1) = b_i$

$$W(n-k-i) = W_{n-k-i} \quad (n > k+i) \quad (10)$$

are FORTRAN arrays representing the unknowns. We represent these unknowns jointly as ξ (at epoch n)

$$\xi_m = \begin{cases} W(n-m+1) & m \le s \\ b(m-s) & m > s \end{cases} \quad (11)$$

where $1 \le m \le s + q + 1$

s is the number of unknown W
$q + 1$ is the number of unknown b

We write our problem (at epoch n) as

$$\delta \left\{ \sum_{k=0}^{N} (F_{n-k}(\xi) - e_{n-k})^2 + \sum_{p=0}^{s-1} \lambda_p (R_p - C\delta_{po}) \right\} = 0 \quad (12)$$

where λ_p are Lagrange multipliers.

The normal equations are:

$$2 \sum_{k=0}^{N} \left[(F_{n-k} - e_{n-k}) \frac{\partial F_{n-k}}{\partial \xi_m} + \sum_{p=0}^{s-1} \lambda_p \frac{\partial R_p}{\partial \xi_m} \right] = 0 \quad (13)$$

$$R_p(\xi) = C\delta_{po} \quad (14)$$

These equations must be solved for ξ (using the constraints to get λ_p), but are nonlinear. We use the Gauss-Newton iteration method which ignores certain second derivatives to obtain

$$\sum_t \left[2 \sum_{k=0}^{N} \frac{\partial F_{n-k}}{\partial \xi_m} \frac{\partial F_{n-k}}{\partial \xi_t} + \sum_{p=0}^{s=1} \lambda_p \frac{\partial^2 R_p}{\partial \xi_m \partial \xi_t} \right]_i (\xi^{i+1} - \xi^i) + \sum_{p=0}^{s-1} \frac{\partial R_p}{\partial \xi_m} (\lambda_p^{i+1} \lambda_p^i) = - \left[2 \sum_{k=0}^{N} (F_{n-k} - e_{n-k}) \frac{\partial F_{n-k}}{\partial \xi_m} + \sum_{p=0}^{s-1} \lambda_p \frac{\partial R_p}{\partial \xi_m} \right]_i \quad (15)$$

where i refers to the iteration number.

And the constraints are linearized to

$$\sum_t \frac{\partial R_p}{\partial \xi_t} (\xi_t^{i-1} - \xi_t) = - R_p^i \quad (16)$$

This matrix equation is solved. And the results are used to update the iterates

$$\xi^{n+1} = \xi^n + \Delta\xi, \textit{ etc.} \tag{17}$$

The second refinement addressed in Task 2 was the signal cancellation phenomena, which is a consequence of adaptive interaction between the desired signal and interference. As a result, a sophisticated slaved algorithm based on previous work by Duvall (4) was built into Stage One of TRAPS. Additionally, the order of Stage One and Two of TRAPS were varied to best handle the respective noise or signal statistics. The influence of a possible different adaptation time for each phone in Stage One was studied for its ability to remove bias in the data. Initial results were excellent.

The purpose of Task 3 was to decrease the false alarm rate of TRAPS and to enhance FK space definition by means of a signal characterization mode. In order to demonstrate the logic for the direction taken in Task 3 attention should be given to the fact that the ARMA coefficients, poles and zeroes of the process, *etc.* completely determine the shape of the power spectrum. The supposition that these parameters characterize an event is a valid one (5-6). The similarity of one event to another for this research project was identified by comparing the parameters for each event innate to Stage 2 of TRAPS. How "close" the signature of one set of coefficients is to the signature of a reference set was made by comparing the weighted linear prediction error residual (WLPR) resulting from each set. These WLPR's then served as input to a combined statistical/structural classification system. The purpose of the classification was twofold. First, such a pattern recognition algorithm (PRA) would be able to discriminate between various types of explosions and earthquakes. Also, the information, resulting from the PRA in an iterative mode with TRAPS, isolated and then classified the various waves of an event despite "missing" data, thus enhancing the range and bearing estimate. Once confirmation was made of the validity of the technique, the PRA was extended to identify phase irregularities that characterize a field.

Each innovational refinement to TRAPS was first evaluated on simulations. Once the intrinsic properties of each solution were identified, a revised TRAPS was created. Initial results on a small data base showed the revised TRAPS to have a 15% accuracy improvement over the original TRAPS in location ability. A larger data base is presently being used to produce ROC curves which will be included in the final report of this contract.

References

1. Schnitta-Israel, B., Fletcher, D. and Dorman, J., "Hybrid Adaptive Filtration for Seismic Event Location," *JASA* **73(1)**, Jan. 1983, pp 230- 241.
2. S.L. Marple, Jr., "Conventional Fourier, AR and Special ARMA Methods of Spectrum Analysis," *Thesis*, Stanford U., Jan 1977.

3. Cadzow, C.A., "ARMA Spectral Estimation: A Model Equation Error Procedure," *IEEE Trans.*, **19(1)**, Jan 1981, pp 24-28.
4. Duvall, K., *Signal Cancellation Phenomena in Adaptive Atennas: Causes and Cures*, PhD dissertation, Stanford University., 1982.
5. Harjes, H., "Spektral Analytische Interpretation Seismischer Aufzeichnungen," *Geol. Jahr.*, Reihe E Heft **17**, Hannover, 1979.
6. Bois, P., "AR Pattern Recognition Applied to the Delimitation of Oil and Gas Reservoirs," *Geoph. Pros.*, **28**, 1980.

Earthquake or Explosion: Teleseismic Monitoring Where Are We Now?

P. D. Marshall and A. Douglas

Introduction

At the start of the CTBT negotiations in 1958 the technical experts had very little observational data on which to make recommendations. In truth there was no adequate theory of how explosions and earthquakes generate seismic waves and the knowledge of earth structure was not detailed enough to allow predictions to be made on how seismic signals are distorted on propagation through the earth. That was over 25 years ago; since then seismology has come a long way. In 1958 Sir William (now Lord) Penny described seismology as "a stone age science" but a number of significant national programs, of which VELA Uniform is the largest, have dragged the science willingly into the 20th century.

Forensic seismologists, for the last 20 years or so, have focused successfully on two principal problems: one is understanding the seismic effect of explosions and earthquakes (getting to grips with the physics of the problem) and determining the structure of the earth; and the other is that of improving methods for the detection, location and identification of underground explosions in the presence of the vast number of naturally occurring seismic disturbances.

Seismological research is in many ways more difficult than most other branches of scientific research: it is essentially an inferrential science. Experiments have to be designed to *infer* earth structure since we cannot drill 2000 km into the earth to recover samples for study in the laboratory. The major source of elastic wave energy which is used to probe the earth is uncontrolled in that earthquakes occur where and when they have to. The controlled source of elastic wave energy, the underground explosion, can only be fired by Western nations at a very limited number of test sites. Thus, the availability of basic data, such as location, depth, yield, *etc.*, are limited. Seismologists have virtually no information on the basic data of Soviet or Chinese explosions which makes the design of experiments to resolve the problems of verification of Soviet compliance with a treaty very difficult. Even the acquisition of the observational data to resolve the problems is difficult; the USSR is a vast land mass and data from stations within the USSR are unattainable; so data

for underground explosions is available only at teleseismic distances. It is a credit to the USA that basic data from numerous U.S. explosions, as well as observational data, are freely available to seismologists of all nationalities. Much of the observational data are available from the VELA Uniform world-wide network of seismic stations, a network once described by Thirlaway as the "giga volt tool of the earth scientist."

It was to overcome the difficulties of verification of compliance with a CTBT that led to the establishment of the VELA Uniform program. Briefly, its objective was to fund research to solve the problems of the detection, location and identification of underground nuclear explosions even in the presence of attempts to conceal the explosion in such a way as to evade either detection or identification.

It is our belief that the VELA Uniform program, with contributions from other national programs, has made enormous progress in resolving some, but not yet all, of the discrimination problems and of understanding the physics of the seismic source and the propagation of elastic wave energy through the earth. Let us then see where, as a result of this research, we now stand on the question: Earthquake or Explosion?

The decision making process starts with the detection of a seismic disturbance followed by its location. Any diagnostic evidence available is then analysed to identify the nature of the seismic disturbance.

Detection of Seismic Disturbances

The first evidence of a seismic disturbance that is observed at teleseismic* distance is the *P* wave. The detection of a *P* wave depends on several factors which include:

(1) the amplitude and period of the *P* wave
(2) the amplitude and period of the ambient seismic noise
(3) the characteristics of the recording instrument

In 1958 it was proposed to monitor seismic activity with a network of 180 small (3 km aperture) arrays of seismometers spaced at intervals of 500 km. (It is of interest to speculate on what such a network would have done for discrimination but such speculation is more in keeping with a study of regional verification). Such a network was not to be; instead we have seen the deployment of small, medium and large aperture arrays of seismometers, single stations, borehole systems both on land and under the sea floor. Much of the successful development of seismometers and arrays has been due to the impetus and funding provided by national programs such as VELA Uniform. A review of instrumental

*Teleseismic indicates a distance greater than 25° or about 2750 km.

development under such programs has already been given so no further discussion is presented here. Since 1958 we have learned a great deal about site selection procedures and whether a single station will suffice or whether an array is required at a particular location to satisfy proposed detection needs. Perhaps most of all we have defined a clear limit for detection capacity at teleseismic distances. The noise level at the quietest surface installations in the world is around 1 nm; given arrays or adequate borehole installations it may be possible to achieve a network of stations each with a noise level of about ½ nm, which at teleseismic distances is equivalent to a m_b of about 3½. Such a network does not yet exist, indeed may never, because to achieve a *global* detection capacity of m_b ~3½ would require, in addition to land based systems, ultra-quiet ocean bottom or island sites in the Southern hemisphere. This represents a limit which, in theory, could be achieved at teleseismic distances for the major land masses though the network would be very expensive and probably politically difficult to deploy..

Reliance on totally teleseismic systems with existing stations reporting to, say, the NEIS or ISC, gives a detection capacity of about 4½ in the northern hemisphere but nearer 5½ in the southern hemisphere. The detection capacity of any network is very much a function of the type of station, the number of stations, their location and the radiation of elastic wave energy from seismic sources to that network of stations.

The seismological objectives of a network should be defined and a network tailored to meet those objectives. In some areas of the world these objectives may not be met and we are faced with a "detection deficit," a grey area in which the science and technology will not be able to help the politicians in their assessment of the level of risk to national security. It is imperative to know whether the objective is global monitoring or only specially targeted areas such as nuclear weapon states territories. There is a vast difference in the order of magnitude of the task and of cost of these different objectives.

In 1958 the detection capacity for sources located in the northern hemisphere was close to m_b 5½. By 1963 this number had dropped to about 5. With the deployment of the WWSSN and numerous array stations the figure quickly dropped to about 4¾; today it is nearer 4½ but to achieve this level regional data are invariably included. Without a massive effort we can probably achieve teleseismic detection at m_b 4 for targeted areas but to go lower would require the installation of regional or internal stations — this should be more readily achieved than attempting to go for the more difficult theoretical limit of m_b 3½ possible, perhaps, at teleseismic distances.

There are still areas where further research may prove beneficial

for detection. For example, at the PKP focus the amplitude is similar to or greater than amplitudes in the teleseismic window and may provide additional evidence of a seismic disturbance in an area difficult to monitor in the 30° - 90° range. Another, and more promising, observation is the kind made at NORSAR where very small disturbances north of the Caspian Sea have been detected and located using the NORSAR array by taking advantage of $dT/d\Delta$ variations in the triplications associated with the distance range to assist location. This observation is an unexpected bonus but hard to predict where else it may occur. To be sure a potential violator of a treaty would need to know whether or not such a pipeline to his proposed test site existed; it has a certain deterrence value.

Finally, the good work on signal detection and enhancement, such as prediction filtering, multichannel analysis, *etc.*, must be acknowledged. The literature abounds with techniques and their applications to seismic data and some show significant improvements in S/N ratios and improved detection levels. Many of these techniques have been developed and tested under the VELA Uniform program and the transition from film to analogue magnetic tape to digital data have facilitated the application of these techniques.

So, where are we now? Should the requirement arise to monitor a particular region we know what we would need to do. Much would depend on the location of the region. It could be prohibitively expensive but the technology exists to monitor any region on earth. Looking to the future it is hard to see where additional research effort would lead to any large improvements in detection capacities.

A major difficulty of verifying compliance with a test ban treaty is how to handle the vast amount of data that will accrue in a day from high sensitivity networks. It is imperative that the seismic source is located fairly quickly after detection. But how many events will be detected by a station, an array or a network of stations, in a day or a year? One would think that this is a fairly easy question to answer but in reality it has proved very difficult. In 1958 western estimates of the number of seismic disturbances above a specific magnitude were made but after more research the number was modified downwards. For certain regions of the earth we are in a position, by virtue of highly sensitive stations, to make reasonable estimates of the number of seismic disturbances in that region but a global estimate is not yet agreed. Current assessments of global seismicity indicate that there are at least 8,500 seismic disturbances *per annum* at magnitude 4 and above; however, there is some evidence to suggest that the number may be larger. It is an important number to determine and it is time that such an estimate was made to define data analysis needs. Once a seismic disturbance is detected its source must be located.

Location of Seismic Disturbances

An essential facet of any detection network is the ability to provide accurate source locations. The only way to positively or uniquely identify an underground nuclear explosion is to produce radioactive debris from the explosion. To find this evidence you have to be able to go to the precise location of the test. Given the arrival times of *P*-wave signals from a seismic disturbance at several stations, ideally well-distributed in azimuth and distance from the epicentre, estimates can be made of the epicentre and origin time of the disturbance.

In 1958 the Conference of Experts stated that given good azimuth coverage and regional travel time curves the area within which an epicentre is localized can be assessed as approximately 100-200 square kilometres. It was quickly found that similar epicentral location accuracies could be achieved using teleseismic data obtained from an appropriate network. Much effort was made to improve teleseismic location capacity. Refined travel time studies were carried out, the use of a master event and least squares multiple epicentre techniques developed, all of which led to greater accuracy and confidence in epicentral locations.

A very important contribution to test ban seismology (or forensic science) made under the VELA program was the LONG SHOT underground nuclear explosion in the seismically active area of the Aleutian Isles. Epicentre location became a growth industry, experts in source bias emerged, all ultimately to add to our understanding and knowledge of problems associated with epicentre location. Given the benefit of this research how accurately can we estimate epicentres? It depends on the detection network, its distribution in distance and azimuth relative to the epicentre. It is also a function of its location: seismic disturbances in the middle of stable uniform regions can be located with an accuracy of a few kilometres whereas sources in or close to seismically active regions in areas of strong lateral variations in velocity may be mislocated by more than 25 km. In attempting to monitor compliance with a treaty on a global basis much care will be needed to ensure adequate station coverage to assure detection and location of the seismic disturbances.

Certainly, location of the hypocentre has a role to play in discrimination between earthquake and explosion sources but this will be discussed later. Refinements of hypocentre location techniques are continually being investigated, further refinements to *P*-wave travel times are being actively investigated at the present time, regional travel-time data can also be integrated into our hypocentre location programs to improve location capacity. However, the fact remains that location accuracy is a function of magnitude, the confidence ellipses increase quite significantly around

m_b 4 and location capacity is a function of the network and how well it is distributed in azimuth and distance from an epicentral region.

A treaty can only be violated by states party to that treaty. It is conceivable that not every nation, nuclear or non-nuclear weapon state, would sign such a treaty and in these circumstances it would be quite critical to decide whether a suspicious seismic disturbance originated within a territory not party to the treaty or a neighbouring state party to the treaty. This either/or situation would be of considerable political importance and the forensic seismologist would be under pressure to make a positive and correct decision.

At present we are in a position to suggest a network of stations, arrays, borehole systems land based or on the ocean bottom, which, given the appropriate financial resources, could be deployed to detect and locate seismic sources down to 4 or possibly lower in the northern hemisphere. We are unaware of any studies that make it possible to assess a capacity for the southern hemisphere but it is likely that a capacity close to m_b 4 for the principal areas of interest, *i.e.*, continental land masses, could, with truly international co-operation and participation, be achieved. This is by no means certain.

The next stage of the verification process is to identify the nature of the source that has been detected and located.

Identification of Seismic Disturbances

In an ideal world one would hope that the sources of all seismic signals detected could be located and identified; in practice there will always be some signals which are so small or weak that identification with a significant degree of probability is just not possible. Thus, there is a gap between the detection and identification level of any high sensitivity network of monitoring stations.

In the absence of radioactive debris it is not possible to positively identify a seismic source as a nuclear explosion. We can *presume* the source of seismic signals was nuclear. We can also presume that the source was an explosion, but would our evidence stand up in an international court of law? In other words, what do we mean by identification? In national terms expert forensic seismologists need to be able to satisfy their own government that in all probability a seismic source was a nuclear explosion and that, we believe, is their principal role. How a government would respond in that situation is a political decision and not one for scientists.

It is possible to tabulate what we seek in any identification criterion:

(1) Absolute separation between earthquake and explosions.

(2) An understanding of the physics of the processes enabling identification to be made. This would give the criterion predictive properties should we need to apply the criterion to low magnitude sources located anywhere in the world.

(3) Confidence that evasion is difficult.

With these requirements we can now examine the most significant criteria, applicable at teleseismic distances, that have been available or developed since 1958.

Location and Depth. It has been suggested that if the epicentre of a seismic disturbance lies over the sea then the source is either an earthquake below the seabed or an explosion in the water. It is further suggested that the explosion will generate a hydroacoustic signal and be uniquely identified as an explosion. Whereas an absence of hydroacoustic signal indicates an earthquake source and in this way the large majority of shallow earthquakes located at sea can be identified. The suggested criterion is that there is a high probability that the epicentre is more than 25 km from land. This distance is chosen to allow for the possibility of source bias in the epicentre location.

There certainly is merit in the argument but in the absence of data to verify the efficiency of the technique uncertainties may, of course, still remain. Can holes of sufficient diameter and depth be drilled in the seabed and used to detonate a device below the seabed? Underwater, or seabed, technology is an area in which much progress is being made and what is not possible today may be tomorrow. It may be possible to detonate nuclear devices below the sea floor. Perhaps we should address the question and seek answers: under what circumstances can the epicentre of a seismic disturbance be used to indicate that the source is probably an earthquake?

It was recognized in the 1958 discussions that the depth of a seismic disturbance is a very useful diagnostic aid. If a source is located at some depth beyond, say 10 km, it can be assumed that in all probability the source is an earthquake. But as a diagnostic aid it depends on our ability to determine the depth of seismic disturbances with considerable accuracy. Although much effort has been made since the VELA program began to refine hypocentre locations, using only the travel times leads to uncertainties such that at low magnitudes only sources located deeper than, say 50 km, can be assumed to be natural in origin. The use of *pP* to determine depth can be more precise. At teleseismic distances the time between *pP*, *sP* and *P* are short and often very difficult to identify in the presence of crustal reverberations, mode conversion, upper mantle

reflections and scattering close to the source. The difficulty of estimating *pP* times for shallow sources is such that the technique has proved to be of little value. A further difficulty is the possibility that an observed second arrival could, of course, be a second explosion so diagnostic procedures have to be applied to later phases to remove this possibility.

Improvement in hypocentre location is possible using the master event or multiple hypocentre location methods. A region may be calibrated by using earthquakes that have clear identifiable *pP* and *sP* phases. There are still reservations of the global applicability of the technique due, not least, to the availability of earthquakes exhibiting the desired clear surface reflections. Even our knowledge of *pP* from explosions is still very poor. It would be very useful for many reasons to be able to determine the depth of explosions with some certainty. However a very shallow source depth estimate does little to help identify the nature of the source. This is probably a greater problem for seismologists in the USSR since approximately 90% of North American earthquakes would appear to be at depths of 20 km or less whereas in the USSR 90% of earthquakes would appear to be at depths greater than 20 km.

Thus, the use of depth as a diagnostic aid is very valuable; there are limitations to its applicability and further research is required to improve depth estimates.

The use of regional and first zone data will be of value in refining hypocentre location particularly for seismic disturbances within the crust but hypocentre location for shallow focus disturbances from teleseismic data is not sufficiently well restrained to serve as a discriminant over the whole detection range. The accuracy of the location and depth estimation decreases with magnitude (or signal to noise ratio) and below magnitude 5 it is probable that reliable depth information will not be available.

Identification Criteria. An explosion is, in theory, a shallow focus radially symmetric source of elastic wave energy. A simple view of an earthquake is the movement, along a fault plane, of one mass of rock relative to another. The source may be deep, the release of energy less rapid, than in an explosive source and with a quadripolar distribution of energy. It is these intrinsic differences in the nature of the source that are exploited to identify the nature of the source. The differences in the direction of first motion of the *P* waves generated by explosions and earthquakes were clearly recognized by the Conference of Experts in 1958 and with information on source depth formed the first diagnostic aids to source identification.

Earthquakes, as shear type sources, generate *S* waves whereas explosions, as pure compressional sources, should not. Thus, attempts have been made to exploit *S*-wave excitation as a diagnostic aid. The rate of

release of energy by the two different sources may manifest itself in the duration of the recorded pulses and hence the spectral content of seismic waves. Much research has been conducted to take advantage of possible spectral differences between the two sources. Finally, a shallow explosive point source should generate simpler seismograms than a shallow earthquake source because of the presence of S to P conversions (absent in the explosion) in the layered structure of the source region.

How successful are attempts to exploit the intrinsic differences between earthquakes and explosions as a means to source identification? This is somewhat difficult to quantify since it depends on the network of stations available to produce the essential data, on the geographical region in which the source is located, and on the magnitude of the disturbances to be identified.

***P*-Wave First Motion.** If the initial motion of a P wave is identified as a rarefaction then the source of that P wave must be an earthquake. Thus, negative first motion identifies earthquakes. Compressional first motions do not identify explosions or earthquakes. At teleseismic distances only a narrow cone of angles from the lower portion of the focal sphere are observed and given a particular location and orientation of the source it is possible that only compressions are observed at teleseismic distances thus the technique is of no help in identifying such sources. However, the principal difficulty of the method is the need for an adequate signal to noise ratio to be certain of the direction of first motion. The technique works well for large magnitude disturbances but its value decreases rapidly as the magnitude decreases. To improve the detection of low magnitude disturbances, the output of a seismometer is usually tightly filtered and the phase distortion tends to delay energy and reduce the amplitude of the initial motion making it more difficult to be certain of the direction of the initial motion. Several deconvolution techniques, *e.g.*, spike filtering, exist which, when applied, give greater confidence in the identification of the direction of first motion.

Certainly this diagnostic aid has proved useful. In one notable investigation of Tibetan earthquakes which proved rather difficult to identify, one sequence of earthquakes could only be identified as earthquakes by use of rarefactional first motion observed on LP seismograms.

The technique has some diagnostic value but in general only for sources greater than say m_b 4½ - 5. This is a result which has not altered significantly since 1958. Improvements in instrumental techniques have led to better seismograms with improved S/N ratios but further exploitation of first motion diagnostics seem limited. The identification of first motion may be difficult but there is a lot more information in a seismogram than first motion. The whole P wave contains diagnostic

information, not least of all its spectral content.

***P*-Wave Spectral Methods.** With an increase in the number of nuclear explosions underground after the 1963 PTBT, it became apparent that many of the explosions in the USSR generated *P* waves with higher predominant frequencies than most shallow earthquakes of similar magnitude. This led to the development of spectral ratios as a diagnostic aid. The idea is simple: a spectral ratio of HF to LF is made for explosion and earthquake *P* waves and the larger the ratio the greater the probability that the source is an explosion. Several other methods have been developed which are based on the spectral content of *P* waves; these, for example, include the determination of the third moment of frequency.

The problem is that the spectral content of the *P* wave is determined not only by the nature of the source but also by the amount of attenuation that the *P* wave is subjected to over the path. Ideally, data from seismic stations located in regions overlying high *Q* are used since they should still contain a large fraction of the HF energy. Unfortunately, when the sources are located in regions of low *Q*, the diagnostic high frequency is preferentially absorbed and the technique becomes less valuable. However, it is a diagnostic aid which is dependent upon the source region. The windows through which we look at the ratio of HF to LF have to be tailored to the source region under investigation and this imposes a limitation to its applicability. The technique provides complete separation for USSR explosions and Eurasian earthquakes but the explosions are, in general, located well away from the earthquakes and it may be that the t^* differences are related to the geographical region rather than any intrinsic source differences. The technique does not work so well in the southwestern United States where the explosions are located much nearer to the earthquake sources and the whole region probably overlays low *Q*.

The technique works very well for some regions of the world and down to magnitudes around m_b 4 we can probably predict the source regions where it will work well; but because the spectral parameters have to be varied to suit the source region it is not easy to test the technique on a global basis because of the limited availability of explosion test sites. Spectral ratios derived from seismic waves other than *P* are, however, useful diagnostic aids. One method which uses the spectral ratio between the 1 s *P* wave and the 20 s Rayleigh wave is better known as the m_b:M_s discriminant.

The m_b:M_s and Surface Wave Discriminants. In the 1958 CTBT exchanges the value of Rayleigh waves as a source diagnostic was discussed. It was suggested on good theoretical grounds that the frequency of Rayleigh waves from explosions would be higher than for most earthquakes and that their amplitude would be lower.

Much research since the early sixties has confirmed this early promise that explosions can be perhaps best identified by their m_b:M_s ratio when compared to m_b:M_s for earthquakes. For the same m_b, the explosion M_s (based on the Rayleigh wave amplitude) will be about one magnitude lower than the earthquake M_s. In other words, for the same m_b explosions generate weaker surface waves, it is more correct to say that for the same M_s value explosions generate much higher m_b values than an earthquake.

The method evolved from observations of surface waves from earthquakes and explosions in the southwestern United States. It was possible to separate the explosions from the earthquakes by measuring the area of the envelope of the surface waves recorded on 3-component LP systems and plotting the area, defined as AR, against the *P*-wave amplitude both observations being normalized to a fixed distance. These early observations were made at regional distances and it was not long after that surface waves from underground explosions were recorded at teleseismic distances, distances at which Gutenberg's distance dependence term for T = 20 s Rayleigh waves was applicable. Teleseismic m_b and M_s were measured and

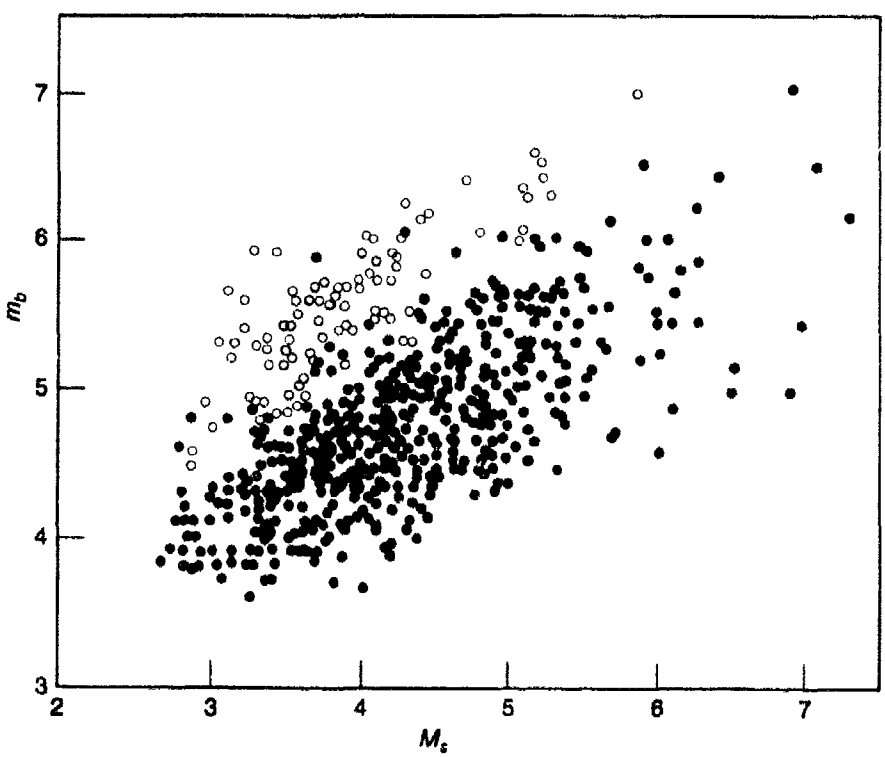

m_b:M_s data collected from numerous sources by Weichert and Basham (*BSSA* 63, No. 3, p. 1124) 1973. Open circles are presumed explosions.

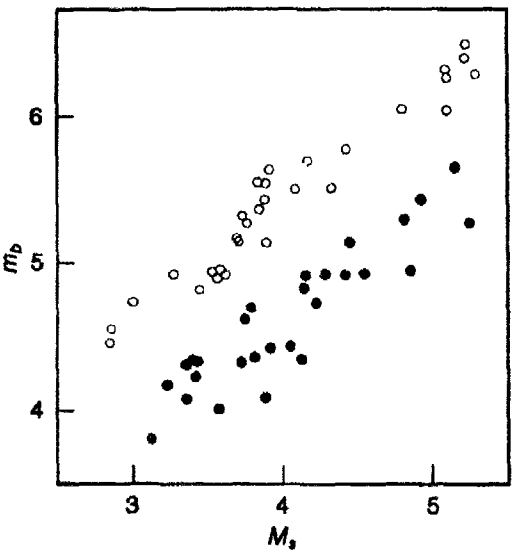

m_b:M_s for western North America. (Weichert and Basham, 1973)

a plethora of almost simultaneous $m_b : M_s$ studies demonstrating the success of the technique were published. It gained general acceptance after the VELA LONG SHOT explosion in the Aleutians and is yet another example of the value of the LONG SHOT explosion to scientists engaged in forensic seismology.

The technique appears to be one of the best identifiers of explosion sources. Most studies show separation of the two populations, but the separation has decreased with time. The earliest studies, usually focused on one geographical region, showed large separation but generally the data base was small, with data available for only a few explosions. Since the early studies many more explosions at widely separated test sites have occurred and, with the dramatic increase in the magnification of LP systems since the early 60's, many more explosions have been detected at teleseismic distances with sufficient amplitude to enable M_s to be determined. The increased data base and lower detection threshold has led to a discriminant which, like many others, appears to decrease in value as the magnitude decreases.

Most published studies have been made on explosions and earthquakes in the same general region. Seismic disturbances located within the USSR appear to be well identified but most of the explosions are located remote from the earthquake region so are the m_b:M_s differences due to location rather than differences in the source function? The answer is probably no, based on observations of m_b:M_s for explosions and earthquakes in the Aleutian Isles where the explosions are located very close to the earthquake epicentres. It would appear then that the m_b:M_s

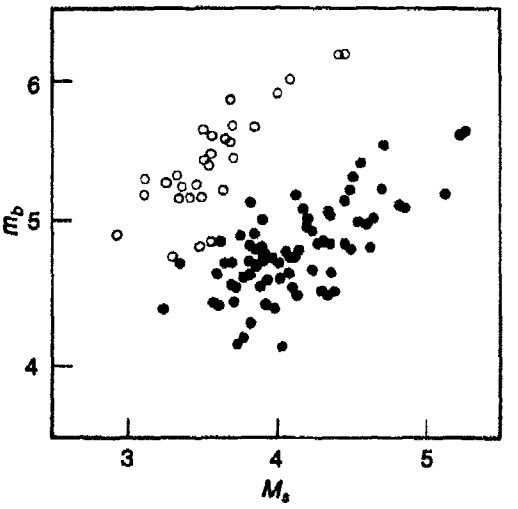

m_b:M_s for Eurasia. (Weichert and Basham, 1973)

criterion works because of differences in the source. The separation between explosions and earthquakes on m_b:M_s plots is not quite so good for explosions in Nevada. This may be due in part to greater attenuation of P-wave energy for explosions in Nevada giving a lower m_b than identical explosions in the USSR. A contributing factor is also the effect the shot medium has on P-wave amplitudes. The slope of the m_b:M_s may be, to some degree, a function of the network used to determine them. The m_b:M_s relationships for explosions appears to be a function of the detonation medium principally due to the variations in m_b:yield. Thus a combination of m_b:M_s observations from different test sites may well increase the scatter and cause populations to approach or even overlap each other. In other words a m_b:M_s plot of a global suite of explosion and earthquake data may well demonstrate some overlap which is not observed when the data are treated on a regional basis.

The major question still unanswered is how far down in magnitude do we have to go before separation is no longer achieved. This again is not any easy question to answer. It would help if agreement could be reached within the seismological community on what are the requirements for robust m_b and M_s estimates. Clearly one observation of m_b or M_s is not enough, 4 is better but of no more use if restricted to the same azimuth. To determine m_b and M_s requires good azimuthal coverage to minimize the effects of the radiation pattern from earthquakes. It would be useful if the number of stations required to determine magnitude reliably could be more clearly defined and thus enhance our confidence in the value of m_b:M_s curves as a discriminant.

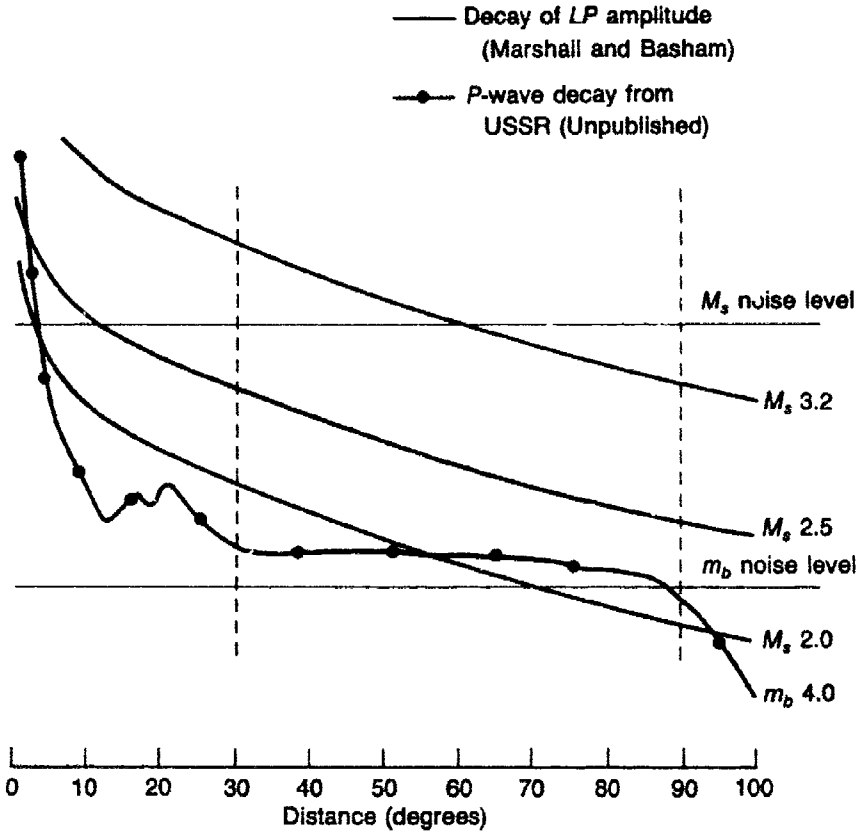

P and Rayleigh wave amplitudes as a function of distance compared to typical low noise levels. This illustrates the range at which the waves may be observed.

The m_b:M_s technique for discrimination works well at larger magnitudes but we need to know down to what magnitude it can be used with confidence. At teleseismic distances *P* waves can be detected down to, say, m_b 4. The surface waves from an explosion in hard rock of m_b 4 is approximately equivalent to a M_s of 2 for explosions and 2½ plus for earthquakes. It is not possible to detect M_s 2 events at teleseismic distances. Given the deployment of numerous high quality LP stations, including arrays, improves detection (at, say, 4 stations) down to about M_s 3½ or m_b 5+. To lower the detection threshold stations at regional distances must be employed. At short ranges the technique still appears to be useful; observations made in California and Nevada of NTS explosions indicate that at some stations, but not all, the technique works down to quite low magnitudes which is, in a way, an endorsement of the earlier success of the AR:m_b method.

There is, however, some theoretical and observational evidence to suggest that there is convergence of the earthquake and explosion population with some overlap of the populations at lower magnitudes. This is certainly a subject where further research can incorporate our understanding of the physics of the source and our understanding of how well the technique will work at low magnitudes and also, perhaps, add the essential predictive element so that some estimate may be made of the applicability of the technique in areas where underground tests have not yet been conducted but which need to be monitored under a treaty.

Research has demonstrated that 45° dip-slip earthquakes generate *P* and *LR* waves such that on a m_b:M_s plot they will lie close to the explosion population, not least because the maximum *P*-wave radiation is directed towards the teleseismic region and produces a relatively high m_b.

The m_b:M_s discriminant is one of the most significant improvements in diagnostic aids since the 1958 talks. Its use is limited at teleseismic distances by the detection capacity of a network to detect surface waves. Realistically this figure lies between M_s 3 and 3½ beyond about 30°. To identify sources down to m_b 4½ requires *LR* detection at shorter ranges than the teleseismic distance range. But perhaps the largest drawback to its application lies in the obscuration of the surface waves of interest by surface waves from large earthquakes. One study indicates that about 15% of the surface waves could not be measured for sources at the $m_b \geq 4¾$ level. Other studies have suggested that the problem is not quite so severe. Efforts should be made to define what loss of surface waves may be expected in order to assess to what degree confidence in the m_b:M_s criterion is lowered.

Other types of surface waves, namely Love waves, may well have diagnostic potential. It is, however, rather difficult to be very specific as to their proven value. In theory explosions do not excite Love waves but earthquakes may. However, Love waves are often observed from underground explosions; it may be that the origin of the Love waves is due to secondary sources originating from tectonic release triggered by the explosion. Incidentally, it appears that Love waves are seen more often from explosions at NTS and the Aleutian Isles than from explosions in the USSR. To exploit the relative Love wave excitation it would be useful to understand the mechanism and reasons for their presence in explosion signals although plausible explanations exist. Discrimination based on Love waves has been attempted but only for small sample populations. There is a need for more research here and tests made on large populations of earthquakes and explosions to ascertain their potential. It is not possible to define detection levels for Love waves from a specific area until a network is deployed: horizontal component instruments are necessary and they should be located

in well-controlled environments in boreholes, otherwise their value may be limited to the identification of large magnitude events which may be readily identified by other criteria.

The spectra of surface waves have not been thoroughly investigated as a diagnostic aid. At teleseismic distances the value of surface wave spectra is limited again by the detection capacity of the monitoring network. Good S/N ratios are required for reliable spectral estimates, given a good S/N ratio the chances are, again, that the source can be identified on other criteria. To my knowledge no extensive study has been made of the value of spectral ratios determined from surface waves which perhaps is an indication that the seismological community does not rate the technique highly, yet Eurasian explosion- generated surface waves, recorded at up to about 40°, have more high frequency energy when compared to *most* shallow earthquake Rayleigh wave trains. Remember, 90% of earthquakes in the USSR occur at depths greater than 20 km so it is, perhaps, not surprising.

S-Wave Criteria. The theory of the explosion and earthquake source suggests that the ratio of shear to compressional energy would be a particularly useful diagnostic aid. However, high frequency *S*-wave energy is rapidly attenuated in the earth and is difficult to detect from shallow focus teleseismic sources which limits its value, particularly at teleseismic distances, as a diagnostic aid. At much shorter range it has definite applications including restraints on hypocentre location. It is difficult to see how, for low magnitude seismic disturbances, *S*-wave excitation can be of value for teleseismic discrimination. It is, of course, a great tool for studying attenuation in the earth, knowledge of which will greatly improve modeling and synthesis of waveforms. However, shallow sources rich in *S* waves, such as earthquakes, can produce quite complex teleseismic signals due to numerous *S-P* conversions in the crust and upper mantle of the source region. Such complexity should not be observed from simple compressional explosive sources.

Complexity. In 1958 attention was principally focused on detection and identification of seismic disturbances at relatively short range. As the yield of underground tests increased more and more, teleseismic *P*-wave signals were recorded and it was observed that signals from underground explosions were very simple in appearance compared to most shallow earthquake source signals. The "lonesome *P*" became a vogue phrase. In the early sixties it appeared that it was possible to discard some 90% of the detected signals as earthquakes simply because of their complexity. The rush to the third, or teleseismic, zone was on; it produced a radical change in the concepts of monitoring CTBT. By placing recording stations within the teleseismic window, *i.e.*, the third zone, it was possible to obtain a clean look at the source and this should have been

a large bonus since the key to discrimination between explosions and earthquakes lay in their source differences. The initial excitement created by the extremely simple *P*-wave recordings of Russian and French explosions (and only slightly less simple NTS explosion recordings) at teleseismic distances suffered a serious setback when very complex recordings were made in North America of two small explosions at Novaya Zemlya. Complexity has been defined in a number of different ways but it is essentially an energy ratio: the ratio of the area under the smoothed curve in the first 5 s of the signal to the area under the curve from 5-35 s. For simple explosion-like signals this ratio is near unity but for complex records the ratio is much less than 1.0. (Strictly, this particular definition is a simplicity factor rather than a complexity factor).

Even redefining the complexity criterion to allow identification of Novaya Zemlya, explosions allow a small percentage of earthquakes to be identified on complexity but today it is, and should be, regarded more as a diagnostic aid than an identifier.

The efficacy of complexity is reduced even further if we consider what happens if multiple explosions are detonated since these would produce complex records in all azimuths.

Complexity, however, stimulated a great deal of research. Many researchers have looked for the causes of complexity in explosion and earthquake recordings and our understanding of the earth as a transmission path has benefited significantly. Much of the complexity can be explained in terms of signal generated noise, the presence of random scatterers in the mantle beneath the source and recording station, lateral variations in Q and in velocity in addition to any S to P conversions.

Complexity did have an impact, it led to:

(1) The concept that it may be possible to monitor a CTBT at teleseismic distances which overcomes any political difficulty of negotiating internal stations, often described as intrusive verification.

(2) It stimulated much worthwhile research to explain complexity which led to a much greater knowledge of the transmission path and its properties.

The preceding discussion has commented on our ability to detect and identify seismic sources at teleseismic distances. To verify compliance with any treaty banning or limiting underground nuclear explosions to low yield or magnitude would require additional seismic stations to gather all the necessary information. It could, of course, be targeted on the principal areas of interest but to monitor the whole world is a rather daunting task bearing in mind the vast number of detections, the processing

of the data and the decison making processes which would have to be employed. The problem becomes at least a whole order of magnitude worse given that a potential violator of the treaty could emplcy evasion techniques to avoid either detection or identification of his clandestine test.

Evasion of Detection or Identification

The aim of a potential violator of a CTBT is to detonate a nuclear explosion in such a way that the provisions of the treaty are evaded and no challenges made. If a violator decides to conduct a test underground what options are available to him? Much would depend on the yield of the device, the location and sensitivity of the network deployed to monitor that nation's compliance with the treaty.

To avoid detection the size of the radiated *P*-wave signals must be reduced so that the amplitude remains below the detection capacity of the network. For very low yield tests this could possibly be achieved by firing in a dry low-coupling medium which would give a reduction of about a factor of 10 over hard-rock, close-coupled detonations.

To avoid detection of up to a few tens of kt a potential violator may attempt decoupling the explosion by firing in a cavity. This is the technique which caused so much discussion in the 1958-1962 CTBT talks. Theoretical calculations and subsequent experimental work indicated that decoupling factors, relative to hard-rock coupling, of about 100 were possible. The debate on how high a yield could be successfully decoupled continues but there appears to be a concensus that an upper limit of 50 kt is about right. Fully decoupled, this would be equivalent to say ½ kt close coupled in hard rock — a yield difficult to detect and identify, certainly at teleseismic distances. A yield of 50 kt would, we suspect, be deemed a very significant and useful level at which no nation should be able to evade. As far as we are aware the experimental confirmation of decoupling has only been achieved at the sub-kiloton range. This was the STERLING explosion fired in the SALMON cavity. There is no reason to believe that the theory will break down at higher yields but it is a risk, in the absence of experimental data, that a potential violator must assess. Successful decoupling would depend on the yield to be tested and the availability of appropriate cavities. It is certain that as the yield decreases the task becomes easier and the availability of ready-made suitable cavities increases. At low yields full decoupling of factors of 100 may not be necessary; partial decoupling by factors of say 20 or less may be adequate to evade identification.

Another method to avoid identification is to detonate a device shortly after an earthquake has occurred in the hope that the earthquake coda signals mask the explosion signals. Various scenarios have been proposed

but again, to our knowledge, there has been no attempt to verify the technique. The nearer the test site is to the earthquake epicentre the more difficult it will be to extract the explosion signal. It has been suggested that yields of about 50 kt could be hidden in the coda of a nearby large earthquake but as with all evasion techniques the chances of success increase as the yield decreases. There may be problems associated with the nuclear device if it is to be kept at the bottom of a very deep borehole or in a mountain side for many months, but assuming there are none the detection and identification of such a test would be extremely difficult at teleseismic distances. Like cavity decoupling, the hide-in-earthquake evasion method would require stations to be sited close to areas in which such opportunities present themselves.

A third method of evasion which allows for detection, but which attempts to avoid identification as an explosion, is the multiple shot technique. Here, a series of explosions are detonated over several seconds; the first explosion is low yield to cloud precise onset times, to confuse the epicenter location, make identification at first motion difficult and produce low m_b values. Larger yield explosions are detonated after a few seconds to create a complex seismogram and generate surface waves which interfere constructively to enhance M_s, thus confusing the m_b:M_s discriminant. In theory the technique looks attractive but the violator is taking a much greater risk with this evasion technique. He would need to have total confidence in his containment, not a trivial consideration in the light of experience such as BANEBERRY. It also assumes that the violator knows the identification procedures used by the monitoring networks and is confident he will not be observed on broadband recording systems. Both the hide-in-earthquake and multiple shot method require an assumption to be made by a potential violator about the transmission path between the source and network of receivers. It would appear then that the most serious problems for verification of compliance with test ban treaties are posed by cavity decoupling in which full or partial decoupling is achieved.

Conclusions

Based on the evidence currently available some conclusions can be drawn about our ability to verify compliance with a treaty banning underground nuclear tests. In a way they represent the culmination of some 25 years research effort.

1. In the absence of a positive identifier of earthquake or explosion signals based solely on short period P-wave discriminants there is little prospect that a purely teleseismic system for detecting and identifying underground explosions down to a

politically acceptable level will be possible. However, as modeling of earthquake and explosion-generated P waves improves, it may one day be possible to use only teleseismic P waves for adequate verification. If identification by successful modeling is achieved the identification level would be close to the detection level.

2. The most successful diagnostic aids to discrimination are depth of focus and m_b:M_s. At purely teleseismic distances this suggests a convincing identification threshold of about m_b 5. If teleseismic SP data are supplemented by LP data recorded at shorter ranges such a data base should provide adequate assurances on compliance down to about m_b 4½. To lower the threshold further would require regional networks of seismic stations and the monitoring system is then no longer a teleseismic network.
3. Apart from seismic disturbances which remain unidentified because of obscuration of essential verification evidence, it would appear from available studies that there are some earthquakes which are only identified by the direction of their first motion. If the polarity of first motion had been in the opposite sense the earthquake would have remained unidentified.
4. There is still no concensus in the seismological community as to what adequately defines the identity of a seismic disturbance. Almost all diagnostic measurements are estimates with associated errors but there is, as yet, no adequate statistical assessment to define discrimination capacity.
5. Further research remains to be done but much has been achieved. Our understanding of the source, earth structure, attenuation within the earth, scattering, *etc.*, has increased enormously over the years. Our understanding of much of the physics has enabled us to do modeling and waveform synthesis which has provided excellent insight and additional understanding of the problems associated with the detection and identification of underground nuclear explosions. A solution to the outstanding problems may well be resolved by further success of modeling techniques which encompasses all the physics of the source and transmission path.

Verification of a Threshold Test Ban Treaty

A CTBT can be regarded as a zero yield threshold test ban treaty but in practice verification is only possible down to some technical

threshold. A TTBT, like CTBT, is a treaty limited by some technical threshold. To verify compliance with a threshold test ban there is an additional task beyond identification of the nature of the source: once an underground explosion has been identified an estimate must be made of the yield. This particular problem was not one faced by the Conference of Experts in 1958, but in recent years it has received considerable attention from seismologists as a result of the bilateral TTBT and PNET.

At present the approach to yield estimation is to attempt to relate the seismic magnitude of an explosion to yield via calibration data. Problems arise because of shortcomings in the transportability of the magnitude-yield relationship established for one or more rock types at a test site where the yields are known, to a remote, foreign test site where the test site characteristics are less well known. This is by no means a trivial problem.

The first area of uncertainty is the determination of the seismic magnitude of an explosion. The original m_b magnitude scale in current use was devised to estimate the relative sizes of earthquakes. By today's standards these earthquakes would be regarded as fairly large and as such the source spectra and the spectral distribution of the radiated energy are very different to those from the extremely short duration explosive sources that we wish to investigate using this magnitude scale.

The SP formula for the determination of m_b is:

$$m_b = \log_{10} A/T + B(\Delta)$$

where A is the amplitude of the P wave, T its predominant period and $B(\Delta)$ a distance normalizing term. The use of A/T for large earthquakes seems to work quite well. But is it still applicable for sources which have a much higher corner frequency? Attempts have been made to use A instead of A/T but discarded because it does not result in a significant reduction in the variance of the magnitude estimate. The variance is due mainly to the effects of the transmission path and to reduce this variance is difficult. A is determined initially by the source; attenuation over the path and the effects of the recording instrument response will determine the final values of A and T.

It is probable that P waves from explosions detonated in a shield region are less attenuated than P waves from a source in a tectonic province. Thus, the ration A/T may in effect be enhanced for a shield explosion because a large amplitude is further amplified by dividing by a number less than unity. In short, it should be established by further research that the conventional magnitude used to estimate yield is adequate for the task and that it can be used to a level of accuracy to satisfy

the conditions of any treaty limiting the size of underground nuclear explosions.

Current and conventional wisdom determines that the $B(\Delta)$ curve used to normalize the distance effects on A/T for magnitude determination shall be that devised by Gutenberg and Richter (G&R° before even CTBT talks started in 1958. Almost every subsequent study of P-wave amplitudes as a function of distance show very significant departures from the G&R curve, particularly in the 35° - 45° range. Errors in $B(\Delta)$ will manifest themselves not only as possible changes in mean m_b value but in variance associated with the estimate.

Uncertainties in the adequacy of the magnitude formula are only part of the problem. At present we have no consensus on how the final estimate of the magnitude of a seismic source should be made; individual magnitudes of a network are simply averaged and a variance estimated. There is still no consensus on the minimum number of stations needed to estimate a consistent and stable magnitude.

Station corrections are usually a function of azimuth and distance and applicable only for sources from a specific region. Regular use of a test site can lead to highly stable station corrections and provide magnitude estimates with low variances. It is very important for yield determination to know that the absolute level of the magnitude is not biased in some way. The mean magnitude from a network of stations depends to a degree on the location of the stations relative to a test site. Thus, a network deployed to monitor one test site may not be well located to monitor another and it is essential to know what the base-line shift or bias between the two networks is. The two main sources of bias to contend with in relating magnitude to yield are:

(1) Network bias

(2) Source bias

Neither of these are easy to determine but the difficulties must be resolved to establish confidence in the seismologist's ability to provide the answers so that a treaty can be adequately monitored.

Some network bias may be attributable to the recording system deployed in the network. The network of stations should have recording systems with similar frequency responses. Experiments indicate that the conventional SP instruments of the WWSSN or LRSM type show little or no variation in A/T measurements between the two responses. For yield estimation the passband of the instrument should be such that the peak of the P spectra should lie close to the centre of the passband. Broadband instruments may have a role to play in allowing consistent A/T measurements to be made but they will have little or no value if the yield

threshold to be monitored is less than about 50 kt. It is probable that variations in SP instrument responses contribute little to network bias.

Source, or regional bias, causes a shift in the base line of m_b. Attenuation beneath the source region will reduce the mean magnitude and to make magnitude-yield curve transportable it is imperative that the base line be fixed so it is necessary to estimate, and correct for, source bias. Resolution of this problem has taxed forensic seismologists for some while. Estimates of t^* can be used to predict bias but the bias indicated from t^* measurements is usually at variance with time domain estimates based on observed amplitudes. To be sure, time will resolve these differences and the problem of estimating source bias will be solved. If source bias can be estimated the same technique can probably be applied to a station receiver region and this may go some way to the resolution of the network bias problem.

Perhaps the greater area of ignorance in our knowledge of what is happening in the source region is concerned with the free surface reflection pP. There are serious shortcomings in our attempts to model its behavior. Seismic waveforms from deep explosions can usually be modeled on the assumption that pP is a mirror image of P but this approach fails for shallow explosions and further research is vital to resolve this problem. A solution to the problem of pP will be of considerable value to the refinement of source identification techniques for CTBT monitoring and may prove vital if the accuracy of yield estimation is to be improved. There is much evidence to suggest that pP can add constructively or destructively to the P wave and the resultant amplitude of the P from a fully contained explosion may be altered by a factor of up to about 2 simply by the addition of pP. The refinement of corrections for pP may make m_b estimates more robust and aid not only yield estimation but interpretation of m_b:M_s curves. Whilst some progress has been made in recent years on pP it is clear that there is a long way to go. It is one of the most important outstanding problems yet to be resolved.

Given a final, robust estimate of m_b, this can be related to yield by reference to a magnitude-yield curve for the appropriate shot medium. Unfortunately there is a dearth of robust m_b and yield data for some important rock types. For example, the available information on granite comes from three explosions in the United States and a little data for the French tests at Sahara published in the SIPRI report. All but one of the explosions are less than about 60 kt and are pre 1967 which means the available m_b data are sparse. Use of such data to predict m_b at, say, 150 kt requires extrapolation into a region for which there is no data and this is always a somewhat risky procedure. Theoretical studies, such as modeling P, will play an important part in predicting what may happen for

different yields in different environments for which we have no observational data. Our ability to do this will demonstrate how much we have learned of the physics of the problem over the years.

The surface wave magnitude M_s can also be used to estimate the yield of an underground explosion. There is still a paucity of good teleseismic data even at the 150 kt yield level. Special procedures will be needed if M_s is to be used to aid verification of compliance with a low threshold TTBT since internal stations located at short ranges from a test site will be essential.

The problems of determining a robust M_s are mainly due to lack of observations rather than source or network bias. Path corrections of M_s are somewhat more readily computed and it is possible that M_s will prove to be a good indicator of the yield of an explosion.

A recent, additional factor has to be taken into account when relating M_s to yield and that is the effect on the observed surface wave train of tectonic release immediately after the explosion. Much good modeling work has already been used to explain many of the observations. Further research will demonstrate whether or not the explosion source can be deconvolved with adequate assurance for yield estimation from M_s. This is a good example of where the forensic seismologist was able to respond quickly. Such a response should be somewhat reassuring to politicians because who knows what problems may arise in trying to verify global compliance with test ban treaties.

The verification of compliance with a threshold test ban treaty poses some additional difficulties for the scientist *vis-a-vis* the politician. A politician needs to know whether the yield of an explosion is a violation of the terms of a treaty threshold or not: it seems they want to know whether the yield is 149 kt. Such precision is not possible from seismological evidence. The politicians need educating on the meaning of the variance associated with an estimate

Our experience is that for NTS explosions given all the available geophysical evidence, which is extensive, the yield of explosions below the water table can be estimated to better than a factor of 2 at the yield level of 100 - 150 kt. This factor increases as the magnitude or yield decreases. Without special verification procedures we can, at best, estimate the yield of foreign explosions to within a factor of three.

Down-hole facilities give an answer around $\pm$ 10%. This represents the best estimate that can be made. Seismological evidence *alone* may not, even in ideal circumstances, do better than $\pm$ 50%. The advice that seismologists give to politicians should reflect this uncertainty.

Clearly much work remains to solve the outstanding problems of yield verification. How we combine yield estimates from surface waves with

estimates from body waves is uncertain but such uncertainty may be removed by the application, again, of our increasing understanding of the physics of the source. We also need consensus on what information would be required, in advance, to define a geophysically distinct region within a designated test site so that yield can be adequately estimated to satisfy the conditions of a TTBT.

It is thus clear that there are a number of areas of uncertainty in which further research will provide clarification and add to our understanding and resolution of the scientific and technical problems associated with the teleseismic verification of compliance with underground nuclear test ban treaties. It is unlikely in the near future, but not impossible, that a low yield threshold treaty can be monitored adequately using only teleseismic data. In the absence of internal stations, or stations located within 10's or 100's of km of an area of interest it is unlikely that the level of deterrence, let alone verification capacity, will provide the assurance required by those responsible for the assessment of the risk to national security that would arise from a treaty which allows one nation to test even at a very low yield to the detriment of the other.

It should be remembered that monitoring of nuclear tests in space, in the atmosphere and underwater was fraught with problems in 1963. However, the verification deficiencies were swept aside with the political will to achieve PTBT. It could happen again, although it is most unlikely, for the PTBT had virtually no effect on a nuclear weapons state's ability to develop weapons or maintain its stockpile reliability. A CTBT will require adequate verification procedures, each state party to the treaty will require assurance that the procedures adopted are adequate to ensure its confidence in the treaty. Our task, and responsibility, as scientists is to provide the politicians with a clear statement of our capacity to verify compliance with any proposed treaty limiting underground nuclear weapon tests. This capacity should be defined, with the uncertainties, so that the benefits and risks of a proposed treaty can be reliably assessed and that any special verification procedures that may be necessary are defined and negotiated in advance of the treaty such that confidence in the treaty is maintained during its existence. This is what the VELA Program is and has been all about.

Relative Magnitude Analysis of Short-Period P, P-coda and L_g Waves

Douglas R. Baumgardt

Summary

P-coda magnitudes, measured at NORSAR for presumed Soviet explosions, have lower standard deviations around the array than P-wave magnitudes. Analysis of P-coda characteristics indicates that coda waves are caused by P-wave and surface-wave (fundamental and L_g) scattering in source, propagation-path, and receiver regions. Preliminary analysis of relative L_g and P-coda magnitudes for the largest Soviet explosions between 1976 and 1982 suggests that these events may have a smaller range of yield by approximately a factor of two than indicated by network averaged P-wave magnitudes.

Conclusions

The following conclusions were reached regarding the measurements on codas recorded at NORSAR for presumed Russian explosions in western Kazakh:

(i) NORSAR P-coda magnitudes for Semipalatinsk events vary across the array by about 0.1 magnitude units as compared with about 0.2 to 0.3 units for P-wave magnitudes. Also, array-averaged estimates of coda magnitude varied more smoothly with time into the coda than single-channel estimates [Figs. 1(a) and 1(b)]. The same result was obtained for Azgir-Astrakhan events. These results suggest that local subarray scattering causes random perturbations in coda levels which are smoothed out by the averaging process.

(ii) We find that NORSAR P-coda magnitudes, like the L_g measurements of Ringdal (1983), are more consistent with network averaged P-wave magnitudes than NORSAR single-channel magnitudes (Fig. 2). There is some indication that L_g measurements may be slightly better than P-coda measurements in terms of reducing scatter and bias.

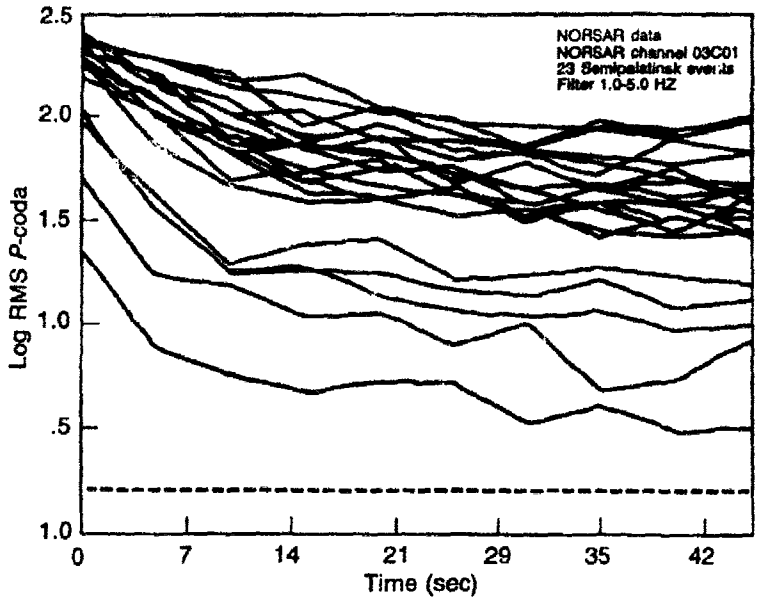

Fig. 1(a). Log RMS amplitude levels in 10 adjacent 5-second time windows on channel 03C01 starting at the *P* first arrival for 23 Semipalatinsk events. Dashed horizontal line is mean noise level before *P* onset.

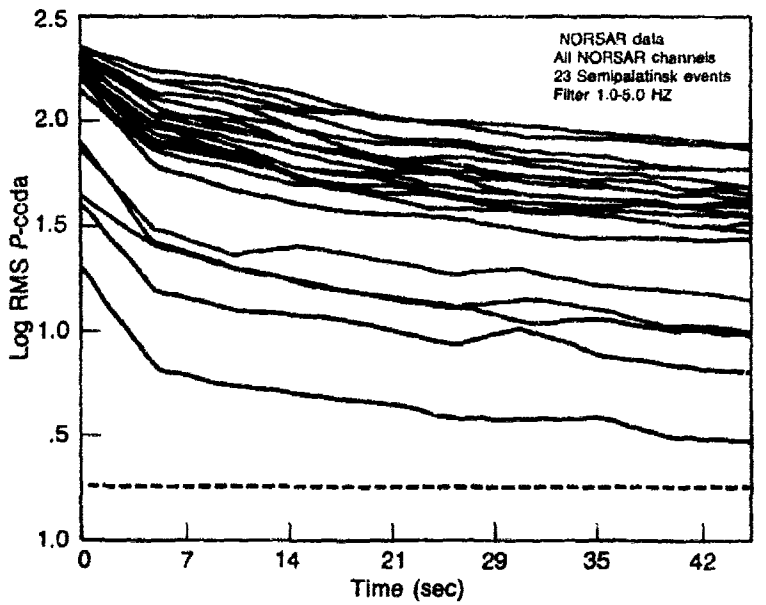

Fig. 1(b). Same as Fig. 1(a) except the *P* and log RMS coda levels are averaged over all usable NORSAR subarray channels. Dashed horizontal line is mean noise level averaged over all channels and events.

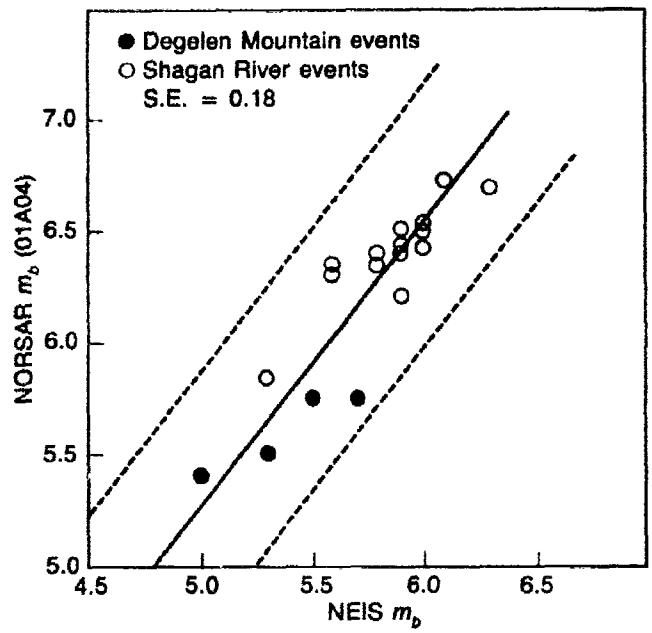

Fig. 2(a). NORSAR magnitudes, measured on channel 01A04, plotted against NEIS magnitudes for Semipalatinsk events. Dashed lines represent plus and minus two standard deviations.

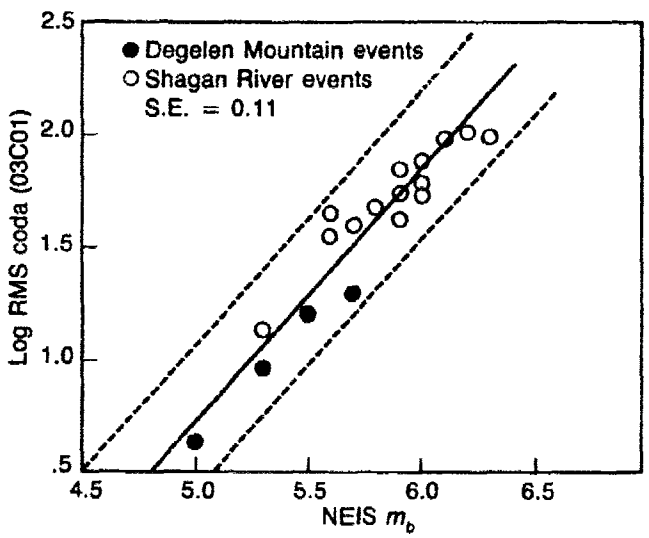

Fig. 2(b). Single-channel (03C01) NORSAR subarray log RMS coda magnitude estimates plotted against NEIS magnitudes for Semipalatinsk events. Dashed lines represent plus and minus two standard deviations.

(iii) *P*-wave scattering in the source and receiver regions produces most of the coda energy between *P* and *PP* for Semipalatinsk events recorded at NORSAR. Comparison of coda measurements in this part of the coda and L_g and L_g-coda measurements (Fig. 3) indicate that fundamental and higher-mode scattering in the Semipalatinsk source region is less important than body-wave scattering in producing long-term coda between *P* and *PP*.

(iv) Since there is such a close correlation between later L_g-precursor coda magnitudes and L_g (Fig. 4) and because the first flat part of the coda is about 0.1 to 0.2 magnitude units above the L_g level, coda magnitudes measured in the flat part of the coda before L_g (Fig. 5) may be more stable for yield estimation than either *PP*-precursor coda measurements or L_g and L_g-coda measurements.

(v) The coda between *PP* and L_g, or the L_g precursor coda, where the *P* coda envelope appears to flatten (see Fig. 5), arises from L_g-to-*P* scattering and other regional phases, such as shear

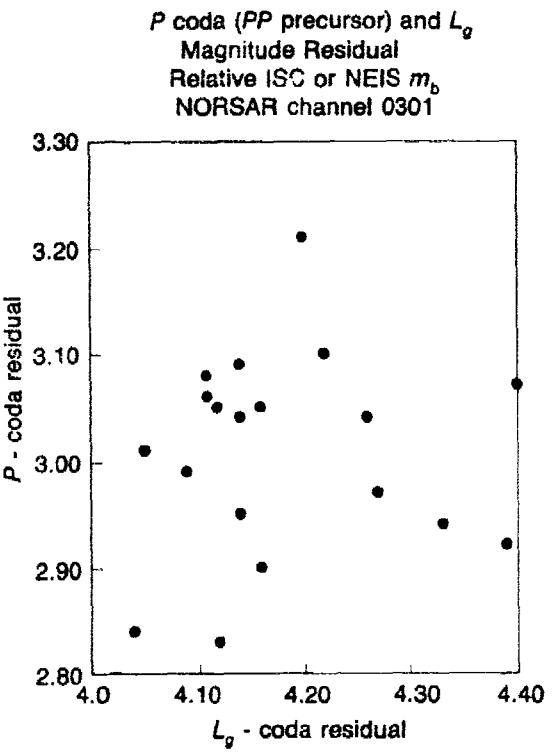

Fig. 3. Residual, with respect to ISC or NEIS m_b, of the RMS coda magnitude versus the L_g residuals for channel 03C1.

waves. The time between the energy burst in the coda and L_g is consistent with the burst being P waves produced by L_g-wave scattering in the vicinity of the southern Ural Mountains (Fig. 5).

We have begun a relative magnitude analysis of P, P-coda, and L_g magnitudes for the largest Shagan River explosions between 1976 and

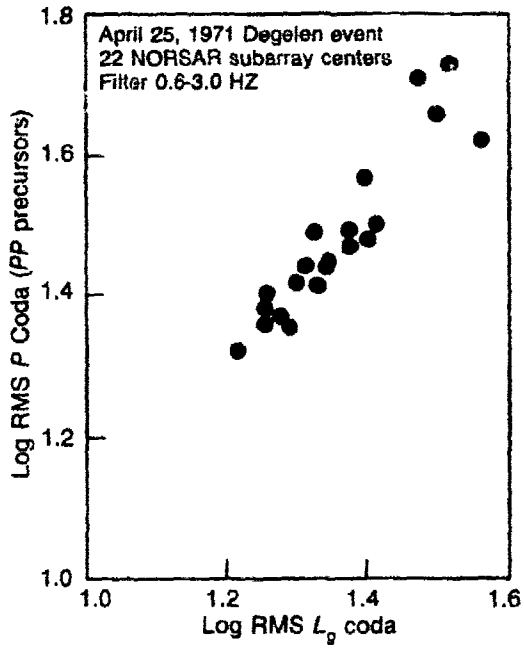

Fig. 4(a). Plot of measurements of *PP*-precursor coda (window 1) against those of L_g and L_g-coda (window 3).

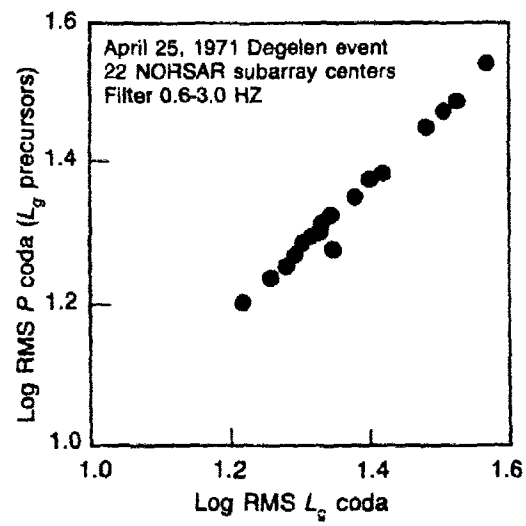

Fig. 4(b). Plot of measurements of L_g-precursor coda (window 2) against those of L_g and L_g-coda (window 3).

1982 in order to check the contention of Sykes and Cifuentes (1983) that these events were detonated at nearly the same yields. Our very preliminary conclusions, based on initial results summarized in Table 1, are:

(i) Relative NORSAR L_g and P-coda magnitudes for these events vary by ± 0.04 to ± 0.05 logarithmic units as compared with ± 0.08 to ± 0.10 for P-wave magnitudes. Assuming a magnitude-yield

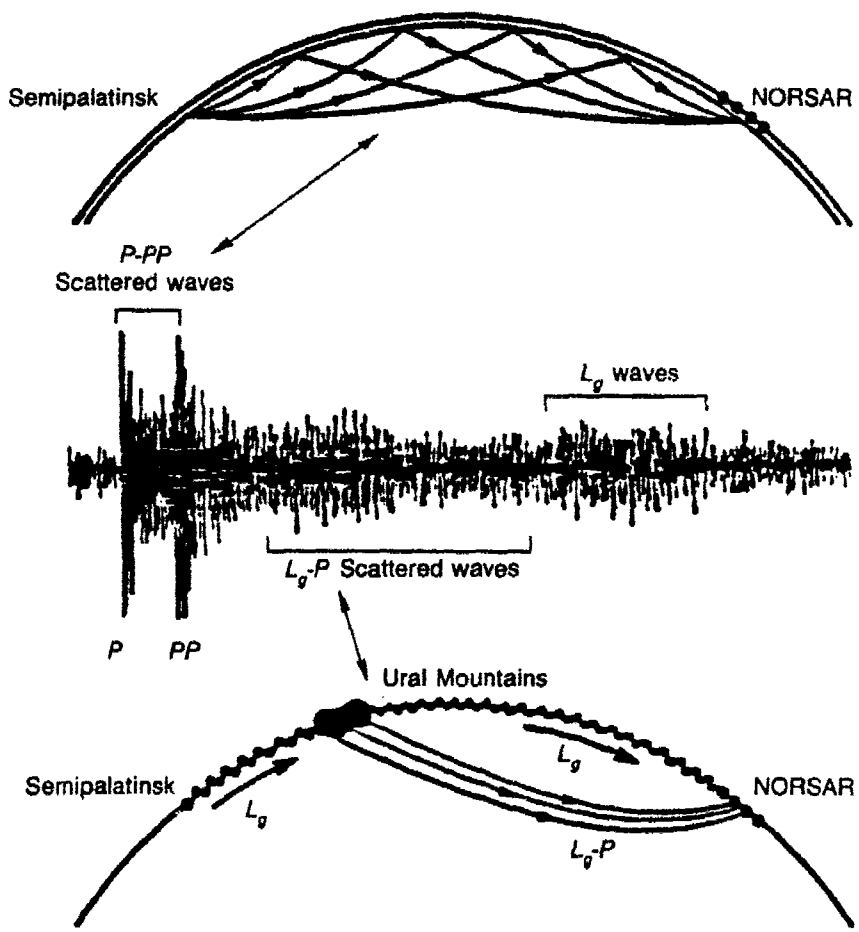

P Coda Generation Mechanisms for
Semipalatinsk Explosions Recorded at NORSAR

Fig. 5. Schematic illustration of postulated model for *P*-coda wave excitation from Semipalatinsk.

Table 1. Means and Standard Deviations for Magnitude Measurements of Largest Soviet Explosions, 1976-1982.

	Method	Mean	Standard Deviation	No. of Events
1.	Single-Channel L_g NORSAR†	3.11	0.04	5
	Multi-Channel L_g NORSAR††	3.01	0.05	5
	NEIS m_b Corresponding Events	6.12	0.13	5
	Corrected m_b Corresponding Events*	6.143	0.092	5
2.	Multi-Station L_g WWSSN**	6.01	0.07	4
	NEIS m_b Corresponding Events	6.18	0.10	4
	Corrected m_b Corresponding Events*	6.167	0.036	4
3.	Single-Channel P-coda NORSAR‡	1.97	0.05	6
	Multi-Channel P-coda NORSAR‡‡	1.96	0.06	6
	NEIS m_b Corresponding Events	6.17	0.10	6
	Corrected m_b Corresponding Events	6.160	0.082	6

† Log-RMS amplitude on channel 03C01 (Ringdal, 1983).
†† Log-RMS amplitude averaged over all NORSAR channels (Ringdal, 1983).
* Station corrections derived by analysis of variance (Sykes and Cifuentes, 1983).
** Absolute m_b (L_g) magnitude estimates (Nuttli, 1983).
‡ Log-RMS amplitude-channel 03C01 (Baumgardt, 1984).
‡‡ Log-RMS amplitude averaged over all NORSAR channels (Baumgardt, 1984).

slope of 1, the corresponding yield ranges near 150 kt are ±17 kt for L_g and *P*-coda measurements as compared to ±35 kt for *P*-wave magnitudes.

(ii) The variation in L_g magnitudes, estimated by Nuttli (1983), and the corresponding *P*-wave magnitudes are more comparable.

(iii) We conclude overall that the yield range for these events, based on L_g and *P*-coda measurements, is smaller by approximately a factor of 2 than the yield range indicated by corresponding *P*-wave magnitudes. However, these conclusions must be considered preliminary until more data can be examined.

Recommended Future Research

Based on the results of this study, we recommend that the following studies be carried out:

(i) Redo the comparison of *P*-coda and L_g magnitudes using a consistent measurement methodology, *i.e.*, same averaging window lengths and start points.

(ii) Investigate the effect of averaging-window length on the stability of coda and L_g magnitudes.

(iii) Investigate the short-term coda (5 to 10 seconds after *P*) for Russian events to determine if fundamental-mode scattering is important in producing short-term coda phases.

(iv) Compare coda magnitudes with fundamental-mode magnitudes on intermediate band seismograms, such as the mid-period RSTN band, to determine if high-frequency fundamental mode scattering generates long-term *P*-coda.

(v) Detailed analytical studies of the surface-wave scattering mechanism need to be made. These studies need to address specifically how fundamental- and higher-mode waves scatter to produce diving *P* waves. For example, can topographic expression scatter L_g waves as effectively as fundamental modes or do L_g waves scatter off of deeper seated structures, such as vertical impedance contrasts produced by deeply penetrating faults? Is L_g scattering more effective at producing long-term coda than fundamental-mode waves?

(vi) Compare coda measurements in the flat part of the coda, which may be caused by L_g to P scattering, with L_g measurements for several events to see if they are as correlated as were the multichannel measurements for a single event in Fig. 3. Measure the slowness and azimuths of the coda phrases to see if they are consistent with P phases arriving from the Ural Mountains.

(vii) Investigate whether or not coda magnitudes measured in the flat part of the coda are more stable than those measured in the coda between P and PP.

(viii) Apply Nuttli's method to determine absolute L_g magnitudes for NORSAR and investigate relative L_g magnitudes for the largest Soviet explosions.

References

Baumgardt, D. R., *Analysis of Short-Period P-Coda Measurements for Presumed Underground Nuclear Explosions in Eurasia*, AFOSR Final Report, SAS-TR-84-01, ENSCO, Inc., Springfield, Virginia, 1984.

Nuttli, O. W., *A Methodology for Obtaining Seismic Yield Estimates of Underground Explosions Using Short-Period L_g Waves*, AFOSR Semiannual Report, 31 March 1983.

Nuttli, O. W., *Illustration of Use of Coda Q Method of Obtaining Anelastic Attenuation Values for Paths from SALMON (Mississippi) and NTS Events*, AFOSR Semiannual Report, 30 November 1983.

Ringdal, F., *Magnitudes from P-Coda and L_g Using NORSAR Data*, NORSAR Semiannual Technical Summary, 1 October 1982-31 March 1983, 1983.

Sykes, L. R. and I. L. Cifuentes, "Yields of Soviet Underground Explosions from Seismic Surface Waves: Compliance with Threshold Test Ban Treaty," submitted to *Proc. National Academy of Sciences of U.S.A.*, 1983.

The Relative Performance of m_b and Alternative Measures of Elastic Energy in Estimating Source Size and Explosion Yield

J.T. Bullitt and V.F. Cormier

Abstract

A comparison has been made of the relative scatter of classical m_b and alternative measures of P wave energy from underground explosions at test sites in East Kazakh, USSR. The scatter of the energy measures is observed among stations in teleseismic arrays of short period GDSN and the local broadband array at Graefenburg, F.R.G. Four measures of A in log (A/T), spectral magnitudes, peak velocity, rms coda, and integrated velocity-squared are compared. The measures are constructed to be in equivalent units of the flux rate of radiated elastic energy. All measures are assumed to have the same slope in a linear regression of log (yield) versus log (measure). Three independent tests were made of the stability of the yield estimators: the scatter of the measures using (1) Graefenburg array data, (2) GDSN data normalized to a reference station, and (3) GDSN data normalized to a reference event. The difference among the standard deviations are small (≤ 0.1 m_b units), making it difficult using a small database to conclude whether the performance of one estimator is significantly better than another. The relative order in the performance of the yield estimators, however, is preserved in each of the three tests. The coda measure is the most stable, followed by the spectral and time-domain A/T measures. The relations observed at Graefenburg between (1) the amplitude of direct P versus P coda, (2) the apparent azimuth of direct P, and (3) complexity, suggest that amplitude variations across an array are a product of scattering along the entire ray path as well as scattering, focusing, and defocusing localized in the lithosphere beneath the source and receiver sites.

Graefenburg Array

The Graefenburg array consists of ten vertical-component and three three-component seismometers arranged in a semicircular arc approximately 150 km long. The instruments are Wielandt seismometers with an output designed to be flat to ground velocity over the frequency band .05 to 5 Hz. The broadband nature of the seismometer output simplifies

the testing of a variety of amplitude measures, because instrument deconvolution is unnecessary.

Summary of Graefenburg Results. The scatter of the amplitude measures tested at Graefenburg is summarized in Fig. 1. The error bars show the estimated experimental errors associated with the each measure type.

The coda RMS measure performs slightly better than the peak amplitude measures when long (60 seconds) time windows are used. Exclusion of the direct *P* wave from the averaging window in the RMS coda measure increases the scatter slightly. Frequency-domain methods perform only about as well as the best of the peak-amplitude measures.

At Graefenburg the energy associated with the direct *P* wave, whether measured in ter of peak amplitude or of RMS velocity in the first 5 seconds, varies from station to station in the same way as the coda energy. In other words, stations with high peak amplitudes tend to exhibit large coda amplitudes, and *vice-versa*. This observation supports the interpretation that a large fraction of the coda is generated before the *P* wave encounters the lithosphere beneath the array. In this case the direct *P* wave propagates upward to the structure beneath the array

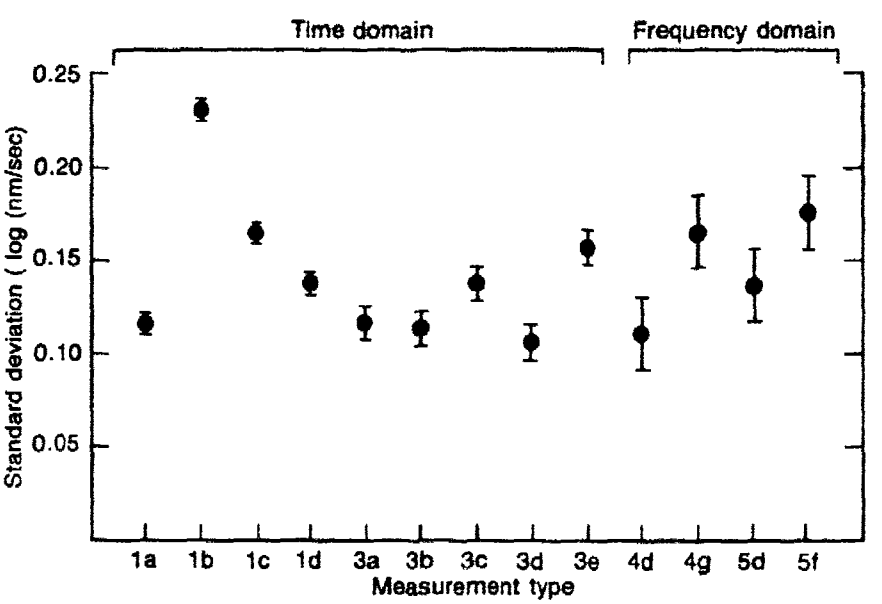

Fig. 1. Summary of relative performance of all measures tested at Graefenburg. Time-domain measures were applied to high-pass filtered records (cutoff frequency 0.3 Hz). For the two frequency-domain methods, scatters are shown only for the averaging windows that yielded the greatest and least scatter.

followed immediately by previously-generated coda energy. The *P* wave and coda energy are then focused and defocused in the same fashion by heterogeneities beneath the array.

The relationship between direct and scattered *P* amplitudes is not, however, simply one-to-one. In general, the coda level tends to increase more rapidly than the peak amplitude. This is confirmed by the observed positive correlation at Graefenburg between the complexity (the reciprocal of the ratio of integrated amplitude in the first 5 seconds to that in the next 30 seconds; Douglas *et al.*, 1973) and the RMS coda amplitude. The often-observed stability of *P* coda amplitudes relative to direct-*P* amplitudes has been interpreted in terms of multiple scattering by small-scale heterogeneities in the earth (*e.g.* Aki. 1973; Douglas, *et al.*, 1973). The *P* coda presumably becomes stable as a result of averaging over a large number of scattering paths (Aki, 1982). At Graefenburg, however, the coda appears not to be as "saturated" with scattered energy as would be expected for waves propagating over the long scattering paths. Thus some of the coda energy appears to have been generated along a relatively short path in the crust below the receiver.

These features of the scattered *P* energy present in the Graefenburg records are highlighted in Fig. 2. High-pass filtered broadband records from three stations are shown with their corresponding peak amplitudes, coda amplitudes (RMS velocity in the 30 second time window beginning 5 seconds after *P*), and complexity. Stations B2 and B3 are separated by no more then 15 km, while station C2 is about 55 km to the south of the other two. These seismograms are representative of the trend seen across the array: as peak amplitude increases, so does coda amplitude, but at a much faster rate.

These observations suggest that while the *P* coda amplitudes are slightly more stable than direct *P* amplitudes, they may also be subject to the same focusing/defocusing effects that affect direct *P*. Focusing/defocusing beneath the NORSAR array, however, seems to affect direct *P* more strongly than *P* coda, and *P* coda amplitudes can be significantly more stable than direct *P* amplitudes there (Baumgardt, 1983; Ringdal, 1983). Stability of *P* coda relative to direct *P* is thus a regional effect which is not observed at all seismic arrays.

At Graefenburg, then, we see evidence of scattering taking place at two sections along the source-receiver path: in the crust immediately beneath the receivers, and somewhere along the path extending from the source to the bottom of the crust beneath the array. It is not possible, however, to determine from these observations alone what relative proportions of the coda energy are generated near the source and along the teleseismic ray path (Dainty, personal communication, 1983). The

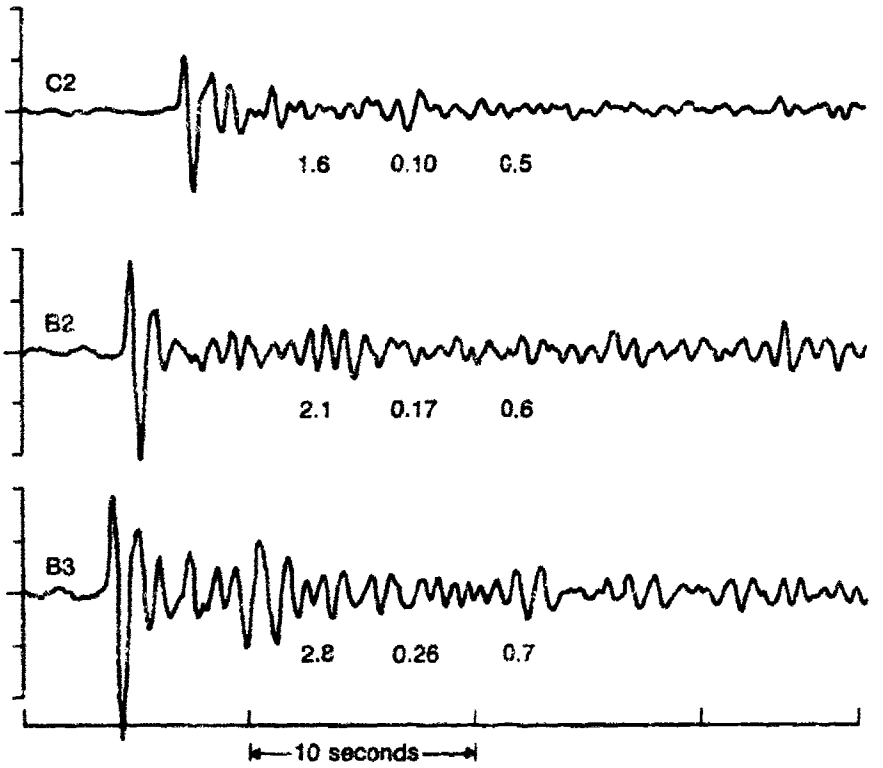

Fig. 2. Seismograms from three stations in the Graefenburg array, showing the large variation of peak and coda amplitudes of the *P* wave. The numbers shown below each seismogram are, respectively, peak velocity, coda amplitude (RMS velocity in the 30-second time window beginning 5 seconds after the *P* arrival), and complexity. Velocities are in units of nm/sec.

observed instability of all yield measures tested at Graefenburg is strongly affected by three-dimensional structural heterogeneities beneath the array.

GDSN Network

Guided by the results of the tests made on the Graefenburg data, we tested a subset of the Graefenburg yield measures on data from the GDSN (Global Digital Seismic Network). Short-period GDSN records of underground nuclear explosions at the Soviet test site in East Kazakh, USSR, were deconvolved to remove the effect of the instrument response and converted to velocity records prior to all subsequent processing. All seismograms were high-pass filtered at 0.5 Hz to equalize the level of microseismic noise among stations of the network. *P* wave amplitude measures 1d, 3b, 3c, and 4a, (Table 1) were calculated for each seismogram.

Table 1. Description of amplitude measures tested in this study. All measures shown were tested on the Graefenburg array data; measures marked with a single asterisk were also tested on GDSN data.

Amplitude Measures Tested on GRF and GDSN data		
Measure	**Type**	**Time or Frequency Window**
1	$\log(V)$	Peaks: a) zero to first peak b) first peak to first trough c) maximum peak-to-peak amplitude d) maximum trace amplitude*
2	$\log(A/T)$	Peaks: a) zero to first peak b) first peak to first trough c) maximum peak-to-peak amplitude d) maximum trace amplitude
3	log (RMS velocity)	Time Windows: a) P to $P+5$ sec b) P to $P+30$ sec* c) $P+5$ sec to $P+35$ sec* d) P to $P+60$ sec e) $P+5$ sec to $P+65$ sec
4	log ($\hat{V}$) (smoothed FFT)	Frequency Bands: a) 0.4 - 4.0 Hz* b) 0.47 - 0.78 Hz c) 0.5 - 2.0 Hz d) 0.3 - 3.0 Hz** e) 0.6 - 3.0 Hz f) 1.0 - 3.0 Hz g) 1.0 - 2.0 Hz** h) 0.5 - 1.0 Hz
5	log ($\hat{V}$) (narrow-band filters)	Frequency Bands: a) 0.4 - 4.0 Hz b) 0.47 - 0.78 Hz c) 0.5 - 2.0 Hz d) 0.3 - 3.0 Hz** e) 0.6 - 3.0 Hz f) 1.0 - 3.0 Hz** g) 1.0 - 2.0 Hz h) 0.5 - 1.0 Hz

* Tested on GDSN data.
** Best of worst frequency band; scatter shown in Figure 1.

Summary of GDSN Results.

Reference Station. A reference station normalization was applied to the four selected amplitude measures at stations ANMO, CTAO, KAAO, and MAJO. The scatter of each measure was calculated for each station after averaging over a suite of 10 East Kazakh events. The scatter of the four measures for two reference stations (ANMO and MAJO) are shown in Figs. 3 and 4. The uncertainty in the value of the scatter for a given measure is estimated from the experimental errors encountered in the Graefenburg study. We assume the experimental error in the estimate of the scatter of a given unnormalized measure is the same for both Graefenburg and GDSN data, as amplitudes were calculated using identical procedures. When the data are normalized in the case of the GDSN data, however, both the numerator and denominator in the normalization contribute equally to the error, with the result that the error in the normalized amplitude is approximately $\sqrt{2}$ times that of each of the unnormalized amplitudes. We conclude that the uncertainties in our estimates of the scatters are approximately ± 0.02 for the RMS coda measures, ± 0.01 for the peak amplitude measures, and ± 0.03 for the spectral measures. These uncertainties are indicated in Fig. 3 by the error bars.

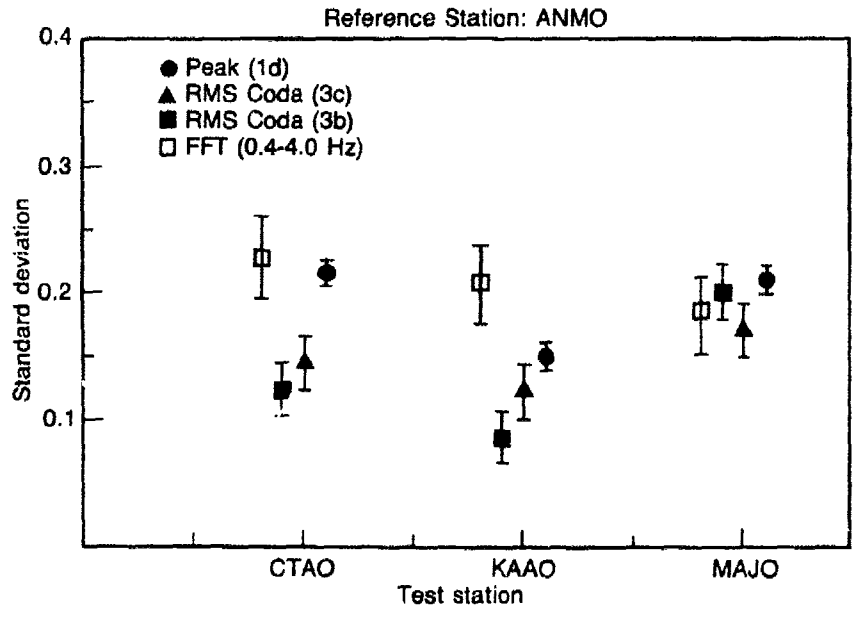

Fig. 3. Relative performance of four amplitude measures tested on deconvolved SRO records of 10 East Kazakh explosions. Data normalized to reference station ANMO. See text for details of data normalization procedure.

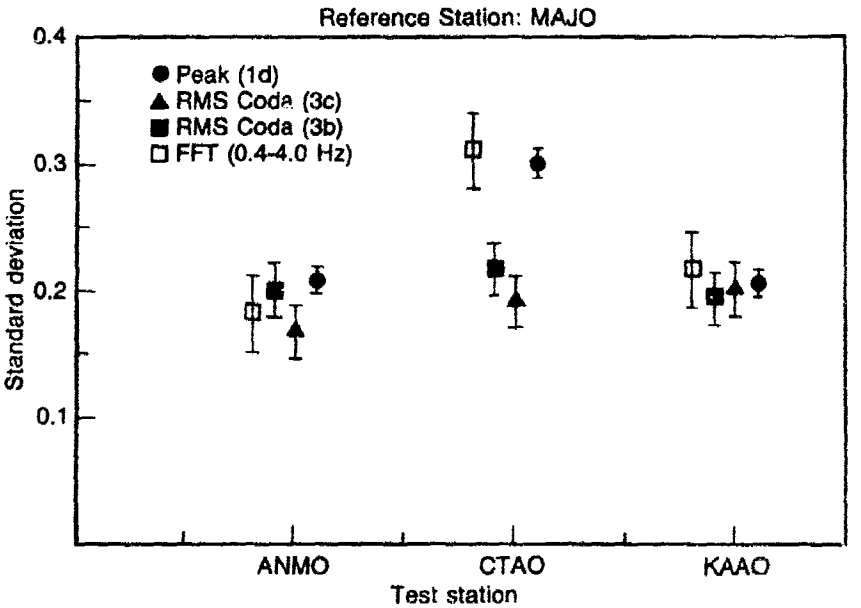

Fig. 4. Same as Figure 3, but normalized to reference station MAJ

The two coda measures generally perform better than either the peak time-domain amplitude or the spectral magnitude. The difference between the four measures at station MAJO is considerably smaller than at the other stations. The behavior of the measures at MAJO may be anomalous because of the relatively complex waveform of East Kazakh events observed at this station. The complexity at MAJO may be a product of multipathing in the Japanese slab. At no station does the spectral amplitude measure perform significantly better than the peak time domain measure. There is a suggestion that the coda measure performs better when the *P* wave is excluded from the averaging window, although this may not be significant.

Reference Event. Normalization of the data to a reference event yields similar results. The normalized amplitudes were averaged over 9 stations in the network and the standard deviations calculated. The results from two typical reference events (events 10 and 31) are shown in Figs. 5 and 6. The error bars show the estimated experimental errors as previously described. Here the pattern is more consistent: the two coda measures perform better than the other measures. The spectral magnitude usually performs better than the peak time-domain amplitude. Similar results were obtained with other events selected as reference events.

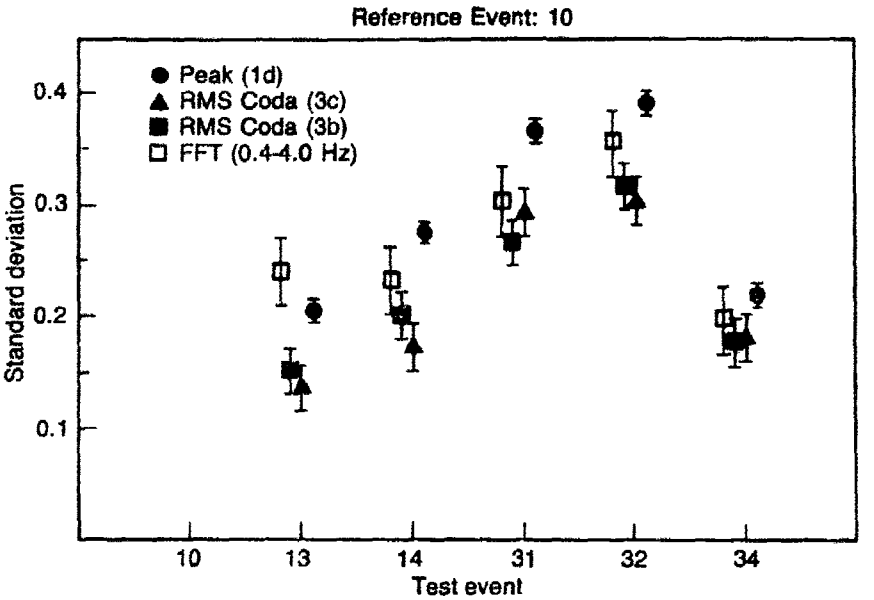

Fig. 5. Relative performance of four amplitude measures tested on deconvolved SRO explosion records from 9 stations. Data normalized to reference event 10.

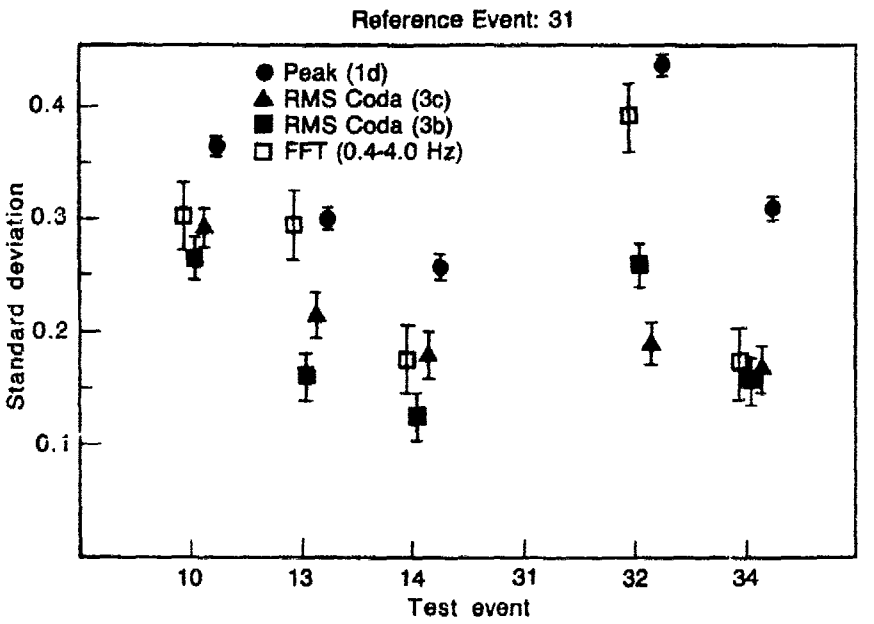

Fig. 6. Same as Figure 5, but normalized to reference event 31.

The GDSN seismograms were high-pass filtered at 0.3 Hz to reduce the microseismic noise level. At some GDSN stations, however, considerable microseismic energy may be present at frequencies above 0.3 Hz. If a large amount of microseismic energy passes through the filter, the RMS coda amplitude measure may exhibit spuriously small scatter, because the noise level may in fact be the most stable feature in the seismograms. In order to test whether the observed stability of the RMS coda amplitudes was, in fact, an artifact of the high noise levels, the GDSN records were high-pass filtered again at 0.5 Hz, and the four amplitude measures recalculated. The resulting scatters are slightly different at all stations for each measure, but the relative performance of measure types is preserved: coda RMS performs better than the peak amplitude or spectral methods, and the spectral method does not perform significantly better than the peak amplitude measure.

Conclusions

Digital broadband velocity seismograms facilitate computation of a wide range of physically meaningful measures of radiated elastic energy. Three independent tests of the stability of several estimators of yield were conducted using (1) amplitudes from a local array at teleseismic distance, (2) amplitudes from a teleseismic network, normalized to a reference station, and (3) amplitudes from a teleseismic network, normalized to a reference event. In each case spectrally averaged magnitudes perform only about as well as the best measure of amplitude in the time domain, the maximum peak or trough of broadband velocity in the first 5 seconds. The root-mean-square amplitude of broad-band velocity in a long time window in the *P* coda is slightly more stable than the other measures tested. These conclusions assume a constant slope, for all measures, in the log yield-log amplitude relations. The amplitude scatters must be adjusted by the corresponding slope factor in order to make direct comparisons of yield scatter.

While comparisons of the stability of various yield estimators are much more difficult for a global array when yield data are unavailable, it is still possible to draw meaningful inferences of the relative performance of yield measures by normalizing the measures to reference stations and reference events. Across an array having an aperture of 100 km, or for an array of sources of the same dimension across a test site, all measures still exhibit scatter, including the best coda and spectral measures. The behavior of travel time, azimuth, and slowness anomalies observed at local arrays suggest that this scatter in amplitudes is due to focusing/defocusing effects of three-dimensional structure beneath the source and receiver. For some source-receiver paths focusing/defocusing can

affect the coda level in the same way as it affects the amplitudes in the first several cycles. When the amplitude of the first several cycles is large or small, so is the coda amplitude, although the relationship is not one-to-one. This suggests that a significant fraction of the coda energy is generated by scattering along the ray path at points other than in the crust beneath the receiver.

Acknowledgements

The reader is referred to the published version of this report (*Bull. Seism. Soc. Am.*, **74**, 1863-1882, 1984) for further details. Tae Im assisted with the GDSN data analysis. The Graefenburg data were collected and supplied by George Choy. This research was supported by the Advanced Research Projects Agency of the Department of Defense and was monitored by the Air Force Office of Scientific Research under contract No. F49620-83-C-0038.

References

Aki, K., (1973), "Scattering of *P* Waves Under the Montana LASA," *J. Geophys. Res.*, **78**, pp. 1334-1346.

Baumgardt, D.R. (1983), *Teleseismic P-Coda Stability and Coda Magnitude Yield Estimation*, SAS-TR-83-01, ENSCO Signal Analysis Systems Division, Springfield, Virginia.

Douglas, A., P.D. Marshal, P.G. Gibbs, J.B. Young and C. Blamey (1973), "*P* Signal Complexity Reexamined," *Geophys. J. Roy. Astr. Soc.* **33**, pp 305-324.

Ringdal, F., (1983), "Magnitudes from *P* Coda and L_g Using NORSAR Data," DARPA /AFOSR Seismic Research Symposium, 16-18 May 1983, Rosario Resort, Eastsound, Washington.

Estimation of t^* for Asian Travel Paths Using sP and sS Phases

L.J. Burdick and S.P. Grand

Summary

A data set of short period sP and sS observations has been collected from four strike slip earthquakes in Asia. The value of t^* can be determined from such observations by measuring the value of $\Delta t^* = t^*_\beta - t^*_\alpha$ which is required to explain the shift in frequency content between sP and sS. The additional relationship that $t^*_\beta = 4t^*_\alpha$ in the earth provides two equations in two unknowns from which t^*_β and t^*_α can be determined. The average measured value of t^* from 22 sP-sS pairs was 0.99 sec. The range in the measured values is from 0.42 to 1.3 sec. Two of the earthquakes studied occurred in southern Asia. The central Asian source region appeared to have a negative attenuation bias of −0.14 sec with respect to the average, while more tectonically active southern Asia appeared to have a positive bias of +0.27 sec.

Introduction

In experiments to measure body wave t^*, it is important to find ways to account for the very crucial unknown of the initial source excitation. One widely recognized experiment in which this is accomplished in a very clever way is the measurement of t^* from multiple *ScS* phases (Jordon and Sipkin, 1977). This approach does not yield information about t^* at frequencies near 1 Hz., however, so other methods need to be developed. Two approaches that do provide information at these frequencies are t^* measurements from *ScP* and *ScS* phases (Sacks, 1980; Kanamori, 1967; Burdick, 1984) and from *Sp* and *sS* phases (Burdick, 1978). The data set used by Burdick (1978) was limited, however, and additional observations are needed to substantiate his results. The t^* measurment from the *sP* and *sS* approach offers an important analog to the *ScP-ScS* approach. As in the *ScP-ScS* experiment, it is assumed that the two phases leave the source with the same initial spectrum. The difference in the amount that *sS* has been attenuated with respect to *sP* ($t^*_\beta - t^*_\alpha$) is measured from the difference in frequency content of the arriving

teleseismic signals. The relative rate of P and S wave attenuation is known with good confidence to be $t^*_\beta / t^*_\alpha = 4$ (Cormier, 1982). Thus we have two equations in two unknowns from which the absolute levels of t^*_α and t^*_β can be determined. The difficulty with the *ScP-ScS* experiment is that the phases penetrate the laterally varying and poorly characterized region of the mantle just above the core-mantle boundary. The *sP* and *sS* phases do not. The difficulty with the *sP-sS* experiment is that the phases are not as well isolated on the record as *ScP* and *ScS* phases, and they generally come from seismic sources with more complex mechanisms. The *ScP-ScS* and *sP-sS* experiments in tandem, however, offer one of the most reliable approaches to measuring t^* in the short-period body-wave band. We here present the results of t^* measurements from 22 *sP-sS* pairs from four earthquakes that occurred in Asia. This study increases the number of *sP-sS* pairs which have been analyzed up to a level similar to the number of previously analyzed *ScP-ScS* pairs.

The *sP-sS* Experiment

The basic geometry of the *sP-sS* experiment along with the salient assumptions in the analysis are outlined in Fig. 1. Panel *a* depicts the two most important considerations in the experimental design. The first is that the *sP* and *sS* phases are both generated as *S* waves with initial upward take-off angles which are similar enough so that we can assume that their initial excitation is the same. The second is that it is necessary to work with shallow, near-vertical strike-slip earthquakes. For this fault orientation, the *sP* phase is perhaps four or five times larger than the direct *P* or *pP* phases at some azimuths (Langston and Helmberger, 1975; Burdick and Mellman, 1976; Ebel *et al.*, 1978). The *sS* can be perhaps twice as large as the direct *S* phase and is lagged far enough behind so that it can be separated from it.

Panel *b* in Fig. 1 illustrates the assumption that the *sP* and *sS* raypaths are essentially identical in their geometry after reflection at the free surface and that the structure near the turning point does not affect the waveshapes. These assumptions are generally valid for epicentral ranges between 30° and 90°. It is also noted in Panel *b* that we assume that $t^*_\beta \sim 4t^*_\alpha$ (Cormier, 1982). Typical *sP* and *sS* arrivals of the type analyzed in this study are shown in Panel *c* of Fig. 1. The signals shown are digitized WWSSN vertical (*P*) and tangential (*SH*) components. Note that the *sP* arrival is much larger than the *P* or *pP* and the *sS* arrival is larger than *S* because of the source radiation pattern. The shift in the frequency content of *sS* with respect to *sP* is very strong, is very clear in the data and therefore can be reliably measured. The value of $\Delta t^* = t^*_\beta - t^*_\alpha$, where β and α refer to *S* and *P* wave t^* respectively, can be determined

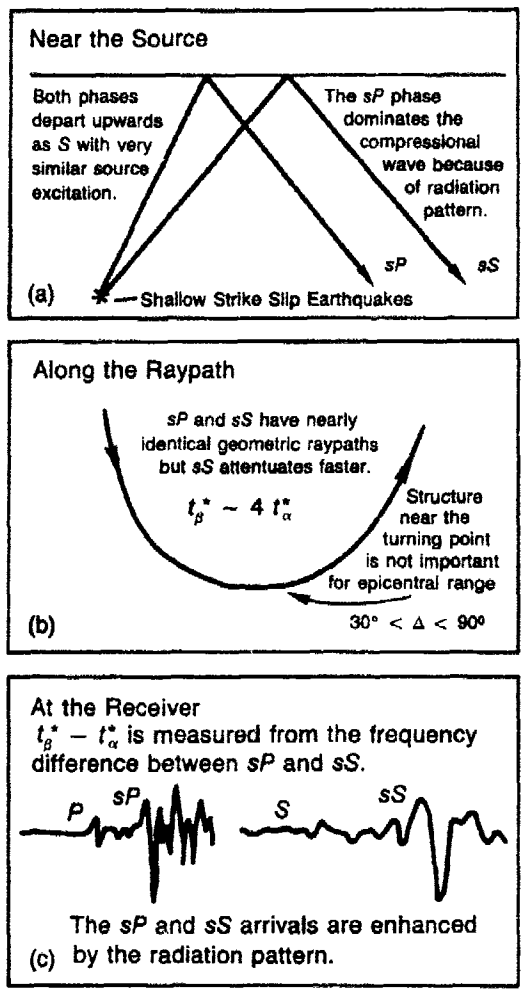

Fig. 1. Schematic diagram of the *sP-sS* experiment.

from just the relative change in the *sP* and *sS* frequency content. Absolute amplitude information is not required. This eliminates uncertainties associated with the source radiation, free surface reflection, geometric spreading and site amplification effects.

The procedure for measuring t^* can be formulated as follows. The standard time domain representation for the *sP* arrival is

$$sP(t) = I(t) * A_P(t) * [S(t) \cdot R_{sP}] \tag{1}$$

$I(t)$ is the instrument operator, $A_P(t)$ is the P wave attenuation operator, $S(t)$ is the source time function including the radiation pattern

term, R_{sP} is the free surface conversion coefficient and * represents convolution. The *sS* arrival is

$$sS(t) = I(t) * A_S(t) * [S(t) \cdot R_{sS}] \tag{2}$$

where R_{sS} is the free surface reflection coefficient and $A_S(t)$ is the *S* wave attenuation operator. We assume that the source time function is the same for both phases. The ratio of the expressions show

$$sS(t) = c \cdot T(t) * sP(t) \tag{3}$$

where c is a constant related to the ratio of the free surface coefficients and the radiation pattern terms and T is a transfer function defined in frequency domain as the spectrum of A_S divided by the spectrum of A_P. We wish to consider both frequency independent and frequency dependent representations for the attenuation operator in this investigation. The formulation for a causal attenuation operator in which Q is independent of frequency in the band of interest was developed by Futterman (1962). The expression for the operator which we denote as A_1 in frequency domain is

$$\ell n\, A_1\,(\omega,t^*) = \frac{\omega t^*}{2}\left\{-1 + \frac{2i}{\pi}\left[\ell n\left(\frac{\omega}{\omega_o}\right) - 2\right]\right\} \tag{4}$$

where ω_o is the Nyquist frequency used in the digital evaluation of the equation. t^* is formally defined as

$$t^* = \int_{\text{Path}} Q^{-1}\,(s)\; V^{-1}\,(s)\; ds \tag{5}$$

The frequency dependent representation for the attenuation operator which we will consider was developed by Minster (1978a, b). It is the attenuation operator for a standard linear solid and it is represented in frequency domain as

$$\ell n\, A_2(\omega,\, t^*,\, \tau_m) = \frac{\omega t^*}{2}\left\{-\frac{2}{\pi}\tan^{-1}\left[\frac{\omega(\tau_M - \tau_m)}{1 + \omega^2 \tau_m \tau_M}\right]\right\} \tag{6}$$

It is assumed in this representation that absorption occurs at an almost frequency independent rate within some absorption band. However, Q increases (absorption decreases) rapidly outside the band. t^* has the same

meaning as in the Futterman representation at the midpoint of the absorption band. The increase of Q at high frequency is controlled by τ_m and at low frequency by τ_M. The increase of Q at low frequency must occur well outside the body wave band. The value of τ_M was therefore simply fixed at 1000 sec. and neglected throughout the course of this study. The purpose of the investigation was to determine which values of t^* and τ_m in the standard linear solid operator or t^* in the Futterman operator best explain the *sP-sS* frequency shift.

Strike Slip Earthquakes In Asia

The pattern of seismicity in Asia is different than in most other regions of the world. Tectonic deformation appears to occur throughout the southern half of the continent rather than being concentrated in narrow zones near plate boundaries. Moderate or large-sized earthquakes occur on many widely scattered small faults rather than on a few large ones as in other areas. Moreover, many of the events are strike-slip, which makes them useful for measuring t^*. Das and Filson (1975) and Molnar and Chen (1983) have provided discussions of the tectonics and many fault plane solutions for the earthquake source regions considered in this study.

The WWSSN records of many events in Asia were scanned first to determine whether the events had near-vertical strike-slip mechanisms and second whether the short period records showed clear *sP* and *sS* phases which were much larger than *P*, *pP* or *S*. Four events which provided good *sP* and *sS* observations were found. The epicenters are plotted on the tectonic map of Alverson *et al.* (1966) in Fig. 2.

Figure 2 also shows how patterns in the tectonics of Asia might be expected to cause lateral variations in t^*. Such lateral variations are of importance since they can cause systematic errors in estimation of the yields of nuclear events. The continent is divided into platforms and fold systems. The large Russian and Siberian platforms in the north of the continent have had the longest period of tectonic quiescence and should be very comparable to the central U.S. or Canadian shield. The southernmost fold belts have been strongly deformed in the recent past and should be comparable to the recently deformed portions of the western U.S. Strong similarities in the seismic character of the central U.S. and northern Asia and the western U.S. and southern Asia have been confirmed by Burdick *et al.* (1983). This should mean that t^*_α differences between the northern platforms and the southern fold belts should be about 0.2 sec. It is not clear, however, what level of attenuation bias might exist between the more stable fold systems of central Asia and those of Southern Asia.

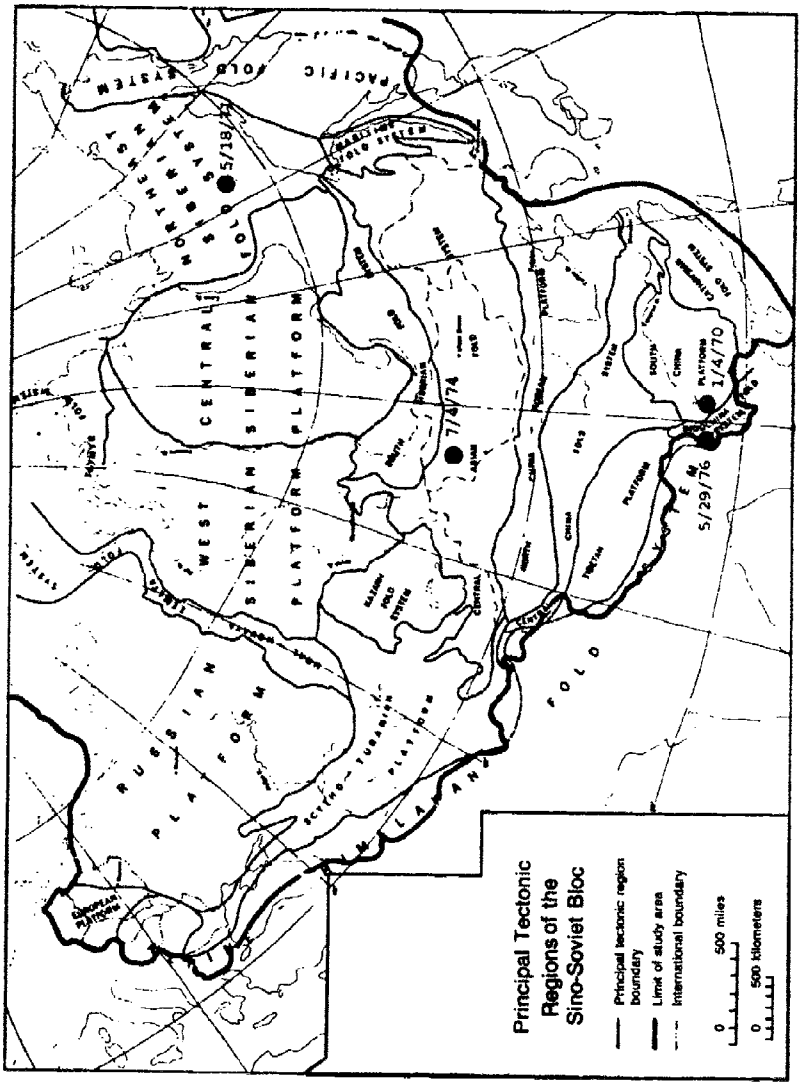

Fig. 2. Tectonic map of Asia (after Alverson *et al.*, 1966).

Figure 2 shows that two of the events studied are well to the south. One is in the Indochina fold system and one in the south China platform. The other two are in the more stable Asian fold system and northeast Siberian fold system. The former is obviously very similar to the Kazakh fold system where the Soviet nuclear test sites are located. At any rate, it should be expected that the southern events in Fig. 2 should yield higher t^* measurements than those to the north. Furthermore, t^* values for the northern two events should be appropriate for the nuclear test sites in the Kazakh fold system. The WWSSN first motion data has been gathered from the four earthquakes. This data and corresponding fault plane solutions are shown in Fig. 3.

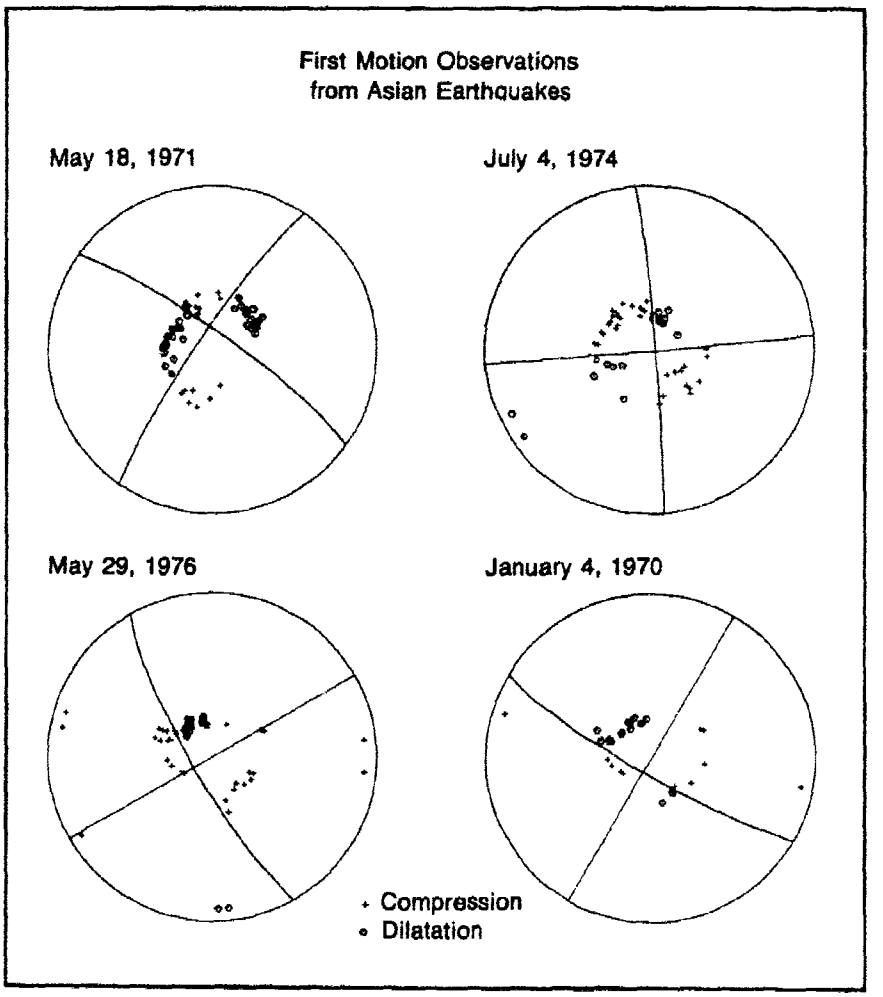

Fig. 3. First motion observations for events 1 through 4.

Identification of the *sP* and *sS* Arrivals

The first step in the data search procedure was to examine the WWSSN long period records from candidate events. The body wave shape for a near-vertical strike slip earthquake is very distinctive. At some azimuths, the *P* and *pP* arrivals appear as small precursors to the much larger *sP* arrival. The *S* appears as a small precursor to the *sS* on the transverse component. Figure 4 shows sample *P* and *SH* waveforms from

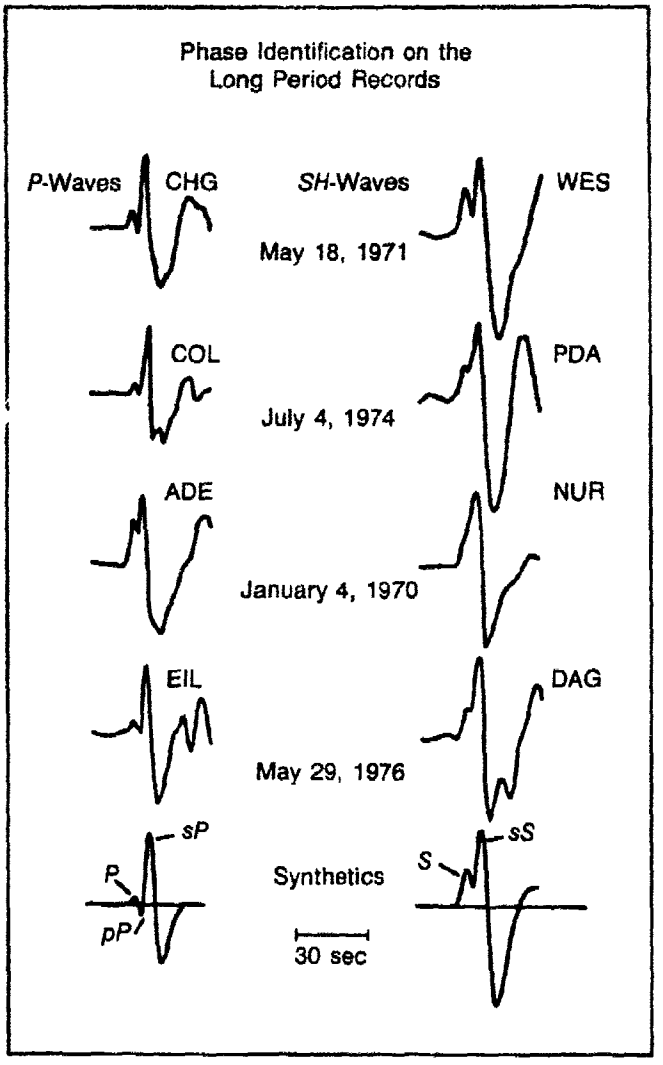

Fig. 4. Sample long period *P* and *SH* waveforms from the 4 strike-slip earthquakes. The major arrivals are identified in the synthetic waveforms at the bottom.

each of the four events used in this study. We adopt the convention in Fig. 4 and throughout the remainder of this paper of displaying all waveforms with positive polarity so that they can be more easily compared to each other. At the bottom of the figure are synthetic waveforms for a 10 km deep strike slip earthquake with a 15° dip on one fault plane. The *P* waves all have a very similar shape which is well matched by the synthetic. We can confidently identify *P*, *pP* and *sP* in the synthetic. The *SH* waves are all also very similar and are matched by the synthetic. We thus can identify *S* and *sS*. The waveforms for the January 4, 1970 earthquake differ the most from the others because this event was significantly larger and had a more complex time function.

Once the *sP* and *sS* arrivals have been identified on the long period records we can identify them through their timing on the short period records. Figure 5 shows some long and short period records from the May 18, 1971 event displayed on the same time scale. The left column

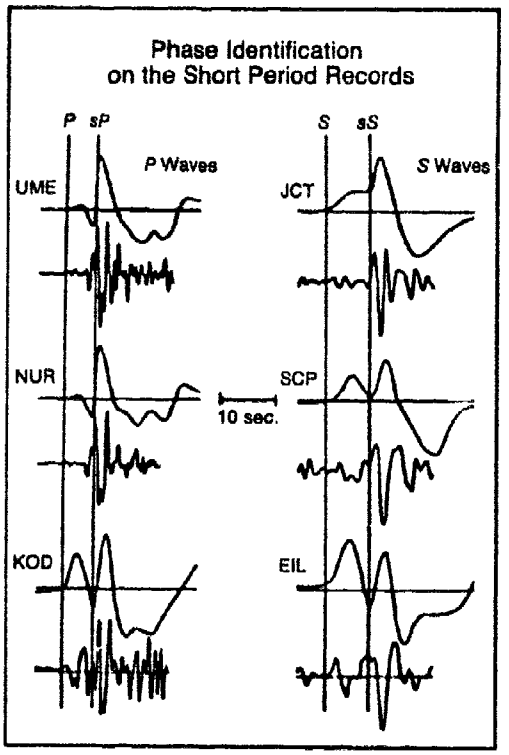

Fig. 5. Sample long period and short period *P* and *S* waves from the May 18, 1971 earthquake. The *sP* and *sS* arrivals in the short period records are identified through their timing.

shows *P* waves and the right shows *S*. There is no difficulty in identifying the *sP* and *sS* arrivals. The *pP* can be clearly seen as a precursor to *sP* in the short period records at UME and NUR. The strong frequency shift between *sP* and *sS* is very clear, so that from it we can accurately measure $t^*_\beta - t^*_\alpha$. It can be noted on the *S* wave records at JCT and SCP that the *sS*/*S* amplitude ratio appears even larger on the short period than it appears on the long period. This is, of course, favorable for the *sP*-*sS* experiment. This enhancement of upgoing short period *S* waves with respect to downgoing was observed in three of the four events used in the study. The most likely explanation for it is upward directivity at the source. It would appear from our data search that unilateral upward rupture propagation is fairly common in strike slip earthquakes.

For each event, a suite of short period *P* waves and a suite of short period *S* waves was digitized. Each trace was hand digitized six times and the results were averaged to suppress digitizing noise. The traces were evenly interpolated at a time step of .02 sec.

In the ideal *sP*-*sS* experiment, the two phases should be recorded at the same station. However, this requirement was too stringent to allow us to compile a large data set. We therefore adopted the procedure of also measuring the frequency shift between good *sS* observations and good *sP* observations from the nearest possible station. It is well known that the frequency content of short period body waves from earthquakes varies substantially with azimuth from the source because of directivity (Ebel and Helmberger, 1982). However, stations within 20° or so of the same azimuth from the source generally receive very similar radiated pulses. We also made the approximation of simply treating the horizontal record closest to being transverse as the *SH* record. This approximation is necessary because digitizing and rotating short period records is such an unstable and noisy process that the results are seldom reliable. There were 22 *sP*-*sS* pairs analyzed in the course of the study.

The short period data for the May 18, 1971 earthquake in the northeast Siberian fold system (Fig. 2) is shown in Fig. 6. In the top three instances, both the *sP* and *sS* observations came from the same station. In the lower four they came from nearby stations. The stations SCH and GWC are part of the Canadian network which has a higher frequency instrument than the WWSSN. Note the coherency between the arrivals even in this higher frequency band. The NUR, UME and KOD arrivals from this event also showed good coherency in Fig. 5. The *pP* arrival can clearly be seen in the IST and NUR records at the bottom of the figure. The *sS* arrival is simple and relatively coherent at all stations.

The *sP* waves from all the events exhibit the waveform complexity and azimuthal instability typical of short period data. They have, however,

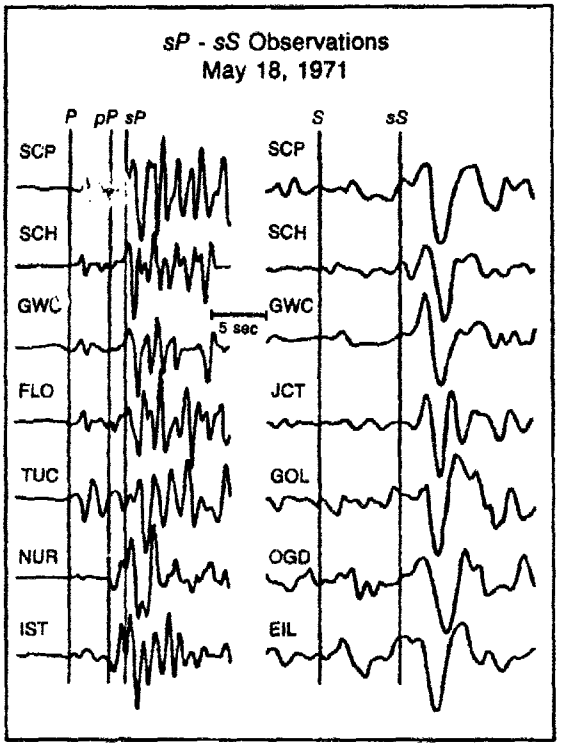

Fig. 6. The data set for event 1.

enough stable characteristics to indicate the analyses of them would be meaningful. In all cases, *sP* is a large impulsive arrival with consistent timing with respect to *P* and *pP* and with an amplitude consistent with the radiation pattern. The interaction of *pP* and *sP* is remarkably stable. The *sS* waves are stable and consistent in all the data sets. The frequency shift between *sP* and *sS* is so strong and clear in all instances that it seems apparent that this data set can be used to place some important constraints on t^*.

The Measurement Procedure

The *sP* and *sS* data sets shown in the previous section present some clear difficulties to further analysis. Identifying the exact onset of the arrivals of interest is not always possible, which makes windowing them out correctly an ambiguous procedure. The coda generated by *P* and *pP* within the *sP* pulse and by *S* within the *sS* represent noise in our analysis. An examination of the records indicates that this noise is probably substantial in some cases. A procedure for measuring t^* which is

stable in the presence of timing errors and noisy signals is therefore required. It would also be desirable to use an analytic way of comparing signals to keep the results as objective as possible. Burdick (1984) developed such a procedure in his analysis of *ScP* and *ScS* waves. We adopted the same procedure for use in this investigation so we could easily compare the results of these two analagous studies.

The procedure relies on a normalized cross correlation coefficient for analytically comparing waveforms to each other. A similar technique was used by Burdick and Mellman (1976) and Lay *et al.* (1984). However, such coefficients are unstable for comparing complex, noisy signals. This instability is removed in the procedure of Burdick (1984) by cross correlating autocorrelations of signals rather than the signals themselves. In this investigation, the procedure was to first window out as accurately as possible the *sP* and *sS* arrivals and to bandpass filter them. The *sP* arrival was then filtered by a suite of transfer functions [$T(t)$ in Eq. 3] corresponding to the possible range of t^* in the Futterman or τ_m in the standard linear solid operator. The autocorrelation of the *sS* to define the optimal values of τ_m and t^*.

It is important to emphasize that the normalized cross correlation coefficient being used defines a best fit in time and frequency domain simultaneously. Therefore, though we display our results in time domain, our conclusions would not change if we had chosen to display their spectra instead. The expression for the cross correlation norm for comparing two waveshapes, $a(t)$ and $b(t)$, defines a best fit between them as the maximum value of

$$N(a,b) = a(t) \underline{cc}\, b(t) \tag{7}$$

where $\underline{cc}$ represents cross correlation. The signals are normalized so that $N(a,a) = N(b,b) = 1$. Maximizing N is the same as minimizing

$$2(1-N) = \int [a(t) - b(t)]^2\, dt \tag{8}$$

or by Parseval's theorem

$$2(1-N) = \int [a(\omega) - b(\omega)]^2\, d\omega \tag{9}$$

Thus a maximum of N defines a best fit in both time and frequency domain. The norm can be recognized in Eqs. 13 and 14 as a least squares norm evaluated at the phase shift of maximum correlation. The norm is unstable for complex (multi-peaked) data because the wrong peaks may

begin to correlate with each other. When $a(t)$ and $b(t)$ are autocorrelations of the signals rather than the signals themselves, the central autocorrelation peaks are always compared to each other.

The measurement procedure was applied to the 22 usable *sP-sS* pairs located in our data search. For each pair, standard linear solid operators were tested for τ_m ranging from 0.01 sec. to 0.90 sec. The long period t^* levels in the operator (see Eq. 6) were readjusted for each data pair according to the model of Anderson and Hart (1978). The fact that in some instances the *sP* and *sS* phases came from different ranges was explicitly taken into account in this correction. The sampling interval in τ_m was .025 sec., which proved to be sufficient for good resolution of the peak value of the cross correlation coefficient. Futterman operators were tested for each *sP-sS* pair at even increments of Δt^*. The values of Δt^* are related to t^*_α and t^*_β through $t^*_\alpha = \Delta t^*/3$ and $t^*_\beta = 4\Delta t^*/3$. The step size in Δt^* was 0.25 sec. and the range investigated was from 0.25 to 4.0 sec.

The results for one of the two central Asian events (Fig. 2) are shown in Fig. 7. For each station pair, the windowed and filtered *sP* and *sS* traces are shown first in dark line. Next follows the autocorrelated *sS* and then the best fitting, attenuation-filtered *sP* waves. The best fitting values of τ_m are indicated. The values of Δt^* for the central Asian events range from 1.25 to 4.0 sec. with an average of 2.6 sec. The τ_m values range from .01 to .20 sec. with an average value of .10 sec. As should be expected, higher values of τ_m correlate with lower values of Δt^* since these both imply less attenuation in the passband of the data. The results of the τ_m and t^* measurements are summarized in Table 1.

The Δt^* values for the two south Asian events range from 3.0 sec. to 4.0 sec. with an average value of 3.8 sec. The τ_m values range from .01 to .05 sec. with an average value of .015 sec. It appears that there is a strong attenuation bias between central and southern Asia as might be expected from the tectonics. The results from southern Asia are also summarized in Table 1. They are always very comparable to each other for any given *sP-sS* pair. This means that the *sP-sS* experiment does not in and of itself resolve any frequency dependence in t^*. This dependence can only be inferred by comparing the results from the *sP-sS* frequency band to results from other types of t^* measurements in other frequency bands.

Conclusions

It has been demonstrated in this investigation that the *sP-sS* experiment is a viable way to measure t^*. It has been shown that appropriate strike slip earthquakes occur often enough so that a substantial data set

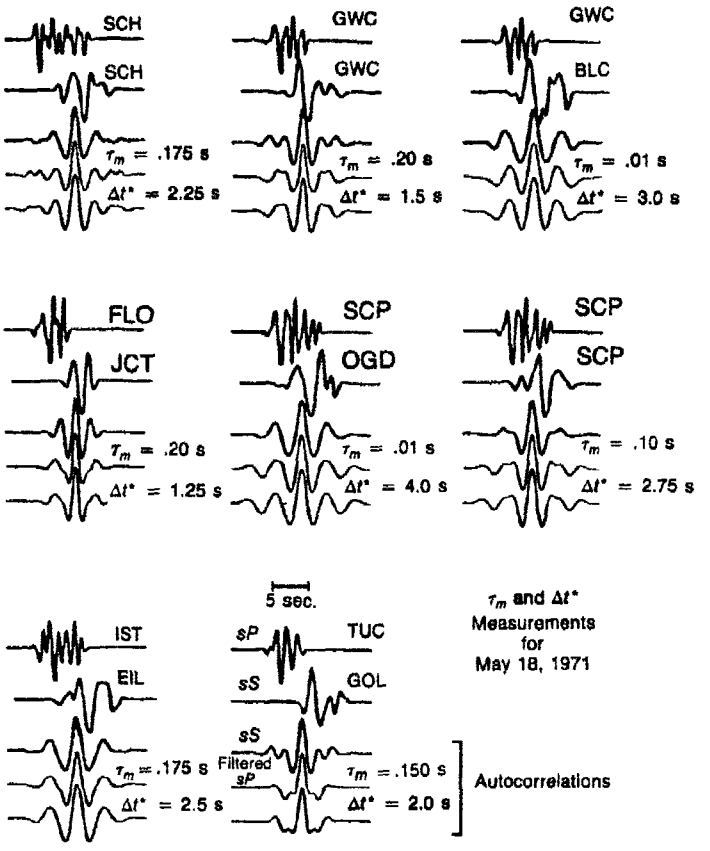

Fig. 7. Best fitting values of τ_m and t^* for event 1.

can be collected. The data set collected here appears to give estimates of t^* for Asia which are consistent with previous estimates and indications of lateral variations in t^* which are consistent with the tectonics. The average value of t^*_α for the earth was found to be .99 sec. The central Asian fold belts have an attenuation bias of $-.14$ whereas more tectonically active southern Asia has a bias of $+.27$ sec. A frequency dependent (standard linear solid) attenuation operator was tested as well as a frequency independent (Futterman) one. The two operators fit the data equally well. Some frequency dependence of t^* was required, however, to reconcile the *sP*-*sS* observations with t^* from a standard Q model based on low frequency observations.

Table 1. Results of the Measurements of t^* and τ_m.

Event Number	STN for *sP*	STN for *sS*	Best Fitting Δt^* (sec.)	Cross Correl. Coeff.	Long Period t^*_α (sec.)	Long Period t^*_β (sec.)	Best Fitting τ_m (sec.)	Cross Correl. Coeff.
1	SCH	SCH	2.25	.943	.94	4.53	.175	.939
	GWC	GWC	1.50	.890	.94	4.46	.200	.862
	GWC	BLC	3.00	.879	.94	4.16	.010	.873
	FLO	JCT	1.25	.875	.91	4.16	.200	.813
	SCP	OGD	4.00	.956	.90	4.32	.010	.935
	SCP	SCP	2.75	.959	.90	4.32	.100	.958
	IST	EIL	2.50	.993	.91	4.20	.175	.994
	TUC	GOL	2.00	.835	.91	4.48	.150	.773
2	ESK	KON	2.00	.952	.94	4.37	.125	.943
	ESK	NUR	2.50	.938	.94	4.30	.100	.927
	NAI	NAI	1.75	.946	.91	4.35	.175	.927
	IST	JER	3.75	.891	.93	4.28	.010	.852
	IST	IST	3.00	.928	.93	4.22	.050	.926
	IST	ATU	3.50	.830	.93	4.40	.010	.835
	IST	SHI	3.00	.815	.93	3.80	.010	.816
3	KEV	KEV	3.00	.820	.93	4.47	.050	.812
	JER	JER	4.00	.934	.94	4.51	.010	.918
	JER	SHI	4.00	.890	.94	4.51	.010	.885
	JER	HLW	3.75	.934	.94	4.51	.010	.934
4	NUR	COL	4.00	.969	.93	3.96	.010	.916
	NUR	DAG	4.00	.921	.93	4.22	.010	.883
	NUR	UME	4.00	.831	.93	4.46	.010	.753

References

Anderson, D.L. and R.S. Hart, "Attenuation Models of the Earth," *Phys. Earth and Plan. Int.*, **16**, 289-306, 1978.

Burdick, L.J., "t^* for *S* Waves with a Continental Raypath," *Bull. Seism. Soc. Am.*, **68**, 1013-1030, 1978.

Burdick, L.J., "Estimation of the Frequency Dependence of *Q* from *ScP* and *ScS* Phases," *Geophys. J. R. Astr. Soc.*, (in press), 1984.

Cormier, Vernon F., "A Review of the Effect of Attenuation On Yield Estimation From Seismic Body Waves," *Bull. Seis. Soc. Am.*, **72**, 169-200, 1982.

Ebel, J., L.J. Burdick and G.S. Stewart, "The Source Mechanisms of the August 7, 1966 El Golfo Earthquake," *Bull. Seism. Soc. Am.*, **68**, 1281-1292, 1978.

Ebel, J.E. and D.V. Helmberger, "*P* Wave Complexity and Fault Asperities: the Borrego Mountain, California, Earthquake of 1968," *Bull. Seism. Soc. Am.*, **72**, 413-423, 1982.

Futterman, W.I., "Dispersive Body Waves," *J. Geophys. Res.*, **67**, 5279-5291, 1962.

Jordan, T.H. and S.A. Sipkin, "Estimation of the Attenuation Operator for Multiple *ScS*

Waves," *Geophys. Res. Lett.*, **4**, 167-170, 1977.

Kanamori, H., "Spectrum of Short-Period Core Phases in Relation to the Attenuation in the Mantle," *J. Geophys. Res.*, **72**, 2181-2186, 1967.

Langston, C.A. and D.V. Helmberger, "A Procedure for Modeling Shallow Dislocation Sources," *Geophys. J. R. Astr. Soc.*, **42**, 117-130, 1975.

Lay T., L.J. Burdick, D.V. Helmberger, C.G. Arvesen, *Estimating Seismic Yield and Defining Distinct Test Sites*, WCCP-R-84-01, Woodward-Clyde Consultants, Pasadena, CA, 1984.

Minster, J.B., "Transient and Impulse Responses of a One-Dimensional Linearly Attenuating Medium; Part I. Analytical Results," *Geophys. J. R. Astr. Soc.*, **52**, 479-501, 1978a.

Minster, J.B., "Transient and Impulse Response of a One-Dimensional Linearly Attenuating Medium; Part II. A Parametric Study," *Geophys. J. R. Astr. Soc.*, **52**, 503-524, 1978b.

Sacks, I.S., "Mantle *Q*s From Body Waves—Difficulties in Determining Frequency Dependence," *EOS, Trans. Am. Geophys. Un.*, **61**, 298, 1980.

Frequency Dependence of Q in the Mantle Under the Shield Areas of Eurasia

Z.A. Der, A.C. Lees, L.M. Anderson, J.A. Burnetti, M.E. Marshall, T.W. McElfresh, and R. Wagner

Summary

A large set of broadband digital data has been analyzed in both the time and frequency domains to determine the frequency dependence to t^* under the Eurasian shield. We find that t^* in this region has a distinct frequency dependence, with t^* increasing with period. For P waves, we find $t^* \approx 0.2$ seconds in the 1-9 Hz band, $t^* \approx 0.5$ seconds in the 0.3-1 Hz band, and $t^* \approx 0.75$ seconds in the 0.02-0.2 Hz band, in all cases lower than the global average of $t_p^* = 1.0$ second from long period data. The Q model with the best fit to our data has an absorption band which shifts with depth in the mantle; it includes a relatively low Q in the upper 400 km of the mantle, high Q's through the rest of the mantle, and no low Q zone at the base of the mantle.

Introduction

As seismic signals have been recorded over broader frequency ranges, it has become apparent that Q values derived from long period observations cannot be applied to short period signals. The Q's measured from low frequency observations predict amplitudes for high frequency arrivals that are practically undetectable. However, high frequency arrivals are commonly and clearly observed; teleseismic short period P waves often contain significant energy up to 8-10 Hz and high frequency S waves from deep earthquakes may contain 2 Hz energy above the noise (Der *et al*, 1982a, 1982b). Thus, significant differences are beginning to appear between the attenuation observed in high and low frequency bands.

A natural explanation for these apparent discrepancies is that Q is frequency dependent in the Earth (Solomon, 1972; Der and McElfresh, 1977; Lundquist and Cormier, 1980). Clearly, the specific forms of this frequency dependence for various parts of the Earth's mantle would provide valuable information about the physical processes occurring in the Earth. Moreover, accurate estimation of yields of nuclear explosions also requires the knowledge of attenuation properties of the mantle. This study

is an attempt to obtain a frequency dependent Q model for the mantle underlying the northern shield areas of Eurasia.

General Methodology

The Eurasian shield is especially suitable for an initial regional study of the frequency dependence of Q. Since shields tend to have a higher Q than active tectonic regions, observations can be made over the widest possible frequency range. Such a study is also aided by the fact that both events and seismic receivers are available within the shield area.

To examine the possibility of frequency dependence in mantle Q, data covering a wide range of frequencies must be available for the specific region studied. The data we utilize includes various types of recordings of seismic events with paths crossing the northern part of Eurasia. Information at the highest seismic frequencies (up to 10 Hz) is furnished by short period P wave recordings of nuclear explosions across the USSR obtained from stations located in northern Europe. Intermediate band information (0.25-2 Hz) is given by S, SS, ScS, ScP, P, and PP phases from short period WWSSN records of deep events in the Far East and Hindu Kush, as recorded in northern Europe. To obtain long period information, we use digital recordings, again from northern European stations, of multiple S and ScS from Far Eastern deep earthquakes.

We have used a variety of mutually complementary techniques to analyze our data: relative time domain amplitudes, waveform modeling, and spectral methods. The individual spectral components of signals in attenuating media are reduced proportionally to $\exp(-\pi f t^*(f))$, a factor which thus determines the relative amplitudes of most band-limited signals. The waveforms and spectral ratios, on the other hand, will mostly be shaped by the apparent t^*, $\overline{t^*}$, which for a limited frequency band may be written as

$$\overline{t^*} = t^* + f\,(dt^*/df)$$

We use a combination of t^* and $\overline{t^*}$ measurements to determine Q over a wide frequency range.

Spectral ratios as functions of frequency have been used to derive $t^*(f)$ from spectra of P waves arriving from narrow ranges of azimuths (Lundquist and Samowitz, 1981, 1982), *i.e.* from known test sites to a set of SRO stations. It can be shown however that such spectral ratios are dominated by effects of lateral heterogeneities near the recording stations, because they vary drastically depending on the particular sensor pair chosen within the same array.

Therefore, we cannot depend much on the details of spectral shapes in narrow frequency bands to specify $t^*(f)$; we have decided instead

to outline the frequency and depth dependence of Q by a combination of time domain and spectral measurements, each of which gives an estimate of t^* or $\bar{t}^*$ most appropriate to a limited frequency band. In this paper we shall assume that anelastic losses occur in shear deformation only, and not in compression, which, of course, needs independent verification. However, our preliminary results in this band can be explained without anelastic losses in compression.

Analyses of Short Period *P* Waves from Nuclear Explosions

For the studies of high frequency attenuation we have utilized P waves from nuclear explosions in the Soviet Union as recorded at NORSAR and other Scandinavian and northern European stations. Spectra of P waves were computed for the first arrivals of a whole suite of events, and show high frequency signal energy above the noise level up to the frequencies of 8-10 Hz. Due to the sensitivity of high frequency energy to Q, these spectra provide a robust constraint on any frequency dependent Q models of the upper mantle almost irrespective of the source model. At NORSAR, the assumption of a cube-root scaled source according to the von Seggern and Blandford (1972) source model yielded $\bar{t}^*$ values of 0.1-0.25 seconds as average estimates for the 0.5-10 Hz band. Other explosion source models yield essentially the same or lower $\bar{t}^*$ estimates. The P-wave spectra can be easily matched in gross shape with a constant frequency-independent t^*, which indicates that t^* varies very slowly with frequency (Der *et al*, 1982; Shore, 1983, Bache, 1984).

In order to outline a Q structure of the upper mantle in the short period band we have assembled the NORSAR recordings of these events into profiles following the approach of Masse and Alexander (1974) and King and Calcagnile (1976), and shall focus on changes in the upper mantle triplications with frequency (Fig. 1). The model by King and Calcagnile (1976), which is superimposed on the profiles, was used in our interpretation because of its relative simplicity and because it fits all of the more obvious arrivals. Figure 1 shows little change in the patterns of arrivals between the 0.5-1.5 and 5.0-8.0 Hz bands. This is an indication of a high Q environment in the upper mantle.

To measure more subtle changes in the frequency contents of the various travel time branches we have computed spectral ratios between a few selected branches using several non-overlapping time windows within the same seismic traces. This has the advantage that source and receiver effects cancel, and using many traces one can assess the repeatability of the results. An example of such spectral ratios is shown in Fig. 2(a). Although the spectral differences are small, the overall slopes

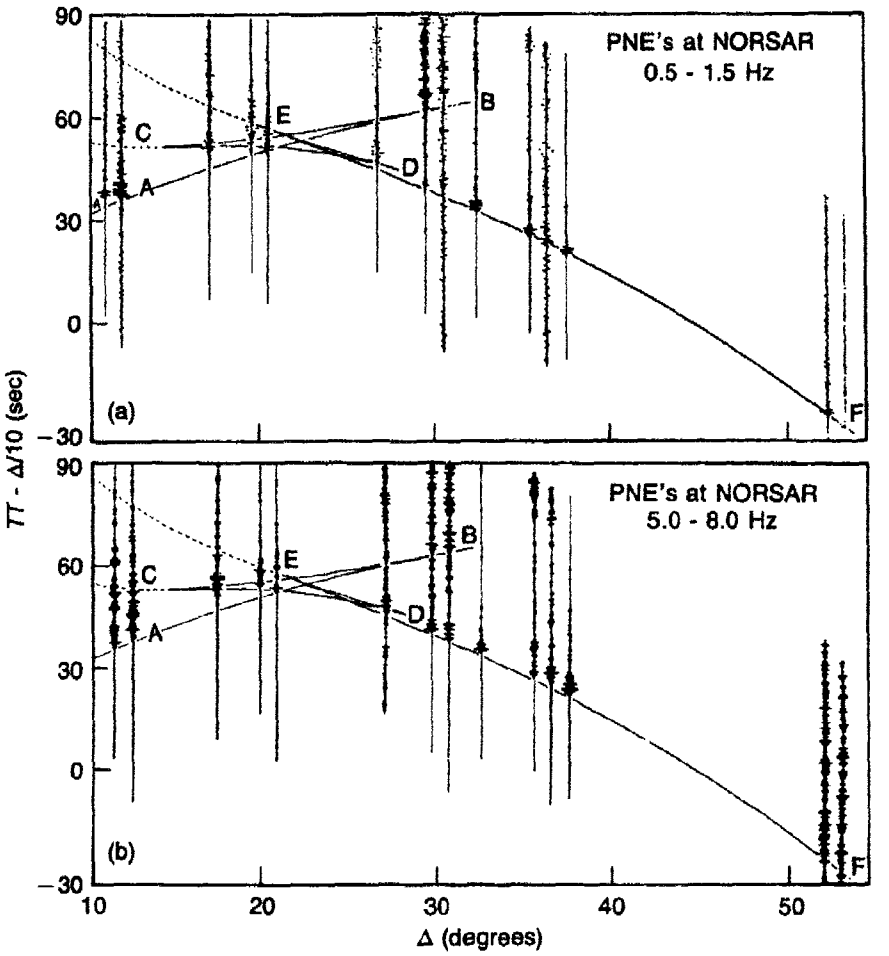

Fig. 1. (a) Reduced travel time curve of seismic profiles from Soviet PNE's at NORSAR, filtered into the 0.5-1.5 Hz frequency band. The travel time triplications from the model of King and Calcagnile (1976) are superimposed. (b) Same as (a) with the seismic profiles filtered into the 5.0-8.0 Hz frequency band.

are fairly consistent and repeatable for the same pairs of arrivals. By raytracing, a Q versus depth model was derived that generally agrees with our observations as well as with the t^* estimates from direct, first arriving P waves is shown in Fig. 2(b). The t^* values predicted by this model are shown in Fig. 2(c) for the branches of the travel time curve. The predicted t^* differentials between the branches of the P travel time curve are consistent with the t^* differentials determined from the spectral ratios. It is also interesting to note that although the Q model in

Fig. 2(b) has a low Q layer in the upper mantle, the Q_P value there is about an order of magnitude higher than those derived for the same depth under the western United States (Der and McElfresh, 1977).

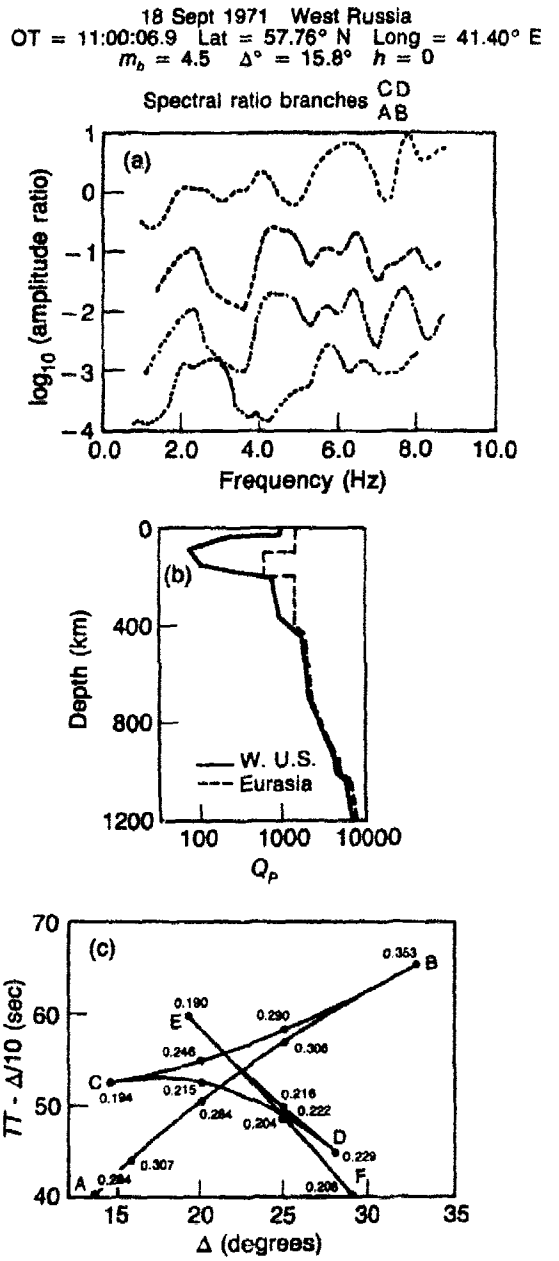

Fig. 2. (a) Spectral ratios between windows centered on the CD and AB branches of *P* wave observations at NORSAR such as those in Figure 1. (b) Model of *Q versus* depth that satisfies the spectral characteristics of the *P* wave profiles such as those in Fig. 1 (dashed line) as compared to a model of the western United States (Der and McElfresh, 1977). (c) Values of t^* predicted by the *Q* model in (b) and the velocity model of King and Calcagnile (1976). The t^* values are labeled for various points on the travel time curve. The t^* differentials between the various branches of the travel time curve in (c) are consistent with the t^* differentials obtained from spectral ratio measurements such as those in (a).

Analyses of Intermediate Period Phases

In the following we describe several constraints on the possible range of $t^*(f)$ in the 0.5-2 Hz band. Measurements of period, rise time, and short period to long period amplitude ratios were used in the analyses. We assumed that all losses are in shear deformation, and we used the empirical relation, $t_S^* = 4t_P^*$.

Short period S waves observed at WWSSN stations in Scandinavia from Far Eastern deep earthquakes usually have very short periods (between 1 and 2 seconds). If source pulses of reasonable length are assumed for these fairly large events (for instance triangular pulses of 1-2 seconds duration), the short periods cannot be reproduced for $\overline{t_S^*}$'s much larger than 1 second, as shown in Fig. 3. Doubling this value gives an upper limit of $\overline{t_S^*} = 2$ seconds for a double pass through a Scandinavian type of upper mantle, corresponding to $\overline{t_P^*} = 0.5$ seconds.

Short period S-SS pairs can also be used to define limits on t^* in the mantle. A pronounced low Q zone in the mantle should cause a very noticeable difference in the waveforms and amplitudes of the short period S and SS. For a number of S-SS pairs, we have found that the changes in period as compared with synthetic simulations give $\overline{t_S^*}$ differentials of less than 3 seconds in the 0.3-1 Hz range. Similar comparisons of the periods of P and PP on short period vertical records gives an estimate of $\overline{t_P^*} \approx 0.5$ seconds.

Following the approach of Burdick (1983), we also compared the periods of ScS-ScP pairs on short period records of deep earthquakes. Since the downgoing legs of the two phases are nearly identical, they cancel when spectral comparisons are made, and thus variations due to structural complexities in the source region are eliminated. The two

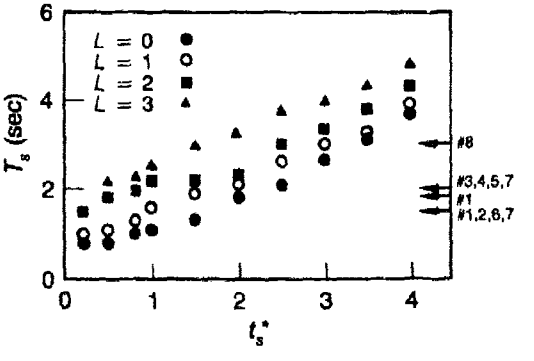

Fig. 3. $\overline{t_s^*}$ compatible with the dominant periods of observed short period S waves recorded across Fennoscandia from deep events in the Far East and the Hindu Kush (marked on the right edge of the figure). The periods of synthetics for triangular sources of various lengths (0, 1, 2, and 3 seconds) are plotted *versus* $\overline{t_s^*}$. For reasonable source durations, $\overline{t_s^*} \sim 1$ second for these deep events, which corresponds roughly to $\overline{t_s^*} \sim 2$ seconds for shallow events.

phases do have different bounce points at the core-mantle boundary, and all reflection coefficients are assumed to be frequency independent. Our observations give $\overline{t_P^*} \approx 0.6$ seconds for a double pass through the mantle, which is lower than Burdick's result.

A time domain approach to the estimation of Q for body waves is the matching of rise times (Stewart, 1984). t^* is taken to be the controlling factor that determines the time between the first arrival break and the first maximum in the P waveform. Other factors that may influence the rise time are the shape of the initial source pulse and the time lag between P and pP. We have measured the rise times for a set of USSR and one Indian nuclear explosion at NORSAR. The theoretical rise times were computed by using the cube-root scaled von Seggern-Blandford (1972) granite source model, the minimum containment depth, and a range of t_P^*'s. The results indicate an overall *upper limit* for $\overline{t_P^*}$ around 0.5 seconds for frequencies between 0.5 and 5 Hz. It is interesting that the estimate of $\overline{t_P^*}$ from the initial rise times is considerably larger than the estimate for the same data from spectral measurements. This may be due to some sort of frequency-dependent scattering phenomenon which causes the high frequency energy to come in later in the wavetrain as suggested by McLaughlin and Anderson (1984).

The matching of observed and theoretical rise times was also used to estimate t^* from short period S waves. Comparison of the observed rise times with the rise times of realistic synthetic pulses gives $\overline{t_S^*}$ approximately 2-3 seconds for a double pass through the mantle.

In the time domain, amplitude ratios of SS/S from corresponding long and short period records provide an estimate of $\overline{t^*}$ across the 0.07 to 0.5 Hz frequency range. Even when the short period SS is not seen, this measurement can put a lower limit on t^* if the amplitude of the noise is used as an upper limit on the SS amplitude. Nine sets of these measurements give $\Delta\overline{t_S^*} < 2.5$ seconds.

Analyses of Long Period S Waves

Estimates of attenuation in the long period band were derived from recordings of deep earthquakes in the Far East. The most suitable phases for studies of Q are the multiple S and ScS arrivals. To simplify our analyses we have utilized only the SH components. Both spectral ratios and waveform modeling were used to estimate t^*; amplitude studies in the time domain were inconclusive, most likely because a simple double couple is not an adequate fit to the source model.

Spectral ratios of long period S phases give $\overline{t_S^*} \approx$ 2-4 seconds for a double pass through the upper mantle. For multiple ScS phases, the spectral ratios only gave positive $\overline{t_S^*}$ differentials in a few cases, and in

these there is a lot of variability in the results. While the results with *ScS* are inconclusive, they suggest that, if anything, since the multiple *ScS* phases are broadened less than the multiple *S* phases, there is not a highly attenuating layer in the lower mantle. Figure 4(a) shows some of the spectral ratios.

Figure 4(b) is an example of the waveform modeling used to get another handle on the differential t^* between long period multiple *S* and *ScS* phases. The top trace is one arrival and the bottom trave is another multiple *S* or *ScS* from the same record. In between, various t^* operators, and a Hilbert transform if necessary, are applied to the first arrival to find the $\overline{t^*}$ which best characterizes the waveform broadening between the two phases. For the multiple *S* phases, we find $\Delta\overline{t_S^*} \approx$ 3-4 seconds, similar to that from the spectral ratios. However, as with the spectral ratios, there is very little visible broadening between the multiple *ScS* phases.

Interpretation of the Results and Conclusions

The compilation of the t^* and $\overline{t^*}$ determinations above is shown in Fig. 5. Under the Eurasian shield, t^* is clearly frequency dependent, even when the scatter in the data is taken into account. Note that t^* increases

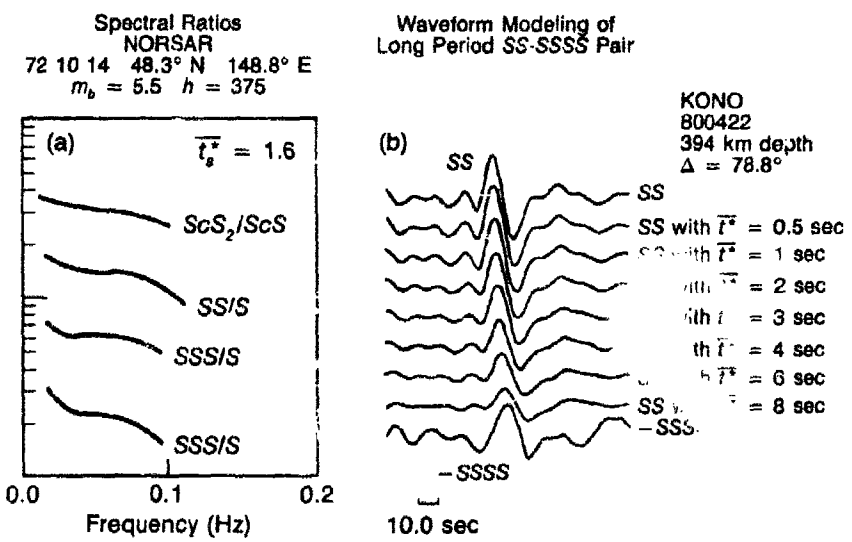

Fig. 4(a). Spectral ratios of long periods *S* and *ScS* phases at NORSAR. From top to bottom, t_s^* = 1.1 seconds, t_s^* = 1.9 seconds, t_s^* = 0.9 seconds, and $2t_s^*$ = 2.1 seconds or t_s^* = 1.1 seconds. (b). Waveform modeling of long period *SS-SSSS* pair. The minus sign has been applied to the *SSSS* phase to account for the two Hilbert Transforms that *SSSS* has undergone relative to *SS*. The best fit is $2t_s^* \approx 6$ seconds.

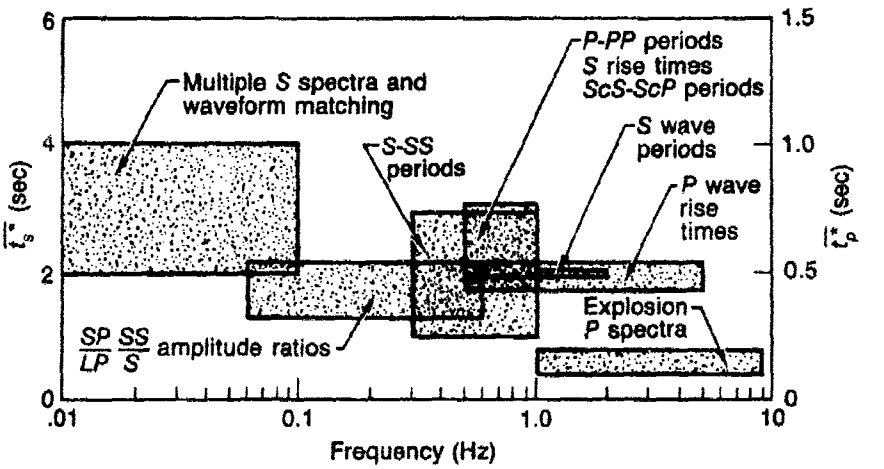

Fig. 5. Summary of observations of $\overline{t_s^*}$ *versus* frequency. The data have been adjusted to give upper limits on $\overline{t_s^*}$ for the double passage of S waves through the upper mantle. Each stippled area has been labeled with the appropriate type of observation.

as period increases, and that $t_P^* < 1$ second and $t_S^* < 4$ seconds, where 1 second and 4 seconds are the generally accepted worldwide averages for t_P^* and t_S^* from free oscillation data.

We have compared our results with the t^*'s predicted by six Q models for the mantle. Two of these are constant, frequency-independent Q models, which are clearly inconsistent with the observations shown in Fig. 5. Four models are modified versions of the frequency-dependent Q model AM of Anderson and Given (1982), models AGM1-AGM4. AGM1-AGM4 span a range of Q models including high and low Q's in the upper mantle and the possibility of a low Q region in the lowest several hundred kilometers of the mantle. The Q models were used in a raytracing program to determine t^* and $\overline{t^*}$ for the various seismic arrivals that were studied above. The t^*'s were used to test the fit of the models to our observations.

The closest fit to our observations is obtained by model AGM4, which is shown in Fig. 6(a); the predictions of AGM4 are shown with our observations in Fig. 6(b). AGM4 is a modification of the AM model of Anderson and Given (1982). AM and AGM4 both have an *absorption band which shifts with depth*, which is consistent with our observation of large $\overline{t^*}$ differentials in the long period band and much smaller $\overline{t^*}$ differentials in the short period band. AGM4 has a low Q region in the upper 400 km of the mantle. The model does not have a low Q zone at the base of the mantle; the 500-km thick zone of Anderson and Given is incompatible

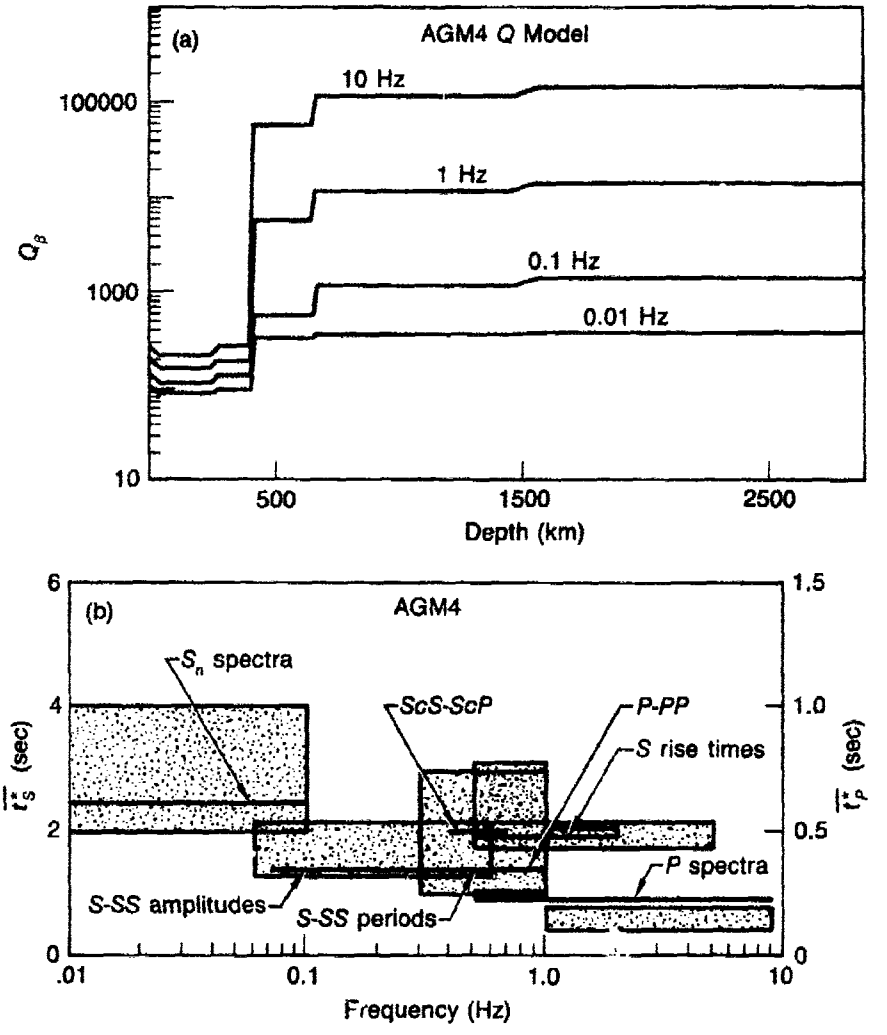

Fig. 6(a). Plot of the AGM4 model, Q_β *versus* depth. (b). $\overline{t_s^*}$ predictions of the AGM4 Q model superimposed on the observations from Fig. 5.

with our observations, especially a long period S *versus* ScS phases, though we cannot rule out the possibility of a thinner Q region at the core-mantle boundary.

In the continuation of this work, we shall further refine the t^* observations and the frequency and depth dependent Q models to more closely match the observations. Observationally, we plan more studies of the long and intermediate period phases. In addition to the amplitude and spectral ratio measurements that we have used to analyze the data, more

extensive waveform modeling of both individual arrivals and the whole *SH* wavetrain will help to refine the observed frequency dependence of t^*.

Recommendations for Future Work

This study is a natural starting point for future studies of attenuation under other regions of the Earth. With the frequency dependence of t^* fairly well established for a shield region where energy is observed to frequencies as high as 10 Hz, the Eurasian shield can be used as a comparison or reference region when doing studies of smaller regions or regions where both sources and receivers are not contained within the region. Also, in a very attenuating region, more information can be obtained about Q from a seismic ray if it only passes once through the region (*i.e.* from a source in the region to a receiver in a high-Q region or vice versa) instead of twice (from a source to a receiver in the same region).

This study also suggest that the frequency dependence of Q should be taken into account when waveform modeling is done to estimate the yield of an explosion.

References

Anderson, D.L. and J.W. Given (1982). "Absorption Band Q Model for the Earth," *J. Geophys. Res.* **87**, 3893-3904.

Bache, T.C. (1984). "The Effect of Q On the Spectrum of Teleseismic P Waves In the 2-8 Hz Band (Abstract)," *Geophys. J. R. Astr. Soc.*, **77**, 297-298.

Burdick, L.J. (1983). *Estimation of the Frequency Dependence of Q From ScP and ScS Phases*, WCCP-R-83-06, Woodward-Clyde Consultants, Pasedena, California.

Der, Z.A., and T.W. McElfresh (1977). "The Relationship Between Anelastic Attenuation and Regional Amplitude Anomalies of Short-Period P Waves in North America," *Bull. Seism. Soc. Am.* **67**, 1303-1317.

Der, Z.A., T.W. McElfresh, and A. O'Donnell (1982a). "An Investigation of the Regional Variations and Frequency Dependence of Anelastic Attenuation in the Mantle Under the United States in the 0.5-4 Hz Band." *Geophys. J. R. Astr. Soc.*, **69**, 67-100.

Der, Z.A., W.D. Rivers, T.W. McElfresh, A. O'Donnell, P.J. Klouda, and M. E. Marshall (1982b). "Worldwide Variations In the Attenuative Properties of the Upper Mantel as Determined From Spectral Studies of Short-Period Body Waves," *Phys. Earth Planet, Int.* **30**, 12-25.

King, D.W. and G. Calcagnile (1976). "P-Wave Velocities In the Upper Mantle Beneath Fennoscandia and Western Russia." *Geophys. J. R. Astr. Soc.* **46**, 407-432.

Lundquist, G.M. and V.C. Cormier (1980). "Constraints On the Absorption Band Model of Q," *J. Geophys. Res.*, **85**, 5244-5265.

Masse, R.P. and S.S. Alexander (1974). "Compressional Velocity Distribution Beneath the Scandinavia and Western Russia," *Geophys. J. R. Astr. Soc.*, **36**, 705-716.

Mclaughlin, K.L. and L.M. Anderson (1984). "Stochastic Dispersion of Seismic Waveforms Due to Scattering and Multipathing (Abstract)," *Earthquake Notes*, in press.

Shore, M.J. (1983). "Short Period P-Wave Attenuation In the Middle and Lower Mantle of the Earth," VSC-TR-83-7, VELA Seismological Center, Alexandria, Virginia.

Sipkin, S.A., and T.H. Jordan (1979). "Frequency Dependence of Q_{ScS}," *Bull. Seism. Soc. Am.* **69**, 1055-1079.

Sipkin, S.A. and T.H. Jordan (1980). "Regional Variations of Q_{ScS}," *Bull. Seism. Soc. Am.* **70**, 1071-1102.

Solomon. S.C. (1972). "Seismicc-Wave Attenuation and Partial Melting In the Upper Mantle of North America," *J. Geophys. Res.*, **77**, 1483-1502.

Stewart, R.C. (1984). "*Q* and the Rise and Fall of a Seismic Pulse," *Geophys. J. R. Astr. Soc.* **76**, 793-805.

von Seggern, D.H. and R.R. Blandford (1972). "Source Time Functions and Spectra from Underground Nuclear Explosions," *Geophys. J. R. Astr. Soc.*, **31**, 83-97.

Source Parameters of Shagan River East Kazakh, USSR Events Using Surface Wave Observations

Jeffrey W. Given and George R. Mellman

Summary

The surface waves from 12 events in the Shagan River region USSR have been inverted for the three observable source parameters using the best available corrections for propagation. The non-isotropic radiation for all of the events can be explained by thrust faulting coincident with the explosion with fault strike generally between 310°-330°. The occurrence of simultaneous thrust typically results in a decrease of M_s by approximately 0.2 units.

Analysis

In most source models of underground nuclear explosions, measurements of the long period source amplitude is essential to accurately estimate the yield. Measurement of the long period source strength is, in many cases, contaminated by non-isotropic seismic radiation, which is observed as *SH* waves (including Love waves) and azimuthal variations in the Rayleigh wave amplitudes and phase. Non-isotropic sources coincident with nuclear tests have been large enough to completely reverse the polarity of the Rayleigh wave radiation. For such events, conventional measures of the long period source amplitude, for instance M_s, bear little relation to the explosion strength.

If we can consider a nuclear explosion and accompanying non-isotropic source as being co-located in space and as having identical time functions, then a moment tensor source is a reasonable model for interpreting the long period seismic radiation. However, when the source is near the free surface, only three linear combinations of the six moment tensor elements can be resolved from observations with wavelengths that are long compared to the source depth. These three parameters are:

$$S_0 = \frac{M_{xx} + M_{yy}}{2} - \frac{M_{zz}}{3}$$

$$S_1 = \frac{M_{xx} - M_{yy}}{2}$$

$$S_2 = M_{xy}$$

where we have defined a local cartesian coordinate system at the source with x directed north, y east, and z, down. The azimuthal radiation pattern for the *P-SV* system (including Rayleigh waves) can be written as

$$U_R(\omega) = P_R^1(\omega)\,(S_0 + S_1 \cos 2\phi + S_2 \sin 2\phi)$$

where $U_R(\omega)$ is the source amplitude and $P_R^1(\omega)$ is an excitation function that depends on the source region elastic structure and source depth. Similarly for the *SH* waves:

$$U_L(\omega) = P_L^1(\omega)\,(S_1 \sin 2\phi - S_2 \cos 2\phi)$$

In both cases, if the source has a step function time dependence, U_R, U_L, P_R, P_L, are real numbers, and the source initial phase is 0 or π.

With only three observable parameters, there is a substantial ambiguity present when attempting to estimate the isotropic component, $\frac{1}{3}(M_{xx} + M_{yy} + M_{zz})$. As a simple example consider an explosion with strength M_I coincident with an earthquake with moment $M_{DC} = FM_I$. If the earthquake is a 45° dipping thrust with $M_{DC}^t = 0.3\,M_I^t$, then the radiation pattern is identical to an explosion accompanied by a vertically dipping, left lateral, strike slip fault with $M_{DC}^S = 0.24\,M_I^S$ and $M_I^S = 0.625\,M_I^t$. An identical radiation pattern is also seen from a 45° dipping normal fault striking east-west with $M_{DC}^n = 1.2\,M_I^n$ and $M_I^n = 0.25\,M_I^t$. Without further constraints on the source mechanism, the explosion size (or yield) can vary by a factor of 4. This is not a worst case example; the source models in the above example have a radiation pattern that is typical of observations from events in the East Kazakh region of the USSR.

We have investigated the Rayleigh and Love waves observed on SRO and ASRO instruments from presumed underground nuclear explosions in the Shagan River region, East Kazakh, USSR. The source radiation pattern was determined after correction for propagation effects using the phase velocity and attenuation measurements of Stevens *et al.*, 1982. Table 1 gives the resulting observables, S_0, S_1, S_2 for 12 events. We briefly discuss four examples.

Table I. Inversion results.

Event	Type	S_0	S_1	S_2	M_I	F	M_{DC}	Strike	δM_S
09/15/78	A	2.82	0.17	−0.85	6.4	0.27	1.7	320	0.19
11/04/78	B	−0.09	0.44	−1.98	4.9	0.82	4.1	321	0.51
11/29/78	A	2.54	0.52	−0.99	6.6	0.34	2.2	329	0.25
06/23/79	A	3.28	0.82	−2.22	10.8	0.44	4.7	325	0.48
07/07/79	C	−5.97	−0.68	−5.27	4.3	2.45	10.6	318	0.03
08/04/79	A	4.44	−0.04	−1.69	10.9	0.31	3.4	314	0.22
08/18/79	B	−1.93	0.17	−3.68	6.3	1.16	7.4	316	0.35
10/28/79	A	4.10	1.77	−1.29	11.6	0.38	4.4	342	0.32
12/02/79	A	5.33	0	0	8	0	0	---	0
12/23/79	A	2.03	−0.04	−0.94	5.4	0.35	1.9	313	0.28
09/14/80	B	−0.96	0.76	−5.06	11.3	0.90	10.2	319	0.47
10/12/80	A	3.94	0.63	−0.85	8.6	0.24	2.1	333	0.15

Units of S_0, S_1, S_2, M_I, and M_{DC} are 10^{15} N-m.

Type A events have initial phase of π at all azimuths, which is appropriate for an explosion. B events are four lobed with alternating normal and reversed polarity. C events are reversed at all azimuths relative to the Type A event.

Figure 1 shows the results for the event of 2 December 1979. This event is very nearly isotropic as seen by the near azimuthal invariance of the Rayleigh wave amplitudes and the very small Love wave amplitudes. Although the path corrections of Stevens *et al.* (1982) give source amplitudes that are reasonably consistent, we observe that stations with similar or opposite azimuths show amplitudes that differ by almost a factor of 2. Since the network coverage is very sparse and almost never complete we found it necessary to introduce an additional frequency independent amplitude correction to the Rayleigh waves. This correction is derived by assuming that the 2 December 1979 event was isotropic and is simply the ratio of the computed to observed Rayleigh wave amplitude averaged over the period band of interest. A similar correction is desirable for the Love waves but is more difficult to derive since the source of the Love waves cannot be constrained as easily. The Rayleigh wave amplitude corrections have been included in all of the other results.

Figure 2 shows the results from the event of 4 August 1979. Substantially more Love wave radiation can be observed, and an azimuthally varying radiation pattern can be seen in the Rayleigh wave. The observed Rayleigh wave seismograms for this event are very similar in shape to the observed seismograms from the event of 2 December 1979.

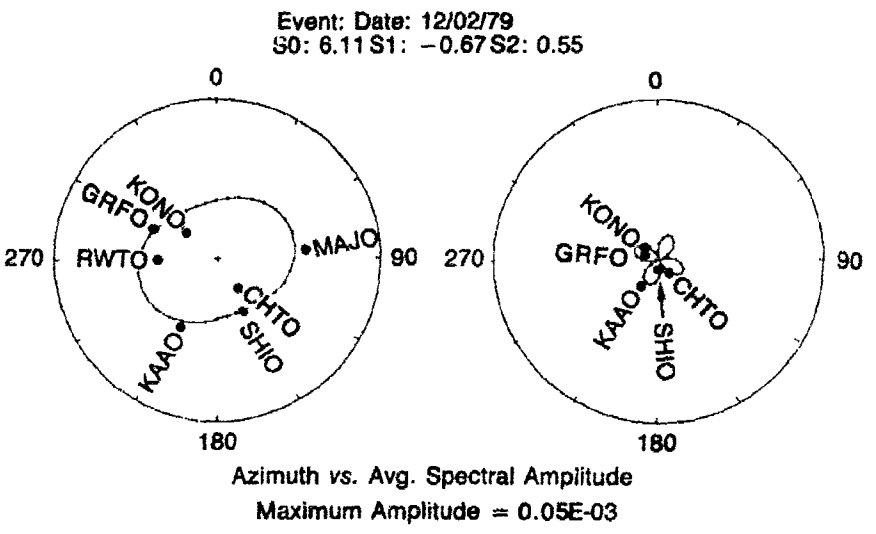

Fig. 1. Observed and computed source radiation patterns for Rayleigh waves (right) and Love waves (left) for the event of 12/02/79. The amplitude scale is linear with the value at the outer circle given below each plot. The amplitude scale is the same for each radiation pattern; note low level of Love wave excitation.

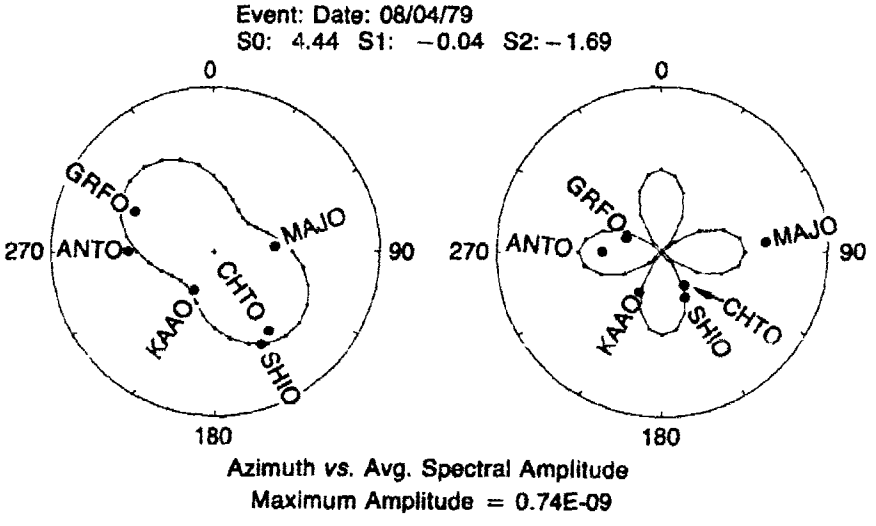

Fig. 2. Observed and computed radiation pattern for event of 4 August 1979. See caption, Fig. 1 for description. Amplitude corrections described in text have been applied.

In Fig. 3 we show the results from the event of 14 November 1980. In this event, although the Rayleigh wave shapes are very similar to those from the previous examples, at station MAJO and KAAO the polarity is apparently reversed. Love wave radiation is large for this event and the apparent initial Love wave phase is identical to the event of 4 August 1979.

In Fig. 4 we present results from an event on 7 July 1979. The polarity of the Rayleigh waves appears to be opposite that of the 2 December 1979 event at all stations. The Love wave radiation is large and with the same polarity as with the preceding two events.

If we assume that the mechanism of the non-isotropic radiation in the Shagan River is the same for all events, and varies only in size relative to the explosions, then a possible explanation of these results is the triggering of thrust faults by the explosion. This is the only double couple plus explosion model that can explain all of the observations with a consistent double couple orientation. In Table 1 we present the derived parameters assuming a 45° dipping thrust event coincident with the explosion. The strike of the assumed thrust fault is very consistent from event to event, usually between 310° and 330°.

The addition of thrust faulting tends to reduce the observed Rayleigh wave amplitudes relative to an explosion alone, and therefore observed M_s values are reduced. In Table 1 we give M_s corrections necessary

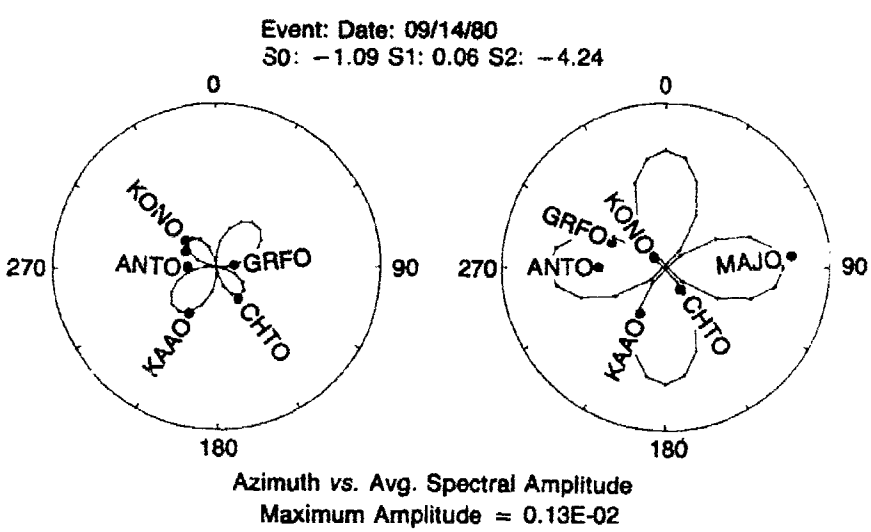

Fig. 3. Observed and computed radiation pattern for event of 14 September 1980. See caption, Fig. 1 for description. Amplitude corrections described in text have been applied.

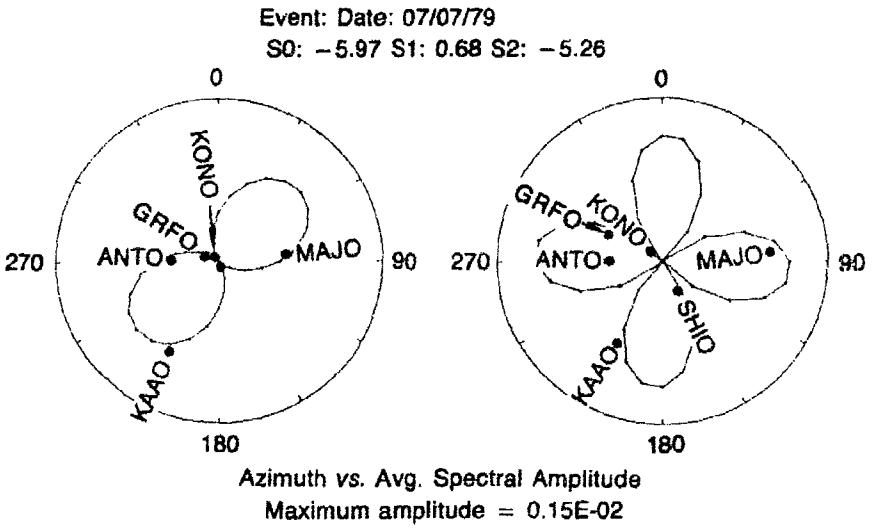

Fig. 4. Observed and computed radiation pattern for event of 7 July 1979. See caption, Fig. 1 for description. Amplitude corrections described in text have been applied.

to remove the effects of the thrust faulting. The correction, to be added to the observed M_s, is about 0.2 units for the typical event. The corrected M_S or similarly M_I can be used to place an upper bound on the size of the explosion, relative to any other double couple plus explosion source model.

Conclusions and Recommendations

With accurate path corrections and high quality data, surface waves can be routinely used to extract three source parameters for shallow events. Further constraints are necessary to estimate explosion yield because of the presence of long period, non-isotropic, radiation. Future work should include using any additional long period data to resolve the source as well as continuing research on combining short-period body and surface wave data. The analysis should be extended to include a sizeable number of U.S. and USSR events for comparisons with additional seismic data.

References

Stevens, J.L., W.L. Rodi, J. Wang, B. Shkoller, E.J. Halda, B.F. Mason and J.B. Minster, 1982, *Surface Wave Analysis Package and Shagan River to SRO Station Path Corrections*, VSC Topical Report VSC-TR-82-21.

Use of *P* Coda for Explosion Medium and Improved Yield Determination

I.N. Gupta, R.R. Blandford, R.A. Wagner and J.A. Burnetti

Abstract

Spectral analyses of P and P coda on teleseismic recordings of nuclear explosions at Yucca Flats and Pahute Mesa regions of the Nevada Test Site (NTS) seem to provide explosion source medium information. The spectral ratio P/P-coda on short-period vertical component records at NORSAR show significant correlation with both explosion medium velocity and transit time between the shot point and the surface. The initial P waves from an explosion within a low velocity medium are richer in low frequencies as compared to those from an explosion within a high velocity medium. The P codas, on the other hand, are relatively insensitive to the near-source velocity differences from one shot to another. Near-source scattering of explosion-generated fundamental-mode Rayleigh waves into teleseismic P appears to be important. Evidence for this comes from the analysis of arrivals immediately following pP and from comparison of P-wave spectra of adjacent explosions with somewhat different depths. The results offer the exciting possibility of extracting near-source information from teleseismic observation of P waves.

Magnitudes based on spectral integration of the initial P, when plotted against log yield, indicate considerable separation between the Yucca Flats and Pahute Mesa events whereas P coda shows no such evidence of source bias. Coda magnitudes provide a significantly more reliable measure of yield than the initial P. Moreover, after correcting the spectral displacement values for the effects of attenuation in the upper mantle and for source function spectrum based on knowledge of approximate yield or m_b, a plot of P-coda magnitude versus log yield appears to have a slope of unity. This implies that P coda from several stations (with different but known t^* values) can be combined to further improve the yield determinations.

Introduction

Scattering of seismic waves due to departure from plane stratified media appears to play a vital role in the observed ground motion from

nuclear explosions. A striking example is the transverse component L_g which is generally larger than the vertical or the radial component (Gupta and Blandford, 1983a). At teleseismic distances, significantly greater stability of P coda as compared to teleseismic P has been established in numerous recent studies (see *e.g.* the review articles by Aki, 1982 and Bache, 1982) so that P coda can be used to obtain stable and reliable measures of yield. Preliminary results from analysis of NORSAR records of NTS explosions also offer the exciting possibility of determining source medium properties from teleseismic observations of P and its associated coda (Gupta and Blandford, 1983b, Gupta *et al.*, 1984).

Variation of Spectral Ratio *P*/*P*-Coda with Overburden Velocity and Depth

Short-period, vertical component NORSAR records of fourteen (14) underground nuclear explosions were first selected for spectral analysis of initial P and the associated codas. Figure 1 shows typical waveforms for the explosions STRAIT at Yucca Flats and POOL at Pahute Mesa. The yields of the two explosions are nearly equal (POOL is somewhat bigger). Both records have nearly the same peak amplitude values but the frequency contents of the initial P wave train appear to be quite different. The P codas on the two records, however, do not seem to be significantly different. The time windows used for spectral analyses of initial P and P coda, as indicated in Fig. 1, are 12.8 sec and 25.6 sec

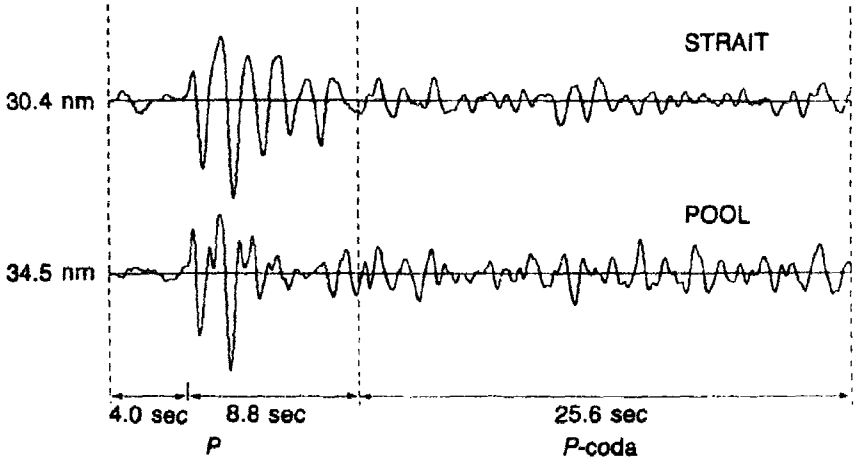

Fig. 1. NORSAR records of P and P coda from STRAIT and POOL showing time windows selected for initial P and P coda. Note that the energy in the initial P for the two explosions with nearly equal yields is considerably different whereas the P coda levels do not appear to be much different.

long with the *P* window starting 4 sec before the onset of direct *P*. The spectral ratios *P*/*P*-coda were obtained after correcting for noise by subtracting the power in noise from the power in observed signal. Results for STRAIT and MAST are shown in Fig. 2 in which the least squares mean slopes of the *P*/*P*-coda spectral ratios for the frequency range 0.5 to 3.0 Hz are indicated.

A comparison of the spectral ratios in Fig. 2 shows interesting features. The spectral ratio *P*/*P*-coda, on the average, decreases with frequency for STRAIT and increases with frequency for MAST. In other

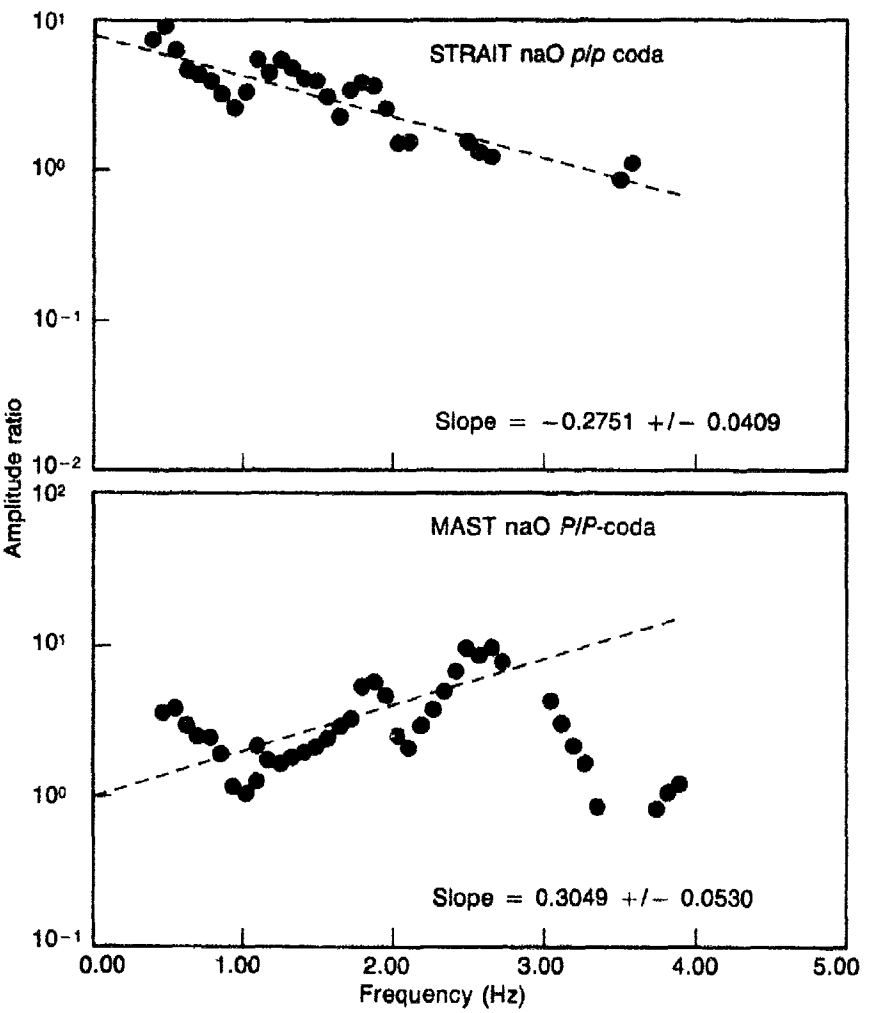

Fig. 2. Spectral ratios *P*/*P*-coda, corrected for noise, for STRAIT and MAST. Points for which the signal to noise power ratio is less than 2 are not plotted. The dashed lines show mean slopes for the frequency range 0.5 or 3.0 Hz.

words initial P for STRAIT, an explosion in a low velocity medium is richer in low frequencies compared to P coda whereas the opposite is true for MAST, an explosion in a much higher velocity medium. The frequency dependence of spectral ratio P/P-coda appears to be related to the medium velocity and probably other properties of the near-field medium. The spectral ratios P/P-coda were also obtained for 12 other explosions for which the average overburden velocities were known. The least-squares mean slopes on P/P-coda are plotted against overburden velocity in Fig. 3 for all 14 explosions. There is considerable scatter among the data points but an approximately linear trend with correlation coefficient of 0.896 is obtained.

Knowing the explosion depth, d and overburden velocity, α one can obtain the delay time, $t_d = 2d/\alpha$ for each explosion. This delay time represents the time interval by which pP will be delayed with respect to P for waves propagating vertically downwards or for large (teleseismic) epicentral distances. Figure 4 shows a plot of P/P-coda slope versus t_d. If one excludes the four data points in the upper right section of the figure which belong to explosions with d > 1 km, an approximately linear relationship (correlation coefficient = 0.872) is obtained for the remaining ten explosions.

A Possible Mechanism

A possible qualitative explanation for the dependence of the spectral ratio P/P-coda on the overburden velocity can be offered by comparing records from shots in low and high velocity media, such as those in Fig. 1 for STRAIT and POOL. The initial P, as defined in Fig. 1, may

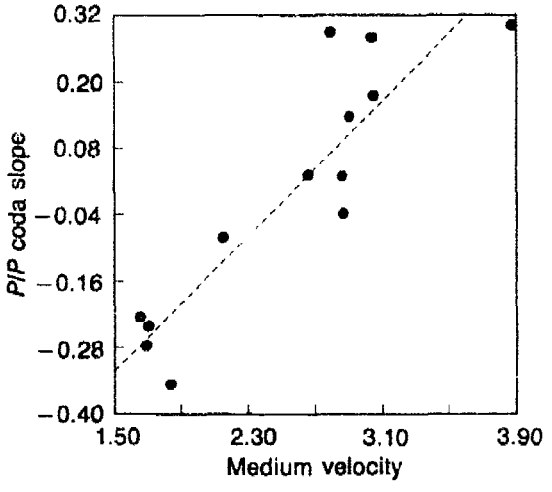

Fig. 3. Mean P/P-coda spectral slope for the frequency range 0.5 to 3.0 Hz *versus* average shot-point to surface or overburden velocity for 14 explosions. The linear trend (dashed line) shows correlation coefficient of 0.896.

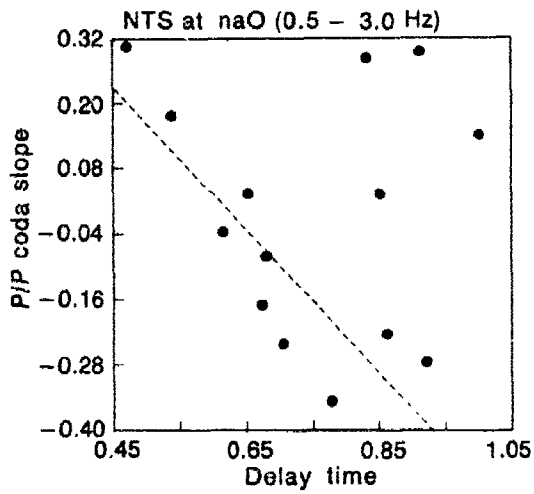

Fig. 4. Mean *P*/*P*-coda spectral slope *versus* computed *pP*-*P* delay time for 14 explosions. If one excludes the four data points in the upper right section of the figure which belong to explosions deeper than 1 km, the linear trend (dashed line) for the remaining ten explosions has a correlation coefficient of 0.872.

consist mainly of direct P, pP and P waves derived from conversion of near-source Rayleigh waves (called $R \rightarrow P$ waves, hereafter.) A review of available free field seismic data from underground nuclear explosions (Murphy and Bennett, 1979; Murphy, 1978) show that the RDP's for explosions in hard rock generally have smaller rise times and greater overshoots than those in soft rock. This means that, for a given yield, the first P as well as pP for a shot within a lower velocity medium should be richer in low frequencies as compared to a shot in higher velocity medium. This effect will explain the lower-frequency content of the first cycle of P on STRAIT as compared to POOL in Fig. 1.

For an explosion source with source function $S(f)$ within a homogeneous half space with compressional velocity α, the fundamental-mode Rayleigh wave amplitude, R is given by the expression (*e.g.* Hudson and Douglas, 1975)

$$R = \frac{C_1 S(f)}{r^{0.5} \rho \alpha^{3.5}} f^{1.5}\, 10^{-2.18 t_d f} \qquad (1)$$

where a Poisson's ratio of 0.25 is assumed, ρ is the density, r is the epicentral distance and C_1 is a numerical constant. It follows that for an explosion within a low velocity medium (such as STRAIT), R will be richer in low frequencies because, for a given shot depth, t_d will be larger. If the scattering process responsible for $R \rightarrow P$ is nearly the same (in both its amplitude and frequency dependence) for shots in low and high velocity media, then $R \rightarrow P$ for a shot within a low velocity medium can also be of larger amplitude and richer in low frequencies.

The P coda used in this study, starting 8.8 sec after the first P and lasting for 25.6 sec (see Fig. 1), is perhaps sufficiently delayed with respect to the first P so that its spectrum represents an average over such a large volume around the shot point that the scattering effects of localized low or high velocity regions lose most of their significance. The spectral ratio P/P-coda may therefore have a negative slope for explosions with low overburden velocity and the opposite may be true for shots in high velocity media, in agreement with Fig. 3. Similarly, the spectral ratio P/P-coda in which P includes $R \rightarrow P$ waves should show some correlation with t_d because the spectral characteristics of $R \rightarrow P$ are strongly dependent on t_d [see Eq. (1)]. This seems to explain the results in Fig. 4 in which the lack of a linear relationship between P/P-coda slope and t_d for the four deeper explosions is perhaps due to the much larger excitation of higher mode Rayleigh waves as compared to the fundamental-mode Rayleigh wave. Note that since short period surface waves are confined to a shallow surface layer, we expect that the short-period part of the Rayleigh wave spectrum for a shallow source will have amplitudes similar to those for a source in a homogenous half-space (Hudson and Douglas, 1975). In other words, the assumption of a homogeneous half-space for short-period fundamental-mode Rayleigh waves may be approximately valid only for very shallow sources.

Results From Neighboring Explosions

A somewhat more convincing test for the presence of $R \rightarrow P$ waves can be performed by comparison of records from pairs of explosions nearby locations but somewhat different depths and delay times. Hannon (1972) considered the problem of generation of fundamental-mode Rayleigh waves from a compressional source and found that the initiation of the Rayleigh wave takes place when the P wave strikes the free surface after traveling a distance of about $2.5d$, where d is the source depth. The angle of incidence at the free surface (about 66%) is such that most of P is converted to SV. If conversion of Rayleigh wave to P occurs mostly near the free surface, the $R \rightarrow P$ pulse should be delayed by approximately $2t_d$ with respect to the direct P at teleseismic distances. The dominant $R \rightarrow P$ may therefore be assumed to lie within a window starting at a time $2t_d$ after the first P. The spectral ratios of such windows for two explosions 1 and 2, where 1 is shallower, gives, assuming that the scattering function (which converts R to P) is the same

$$\frac{(R \rightarrow P)_1}{(R \rightarrow P)_2} = C_2 \frac{S_1(f)}{S_2(f)} 10^{2.18(t_{d2} - t_{d1}) f} \tag{2}$$

where C_2 is independent of frequency. In deriving Eq. (2), the differences in α and ρ between the two explosions are also ignored (see Eq. (1)). These assumptions are perhaps approximately valid for nearby explosions. One may evaluate $S_1(f)/S_2(f)$ by using von Seggern and Blandford's (1972) source function for known yields of the two explosions. Note that Eq. (2) indicates that the observed spectral ratio of $R \rightarrow F$' waves for shallow/deep explosions should have a positive slope of about 2.18 times the difference in delay times, if only fundamental-mode Rayleigh waves are excited. Higher-mode Rayleigh waves based on realistic crustal models would also indicate a positive slope but of generally smaller value (see, *e.g.* Herrmann and Nuttli, 1975; Hanka, 1982.)

Results from two pairs of explosions TOPGALLANT/STRAIT and INLET/POOL from NORSAR records are shown in Fig. 5. The Rayleigh pulse window is about 5 sec long for each explosion. TOPGALLANT and STRAIT were at the Yucca Flats region, within less than 1 km of each other, and with t_d values of 0.863 and 0.923 sec, respectively. INLET and POOL were at Pahute Mesa region, within about 5 km of

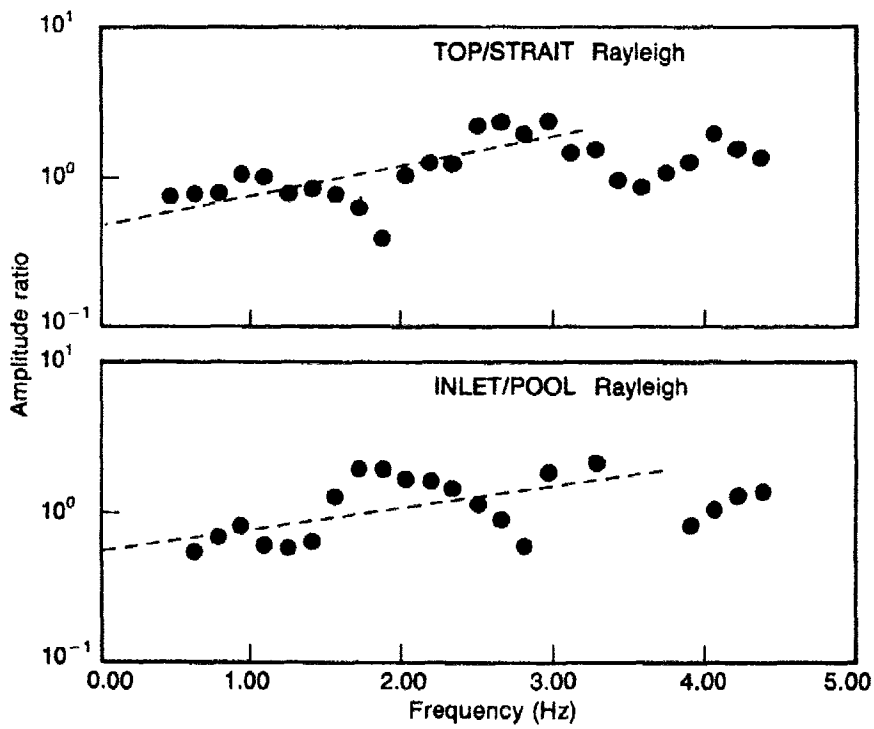

Fig. 5. Spectral ratios of Rayleigh pulses for pairs of nearby explosions, TOPGALLANT/STRAIT and INLET/POOL. Mean slopes for the frequency range 0.5 to 3.0 Hz are shown (dashed lines).

each other, and with t_d values of 0.538 and 0.614 sec, respectively. The spectral slopes are corrected for source function because of their somewhat different yields. Figure 7 shows a mean slope of about 0.20 ± 0.06 per Hz for TOPGALLANT/STRAIT. This is in good agreement with a slope of about 0.13 per Hz predicted by Eq. (2). For INLET/POOL, a mean slope of 0.14 + 0.06, is obtained, this is again in good agreement with the expected value of about 0.17 per Hz. Similar results have been obtained for several other pairs of nearby explosions recorded at NORSAR as well as at a few other distant stations.

P and *P* Coda Magnitudes Based on Spectral Integration

Using *P* and *P* coda windows specified earlier, spectra corrected for noise and instrumental response were first obtained for the 14 NTS explosions. Spectral particle velocities integrated over several frequency ranges (*e.g.* 0.5 to 3.0 Hz, 0.5 to 2.0 Hz, 1.0 to 3.0 Hz) were obtained and plotted against the known yield of explosions on a log-log scale. The signal to noise ratio for most explosions fell off rapidly beyond 3 Hz so that frequencies higher than 3 Hz were not considered to be useful. The frequency range 0.5 to 3.0 Hz appeared to provide better correlation with yield than the other frequency ranges. The data for *P* showed a large scatter and the Yucca Flats and Pahute Mesa events appeared to separate out. For *P* coda, there was no clear distinction between the Yucca Flats and Pahute Mesa events.

The integrated spectral magnitudes are subject to variations similar to those for time domain measurements. The effect of *pP*, which has a modulating effect on the spectra, will in general be somewhat smoothed out as compared to its time domain counterpart. *P* coda should be nearly free from the effects of *pP*. The effect of attenuation due to the upper mantle structure is also important (Blandford, 1976; Marshall *et al.*, 1979) and should equally apply to *P* and *P* coda. A correction for the effects of attenuation was therefore applied to the spectral data by assuming $t^* = 0.4$, the value appropriate for NTS shots recorded at NORSAR (Der, *et al.*, 1983). The particle displacement value for each frequency, f was therefore multiplied by the term $\exp(\pi f t^*)$. Finally, a correction for the source function was applied using the von Seggern and Blandford (1972) source time function for the known yields of the 14 NTS explosions. With these two corrections, the integrated spectral magnitude *versus* yield plots should ideally have a slope of unity.

The actual results with data points are not shown in this paper because the yield values are classified. The integrated spectral magnitude *versus* yield for the initial *P* had a standard deviation, σ of 0.14 magnitude

units when a slope of 1 was fitted to the data points. The integrated spectral magnitude *versus* yield plots indicated a slope of unity. Obtaining a slope of unity has practical significance since it suggests that corrections for source function and t^* can appropriately be applied to P coda so that results from several stations (each with its own t^* value) can be properly combined to further improve the yield determinations.

The results for P coda showed significantly less scatter than initial P, with $\sigma \sim 0.07$ m.u. Note that this low value of σ is nearly the same as for yield estimates from regional L_g waves for NTS explosions when results from several stations were combined (Nuttli, 1983).

Conclusion

Our preliminary results suggest that the spectral analysis of P and P coda for NTS explosions can provide near-source information such as overburden velocity and shot depth. Near-source scattering of explosion-generated Rayleigh waves into teleseismic P seems to play an important role in characterizing the observed compressional arrivals. It will be very useful to continue this work by using more sophisticated techniques so as to verify the preliminary findings and to determine the best procedures for obtaining near-source parameters from teleseismic observations.

Magnitudes based on spectral integration of P coda from NTS explosions provide a much more reliable measure of yield than the initial P. Furthermore, the spectral displacement of P coda seems to be linearly related to yield after corrections for the effects of attenuation in the upper mantle and source function based on knowledge of approximate yield (m_b) have been applied. Slope of 1 on spectral displacement *versus* yield plots (on a log-log scale) suggests that results from several stations can be combined to further improve the yield determinations. It is also hoped that near-source information, such as that derived from the spectral ratio P/P-coda, can also be used to further improve the yield estimates.

References

Aki, K. (1982). "Scattering and Attenuation," *Bull. Seism. Soc. Am.* **72**, S319- S330.

Bache, T. (1982). "Estimating the Yield of Underground Nuclear Explosions," *Bull. Seism. Soc. Am.*, **72**, S131-S168.

Blandford, R.R. (1976). *Experimental Determination of Scaling Laws for Contained and Cratering Explosions*, SDAC-TR-76-3, Teledyne Geotech, Alexandria, Virginia.

Der, Z.A., T.W. McElfresh, R. Wagner and A. O'Donnell (1983). "Global t^* Measurements for the Magnitude Yield Experiment," SDAC-TR-82-3, Teledyne Geotech, Alexandria, Virginia.

Greenfield, R.J. (1971). "Short-Period P-Wave Generation by Rayleigh-Wave Scattering at Novaya Zemlya," *J. Geophys. Res.*, **76**, 7988-8002.

Gupta, I.N. and R.R. Blandford (1983a). "A Mechanism for Generation of Short-Period Transverse Motion from Explosions," *Bull. Seism. Soc. Am.* **73**, 571-592.

Gupta, I.N. and R.R. Blandford (1983b). "Spectral Analysis of Teleseismic *P* and *P*-Coda at NORSAR," paper presented at VSC Research Conference, 28 September.

Gupta, I.N., R.R., Blandford, R.A. Wagner and J.A. Burnetti (1984). "Use of *P* Coda for Explosion Medium and Improved Yield Determination," *Seismol. Soc. Am.* meeting, Anchorage, Alaska, May 30.

Hanka, W. (1982). "Analysis of Broad-Band Rayleigh Waves: A Possibility for Seismic Discrimination," *Jour. of Geophysics*, **51**, 165-179.

Hannon, W.J. (1972). *An Examination of Rayleigh Waves Produced by Shear and Compressional Line Sources*, UCRL-51233, Lawrence Livermore Laboratory, Livermore, California.

Herrmann, R.B. and O.W. Nuttli (1975). "Ground Motion Modelling at Regional Distances for Earthquakes in the Continental Interior, II, Effect of Focal Depth, Azimuth and Attenuation," *Earthquake Eng. Struct. Dyn.*, **4**, 59-72.

Hudson, J.A. and A. Douglas (1975). "On the Amplitudes of Seismic Waves," *Geophys. J.*, **42**, 1039-1044.

Marshall, P.D., D.L. Springer and H.C. Rodean (1979). "Magnitude Corrections for Attenuation in the Upper Mantle," *Geophys. J.*, **57**, 609-638.

Murphy, J.R. (1978). *A Review of Available Free-Field Seismic Data from Underground Nuclear Explosion in Salt and Granite*, CSC-TR-78-0003, Computer Science Corporation, Falls, Church, Virginia.

Murphy, J.R. and T.J. Bennett (1979). *A Review of Available Free-Field Seismic Data from Underground Nuclear Explosions in Alluvium, Tuff, Dolomite, Sandstone-Shale and Interbedded Lavea Flows*, SSS-R-80-4216, Systems, Science and Software, La Jolla, California.

Nuttli, O. W. (1983). *A Methodology for Obtaining Seismic Yield Estimates of Underground Explosions Using Short-Period L_g Waves, in Attenuation of Seismic Waves at Regional Distances*, Semi-annual Report (31 March 1983), Saint Louis University, St. Louis, Missouri.

von Seggern, D.H. and R.R. Blandford (1972). "Source Time Functions and Spectra for Underground Nuclear Explosions," *Geophys. J.*, **31**, 83-97.

Path-Specific Properties of Teleseismic Body Waves

Gary M. Lundquist and Ilene R. Samowitz

A model of the material properties of seismic raypaths is of fundamental importance to studies of both seismic sources and wave propagation. However, the classic tradeoff between source and propagation means that neither may be determined precisely until the other is out of the problem. This research uses a spectral ratio, or "transfer function" technique to eliminate the source and determine accurate relative path properties, with emphasis on paths about Russian and American nuclear explosion test sites. Each transfer function contains information on anelastic attenuation, geometric attenuation and receiver crustal properties, including acoustic impedance contrast and laterally refracted and scattered arrivals. Thus, transfer functions become high-quality data sets for a variety of forward and inverse problems.

Transfer function technology is applied to arrays characterized by apertures of local and global dimensions. The Warramunga Array in Australia is used to demonstrate local array behavior, but the major emphasis of this paper is arrays of digital stations located 30° – 90° about the Eastern Kazakh (Semipalatinsk) and Nevada Test Sites. These digital stations include arrays operated by the UK and stations in the Global Digital Seismic Network. The method is always applied to arrays relative to a reference station. Thus, N transfer functions are produced to model the relative seismic properties of $N + 1$ paths.

Transfer functions may be used directly as frequency dependent station corrections, replacing scalar station corrections in m_b estimation. Seismograms from all channels in a local array or all stations in a global array are filtered to have the same path properties as the reference path. For local arrays, this optimizes waveforms for either m_b estimation or beamforming. For global arrays, the effects of source asymmetry are displayed on a consistent reference station waveform. In both cases, significant reduction in m_b scatter is obtained by application of transfer functions as frequency dependent station corrections.

The ideal end result of transfer function research is two filters for each path: a receiver function which models all near receiver contributions to observed seismograms and a Q filter which models anelastic properties of the path. The fact that any component common to both paths

is lost in the ration process, however, means that the results will be relative receiver functions and relative path attenuation filters unless outside constraints are used.

Estimation of $N+1$ separate receiver functions from N transfer functions requires an additional assumption. A simplicity criterion is implemented to enable estimation of the $N+1$ relative receiver functions, and the results are verified using comparison of synthetic seismograms to observation and comparison of synthetic seismogram m_b to standard scalar station corrections. The receiver functions for Eastern Kazakh (Semipalatinsk) and Global Digital Seismic Network comprise a very significant advance to the state-of-the-art of seismogram modeling. The success here of seismogram synthesis demonstrates the importance of modeling specific path propagation behavior. In particular, studies of source asymmetry or source-time function must include receiver functions or their equivalent.

Inversion for t^* has been significantly improved over results previously presented. First, the high quality Yield Experiment Data set was used and a thorough noise study was done to determine effective bandwidths for t^* estimation. Second, the inverse technique, which is still based upon the absorption band model for t^*, was enhanced as follows. A new weighting scheme was applied to remove any dependence upon choice of reference path by considering all possible spectral ratios equally. Further, a low frequency gain factor was estimated for each path to remove effects of acoustic impedance contrast, residual goemetric attenuation and low frequency focusing from the t^* estimates. Finally, the criterion was added that the resulting t^* filters be compatible with ω^{-2} slopes on observed explosion seismogram spectra.

Inclusion of the slope constraint is the same as adding a second spectral ratio into the inverse for each path. Both instrument and source (ω^{-2} slope) are deconvolved from observed explosion seismogram spectra, leaving the path Q filter in the presence of noise. The objective then is to find a set of Q filters which are compatible with both the transfer functions and the residual seismogram spectra. Experience with the dual constraints shows that not only can both criteria be satisfied, but that the tradeoff between absorption band parameters is very significantly reduced.

Results of enhanced methods applied to improved data sets confirm previous conclusions that t^* must vary as functions of both path and frequency. Relative to the Chiang Mai, Thailand station, δt^* at 2.0 Hz varies from $+.1$ to $+.9$ sec, with most stations falling in the range $+.3$ to $+.6$ sec. Significant consistency is found in the frequency dependence, implying that absorption bands along higher attenuation paths are shifted

to somewhat lower frequencies than those observed for small attenuation paths. This can be an important new constraint on the anelasticity of the earth.

Magnitude Anomalies in French Polynesia

P. Mechler and N. Raviau

Introduction

The P wave amplitude, and so the magnitude, of earthquakes recorded in several seismic stations, show a very large scatter. Even if the radiation pattern of the seismic source may play a role in the scatter, the main part of it is attributed to lateral heterogeneities in the earth: variations in the upper mantle attenuation, or crustal structure beneath the seismic station.

It should so be possible to use the observed magnitude variation to increase our knowledge of the earth's structure. In fact, the results seem so randomly distributed that this was never done, and, for a long time, only single station's corrections were computed.

Recently, A. C. Chang and D. H. von Seggern (1980) examined whether magnitude bias can be explained by regional and local effects in LASA subarray's data. They computed a magnitude anomaly, difference between the actual value of the magnitude in one subarray and the magnitude published by the National Earthquake Information Service (NEIS). A smoothing of the results was achieved by averaging together all quakes which occurred in the same azimuthal sector (a total of 10 sectors around Montana was used). Such an averaging is strongly dependent upon the earth's seismicity, in this case most of the quakes occurred in only 2 or 3 of the 10 sectors. In this paper, using the seismic data of French Polynesia, we will examine whether azimuthal variations of magnitude anomalies can be explained. The "Laboratoire de Géophysique" (LDG) maintains a seismic network in French Polynesia, with mainly two subarrays (Fig. 1). Five stations in Tahiti, a volcanic island, with two sub-actual volcanoes on Tahiti itself and one in the nearby island of Moorea (and at least 3 active submarine volcanoes at less than 100 kilometers to the East of Tahiti). Four stations in Rangiroa, an atoll, the second largest in the Pacific Ocean, 350 kilometer to the North-East of Tahiti. Rangiroa is in the northern part of Tuamotu archipelago.

As French Polynesia is in the middle of Pacific Ocean, its network records all major earthquakes of the Circum Pacific Belt. The world's seismicity as seen from Tahiti is relatively homogenous in azimuth, with exception of the south direction.

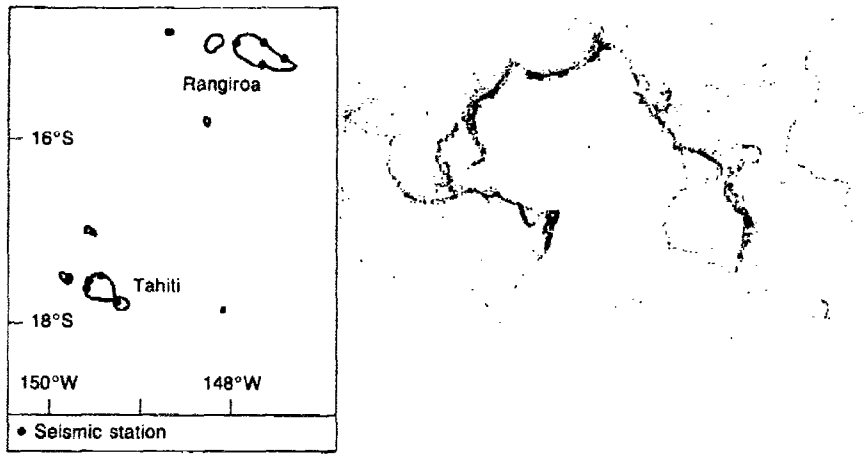

Fig. 1. World seismicity map (Barazangi, M. and Dorman, J., 1969) and location of the French Polynesia array. The star indicates the location of the French Polynesia array. The left part represents in detail a view of the French Polynesia array.

After a short description of our data set, the paper will have three main parts: comparison with NEIS magnitude, definition of local magnitude anomaly to describe in more detail the effects inside the seismic array and finally a comparison between magnitude anomalies and travel time anomalies.

Data Set

The first part of the data set used in this study is given by all quakes, between January 1978 and July 1979 and recorded in, at least, one of the nine stations of LDG seismic network in French Polynesia. It appears that a one-and-a-half year period was not long enough to give a good azimuthal coverage. Selected events, from 1975 to 1981, which occurred in less seismic areas were added to the set.

Our final data set contains 733 events among which 299 were recorded in all nine stations.

The parameters of the events were taken in the NEIS publications, the amplitude and period in the LDG bulletin. The re-reading of some hundred records convinced us of the quality of this bulletin, and the use of ISC magnitude instead of NEIS magnitude do not change our conclusions. For each quake, in each station, we computed the magnitude by the well known formula:

$$m_b = \log\left(\frac{A}{T}\right) + B\,(\Delta, h)$$

The depth-distance correction function B used was the same as used in NEIS magnitude computation.

Finally the magnitude of the earthquakes of our data set are in the range 4.6 to 6.8. This is compatible with the 50% detection threshold of this network which is around $m_b = 5$.

Comparison with NEIS Magnitudes

For each earthquake, and each station, a magnitude anomaly Δm_b

$$\Delta m_b = m_b \text{ (station)} - m_b \text{ (NEIS)}$$

was computed. With this definition, a positive anomaly corresponds to an earthquake recorded with an amplitude larger than expected from the published magnitude.

Table I gives the average of m_b for all earthquakes; this is the usual "station correction". The second column gives the standard deviation and the third the number of events of our set recorded in the corresponding stations. In the mean, Polynesian magnitudes are very similar to NEIS values (maximum station correction 0.175 to TVO and minimum −0.115 for PPN) and this bias is small compared to standard deviations, of the order of 0.3 magnitude unit.

If we suppose NEIS magnitudes to be a good reference (which is certainly not the case even if we are not able to propose a better one), it is important to see if there exists a systematic relation between the

Table 1. Mean magnitude bias and standard deviation of the French Polynesia stations and subarrays. Magnitude biases are computed against NEIS magnitudes with the formula: $\Delta m_b = m_{b\,\mathrm{LDG}} - m_{b\,\mathrm{NEIS}}$.

Stations	Mean values of magnitude bias	Standard deviation	Number of events
AFR	+0.133	0.266	436
PAE	+0.033	0.299	466
PPT	+0.122	0.296	496
PPN	−0.115	0.266	466
TVO	+0.175	0.282	495
Tahiti	+0.070	0.269	299
PHO	+0.021	0.297	639
VAH	−0.015	0.306	584
TPT	+0.035	0.267	643
RUV	+0.070	0.309	653
Rangiroa	+0.044	0.266	299

magnitude's anomalies and some parameters: epicenter's depth, magnitude, epicenter's distance or azimuth.

The seismic zone number 12 in the Flinn and all, zonation, the Tonga islands, is well recorded in French Polynesia at a distance of some 40 degrees. By looking at this set of quakes, at same distance and azimuth, and probably with similar focal mechanism, we were unable to find a systematic variation with either depth or magnitude.

From Tonga Islands (40 degrees) to Sunda Arc (90 degrees), an all subset of our quakes is recorded in the same azimuth. Again we were not able to find a systematic effect of distance.

And so the main parameter of our study will be azimuth.

Figure 2 shows a plot of all magnitude's anomalies *versus* azimuth for one of the nine stations (AFR, Tahiti subarray). The 0.3 magnitude unit scatter from Table 1 is clearly seen on the plot. We smoothed the raw data by replacing each of it by an average between all nearby values (the weighting is a triangular function with an angle of 2.5° at 3 dB). The shape of the averaged curve is not an artifact of our particular data base; the shape is the same in one station if we use only the 299 quakes recorded in all nine stations or all quakes recorded in this particular station. This shape of the averaged curve is very similar for all nine stations. In Fig. 3 we plotted the results for Tahiti's subarray.

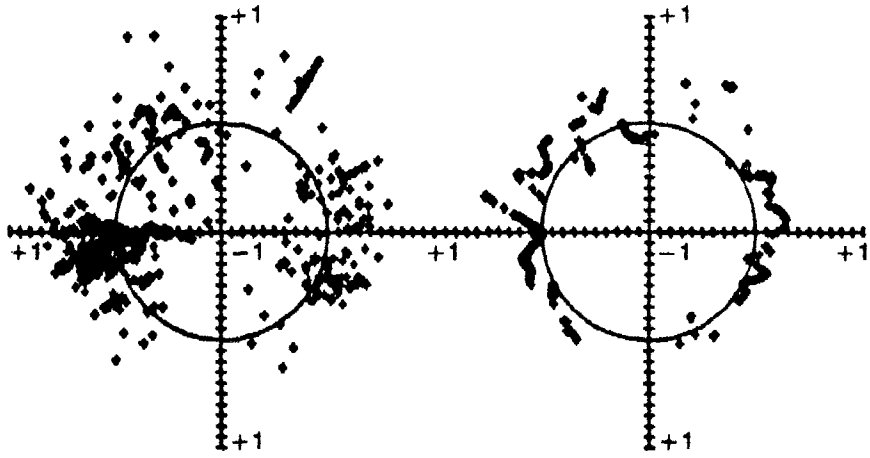

Fig. 2. Magnitude bias *versus* azimuth in the AFR station. Magnitude biases are computed against NEIS magnitudes with the formula: $\Delta m_b = m_{b\,\mathrm{LDG}} - m_{b\,\mathrm{NEIS}}$. On the left part, raw data are plotted. Circle represents zero m_b bias. Inside the circle negative m_b bias is represented, and positive m_b bias is represented outside the circle. A smoothed curve is represented on the right part.

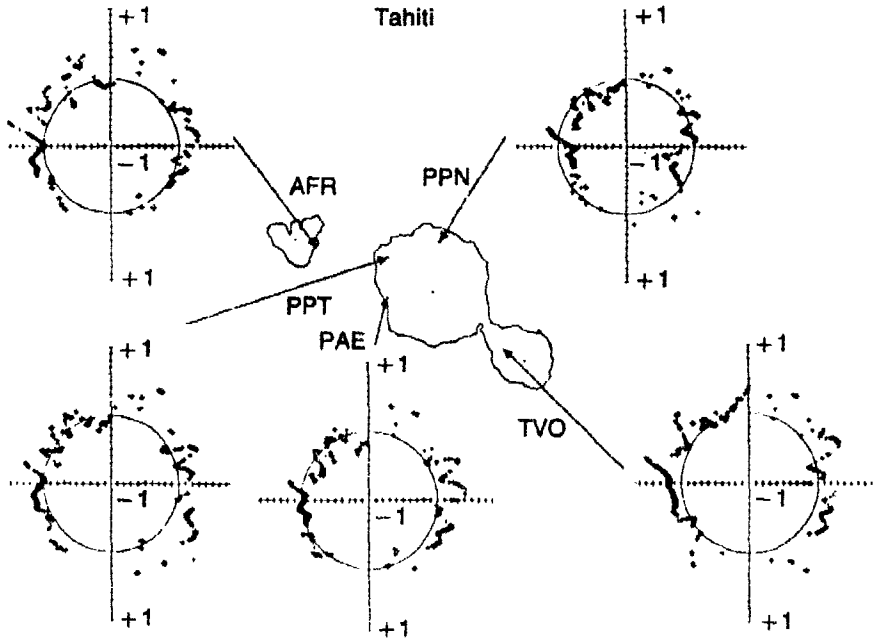

Fig. 3. Smoothed curve of magnitude bias ($m_{b\,\mathrm{LDG}} - m_{b\,\mathrm{NEIS}}$) *versus* azimuth for all Tahiti stations.

A first interpretation is that, in a given station, the magnitude anomaly is the sum of a constant for the station (quality of the rocks on which the seismometer is installed) and of a function of azimuth which seems to be nearly the same for all our nine stations in French Polynesia. This fact had been already found in a preliminary study of our data, in which all quakes occurring in the same seismic zone had been averaged together.

These results seem to us rather unsatisfactory: it implies there is no effect of the structure of the islands, which is rather puzzling for five stations installed around a volcano and in contradiction with the visual observation of seismic records (*e.g.* some Aleutian quakes are specially well recorded in the AFR station). If the local effects which, by experiment we know exist, are not seen in the plots of magnitude's anomalies, it means our processing of the data is not efficient enough. The scatter of the anomalies is too large but a part of it is produced by the poor quality of the published magnitude used for reference.

Regional and Local Magnitude Anomalies

To suppress all influences of a reference value for magnitude we defined the regional anomaly between Tahiti and Rangiroa as the difference

between the mean magnitude measured in Tahiti and in Rangiroa. Inside one of the two subarrays the local anomaly of one station is the difference between the magnitude in this station and the averaged value of its subarray. We defined so relative anomalies but without need of a reference magnitude and so without influence of a possible error in this magnitude. We have also to point out that, in a given azimuth, most of the quakes are coming from the same seismic area (except for west direction). The influence, if any, of a special focal mechanism will not be important.

Figure 4 shows the regional effects *versus* azimuth, differences between Tahiti and Rangiroa. Figure 5 gives one example of local effects, inside a subarray, we chose the same AFR station as in Fig. 3.

For both figures, on the left part are plotted the raw data and on the right one the average curve, with the same weighting function as in Fig. 3.

A first look clearly indicates a decrease in the scatter of the raw data (compared with Fig. 3). It indicates that a large part of the scatter was induced by the poor reference magnitude.

The local variations of magnitude were hidden in the scatter of the previous plot of magnitude anomalies versus NEIS values. Those local variations were checked to be in very good correlation with the visual amplitude's anomalies observed on the graphics records.

Correlations Between Magnitude Anomalies and Travel Time Anomalies

Several possible explanations were given for magnitude anomalies inside an array. Among them, local variation of attenuation, focusing and

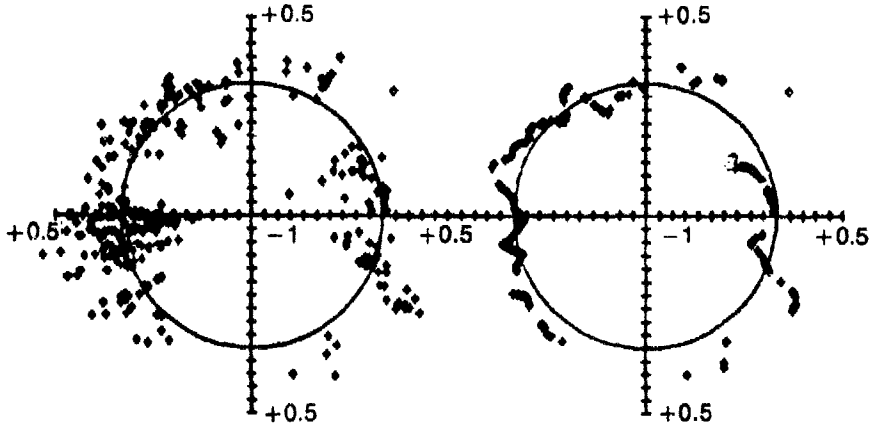

Fig. 4. Regional magnitude bias *versus* azimuth (m_b mean Tahiti minus m_b mean Rangiroa). On the left part raw data are plotted and on the right part a smoothed curve is presented (see Fig. 2).

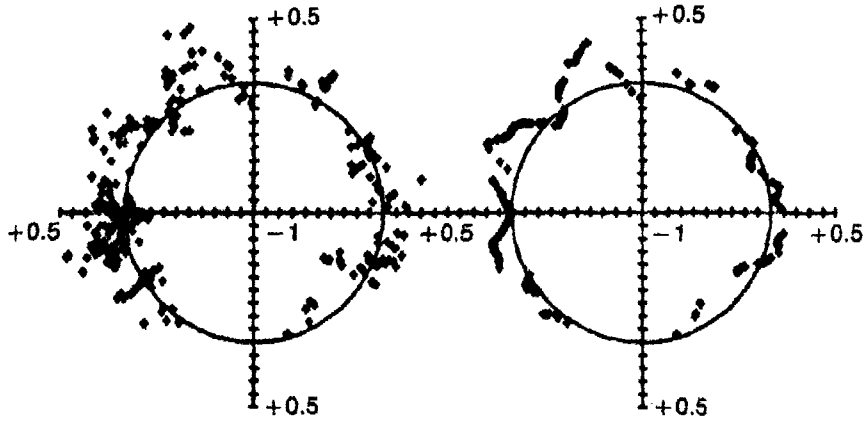

Fig. 5. Local magnitude bias (m_b station minus m_b mean Tahiti) in AFR station *versus* azimuth. The representation is the same as Fig. 2.

defocusing of seismic waves, and more recently, scatter of seismic waves due to heterogeneities inside the mantle.

The first effect to look at to support one of these explanations is to see if there is any correlation between the travel time anomalies and the magnitude anomalies.

A study of travel time anomalies in French Polynesia was made recently by P. Marie (1981). All time anomalies values were taken in this work and only replotted in a format similar to the one we chose for magnitude anomalies.

The travel time anomalies are observed minus computed time. The computations were made from the NEIS epicenter's parameters using the Jeffreys and Bullen *Seismological Tables*.

A positive travel time anomaly corresponds to a wave arriving later than expected, as a positive magnitude anomaly corresponds to an amplitude larger than expected.

For each station, we compared the travel time anomalies *versus* azimuth with the magnitude anomalies (magnitude minus NEIS value). Figure 6 shows a typical plot for one station, the same as above: AFR. There is no clear correlation with Fig. 2. In both cases the scatter of the data is very large and in both cases the reference value defining the anomaly (NEIS magnitude or origin time). It is certainly not accurate enough to be used in such study.

We explained earlier how we suppressed the influence of magnitude reference by defining a local magnitude anomaly; the same procedure may be applied to travel time anomalies.

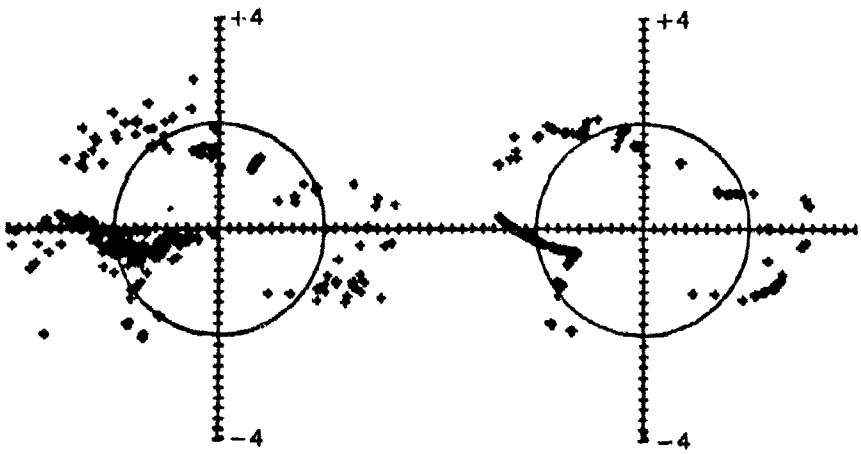

Fig. 6. Travel time anomalies *versus* azimuth. The travel time anomalies are observed minus computed time. The computations were made from the NEIS epicenter's parameters using the Jeffreys and Bullen *Seismological Tables*. On the left part the raw values are plotted. Circle represents zero travel time anomaly. The travel time anomaly is positive outside the circle and negative inside the circle. A smoothed curve is represented on the right part.

Figure 7 gives the results of a regional anomaly, difference between the mean travel time anomaly in Tahiti minus anomaly in Rangiroa. The correlation with the plot of Fig. 4 is rather good. If the magnitude is larger in Tahiti, the waves of this quake arrive later in that subarray.

In a similar way, we have plotted the local anomalies. Figure 8 shows the results of AFR and has to be compared with Fig. 5. We notice a very strong correlation between both curves. When azimuth changes, if magnitude bias increases the value of travel time anomalies increase and *vice versa*. This good correlation is available for all Polynesian stations (see Fig. 9 for Tahiti subarray's stations).

This correlation supposes strong focusing and defocusing of seismic waves in the immediate vicinity of the stations.

Conclusion

In this experimental study of magnitude anomalies in French Polynesia, we were led to divide the anomaly in one station into the sum of 4 main effects:

- A station's constant depending on the geological quality of the site.
- A very local effect, function of azimuth and strongly correlated with local travel time anomalies. An earthquake being recorded with

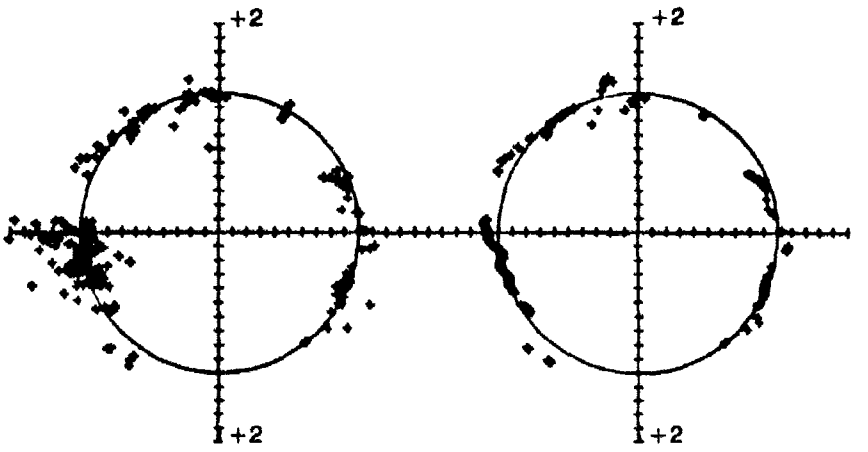

Fig. 7. Regional travel time anomalies *versus* azimuth (difference between the mean travel time anomaly in Tahiti minus mean travel time anomaly in Rangiroa. The presentation is the same as Fig. 6.

a large amplitude if it arrives late in this station compared to nearby stations. This supports the hypothesis of focusing and defocusing effects in the immediate vicinity of the station, probably at the Moho level which is relatively shallow in this part of the world.

• A regional effect, again function of azimuth, observed between the two subarrays of Tahiti and Rangiroa. This regional effect is in good correlation with travel time anomalies between the two

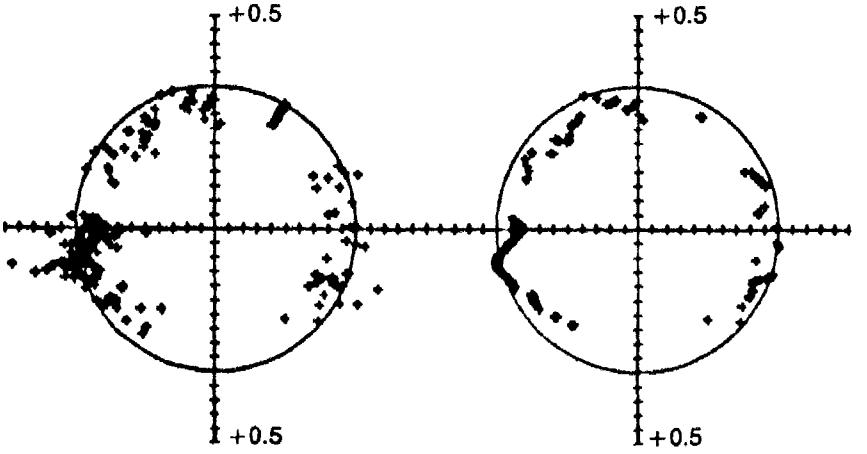

Fig. 8. Local travel time anomalies in AFR station *versus* azimuth (travel time anomaly in AFR minus mean travel time anomaly in Tahiti). The representation is the same as in Fig. 6.

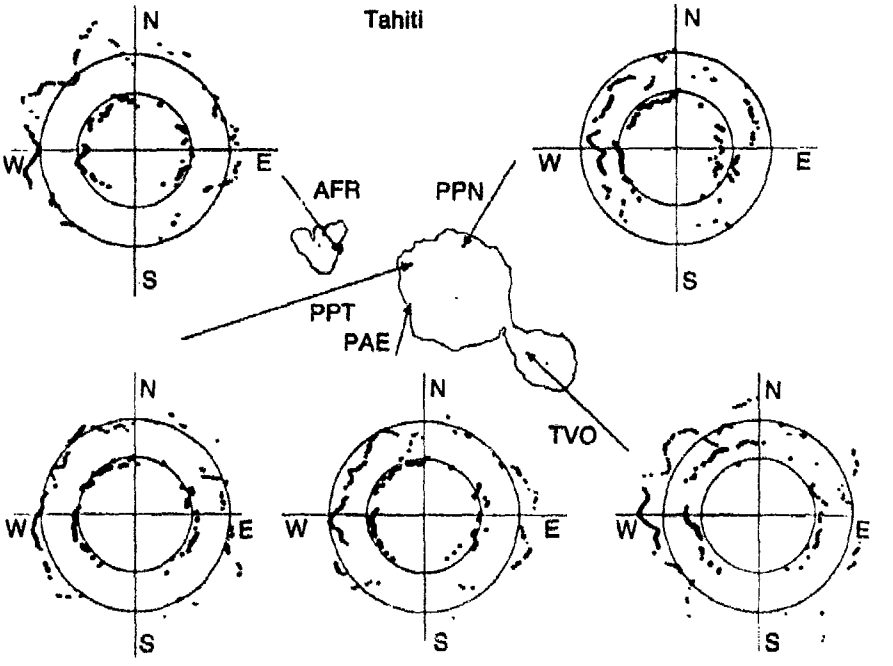

Fig. 9. Correlation between local magnitude and travel time anomalies *versus* azimuth in Tahiti subarray. The five stations are represented. For each station two smoothed curves are presented:

1) magnitude biases correspond to the exterior curve (see Fig. 5 for AFR)

2) travel time anomalies correspond to the interior curve (see Fig. 8 for AFR).

islands. Again, this fact supports the hypothesis of focusing and defocusing but at a greater depth inside the upper mantle.

- A global effect, the same for all stations we used in this study. We are not in a position of giving an explanation for this global effect (focal mechanism, heterogeneity in the deep mantle or in the source area ...). The large scatter usually observed in magnitude anomalies study is mainly concentrated in this last effect, and is certainly induced by the difficulty of defining a good reference value for the magnitude of an earthquake.

The four effects we observed are roughly of the same order of magnitude, of the order of a few tenths of a magnitude unit.

The French Polynesian Network is, at least on a geographical basis, very suitable for such a study: located in the middle of Pacific Ocean it records earthquakes from a large variety of azimuths, and this network consists of very well calibrated and identical seismic stations. On the other

hand, the number of stations is limited and difficult to increase without using ocean bottom seismometers. If we were able to show the feasibility of interpreting at least part of the observed anomalies in term of geological structure, we are not in a position to really propose a model of the islands explaining our observations.

Acknowledgements

We thank the Laboratoire de Geophysique for both the data and the fruitful discussion with it's members, specially Dr. J. Talandier and Dr. J.P. Massot. This research was partly supported by the Advanced Research Projects Agency and monitored by the Air Force Office of Scientific Research under contract No. AFOSR 80-0082.

References

Aki, K., (1982). "Scattering and Attenuation." *B.S.S.A.* **72** No. 6 P. S319-S330 December 1982.

Barazangi, M., and Dorman, J., (1969). "World Seismicity Maps Compiled from ESSA, Coast and Geodetic Survey, Epicenter Data 1961-1967." *B.S.S.A.* **59**, No. 1 p 369-380.

Chang, A.C. and von Seggern, D.H. (1980). "A Study of Amplitude Anomaly and m_b Bias at LASA Subarrays." *Journal of Geophysical Research* **85**, No. B9 p. 4811-4828.

Gutenberg, B., and Richter, C.F. (1956). "Magnitude and Energy of Earthquakes." *Annali di Geofis.* **9** (1956b) p. 1-15.

Jeffreys, H. and Bullen, K.E. (1948). *Seismological Tables*. Office of the British Association. Burlington House, W. I. London.

Marie, P., (1981). *Structures de Zones Volcaniques Relevees par la Geophysique. Application a la Polynesie (Sismique) et au Mont-Dore (Magnetotellurique).* These Paris VI No. 81-41.

Ravaiau, N., (1983). *Etude Experimentale des Anomalies en Magnitude des Teleseismes Enregistres en Polynesie Francaise.* These Paris VI No. 83-39.

Focal Mechanism Analysis as a Method for Teleseismic Discrimination

K.L. McLaughlin, D.W. Rivers, M.E. Marshall, and R.A. Wagner

Summary

The Pearce (1977) algorithm has been shown to be a valid method for testing the earthquake hypothesis when teleseismic data does not show adequate pP-P move-out for shallow events. Improved depth estimates are available when these depth phases are reliably shown to yield double-couple solutions. The method has been shown to apply to small events when array data is available at 3 or 4 stations. Large explosions consistently fail the earthquake hypothesis when coda levels are taken for maximum pP amplitudes. Small explosions have not been adequately tested in this regard. Evaluation of film data of small events has demonstrated the importance of the seismic analyst's need to compare signals from the common event at different sites for the purpose of picking pP and sP phases. The utility of digital data in this regard is greatest in the presence of multiple events with similar focal mechanisms in the same region, and with origin times occurring within the pP-P time of each other. As was found by Pooley et al., (1983), comparison of digital data to synthetic seismograms is also useful in evaluation of the output of exhaustive search procedures such as Pearce (1980).

As a continuing direction of research, we have been evaluating the efficacy of the Pearce (1977) algorithm as an aid to the discrimination process. In a recent study McLaughlin et al., (1982) concluded that large explosions consistently violated the "double-couple at depth" hypothesis when coda levels were chosen for maximum pP amplitudes. Limitations of the method were found when data was not available from one or more azimuthal quadrants. Given the same constraints, earthquakes were found to always have focal mechanisms. Due to the detection threshold of the GDSN network, it was not possible to examine small earthquakes and small explosions simultaneously. Current work along these lines evaluates the data for small unidentified events using film chip data. Although, the small events in the present data set are not definitively known to be explosions or earthquakes, we feel that the preliminary results indicate that the algorithm can be applied to small events.

Complications due to the nature of film chip data make the full utilization of the technique difficult. It is difficult to align seismograms from different sites to compare waveforms and choose the most likely pP, sP combinations that will ultimately give the most likely depth and double-couple estimates. This is the most difficult when multiple events produce a profusion of depth phases that are intertwined. Goncz and Barker (1978) showed that it is easier to make pP picks on a screen full of traces than on each trace individually. A consistent set of pP-P times then results in greatly improved locations.

Definition of the Method

The Pearce algorithm (Pearce, 1977) is a systematic method for the examination of possible double-couple source mechanisms, using amplitude ratio bounds of *pP*-to-*P* and *sP*-to-*P* from a network of stations in an exhaustive search procedure. The method may be used with or without polarity data. The use of amplitude ratios at a given station helps to eliminate the requirements for station amplitude corrections. The method uses the extremal bounds estimated for the *P*, *pP*, and/or *sP*, phases to infer extremal bounds for the amplitude ratios of *pP*-to-*P* and/or *sP*-to-*P*. Since only the extremal bounds of prospective depth phases are used, the method may be used down to the detection threshold of *P*. In the event of no depth phase detection, the *P* coda amplitude is read as the upper bound for the depth phase amplitude. The method makes maximum advantage of low noise stations, and filtering to improve the *P* wave and *P* coda amplitudes with respect to ambient noise.

In the event that no double-couple can be found for the *P* coda levels of an event, then it is declared a non-earthquake. In this manner, the method may be used to window the population of unidentified events by testing the hypothesis of an earthquake at depth. This method of discrimination can be applied to small events near the detection threshold because the method can use the noise levels behind the *P* wave detection for depth phase amplitude bounds.

An Example

The Pearce method has shown its utility in selecting from a number of hypotheses when multiple events occur. Seismograms and inferred possible focal mechanisms of a couple of earthquakes in the Lake Baikal region are shown in Figs. 1, 2, and 3. The seismograms offer the alternatives of either (1) two very shallow earthquakes, or (2) two somewhat deeper earthquakes (indicated by the labeled *P*'s and *pP*'s). However, the relative amplitude ratios of ½ to ⅓ for the first two phases (labeled

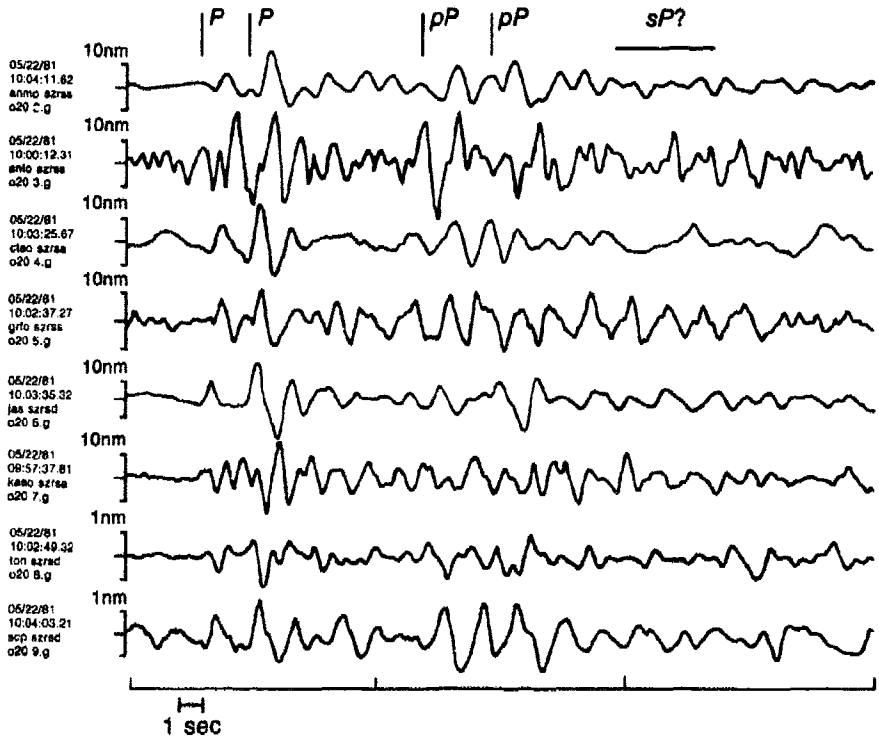

Fig. 1. Short period seismograms of an earthquake 05/22/81 in the Lake Baikal Region. The event appears to have double *P* and *pP* waves. An alternative explanation is the possibility of a very shallow earthquake. Seismograms are only crudely lined up on the initial *P* wave.

P and *P*) are consistently the same across the network of stations, and the Pearce algorithm rejects the hypothesis that these may be interpreted as *P* and *pP* of a very shallow earthquake. The repetition of the two events as $P+P$ and $pP+pP$ is clearer in the filtered seismograms of Fig. 2. The *sP* depth phases are not clearly visible. Possible focal mechanisms are shown in Fig. 3. From the similarity of *P* waveforms, it can be argued that the mechanisms that place nodal planes between the stations are not reasonable. We can make such an argument based on the entire waveform, although the "first motion" of each waveform is not clearly visible.

Extensions and Improvements

Several refinements to the systematic study of focal mechanisms may be implemented at this juncture. Most of these methods are best applied to digital data.

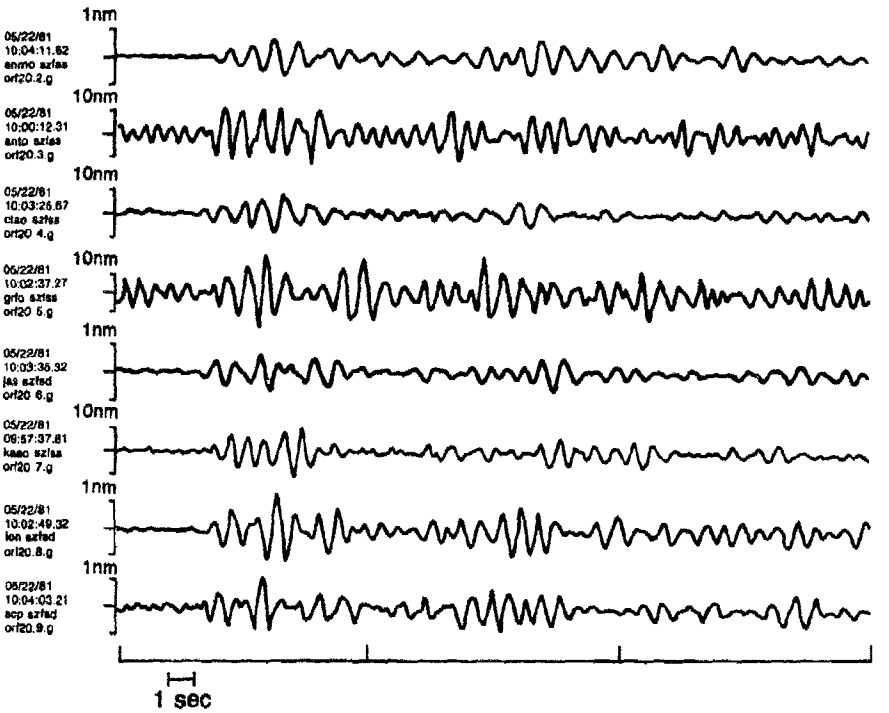

Fig. 2. Filtered short period seismograms for the event of Fig. 1. Double nature of the event is more evident in the filtered depth phases.

As demonstrated in the above example, although the "first motions" of two waveforms are not visible, we can use the correlation of two waveforms to argue that they have the *same or opposite polarity*. This is a valuable constraint in the analysis of focal mechanisms of small earthquakes. The method could also be used as a discriminant, when two or more P waves are demonstrably *reversed* with respect to each other. Even though the net dilatation or compression of each seismogram may not be readable, the reversed nature of the waveforms would argue against an explosion source. The application of prediction error filtering to this possible discriminant is proposed in an accompanying proposal, but it is clear that the Pearce method of focal mechanisms analysis could use the results of such a research effort.

The Pearce algorithm as presently implemented only eliminates unacceptable mechanisms. Although the Pearce algorithm often results in a well constrained set of acceptable focal mechanisms, it is desirable to incorporate an estimate of "best-fit double-couple" to the procedure. This procedure would aid in the selection of acceptable focal mechanisms

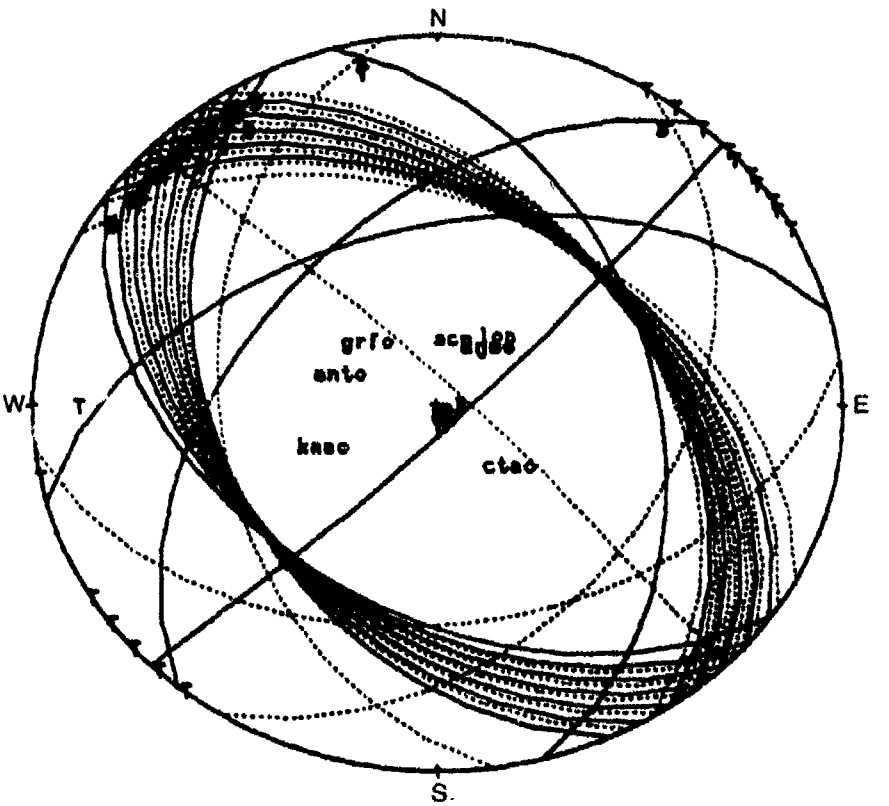

Fig. 3. Focal mechanisms for the double event consistent with the amplitude ratios of *pP/P* taken from Figs. 1 and 2. Polarity data from only one station, LON, was used to construct the solution set.

for comparison to synthetic seismograms, as well as indicate how well the mechanism is constrained by the data. The present algorithm would act as a filter to eliminate those mechanisms that are not worth considering.

The use of synthetics to model small shallow earthquakes has been demonstrated by Pooley *et al.* (1983). The method of relative amplitude bounds and polarities can be used as a "front-end" together with the improvement to obtain a best-fit double-couple mechanism to calculate synthetics.

References

Goncz, J.H. and B.W. Barker (1978). *Detection of Depth Phases Using Computer Graphics*, SDAC-TR-78-8, Teledyne Geotech, Alexandria, VA.

McLaughlin, K.L., D.W. Rivers, and M.A. Brennan (1983). *Pearce Focal Sphere Analysis of Explosion and Earthquake Mechanisms*, Teledyne-Geotech, report SDAC-TR-83-4, Alexandria, VA.

Pearce, R.G. (1977). "Fault Plane Solutions Using the Relative Amplitudes of *P* and *pP*." *Geophys. J. Roy. Astr. Soc.* **50**, 381-394.

Pearce, R.G. (1980). "Fault Plane Solutions Using Relative Amplitude of *P* and Surface Reflections: Further Studies," *Geophys. J. Roy. Astr. Soc.* **60**, 459-487.

Pooley, C.I., A. Douglas and R.G. Pearce (1983). "Research Note: The Seismic Disturbance of 1976 March 20, East Kazakhstan: Earthquake or Explosion?" *Geophys. J. Roy. Astr. Soc.* **74**, 621-631.

Depth Corrections for Yield Estimation of Underground Nuclear Explosions

G.R. Mellman, S.K. Kaufman, W.C. Tucker

Abstract

Any seismic source at depth will produce a variety of reflections, both from the free surface and from near source structural discontinuities. The interference effects produced by these reflections can produce major changes both in the waveforms and amplitudes of observed teleseismic seismograms. We have employed a combination of waveform modeling, relative waveform inversion, deconvolution and spectral techniques to determine the arrival times and amplitudes of pP and other early arrivals, and to assess the effect of these arrivals on the observed magnitude of selected events at the Shagan River test site.

For the Shagan River events, the presence of early arrivals with arrival times and amplitudes which vary as a function of both event location and receiver azimuth make determination of pP times and amplitudes quite difficult. By prefiltering and windowing, it is possible to separate pP from later arrivals. Then, using inversion and deconvolution methods, we have removed the effects of pP to obtain magnitude estimates based only on the amplitude of the direct P wave. Results indicate that for the events studied, pP and later arrivals produce significant magnitude enhancement at most stations.

Analysis

A seismic source at depth in a realistic earth structure will produce reflections, both from the free surface and from velocity contrasts at depth. For a shallow explosion source, these reflections together with late arrivals caused by non-elastic source phenomena, interfere with the direct arrival, causing bias in yield estimation depending on source depth and near source structure. In this study, we examine the effects of those depth phases on yield estimation for underground explosion in the Shagan River test area.

We may, in general, wish to consider separately the problems of estimating the absolute effects of depth on yield and the relative effects on events within a specific test site. In cases where there is no clear spectral null associated with *pP*, as is the case for Shagan River events,

the estimation of depth effects will depend on estimates of receiver effects and t^*. Uncertainties in these estimates lead to uncertainties in pP times and amplitudes that are sometimes greater than the total variation in pP observed at a test site. It is therefore useful to consider the data in a relative sense, where only assumptions of the stationarity of t^* and receiver effects are necessary. This allows much finer resolution of pP effects and provides a means of verifying in detail the validity of the assumptions used in our depth effect estimates.

We have used several methods to estimate absolute pP times and amplitudes and the effects of these on yield estimation for a suite of Shagan River explosions in the 5.8 to 6.3 m_b range. These techniques produce estimates of pP times of between .25 and .40 sec, pP amplitude between .5 and .8 and amplification effects of .15 to .25 magnitude units compared to expected amplitudes for events without pP.

The simplest technique used to estimate pP effects was to construct synthetic seismograms, using the best available estimates of receiver effects (Lundquist *et al.*, 1981), path effects, and a scaled von Seggern-Blandford time function. By varying pP times and amplitudes, and measuring magnitudes for the synthetic seismograms produced, depth correction curves were produced for some 19 stations. Figure 1 shows an example for station ANTO. The peak at .3 sec. is typical of high frequency, low attenuation paths. In general, good agreement between synthetics

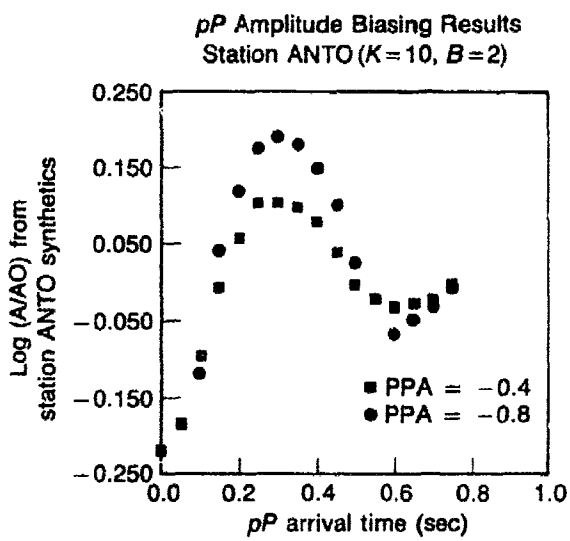

Fig. 1. Magnitude correction curve for station ANTO for Shagan River source. Magnitudes of synthetics for specified pP time and amplitude are referenced to zero pP amplitude synthetics.

and data was obtained for *pP* times of .25 to .40 sec. This produces amplification relative to the zero amplitude *pP* case of about .2 m_b units for this station, assuming a *pP* amplitude of .8. For this range of *pP* times, there is relatively little variation of amplification effects, so that exact *pP* time estimates are not critical in determination of m_b bias.

The depth correction curves make the assumption that *P* and *pP* are the dominant arrivals for Shagan River events and that the receiver source and path estimate are not seriously in error. To test the validity of these assumptions, we have deconvolved *P-pP* pairs from data, once again varying *pP* times and amplitudes. The results for station ANTO for *pP* amplitudes of .8 are shown in Fig. 2. The changes in amplitude as a function of *pP* time are quite consistent with the correction curve of Fig. 1. We also note that waveform changes as a function of *pP* are useful in limiting allowable *pP* times. Using results for a variety of short period and broad band stations, a good case can be made for *pP* times

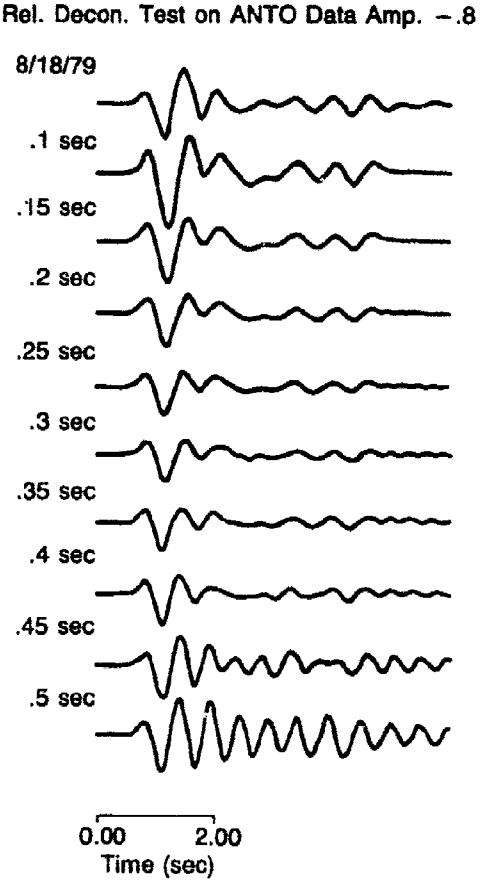

Fig. 2. Deconvolution of *P-pP* pairs for recording of 08-18-79 Shagan River event at ANTO. Note evolution of waveform and stability of amplitude as *pP* time varies from .2 to .4 sec.

in the .25 to .40 sec range. Once again, in this range relatively little change in amplification effect is seen.

A third method used to estimate *pP* times and amplitudes, as well as times and amplitudes of later arrivals, is L1 deconvolution. In this method, a wavelet consisting of instrument, t^*, and source time function estimate is formed. Receiver function estimates may also be included. The L1 deconvolution finds a spike sequence containing the minimum number of spikes which, when convolved with the wavelet, reproduces the data seismogram to some specified accuracy.

Figure 3 shows the application of this technique for the 08-04-79 Shagan River event as recorded at YKA. A slightly broadened *pP* with amplitude .6 is present at .4 sec. Additional large negative arrivals, starting at .75 sec are evident both in the deconvolution and the original seismogram. Note that the wavelet in this case does not include a receiver estimate, so that the spike sequence also includes receiver effects.

Results of L1 deconvolutions to this point in time have produced *pP* estimates of .3 to .4 sec. Reasonable changes in time function and t^* have been tried. Decreases in t^* lead to broadening of the spikes, while increases lead to a loss of the simple spike-like character of the deconvolution. Time function changes have somewhat less effect. Thus, the L1 results seem to strongly support *pP* times of .3-.4 sec, although more research on possible tradeoffs is needed.

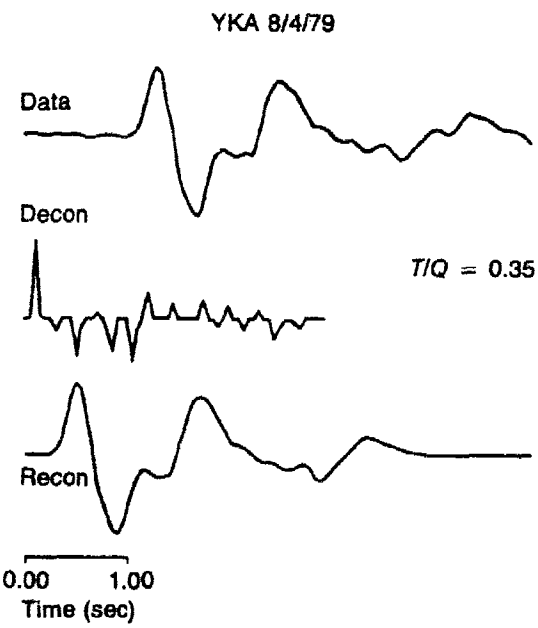

Fig. 3. *L1* deconvolution of YKA broadband data (top) for Shagan River event of 8-4-79. Wavelet used has t^* of .35 and von Seggern-Blandford time function. No receiver estimate was used. Middle trace shows estimate of source spike sequence, while bottom trace shows convolution of spike sequence with source wavelet.

High resolution relative P and pP estimates where obtained using Relative Waveform Inversion methods (Mellman and Kaufman, 1982) for a suite of eight short period and broadband stations and 12 Shagan River events. This processing was complicated by the existence of a large arrival at ~ .8 sec, which varies in amplitude from event to event and azimuth to azimuth. This necessitated prefiltering of the data to extend the bandwidth to both higher and lower frequencies. Using this pre-filtered data, it was impossible to eliminate the effects of the later arrivals, both in the RWI procedure and in convention magnitude determination. This necessitated using a quite short (.8 sec) time window. With this time window, azimuthally consistent, stable results were obtained. Larger time windows tended to give azimuthally varying pP estimates.

Figure 4 shows the filtered data for Station ANTO. The later arrival, though fairly small for this station, is evident. Note that there is very little variation in the early portions of these waveforms. This is a reflection of small variation in pP times for these events.

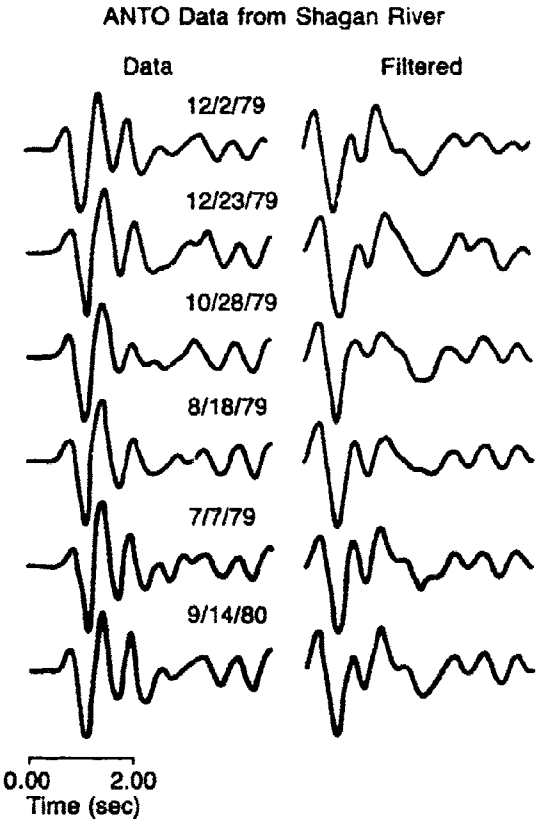

Fig. 4. Data set of Shagan River explosions at ANTO and filtered data. Note consistency of the early portion of the filtered waveforms.

The log of the *P* amplitudes, relative to the 12-02-79 amplitude, *pP* times and amplitudes as derived from the relative waveform inversion are given in the Table 1. We note that the largest variation in *pP* time is .06 sec. This is about as expected for events with this variation in size, assuming constant scaled depth of burial. There does appear to be fairly good correlation between *pP* time and event size.

Since these results represent our best estimates of depth corrected relative yield, it is interesting to compare these estimates with the tectonic corrected surface wave estimates of Given *et al.*, 1984. This is done in Fig. 5, with all results referenced to 12-02-79. A line with unit slope has been drawn through the 12-02-79 event for reference. Agreement between the body and surface wave estimates is quite good, with eight of eleven events within .15 magnitude units of the reference line and six events within .05. Three events lie about .25 magnitude units above the reference line. We note that two of these events are very high tectonic release events.

One possible explanation of the three anomalous events is a change in the overshoot of the source time function, caused by a change in the material in which these devices were buried. A second line has been added to Fig. 5 to illustrate the change expected by varying the von Seggern-Blandford overshoot parameter from 1 to 2. This change is well within the changes observed for NTS shots and is not resolvable in the far field body wave data. More study of additional events in needed, however, before any definitive statement can be made as to whether Fig. 5 does indeed show two populations, or whether we are just looking at statistical variation in a single population.

Table 1. RWI *pP* Times and Amplitudes for 13 Shagan River Explosions.

Event RWI	*pP* Time	*pP* Amplitude	Δm_{RWI} Relative to 12/2/79
12/02/79	.34	−.68	.0
10/12/80	.36	−.79	−.10
09/15/78	.34	−.69	−.10
12/14/80	.39	−.76	−.05
12/23/79	.35	−.76	.09
10/28/79	.36	−.78	.06
08/04/79	.38	−.79	.14
08/18/79	.37	−.84	.14
07/07/79	.34	−.76	−.07
06/23/79	.37	−.77	.16
09/14/80	.37	−.78	.20
06/12/80	.34	−.82	.42
11/04/78	.31	−.67	−.39

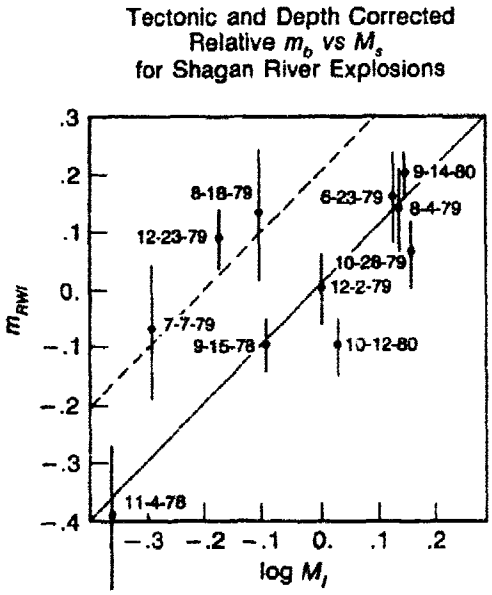

Fig. 5. Comparison of the log of the isotropic moment based on surface wave moment tensor study with log of direct *P* amplitudes based on RWI study for 11 Shagan River events. All events are referenced to 12-2-79. Solid line is referenced line with unit slope passing through 12-2-79 event. Dashed line represents synthetic change of solid line for change in overshoot parameter *B* from 1 to 2.

Conclusions and Recommendations

There is strong although not necessarily conclusive evidence for *pP* times of .25-.40 sec for Shagan River events in the range of magnitude 6. These arrivals produce significant m_b enhancement. Additional large later arrivals, which show significant azimuthal variation, may be removed from consideration by prefiltering of the data. Relative depth corrected m_b shows good agreement with tectonic corrected M_s for most events considered.

Processing of additional events is necessary to determine whether time m_b *vs* M_s relationship is in fact bimodal. Similar studies are also necessary for NTS, to provide calibration of direct arrival amplitudes.

References

Given, J.W. and G.R. Mellman, *Corrections to Surface-Wave Amplitude Measurements From Shagan River Events Based on Moment Tensor Inversion Method*, Sierra Geophysics, Inc. Report SGI-R-84-104, Redmond, WA. 1984 (SECRET).

Lundquist, G.M., M.N.S. Kam, G.R. Mellman and D.M. Hadley, *Relative Receiver Functions For the NTS Global Array*, Sierra Geophysics Report for VELA Seismological Center, VSC-TR-81-26, 1981 (SECRET).

Mellman, G.R. and S.K. Kaufman, *Relative Waveform Inversion*, Sierra Geophysics Report R-82-048, 1981.

Evaluation of the Results of the DARPA Yield Experiment

J.R. Murphy, B.W. Barker and A. O'Donnell

Summary

Over the past several years, DARPA has been supporting a yield estimation experiment in which various innovative procedures are being tested using a large, digital explosion data base assembled for that purpose. These seismic data, together with preliminary results of the research, have been transferred to the CSS where they are currently being evaluated.

The indirect estimation of the energy release of underground nuclear explosions relies primarily on analyses of the seismic waves generated by the explosions and recorded on specially designed monitoring networks located at great distances from the source area. This inferential procedure involves two distinct steps. The first is the determination of a "source size" related parameter from the observed seismic data; the second is the correlation of this seismic parameter with energy release at the source using scaling laws calibrated with data from explosions of known yield. Although the various aspects of this estimation procedure have been subjected to critical review and revision over the years, the primary seismic measures of source size have continued to be the classical time domain m_b and M_s magnitudes whose definitions date back to the early days of instrumental seismology. However, it has long been recognized that these classical magnitudes may not be optimum measures for yield determination purposes, particularly now that digital seismic data is becoming routinely available. As a result, a program has recently been initiated by DARPA to investigate the utility of alternate seismic magnitude measures. The goals of this program are to employ modern seismological procedures to determine a variety of magnitude measures from a suitable sample of explosion seismograms and to assess the advantages and disadvantages of these alternate measures, relative to classical m_b and M_s, for yield estimation purposes.

The yield estimation experiment involves two principal features: corrections applied to the seismic data using deterministic models which have been calibrated against appropriate explosion data and derivation of alternate magnitude measures (primarily spectral) through sophisticated signal

processing of the corrected and uncorrected digital data. The deterministic corrections for body waves focus on the effects of source depth, inelastic attenuation in the upper mantle beneath the source and receiver, and variations in crustal structure beneath the various observation points. The deterministic corrections being applied to the surface wave data are path corrections which attempt to compensate for variations in dispersion and attenuation characteristics along the propagation paths to the stations of interest. For both body and surface waves, alternate spectral magnitudes are defined in terms of linear combinations of the outputs of a series of narrowband filters covering the frequency windows characteristic of teleseismic P and surface wave arrivals. The other alternate magnitude measure selected for analysis is the scalar moment, M_0, of the isotropic component of the moment tensor corresponding to the explosion component of the source as deduced from inversion of the observed surface waves.

The flow diagram for the body wave data is illustrated schematically in Fig. 1 where it can be seen that classical m_b as well as spectral $\hat{m}_b$ values are being derived from both the uncorrected and corrected data. Correction procedures designed to account for propagation path effects (receiver functions), variations in inelastic attenuation in the upper mantle beneath the source areas and receiver sites and effects of variations in source depth (pP interference effects) are being evaluated. The receiver function corrections, developed by Lundquist and Kam (1982) are being determined from the short period data by Sierra Geophysics, Inc. and can be viewed essentially as frequency-dependent station corrections which are designed to account for the fact that the relative spectral composition of P waves observed at specific sites can be expected to vary due

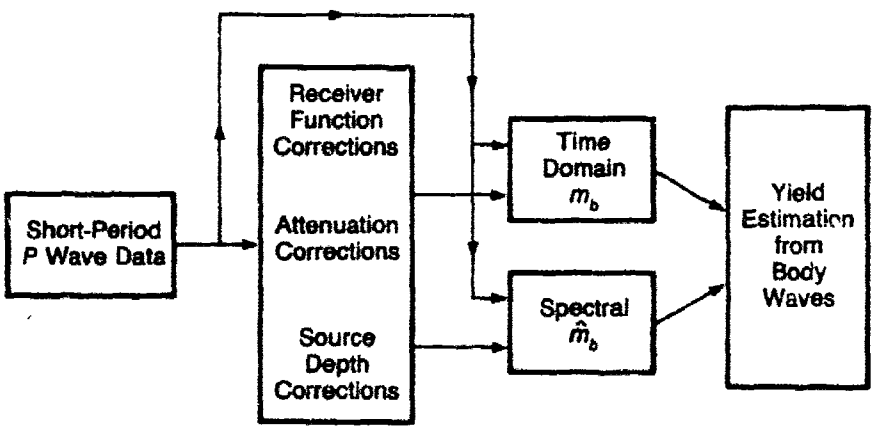

Fig. 1. Flow diagram for body wave data.

to changes in yield, source depth of burial, and source medium physical properties. For each testing area to be investigated, the objective is to estimate receiver functions at each recording station which has recorded a required minimum number of explosions from that area and then apply these corrections to all the remaining data.

The attenuation corrections are designed to compensate for variations in upper mantle inelastic attenuation beneath the various testing areas and recording stations. These corrections are being determined by Teledyne Geotech using their well-documented spectral decay estimation procedures for the attenuation parameter t^* (Der *et al.*, 1981). The objective of this phase of the investigation is to define attenuation corrections for each testing area to be studied and also for each recording station which has recorded a suitable sample of explosion data from that area.

The source depth corrections are designed to account for effects due to variations in *pP* amplitude and time delay with respect to *P* and are being carried out by Sierra Geophysics, Inc., using techniques developed both by them (Mellman and Kaufman, 1981) and by others to characterize the *pP* arrivals. The objective of this phase of the investigation is to estimate *pP* amplitudes and delay times for each explosion under investigation and to define the frequency-dependent effects of this arrival on the *P* waves observed at the stations which recorded these explosions.

Once these corrections have been defined and applied to the raw data, traditional time domain (m_b) and spectral ($\hat{m}_b$) body wave magnitudes will be determined for all the observations. The spectral $\hat{m}_b$ determinations are being carried out by S-CUBED using their well-documented narrow-band filtering procedure (Bache *et al.*, 1979; Farrell *et al.*, 1982). The output of this process consists of body-wave magnitude estimates as a function of frequency in a number of bands which cover the usable teleseismic passband.

The flow diagram for the surface wave data is illustrated schematically in Fig. 2 where it can be seen that, as with the body waves, classical M_s as well as spectral $\hat{M}_s$ magnitudes are being determined from both the corrected and uncorrected long-period surface waves. In this case, an additional alternate magnitude measure, M_0, based on moment tensor inversion of the path-corrected surface waves is also being considered. The long period data are being corrected by S-CUBED using their surface wave path correction procedure (Stevens *et al.*, 1982) which is designed to account for differences in the effects of propagation (*i.e.*, dispersion, attenuation) along the variety of paths characteristic of the propagation from a specific testing area to the stations of the monitoring network.

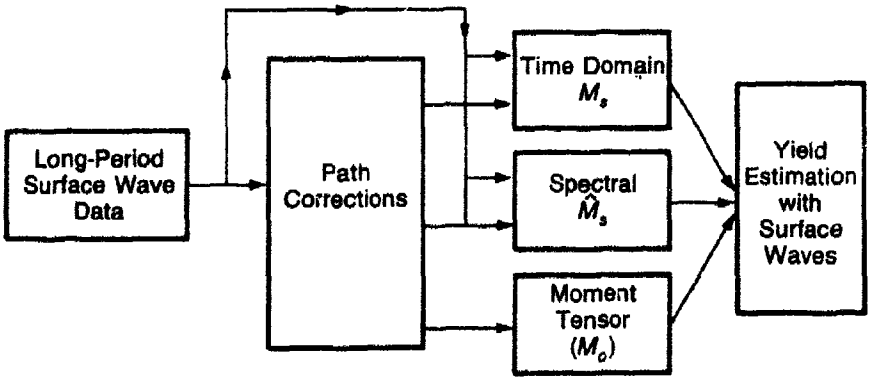

Fig. 2. Flow diagram for surface wave data.

As the corrected data become available, they are being processed by S-CUBED and Sierra Geophysics, Inc., to obtain spectral M_s and scalar moment M_0 estimates, respectively. The surface wave spectral estimates are being determined using a procedure completely analogous to that employed with the body waves (Farrell *et al.*, 1982). That is, the arriving surface wave energy is compressed into a pulse by analytically removing the effects of dispersion estimated from the path correction analysis and the resulting pulse is bandpass filtered to give a surface wave magnitude estimate as a function of frequency. The moment tensor representation of the effective explosion source function is being obtained using surface wave inversion procedures which have been developed over the past decade. The results of this analysis are quantitative estimates of the isotropic and deviatoric components of the moment tensor and, ultimately, estimates of the explosion component of the scalar moment, M_0, for each explosion studied.

For the purpose of the experiment, an explosion seismic data base consisting of nearly 10,000 digital short-period and long-period seismograms has been assembled on the classified computer system at the DARPA Center for Seismic Studies, (CSS), together with cross-reference files containing the best available station and event information. These correspond to data recorded on the AEDS, SRO and WWSSN networks from 65 NTS, 58 Semipalatinsk and 7 French Sahara explosions. Subsets of these data are being processed by various DARPA contractors to derive the alternate magnitude measures and correction procedures described above. As they become available, results of these analyses are being transmitted to the CSS where they are being evaluated using the entire yield data set. The evaluation phase of the experiment is still in progress, and only preliminary results are available at the

present time. In the following discussion, we will briefly discuss some of the results of the short-period attenuation study in order to illustrate some aspects of this evaluation effort.

From the perspective of seismic yield determination, the value of short-period attenuation (*i.e.*, t^*) estimates for teleseismic *P*-wave paths of interest rests primarily on their ability to provide accurate estimates of the magnitude biases introduced by variations in upper mantle attenuation beneath test sites and stations of interest. However, it is important to recognize that there are other factors, such as focusing and crustal amplification, which can significantly affect short-period *P*-wave amplitudes and, in some cases, mask the effects of attenuation. This is illustrated in Fig. 3 which shows selected SRO m_b station correction factors computed with respect to reference station CHTO using data from Shagan River explosions, plotted as a function of the corresponding differences in t^* values with respect to CHTO as estimated by Der *et al.*, (1983). The straight line on this figure shows the nominal attenuation effect, $\Delta m_b = -1.5\Delta t^*$, which should be approximately applicable to explosion *P* waves. It can be seen that the variation in m_b station corrections is much larger than that which would be expected from the differences in t^*, and shows little or no correlation with the predicted trend. Another illustration of this effect is provided by the relative receiver functions, which represent average *P* wave spectral ratios between pairs of stations. Figure 4 shows some representative relative receiver functions for four different SRO stations, computed with respect to reference station CHTO using Shagan River explosion data (Lundquist and Samowitz, 1983). The straight lines on these figures correspond to the spectral amplitude differences expected on the basis of the differences in t^* (with respect to CHTO)

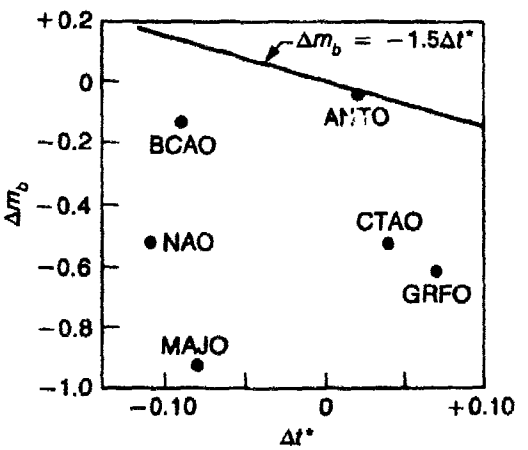

Fig. 3. Comparison of observed SRO m_b station corrections for Shagan River explosions with variations in station t^* values determined by Der *et al.* (1983).

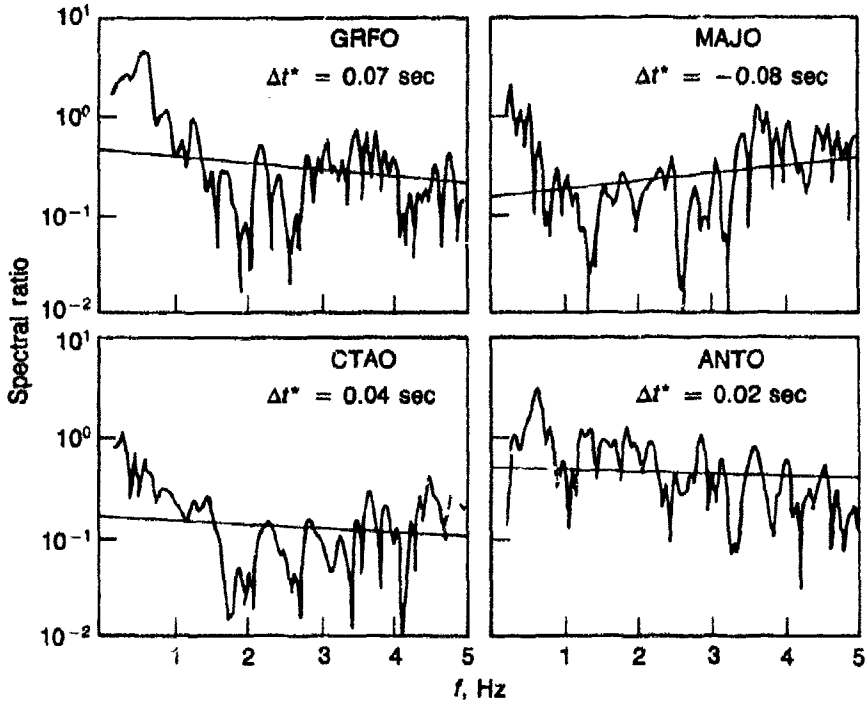

Fig. 4. Comparison of the amplitude spectra of the relative receiver functions for selected SRO stations with respect to reference station CHTO determined by Lundquist and Samowitz (1983) with spectral trends predicted by the corresponding t^* differences (straight lines).

inferred by Der *et al.* (1983) normalized to an amplitude level which provides the best overall fit to the spectral ratio data. It can be seen that the trend of the spectral ratios with increasing frequency generally agrees fairly well with the trends predicted by the inferred differences in t^*, as they should. Again, however, it can be seen that in some cases (*e.g.*, CTAO), the nearly frequency-independent offset in amplitude level completely overwhelms the relatively small effects predicted by the differences in t^*. That is, in these cases the elastic propagation effects are large and mask any correlation which may exist between t^* and m_b. This observation that there is no one-to-one relation between m_b anomalies and variations in t^* is not a new one and, in fact, was previously noted in the analysis of the results of the NTS reciprocal experiment (Der *et al.*, 1981). However, it does emphasize the fact that there are unresolved issues concerning the relative importance of variations in short-period attenuation on m_b which remain to be considered in the context of yield estimation.

Conclusions and Recommendations

The DARPA yield experiment is now well underway and significant progress is being made toward the objective of identifying improved alternate procedures for use in yield estimation. However, much work remains to be done to complete a definitive evaluation of the various procedures being tested, particularly in the area of surface wave analysis.

References

Bache, T. C. (1979), *m_B, a Spectral Body Wave Magnitude (U)*, S-CUBED Report SSS-CR-79-3901 (SECRET).

Der, Z. A., T. W. McElfresh and A. O'Donnell (1981), *Results of the SDCS (Special Data Collection System) Attenuation Experiment*, Teledyne Geotech, VSC-TR-81-14.

Der, Z. A., T. W. McElfresh, R. Wagner and A. O'Donnell (1983), *Global t^* Measurements For the Magnitude Yield Experiment (U)*, Teledyne Geotech, SDAC-TR-82-3 (SECRET).

Farrell, W. E., J. L. Stevens, L. B. Bache, A. O'Donnell and B. Shkoller (1982), *Spectral Magnitudes and Seismic Discrimination*, S-CUBED SSS-R-83-5831 (Draft).

Lundquist, G. M. and M. N. S. Kam (1982), *Preliminary Relative Receiver Functions For the Eastern Kazakh Global Array and the Nevada Test Site Global Array (U)*, Sierra Geophysics, SGI-R-82-071 (SECRET).

Lundquist, G. M. and I. R. Samowitz (1983), *Path-Specific Properties of Teleseismic Body Waves (U)*, Sierra Geophysics, SGI-R-83-098 (Draft) (SECRET).

Mellman, G. R. and S. K. Kaufman (1981), *Relative Waveform Inversion*, Sierra Geophysics, Inc., SGI-R-81-048.

Stevens, J. L., W. L. Rodi, J. Wang, B. Shkoller, E. J. Halda, B. B. Mason, J. B. Minster (1982), *Surface Wave Analysis Package and Shagan River to SRO Station Path Corrections*, S-CUBED, VSC-TR-82-21.

Experimental Study of Magnitude Anomalies in French Polynesia

F. Navarre

The French Polynesia seismic network, right in the middle of the Pacific Ocean is well situated to study an azimuthal variation of magnitude anomalies.

We computed these anomalies for 733 events among which 299 were recorded in all the nine stations used for this study. We first looked the magnitude's anomalies between the actual records and the magnitudes published by NEIS. As expected, the scatter of those anomalies is very large. Nevertheless, we obtained a function of azimuth which is the same for all nine stations. More interesting is the variation of magnitude inside the network. The local anomalies may be divided in a constant factor, function of the quality of the very near geological environment of each station and a function of azimuth.

This last term is very well-correlated with the local travel time anomalies. The larger the recorded magnitude, the later the seismic waves arrive.

This confirms the existence of focusing and defocusing effects in the propagation of waves through the earth's crust.

Study of Regional Phases

Propagation of Regional Phases in Western Europe. In a former study an attempt to evaluate the attenuation of L_g phases was made by filtering process on local data for six earthquakes in western Europe. ("Attenuation of Regional Phases in Western Europe" by M. Nicolas *et.al.*, BSSA vol. **72** 6 pp. 2089-2106, December 1982).

By using more quakes in this area and more adequate methods of investigation, we try to improve the evaluation of anelastic attenuation (and determination of Q factor) for L_g phases in order both to better understand the propagation anomalies and to get some information on the sources and station functions.

Method: Spectral amplitudes of L_g phases are computed in each station from 0.5 to 15 Hz after having made a seismic noise correction. For each frequency of any L_g phase the amplitude $A\ (f,D)$ is expressed as follows:

$$\log A\,(f,D) = \log A_o(f) - \alpha \log D - \frac{\Pi Df}{QV} + \delta T(f)$$

D:	distance epicenter - station
$A_o(f)$:	source amplitude
α:	geometrical spreading attenuation coefficient
V:	group velocity
$\delta T(f)$:	station correction

By least-square method. $A_o(f)$, $Q(f)$, and $\delta T(f)$ are computed.

Data: 18 earthquakes in France and other parts of western Europe have been selected. The range of magnitudes M_L is 3.3 to 4.7. They have been recorded in 20 to 25 short period stations from 100 to 1500 km. Three time windows have been selected on the L_g signals according to their group velocities: 3.6 - 3.1 km/s; 3.1 - 2.6 km/s; 2.6 - 2.1 km/s.

Main results: The first result we have obtained is an evaluation of the station transfer function, $\delta T(f)$ in good agreement with the local seismic noise spectrum. This $\delta T(f)$ gives an efficient correction on the function dispersion versus frequency.

The second result concerns the Q function itself. Obtained for the 18 earthquakes globally, it is expressed as:

$$Q = Q_o f^{0.6}$$

with $Q_o = 300$. The scatter is rather important nevertheless, but should be largely interpreted in terms of regional anomalies.

This part of the work is now to be done. The last result is an evaluation of the source function $A_o(f)$ in good agreement with the Brune function. More work is necessary to better define this source function and see if it possible by this method to reach some of its main characteristics.

Regional Seismograms Modeling. A theoretical study of the generation and geometrical attenuation of regional crustal phases has been carried on. It has been done through the computation of seismograms in the epicentral distance range from 60 to 500 km. The geometrical attenuation of L_g waves with epicentral distance is of the form $r^{-0.8}$. P_g wave amplitudes display a much stranger decay of the form $r^{-1.5}$. The spectral density of the crustal transfer function for P_g waves is relatively flat for frequencies between 0.1 and 5 Hz while L_g wave spectra strongly fall off beyond 2 to 3 Hz.

The excitation of P_g wave is insensitive to the depth of the source within the crust while the L_g amplitude is about 50% higher for a source in the upper or middle crust than in the lower crust. The amplitudes of these two waves drastically decrease when the source is below the moho. These results illustrate the important role of wave guide played by the crust for the propagation of L_g and P_g.

We find that the geometrical attenuation of P_g and L_g waves is independent of source mechanism. In the case of an explosion the excitation of P_g is insensitive to the source depth. The L_g wave amplitude is small in comparison to P_g and Rayleigh waves and depends on the closeness of the source to an interface or to the free surface. (M. Bouchon *et al.*, "Theoretical Study of the Excitation, Spectral Characteristics and Goemetrical Attenuation of Regional Seismic Phases", submitted to the BSSA, 1983).

***T* Phases Detection by Seismographs.** *T* phases converted in seismic waves have been propogated along hundreds of km through the crust and recorded in different stations of the LDG network. These *T* phases were generated by large offshore quakes as the Azores Islands quakes (1/1/1980 - M_s = 6.9).

Using these data and data from offshore chemical blasts recorded on the LDG network, a comprehensive study of the acoustic- to -seismic-wave conversion at the continental slope has been carried out.

We found that the wavetrain commonly recorded at the station is composed essentially of P_g and S_g waves which reach the seismometer under different azimuths.

Assuming the signal is the sum of discrete arrivals due to different rays crossing the continental slope at different points, synthetic seismograms are computed and compared to the recorded data.

The transmission of energy from the ocean to the earth is mainly due to diffraction effects. We point out the influence of the continental slope on the duration and the amplitude of the *T*-phase.

A better understanding of the *T* waves' complexity has been partly achieved. (Y. Cansi *et al.*, "*T* Waves with Long Inland Paths: Synthetic Seismograms", submitted to the *JGR*, 1984).

MSS and OBS Data from the Ngendei Experiment in the Southwest Pacific

John Orcutt and Thomas H. Jordan

Summary

An extensive set of noise, explosion, and earthquake data was collected by the Marine Seismic System (MSS) and ocean bottom seismometer (OBS) arrays during the 1983 Ngendei experiment in the Southwest Pacific Basin. The MSS was emplaced in a drill hole 124 m below the sediment-water interface. Noise levels in the frequency band 0.5-2.0 Hz observed on the MSS were 20-30 dB less than those recorded on the OBSs, consistent with models in which seafloor noise propagates primarily as interface waves. The refraction data require directional anisotropy in the upper crust and uppermost mantle; the latter implies a fossil seafloor—spreading direction of N30°E in this part of the Pacific. Clear S_n phases, with an apparent velocity of 4.7 km s^{-1}, are observed in the refraction data. A number of earthquake signals at regional and teleseismic distances were recorded by the MSS and OBSs. Intermediate focus and deep-focus events from the Tonga-Kermadec seismic zone show complex P arrivals: these provide new information about the attenuation and velocity structure of the oceanic upper mantle. In particular, the sub-lithospheric mantle beneath the Ngendei site is highly attenuating, with an average apparent Q_P of about 300. Because of this attenuation, the detection threshold of the MSS for distant ($\Delta > 30°$) teleseismic events is relatively high ($m_b \approx 5.0$). At regional distances ($\Delta < 15°$), however, where signals propagate through the high-Q lithospheric waveguide, events with body wave magnitudes as small as 4.0 are well recorded on the MSS, and the detection threshold is lowered to about 3.7.

During January-April, 1983, the *D/V Glomar Challenger* and the *R/V Melville* deployed and recovered the NORDA/DARPA Marine Seismic System (MSS) and a six-element ocean bottom seismometer (OBS) array at a site in the southwest Pacific (23°49'S, 165°32'W), approximately 900 km east of the Tonga Trench. The expedition was named Ngendei after a Polynesian deity associated with volcanoes and earthquakes. Instrument emplacement and recovery were accomplished as planned, and the major scientific objectives were achieved; three basic types of

seismological data — noise, refraction, and earthquake — were successfully recorded by both the MSS and the OBS array.

The data analysis program has four primary objectives: (a) comparison of noise levels and signals recorded by the MSS and OBS sensors to assess the signal-to-noise improvement attainable by burial of seismometers below the sediments in a deep-ocean environment, (b) use of noise data to investigate the mode of noise propagation on the sea floor and to test physical models of noise generation in the deep ocean, (c) analysis of refraction data to study the structure of the crust and upper mantle, in particular, the anelastic and anisotropic structure of the oceanic lithosphere, and (d) use of earthquake data to examine the propagation of seismic signals to regional and teleseismic distances over purely oceanic paths and to constrain elastic and anelastic models of the sublithospheric mantle.

Noise Data

The comparison of absolute values of seismic noise at the sea floor, as measured by the OBSs, with values recorded by the sub-bottom MSS is a major component of this study. The MSS was deployed in DSDP hole 595B at a depth of 124 m below the sediment-water interface, approximately 54 m into basaltic basement. It was anticipated that noise levels would decrease substantially with depth of burial given the working hypothesis that high-frequency ($\sim$ 1 Hz) noise travels largely as a fundamental-mode Stoneley wave along the sea floor. The Leg-78B deployment of the MSS yielded results which supported this hypothesis (Adair *et al.*, 1984), but a full-fledged test of noise models was not possible with the data from this experiment because of the lack of OBS array measurements at the time of MSS recording.

Figure 1 depicts the response of the OBS and MSS instrumentation employed during Ngendei. The MSS mid-period channel has a much lower gain than the short-period channel. The high end of the MSS short-period response was substantially modified over that illustrated by the Gould anti-aliasing FIR filter, which essentially eliminated all energy above about 18 Hz. The Nyquist frequency was 20 Hz for the MSS and 64 Hz for the OBSs.

Figure 2 illustrates the absolute ground-motion noise levels for the period beginning at 0635 Z on 8 February 1983. The spectra from the MSS and Suzy (one of the OBSs) were stabilized by stacking ten spectral realizations from contiguous, tapered windows of 13-second duration. Both the *Glomar Challenger* and the *Melville* were on station near the drill site at this time; a 10 Hz peak associated with the thrusters on the *Challenger* can be seen in both data sets. The spectra differ by only

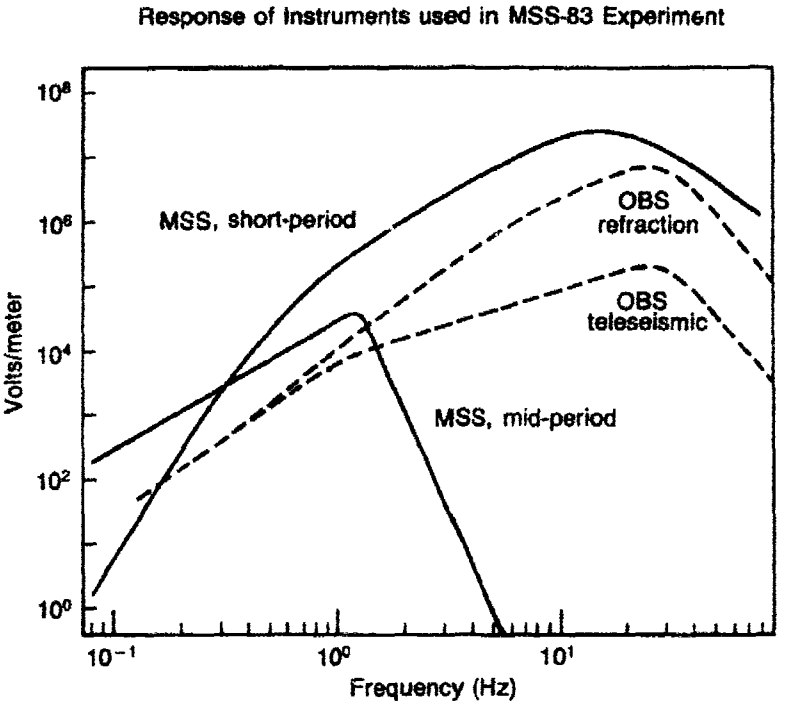

Fig. 1. A comparison of the MSS and OBS response functions used in the Ngendei experiment. The MSS Nyquist frequency was 20 Hz; the response of the MSS was modified by a low pass FIR filter (not shown) to prevent aliasing. The OBS response is broader band and has a Nyquist frequency of 64 Hz.

a small amount in the vicinity of the microseism peak at 3-4 s period, but the difference increases at higher frequencies, reaching approximately 20 dB at a frequency of 2 Hz. Figure 2 also shows several continental noise spectra for comparison. The Brune-Oliver upper bound is taken from Brune and Oliver (1959), as normalized by Melton (1976), and represents the highest noise levels expected for a continental site. The MSS/OBS levels are lower than this bound (the penetration of the bound at a frequency of 0.17 Hz by the Suzy spectrum is largely owing to the increasing OBS electronic instrument noise generated by low-power CMOS amplifiers). The Lajitas, Texas, spectrum, the lowest ever documented on continents (Herrin, 1982), and the very quiet Queen Creek, Arizona, measurement (Melton, 1976) are also plotted. (The Queen Creek spectrum, as noted by Herrin (1982), is nearly identical to Lajitas at frequencies below about 0.7 Hz.) The Ngendei noise levels are higher than at these continental sites but, above 1 Hz, are substantially less than those of average continental stations. The uncorrected

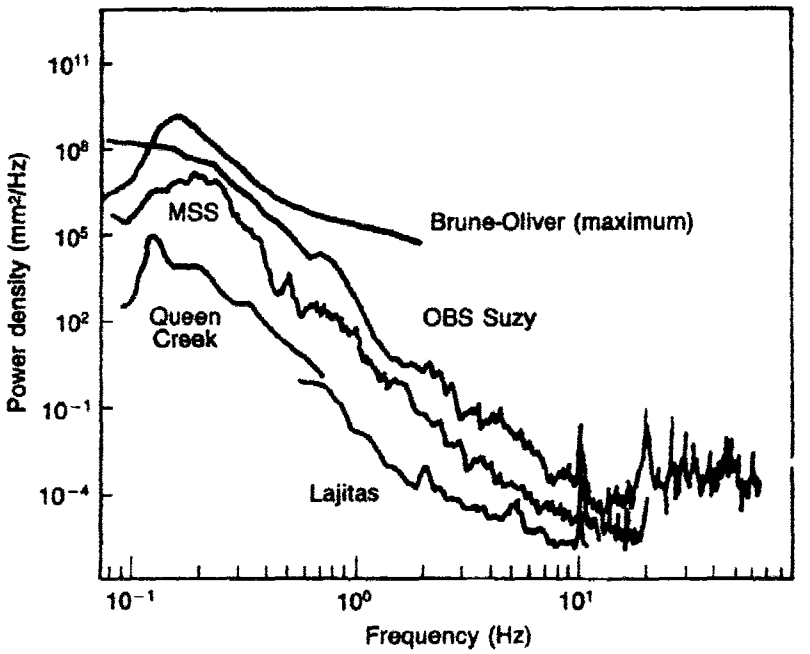

Fig. 2. Power spectra of simultaneous sea-floor noise estimates for the MSS and OBS Suzy. These power spectra are compared to the Brune and Oliver continental upper bound and to two extremely quiet continental measurements described in the text. The 10-Hz (overtone) peaks are ship noise from the *D/V Glomar Challenger*.

noise levels before and after *Challenger* departure are illustrated in Fig. 3; substantial improvements are realized in the OBS levels at frequencies above 3 Hz and in the MSS levels above 10 Hz.

Refraction Data

The seismic refraction experiment conducted at the Ngendei site consisted of a star pattern (4 split profiles) with legs extending to approximately 60 km range. Two legs, normal to one another, were extended to 250 and 150 km to evaluate deeper lithospheric structure. Figures 4 and 5 illustrate the MSS and OBS data for one of the lines; topographic corrections have been applied.

The OBS seismograms show clearly the high-frequency noise generated by *Challenger* (*cf.* Fig. 3) and, because of the broader bandwidth of the OBS response (Fig. 1), contain substantially more energy at high frequencies. The OBS signals fell below the noise level beyond a range of about 70 km, whereas the MSS yielded observable signals out to 250 km.

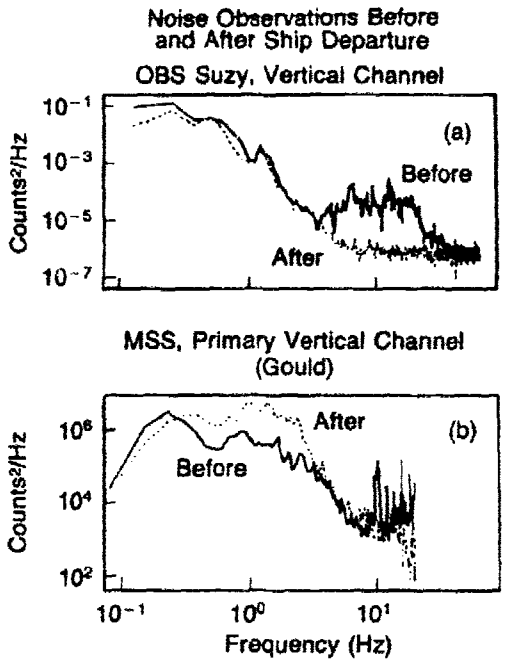

Fig. 3. Power spectra, uncorrected for instrument response, illustrating the effect of ship noise on estimates such as those in the previous figure. At the sea floor, the ship noise is a significant contributor above a frequency of 3 Hz. The flat spectrum from OBS Suzy above a frequency of 8 Hz in the absence of ships is due to the digitizing noise associated with a 12-bit A/D converter.

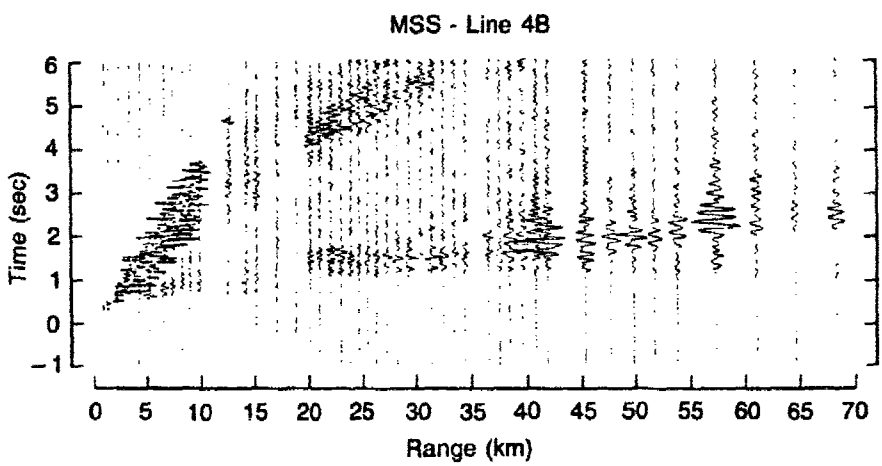

Fig. 4. Marine Seismic System data from an explosion seismology line extending from the MSS/OBS array to the southwest reduced at 8 km s^{-1}. The MSS began its first recording when the epicentral distance was about 20 km. The events between 0 and 20 km were shot at a later time and, hence, cannot be directly compared to the OBS records in Fig. 5. The crossover between P_n and crustal phases occurs at about 35 km. Note the larger shear waves arriving at later times.

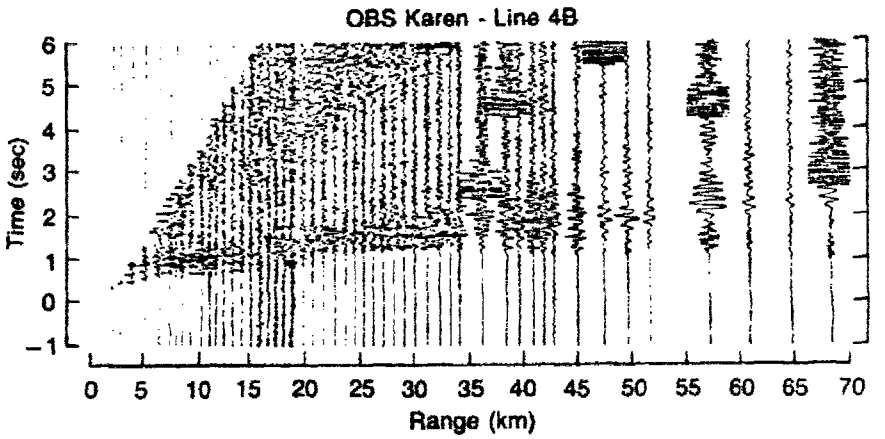

Fig. 5. Same as Fig. 4 as recorded by an OBS. The OBS records are noisier due to the presence of the *D/V Challenger*, and sediment reverberations contaminate the later portions of the record. The large impulses in some records (*e.g.* at 36.5 km) are caused by tape recorder turn-on transient after the OBS CMOS memory buffer has been filled.

Figures 6 and 7 contrast two of the distant events from the refraction line in Figs. 4 and 5. The OBS and MSS seismograms have been aligned by a correction for the depth differences. The two data sets are nearly identically in phase with the MSS appearing largely as a filtered version of the OBS data. The OBS data have higher signal amplitudes after the arrival of the initial compressional wave; we attribute this signal to reverberations within the gelatinous sediment layer.

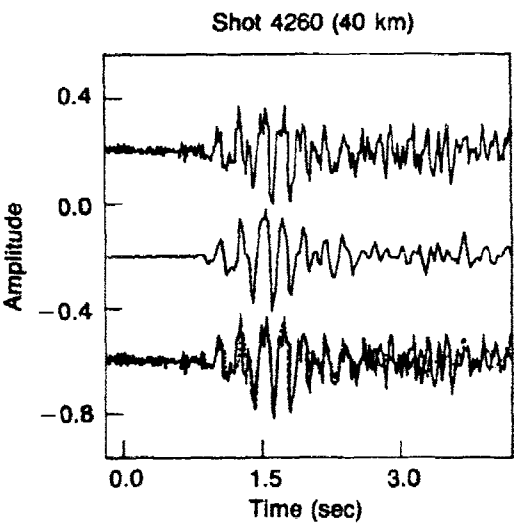

Fig. 6. An event from profile 4B as recorded by an OBS (top trace) and the MSS (middle trace). The OBS record, with a greater bandwidth, contains a great deal of noise from *D/V Challenger*. The two seismograms are overlain in the bottom trace to emphasize the coherence of the *P* wave. The coherence deteriorates after 1.0-1.5 s as low-velocity shear-wave reverberations in the sediment are sensed by the OBS.

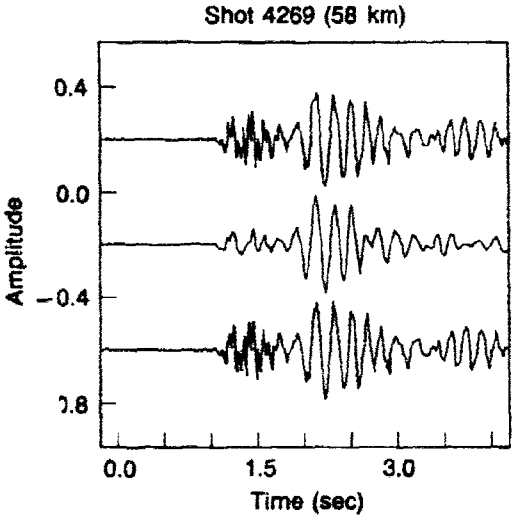

Fig. 7. Another trace from profile 4B. The initial arrival is P_n while the large second arrival is a 'reflection' from the Moho. Again the MSS appears as a low-passed version of the OBS data.

The gross velocity structure of the crust at this site is typical of the older parts of the Pacific Basin. Strong compressional-wave anisotropy (8.0 to 8.4 or 8.5 km s^{-1}) is observed in the uppermost mantle, with a direction of maximum velocity (and, by inference, a fossil direction of seafloor spreading) oriented 30° east of north. An anisotropy of somewhat smaller magnitude is required by the data for the shallow crust. The direction of crustal anisotropy is rotated by almost exactly 90° from the mantle anisotropy; we propose the former is associated with the sheeted dike complex underlying the surface volcanics, as hypothesized from the ophiolite model of oceanic crustal structure. Clear S_n phases are observed on the MSS profiles and are characterized by a phase velocity near 4.7 km s^{-1}. The phase velocity appears to be independent of azimuth.

Teleseismic and Regional Events

Approximately five days of MSS data were recorded on the deck of the *D/V Glomar Challenger* during its occupation of Site 595. At the end of this period, which included the refraction experiment and engineering tests of the MSS, the downhole sensors were connected via an electromechanical cable to the Gould Bottom Processing Package (BPP), and the continuously recording BPP was deployed for a planned 45-day experiment. The six-element OBS array was recovered by the *R/V Melville* and redeployed for simultaneous recording of teleseisms (triggered) and ambient seismic noise (at present intervals) over this period. All six OBSs functioned nearly perfectly, but, unfortunately, the extended MSS

experiment was cut short by a power failure in the BPP only 40 hours after its deployment.

Nevertheless, a number of earthquake signals from events at regional and teleseismic distances were recorded by the MSS, and the analysis of these signals is providing new information about seismic wave propagation in the ocean basins. During the five days of on-deck recording, for example, 64 natural seismic events occurred which were large enough to be identified on the low-gain, strip-chart recorders used for real-time monitoring of the MSS. Most of these were regional events from various depths in the Tonga-Kermadec seismic zone.

Figure 8 shows a typical shallow-focus (h = 52 km) earthquake from the Kermadec Trench. The initial arrival (Fig. 9) is dominated by high-frequency, incoherently scattered energy characteristic of P_n propagation through the high-Q oceanic lithosphere at this distance (12.5°). Waveforms from deeper events are more complex. Figures 10 and 11, for example, display an earthquake at about the same distance (12.9°) with a focal depth of 293 km. In this case the initial wave group is not P_n but rather comprises the P waves triplicated by interaction with the 400-km discontinuity. Because the sublithospheric mantle beneath this part of the Pacific Basin is highly attenuating, these arrivals are relatively depleted in high frequencies. After 10 s, however, the amount of high-

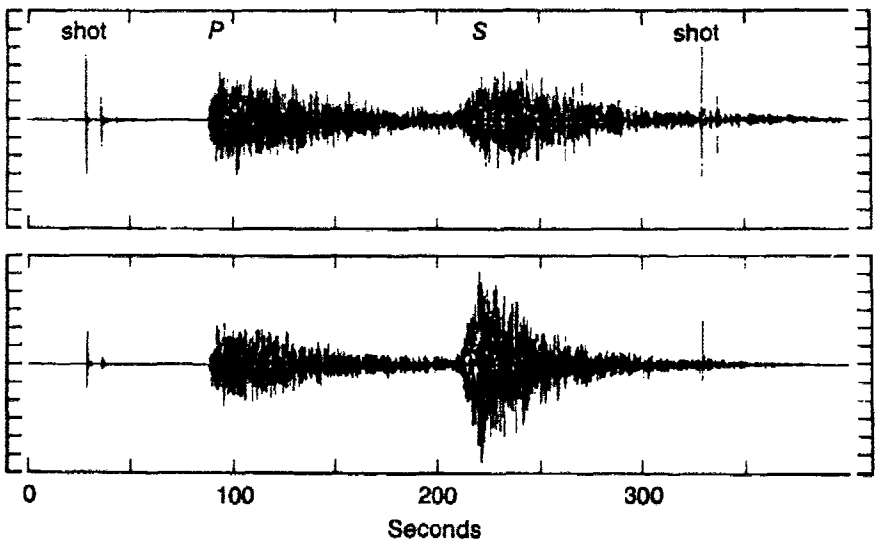

Fig. 8. Short-period vertical (top panel) and horizontal (lower panel) seismograms recorded on the MSS from the shallow-focus (h = 52 km) Kermadec earthquake of 7 Feb 83 (m_b = 6.0, Δ = 12.46°). Time is in seconds after 18:24:34.49 Z; tic-mark interval on vertical axis is 5 × 10^4 counts. Spikes near 30 s and 330 s are refraction shots.

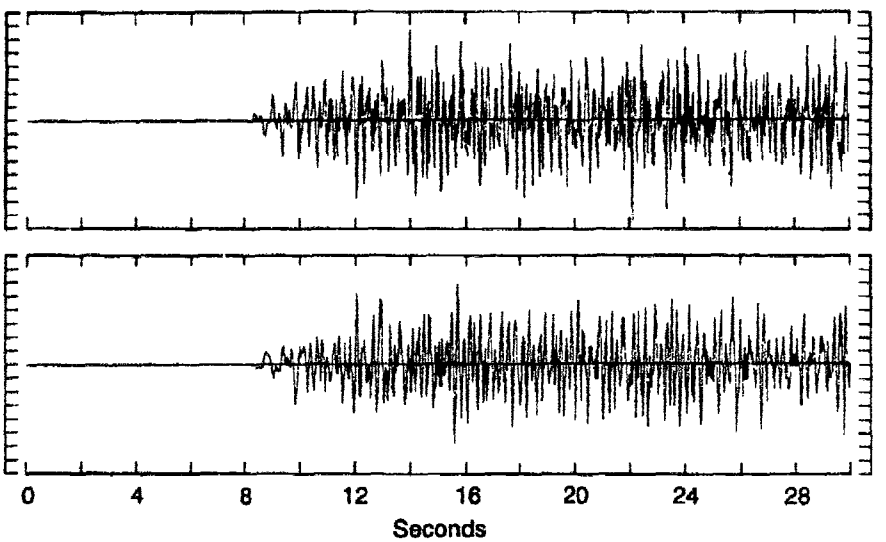

Fig. 9. Short-period vertical (top panel) and horizontal (lower panel) seismograms from the shallow-focus earthquake of Fig. 8, showing *P*-wave arrival on expanded time scale. Time is in seconds after 18:25:54.49 *Z*; tic-mark interval on vertical axis is 2×10^4 counts. The high-frequency, incoherently scattered energy observed on this record is characteristic of oceanic P_n at this distance $\Delta = 12.46°$).

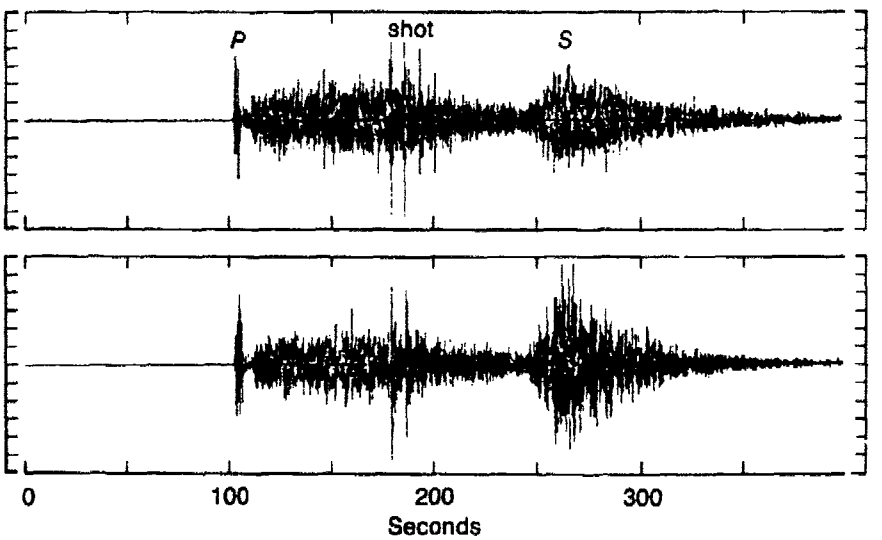

Fig. 10. Short-period vertical (top panel) and horizontal (bottom panel) seismograms recorded on the MSS from the intermediate-focus (h = 293 km) Kermadec earthquake of 7 Feb 83 (m_b = 5.0, Δ = 12.91°). Time is in seconds after 17:57:04.49 *Z*; tic-mark interval on vertical axis is 5×10^3 counts. Spikes between 175 s and 205 s are arrivals from a refraction shot.

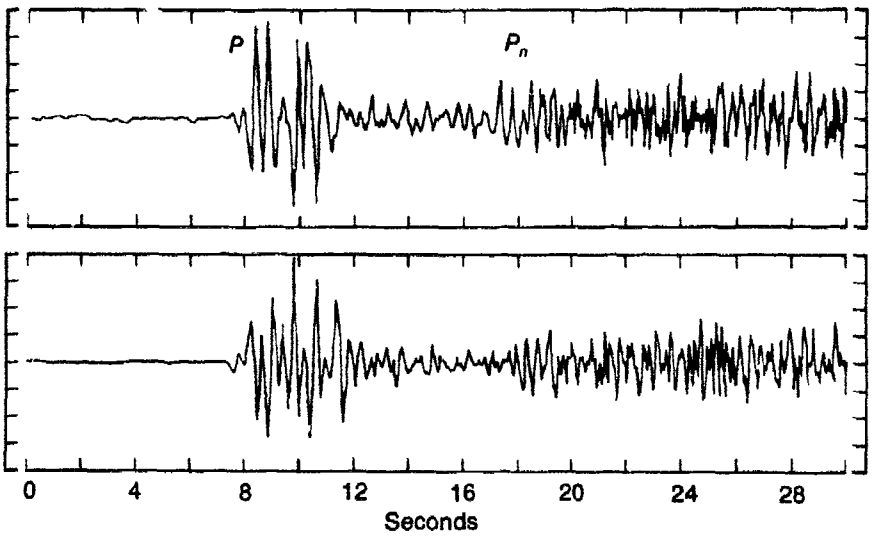

Fig. 11. Short-period vertical (top panel) and horizontal (lower panel) seismograms from the intermediate-focus earthquake of Fig. 10, showing P-wave arrivals on expanded time scale. Time is seconds after 17:58:39.49 Z; tic-mark interval on vertical axis is 5×10^3 counts. Complex P waveform between 7 s and 12 s is a triplication from the 400-km discontinuity. Arrivals following 18 s are P_n waves refracted up and around the corner of the lithospheric waveguide; their enrichment in high frequencies relative to P is indicative of the low Q of the sub-lithospheric mantle beneath the Southwest Pacific Basin.

frequency energy increases, corresponding to the arrival of the P_n wave refracted up and around the corner of the descending slab. (Similar signals were observed by Oliver and Isacks (1967) and Barazangi *et al.* (1972) at the WWSSN station on the island of Rarotonga and were used as evidence for the existence of subducted lithosphere during the development of the plate-tectonic model.)

The spectral ratios of these two types of signals give quantitative information on the differences in attenuation along lithospheric and sublithospheric paths. An analysis of OBS records from the intermediate-focus Tonga earthquake of 1/26/83 ($\Delta = 14°$, $h = 238$ km), which show similar arrivals, yields an apparent differential attenuation of $\Delta Q_P^{-1} \approx 2.5 \times 10^{-3}$. Assuming the attenuation is frequency independent and the Q_P of the lithosphere is ~ 1000 (Oliver and Isacks, 1967), we obtain an average quality factor for the sub-lithospheric path of $\overline{Q}_P \cong 300$.

The effect of this relatively high attenuation in the upper mantle beneath the Ngendei site is manifested in the spectral content and

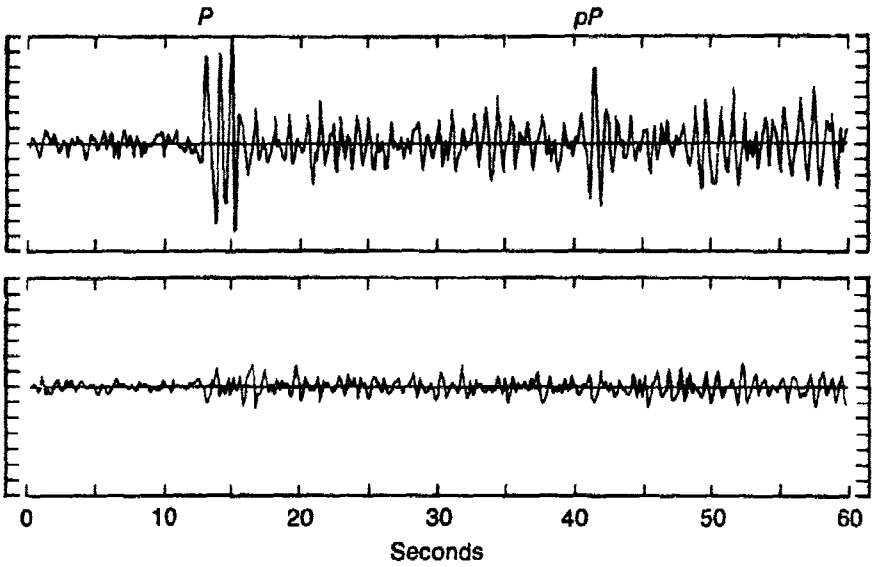

Fig. 12. Short-period vertical (top panel) and horizontal (lower panel) seismograms recorded on the MSS at a distance of 61.2° from a teleseism in the Marianas Islands (13 Feb 83, h = 105 km, m_b = 5.7) showing P and pP arrivals. Tic-mark interval on vertical axis is 5 × 10^3 counts.

amplitudes of teleseismic P waves from events at distances greater than 30°. Figure 12 shows the P and pP waveforms from an intermediate-focus earthquake (m_b = 5.7) at Δ = 61°, which again are relatively depleted in high frequencies. The detection capabilities of the MSS with respect to earthquakes located by the National Earthquake Information Service are summarized in Fig. 13. No events with body-wave magnitude below 5.1 were detected at distances beyond about 30°.

At regional distances, however, where signals propagate through the high-Q lithospheric waveguide, this threshold is considerably reduced. All events at distances less than 30° located by the NEIS were observed on the MSS (unless the record was obscured by refraction shots or other earthquakes). In addition, many smaller, unlocated events from the Tonga-Kermadec seismic zone with S-P times less than 170 s ($\Delta \lesssim 15°$) were recorded with a good signal-to-signal ratio. We estimate the detection threshold for shallow-focus events at these distances to be on the order of 3.7.

Conclusions and Recommendations

The Ngendei seismic experiment has demonstrated the capability of the MSS and OBS instruments to record earthquakes at regional

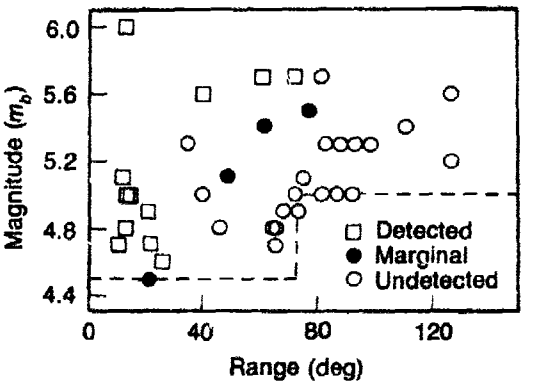

Fig. 13. Diagram of body-wave magnitude versus epicentral distance showing NEIS-catalogued earthquakes detected by the MSS. Each symbol represents an earthquake located by the NEIS in the time interval of MSS recording (6 Feb 83, 14:37 *Z* through 13 Feb 83, 15:11 *Z*). Open squares are events recorded with good signal-to-noise ratio; closed circles are marginal detections with signal-to-noise ratios near unity; open circles are events undetected by the MSS. Events with $m_b < 4.5$ at $\Delta < 72°$ and $m_b < 5.0$ at $\Delta > 72°$ were not included in the sample, nor were those whose signals were obscured by refraction shots and local earthquakes or whose records were missing because of deployment operations and engineering tests. As discussed in the text, the detection threshold for regional events ($\Delta < 15°$) is less than magnitude 4.0.

distances in the deep-ocean environment. These events, especially the intermediate-focus and deep-focus earthquakes, show waveform complexities which are proving useful in constraining attenuation and velocity models of oceanic upper-mantle structure. As demonstrated by Hales *et al.* (1980), the signals from deeper events yield information about upper-mantle structure not attainable from shallow-focus sources, and additional experiments to collect these data should be conducted. For this purpose, arrays of OBSs distributed on profiles normal to the Tonga Kermadec Trench and operated for intervals of 30-90 days would provide the density of coverage required for detailed modeling work.

Acknowledgements

We thank the captains, crews, and scientific parties of the *D/V Glomar Challenger* and *R/V Melville* for their efforts during the complex field operations of the Ngendei seismic experiment. R. Adair, M. Burnett, P. Shearer, C. Van Bruggen, and R. Whitmarsh assisted in the preparation of these results. This research was sponsored by the Defense Advanced Research Projects Agency, The Office of Naval Research, and the Air Force Office of Scientific Research under contracts ONR-N0014-83-K-0151 and AFOSR-84-0043.

References

Adair, R.G., J.A. Orcutt and T.H. Jordan, 1984. "Analysis of Ambient Seismic Noise Recorded by Downhole and Ocean Bottom Seismometers on Deep Sea Drilling Project Leg 78B," *Initial Reports Deep Sea Drilling Project*, **78**, 767-781.

Barazangi, M., B. Isacks, and J. Oliver, 1972. "Propagation of Seismic Waves through and beneath the Lithosphere that Descends under the Tonga Island Arc," *J. Geophys. Res.*, **77**, 942-958.

Brune, J.N. and J. Oliver, 1959. "The Seismic Noise of the Earth's Surface," *Bull. Seism. Soc. Am.*, **49**, 349-353.

Hales, A.L., K.J. Muirhead and J.M.W. Ryan, 1980. "A Compressional Velocity Model for the Upper Mantle," *Tectonophysics*, **63**, 309-348.

Herrin, E., 1982. "The Resolution of Seismic Instruments Used in Treaty Verification Research," *Bull. Seism. Soc. Am.*, **72**, 561-567.

Melton, B.S. 1976. "The Sensitivity and Dynamic Range of Inertial Seismographs," *Rev. Geophys. Space Phys.*, **14**, 93-116.

Oliver, J., and B. Isacks, 1967. "Deep Earthquake Zones, Anamalous Structures in the Upper Mantle, and the Lithosphere," *J. Geophys. Res.* **72**, 4259-4275.

Statistical Analysis of Explosion Magnitudes and Yields

D.W. Rivers, R.H. Shumway, R. Wagner

Summary

Statistical models have been applied to the computation of station corrections for m_b and M_s, the estimation of yields from these magnitudes, and the investigation of TTBT compliance.

Introduction

Although the estimation of explosion yields from observed seismic magnitudes is a standard problem which has been investigated throughout the history of the VELA program, certain questions remain about whether the procedures which are currently used for this purpose are in every case the best ones, and the estimation of the uncertainty which is involved in the process is still the subject of some controversy. The ongoing study described herein is aimed at applying rigorous statistical models to three procedures which are involved in magnitude-yield analysis, namely the determination of seismic magnitudes which are free of biases in the estimated station corrections, the performing of multivariate magnitude-yield regressions for calibration events of known yields, and the use of estimated yields for testing whether there has been compliance with the Threshold Test Ban Treaty (TTBT). Using the statistical models for these procedures gives them a firm theoretical basis and permits measurements of uncertainty to be determined for them.

Magnitude Estimation

One of the most important problems in determining the yield of an explosion is the apparently simple one of obtaining an unbiased seismic magnitude for the event. The first contribution to this question in recent years was due to Ringdal (1976), who showed how a maximum-likelihood technique can be used to estimate the magnitude of an event based on measurements made at a network of stations when the signal from that event is too small to be observed at all stations. Simply ignoring the stations which failed to detect the signal, as had traditionally been done, resulted in an event magnitude which was biased too high. Ringdal showed

that a maximum-likelihood estimator for magnitude substantially reduces that bias. This technique was later extended to include clipped signals as well as undetected signals.

Another important aspect of the problem of determining unbiased magnitudes is that of correcting the measurements for station effects. The traditional method of making this correction is the decomposition of a suite of explosion magnitudes into station and site effects by means of a generalized linear model (GLM). The GLM analysis, however, could not be performed in those cases for which the maximum-likelihood estimator was required to calculate an event magnitude which was not biased by undetected or clipped signals. Applying the GLM without taking into account the data which were censored by the detection and clipping thresholds results once again in biased event magnitudes and hence in unreliable station corrections. Blandford and Shumway (1982) corrected this deficiency by extending the GLM techniques so that explosion magnitudes and station corrections could be estimated simultaneously in spite of individual station data which were missing on account of signal nondetection or clipping. The GLM was extended further by Blandford *et al.* (1983), who considered that the computation of station corrections may be biased by the use of several explosions at the same test site, since the amplitudes of the signals from those events as measured at any given station may not be independent. This problem was addressed by the introduction into the GLM of a correlation structure for the intra-site effects.

The previous studies involving the GLM have been restricted to measurements of the *P*-wave magnitude m_b. In the present study we are applying the GLM technique to measurements of the surface-wave magnitude M_s also. Long-period WWSSN film records have been read for 8 explosions in the NTS, 4 at other sites in the western US, 3 at Amchitka, and 1 each in the eastern US, Semipalatinsk, Azgir, Novaya Zemlya and Algeria. For each record, the Rayleigh-wave amplitude has been measured if the signal could be detected, and the noise level has been measured if no signal was visible. These data will be used to compute M_s values for each event, along with a set of long-period station corrections, via the GLM. The short-period data base of the previous studies has been expanded by reading WWSSN film records for explosions at the French Sahara Test Site. These data will be combined with the measurements made in the previous studies to calculate a new set of m_b values and short-period station corrections.

The GLM statistical model provides a sound framework for estimating the magnitudes, either m_b or M_s, of a suite of explosions. We are in the process of applying it to the long-period data in various manners, such

as restricting the data to those measurements made at certain distance ranges from the events and testing different functional relations for the decay of amplitude with distance. It is of course important that an estimate be made of the uncertainty in the resulting event magnitudes and station corrections. For this purpose, the non-parametric statistical technique of "bootstrapping", *i.e.*, or repeating the analysis using re-sampled subsets of the original data, has been added to the GLM algorithm. We thus have a statistical model which reduces the biases in the estimation of the event magnitudes and permits uncertainty estimates to be made. The application of this model to the long-period data and to the newly measured short-period data is currently being performed.

Yield Estimation

After the magnitudes m_b and/or M_s have been calculated for each of a suite of explosions, the next stage in the analysis is to use those magnitudes to estimate the yields of the events. Thus far in this study our estimation of yields has been based on values of m_b reported by the AEDS network, but this will soon be extended to use the values of m_b and M_s which result from applying the GLM to WWSSN data, as was described in the previous section.

In yield estimation it is conventionally assumed that the P-wave magnitude m_b is a linear function of the logarithm of the yield. We shall restrict the form of this linear function by considering the particular case of explosions detonated in granite, in order to reduce the variability due to differences in m_b due to different source media for the explosions under consideration. We take as our model of the generation of the seismic magnitudes by the n explosions in a common medium at a common test site

$$m_j = \alpha + \beta W_j + e_j + \epsilon_j$$

for $j = 1, \ldots, n$. Here the intercept α is strongly dependent on the test site since it includes the effect of the average of the anelastic attenuation parameters t^* for the paths to the stations in the network. W_j is the log yield of the jth event, and e_j is the estimation error in the magnitude m_j. ϵ_j is an error term which accounts for the variability in coupling among the events. (This variability arises on account of geologic heterogeneity within the test site, even for explosions detonated in the same source medium). We assume that the log yields are known for these events, which are to be used to calibrate the magnitude-yield relation so that it can subsequently be applied to the events of unknown yield. The variables W_j are thus assumed to have Gaussian distributions with known means μ_j (the logarithms of the radiochemical yields) and known variances τ_j^2

(the uncertainties in making the radiochemical measurements.) The magnitude estimation error e_j has zero mean and a known variance σ_j^2 which is inversely proportional to the number of stations detecting the jth event. The coupling error term ϵ has zero mean and a common variance σ_ϵ^2 for all the events. We wish to use the measured magnitudes m_j to estimate the intercept and slope α and β of the magnitude-yield relation, the coupling scatter σ_ϵ, the log yields W_j, the magnitude estimation errors e_j, and the mean square errors of the estimates of W_j.

Our statistical model of the magnitude-yield relation is thus one in which both the magnitude and yield are assumed to be random from the prediction point of view, with the variances of both variables being known quantities. We believe this model to be a more realistic one than a regression which is performed using least squares under the assumption that either the magnitudes or the yields are fixed quantities. We shall estimate the unknown parameters in the model by an iterative approach. As the initial values in the iteration we shall use a guess for σ_ϵ and the values for α and β which result from solving the linear relation by the technique of weighted least squares. The iteration then proceeds to re-estimate the parameters by the method of maximum likelihood. The maximum-likelihood regression is then allowed to continue through as many iterations as are required to obtain convergence.

The statistical model described above considers only a single measurement of the seismic magnitude for each event, m_j. It may easily be extended to consider I such measurements m_{ij} for each event. The I measurements may be considered replications over different stations, whereupon the coefficient α_i would be made to include station effects as well as the intercept of the magnitude-yield relation. We adopt an alternative approach of using the GLM to combine the individual magnitudes measured at each station into a single magnitude averaged over the entire network, which is then used in the magnitude-yield regression. The I replications are then taken to be different types of measurements of the magnitudes m_j. Specifically, we can set $m_{1j} = m_{b,j}$ and $m_{2j} = M_{s,j}$. We can then use both of the magnitudes calculated by this GLM in a unified estimation procedure for the yields. Thus far in this study, however, we have used only m_b values.

Estimation of the yields for the events with unknown radiochemical yields, which is of course the case of practical interest for all explosions except for the calibration events so far considered, can proceed in two ways, one of which may be considered as a limiting case of the other. One method of estimating unknown yields is to make an educated guess about the unknown yield by assigning some value to the mean μ_j of the random variable W_j and allowing its variance τ_j^2 to be large, indicating

that we have little confidence in the value which was assigned to μ_j. We can then perform the maximum-likelihood regression as before, this time using data from both the calibration and unknown events. In the regression the data from the unknown events will carry less weight on account of their larger values of the variance τ_j^2. The maximum likelihood regression will, as before, result in estimates of the log yields W_j^{est} for all events, including the unknowns. It should be noted that the magnitudes for the unknown events would have to be adjusted for differences in the value of α between the test site of the calibration events and that of the unknowns unless the attenuation parameter t^* is believed to be the same for both cases, and a new error term would have to be added to the magnitude-yield relation to account for the coupling scatter within the test site of the unknown events, which would probably be different from the value σ_ϵ for the calibration test site. This procedure is a Bayesian estimator of the yield, since the *a posteriori* estimate W_j^{est} depends not only on the observed magnitudes m_j, but also on the means μ_j and variances τ_j^2 of the *a priori* yield estimates W_j. Since it may be considered undesirable that the estimated yields W_j and particularly the estimated slope and intercept α_0 and β_0 of the magnitude-yield relation be sensitive to yield estimates which are made *a priori*, an alternative approach can be used of simply performing the maximum-likelihood magnitude-yield regression using only the calibration events which have radiochemical yields, and then using the resulting estimates of the slope and intercept of the relation to estimate the yields of the unknown events via the formula

$$W_j^{est} = \frac{m_j - \alpha_0}{\beta_0}$$

Applying this formula is equivalent to including the unknown events in the maximum-likelihood regression but assigning them zero weight by replacing the assumed Gaussian prior distributions of W_j by uniform distributions (or equivalently by retaining the Gaussian priors but making the variances τ_j^2 infinite), in which case the estimator is insensitive to the *a priori* estimates μ_j.

Investigation of TTBT Compliance

When explosion yields have been estimated by the previously described technique, or by any other method, they may then be examined to determine whether they are in compliance with the TTBT threshold of 150 kt. We may use the fact that the estimated yield of the jth event is normal with mean W_j and variance

$$\mathrm{var}(W_j^{est}) = (\sigma_\alpha^2 + 2\sigma_{\alpha\beta} W_j + \sigma_\beta^2 W_j^2 + \sigma_j^2) / \beta_0^2$$

which depends on the true log yield W_j and on the variances and covariance of the slope and intercept of the magnitude-yield relation; these may be obtained from the maximum-likelihood regression, although in this study we have so far used values which were recently obtained by Heasler and Nicholson (1984) from an analysis of individual station and pooled magnitude measurements. In order to derive a 100 $(1-\alpha)$% confidence interval, we substitute the right-hand side of this equation into the denominator of the inequality

$$\frac{|W_j^{est} - W_j|}{\sqrt{\mathrm{var}(W_j^{est})}} \leq Z_{\alpha/2}$$

where $Z_{\alpha/2}$ is the upper $\alpha/2$ percentage point in the normal distribution. (Note that α in this context is not the same variable as the intercept α of the magnitude-yield relation). This substitution results in a quadratic expression for W_j, the two roots of which bound the confidence interval. A possible compliance testing procedure would be to challenge any yield for which the lower bound on the 95% confidence interval was greater than the compliance yield of 150 kt. This procedure works very well for testing one yield at a time but would be difficult to extend to ensembles of events since the estimated yields are highly correlated. This correlation comes about because the estimated yields were all calculated using the same values α_0 and β_0 of the random variables α and β. Even if α_0 and β_0 are regarded as fixed parameters rather than as samples of the random variables (in which case the estimated yields are to be regarded as conditional upon the values α_0 and β_0), the yield estimates will nevertheless be correlated because the variance σ_α^2 of the intercept will still be non-vanishing. This parameter is greater than zero because there is a variance associated with the estimate of the difference in the attenuation parameter t^* between the calibration test site and that of the events with the unknown yields. We thus see that TTBT compliance for an ensemble of events cannot be determined by examining the confidence regions surrounding the yield estimates.

By taking into account the variance-covariance structure of the yield estimates (which is a function of σ_α and σ_j if the parameters α_0 and β_0 are taken to be fixed), it is possible to derive an analytic expression for the probability that each of the yields is less than a 150 kt threshold. On

account of the correlation of the estimated yields, this probability is not equal to the product of the separate probabilities that each yield is individually less than the threshold. Although evaluation of this analytic expression is straightforward, its interpretation as being the probability of TTBT violation is misleading. As σ_α increases, *i.e.*, as the uncertainty in the attenuation correction t^* increases, the calculated probability that the yield of at least one event exceeded the 150 kt threshold (or, for that matter, any greater threshold) increases. This can be seen by considering the fact that for a single event, as σ_α approaches infinity the estimated yield becomes indeterminate, so the probability that it exceeds the 150 kt threshold approaches one half. Even if the yields are actually all in compliance, the computed probability that they are all less than 150 kt will therefore be quite low unless σ_α is very small. The computed probability is thus seen to reflect not so much the compliance situation as our capability of verifying it, and hence it leads to an unacceptable value of the probability of compliance. About the best that can be done with this probability calculation is to show that the probability is small that any event exceeded a threshold which is about two standard deviations ($= \sqrt{\sigma_j^2 + \sigma_\alpha^2/\beta_0}$) greater than the largest estimated yield.

A more satisfactory statistical analysis is a classical test of the null hypothesis that all the yields are less than the 150 kt threshold. We must specify some criterion for rejecting this null hypothesis of TTBT compliance, given the observed magnitudes. We have investigated two such criteria: (1) compliance is rejected if one or more estimated yields exceed some threshold T, and (2) compliance is rejected if two or more estimated yields exceed a different threshold T. It can be shown that neither of these criteria is optimum, but the optimum (*i.e.*, most powerful) criterion given by the Neyman-Pearson lemma leads to intractable computations. The thresholds T will of necessity exceed the 150 kt threshold for compliance, *i.e.*, we cannot reject the hypothesis of compliance with the 150 kt threshold unless one or more of the estimated yields (for one test, or two or more for another test) exceed some significantly higher threshold.

In order to set appropriate values for T for each of the two criteria, we create from the observed data an artificial data set which conforms to the null hypothesis by adjusting the estimated yields so that they are all less than 150 kt. The probability is then computed that the magnitudes which would result from this "compliance" yield distribution would cause the null hypothesis to be rejected for various values of the threshold T. The probability of rejection of the null hypothesis for the "compliance" data set is the false alarm probability, and the thresholds T are then chosen so that this probability attains some suitably low value. Once the thresholds

T have been set, we may construct other artificial data sets for which the yields are all in compliance with the TTBT except for some particular pattern of violation events, say two events with yields of 300 kt. The same probability calculation as was performed before for the false alarm case may now be applied to this "violation" data set. This time, the resulting probability is the signal (*i.e.* violation) detection probability for the particular violation pattern. By changing the yields of the violating events, we may evaluate the power of the hypothesis test by constructing plots of the signal detection probability versus the violating yield(s), all at a fixed false alarm probability. The false alarm and signal detection probabilities are all functions of the integral

$$\text{Prob}\ (W_1^{est} \leq T, \ldots, W_n^{est} \leq T)$$

$$= \int\int \text{Prob}\ (W_1^{est} \leq T, \ldots, W_n^{est} \leq T \mid \alpha,\beta)\, f\,(\alpha,\beta)\, d\alpha d\beta$$

$$= \int\int \prod_{j=1}^{n} \Phi\left[\frac{(\alpha_0 + \beta_0 T) - (\alpha + \beta W_j)}{\sigma_j}\right] f\,(\alpha,\beta)\, d\alpha d\beta$$

evaluated under a fixed yield configuration $W_1, \ldots, W_n$, where $f\,(\alpha,\beta)$ is the joint density of α and β, assumed here to be bivariate normal with means α_0 and β_0 and with variances σ_α^2 and σ_β^2 and covariance $\sigma_{\alpha\beta}$, as was discussed before. In order to apply the hypothesis tests to the observed data, we simply check the observed magnitudes to see whether one or more (or two or more) magnitudes exceed the value which corresponds to the yield threshold T for the chosen false alarm probability. If so, then we reject the null hypothesis that the observed magnitudes were drawn from a population of events all of which have yields of less than 150 kt.

Conclusions and Recommendations

We have developed statistical methodology for seismic magnitude determination, yield estimation, and TTBT compliance testing which is rigorous and which permits the uncertainty in the analysis to be estimated. The investigation is not complete, since it has thus far relied primarily on magnitudes reported by the AEDS network rather than on magnitudes calculated and applied to an expanded data base consisting of more events at as many test sites as possible and a larger network of stations. In particular, it is important that the GLM be applied to the WWSSN and AEDS networks simultaneously in order to derive a consistent set of global station corrections for all these stations.

References

Blandford, R.R., and R.H. Shumway (1982), *Magnitude: Yield for Nuclear Explosions in Granite at the Nevada Test Site and Algeria; Joint Determination with Station Effects and with Data Containing Clipped and Low-Amplitude Signals*, VSC-TR-82-12, Teledyne Geotech, Alexandria, Virginia.

Blandford, R.R., and R.H. Shumway, and R. Wagner (1983), *Magnitude Yield for Nuclear Explosions at Several Test Sites with Allowance for Station Effects, Truncated Data, Amplitude Correlation Between Events Within Test Sites, Absorption, and pP*, VSC-TR-83-15, (in press), Teledyne Geotech, Alexandria, Virginia.

Heasler, P.G. and W.L. Nicholson (1984), *Statistical Analysis of Individual AEDS Station m_b Data (U)*, PNL-X-385, (in press), Pacific Northwest Laboratory, Richland, Washington.

Ringdal, F. (1976), "Maximum Likelihood Estimation of Seismic Magnitude," *Bull. Seism. Soc. Am.* **66**, 789-802.

Focusing Effects on m_b at Small Arrays

E. Smart, J.A. Burnetti, and R. Wagner

Summary

Mechanical waves propagating in an elastic medium are subject to focusing by inhomogeneities in the medium velocity. This effect is analogous to optical focusing in which the velocity inhomogeneity is introduced by a glass lens. One implication of the effect is that focusing bias in the amplitudes of seismic signals from a specified geographical source region, as observed at a given seismological station, can be measured directly from the magnification of the image field. Seismologically, magnification means that computed locations of events in the selected source region will be dispersed over a larger (or smaller) area than are the actual locations.

Introduction

One of the two major causes of large variation in measurements of the body-wave magnitude of a given seismic event, from one seismological observatory to another, is focusing of the seismic waves by lateral variations in the propagation velocity of the earth in the vicinity of the event and also in the vicinity of the observatory. (The other major cause is t^* variation). Diagnosing and correcting for such effects would lead to very considerable improvements in the reliability of estimates of the energy yielded by underground nuclear explosions, which are based on the data of a worldwide network of seismic observatories, by increasing the accuracy of the individual observatory estimates that go into those magnitude determinations. The causal relation between location bias and amplitude bias, both of which are effects of focusing, provides the key to making those corrections. The remarkable insight of this present study is the recognition that amplitude bias due to focusing can be computed directly from location bias. Estimates so made are accurate in a way that previous amplitude bias measurements could not be, since previous estimates were simply of the relative bias with respect to a network mean. Estimates computed from location bias are measurements of the total, absolute amplitude bias due to focusing, and they are made quite independently of network yield determinations and indeed of other amplitude measurements made around the network. Quite unlike previous bias estimates, these would reflect the presence of such phenomena as uniform focusing under a test site, as, for

example, in the case hypothesized in recent studies by Der, *et al.* (1981) to account for the discrepancy in m_b and t^* as measured at NTS. The method is well-adapted to use in a network which possesses several small arrays.

Discussion

The factor responsible for most of the distortion of short-period teleseismic body-wave amplitudes is focusing by local, small-scale inhomogeneities. This effect produces large, systematic variations in the waveforms and amplitudes of teleseismic P waves and is the main cause of scatter in m_b measurements. These variations are functions of the azimuth and distance to the source. The most common range of variation in amplitude across LASA or NORSAR for a given P wave is a factor of three or four, but factors of up to twenty have been observed. Such fluctuations in P-wave amplitudes probably exist at most locations, and constitute the greatest obstacle for the precise determination of small explosion yields. They are most easily observed at array stations, where variation in amplitude across the array as a function of azimuth can be mapped out, and regions within the array that are anomalously high or low with respect to the whole can be identified, as has been done, for example, in the study of Chang and von Seggern (1980). This technique makes receiver focusing visible but it is not effective for revealing focusing effects at the source. Of course, no comparable technique is available for the isolated, one-site seismic station even for receiver focusing.

At present, amplitude correction factors as a function of source region and receiver are estimated empirically by comparing the amplitudes of historic events, as measured at the given receiver, with the amplitudes predicted for it from the corresponding network magnitudes. The correction factor assigned for a given source-receiver path is such that the mean of the receiver magnitude errors for the historic set of events is zero. This approach is not always satisfactory since it requires that for each source region and receiver there be at least one historic event large enough to have been recorded at enough of the stations in the network (*e.g.*, WWSSN) to yield an "unbiased" estimate. ("Unbiased" means that for the given event the mean of the individual station yield estimates is such that the station biases cancel out.) In some cases of interest there are only a few small shots at a given site available in the archives, so that this approach is inapplicable. More significantly, there may be symmetrical focusing under a given test site in which case the network magnitudes themselves will have a systematic bias in them even though the apparent receiver biases are corrected for. The danger here is that the systematic bias may be unsuspected if independent corroborative magnitude estimates are not available.

As it happens there is an alternative and completely independent method for estimating amplitude correction factors which does not depend upon these boot-strap techniques. It is based upon location bias and the fact that location bias and amplitude bias are both manifestations of the same phenomenon, that is, focusing. That method is discussed here.

The optical analogy is convenient to illustrate a simple but important principle of seismology. In optics, two observable effects result from the same lens phenomenon. The refraction of light through a converging lens (1) intensifies the light, and (2) disperses objects in the image field. The converse is true for a diverging lens: the amplitude, or intensity, of light passing through it is diminished, and objects in the field of vision are displaced so as to seem to crowd together. Both effects, the change of intensity and the displacement of images, are produced by the same phenomenon: the refractive bending of ray paths, either convergently or divergently.

These same effects are, of course, present in seismology, but the relation between them, that is, the relation between amplitude anomalies and location anomalies, has been neglected in the seismological literature. Nevertheless, the mapping of the two, in juxtaposition, will readily reveal their interdependence. Moreover, because the location errors (the differences between the locations estimated by an individual seismic station and the corresponding estimates of a global network) can be measured and mapped more precisely than amplitude errors, and because the latter can be predicted from the former, station amplitude corrections as a function of source region can most likely be determined with greater precision and accuracy from a location-error map than can be done directly from estimated amplitude errors.

Therefore, this present study was indicated to demonstrate the interdependence of location and amplitude errors, and to test the hypothesis that station source-region corrections for amplitude, as determined from location errors, are more accurate than those computed from estimated amplitude biases.

A study to demonstrate the interdependence of location and amplitude errors can be made without resort to waveform data, initially. Uncorrected location and amplitude measurements from the bulletin of a given seismic station can be compared to locations and magnitudes for the corresponding events as published in the bulletin of a worldwide network, and the differences plotted on a world map. Amplitude correction factors computed from the degree of convergence or divergence of the location error vectors on the map would then be tested for validity by plotting corrected amplitudes against those predicted from the network magnitudes, or by plotting them against P-coda amplitudes. (Note that much, perhaps most, of the energy in the P coda has not arrived over the direct path from the source to the sensor, but has been scattered to the sensor from over a

wide region surrounding the seismic station. This has been demonstrated with LASA LONGSHOT data in current research at Geotech. Therefore, much of the coda energy has not traveled the narrow path through a possible seismic lens beneath the station, but through a wide cone of diversified rock and thus will be a more unbiased estimator of magnitude than the uncorrected P amplitud. Gupta and Blandford, 1983).

This initial study based on station and network bulletins, of course, applies only to arrays, since event locations are not ordinarily computed from the records of a seismic station with only one sensor site, albeit a 3-component station. But by application of the Smart processor, (Smart and Sproules, 1981), the waveform data of individual, single-site, 3-component seismic stations can be made to yield estimates of signal azimuth and emergence angle of arriving P waves and, thus, estimates of the P source locations. Then similar maps of location and amplitude errors can be constructed for these stations too, and amplitude correction factors estimated and applied to them. Thus the use of location bias for estimating amplitude correction factors is a principle that can be applied both to array data and to single-site, 3-component records as well.

Amplitude correction factors are computed from location error maps in an uncomplicated manner. Straight lines joining the epicenters of the outermost members of a suite of seismic events in a given source region will, of course, form a polygon. The square root of the ratio of the area within the polygon formed by the available global network locations, within a given source region, to that of the corresponding locations of a given receiver station is taken to be the amplitude correction factor for that station and that source region. Of course, in practice greater accuracy and statistical stability can be achieved if instead of using the areas of the polygons one makes the computation for each of the $n(n\text{-}1)(n\text{-}2)/6$ triangles that can be drawn by connecting all the n epicenters with straight lines and taking the square root of the mean of all the area ratios of the resulting triangle pairs.

Observations

In a study of this relation we selected as a seismic data base 6 small suites of large events in Novaya Zemlya, Kazakh, Hindu Kush, southeastern Alaska, the Nevada test site, and Central America. About half of these events are nuclear explosions. We have mapped several of the selected source regions using the NORSAR array bulletin. This contains signal azimuth and velocity across the array as well as P wave maximum amplitude and period so that locations and magnitudes can be recomputed without bias correction.

A significant result is that from measurements of the magnification and the amplitude bias, at NORSAR, of a collection of large (5.5 m_b or greater) Kazakh events. That is a high Q path, and therefore any amplitude bias

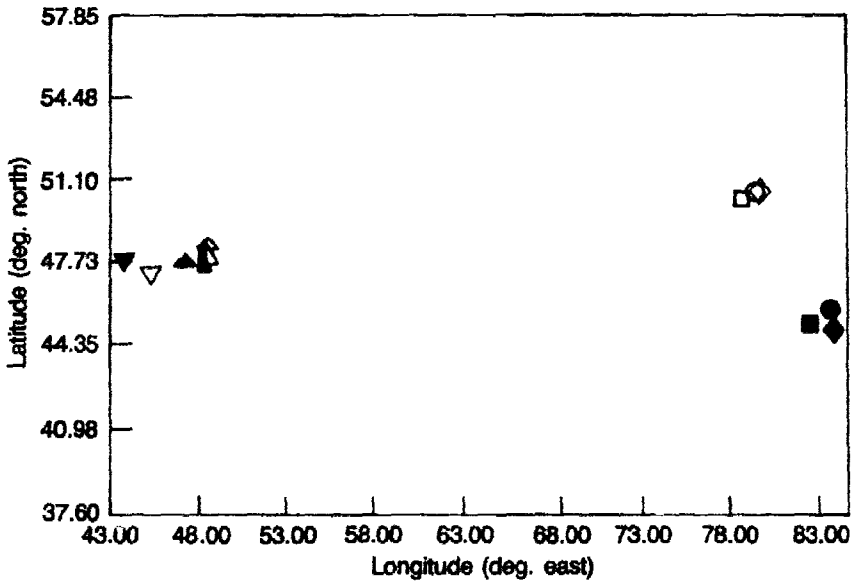

Fig. 1. A map of 6 presumed nuclear underground explosions in Kazakh. The open data points show the locations of the events as computed from network data. The solid data points show the locations of the same events as inferred from NORSAR data.

should be due only to focusing. The measured image magnification is 1.22. That is, distances between Kazakh events, as measured on the map of epicenters inferred from NORSAR data, are on the average 1.22 greater than those measured on the map of network epicenters. The standard deviation is a small 0.02. The measured amplitude bias factor for these events is 1.26, which is close to the image magnification. But the standard deviation is large. The amplitude bias estimate is derived from the average difference in magnitude between the array and the network, since it is the magnitudes, not the amplitudes, which are normally distributed (Freedman, 1967, and von Seggern, 1973). The magnitude bias is 0.10, with standard deviation 0.30. The base 10 raised to 0.10 gives the amplitude bias factor of 1.26. But the magnitude standard deviation of 0.30 translates into a 90% confidence interval, for the amplitude bias factor, which is very broad, *i.e.*, from 0.6 to 2.5. This confirms only the sense and order of magnitude of the bias measured rather precisely from image magnification. Since magnitudes in general have such broad distribution it may be that that is all that can be expected in this present study, that is, confirmation of agreement in the sense and order of magnitude between image magnification and amplitude bias. Some alternative methods of magnitude determination,

such as that described by Gupta (1983), measuring magnitude in the signal P coda, appear to have narrower distributions and may be proven to be more suitable tools in a study of this sort.

Conclusions and Recommendations

This present study is still in its initial phases, but it is already apparent that estimates of the magnification due to focusing made from location bias may be markedly more precise than those made from amplitude bias. It may be that measurements of amplitude bias will only be precise enough to confirm the sense and order of magnitude of magnification as measured by location bias. However, if, in a significant number of cases of station-source region pairs in which the travel path is a high Q path (essentially no attenuation), the relative amplitude bias determined from station-network magnitude differences does confirm, if only in sense and magnitude, the amplitude bias as inferred from location bias, then amplitude correction factors from location bias, which are much more precise, will be used with confidence in place of the relative correction for whatever path. This would be significant not only for improving magnitude-yield estimates, but also for improving attenuation measurements by clearly separating attenuation amplitude bias from that due to focusing.

If these initial positive correlations (of location bias with amplitude bias) persist through the completion of our present study, then a systematic evaluation of magnification at areas of interest, as seen from array and 3-component stations, is required to map amplitude-bias due to focusing worldwide. This knowledge will not only refine magnitude determinations by its direct application, but will also make it possible to separate amplitude bias due to attenuation from that due to focusing, and thus refine attenuation measurements which must at present necessarily (and erroneously) include effects of focusing.

References

1. Chang, A.C. and D.H. von Seggern (1980), "A Study of Amplitude Anomaly and M_b Bias at LASA Subarrays," *J. Geophys. Res.* **85**, pp 4811-4828.
2. Der, Z.A., T.W. McElfresh, and Anne O'Donnell (1981), "Results of the SDCS (Special Data Collection System) Attenuation Experiment," *SDAC-TR-80-4 (VSC- TR-81-14).* Teledyne Geotech, Alexandria, Virginia.
3. Freedman, H.W. (1967), "Estimating Earthquake Magnitude," *Bull. Seism. Soc. Am.* **57**, pp 747-760.
4. Gupta, I. and R.R. Blandford (1983), "Spectral Analysis of Teleseismic P and P-coda at NORSAR," Vela Seismological Center conference, 28 September, 1983, Alexandria, Virginia.
5. Herrin, E. and W. Tucker (1972), *On the Estimation of Bodywave Magnitude*, Technical Report to AFOSR, October 1972, Dallas Geophysics Laboratory, Southern Methodist University, Dallas, Texas.

6. Ringdal, F. (1976), "Maximum-Likelihood Estimation of Seismic Magnitude," *Bull. Seism. Soc. Am.* **66**, pp 789-802.
7. Smart, E. and E. Sproules (1981), "Regional Phase Processors," *SDAC-TR-81-1 (VSC-TR-81-19)*, Teledyne Geotech, Alexandria, Virginia.
8. von Seggern, D. (1973), "Joint Magnitude Determination and the Analysis of Variance for Explosion Magnitude Estimates," *Bull. Seism. Soc. Am.* **63**, pp 827- 845.

Regional Detection, Location, Discrimination and Yield Determination

Robert Blandford

I. Introduction

Blandford (1981) and Pomeroy, Best, and McEvilly (1982) have recently published reviews of detection, location, and discrimination using regional data. In this review I shall only give a brief overview of the subject covered in those papers and shall concentrate on papers and reports which have recently appeared. Subjects to be discussed include high-frequency earth noise, absorption, and decoupling; comparative P spectra for earthquakes and explosions; discrimination using P_{max}/L_g amplitude ratios and L_g spectral shapes; and recent theoretical studies which appear to offer explanations for some of the observations. In addition I shall briefly mention studies appearing in this volume which seem naturally to extend the work which has gone before. These last remarks cannot, naturally, be very complete because the studies have just appeared.

II. Outline of Recent Reviews

Blandford (1981) discussed the qualitative features of regional phases by means of a detailed examination of signals from SALMON and the 18 February 1964 Alabama earthquake as recorded at a string of LRSM stations up the Appalachians. He concluded that the P wave spectra from the two events were indistinguishable, and that the L_g spectrum was of substantially lower frequency than the P wave spectrum which, except for absorption, faithfully reflected the source spectral shape. The transverse L_g from the earthquake had a sharper, lower frequency start than did that from SALMON. The L_g spectrum was also of lower frequency than the spectrum of the P_g coda which just preceded the L_g arrival time, and the spectrum appeared to "plunge into" the P_g coda spectrum near 2-3 Hz.

These spectral features were also noted to be characteristic of a USSR explosion recorded at NORSAR from a distance of about 12 degrees. Topics of phase and group velocity of regional phases as seen at arrays were discussed, along with questions of array design.

P_{max}/L_g as a discriminant was also discussed, together with some information suggesting that 30 Hz signals could be seen at a distance of 3 degrees on the Canadian Shield. Studies of amplitude distance for P_g and L_g were reviewed showing that P_g falls off more rapidly than L_g in the eastern United States (EUS), $r^{-2.5}$ for P_g and r^{-2} for L_g. It was also shown that these formulas were approximately the same as found within the USSR.

Pomeroy, Best, and McEvilly covered some of the same topics as above, and also discussed the many observations giving gamma and Q estimates for the regional phases, especially L_g. They discussed various efforts for determining depth from use of regional phases in location programs. They gave a comprehensive discussion of many regional discriminants which have been proposed in the literature and conclude with a list of discriminants ordered by degree of promise.

"1. The most promising discriminants appear to be

   a. regional variant of the M_s:m_b criterion
   b. the excitation of short-period *SH* waves
   c. generation of higher mode surface waves
   d. long-period surface-wave energy density
   e. spectral ratios in P_g and L_g
   f. arguably, L_g/P amplitude ratios

2. Proposed discriminants requiring additional documentation include

   a. L_g/R_g amplitude ratios
   b. excitation of S_n
   c. third moment of frequency
   d. long-period *S*-to-Rayleigh wave amplitudes
   e. arguably, the spectral ratio of long-period Love to long-period Rayleigh waves

3. Proposed discriminants which probably should be abandoned include

   a. first motion
   b. *P*2/*P*1 ratio
   c. L_g group velocity and energy ratios
   d. prevailing period of long-period Love waves."

III. Implications of Low-Amplitude High Frequency Noise

In the same issue of the Bulletin of the Seismological Society of America in which appear the Pomeroy, Best, and McEvilly review paper also appeared a paper by G. Herrin giving the noise spectrum shown in Fig. 1. We see here a high-frequency amplitude noise spectrum spectacularly lower than that observed previously at such quiet sites as Queen Creek Arizona. In Fig. 2 we see that many seismometers currently deployed have system noise well above the earth noise at such quiet stations. Recent studies at NORSAR have confirmed these low values.

These observations raise the question of whether it is possible to detect signals at very high frequencies at these stations. Obviously in

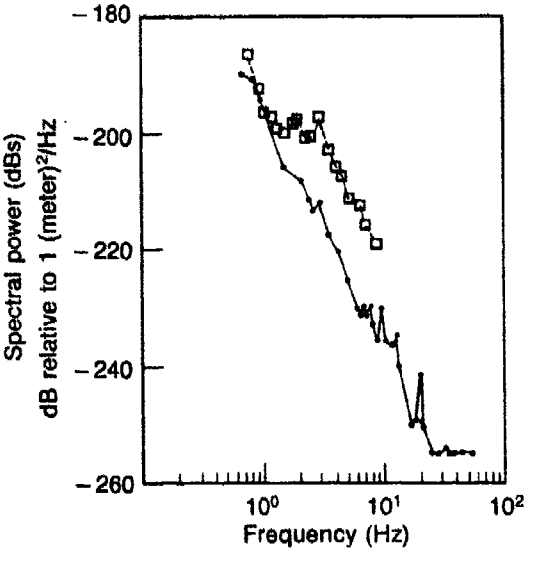

Fig. 1. Spectra of Lajitas background noise (•) and Queen Creek noise (□).

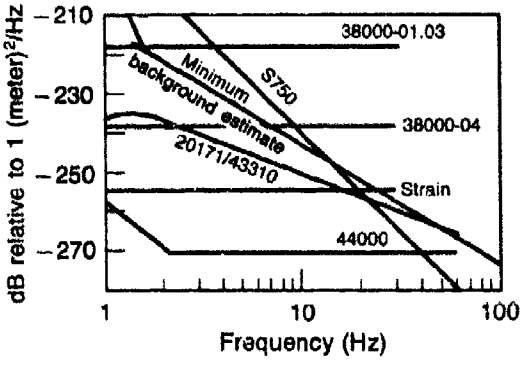

Fig. 2. Limiting displacement resolution of a number of systems based on the calculated self-noise levels (calculations by O. D. Starkey, 1982).

this case the question of signal absorption is crucial. Probably it would be worthwhile to separate the problem into two cases, phases which are confined to the crust, such as P_g and L_g; and phases which penetrate to the mantle P_n and S_n.

Figure 3 shows a map of stations which recorded the event SALMON. Figure 4 shows the P wave signals at these stations, and Fig. 5 shows the reduced displacement potential measurements for SALMON. Using the indicated average of these measurements to give a source spectrum Der *et al.* (1976) obtained the ratio of P wave spectrum to source spectrum indicated in Fig. 6. These give t^* values ranging from 0.0 at BLWV in West Virginia to 0.7 at KNUT in Utah.

A summary of measurement of this type is given by Fig. 7 which shows that for shield-to-shield paths t^* increases from 0.0 at 0 degrees

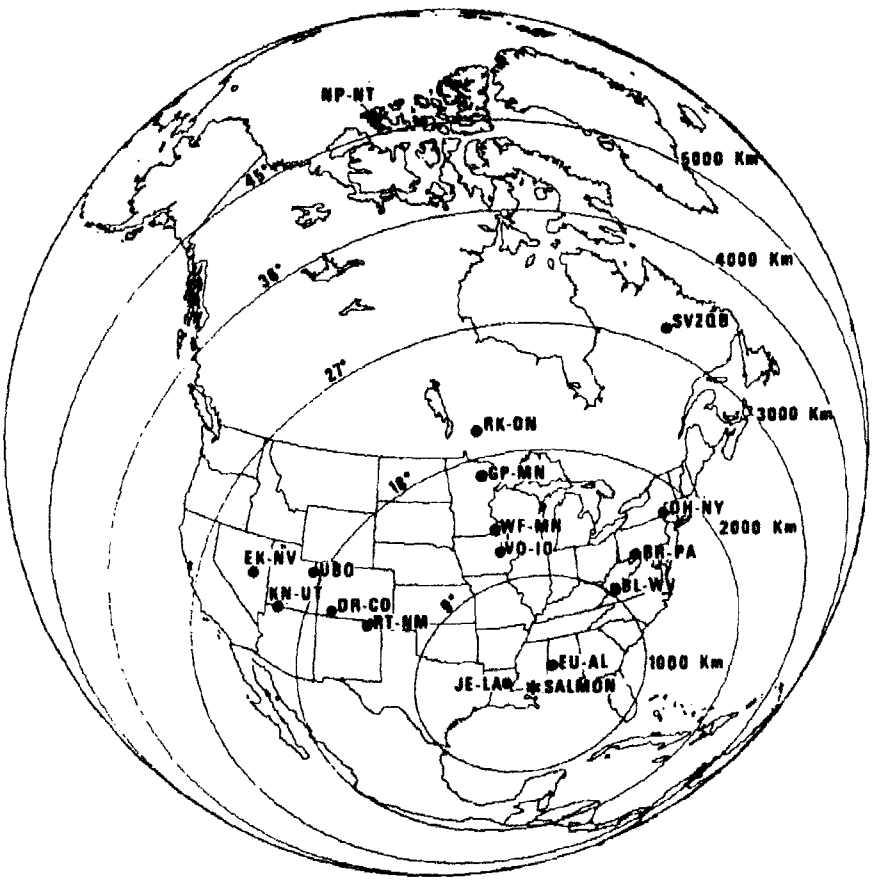

Fig. 3. Location of SALMON and stations used in the study.

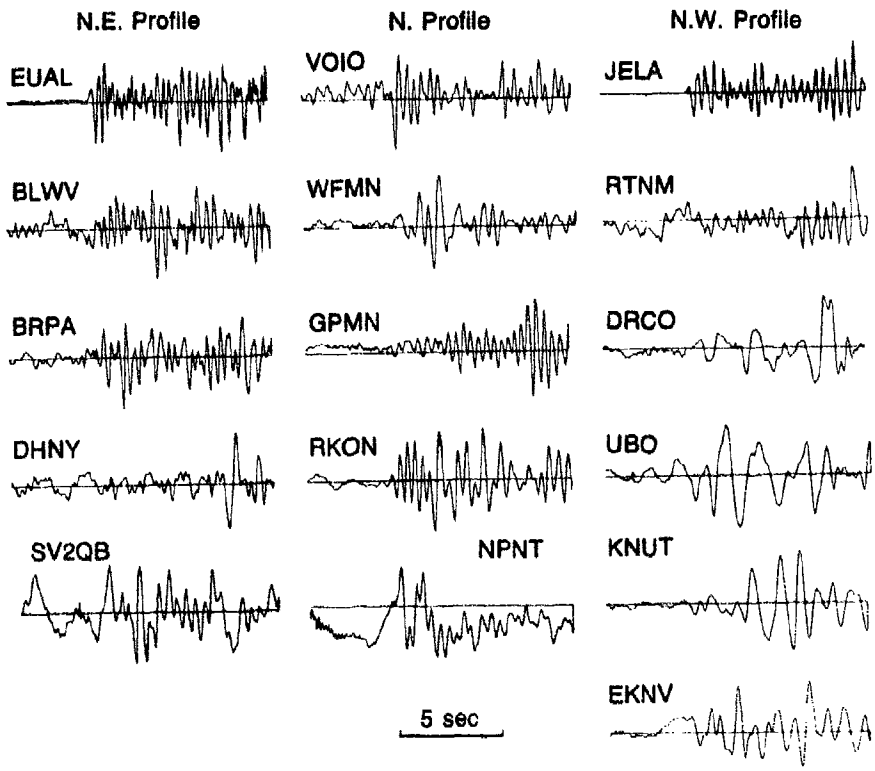

Fig. 4. *P*-wave seismograms used.

to perhaps 0.1 at 12 degrees and to 0.2 at 20 degrees. For WUS-to-shield paths t^* increases to perhaps 0.5 by 20 degrees. These values of t^* were determined by spectral ratios out to approximately 4 Hz, and as such offer a convenient method of computing the signal amplitude at frequencies up to 4 Hz. In this volume T. Bache presented spectral ratios of P waves for several teleseismic shield to shield paths which range up to 8 Hz and give t^* values typically equal to 0.15. These are, perhaps,

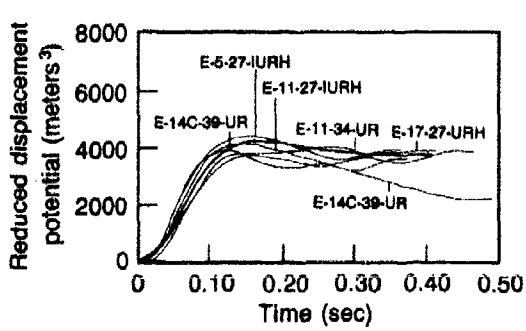

Fig. 5. Reduced displacement potentials for SALMON as given by Patterson at various close-in observing stations and the reduced displacement potentials used to derive the close-in source spectrum.

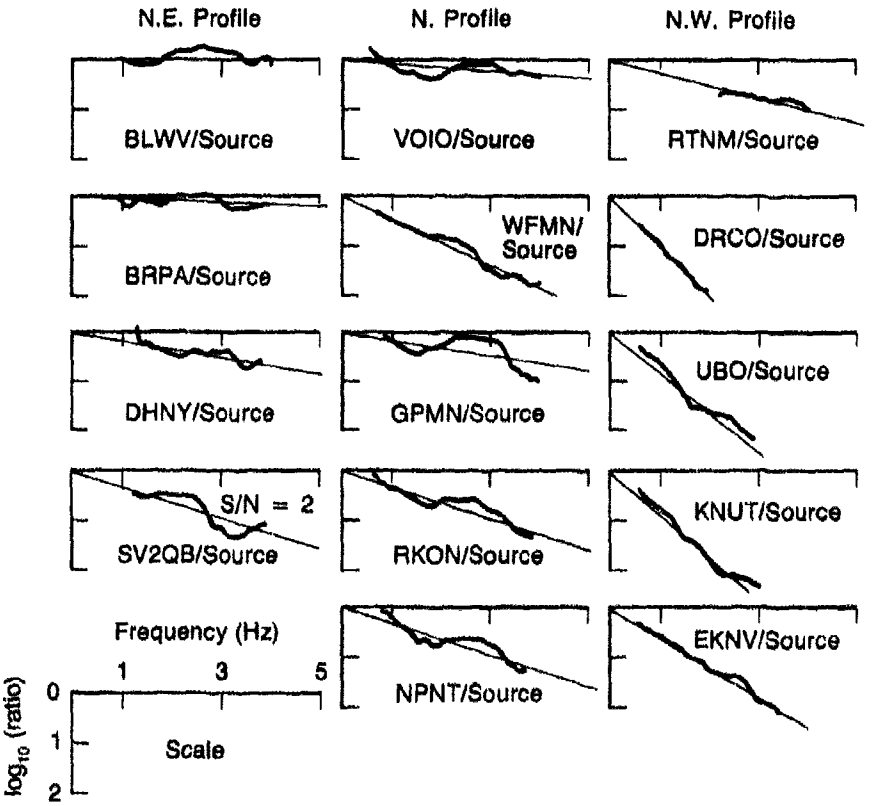

Fig. 6. Ratios of *P*-wave amplitude spectra at the individual stations to the source spectrum directly derived from the displacement potential.

not significantly different from those found in Fig. 7, so we may imagine that at regional distances the corresponding lower values for t^* seen in Fig. 7 will hold for those paths also.

The most important application of high frequency propagation is probably in the detection of decoupled nuclear explosions. The only data available on this subject is that from the SALMON-STERLING nuclear explosion experiment. Figure 8 shows the SALMON *P* wave signal and amplitude spectrum as recorded at station PLMS at a distance of approximately 30 km. Figure 9 shows the STERLING signal and spectrum with the SALMON spectrum superimposed after having been divided by 1000. We see that the spectral ratio varies from 1000 at 1 Hz to approximately 17 at 20 Hz. Scaling of SALMON to STERLING yield by cube-root scaling gives a factor of 70 decoupling at low frequencies, declining to a factor of 7 at high frequencies. These plots are from Blandford and Woolson

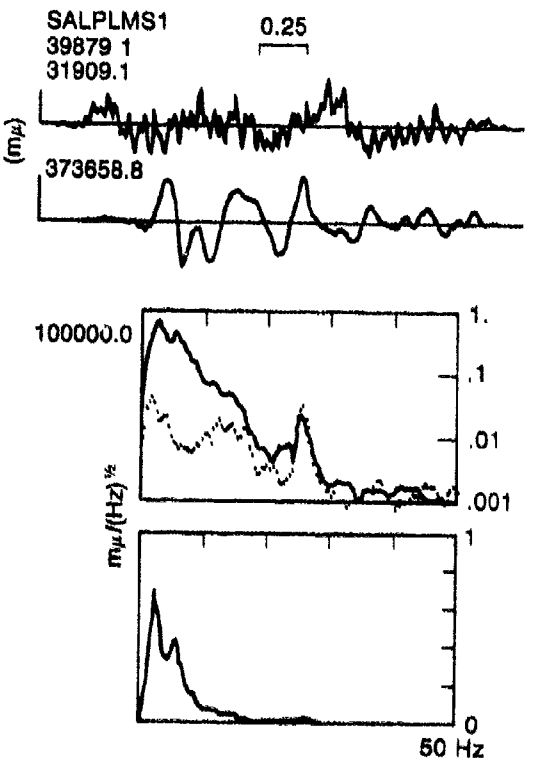

Fig. 7. Upper trace is noise in front of signal, lower trace is signal. Units of millimicrons at 1.0 Hz. Data sampled at 100 sps. Upper spectrum is square root of power spectrum with units millimicrons/(Hz)$^{1/2}$. Solid line is signals, dashed line is noise. Lower spectrum is the same except with a linear rather than logarithmic vertical scale, and without the noise spectrum.

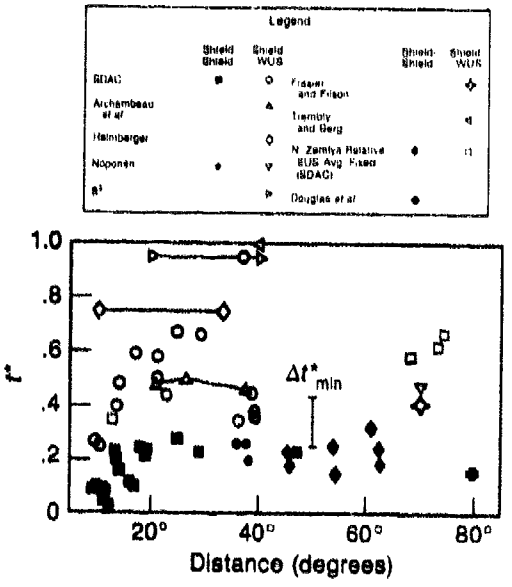

Fig. 8. t^* values *versus* distance. Δt^*_{min} is the t^* differential needed to explain the magnitude differential 0.25 at 1 Hz. Hollow symbols involve paths crossing the mantle under the WUS; the rest of the symbols denote t^* values derived from pure shield (stable platform) type paths.

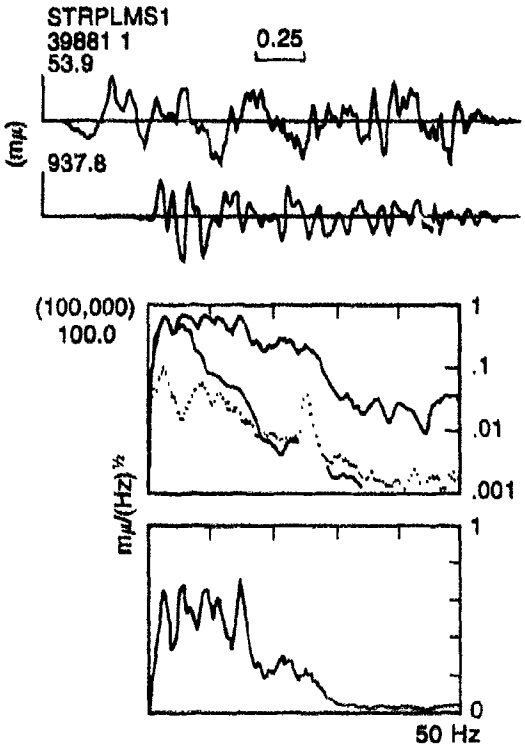

Fig. 9. Upper trace is noise in front of signal, lower trace is signal. Units of millimicrons at 1.0 Hz. Data sampled at 100 sps. Upper spectrum is square root of power spectrum with units millimicrons/(Hz)$^{1/2}$. Solid line is signals, dashed line is noise. Lower spectrum is the same except with a linear rather than logarithmic vertical scale, and without the noise spectrum channel 1. The maximum amplitude in parentheses is appropriate for the SALMON spectrum.

(1979) and give a smaller decoupling ratio at high frequencies than earlier studies for two reasons. First, only the *P* waves were included in the spectral ratio; Blandford and Woolson show that the later phases were better decoupled. Secondly, earlier spectral ratios were contaminated by system noise in the SALMON spectrum leading to an overestimate of decoupling at high frequencies. It is noteworthy in this regard that, as can be seen by comparing Figs. 8 and 9 that the noise problem occurred for SALMON and not for STERLING even though the SALMON signal at low frequencies was 1000 times larger, and at high frequencies 17 times larger. This shows the importance of proper prewhitening in signal acquisition. The lower corner frequency of SALMON would have required that the recording system be peaked at higher frequencies than for STERLING. Had this been done we would have decoupling data for several stations out to 50 Hz instead of data out to 20 Hz at one station.

The result of this refined analysis may be seen best, perhaps, in Fig. 10, from Springer *et al.* (1968). The dashed line, emerging from the original heavy line, shows the changed high frequency spectral ratio determined by Blandford and Woolson. We see that this ratio does not appear to fit in naturally with the theoretical spectral ratios determined

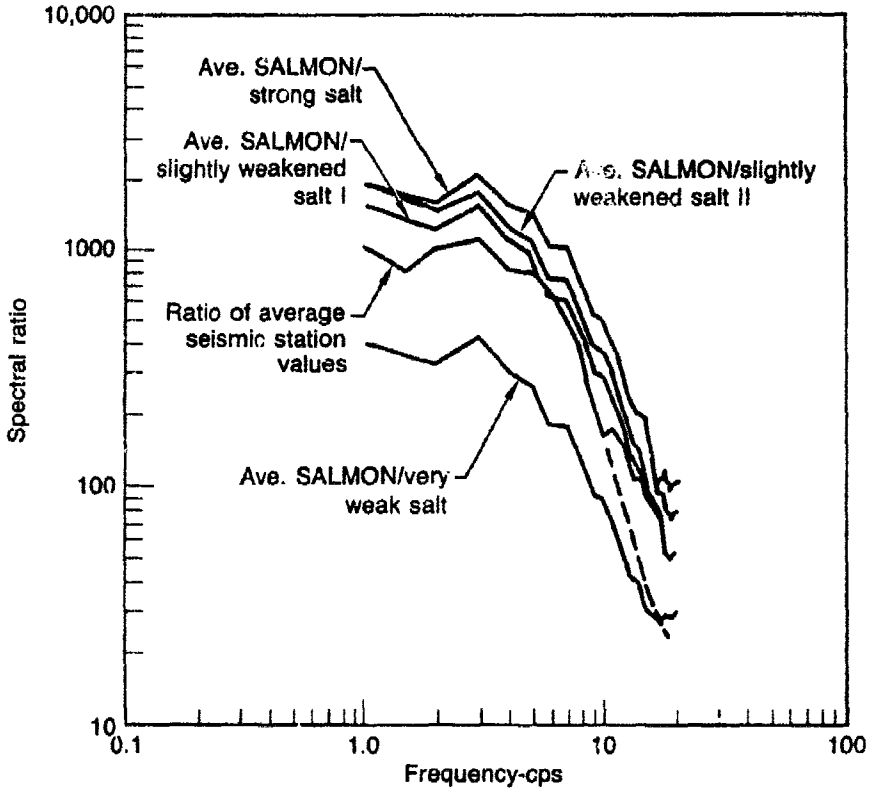

Fig. 10. Theoretical spectral ratios for SALMON/STERLING from Patterson (1966) together with the observed spectral ratios plotted by Springer *et al.* (1968).

by Patterson (1966), it has too little high frequency decoup r th low frequency level. It is as if the salt were weaker at high fr cies than at low frequencies. Although these are the only available experi l data on nuclear explosion decoupling, it should be remembered that t y are from a cavity created by a nuclear explosion. This may have weakened the salt. An explosion in mined cavity may well offer better dec pling, perhaps much like that in the upper curve in Fig. 10. Once again, however, we must remember that our knowledge of the relevant material properties at high strains is very poor. Prudence might dictate relying on the experimental data until data from a mined cavity is known to be available. It is obviously important that any remaining data from the SALMON/STERLING experiment be analyzed to verify this high frequency limit.

Thus we have the three elements needed to calculate the detectability of decoupled explosions at high frequencies, the noise level, the signal

absorption, and the decoupling ratio. Also obviously there are weaknesses in each data set. The universality of these low noise levels needs to be investigated; as is the kind of array needed to improve the S/N ratio. There is not enough data on the question of whether t^* decreases with frequency at these high frequencies; and we have not touched on the t^* or Q values for regional phases, a subject which we will discuss further in the section below on theoretical calculations of regional phases. Finally the decoupling ratio as a function of frequency needs further investigation both theoretically and via further analysis of SALMON/STERLING data; and possibly via cooperative experiments with other countries.

III. Recent Experimental Analyses

Figure 11, from Werth *et al.* (1963), illustrates the importance of scattering in regional phases. We see that the ratio of transverse to radial and vertical amplitudes from SALMON increases from approximately 1:10 at 0.5 km to 1:1 at 30 km. These observations were made at a frequency of approximately 5 Hz.

Figure 12 shows stations which recorded both SALMON and an Alabama earthquake of 18 February 1964. We see that station EUAL

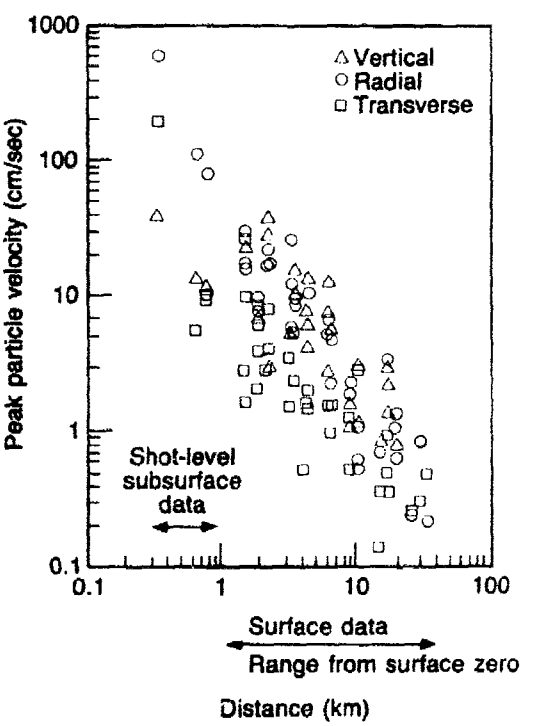

Fig. 11. Peak particle velocity *versus* distance for the vertical, radial, and transverse components of motion due to SALMON. Note that for shot-level subsurface data, vertical motion is also "transverse" to the source-receiver direction.

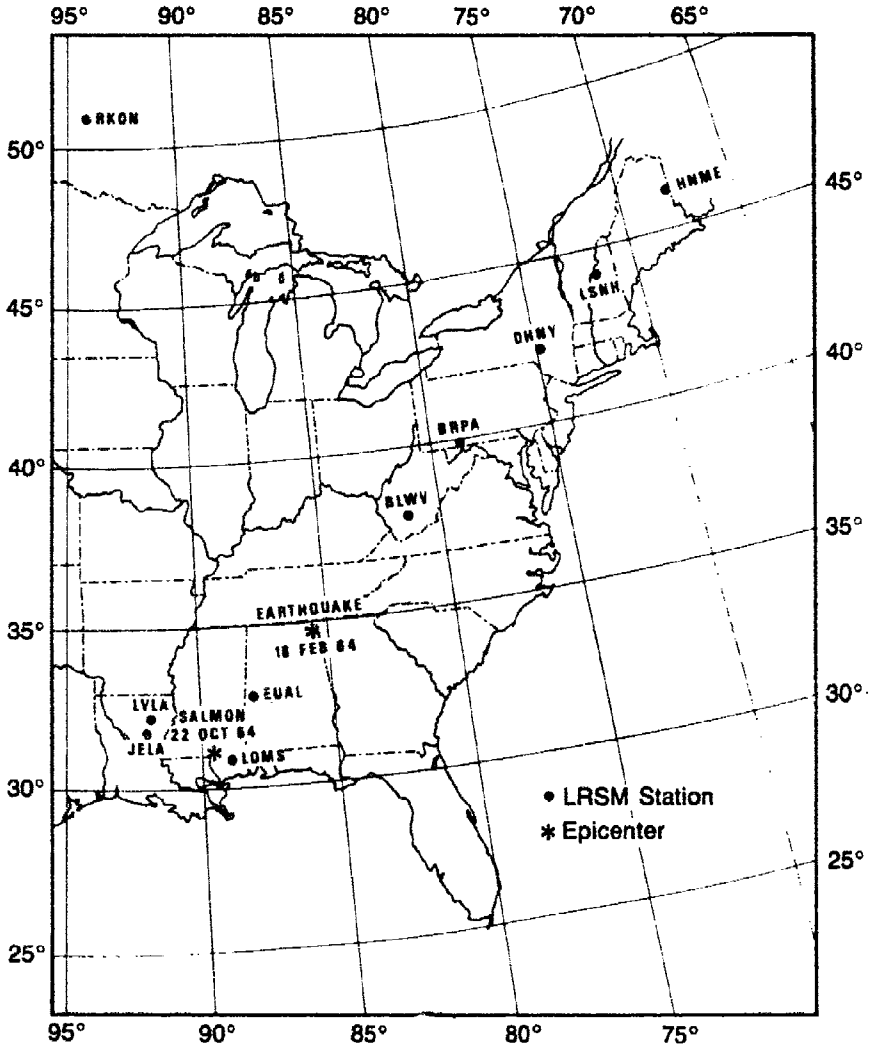

Fig. 12. Epicenters of the 18 February 1964 earthquake and SALMON (22 October 1964), and locations of some LRSM stations in the EUS.

is approximately equidistant from the two events. In Fig. 13 we see the P wave spectrum of the two events, we see that there is no discernable difference between the two, and Blandford *et al.* (198) show that this is true also for the other high-Q paths. On the other hand Fig. 14 shows that the L_g spectra are quite different — the explosion has the lower frequency L_g. Gupta and Blandford (1983) suggest that this is due to the fact that L_g is composed of shear waves which must have been created

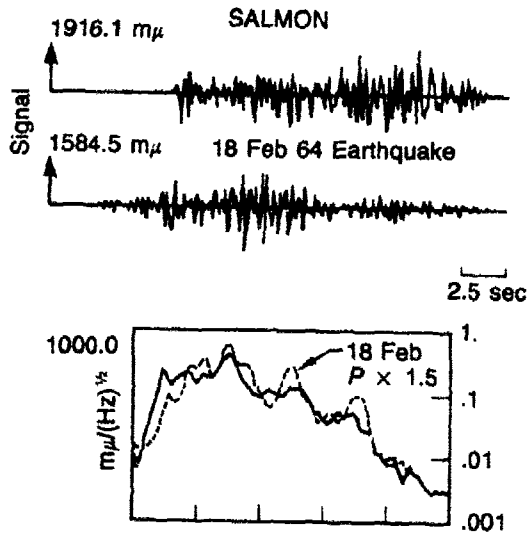

Fig. 13. Similar to Figure 8 but for the compressional wave arrivals (25.6-sec windows) and the earthquake spectral amplitudes multiplied by a factor of 1.5 (from Blandford *et al.*, 1981).

from P waves; and that the conversion is more efficient at lower frequencies than at high frequencies. Gupta and Blandford also show that if SH amplitudes are equal to SV amplitudes in L_g, then the effect of the free surface is to make the transverse component have twice the amplitude of SV.

Murphy and Bennett (1982), and Murphy, Bennett and Tzeng (1981) made similar observations. Figure 15 gives their comparison of SALMON and the Alabama earthquake at JELA and EUAL, which are at approximately equal distances. The spectra are seen to be roughly equal although

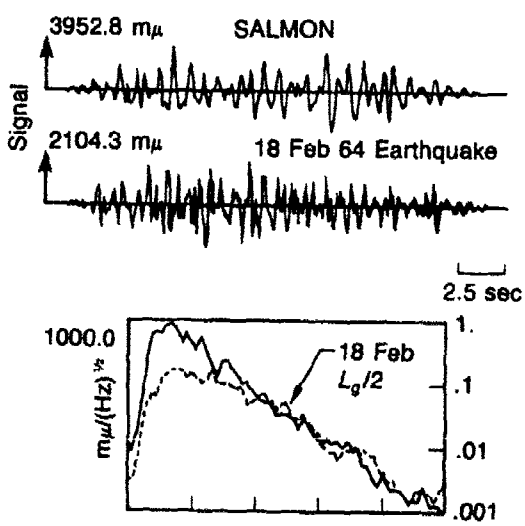

Fig. 14. Vertical-component EUAL records of L_g wave train (25.6-sec windows) from SALMON and the 18 February 1964 earthquake. The lower section shows the displacement spectra (corrected for instrument response only at 1 Hz) for the two signals with the earthquake spectral amplitudes divided by 2.0 (from Blandford *et al.*, 1981).

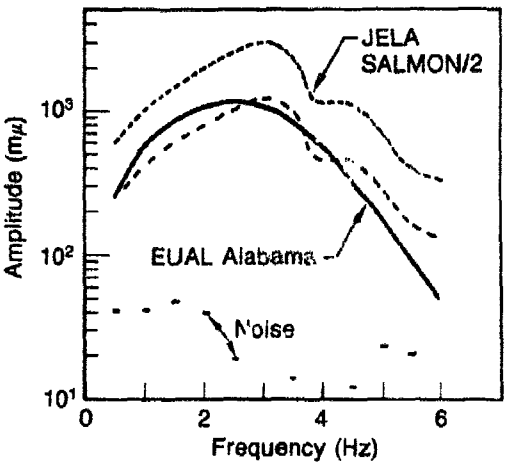

Fig. 15. Narrow band filter generated P_n spectra at EUAL and JELA for the Alabama earthquake and the SALMON explosion.

there is some suggestion that the explosion has higher frequency. This could be due to a site effect since the stations are different.

Murphy and Bennett also analyzed the P wave spectra at TFO from NTS explosions and from earthquakes surrounding NTS as seen in Fig. 16. Figure 17 shows that the average spectra are nearly identical. This analysis may be criticized on the grounds that most of the explosions are in unconsolidated alluvium and so their corner frequencies may be lower than might be the case in a true test ban situation where hard rock would be required to avoid generation of collapse craters. Also the average explosion magnitude is perhaps 0.7 m_b units higher than the average earthquake, perhaps this also leads to a bias, the data should be reanalyzed

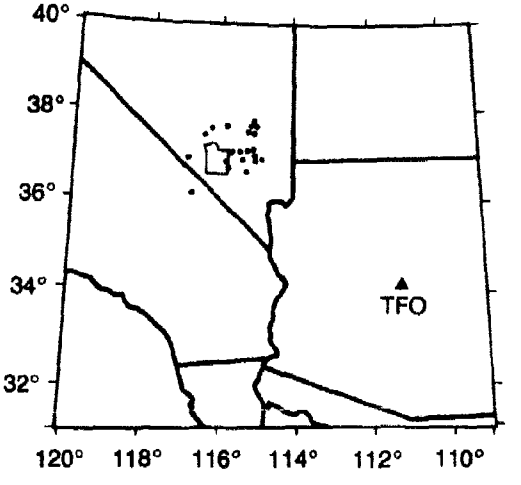

Fig. 16. Earthquake sample from the vicinity of NTS with regional phases recorded at TFO. Circles indicate epicenters; triangle is the station location.

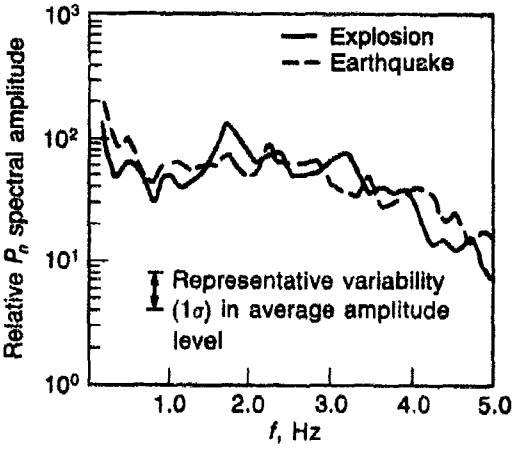

Fig. 17. Comparison of average earthquake and explosion P_n spectra ($3.7 \leq m_b \leq 4.3$) derived from NTS events recorded at TFO.

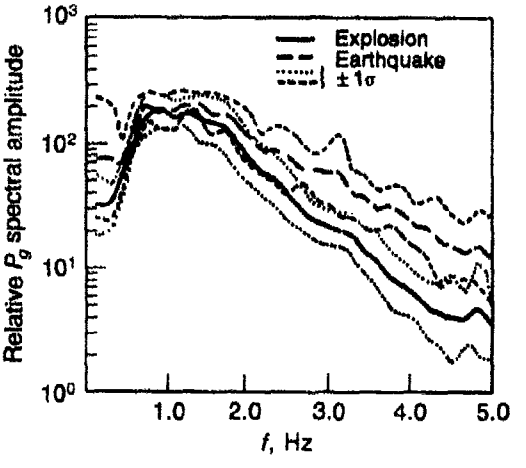

Fig. 18. Comparison of average earthquake and explosion P_g spectra ($3.7 \leq m_b \leq 4.3$) derived from NTS events recorded at TFO.

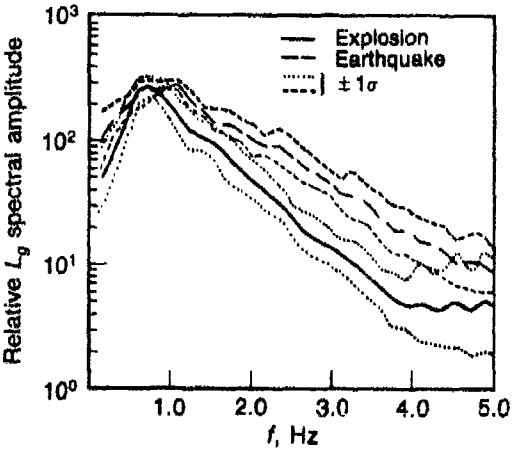

Fig. 19. Comparison of average earthquake and explosion L_g spectra ($3.7 \leq m_b \leq 4.3$) derived from NTS events recorded at TFO.

using only those events which overlap in magnitude. However, the agreement of this result with that of SALMON and the Alabama earthquake is striking. These two data sets are about as well controlled for path and source effects as any in the literature, and they show nearly identical P wave spectra, suggesting that short period P wave discriminants would not be useful.

Although the P-wave spectra seem provisionally identical, the same is not true for other regional phases, as we have seen already for the SALMON/Alabama L_g phases. Figure 18 shows that the average earthquake L_g spectrum (NTS to TFO), according to Murphy and Bennett, is higher frequency than the average explosion spectrum. Figure 19 shows that the same is true of L_g. For L_g this difference may be exploited to form a discriminant, Fig. 20 shows only a one-event overlap near magnitude 4.3. This is the Massachusetts Mountain earthquake which occurred at NTS. (As a side issue, note that there is no apparent trend of the spectral ratio with frequency, suggesting that corner frequency effects are not significant.) Even this event may be well discriminated at another station, examination of the broadband signals in Fig. 21 shows that the S_n from the earthquake is of higher frequency than the S_n from the explosion.

Murphy and Bennett also calculated theoretical L_g spectra in an attempt to understand this phenomenon, but as Fig. 22 reveals, for point step sources in a Basin and Range structure, there is no apparent spectral difference between a dilatation source at 200 meters and a double-couple source at 4 km.

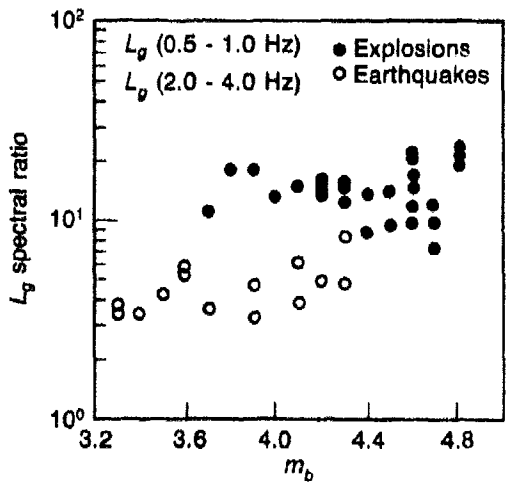

Fig. 20. Comparison of vertical-component L_g spectral ratio discriminant (ratio of average amplitude levels in 0.5 to 1.0 Hz and 2.0 to 4.0 Hz passbands) for NTS explosions and earthquakes ($3.3 \leq m_b \leq 4.8$).

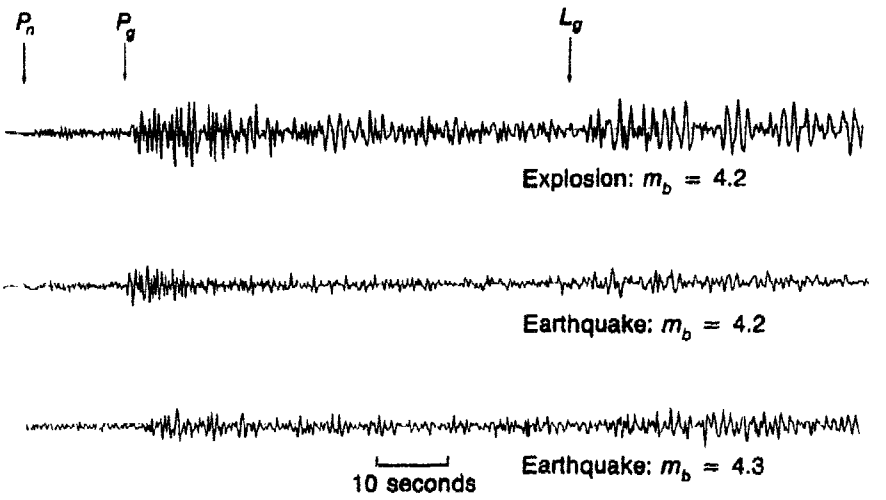

Fig. 21. Comparison of vertical-component seismograms recorded at TFO from an explosion and two nearby earthquakes of about the same magnitude.

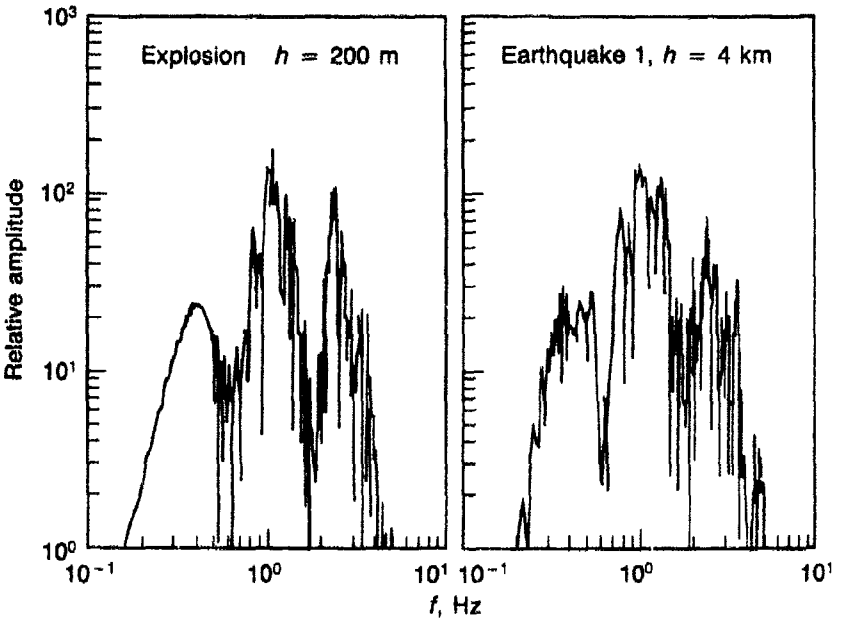

Fig. 22. Comparison of theoretical L_g spectra from a shallow explosion (left) and an earthquake (right) with a focal depth of 4 km.

Murphy and Bennett also examine the possibility that a simple amplitude ratio of L_g to P can serve as a discriminant for these events. Figure 23 shows that at a single station the discriminant performs poorly.

However, poor single station performance can also be found to be the case for the classical M_s:m_b discriminant at regional distances in the WUS. Figure 24 shows single station M_s:P_n discrimination at MINA and KANAB as reported by Peppin and McEvilly (1974). For the earthquakes the separation seems quite good although at KANAB there is some suggesting of earthquake convergence. However, Fig. 25 from Lambert *et*

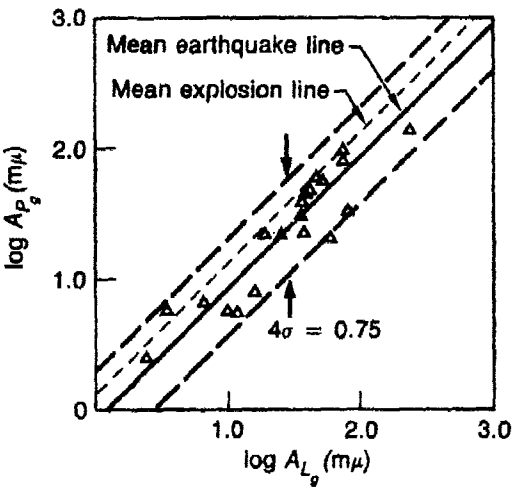

Fig. 23. Comparison of P_g and L_g amplitudes recorded at TFO from earthquakes near NTS. Triangles indicate data points and the solid line is a regression line through the data.

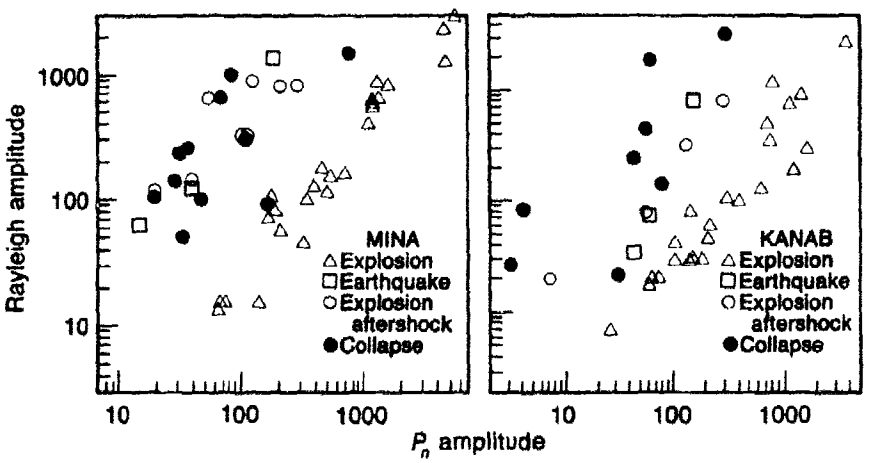

Fig. 24. Long-period Rayleigh wave amplitude *versus* short-period P_n amplitude for an NTS explosion and earthquake sample recorded at MINA and KANAB (after Peppin and McEvilly, 1974).

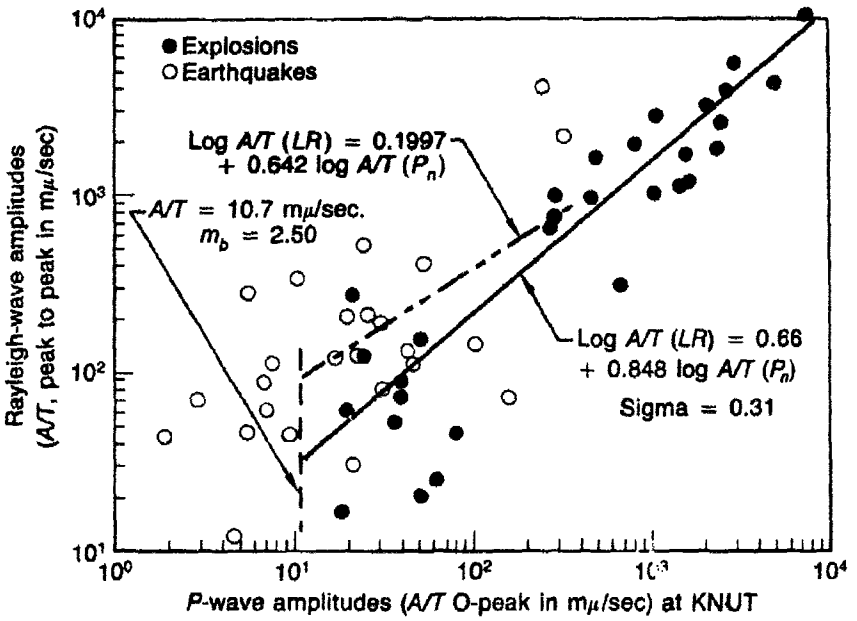

Fig. 25. Rayleigh and P_n-wave amplitudes at KNUT for Nevada earthquakes and explosions.

al. shows greater overlap at the same station in the same magnitude range, as does Fig. 26 from Murphy, Bennett and Tzeng. If this overlap is accurate then the good performance of teleseismic M_s:m_b as a discriminant for WUS earthquakes may well be the result of network averaging; and so network averaging may also help the L_g:P discriminant. However, it is important to have a discriminant which will work well at a single station because in analysis of decoupled explosions it is possible that there will be only 1 or 2 stations with good data.

Since P_g and L_g generally are more easily detected in the WUS than is P_n, Murphy, Bennett and Tzeng plotted these phase amplitudes *versus* L_R amplitude, as can be seen in Figs. 27 and 28. In general the separation is better although still far from perfect.

In this volume Murphy and Bennett present new results which in general terms confirm their earlier results, as discussed above, with more data.

V. Theory

Bache *et al.* (1981) performed extensive calculations of L_g waves by means of modal superposition. One of the most interesting results

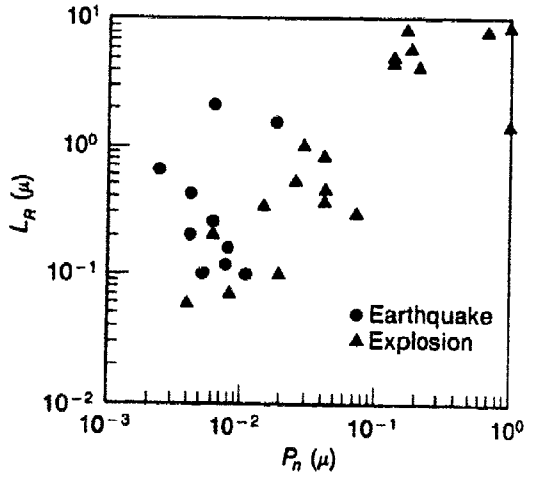

Fig. 26. Amplitudes of long-period Rayleigh wave pulses *versus* short-period P_n for NTS explosions and earthquakes.

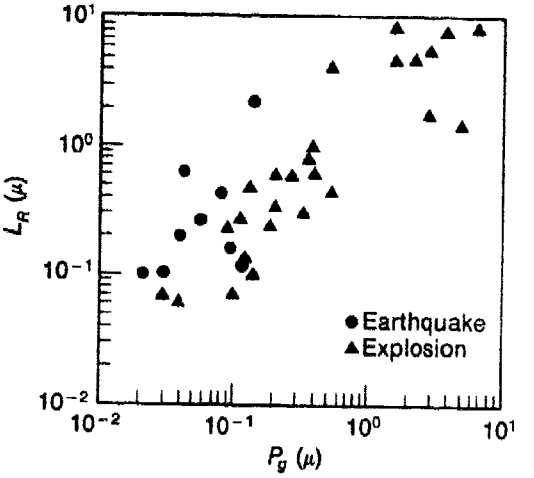

Fig. 27. Amplitudes of long-period Rayleigh wave pulses *versus* short-period P_g for NTS explosions and earthquakes.

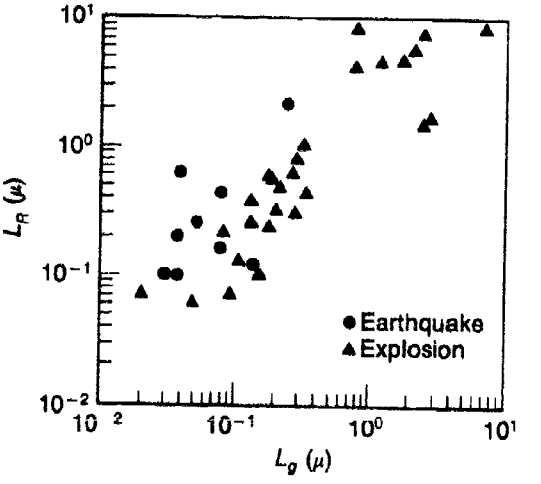

Fig. 28. Amplitudes of long-period Rayleigh wave pulses *versus* short-period L_g for NTS explosions and earthquakes.

was that the explosion L_g spectrum differed greatly depending on whether the explosion was near a layer interface or not. For example in Fig. 29 the L_g spectra at depths 8 and 11 km are far from internal layer interfaces whereas depths 6 and 14 are close to interfaces. The spectra from 8 and 11 km are shifted to low frequency. This effect was not observed for earthquakes. This is reminiscent of the "low L_g spectrum" discriminant discussed above. Perhaps it may be interpreted, as was done by Gupta and Blandford (1983), by saying that a large part of the low frequency P was converted to S by detonations near the interface; but for the earthquakes the converted P wave energy was small compared to the S wave emitted from the double couple source.

This calculation also offers a clear warning that the L_g spectrum may not faithfully reflect the source spectrum, and so the use of L_g to determine corner frequencies is suspect. This conclusion was also reached by Blandford (1981) on the grounds that the L_g spectrum appears to disappear into the P_g coda "noise" around 3 Hz, suggesting that even

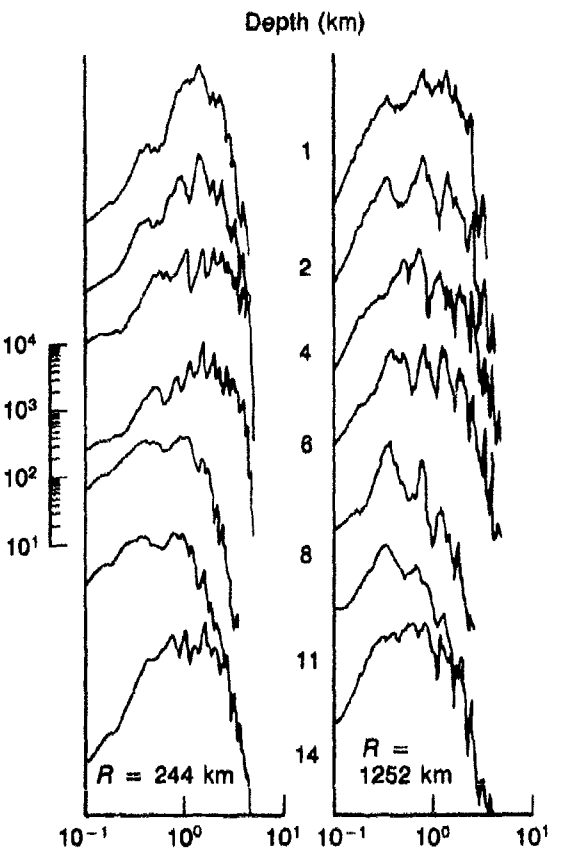

Fig. 29. Smoothed L_g spectra for the center of dilatation source. These spectra are cosine tapered to zero between 4 and 5 Hertz.

if the apparent L_g signal amplitude was greater than earth noise above 3 Hz it may not really be L_g but only P_g coda.

Using a Mueller-Murphy source spectrum, Bache *et al.* (1981) also notes that it is necessary to use a low Q in the near surface layers in order to eliminate the fundamental mode which is not observed but which, for high Q, dominates the theoretical records, and to obtain the correct absolute amplitude of the higher modes at the closest stations. However, they also note that this results in a much higher rate of decay of amplitude with distance than is observed for the higher modes as is illustrated in Fig. 30. The gamma value of 0.34 is much higher than is generally observed by experimental workers in the field.

This conflict could be avoided if we assumed that elastic scattering removes the fundamental mode, and that the true gamma is smaller (perhaps still due to scattering), and that the Mueller-Murphy source function is too large in absolute terms as suggested recently in connection with teleseismic m_b by Trulio. It seems conceivable that overestimation of t^* and gamma may be in part due to the same cause, the fact that the displacement continued to decay rapidly beyond the region where

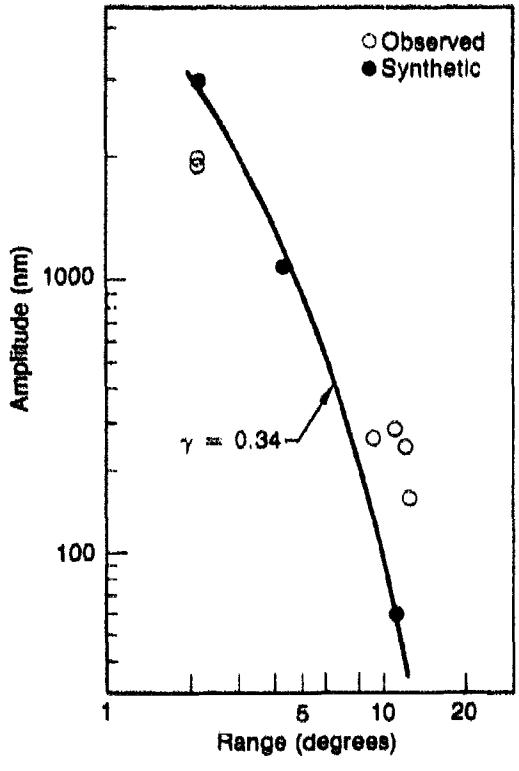

Fig. 30. The synthetic L_g amplitudes from the S1 synthetic seismograms are plotted with the SALMON data.

source function measurements are usually made; that the amplitude decays rapidly out to distances where the strains are as small as 1 bar.

Figure 31, from Bache *et al.*, suggests that amplitude ratios of L_g to other phases will in general be a poor depth determinant because L_g varies with depth in different ways for different focal mechanisms. However, this conclusion cannot be definite because we do not know how P_g varies with depth.

Campillo, Bouchon, and Massinon (1984) have recently performed extensive calculations of full seismograms for earthquakes and explosions at different depths and distances. Figure 32 shows all three components for a vertical strike-slip point source at a depth of 5 km. The model is fully elastic and we see the fundamental mode following the L_g.

Figure 33(a) shows the amplitude decay of P_g and L_g. We see that L_g falls off more slowly than P_g. For this model with no absorption or scattering the L_g decays as $r^{-0.83}$, an exponent very close to the 5/6 value assumed by Nuttli in accordance with his identification of the L_g

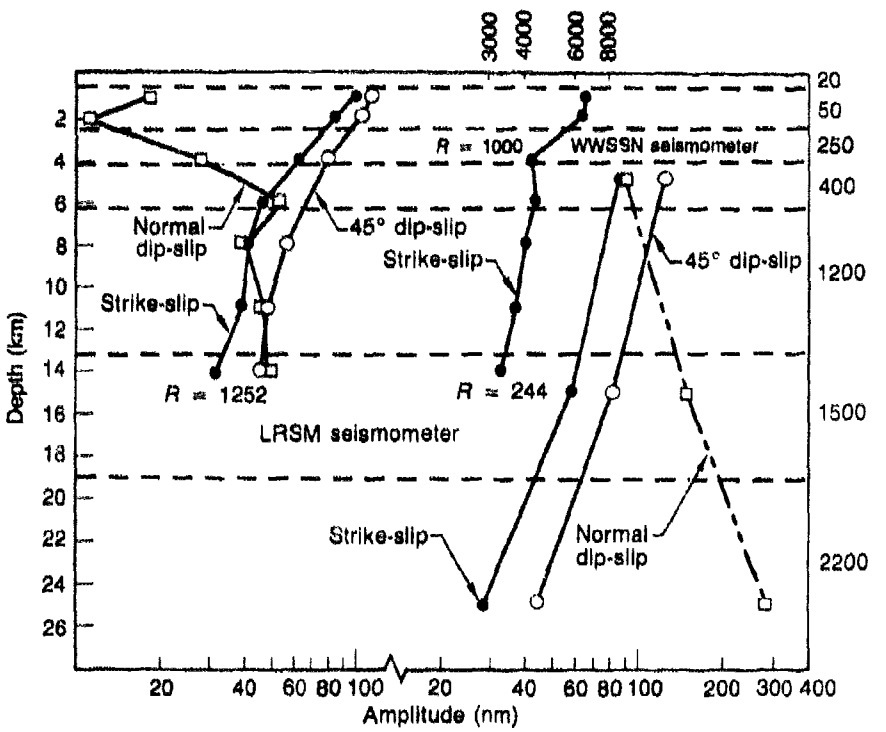

Fig. 31. L_g amplitudes from the synthetic seismograms are plotted *versus* source depth. The interfaces are indicated with a dashed line and the Q in each layer is listed along the right border of the plot. The amplitude scale for the R = 244 synthetics is at the top.

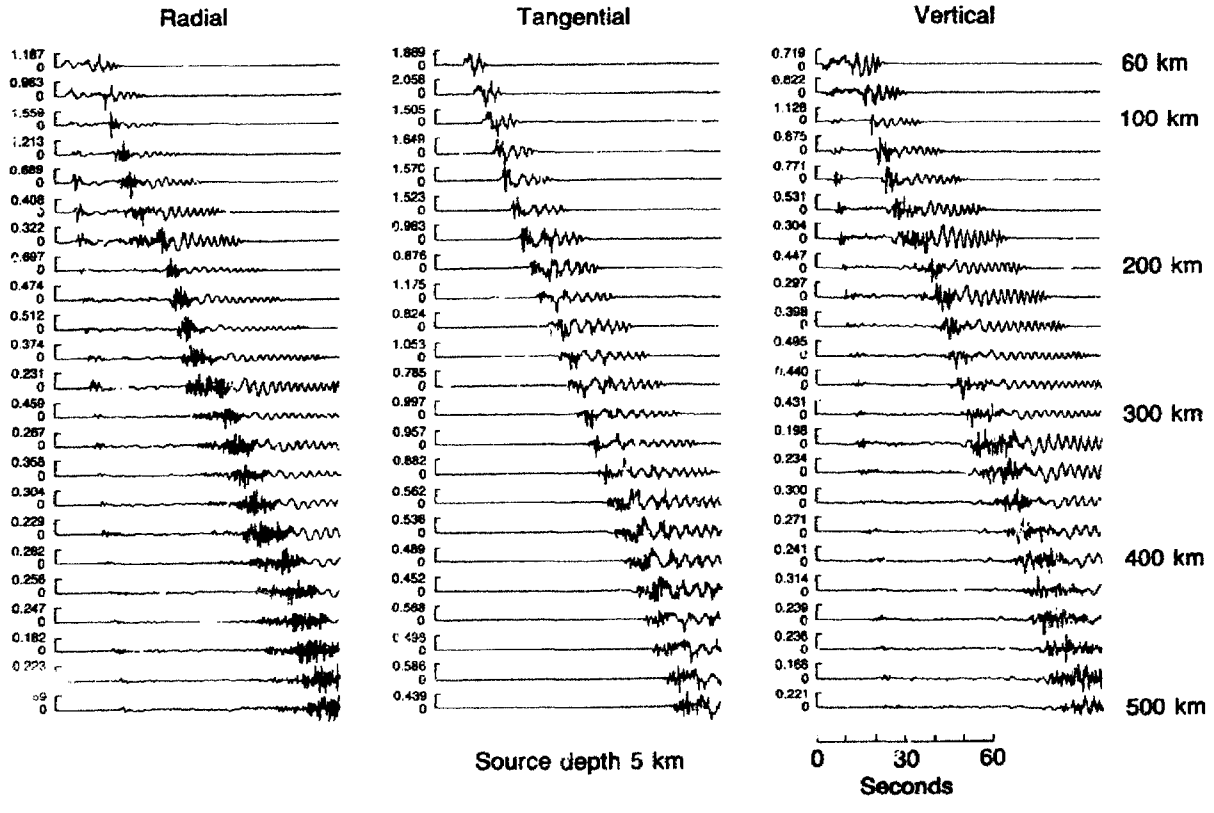

Fig. 32. Synthetic ground displacements produced by a vertical strike-slip point source for epicentral distances between 60 and 500 km at 20-km interval. The source depth is 5 km, and the source time function is defined by $[1 + \tanh (t/t_o)]/2$ with t_o equal to 0.2 sec. The displacements are given in tenths of millimeters for a seismic moment of 10^{23} dyne-cm. The signal duration is 100 sec. Each trace is normalized by the peak value of displacement. The reduction velocity is 8 km/sec.

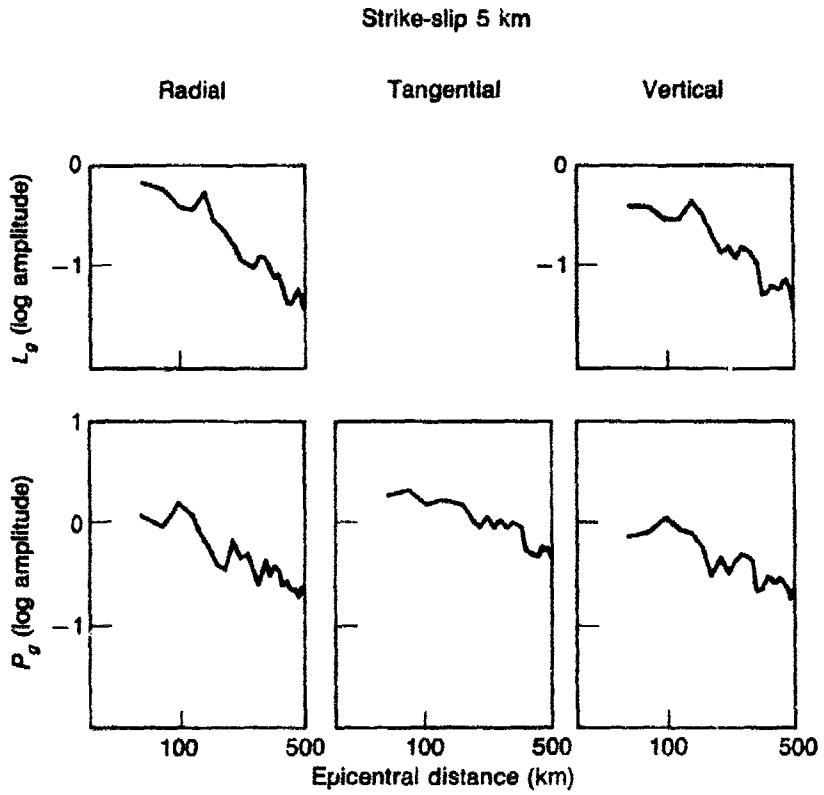

Fig. 33(a). Attenuation curves of P_g and L_g waves for each component of ground displacement for a strike-slip source at a depth of 5 km.

arrival with an Airy phase. The P_g decays as -1.5; the difference is close to values reviewed by Blandford (1981) in the EUS, -2.0 for L_g, -2.5 for P_g. The additional decay is, perhaps induced by scattering or by true absorption.

Careful inspection of Fig. 33(b) will show that the L_g falls off with frequency near 3 Hz while P_g is flat out to 5 Hz, the highest frequency in the model. This shows from a theoretical point of view that the L_g spectrum is not a reflection of the source spectrum and verifies the experimental observation that L_g is of lower frequency than P_g. This should be checked for other mechanisms than vertical strike slip. It would be of interest to have further insight into the physical mechanism behind this spectral difference. It should be noted that the difference is probably somewhat obscured in actual field observations due to the high frequency P_g coda which is inevitably still arriving at the same time as the true L_g.

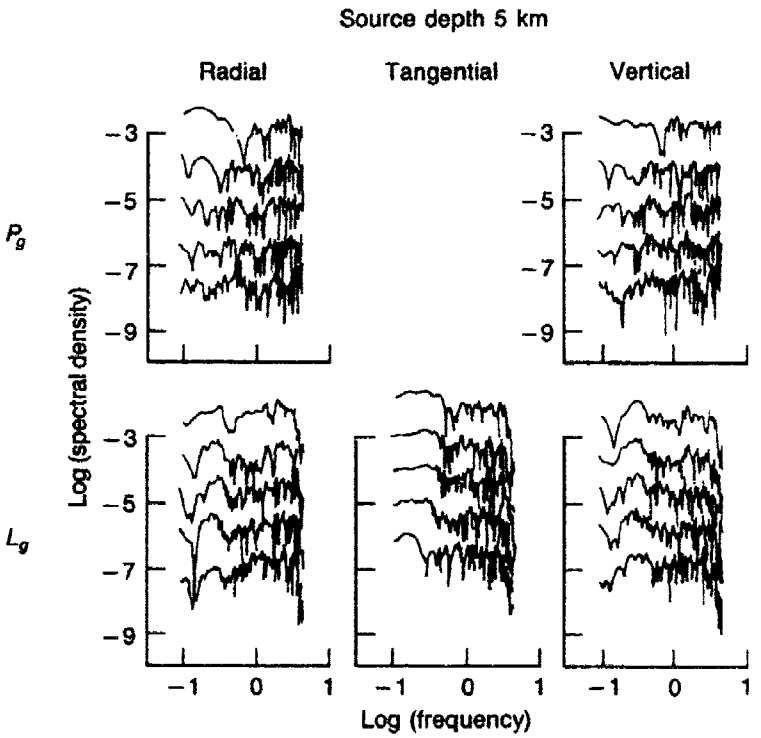

Fig. 33(b). Spectra of the crustal transfer function associated with P_g and L_g waves for a strike-slip source at a depth of 5 km. The time window is defined by group velocity between 6.5 and 4.0 km/sec for P_g and 3.8 and 2.5 km/sec for L_g waves. Five epicentral distances are considered from 100 to 500 km, and the corresponding spectra have been plotted with an arbitrary shift.

Figure 34 shows the vertical displacement for three different mechanisms as a function of depth. Apparently the P_g phase decreases with increasing depth more slowly with depth than does L_g for this strike-slip event (see Fig. 31) so that the earthquakes become more explosion-like as the depth increases. In view of the different behavior of normal dip slip events in Fig. 31, this relation should be checked for the other two canonical earthquake mechanisms.

Notice in Fig. 34 how the P_g/L_g ratio varies with distance, as would be expected due to the different rate of fall off the phases with distance. Obviously any use of these ratios as a network-averaged discriminant must make use of a distance correction before averaging.

Figure 37 shows seismograms as a function of distance for three different mechanisms. The seismograms seem quite similar and prompted Campillo *et al.* to conclude that there was no difference in fall-off rate

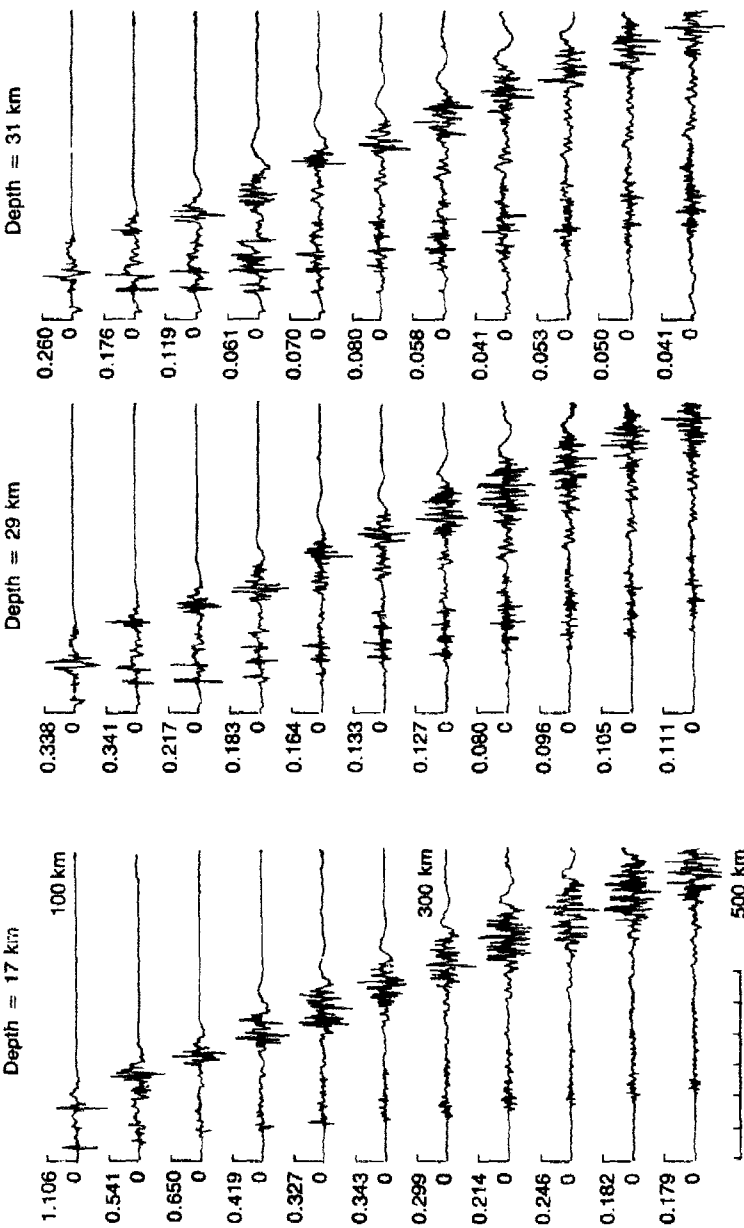

Fig. 34. Effect of the source depth on the seismic radiation from a vertical strike-slip earthquake. The vertical displacements are displayed for epicentral distances between 100 and 500 km at 40-km interval. The scales are the same as in Fig. 32.

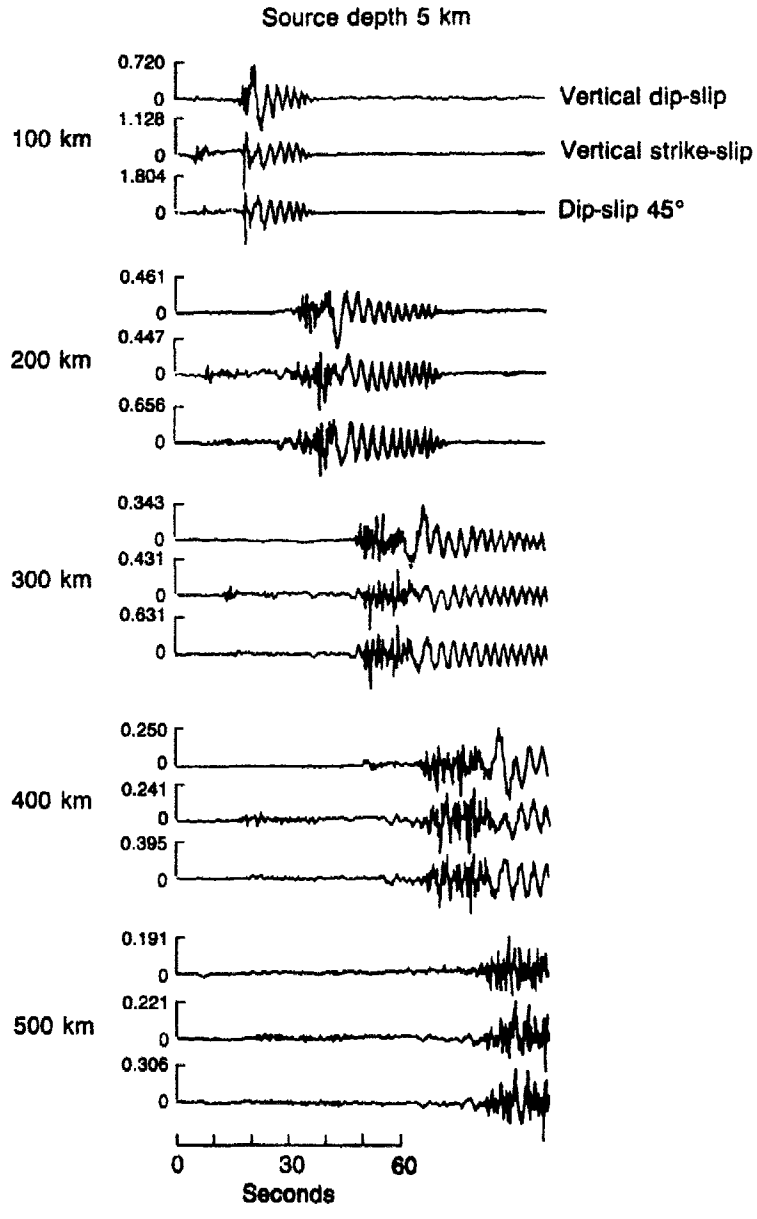

Fig. 35. Synthetic displacements produced by the three elementary types of seismic sources at five epicentral distances between 100 and 500 km. The scales are the same as in Fig. 32. Note the similarity of the L_g waveforms radiated by a vertical strike slip and by a 45° dip slip.

of the different phases as a function of source mechanism, as can be seen by a comparison of Figs. 36 and 33(a).

Comparison of Fig. 37 for an explosion with Fig. 35 at 300 km seems definitely to suggest that P_g/L_g would be an excellent discriminant. However, the vertical strike slip event does seem to have only about a factor of 2 discrimination power; the other mechanisms seem much better. It would seem that further explorations of parameter space are warranted, and some experimental investigations of the range of observed P_g/L_g amplitude ratios for earthquakes of known mechanism to see if a region of parameter space can be reserved for explosions using regionalization techniques.

Also, comparison of Figs. 35 and 37 does seem to indicate that the explosion L_g is of lower frequency than that of the earthquake. More detail on this subject is obviously important; a physical understanding is greatly to be desired.

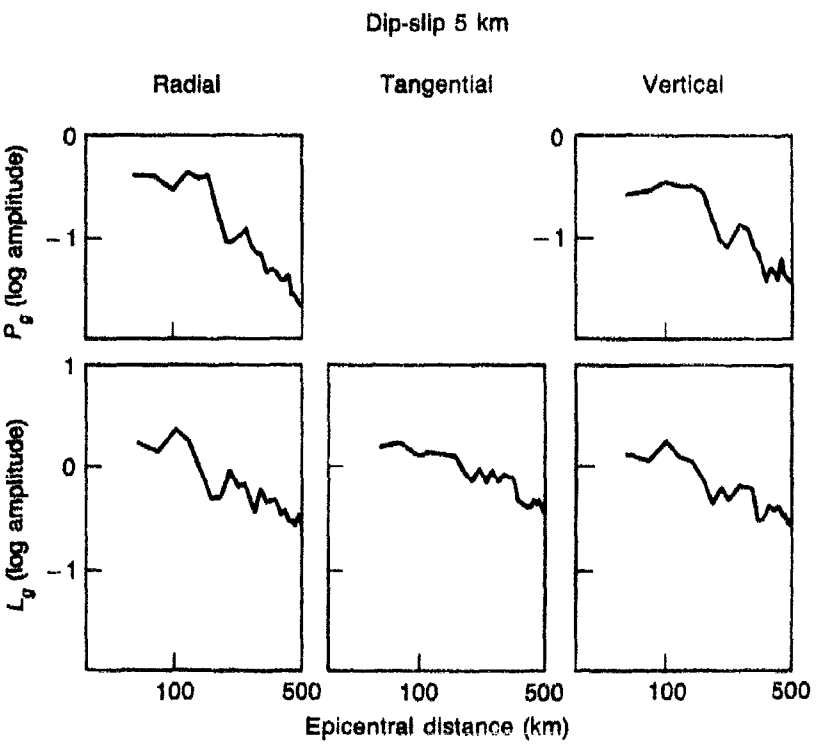

Fig. 36. Attenuation curves of P_g and L_g waves for each component of ground displacement for a thrust with a dip of 45° at a depth of 5 km.

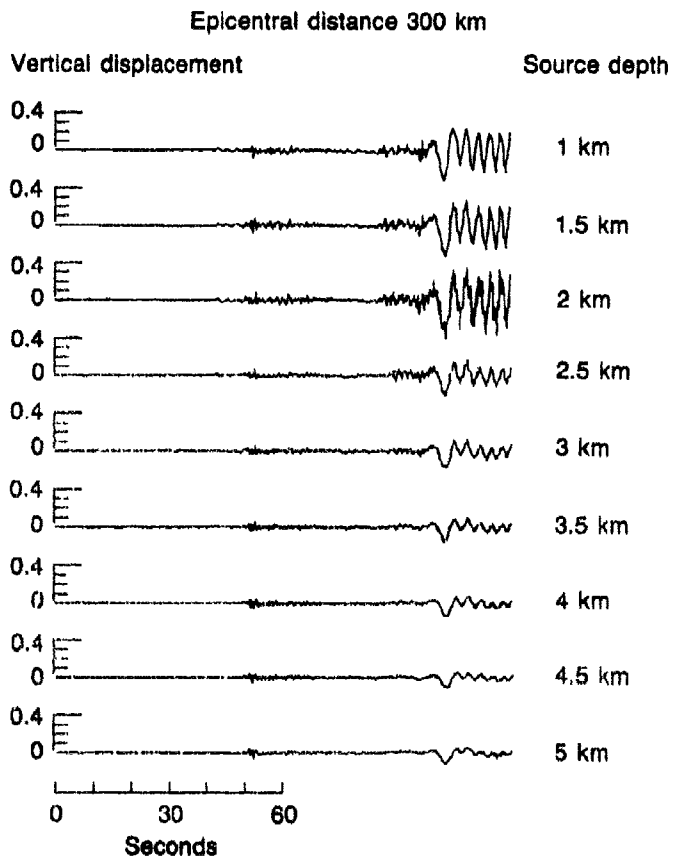

Fig. 37. Effect of explosion depth on vertical displacement produced at 300 km of epicentral distance. There is an interface at a depth of 2 km in the source model considered.

References

Bache, T.C., H.J. Swanger, B. Shkoller and S.M. Day, 1981, *Simulation of Short Period L_g, Expansion of Three-Dimensional Source Simulation Capabilities and Simulation of Near-Field Ground Motion From the 1971 San Fernando, California Earthquake*, S-Cubed Report SSS-R-81-4668.

Blandford, R.R., 1981, "Seismic Discrimination Problems at Regional Distances," in *Identification of Seismic Sources--Earthquake or Underground Explosion*, D. Reidel Publishing Company, Boston, :1.

Blandford, R.R., 1982, "Seismic Event Discrimination," *Bull. Seism. Soc. Am.*, **72**, S69-S88.

Blandford, R.R., and J.R. Woolson, 1979, *Experimental Analysis of SALMON/STERLING Decoupling*, SDAC-TR-79-2, Teledyne Geotech, Alexandria, Virginia.

Campillo, M., M. Bouchon, and B. Massinon, 1984, "Theoretical Study of the Excitation, Spectral Characteristics, and Geometrical Attenuation of Regional Seismic Phases," *Bull. Seism, Soc. Am.*, **74**, 79-90.

Der, Z.A., and T.W. McElfresh, 1976, "Short Period *P* Wave Attenuation Along Various Paths in North America as Determined From *P*-Wave Spectra of the SALMON Nuclear Explosion," *Bull. Seism. Soc. Am.*, **66**, 1609, 1622.

Gupta, I. and R.R. Blandford, 1983, "A Mechanism For Generation of Short-Period Transverse Motions From Explosions," *Bull. Seism. Soc. Am.*, **73**, 531-591.

Lambert, D.G., and S.S. Alexander, 1971, *Relationship of Body and Surface Wave Magnitudes for Small Earthquakes and Explosions*, Seismic Data Laboratory Report 245, Teledyne Geotech, Alexandria, Virginia.

Murphy, J.R., 1975, *Analysis of Near-Field Ground Motion Spectra From Earthquakes and Explosions*, Semi-annual Technical Report to ARPA, Computer Sciences Corporation, February.

Murphy, J.R., and T.J. Bennett, 1982, "A Discrimination Analysis of Short Period Regional Seismic Data Recorded at Tonto Forest Observatory," *Bull. Seism. Soc. Am.*, **72**, 1351-1366.

Murphy, J.R., T.J. Bennett, and T.K. Tzeng, 1981, *A Discrimination Analysis of Regional Seismic Data Recorded at Tonto Forest Observatory from Nevada Test Site Explosions and Nearby Earthquakes*, S-Cubed Report SSS-R-82-5301.

Patterson, D.W., 1966, *The Calculation Sensitivity of a Model Describing the Response of a Nuclear Formed Cavity: The STERLING Event*, Lawrence Livermore Lab., Report UCID-5.25, Livermore, California.

Peppin, W.A., and T.V. McEvilly, 1974, "Discrimination Among Small-Magnitude Events on Nevada Test Site," *Geophys. J.*, **37**, 227-243.

Pomeroy, P.W., W.J. Best, and T.V. McEvilly, 1982, "Test Ban Treaty Verification with Regional Data," *Bull. Seism. Soc. Am.*, **72**, S89-S130.

Springer, D., M. Denny, J. Healy, and W. Mickey, 1968, "The STERLING Experiment, Decoupling of Seismic Waves by a Shot-Generated Cavity," *J. Geoph. Res.*, **73**, 5995-6011.

Werth, G., and P. Randolph, 1966, "The SALMON Seismic Experiment," *J. Geoph. Res.*, **71**, 3405-3414.

Relationship Among Near-Field, Regional, and Teleseismic Observations of Seismic Source Parameters

Shelton S. Alexander

Summary

Analysis of L_g excitation by explosions at NTS, Semipalatinsk, and Hoggar indicates that above about .3 Hz L_g waves are not affected strongly by non-isotropic source excitation and provide a reliable additional means of estimating yield. Transverse component L_g appears to give equally good or better estimates of yield than vertical-component L_g, although combined vertical and transverse L_g may be better than either alone. Differences in modal excitation caused by differences in depth and source mechanism can be observed in L_g signatures from earthquakes in the eastern U.S., although the ensemble, represented by the conventional time-domain m_{bL_g} measurement gives a good estimate of size using single stations. Observations for events in the Semipalatinsk area suggest that L_g/P is a good discriminant between earthquakes and explosions there. Several approaches to overcome biasing effects of non-isotropic source contributions on the long-period Rayleigh wave signals from explosions have been developed and are being tested.

Conclusions and Recommendations

Short-Period Surface Waves. Our recent findings (von Seggern and Alexander, 1982, 1983; Alexander, 1983, and current research) using data for NTS and Soviet explosions suggest that yields estimated from L_g are much less affected by non-isotropic source effects than are the long-period surface wave yield estimates. This holds true for all NTS, Soviet and French events that we have analyzed to date. Figures 1 and 2 illustrate this result for NTS explosions where the L_g source terms derived by von Seggern and Alexander (1983), are shown compared with P-wave source terms and yield. A number of these explosions exhibit significant tectonic release based on the level of long-period Love-wave excitation. Similar results for Shagan River events are discussed below.

Like NTS, explosions in the Shagan River area of the Semipalatinsk test site produce transverse-component L_g signal levels that do not

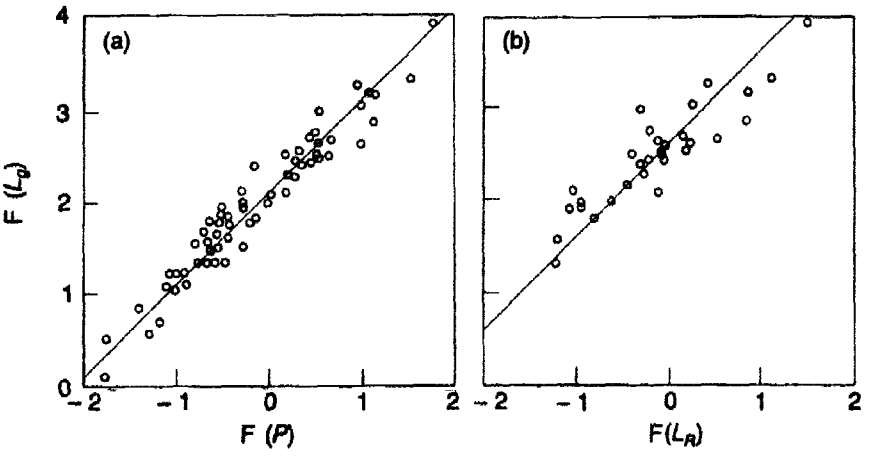

Fig. 1. L_g source terms of NTS explosions *vs* the *P*-wave source terms (a) and the L_R source terms (b).

appear to be correlated with the long-period Love-wave excitation based on observations at the Grafenberg broad-band array, while the vertical component does appear to be slightly reduced when the Love wave signals are large. However, this is not the case for frequencies above 0.3 Hz. We have found that for individual center frequencies in the range 0.5-0.8 Hz log ($L_g(f)$) *vs* m_b is linear and exhibits small scatter. Center frequencies around 0.6 or 0.7 Hz appear generally to be the best as the example in Fig. 3 shows. The observed slope is unity for the paths from Semipalatinsk to Grafenberg (Fig. 3), Konsberg (not shown), and Kabul (not shown), but apparently greater than unity for the path to Meshed (Fig. 8).

Therefore, we recommend that quantitative ways be developed to estimate the relative contributions to transverse L_g from scattering *vs* *SH* source excitation. The frequency dependence of the scattering contributions is especially important for both yield estimation and inferring non-isotropic contributions. Clearly, broad-band 3-component data are essential for such an evaluation, so the addition of broad-band (or short-period) horizontal components at SRO and other digital stations is strongly recommended. An important question to be addressed is whether transverse-component L_g is affected at any frequency by non-isotropic effects. Above about 0.3 Hz there appears to be no significant non-isotropic effects present in the explosion L_g transverse or vertical signals that we have analyzed.

In a recently completed M.S. thesis, Nichols (1984) analyzed the L_g and fundamental mode surface wave signals from the recent New

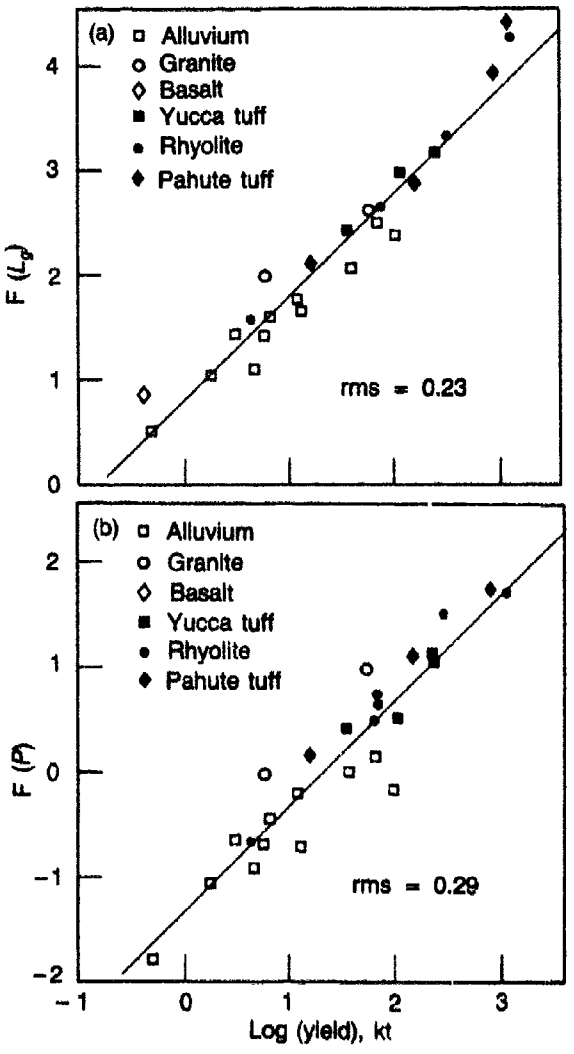

Fig. 2. (a) Transverse L_g source terms *vs* yield for NTS shots in various media, (b) P source terms *vs* yield.

Brunswick sequence of earthquakes, using primarily the digital recordings at SCP at a distance of approximately 1100 km. The source structure and focal mechanisms of the mainshock and several aftershocks were modeled using Harkrider's program to calculate surface wave modal excitation spectra and synthetic seismograms. She found that, unlike propagation from NTS to regional distances, these events exhibit significant spectral differences among both vertical and transverse L_g

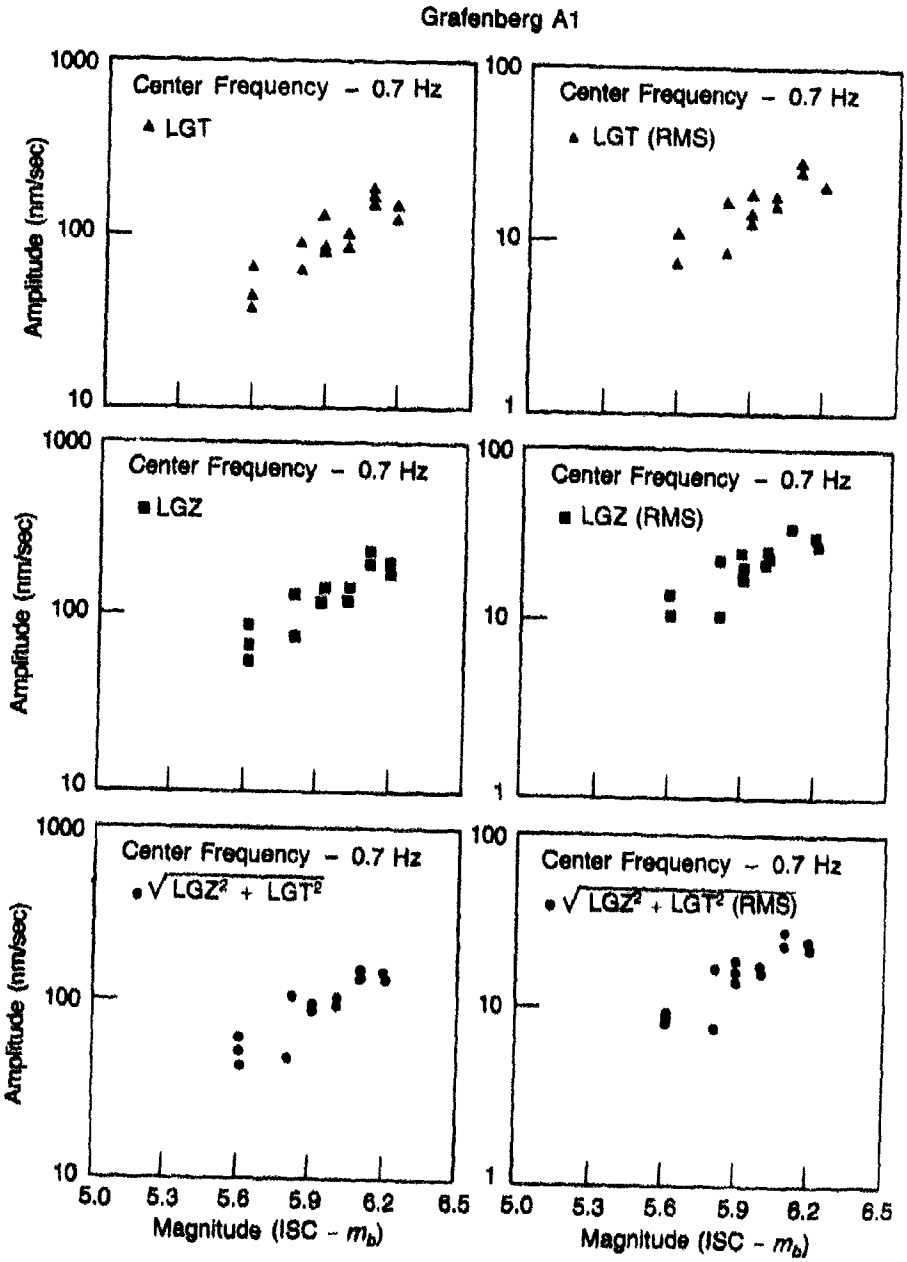

Fig. 3. Observed L_g amplitude *vs* m_b for the center frequency indicated for Semipalatinsk explosions. Left-hand figure is the maximum amplitude and the right-hand figure is the RMS in the L_g velocity window.

signatures as a function of changes in source mechanisms and focal depths; these differences persist to frequencies well above 1 Hz. This suggests significantly less heterogeneity, hence less scattering, for propagation paths in the eastern United States compared to propagation from NTS; work is in progress to compare results at other eastern North American stations with the SCP results. However, L_g measured in the usual way at SCP still gives excellent estimates of magnitude (Table 1). From the modeling of the different source mechanisms of New Brunswick events (Nichols, 1984), we conclude that even though individual higher modes

Table 1. Comparison of Short- and Long-Period Magnitude Estimates for New Brunswick Earthquakes

Month/Day/Event 1982	m_b	m_{bL_g}*	M_s*	m_{bL_g}***	M_s**
1/9 main	5.7	5.8	5.2	5.9	4.9
1/9 aftershock	5.1	5.3	3.9	5.2	3.6
1/11 aftershock	5.4	5.5	4.5	5.5	4.25
6/16 aftershock	4.7	4.6	-	4.3	-

* Reported in Wetmiller *et al.* (1983). m_{bL_g} values are from the Canadian Network; M_s are from NEIS.

** As measured from the photographic records at SCP.

*** As measured from the digital records at SCP. m_{bL_g} for the clipped mainshock signal was calculated from a short period record simulated from the intermediate period record.

are excited differently the *ensemble* gives nearly the same maximum L_g signal level from event to event when the m_b's are similar.

Additional GDSN, (SRO, DWWSN, and RSTN) teleseismic and regional digital data for these earthquakes have been obtained from the Center for Seismic Studies. They are being used for similar spectral analyses for other paths in eastern North America to characterize the path effects and source effects that can be distinguished as compared with NTS and Eurasia. Direct comparison of these events with observations for the earthquake of March 20, 1976, (Fig. 6) located near Degelen in Semipalatinsk and other nearby explosions will provide an excellent test of the similarity of source and propagation characteristics in these two regions.

We recommend that these important findings be pursued both to document more completely the degree of variability for various test sites

and to gain understanding of the mechanism(s) involved that explain why L_g with its complicated wave character is such a good estimator of source moment or yield. Where possible three-component recordings should be analyzed to permit comparison of transverse (Love) *vs* vertical (Rayleigh) L_g excitation; one important unresolved question is the mechanism(s) that consistently produce transverse-component L_g signals comparable to or greater in energy content than vertical-component L_g for NTS explosions and cavity collapses and for Soviet explosions. As the results of von Seggern and Alexander (1983), Fig. 2, and current research show, transverse L_g observations give good yield estimates for NTS events and they are essentially unaffected by non-isotropic source contributions as far as event magnitude (moment) is concerned.

Several approaches might be used to obtain improved absolute estimates of yield from L_g. One is the approach of von Seggern and Alexander (1983) where path effects are estimated and automatically taken into account to obtain the source moment (yield) for each event. Another is to use a local array such as Grafenberg or NORSAR (NORESS) to obtain the mean, noise-corrected L_g spectrum (with station structure effects averaged out) from which path Q can be estimated, provided the source spectral shape for L_g modes can be inferred. Figure 4 shows an example of the mean, noise-corrected L_g spectrum for the Grafenberg array (12 stations) for a m_b 5.9 Shagan River explosion. Assuming the source spectral excitation is flat in the range 0.3-0.9 Hz the average path Q is inferred to be slightly less than 1000. This is consistent with the individual station spectral amplitude decay obtained by narrow band filtering as shown by the example in Fig. 5. Another is Nuttli's approach where the L_g coda decay gives an estimate of average path Q and the observed L_g signal can then be corrected to give the source excitation (yield); in applying this method filtering of digital seismograms around the dominant frequency of the L_g signal may give an improved estimate of the average path Q, hence yield. Averaging the coda Q values obtained from individual stations in a local array (such as GRF or NORESS) may give a still better estimate of yield.

With regard to *discrimination*, it appears that in the western U.S. P_g/L_g is the most powerful short-period regional discriminant whereas in the eastern U.S. P_n/L_g may be more diagnostic. L_g/P also appears to be a powerful regional discriminant for events near Semipalatinsk as indicated in Fig. 6 and Figs. 7 and 8. There is approximately an order-of-magnitude difference in the L_g/P excitation for the earthquake and a nearby explosion of comparable m_b (5.1 and 5.2 respectively) shown in Fig. 6. Figure 7 confirms that the pattern of L_g/P spectral energy distribution for the m_b 5.2 explosion is typical of others in the

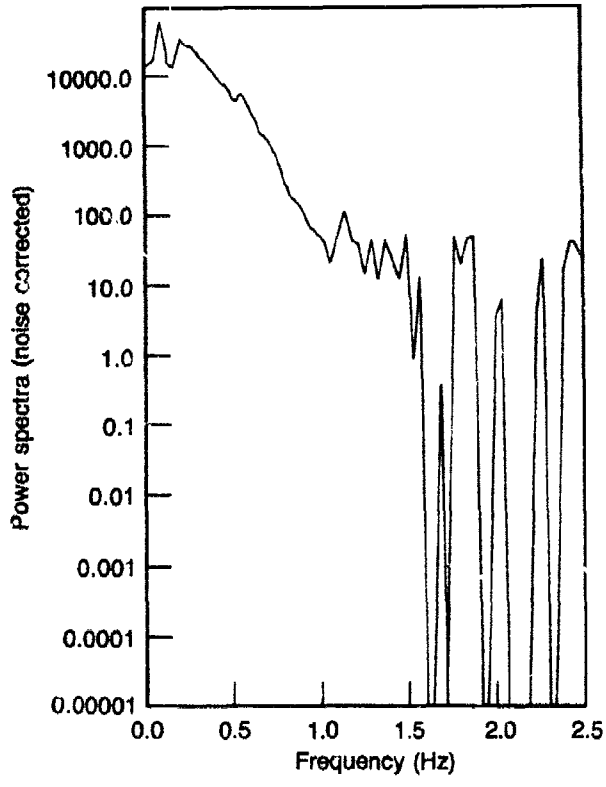

Fig. 4. Noise-corrected mean power spectrum for the event of 4/22/81 for the Grafenberg array (12 stations included in the average).

Semipalatinsk source region. This result is significant because other studies comparing L_g from earthquakes and explosions in Eurasia have suggested that L_g/P may not be a good discriminant. In those studies the earthquakes and explosions typically were rather widely separated spatially, so possibly differences in propagation paths or local source structure differences contributed to the variability.

An extension of the decomposition method used by von Seggern and Alexander (1983) should be incorporated into existing discrimination algorithms to allow simultaneous discrimination and source moment (yield) estimation from combined regional and teleseismic phases observed over a network, with source terms isolated from propagation and station terms.

Long-Period Surface Waves. Various methods can be considered to overcome the biasing perturbations caused by non-isotropic effects. In settings dominated by strike-slip faulting M_s bias can be minimized simply by averaging over azimuth or utilizing observations on favorable

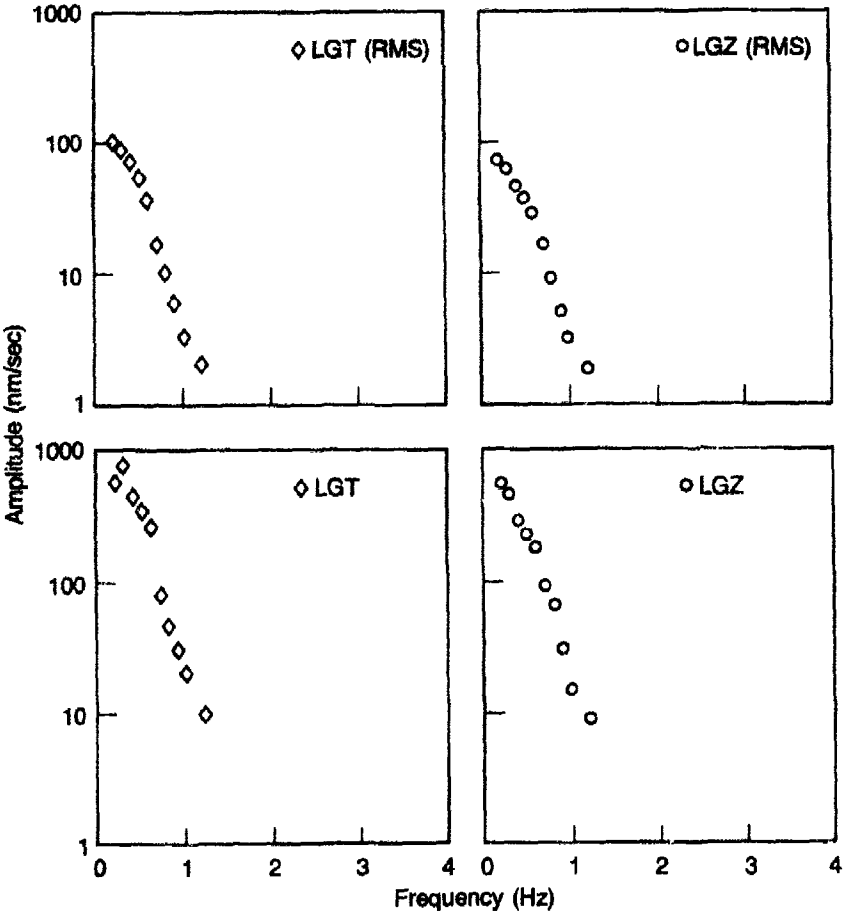

Fig. 5. L_g spectral amplitude *vs* frequency for transverse and vertical components of the event of 4/22/81 at Grafenberg station A1.

source-receiver azimuths (where Love-waves are maximum), whereas in areas dominated by thrust or normal faulting a systematic amplitude bias that is weakly dependent on azimuth is introduced into the Rayleigh signal. In those settings determinations of M_s bias must be made based on the orientation of the tectonic stress field (principal stress directions) and on the level of Love-wave excitation at several stations, assuming the bias is mostly "earthquake-like".

If there is sufficient azimuthal coverage, a formal moment tensor decomposition (properly constrained) can be used to estimate the isotropic (explosion) contribution. However, in many instances surface wave data from relatively few stations are available, so other techniques are needed.

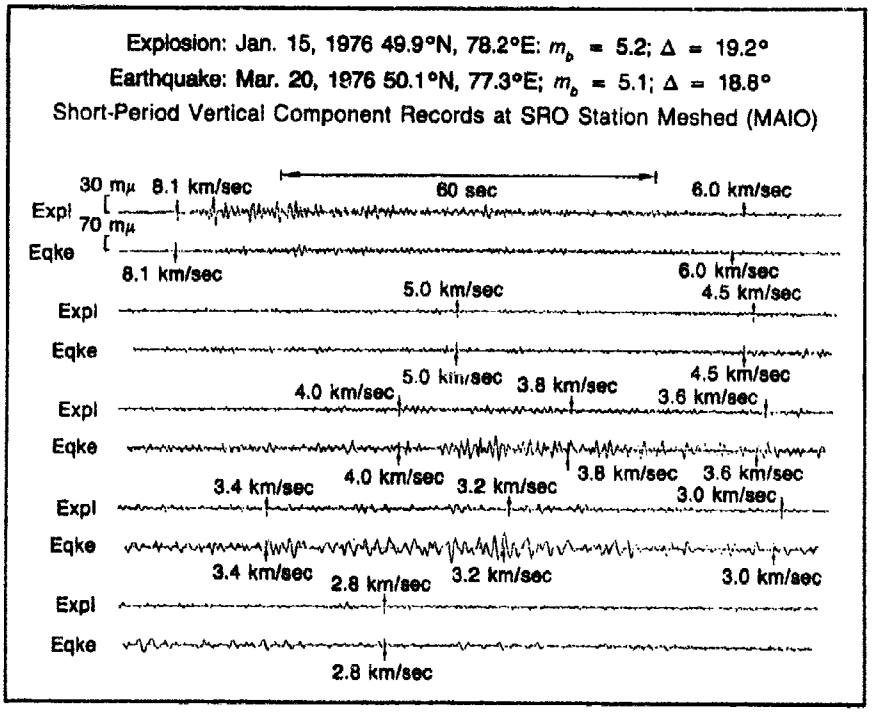

Fig. 6. Comparison of signatures of a m_b 5.2 nuclear explosion at Degelen and a nearby m_b 5.1 earthquake recorded at the SRO station MAIO. Note that the L_g/P ratio for the earthquake is approximately 8 times that for the explosion indicating that L_g/P is a good discriminant. L_g/P for the explosion is comparable to that observed at a similar distance for the Hoggar explosions. The m_{bL_g} for this earthquake using Nuttli's formula for the eastern U.S. is 5.25.

In the case of strike-slip tectonic contributions, averaging Rayleigh waves over azimuth will reduce or eliminate the biasing effect on M_s. An alternative is to estimate M_s using only Rayleigh waves at stations which have *maximum* Love wave amplitude; theoretically at that azimuth there is no Rayleigh-wave contribution from the strike-slip source. For example, for NTS events, stations such as SCP would be near a Love wave maximum. However, for tectonic areas characterized by dip-slip (thrust or normal faulting) contributions, other techniques must be used, because the Rayleigh wave bias is systematic with a weak dependence on azimuth and frequency. In this case the use of the Love waves is crucial. One approach that we are now pursuing for the Shagan River area is to use several very low tectonic release events to obtain an empirical "pure explosion" Rayleigh signature (shape), which then is incrementally scaled

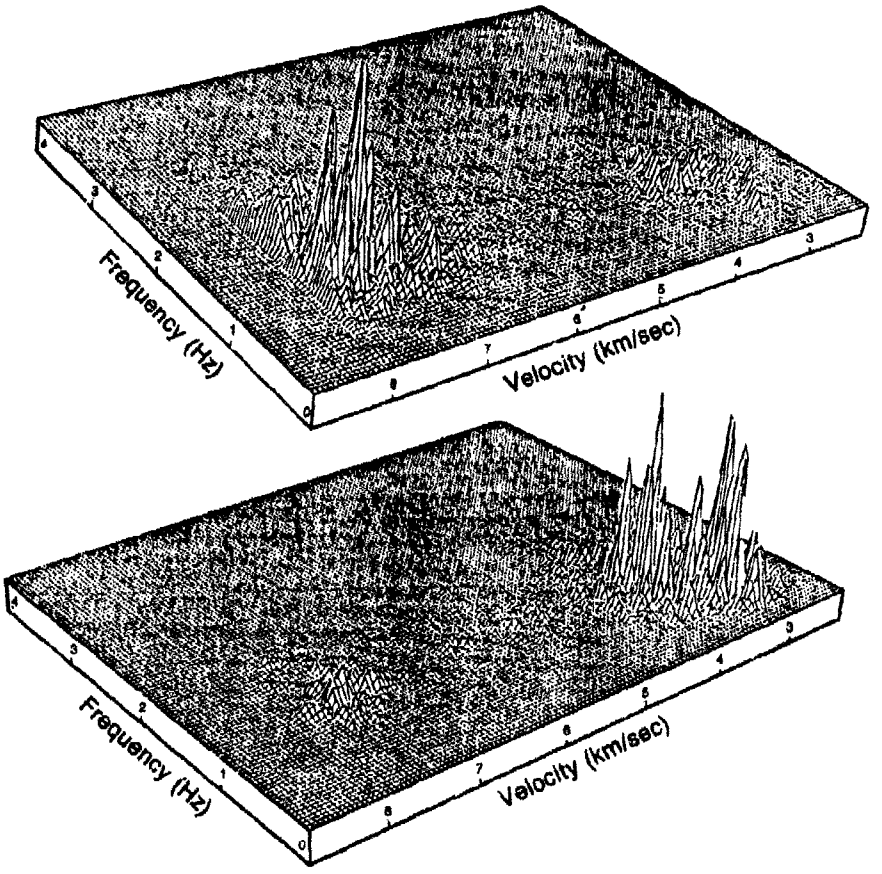

Fig. 7(a). Comparison of spectral (power) signatures displayed as a function of frequency and velocity for the explosion (top) and earthquake (bottom) for the seismograms shown in Fig. 6.

and subtracted from the total Rayleigh wave signature of high tectonic release events until the best double-couple solution is found (*i.e.*, when the trace of the moment tensor is closest to zero). This scale factor times the "pure explosion" signature then gives the equivalent Rayleigh wave for the explosion without tectonic release. For each event, these derived "pure explosion" Rayleigh waves for the network stations are then used to estimate M_s (yield). The assumptions in this approach are (a) that "pure explosion" Rayleigh waveform shapes are the same for events of comparable yield in the same source region and (b) the long-period Rayleigh and Love-wave signatures generated by non-isotropic source effects can be represented by a double-couple earthquake source. This

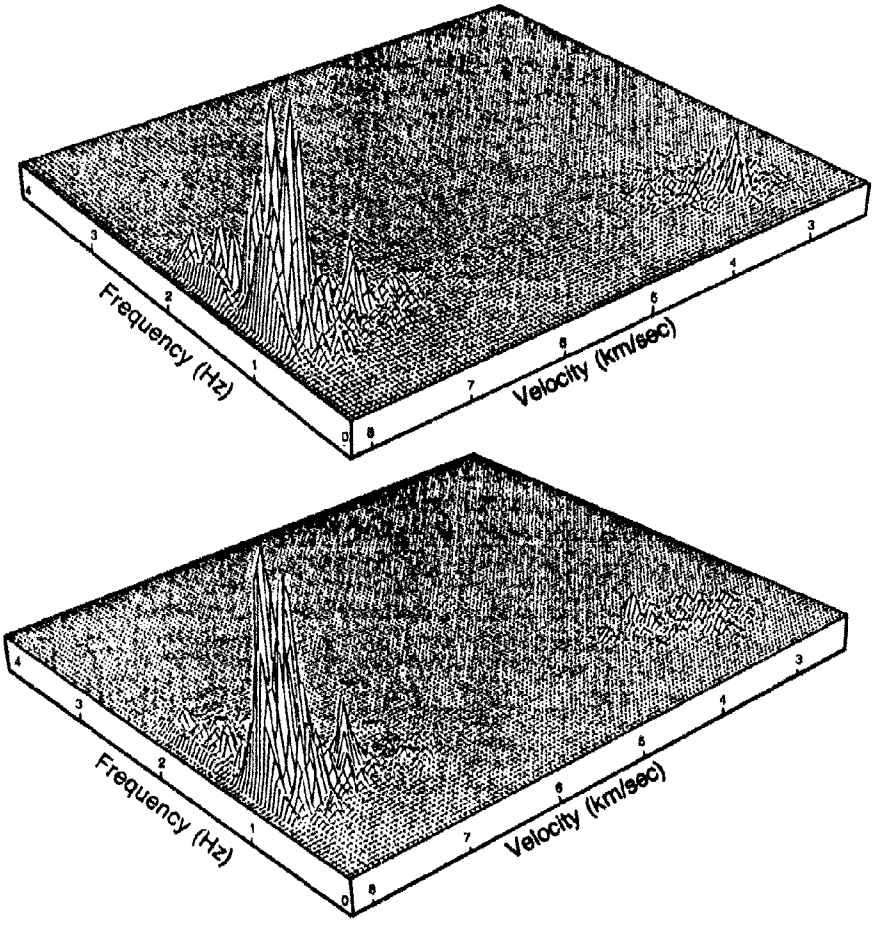

Fig. 7(b). Displays for two other explosions at Semipalatinsk as given in Table 2. Note the striking difference in the L_g energy distribution compared to the *P*-wave energy for the earthquake *vs* the explosions and the close similarity among explosions. Top display is for the event of 9/15/78 and bottom is for the event of 7/05/78 as recorded at MAIO. See Table 2 for event information.

latter assumption is least likely to hold in general but appears to be acceptable for the Shagan River source region and NTS. The remaining "pure earthquake" Rayleigh and Love-wave signals for each event interpreted in terms of a best-fitting equivalent earthquake model (strike, dip, rake, depth, moment) will also characterize the corresponding tectonic stress field at the source. Comparison of the inferred stress field with the known geologic features at each source location may increase our understanding of the nature of non-isotropic source generation at Semipalatinsk. We will continue with this approach and look particularly

Table 2. Events Analyzed for SRO Station MAIO

Date	Origin Time h m s	Location (ISC) Lat.	Long.	m_b (ISC)
09/29/78	02: 37: 06.4	49.98°N	79.02°E	5.9
11/23/76	05: 02: 57.5	49.97°N	79.01°E	5.8
07/05/78	02: 46: 57.5	49.84°N	78.91°E	5.8
05/29/77	02: 56: 57.5	49.86°N	78.84°E	5.8
06/11/78	02: 56: 57.8	49.88°N	78.81°E	5.9
09/15/78	02: 36: 57.5	49.91°N	78.94°E	6.0
03/20/76	04: 03: 39.9	50.02°N	77.37°E	5.1
01/15/76	04: 46: 57.3	49.80°N	78.25°E	5.2

at the frequency dependence of the tectonic contribution. The frequency dependence is important because we now know that high-frequency higher mode surface waves (L_g) and body-waves typically do not have significant tectonic contributions, and the explanation may rest on the nature of this frequency dependence (*e.g.* different and longer source-time function versus scattering dependence).

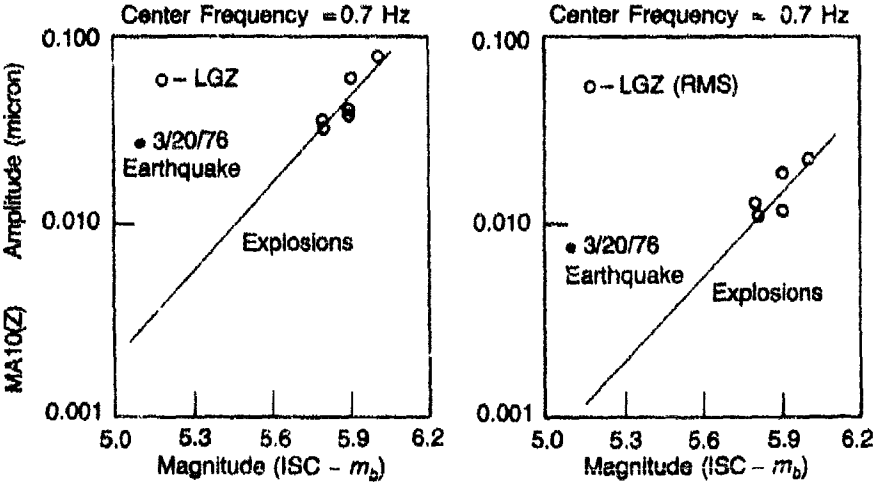

Fig. 8. Observed L_g amplitude *vs* m_b for the center frequency indicated for Semipalatinsk explosions. Left-hand figure is the RMS in the L_g velocity window. (See Table 2 for event information.)

References

1. Alexander, S.S., "Relationship Between Near-Field and Teleseismic Observations of Seismic Source Parameters," *Semi-Annual Technical Report, Grant AFOSR-82-0054*, 1 March 1982-28 February 1983, The Pennsylvania State University.
2. Alexander, S.S., "Relationship Between Near-Field and Teleseismic Observations of Seismic Source Parameters," *Semi-Annual Technical Report, Grant AFOSR-82-0054*, 1 March 1983-31 August, 1983, The Pennsylvania State University.
3. Alexander, S.S., and D. von Seggern, "Spectral Estimates of Source, Path (Q), and Receiver Contributions to L_g Signal from Earthquakes," *EOS*, **64**, No. 18, p 260, 1983.
4. Gupta, I.N., and R.R. Blandford, "A Mechanism for Generation of Short-Period Transverse Motion from Explosions," *Bull. Seis. Soc. Am.* **73**, pp 571-593, 1983.
5. Ng, Carolyn, *Combined Use of Wavenumber Analysis of Landsat Digital Imagery and Seismic Data to Infer the Orientation of Tectonic Stress in the Hoggar Region in Africa*, Master's Thesis, The Pennsylvania State University, Department of Geosciences, University Park, PA, 1983.
6. Nichols, C., and S.S. Alexander, "Long-period and L_g Surface Wave Excitation by Recent Earthquakes in the Northeastern United States," *EOS*, **63**, No. 18, p 384, 1982.
7. Nichols, C., *Analysis of the New Brunswick, 1982, Earthquake Sequence with Inferences on Source Parameters from Multi-Mode Surface Wave Dispersion and Spectral Excitation*, Master's Thesis, The Pennsylvania State University, Department of Geosciences, University Park, PA, 1984.
8. Pooley, C.I., A. Douglas and R.G. Pearce, "The Seismic Disturbance of 1976 March 20, East Kazakhstan: Earthquake or Explosions?", *Geophys. J. R. Astr. Soc.*, **74**, pp 621-631, 1983.
9. Sandvin, O., and D. Tjostheim, "Multivariate Autoregressive Representation of Seismic P-wave Signals with Application to Short-Period Discrimination," *Bull. Seis. Soc. Am.*, **68**, pp 735-756, 1978.
10. von Seggern, D.V., and S.S. Alexander, "Aspects of L_g Excitation and Propagation in Eastern North America," *EOS*, **63**, No. 45, pp 1035-1036, 1982.
11. von Seggern, D.V., and S.S. Alexander, "Investigation of Source, Path and Receiver Effects for L_g Waves from Nevada Test Site Explosion," submitted to *Bull. Seis. Soc. Am.*, 1983.
12. von Seggern, D.V., and S.S. Alexander, "Study of L_g Excitation and Propagation in Eastern North America," submitted to *Bull. Seis. Soc. Am.*, 1983.

An Evaluation of Seismic Decoupling and Nuclear Test Monitoring Using High Frequency Seismic Data

Charles Archambeau

Summary

The possibility of successful evasion of a Comprehensive Test Ban Treaty (CTBT) or a Low Threshold Test Ban Treaty (LTTBT) at yields up to several kilotons by cavity decoupling (Latter et al., 1961) has greatly influenced all estimates of the monitoring capabilities attainable by reasonable seismic networks, even when including stations within the USSR and USA. However, observations of regional distance signals at NORSAR and in the eastern U.S. indicate high S/N ratios, near 30, are to be expected for small events (e.g., fully decoupled 1 kt explosions) at distances up to around 300 km. This appears to be a consequence of the rapid falloff of high frequency noise at selected sites (varying as f^{-2}) and the very high effective Q paths for the high frequency signals. Given that the theoretical, and observed, decoupling factor is strongly frequency dependent; in particular, for a 1 kt decoupled explosion in salt it is near 200 at low frequencies and is 10 or less at frequencies greater than 20 Hz, then it is possible to detect and discriminate decoupled explosions to much lower magnitude levels than previously thought, provided a properly designed in-country array recording high frequency data is used. In particular, with a 25 station network in the USSR and 15 stations in surrounding areas, it is estimated that four or more stations will detect all 1 kt fully decoupled explosions, essentially anywhere within the USSR, when high frequency data is employed. Further, it is inferred that spectral discrimination methods, such as variable frequency magnitude discrimination (VFM) methods, which exploit spectral differences between explosions and earthquakes, can be applied to routinely identify any such events as well as small tamped explosions. Therefore, one conclusion to be drawn from this analysis is that in-country networks operating in the high frequency range can greatly enhance detection/identification of decoupled explosions, to a degree that 1 kt, or even lower yield, decoupled as well as tamped explosions could be detected and identified with high probability.

Decoupling of an explosion requires emplacement in a cavity of sufficient size that all stresses produced by the explosion at the cavity walls are within the elastic limit. As was pointed out by Latter *et al.* (1961), the size of such a cavity can be predicted using relatively simple hydrodynamic estimates and is within the range of mining capability for small yield explosions of a few kilotons and less. For such a decoupled explosion, the simple elastic solution for a pressurized cavity in an elastic medium, wherein a step function in pressure may be assumed as a reasonable approximation for the pressure at the cavity wall, provides a reasonably accurate prediction of the direct elastic wave field in the surrounding medium. In particular, for a spherical cavity of radius R_d, the predicted displacement spectrum in a Poisson solid, at a radial distance r, will be given by (*e.g.* Sharpe, 1942)

$$u(r,\omega) = \frac{R_d^3 P_0}{4\mu}\left(\frac{v_p}{v_p^2 - .75R_d^2\omega^2 + iv_pR_d\omega}\right)\frac{e^{-i\omega r/v_p}}{r} \qquad (1)$$

where v_p is the compressional wave velocity, μ the material rigidity, ω the angular frequency and P_0 the magnitude of the pressure step.

On the other hand, tamped explosions can be viewed in terms of an "equivalent elastic source", described approximately in terms of a simple pressure step at an "equivalent elastic radius," R_e, the radius at which the shock wave in the material has decayed to a level where elastic behavior occurs. In this case the direct elastic solution given in Eq. 1, but with the radius replaced by R_e and pressure magnitude by P_e, the "equivalent elastic pressure" at the elastic radius. Both R_e and P_e will be strongly dependent on the surrounding material properties, in particular on strength, porosity, water content, *etc.*, and must be determined emperically or estimated from nonlinear finite difference calculations. In general, however, $P_e \sim P_d$ while the elastic radius is always much larger than the decoupling radius, so

$$R_e \gg R_d\,.$$

In view of these relationships involving the expressions for the radiated elastic wave fields from coupled and decoupled explosions, a decoupling factor D may be defined as the ratio of the amplitudes of the two source types, so one has:

$$D = \frac{R_e^3 P_e}{R_d^3 P_0}\left|\frac{(v_p^2 - .75R_d^2\omega^2)^2 + (v_pR_d\omega)^2}{(v_p^2 - .75R_e^2\omega^2)^2 + (v_pR_e\omega)^2}\right|^{1/2} \qquad (2)$$

Figure 1 shows predicted spectral characteristics of tamped and decoupled explosions for a salt environment (SALMON data used) using the simple relation of the form of Eq. 1. The spectra of both types of explosions is characterized by a flat spectral level up to a corner frequency, beyond which the amplitude spectrum decays as f^{-2} with increasing frequency. The corner frequencies scale with yield (W) as $W^{1/3}$, so that the loci of explosion corner frequencies lie along a line of f^{-3} slope in the spectral plane. Clearly the decoupled explosions are much reduced in low frequency amplitude from tamped explosions of the same yield. For example the 5 kt decoupled explosion has a low frequency amplitude which is roughly a factor of 200 less than that of the tamped 5 kt explosion. However, at higher frequencies the decoupled effect is much less, at 30 Hz the decrease is only about a factor of 10 between the spectral amplitudes for the 5 kt tamped and decoupled explosions.

The reduction in coupling as a function of frequency for a 1 kt explosion in salt is shown in Fig. 2 for various cavity radii, with the larger radii producing over-decoupling with cavity sizes much larger than is necessary for elastic behavior at the cavity wall. The rather rapid decrease

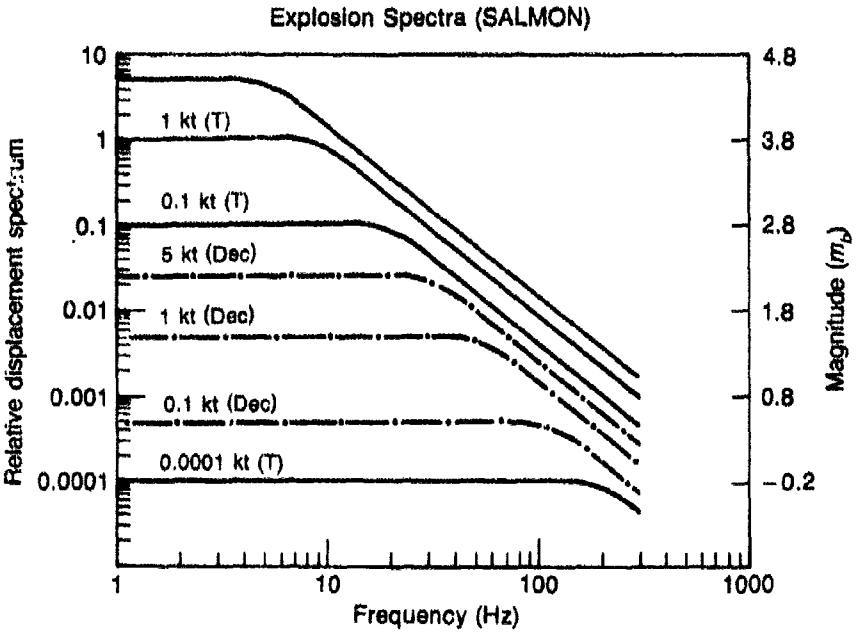

Fig. 1. Predicted source *P* wave displacement spectra of underground explosions in salt (Sharpe model, SALMON conditions). Left hand scale: displacement in arbitrary units. Right hand scale: magnitude scale in m_b units. "T" = tamped. "DEC" = decoupled.

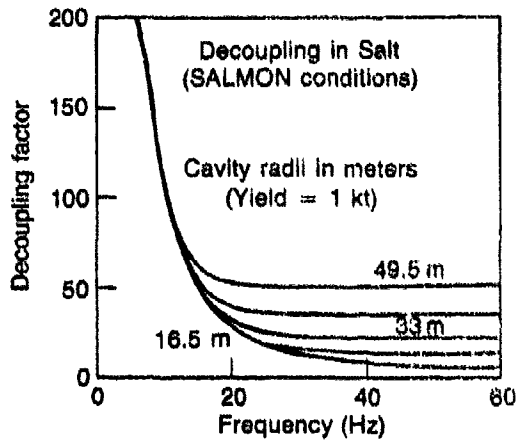

Fig. 2. Decoupling factor for explosions in salt (SALMON conditions) as a function of frequency and radius of cavity. Smallest radius is for "fully-decoupled" explosion. For yields (W) of other than 1 kt, scale frequencies as $W^{-1/3}$ and radius as $W^{1/3}$.

in the decoupling factor from over 200 at low frequencies to less than 10 at high frequencies for the decoupled explosion in the smaller decoupling cavity indicates the rapidity of the decrease in decoupling at high frequencies. The figure also shows that rather large decoupling radii are necessary in order to increase the decoupling to around 50 at high frequencies, with such large cavities being very difficult to construct and maintain.

Because of the decrease in decoupling at the higher frequencies, there is a clear possibility of detecting and discriminating decoupled explosions, as well as small tamped explosions, using signals in the high frequency range (*e.g.* from 5 to 50 Hz) recorded at regional distances. Figure 3 shows predicted earthquake spectra, based on first order relaxation theory models (*e.g.* Archambeau, 1968), superposed on the spectra for low yield tamped and decoupled explosions. Clearly, if it is possible to observe and reliably measure the high frequency signals, it should be possible to discriminate all types of explosions from earthquakes using a high versus low spectral difference (or ratio). In particular, if signals from a few Hertz out to 30 Hz can be measured with good signal-to-noise ratio in the regional distance range, then measuring P wave magnitudes at (say) 5 Hz and 30 Hz would show all explosions, including all decoupled explosions down to 1 kt, to have much higher 30 Hz magnitudes than all comparable earthquakes with the same low frequency magnitude. This corresponds to discrimination down to about the magnitude 1.5 level. At lower magnitude levels it would be necessary to employ a yet higher frequency magnitude measurement to achieve spectral discrimination by this approach, since earthquakes with stress drops above about 100 bars and explosions with magnitudes (m_b) below about 1.5 have nearly flat spectra over the entire range from 1 to

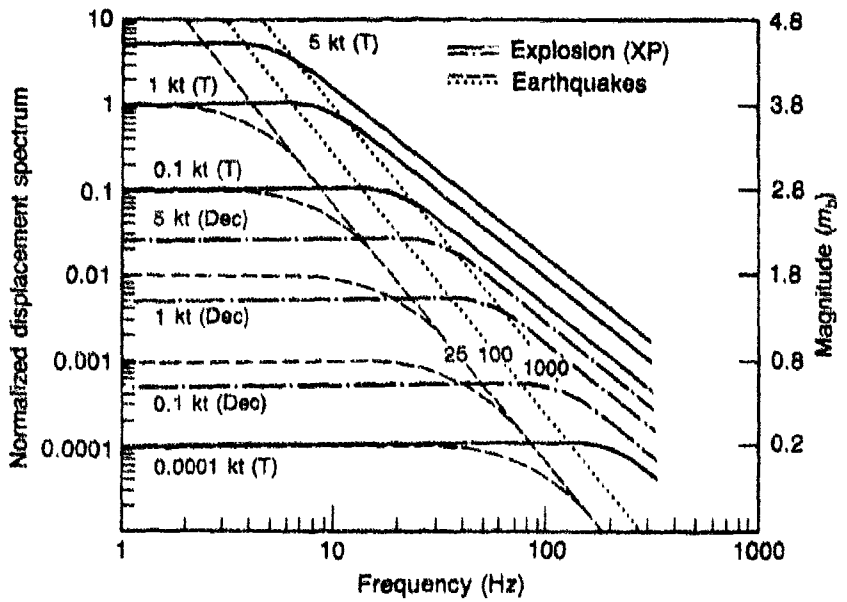

Fig. 3. Predicted event *P* wave displacement spectra of earthquakes and explosions (in salt). Left hand scale: displacement in arbitrary units. Right scale: magnitude in m_b units. Earthquakes have variable length with fixed rupture rate (less than but near the shear velocity) and fixed stress drop of 25 bars. The lines labeled "100" and "1000" are corner frequency lines for earthquakes with stress drops of 100 and 1000 bars. (Spectra for such earthquakes are similar to those shown for 25 bar stress drops, but shifted such that their *P* wave corner frequencies lie along the corner frequency loci indicated.)

30 Hz. (Therefore, both event types would have the same low to high-frequency spectral ratio, and occupy the same region in the low frequency magnitude *versus* high frequency magnitude plane.)

In shield-like stable continental areas there is a good evidence that sufficiently large high-frequency signals can be recorded at properly chosen, low noise, stations out to distances of the order of 1000 km. Figure 4 shows *P* wave spectra recorded at a distance of 190 km from an eastern Canadian earthquake. The high frequency noise level for the recording site is well below the lowest signal power shown on the figure out to 50 Hz. Similar high frequency signal data has been recorded at NORSAR during special recording periods when high digitization rates were implemented (Trourud, 1983; Bungum, 1983).

In these latter studies the observed signal-to-noise ratio of a small Semipalatinsk explosion (m_b = 4.2), at a distance of 38°, was from 8

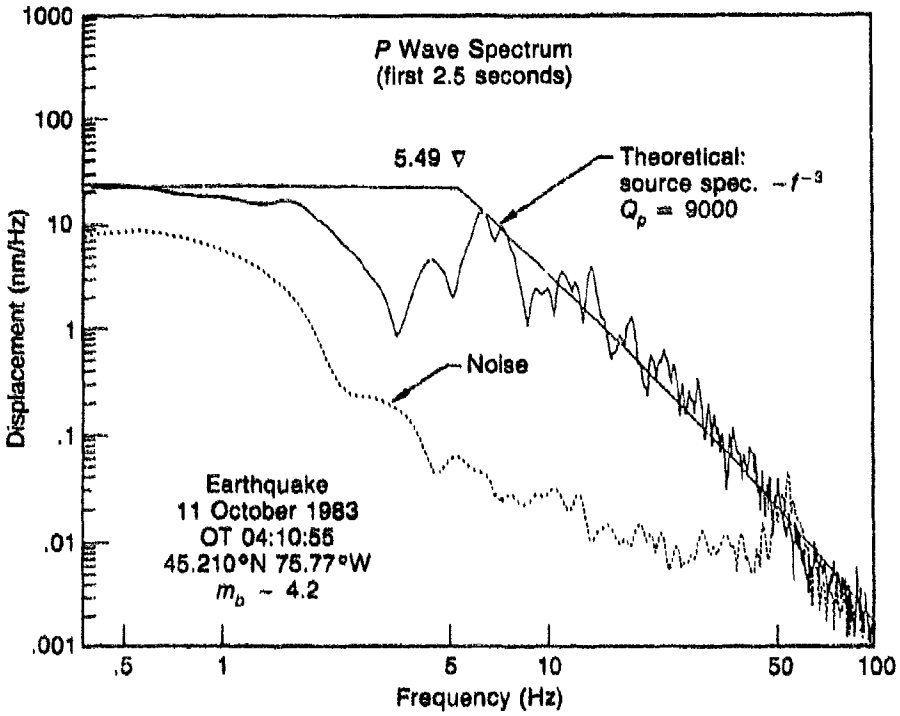

Fig. 4. Observed displacement spectrum of a $m_b \cong 4.2$ earthquake in Canada, as observed at a range of 190 kilometers in New York. "Theoretical" lines shown indicate a fit to the observed spectrum based on relaxation source model predictions and an attenuation Q factor of 9000 for P_n in the eastern U.S.

to 10 in the frequency range from 1 to 10 Hz, with both the high frequency noise and signal also established to fall-off with increasing frequency at a rate of from 40 to 50 dB per decade (*i.e.* as f^{-2} to $f^{-2.5}$). The noise was also shown to continue at about this fall-off rate out to 40 Hz.

Given these results, it is possible to predict the signal spectra to be observed at a NORSAR-like station (*i.e.* a station having noise characteristics like NORSAR) for various sized events. Figure 5 shows the event spectra of Fig. 3 relative to scaled noise, for events at various distances Δ. Thus, for events observed at a distance of 10°, we would expect a signal-to-noise displacement amplitude ratio of about 30, at 30 Hz, for a 5 kt decoupled explosion and a S/N ratio slightly above one for a 1 kt decoupled explosion at this distance. However, for events at distances of around 6° the signal to noise amplitude ratio for a 1 kt

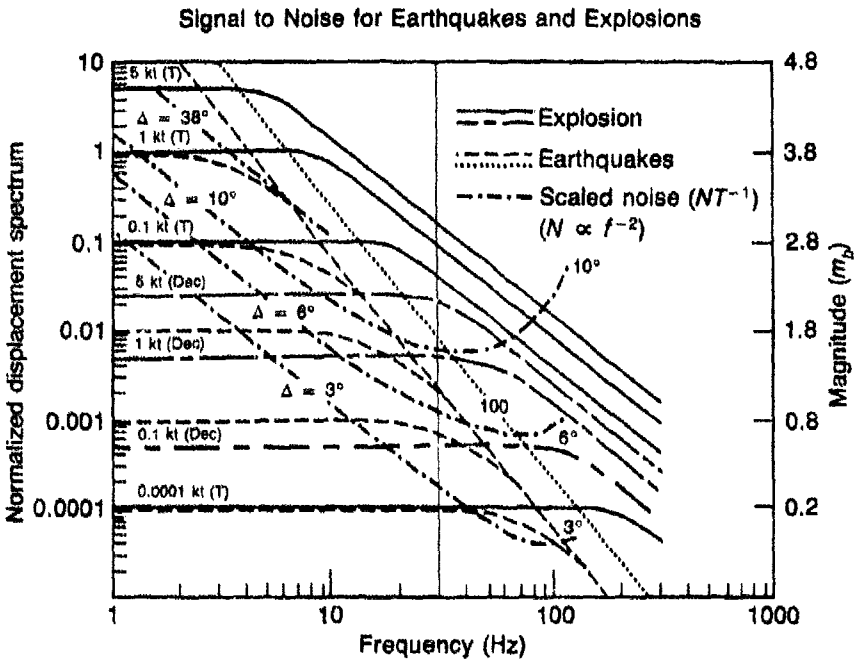

Fig. 5. Predicted source *P* wave displacement spectra of explosions and earthquakes *versus* scaled noise levels. Left hand scale: arbitrary units. Right hand scale: m_b units (measured at 1 Hz). Lines labeled "Δ = 38°", "Δ = 10°" etc. are scaled noise level curves at particular distances from the source obtained by multiplying observed noise spectra, varying approximately as f^{-2}, at frequencies above 1 Hz, by the inverse of the transfer function for *P* waves. The transfer function used is that appropriate to the eastern U.S., with $Q_p \approx 9000$ for P_n and with a "geometric" decrement varying as Δ^{-2}.

decoupled explosion would be about 5 near 30 Hz (*i.e.*, a displacement power ratio of 25 at 30 Hz).

Therefore, for low noise recording sites similar to NORSAR, one would expect to be able to detect 1 kt and smaller decoupled explosions and to obtain signal spectrum information over a wide high frequency range, up to 30 Hz or higher, in the original distance range. Further, in view of the spectral differences between earthquakes and explosions at high frequencies, it would be possible to discriminate the explosions from earthquakes.

If twenty-five high frequency recording sites of this (low noise) type were to be located in the USSR, as indicated by solid triangles on the map in Fig. 6, then detection levels as indicated on this map could be obtained with a detection probability of .9 using 30 Hz signal data. Here it was assumed that decoupling could occur in areas with salt deposits

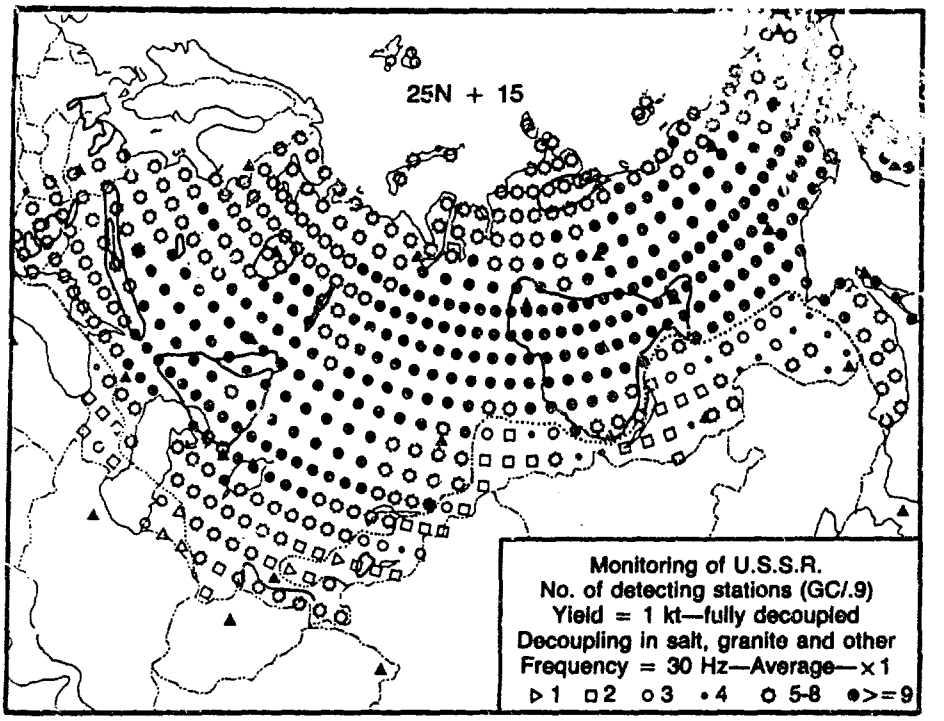

Fig. 6. Predicted number of detecting stations at 0.9 probability for a 1 kt explosion with full decoupling assumed in all hard rock locations. Detection estimates at 30 Hz. Solid triangles: seismological stations. Decoupling assumed possible in salt and other strong rocks throughout the USSR. At each point on a 1 degree latitude/longitude grid, a 1 kt explosion is assumed to occur. The symbols located on this grid indicate the number of stations detecting signals at 30 Hz from the events at that location. Noise levels at all stations are assumed comparable to those at NORSAR. Tectonic areas are assumed to have western U.S. characteristics for signal transmission.

or near surface hard rock environments (*e.g.* granite) and that signal propagation in the non-tectonic areas of the USSR is the same as in the eastern U.S. In tectonic areas it was assumed that *P* wave propagation was similar to that observed in the western U.S. Figure 7 shows the detection capability for the case of a fully decoupled 1 kt explosion with a higher noise environment existing at all stations. (In this example the noise levels are assumed to be about 12 dB above that observed at NORSAR.) In spite of the high noise levels assumed for all stations, it is still predicted that most such explosions within the USSR would be detected at from 4 to 5 stations, with only a few explosion locations occurring within the relatively small tectonic areas, where only two or 3 stations would detect such an event. These results therefore illustrate that: (1) if a sufficient number of low noise sites can be located in the USSR; and (2) if propagational

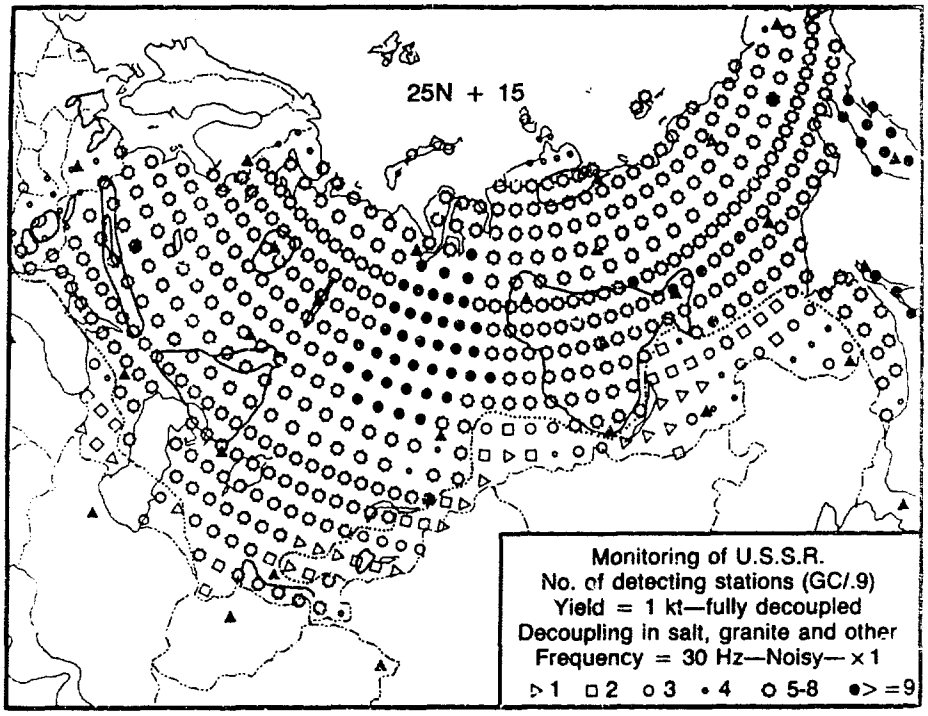

Fig. 7. Predicted number of detecting stations at 0.9 probability for 1 kt decoupled explosions under high noise conditions. Detection at 30 Hz under signal transmission characteristics like those of the eastern U.S. in shield and stable areas, and like the western U.S. in tectonic areas.

paths are typically similar to those in eastern North America, or similar to the NORSAR to Semipalatinsk path, wherein very high effective Q values predominate; then one can fully expect to be able to detect and identify decoupled explosions down to the 1 kt level, as well as tamped explosions to much lower yield levels.

References

Archambeau, C.B., "General Theory of Elastodynamic Source Fields," *Rev. of Geophys.*, **6**, 241-248 (1968).

Bungum, H., "Special NORSAR Study of High Frequency Noise," Communicated to L. Sykes (1983).

Latter, A., R. Le Levier, E. Martinelli and W. McMillan, *JGR*, **66**, 943 (1961).

Sharpe, H., *Geophysics*, **7**, 144 (1942).

Trourud, L., Scientific Report No. 1-82/83, NORSAR, Kjeller, Norway (1983).

Evernden, J.F. C.B. Archambeau and E. Cranswick, "An Evaluation of Seismic Decoupling and Underground Nuclear Test Monitoring Using High Frequency Seismic Data," submitted to *Reviews of Geophysics*, 1985.

Discrimination With Regional Phases in the Western U.S. and Eurasia

T.J. Bennett, J.R. Murphy, D.G. Lambert and J.M. Savino

Summary

The objective of the S-CUBED research program has been to systematically identify and assess the value of regional phase measurements for discriminating Soviet events. Our approach has included the following elements: (1) Use of a well-controlled earthquake and explosion sample for the vicinity of the Nevada Test Site to test the reliability of various proposed regional phase discriminants; (2) Development of a basis for extending the results to apply to Soviet events; and (3) Testing of the regional discriminant measures on available data from Soviet events.

Over the years, a wide variety of regional phase discriminant measures have been proposed and tested on various data bases, and Blandford (1981) and Pomeroy *et al.* (1982) have recently provided extensive reviews describing these studies. A common problem shared by many of these previous investigations has been that it has been difficult to unambiguously interpret the observations due to the fact that the epicentral locations of the earthquake and explosion sources being compared have typically not coincided very closely. That is, given the well-documented variability of regional phase characteristics with changes in propagation path, it has been difficult to attribute observed differences between the earthquake and explosion populations to characteristic differences in source excitation with any real degree of confidence. Consequently, in our regional discrimination studies, we have focused our attention on the analyses of well-controlled data bases recorded from explosions and nearby earthquakes. Thus, for the western U.S., our sample consists of regional data recorded from a large sample of Nevada Test Site (NTS) explosions and nearby earthquakes located within about 1° of NTS. Data from these events recorded at the Tonto Forest Observatory (TFO) in Arizona, the Uinta Basin Observatory (UBO) in Utah and the Blue Mountains Observatory (BMO) in Oregon have been used to test a variety of proposed discriminants. The approximate distances

and azimuths of these stations with respect to NTS are: 530 km and 124° for TFO, 670 km and 55° for UBO and 900 km and 353° for BMO.

One simple, time-domain regional discriminant which has received considerable attention over the years is the L_g/P_g amplitude ratio. That is, it has been observed that, at least in some cases, the L_g amplitude level for earthquakes is significantly larger than that for explosions having comparable P_g amplitude levels. Figure 1 shows comparisons of P_g versus L_g peak amplitude measurements for stations TFO, UBO, and BMO, derived from our sample of NTS explosions and nearby earthquakes. As has been noted previously (Murphy and Bennett, 1982), the L_g/P_g amplitude ratio at TFO is, on the average, somewhat larger for the earthquakes than for the explosions. However, the scatter in these earthquake observations is sufficiently large that the 2σ error bounds

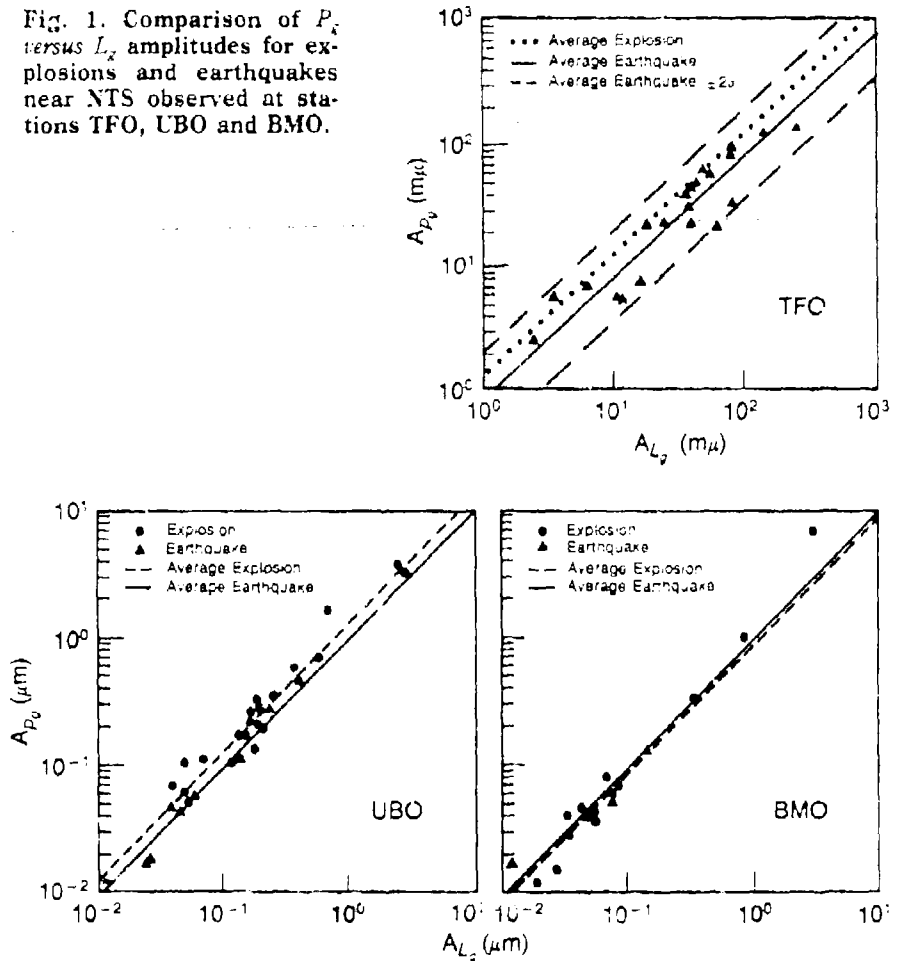

Fig. 1. Comparison of P_g versus L_g amplitudes for explosions and earthquakes near NTS observed at stations TFO, UBO and BMO.

envelope the mean explosion line as well as most of the explosion data. Moreover, it can be seen from this figure that the results obtained using data recorded from subsets of these same events at stations UBO and BMO show even less separation, indicating that network averaging can't be expected to significantly improve the performance of the L_g/P_g discriminant. We conclude that the L_g/P_g discriminant is not capable of consistently separating NTS explosions from nearby earthquakes.

One promising new regional discriminant which has been tested on this western U.S. data set, is based on observed differences in the relative spectral composition of the regional phases recorded from the two source types (Murphy and Bennett, 1982). That is, it has been found that the L_g, and to some extent the P_g, signals from earthquakes are relatively richer in high frequency content than the corresponding signals from explosions. On the basis of this observation, an L_g spectral discriminant, defined as the ratio of the average spectral amplitude level in the 0.5 to 1.0 Hz passband to the average spectral amplitude level in the 2.0 to 4.0 Hz passband, has been applied to the available western U.S. data sample. The results for stations TFO and UBO are shown in Fig. 2. It

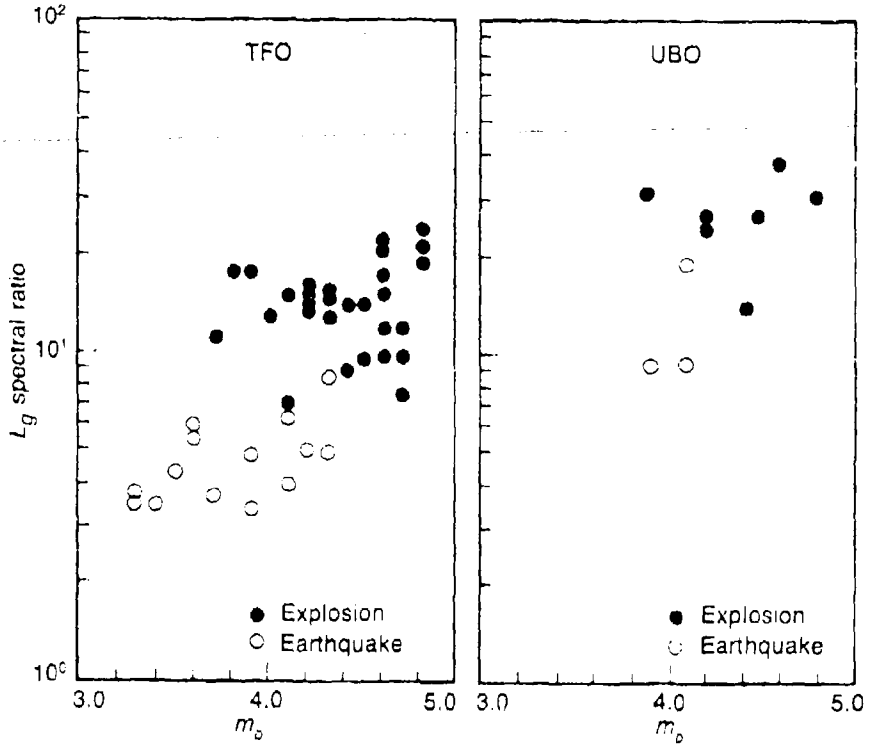

Fig. 2. L_g spectral ratio as a function of m_b for NTS explosions and nearby earthquakes recorded at TFO (left) and UBO (right).

can be seen that at TFO, where a representative sample of results are available, the discriminant works quite well, with an average separation between the earthquake and explosion populations of more than a factor of 3. The corresponding results for station UBO (and also BMO) tend to support this conclusion, although the sample of earthquake data available for analysis from this station is currently too small to permit definitive conclusions. In any case, these preliminary results are encouraging enough to suggest that the L_g spectral discriminant is worth testing on other data sets.

With regard to application of regional discriminants to Eurasian events of interest, we have recently been focusing our investigations on the analysis of regional phases recorded at selected SRO stations from nearby earthquakes and explosions within the Soviet Union (Bennett *et al.*, 1984). In this case, it is even more difficult to obtain well-controlled data samples than it is in the western U.S. due to the fact that the principal underground nuclear test site at Semilpalatinsk is located in a largely aseismic region. Figure 3 shows the map locations of our sample of earthquakes located within about 7° of Semipalatinsk with respect to the location of the SRO station KAAO located about 17° south of the test site in Kabul, Afghanistan. The short-period, vertical component seismograms recorded at KAAO from these six earthquakes and four Semipalatinsk explosions are shown in Fig. 4. The vertical arrows on these figures denote the expected arrival times of phases traveling with group velocities of 4.5 km/sec (*i.e.*, S_n) and 3.5 km/sec (*i.e.*, L_g). It can be seen from this figure that four of the six earthquakes show S and L_g amplitudes which are significantly larger than those observed from explosions with comparable

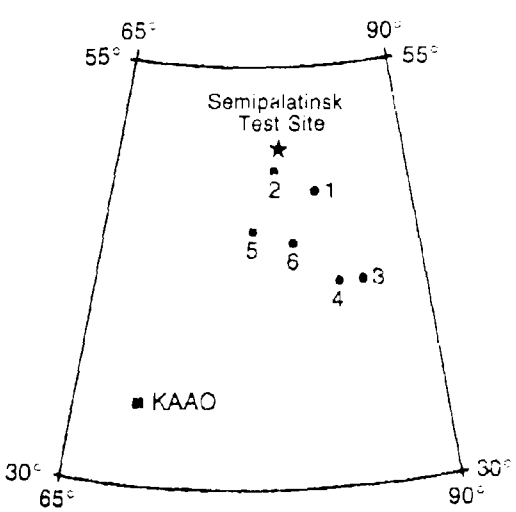

Fig. 3. Locations of Semipalatinsk test site and correlative earthquake sample with respect to station KAAO.

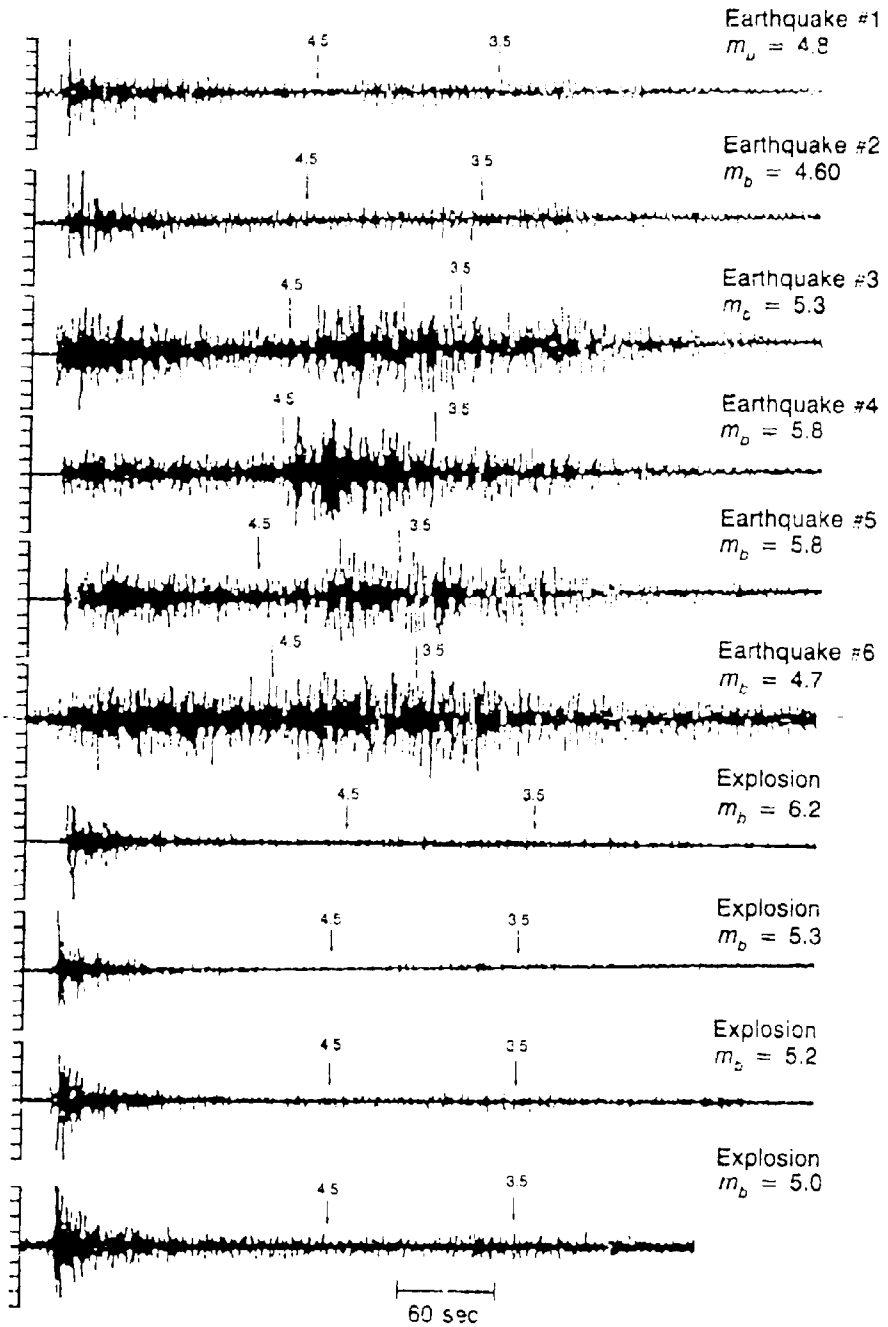

Fig. 4. Comparison of earthquake and explosion seismograms observed at KAAO for Semipalatinsk explosions and several nearby earthquakes.

P wave amplitudes. However, the two remaining earthquakes (*i.e.*, #1, #2) produced relatively weak S and L_g signals only marginally larger than those of the explosions. With reference to Fig. 3, it can be seen that these are also the earthquakes which are located closest to the explosion epicenters at Semipalatinsk. Thus, as in the western U.S., the question arises as to whether these differences in L_g excitation are due to differences in source type or simply to differences in propagation path characteristics. We are currently investigating data recorded at other SRO stations from these events in an attempt to answer this question. In any case, it seems clear that in Eurasia, as in the western U.S., there are shallow focus earthquakes which are associated with L_g/P ratios comparable to those characteristics of explosions.

Finally, Fig. 5 shows some preliminary comparisons of L_g spectra derived from data recorded at KAAO from a Semipalatinsk explosion and three fairly proximate earthquakes. In this case, because of the longer propagation path, the available bandwidth at KAAO is limited to frequencies below about 3 Hz as opposed to the 5 Hz cut-off characteristic of the western U.S. stations TFO, UBO and BMO. Nevertheless, it can be seen that when the L_g spectra for the earthquakes are normalized to a common level at frequencies below 1 Hz, the earthquake spectra are found to be somewhat richer in high frequencies than the explosion spectrum, similar to the findings for the western U.S. cited above.

Conclusions and Recommendations

Based on analyses of a large sample of data from stations at regional distances for explosions and earthquakes near NTS and the Soviet test areas, we conclude that some regional discriminants look promising for event identification in certain areas (*e.g.*, L_g spectral ratio in the western U.S. and possibly L_g/P_{max} amplitude ratio and L_g spectral ratio in the Soviet Union). However, none of the regional discriminants which have been tested produces correct identification in all cases. It is our view that regional discriminants will not be established as reliable tools without additional theoretical insight into the physical behavior of regional phases. In particular, a better theoretical basis needs to be developed for explaining how source and propagation path differences affect the observed signals and discriminant measures. These theoretical studies should help to identify which regional discriminant measures should be pursued.

References

Bennett, T., J. Murphy, D. Lambert and J. Savino (1984), *Regional Discrimination (U)*, S-CUBED Report submitted to Air Force Technical Applications Center, April, 1984.

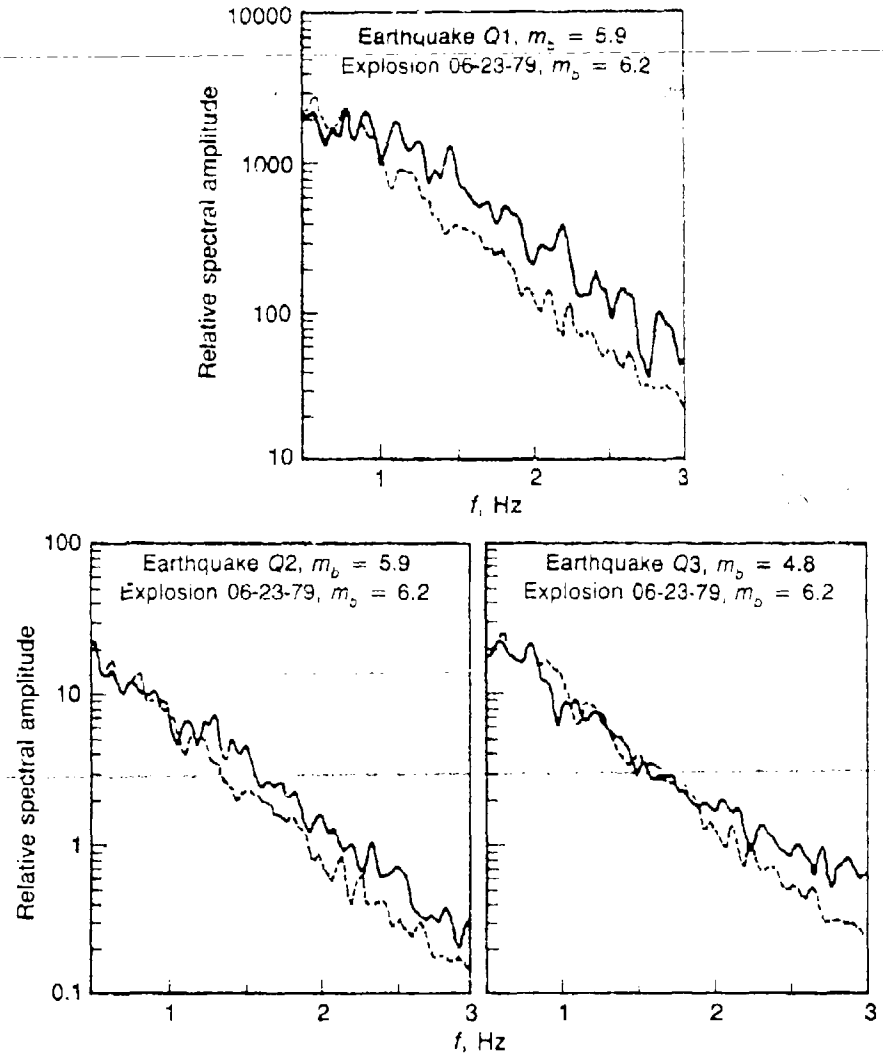

Fig. 5. Comparison of L_g spectral composition in the frequency band of 0.5 to 3.0 Hz for a Semipalatinsk explosion (dashed lines) and nearby earthquakes (solid lines) recorded at KAAO.

Blandford, R.R. (1981), *Seismic Discrimination Problems at Regional Distances*, NATO, Advanced Study Institutes, Series C, 74, D. Reidel Publishing Company, Dordrecht, Holland.

Murphy, J. and T. Bennett (1982), "A Discrimination Analysis of Short-Period Regional Seismic Data Recorded at Tonto Forest Observatory," *Bull. Seism. Soc. Am.*, **72**, pp. 1351-1366.

Pomeroy, P.W., W. Best and T. McEvilly (1982), "Test Ban Treaty Verification with Regional Data — A Review," *Bull. Seism. Soc. Am.*, **72**, pp. S89-S130.

Theoretical Modeling of L_g Wave Attenuation

M. Bouchon and M. Campillo

1. Spatial Attenuation

We compute the theoretical seismograms and the L_g wave spectra for a crustal structure where Q obeys the experimentally derived law for attenuation of regional phases in France. The velocity model chosen is based on long range refraction experiments and is thought to approximate the crustal structure in Central France where most of the recording stations are located.

The model parameters are given in Table 1. Q is assumed to be uniform throughout the crust and of the form $Q = 290f^{0.5}$ where f denotes the frequency. The seismic source is a vertical strike-slip dislocation point located at a depth of 10 km. The source time dependence is a step function. The synthetic vertical displacements in the range 180 to 700 km are shown in Fig. 1. The frequency cut-off is 5 Hz. The attenuation of the high frequencies with increasing epicentral distance is clearly visible. The corresponding L_g wave spectra taken in the group velocity range 3.8 to 2.5 km/s and deconvolved from the source time function are displayed in Fig. 2. As shown by Campillo *et al.* (1984), a 45°dip-slip dislocation would yield the same spectra. From these results we can infer the amplitude fall-off with distance at various frequencies (Fig. 3).

Table 1. Crustal model

Layer thickness (km)	*P*-wave velocity (km/sec)	*S*-wave velocity (km/sec)	Density (gm/cm^3)
2	4.5	2.6	2.6
16	6.0	3.5	2.8
6	6.3	3.65	2.9
6	6.7	3.9	3.1
	8.2	4.7	3.3

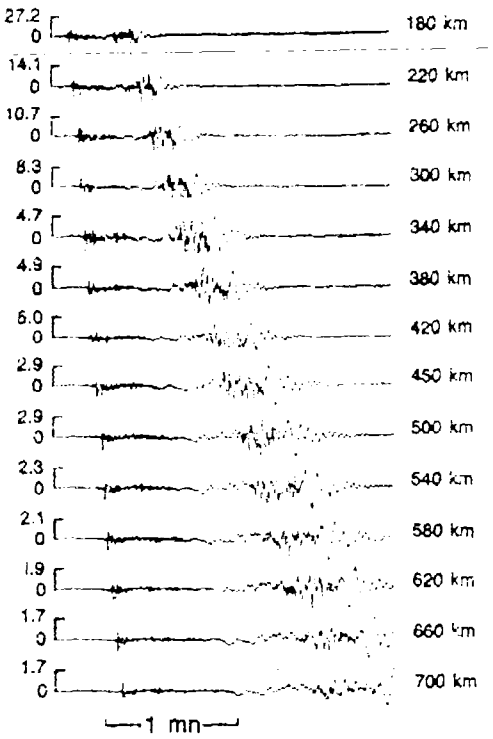

Fig. 1.

The comparison with the data (Fig. 4) shows a very good agreement between observations and calculations which supports the interpretation of L_g wave attenuation as an average shear wave crustal attenuation.

2. Influence of Source s Depth

As L_g waves are made up of multiple subcritically reflected S waves (*e.g.* Bouchon 1982), the shear wave velocity in the source region should affect their propagation. An illustration of this dependency is presented in Fig. 5. We have drawn in this figure all the subcritically reflected rays (that is the individual contributions to the L_g wave group) radiated by sources located at 1 km, 10 km and 29 km depth. Clearly, the L_g waves radiated by the three sources sample with different weight different regions of the crust. A deeper source will sample the crust more uniformly than a source located in the upper crust.

Another related phenomenon is depicted in Fig. 6. We have traced all the subcritically reflected rays radiated by a 10 km deep source and

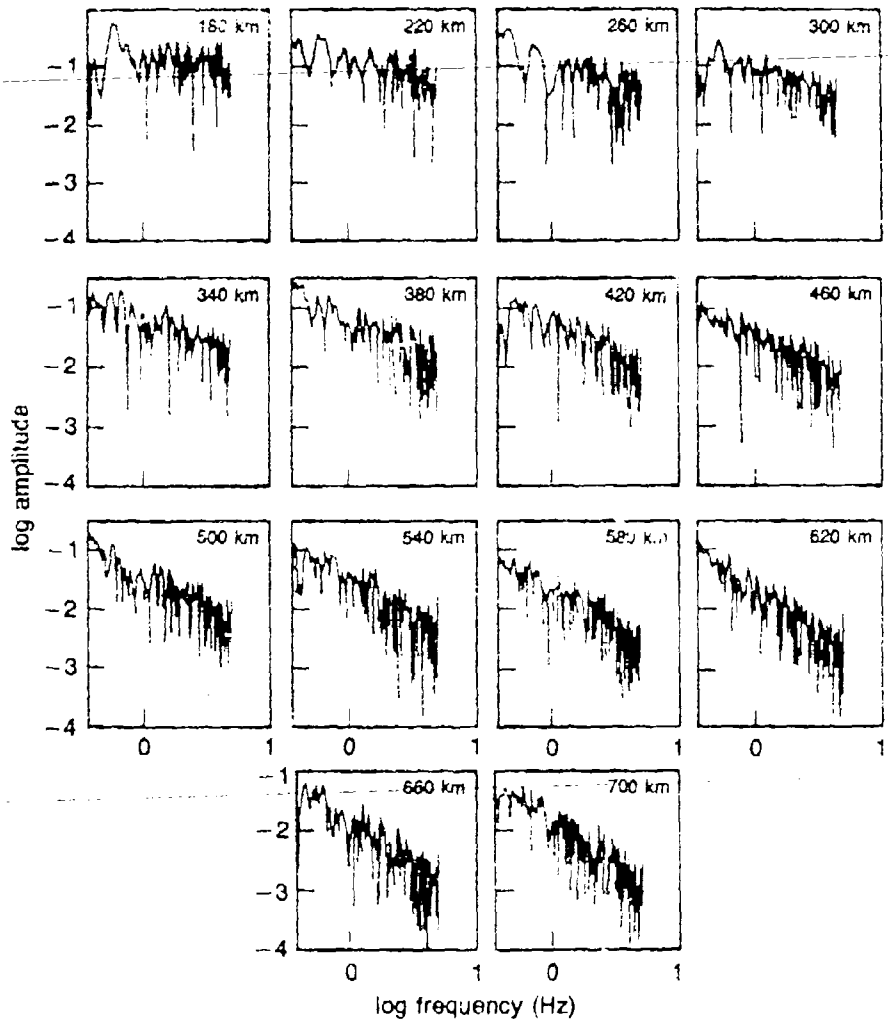

Fig. 2.

leaving the source in three different ranges of take off angles: 0-60°, 60°-120°, and 120°-180°. The shallowest rays do not sample the lower crust while the more oblique ones which are associated with longer travel time sample the crust quite uniformly.

In Fig. 7 we investigate the effect of a low Q in the upper sedimentary layer on the attenuation of L_g waves. We assume that all the attenuation occurs in the 2 km thick upper layer and is of the form $Q = 100f^{0.5}$. The corresponding synthetic seismograms show that the high frequencies attenuate only slightly with distance and suggest that a zone

Fig. 3.

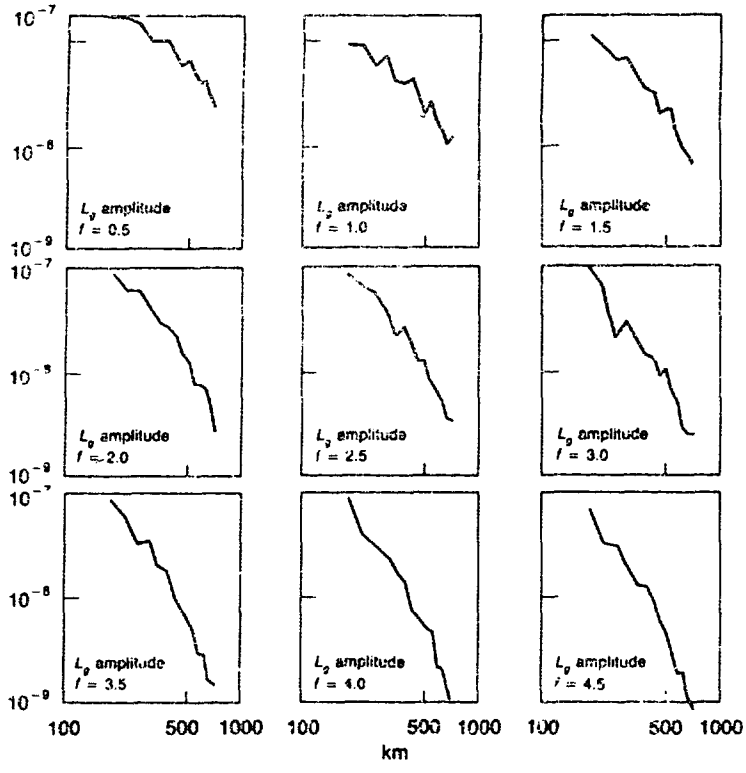
10^{-7}
10^{-8}
10^{-9}
L_g amplitude
f = 0.5
L_g amplitude
f = 1.0
L_g amplitude
f = 1.5
L_g amplitude
f = 2.0
L_g amplitude
f = 2.5
L_g amplitude
f = 3.0
L_g amplitude
f = 3.5
L_g amplitude
f = 4.0
L_g amplitude
f = 4.5
100
500
1000
km

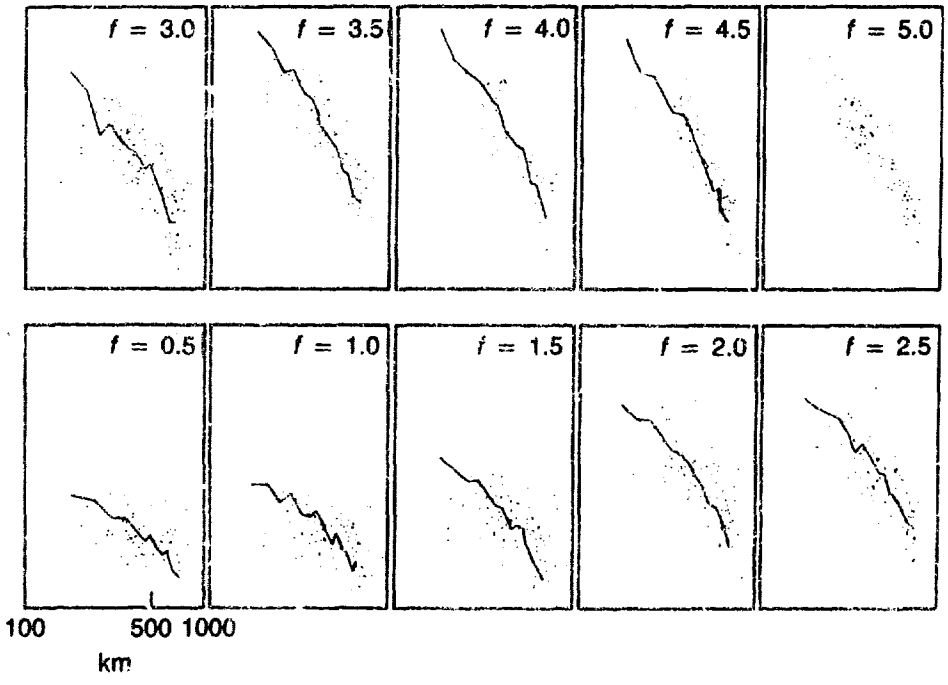
f = 3.0
f = 3.5
f = 4.0
f = 4.5
f = 5.0
f = 0.5
f = 1.0
f = 1.5
f = 2.0
f = 2.5
100
500 1000
km

Fig. 4.

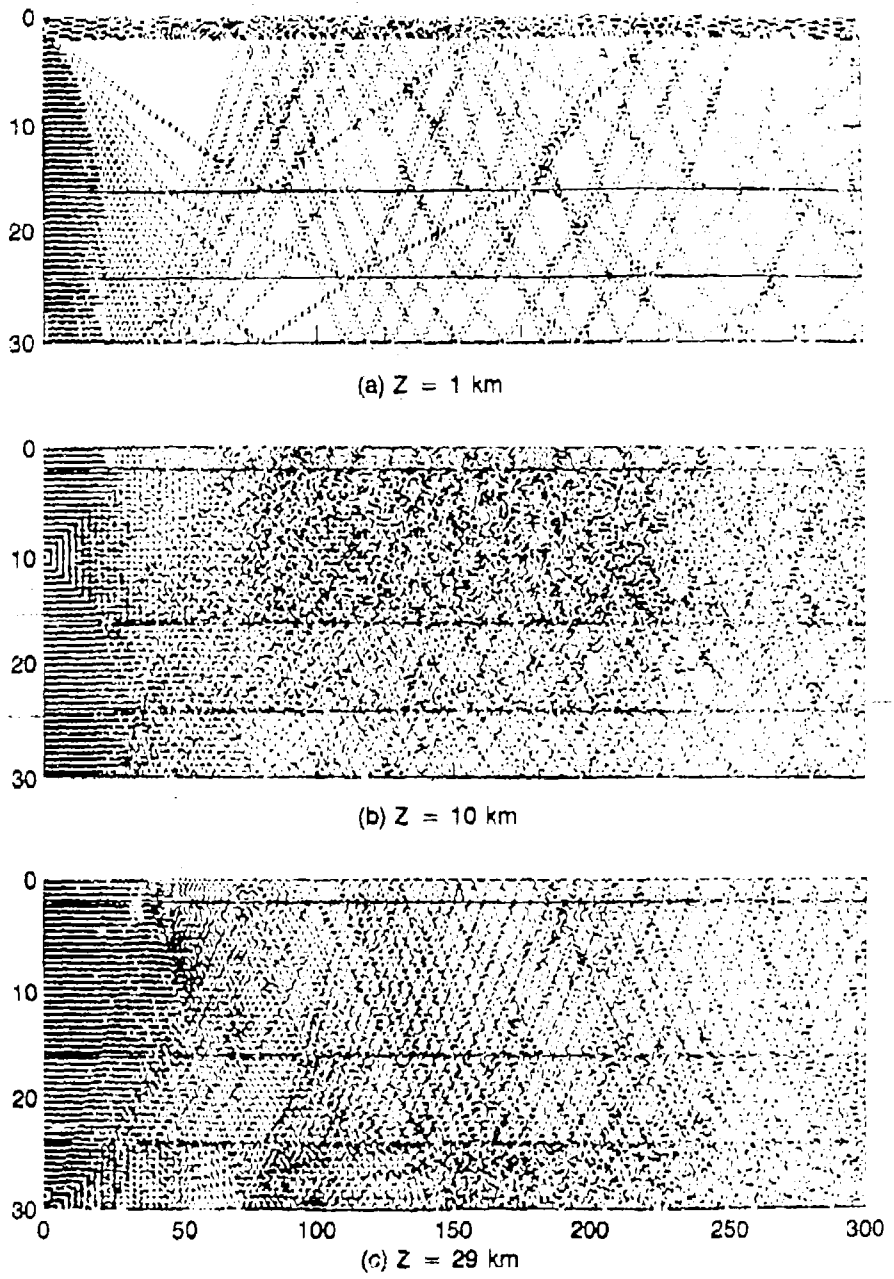
0
10
20
30
(a) Z = 1 km
0
10
20
30
(b) Z = 10 km
0
10
20
30
0
50
100
150
200
250
300
(c) Z = 29 km

Fig. 5.

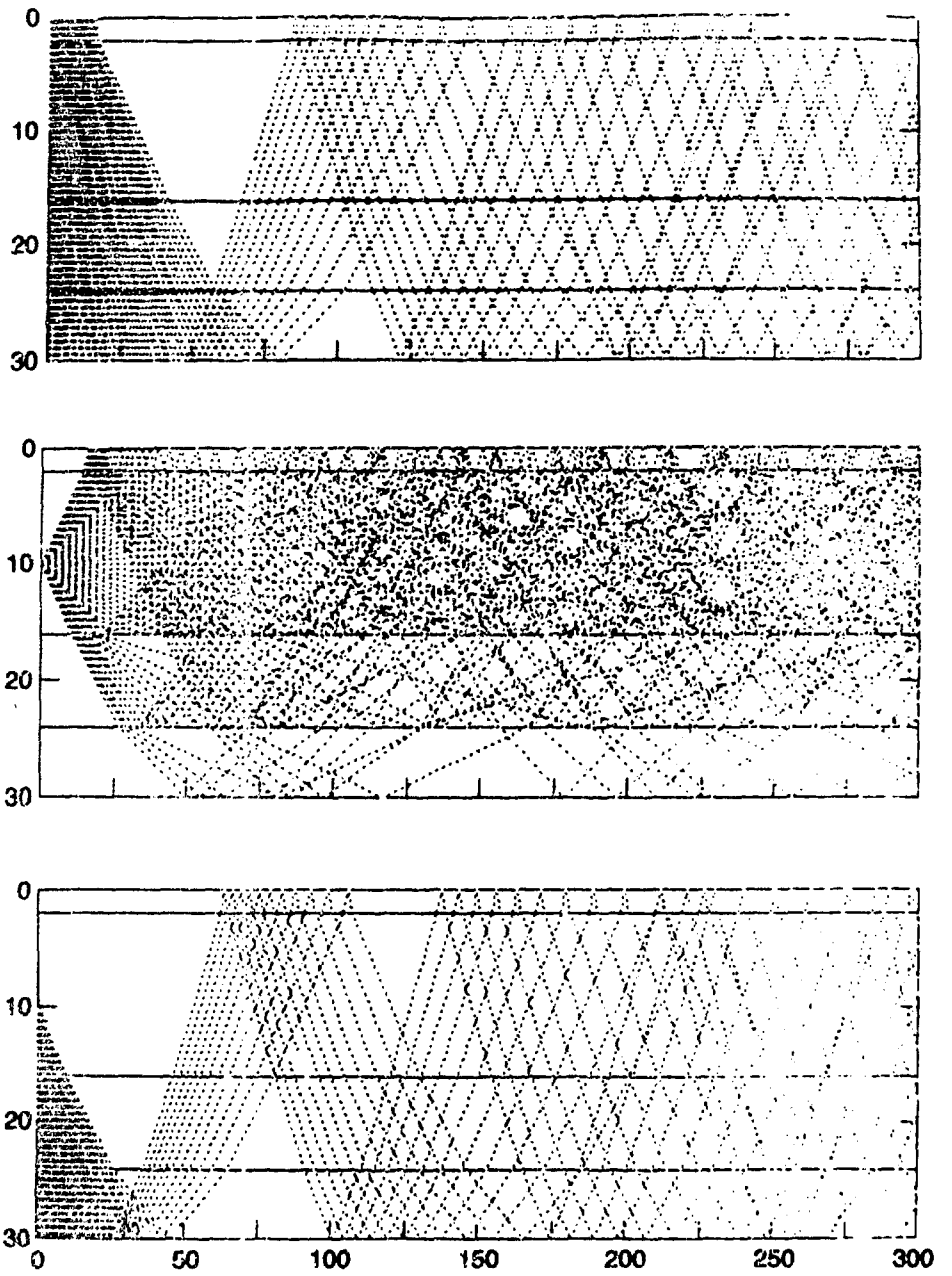

Fig. 6.

of low Q in the sediments or at shallow depth would have little effect on the attenuation of L_g waves.

It is also interesting to investigate the effect of a zone of high attenuation at the base of the crust as such models have been proposed by several authors.

For this purpose, and in order to separate such effects, we consider a model where all the attenuation occurs in the bottom crustal layer. We again assume $Q = 100f^{0.5}$. The resulting seismograms are presented in Fig. 8. They show a sharp attenuation of the L_g coda. The comparison with Fig. 7 is particularly striking in this respect: the L_g wave coda is quite insensitive to the presence of highly attenuating sediments but will be strongly affected by attenuation or scattering at the base of the crust.

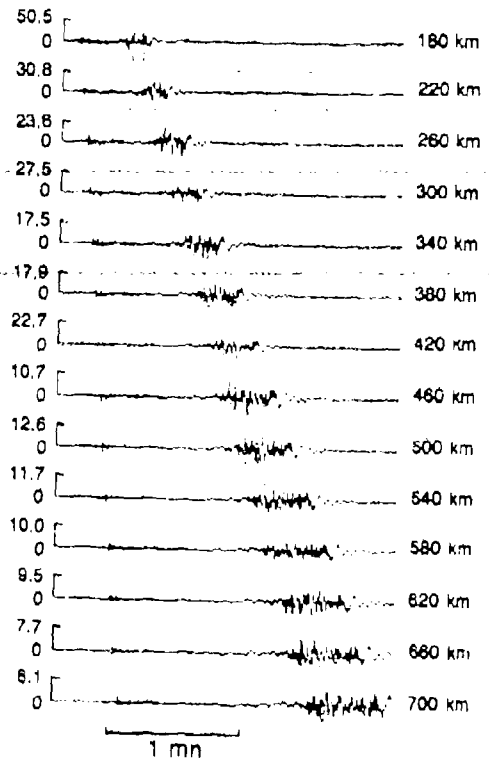

Fig. 7.

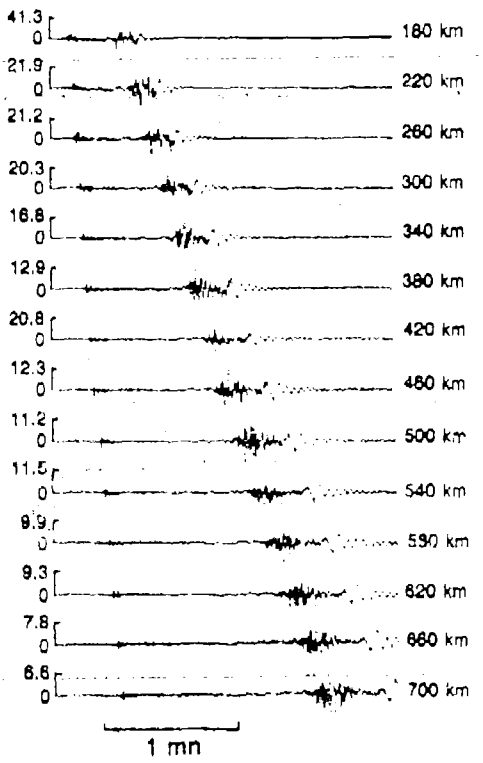

Fig. 8.

References

Bouchon, M., "The Complete Synthesis of Seismic Crustal Phases at Regional Distances," *J. Geophys. Res.*, **87**, 1735-1741, 1982.

Campillo M., M. Bouchon and B. Massinon, "Theoretical Study of the Excitation, Spectral Characteristics, and Geometrical Attenuation of Regional Seismic Phases," *Bull. Seism. Soc. Am.*, **74**, 79-90, 1984.

Hide-In-Earthquakes (HIE) Studies Using Broadband Data

J.A. Burnetti and D.W. Rivers

Summary

A detailed examination of seismicity rates before and after large earthquakes is to be performed. Superposition of earthquake and explosion broadband seismograms will be used to evaluate the effectiveness of the Hide-in-Earthquake (HIE) evaluation scenario for regional networks. This study is still in the preliminary stages of investigation.

Background

An evasion scenario which has attracted considerable attention in previous studies is the possibility of disguising a clandestine nuclear test by setting off the explosion shortly after the occurrence of a large earthquake. These studies of the hide-in-earthquake (HIE) evasion technique have utilized seismicity patterns to predict the number of opportunities per year for the detonation of an explosion which could not be de ected on account of interfering signals from the preceding, larger earthquake. Such studies may tend to underestimate the possible effectiveness of the HIE technique, since some secondary signals within seismic codas which are detectable in theory may nevertheless go unreported in actual practice if particular attention is not paid to the possibility of evasion. Furthermore, even if signal arrivals are detected in the earthquake coda, it is not guaranteed that they will be correctly associated so that an analyst can form the second event correctly. One method of avoiding these pitfalls in the estimation of HIE effectiveness is to use only seismic bulletin data which have already been processed without special regard to signals buried within codas. These bulletin data would be used to test the hypothesis that earthquakes may get hidden in the codas of other earthquakes. If this hypothesis turns out to be true, then one would be led to conclude that the HIE technique would be successful under the same set of conditions (*i.e.* data availability and routine analysis procedures) as prevailed during the creation of the bulletin.

An important aspect of previous HIE studies has been the determination of how small a signal may be detected within the coda of a larger

earthquake. This determination has been performed by synthesizing composite seismograms consisting of explosion and earthquake signals added together at various time separations with various relative amplitudes. These synthetic seismograms were examined by an analyst, who attempted to identify the explosion signals which were imbedded within the earthquake codas. As was noted earlier, this procedure may tend to overestimate the analyst's effectiveness in performing this task in more nearly routine circumstances. These studies are nevertheless useful as a determination of how small a signal is at least possible, if not actually likely, to be detected within an earthquake coda. These studies (*e.g.*, Jeppson, as reported by Dahlman and Israelson, 1977) have utilized the response of short-period instruments in generating the synthetic seismograms, since signal detection is customarily performed on short-period traces. Modern seismic networks such as the RSTN, however, also employ broadband instruments which may impart information useful for HIE counterevasion. In particular, the characteristic period difference between earthquakes and explosions may be more nearly evident on broadband traces. The RSTN is envisioned as a prototype for a network which would be deployed within the USSR, so it is an appropriate system to use as a model in an HIE investigation which is designed to determine the counterevasion value of stations located at regional distances to the explosions and/or interfering earthquakes. Such an investigation should utilize the broadband as well as the short-period RSTN instrument responses.

Seismicity Survey For HIE Analysis

A survey is planned of global seismicity rates before and after large earthquakes. This survey will be aimed at determining whether small earthquakes tend to get hidden in the codas of larger ones which are located either nearby ($\Delta \leq 500$ km) or at large distances from them. It will be necessary to exclude earthquakes occurring within 50 km of each other in order to avoid biasing the count of the seismicity rate by including aftershocks and earthquake swarms. Since earthquakes outside the aftershock zone presumably are distributed randomly in time and space with respect to the preceding large earthquake, if it does in fact turn out that some of them are by chance obscured by the larger event, then this observation would tend to lend credence to the possibility that an HIE evasion attempt which was carefully designed to take advantage of the distribution of seismic regions and monitoring stations might enjoy a good chance of success. Particular attention will be paid to the inferred magnitude distribution of the "missing" events (if any) following earthquakes of various magnitudes. It is doubtful that statistically

significant results can be obtained without examining many years' worth of seismic bulletin data, so it is to be anticipated that the examples of earthquakes hidden by other earthquakes, if any are found, will be anecdotal evidence for the potential success of HIE.

In addition to this anecdotal evidence about "missing" earthquakes, the examination of seismic bulletin data will reveal certain information which is of more direct importance in analyzing the potential for HIE evasion. Specifically, a detailed examination will be made of those events which actually are detected following a large earthquake in spite of interference from the seismic coda. This examination will be aimed at determining which stations fail to report a signal arrival from the second (smaller) earthquake, as compared with those stations which would have reported a signal arrival for an event occurring at the same epicenter and having the same magnitude if it were not for the preceding large event. In order to simulate the HIE scenario, this investigation should be confined to earthquake pairs in which the second, smaller earthquake is shallow. Statistics will be compiled on the number of detecting stations (and by inferrence, non-detecting stations) and their distribution with respect to both of the interfering events, as a function of the following parameters: magnitude difference between the two events (assuming that there are enough detections of the second event to permit its magnitude to be determined reliably), distance between the two events, distance between each event and the station, and the time interval between the two events. By comparing the lists of detecting stations for a large number of interfering events with those of matched isolated events, patterns will be constructed which show how the aforementioned parameters interact to determine whether the second one of a pair of earthquakes will be detected at a given station. Using this information, conclusions will be drawn about the configurations of seismic networks which would, and which would not, be vulnerable to evasion by the HIE technique in various circumstances.

The seismicity investigation is so far in only a preliminary stage, since the necessary ISC bulletin data has not yet been loaded onto the computer system. When the signal arrival files are installed, they will be searched automatically to extract the desired information about detection patterns for pairs of interfering events.

The Simulation With Broadband Seismograms

A simulation of the HIE scenario can be performed by taking seismic records from "normal" days containing explosions and superimposing on them seismograms from large earthquakes. The superposition of the seismograms is to be carried out in such a way that certain of the codas

of the added earthquakes obscure the pre-existing explosion signals on the "normal" records. Since this can be done independently for the records from each station in the network, it is possible to simulate the large earthquakes' occurring at any desired epicenters. The choice of the delay and magnitude difference between the interfering events can be made in accordance with the circumstances which were found to be favorable for HIE evasion on the basis of the seismicity investigation. The composite seismograms will be examined to determine whether the explosion signals on the original record can still be recognized.

As we have pointed out in the previous discussion, studies such as this one have been performed before, and they may tend to overestimate the effectiveness of secondary signal detection within codas as it is performed in normal practice. Nevertheless, this procedure is valuable for establishing at least a lower limit on the effectiveness of HIE. The difference between this study and the previous ones is that the usual short-period seismograms are to be supplemented with broadband records. We are especially interested in the HIE evasion technique as it might be applied to networks of stations located at regional distances to the explosions and to many of the earthquakes. We are therefore interested in the HIE counterevasion capabilities of the RSTN stations, which are prototypes of stations designed to be deployed at regional distances from nuclear tests and from seismically active regions within the USSR. Two important features of the RSTN are the extended dynamic range of the instruments and the inclusion of broadband instrumentation. Our investigation of HIE simulation by seismogram superposition will focus on whether these features make the RSTN less vulnerable to HIE evasion than would be the case if conventional short-period instruments were to be used for monitoring at regional distances. We shall investigate various filtering techniques for the broadband data to see whether the capability of detecting the hidden explosion signals can be enhanced.

This investigation is also at a preliminary stage, since we are currently retrieving particular short-period and broadband seismograms from the RSTN archival data base which are deemed to be useful for the seismogram superposition. Regional waveforms of events with various magnitudes, and hence a range of corner frequencies, have been selected for use in this analysis.

Conclusions And Recommendations

Since this study is currently in the data acquisition phase, no conclusions can be made about the utility of broadband data for use against an HIE evasion scheme, and no recommendations can be made for additional study until the present investigation has progressed further.

References

Dahlman, O., and Israelson, H. (1977). *Monitoring Underground Nuclear Explosions*, Elsevier North-Holland, Inc. New York.

T-Waves with Long Inland Paths: Synthetic Seismograms

Yves Cansi and Nicole Bethoux

Abstract

In order to provide more insight into the T-phase land propagation, signal analysis has been carried out. We found that the wavetrain is composed mainly of P_g- and S_g-waves which reach the seismic station under different azimuths. With the hypothesis that the signal is the sum of discrete arrivals due to different rays crossing the continental slope in different points, synthetic seismograms of T-waves are computed inducing variation of the conversion point along the slope. We show that the transmission of energy from the ocean to the solid medium is mainly due to diffraction effects. We point out the influence of the continental slope on the duration and the amplitude of the T-phase which are different criterions used to evaluate the tsunami risk.

Introduction

T-waves are propagated along oceanic paths as compressional waves in water, generally in the SOFAR channel. Following Northrop (1974) and Bath *et al.* (1971) we will not study these waves strictly speaking, but the seismic waves generated by their conversion along a continental slope and propagated in the earth to the recording station. We have used *T*-phases generated by underwater shots in the Atlantic Ocean at about 1200 km from the slope (see Fig. 1 and Table 1 for location) and recorded on the French L.D.G. Network and on a three-axial short-period seismograph station implemented near the coastline for the experiment.

The typical shape of *T*-waves with long inland paths is well documented in Fig. 5. In some stations (for example RJF and LOR), the

Table 1. Events studied in this paper.

	Latitude	Longitude	Date	Origin Time UTC
Chemical blast	41.893 N	17.885 W	Oct 11, 1981	20h 54m 38.15s
Algerian earthquake	36.589 N	5.271 E	June 28, 1974	11h 09m 40.0s
Tanker explosion near Corsica	41.20 N	7.10 E	July 5, 1981	11h 26m 15s

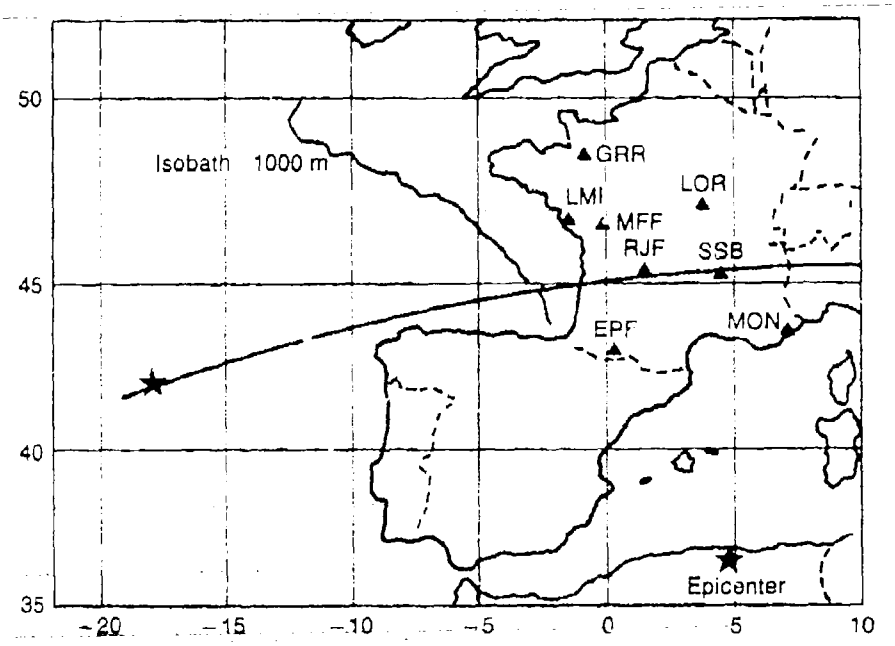

Fig. 1. Locations of the seismic stations of the L.D.G. Network used in this study. Epicenters are shown by ★. The great circle determines the southern limit of the useful isobath due to the northern part of Spain.

signal is separated in two parts. A numerical polarization filter applied on three dimensional records leads to results involving the hypothesis of a double conversion into P_g and S_g waves along different azimuths corresponding to different points of the conversion slope. The rather important duration of the recorded signal (between 3 and 4 minutes) contrasting with the supposed short one of the source (less than 1 s) suggests that the acoustic to seismic conversion takes place on different points of the continental slope. This fact has been already pointed out by many authors (Aubrat, 1963; Northrop, 1974; Talandier and Okal, 1979; Cansi, 1980). The purpose of this paper is to better understand this influence. Under the hypothesis that the T-wave train recorded in a station is the sum of discrete arrivals due to rays crossing the continental slope at different points, synthetic seismograms are computed inducing variation of the conversion point along the slope. Diffraction theory is used to compute transmission effects.

Signal Analysis

In order to evaluate the importance and direction of polarization of the recorded signals, we have drawn the ground motion in different planes.

The results are displayed in Fig. 2. Within the first figure, polarized signals in the east-western vertical plane are seen, which are identified as P_g-waves, according to the epicenter-station direction. Then the increase of the polarized signal in the horizontal plane suggests the presence of S_g-waves. For a more detailed analysis, we have used a numerical polarization filter called "REMODE" filter. The main part of the theory is described in Kanasewich (1975) and will be now briefly summarized.

The vertical Z and radial R components of seismic records are rotated so that the expected direction of the incident wave bisects the angle between the two orthogonal components $\bar{R}$ and $\bar{Z}$. The filter operator is obtained by a cross-correlation function $C(T)$ of $\bar{R}(t)$ and $\bar{Z}(t)$ over a window centered at some time t of the record. By convolving $C(T)$ with the original time series, motion of high rectilinearity is enhanced. Then the output series are given by $Y_R = pKR*C$ and $Y_Z = pKZ*C$ where K is a normalizing factor and p is a polarization one choosing

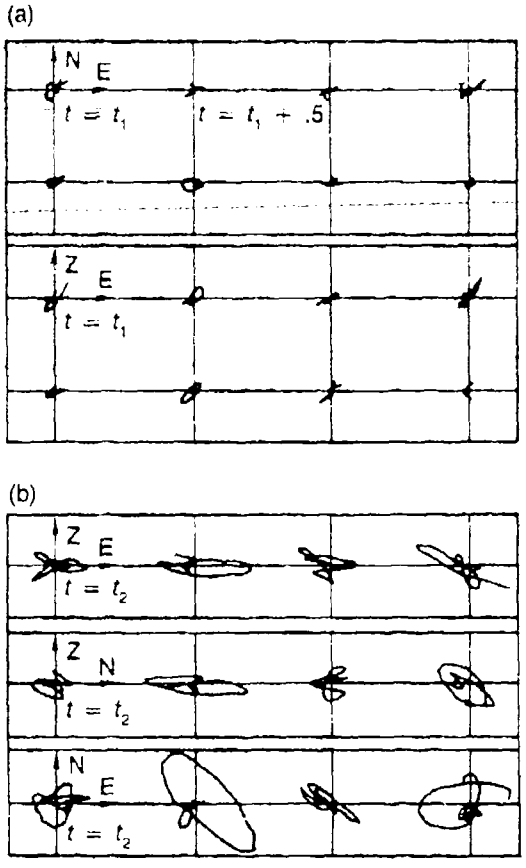

Fig. 2. Ground motion deduced from the 3-axial station LMI for the chemical blast recorded on October 12, 1981. N, E and Z stand for North, East and Vertical upward direction. Figure (a) shows P_g-polarized phases at the beginning of the signal ($t_1 = t_0 + 13' 40''$) and Fig. (b) shows S_g-polarized phases at the end of the signal: ($t_2 = t_0 + 14' 20''$). For each figure, one frame represents 0.5 s and the figures are to be read from left to right and from top to bottom.

between P and S type (Kanasewich, 1975). The * denotes convolution. In order to smooth the output signals, we have computed the energy by integrating it over a 5-second time window. In Fig. 3, we observe at the beginning of the signal a highly polarized P-phase, prevailing in the azimuths close to the epicenter-station direction. In the further part of the signal, groups of S-waves are identified. All these phases follow different azimuths which means a conversion at different points of the continental slope.

Synthetic Seismograms: Method

The method is based upon the knowledge of the continental slope. According to the fact that T-waves reach the coast at the SOFAR depth (about 1000 m in the Atlantic Ocean) this isobath has been digitalized

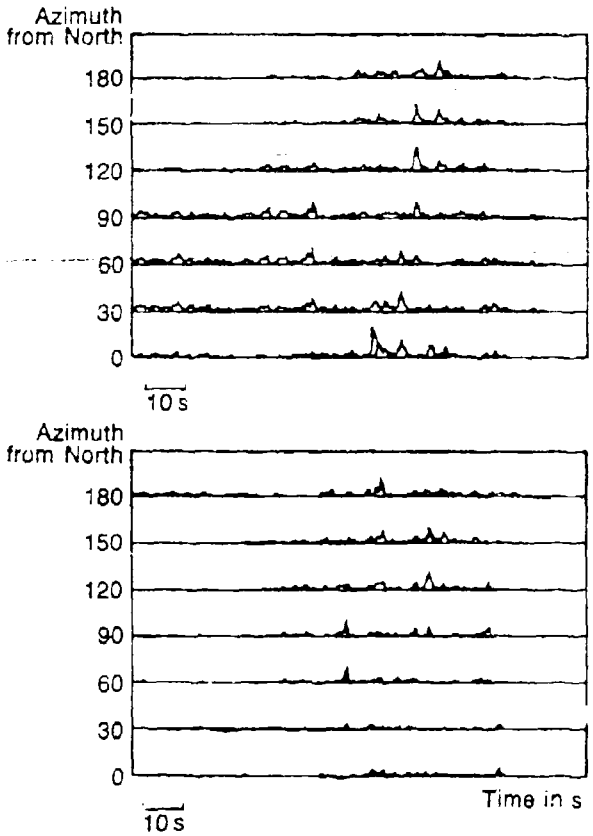

Fig. 3. Energy of the REMODE-filtered signal of the chemical blast recorded at LMI. Each trace represents the energy obtained in the azimuth displayed on the left. (a) P_g-polarized filtered signal (b) S_g-polarized filtered signal.

with an accuracy of about one point each kilometer (for instance 583 points for the French Atlantic continental slope 600 km long). It is convenient to cut off the isobath at some point in the South because of the shadow-zone due to the northern part of Spain (see Fig. 1).

1. Travel-time. In the case of an underwater blast, denoting by E the epicenter, S the station and P_n the n-th point of the digitized isobath, travel-time of the two types of converted waves can be written in the form:

$$t_{jn} = \frac{1}{V_T}^{d_n} + \frac{1}{V_j}^{d'_n} + \tau_j \,. \tag{1}$$

d_n denotes the distance between E and P_n, d'_n the one between P_n and S and τ_j is the time-term of the j-th hodochrone according to the crustal model displayed in Table 2 ($j = 1$ for P_g-phase and $j = 2$ for S_g-phase). V_T is the T-phase velocity in water (1484 m/s in the Atlantic Ocean). In the case of an inland event, we have taken into account first a seismic to acoustic conversion at the coastline close to the epicenter and then an acoustic to seismic one close to the station.

2. Amplitudes. Assuming that the T-waves reaching a rectangular elementary surface Σ_n of the slope centered at same point P_n, are diffracted into the ground, we have used diffraction theory developed by N. and S. Tjotta (1981) to compute the transmission effects of an acoustic beam into a solid medium.

Denoting by φ the angle of incidence of the SOFAR T-wave measured in the vertical plane from the horizontal direction, the incident beam reaches the interface plane π_n containing Σ_n with an angle of incidence δ_n depending on φ and the slope β_n of Σ_n. The local reference system is defined at the point P_n by $z = 0$ for the interface plane π_n, and

Table 2. Crustal model used to compute the inland propagation.

Layer thickness	*P*-wave velocity (km/s)	*S*-wave velocity (km/s)
0.9	3.00	1.73
25.0	6.03	3.56
	8.16	4.65

This leads to the following hodochrones:

$t = 0.52 + \Delta/6.03$ for P_g-phase

$t = 0.91 + \Delta/3.56$ for S_g-phase

$y = 0$ for those plane of incidence Q_n (see Fig. 4). The observation direction is located by its cartesian and spherical coordinates (x_n, y_n, z_n) and $(r_n, \theta_n, \varphi_n)$.

Following N. and S. Tjotta, we write down the frequency response of the point P_n:

$$S_{jn}(x_n, y_n, z_n; \omega) = S_0 T_{jn} ik_j \cos\theta_n (\pi r_n)^{-1} \exp(ik_j r_n)$$
$$\iint_{\Sigma_n} \exp[-ik_j (ux_n + vy_n)/r_n] \exp[ik' \sin\delta_n u] \, du \, dv \qquad (2)$$

with $k_j = \omega/V_j$ and $k' = \omega/V_T$. T_{jn} is the complex transmission coefficient for a plane wave which depends on δ_n (see McKenzie, 1960).

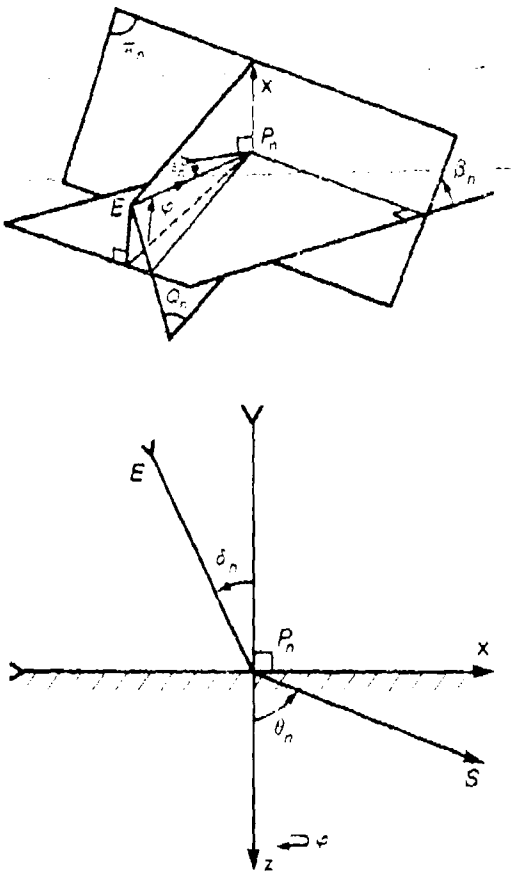

Fig. 4. Geometry and notations used in the diffraction formula. π_n is the interface plane and Q_n the incidence one. EP_n is the T-wave ray from epicenter E to the n-th transform point P_n. The transmitted ray P_nS is defined by its spherical coordinates θ_n, φ_n relative to the local reference system (P_n, x, y, z).

Denoting by P (respectively $\bar{P}$) the middle point of the segment $[P_{n-1}, P_n]$ (respectively $[P_n, P_{n+1}]$) Σ_n is delimited by the two vertical planes containing P and $\bar{P}$ and the horizontal ones delimiting the thickness of the SOFAR channel.

Assuming that the angle φ can vary from $-14°$ to $14°$ (Officer, 1968) in the Atlantic Ocean, summation is made for all these directions. The converted signal $S_{jn}(t)$ at the point P_n is then computed by performing an inverse Fourier transform on the function $S_{jn}(\omega)\ s(\omega)\ A_{jn}(\omega)$ where $s(\omega)$ is a source function, $A_{jn}(\omega) = r_n^{-1/2} \exp[-r_n\omega/(2Q_jV_j)]$ an attenuation factor. The numerical values for Q_j have been derived from Nicolas *et al.* (1982). The global wavetrain is then computed by:

$$S(t) = \sum_{j=1}^{2} \sum_{n=1}^{N} S_{jn}(t - t_{jn}) \tag{3}$$

To compare with real signals, we take the convolution of $S(t)$ with the impulse instrumental response $I(t)$.

3. Numerical Results. Synthetic seismograms and the original dataset are presented on Fig. 5 for the oceanic shot displayed on Fig. 1.

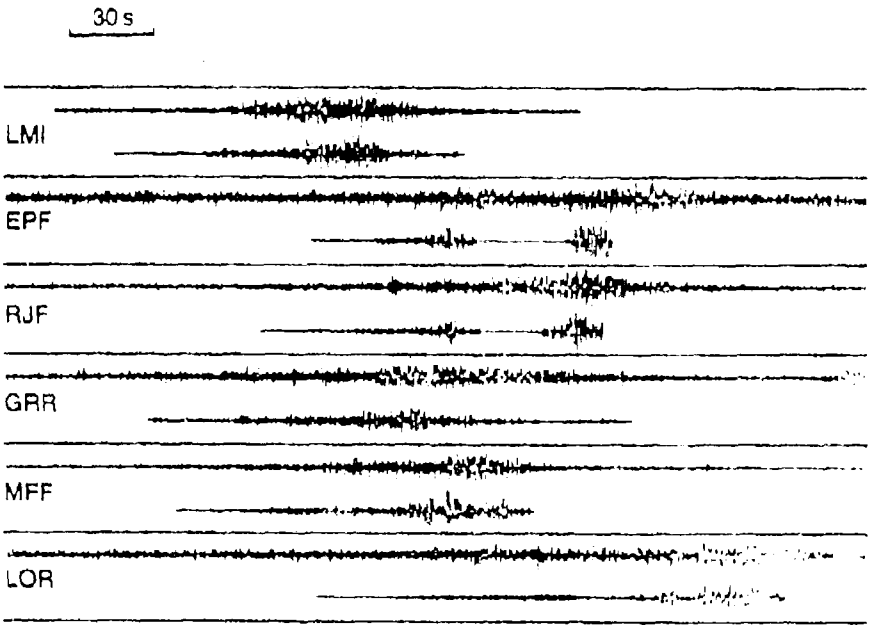

Fig. 5. For each station, the top trace is the recorded signal filtered in the 2 - 7 Hz band and the bottom one is the synthetic. Each signal is normalized.

We can see the good agreement with the data, especially for the northern stations (for example GRR, LMI*, MFF). On the other hand, for the southern stations like RJF and EPF, synthetic seismogram breaks down more rapidly than the original record. This difference might be explained by the fact that effects of inland propagation are not included in our synthetics. M. Bouchon (1981) has shown that in a multi-layered medium, L_g waves are multi-reflected S_g waves so that the ground response is slightly different from the simple one used in our computation.

However, for the northern stations like GRR, the last part of the signal is made up of discrete arrivals converted far from the station in the southern part of the slope (Fig. 5) so that the amplitude decreases slowly. On the other hand, for southern stations, the main part of the slope produces signals which arrive all together at the seismic station in a short time-window at the end of the signal. Then its last part ends abruptly and the lack of the propagation effects is clearly apparent.

Another example has been studied: an Algerian earthquake which occurred close to the Mediterranean coastline (see Table 1) and recorded at the triaxial station SSB (Fig. 1). Oceanic T-wave propagation in the Mediterranean Sea lies at about 100 m deep and we have used this isobath to compute the transmission. In this case, $V_T = 1509$ m/s (Porter, 1973). On this record, the existence of the two groups of converted seismic waves is well illustrated in Fig. 6. The first one can be seen in the vertical-radial plane (*i.e.*: vertical north-south) and corresponds to the T-P_g phase. The second one is predominant in the vertical-tangential plane (*i.e.*: vertical east-west) and might be interpreted in the T-L_g wavetrain. The synthetic signal has been separated into two groups and we can see the good agreement with the recorded data especially for the T-P_g wavetrain. As in the precedent case the lack of signal in the T-L_g coda is dramatically shown in the present example. In order to minimize the inland propagation effects, we have studied another case with the station standing near the continental slope (at about 1 or 2 km). It is the signal produced by the explosion of a tanker wreck off South Corsica and recorded at the seismic station of Monaco (MON) on July 5, 1981. Equation 2 can not be used because it is an equation for very far field (*i. e.*, $r_n \gg ka^2/(2\cos\delta_n)$ where a is the characteristic length of Σ_n.

N. and S. Tjotta give in their paper another formula for near field but for a direction of measure lying in the incidence plane:

* Provisory station.

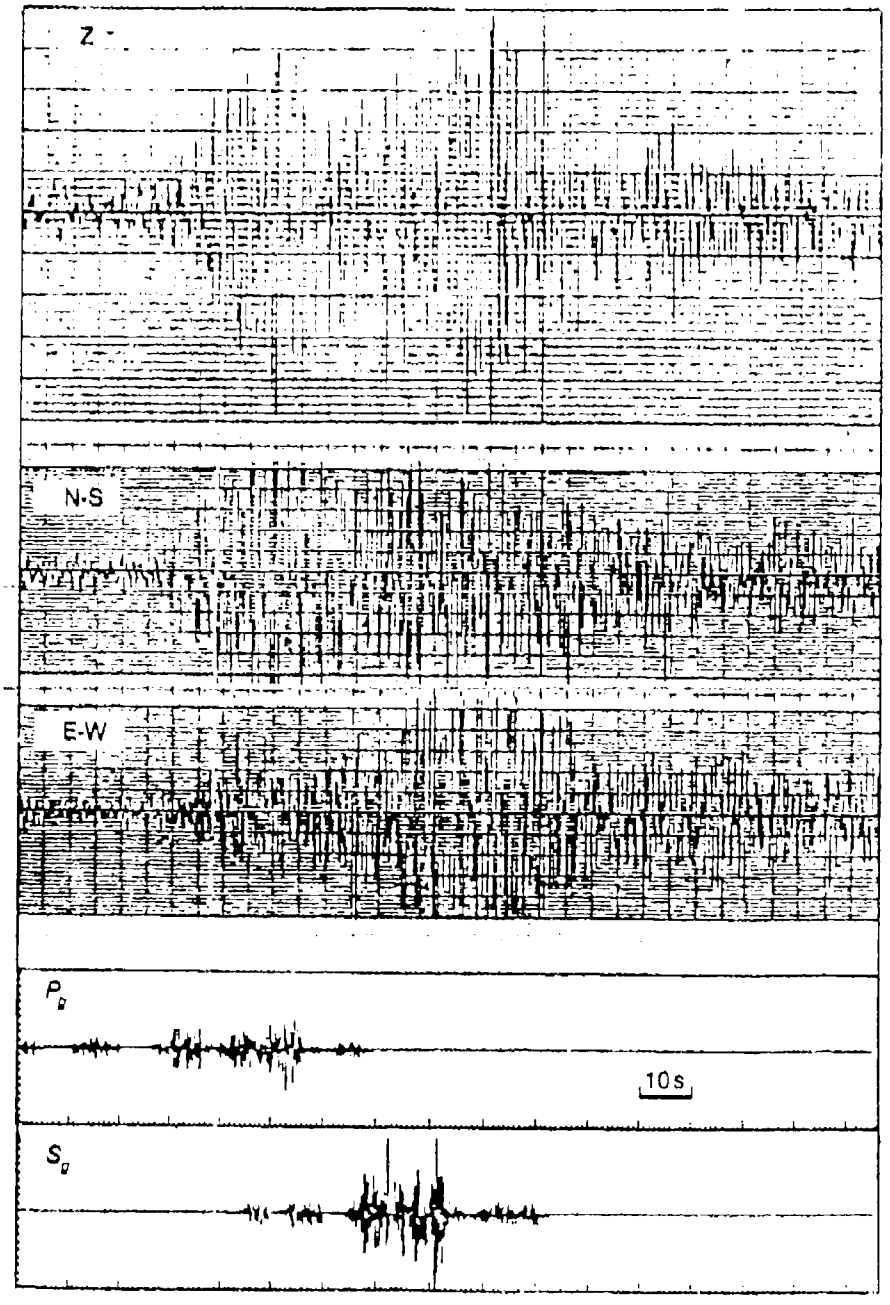

Fig. 6. The three top traces represent the seismic event of June 28, 1974 recorded at the three axial station SSB. The two groups correspond to the P_g and S_g wavetrain. The two traces at the bottom represent the synthetic signal in P_g-phase at the top, and S_g-phase at the bottom.

$$S_{jn}(x_n, y_n, z_n; \omega) = S_0\, T_{jn} \left(\frac{k' \sin\delta_n}{2\pi}\right)^{1/2} z_n \exp\left(ik' \sin\delta_n x_n - i\frac{\pi}{4}\right)$$
$$\int \exp\left\{\frac{ik' \sin\delta_n}{2}\left[\frac{z_n^2}{x_n - u} - \left(\frac{k_{jn}}{k' \sin\delta_n}\right)^2 (x_n - u)\right]\right\} \frac{du}{(x_n - u)^{3/2}} \tag{4}$$

with $k_{jn}^2 = (k' \sin\delta_n)^2 - k_{jn}^2$.

For all the points of the slope which are very close to the station, and which produce the main part of the signal, the station is also very close to the plane of incidence. This allows us to use this formula in our computation. Results are shown in Fig. 7 and we can see the good agreement with the recorded data despite the new approximation.

Conclusion

In order to explain the long-time direction of T-waves with long continental paths, an appropriate analysis has allowed us to conclude that acoustic waves are converted simultaneously into P_g and S_g (or L_g) waves along the continental slope. These signals have been interpreted as the summation of elementary waves corresponding to various transmission points. Under the hypothesis that this transmission is mainly due to diffraction effects, we have computed synthetic seismograms. The duration and the typical shape of the signal, although simplified, are in good agreement with the observed records. These records emphasize the main

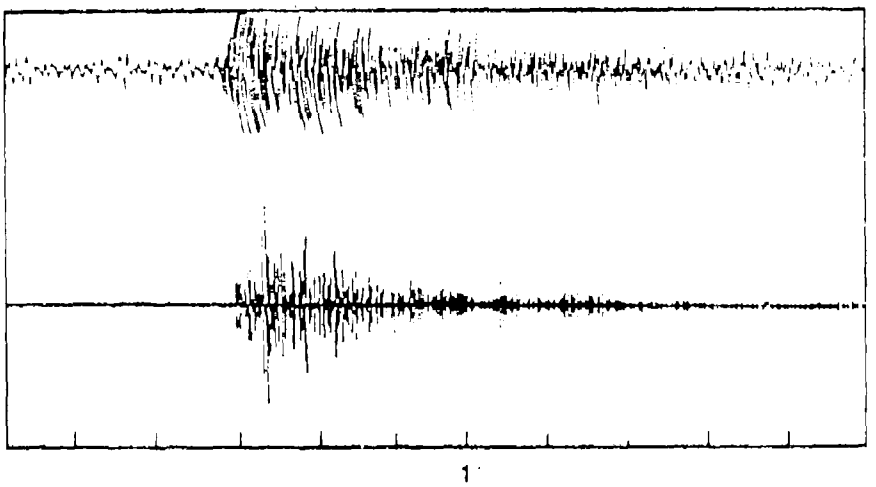

1

Fig. 7. The top trace is the signal recorded at Monaco station (MON) and produced by the explosion of a tanker. The bottom one is the synthetic computed with the Tjotta's formula for near field.

influence of the length and the shape of the continental slope versus the station location on the seismogram. Local parameters have to be taken into account in order to investigate empirical relations between the magnitude of earthquake, the amplitude or duration of the T-wave and the tsunami height. (Talandier, 1971; Comer, 1980; Johnson and Northrop, 1966).

References

Aubrat, J., "Ondes *T* Reflechies dans la Mer des Antilles," *Ann. Geophys.* **19**, F4, 1963.

Bath, M., and M. Shahidi, "*T* Phases from Atlantic Earthquakes," *Pure and Appl. Geophys.*, **92**, 74-114, 1971.

Bouchon, M., "The Complete Synthesis of Seismic Crustal Phases of Regional Distances," *J. Geophys. Res.*, **87**, 1735-1741, 1982.

Brekhovskikh, L.M., "Waves in Layered Media," *Applied Mathematics and Mechanics*, **16**, 2nd edition, Academic Press.

Cansi, Y., *Etude Expérimentale des Ondes T*, Thèse de 3e Cycle, Université Paris XI, (Orsay), 1981.

Kanasewich, E.R., *Time Sequence Analysis in Geophysics*, The University of Alberta Press, 2nd edition.

MacKenzie, K.V., "Reflection of Sound from Coastal Bottoms," *J. Acoust. Soc. Am.*, **32**, 221-231, 1960.

Nicolas, M., B. Massinon, P. Mechler, and M. Bouchon, "Attenuation of Regional Phases in Western Europe," *Bull. Seism. Soc. Am.*, **72**, 2089-21106, 1982.

Northrop, J., "*T* Phases from the Hawaiian Earthquake of April 26, 1973," *J. Geophys. Res.*, **79**, 5478-7958, 1974.

Officer, C.B., *Introduction to the Theory of Sound Propagation*, Mac-Graw Hill, ed. New York, 1968.

Porter, R.P., "Dispersion of Axial SOFAR Propagation in the Western Mediterranean," *J. Acoust. Soc. Am.*, **53**, 181-191, 1973.

Talandier, J., and E.A. Okal, "Human Perception of *T* Waves: the June 22, 1977 Tonga Earthquake felt on Tahiti," *Bull. Seism. Soc. Am.*, **69**, 1475-1486, 1979.

Tjotta, N., and S., "Theoretical Study of the Penetration of Highly Directional Acoustic Beam Into Sediments," *J. Acoust. Soc. Am.*, **69**, 998- 1008, 1981.

Tolstoy, I., and M. Ewing, "The *T* Phase of Shallow Focus Earthquakes," *Bull. Seism. Soc. Am.*, **40**, 25-50, 1950.

Discrimination between Quarry Blasts, Nuclear Explosions, and Earthquakes—Preliminary Results

I.N. Gupta, J.A. Burnetti and M. Marshall

Abstract

Regional phases from quarry blasts and earthquakes, observed at RSTN stations, show significant spectral differences on both the short-period and mid-period instrument records. Limited data from quarry blasts and earthquakes indicates that the spectral ratio of transverse component initial to later L_g may work as a discriminant. Furthermore, quarry blasts seem to generate strong surface (both Love and Rayleigh) waves in the mid-period band.

Spectral characteristics of regional phases have also been examined on short-period, three component records of several closely spaced (within a few km) nuclear explosions from the NTS. The objective is to understand the influence of localized near-source variations on the characteristics of regional phases when the source-receiver path is essentially common. Preliminary results indicate surprisingly large differences in both the amplitude and frequency content of both P_g and L_g phases, even for two explosions within a few hundred meters of each other and of nearly equal yields.

Introduction

A number of promising avenues for discrimination at regional distances follow from recent research, especially by Gupta and Blandford (1983a) and Murphy and Bennett (1982). Explosion shear waves seem to be primarily generated by near source $P \rightarrow SV$ scattering which is more efficient at low frequencies (Gupta and Blandford, 1983a). This explains why the spectra of shear waves, including L_g from an explosion are significantly deficient in higher frequencies so as to be useful for source discrimination (Murphy and Bennett, 1982). The transverse component of shear waves or *SH* from an explosion is mainly due to the scattering of *SV* into *SH* by small heterogeneities perturbing a nearly plane stratified medium (Gupta and Blandford, 1983a). This results in the short-period *SH* having an emergent beginning with small amplitudes but rich in high

frequencies so that the first arrivals on the transverse component of L_g from explosions are richer in high frequencies than the later arrivals. Short-period *SH* motion from earthquakes, on the other hand, generally has a sharp onset and the spectra of the initial and later arrivals in L_g are not expected to be much different. These ideas appear to be supported by data from several nuclear explosions and earthquakes recorded at local and regional distances. Limited data from small chemical explosions (see *e.g.* Kisslinger *et al.*, 1961) also show the initial *SH* motion to be generally richer in higher frequencies than the later arrivals.

In this study, we have carried out a preliminary analysis of the spectral characteristics of regional phases generated by quarry blasts, nuclear explosions and small earthquakes. Three component records of quarry blasts and earthquakes have been examined at several RSTN stations. Short-period, three component records of several closely spaced nuclear explosions recorded at a common station have also been analyzed in an attempt to understand the influence of near-source variations on the generation of regional phases.

Quarry Blasts and Earthquakes

Whereas the available data from quarry blasts is still too limited to draw any general conclusions, preliminary results seem interesting. Short-period, three component rotated records from the RSTN stations RSCP for a quarry explosion in Kentucky on June 21, 1983 with epicentral distance of about 300 km are shown in Fig. 1. The letters *Z*, *R*, and *T*

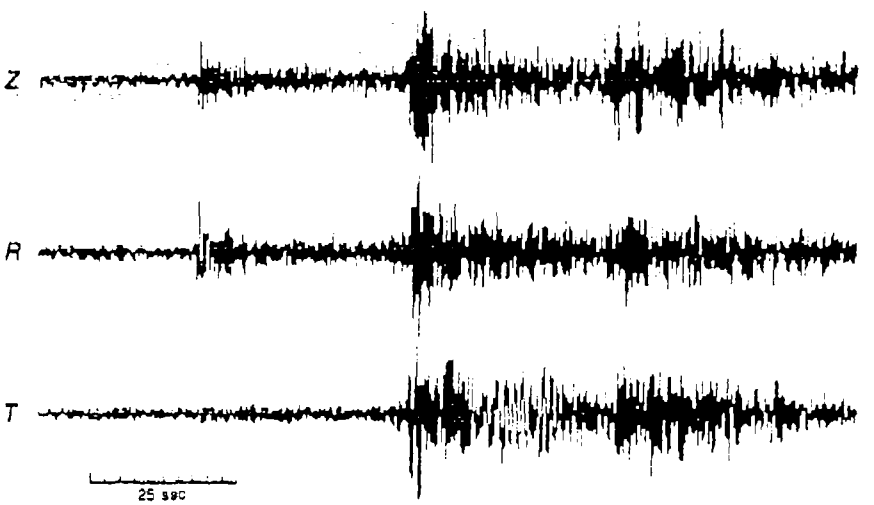

Fig. 1. Rotated, short-period three component records of a quarry explosion in Kentucky recorded at the RSTN station RSCP. *Z*, *R*, and *T* refer to these vertical, radial and transverse components, respectively.

refer to the vertical, radial and transverse component respectively. The spectral ratio of initial to later transverse L_g, shown in Fig. 2, shows a sharp increase with frequency, in agreement with Gupta and Blandford's (1983a) proposed mechanism for the generation of shear waves from explosions. This result is similar to that obtained earlier for SALMON and an earthquake, reproduced in Fig. 3 (Gupta and Blandford, 1983b). The upper figure shows the spectral ratio for the initial 12.8 sec of transverse L_g to the subsequent 12.8 sec signal from SALMON as recorded at EU-AL, at an epicentral distance of 242 km. The lower figure shows similar results from the Alabama earthquake of 18 February 1964, again recorded at EU-AL at an epicentral distance of 311 km. The signal to noise ratios are such that results for frequencies higher than 5 Hz are not reliable. There is a clear distinction between the two spectral ratios. The increase with frequency for the quarry blast (Fig. 1) appears, however, to be considerably faster than for SALMON (Fig. 3), probably because of greater scattering due to the shallower depth of the blast.

The rotated mid-period records for the same quarry blast as in Fig. 1 are shown in Fig. 4. The most striking feature seems to be the large amplitude Love waves. A few other blast records showed large-amplitude surface waves (Rayleigh and Love). The three-component waveforms appear similar to the fundamental-mode Rayleigh and Love

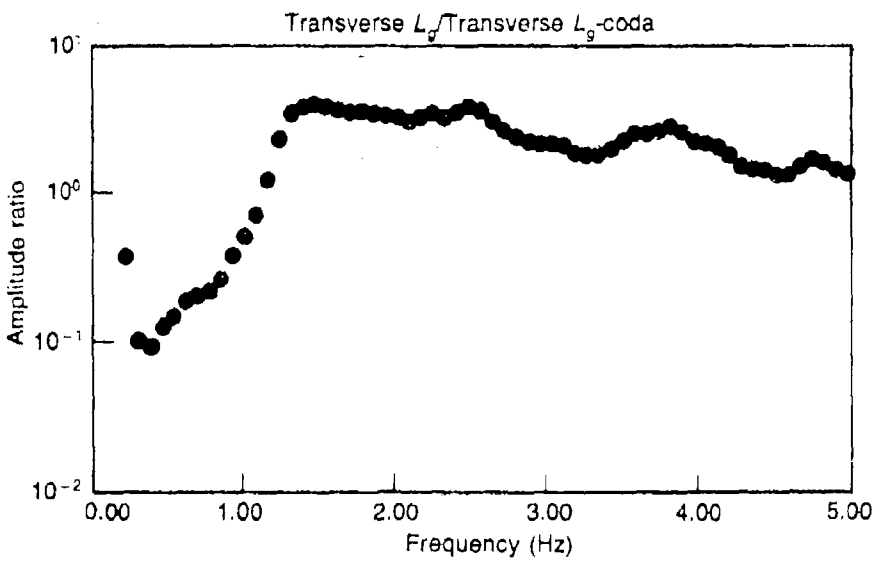

Fig. 2. Spectral ratio of transverse component initial to later L_g (each 12.8 sec long) obtained from the quarry blast records shown in Fig. 1. Note the sharp increase in the amplitude ratio with frequency for frequencies up to about 1.4 Hz.

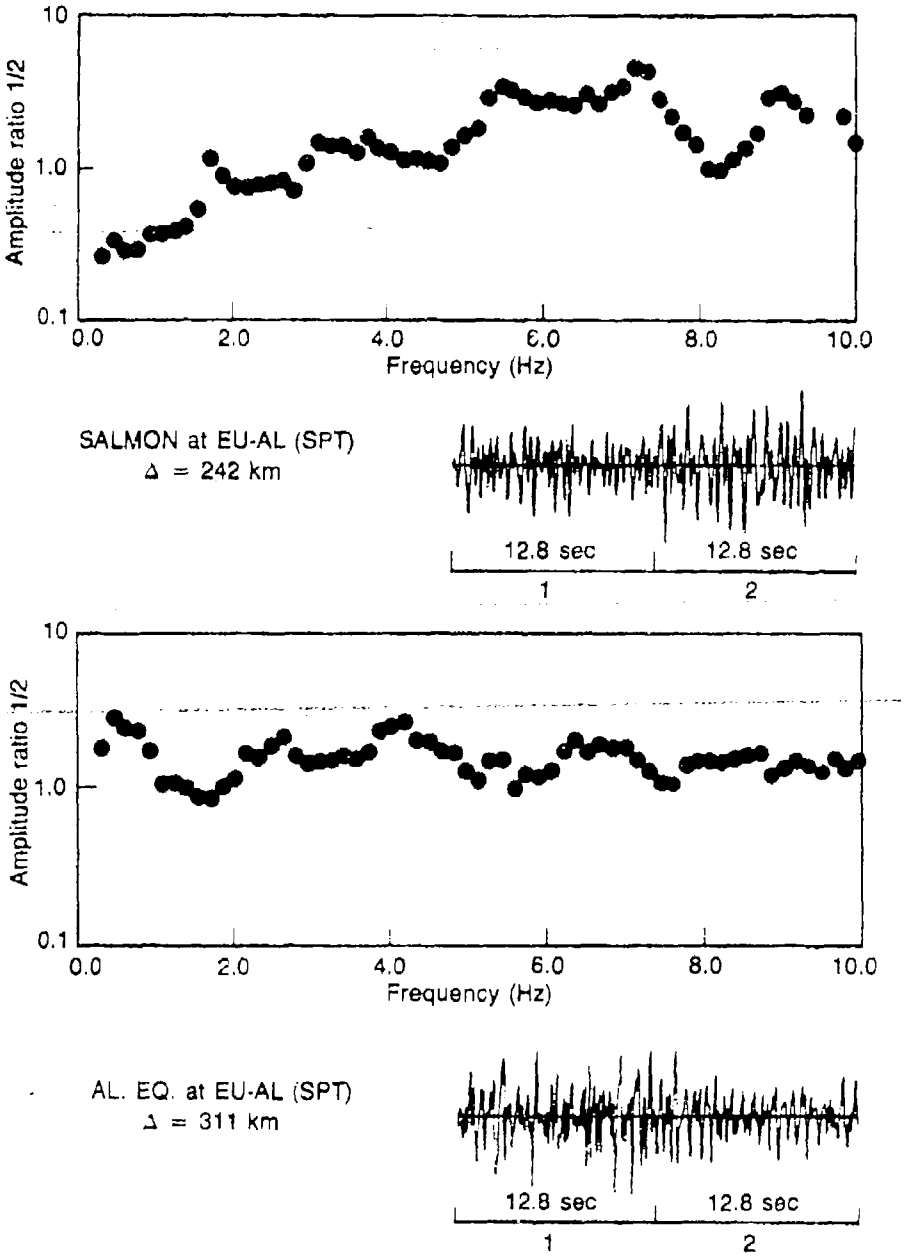

Fig. 3. Spectral ratio of transverse component initial to later L_g (each 12.8 sec long) at EU-AL from SALMON (upper figure) and the Alabama earthquake of 18 February 1964.

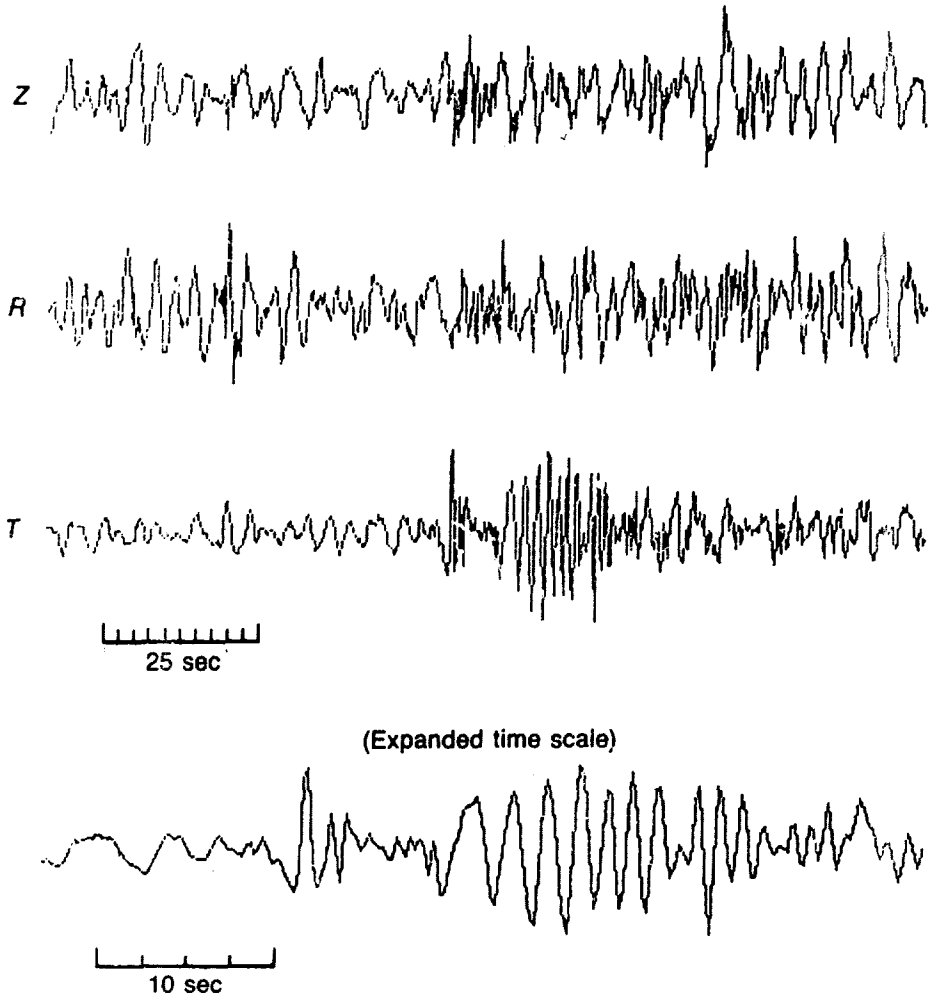

Fig. 4. Rotated, mid-period, three component records of a quarry explosion in Kentucky recorded at the RSTN station RSCP. *Z*, *R*, and *T* refer to the vertical, radial and transverse components respsectively. The bottom trace is an expanded view of the Love wave portion of the transverse component

waves observed from surface explosions at a hard rock site in an earlier study (see Fig. 2, Gupta and Hartenberger, 1981). The earthquake records generally did not show any appreciable surface wave energy on the mid-period records. Note that quarries are generally at shallow depths where effective Q is generally low due to factors such as greater scattering efficiency because of greater impedance contrasts. High strain rates at shallow depths where the hydrostatic pressure is low also lead to low Q (Stewart *et. al.*, 1983). The low frequency of quarry events could thus be due to low Q within and near the source region. Detailed analysis of many more events will be carried out in order to understand the

mechanism of generation of large amplitude, low frequency surface waves from quarry blasts.

Results From Neighboring Explosions at TFO

We examined the spectral characteristics of several closely spaced NTS explosions recorded at TFO, at an epicentral distance of about 530 km. The objective was to understand the influence of near-source variations, such as shot depth and overburden velocity, on the excitation of regional phases when the source-receiver path is essentially the same. We also looked at several earthquakes at similar epicentral distances.

The regional discriminants such as the spectral ratio of initial to later transverse L_g (Gupta and Blandford, 1983b) and the ratio of L_g spectral energy in the 0.5 to 1.0 Hz passband to that in the 2.0 to 4.0 Hz (Murphy and Bennett, 1982) worked well for most events. The most surprising result is the large variability found among the regional phases from one shot to another, even for closely spaced explosions.

Figure 5 shows the rotated three component records from CHOCOLATE (m_b = 4.3) and PLIERS (m_b = 4.7); the letters Z, T, and R refer to the vertical, transverse and radial components, respectively. These two explosions had nearly the same shot depths (about 240 m) and their shot points were separated by only about 250 m. On CHOCOLATE records, P_n is emergent and of much smaller amplitude compared to the P_g and L_g amplitudes, whereas on PLIERS, P_n is sharp and of much larger amplitude, comparable to the amplitudes of P_g and L_g phases. The transverse component of P_g from PLIERS is also much larger and with sharper onset than that from CHOCOLATE. The spectral ratios of initial to later transverse L_g for the two explosions, shown in Fig. 6, also seem to have opposite trends. The spectral ratio for CHOCOLATE (Fig. 6a), is typical of those from most explosions. Perhaps the fact that the later explosion, PLIERS was detonated very close to the pre-existing cavity created by CHOCOLATE may be responsible for the anomalous results from PLIERS. The subsurface geology in this region is, however, complicated by the presence of a fault and other variations.

Conclusion

The regional phase from quarry blasts, nuclear explosions and small earthquakes seem to have spectral characteristics which can be exploited for source discrimination. The regional phases do, however, seem to have large variability from one event to another. Much more detailed analysis with considerably more data will be necessary before reliable source discriminants can be established.

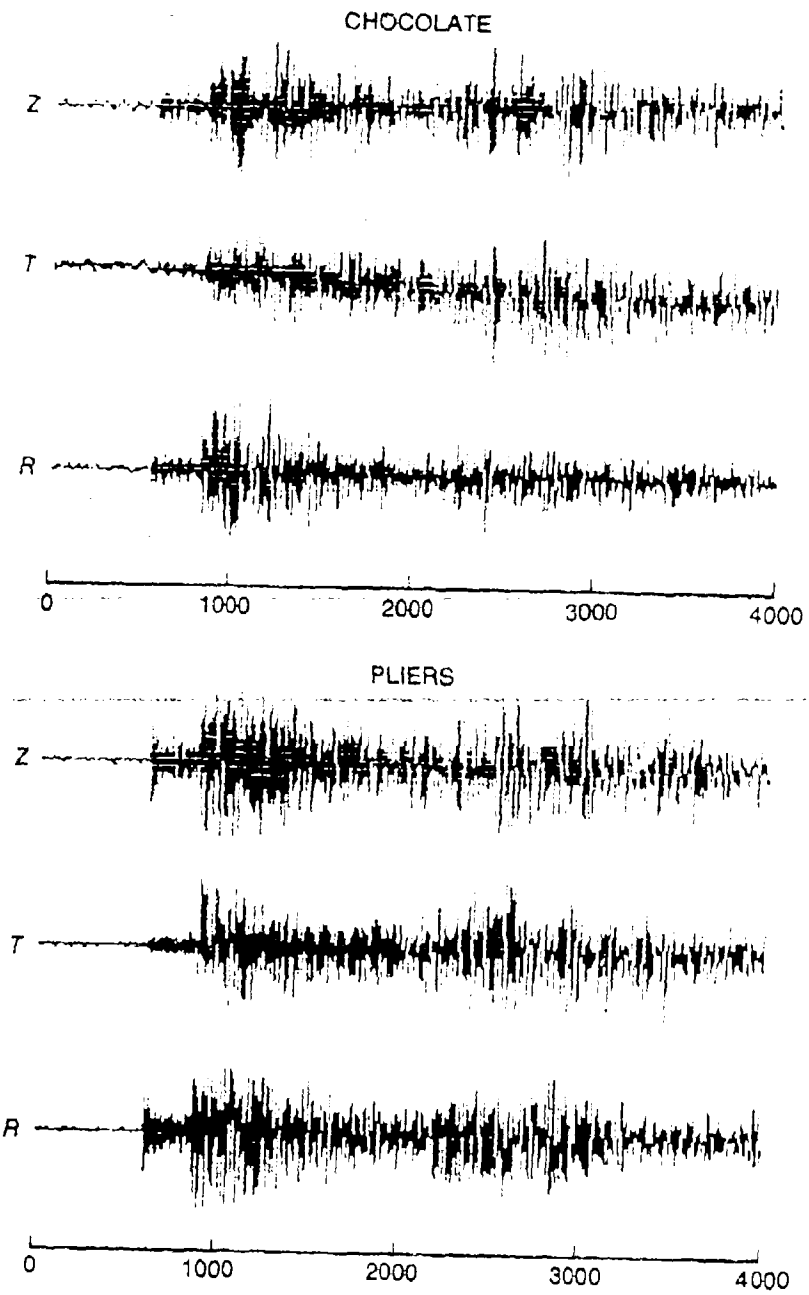

Fig. 5. Rotated, short-period three component records of the nuclear explosions CHOCOLATE and PLIERS at TFO. *Z*, *T*, and *R* refer to the vertical, transverse and radial components, respectively. The two explosions were within about 250 m of each other.

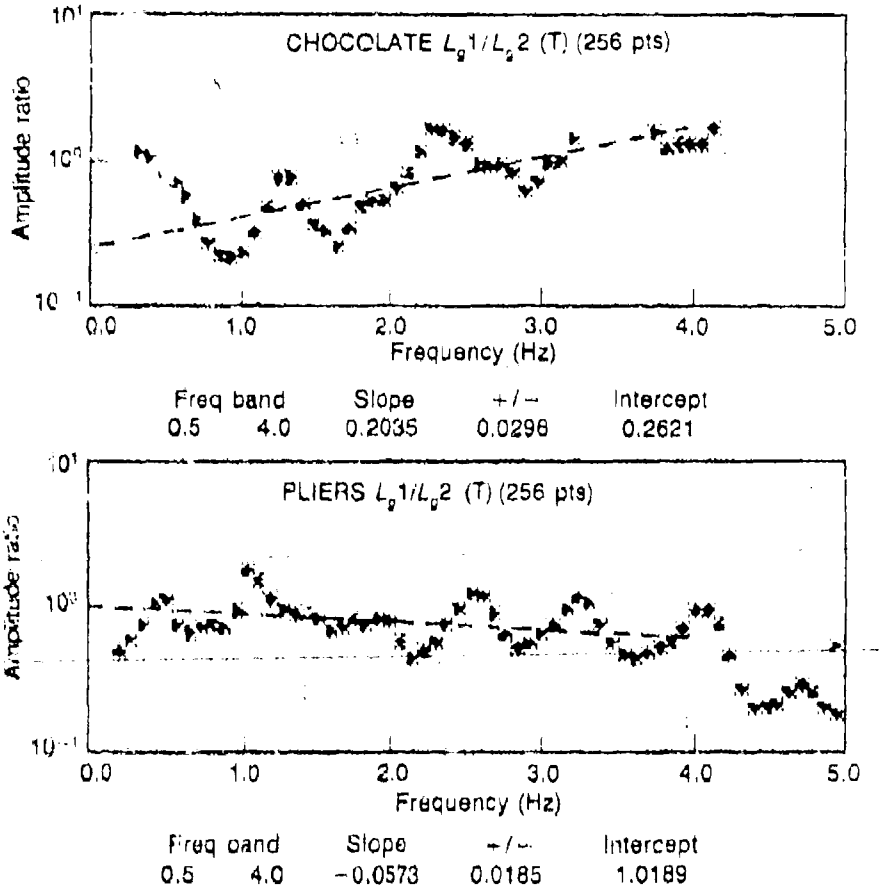

Fig. 6. The spectral ratios of transverse component initial to later L_g (each 12.8 sec long) for CHOCOLATE and PLIERS recorded at TFO. The dashed lines show the mean slopes for the frequency range 0.5 to 4.0 Hz.

References

Gupta, I.N. and R.R. Blandford (1983a). "A Mechanism For Generation of Short-Period Transverse Motion From Explosion," *Bull. Seism. Soc. Am.*, **73**, 571-591.

Gupta, I.N. and R.R. Blandford (1983b). "Short Period *SH* Motion From Explosions—A Possible Discriminant?" American Geophysical Union Meeting, May 1983.

Gupta, I.N. and R.A. Hartenberger (1981). "Seismic Phases and Scaling Associated with Small High-Explosive Surface Shots," *Bull. Seism. Soc. Am.*, **71**, 1731-1741.

Kinslinger, C., E.J. Mateker, Jr. and T.V. McEvilly (1961). "*SH* Motion from Explosions in Soil," *J. Geophys. Res.*, **66**, 3487-3496.

Murphy, J.R., and T.J. Bennett (1982). "A Discrimination Analysis of Short-Period Regional Seismic Data Recorded at Tonto Forest Observatory," *Bull. Seism. Soc. Am.*, **72**, 1351-1366.

Stewart, R., M.N. Toksöz and A. Timur (1983). "Strain Dependent Attenuation: Observations and a Proposed Mechanism," *J. Geophys. Res.*, **88**, 546-554.

Crustal Phase Variations — L_g and P_g

Wayne Helterbran

Summary

A preliminary evaluation of L_g and P_g observations from explosions at the Nevada Test Site has resulted in formulations for L_g and P_g magnitudes over the range from 2.62 to 6.03 with a correlation coefficient of 0.985.

Abstract

A database of approximately 8000 arrivals obtained from the series of shot reports prepared from the Long Range Seismic Measurements (LRSM) and Geneva Observatory programs has been established in the Ingres data management system at the Center for Seismic Studies. Efforts are continuing to review and evaluate these data and to integrate it with the more formally established data base structure at the Center. Data from approximately 90 events recorded by as many as 250 stations are included. Most of the data are from underground nuclear explosions conducted at the Nevada Test Site but additional off-site and chemical explosions are also included.

Primary emphasis is on the crustal phase observations and the associated long period data. The data set includes numerous other secondary and core phases which are being reviewed and incorporated into the files for future reference. Approximately 10 percent of the data set is missing either the period or amplitude measurement required for the conventional magnitude determination. Although the data are extensive the relocation of stations and the long time interval over which the data were collected rapidly degrades the available comparative sets when common observations of a specific nature are required. The L_g phase represents the predominance of the individual phase observations with some 1800 included in the data set. A large majority are from the transverse horizontal component. When these are paired with other observations the base now includes about 900, 800, 300, 250 and 450 direct comparisons with P_g, P_n, P, LQ and LR phases respectively. The number of observations ranges from many single points to over sixty observations at stations like Mina, Nevada, and Kanab, Utah, which were in continuous operation over a long period of time. The Geneva Observatory

data are presently limited but can and will be supplemented with other currently available readings for the Tonto Forest Observatory for all NTS events recorded at that location.

Introduction

Using a database of 670 paired observations of P_g and L_g at 45 stations from 60 explosions at the Nevada Test Site a preliminary evaluation has been completed. An absolutely straight-forward application of theoretically sound magnitude estimation techniques for P_g and L_g results in determinations over a magnitude range from 2.62 to 6.03 with a correlation coefficient of 0.985. This is achieved without recourse to station corrections, data screening or rejection other than requiring five or more observations at distances less than nine degrees. The resulting data set includes almost every type of explosion source available from most of the test areas at NTS including near-surface atmospheric, cratering, alluvium, tuff, basalt, granite, and all ranges of water saturation. The test areas include Yucca Flat. Frenchman Flat, Pahute Mesa, Rainier Mesa, Buckboard Mesa and the Shoshone Mountain. It is further completely compatible with the correspondence between M_L and *mblg* reported by Herrmann and Nuttli (1982) and, oddly enough, the observations of Iranian earthquakes reported by Nuttli (1980) which initiated the course of this study.

Analyses

The preliminary review of the present paired L_g and P_g data set showed very high correlations when the data were viewed both station by station and event by event. In fact, the overall dataset of 894 observations have a correlation coefficient of .929 with the L_g amplitude a factor of 1.62 larger in the overall set. The gross characteristics of the observations seemed remarkably similar to the observations reported by Nuttli (1980) for the Iranian earthquake dataset. In that data set the uniformly-high amplitude of P_g as compared to L_g was markedly different from the eastern United States experience but noted to be similar to western U.S. observations. This lead to an initial belief that perhaps the data could be treated in an analogous fashion to the Iranian earthquake data, *i.e.* both L_g and P_g as dispersive wavetrains with approximately equivalent source and propagation parameters. The further evaluation of M_L and *mblg* for the western U.S. reported by Herrmann and Nuttli (1982) provided a rational numeric basis for an initial evaluation of the present dataset. The definition presented for this evaluation is given as:

$$mblg = 3.81 + 0.83 Log\,\Delta + \gamma(\Delta - 0.09) Log\,e + Log\,A$$

where Δ is in degrees, A in microns. In this form the data were to be restricted to $T = 1.0 + 0.2$ seconds and the intercept was chosen such that a $mblg = 5.0$ earthquake is one with an amplitude of 115 μm at an epicentral distance of 10 km. This further relates directly to an equivalent $M_L = 5.0$ event. The evaluation of the average γ for the western U.S. lead to a value of $\gamma = 0.0035$ km^{-1} or 0.39 deg^{-1}. For the Iranian dataset a value of $\gamma = 0.0045$ km^{-1} or 0.50 deg^{-1} had been found appropriate with a 10 km intercept of 270 μm for the L_g data and no significant difference for P_g. It should be noted that these formulations are all in terms of vertical component observations near 1.0 second period. The present data are generally centered on 0.6 sec period and in the case of L_g are peak amplitude measurements on the horizontal transverse component.

As an initial step the dataset were evaluated using the formulations:

$$mpgi = 0.81 + 0.8333 Log\,\Delta + (0.5)(0.4343)(\Delta - 0.09) + Log\,A$$

$$mlgi = 0.81 + 0.8333 Log\,\Delta + (0.5)(0.4343)(\Delta - 0.09) + Log\,A$$

$$mlgw = 0.81 + 0.8333 Log\,\Delta + (0.4)(0.4343)(\Delta - 0.09) + Log\,A$$

where the intercept has been adjusted to $m\mu$ and $Log\ A$ is in terms of $m\mu$, the i indicating Iranian parameters and w the western U.S. earthquake parameters. Noting that the Iranian dataset required a break at 1000 km and also that relative to the Nevada Test Site a distance of 1000 km (9 deg) closely approximates the boundary of the "western U.S." in terms of the station distribution, the magnitudes were calculated for all events with more than four observations at distances less than 9 degrees.

Results

The resulting magnitudes for 60 events observed at 45 stations with 670 observations remaining out of the 894 available have a correlation coefficient of 0.985 relating either *mpgi-mlgi* or *mpgi-mlgw*. The data are shown in Table 1 and the *mpgi-mlgw* data set is plotted in Fig. 1. The average magnitude over the entire data set are: $mpgi = 4.32$, $mlgi = 4.49$ and $mlgw = 4.31$. At this stage of the analysis it seems allowable to select the *mpgi-mlgw* relationship as providing a highly systematic and numerically equivalent mechanism for relating magnitudes from NTS explosions — determined from P_g and L_g. This selection further, by inference, relates either or both, at least numerically, to M_L via the work of Herrmann and Nuttli. It further appears unnecessary to restrict to distances greater than 400 km as was the case in the Iranian data. The present data

Table 1. Magnitude Determinations from Paired Pg and Lg Observations Within Nine Degrees of the Nevada Test Site, Five or More Observations.

Name	Log Yield (tons)	No.	mpgi	sd	mlgi	sd	mlgw	sd
aardva	4.60	11	5.04	0.34	5.36	0.19	5.15	0.17
acushi	-1.00	14	4.15	0.30	4.43	0.39	4.23	0.41
agouti	3.81	16	4.15	0.32	4.22	0.29	4.02	0.24
allegh	-1.00	10	3.79	0.40	3.98	0.38	3.80	0.36
antler	3.41	5	3.99	0.16	4.16	0.22	4.01	0.27
armadi	3.85	14	4.23	0.35	4.59	0.28	4.40	0.25
auk	-1.00	12	5.05	0.25	4.99	0.38	4.80	0.35
[illegible]ilby	5.40	7	5.78	0.28	5.70	0.27	5.49	0.23
bobac	-1.00	9	3.82	0.23	4.03	0.23	3.85	0.22
boxcar	6.11	7	6.30	0.44	6.15	0.50	6.03	0.50
bronze	-1.00	5	5.63	0.26	5.49	0.14	5.30	0.18
[illegible]ssel	-1.00	13	4.15	0.30	4.37	0.20	4.20	0.22
chena	-1.00	8	3.37	0.40	3.60	0.52	3.39	0.51
chin 2	-1.00	19	3.40	0.24	3.72	0.34	3.55	0.33
chinch	3.28	16	3.76	0.34	3.86	0.25	3.69	0.24
clearw	-1.00	9	5.34	0.47	5.36	0.48	5.16	0.44
codsaw	-1.00	17	3.80	0.37	4.06	0.24	3.88	0.22
cup	-1.00	11	5.45	0.27	5.52	0.18	5.34	0.20
dannyb	2.63	13	3.41	0.26	3.68	0.34	3.51	0.32
desmoi	-1.00	10	4.01	0.35	4.18	0.37	4.00	0.36
dilwat	-1.00	6	4.82	0.21	4.91	0.32	4.68	0.28
dormou	-1.00	19	4.38	0.36	4.44	0.38	4.24	0.38
dorpri	4.03	15	4.50	0.33	4.60	0.33	4.39	0.32
feathe	-1.00	7	2.53	0.44	2.76	0.27	2.62	0.27
fisher	4.13	16	4.53	0.39	4.58	0.28	4.38	0.29
fore	-1.00	10	5.23	0.27	5.52	0.36	5.34	0.33
hardha	3.76	16	4.92	0.36	4.98	0.32	4.78	0.31
haymak	4.83	12	5.14	0.25	5.31	0.27	5.10	0.25
hyrax	-1.00	10	4.01	0.36	4.22	0.43	4.04	0.42
kaweah	-1.00	13	3.84	0.30	4.04	0.33	3.85	0.32
klick	-1.00	9	5.07	0.28	5.29	0.33	5.11	0.30
mad	2.70	12	3.08	0.50	3.45	0.41	3.26	0.41
madiso	-1.00	9	4.15	0.23	4.52	0.29	4.32	0.27
marshm	-1.00	11	4.49	0.19	4.59	0.22	4.37	0.16
merrim	-1.00	10	4.47	0.30	4.72	0.28	4.52	0.28
minx	-1.00	7	3.20	0.47	3.28	0.51	3.11	0.49
missis	5.06	8	5.31	0.30	5.59	0.26	5.40	0.28
packra	-1.00	8	4.08	0.25	4.26	0.32	4.08	0.31
pampas	-1.00	13	4.49	0.43	4.55	0.33	4.33	0.31
par	4.58	12	4.91	0.16	4.97	0.22	4.79	0.22
passai	-1.00	23	4.40	0.33	4.63	0.35	4.47	0.35
peba	-1.00	8	4.22	0.22	4.34	0.21	4.17	0.19
planqn	3.63	10	4.32	0.21	4.55	0.30	4.35	0.29
redhot	-1.00	7	3.43	0.27	3.68	0.22	3.54	0.24
ringta	-1.00	16	3.94	0.29	4.10	0.24	3.91	0.27
roanok	-1.00	10	3.52	0.22	3.83	0.25	3.64	0.26
sacram	-1.00	9	3.77	0.49	4.23	0.24	4.04	0.23
santee	-1.00	9	3.95	0.30	4.12	0.27	3.94	0.26
scroll	-1.00	8	4.16	0.25	4.05	0.17	3.94	0.19
sedan-	5.02	10	4.47	0.35	4.93	0.43	4.74	0.42
smallb	-1.00	7	3.22	0.22	3.38	0.33	3.21	0.33
stillw	3.49	16	4.05	0.49	4.27	0.30	4.07	0.28
stoat	3.71	11	4.01	0.38	4.10	0.23	3.89	0.28
stones	-1.00	15	4.80	0.27	4.91	0.36	4.75	0.33
turf	-1.00	11	5.04	0.14	5.22	0.23	5.03	0.24
wagtai	-1.00	7	5.32	0.18	5.50	0.18	5.31	0.14
wichit	-1.00	10	4.00	0.22	4.05	0.31	3.87	0.30
wisbon	-1.00	10	4.69	0.24	5.04	0.28	4.83	0.28
york	-1.00	9	4.27	0.32	4.49	0.22	4.31	0.23
yuow	-1.00	15	4.01	0.32	4.15	0.34	3.98	0.33
Average		11	4.32	0.31	4.49	0.30	4.31	0.29

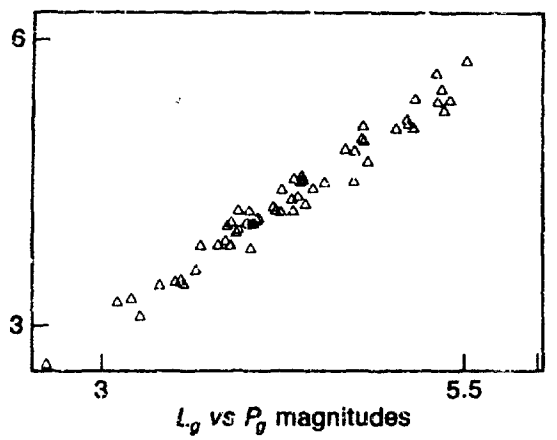

Fig. 1. L_g magnitude from the transverse horizontal component *versus* P_g magnitude from the vertical component.

include many observations at the smaller distances with no apparent impact on the correlation. The resulting magnitudes for the nineteen explosions with announced yields are plotted in Figs. 2 and 3. While the L_g data appear rather closely related to the yields of the widely varying source types included in this preliminary analysis it seems potentially significant that the large outliers in the P_g plot are the HARDHAT event in granite (lower), and the SEDAN cratering experiment (upper).

Conclusions

The preliminary results limited to the investigation of a highly selected subset of the available data are very encouraging. Obviously, it remains to further investigate the real geophysical implications of these initial numeric agreements. Additionally, there remain numerous vertical L_g observations and the Geneva Observatory data which includes both horizontal components of L_g motion and the extensive TFO dataset

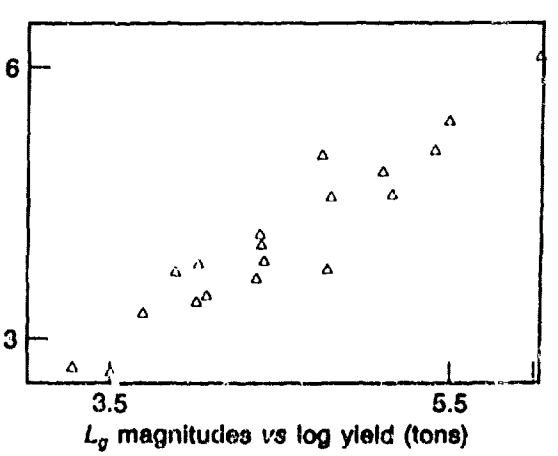

Fig. 2. L_g magnitude *versus* log yield for the nineteen events with announced yields contained in the dataset.

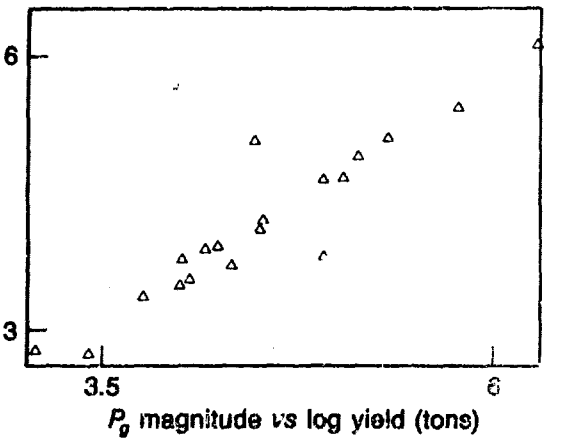

Fig. 3. P_g magnitude *versus* log yield for the nineteen events with announced yields contained in the dataset. Note HARDHAT, in granite, the lower outlier and SEDAN, the cratering experiment, the upper.

which has not been incorporated yet. There are further paired observations of P and P_n which in many instances show comparable correlations as those of the analyses reported here. It would appear that a much better understanding of the characteristics of propagation from the Nevada Test Site can be gained by extension of this analysis.

References

Nuttli, O.W. (1980). "The Excitation and Attenuation of Seismic Crustal Phases in Iran," *Bull. Seism. Soc. Am.* **70**, 469-485.

Herrmann, R.B. and O.W. Nuttli (1982). "Magnitude: The Relation of M_L to *mblg*," *Bull. Seism. Soc. Am.* **72**, 389-397.

Estimation of Explosion Yield and m_b Bias by Regional L_g Waves

Otto W. Nuttli

Summary

A methodology has been developed, using the amplitudes of vertical-component L_g waves of frequency near 1 Hz, to estimate $m_b(L_g)$. In order to apply the method, precise values of the coefficient of anelastic attenuation must be determined for each source-to-station path. A first approximation of attenuation values is obtained from the frequency variation with travel time of the waves comprising the coda of L_g. This is best determined by using explosions that give relatively small amplitude coda waves, which ensures that the source-spectrum corner frequency is greater than 1 Hz. It also makes it easier to select wavelets that are near-sinusoidal in shape. These attenuation values then are adjusted to minimize the residuals of $m_b(L_g)$ as determined from a set of stations. If stations are selected so that the epicentral distances are unequal, the revised values will not depend strongly on the original values obtained from the coda-Q method. And, once they are found, they do not need to be redetermined for each explosion.

L_g waves were first used on a routine basis to determine m_b values about 10 years ago, when they were employed to estimate magnitudes of small to moderate sized earthquakes in eastern North America (Nuttli, 1973). Since then L_g waves have been used for similar purposes in other continental areas, in regions where they propagate efficiently through the crust. For such earthquake studies there was no attempt to determine m_b with an accuracy beyond the first decimal point. Typical values of standard deviation of $m_b(L_g)$ were 0.2 to 0.3, the same or a little less than when teleseismic P-wave amplitudes of earthquakes were used. L_g waves have an advantage over P waves in that they do not show as large an azimuthal variation in amplitude due to the source mechanism. Thus they give better magnitude estimates when data from only a small number of stations or from a limited azimuthal range are available.

The relatively large standard deviations (0.2 to 0.3) associated with $m_b(L_g)$ estimates for earthquakes principally are the result of difference

of the anelastic attenuation coefficient value for the source-to-station path from the average attenuation value for the region, which is further complicated by the fact that the attenuation is frequency dependent for frequencies near 1 Hz. One way to treat this problem is to use the empirical approach employed for improving m_b and M_S estimates of explosions using P-wave amplitudes and Rayleigh-wave amplitudes, respectively. That is, assume the anelastic attenuation does not vary geographically, use explosions recorded by as large a number of stations as possible as calibration events, and then determine source-to-station departures from the average magnitudes for individual stations and specific source areas. These corrections then are applied to the P-wave and Rayleigh-wave of other explosions for which m_b and M_S are to be determined. For particular source areas the station corrections can be as large as one-half a magnitude unit at certain stations.

A similar approach could have been used to determine $m_b(L_g)$ for explosions. However, the author felt a better procedure was available, which makes use of elastic wave theory to substantially reduce the size of the source-to-station corrections for getting $m_b(L_g)$ estimates. Instead of using an average value for the coefficient of anelastic attenuation over a large geographic region, specific values of Q_0 (1-Hz value of Q) and the parameter ξ (which measures the frequency dependence of Q by the relation $Q(f) = Q_0 f^{\xi}$) are determined for each source-to-station path from the variation of the coda-wave frequency with travel time, using a method developed by Herrmann (1980). Although there still is some concern about the best mathematical-physical model to use for explaining the coda waves and of the best choice of "master curves" to be used in obtaining estimates of Q_0 and ξ for specific source-to-station paths, the important point is that the values obtained by using any of the models will be relatively close to the "correct" value, much more so than by using an average regional value for Q_0 and ξ.

The next step in the procedure is to use the coda estimates of Q_0 and ξ to obtain $m_b(L_g)$ estimates at individual stations for a number of explosions located in a common source area. Then a station correction is obtained for each station, depending on departure of individual station $m_b(L_g)$ values from the average value of $m_b(L_g)$ for an explosion. However, unlike the station corrections used for estimating $m_b(P)$ or M_S, the L_g correction is not taken to be a simple additive term to individual station magnitude estimates, but rather is taken to be a small correction to the Q_0 value obtained originally by means of the coda-wave method. This procedure enables us to estimate m_b (L_g) values to the nearest hundredth of a magnitude unit.

When the $m_b(L_g)$ method was applied to data from NTS explosions

of announced yield, it soon became apparent that there was a different relation between $m_b(L_g)$ and explosion yield for explosions in alluvium and in other media. The available data suggest also that explosions in dry tuff have somewhat smaller $m_b(L_g)$ values than explosions of the same yield in water-saturated tuff or more competent rocks, the differences not exceeding about 0.1 magnitude unit. Similarly, explosions in granite in Nevada give data that suggest that the $m_b(L_g)$ may be about 0.1 unit larger in granite than for explosions of the same yield in other competent rocks of NTS. The empirical relation obtained from the data of NTS explosions of announced yield, excluding data from alluvium and granite shots, is

$$m_b(L_g) = 3.868 + 1.181 \log Y\,(\text{kt}) - 0.0938\,(\log Y)^2$$

with a standard deviation of 0.060 for $m_b(L_g)$.

There does not appear to be any strong dependence of the NTS yield versus $m_b(L_g)$ relation on the particular area of NTS in which the explosion occurs. Given that observation, the next logical questions concern the applicability of the empirical relation to other test sites throughout the world. Unfortunately the data are limited. The available data are summarized in Table 1.

The available data, although limited, come from a number of different geological environments. SALMON was shot in salt in the Gulf Coastal Region of the United States, with the source-to-station paths for some stations in young coastal sediments and for others principally in the low-attenuating cratonic region of eastern North America. GASBUGGY, RULISON, and RIO BLANCA were in geologic environments rather

Table 1. Yield estimates obtained by using the $m_b(L_g)$ *versus* yield relation for NTS events.

Event	Location	$m_b(L_g)$	m_b(*P*-ISC)	Announced Yield (kt)	Yield from $m_b(L_g)$ (kt)
SALMON	Mississippi	4.66	4.6	5.3	5.1
GASBUGGY	New Mexico	5.38	4.8	29	28
RULISON	Colorado	5.56	5.0	40	45
RIO BLANCA	Colorado	5.71	5.1	90*	66
RUBIS	French Sahara	5.72	not given	52**	68
SAPHIR	French Sahara	5.89	not given	120**	111
Jan. 15, 1965	Shagan River East Kazakh	5.87	5.8	125**	105

* Three 30-kt shots.

** Announced yield values. Revised values have not been announced.

*** Cratered event.

similar to NTS, and the paths to the stations also were in a highly attenuating region. RUBIS and SAPHIR were shot in granite, and the ray paths to northeast and southwest Africa were marked by extremely low attenuation. The geological environment of the 1965 Shagan River event (it cratered a water-saturated sandstone) likely is more similar to that of eastern North America than to that of western North America. Good L_g waves were seen at only two WWSSN stations, SHL and NDI, both in India, for this event. The paths were highly attenuating with relatively low Q values, but not as low as in western North America. In general, we can conclude that the geologic environments of the source regions and of the transmission paths for the explosions listed in Table 1 are about as varied as one might expect throughout the continental crust of the world. This leads to the conclusion that the NTS-derived $m_b(L_g)$ versus yield relation likely is applicable to all continental areas of the world.

In addition to being used for a direct estimation of explosion yield, L_g wave amplitudes also can be used to estimate the $m_b(P)$ bias between different explosion test sites. If $m_b(L_g)$, or the excitation of L_g waves, for an explosion of a given yield is independent of geographic location, as suggested above, then the difference in values of $m_b(P)$ and $m_b(L_g)$ at different geographic areas can be used to obtain the $m_b(P)$ bias between the areas. In this study, $m_b(P)$ values as given in the ISC bulletin were used, as they are considered to be the best available unclassified $m_b(P)$ values.

For 30 Shagan River explosions, $m_b(\text{P-ISC}) - m_b(L_g) = +0.10 \pm 0.14$, for 24 Degelen Mountain explosions the difference is $+0.24 \pm 0.14$, and for 19 hard rock NTS explosions it is -0.30 ± 0.09. Assuming the L_g excitation is the same for an explosion of the same yield at the three test sites, this suggests an $m_b(P)$ bias of 0.40 ± 0.17 units between NTS and Shagan River, and of 0.54 ± 0.17 units between NTS and Degelen Mountain.

Biases of 0.40 and 0.54 between NTS and the East Kazakh sites are larger than those obtained by more traditional methods. Special attention, therefore, should be paid to the assumptions that lead to these conclusions and to the quality of the data. As previously noted, the success in estimating yield at non-NTS sites using an NTS-derived yield curve suggests that the $m_b(L_g)$ *versus* yield relation is independent of geographic region. More data of this type would be desirable, but likely are unobtainable. Therefore numerical modeling may have to be resorted to. If there is a focal depth effect on L_g excitation, it should reveal itself in explosions of different size, inasmuch as the large contained explosions are at greater depth. Most of the recent Shagan River events are in the $m_b(L_g)$ range of 5.5 to 6.2. If only NTS events of similar

magnitude are used, m_b(P-ISC) $- m_b(L_g)$ for 15 NTS events is -0.30 ± 0.08, the same as before. Therefore a depth effect appears to be ruled out.

One possible source of error concerns the $m_b(P$-ISC) values. Because the data from different seismograph stations are used to determine $m_b(P$-ISC) for NTS and East Kazakh events, it might be possible for different station-site effects to produce an $m_b(P)$ bias in addition to that caused by source conditions. It would require that, on average, because of conditions at the recording seismograph stations, the P-wave amplitudes are larger for East Kazakh explosions than for NTS explosions of the same yield (assuming the source effects have been removed.)

Future work will be concerned with obtaining reliable $m_b(L_g)$ estimates for additional NTS and East Kazakh explosions in the m_b range of 5.5 to 6.2. Their yields need not be known, but it is necessary to have $m_b(P$-ISC) values for all of them. It is hoped that this will lead to a reduction in the standard deviation of the m_b bias values, and possibly it might result in different values for the estimated bias between NTS and the East Kazakh sites.

References

Herrmann, R.B. (1980). "Q Estimates Using the Coda of Local Earthquakes," *Bull. Seism. Soc. Am.*, **70**, 447-468.

Nuttli, O.W. (1973). "Seismic Wave Attenuation and Magnitude Relations for Eastern North America," *Jour. Geoph. Res.*, **78**, 876-885.

The Utility of Regional Chinese Seismograms for Source and Path Studies in Central Asia

Howard J. Patton, Steven R. Taylor, David B. Harris, and Joseph M. Mills, Jr.

Abstract

Broadband seismograms from the National Seismic Network of the People's Republic of China (PRC) have recently become available through a data exchange program between NOAA and the State Seismological Bureau of the PRC. In this study, regional surface waves recorded at the Urumchi station located about 700 km north of the Tibetan Plateau in the Sinkiang Province are used to study East Kazakh explosions and wave propagation in central Asia. The data consist of broadband (flat to displacement between 0.1 and 10 Hz) photographic records from an SK Kirnos galvanometric system. Simultaneous inversion of Rayleigh wave phase and group velocities for the path from East Kazakh through the Dzhungarian Basin yields a crustal model dominated by the presence of very low velocities and a strong positive velocity gradient above 15 km depth. Velocities below 15 km depth are not significantly different from other continental structures underlain by Paleozoic or Precambrian basement. This model is consistent with geologic evidence indicating that most of the path is characterized by the presence of up to 10 km of sediments overlying a Paleozoic basement. Source studies were made on seven East Kazakh explosions detonated in the time period between June, 1980 and April, 1981. These studies involved estimation of seismic moments using models of explosion sources with associated tectonic release. The largest explosion studied occurred on 9/14/80 and has an m_b of 6.2 and a seismic moment of 2.7×10^{23} dyne-cm. The observed amplitude spectra of Rayleigh waves are richer in high frequencies than predicted by explosion source models with tectonic release. This could be caused by a path effect involving seismic wave focusing by the large sedimentary basin between East Kazakh and the Urumchi station, although source medium effects cannot be ruled out.

Introduction

Recently, the National Oceanic and Atmospheric Administration (NOAA) initiated a data exchange program with the State Seismological

Bureau of the People's Republic of China (PRC). Seismograms are becoming available from the 17-nation PRC national network beginning from 1979. These new data are of considerable interest to both source and structural studies in Asia and to seismic verification programs, since two of the Chinese stations are within regional distance of the Soviet test site near Semipalatinsk. The stations are located in Sinkiang Province, at Urumchi, approximately 950 km from the test site, and at Kashi, approximately 1200 km distant. The map in Fig. 1 indicates their positions relative to the test site. The stations are at a distance comparable to those expected for in-country monitoring stations designed to verify

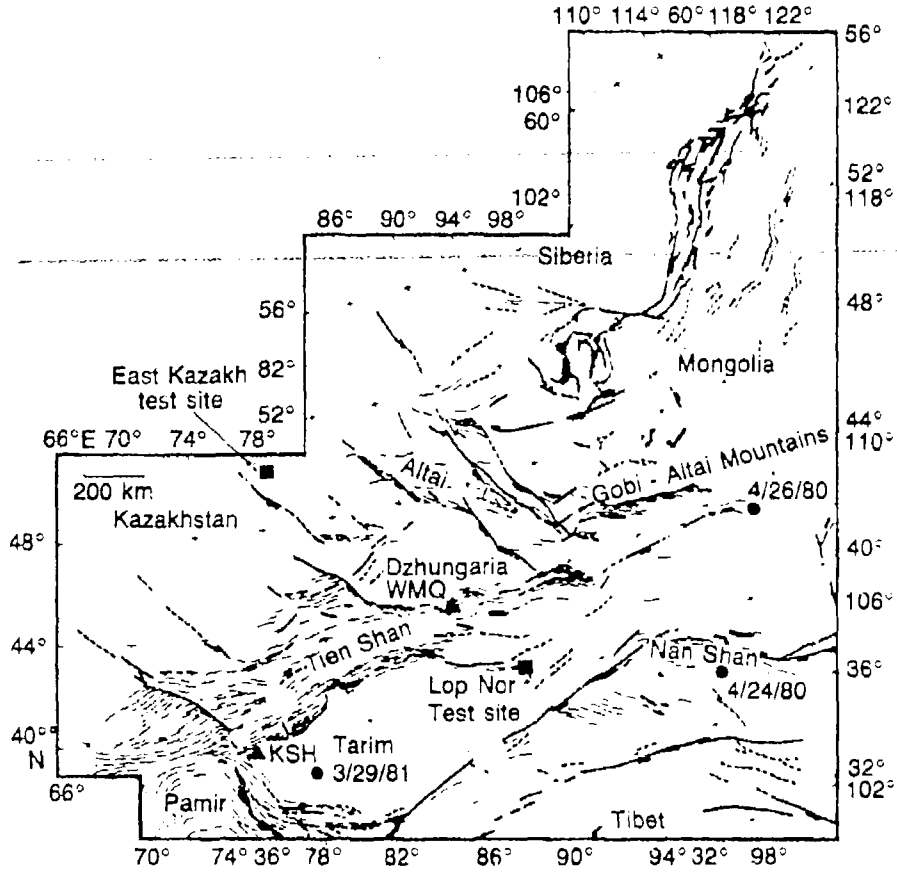

Fig. 1. Map of central Asia showing locations of test sites (solid squares), events (solid circles), and the Urumchi (WMQ) and Kashi (KSH) stations (triangles). The base map is reproduced from Figure 17 of Tapponnier and Molnar (1979). Bold lines indicate major active faults, and dashed lines are ancient and less certain faults. Thin dashed lines indicate regions of intense late Cenozoic crustal shortening.

compliance with test ban treaties. As such, data from the Chinese stations may be useful for evaluating detection, location and identification capabilities of monitoring networks in the central Asia region.

Shortly after receiving the announcement of data availability, we obtained recordings made at the Sinkiang stations of seven presumed Soviet nuclear tests at the East Kazakh Test Site, three regional earthquakes, and an atmospheric explosion at Lop Nor (Fig. 1). This report presents an investigation of these events using the data from the station at Urumchi. In this paper, we first describe the instrument and data characteristics at the Chinese stations and include a discussion of data limitations. We then discuss the measurement and inversion of Rayleigh wave phase and group velocities concentrating on the path between the East Kazakh test site and Urumchi. Finally, analysis of source characteristics for the seven Soviet explosions as recorded at Urumchi is presented. Although much additional work is warranted, the main purpose of this initial study is to describe a useful new source of seismic data from a relatively unexplored region. More detailed description of the analyses is presented in Harris *et al.* (1982) and Patton and Mills (1984).

Instrument and Data Characteristics

The PRC data are recorded on three-component SK Kirnos galvanometric seismographs and the instrument parameters are published by NOAA who distributes the records on 70 mm film chips. The instrument response is nearly flat to displacement between frequencies of 0.1 and 10 Hz which is well-suited to recording regional seismic waves (Fig. 2). Many of the difficulties encountered with handling the Chinese data are related to the usual problems with digitization of photographic records. The high frequencies are nearly impossible to accurately digitize and timing

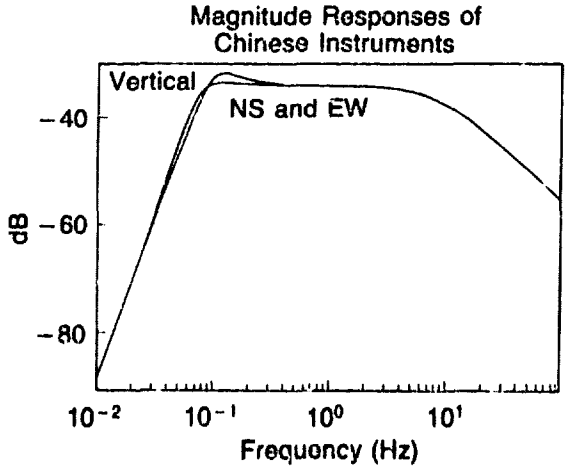

Fig. 2. Displacement response for the Urumchi instruments using the nominal instrument parameters supplied by NOAA (Harris *et al.*, 1982).

marks are often difficult to properly register. With the recording speed provided (30 mm/min), errors in timing registration between components were sometimes estimated to be approximately 2 seconds (Harris *et al.*, 1982). Additionally, absolute times were often in question and extremely large clock corrections (40 s) were sometimes encountered. However, with the supplied clock corrections, timing errors were reduced substantially. The third main problem encountered with the data was related to the lack of calibration pulses on all of the seismograms analyzed for the study. Thus, it was necessary to use the nominal instrument parameters supplied by NOAA.

The eleven events analyzed in this study consist of seven Soviet explosions from the East Kazakh test site near Semipalatinsk, one explosion from the Chinese test site at Lop Nor, and three regional earthquakes (Fig. 1; Table 1). The earthquakes are located to the east of Urumchi in southern Mongolia, to the southeast in the Nan Shan foldbelt, and to the southwest on the Tarim Basin. Epicentral distances to the Urumchi station are about 955 km from the East Kazakh Test Site, 362 km from Lop Nor Test Site and 1347 km, 1190 km and 951 km from the three earthquakes, respectively. Surface-wave signals from these events were manually digitized from paper records made from the 70 mm film chips obtained from NOAA. Time windows were selected to include Love and Rayleigh waves; however, for the East Kazakh events it was impossible to digitize the entire wavetrain because of the faint L_g portion of the record. The raw digitized data were detrended and resampled

Table 1. Epicentral data for events used in this study.

Date	Origin Time	Latitude (°N)	Longitude (°E)	m_b
East Kazakh Explosions				
4/25/80	03:56:57.4	49.95	78.81	5.5
6/12/80	03:20:57.5	49.94	79.04	5.6
9/14/80	02:42:39.3	49.94	78.86	6.2
10/12/80	03:34:14.0	49.91	79.05	5.9
12/14/80	03:47:06.6	50.01	79.03	5.6
3/29/81	04:03:50.0	50.01	79.03	5.6
4/22/81	01:17:11.4	49.90	78.90	5.9
Other Events				
4/24/80	07:59:38.1	37.82	99.40	4.7
4/26/80	03:22:32.3	43.26	104.38	4.6
10/16/80	04:30:28.9	41.04	89.99	4.4
3/29/81	19:21:15.0	38.16	79.19	4.8

to a constant rate of four samples/sec. The data were scaled to a trace amplitude in centimeters and, when necessary, adjusted for clock errors. The instrument deconvolution was made using the nominal instrumental parameters, and the resulting trace was bandpass filtered between 0.05 Hz and 0.3 Hz to remove long-period noise arising from the deconvolution and inaccuracies at high frequencies arising from digitization. The instrument-corrected data were rotated to apparent backazimuths as determined from particle motion analyses as described in Harris *et al.* (1982). Examples of the rotated data are plotted in Fig. 3, where positive deflection on the radial is away from the source and positive on transverse is counter-clockwise. All signals from East Kazakh explosions show large amplitudes, highly dispersed Rayleigh waves on the vertical component. Rayleigh waves on the radial component are significantly smaller in amplitude and are poorly correlated with the vertical channel at frequencies above 0.2 Hz. It is also apparent that Rayleigh waves on the radial

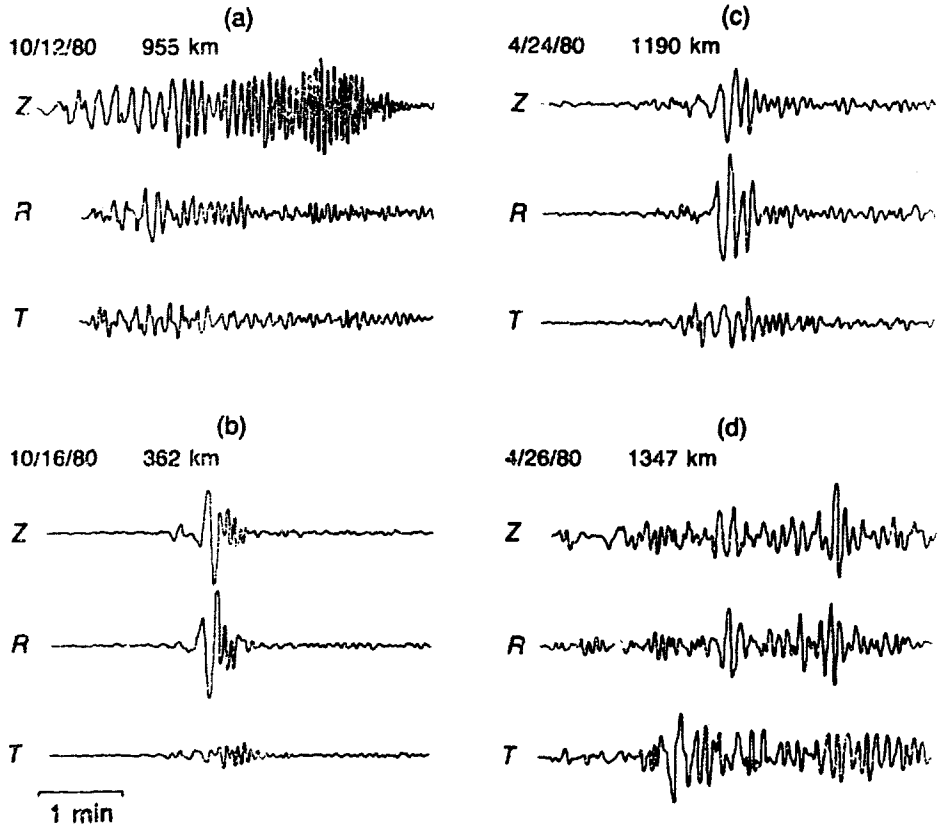

Fig. 3. Examples of rotated and instrument-corrected waveforms for the events in this study. (a). 10/12/80 East Kazakh explosion. (b). 10/16/80 Lop Nor atmospheric explosion. (c). 4/24/80 Qinghai Province earthquake, and (d). 4/26/80 Mongolia earthquake.

component and Love waves have been truncated at the beginning of the record due to the restricted digitization window. Records of the Chinese atmospheric explosion show a classic Rayleigh-wave pulse and no Love waves. Records of the Mongolian earthquake show clear Love waves and very weak Rayleigh waves, probably indicating that the station lies near a node in the Rayleigh-wave radiation pattern.

Geologic Setting

The area of interest in this study is located in a complex region of Asia characterized by deformation during a number of different episodes. In general, Asia represents a classic example of accretionary tectonics involving the suturing of numerous continental blocks and arc terrains about a central Precambrian core (the Siberian Craton: Burke *et al.*, 1977). The major collisional-episodes occurred intermittently throughout much of geologic time and climaxed with the Eocene (40 m.y.) collision of India with Asia. Since that time, India has continued to converge upon Asia at the rate of approximately 5 cm/year causing extensive crustal shortening and lateral displacement along major strike-slip faults (Tapponnier and Molnar, 1976; 1977). The resulting picture consists of a set of marginal fold-and-thrust belts wrapping around a Precambrian core with intervening Precambrian micro-continents.

The path separating the East Kazakh Test Site from Urumchi is relatively complex and can be divided into two different segments of nearly equal length. The northwestern half of the path consists mainly of early to middle Paleozoic rocks covered in many areas by a thick Carboniferous sequence, while the southeastern segment consists of a large sediment-filled depression (the Dzhungarian Basin; Fig. 1).

The structural trends in the region are predominantly northwest-southeast and the basement along most of the path is composed mainly of Paleozoic sediments and metasediments with numerous granitic intrusives of similar age. The Paleozoic rocks can be subdivided into early Paleozoic (Caledonian), middle Paleozoic (Hercynian), and Carboniferous sequences (Nalivkin, 1962). The Carboniferous rocks found along the northwestern portion of the path unconformably overlie the pre-Devonian basement and consist mainly of thick (up to 9 km), relatively undeformed, sedimentary sequences.

The Dzhungarian Basin is one of the many large Cenozoic basins found in northern China that are thought to be filled with 7-10 km of continental sediments of Tertiary and Quaternary age (*cf.* Tapponnier and Molnar, 1977; Chen and Yoshii, 1977). The Dzhungarian Basin is bounded to the south by the Tien Shan mountain range and to the northeast by the Altai foldbelt. The projection of structures into the basin suggests

that it is floored at depth by Paleozoic rocks similar to those found at the surface in eastern Kazakh described above. The seismic structure along the path separating East Kazakh from Urumchi can be inferred by combining Deep Seismic Sounding (DSS) results with surface wave studies in the region. Two seismic profiles in southeastern Kazakh located about 100 km southeast of Semipalatinsk are probably representative of the northwestern half of the travel path (Bulin *et al.*, 1969). The crustal thickness varies between 42-50 km, and P_n velocities are about 8.2 km/s (see also summaries in Piwinskii, 1979). Within the crust, a strong conversion boundary was observed to lie between 3-9 km depth. This boundary was interpreted to separate less dense upper strata (presumably of Carboniferous age: with *P*-wave velocities interpreted to separate less dense upper strata (presumably of Carboniferous age) with *P*-wave velocities (V_p 5.6-5.7 km/s) from more consolidated and metamorphosed pre-Devonian rocks (V_p 5.9-6.1 km/s). Additional velocity discontinuities were observed at 14-19 km depth (the A-horizon: V_p 6.1-6.2 km/s) and at 23-27 km depth (the B-horizon or 'Conrad' discontinuity: V_p 6.7-6.8 km/s). Also, numerous deep fracture zones were observed that extended into the upper mantle. A number of blind zones were observed showing no discontinuities at depth. The blind zones usually coincide with granitic surface outcrops and probably represent disturbed crust from upwelling of crustal magmas.

A first approximation to the structure of the Dzhungarian Basin can be obtained from examination of Rayleigh-wave phase and group velocities across another large Tertiary basin located southwest of Lake Balkhash (about 1000 km west of the Dzhungarian Basin: Savarenskiy and Peshkov,1968: Arkhangelskaya and Kuznetsova. 1969). The Rayleigh waves traversing the basin showed evidence of strong dispersion, especially for periods less than about 6 seconds. Measured phase and group velocities were very low and simple models of the basin structure indicated a 10 km thick sedimentary layer with V_p 4.0 km/s overlying a 15 km thick layer with V_p 6.0 km/s.

In summary, it appears that the travel path separating East Kazakh from Urumchi can be divided into two sections of nearly equal length. A thick sedimentary sequence appears to lie along the entire path, and the basement beneath much of the path (below 15 km depth) is probably composed of early and middle Paleozoic lithologies. In general, the mid-to-lower crust is typical of that expected for a Paleozoic foldbelt with crustal thicknesses of greater than 40 km and P_n velocities of about 8.0-8.2 km/s. The sediments along the northwestern segment are predominantly Carboniferous in age with thickness of 3-9 km and *P*-velocities slightly greater than 5 km/s. These sediments contrast

markedly with Cenozoic sediments filling the Dzhungarian Basin which are probably characterized by very low velocities (< 4 km/s) and extreme thicknesses (~ 10 km).

Inversion of Rayleigh Wave Phase and Group Velocities

In order to derive an average velocity structure between the East Kazakh Test Site and Urumchi, fundamental-mode Rayleigh wave phase and group velocities were measured and inverted simultaneously. The strong dispersion exhibited on the vertical component seismogram at periods less than 10 seconds suggests the existence of a large positive velocity gradient in the upper-most crust.

The group velocities were measured using both the multiple filtering technique (Dziewonski *et al.*, 1969) and the phase-matched filter technique (Herrin and Goforth, 1977) which gave similar results. No corrections were made for source group delays, because errors as large as 4 seconds will only produce errors of 1% for periods of 20 seconds. The phase velocities were calculated from the unwrapped phase spectrum, uncorrected for source initial phase. At a distance of 950 km, an error of half a cycle will cause a phase error of ±3% at a period of 20 seconds. The measured phase and group velocities are shown in Fig. 4(a). As discussed by Harris *et al.* (1982), the velocities along this path are quite close to those of Arkhangelskaya and Kuznetsova (1969) and are markedly lower than those of other tectonic regions, including the Basin and Range Province. Also, the group velocity curve is consistent with the strong dispersion exhibited on the seismogram, especially for periods less than about 7 seconds.

The phase and group velocities were inverted simultaneously for shear velocity structure using a technique described in Taylor (1980). The observed and calculated phase and group velocities are shown in Fig. 4(a) and the RMS error of the fit was about 0.05 km/s for both sets of measurements. The compressional velocity was adjusted using the shear velocity and assuming a Poisson's ratio of 0.25. The final shear velocity with model standard errors is shown in Fig. 4(b). Resolution calculations indicate resolving lengths of about 5 km in the upper layers. Below depths of about 15 km, the path to Urumchi is similar to those from many other regions typical of eastern North American (Harris *et al.*, 1982). However, as expected from the high degree of dispersion exhibited on the surface wave train, a strong positive velocity gradient is observed above depths of 15 km.

From geological considerations discussed earlier, the low velocities and large velocity gradient observed in the upper crust are presumably

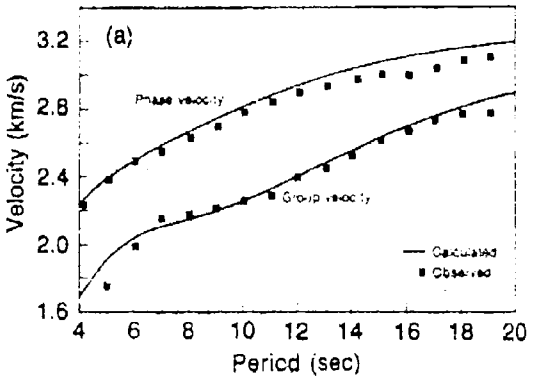

Fig. 4(a). Calculated and observed Rayleigh-wave phase and group velocities between the East Kazakh Test Site and Urumchi for the 10/12/80 event.

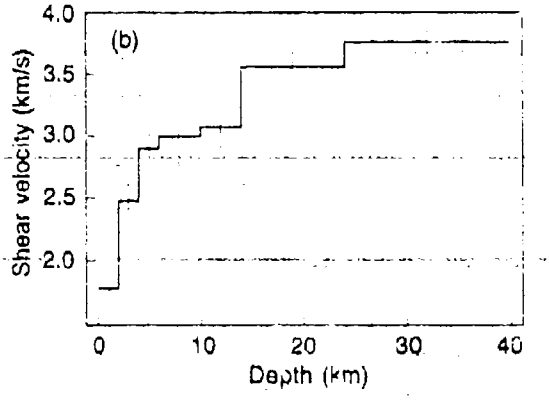

Fig. 4(b). S-velocity as a function of depth from inversion of phase and group velocities shown in 4(a). Vertical lines indicate model standard errors.

due to the great thickness of sediments along much of the travel path. Because the surface wave dispersion curves represent an average over the total travel path, it is expected that the upper crustal velocities are probably slightly greater than those shown in Fig. 4(b) for the northwestern portion of the path (in the older Carboniferous sediments) relative to the southeastern portion (in the younger Cenozoic sediments).

Spectral Amplitudes and Seismic Moment Estimates

In this section, we analyze the recordings of East Kazakh explosions at Urumchi to calculate source characteristics such as seismic moments and to estimate the relative amounts of tectonic strain release. The vertical-component seismograms were Fourier transformed, and the resulting amplitude spectra were smoothed using a five-point mean. The spectra were normalized for geometric spreading to a distance of 500 km and corrected for attenuation assuming the decay rate for eastern and central United States (Mitchell, 1973). The corrected Rayleigh-wave spectra for the explosion on 9/14/80 is plotted in Fig. 5 for frequencies

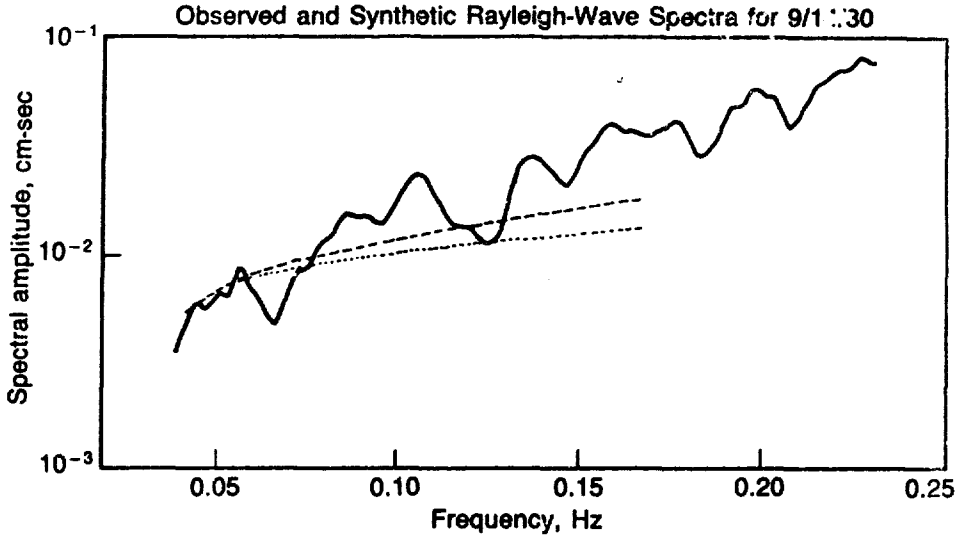

Fig. 5. Amplitude spectra of Rayleigh waves from the 9/14/80 East Kazakh explosion and synthetic spectra for the models described in the text. Observed spectrum is shown by solid line and synthetic spectra are shown by short-dashed and long-dashed lines for pure-explosion and explosion with associated tectonic release, respectively.

where the S/N is believed to be good. Also plotted in Fig. 5 are synthetic spectra calculated from source models discussed below.

The first source model is the spherically-symmetric explosion buried 1 km deep in the Gutenberg continental earth model. The Gutenberg earth model was chosen because of its hard-rock, thick-crust characteristics. The source-time function of Von Seggern and Blandford (1972) was used in the calculation, where K, which is inversely proportional to the rise time, was set to a value of 5 sec^{-1} and B, the overshoot, was set to a value of 2. Plausible K-values have little effect on the amplitude spectrum in the frequency range of interest in this study (Patton and Vergino, 1982). However, the overshoot parameter is important. Von Seggern and Blandford (1972) found that B-values near 2.0 satisfied the granite observations of Werth and Herbst (1963). Burdick and Helmberger (1979) found that body-wave synthetics with B-values between 2.0 and 7.0 matched observations of explosions at Novaya Zemlya. Recent arguments by Douglas and Hudson (1983) claim that the large B-values obtained by Burdick and Helmberger are in fact not required by their data. In light of the results of these studies, a B-value near 2.0 is probably a good assumption.

Synthetic spectra were computed for this source model and were fit to the observed amplitude spectra for the East Kazakh explosions.

As the purpose of this experiment was to estimate seismic moments, particular care was taken to fit amplitudes at the lowest frequencies. The moments obtained in this manner are listed in the first column in Table 2, and the synthetic spectrum for the 9/14/80 event is plotted with the observed in Fig. 5. It is apparent from Fig. 5 that the observed spectrum is considerably richer in high frequencies than the synthetic spectrum.

In order to explain these high frequencies, we first investigated the effect of tectonic strain release on the surface wave amplitude spectra. Explosions at East Kazakh have been known to exhibit significant non-isotropic source effects, such as large Love waves and reversed polarity Rayleigh waves, which indicate that the explosions are triggering tectonic strain release (Rygg, 1979; North and Fitch, 1984). A dip-slip thrust mechanism appears to be consistent with many observed effects (Patton,1980).

Sykes and Cifuentes (1983) measured Love-to-Rayleigh-wave amplitude ratios (LQ/LR) at 20 sec period for many East Kazakh explosions including some in this study. These amplitude ratios were used to infer F-values (see below) of explosions with associated tectonic release. North and Fitch (1984) determined fault azimuths for nine East Kazakh explosions, unfortunately, none of which were used in this study. The average fault strike for their nine events was 127° with a standard deviation of about 20°. Preliminary results for the fault strike associated with the explosion on 9/14/80 based on teleseismic surface waves (Mellman. 1983; Smith *et al.*, 1984) indicate a value near 135°. In the

Table 2. Explosion seismic moments (in units of 10^{23} dyne-cm) for a pure explosion and for plausible F-values.

Date	Pure Explosion	F-Value			
		0.5	1.0	1.5	2.0
4/25/80	0.15	0.15	0.19	0.23	0.3
6/12/80	0.4	0.5	0.5	0.65	0.8
9/14/80	1.6	1.9	2.2	2.7*	3.6
10/12/80	1.6	1.9*	2.2	2.7	3.2
12/14/80	1.3	1.5*	1.7	2.2	2.8
3/29/81	0.3	0.35	0.4	0.5	0.6
4/22/81	1.6	2.0*	2.2	2.8	3.2

* Preferred values based on F-values deduced from LQ/LR observations.

following, we assume that the fault strike is on azimuth with the Urumchi station, which is 133°.

Synthetic spectra were calculated for different F-values using the earthquake trigger model (Aki and Tsai, 1972) where a pure dip-slip thrust earthquake is superimposed on an explosion. Here we use F-value defined by Muller (1973):

$$F = \frac{\alpha^2 M_Q}{2\beta^2 M_X}$$

where M_Q and M_X are seismic moments of the thrust event and explosion, respectively, and α and β are P- and S-wave velocities in the source region, respectively. The synthetic spectra for the combined model were fit to the observed spectra in the same manner as was done with the synthetic spectra for a pure explosion model. The resulting explosion moments are listed in Table 2 for F-values as large as 2.0. Adopting the F-values inferred by Sykes and Cifuentes (1983), we find that the seismic moment determined from the combined model for the explosion on 9/14/80 increased by 69% over the moment obtained assuming a pure explosion model. Likewise, moments increased for the explosions with F-values around 0.5, but only by about 20%. If we assume an F-value as large as 2.0 for the remaining events with no F-value data, there is about a factor of two increase in the moment over that for a pure explosion. Above an F-value of 2.0, the model predicts Rayleigh-wave phase reversals for this station. On the assumption that the event on 10/12/80 is a small F-value event, phase reversals are not supported for any of the events by the results of a differential source phase analysis (Patton and Mills, 1984).

Synthetic spectra for the tectonic release model are richer in high frequencies than the spectra for a pure explosion as can be seen in Fig.5 for the event on 9/14/80. Nevertheless, the large F-value event on 9/14/80 still has more high frequencies than the model predicts. The observed spectra for events on 10/12/80, 12/14/80 and 4/22/81 were also richer in high frequencies.

There are a number of source parameters of the tectonic release model that can affect the frequency content of computed spectra. Fault strike is a very important parameter because the Urumchi station lies on a minimum of the radiation pattern of the tectonic release for our choice of fault strike, and even small changes in the strike can increase the amplitude of the tectonic contaminant significantly. For the small F-values events though, the effect of changing fault strike alone cannot account for the high frequencies. We considered relaxing the assumption that the tectonic event occur simultaneously with the explosion. Observation of

time delays in reversed Rayleigh-waves for East Kazakh explosions (Rygg, 1979; Cleary, 1981) suggest the possibility of a few seconds delay in the triggering of the tectonic event. A two-second delay will introduce a frequency-dependent phase perturbation such that low frequencies are cancelled, but frequencies above 0.12 Hz are actually enhanced by the tectonic contaminant. Numerical experiments show that if the strike of a delayed event is rotated by 40° to 50°, it is possible to fit the observed frequency content of the low F-value explosions. This suggests the possibility that tectonic release was delayed and occurred on more east-west oriented faults for these low F-value explosions, and we have looked for evidence in the teleseismic surface wave data to support this. Preliminary results of several studies currently in progress (*e.g.*, Mellman, 1983; Smith *et al.*, 1984) indicate that fault strikes for these events are not much different from the strike of the 9/14/80 explosions, which is estimated to be 135°.

Other possibilities that could explain the frequency content of the observed spectra are: (1) source medium (*e.g.* more high frequencies in the Green's functions), and (2) energy focusing or amplification at the Urumchi station. Energy focusing is a good possibility considering the large contrast in Rayleigh-wave group velocities between basin and foldbelt structures (Patton and Mills, 1984) and that the Dzhungarian Basin between the East Kazakh Test Site and the Urumchi station (Fig. 1) would be an effective seismic lens for short-period surface waves.

Conclusions

Seismograms from the PRC National Seismic Network are available through a data exchange program between NOAA and the State Seismological Bureau of the PRC. The data consist of three-component, broadband (flat to displacement between 0.1 and 10 Hz) photographic records from an SK Kirnos galvanometric system, which is well suited for recording regional seismic waves. Most of the difficulties encountered with handling the Chinese data were related to the usual problems associated with digitization of photographic records. It was necessary to use the nominal instrumental parameters supplied by NOAA since calibration pulses were not available for the time period analyzed. Nevertheless, the results of this paper suggests that these data will be useful for source and structural studies in Asia and for seismic verification studies, since two of the Chinese stations are within regional distance of the Soviet East Kazakh Test Site.

Rayleigh-wave phase and group velocity dispersion were measured on the path between East Kazakh and the Urumchi station in Sinkiang

Province of western China. Previous work on earth structures in central Asia similar to this path indicates the presence of thick sedimentary deposits underlain by Paleozoic rocks of pre-Devonian age. The depth to Paleozoic rock can be as great as 10 km. Based on surface geology, the path may be divided equally into a northwest and southeast segment, with thick Carboniferous sediments, 3-9 km thick, in the northwest, and Tertiary and Quaternary sediments in the Dzhungarian Basin in the southeast. The inversion of phase and group velocities confirms the presence of thick sedimentary deposits. The upper 15 km of the crust show a strong velocity gradient with extremely low velocities compared to any known structure on the North American continent. Velocities in the crust below 15 km depth are not significantly different from other continental structures.

Amplitude spectra of Rayleigh waves from seven East Kazakh explosions were computed, and the seismic moments were estimated based on models of the explosion source triggering tectonic release. These models incorporated independent estimates of the overshoot parameter, B, the F-value and the fault strike. The largest explosion studied in this paper occurred on 9/14/80 and had an m_b of 6.2 and a seismic moment of 2.7×10^{23} dyne-cm. We found that the observed spectra were richer in high frequencies than predicted by the model. This could be caused by a path effect involving seismic wave focusing by the Dzhungarian Basin between East Kazakh and the Urumchi station, although source medium effects cannot be ruled out. It is noteworthy that the Chinese data provide estimates of the seismic moment for a frequency range bridging the teleseismic surface-wave and body-wave observations. In principal, the results from studies of the Chinese data and teleseismic data could be used to construct a broadband moment spectrum for explosions at East Kazakh. Such a synthesis may be helpful to further understand the nature of the explosive source in hard rock media.

Acknowledgments

We wish to thank Jim Hannon, Keith Nakanishi, and Al Smith for critical reviews of the manuscript. We also thank George Mellman for providing results of teleseismic surface-wave studies prior to release of the Sierra Geophysics Report. Bob Rohrer digitized many of the seismograms used in this study and Eileen Vergino assisted in the data processing. This work was performed under the auspices of the U.S. Department of Energy by the Lawrence Livermore National Laboratory under Contract W-7405-ENG-48.

References

Aki, K., and Y.B. Tsai. "Mechanism of Love-wave excitation by explosive sources." *J. Geophys. Res.*, **77**, 1452-1475, 1972.

Arkhangei'skaya, V.M. and I.M. Kuznetsova, "Study of the upper portions of the earth's crust in central Asia from dispersion of surface waves," *Izv., Earth Physics*, **5**, 61-65, 1969.

Bulin, N.K., E.A. Propvaka, V.I. Bubnova, V.I. Tolmanov, and E.I. Erglis. "Deep structure of the southwest Altai region according to seismological data," *Sov. Geol.*, **12**. 97-109, 1969.

Burdick, L.J. and D.V. Helmberger, "Time function appropriate for nuclear explosions," *Bull. Seism. Soc. Am.*, **69**, 957-973. 1979.

Burke, K., J.F. Dewey, and W.S.F. Kidd. "World distribution of sutures — The sites of former oceans," *Tectonophys.*, **40**, 69-99, 1977.

Chun, K.Y. and T. Yoshii. "Crustal structure of the Tibetan Plateau: A surface-wave study by a moving window analysis," *Bull. Seism. Soc. Am.*, **67**, 735-750. 1977.

Cleary, J.R., "Anomalous Rayleigh waves from presumed explosions in East Kazakh," in *Identification of Seismic Sources — Earthquake or Underground Explosion*, F.S. Husebye and S. Mykkeltveit (eds.) D. Reidel. Dordecht, 191-199, 1981.

Douglas, A. and J.A. Hudson, "Comments on 'Time functions appropriate for nuclear explosions' by L.J. Burdick and D.V. Helmberger," *Bull. Seism. Soc.Am.*, **73**, 1255-1264, 1983.

Dziewonski. A., S. Bloch, and M. Landisman. "A technique for the analysis of transient seismic signals," *Bull. Seism. Soc. Am.*, **59**, 427-444, 1969.

Harris, D.B., S.R. Taylor, and H.J. Patton. *Analysis of an Eastern Kazakh explosion using regional Chinese seismograms: A pilot study*, UCID-19503, Lawrence Livermore National Laboratory, CA 1982.

Herrin, E. and T. Goforth, "Phase-matched filters: Applications to the study of Rayleigh Waves," *Bull. Seism. Soc. Am.*, **67**, 1259-1275, 1977.

Mellman, G., Sierra Geophysics, Redmond, WA., private communication, 1983.

Mitchell, B.J., "Surface-wave attenuation and crustal anelasticity in central North America," *Bull. Seism. Soc. Am.*, **63** 1057-1071, 1973.

Muller, G., "Seismic moment and long-period radiation of underground nuclear explosions," *Bull. Seism. Soc. Am.*, **63**, 847-857, 1973.

Nalivkin, D.V., *Geology of the U.S.S.R.* (Translated by N. Rast), University of Toronto Press, 855 pp, 1962.

North, R. and T. Fitch, "Surface-wave generation by underground nuclear explosions," *J. Geophys. Res.*, in press, 1984.

Patton, H.J., *Surface-wave generation by underground nuclear explosions releasing tectonic strain*, UCRL-53062. Lawrence Livermore National Laboratory Livermore, CA 1980.

Patton, H.J. and E.S. Vergino, *Source effects on surface waves from Nevada Test Site explosions*, UCRL-53247, Lawrence Livermore National Laboratory, Livermore, CA 1981.

Patton, H.J. and J.M. Mills, Jr., *A study of East Kazakh explosions and propagation in Central Asia using regional Chinese seismograms*, UCID in preparation, Lawrence Livermore National Laboratory, Livermore, CA 1984.

Piwinskii, A.J., *Deep structure of the Earth's crust and upper mantle in the U.S.S.R. according to the geophysical and seismological data, Part 1*, Univ. Calif. Int. Dist., 18099, 69 pp, 1979.

Rygg, E.,"Anomalous surface waves from underground explosions," *Bull. Seism. Soc. Am.*," **69**, 1995-2002, 1979.

Savarenskiy, Y.F. and A.B. Peshkov, "The use of surface wave velocities for selection of models of crustal structure" (translated by D.G. Fry) *Earth Physics*, **10**, 79-87, 1968.

Smith, A.T., D.L. Springer, and E.S. Vergino, *Isolating tectonic strain release in East Kazakh explosions using body and surface waves.* UCID in preparation 1984.

Sykes, L. R. and I. Cifuentes, "Determinations of yields of underground nuclear explosions using seismic surface waves," *Abstr. EOS*, **64**, p. 194. 1983.

Tapponnier, P. and P. Molnar, "Slip-line field theory and large-scale continental tectonics," *Nature*, **264**, 319-324, 1976.

Tapponier, P. and P. Molnar, "Active faulting and tectonics in China," *J. Geophys. Res,"* **82**, 2905-2920, 1977.

Tapponnier P. and P. Molnar, "Active faulting and Cenozoic tectonics of the Tien Shan, Mongolia, and Baykal regions," *J. Geophys. Res.*, **84**, 3425-3459, 1979.

Taylor, S.R., *Crust and upper mantle structure of the northeastern United States*, Ph.D. thesis, Masachusetts Institute of Technology, 288, pp., 1980.

Von Seggern, D. and R. Blandford, "Source time functions and spectra for underground nuclear explosions," *Geophys. J.R. Astr. Soc.*, **31**, 83-97, 1972.

Werth, G.C. and R.F. Herbst, "Comparison of amplitudes of seismic waves from nuclear explosions in four mediums," *J. Geophys. Res.*, **68**, 1463-1475, 1963.

Propagation of L_g Phases in Western Europe

J. L. Plantet and B. Massinon

Introduction

For intermediate distances (150-1500 km) along continental propagation, seismograms are mostly dominated by L_g phases, as far as amplitudes and durations are concerned.

These waves, built up by a complex composition of multi-reflected S waves within the crust (Bouchon 1982), convey information on the source itself, the propagation path and the reception function. In the frequency domain, the L_g wave amplitude is represented by the product of these three functions: source function, propagation function (or attenuation function), and station transfer function.

An earthquake model can be described by a dislocation model (Brune 1970) which explains spectra with a low frequency constant level connected to the seismic moment, and with a corner frequency over which amplitudes decrease as $\propto f^b$. The propagation function is the product of two factors:

- one which represents the attenuation due to geometrical spreading
- one which represents the anelastic attenuation

The reception function, a generally neglected term, allows taking into account the influence of superficial layers beneath the recording station.

The purpose of this study is to evaluate the effect of these three factors by computing L_g waves spectra recorded in the French seismic network of LDG.

1. Data and Data Processing

1.1 Data. This study has used the L_g waves generated by 18 earthquakes and recorded by the French seismic network. Essentially localized around France (Fig. 1), these earthquakes have local magnitudes M_l between $M_l = 3.2$ and $M_l = 4.8$ (Table 1). Their hypocenters, always within the crust, are mostly computed with an uncertainty larger than 5 km. Wave paths cross various geological structures and epicentral distances range from 150 km to 1200 km. For the same quake, the

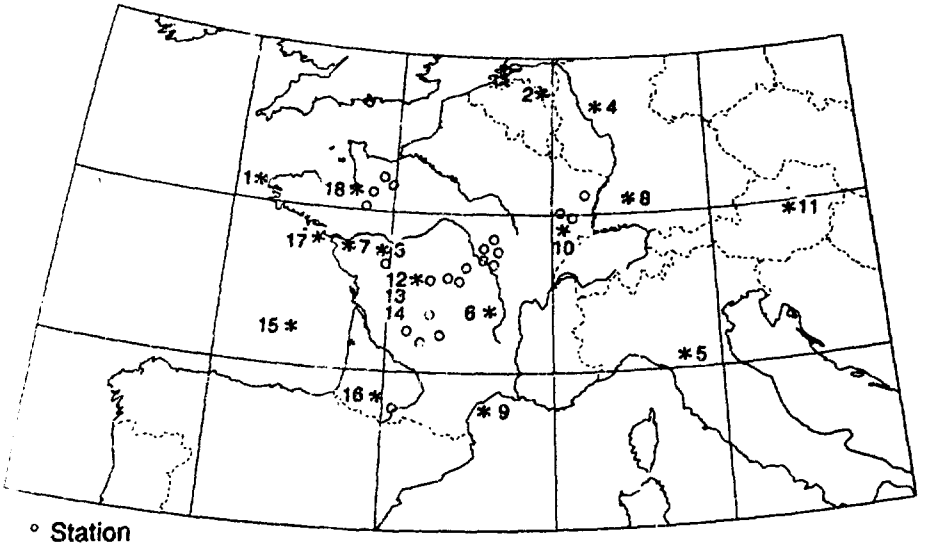

Fig. 1. Map of earthquakes (stars) and stations (open circles) used in this study. Numbers are numbers of earthquakes as described in Table 1.

Table 1

	Date	Origin Time	Coordinates	M_l	Region
1 —	04/09/81	04h 41 59.2	48.48N 05.11W	4.2	Brest
2 —	02/03/82	01h 27 26.3	51.01N 05.77E	4.0	Anvers
3 •	28/05/82	04h 50 24.7	46.96N 00.11W	3.3	La Rochelle
4 —	28/06/82	09h 57 33.3	50.69N 07.84E	4.9	Francfort
5 —	26/07/82	15h 07 29.5	44.26N 10.88E	4.3	Emilie
6 •	08/10/82	13h 19 46.3	45.51N 03.66E	3.3	Clermont-Ferrand
7 •	09/11/82	13h 44 47.3	47.07N 01.73W	3.9	Nantes
8 —	28/11/82	04h 34 05.0	48.31N 09.05E	3.9	Jura Souabe
9 •	23/12/82	14h 46 13.4	43.02N 03.75E	4.1	Montpellier
10 —	03/02/83	02h 48 30.1	47.34N 06.53E	3.4	Vesoul
11 —	14/04/83	14h 52 15.2	47.75N 15.10E	4.8	Salzbourg
12 •	21/04/83	01h 53 07.9	46.20N 00.96E	4.0	Bellac
13 •	21/04/83	19h 07 02.1	46.19N 00.96E	3.6	Bellac
14 •	21/04/83	23h 31 13.8	46.20N 00.96E	3.8	Bellac
15 —	08/05/83	17h 47 51.4	44.97N 03.47W	4.0	Ouest-Rochefort
16 —	06/06/83	01h 29 50.3	43.27N 00.30W	4.1	Pyrenees
17 •	03/07/83	20h 47 11.2	47.21N 02.50W	3.2	Loriert
18 —	07/07/83	03h 52 25.2	48.41N 01.30W	4.2	Fougeres

— CSEM location
• LDG location
M_l LDG local magnitude

useful distance range is reduced even further due to the dynamic range of the recording process (60 dB): the maximum distance without amplitude clipping is generally between two and three times the minimum distance.

In order to point out eventual modifications of the attenuation, the L_g wave train is divided in 3 parts according to their group velocities (Fig. 2):

L_g1 : 3.1 km/s $< V <$ 3.6 km/s	maximum of L_g
L_g2 : 2.6 km/s $< V <$ 3.1 km/s	coda of L_g
L_g3 : 2.3 km/s $< V <$ 2.6 km/s	end of L_g coda

For each of the digital signals recorded with a sampling rate of 50 samples/s, amplitude spectra are computed by FFT, between 0.5 Hz and 15 Hz (Fig. 3). Seismic noise spectra 30 sec before the P_n wave arrivals are also computed. For each frequency, the L_g spectrum is corrected from seismic noise spectrum.

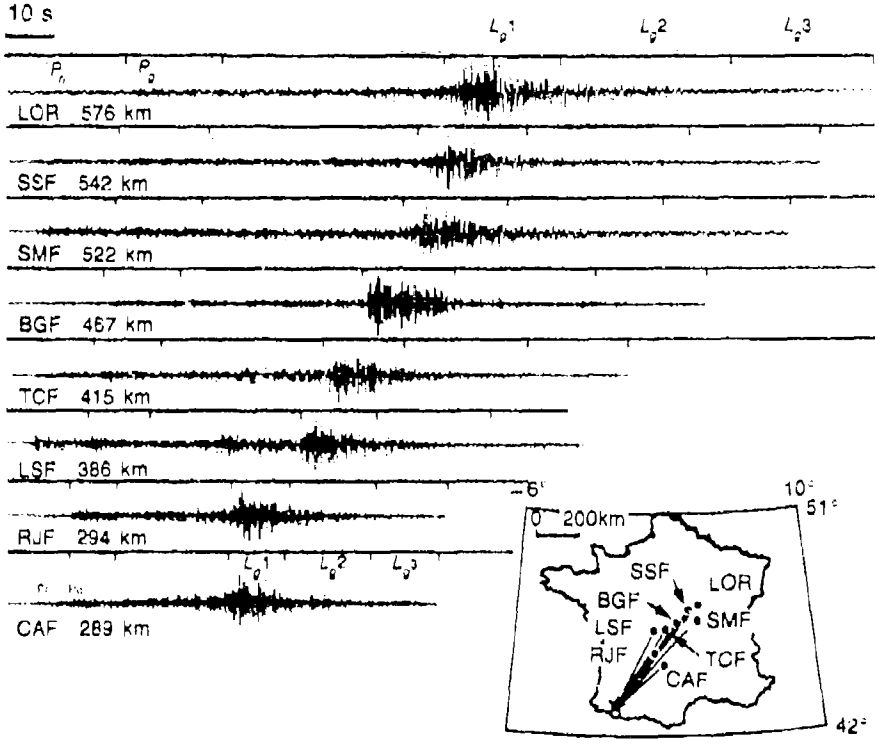

Fig. 2. Seismograms recorded by 8 stations for the Pyrenees earthquake (number 16 - 06/06/83 - M_L = 4.1). Amplitudes are normalized to the maximum amplitude on each trace.

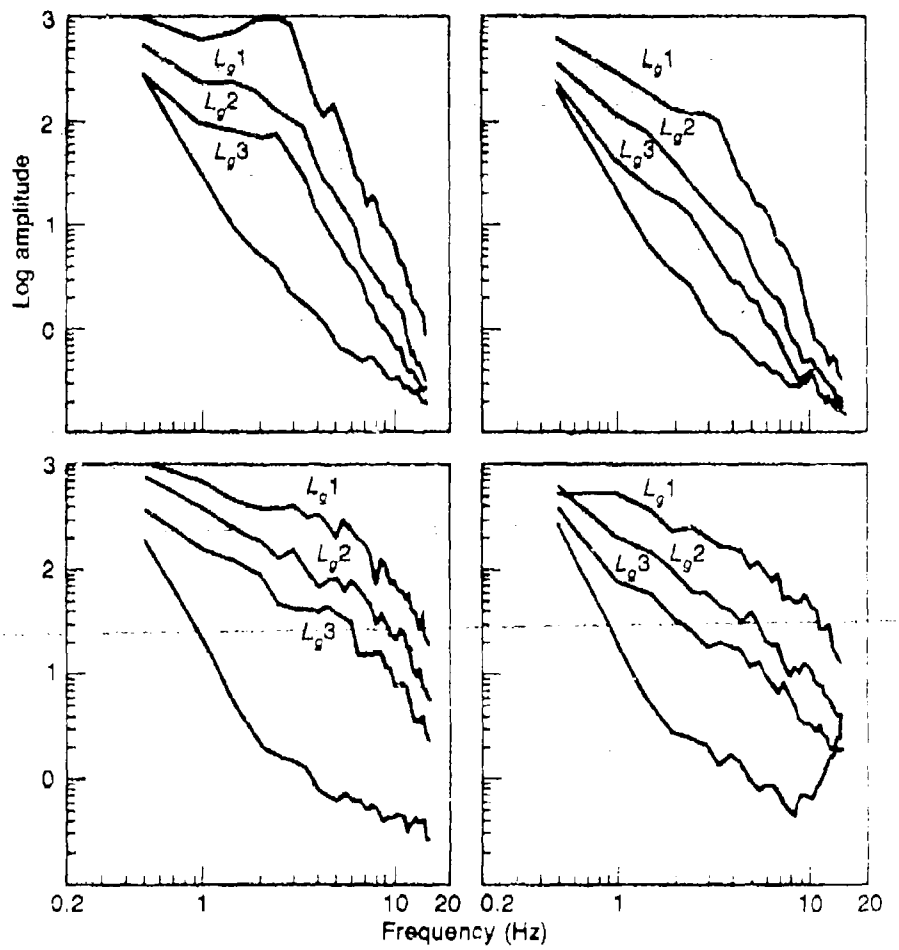

Fig. 3. Amplitude spectra computed for seismic noise (lower trace) and L_g phases (L_g1, L_g2, L_g3) recorded in four stations BGF, LOR, CAF, LSF for the Pyrenees earthquake (number 16 - 06/06/83 - M_l = 4.1) Amplitudes are normalized to the maximum spectral amplitude at station BGF.

1.2 Data Processing. The spectral amplitude of a recorded wave at the ith station, at distance d_{km} from the jth earthquake is:

$$A_{ij}(f,d) = S_j(f) \bullet R_j(\theta_i, \varphi_i) \bullet \mathrm{EXG}(d) \bullet \mathrm{AI}(f,d) \bullet \mathrm{TFS}_i(f) \quad (1)$$

with:

$S_j(f)$: source amplitude spectrum of the jth earthquake
$R_j(\theta_i, \varphi_i)$: radiation pattern of the jth earthquake to the ith station
$\mathrm{EXG}(d)$: attenuation factor due to the geometrical spreading

$AI(f,d)$: anelastic attenuation factor
$TFS_i(f)$: transfer function at the ith station

Each of these terms can be modeled.

a) Source $S_j(f)$. The S wave spectrum generated by a seismic source is described by the amplitude at $f = 0$ Hz ($S_j(0)$), the corner frequency fc_j; and the asymptotic decrease expressed by the coefficient γ of the spectrum (Brune 1970)

$$S_j(f) = S_j(0) \bullet \left(1 + (f/fc_j)^{2\gamma}\right)^{-1/2}$$

(Johnson-McEvilly 1974)

b) Radiation pattern $R_j(\theta_i, \varphi_i)$. The radiation pattern is a function of the source mechanism. Concerning most of the earthquakes used in this study, source mechanisms are poorly determined. Consequently, $R_j(\theta_i, \varphi_i)$ is set equal to 1.

c) Geometrical spreading EXG (d): This factor is independent of frequency. For L_g phases Nuttli (1973) proposed, after theoretical and empirical considerations, to express it as:

$$EXG(d) = d^{-1/3} \bullet (\sin d)^{-1/2}$$

Campillo (1984) computes synthetics of L_g phases propagating through a European crust and obtains:

$$EXG(d) = d^{-0.83}$$

Since distances are small ($d \leq 10°$), these two formulas are equivalent ($\sin d = d$). We use the second one.

d) Anelastic attenuation factor AI (f,d). The anelastic attenuation factor can be written as:

$$AI(f,d) = e^{-\frac{\pi f d}{Q(f)v}}$$

with:

$Q(f)$: quality factor, function of frequency f
v : group velocity of the wave

$Q(f)$ is expressed for a limited frequency band (0.5 Hz - 15 Hz) by

$$Q = Q_0 f^b$$

(Mitchell, 1980)

e) Transfer function at the *i*th station: $TFS_i(f)$: This factor is the frequency response of the superficial structures beneath the station. Impossible to model *a priori* because these structures are not known with sufficient accuracy, it will be computed.

1.3 Resolution of Equation 1. Distance range (150-1200 km) and frequency range (0.5 Hz-15 Hz) being too narrow, they lead to a numerical indetermination between geometrical and anelastic attenuation. Consequently, the geometrical spreading factor is fixed as:

$$d^{-0.8}$$

Equation 1 can be linearized by taking logarithms to form:

$$\log\left(A_{ij}(f,d)\right)+0.8\log d = \log\left(S_j(f)\right)-\frac{\pi d}{Q(f)v}f+\log\left(\mathrm{TFS}_i(f)\right) \quad (2)$$

Equation 2 can be solved by iterative process:

a) by least squares, estimate for each frequency and for each quake the two factors $S_j(f)$ and $Q(f)$, using an estimation of the TFS factor. (At the first iteration TFS is taken as 1.)

b) model for the whole set of quakes: $Q = Q_0 f^b$

c) evaluate the perturbations to bring to the transfer functions TFS as the r.m.s. to each station, with the additive hypothesis:

$$\sum \mathrm{TFS}_i(f) = 1$$

The process is stable and convergent after few iterations.

2. Results

2.1 Transfer Function at the *i* th Station. By taking into account the TFS or transfer function of the stations, the estimation of the Q factor is significantly improved and the scattering reduced.

The transfer functions of the 22 seismic stations are essentially representative of any attenuation or magnification for high frequencies ($f > 5$ Hz) by factors up to 3 (Fig. 4). They are relative to mean $\overline{\mathrm{TFS}}$ defined previously as

$$\overline{\mathrm{TFS}} = \frac{1}{n}\sum_{i=1}^{n} \mathrm{TFS}_i(f) = 1$$

These TFS obtained by L_g wave spectra are rather well correlated with seismic noise spectrum variation, specially for high frequencies (Fig. 5) which confirms its origin associated with superficial layers.

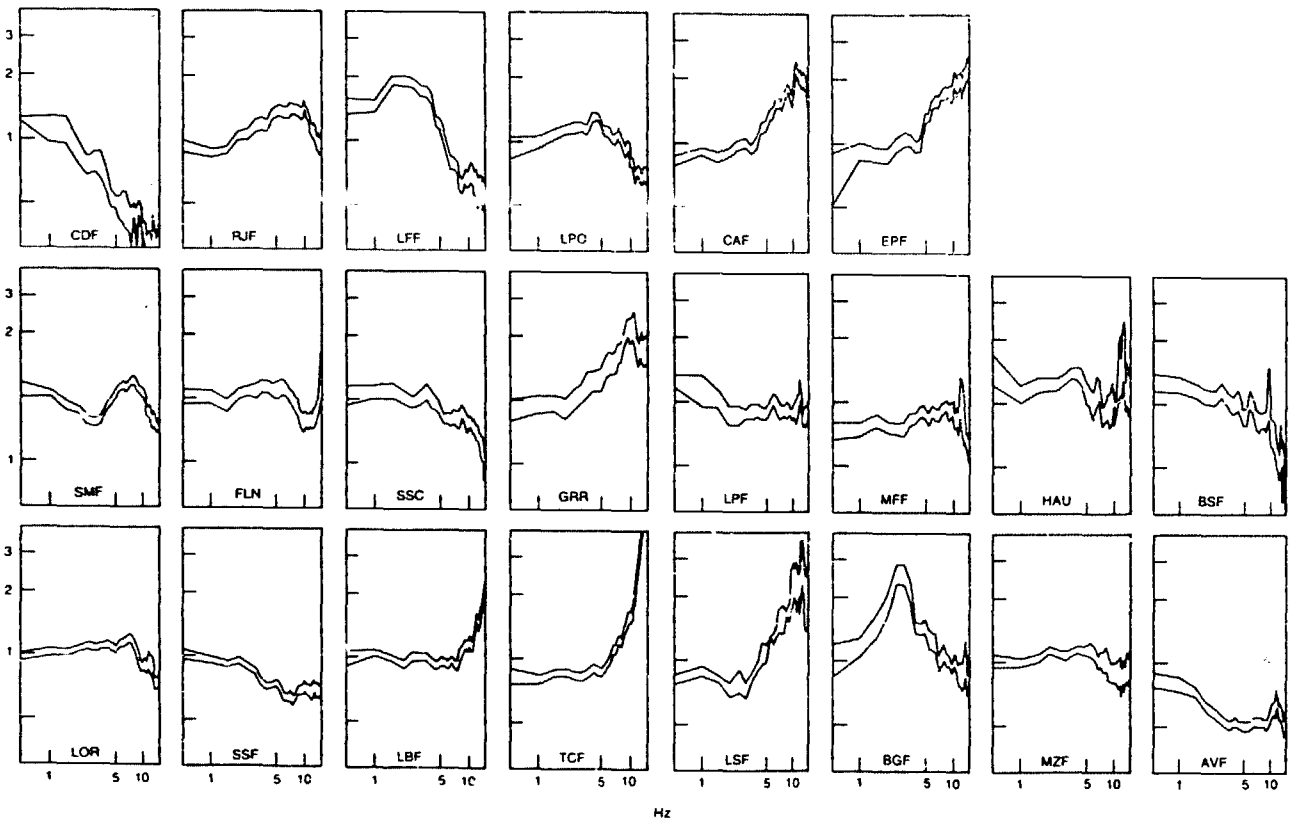

Fig. 4. Transfer functions of station TFS between 0.5 Hz and 15 Hz. Both curves represent TFS ± σ (TFS) for 22 stations of the French SP network.

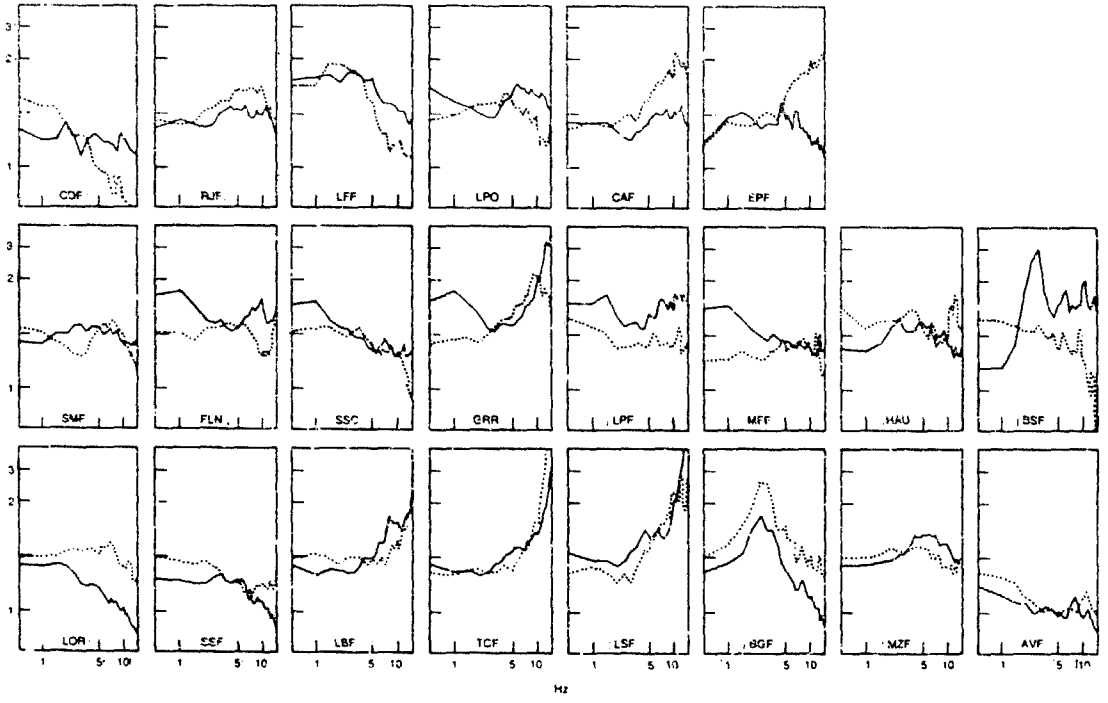

Fig. 5. Comparison between the transfer function of station TFS and the seismic noise spectrum between 0.5 Hz and 15 Hz for 22 stations of the French network. The dotted line is the TFS variation for the *i*th station. The solid line figures for this *i*th station:

$$\log B_i(f) - \log\left(\frac{1}{n}\sum_{i=1}^{n} B_i(f)\right)$$

where $B_i(f)$ is the seismic noise spectrum.

2.2 Quality Factor — Frequency Variations. The quality factor Q is estimated for each quake at each frequency independently. After TFS correction, the Q factor is given with an uncertainty of about 30% or less (Fig. 6).

For each quake and the three L_g phase groups, the Q factor varies significantly with the frequency and these variations are correctly

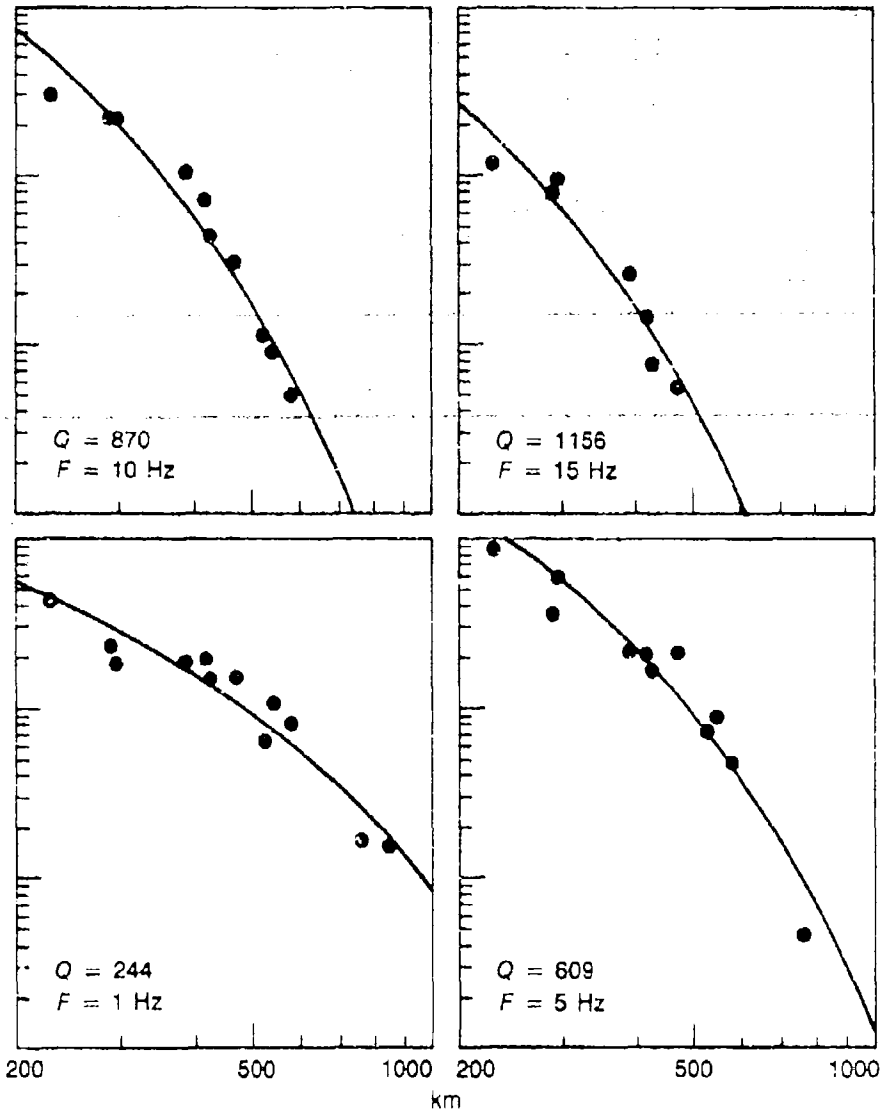

Fig. 6. Spacial attenuation of the L_g waves for the Pyrenees earthquake (number 16 - 06/06/83; $M_l = 4.1$) for different frequencies: $f = 1$ Hz, 5 Hz, 10 Hz, 15 Hz. Attenuation due to geometrical spreading is modeled by $d^{-0.8}$

described by the relation (Fig. 7): $Q = Q_0 f^b$ where b can take values between $b = 0.2$ and $b = 0.8$ depending on the earthquakes. Most of these values are nevertheless concentrated between:

$$b = 0.4 \text{ and } b = 0.6 \text{ (Fig.8)}$$

The mean values for b are finally the following according to the type of L_g:

L_g1	$b = 0.46$	$\sigma_b = 0.10$
L_g2	$b = 0.53$	$\sigma_b = 0.08$
L_g3	$b = 0.54$	$\sigma_b = 0.13$

Discrepancies in b values obtained for three Bellac earthquakes (numbers 12, 13, and 14) point out that the standard errors, σ_b, are not clearly associated to regional differences (Table 2).

For western Europe an estimation of $\overline{Q}$ or mean quality factor is obtained by using the whole set of earthquake data (Fig. 9).

L_g1	$Q = 290\, f^{0.52}$	
L_g2	$Q = 295\, f^{0.55}$	Relations A
L_g3	$Q = 350\, f^{0.50}$	

result similar to the one already obtained by Nicolas *et al.* (1982). If the same frequency variation is selected for each L_g phase, that is to say the same b:

$$b = 0.53$$

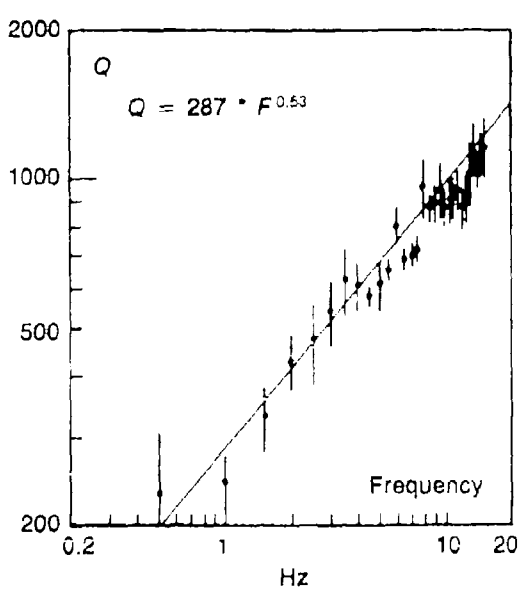

Fig. 7. Variations of Q factor versus frequency for L_g1 waves of the Pyrenees earthquake (number 16 - 06/06/83 - $M_l = 4.1$). Error bars correspond to 66% of confidence limit.

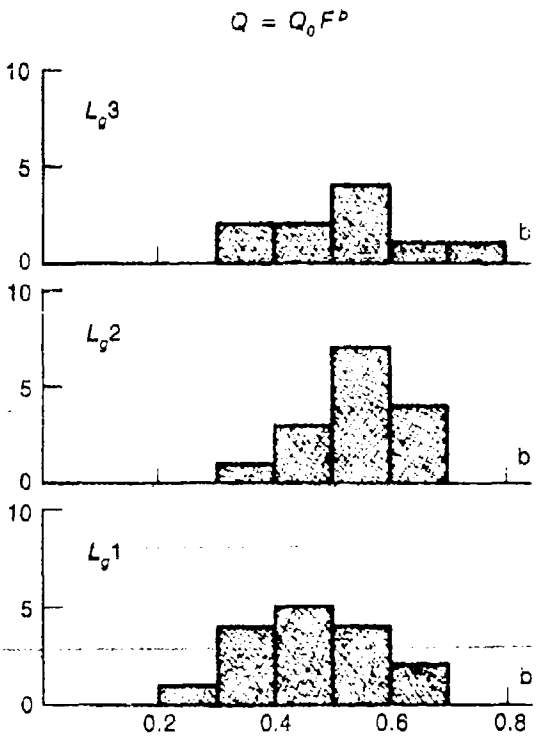

Fig. 8. b histograms from $Q = Q_c f^b$ computed for L_g1, L_g2, L_g3 waves from the whole set of 18 earthquakes.

we obtain:

L_g1	$Q = 290\, f^{0.53}$	
L_g2	$Q = 310\, f^{0.53}$	Relations B
L_g3	$Q = 330\, f^{0.53}$	

which means that the L_g waves and their coda have the same anelastic attenuation and confirm the association of the Q factors with S waves and their coda (Aki 1980). Nuttli (1983) obtains $b = 0.6$ for L_g attenuation in the central U.S.

3. Source Spectrum

Source spectrum is defined as the mean of the spectra computed for each station signal, after transfer function correction (TFS) and propagation correction. The attenuation correction term is the one computed for the whole set of earthquakes (Relations B).

The spectra, after corrections, present a dispersion (Fig. 10) probably due to a rough modeling of propagation which does not take into account differences between local structures.

Table 2. *b* values for L_g1, L_g2, and L_g3 waves recorded from earthquakes numbers 12, 13 and 14 which occurred in the same region of central France (Bellac).

Number	M_l	$b\ L_g1$	$b\ L_g2$	$b\ L_g3$
12	4.0	0.35	0.62	0.48
13	3.6	0.35	0.58	0.34
14	3.0	0.21	0.57	0.59

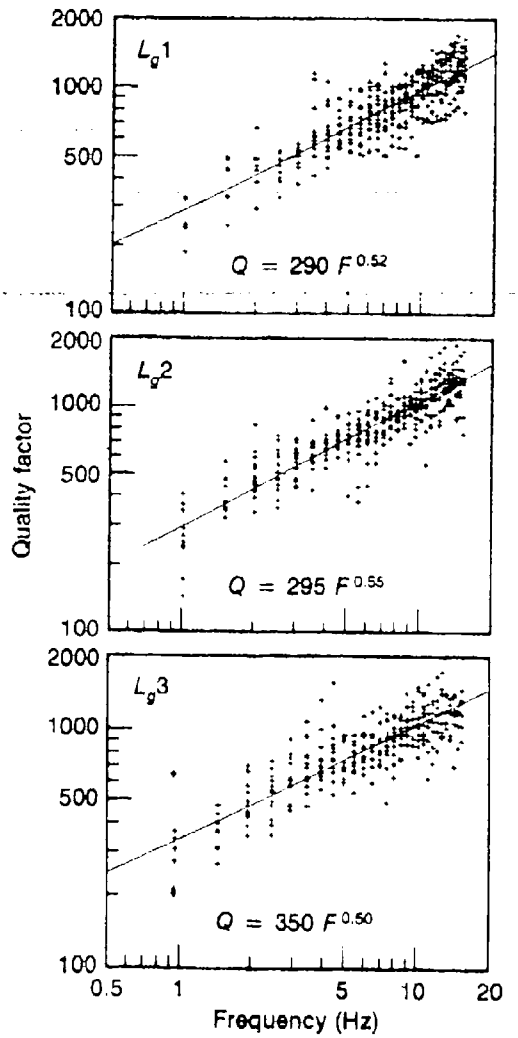

Fig. 9. Variations of Q factor for L_g1, L_g2, and L_g3 for the whole set of 18 earthquakes.

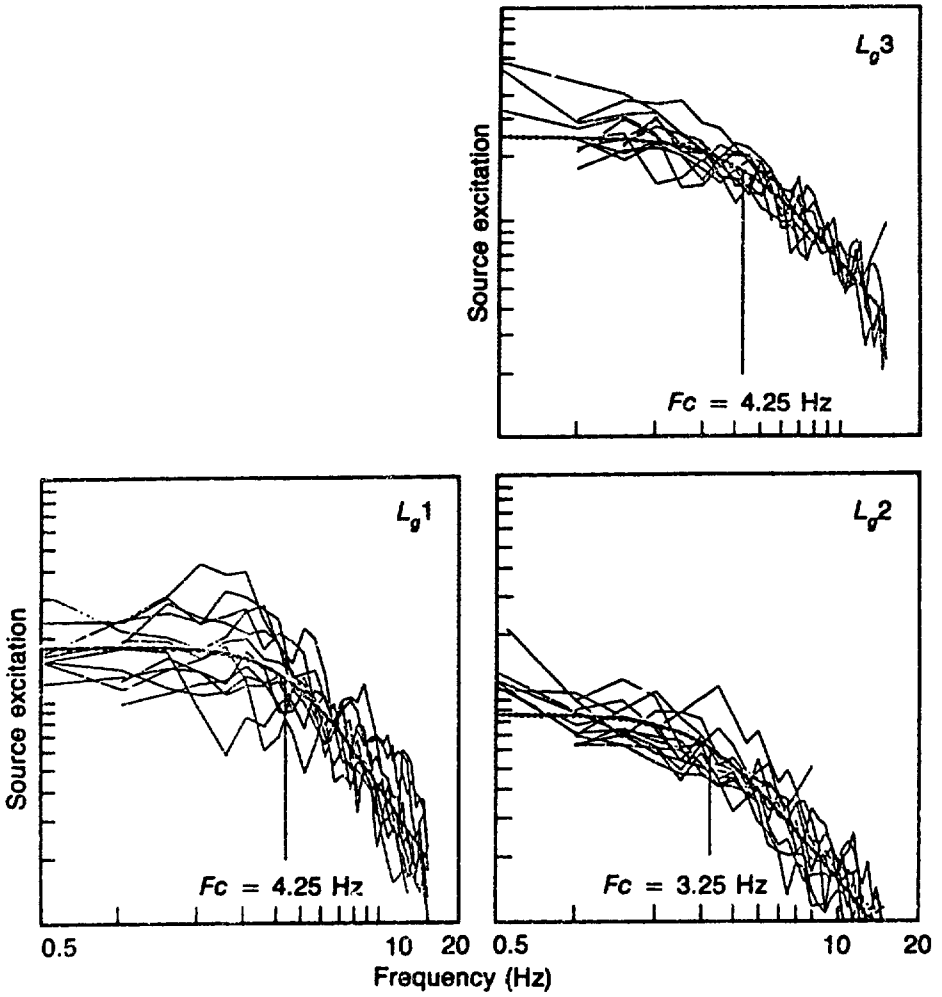

Fig. 10. Source spectra obtained from L_g1, L_g2, L_g3 waves for the Pyrenees earthquake (number 16 - 06/06/83 - M_l 4.1). Each solid line represents the spectrum at each station after propagation correction and transfer function correction (at the station). Dotted lines figure the spectrum:

$$S(f) = S_0(0) / \left[1 + (f/f_c)^{2\gamma} \right]^{1/2}$$

Nevertheless, these spectra pointed out the main features of a Brune source (Brune 1970). L_g phases (L_g1) and their coda (L_g2) and L_g3) lead to similar source spectra (Fig. 10 and Fig. 11). The asymptotic decrease of the spectra for high frequencies is in between $f^{-1.5}$ and $f^{-2.25}$, and corner frequencies are in the range 1.25 Hz to 10 Hz. Assuming a relation between fc and M_l of the form:

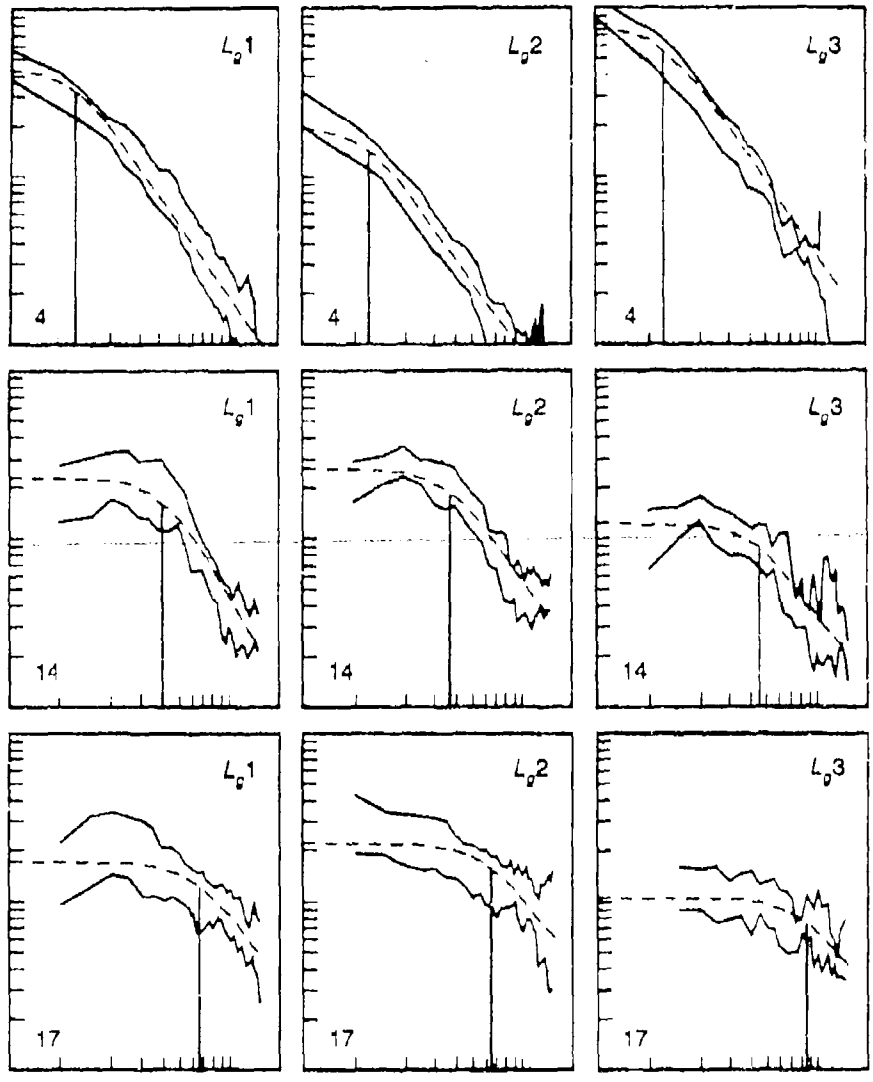

Fig. 11. Source spectra obtained for the following three earthquakes:

number 17 Lorient M_l = 3.2
number 14 Bellac M_l = 3.8
number 4 Francfort M_l = 4.9

Corner frequencies are also given.

$$\log fc = A + B M_l$$

a least squares fit to the data yields: (Fig. 12)

$$\log fc = 1.98 - 0.33 M_l$$

On the other hand, $S_0(0)$, low frequency level of the source spectrum is connected to the earthquake magnitude M_l as follows:

$$\log S_0(0) = C + 1.5 M$$

and this, for each L_g1, L_g2, L_g3 wave spectrum.

The slope 1.5 is similar to the one obtained by Johnson and McEvilly in their relation:

$$\log M_0 = 17.0 + 1.4 M$$

with the relationship: $M_0 = 4\pi\varrho\beta^3 R S_0(0)$, where ϱ is the density, β is the shear wave velocity of the medium, and R is the hypocentral distance (L.R. Johnson and McEvilly, 1974).

Conclusion

This study which used the L_g waves generated by 18 local earthquakes recorded on the French seismic network, gives information on the source itself, the L_g wave propagation and the reception function.

A reasonable evaluation of the source spectrum similar to the Brune dislocation model is obtained for each quake.

Anelastic attenuation term both for L_g and its coda leads to an estimation of the Q factor of the form:

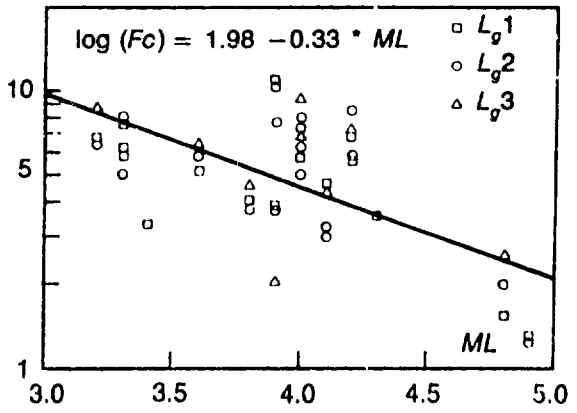

Fig. 12. Variations of the corner frequency f_c *versus* the local magnitude M_l.

$$Q = 300 f^{0.5}$$

between 0.5 Hz and 15 Hz, assuming a geometrical spreading attenuation factor as $d^{-0.8}$ *versus* distance. The reception response is also obtained. It correlates specially for high frequencies with the seismic noise spectrum recorded at the station.

This confirms the influence of local superficial layers on the transfer function of the station.

References

Bouchon, M., "The Complete Synthesis of Seismic Crustal Phases at Regional Distances," *J. Geophys. Res.*, **87**. 1982.

Brune, J.N., "Tectonic Stress and the Spectra of Seismic Shear Waves from Earthquake," *J. Geophys. Res.*, **75**, 1970.

Johnson, L.R. and T. McEvilly, "Near-Field Observations and Source Parameters of Central California Earthquakes," *Bull. Seism. Soc. Am.*, **64**, No. 6, 1974.

Nuttli O.W., "Seismic Wave Attenuation and Magnitude Relations for Eastern North America," *J. Geophys. Res.*, **78**. 1983.

Campillo, M., *et al.*, "Study of the Excitation, Spectral Characteristics and Geometrical Attenuation of Regional Seismic Phases," *Bull. Seism. Soc. Am.*, **74**, 1984.

Mitchell B.J., "Frequency Dependence of Shear Wave Internal Friction in the Continental Crust of Eastern North America," *J. Geophys. Res.* **85**, 1980.

Aki, K., "Scattering and Attenuation of Shear Waves in the Lithosphere," *J. Geophys. Res.*.

Nicolas, M., *et al.*, "Attenuation of Regional Phases in Western Europe," *Bull. Seism. Soc. Am.*, **6**, 1982.

The Use of L_g for Yield Determination

Paul W. Pomeroy and Lynn L. Peseckis

Summary

The amplitudes of regional phases provide an additional constraint on the determination of explosion yield. $L_g(Z)$ may be used to determine yield once significant problems associated with the determination of Q and the selection of the appropriate m_{bLg} versus yield curves are resolved.

Introduction

One of the most exciting advances in yield determination in recent years involves the use of regional waves, particularly $L_g(Z)$, as a measure of yield. The use of regional seismic waves such as L_g provides a measurement that is partially, at least, independent of the teleseismic body and surface wave methodologies.

The determination of yield using L_g (Z) involves the following steps:

1. Determine the frequency-dependent attenuation from measurements of the predominant frequency as a function of travel time. The frequency dependence of attenuation may be of the exponential form $Q = Q_0 f^{\zeta}$ (Mitchell, 1980) or the linear form $Q = Q_0 + \alpha f$.

2. Measure the sustained amplitude of the $L_g(Z)$ wavetrain for group velocities between 3.3 and 3.8 km/sec at frequencies near 1 Hz.

3. Using the m_{bLg} formulation of Nuttli (Nuttli, preprint 1) to determine m_{bLg}.

4. At this point, there are two options:

a. Combine the individual station m_{bLg} determinations to determine a network m_{bLg} and then determine the yield from a composite m_{bLg}-yield curve (derived for known yield events at NTS in this case) or

b. Determine the yield at each station from each station m_{bLg} using a m_{bLg}-yield curve (derived for known yield events at NTS). That curve could be derived only for the individual station or it could be a composite curve as in paragraph *a*.

5. For application in other geographic regions, the "correct" m_{bLg} versus yield curve must be utilized in Step 4.

In this determination of yield, there are several possible sources of error and/or uncertainty. The primary purpose of this study is to evaluate and quantify these uncertainties to determine the ultimate accuracy of

the m_{bLg} methodology for yield determination as well as to evaluate the independence of this methodology. An additional objective of the RAI program is to evaluate other regional phases for possible use as yield determinants. This paper deals only with the evaluation of the m_{bLg} method and quantification of its uncertainty.

Each step of the methodology will be dealt with separately in the following sections.

1. Evaluation of Methodology.

Determination of $Q(f)$. This first step of the process involves the greatest source of uncertainty and/or potential error in the determination of yield. To evaluate this, twelve (12) Nevada Test Site events were chosen as recorded at the WWSSN stations BKS, DUG, and TUC. For each recording, the predominant frequency f_p in the coda was determined as a function of travel time (t). In all, 70 data points were obtained at BKS, 75 at DUG, and 55 at TUC. $Q(f)$ is determined by fitting the f_p versus t data to theoretical curves which depend on the type of frequency dependence assumed, the amount of frequency dependence, and the characteristics of the recording instruments. In this study, two types of frequency dependence were assumed:

1. exponential dependence $Q = Q_0 f^{\zeta}$ and
2. linear dependence $Q = Q_0 + \alpha f$.

Each of these is examined in the subsequent paragraphs.

In Figs. 1 and 2, f_p versus t data for BKS are presented together with the theoretical curves for the exponential dependence $Q = Q_0 f^{\zeta}$. In Fig. 1, values of ζ of .2 and .4 are used while in Fig. 2, ζ values of .6 and .8 are assumed. Note that increasing ζ increases the slope of the curves at lower frequencies and increase the curvature at higher frequencies. The choice of ζ is critical to the determination of Q_0 and, as can be seen in these two figures, the scatter of the f_p versus t data coupled with the similarity of the different curve ensembles makes the choice of curves difficult. The data cut across the higher sloping $\zeta = .6$ and $\zeta = .8$ curves indicating a lower slope then these theoretical curves. For the BKS station, the RAI choice would be $\zeta = .2$ and $Q_0 = 225$. Earlier, Nuttli, on the basis of a smaller data set, had chosen a $Q_0 = 139$ (Nuttli, preprint) following his selection of a ζ of .6 based on other western US data.

In Figs. 3, 4, and 5, the RAI f_p *versus* t data are presented for the stations BKS, DUG, and TUC, respectively. In these figures, we have plotted the curves for a) the best exponential ($Q = Q_0 f^{\zeta}$) fit to the data with the parameters indicated; b) the best linear fit ($Q = Q_0 + \alpha f$); and

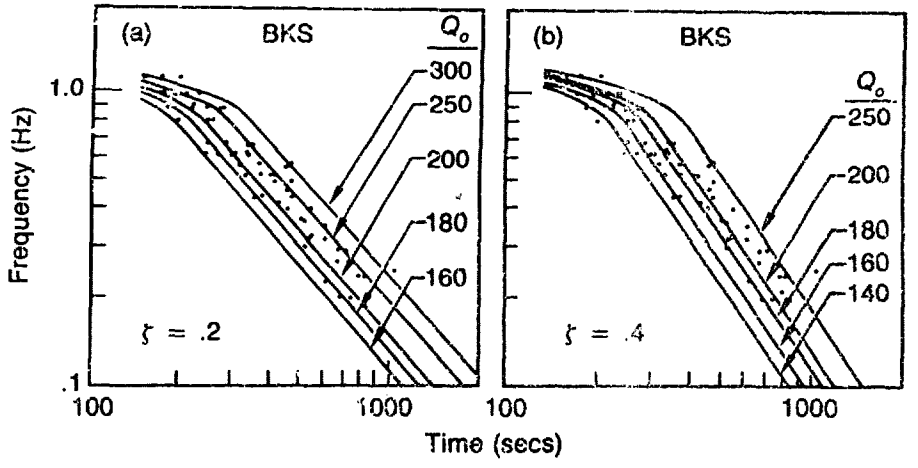

Fig. 1. Predominant frequency (*fp*) *versus* travel time (*t*) data for BKS are shown with the theoretical curves for an exponential dependence of Q on frequency ($Q = Q_o f^{\zeta}$) with (a) ζ = .2 and (b) ζ = .4. The scales are the same.

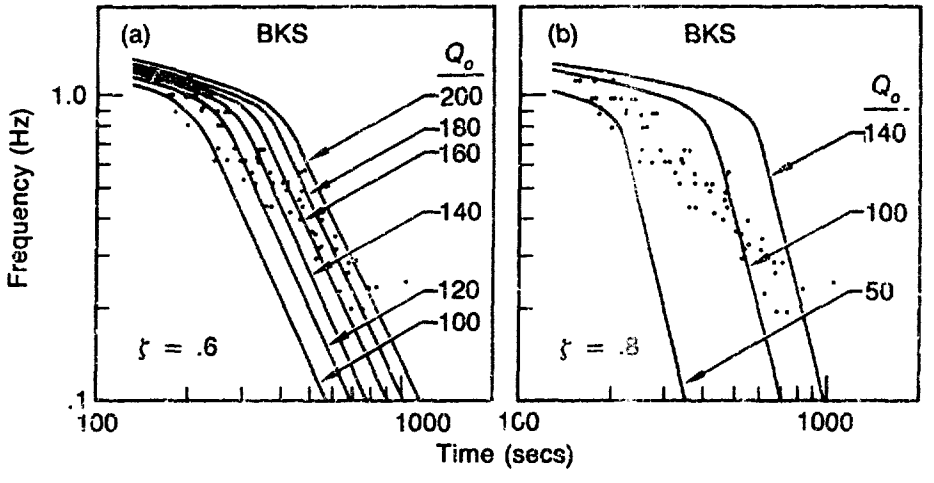

Fig. 2. *fp versus t* data for BKS with (a) ζ = .6 and (b) ζ = .8. Note the apparent lower slope of the data compared to these curves. The scales in both (a) and (b) are the same.

c) the curve chosen by Nuttli to fit his data. Standard deviations for the RAI data from each of the selected models are indicated by the σ values in these figures. The reader should note that the linear model provides a better fit then the exponential model to the RAI data at BKS and TUC but the fit of the linear model is slightly worse than the exponential model at DUG.

The resultant variability of Q_o from alternative fits to the data result in major changes in m_{bLg} and thus differences in the yield values. For

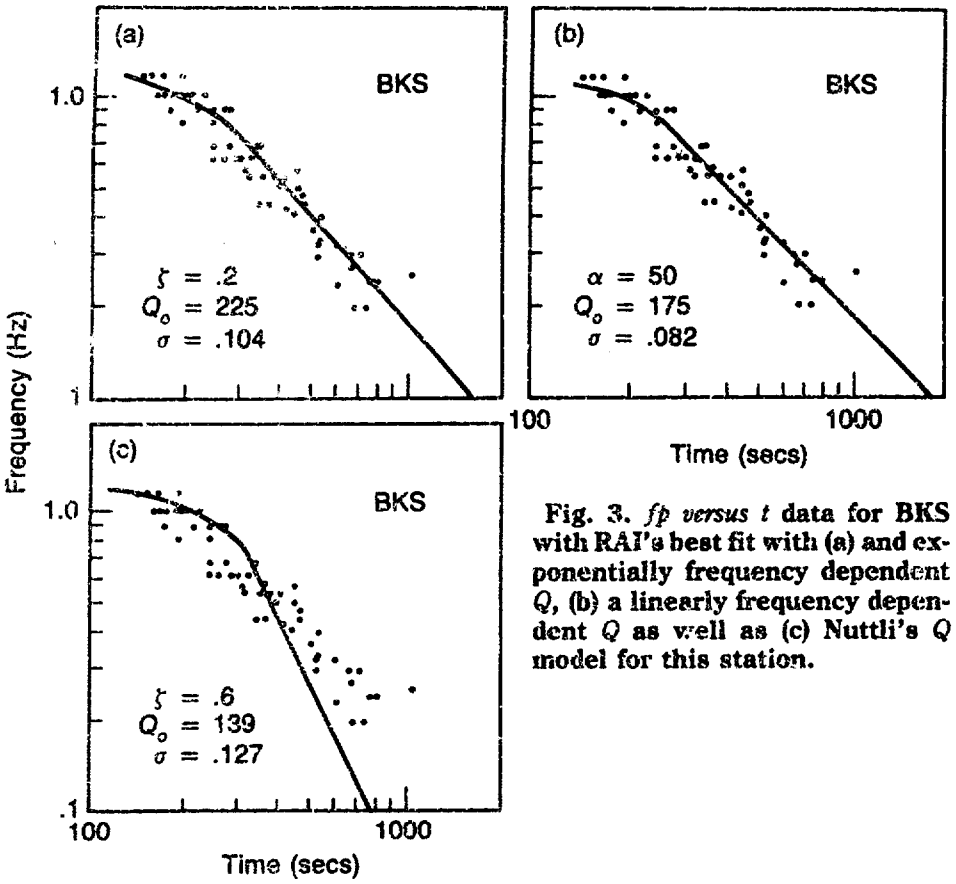

Fig. 3. *fp versus t* **data for BKS with RAI's best fit with (a) and exponentially frequency dependent Q, (b) a linearly frequency dependent Q as well as (c) Nuttli's Q model for this station.**

instance, at DUG, our best fit has $\zeta = .3$, $Q_0 = 230$ compared to Nuttli's $\zeta = .6$, $Q_0 = 155$. For the CHARTREUSE explosion these correspond to $m_{bLg} = 5.24$ and $m_{bLg} = 5.79$, respectively. Converting them m_{bLg}'s to yield on the same m_{bLg} *versus* log-yield curve gives yields of 14 kt and 80 kt. However, a different curve is derived from our data (seen Section 4 below and Fig. 6). When this curve is used, a yield of 72 kt (rather than 14 kt) is derived. These compare well to the announced yield of 70 kt.

2. Amplitude Measurements. Although there are small but real differences in measurements of "sustained" amplitudes by different observers, this study indicates that those differences produce relatively small changes in yield compared to the variations in Q values discussed above. As an average example, using Nuttli's Q model for BKS and our amplitude measurement, we calculate for STARWORT $m_{bLg} = 5.89$ compared to Nuttli's $m_{bLg} = 5.92$ (Nuttli, written communication).

3. Determination of m_{bLg}. This portion of the methodology is a simple numerical calculation and errors are not introduced. The Nuttli

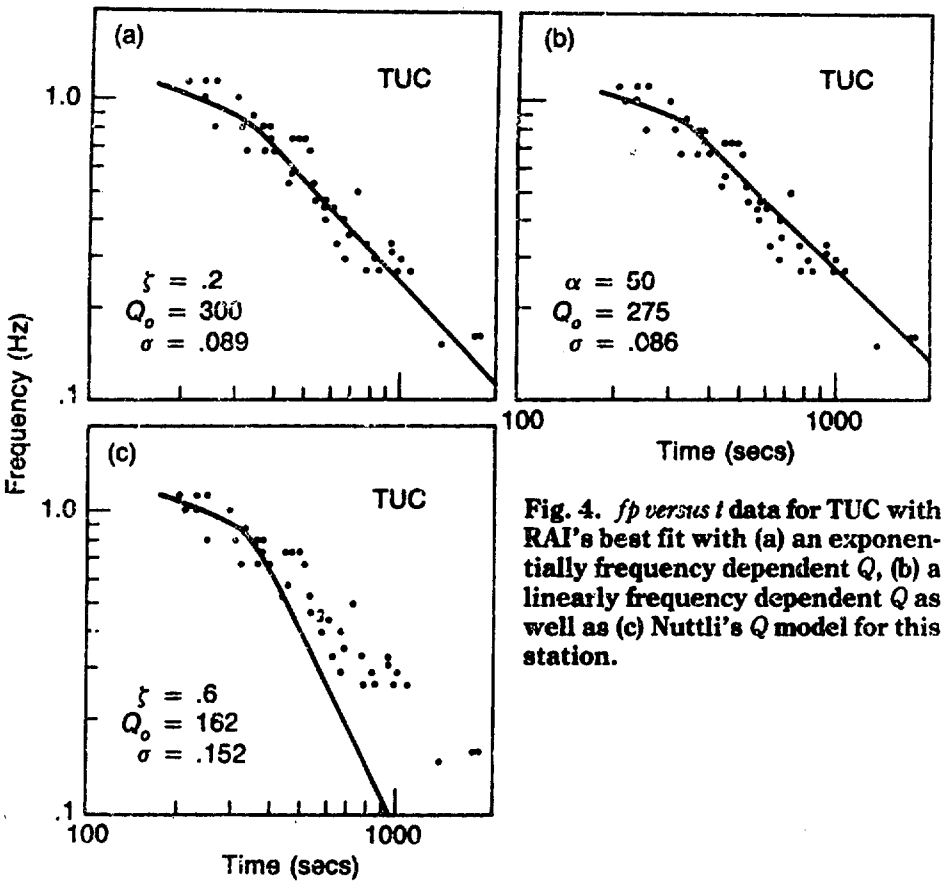

Fig. 4. *fp versus t* **data for TUC with RAI's best fit with (a) an exponentially frequency dependent Q, (b) a linearly frequency dependent Q as well as (c) Nuttli's Q model for this station.**

formulation assumes, however, Airy phase propagation in L_g, a hypothesis that remains to be tested. However, strict application of the methodology in determination of the m_{bLg}-yield curve and in the determination of m_{bLg} for unknown yield events should lead to the correct answer. The RAI m_{bLg} is used in the following section were derived as follows:

a. BKS, TUC, and DUG recordings of 11 NTS events were utilized.

b. The best exponential and linear fits to the f_p *versus* t curves were determined to determine Q_o, ζ, and α.

c. The m_{bLg} values measured for all events at all on-scale stations were submitted to LSMF to obtain event m_{bLg}'s with 95% confidence limits. Nuttli's m_{bLg} values were treated in the same way.

4. m_{bLg}-Yield Curves. There are several aspects to this portion of the problem. First, for events of known yield, the choice of $Q(f)$ in effect determines the m_{bLg} and thus different choices of $Q(f)$ result in

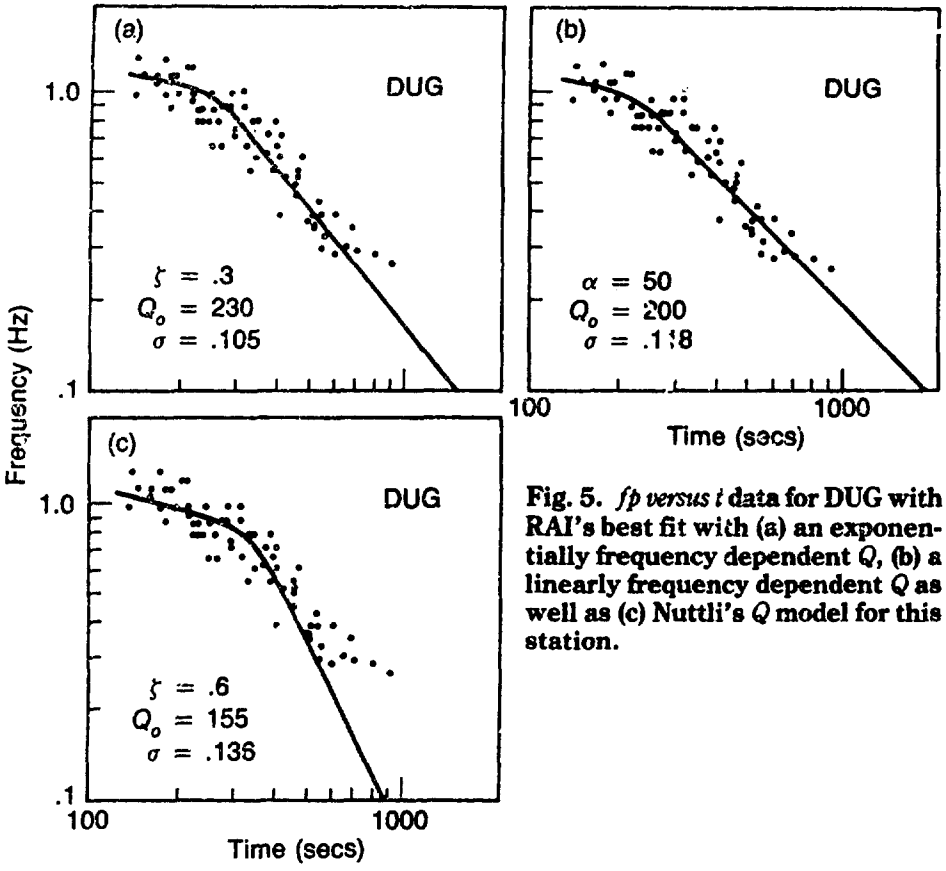

Fig. 5. ***fp versus t*** **data for DUG with RAI's best fit with (a) an exponentially frequency dependent Q, (b) a linearly frequency dependent Q as well as (c) Nuttli's Q model for this station.**

different m_{bLg} curves. In Fig. 6, network m_{bLg} *versus* yield data are plotted for different $Q(f)$'s. In Fig. 6(a), RAI data on m_{bLg} (using the exponential form of frequency dependence of Q) for known yield events at the Nevada Test Site are plotted with the least squares linear fit to the data. Error bars from LSMF are plotted on all the individual data points and the $\pm$ 1 σ curves are plotted as dashed lines. Similarly, in Fig. 6(b) RAI data using linear frequency dependence of Q are plotted, while in Fig. 6(c) Nuttli's data for NTS (with some of his data edited out) are plotted. The use of these three different curves result in different yield values *e.g.* DURYEA (4/14/66).

Model	m_{bLg}	Yield	Curve
RAI Exponential	5.09	43 (29-66)	Fig. 6(a) using RAI m_{bLg}
RAI Linear	5.06	42 (28-62)	Fig. 6(b) using RAI m_{bLg}
Nuttli	5.67	55 (42-72)	Fig. 6(c) using Nutli's m_{bLg}

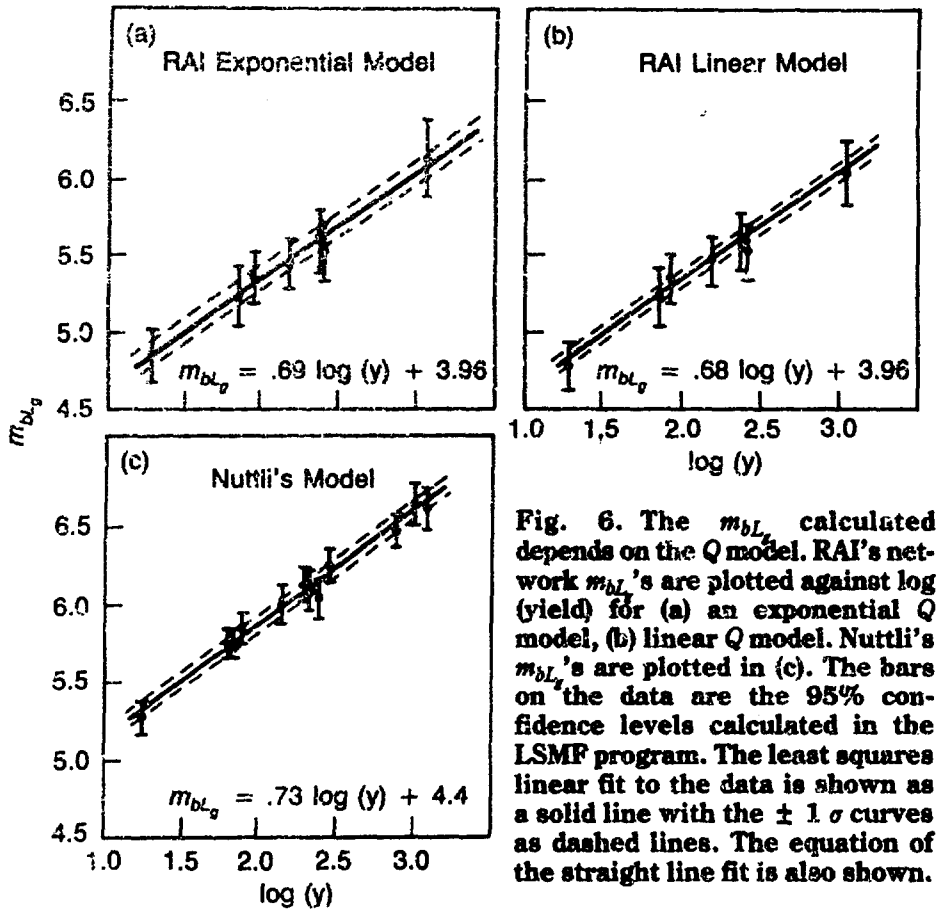

Fig. 6. The m_{bL_g} calculated depends on the Q model. RAI's network m_{bL_g}'s are plotted against log (yield) for (a) an exponential Q model, (b) linear Q model. Nuttli's m_{bL_g}'s are plotted in (c). The bars on the data are the 95% confidence levels calculated in the LSMF program. The least squares linear fit to the data is shown as a solid line with the ± 1 σ curves as dashed lines. The equation of the straight line fit is also shown.

The announced yield for DURYEA is 65 kt.

If the other option is used at this point in the methodology, that is m_{bLg}'s at each station are determined using the RAI models of the frequency dependence of Q and the yield is determined by averaging the station yields, the following results are obtained for DURYEA.

Exponential			Linear		
Station	m_{bL_g}	Yield	Station	m_{bL_g}	Yield
BKS	5.14	51	BKS	5.14	54
TUC	4.86	20	TUC	4.86	21
DUG	5.26	77	DUG	5.19	64
Average Yield (DURYEA):		49 kt			49 kt

The alternative of using station m_{bLg} versus yield curves rather than network m_{bLg} versus yield curves is currently under investigation.

5. Transportability of Other Test Areas. The key question here is, of course, what is the "correct" m_{bLg}-yield curve given the questions regarding the frequency dependence of Q. That question is currently being evaluated in the classified portion of this research.

Conclusions and Recommendations

1. The use of regional phases (such as $L_g(Z)$ discussed here) shows great promise as a quasi-independent measurement of yield.

2. In the $L_g(Z)$ methodology, there are two key issues:

a. Selection of the appropriate form of the frequency dependence of Q and the selection of constants in that form.

b. The use of the appropriate m_{bLg} versus yield curve in different geographic regions. Detailed evaluation of these issues should be carried out.

In addition, other L_g measurements ($L_g(T)$) and other regional seismic phases such as P_g both provide additional measurements of yield and follow-on studies of those additional constraints on yield should be carried out.

References

Herrmann, R.B., 1980, "Q Estimates Using Coda of Local Earthquakes," *B.S.S.A.*, **70**, no. 2, pp. 447-468.

Herrmann, R.B. and A. Kijko, 1983, "Modeling Some Empirical Vertical Component L_g Relations," *B.S.S.A.*, **73**, no. 1, pp. 157-171.

Herrmann, R.B. and A. Kijko, 1983, "Short-Period L_g Magnitudes: Instrument, Attenuation, and Source Effects," *B.S.S.A.*, **73**, no. 6, pp. 1835-1850.

Herrmann, R.B. and C.Y. Wang, 1983, *L_g Wave Excitation and Propagation with Application to Nuclear Yield Determination*, Semi-Annual Report Contract F49620-83-C-0087.

Mitchell, B.J., 1980, "Frequency Dependence of Shear Wave Internal Friction in the Continental Crust of Eastern North America," *Jour. Geophys. Res.*, **85**, no. B10, pp. 5212-5218.

Mitchell, B.J. and O.W. Nuttli, 1982, *Attenuation of Seismic Waves at Regional Distances*, Semi-Annual Report Contract F49620-83-C-0015.

Nuttli, O.W., *Seismic Yield Determination for NTS Events Using Regional L_g Waves.* (preprint 1; also contained in Mitchell and Nuttli, 1982).

Nuttli, O.W., *A Methodology for Obtaining Seismic Yield Estimates of Underground Explosions Using Short Period L_g Waves*, (Preprint 2).

Nuttli, O.W., *Illustration of Use of Coda Q Method to Obtain Anelastic Attenuation Values for Paths for SALMON (Mississippi) and NTS Events.* (Preprint 3; also contained in Mitchell and Nuttli, 1983).

Singh, S. and R.B. Herrmann, 1983, "Regionalization of Crustal Coda Q in the Continental United States," *Jour. Geophys. Res.*, **88**, n. B1, pp. 527-538.

Source Mechanism, Surface Wave Excitation, and m_b-M_s Analysis of the Mammoth Lakes Earthquakes

Keith F. Priestley

Summary

Evaluation of the parameters relating to the m_b-M_s relationships for the Mammoth Lakes earthquakes.

Introduction

The observation that earthquakes generate relatively greater surface wave amplitudes than do underground nuclear explosions of the sample local or teleseismic body-wave magnitude has led to the discrimination technique based on the ratio of body-wave magnitude (m_b) to surface wave magnitude (M_s). On a plot of m_b *vs* M_s, earthquakes and explosions cluster in two groups separated by approximately one unit of magnitude, each group scattering about a line with slope of 1-1.8, depending on the m_b range (Evernden *et al.*, 1971). The success of the m_b-M_s discrimination technique is believed to be the result of one or a combination of the following factors: (1) Source dimension, (2) Source rupture duration, (3) time function of the displacement at various points on the fault for an earthquake, or at the elastic radius for an explosion, and (4) source symmetry, *i.e.*, symmetric dilation for an explosion and shear dislocation for an earthquake. Gilbert (1973) found that the effects of source symmetry alone can account for approximately 0.5 surface wave magnitude units between earthquakes and explosions.

In a number of recent studies (*e.g.* Tucker and Brune, 1977) it has been found that estimates of seismic moment based on long period data were 4-10 times higher than estimates of short-period records for the same earthquakes. This has led to the hypothesis that faulting in shallow earthquakes begins in a relatively small region of high stress drop and nigh rupture velocity, and propagates into regions of lower stress drop and lower rupture velocity. The first stage of faulting controls the short-period radiation, and the second stage of faulting adds to the long-period

radiation while being a weak source of high-frequency waves. This process will also lead to the disparity between m_b and M_S for shallow focus earthquakes.

With adequate, high quality, near-source data, it should be possible to examine the various factors leading to the m_b-M_S discriminant. From near source spectra it should be possible to predict the observed m_b values at teleseismic distances, from the spectral amplitudes near 1 Hz, and the M_s values from the inferred moment. The Mammoth Lakes, California, earthquake sequence provides a unique opportunity for such a study. There are a large number of broad-band digital and strong motion recordings available in the source region for averaging the near-source spectra over the focal sphere. The epicentral region is surrounded by an array of long-period seismographs at regional distances for determining M_s; and is located more than 20° from most of the sensitive short-period stations of the Canadian network, which is important for consistent determination of m_b (Evernden, 1967). In addition, the propagation paths from all of the epicenters to a given regional or teleseismic station are essentially identical, and very similar for waves from NTS explosions to many of those same stations.

The Mammoth Lakes Earthquake Sequence

The Mammoth Lakes earthquake sequence comprises the largest episode of seismic strain release to occur in the western United States in the last decade. The earthquakes are associated with the intersection of the Sierra Nevada frontal fault system and the Long Valley Caldera. The Long Valley Caldera was formed 0.7 million years ago by collapse and subsidence associated with the eruption of the Bishop tuff (Bailey *et al.*, 1976), and volcanic activity has continued on a reduced scale into the Holocene. The dominant fault of the area is the Hilton Creek Fault along which several hundred meters of pure normal fault displacement has occurred since the formation of the Long Valley Caldera (Bailey *et al.*, 1976).

During the present century, the area just south of the Long Valley Caldera has experienced the largest concentration of earthquakes with local magnitude greater than 5 of any region along the entire length of the Sierra Nevada frontal fault system. This may be in response to stress concentration at the north end of the zone of faulting accompanying the 1872 Owens Valley earthquake (Cramer and Toppozada, 1980). The region experienced a lower than normal level of seismicity during the mid-to-late 1970's, primarily during the period October, 1977 to September, 1978 (Van Wormer and Ryall, 1980; Ryall and Ryall, 1980). The earthquake sequence clearly began with an event of local magnitude

(M_l) 5.8, beneath Wheeler Crest 30 km northwest of Bishop, California on October 4, 1978. Following this event, activity gradually spread to the west. The main period of energy release began on May 25, 1980. This was preceded for over a year by M_l 3.5-4.5 earthquake swarms in the region of the magnitude 6 events of May 25, 1980. These swarms generally clustered near the southern boundary of the Long Valley Caldera, and migrated eastward towards the eventual epicenter of the first magnitude 6 event (Cramer and Toppozoda, 1980). The main episode of strain release commenced with a $M_l = 6$ event at 1633 on May 25 and was followed by a second $M_l = 6$ event at 1649. These initial events occurred along an east-west trend near the southern boundary of the Long Valley Caldera. The seismicity then migrated southward from the Caldera boundary. Lide (1984) has shown that in the two months period following the main events, aftershocks and continuing swarms occurred along the trend of the southern caldera boundary, and along several northeast-southwest trends orthogonal to the caldera boundary. Mayo (1937) has found the fracting pattern to have a similar trend. Nearly all of the events lie well west of the projection of the Hilton Creek Fault to depth indicating that this is not the causative fault for the earthquake sequence.

Considerable controversy has arisen regarding the source mechanisms of the larger events. Focal mechanisms derived from local and regional first motion data indicate strike-slip motion with a NE-SW tensional axis and a NW-SE compressional axis (Cramer and Toppazada, 1980; Ryall and Ryall, 1980). This implies right lateral motion on east-west trending faults, or left-lateral motion on north-south trending faults. Moment-tensor inversion of long-period teleseismic body and surface waves recordings of the largest events require a solution different from the first motion data. These mechanisms have been interpreted as left-oblique slip of planes striking NNE and dipping eastward or a non-double-couple mechanism. Given *et al.* (1982) and Wallace (1983) have suggested the discrepancy in the mechanisms arise from structural effects which distort the teleseismically-observed radiation pattern, or from complex rupture during the events. The structural distortion of the outgoing rays may result from the presence of magma chambers as has been proposed in a number of studies (Steeples and Iyer, 1976; Hill, 1976; Ryall and Ryall, 1981b). Reversals of polarity observed on short- and long-period instruments at the same site suggest a complex source time function with the short-period arrivals representing the failure of an asperity and the long-period arrivals due to the overall response of the faulting episode. The repeatability of the observations is difficult to explain with source complexity. Barker and Langston (1983), Julian (1983), Ekstrom and

Dziewonski (1983) and Aki (1984) have explained the discrepancy in local and teleseismic mechanism as indicating a non-double-couple source or a compensated linear vector dipole. Such a source could arise from tensile failure due to fluid injecting at depth along vertical fractures striking northwest—*i.e.* possibly the formation of dikes.

Analysis of Surface Wave Delta

Many of the events with local magnitude (M_l) greater than 3.5, produce surface wave recordings at regional long-period stations. Data were available from stations for the World Wide Network, the long-period stations operated by California Institute of Technology, long-period stations in northern Mexico operated by Scripps Institution of Oceanography, and broad-band stations operated by the University of Nevada and the Lawrence Livermore Laboratory.

The surface wave magnitude (M_s) defined by the formula (Marshall and Basham, 1972)

$$M_s = \log A + B'(\Delta) + P(T)$$

has been determined for a large number of events for which there were two or more recordings. In this formula, A is one-half the peak-to-peak ground amplitude of the maximum amplitude Rayleigh wave with period T at distance Δ. $B'(\Delta)$ corrects for the average effects of attenuation, scattering, geometrical spreading and refraction; $P(T)$ is a correction factor for dispersion and allows measuring the surface wave amplitude at any period. Marshall and Basham (1972) have tabulated $P(T)$ for continental North America for periods ranging from 10 to 40 seconds. In some cases the maximum surface wave amplitude was in the period range 8 to 10 seconds for the Mammoth Lakes observations. Since $P(T)$ is a smoothly varying function, we have extrapolated $P(T)$ to 8 seconds periods. Marshall and Basham have also provided for correcting M_s for source depth by comparing M_s determined for an event at different periods. However, most of the surface wave observations made in this report have consisted of a single pulse, and thus such a comparison could not be made. The exception was for events recorded at station BRK where a more dispersed wave train was normally observed.

Twenty-two of the events were chosen for presentation in this report. The hypocentral parameters for these events appear in Table 1. These events range in local magnitude M_l from 4.2 to 6.2 and range in depth from 1 to 16 km. The surface wave data for these events is summarized in Table 2.

Table 1

Event	Date	Time	Latitude	Longitude	Depth	M_l	m_b	M_s
1	10/04/78	16:42:48.6	37.5	118.7	10	5.8	5.6	5.94
2	05/25/80	17:48:30.0	37.6	118.9	4	4.6	3.9	3.92
3	05/25/80	19:44:51.0	37.5	118.8	13	6.1	5.3	5.53
4	05/25/80	20:35:48.0	37.6	118.9	5	5.7	4.9	5.11
5	05/25/80	20:59:22.6	37.6	118.8	8	5.0	4.4	3.75
6	05/26/80	00:57:02.3	37.6	118.9	1	4.5	4.1	3.51
7	05/26/80	01:19:02.2	37.6	118.9	7	4.6	4.3	3.68
8	05/26/80	05:56:26.3	37.6	118.9	7	4.7	4.0	3.09
9	05/26/80	12:24:25.1	37.6	118.9	7	5.1	4.7	4.17
10	05/26/80	14:37:30.8	37.5	118.9	8	4.5	4.8	2.71
11	05/26/80	16:20:21.6	37.5	118.9	5	4.8	4.6	3.88
12	05/26/80	18:57:55.9	37.5	118.9	8	5.7	4.9	4.37
13	05/27/80	13:27:07.1	37.5	118.9	7	4.3	3.9	2.82
14	05/27/80	14:50:56.6	37.5	118.8	16	6.2	5.5	5.55
15	05/27/80	10:01:07.9	37.6	118.8	6	4.2	4.3	3.49
16	05/28/80	05:16:23.0	37.6	118.9	4	4.9	4.2	3.75
17	05/28/80	05:48:29.5	37.6	118.9	6	4.6	4.0	3.43
18	05/31/80	00:58:17.3	37.5	118.9	9	4.5	4.1	2.75
19	05/31/80	15:16:11.4	37.6	118.8	8	4.9	4.2	3.71
20	06/01/80	06:47:36.0	37.5	118.9	8	4.7	3.7	2.87
21	06/11/80	04:40:58.5	37.5	118.9	8	4.7	4.1	3.09
22	07/05/80	11:58:59.0	37.6	118.8	9	4.3	4.2	3.27

Table 2

Event	BRK	COR	LON	MSO	DUG	COL	JCT	ALQ	PAS	AVG
1			5.41	4.75		4.61	5.46	4.98		5.04
2				3.92						3.92
3				5.46			5.59			5.53
4			5.14	4.92			5.26			5.11
5			3.75							3.75
6	3.57	3.58	3.63	3.44	3.75		3.41		3.21	3.51
7	3.73	3.72	3.74	3.69	3.95		3.46		3.49	3.68
8		3.05	3.18	3.10	3.26		2.94		3.00	3.09
9		4.25	4.28	3.99			4.27		4.05	4.17
10				2.72					2.70	2.71
11	4.00	3.67		3.74	4.18		4.19	4.04	3.37	3.88
12	4.87		4.42					4.45	4.04	4.37
13				2.63	3.01			2.94	2.68	2.82
14							5.55			5.55
15			3.56	3.42	3.95		3.11	3.45	3.51	3.50
16		3.59	3.55	3.98	4.20		3.62	3.74	3.58	3.75
17		3.29	3.12	3.73	3.99		3.24	3.39	3.27	3.43
18			2.92	2.63					2.70	2.75
19		3.67	3.87	3.62	3.98		3.71	3.63	3.49	3.71
20			3.00		2.83		2.94		2.70	2.87
21		2.96	2.76	3.31	2.91		3.08	3.27	3.37	3.09
22	3.17	3.45	3.26		3.26		2.94	2.94		3.17

Figure 1 is a comparison of the data from Fig. 6 of Marshall and Basham (1972), the m_b-M_s data for the San Fernando aftershocks from Tucker and Brune (1977) and the m_b-M_s data for the Mammoth Lakes earthquakes from Tables 1 and 2. All of the explosion and earthquakes data reported in Fig. 6 of Marshall and Basham (1972) are from North America. In their study they have used Canadian network data for determining both m_b and M_s. In this study and the study of Tucker and Brune (1977), Canadian network data were used to determine m_b, but data from WWSSN long-period stations in the western United States were used to determine M_s. This could produce systematic differences between the M_s determinations of Marshall and Basham and the M_s determinations for the Mammoth Lakes and San Fernando data. This does not seem to have a strong effect since the paths overlap to a large extent, and the data sets in Fig. 1 overlap. All of the 22 Mammoth Lakes events fall within the earthquakes population and discriminate from explosions, although two events (14 and 22 of Table 1) are well offset from the earthquake mean towards the explosion population.

For comparison with the near-source spectral moments to be discussed below, surface wave moments were determined for all events listed

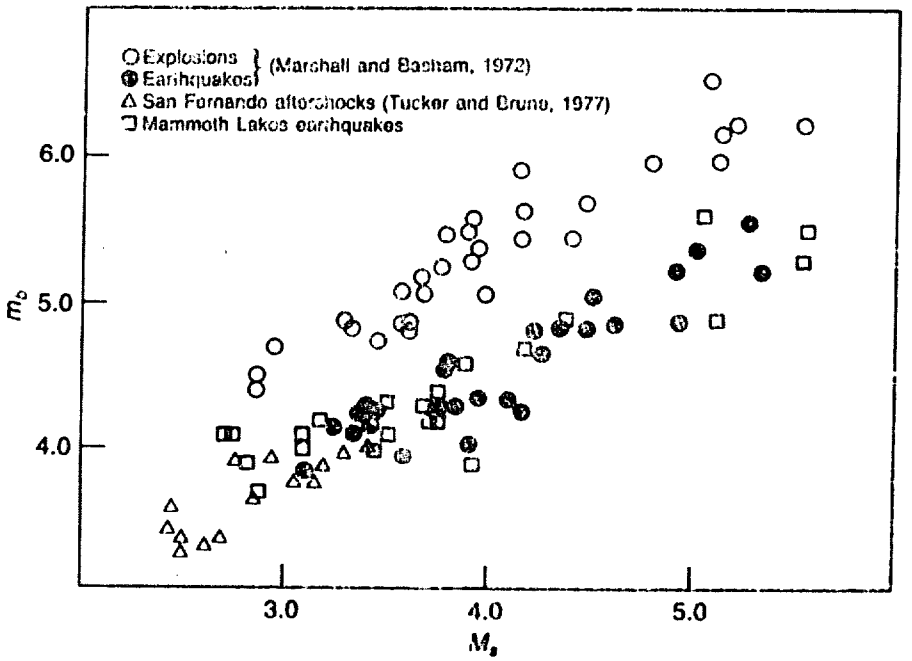

Fig. 1. Body-wave magnitude (m_b) measured on short-period instruments of the Canadian network *vs.* surface-wave magnitude (M_s) measured on WWSSN stations in the western United States and determined with Marshall and Basham (1972) formula.

in Table 1. The surface wave-moment relationship was originally established by Wyss and Brune (1968) for events less than magnitude 6.

For these events, Wyss and Brune found the 13 earthquakes studied defined a moment-versus-magnitude relation

$$\log M_0 = 1.7M_l + 15.1 \qquad 3<M_l<6$$

We have determined a moment-versus-magnitude relationship for the Mammoth Lakes earthquakes in the following way. The surface wave moment is linearly related to the surface wave amplitude and thus to the surface wave magnitude. Surface wave synthetics were generated by the method of Masters (written communication) for an earthquake of 10^{21} dyne-cm, at each of the regional seismographs. For the stations within and along the eastern boundary of the Basin and Range, we have used the Great Basin model (Priestley and Brune, 1978; Priestley *et al.*, 1980), and the crust and upper mantle Q structure of Patton and Taylor (1982). Focal mechanisms and hypocentral coordinates used in computing the synthetics were supplied by Vetter (written communication, 1984) and Lide (written communication, 1984) respectively. When focal mechanisms for specific events were not available, the focal mechanism of an event with a similar hypocenter was used. From the synthetic amplitudes, the M_s magnitude was determined in the same method as for the observed data. The moment of the events could then be determined from the observed surface wave amplitude by scaling to the surface wave amplitude of the synthetic seismograms. The resulting relationship between surface wave magnitude M_s and moment M_0 is given by the equation

$$\log M_0 = M_s + 19.4$$

Figure 2 shows the relationship between the moments determined in this study from the surface wave magnitude using the above relationship, and the moments determined from the local magnitude using Eq. 10 of Archuleta *et al.* (1982).

Analysis of Local Data

We have collected a large number of strong-motion and broad-band digital recordings from within the source region of the Mammoth Lakes earthquake sequence. Archuleta *et al.* (1982) have published spectral parameters from digital velocity and acceleration recordings for 67 events and have recorded a large number of additional events. Peppin (written communication) has determined spectral parameters from broad-band digital records for approximately 350 events both prior to and following

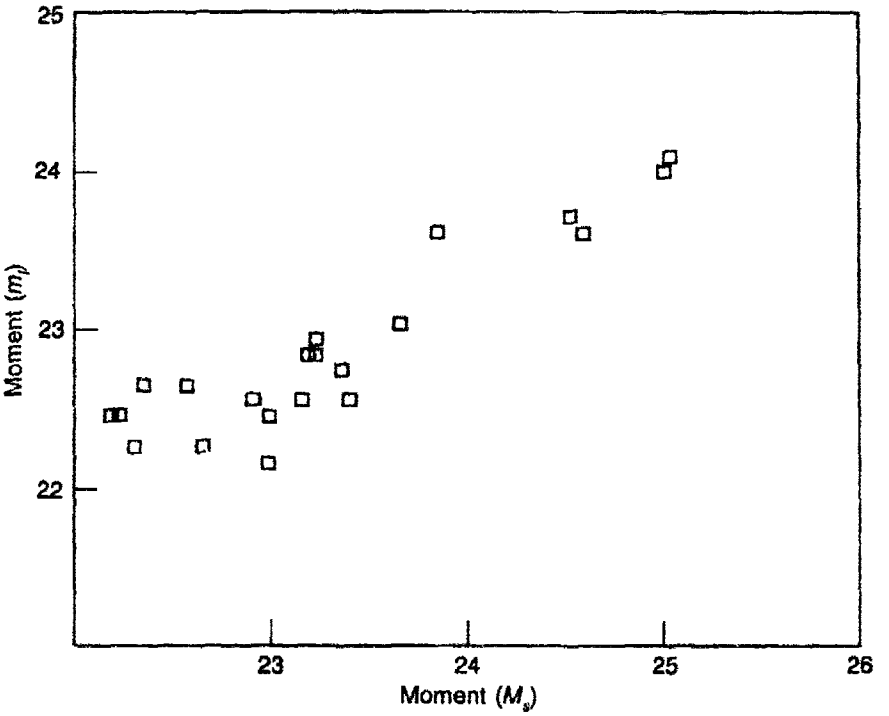

Fig. 2. Comparison of Moment determined from local magnitude using the M_o-M_l relationship of Archuleta *et al* (1982), and the moment determined from the surface wave magnitude using the relationship determined in this study.

the main events of the Mammoth Lakes sequence in May of 1980. Anderson (personal communications) has analog strong-motion recordings from eight stations in the vicinity of Mammoth-Lakes and the California Division of Mines and Geology and has analog strong-motion recordings from an additional four stations. In total there are 29 strong-motion and digital seismographs. In the epicentral region of the Mammoth Lakes sequence with on scale recording for a range of local magnitude M_l from 6.2 to below 1.

We have selected a number of the events for which we have m_b and M_s measurements, and computed the spectral parameters from the local data. Three of those events will be discussed in this report. Displacement amplitude spectra were computed by transforming the seismograms directly, and dividing the acceleration spectra by ω^2 and the velocity spectra by ω, where ω is the angular frequency.

In order to compare the parameters for the events, it is important to consider the frequency associated with each measurement . Values of the parameters and the frequencies at which the measurements were

made have been converted into spectral values and are plotted in Fig. 3, together with values from the actual measured spectra, to illustrate the relationship of the measured parameters to the spectra. All observations were converted into spectral values corresponding to a distance of 10 km and an average azimuth in a homogeneous full-space characterized by a density of 2.7 g/cc and a shear wave velocity of 3.7 km/s.

Figure 3(a) shows the displacement spectra for the event occurring at 1516 on May 31, 1980 (Event number 19 in Table 1), normalized to 10 kilometers. For this event, the accelerometer spectrum (converted to displacement) is the log average of the spectra observed at seven sites (14 records), and the displacement spectrum (Peppin) is the log average of spectra observed at two sites (4 records). As pointed out by Archuleta *et al.* (1982), in averaging the spectra it is important to compute the log-average of the spectra and not the simple arithmetic average since the errors associated with Ω_0 and M_0 are lognormally distributed. These spectra are compared with the spectrum inferred from the results reported by Archuleta *et al.* (1982), and with the moment determined from the surface wave measurements. In plotting the spectrum from Archuleta *et al.* we have plotted the Ω_0 and f_c (with error bounds) reported in their Table 4, and assumed a ω^{-2}

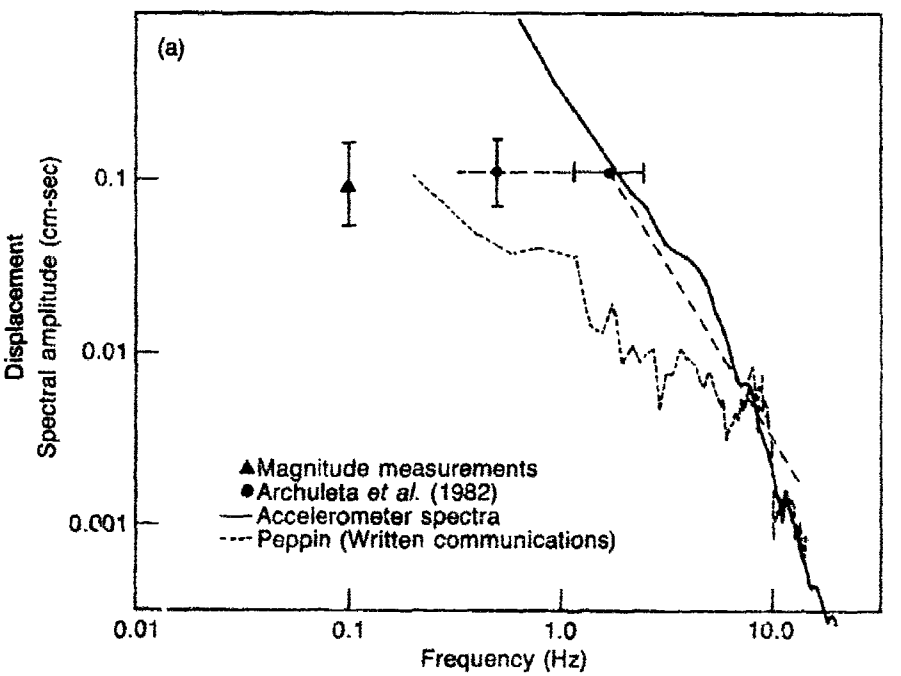

Fig. 3a. Inferred equivalent full-space spectral values for the event of 1516, May 31, 1980 normalized to 10 km.

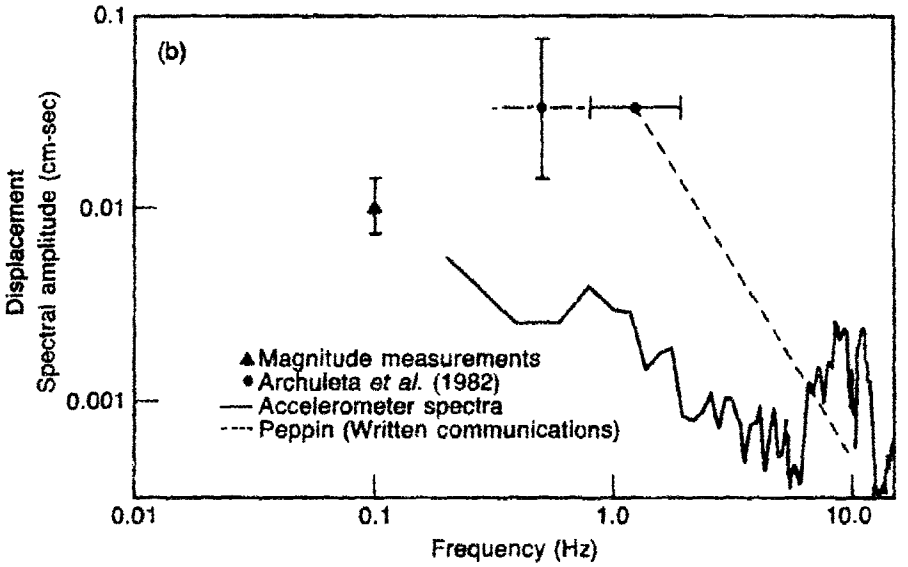

Fig. 3b. Inferred equivalent full-space spectral values for the event of 0056, May 31, 1980 normalized to 10 km.

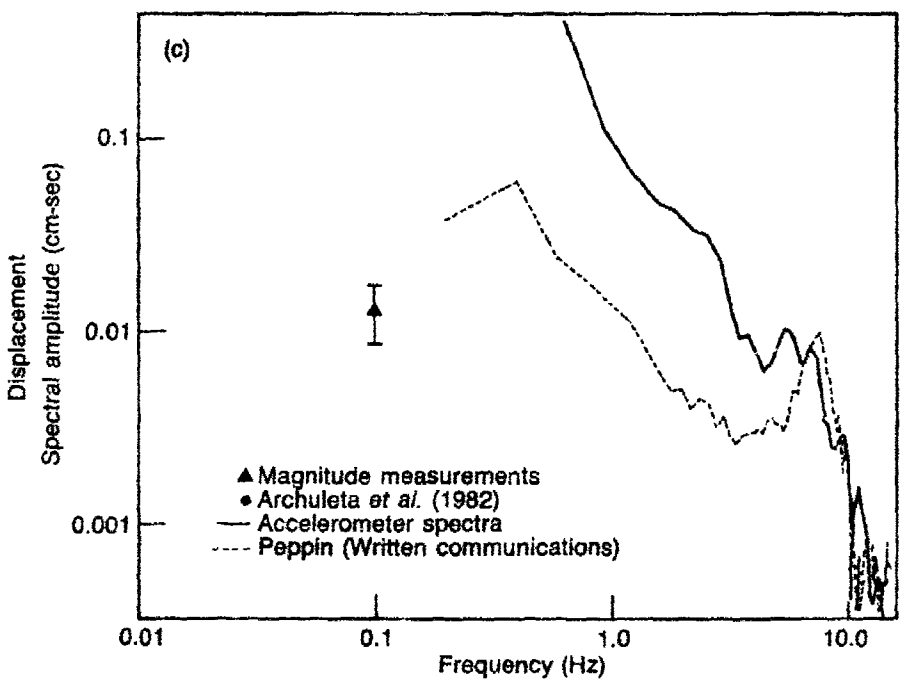

Fig. 3c. Inferred equivalent full-space spectral values for the event of 0647, June 1, 1980 normalized to 10 km.

slope for the high frequency falloff. The long period spectral level (Ω_0) and corner frequency (f_c) inferred from the combination of the surface wave and accelerometer data are in excellent agreement with the spectrum inferred from the results of Archuleta *et al.* However, the displacement spectrum of Peppin indicates a much higher corner frequency (9 Hz *vs* 1.7 Hz) and a much lower long-period spectral level (0.008 cm-sec *vs* 1.11×10^{-1} cm-sec.)

We have gone to considerable length to check the source of this discrepancy. The displacement spectra have been recomputed a number of times by both Peppin and Priestley, using different routines, different sample lengths, and different tapers, all of which yield comparable results. Peppin has carefully calibrated the instrument by fitting synthetic calibration pulses to those recorded on the instrument during the field experiment, and by shake table tests. We have compared coherent signals at the McGee Creek Station and the McGee Creek accelerometer (approximately 1 km separation and both essentially on bedrock) and find the amplitude of the two signals to be closely matched. Surface waves from the nuclear explosion which occurred on June 12, 1980 were recorded at McGee and have a spectral amplitude within a factor of two of the spectral amplitude observed on the WWSSN station at Dugway, Utah. These tests have led us to the conclusion that the differences are not the result of erroneous calibration of the University of Nevada digital event recorders, but arise through the interpretation of the data.

We have yet to determine the source of the discrepancy. The discrepancy may have arisen from the presence of two corner frequencies in the data, and a misidentification of the higher corner frequency in the data of Archuleta *et al.* Tucker and Brune (1977) found that all of the small (M_l 1-3.5) and about half of the larger (M 3.5-4) events had a single corner frequency below which they are approximately constant and above which they are proportional to ω^{-2} or ω^{-3}. The remaining spectra of the large events have two corner frequencies, one between 0.1 and 1 Hz, below which they were constant, and another between 3 and 10 Hz, above which they are proportional to about ω^{-2} or ω^{-3}. For these events, the spectral amplitude at the low frequency corner was two to eight times larger than at the higher frequency corner. All of the Mammoth Lakes events we have examined to date are larger than $M_l = 4$. The spectra of Peppin, and the Ω_0 values determined from the regional surface wave observations suggest a similar character for the spectra of the Mammoth Lakes earthquakes. We defer further comment on this subject until we have completed the analysis of all our data, and have incorporated the data being supplied by Archuleta in our analyses.

Figures 3(b) and 3(c) show the spectral parameters for the events

occurring at 0058 on May 31, 1980, and at 0647 on June 1, 1980, respectively. Both events are of similar body wave magnitude, however, the event of 0058 has anomalously small surface wave and discriminates poorly from nuclear explosions (see Fig. 1) while the event of 0647 is well separated from the explosion population on the basis of m_b-M_s. Unfortunately, we have no acceleration data for the event at 0058, and do not yet have Archuleta's data for the event of 0058. From the spectra of the 0647 event inferred from the results of Archuleta *et al.* (1982), the spectral amplitude near one second where m_b is determined is approximately five times higher than the spectral amplitude at 0.1 Hz where we have determined M_s. However, as for the case of the event at 1516, Peppin's spectrum is approximateley a factor of 10 lower than the spectrum of Archuleta *et al.* near 1 Hz. In contrast, the spectral amplitude near 1 Hz for the event at 0647 is comparable to the spectral amplitude at 0.1 Hz.

References

Aki, K., "Evidence For Magma Intrusion During the Mammoth Lakes Earthquakes of May, 1980 and Implications of the Absence of Volcanic (Harmonic) Tremor," submitted to *Jour. Geophys. Res.*, 1984.

Archuleta, Ralph J., Edward Cranswick, Charles Mueller, and Paul Spudich, "Source Parameters of the 1980 Mammoth Lakes, California Earthquake Sequence," *Jour. Geophys. Res.*, **87**, 4595-4607, 1982.

Bailey, R.A., G.B. Dalrymple, and M.A. Lamphere, "Volcanism, Structure, and Geochronology of Long Valley Caldera, Mono County, California," *J. Geophys. Res.*, **81**, 725-744, 1976.

Barker, J.S. and C.A. Langston, "A Teleseismic Body Wave Analysis of the May, 1980 Mammoth Lakes, California Earthquakes," *Bull. Seism. Soc. Am.*, **73**, 1983, in press.

Cramer, C.H., and T.R. Toppozada, "A Seismological Study of the May, 1980 and Earlier Earthquake Activity Near Mammoth Lakes, California," *Calif. Div. Mines Geol. Spec. Rep.*, **150**, 91-130, 1980.

Ekstrom, G., and A.M. Dziewonski, "Moment Tensor Solutions of Mammoth Lakes Earthquakes, *EOS, Trans. Am., Geophys. Un.*, **64** 262, 1983 [abstract]

Evernden, J.F., "Magnitude Determination at Regional and Near-Regional Distances in the United States," *Bull. Seism. Soc. Am.*, **57**, 581-639, 1971.

Evernden, J.F., "Variation of Rayleigh-Wave Amplitude with Distance," *Bull. Seism. Soc. Am.*, **61** 231-140, 1971.

Evernden, J.F. W.J. Best, P. W. Pomeroy, T.V. McEvilly, J.M. Savion and L.R. Sykes, "Discrimination Between Small-Magnitude Earthquakes and Explosions," *J. Geophys. Res.*, **76**, 8042-8055, 1971.

Gilbert, F., "The Relative Efficiency of Earthquakes and Explosions in Exciting Surface Waves and Body Waves," *Geophys. J.R. Astr. Soc.* **33**, 487-488, 1973. 1976.

Julian, B.R., "Evidence For Dyke Intrusion Earthquakes Mechanisms Near Long Valley Caldera, California," *Nature*, **303**, 323-325, 1983.

Lide, C.S., *Precise Relocation of Aftershocks of the May 1980 Mammoth Lakes Earthquakes*, Univ. Nev. MS Thesis, 1984.

Marshall, P.D. and P.W. Basham, "Discrimination Between Earthquakes and Underground Explosions Employing and Improved M_s Scale," *Geophys. J.R. Astr. Soc.* **28**, 431-458, 1972.

Patton, Howard J. and Steven R. Taylor, *Q-Structure of the Basin and Range from Surface Waves*, Lawrence Livermore Laboratory, Livermore, California, UCRL-87381, 1982.

Ryall, A. and F. Ryall, "Attenuation of *P* and *S* Waves in a Magma Chamber in Long Valley Caldera, California," *Geophys. Res. Letters*, **8**, 557-560, 1981a.

Ryall,A.and F. Ryall, "Spatial-Temporal Variations in Seismicity Proceding the May, 1980, Mammoth Lakes, California, Earthquakes, Quakes," *Bull, Seism. Soc. Am.*, **71**, 27-39, 1981b.

Steeples, D.W. and H.M. Iyer, "Low-Velocity Zone Under Long Valley as Determined From Teleseismic Events," *Jour. Geophys. Res.*, **81**, 849-860, 1976.

Tucker, B.E. and J.N. Brune (1977). "Source Mechanisms and Surface-Wave Excitation for Aftershocks of the San Fernando Earthquake, Ven," *J. Geophys. J.R. Astr. Soc.* **49**, 371-426.

Wallace, T.C., *Long Period Regional Body Waves*, Calif. Inst. Technology, PhD Dissertation, 180 pp. 1983.

Wyss, M. and J.N. Brune, "Seismic Moment, Stress and Source Dimensions for Earthquakes in the California-Nevada Region," *J. Geophys. Res.*, **73** 4681-4694, 1968.

Analysis of Digital Data from Eastern U.S. and Central Pacific

George H. Sutton and Jerry A. Carter

Summary

The capabilities of CSA, WHA, and other digital data for detection, discrimination, and yield determination of regional and teleseismic events are being found.

The objectives of this research are to determine the utility of short-period (less than about 3 sec) oceanic and continental guided waves and body waves in resolving depth and of short-period spectra for discrimination and yield determination. The research primarily has involved analysis of digital data from the Wake Island ocean bottom hydrophone array (WHA) and from the Catskill Seismic Array (CSA). Presently, we also are using data archived at CSS from RSTN stations and other stations of the GDSN. In this report, we shall summarize some results using WHA and CSA data and their comparison with synthetic data.

The WHA broadband digital recording system is producing unique seismic data continuously from an oceanic environment. It happens to be at a favorable distance for the reception of teleseismic *P* waves from known nuclear explosion test sites. In addition, it is a very quiet location for frequencies above about 2.5 Hz (McCreery *et al.*, 1983). In the McCreery *et al.* paper, we presented and compared spectra of nuclear explosions, shallow earthquakes and background noise as recorded at WHA. Significant differences were found between the spectra of *P* phases from explosions and shallow focus earthquakes of similar magnitude at 61-71° distance.

Figure 1 illustrates spectral ratios for explosions at NTS, Tuamotus, and Eastern Kazakh recorded at WHA. The events are of similar magnitude and, as mentioned earlier, similar distance (Table I). Also shown in Fig. 1 is a seismogram and its spectrogram from the Eastern Kazakh event. Note that the signal is well above background at 10 Hz, the limit of the figure. The record shown includes the direct *P* and the first water surface reflection of *P*, *PsP1*. Although the amplitude of the first cycle and a half is greater than three times the following coda, the

Table I. Explosion source data.

Location	Date	m_b	Distance to WHA
Eastern Kazakh	8/4/79	6.1	73°
Tuamotu	7/25/79	6.0	68°
NTS	9/6/79	5.8	68°

signal remains well above background to beyond *PsP2* and a time interval of 20 sec, including *P* through *PsP2*, was used to produce the spectral ratios.

The spectral ratios EK-TU and EK-NTS (dB) increase fairly regularly from 0.6 to 2.8 Hz; the EK-NTS ratio being the greater with more than 20 dB increase. Above 3.4 Hz the ratios both generally decrease with frequency until cut off by noise at 4.0 and 5.6 Hz for NTS and TU, respectively.

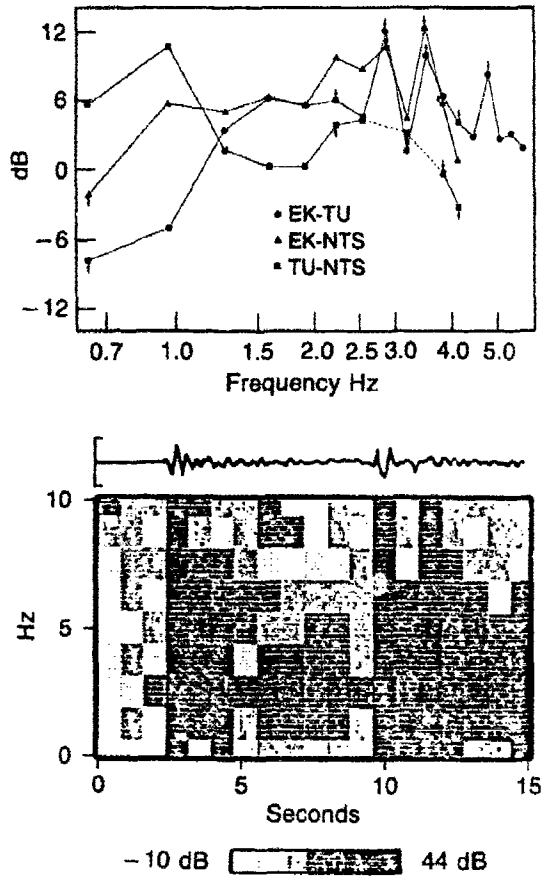

Fig. 1. Upper: Spectral ratios (dB differences) of *P* arrivals among Eastern Kazakh (EK), Tuamotu (TU), and NTS explosions (listed in Table I) recorded at WHA. Spectra are for 20 sec of data including *P* through *PsP2*. Points are from averages of 8 spectral estimates. Arrows indicate minimum or maximum values where one of the arrivals is less than 3 dB above noise. Lower: Spectrogram of *P* and P_sP_l from the Eastern Kazakh event uncorrected for instrument response (designed to flatten background spectrum) 6 dB contour interval. Note that signal maxima are well above background at 10 Hz with peak recorded energy between 2 and 3 Hz. Arrivals and coda are above background in the interval shown.

Previously reported results using explosion *P*-wave spectra to obtain path-averaged t^* as a function of frequency for paths from NTS and three Russian sites to WHA and CSA are given in Table II.

Coherent signals across the WHA bottom array (40 km across) enable reliable determination of *P*-wave phase velocities for earthquakes and nuclear explosions. This is demonstrated in Figs. 2 and 3 where seismograms and slowness (reciprocal velocity) stacks for the Eastern Kazakh explosion and a deep Philippine Islands earthquake, $m_b = 5.1$ are shown. The slowness stacks are produced by delay-sum of the array elements at each value of slowness. (Traces are at equal intervals of slowness). The phase velocities are clearly resolved and agree with expected values for the given epicentral distances. Figure 3 also demonstrates the high correlation between *P* and *PsP1*.

Spectral characteristics of high-frequency oceanic guided waves P_n and S_n are discussed in Walker *et al.*, 1983. Most of this work has been presented at earlier AFOSR/DARPA briefings. Efforts continue on the problems of determining $Q(f)$ of the oceanic lithosphere using these waves.

Most of the regional earthquakes from the eastern United States recorded on the Catskill Seismic Array (CSA) have been analyzed to some extent including frequency and polarization filtering, beam forming, and slowness stacking and the generation of various spectra.

Array processing and polarization filtering improve signal to noise ratio, sharpen signal onsets, and help in arrival identification. Suppression (or identification) of laterally refracted and scattered arrivals (or arrivals from different events) facilitates the comparison of data with synthetic seismograms as most practically useful programs for synthetics assume lateral homogeneity.

Table II. $t^*(f)$ for explosion *P* waves to CSA and WHA ($t^* = t/Q$).

Path	Distance	t (sec)	m_b	t^* 1 Hz	t^* 5 Hz	t^* 10 Hz
NZ-CSA	60°	611	5.8	.49	.33	.24
NZ-WHA	77°	716	5.8	.65	.42	.29
EK-CSA	85°	759	6.1	.69	.45	.31
WS-WHA	77°	716	4.5	.72 ±	.48 ±	.29 ±
EK-WHA	73°	693	6.1	.82	.48	.32
NTS-WHA	68°	663	5.8	1.02	.53	.33
NTS-CSA	33°	399	5.6	1.60	.67	.40 ±

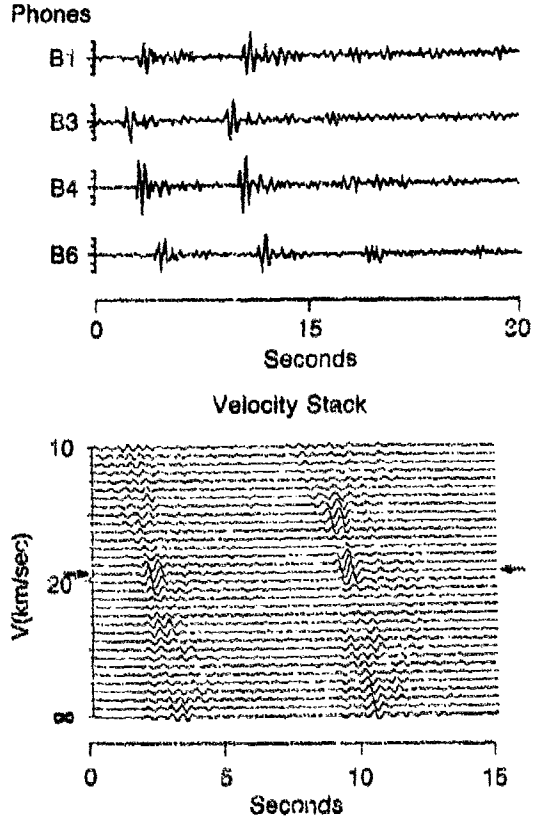

Fig. 2. East Kazakh explosion, m_b = 5.7, recorded at WHA, Δ = 73.0°, θ = 317.7°. Seismograms and velocity stack from Phones B1, B3, B4, and B6, filtered 1-5 Hz bandpass. Arrows indicate arrival phase velocity. Second and third arrivals are ocean surface reflection and its multiple. Note high coherence of *P* and surface reflection across 40 km array.

Analysis of the *P* wave from a Long Island Sound earthquake recorded at CSA (Δ = 1.4°, m_b = 3.5) is shown in Fig. 4. The wave type, direction of approach, apparent angle of incidence, and phase slowness are obtained using three different procedures. Methods A and B use three-component data at a single station and Method C uses a single component of motion at three stations. The angle determinations in the instantaneous polarization method, A, are unstable when the particle motion passes through zero. This instability is avoided in the adaptive method, B, which uses the angles giving zero cross-covariance at zero lag, in a moving time window, between orthogonal horizontal components and between vertical and (adaptive) radial components as estimates of azimuth and angle of incidence, respectively. Beam forming, C, uses the lags of the maxima of the three cross-correlations among the three elements of CSA to obtain azimuth, slowness, and an error term. (Only two lags are needed for slowness and θ; the three lags should sum to zero).

The "whole" seismogram synthesis program of Harvey, 1981, has been used (on CSS computers) for generation of synthetic seismograms.

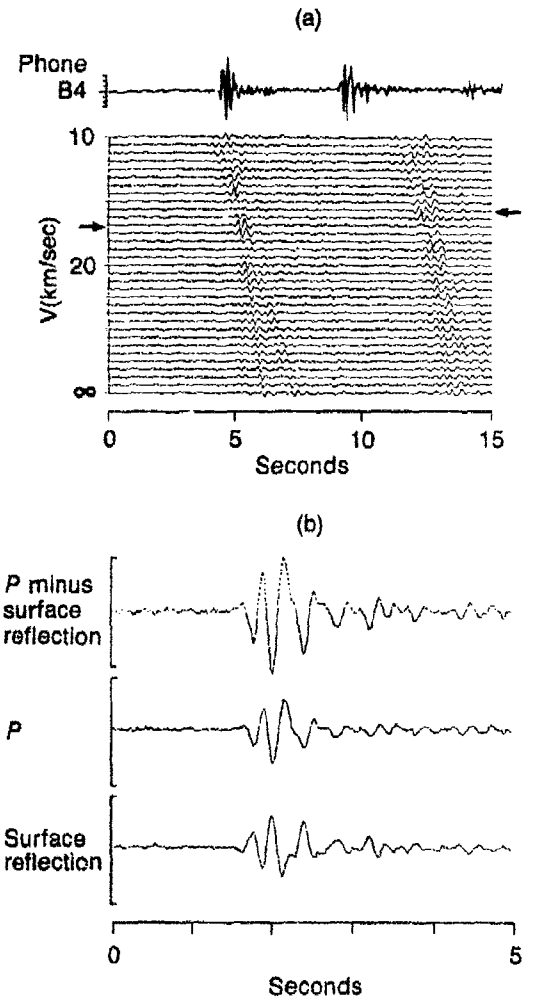

Fig. 3. Mindanao, PI earthquake, m_b = 5.1, H = 601 km recorded at WHA, Δ = 43.8°, θ = 257.1°. (a) Seismogram from phone B4 and velocity stack of phones B1, B3, B4, and B6. Filtered 1-6 Hz bandpass. Arrows indicate arrival phase velocities. Second and third arrivals are ocean surface reflection and its multiple. (b) Delayed difference of P and first surface reflection, unfiltered.

The two velocity/attenuation models in Fig. 5 have been used at RAI for eastern United States source and propagation studies. They produce quite difference synthetic seismograms and the Pulli model appears to be a better fit to the observational data. Both models exhibit strong depth dependence, both in specific arrivals, such as surface reflected "depth" phases, and in the general character of the "whole" seismogram. This latter point is strongly exhibited in the difference in seismograms and spectrums between 0 and 5 km depth for explosion sources (Fig. 6). For small events, the P waves at regional and teleseismic distances recorded with high quality digital instruments do not have adequate signal to noise ratios for detailed analysis of the compressional arrivals and more reliance

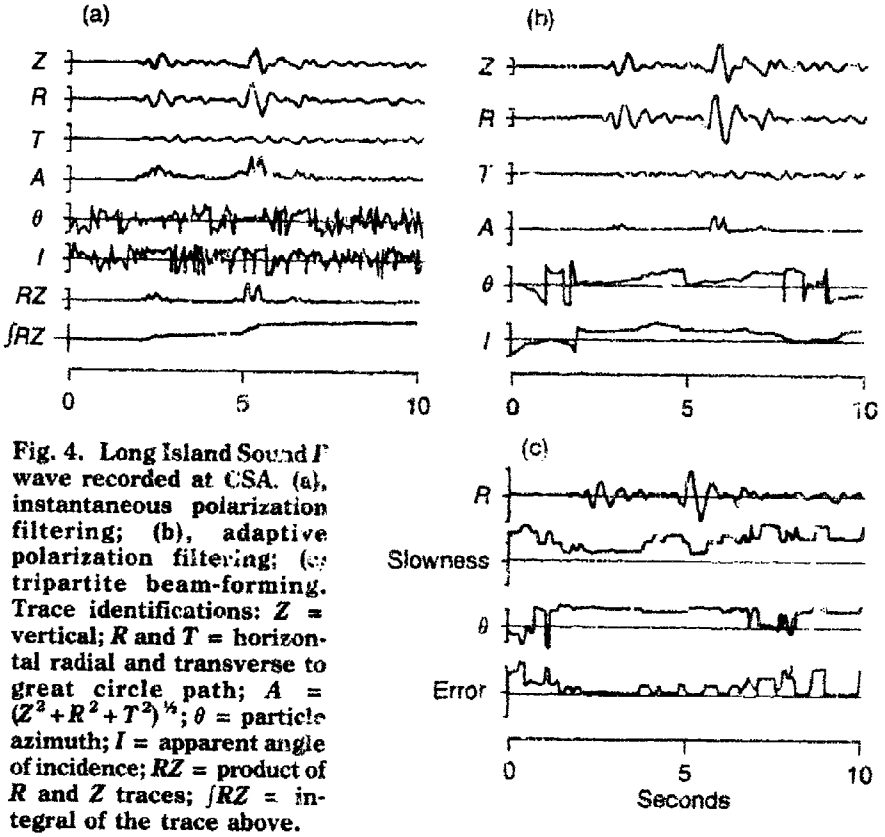

Fig. 4. Long Island Sound *P* wave recorded at CSA. (a), instantaneous polarization filtering; (b), adaptive polarization filtering; (c) tripartite beam-forming. Trace identifications: *Z* = vertical; *R* and *T* = horizontal radial and transverse to great circle path; *A* = $(Z^2+R^2+T^2)^{1/2}$; θ = particle azimuth; *I* = apparent angle of incidence; *RZ* = product of *R* and *Z* traces; *∫RZ* = integral of the trace above.

Eastern U.S. Crustal Models

Bache

Depth	V_p	Q_p	V_s	Q_s
	6.1	250	3.3	125
-10-	6.6	250	3.6	125
-20-	6.6	2000	3.6	1000
-30-	8.1	2000	4.5	1000
-40-				

Pulli

Depth	V_p	Q_p	V_s	Q_s
	6.0	1000	3.5	500
-10-	6.4	3000	3.9	1000
-20-	7.0	5000	4.0	2500
-30-	8.2	5000	4.7	2500
-40-				

Fig. 5. Velocity/attenuation models used for generation of synthetic seismograms: Bache, *et al*., 1980; Cuttain *et al*., 1983 (Pulli).

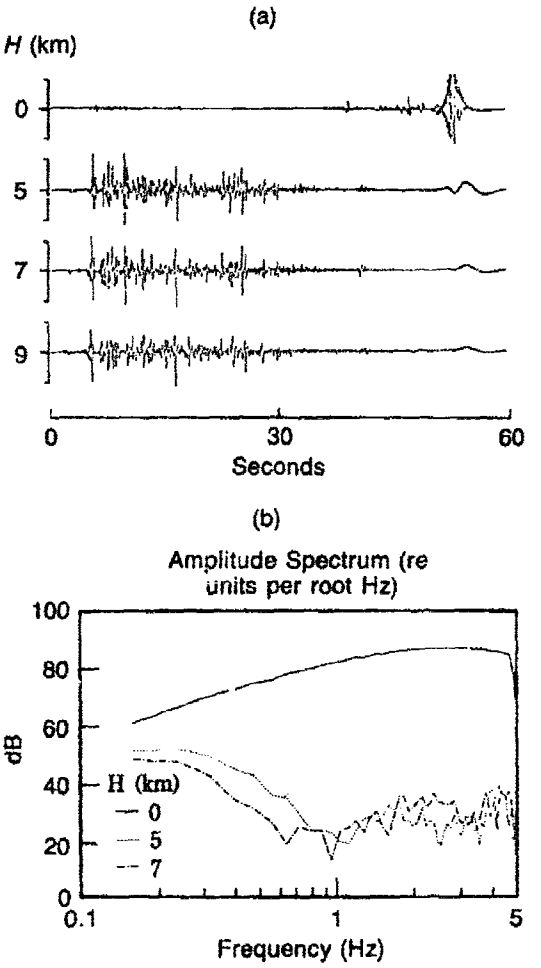

Fig. 6. Synthetic seismograms and spectra for explosion source at different depths, Pulli model, Δ = 300 km, 0-5 Hz bandpass. (a) Seismograms (note that late arrival for $H = 0$ is clipped); (b) Spectra of S/L_g.

must be placed on analyses of the "whole" seismogram, since signal to noise is much greater for later phases.

The entire 1-5 Hz record from the Long Island Sound earthquake and a smaller Rhode Island earthquake are compared with synthetics in Fig. 7. Using the details of the *P* and *S* arrivals, focal depth can be estimated to about ± 0.5 km. Of course, the depth determination is model-dependent and misidentification of phases can lead to unreliable results.

The analysis techniques mentioned above; beamforming, instantaneous and adaptive polarization filtering, and slowness stacking were developed for use at CSS and are being implemented on the SUN computer. Programs already in use on the SUN include spectral analysis, spectrogram (frequency *versus* time *versus* dB), and waveform operations

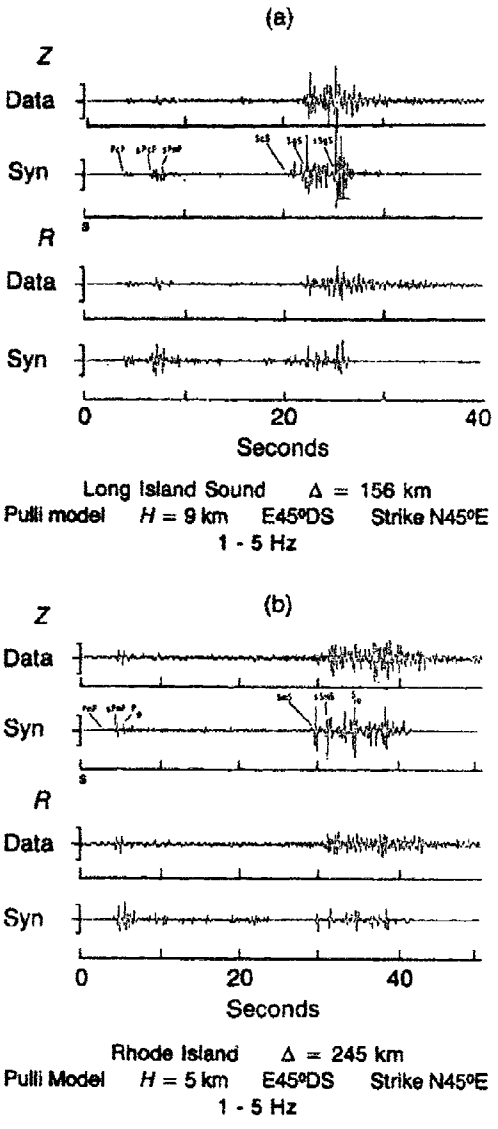

Fig. 7. Comparison of data with synthetic ground motion: (a) from the Long Island Sound earthquake; (b) from a Rhode Island earthquake (m_b = 2.7). *o*, *g*, *c*, and *m* identify the direct arrival and the three successively deeper crustal reflections, respectively. Prefix *s* leaves the source upward as an *S* wave.

(addition, subtraction, multiplication, or division of waveforms) and take full advantage of the available interactive graphics. Data transfer between "seismo" at CSS and "raisun" at RAI through the leased phone line is routine and even large files are easily transferred overnight. Large, computer-intensive programs such as synthetic seismograms are run directly on seismo at CSS.

Conclusions and Recommendations

An array of bottom hydrophones is an excellent receiver for short-period components of teleseismic P waves, and oceanic guided waves P_n and S_n. The unique WHA data are being used to study attenuation as a function of frequency needed for better estimation of yield, and the short-period characteristics of explosion and earthquake signals that are useful in discrimination. Further research along these lines should be rewarding.

Preprocessing of high-quality short-period (< 3 sec) digital data to reduce effects of scattering and lateral refraction facilities comparison with synthetics in an attempt to improve depth determination of shallow events from one or a few regional stations. Use of the "whole" seismogram is necessary for smaller events whose early arrivals are not well recorded. More comparisons between processed data and synthetics are needed to establish optimum procedures and their reliability and accuracy.

Data transfer and computation between CSS and RAI through the leased phone line to CSS and on the SUN computer at RAI are working well and improving.

References

Bache, T.C., H.J. Swanger, and B. Shkoller, 1980, *Synthesis of L_g in Eastern United States Crustal Models with Frequency Independent Q*, Semi-Annual Technical Report to DARPA, Systems, Science, and Software, SSS-R-81-4668, 114p., La Jolla, California.

Curtin, P.L., JJ. Pulli and C.B. Godkin, 1983, "A New Crustal Model for Central New England — Implications for Hypocentral Calculations and Fault Plane Solutions," Presented at the 55th Annual Meeting of the Seismological Society of America Eastern Section, September 1983 (Abstract).

Harvey, D., 1981, "Seismogram Synthetics Using Normal Mode Superposition: The Locked Mode Approximation Method," *Geophys. J. Roy. Astron. Soc.* **66**, 37-39.

McCreery, C.S., D.A. Walker, and G.H. Sutton, 1983, "Spectra of Nuclear Explosions, Earthquakes, and Noise from Wake Island Bottom Hydrophones," *Geophys. Res. Let.*, **10**, no. 1., 59-62.

Walker, D.A., C.S. McCreery, and G.H. Sutton, 1983, "Spectral Characteristics of High-Frequency P_n, S_n Phases in the Western Pacific," *J. Geophys. Res.*, **88**, 4289-4298.

Tools for Seismic Data Analysis and Management for Research and International Data Exchange

Ann U. Kerr

DARPA has initiated a program to develop a number of tools for more effective analysis and management of seismic data. This development program is motivated by two basic needs: the support of geophysical research for the development and testing of new signal processing techniques appropriate to the emergence of high quality digital data and the development of capability to participate in future treaty agreements on international seismic data exchange such as those currently under discussion by the Ad Hoc Group of Scientific Experts of the Conference on Disarmament. The needs differ in that research support requires a test bed for unproven research ideas for automated and interactive analysis while treaty support requires standardized methods for signal detection, event association and location. Neither can be supported without efficient methods for acquisition, processing, management, storage and distribution of large volumes of diverse seismic data.

Center for Seismic Studies

A prototype test bed is being developed to incorporate the tools required to support both geophysical research and international data exchange for treaty support. It is housed in the recently established DARPA Center for Seismic Studies which includes a resident research and operations staff and provision for visiting scientists. To date, scientists from several U.S. agencies and universities as well as research institutions in Germany, Norway and Sweden have resided at the Center as visiting scientists.

United Nations International Data Exchange Experiment

In 1985, the Conference on Disarmament Group of Scientific Experts sponsored a United Nations International Data Exchange Experiment to test some of the procedures being developed by the Group to support international data exchange anticipated under a future nuclear

test ban treaty. The United States participated in this experiment by successfully operating a prototype National and International Datacenter developed and located at the Center for Seismic Studies. Almost forty countries participated and contributed data from over 75 seismic stations. Data from six U.S. stations was collected and prepared for exchange. The processing involved the automatic and interactive analysis of waveforms needed to measure detection and other parameters.

As part of this experiment, Sweden and Moscow also operated International Data Centers which collected and rapidly processed all participant data. Daily lists of events with associated identification parameters were distributed to all the participant countries. This first practical test of a possible global data collection and exchange system was overall very successful. It also provided new insight into some of the potential problems in an operational data exchange environment.

Data Management Problem

The data management requirements for research and treaty monitoring can be sized in terms of the type of global network proposed for a Comprehensive Test Ban Treaty to achieve a worldwide detection threshold of about m_b 4.0: about 50 high-quality stations and small arrays. Modern three-component digital stations generate about 2,400 bits of data per second and arrays generate about 30,000 bits per second. This 50-station network would generate about 5,000 detections per day assuming about 100 detections per station. The collection and processing of this data would be a major task for an International Data Center and would probably result in a global bulletin containing about 10 to 20 events of m_b 4 or greater. In addition, a large number of the reported signals would be unassociated to events in the bulletin, as was the experience in the UN experiment.

Better techniques for automatically collecting and processing the volume of data anticipated from a global exchange are needed to minimize the task of the national and international datacenters. Further realization of the potential of digital seismic data requires the development of algorithms to automatically process this volume of data to detect signals, measure signal parameters, identify phases and associate signals to events. Human judgement is required for complete processing of the data which requires development of responsive high resolution graphical analysis. A centralized data facility solves the problem of efficient collection, organization and provision of data in a uniform format to numerous researchers and treaty participants, if combined with effective remote access. These problems are all being addressed in the research program, primarily at the Center for Seismic Studies.

DARPA Scientific Workstation

An important new tool was developed to faciliate remote access to the data archive at the Center and to provide scientific workstation capability local to the various research institutions. A small computer system incorporating recent advances in microprocessor technology has been developed which incorporates large memory, standard magnetic tape and large capacity disc. It is fully compatible with the Center software and allows researchers to access the computing and data resources at the Center to create and extract specialized data sets. While still under development, it is being used by many of the researchers in the program and by research institutions in four other countries.

During the data exchange experiment it supported all the functions of the U.S. National Datacenter and is serving as a model for many countries in their development of similiar capability. The workstation is expandable to accommodate multiple processors and other peripherals such as laser printers, optical disc and small satellite data receivers. Under a joint program with Australia, a version of the workstation is being developed to serve all the functions of a seismic station processor. It is being developed and tested to acquire analog data from the seismic array at Alice Springs, digitize, filter, beamform the data and detect, in realtime. Upon completion of the program, the workstation system design and software will be widely available and be a valuable resource to the seismological community as a prototype for many data collection and processing applications. The major contribution will be in the software compatibility and the informal network of researchers that has developed and will be able to exchange data and software with standard tools.

Acknowledgements

A number of university and industrial organizations have been instrumental in the DARPA development program and should be specially mentioned. The Applied Seismology Group of MIT-Lincoln Laboratory, under the direction of Dr. Michael Chinnery, developed the framework for the treaty research requirements and initiated the design and development of the system which evolved into the Center for Seismic Studies. The Computer Science and Applied Mathematics Department of Lawrence Berkeley Laboratories, under the direction of Dr. Carl Quong, provided computer science expertise and developed the concept and design for the relational database and developed some of the early graphics design. Systems Science and Software, under the direction of Dr. Bernard Minster and Dr. Jon Berger, developed the interactive waveform and non waveform graphics systems, the seismic database, and developed the pre-prototype workstation. Science Horizons, under the direction of Dr.

Ted Cherry and Mr. Robert Goff, has developed the full workstation system with its full set of capabilities and is developing the seismic station processor.

Teledyne Geotech, under the direction of Dr. William Dean, established the Center for Seismic Studies systems, facilities and operation. Science Applications International Corporation, under the direction of Dr. Carl Romney, Technical Director of the Center for Seismic Studies, fully established the Center as the research and treaty support testbed and continues to direct its development.

In the early development of the Group of Scientific Experts System, Dr. Roger Booth, Arms Control and Disarmament Agency, conceived of the need for some countries to have capability to more easily participate in treaty exchange and initiated a new concept, the Remote Seismic Terminal. Under a joint program with ACDA, Dr. Richard Moroney of CAC Sanford developed the first Remote Seismic Terminal system and demonstrated its practical use to the Group of Scientific Experts in Geneva.

Appendices

DARPA Office Directors

The following individuals served as Directors of the DARPA VELA Program Office throughout its history. The name of the office changed over the years from Nuclear Test Detection to Nuclear Monitoring Research Office to the current Geophysical Sciences, as the program evolved.

1959-1961

Dr. Carlton M. Beyer
First Director Nuclear Test Detection Office

1961-1963

Dr. George F. Bing

1963

Dr. Jack Ruina
Director of ARPA and Acting Director of Nuclear Test Detection Office
Established the VELA Seismological Center

1963-1966

Dr. Robert Frosch

1966-1968

Dr. Steven J. Lukasik
Served in dual capacity as Director of ARPA and
Acting Director Nuclear Monitoring Research Office (1968-1970)

1970-1975

Dr. Eric H. Willis

1975-1980

Dr. Carl F. Romney
Director of Nuclear Monitoring Research Office and
Deputy Director DARPA (1980-1981)

1980-1981

Col. George V. Bulin

1981 —

Dr. Ralph W. Alewine, III

DARPA Program Managers*

Ralph Alewine
Tom Bache
Charles Bates
Joe Berg
Rudy Black
Bob Blandford
Robert Brouns
George Bulin
Don Chandler
Don Clements
John DeNoyer
Jack Evernden
John Filson
Verne Fryklund
Ted George
Bob Harris
Ted Jones
Ann Kerr
George Lasche
John LeRohl
Austin Lowrey
Nick Orsini
Jack Pearce
John Poulson
Stan Ruby
Dave Russell
Alan Ryall
Alois Schardt
Harry Sonneman

* The above list is as complete as could be compiled from the available records.

Directory of Contributing Authors

Abdel-Gawad, M.
Rockwell International Science Center
P.O. Box 1085
Thousand Oaks, CA 91360

Aki, K.
Geophysics Department
University of Southern California
Los Angeles, CA 90007

Alewine, R.W., III
Defense Advanced Research
Projects Agency
1400 Wilson Blvd.
Arlington, VA 22209

Alexander, S. S.
Penn State University
403 Deike Bldg.
University Park, PA 16801

Anderson, D.L.
Director, Seismological Lab.
Mail Code 252-21
California Institute of Technology
Pasadena, CA 91125

Anderson, L.M.
Teledyne Geotech
314 Montgomery Street
Alexandria, VA 22314

Archambeau, C.B.
CIRES
University of Colorado
Boulder, CO 80309

Arvensen, C.G.
c/o D.V. Helmberger
Mail Code 252-21
Seismological Laboratory
California Institute of Technology
Pasadena, CA 91125

Bache, T.C.
Science Applications Int'l Corp.
10210 Campus Point Road
San Diego, CA 92121

Barker, B.W
S-Cubed
11800 Sunrise Valley Dr., Suite 1212
Reston, VA 22091

Barker, J.S.
Woodward-Clyde Consultants
566 El Dorado St.
Pasadena, CA 91101

Basham, P.W.
Earth Physics Branch Observatory Cr
Ottawa, Ontario KIA0Y3

Baumgardt, D.M.
ENSCO, Inc.
5400 Port Royal Road
Springfield, VA 22151

Bennett, T.J.
S-Cubed
11800 Sunrise Valley Dr., Suite 1212
Reston, VA 22091

Bethoux, N.
Radiomana
27 rue Claude Bernard
75005 Paris, France

Blandford, R.R.
Defense Advanced Research
Projects Agency
1400 Wilson Blvd.
Arlington, VA 22209

Bouchon, M.
Radiomana
27 rue Claude Bernard
75005 Paris, France

Bulau, J.R.
Rockwell International Science Center
P.O. Box 1085
Thousand Oaks, CA 91360

Bullitt, J.T.
Terrametrics Research
751 Main Street
Waltham, MA 02154

Burdick, L.J.
Woodward-Clyde Consultants
P.O. Box 93245
Pasadena, CA 91109-3245

Burnetti, J.A.
Teledyne Geotech
314 Montgomery St.
Alexandria, VA 22314

Campillo, M.
Radiomana
27 rue Claude Bernard
75005 Paris, France

Cansi, Y.
Radiomana
27 rue Claude Bernard
75005 Paris, France

Carter, J.A.
Rondout Associates
P.O. Box 224
Stone Ridge, NY 12484

Chen, J.J.
Dept. of Earth & Atmos. Sciences
Saint Louis University
P.O. Box 8099-Laclede Station
St. Louis, MO 63156

Claassen, J.P.
Organization 315
Sandia National Laboratories
Albuquerque, NM 87185

Cormier, V.F.
Earth Resources Lab., MIT
Bldg. E34, Room 450
42 Carleton St.
Cambridge, MA 02142

Dainty, A.M.
Earth Resources Lab
M.I.T.
42 Carleton Street
Cambridge, MA 02142

Denny, M.D.
Lawrence Livermore National
Laboratory
P.O. Box 808
Livermore, CA 94550

Der, Z.A.
Teledyne Geotech
314 Montgomery St.
Alexandria, VA 22314

Durham, H.B.
Code 0311
Sandia National Laboratories
P.O. Box 5800
Albuquerque, NM 87185

Dziewonski, A.M.
Department of Geological Sciences
Hoffman Laboratory
20 Oxford Street, Harvard Univ.
Cambridge, MA 02138

Esmersoy, C.
Earth Resources Lab., MIT
Building E34
42 Carleton Street
Cambridge, MA 02142

Farrell, W.E.
Science Applications Int'l Corp.
10210 Campus Point Road
San Diego, CA 92121

Flinn, E.A.
Code EE-8
NASA Headquarters
Washington, DC 20546

Giller, E.B.
Pacific Sierra Research
1401 Wilson Blvd.
Arlington, VA 22209

Given, J.W.
Sierra Geophysics, Inc., Suite 400
15446 Bell-Red Road
Redmond, WA 98052

Goncz, J.H.
Teledyne Geotech
314 Montgomery Sstreet
Alexandria, VA 22314

Grand, S.P.
Woodward-Clyde Consultants
P.O. Box 93245
Pasadena, CA 91109-3245

Greenfield, R.J.
The Pennsylvania State Univ.
403 Deike Bldg.
University Park, PA 16802

Gupta, I.N.
Teledyne Geotech
314 Montgomery St.
Alexandria, VA 22314

Harjes, H.-P.
Lehrstuhl fur Geophysik
Ruhr-Universitat Bochum
Postfach 10 21 48
D 4630 Bochum 1, FRG

Harkrider, D.G.
Assoc. Prof. of Geophysics
Seismological Laboratory
252-21, Cal. Inst. of Technology
Pasadena, CA 91125

Harris, D.B.
Lawrence Livermore National Laboratory
P.O. Box 808
Livermore, CA 94550

Helmberger, D.V.
Mail Code 252-21
Seismological Laboratory
California Institute of Technology
Pasadena, CA 91125

Helterbran, W.
Teledyne Geotech
314 Montgomery Dr.
Alexandria, VA 22314

Herrin, E.
Department of Geophysics
210 Heroy Building
Southern Methodist University
Dallas, TX 75275

Herrmann, R.B.
Dept of Earth & Atmos. Sciences
St. Louis University
P.O. Box 8099-Laclede Station
St. Louis, MO 63156

Husebye, E.S.
NTNF/NORSAR
P.O. Box 51
N-2007 Kjeller, Norway

Ingate, S.F.
NTNF/NORSAR
P.O. Box 51
N-2007 Kjeller, Norway

Johnson, G.W.
TRW R2/2076
One Space Park
Redondo Beach, CA 92024

Johnson, L.R.
Dept. of Geology and Geophysics
Room 485
University of California, Berkeley
Berkeley, CA 94720

Jordan, T.H.
Dept of Earth Atmospheric and Planetary Sciences, Room 54-518
Mass. Institute of Technology
Cambridge, MA 02139

Kaufman, S.K.
Sierra Geophysics, Inc. Suite 400
15446 Bel-Red Road
Redmond, WA 98052

Kemerait, R.C.
1930 Highway A-1A
Indian Harbour, FL 32927

Kerr, A.U.
Defense Advanced Research Projects Agency
1400 Wilson Blvd
Arlington, Va 22209

Lambert, D.B.
S-Cubed
11800 Sunrise Valley Dr., Suite 1212
Reston, VA 22091

Langston, C.A.
Penn State University
403 Deike Building
University Park, PA 16801

Lay, T.
Dept of Geological Sciences
Univ. Of Michigan
1006 C.C. Little Bldg.
Ann Arbor, MI 48109

Lees, A.C.
Teledyne Geotech
314 Montgomery St.
Alexandria, VA 22314

Lundquist, G.M.
Sierra Geophysics, Inc., Suite 400
15446 Bel-Red Road
Redmond, WA 98052

Mandal, B.
Dept. of Earth & Atmos. Sciences
Saint Louis University
P.O. Box 8099-Laclede Station
St. Louis, MO 63156

Marshall, M.E.
Teledyne Geotech
314 Montgomery St.
Alexandria, VA 22314

Marshall, P.D.
Ministry of Defence
Atomic Weapons Research Est.
Blacknest Seismological Center
Brimpton Reading, RG7 4RS UK

Massinon, B.
L. D. G.
Section Traitment de Donnees Geophysique
B.P. 12
91680 Bruyeres-le-Chatel, France

McCartor, G.D.
Mission Research Corporation
P.O. Drawer 719
Santa Barbara, CA 93103

McElfresh, T.W.
Teledyne Geotech
314 Montgomery St.
Alexandria, VA 22314

McEvilly, T.V.
Dept of Geology and Geophysics
Room 485
University of California, Berkeley
Berkeley, CA 94720

McLaughlin, K.L.
Teledyne Geotech
314 Montgomery Street
Alexandria, VA 22314

Mechler, P.
Radiomana
27 rue Claude Bernard
75005 Paris, France

Mellman, George R.
Sierra Geophysics, Inc., Suite 400
15446 Bel-Red Road
Redmond, WA 98052

Mills, J.M., Jr.
Lawrence Livermore National Laboratory
P.O. Box 808
Livermore, CA 94550

Minster, J.B.
Science Horizons, Inc.
710 Encinitas Blvd.
Encinitas, CA 92024

Mitchell, B.J.
Dept. of Earth & Atmos. Sci.
Saint Louis University
P.O. Box 8099 - Laclede Station
St. Louis, MO 63156

Murphy, J.R.
S-Cubed
11800 Sunrise Valley Dr., Suite 1212
Reston, VA 22091

Mykkeltveit, S.
NTNF/NORSAR
P.O. Box 51
N-2007 Kjeller, Norway

Navarre. F.
Radiomana
27 rue Claude Bernard
75005 Paris, France

North, R.G.
Earth Physics Branch Observatory Cr
Ottawa Ontario KIA0Y3

Nowack, R.
Geophysics Department
University of Southern California
Los Angeles, CA 90007

Nuttli, O.W.
Dept of Earth & Atmos. Sciences
St. Louis University
P.O. box 8099-Laclede Station
St. Louis, MO 63156

O'Donnell, A.
S-Cubed
11800 Sunrise Valley Dr., Suite 1212
Reston, VA 22091

Orcutt, J.A.
Geological Research Div (A-015)
Scripps Institution of Oceanography
La Jolla, CA 92093

Patton, H.J.
Lawrence Livermore National Laboratory
P.O. Box 808
Livermore, CA 94550

Peseckis, L.L.
Rondout Associates
P.O. box 224
Stone Ridge, NY 12484

Plantet, J.L.
L. D. G.
Section Traitment de Donnees Geophysique
B.P. 12
91680 Bruyeres-le-Chatel, France

Pomeroy, P.W.
Rondout Associates, Inc.
P.O. Box 224
Stone Ridge, NY 12484

Priestly, K.
Mackay School of Mines
University of Nevada
Reno, NV 89557

Ravaiau, N.
Radiomana
27 rue Claude Bernard
75005 Paris, France

Regan, J.
Seismological Laboratory
252-21, Cal. Inst. of Technology
Pasadena, CA 91125

Richards, P.G.
Lamont-Doherty Geological Observatory of Columbia Univ.
Palisades, NY 10964

Ringdal, F.
NTNF/NORSAR
P.O. Boks 51
N-2007 Kjeller, Norway

Rivers, D.W.
Ministry of Defence
Atomic Weapons Research Est.
Blacknest Seismological Center
Brimpton Reading, RG7 4RS UK

Romney, C.F.
Center for Seismic Studies
1300 N. 17th St., Suite 1450
Arlington, VA 22209

Samowitz, I.R.
Sierra Geophysics, Inc., Suite 400
15446 Bel-Red Road
Redmond, WA 98052

Schnitta-Israel, B.
South Fork Technological Consultants
29 Gann Road
East Hampton, NY 11937

Scott, P.
c/o Dr. D.V. Helmberger, Mail 252-21
Seismological Lab., Cal. Inst. of Tech.
Pasadena, CA 91125

Shumway, R.H.
616 Flamenco Pl
Davis, CA 95616

Smart, E.
Teledyne Geotech
314 Montgomery St
Alexandria, VA 22314

Stump, B.W.
Department of Geological Sciences
Southern Methodist University
Dallas, TX 75081

Sutton, G.H.
Rondout Associates, Inc.
P.O. Box 224
Stone Ridge, NY 12484

Taylor, S.R.
Lawrence Livermore National Laboratory
P.O. Box 808
Livermore, CA 94550

Thirlaway, H.I.S.
18 Speen Lane
Newbury, Berkshire
England

Thoresen, E.
NTNF/NORSAR
P.O. Box 51
N-2007 Kjeller, Norway

Tittmann, B.R.
Rockwell International Science Center
P.O. Box 1085
Thousand Oaks, CA 91360

Toksöz, M.N.
Earth Resources Lab., MIT
Bldg. E34, Room 400
42 Carleton Street
Cambridge, MA 02154

Trulio, J.G.
Applied Theory, Inc
930 S. La Brea Ave.
Los Angeles, CA 90036

Tucker, W.C.
Sierra Geophysics, Inc. Suite 400
15446 Bel-Red Road
Redmond, WA 98052

Wagner, R.A.
Teledyne Geotech
314 Montgomery St
Alexandria, VA 22314

Wallace, T.
Department of Geosciences
University of Arizona
Tucson, AZ 85721

Wang, C.Y.
Department of Geophysics
National Central University
Chung-Li
Taiwan 320 Republic of China

Woodhouse, J.H.
Department of Geological Sciences
Hoffman Laboratory
20 Oxford Street, Harvard Univ.
Cambridge, MA 02138

Wortman, W.R.
Mission Research Corporation
P.O. Drawer 719
Santa Barbara, CA 93101

Wu, R.
Geophysics Department
University of Southern California
Los Angeles, CA 90007